THE UNIVERSITY of ADELAIDE

Linking metals to magmatism: The role of the Hiltaba Suite and Gawler Range Volcanics, Gawler Craton

Claire E. Wade

Department of Earth Sciences
School of Physical Sciences
University of Adelaide

This thesis is submitted in fulfilment of the requirements for the degree of Doctor of Philosophy

2021

Table of Contents

Abstract	5
Declaration	6
Acknowledgements	7
Publications arising from this project	9
CHAPTER 1: INTRODUCTION AND THESIS OUTLINE	11
Introduction	12
Background	14
Thesis aim and outline	16
References	18
CHAPTER 2: HETEROGENEITY OF THE SUB-CONTINENTL LITHOSPHERIC MANTLE AND 'NON-JUVENILE' MANTLE ADDITIONS TO A PROTEROZOIC SILICIC LARGE IGNEOUS PROVINCE	27
Abstract	30
Introduction	30
Regional Geology of the Gawler Craton, South Australia	31
The Gawler Range Volcanics-Hiltaba Suite Silicic Large Igneous Province (GRV-HS SLIP)	35
Sample Descriptions	36
Methods	37
Geochemistry	39
Discussion	42
Conclusions	53
Acknowledgements	54
References	54
CHAPTER 3: SUBCONTINENTAL LITHOSPHERIC MANTLE CONTRIBUTION TO GRANITES IN A SILICIC LARGE IGNEOUS PROVINCE: GEOCHEMISTRY AND ND ISOTOPIC CONSTRAINTS	61
Abstract	64
Introduction	64
Pre-LIP basement geology	65
The 1590 Ma granitoids of the Hiltaba Suite	67
Methods	70
Results	71
Geochemistry	71
Discussion	72
Conclusions	85

Acknowledgements 86
References 86

CHAPTER 4: TEMPORAL, GEOCHEMICAL AND ISOTOPIC CONSTRAINTS ON PLUME-DRIVEN FELSIC AND MAFIC COMPONENTS IN A LARGE IGNEOUS PROVINCE 93
Abstract 96
Introduction 96
Geological Background and Unit Descriptions 99
Analytical Methods 102
Results 103
Discussion 108
Conclusions 121
Acknowledgements 122
References 122

CHAPTER 5: ZIRCON TRACE ELEMENT GEOCHEMISTRY AS AN INDICATOR OF MAGMA FERTILITY IN IRON OXIDE-COPPER-GOLD TERRAINS 133
Abstract 136
Introduction 136
Background 137
Methods and Results 139
Discussion 142
Conclusions 147
Acknowledgements 148
References 148

CHAPTER 6: MAPPING HYDROTHERMAL SYSTEMS IN IOCG DEPOSITS USING APATITE GEOCHRONOLOGY AND GEOCHEMISTRY: AN EXAMPLE FROM VULCAN CU-AU PROSPECT 155
Abstract 158
Introduction 158
The Olympic Cu-Au Province 159
The Vulcan Prospect 160
Methods 163
Results 164
Discussion 178
Conclusions 184

Acknowledgements 184
References 185

CHAPTER 7: DISCUSSION AND CONCLUSIONS 193

Appendix 1 209
Appendix Table A1: The whole-rock geochemical composition for complete filtered dataset for the Hiltaba Suite mafic dykes used in this contribution 210
Appendix Figure A1: Selected major and trace elements versus LOI for the mafic Hiltaba Suite 217

Appendix 2 219
Appendix Table A1 Mantle types identified and their average $\varepsilon_{Nd(1590\ Ma)}$ and Nd average compositions used in the mixing calculations 220
Appendix Table A2 Host rocks to the Hiltaba Suite granitoids and their average $\varepsilon_{Nd(1590\ Ma)}$ and average Nd compositions used in the mixing calculations 221
Appendix Table 2 A3: Host rock types to the Hiltaba Suite granitoids and their average $\varepsilon_{Nd(1590\ Ma)}$ and Nd average compositions used in the mixing calculations 222
Appendix Table A4: The whole-rock geochemical compositions for Hiltaba Suite granite samples collected in this study 223
Appendix Table A5 Hiltaba Suite granitoid groups and their average $\varepsilon_{Nd(1590\ Ma)}$ and Nd average compositions used in the mixing calculations 231

Appendix 3 233
Appendix Table A1:The whole-rock geochemical composition for the Gawler Range Volcanics collected in this study 234
Appendix Figure A1: $\varepsilon_{Nd(i)}$ vs Th, Nb/La and Th/Nb illustrating source composition variation in the SCLM and crustal assimilation traced via Th and decreasing $\varepsilon_{Nd(i)}$ values 252

Appendix 4 253
Appendix 1: Analytical Methods 254
Appendix Table A1: Metadata for LA-ICP-MS U-Pb analyses, University of Adelaide 257
Appendix Table A2: Metadata for LA-ICP-MS U-(Th-)Pb analyses, Boise State University 258
Appendix Table A3: Zircon trace element data for GRV and Hiltaba Suite samples analyzed at the University of Adelaide 259
Appendix Table A4: LA-ICP MS U-Pb data for GRV and Hiltaba Suite zircon analyzed at the University of Adelaide 274

Appendix Table A5: Zircon trace element data for GRV and Hiltaba Suite samples analyzed at Boise State University 282
Appendix Table A6: LA-ICP-MS U-Pb data for GRV and Hiltaba Suite zircon analyzed at the Boise State University 303
Appendix Table A7: LA-ICP MS U-Pb data for standard zircon analyzed at the University of Adelaide 317
Appendix Table A8: LA-ICPMS isotopic U-Pb and trace element concentration data for standards analyzed at Boise State University 325
Appendix Table A9: Standard calibration uncertainties, Boise State University 353
Appendix Figure A1: Total rare earth elements (REE) vs P concentrations for the data indicating inherited and discordant grains (>5% discordance), and 370 ppm P (dashed line). 354
Appendix Figure A2: A) Zircon rare earth element plots used in this study duplicated to include data that was excluded on the basis of discordance >5% and P > 370 ppm. 355
Appendix Figure A2: A) Bivariate plots used in this study duplicated to include data that was excluded on the basis of discordance >5% and P > 370 ppm. 356
Appendix Figure A4: Ti vs Hf for individual samples with ≥5 analyses for rhyolites and granitoids. 357

Appendix 5 357
Appendix Table A1: LA-ICP-MS U-Pb apatite data collected in this study 358
Appendix Table A2: LA-ICP-MS Trace element data collected for apatite from Vulcan Prospect in this study. 371
Appendix Table A3: LA-ICP-MS Trace element florencite data from the Vulcan Prospect, collected in this study. 389
Appendix Table A4: Magnetite and hematite LA-ICP-MS trace element data collected at Vulcan in this study. 399
Appendix Figure A1: Back scatter electron (BSE) and mineral liberation analysis (MLA) maps for thin sections analysed in this study. 435
Appendix Figure A2: Representative time-resolved profiles for apatite 446
Appendix Figure A3: Chondrite-normalised REY plots and transition metals vs total REY including samples below the detection limit 458

Appendix 6 461
Publications arising from this project 462

Abstract

Significant iron oxide-copper-gold (IOCG) and base metal mineralisation developed during a widespread Mesoproterozoic hydrothermal-magmatic event in southern Australia, producing the Olympic Cu-Au Province in the eastern Gawler Craton, IOCG ± Mo deposits in the Curnamona Province and gold and base metal deposits in the central Gawler Craton. Magmatic rocks of the ca. 1594–1586 Ma Gawler Range Volcanics (GRV), the ca. 1595–1570 Ma intrusive Hiltaba Suite and ca. 1595–1580 Ma Ninnerie Supersuite form a silicic-dominated large igneous province (LIP) that shows a consistent spatial relationship with these mineral deposits. Timing of IOCG mineralisation (1594–1590 Ma) overlaps with the early part of GRV and Hiltaba Suite magmatism. Mantle input is considered important in the formation these deposits. Therefore, analysis of the lithospheric mantle is a key step to understanding the greater hydrothermal-magmatic systems and their controls on mineralisation.

This thesis provides a comprehensive geochemical and isotopic framework for the LIP-related Gawler Craton ca. 1590 Ma GRV and Hiltaba Suite. Geochemical and isotopic signatures of mafic intrusive and extrusive rocks are consistent with an enriched, metasomatised subcontinental lithospheric mantle (SCLM) source. Enriched signatures are attributed to a primary metasomatised mantle source region that was altered during earlier subduction events. Geochemical and isotopic compositions of mafic and felsic components of the intrusive Hiltaba Suite show the rocks share a common SCLM source region. This SCLM source can account for the largely oxidised nature of the felsic magmas. The oxidising conditions in the felsic magma generation are of particular importance when considering the metallogenic fertility of the magmas.

Recent work has provided precise absolute timing on eruption of the GRV associated with the Gawler LIP. Detailed petrogenetic work on these temporally constrained lavas best supports generation of the GRV in an intracontinental, plume setting, analogous to a mafic LIP model. Mafic and felsic volcanism shows evidence for significant SCLM input during early stages (ca. 1594–1589 Ma), while volcanism after ca. 1589 Ma shows evidence for increasing crustal input.

Trace element geochemistry of zircons from > ca. 1590 Ma rhyolites and granitoids associated with IOCG mineralisation demonstrate more oxidising magmatic conditions and higher magmatic temperatures when compared with zircon from <1589 Ma mineralisation-absent magmatic rocks. Oxidised and less fractionated features of the older magmas appear to be instrumental to the Cu and Au mineralisation. This result suggests that a link to a metasomatised SCLM source is a fundamental process in the magma fertility and distribution of Gawler Craton IOCG deposits.

Apatite is a common accessory phase formed during the mineralisation process. The geochemical attributes of apatite is also investigated in this thesis using samples from the Vulcan Prospect, a hematite-dominated IOCG mineralising system in the Olympic Cu-Au Province. The U-Pb ages of apatite at the Vulcan Prospect can be related to multiple discrete episodes of hydrothermal activity at ca. 1600, 1100 and 450 Ma. Each apatite phase has characteristic trace and rare earth element compositions that display a transition from magnetite-associated to hematite-associated hydrothermal apatite which point to a multistage hydrothermal history.

I certify that this work contains no material which has been accepted for the award of any other degree or diploma in my name, in any university or other tertiary institution and, to the best of my knowledge and belief, contains no material previously published or written by another person, except where due reference has been made in the text. In addition, I certify that no part of this work will, in the future, be used in a submission in my name, for any other degree or diploma in any university or other tertiary institution without the prior approval of the University of Adelaide and where applicable, any partner institution responsible for the joint-award of this degree.

I acknowledge that copyright of published works contained within this thesis resides with the copyright holder(s) of those works.

I also give permission for the digital version of my thesis to be made available on the web, via the University's digital research repository, theLibrary Search and also through web search engines, unless permission has been granted by the University to restrict access for a period of time.

I acknowledge the support I have received for my research through the provision of an Australian Research Council Linkage Project LP160100578 *Source to spectrum: Finding deposits beyond the Fe oxide-Cu-Au envelope*.

Claire Elise Wade

9 of December, 2020

Acknowledgements

To my dear husband Ben, I thank you for your support, which came in many facets, moral, emotional, domestic, technical and as a mentor. You are always my go to man for advice, you always tell it how it is, so I know I can always get an honest answer from you. Whenever in doubt, “just ask Ben”. I appreciate your patience and understanding, as the last three years were challenging for us both, having big changes in our daily routines, but we made it work and I am grateful for the sacrifices you made for me to achieve this. Thank you for letting me have a life outside of my PhD – netball, swimming, dinner with the girls and watching football. Thank you for being a fantastic father and husband. You are my best friend. You are my love. You are my life.

To my children, Oliver and Isla, who have brought me joy and much needed distractions at times when I needed it most. Your lovely personalities and funny antics have brought humour, balance and enjoyment to my life, and kept me sane during the last three years. Thank you for understanding when I needed to go away for work or was a bit busy at times. I will always have time for you and I am so glad to see you both grow into strong and caring little people. Spending time with you has been, and always will be, filled with laughs, challenges, craziness, unpredictability, questions, silliness, concerts, crazy art and craft projects, fun and the best memories.

My amazing mother in law, Val, you deserve a massive thank you for all of the babysitting, more babysitting and extra babysitting you did. Without your help, I would not have been able to work longer hours in the lab when I needed to, attend and present at conferences and workshops, do field work and socialise with my colleagues. I would not have been able to do this without your willingness to spend time with your (favourite) grandchildren, and help with all of the little things as well. Ben and I appreciate everything you do for us and we love you for it.

I would like to thank my supervisory panel, Karin, Justin and Anthony. I would like to thank you for your guidance, for challenging me, your support and for making the last three years an enjoyable experience. I highly value your friendships and believe this has helped immensely in my journey. Your breadth of knowledge is incredible and I am glad I got to access your amazing minds during my PhD.

To Karin, for keeping me on track with administration and milestones, and reminding me of all the annoying little things that always needed to be done, and also for keeping things fun and interesting, and suggesting all sorts of “out there” ideas, and feeding my Tim Tam addiction.
Justin, I appreciate all of the late night e-mail exchanges we had, and your patience for me to (almost) catch up to your level. Thank you for agreeing to take me on as a student in the first place and being there whenever I needed advice or help, especially with Rhyolite-MELTS.

Anthony, you have always been an inspiration for me in the last 14 years I have been at the survey. Your encouragement and enthusiasm really helped me through the tough times, particularly when you were flying solo supervising, and you always remind me of the bigger picture and life after a PhD.

Acknowledgements

To Steve Hill, the director of the GSSA at the time, and Rian Dutch, GSSA, who were both instrumental in crossing the t's and dotting the lower case j's so that this could happen for me. I appreciate your support and encouragement for me to undertake a PhD, and I am grateful you were willing to give me a chance at proving this could work. Having your endorsement has contributed to my drive and made this possible. Thank you to Rohan Cobcroft, the current direcor of the GSSA for your continuing support.

The CERG group deserve a shout out Renee, Mitchell, Brad, Dillon, Jie and Funny. You have been the best group of people to share this experience with. You are all so helpful and supportive of each other, and it was really great to be part of such a fantastic research group. Thank you for being so inclusive and just being wonderful people in general. Thank you for making me feel young again too!

I would also like to thank the Department of Earth Sciences for awarding me the Eric Rudd Memorial Travel Scholarship for 2019. I had planned to present a paper at Goldschmidt Hawaii, however due to the COVID-19 pandemic I was unable attend the conference in person. I was able to participate in the conference in a virtual manner, and while the experience was new and different, I am sad that I was not able to have seen an olivine sand beach and more volcanoes while I was there. Thanks for the recognition. It would have been an amazing experience but I was able to enjoy the conference in other ways instead.

The GSSA cohort have also been awesome during the last three years. Thank you for your support and interest in my research (and life) and making coming into the office a positive and enjoyable experience. Thank you for inviting me to the writing retreats at Tonsley. Those writing days made a huge contribution to getting things done, and kept my motivation high. Thank you for always including me in meetings, even if I wasn't offering anything, I appreciate being able to contribute in other ways and being kept in the loop about what's been happening at the GSSA since I've been at uni. We too are a great group and the level of respect we have for each other is remarkable. I love being part of such a supportive and forward thinking group. I appreciate all of your friendships, advice, debates we have and support, and will continue to enjoy them.

The core library staff, particularly Dave, Keryn and Dale, you have done an impeccable job at dealing with copious amounts of requests, including numerous rock sample and drill core inspections. In addition, to Dale for even changing a flat tyre while I had a core inspection – thank you! Your efficiency and professionalism makes everyone's jobs easier and I know everyone appreciates the hard work you do.

Technical staff at Adelaide have been tremendous. I would like to thank David Bruce for hours of assistance in the clean lab and on the TIMS. You are ever so helpful and willing to try new techniques and share your ideas about everything. To the staff at Adelaide Microscopy, in particular Sarah and Ben, for assistance on the SEM and Laser, I thank you for your patience, and processing and technical expertise. Morgan Blades, I thank you for assistance with mineral separates and grain mounts and being a great inspiration and support, and a great friend.

JOURNAL ARTICLES

Wade, C. E., Reid, A. J., Payne, J. L. and Barovich, K. M., 2019. The link is in the geochemistry: how we know a metasomatised mantle underlies the mineral systems of the Gawler Craton. MESA Journal, 90: 42-47.

Wade, C. E., Payne, J. L., Barovich, K. M. and Reid, A. J., 2019. Heterogeneity of the sub-continental lithospheric mantle and 'non-juvenile' mantle additions to a Proterozoic silicic large igneous province. Lithos, 340-341, 87-107.

CONFERENCE PRESENTATIONS

Wade, C.E., Payne, J. L., Barovich, K. M., Gilbert, S. E., Wade, B. P. and Reid, A. J. 2020. A comparative study of zircon trace elements in A-type granites: Indicators for magma fertility in Cu and Au metallogenic provinces. Goldschmidt, 21–26 June 2020, Honolulu, USA.

Wade, C.E., Payne, J.L, Reid, A.J. and Barovich, K.M. 2019. The contribution of mafic and felsic magmatism to mineral deposits of South Australia. Iron-oxide copper gold Mineral Systems Workshop. 2–3 December, 2019. Adelaide, Australia.

Payne, J.L, **Wade, C.E.,** Reid, A.J., Crowley, J., Morrissey, L. and Bockmann, M. 2019. Deposits in the central Gawler Craton: the spectrum of processes from mantle to crust. Discovery Day, 28 November 2018, Adelaide, Australia.

Barovich, K. **Wade, C**. Morrissey, L., Payne, J. and Reid, A. 2019. A Nuna-Laurentia-Australia link: Views from Down Under. Geological Society of America Annual Meeting, Arizona, USA.

Wade, C.E., Payne, J.L, Reid, A.J. and Barovich, K.M. 2019. Mantle composition and the links between mineral systems in the Gawler Craton and Curnamona Province. Uncover Curnamona, 24 July, 2019. Broken Hill, Australia.

Wade, C.E., Payne, J.L, Barovich, K.M. and Reid, A.J. 2019. The Gawler Craton mantle and mineralisation from the geochemical and isotopic record. Discovery Day, 8 December, Adelaide, Australia.

Wade, C.E., Payne, J.L, Reid, A.J. and Barovich, K.M. 2018. Mantle input in c. 1590 Ma Gawler Craton mineralizing systems. GSA Earth Science Student Symposium South Australia. 5th December 2018, University of Adelaide, Adelaide.

Wade, C.E. Heterogeneity in the sub-continental lithospheric mantle: Multiple mantle source components identified from ca. 1590 Ma mafic intrusions, Gawler Craton. Australian Geoscience Council Convention, 14-18 October 2018, Adelaide Convention Centre, Adelaide.

Wade, C.E., Payne, J.L., Morrissey, L., LaFlamme, C. and Barovich, K.M. 2018. Mantle input in Gawler Craton mineralizing systems. Solomon Meeting 2018, 21 May – 25 May 2018 Clare Country Club, Clare Valley, South Australia.

Chapter 1

Introduction and thesis outline

INTRODUCTION

Recent studies have greatly expanded our understanding of the origin and evolution of large igneous provinces (LIPs). Much of this work has focussed on the production of the volumetrically dominant mafic rocks in LIPs, particularly in relation to mantle plume vs non-plume models, continental break-up, and their economic significance (e.g. Coffin and Eldholm 1992, Sheth 1999, Pirajno 2004, Ernst *et al.* 2019). However, many continental mafic LIPs also contain volumetrically significant silicic rocks (e.g 1.1 Ga Keweenan LIP, 180 Ma Karoo-Ferrar LIP, 132 Ma Parana-Etendeka LIP and 30 Ma Yemen-Ethiopia LIP; Ewart *et al.* 1998, Ayalew and Gibson 2009, Pankhurst *et al.* 2011). The mechanisms to produce large volumes of silicic magma (>100 000 km^3) in short periods of time (<1–10 Myr) in continental LIPs remain a contentious issue in igneous geology. Silicic large igneous provinces potentially represent significant crustal growth events and are commonly associated with mineralising systems (e.g. Great Bear Magmatic Zone, GRV-Hiltaba Suite). The issues in understanding the formation of silicic magmas in LIPs stem from the complexity in differentiating between various sources of magmas within the event. The mantle components often discussed in relation to LIP formation include plume, subcontinental lithospheric mantle (SCLM) and depleted mantle components (e.g. Chesley and Ruiz 1998, Hawkesworth *et al.* 2000, Kirstein *et al.* 2000, Ewart *et al.* 2004). Silicic magmas in a LIP may be purely mantle derived via fractional crystallisation to purely crustal derived via partial melting of the crust, or a mixed origin (Pearce 1996, Ewart *et al.* 1998, Bryan *et al.* 2002, Yang *et al.* 2004, Pankhurst *et al.* 2011, Ernst 2014).

Geochemical signatures of mafic rocks in continental LIPs reflect a contribution from the continental lithosphere, as evidenced by enriched isotopic ratios and lithospheric trace element signatures (e.g. Baker *et al.* 2000). Enriched geochemical and isotopic signatures may be produced via previous subduction events and mantle metasomatism (e.g. Erlank *et al.* 1987, McKenzie 1989, Turner and Hawkesworth 1995, Wittig *et al.* 2010, Li *et al.* 2014), therefore representing primary source region characteristics. Enriched signatures may also be obtained by processes that occurred after extraction from the mantle (*en route*), i.e. crustal contamination, assimilation and fractional crystallisation processes and wall rock assimilation (e.g. DePaolo 1981, Huppert *et al.* 1985, Sparks 1986, Beard *et al.* 2005). In mafic LIPs, silicic magmas are formed by processes of fractional crystallisation and assimilation of a mafic parent sourced from the convecting mantle or the lithosphere or both (Ewart *et al.* 1998).

Each magmatic rock therefore contains a signature which preserves the history of the deeper levels of the mantle and crust, and their interaction, at a particular location and point in time (e.g. Vielzeuf *et al.* 1990, Pearce 1996, Patiño Douce 1999). With respect to ore formation this is particularly important because it allows the characterisation of the source region and of metallogenetically important rocks and terrains, to be identified (Champion and Huston 2016).

Understanding and determining the source of metals in ore deposits can have significant implications for exploration methods and targets. Magma is regarded as playing a major role in many mineral systems, either by sourcing metals or facilitating the enrichment process in ore deposition (e.g. Feiss 1978, Hedenquist and Lowenstern 1994, Johnson and McCulloch 1995, Kerrich *et al.* 2000, Davidson *et al.* 2005, Pollard 2006, Groves *et al.* 2010, Skirrow *et al.* 2018). Whether the magmas are involved with metal endowment, metal enrichment or metal transport into the upper crust, understanding these processes is imperative to understanding the mineral system as a whole (Hedenquist and Lowenstern 1994). Subtle

differences in the isotopic compositions of magmatic rocks and minerals allows us to characterise the source regions important for geochemical processes such as ore formation.

In southern Australia, significant iron ox-

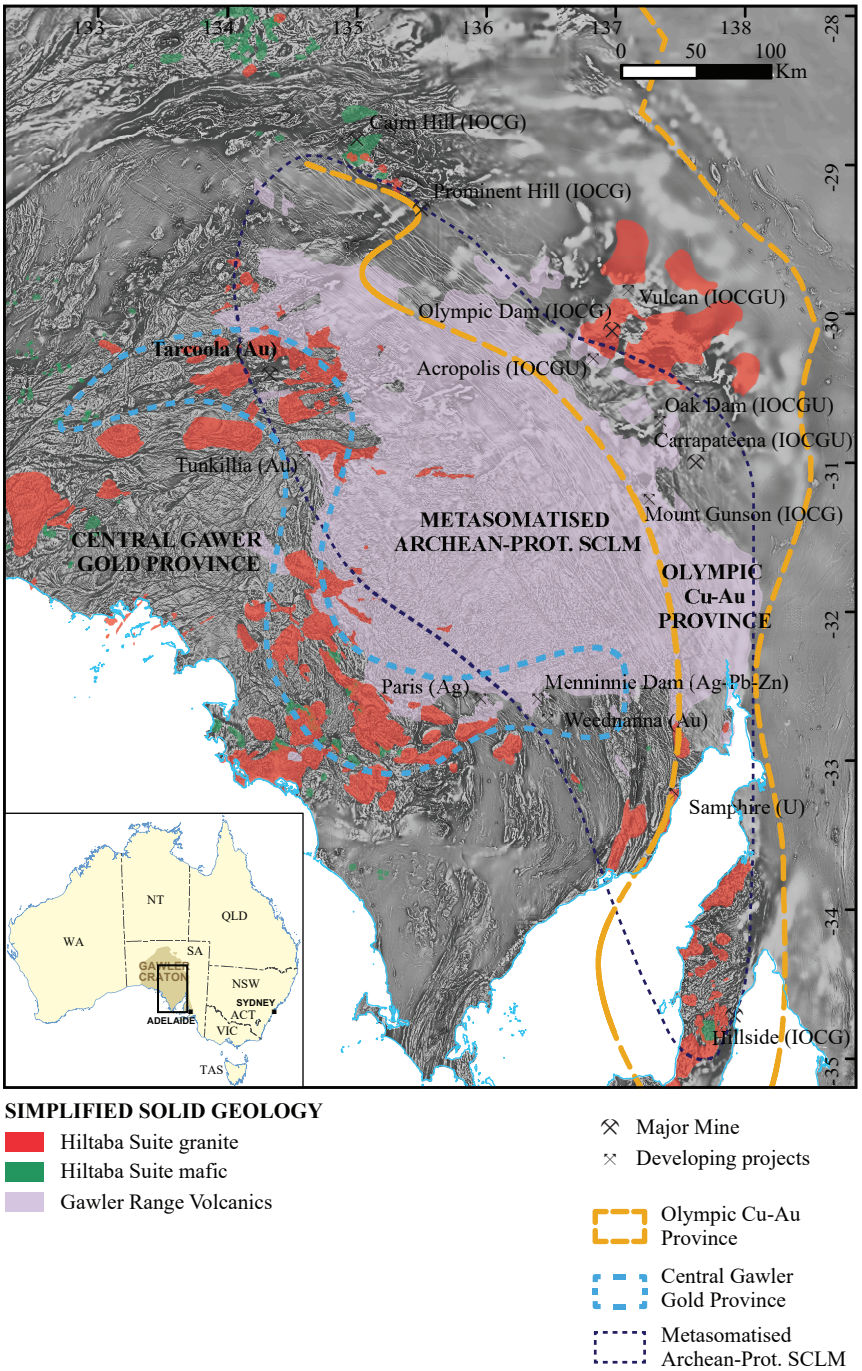

Figure 1: Simplified solid geology map of the Gawler Craton overlain on total magnetic imagery (TMI), highlighting the distribution of the ca. 1590 Ma magmatic rocks, the Gawler Range Volcanics and the Hiltaba Suite in relation to the two mineral provinces of the Gawler Craton, the IOCG Province and the Central Gawler Gold Province. Also shown in the metasomatised Archean to Proterozoic subcontinental lithospheric mantle (SCLM) as identified by Skirrow et al. (2018) and mines and developing projects are indicated. Source for TMI: https://map.sarig.sa.gov.au/

ide-copper-gold (IOCG) and base metal mineralisation was developed during the early stages of a wide-spread Mesoproterozoic hydrothermal-magmatic event in the Gawler Craton, producing a belt of IOCG-dominated deposits in the eastern Gawler Craton, including the world-class IOCG type-deposit Olympic Dam and gold and base metal deposits in the central Gawler Craton (Fig. 1; Budd and Skirrow 2007, Skirrow *et al.* 2007, Nicolson *et al.* 2017). Voluminous silicic-dominant magmatism is temporally and spatially related to these deposits, and magmatic input is considered an important feature into the development of IOCG and base metal mineral systems in the Gawler Craton (Johnson and Cross 1991, Haynes *et al.* 1995, Johnson and McCulloch 1995, Budd and Skirrow 2007, Skirrow *et al.* 2018). The currently known timing of mineralisation (1594–1590 Ma; Johnson and Cross 1995, Cherry *et al.* 2018, Courtney-Davies *et al.* 2020, McPhie *et al.* 2020) overlaps with the early part of Mesoproterozoic extrusive and intrusive magmatism in the Gawler Craton (Jagodzinski *et al.* 2016) This study focuses on the role of magmatism in the hydrothermal-magmatic system that formed ca. 1590 Ma and produced a number of economic iron oxide copper gold (IOCG) and base metal deposits in the Gawler Craton, South Australia. The key areas of investigation include:

- Characterising the composition of the mantle and crust at ca. 1590 Ma
- Assessing the relative contributions of the mantle and the crust to the ca. 1590 Ma magmatic rocks
- Investigating the overall magmatic system and its relationship to a silicic LIP and mantle plume
- Assessing fertility of granites and rhyolites in the ca. 1590 Ma silicic LIP
- Tracing geochemical signatures of minerals associated with mineralisation

Together, these chapters provide a detailed insight into a magmatic system related to hydrothermal-magmatic ore deposits and furthers our knowledge into components critical for ore formation by providing constraints on magmatic sources, magmatic conditions and by assessing magma fertility across a metalliferous region.

BACKGROUND

The association of magmatism and mineralisation in ore deposit formation has been long established (Feiss 1978, Ishihara 1981, Johnson and McCulloch 1995, Tosdal and Richards 2001, Kay and Mpodozis 2002, Pollard 2006). The geochemical signature of deposit-related magmatic rocks and their mineralising systems has been applied as a means to assess potential magma fertility in a variety of mineral deposit types. (e.g. Raveggi *et al.* 2015, Richards 2015, Sun *et al.* 2015, Lu *et al.* 2016, Shu *et al.* 2019, Wade *et al.* in prep). Mineral deposits have predictable and mappable patterns, often attributed to magma source components, fluid chemistry, tectonic settings and hydrothermal processes. Particular signatures linked to these processes can be traced in magma and mineral chemistry which can be used to reconstruct complex magmatic and hydrothermal processes, including ore deposit formation (e.g. Gregory *et al.* 2009, Courtney-Davies *et al.* 2020).

Magmatic-hydrothermal mineral systems include a variety of deposit types. In some instances, magma chemistry is strongly predicted by tectonic setting e.g. porphyry Cu deposits, and in these examples magma characteristics are well understood (Cooke *et al.* 2005, Tosdal *et al.* 2009, Sillitoe 2010, Richards 2011). Other hydrothermal-magmatic mineral systems such as IOCG-iron oxide-apatite (IOA) deposits are enigmatic. IOCG and IOA deposits represent a family of deposits that can form in a range of tectonic settings, leading to wide variety of deposit styles within this family (Groves *et al.* 2010, Corriveau *et al.* 2017, Simon *et al.* 2018). IOCG-IOA de-

posits do show an affiliation with each other in sharing a magmatic-hydrothermal origin, and links to a metasomatised mantle and high temperature oxidized felsic to intermediate magmatism (e.g. Bilenker et al. 2016, Day et al. 2016, Velasco et al. 2016, Storey and Smith 2017, Skirrow et al. 2018, Watts and Mercer 2020). As such, ore formation itself can often be linked to specific events that occurred in the local crust and these events can provide insight into the lithospheric/crustal architecture and geodynamic environment (Champion and Huston 2016).

Since the mid-90's, numerous studies have been carried out on deposits in the Olympic Cu-Au Province (Fig. 1), with particular focus on the Olympic Dam deposit (Johnson and Cross 1995, Johnson and McCulloch 1995, Skirrow *et al.* 2007, Kirchenbaur *et al.* 2016, Krneta *et al.* 2017, Courtney-Davies *et al.* 2019a, Courtney-Davies *et al.* 2019b, Schmandt *et al.* 2019, Verdugo-Ihl *et al.* 2019). These studies have used a range of techniques to understand and address the timing of formation of the deposit, the sources for the metals, the magmatic and hydrothermal conditions during ore deposit formation and subsequent post-mineralisation activity. While these studies have led to significant advances in understanding Olympic Dam and related deposits, the context for the overarching magmatic system and its relationship to ore formation is less well understood.

Significant mineralisation was developed in the Gawler Craton during a magmatic-hydrothermal event ca. 1590 Ma, resulting in a belt of IOCG-dominated deposits in the eastern Gawler Craton and Au-dominated deposits in the central Gawler Craton (Fig. 1; Skirrow *et al.* 2007, Reid 2019). The mineral provinces are known as the Olympic Cu-Au Province and the Central Gawler Gold Province, respectively (Fig. 1). High precision geochronological data indicates hydrothermal alteration and IOCG mineralisation occurred between 1594 and 1590 Ma (Cherry *et al.* 2018, Courtney-Davies *et al.* 2019c, Courtney-Davies *et al.* 2020, McPhie *et al.* 2020). Magmatic rocks of the Hiltaba Suite and Gawler Range Volcanics are intimately associated with much of the ca. 1590 Ma IOCG mineralisation (Haynes *et al.* 1995, Johnson and McCulloch 1995).

Mantle input is considered to be important for metals in the Olympic Dam Cu-Au province (Fig. 1), as evidenced by the association of juvenile isotopes with increasing Cu abundance (Johnson and Cross 1995, Skirrow *et al.* 2007). Central Gawler Gold Province deposits (Fig. 1) also display an association between mafic intrusions and Au (Budd and Skirrow 2007). Heinson *et al.* (2018) demonstrated major IOCG deposits in the eastern Gawler Craton have deep connections to the upper mantle-lower crust, where deep conductivity pathways are mapped to the ore deposit. The existence of a hydrous, metasomatised, heterogeneous and enriched lithospheric mantle is supported by geochemical and geophysical studies of mafic rocks (Thiel and Heinson 2013, Huang *et al.* 2016, Skirrow *et al.* 2018, Wade *et al.* 2019). Using the integration of such data, Skirrow *et al.* (2018) identified mantle domains beneath the Gawler Craton, and importantly identified a metasomatised Archean to Palaeoproterozoic sub-continental lithospheric mantle (SCLM) beneath the central-eastern Gawler Craton (Fig. 1). Its margins align with IOCG deposits in the east and gold deposits in the central Gawler Craton. Authors such as Groves *et al.* (2010) and Storey and Smith (2017) have highlighted the role of subduction modified sub-continental lithospheric mantle (SCLM) in the formation of Precambrian iron-oxide copper gold (IOCG) deposits. Therefore, analysis of the SCLM and its importance in the generation of IOCG and Au mineral systems is a key step to understanding the greater hydrothermal magmatic and mineral system in the Gawler Craton.

THESIS AIMS AND OUTLINE

This project aims to determine the magmatic contribution to iron oxide-Cu-Au, Pb-Zn, Ag and Au-only mineral deposits formed by the c. 1590 Ma fluid system related to the Gawler Range Volcanics (GRV) and Hiltaba Suite in the Gawler Craton. A combination of whole-rock, mineral and in-situ mineral geochemical analysis of magmatic rocks are used to map the spatial and temporal variation of crust and mantle reservoirs across the igneous province. These data will allow an assessment of magmatic potential to contribute to mineralisation, and the relative importance of mantle versus crustal input to ore deposit formation.

Each chapter focuses on a specific aspect related to the GRV–Hiltaba Suite magmatic system, from establishing broad controls on source region compositions and magmatic processes to mineral signatures specific at the deposit scale.

Chapter 2

Chapter 2 is published in Lithos as: Wade, C. E., Payne, J. L., Barovich, K. M. and Reid, A. J., 2019. Heterogeneity of the sub-continental lithospheric mantle and 'non-juvenile' mantle additions to a Proterozoic silicic large igneous province. Lithos, 340-341, 87-107.

This chapter focusses on determining the composition of the mantle at 1590 Ma using whole-rock geochemistry and Sm-Nd isotopic compositions of mafic intrusive rocks. A systematic, craton scale approach is used to map the composition of the subcontinental lithospheric mantle (SCLM) in the Gawler Craton. Common to most mafic Hiltaba Suite units are enrichment in high field strength elements (HFSE) and rare earth elements (REE), with varying degrees of, but generally negative, Nb-Ta-Ti anomalies, and widely variable Nd isotopic compositions. These geochemical and isotopic signatures are interpreted as primary source region signatures, suggesting a heterogeneous and enriched SCLM existed at 1590 Ma. Their compositions can be explained by metasomatism related to ancient subduction, occurring as early as the Archean.

Chapter 3

Chapter 3 is written for submission to Lithos as: Wade, C. E., Payne, J. L., Barovich, K. M., and Reid, A. J. Subcontinental lithospheric mantle contribution to granites in a silicic large igneous province: Geochemistry and Nd isotopic constraints.

This chapter focusses on using felsic intrusive rocks as 'lithoprobes' to determine the composition of the lithospheric column at 1590 Ma and relative contributions of mantle and crustal components in their petrogenesis. The granitic rocks are characterised by enriched high field strength element (HFSE) and rare earth element (REE) compositions and have high Ga/Al*10000 ratios. Coherent trends in major elements suggest fractional crystallisation was a major process in granitoid formation. Felsic Hiltaba Suite rocks have similar trace and RE element patterns to the mafic counterparts, suggesting a common source region. The felsic rocks are distinguished from the mafics by their large negative Ba, Sr, P, Eu and Ti anomalies on primitive mantle normalised trace element diagrams. Nd isotopic compositions are similar to slightly more negative than the mafic Hiltaba Suite, suggesting a source region with similar isotopic composition coupled with crustal contamination. Mixing calculations suggest varying amounts of crustal material were added to mantle-derived magmas to achieve the isotopic compositions in the granitic magmas. A combination of fractional crystallisation and assimilation and fractional crystallisation were involved in granitoid petrogenesis, likely representing a multistage process that varies across the craton. The results suggest mantle plume and mafic underplating played a key role in the formation of felsic magmas in the silicic

large igneous province, providing both a heat source for partial melting of a thickened, dehydrated, lower crust and parent magmas to generate granitic melts. A thickened crust may account for high pressures and temperatures, and the oxidised nature of the Hiltaba Suite.

Chapter 4

Chapter 4 is written for submission to Precambrian Research as: Wade, C. E., Payne, J. L., Barovich, K., Curtis, S. O., Jagodzinski, E., Reid, A. J. and Hill, J. Temporal, geochemical and isotopic constraints on plume-driven felsic and mafic components in a large igneous province.

Chapter 4 focusses on the broader magmatic system using time-constrained contemporaneous extrusive rocks. The volcanic rocks form a felsic large igneous province (LIP) erupted in ~8 Myr, producing >110 000 km^3 of erupted felsic and mafic lava. Newly published high precision geochronology has allowed for a detailed assessment of the geochemical and isotopic evolution of the GRV in this LIP. The magmatic evolution is consistent with other large igneous provinces with appreciable amounts of silicic volcanism related to mantle plume models. Basalts record increasing mantle enrichment followed by enriched juvenile mantle, while rhyolites record increasing mantle input followed by increasing crustal input. The final stages of magmatism represent a waning mantle plume phase. This Chapter quantifies the existence of a mantle plume in the generation of the GRV–Hiltaba Suite magmatic province in an intracontinental setting.

Chapter 5

Chapter 5 has is written for submission to Economic Geology as: Wade, C. E., Payne, J. L., Barovich, K. M., Crowley, J., Jagodzinski, E., Gilbert, S. E., Wade, B. P. and Reid, A. J. Zircon trace element geochemistry as an indicator of magma fertility in iron oxide-copper-gold provinces.

This chapter assesses the utility of trace element geochemistry of zircon as a fertility indicator for IOCG mineralisation. Zircon is ubiquitous in felsic magmas and can carry significant genetic information relating to signatures specific to source region composition and record changes in the crystallization environment (e.g. Hoskin and Ireland 2000, Ballard *et al.* 2002, Belousova *et al.* 2002, Belousova *et al.* 2005, Breiter *et al.* 2014, Kirkland *et al.* 2015, Samperton *et al.* 2015, Lu *et al.* 2016, Loader *et al.* 2017). By using time-constrained rhyolites and granitoids that occur both in metallogenic provinces and outside of these provinces across the Gawler Craton, in this chapter the contents of minor and trace elements in zircon are characterised and used to determine grades of fractionation and potential ore fertility. The study shows that the zircon geochemistry of the GRV and Hiltaba Suite rocks are indicative of oxidising magmatic conditions, which are favourable for Cu and Au mineralisation. Zircon from rhyolites and granitoids associated with mineralisation are distinguished from mineralisation-absent zircon by higher Eu/Eu*, Ce/Ce* and Ti values, and separate magma evolution paths with respect to Hf. These zircon characteristics correspond to lower degrees of fractionation and/or crustal assimilation, more oxidizing magmatic conditions and higher magmatic temperatures, respectively, in magmas coeval with mineralisation. In this respect, higher oxidation state, lower degrees of fractionation and higher magmatic temperatures are considered to be features of fertile magmas in southern Australian IOCG terrains. Similar zircon REE characteristics are shared between magmas associated with southern Australian IOCGs and IOA rhyolites from the St Francois Mountains, Missouri, namely high Ce/Ce* and high Dy/Yb, indicative of oxidized and dry magmas, respectively. The oxidized nature, as indicated by high Ce/Ce* ratios, is considered a key element in magma fertility in IOCG-IOA terrains.

Chapter 6

Chapter 6 is prepared in manuscript format as: Wade, C. E., Payne, Barovich, K. M., Grooby, C., Reid, A. J., Payne, J. L. and Gilbert, S. E,. Mapping hydrothermal systems in IOCG deposits using apatite geochronology and geochemsitry: An example from Vulcan Cu-Au prospect

.

This chapter investigates trace element geochemistry of iron-oxide and phosphate minerals in the Vulcan Cu-Au prospect, Gawler Craton. The Vulcan prospect is a hematite breccia-hosted Cu-Au system that formed ca. 1590 Ma, hosted within ca. 1745 Ma granite (Reid *et al.* 2013). Trace element geochemistry of iron oxides at Vulcan record variation in transition metal and high field strength element distributions. Magnetite is characterised by higher V and Ni, and lower Co, Mg, Mn, Cu, Nb, Y, Th, U, Mo+Sn+W and REY compared with hematite. Uranium and Th are positively correlated with REY in magnetite and hematite suggesting partitioning of U, Th, REE and Y into accessory phases within the Fe-oxides. U-Pb apatite geochronology indicates at least three stages of apatite growth or recrystallisation occurred at the Vulcan Prospect. Each apatite stage has characteristic trace element and REY compositions that can be related to changes in hydrothermal activity and assemblages. Apatite associated magnetite is ca. 1600 Ma apatite and characterised by LREE enrichment and HREE depletions. Two stages of apatite are associated with hematite and recorded U-Pb ages of ca. 1100 Ma and ca. 450 Ma. Hematite-associated apatite is characterised by LREE depletions, which become increasingly depleted as age decreases. LREE depletions in hematite-associated apatite are attributed to breakdown of apatite in acidic fluid conditions accompanied by the new growth of the REE phosphate mineral florencite. The temporal constraints on the geochemistry of apatite show the changing fluid parameters and hydrothermal assemblage hosting the apatite, suggesting apatite geochemistry is able to fingerprint changes in individual assemblages and changes in the REY behaviour during the evolution of the Vulcan Prospect.

Vulcan shares similar attributes with Olympic Dam, including: 1) hematite-sericite-chlorite-carbonate dominated breccias with abundant phosphate accessory minerals; 2) iron-oxides showing similar trace element characteristics; 3) similar geochemical attributes in apatite that can be related to changes in hydrothermal activity; and 4) similar ages relating to the same mineralisation event and subsequent hydrothermal events.

Chapter 7

This chapter provides a broad summary of this thesis. Future work and direction is then discussed in the context of furthering our understanding of hydrothermal magmatic-related mineral systems.

REFERENCES

Ayalew, D. and Gibson, S. A., 2009. Head-to-tail transition of the Afar mantle plume: Geochemical evidence from a Miocene bimodal basalt–rhyolite succession in the Ethiopian Large Igneous Province. Lithos, v. 112, p. 461-476. doi: https://doi.org/10.1016/j.lithos.2009.04.005

Baker, J. A., Macpherson, C. G., Menzies, M. A., Thrilwall, M. F., Al-Kasasi, M. and Mattey, D. P., 2000. Resolving Crustal and Mantle Contributions to Continental Flood Volcanism, Yemen; Constraints from Mineral Oxygen Isotope Data. Journal of Petrology, v. 41, p. 1805-1820. doi: https://doi.org/10.1093/petrology/41.12.1805

Ballard, J. R., Palin, M. J. and Campbell, I. H., 2002. Relative oxidation states of magmas inferred from Ce(IV)/Ce(III) in zircon: application to porphyry copper deposits of northern Chile. Contributions to Mineral-

ogy and Petrology, v. 144, p. 347-364. doi: https://doi.org/10.1007/s00410-002-0402-5

Beard, J. S., Ragland, P. C. and Crawford, M. L., 2005. Reactive bulk assimilation: A model for crust-mantle mixing in silicic magmas. Geology v. 33, p. 681-684. doi: https://doi.org/10.1130/G21470AR.1

Belousova, E. A., Griffin, W. L. and O'Reilly, S. Y., 2005. Zircon Crystal Morphology, Trace Element Signatures and Hf Isotope Composition as a Tool for Petrogenetic Modelling: Examples From Eastern Australian Granitoids. Journal of Petrology, v. 47, p. 329-353. doi: https://doi.org/10.1093/petrology/egi077

Belousova, E. A., Griffin, W. L., O'Reilly, S. Y. and Fisher, N. I., 2002. Igneous zircon: trace element composition as an indicator of source rock type. Contributions to Mineralogy and Petrology, v. 143, p. 602–622. doi: https://doi.org/10.1007/s00410-002-0364-7

Bilenker, L. D., Simon, A. C., Reich, M., Lundstrom, C. C., Gajos, N., Bindeman, I., Barra, F. and Munizaga, R., 2016. Fe–O stable isotope pairs elucidate a high-temperature origin of Chilean iron oxide-apatite deposits. Geochimica et Cosmochimica Acta, v. 177, p. 94-104. doi: https://doi.org/10.1016/j.gca.2016.01.009

Breiter, K., Lamarão, C. N., Borges, R. M. K. and Dall'Agnol, R., 2014. Chemical characteristics of zircon from A-type granites and comparison to zircon of S-type granites. Lithos, v. 192-195, p. 208-225. doi: https://doi.org/10.1016/j.lithos.2014.02.004

Bryan, S. E., Riley, T. R., Jerram, D. A., Stephens, C. J. and Leat, P. T., 2002. Silicic volcanism: an undervalued component of large igneous provinces and volcanic rifted margins. In: Menzies, M. A., Klemperer, S. I., Ebinger, C. J. and Baker, J. (Eds), Volcanic Rifted Margins. Geological Society of America, Special Paper, v. 362, p. 97–118. https://doi.org/10.1130/0-8137-2362-0.97

Budd, A. R. and Skirrow, R. G., 2007. The Nature and Origin of Gold Deposits of the Tarcoola Goldfield and Implications for the Central Gawler Gold Province, South Australia. Economic Geology, v. 102, p. 1541–1563. doi: https://doi.org/10.2113/gsecongeo.102.8.1541

Champion, D. C. and Huston, D. L., 2016. Radiogenic isotopes, ore deposits and metallogenic terranes: Novel approaches based on regional isotopic maps and the mineral systems concept. Ore Geology Reviews, v. 76, p. 229-256. doi: https://doi.org/10.1016/j.oregeorev.2015.09.025

Cherry, A. R., Ehrig, K., Kamenetsky, V. S., McPhie, J., Crowley, J. L. and Kamenetsky, M. B., 2018. Precise geochronological constraints on the origin, setting and incorporation of ca. 1.59 Ga surficial facies into the Olympic Dam Breccia Complex, South Australia. Precambrian Research, v. 315, p. 162-178. doi: https://doi.org/10.1016/j.precamres.2018.07.012

Chesley, J. T. and Ruiz, J., 1998. Crust–mantle interaction in large igneous provinces: Implications from the Re–Os isotope systematics of the Columbia River flood basalts. Earth and Planetary Science Letters, v. 154, p. 1-11. doi: https://doi.org/10.1016/S0012-821X(97)00176-3

Coffin, M. F. and Eldholm, O., 1992. Volcanism and continental break-up: a global compilation of large igneous provinces. Geological Society, London, Special Publications, v. 68, p. 17-30. doi: https://doi.org/10.1144/gsl.Sp.1992.068.01.02

Cooke, D. R., Hollings, P. and Walshe, J. L., 2005. Giant Porphyry Deposits: Characteristics, Distribution, and Tectonic Controls. Economic Geology, v. 100, p. 801-818. doi: https://doi.org//10.2113/gsecongeo.100.5.801

Corriveau, L., C, Potter, E., G, Acosta-Gongo-

ra, P., A, Blein, O., Montreuil, J.-F., F, De Toni, A., A, Day, W., C, Slack, J., F, Ayuso, R., A and Hanes, R., 2017. Petrological Mapping and Chemical Discrimination of Alteration Facies as Vectors to IOA, IOCG, and Affiliated Deposits within Laurentia and Beyond. In: (Eds), SGA Québec 2017. v. p. Page. 408. doi: https://hal-brgm.archives-ouvertes.fr/hal-01488309/document

Courtney-Davies, L., Ciobanu C.L., Verdugo-Ihl M.R., Slattery A., Cook N.J., Dmitrijeva M., Keyser W., Wade B.P., Domnick U.I., Ehrig K., Xu J. and Kontonikas-Charos, A., 2019a. Zircon at the Nanoscale Records Metasomatic Processes Leading to Large Magmatic–Hydrothermal Ore Systems. Minerals, v. 9, p. 364. doi: https://doi.org/10.3390/min9060364

Courtney-Davies, L., Ciobanu, C. L., Tapster, S. R., Cook, N. J., Ehrig, K., Crowley, J. L., Verdugo-Ihl, M. R., Wade, B. P. and Condon, D. J., 2020. Opening the magmatic-hydrothermal window: High-precision U-Pb geochronology of the Mesoproterozoic Olympic Dam Cu-U-Au-Ag deposit, South Australia. Economic Geology, v. p. doi: https://doi.org/10.5382/econgeo.4772

Courtney-Davies, L., Ciobanu, C. L., Verdugo-Ihl, M. R., Dmitrijeva, M., Cook, N. J., Ehrig, K. and Wade, B. P., 2019b. Hematite geochemistry and geochronology resolve genetic and temporal links among iron-oxide copper gold systems, Olympic Dam district, South Australia. Precambrian Research, v. 335, p. 105480. doi: https://doi.org/10.1016/j.precamres.2019.105480

Courtney-Davies, L., Tapster, S. R., Ciobanu, C. L., Cook, N. J., Verdugo-Ihl, M. R., Ehrig, K. J., Kennedy, A. K., Gilbert, S. E., Condon, D. J. and Wade, B. P., 2019c. A multi-technique evaluation of hydrothermal hematite UPb isotope systematics: Implications for ore deposit geochronology. Chemical Geology, v. 513, p. 54-72. doi: https://doi.org/10.1016/j.chemgeo.2019.03.005

Davidson, P., Kamenetsky, V., Cooke, D. R., Frikken, P., Hollings, P., Ryan, C., Van Achterbergh, E., Mernagh, T., Skarmeta, J., Serrano, L. and Vargas, R., 2005. Magmatic Precursors of Hydrothermal Fluids at the Río Blanco Cu-Mo Deposit, Chile: Links to Silicate Magmas and Metal Transport. Economic Geology, v. 100, p. 963-978. doi: https://doi.org/10.2113/gsecongeo.100.5.963

Day, W. C., Slack, J. F., Ayuso, R. A. and Seeger, C. M., 2016. Regional Geologic and Petrologic Framework for Iron Oxide ± Apatite ± Rare Earth Element and Iron Oxide Copper-Gold Deposits of the Mesoproterozoic St. Francois Mountains Terrane, Southeast Missouri, USA. Economic Geology, v. 111, p. 1825-1858. doi: https://doi.org/10.2113/econgeo.111.8.1825

DePaolo, D. J., 1981. Trace element and isotopic effects of combined wallrock assimilation and fractional crystallization. Earth and Planetary Science Letters, v. 53, p. 189-202. doi: https://doi.org/10.1016/0012-821X(81)90153-9

Erlank, A. J., Waters, F. G., Hawkesworth, C. J., Haggerty, S. E., Allsopp, H. L., Rickard, R. S. and Menzies, M. A., 1987. Evidence for mantle metasomatism in preidotite nodules from the Kimberly pipes, South Africa. In: Menzies, M. A. and Hawkesworth, C. J. (Eds), Mantle Metasomatism. Geological Series, Academic Press, v. p. 221-312.

Ernst, R. E., 2014. Large igneous provinces: Cambridge University Press, Cambridge, UK. v. p. availabie at: https://doi.org/10.1017/CBO9781139025300

Ernst, R. E., Liikane, D. A., Jowitt, S. M., Buchan, K. L. and Blanchard, J. A., 2019. A new plumbing system framework for mantle plume-related continental Large Igneous Provinces and their mafic-ultra-

mafic intrusions. Journal of Volcanology and Geothermal Research, v. 384, p. 75-84. doi: https://doi.org/10.1016/j.jvolgeores.2019.07.007

Ewart, A., Marsh, J. S., Milner, S. C., Duncan, A. R., Kamber, B. S. and Armstrong, R. A., 2004. Petrology and Geochemistry of Early Cretaceous Bimodal Continental Flood Volcanism of the NW Etendeka, Namibia. Part 1: Introduction, Mafic Lavas and Re-evaluation of Mantle Source Components. Journal of Petrology, v. 45, p. 59-105. doi: https://doi.org/10.1093/petrology/egg083

Ewart, A., Milner, S. C., Armstrong, R. A. and Dungan, A. R., 1998. Etendeka Volcanism of the Goboboseb Mountains and Messum Igneous Complex, Namibia. Part I: Geochemical Evidence of Early Cretaceous Tristan Plume Melts and the Role of Crustal Contamination in the Paraná–Etendeka CFB. Journal of Petrology, v. 39, p. 191-225. doi: https://doi.org.10.1093/petroj/39.2.191

Feiss, P. G., 1978. Magmatic sources of copper in porphyry copper deposits. Economic Geology, v. 73, p. 397-404. doi: https://doi.org/10.2113/gsecongeo.73.3.397

Gregory, C. J., McFarlane, C. R. M., Hermann, J. and Rubatto, D., 2009. Tracing the evolution of calc-alkaline magmas: In-situ Sm–Nd isotope studies of accessory minerals in the Bergell Igneous Complex, Italy. Chemical Geology, v. 260, p. 73-86. doi: https://doi.org/10.1016/j.chemgeo.2008.12.003

Groves, D. I., Bierlein, F. P., Meinert, L. D. and Hitzman, M. W., 2010. Iron Oxide Copper-Gold (IOCG) Deposits through Earth History: Implications for Origin, Lithospheric Setting, and Distinction from Other Epigenetic Iron Oxide Deposits. Economic Geology, v. 105, p. 641-654. doi: https://doi.org/10.2113/gsecongeo.105.3.641

Hawkesworth, C. J., Gallagher, K., Kirstein, L., Mantovani, M. S. M., Peate, D. W. and Turner, S. P., 2000. Tectonic controls on magmatism associated with continental break-up: an example from the Paraná–Etendeka Province. Earth and Planetary Science Letters, v. 179, p. 335-349. doi: https://doi.org/10.1016/S0012-821X(00)00114-X

Haynes, D. W., Cross, K. C., Bills, R. T. and Reed, M. H., 1995. Olympic Dam ore genesis; a fluid-mixing model. Economic Geology, v. 90, p. 281-307. doi: https://doi.org/10.2113/gsecongeo.90.2.281

Hedenquist, J. W. and Lowenstern, J. B., 1994. The role of magmas in the formation of hydrothermal ore deposits. Nature, v. 370, p. 519–528. doi: https://doi.org/10.1038/370519a0

Heinson, G., Didana, Y., Soeffky, P., Thiel, S. and Wise, T., 2018. The crustal geophysical signature of a world-class magmatic mineral system. Scientific Reports, v. 8, p. 10608. doi: https://doi.iorg/10.1038/s41598-018-29016-2

Hoskin, P. W. O. and Ireland, T. R., 2000. Rare earth element chemistry of zircon and its use as a provenance indicator. Geology, v. 28, p. 627–630. doi: https://doi.org/10.1130/0091-7613(2000)28<627:REECOZ>2.0.CO;2

Huang, Q., Kamenetsky, V. S., Ehrig, K., McPhie, J., Kamenetsky, M., Cross, K., Meffre, S., Agangi, A., Chambefort, I., Direen, N. G., Maas, R. and Apukhtina, O., 2016. Olivine-phyric basalt in the Mesoproterozoic Gawler silicic large igneous province, South Australia: Examples at the Olympic Dam Iron Oxide Cu–U–Au–Ag deposit and other localities. Precambrian Research, v. 281, p. 185-199. doi: https://doi.org/10.1016/j.precamres.2016.05.019

Huppert, H. E., Stephen, R. and Sparks, J., 1985. Cooling and contamination of mafic and ultramafic magmas during ascent through continental crust. Earth and

Planetary Science Letters, v. 74, p. 371-386. doi: https://doi.org/10.1016/S0012-821X(85)80009-1

Ishihara, S., 1981. The granitoid series and mineralization: Economic Geology. v. 75th Anniversay Volume, p. 458-484. availabie at:

Jagodzinski, E. A., Reid, A., Crowley, J., McAvaney, S. and Wade, C., 2016. Precise zircon U–Pb dating of a Mesoproterozoic silicic large igneous province: The Gawler Range Volcanics and Benagerie Volcanic Suite, South Australia. Hornsby, NSW: Geological Society of Australia. Geological Society of Australia Abstracts, v. No. 118, p. doi: https://sarigbasis.pir.sa.gov.au/WebtopEw/ws/samref/sarig1/image/DDD/RB201600032.pdf

Johnson, J. P. and Cross, K. C., 1991. Geochronological and Sm-Nd isotopic constraints on the genesis of the Olympic Dam Cu-U-Au-Ag deposit, South Australia. In: Pagel, M. and Leroy, J. L. (Eds), Source transport and deposition of ore metals. Balkema, v. p. 395-400.

Johnson, J. P. and Cross, K. C., 1995. U-Pb geochronological constraints on the genesis of the Olympic Dam Cu-U-Au-Ag deposit, South Australia. Economic Geology and the Bulletin of the Society of Economic Geologists, v. 90, p. 1046-1063. doi: https://doi.org/10.2113/gsecongeo.90.5.1046

Johnson, J. P. and McCulloch, M. T., 1995. Sources of mineralising fluids for the Olympic Dam Deposit (South Australia); Sm-Nd isotopic constraints. Chemical Geology, v. 121, p. 177-199. doi: https://doi.org/10.1016/0009-2541(94)00125-R

Kay, S. M. and Mpodozis, C., 2002. Magmatism as a probe to the Neogene shallowing of the Nazca plate beneath the modern Chilean flat-slab. Journal of South American Earth Sciences, v. 15, p. 39–57. doi: http://dx.doi.org/10.1016/S0895-9811(02)00005-6

Kerrich, R., Goldfarb, R., Groves, D. and Garwin, S., 2000. The geodynamics of world-class gold deposits: Characteristics, space-time distributions, and origins. Reviews in Economic Geology, v. 13, p. 501–551. doi: https://doi.org/10.5382/Rev.13.15

Kirchenbaur, M., Maas, R., Ehrig, K., Kamenetsky, V. S., Strub, E., Ballhaus, C. and Münker, C., 2016. Uranium and Sm isotope studies of the supergiant Olympic Dam Cu–Au–U–Ag deposit, South Australia. Geochimica et Cosmochimica Acta, v. 180, p. 15-32. doi: https://doi.org/10.1016/j.gca.2016.01.035

Kirkland, C. L., Smithies, R. H., Taylor, R. J. M., Evans, N. and McDonald, B., 2015. Zircon Th/U ratios in magmatic environs. Lithos, v. 212-215, p. 397-414. doi: https://doi.org/10.1016/j.lithos.2014.11.021

Kirstein, L. A., Peate, D. W., Hawkesworth, C. J., Turner, S. P., Harris, C. and Mantovani, M. S. M., 2000. Early Cretaceous Basaltic and Rhyolitic Magmatism in Southern Uruguay Associated with the Opening of the South Atlantic. Journal of Petrology, v. 41, p. 1413-1438. doi: https://doi.org/10.1093/petrology/41.9.1413

Krneta, S., Ciobanu, C. L., Cook, N. J., Ehrig, K. and Kontonikas-Charos, A., 2017. Rare Earth Element Behaviour in Apatite from the Olympic Dam Cu–U–Au–Ag Deposit, South Australia. Minerals v. 7, p. 135. doi: https://doi.org/10.3390/min7080135

Li, X.-Y., Zheng, J.-P., Ma, Q., Xiong, Q., Griffin, W. L. and Lu, J.-G., 2014. From enriched to depleted mantle: Evidence from Cretaceous lamprophyres and Paleogene basaltic rocks in eastern and central Guangxi Province, western Cathaysia block of South China. Lithos, v. 184-187, p. 300-313. doi: https://doi.org/10.1016/j.lithos.2013.10.039

Loader, M. A., Wilkinson, J. J. and Armstrong, R. N., 2017. The effect of titanite crystal-

lisation on Eu and Ce anomalies in zircon and its implications for the assessment of porphyry Cu deposit fertility. Earth and Planetary Science Letters, v. 472, p. 107-119. doi: https://doi.org/10.1016/j.epsl.2017.05.010

Lu, Y.-J., Loucks, R. R., Fiorentini, M., McCuaig, T. C., Evans, N. J., Yang, Z.-M., Hou, Z.-Q., Kirkland, C. L., Parra-Avila, L. A., Kobussen, A. and Richards, J. P., 2016. Zircon Compositions as a Pathfinder for Porphyry Cu ± Mo ± Au Deposits. In: (Eds), Tectonics and Metallogeny of the Tethyan Orogenic Belt. Society of Economic Geologists Special Publication, v. 19, Paper 13, p.

McKenzie, D., 1989. Some remarks on the movement of small melt fractions in the mantle. Earth and Planetary Science Letters, v. 95, p. 53-72. doi: https://doi.org/10.1016/0012-821X(89)90167-2

McPhie, J., Ehrig, K. J., Kamenetsky, M. B., Crowley, J. L. and Kamenetsky, V. S., 2020. Geology of the Acropolis prospect, South Australia, constrained by high-precision CA-TIMS ages. Australian Journal of Earth Sciences, v. 67, p. 699-716. doi: https://doi.org/10.1080/08120099.2020.1717617

Nicolson, B. E., Anderson, J. A. and Cross, K. C., 2017. Menninnie Dam Pb–Zn–Ag and Paris Ag–Pb deposits. In: Phillips, N. (Eds), Australian ore deposits. The Australasian Institute of Mining and Metallurgy, v. Carlton, Victoria, p. 629-630. Available at: https://www.ausimm.com.au/publications/publication.aspx?ID=17223

Pankhurst, M. J., Schaefer, B. F. and Betts, P. G., 2011. Geodynamics of rapid voluminous felsic magmatism through time. Lithos, v. 123, p. 92-101. doi: https://doi.org/10.1016/j.lithos.2010.11.014

Pearce, J., 1996. Sources and settings of granitic rocks. Episodes, v. 19, p. 120-125. doi: https://doi.org/10.4236/jssm.2008.11008

Pirajno, F., 2004. Hotspots and mantle plumes: global intraplate tectonics, magmatism and ore deposits. Mineralogy and Petrology, v. 82, p. 183-216. doi: https://doi.org/10.1007/s00710-004-0046-4

Pollard, P. J., 2006. An intrusion-related origin for Cu-Au mineralization in iron oxide-copper-gold (IOCG) provinces. Mineralium Deposita, v. 41, p. 179-187. doi: https://doi.org/10.1007/s00126-006-0054-x

Raveggi, M., Giles, D., Foden, J., Meffre, S., Nicholls, I. and Raetz, M., 2015. Lead and Nd isotopic evidence for a crustal Pb source of the giant Broken Hill Pb–Zn–Ag deposit, New South Wales, Australia. Ore Geology Reviews, v. 65, p. 228-244. doi: https://doi.org/10.1016/j.oregeorev.2014.09.012

Reid, A., 2019. The Olympic Cu-Au Province, Gawler Craton: A Review of the Lithospheric Architecture, Geodynamic Setting, Alteration Systems, Cover Successions and Prospectivity. Minerals, v. 9, p. 371. doi: https://www.mdpi.com/2075-163X/9/6/371

Reid, A., Smith, R. N., Baker, T., Jagodzinski, E. A., Selby, D., Gregory, C. J. and Skirrow, R. G., 2013. Re-Os dating of molybdenite within hematite breccias from the Vulcan Cu-Au prospect, Olympic Cu-Au Province, South Australia. Economic Geology, v. 108, p. 883-894. doi: https://doi.org/10.2113/econgeo.108.4.883

Richards, J. P., 2011. High Sr/Y arc magmas and porphyry Cu ± Mo ± Au deposits: Just add water. Economic Geology, v. 106, p. 1075-1081. doi: https://doi.org/10.2113/econgeo.106.7.1075

Richards, J. P., 2015. The oxidation state, and sulfur and Cu contents of arc magmas: implications for metallogeny. Lithos, v. 233, p. 27-45. doi: https://doi.org/10.1016/j.lithos.2014.12.011

Samperton, K. M., Schoene, B., Cottle, J. M.,

Brenhin Keller, C., Crowley, J. L. and Schmitz, M. D., 2015. Magma emplacement, differentiation and cooling in the middle crust: Integrated zircon geochronological–geochemical constraints from the Bergell Intrusion, Central Alps. Chemical Geology, v. 417, p. 322-340. doi: https://doi.org/10.1016/j.chemgeo.2015.10.024

Schmandt, D. S., Cook, N. J., Ciobanu, C. L., Ehrig, K., Wade, B. P., Gilbert, S. and Kamenetsky, V. S., 2019. Rare Earth Element Phosphate Minerals from the Olympic Dam Cu-U-Au-Ag Deposit, South Australia: Recognizing Temporal-Spatial Controls On Ree Mineralogy in an Evolved IOCG System. The Canadian Mineralogist, v. 57, p. 3-24. doi: https://doi.org/10.3749/canmin.1800043

Sheth, H. C., 1999. Flood basalts and large igneous provinces from deep mantle plumes: fact, fiction, and fallacy. Tectonophysics, v. 311, p. 1-29. doi: https://doi.org/10.1016/S0040-1951(99)00150-X

Shu, Q., Chang, Z., Lai, Y., Hu, X., Wu, H., Zhang, Y., Wang, P., Zhai, D. and Zhang, C., 2019. Zircon trace elements and magma fertility: insights from porphyry (-skarn) Mo deposits in NE China. Mineralium Deposita, v. 54, p. 645-656. doi: https://doi.org/10.1007/s00126-019-00867-7

Sillitoe, R. H., 2010. Porphyry Copper Systems. Economic Geology, v. 105, p. 3-41. doi: https://doi.org/10.2113/gsecongeo.105.1.3

Simon, A. C., Knipping, J., Reich, M., Barra, F., Deditius, A. P., Bilenker, L. and Childress, T., 2018. Kiruna-Type Iron Oxide-Apatite (IOA) and Iron Oxide Copper-Gold (IOCG) Deposits Form by a Combination of Igneous and Magmatic-Hydrothermal Processes: Evidence from the Chilean Iron Belt. In: Arribas R, A. M. and Mauk, J. L. (Eds), Metals, Minerals, and Society. Society of Economic Geologists (SEG), v. 21, p. https://doi.org/10.5382/sp.21.06

Skirrow, R., van der Wielen, S. E., Champion, D. C., Czarnota, K. and Thiel, S., 2018. Lithospheric artchitecture and mantle metasomatism linked to iron-oxide Cu-Au ore formation: Multidiciplinary evidence from the Olympic Dam region, South Australia. Geochemistry, Geophysics, Geosystems, v. 19, p. doi: https://doi.org/10.1029/2018GC007561

Skirrow, R. G., Bastrakov, E., Barovich, K., Fraser, G., Fanning, C. M., Creaser, R. and Davidson, G., 2007. Timing of Iron Oxide Cu-Au-(U) Hydrothermal Activity and Nd Isotope Constraints on Metal Sources in the Gawler Craton, South Australia. Economic Geology, v. 102, p. 1441-1470. doi: https://doi.org/10.2113/gsecongeo.102.8.1441

Sparks, R. S. J., 1986. The role of crustal contamination in magma evolution through geological time. Earth and Planetary Science Letters, v. 78, p. 211-223. doi: https://doi.org/10.1016/0012-821X(86)90062-2

Storey, C. D. and Smith, M. P., 2017. Metal source and tectonic setting of iron oxide-copper-gold (IOCG) deposits: Evidence from an in situ Nd isotope study of titanite from Norrbotten, Sweden. Ore Geology Reviews, v. 81, p. 1287-1302. doi: https://doi.org/10.1016/j.oregeorev.2016.08.035

Sun, W., Huang, R.-f., Li, H., Hu, Y.-b., Zhang, C.-c., Sun, S.-j., Zhang, L.-p., Ding, X., Li, C.-y., Zartman, R. E. and Ling, M.-x., 2015. Porphyry deposits and oxidized magmas. Ore Geology Reviews, v. 65, p. 97-131. doi: https://doi.org/10.1016/j.oregeorev.2014.09.004

Thiel, S. and Heinson, G., 2013. Electrical conductors in Archean mantle—Result of plume interaction? Geophysical Research Letters, v. 40, p. 2947–2952. doi: https://doi.org/10.1002/grl.50486

Tosdal, R. M., Dilles, J. H. and Cooke, D. R., 2009. From Source to Sinks in Auriferous Magmatic-Hydrothermal Porphyry and

Epithermal Deposits. Elements, v. 5, p. 289-295. doi: 10.2113/gselements.5.5.289

Tosdal, R. M. and Richards, J. P., 2001. Magmatic and structural controls on the development of porphyry Cu ± Mo ± Au deposits. Reviews in Economic Geology, v. 14, p. 157-181. doi: https://doi.org/10.5382/Rev.14.06

Turner, S. and Hawkesworth, C., 1995. The nature of the sub-continental mantle: constraints from the major-element composition of continental flood basalts. Chemical Geology, v. 120, p. 295-314. doi: https://doi.org/10.1016/0009-2541(94)00143-V

Velasco, F., Tornos, F. and Hanchar, J. M., 2016. Immiscible iron- and silica-rich melts and magnetite geochemistry at the El Laco volcano (northern Chile): Evidence for a magmatic origin for the magnetite deposits. Ore Geology Reviews, v. 79, p. 346-366. doi: https://doi.org/10.1016/j.oregeorev.2016.06.007

Verdugo-Ihl, M. R., Ciobanu, C. L., Cook, N. J., Ehrig, K. J. and Courtney-Davies, L., 2019. Defining early stages of IOCG systems: evidence from iron oxides in the outer shell of the Olympic Dam deposit, South Australia. Mineralium Deposita, v. p. doi: https://doi.org//10.1007/s00126-019-00896-2

Wade, C. E., Payne, J. L., Barovich, K. M., Crowley, J., Jagodzinski, E., Gilbert, S. E., Wade, B. P. and Reid, A. J., in prep. Zircon trace element geochemistry as an indicator of magma fertility in iron oxide-copper-gold provinces. xx, v. xx, p. xx. doi: xx

Wade, C. E., Payne, J. L., Barovich, K. M. and Reid, A. J., 2019. Heterogeneity of the sub-continental lithospheric mantle and 'non-juvenile' mantle additions to a Proterozoic silicic large igneous province. Lithos, v. 340-341, p. 87-107. doi: https://doi.org/10.1016/j.lithos.2019.05.005

Watts, K. E. and Mercer, C. N., 2020. Zircon-hosted melt inclusion record of silicic magmatism in the Mesoproterozoic St. Francois Mountains terrane, Missouri: Origin of the Pea Ridge iron oxide-apatite-rare earth element deposit and implications for regional crustal pathways of mineralization. Geochimica et Cosmochimica Acta, v. 272, p. 54-77. doi: https://doi.org/10.1016/j.gca.2019.12.032

Wittig, N., Pearson, D. G., Duggen, S., Baker, J. A. and Hoernle, K., 2010. Tracing the metasomatic and magmatic evolution of continental mantle roots with Sr, Nd, Hf and and Pb isotopes: A case study of Middle Atlas (Morocco) peridotite xenoliths. Geochimica et cosmochimica acta, v. 74, p. 1417-1435. doi: https://doi.org/10.1016/j.gca.2009.10.048

Yang, J.-H., Wu, F.-Y., Chung, S.-L., Wilde, S. A. and Chu, M.-F., 2004. Multiple sources for the origin of granites: Geochemical and Nd/Sr isotopic evidence from the Gudaoling granite and its mafic enclaves, northeast China. Geochimica et Cosmochimica Acta, v. 68, p. 4469-4483. doi: https://doi.org/10.1016/j.gca.2004.04.015

Chapter 2

This chapter is published in *Lithos* as:
Wade, C. E., Payne, J. L., Barovich, K. M. and Reid, A. J., 2019. Heterogeneity of the sub-continental lithospheric mantle and 'non-juvenile' mantle additions to a Proterozoic silicic large igneous province. Lithos, 340-341, 87-107.

Statement of Authorship

Title of Paper	Heterogeneity of the sub-continental lithospheric mantle and 'non-juvenile' mantle additions to a Proterozoic silicic large igneous province.
Publication Status	☑ Published ☐ Accepted for Publication ☐ Submitted for Publication ☐ Unpublished and Unsubmitted work written in manuscript style
Publication Details	Wade, C. E., Payne, J. L., Barovich, K. M. and Reid, A. J., 2019. Heterogeneity of the sub-continental lithospheric mantle and 'non-juvenile' mantle additions to a Proterozoic silicic large igneous province. Lithos, 340-341, 87-107. doi: https://doi.org/10.1016/j.lithos.2019.05.005

Principal Author

Name of Principal Author (Candidate)	Claire Wade		
Contribution to the Paper	Fieldwork and drill core inspections, investigation, visualisation, validation Data collection and modelling, data curation Writing - orginal draft Manuscript writing, editing and review		
Overall percentage (%)	70%		
Certification:	This paper reports on original research I conducted during the period of my Higher Degree by Research candidature and is not subject to any obligations or contractual agreements with a third party that would constrain its inclusion in this thesis. I am the primary author of this paper.		
Signature		Date	21/11/2020

Co-Author Contributions

By signing the Statement of Authorship, each author certifies that:

i. the candidate's stated contribution to the publication is accurate (as detailed above);

ii. permission is granted for the candidate in include the publication in the thesis; and

iii. the sum of all co-author contributions is equal to 100% less the candidate's stated contribution.

Name of Co-Author	Justin Payne		
Contribution to the Paper	Ideas for manuscript, investigation, supervision, conceptulisation, funding acqusition, visualisation, validation Manuscript editing and review Fieldwork		
Signature		Date	29/11/2020

Name of Co-Author	Karin Barovich			
Contribution to the Paper	Ideas for manuscript, investigation, supervision, conceptulisation, visualisation, validation Manuscript editing and review			
Signature			Date	15/11/2020

Name of Co-Author	Anthony Reid			
Contribution to the Paper	Manuscript editing and review Supervision, conceptulisation, visualisation, validation Fieldwork			
Signature			Date	16/11/2020

ABSTRACT

Southern Australia, is host to a ca. 1590 Ma Silicic Large Igneous Province (SLIP) that produced approximately 100 000 km^3 of felsic and mafic magmas within a 20 myr timeframe. Although a minor component, the mafic magmas within the SLIP present an opportunity to investigate the composition of the mantle sources involved in SLIP formation. The mafic rocks are generally characterised by enrichment in high field strength elements (HFSE) and light rare earth element (LREE), negative Nb-Ta-Ti anomalies, and variable Nd isotopic compositions. Enriched geochemical signatures and lack of correlation with crustal proxy elements in the most primitive magmas (high Mg, Cr, Ni and $\varepsilon_{Nd(1590\ Ma)}$) suggest crustal contamination is not significant in the studied samples and the enrichment is a primary source region characteristic. Th/Nb ratios for the suite are mostly greater than 0.2 and the vast majority of $\varepsilon_{Nd(t)}$ values are in the range 0 to -5. In the first instance this means that a large proportion of the mafic magma added to the crust during the SLIP event is effectively isotopically indistinguishable from that considered consistent with Paleoproterozoic reworking of Neoarchean crust. Therefore, continental growth occurring during this event would not be detected by methods that are solely reliant on isotopic datasets (e.g. detrital zircons or bulk sediment compositions). The mantle source for the magma is interpreted to be dominantly sub-continental lithospheric mantle (SCLM) with varying magma compositions interpreted to represent a heterogeneous SCLM. Enrichment of the SCLM is considered to be related to metasomatism during earlier subduction events with the isotopic composition of the magmas suggesting it may have been as early as the Neoarchean.

INTRODUCTION

The composition of continental mafic rocks provides a proxy for the chemical evolution of the deep continental lithospheric mantle and underlying asthenospheric mantle. Studying mantle source components of mafic igneous rocks is essential for improvement in our understanding of mantle derived magmatism through space and time and the interaction between mantle and the crust (Chesley and Ruiz 1998, Jahn *et al.* 1999). Investigations into mafic magmatism have provided important information on tectonic evolution, mantle source characteristics, geodynamic settings and genesis of associated mineralisation (Ernst and Buchan 2001, Bleeker and Ernst 2006, Green and Falloon 2015, Peck and Huminicki 2016, Xia and Li 2019).

Mafic magmatism is believed to play a crucial role in the formation of SLIPs (Xu *et al.* 2017) where the partial melting of the crust is triggered by underplating or intraplating of large volumes of "hidden" mafic magmas (Ernst 2014). However, understanding the source of the mantle-derived magmas is often hindered by the rarity of mafic rocks in SLIPs due to poor exposure and concealment beneath felsic units, potentially due to the low-density felsic magmas inhibiting ascent of the mafic magmas (Ernst 2014). In examples where field relationships are more consistently known (e.g. Chon Aike Province, Whitsundays and Sierra Madre Occidental and South China), mafic rocks associated with SLIPs show compositional variation, characterised by enrichments in incompatible elements and heterogeneous isotopic signatures e.g Li *et al.* (2008) and Xu *et al.* (2017). Mantle sources for the mafic rocks in SLIPs are varied and include depleted lithospheric mantle, previously metasomatised and enriched lithospheric mantle, and oceanic island basalt (OIB) and enriched mid-oceanic ridge basalt (E-MORB) sources, with selective and variable amounts of crustal contamination (Zhou *et al.* 2006, Li *et al.* 2008, Xu *et al.* 2017).

Proterozoic southern Australia contains a SLIP of ~100 000 km^3 of felsic rocks (Allen

et al. 2003, Wade *et al.* 2012) and ~2500 km^3 of mafic rocks. The SLIP is also related to the world's largest iron-oxide copper gold (IOCG) and U deposit, Olympic Dam (Skirrow *et al.* 2007 and references therein). The mafic-felsic magmatic association provides a unique opportunity to study mafic magmas related to a SLIP at a regional scale, providing greater constraints on spatial and compositional variation in the mantle source region.

Early models for the formation of the Proterozoic southern Australian SLIP invoked mafic underplating related to upwelling of a mantle plume (Giles 1988, Blissett *et al.* 1993), similar to typical intraplate magmatism models (e.g. Sharkov *et al.* 2017). More recently, continental margin, back-arc or far-field continental back-arc settings with or without a mantle plume and mafic underplating have been proposed (Hand *et al.* 2008, Wade *et al.* 2012, Rogers *et al.* 2018, Skirrow *et al.* 2018). Limited geochemical signatures available for Mesoproterozoic extrusive mafic rocks from the SLIP (including enrichment in high field strength elements (HFSE) and light rare earth elements (LREE)) have been interpreted as evidence for an enriched lithospheric mantle source (Wade *et al.* 2012, Pankhurst *et al.* 2013, Huang *et al.* 2016, Skirrow *et al.* 2018). Geochemical signatures such as these are typically linked to processes such as: 1) crustal contamination of mafic magmas during ascent (e.g. Huppert *et al*. (1985), Chelsey and Ruiz (1998) and Halama *et al*. (2004); 2) subduction-induced metasomatism of the mantle, i.e. modification of depleted mantle by slab-related fluids and/or subducted sediment melts (e.g. Kelemen et al. (1993), Prouteat *et al.* (2001), Cai *et al.* (2013) and Cheng *et al.* (2018) or; 3) magmas derived from the sub-continental lithospheric mantle (SCLM) e.g. O'Reilly and Zhang (1995). Distinguishing between an enriched mantle source versus a crustally contaminated mantle source is difficult, as similar geochemical and isotopic signatures can be produced (e.g. Kelemen *et al.* (1993).

This contribution uses the geochemical and isotopic composition of mafic intrusive rocks of the Mesoproterozoic southern Australia SLIP to investigate the composition of mantle source components. These rocks are more widespread than their extrusive counterparts and hence provide a spatial understanding of mantle compositions. We propose the enriched geochemical signatures in these rocks originated from a mantle source or sources previously metasomatised by earlier subduction of ancient crust rather than from asthenospheric mantle source contaminated by crustal material. The obtained dataset highlights the heterogeneous nature of mantle sources and demonstrates that the mantle isotopic model (i.e. asthenospheric mantle source) does not represent the composition of mafic material added to the continental crust during SLIP formation.

REGIONAL GEOLOGY OF THE GAWLER CRATON, SOUTH AUSTRALIA

The oldest exposed basement of the Gawler Craton (Fig. 1) is the Mesoarchaean (3150 Ma) Cooyerdoo Granite . It is exposed only on northern Eyre Peninsula but inferred to extend into the middle and lower crust of the central Gawler Craton (Fraser *et al.* 2010, Curtis and Thiel 2019). Volcanosedimentary sequences of the Mulgathing and Sleaford complexes, in the northern and southern Gawler Craton respectively, were deposited during the Neoarchaean to early Palaeoproterozoic (2555–2480 Ma), and were most likely part of a formerly contiguous basin system now dismembered by Proterozoic tectonism (Swain *et al.* 2005, Reid and Payne 2017). A subsequent period of ca. 500 m.y. of geological quiescence was followed by the intrusion of the igneous protolith to the ca. 2000 Ma Miltalie Gneiss (Fanning *et al.* 2007), marking the onset of prolonged basin formation and growth over the period ca. 2000 to 1730 Ma across the entire Gawler Craton (Payne *et al.* 2006, Fanning *et al.* 2007, Szpunar *et al.* 2011, Reid and Payne 2017).

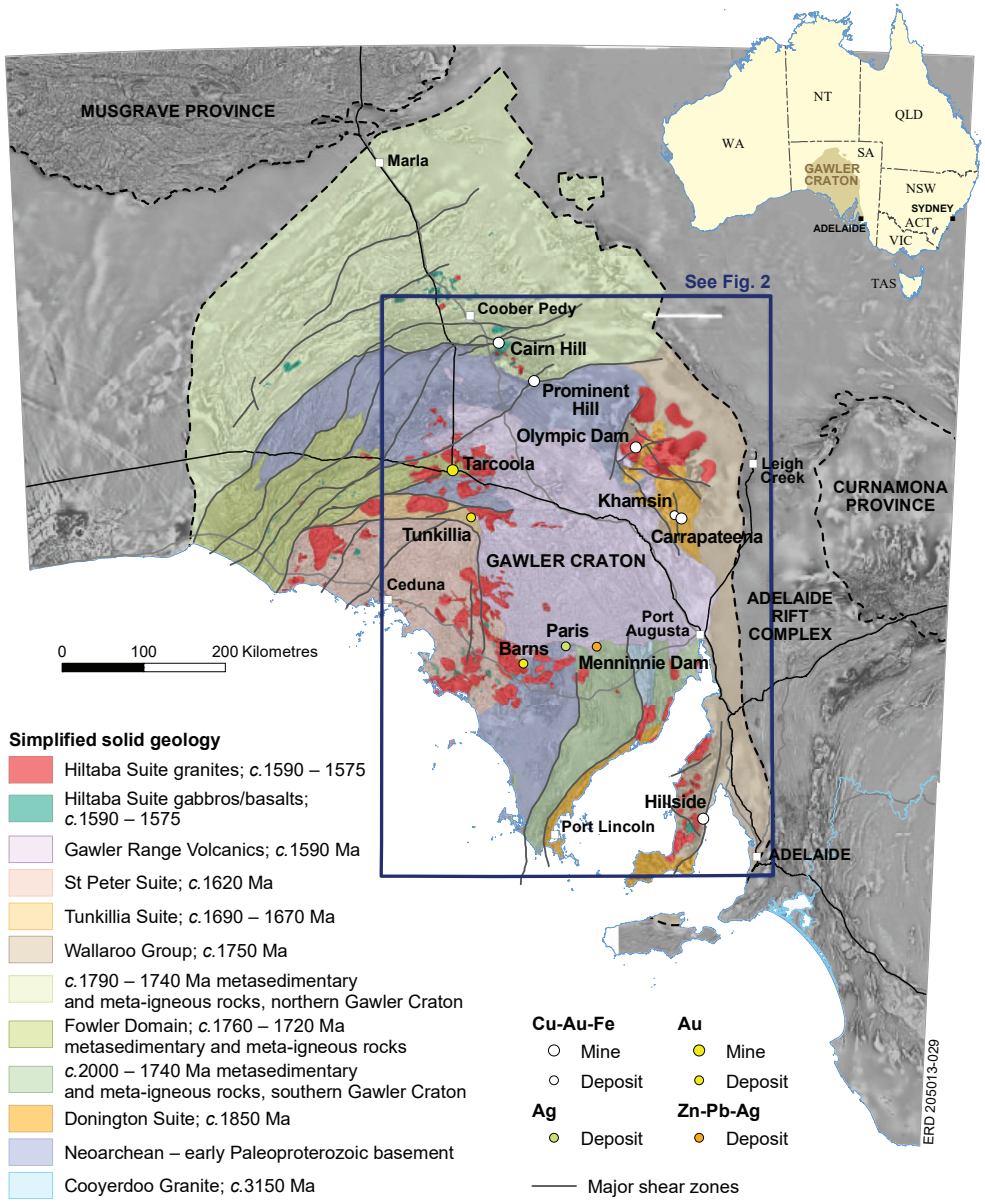

Figure 1: Simplified solid geology map of the Gawler Craton highlighting the main Proterozoic units from ca. 3150–1575 Ma. Study area (Figure 2) represented by box.

Basin formation was punctuated by the Cornian Orogeny and syn-orogenic magmatism of the Donington Suite (ca. 1850 Ma; Reid *et al.* 2008) and ultimately terminated by the craton wide ca. 1730–1690 Ma Kimban Orogeny (Vassallo and Wilson 2002). Widespread felsic and mafic magmatism occurred pre-, syn- and post the Kimban Orogeny and contemporaneous localised sedimentation (1740–1720 Ma) accompanied mafic magmatism in the Fowler Domain in the western Gawler Craton (Howard *et al.* 2011). Following the Kimban Orogeny, only localised sedimentation is preserved in the southern and central Gawler Craton as the ca. 1680 Ma Corunna Conglomerate and the ca. 1655 Ma Tarcoola Formation, respectively (Fanning *et al.* 2007 and references therein).

From 1635–1575 Ma an extended magmatic episode occurred, beginning with the ca. 1630 Ma Nuyts Volcanics and intrusion of

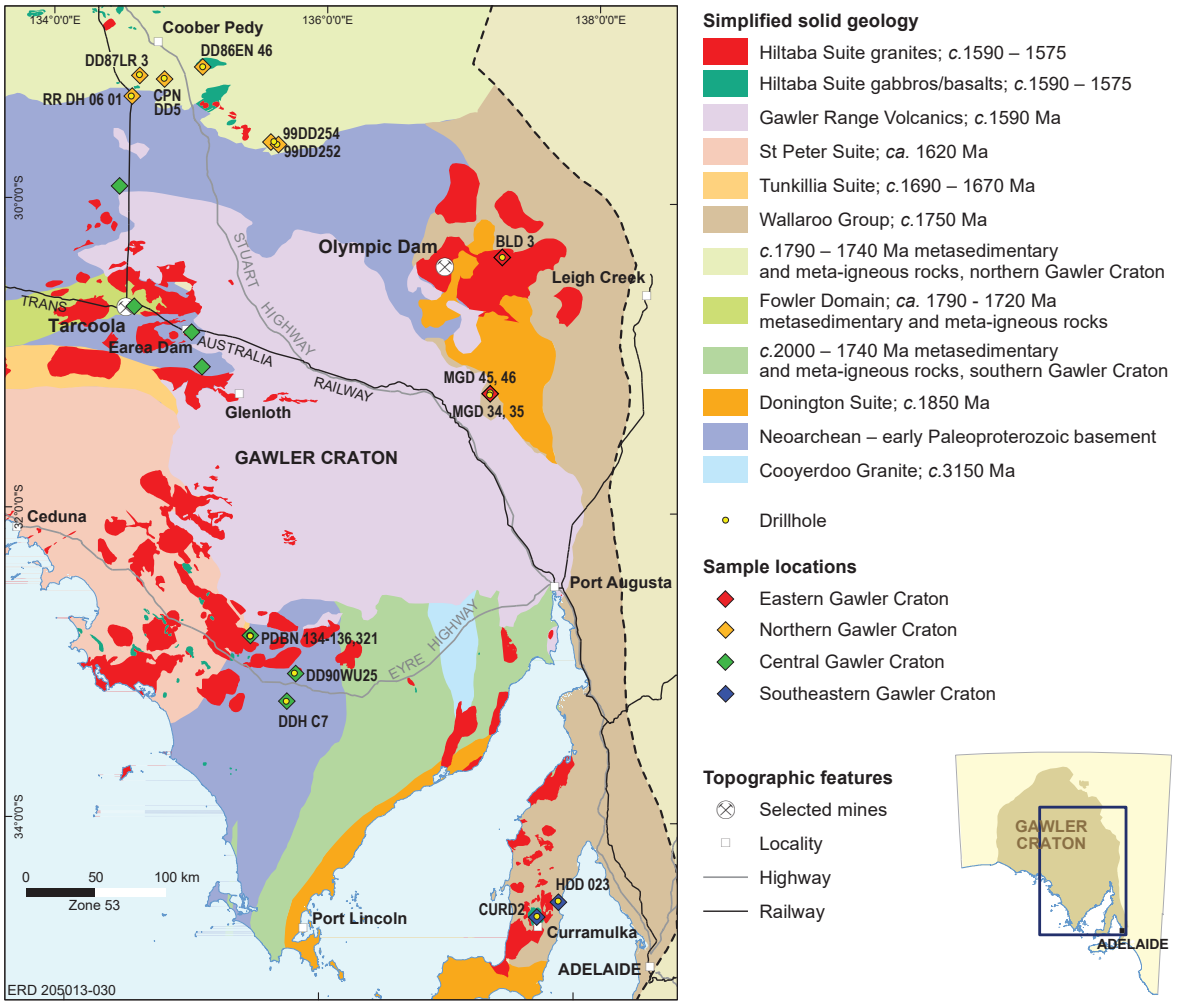

Figure 2: Simplified solid geology map of the study area, showing distribution of Hiltaba Suite and sample locations, including drill holes, used in this study.

isotopically juvenile ca. 1635–1608 Ma St Peter Suite (Swain *et al.* 2008, Reid and Payne 2017). A voluminous, predominantly felsic, magmatic event followed, including the ca. 1592 Ma Gawler Range Volcanics (Blissett *et al.* 1993) and the ca. 1597–1579 Ma Hiltaba Suite granites (Fanning *et al.* 2007 (and references therein), Jagodzinski *et al.* 2007, Zang *et al.* 2007). During the 1600–1570 Ma time period a significant metallogenic episode also occurred, in which IOCG deposits formed largely in the eastern Gawler Craton (Skirrow *et al.* 2007), Au-only ore deposits formed in the central Gawler Craton (Ferris and Schwarz 2003), and Ag-Pb-Zn deposits formed in the southern central Gawler Craton (Nicolson *et al.* 2017).

The Gawler Craton underwent localised deformation via reactivation of shear zones between ca. 1470 and 1450 Ma, particularly in the western Gawler Craton (Fraser *et al.* 2012) and magmatism and granulite facies metamorphism ca. 1450 Ma in the northern Gawler Craton (Morrissey *et al.* 2019). The Gawler Craton was subsequently overlain by various Neoproterozoic, Palaeozoic, Mesozoic and Cenozoic sedimentary successions (e.g. Hou *et al.* 2011).

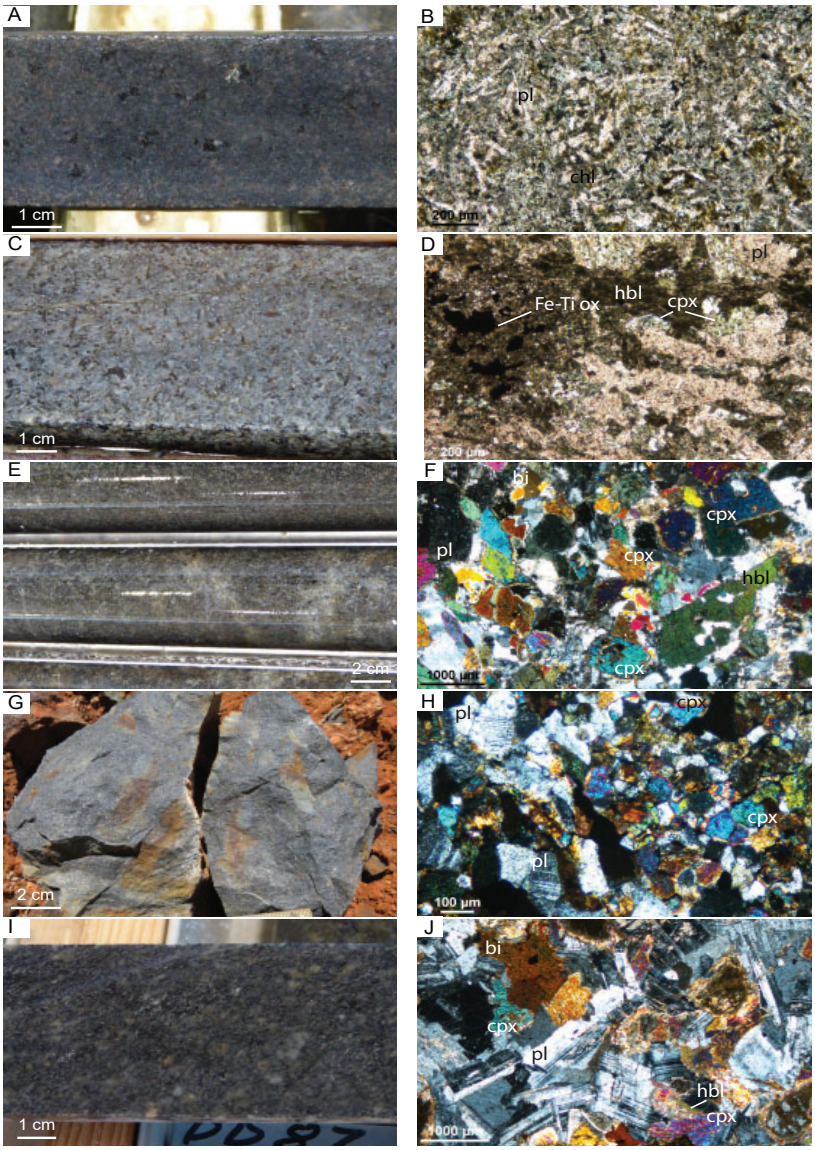

Figure 3: Rock types of the mafic Hiltaba Suite. a) fine-grained, black-grey biotite-quartz-plagioclase gabbro, ~1000 m, drill hole BLD 3, eastern Gawler Craton; b) fine-grained diorite with randomly oriented plagioclase and Fe-Ti oxides in a chlorite-biotite altered groundmass (plane polarised light), sample 2450321, drill hole BLD 3, c) medium-grained, equigranular hornblende-biotite-plagioclase-quartz gabbro with visible pyrite and chalcopyrite, minor chlorite alteration and fracturing, ~55 m, drill hole CURD 2, south eastern Gawler Craton; d) coarse-grained plagioclase-hornblende-clinopyroxene gabbro with Fe-Ti oxides, sample HDD 023-02 (plane polarised light), south eastern Gawler Craton; e) fine-grained, biotite-hornblende-pyroxene-plagioclase gabbro with minor magnetite, pyrite, pyrrhotite and chalcopyrite, ~200 m, drill hole DDH C7, southern central Gawler Craton; f) clinopyroxene-plagioclase-hornblende-biotite dyke with K-feldspar veins and Fe-Ti oxides, sample PDBN 321-02 (cross polarised light), southern central Gawler Craton; g) outcrop sample of fine-grained plagioclase-biotite-quartz mafic dyke, northern central Gawler Craton; h) clinopyroxene-plagioclase-quartz-biotite microgabbro with Fe-Ti oxides, sample 18-Erd-02 (cross polarised light), northern central Gawler; i) coarse-grained gabbro ~91 m, drill hole DD87 LR 3, northern Gawler Craton; and j) plagioclase-hornblende-biotite-clinopyroxene gabbro with Fe-Ti oxides, sample 2442106, drill hole RR DH 06 01 (cross polarised light), northern Gawler Craton. pl: plagioclase; cpx: clinopyroxene; hbl: hornblende, bi: biotite; chl: chlorite, Fe-Ti ox: Fe-Ti oxides.

THE GAWLER RANGE VOLCANICS-HILTABA SUITE SILICIC LARGE IGNEOUS PROVINCE (GRV-HS SLIP)

The Gawler Range Volcanics (GRV) erupted between 1595 and 1587 Ma (Jagodzinski *et al.* 2016). They are divided into two volcanic successions (Blissett *et al.* 1993, Allen *et al.* 2003). The lower succession is a developmental phase comprising basalt, andesite, dacite, rhyodacite, rhyolite and pyroclastic rocks (Blissett *et al.* 1993, Allen *et al.* 2003). Basaltic lavas are volumetrically minor in the lower GRV and crop out as at least three discrete volcanic centres now on the preserved margins of the upper GRV felsic lavas. Subsurface basaltic lavas have been documented at Olympic Dam and Roopena, and were part of isolated sedimentary basins in the eastern Gawler Graton (Curtis *et al.* 2018). Basaltic lavas are aphanitic, porphyritic or amygdaloidal, with olivine (pseudomorphs), clinopyroxene and plagioclase as the major phenocrysts phases (Huang *et al.* 2016). Minor phases include amphibole, Fe-Ti oxides, chromite-Cr-spinels and micro-phenocrysts of phlogopite (Fricke 2005, Huang *et al.* 2016). Basalts of the lower GRV are enriched in high field strength elements (Fricke 2005, Huang *et al.* 2016) and have $\varepsilon_{Nd(1590\ Ma)}$ values that range between -7.0 and 2.5 (Stewart 1994, Fricke 2005) suggesting the assimilation of an older crustal component in the more evolved basalts. Assimilation of the Mesoarchean Cooyerdoo Granite or involvement of a radiogenic metasomatised lithospheric mantle source is also recorded by initial Os isotope ratios (Pankhurst *et al.* 2013). However, initial Hf isotopes suggest a mantle source component for lithophile elements (Pankhurst *et al.* 2013). Rhyolites of the lower GRV are characterised by high concentrations of rare earth elements (REE), Y, high field strength elements (HFSE), Rb and F (Agangi *et al.* 2012). $\varepsilon_{Nd(1590\ Ma)}$ values range between -7.0 and 1.2 (Stewart 1994).

The upper succession (upper GRV) consists of flat-lying and relatively undeformed thick (200–300 m) and regionally extensive (>200 km^3) dacite and rhyolite lavas (Blissett *et al.* 1993, Allen *et al.* 2003). Mineral assemblages in the upper GRV are essentially anhydrous and include phenocrysts of plagioclase (oligoclase-andesine), K-feldspar, orthopyroxene (pigeonite and augite), ferromagnesium phases (olivine (fayalite), clinopyroxene or amphibole and Fe-Ti oxides), ± quartz in a quartz-feldspar groundmass with accessory apatite, magnetite and zircon (Stewart 1994, Allen *et al.* 2003, Agangi *et al.* 2012). The upper GRV is high in silica (>65% SiO_2), enriched in HFSE and REE and has a predominantly crustal signature with $\varepsilon_{Nd(1590\ Ma)}$ values ranging between -5.4 and 1.8 (Stewart 1994).

The intrusive Hiltaba Suite is bimodal, although dominated by granitic compositions. Mapping of surface exposures combined with geophysical interpretations suggest the Hiltaba Suite occurs over an area of approximately 30 000 km^2 at current exposure levels. Major mineral phases of the Hiltaba Suite are typically quartz, K-feldspar, biotite and magnetite with minor plagioclase, zircon, apatite, fluorite, ilmenite and titanite (Stewart and Foden 2003, Agangi *et al.* 2012). Hiltaba Suite granites display considerable geochemical variation and are mostly fractionated, enriched in HFSE, REE, U, Th and K with high SiO_2 (Stewart and Foden 2003). $\varepsilon_{Nd(1590\ Ma)}$ values for the Hiltaba Suite granites range between -13.7 and 2.7 (Stewart 1994, Wurst 1994, Creaser 1995, Johnson and Mcculloch 1995, Stewart and Foden 2003, Brotodewo *et al.* 2018).

The subordinate mafic Hiltaba Suite is mostly known from drill holes or inferred from geophysical imagery (Fig. 2). It occurs across an area of approximately 2500 km^2 in the subsurface. U-Pb zircon geochronology for the mafic Hiltaba Suite yields magmatic crystallisation ages between 1597–1579 Ma (Fanning *et al.* 2007 (and references therein), Jagodzinski *et*

al. 2007, Zang *et al.* 2007). The majority of geochemical investigations into mafic Hiltaba Suite compositions have been focussed in the IOCG province of the Gawler Craton (Johnson and Mcculloch 1995, Skirrow *et al.* 2007, Zang *et al.* 2007) due to their association with mineralisation. One study has focussed on mafic dykes associated with Au mineralisation in the central Gawler Craton (Budd and Skirrow 2007). Johnson and McCulloch (1995) were the first to identify juvenile Nd compositions associated with increasing Cu and Au abundance at the Olympic Dam deposit. This association was followed up and confirmed by Skirrow *et al.* (2007) and Budd and Skirrow (2007) at other IOCG and Au-only deposits in the Gawler Craton. Previous geochemical investigations into the mafic components of the Hiltaba Suite have relied on limited datasets but demonstrated the compositions are enriched in HFSE and REE. The Nd isotopic compositions are widely variable with $\varepsilon_{Nd(1590\ Ma)}$ values ranging from - 8.2 to 4.2 (Johnson and Mcculloch 1995, Budd and Skirrow 2007, Skirrow *et al.* 2007, Zang *et al.* 2007). Authors interpreted these enriched geochemical compositions as being associated with an enriched, metasomatised and heterogeneous lithospheric mantle source region and also being affected by assimilation and fractional crystallisation (AFC) and/or crustal contamination processes, while the mafic dykes with juvenile Nd isotopic compositions have been attributed to an E-MORB-like asthenospheric mantle component (Skirrow *et al.* 2018).

SAMPLE DESCRIPTIONS

Representative samples from mafic intrusive bodies belonging to the Hiltaba Suite were collected from drill hole and outcrop locations distributed throughout the Gawler Craton (Fig. 2). For ease of describing the dataset we have divided it into the following four regions: 1. eastern Gawler Craton; 2. south eastern Gawler Craton; 3. central Gawler Craton; and 4. northern Gawler Craton. A total of 132 samples of mafic Hiltaba Suite were collected from 30 drill holes and various outcrop locations that span these regions. Each was analysed for major and trace whole-rock geochemistry and a subset for Sm-Nd isotopes.

Eastern Gawler Craton

The eastern Gawler Craton region is completely covered by young sedimentary basin sequences (Fig. 1). Drill holes that intersect mafic rocks of the Hiltaba Suite in this region contain fine-grained, black-grey, quartz-plagioclase-biotite-hornblende gabbros (e.g. drill hole BLD 3; Fig. 3a) and grey-green-black aphanitic mafic dykes (drill holes MGD 34, MGD 35, MGD, 45 and MGD 46; Fig. 3b). These dykes and gabbros intrude felsic gneisses of the ca. 1850 Ma Donington Suite and are pervasively altered to haematite, sericite and chlorite, with abundant quartz and haematite-filled veins.

South Eastern Gawler Craton

The southernmost occurrences of mafic Hiltaba Suite occur on Yorke Peninsula (Fig. 2), and include gabbro and gabbronorite. The latter occurs as a subsurface intrusive body approximately 15 x 30 km in size as interpreted from total magnetic imagery (Zang *et al.* 2007). The Curramulka Gabbronorite (drill holes CUR D2, CUR D4 and CUR D6) is fine- to medium-grained, equigranular and hornblende-biotite-plagioclase bearing (Fig. 3c), and gabbro in drill hole HDD 023 (Hillside Fe-Cu-Au deposit) ranges from fine- to coarse-grained hornblende-plagioclase-biotite-quartz-clinopyroxene bearing with disseminated pyrite, chalcopyrite and pyrrhotite, Fe-Ti oxides (Fig. 3d), and quartz veins.

Central Gawler Craton

Central Gawler Craton mafic Hiltaba Suite occurs within six drill holes across three locations on the northern Eyre Peninsula and crops out as thin discontinuous dolerite dykes in the Tarcoola and Earea Dam-Glenloth regions

(Fig. 2). On Eyre Peninsula rock types include: 1) coarse-grained, hornblende, quartz, plagioclase gabbro with minor to pervasive chlorite alteration in hornblende and minor haematite staining in plagioclase and quartz from drill hole DD90WU25 (Wudinna); 2) fine-grained, biotite-hornblende-pyroxene-plagioclase gabbronorite with pyrite, chalcopyrite and pyrrhotite (Fig. 3e) from drill hole DDH C7 (Kimba); and 3) grey-black aphanitic mafic dykes and medium-grained quartz-plagioclase-hornblende-biotite-clinopyroxene (Fig. 3f) dykes with biotite and haematite alteration from the Barns deposit. Aphanitic mafic dykes from the Barns deposit intrude granites of the ca. 1680 Ma Tunkillia Suite. Dolerite dykes from the Tarcoola and Earea Dam-Glenloth regions intrude the ca. 1690 Ma Tarcoola Formation and basement gneisses of the Mulgathing Complex respectively. These dykes are fine- to medium-grained, equigranular, plagioclase, clinopyroxene and biotite bearing (Fig. 3g and 3h), often located adjacent to or nearby quartz veins associated with historical gold workings. Mafic dykes that intrude the Tarcoola Formation at the Tarcoola gold deposit (Perseverence Pit) are variably altered to quartz-sericite-pyrite, epidote and chlorite.

Northern Gawler Craton

Mafic intrusive bodies in the northern Gawler Craton are interpreted from magnetic imagery and intersections in drill holes. The bodies include NW trending dykes (drill holes CPN DD4 and CPN DD5) and roughly circular to elliptical bodies (drill holes DD87LR3, DD88EN46, 99DD252 and 99DD254). The intrusion at Mt Brady (drill hole DD88EN46) is approximately 13 km x 7 km and the White Hill Complex is approximately 15 km x 12 km in size. Rock types include unfoliated to weakly foliated fine-grained to coarse-grained gabbro comprising hornblende-biotite-orthopyroxene-clinopyroxene-plagioclase-quartz with fine-grained disseminated sulphides (pyrite, chalcopyrite and pyhrrotite) and magnetite (Fig. 3i and 3j). The White Hill Complex includes ultramafic lithologies (troctolite, gabbronorite, anorthosite) and may represent a layered mafic intrusion . Northern Gawler Craton mafic rocks display varying degrees of potassic, chlorite and haematite alteration and quartz veining.

METHODS

Analytical Methods

All weathered material was removed from the samples before being crushed, split and milled to a fine powder, with quartz barren wash between samples, at the University of South Australia, the University of Adelaide or at Bureau Veritas Minerals laboratories in Perth, Western Australia. Geochemical analyses were performed by Bureau Veritas Minerals (https://www.bureauveritas.com.au/) in Perth, Western Australia. The samples were cast using a 66:34 flux with 4% lithium nitrate added to form a glass bead. Major elements and chlorine were analysed using X-Ray Fluorescence (XRF) spectrometry. Trace elements were determined by laser ablation-inductively coupled plasma-mass spectrometry (LA-ICP-MS) and Au, Pt and Pd were analysed using fire assay ICP-MS. FeO was determined volumetrically and fluorine was determined using specific ion electrode.

Whole-rock analyses for Sm-Nd isotopic compositions were performed at the University of Adelaide. Approximately 0.2 g of rock powder was digested with a ^{147}Sm + ^{150}Nd mixed spike and evaporated in HNO_3/HF followed by high-pressure digestion in HNO_3/HF for at least 5 days in sealed Teflon high pressure vessels at 200°C. Samples were evaporated to dryness and then redissolved in HCl in high pressure vessels overnight at 180°C.

Samples were loaded on 99.99% Re (standard grade) filaments. Sm and Nd isotopic abundance ratio measurements were carried out on an Isotopx Phoenix thermal ionization mass spectrometer (TIMS) in a three step dynamic

Table 1: Whole-rock geochemical composition for Hiltaba Suite mafic dykes

Sample	2450321	2559254	2559247	2559249	2465592	2465593	PDBN 321-02	GCT 88B	18ErD-02	18ErD-03	18ErD-01	18GL-05	662450
Sample Type	drill core	drill core	drill core	drill core	pulp	pulp	drill core	out crop	out crop	out crop	out crop	out crop	drill core
Drill Hole	BLD 3	MGD 35	MGD 45	MGD 46	PDBN 134	PDBN 134	PDBN 321						DDH C7
Depth From (m)	927.2	412.45	767.05	740.65	53.8	139.49	102.4						186.7
Depth To (m)	927.37	412.6	767.55	740.75	55.7	139.7	103.3						
Data Source	This study	This study	This study	This study	This study	This study	This study	G. Swain	This study	This study	This study	This study	G. Swain
Group	eastern G.C.	eastern G.C.	eastern G.C.	eastern G.C.	central G.C.	central G.C.	central G.C.	central G.C.	central G.C.	central G.C.	central G.C.	central G.C.	central G.C.
Location	Bills Lookout	Chianti	Chianti	Chianti	Barns	Barns	Barns	Bulgunnia	Earea Dam	Earea Dam	Earea Dam	Glenloth	Kimba
Easting	722947	714000	714464	715052	542274	542274	541914	447953	499735	499735	499832	507194	568045
Northing	6637341	6538775	6540377	6540987	6366051	6366051	6366142	6689418	6585307	6585307	6585346	6560233	6319261
Zone	53	53	53	53	53	53	53	53	53	53	53	53	53
Lithology	diorite	aphanitic dyke	aphanitic dyke	aphanitic dyke	aphanitic dyke	aphanitic dyke	diorite	gabbro	gabbro	gabbro	gabbro	dolerite	gab-bronorite
Major elements (wt %)													
SiO_2	42.50	49.21	45.2	45.6	50.62	51.06	50.39	49.70	48.73	48.54	48.95	49.72	45.30
TiO_2	1.72	1.23	1.4	3.3	0.64	1.10	0.71	1.69	1.97	1.93	1.99	1.23	1.72
Al_2O_3	15.78	13.81	14.1	14.9	15.74	11.87	8.90	14.40	13.77	14.04	13.60	14.03	14.60
FeO	10.50	11.80	9.31	10.2	4.46	6.37	6.00		10.00	9.09	8.65	8.81	
Fe_2O_{3T}	14.10	13.89	15.1	17.6	9.55	11.80	8.54	14.90	14.60	14.30	14.40	14.00	16.60
MnO	0.18	0.50	0.4	0.6	0.20	0.69	0.20	0.21	0.21	0.21	0.21	0.26	0.22
MgO	9.91	7.01	7.3	6.9	8.98	8.46	15.80	5.81	6.57	6.65	6.38	6.50	7.62
CaO	6.44	4.06	4.4	1.6	6.34	3.04	8.33	9.43	10.81	10.59	10.56	9.45	10.40
Na_2O	1.58	2.23	1.7	0.2	2.20	0.98	0.69	2.35	2.32	2.33	2.50	2.47	2.30
K_2O	2.86	2.56	2.8	3.1	2.07	2.53	3.47	0.40	0.42	0.54	0.57	1.04	1.09
P_2O_5	0.25	0.12	0.1	0.4	0.20	1.11	0.30	0.13	0.21	0.20	0.22	0.14	0.18
LOI	4.47	4.89	7.2	5.6	3.09	6.94	2.01	0.42	0.31	0.72	0.44	0.99	1.76
F	0.12				0.06	0.19	0.20		0.03	0.03	0.03	0.03	
Trace and rare earth elements (ppm)													
Ga	18.10	17.00	18.1	27.2	16.10	16.20	14.20	24.00	19.80	19.60	19.00	17.10	23.50
Cr	356.00	231.00	195	105	673.00	455.00	1510.00	60.00	62.00	73.00	54.00	94.00	80.00
Ni	215.00	100.00	80	60	265.00	260.00	625.00	76.00	70.00	60.00	45.00	60.00	70.00
Co	54.90	49.80	45.1	176	56.10	47.10	64.70	80.00	54.10	54.20	46.90	48.60	60.00
Sc	36.30	37.60	40.5	46.6	29.60	15.50	22.60		35.70	36.50	36.40	46.50	36.00
Ti	10000.00	7690.00	8230	20200			4300.00		12000.00	11800.00	11800.00	7820.00	
V	311.00	318.00	346	491	193.00	121.00	113.00		307.00	308.00	308.00	297.00	310.00
Cu	95.00	50.00	330	310	35.00	355.00	50.00	195.00	105.00	145.00	135.00	150.00	17.00
Zn	165.00	195.00	390	825	230.00	95.00	105.00	120.00	155.00	140.00	120.00	165.00	115.00
Y	27.50	25.00	29.7	66.5	37.60	31.80	15.50	39.50	23.80	23.40	25.00	28.10	29.00
Rb	146.00	121.00	129	157	131.00	151.00	212.00	31.50	14.80	22.80	64.80	64.00	14.00
Sr	128.00	87.30	75.7	12.4	379.00	299.00	138.00	185.00	218.00	242.00	202.00	262.00	105.00
Cs	9.76	2.38	3.49	6.14	2.90	4.43	9.36	1.40	1.91	1.51	1.35	5.80	0.50
Ba	439.00	2030.00	1720	547	699.00	1320.00	628.00	650.00	85.00	91.00	347.00	149.00	70.00
Th	0.87	3.35	3.08	9.38	3.51	26.90	5.74	1.65	0.85	0.87	0.97	1.45	1.00
U	0.57	1.08	0.86	6.41	0.70	4.62	1.70	0.43	0.19	0.22	0.24	0.22	0.85
Pb	6.00	28.00	535	47	43.00	9.00	5.00	2.50	8.00	10.00	7.00	20.00	5.50
Zr	90.00	97.00	100	305	97.00	383.00	88.50	130.00	124.00	118.00	127.00	86.00	100.00
Hf	2.50	2.76	2.97	8.25	3.04	11.20	2.67	3.00	3.61	3.47	3.43	2.61	3.00
Nb	7.37	5.89	5.98	21	2.84	19.30	7.24	7.00	11.20	10.60	11.10	6.97	13.50
Ta	0.47	0.41	0.42	1.42	0.18	1.00	0.54	<2	0.67	0.63	0.68	0.41	<2
La	6.73	11.20	12.7	32.7	23.70	98.00	41.40	19.00	11.60	11.10	11.30	8.22	11.50
Ce	17.70	24.40	26.9	67.9	45.60	208.00	86.80	36.50	27.50	26.40	27.70	19.00	26.00
Pr	2.53	3.35	3.74	8.91	6.11	26.20	11.80	5.50	4.04	3.88	4.15	2.77	3.90
Nd	11.40	14.70	14.9	37.7	25.90	106.48	47.10	21.50	18.60	17.40	18.60	12.30	17.50
Sm	3.36	3.72	3.89	9.8	4.99	15.00	7.91	6.00	4.91	4.68	4.78	3.28	4.80
Eu	1.05	0.93	0.98	2.32	1.39	3.42	1.82	1.95	1.77	1.59	1.75	1.20	1.35
Gd	4.41	3.97	4.26	11.5	5.87	9.53	5.29	6.00	5.27	4.69	5.03	4.12	4.40
Tb	0.77	0.71	0.8	2.04	0.94	1.16	0.66	1.05	0.79	0.85	0.83	0.73	0.82
Dy	4.69	4.54	5.13	12.4	6.04	6.01	3.45	7.50	4.67	4.86	4.96	4.97	5.00
Ho	1.06	1.02	1.18	2.71	1.39	1.21	0.66	1.45	0.97	0.94	1.02	1.14	1.00
Er	3.23	2.86	3.4	7.54	4.03	3.35	1.63	4.10	2.68	2.54	2.71	3.18	3.10
Tm	0.45	0.45	0.5	1.05	0.55	0.50	0.25	0.60	0.35	0.35	0.35	0.55	0.40
Yb	3.08	2.84	3.2	7.1	3.54	3.26	1.50	4.10	2.24	2.32	2.36	3.20	3.00
Lu	0.44	0.41	0.45	0.96	0.52	0.48	0.17	0.55	0.30	0.31	0.34	0.43	0.41
Eu/Eu*	0.83	0.74	0.74	0.67	0.79	0.87	0.86	0.99	1.06	1.04	1.09	1.00	0.90
$(La/Yb)_N$	1.57	2.83	2.85	3.30	4.80	21.56	19.80	3.32	3.71	3.43	3.43	1.84	2.75
Mg#	43	34	36	32	55	47	67	13	34	35	34	35	48

hopping routine for Nd and a static routine for Sm. Nd ratios are normalised to $^{146}Nd/^{144}Nd = 0.7219$ using an exponential mass fractionation correction.Sm and Nd concentrations are corrected for 100 pg and 50 pg blanks, respectively, although these are insignificant for the volumes measured in this study. The average measured $^{143}Nd/^{144}Nd$ value for JNdi in this study is 0.512106–± 0.000003 (2σ, n= 9). The average $^{143}Nd/^{144}Nd$ value for standard basalt material BCR-2) (basalt, Columbia River) is 0.512623 ± 0.000002 (2σ, n= 4), within uncertainty of 0.512635 ± 0.000029 (GeoRem preferred value, http://georem.mpch-mainz.

Table 1 continued: Whole-rock geochemical composition for Hiltaba Suite mafic dykes

Sample	18WPGTC-04	698127	698129	2465596	2442105	2442091	2442089	364685	HDD023-01	HDD023-02
Sample Type	out crop	drill core	drill core	pulp	drill core	drill core	drill core	drill core	drill core	drill core
Drill Hole		DD90WU25	DD90WU25	DD87LR3	RR DH 06 01	99DD252	99DD254	CUR D2	HDD 023	HDD 023
Depth From (m)		181.05	192.65	163.46	64.2	84.35	142.42	58.2	583	588.7
Depth To (m)				163.86	64.85	84.75	142.7		583.6	589
Data Source	This study	G. Swain	G. Swain	This study	This study	This study	This study	G. Swain	This study	This study
Group	central G.C.	central G.C.	central G.C.	northern G.C.	northern G.C.	northern G.C.	northern G.C.	south eastern G.C.	south eastern G.C.	south eastern G.C.
Location	Tarcoola	Wudinna	Wudinna	Leonard Rise	Robin Rise	White Hill	White Hill	Curramulka	Hillside	Hillside
Easting	455149	573929	573929	462978.78	456993	561459	559079	747769	763149	763149
Northing	6603235	6339271	6339271	6768171.89	6752788	6718232	6720282	6164961	6174298	6174298
Zone	53	53	53	53	53	53	53	53	53	53
Lithology	diorite	gabbro	gabbro	gabbro	gabbro	gabbro	gabbro	norite	gabbro	gabbro
Major elements (wt %)										
SiO_2	48.64	47.00	46.50	49.1	51.00	49.04	50.98	51.9	48.89	49.77
TiO_2	1.20	1.24	1.20	2.4	1.15	0.92	0.56	1.2	1.46	1.37
Al_2O_3	12.92	13.90	13.40	13.5	14.42	11.03	13.77	15.9	14.49	13.90
FeO	5.18			12.9	8.57	8.65	5.42		6.94	7.52
Fe_2O_{3T}	10.30	13.00	13.60	16.1	10.90	14.90	9.69	11.3	12.50	12.20
MnO	0.22	0.22	0.25	0.3	0.20	0.12	0.06	0.2	0.13	0.15
MgO	6.69	8.42	8.68	6.2	8.27	9.69	7.76	6.1	6.65	7.54
CaO	8.02	8.93	9.10	7.7	9.10	9.02	10.53	7.6	5.60	6.04
Na_2O	1.72	2.07	2.05	1.8	2.42	2.98	4.41	3.1	4.41	4.21
K_2O	1.70	2.08	2.12	2.0	1.65	0.90	0.79	1.6	1.53	1.48
P_2O_5	0.30	0.54	0.44	0.7	0.26	0.26	0.13	0.3	0.14	0.12
LOI	7.82	2.75	2.58	-0.1	0.66	0.99	0.72	1.0	3.78	3.14
F	0.07			0.04	0.08	0.26	0.13		0.08	0.08
Trace and rare earth elements (ppm)										
Ga	17.20	21.00	21.00	18.0	16.90	14.70	12.80	20.0	21.00	19.80
Cr	412.00	160.00	160.00	233.0	387.00	133.00	302.00	80.0	181.00	156.00
Ni	90.00	68.00	72.00	50.0	150.00	210.00	155.00	39.0	60.00	60.00
Co	43.90	60.00	56.00	57.2	43.80	63.40	29.80	27.0	50.40	48.70
Sc	31.70			26.3	31.10	29.30	24.60	30.0	42.40	38.70
Ti	7310.00			13700.0	6910.00	5160.00	2950.00		9200.00	8610.00
V	247.00			214.0	188.00	241.00	120.00	220.0	361.00	345.00
Cu	85.00	130.00	115.00	50.0	35.00	85.00	50.00	60.0	90.00	225.00
Zn	200.00	110.00	120.00	145.0	100.00	15.00	10.00	39.0	45.00	70.00
Y	23.10	28.50	29.00	32.9	25.80	26.40	17.50	29.0	34.60	29.00
Rb	41.60	74.00	82.00	41.2	107.00	32.30	34.90	52.0	94.50	82.70
Sr	326.00	600.00	600.00	198.0	155.00	596.00	421.00	280.0	54.90	34.60
Cs	1.67	0.40	0.50	1.0	7.57	0.88	2.39	<3	0.74	0.43
Ba	519.00	600.00	700.00	979.0	224.00	254.00	100.00	550.0	234.00	206.00
Th	3.09	5.50	11.00	2.9	7.31	19.90	14.00	9.0	3.26	2.83
U	0.97	1.25	2.80	0.7	1.48	2.41	3.32	1.5	1.69	2.67
Pb	20.00	17.00	13.50	22.0	15.00	3.00	2.00	<3	2.00	2.00
Zr	130.00	80.00	110.00	250.0	133.00	158.00	93.00	140.0	118.00	92.50
Hf	3.64	2.00	3.00	6.4	3.56	4.32	2.67	6.0	3.46	2.80
Nb	9.22	8.00	9.50	16.4	8.06	12.80	6.64	15.0	8.40	6.39
Ta	0.53	<2	<2	1.1	0.53	0.80	0.56	2.0	0.57	0.55
La	18.80	30.50	36.50	50.3	25.40	47.60	40.90	38.0	11.00	11.00
Ce	39.50	64.00	74.00	94.7	52.00	104.00	73.30	69.0	24.40	23.60
Pr	5.49	9.50	10.50	11.9	6.47	11.80	9.68	8.0	3.40	3.15
Nd	23.80	40.00	41.50	44.9	26.70	43.80	32.30	42.5	15.50	14.10
Sm	5.54	9.50	9.00	7.9	5.19	7.93	5.19	6.0	4.32	4.00
Eu	1.68	2.20	2.20	2.3	1.26	1.51	1.20	1.5	1.06	1.13
Gd	5.35	7.00	7.00	7.3	4.78	5.94	3.99	6.0	4.66	4.67
Tb	0.88	1.00	0.99	1.1	0.76	0.86	0.57	1.0	0.81	0.80
Dy	4.67	6.00	6.00	6.4	4.44	5.00	3.16	6.0	6.22	5.64
Ho	0.96	1.05	1.10	1.4	0.92	1.07	0.63	1.0	1.30	1.17
Er	2.38	2.80	2.80	3.9	2.74	2.96	1.92	4.0	3.85	3.17
Tm	0.40	0.35	0.35	0.5	0.40	0.45	0.25		0.65	0.50
Yb	2.30	2.30	2.50	3.4	2.42	2.62	1.86	3.0	4.20	3.40
Lu	0.35	0.30	0.34	0.5	0.36	0.38	0.23		0.61	0.47
Eu/Eu*	0.94	0.82	0.85	0.91	0.77	0.67	0.81	0.76	0.72	0.80
$(La/Yb)_N$	5.86	9.51	10.47	10.67	7.53	13.03	15.77	9.09	1.88	2.32
Mg#	45	56	56	29	45	44	49	52	39	42

$Eu/Eu^* = (Eu/(Sm \times Gd))_N^{0.5}$
Normalising values from Taylor and McLennon (1995)
Mg# = (Mg/[Mg+Fe]x100)
G.C. = Gawler Craton

gwdg.de/sample_query_pref.asp). Average calculated concentrations for Nd and Sm for BCR-2 measurements are 29.04 ppm and 6.58 ppm, respectively, comparable to the recommended United States Geological Survey values of 28 ± 2 ppm and 6.7 ± 0.3 ppm respectively (https://crustal.usgs.gov/geochemical_reference_standards/basaltbcr2.html).

GEOCHEMISTRY

One hundred and thirty two samples of mafic to intermediate Hiltaba Suite lithologies, collected from 30 drill holes and various outcrop locations, were analysed for whole-rock ma-

Table 2: Sm Nd isotopic composition for mafic Hiltaba Suite samples

Sample	Group	Location	Age (t)	Nd ppm	Sm ppm	$^{143}Nd/^{144}Nd$	2σ	$^{147}Sm/^{144}Nd$	$\varepsilon_{Nd\ (0)}$	$\varepsilon_{Nd\ (t)}$
2450321	eastern G.C.	Bills Lookout	1.59	11.10	3.31	0.512187	0.000002	0.1803	-8.8	-5.5
2559254	eastern G.C.	Chianti	1.59	13.70	3.40	0.512137	0.000010	0.1531	-9.8	-0.9
2559247	eastern G.C.	Chianti	1590	14.40	3.70	0.512087	0.000008	0.1530	-10.7	-1.9
2559249	eastern G.C.	Chianti	1590	36.70	9.00	0.512009	0.000008	0.1477	-12.3	-2.3
PDBN321-02	central G.C	Barns	1.59	46.48	7.94	0.511624	0.000002	0.1033	-19.8	-0.8
2465592	central G.C.	Barns	1.59	25.51	5.12	0.511763	0.000002	0.1214	-17.1	-1.7
2465593	central G.C.	Barns	1.59	106.48	15.69	0.511563	0.000002	0.0891	-21.0	1.0
GCT 88B	central G.C.	Bulgunnia	1.59	21.50	5.65	0.512250	0.000009	0.1586	-7.6	0.2
18ErD-02	central G.C.	Earea Dam	1.59	18.56	4.72	0.512236	0.000002	0.1536	-7.8	0.9
18ErD-03	central G.C.	Earea Dam	1.59	18.09	4.62	0.512250	0.000002	0.1543	-7.6	1.1
18ErD-01	central G.C.	Earea Dam	1.59	19.05	4.95	0.512235	0.000006	0.1570	-7.9	0.2
18GL-05	central G.C.	Glenloth	1.59	11.70	3.26	0.512335	0.000002	0.1686	-5.9	-0.2
662450	central G.C.	Kimba	1.59	17.14	4.43	0.512153	0.000003	0.1563	-9.5	-1.3
18WPGTC-04	central G.C.	Tarcoola	1.59	23.31	5.40	0.512146	0.000002	0.1400	-9.6	1.9
698127	central G.C.	Wudinna	1.59	43.29	9.34	0.511837	0.000009	0.1304	-15.6	-2.1
698129	central G.C.	Wudinna	1.59	44.75	9.44	0.511783	0.000010	0.1276	-16.7	-2.6
2465596	northern G.C.	Leonard Rise	1590	68.76	12.29	0.511432	0.000002	0.1081	-23.5	-5.5
2442105	northern G.C.	Robin Rise	1.59	23.94	4.70	0.511570	0.000002	0.1187	-20.8	-5.0
2442091	northern G.C.	White Hill	1.59	43.61	7.43	0.511487	0.000002	0.1030	-22.4	-3.4
2442089	northern G.C.	White Hill	1.59	33.07	5.30	0.511428	0.000002	0.0970	-23.6	-3.3
364685	south eastern G.C.	Curramulka	1590	31.66	6.01	0.511611	0.00001	0.1148	-20.0	-3.4
HDD023-01	south eastern G.C.	Hillside	1.59	14.50	3.94	0.512229	0.000006	0.1643	-8.0	-1.4
HDD023-02	south eastern G.C.	Hillside	1.59	13.71	3.93	0.512276	0.000003	0.1732	-7.1	-2.3

Errors on $^{143}Nd/^{144}Nd$ measurements are 2σ (mean) and refer to the last significant figure(s).

Measured εNd values calculated with present-day CHUR $^{143}Nd/^{144}Nd$ and $^{147}Sm/^{144}Nd$ ratios of 0.512638 and 0.1966.

Depleted mantle Nd model ages calculated as in Goldstein et al. (1984).

jor and trace element geochemistry [dataset] (Wade 2019). Samples were filtered by SiO_2 and MgO to include samples with 41–52 wt. % SiO_2 and MgO contents > 5 wt. % as an initial screen for removing samples likely affected by crustal contamination. Samples with high Fe_2O_{3t} (> 18 wt. %, as an indication of hematite alteration) and K_2O > 4 wt. % (as an indication of post-emplacement alteration) were also omitted, leaving 69 of the 132 samples. Twenty-three samples were selected for whole-rock Sm-Nd isotope analysis.

Whole-rock geochemistry and Sm-Nd isotope data

Major and trace element geochemistry for 23 mafic Hiltaba Suite samples that were analysed for Sm-Nd isotope compositions are listed in Table 1 with the complete dataset available in Appendix 1 Table A1. Twenty-three new Nd isotope analyses from mafic Hiltaba Suite are recorded in Table 2. Initial $\varepsilon_{Nd(t)}$ values are calculated at 1590 Ma.

Mafic intrusions of the Hiltaba Suite display a variety of major element compositions with significant variation in Mg# (26–67; Mg# calculated as molar Mg# = (Mg/ [Mg+Fe] x100)), CaO (0.7–12.7 wt. %), K_2O (0.5–3.5 wt. %), Na_2O (0.2–44 wt. %) and P_2O_5 (0.1–1.6 wt. %; Fig. 4). Mafic dykes from the central Gawler Craton have a wide range of Mg# (Mg# = 28–67), with several high-Mg dykes (Mg# = 47–67) from the Barns Au deposit. In contrast, the eastern Gawler Craton, south eastern Gawler Craton and northern Gawler Craton samples have similar and low to moderate ranges of Mg#(Mg# = 26–52). Mafic dykes from the south eastern Gawler Craton are distinguished by higher Na_2O abundances relative to mafic intrusions from the other regions (Fig. 4). Similar degrees of scatter are observed in major elements such as SiO_2, Al_2O_3, CaO, K_2O and Na_2O in samples from all regions. Coherent trends are formed between Fe_2O_{3t} and TiO_2 with Mg# in all four sample groups (Fig. 4).

Significant variation is observed in trace element abundances (Fig. 5) between mafic

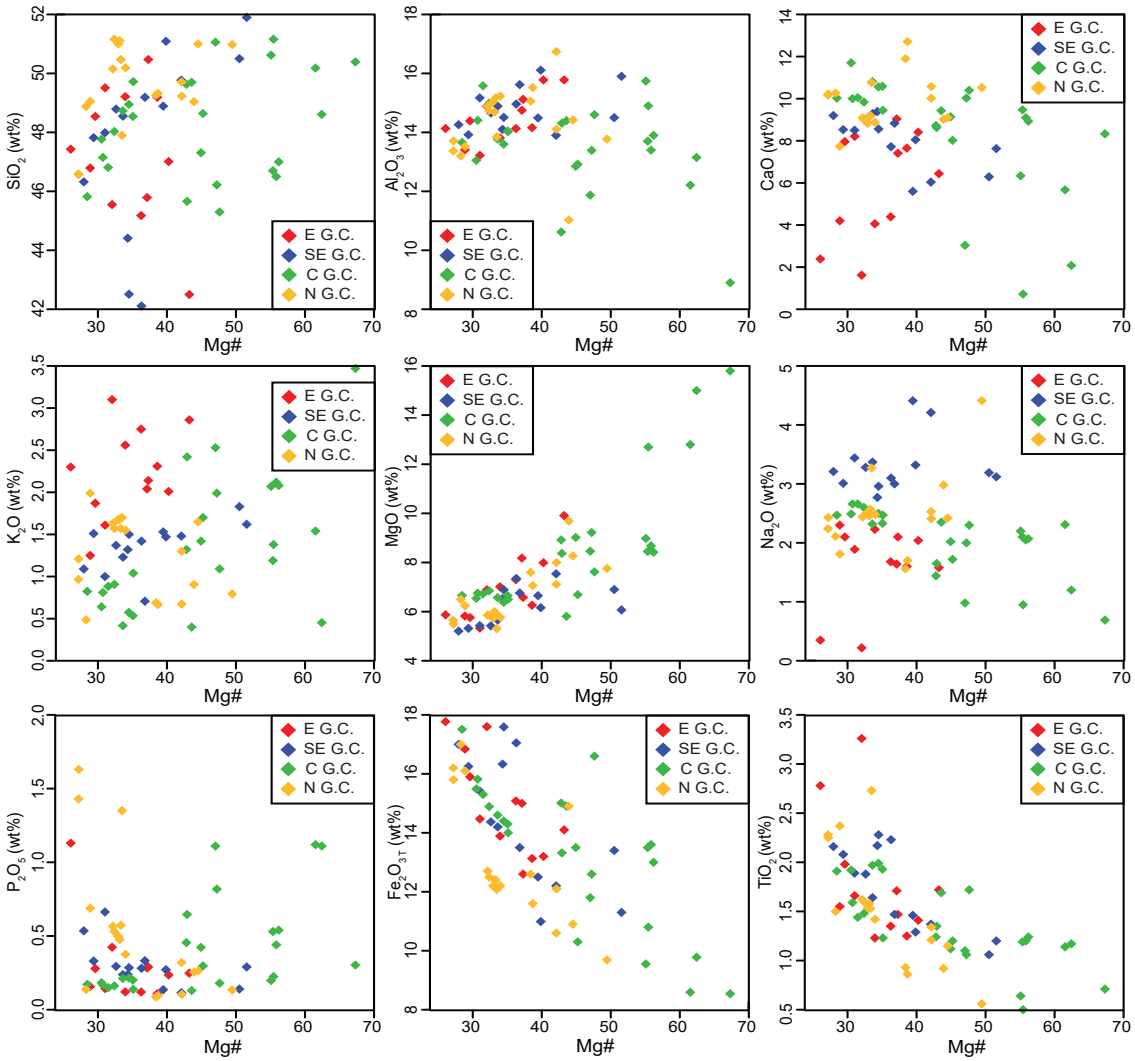

Figure 4: Selected major elements vs the fractionation index Mg# (Mg# = (Mg/ [Mg+Fe] x100)) for the mafic Hiltaba Suite, to assess whether magmatic differentiation trends are evident, divided by geographical regions. E G.C. = eastern Gawler Craton, SE G.C. = southeastern Gawler Craton, C G.C. = central Gawler Craton and N G.C. = norhtern Gawler Craton.

Hiltaba Suite intrusions from each locality. Several of the high-Mg dykes of the central Gawler Craton are separated from the other groups by significantly higher Cr, La, Zr, Th and Nb (Fig. 5). Central Gawler Craton mafic dykes have some of the highest Cr and Ni abundances (54–1510 ppm and 35–640 ppm respectively; Fig. 5). Two coherent trends are formed between Cr and Mg#. A steep trend including the eastern Gawler Craton mafic dykes and some northern Gawler Craton mafic intrusions with the high-Mg central Gawler Craton dykes as the end members, and a flat trend including the south eastern Gawler Craton intrusions and the remaining northern Gawler Craton intrusions with moderate Mg-Cr mafic dykes from the central Gawler Craton forming the end member. Aside from Cr (and Ni not shown), correlations are not observed between trace elements and Mg# in the mafic Hiltaba Suite (Fig. 5).

Common to most of the units are enrichment in HFSE including Zr, Nb, Th and Y and LREE relative to heavy REE (HREE) $(La/Yb)_N$ = 1.6–31.8). There are varying degrees of, but generally negative, Nb-Ta-Ti-Sr anoma-

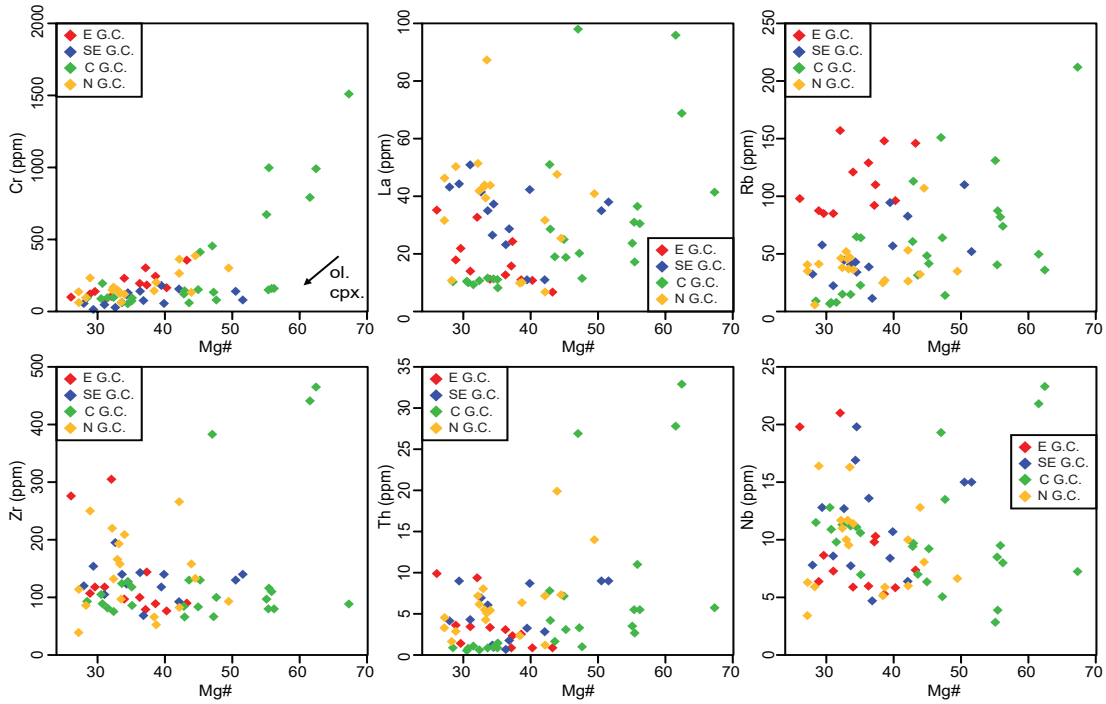

Figure 5: Selected trace elements vs Mg# for the mafic Hiltaba Suite, divided by geographical region. E G.C. = eastern Gawler Craton, SE G.C. = southeastern Gawler Craton, C G.C. = central Gawler Craton and N G.C. = norhtern Gawler Craton.

lies (Fig. 6). Eu anomalies are minor if present (Eu/Eu* = 0.54–1.09; Fig. 7). Scatter in large ion lithophile elements (LILE) such as Rb, Ba and K is also common. Two aphanitic dykes from the eastern Gawler Craton have the most profound negative Sr anomalies and highest degree of enrichment in U and REE relative to the other groups (Fig. 6). A group of samples from the central Gawler Craton (gabbros samples 18-ErD-01, -02, -03 and gabbronorite samples from drill hole DDH C7) are distinguished from other Hiltaba Suite samples by their lower Rb, Ba, Th, U, Zr and Hf abundances, absence of negative Nb-Ta-Ti anomalies and flatter REE patterns (La/Yb = 1.8–3.7 (Figs. 6 and 7). These patterns closely resemble E-MORB in their shape.

By contrast, the high-Mg aphanitic mafic dykes of the central Gawler Craton have profound negative Nb-Ta-Ti anomalies, positive Zr-Hf anomalies and are LREE enriched ($(La/Yb)_N$ = 4.8–31.8). While the trace and REE in the high-Mg dykes are enriched, relative patterns are similar to rest of the mafic Hiltaba Suite and closely resemble bulk crust and global subducted sediment (GLOSS) patterns (Figs. 6 and 7).

Sm-Nd isotopic compositions are recorded in Table 2. $\varepsilon_{Nd(t)}$ values are variable, ranging from -5.5 to -0.9 in the eastern Gawler Craton, from -2.6 to 1.9 in the central Gawler Craton, from -3.4 to -1.4 in the south eastern Gawler Craton and from -5.5 to -3.3 in the northern Gawler Craton. Mafic dykes from the central Gawler Craton with trace element patterns similar to E-MORB are the only samples to have $\varepsilon_{Nd(t)}$ values greater than 0. The northern Gawler Craton intrusions collectively have the most negative $\varepsilon_{Nd(t)}$ values.

DISCUSSION

Source composition or fractional crystallisation and crustal contamination?

Evaluation of the composition of mantle

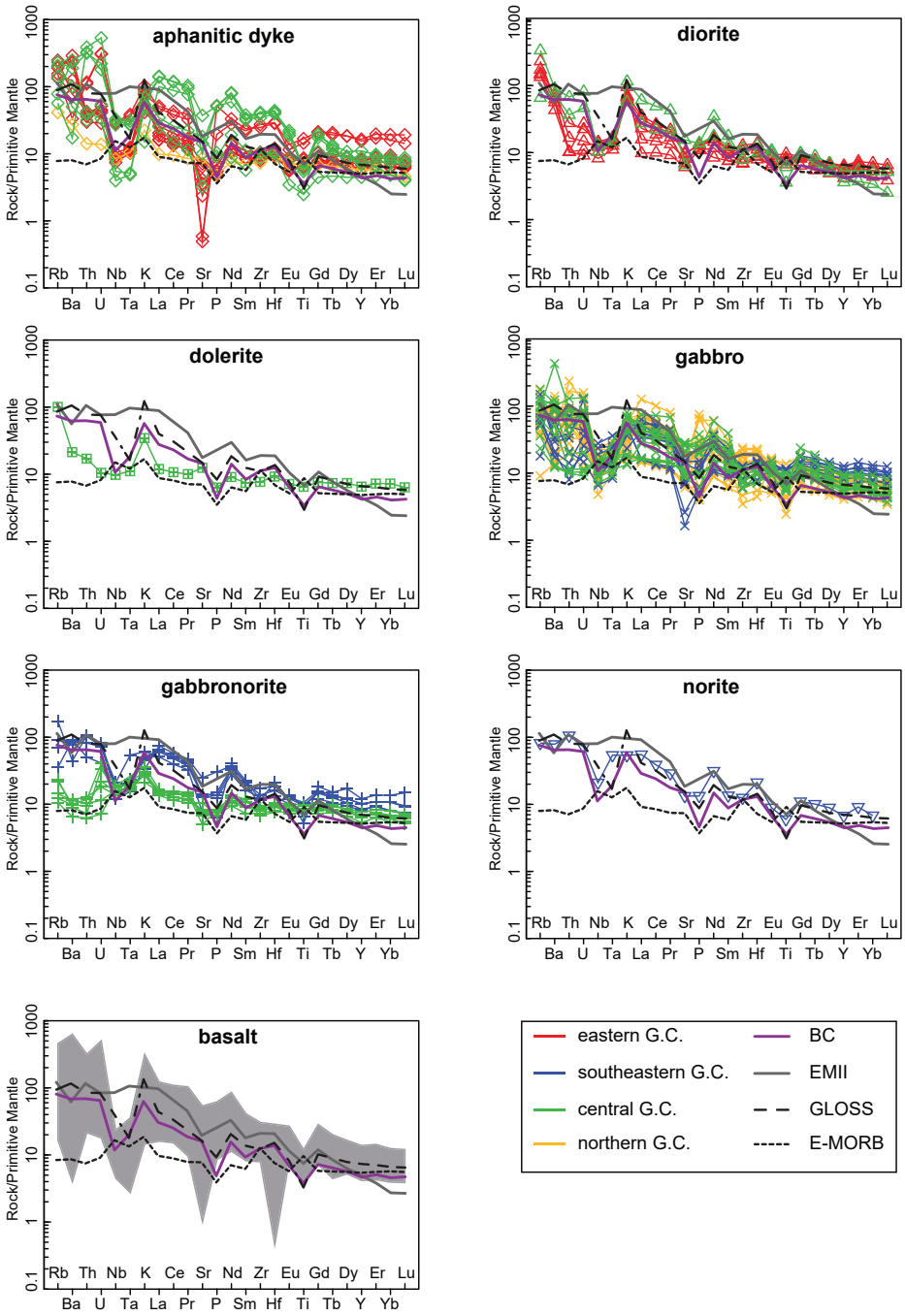

Figure 6: Primitive mantle-normalised trace element diagrams for the mafic Hiltaba Suite and mafic Galwer Range Voclanics (GRV), divided by lithology. Colours for mafic Hiltaba Suite refer to geographic region. Data sources for mafic GRV: Giles (1980), Stewart (1994), Fricke (2005), Agangi (2011), Geoscience Australia (http://www.ga.gov.au/metadata-gateway/metadata/record/65464/ 2007, OZCHEM database and references therein) and Government of South Australia (https://map.sarig.sa.gov.au). Data sources for bulk crust (BC): Rudnick and Gao (2003); Global Subducting Sediment (GLOSS): Plank and Langmuir (1998); enriched mantle 2 (EMII): Workman et al. (2004); and enriched mid-ocean ridge basalt (E-MORB): Kelin (2004). Normalising values for primitive mantle from Sun and McDonough (1989).

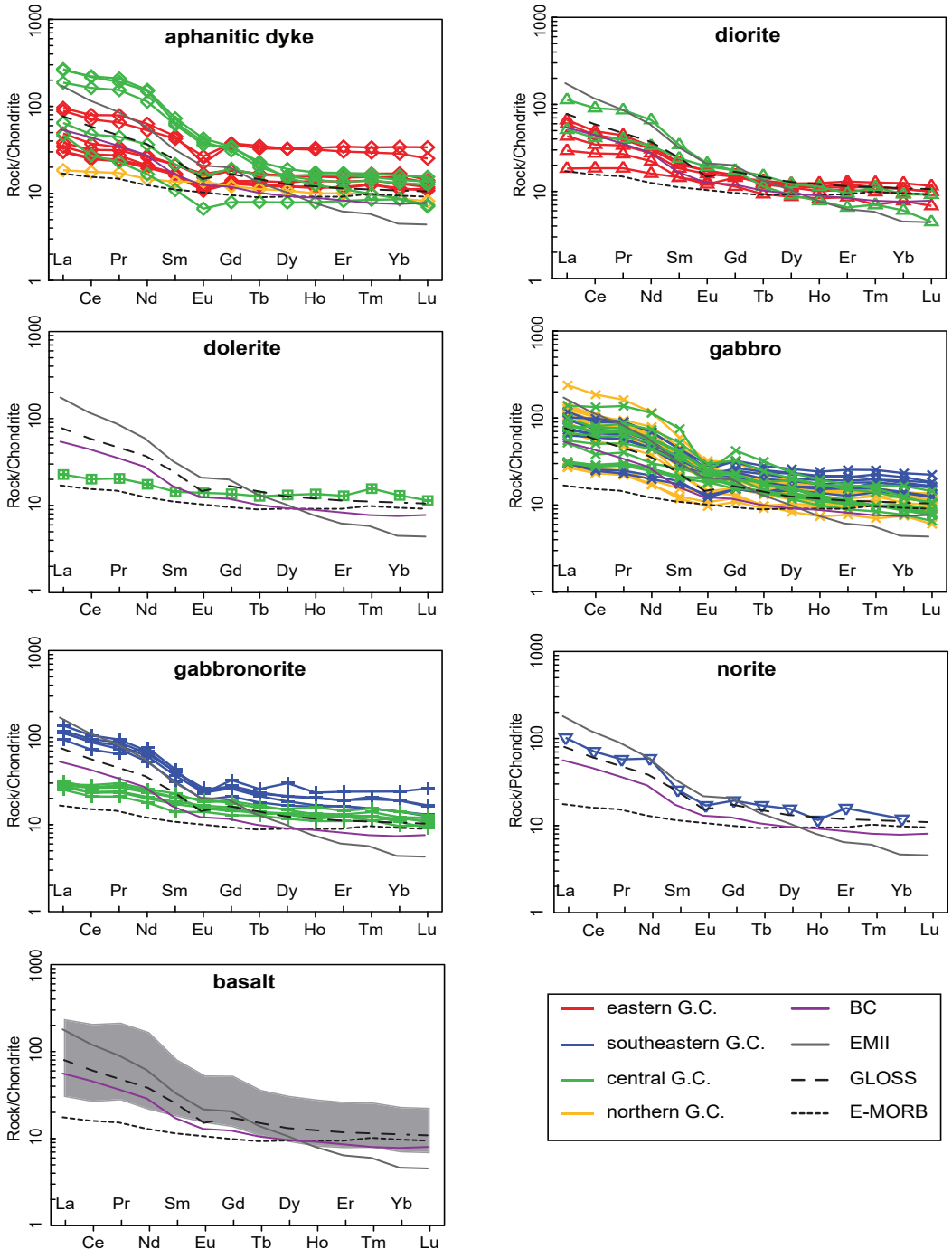

Figure 7: Chondrite-normalised rare earth element diagrams for the mafic Hiltaba Suite and mafic Gawler Range Voclanics (GRV), divided by lithology. Colours for mafic Hiltaba Suite refer to geographic region. Data sources for mafic GRV and mantle and crust reservoirs are the same as Figure 7. Normalising values for chondrite from Taylor and McLennon (1985).

sources from mafic magmas emplaced in the continental crust requires accounting for the influence of crustal contamination and/or fractional crystallisation. This is challenging in the Gawler Craton due to the lack of coherent outcrops that provide a range of compositions

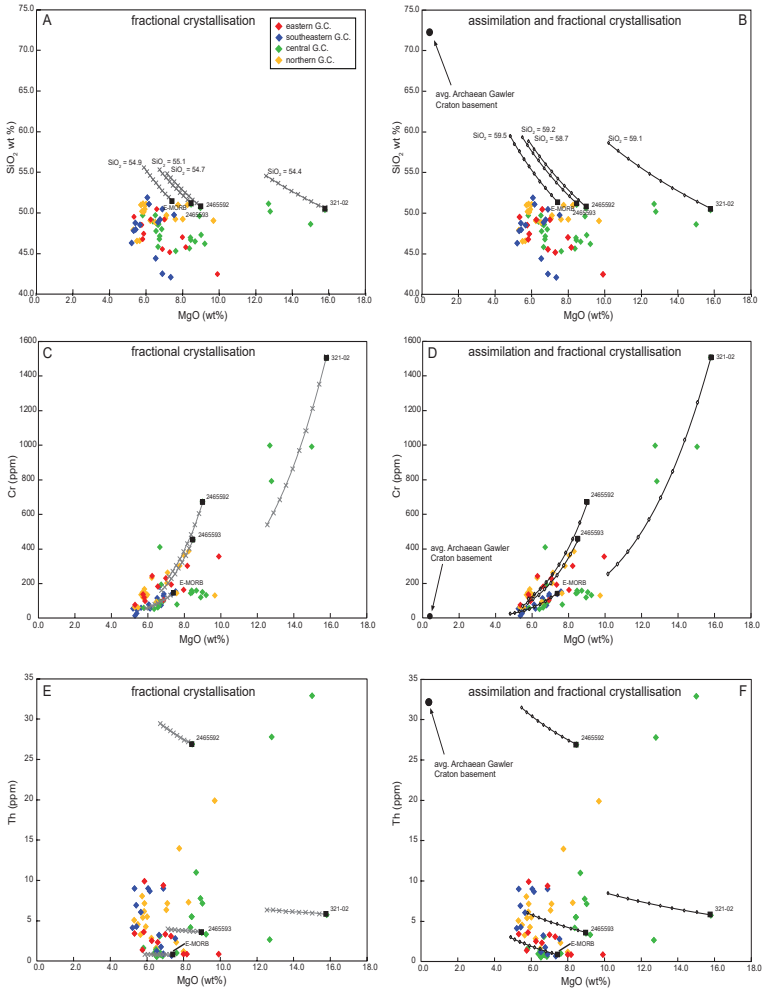

Figure 8: Fractional Crystallisation (FC) (a, c, e) and Assimilation- Fractional Crystallisation (AFC) (b, d, f) lines of descent for three high Mg-Ni-Cr mafic dykes from the Barns Au prospect (black squares) and mafic Hiltaba Suite samples, divided by lithology. Average Archaean Gawler Craton basement (Cooyerdoo Granite) composition represents the crustal end member assimilant (black circle) on Figs. B, d and f. Increments are at 1%. Crystallisation ends at 9 %. r value = 0.4. A) Fractional Crystallisation (FC) (grey crosses) lines of descent between MgO and SiO_2 for samples 321-02, 2465592 and 2465593. B) Assimilation-Fractional Crystallisation (AFC) curves between MgO and SiO_2 for samples 321-02, 2465592 and 2465593. Crystallisation ends at 9%, at 54.4 wt% SiO_2 for sample 321-02, 54.7 wt% SiO_2 for sample 2465592 and 55.1 wt% SiO_2 for sample 2465593. Assimilant is average Archaean Gawler Craton basement represented by the Cooyerdoo Granite. Crystallisation ends at 9%, at 59.1 wt% SiO_2 for sample 321-02, 58.7 wt% SiO_2 for sample 2465592 and 59.2 wt% SiO_2 for sample 2465593. r value = 0.4. C) Fractional Crystallisation (FC) lines of descent between MgO and Cr for samples 321-02, 2465592 and 2465593. Inset shows enlargement of E-MORB curve (boxed area on plot). D) Assimilation- fractional crystallisation (AFC) lines of descent between MgO and Cr for samples 321-02, 2465592 and 2465593. Inset shows enlargement of E-MORB curve (boxed area on plot). E) Fractional Crystallisation (FC) lines of decent between MgO and Th for samples 321-02, 2465592 and 2465593. F) Assimilation-fractional crystallisation curves between MgO and Th for samples 321-02, 2465592 and 2465593. Modelling based on fractionating phases = Olivine 25%, Orthopyroxene 10%, Clinopyroxene 20%, Garnet 5%, Amphibole 10%, Biotite 10% and Plagioclase 20%. Modelling done with the FC-AFC-FCA and Mixing Modeler of Ersoy and Helvaci (2010). E G.C. = eastern Gawler Craton, SE G.C. = southeastern Gawler Craton, C G.C. = central Gawler Craton and N G.C. = norhtern Gawler Craton.

within a single intrusive complex that could assist with determining the role of assimilation or fractional crystallisation. The possibility of crustal contamination is highlighted by enrichments in HFSE and LREE and depletions in Nb-Ta-Ti on primitive mantle normalised trace element diagrams. When accompanied by negative $\varepsilon_{Nd(t)}$ compositions ($\varepsilon_{Nd(t)}$ = -5.5 to + 1.9) the case for crustal contamination can be easily made.

Mg# values for the majority of analysed samples are lower than is considered typical for melts in equilibrium with a depleted mantle (i.e. primary melts) and some samples with the highest Mg# are slightly altered as indicated by elevated loss on ignition (LOI) contents. Elevated LOIs for some samples do not show a correlation with any elements with the exception of a negative correlation with CaO and a weak positive correlations with mobile elements such as K_2O, U, Ba and Rb (Appen-

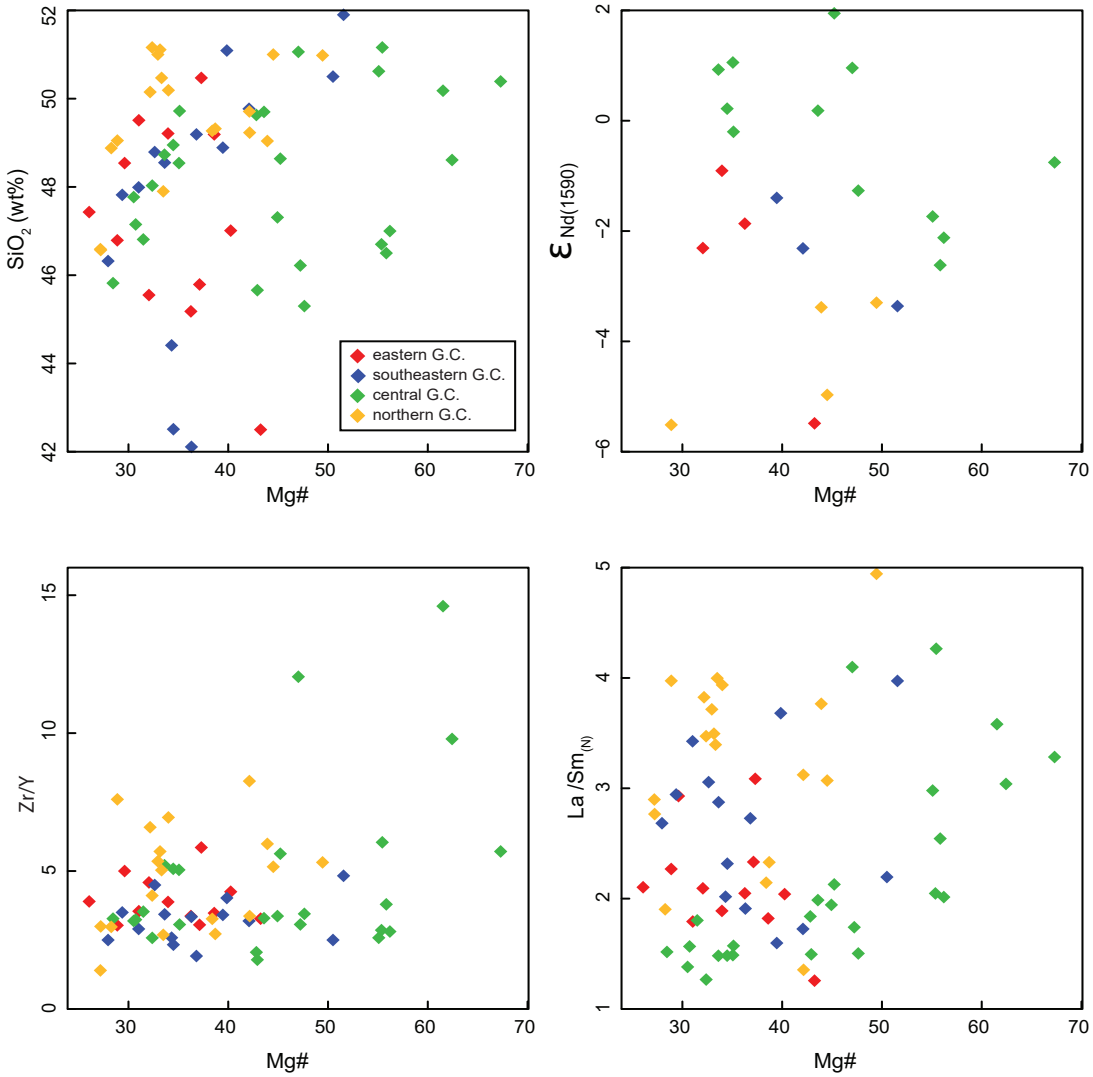

Figure 9: Mg# vs proxies for crustal assimilation. A) Mg# vs SiO_2, B) Mg# vs $\varepsilon_{Nd(t)}$, C) Mg# vs Zr/Y and D) Mg# vs $La/Sm_{(N)}$. Lack of correlation between Mg# and these crustal proxies suggests crustal contamination was minimal. E G.C. = eastern Gawler Craton, SE G.C. = southeastern Gawler Craton, C G.C. = central Gawler Craton and N G.C. = norhtern Gawler Craton.

dix 1 Figure A1). The major element changes suggest (supported by petrography) that the primary effect of the alteration is influx of K_2O and replacement of hornblende with biotite. These major element relationships (negative correlation with CaO and weak positive correlations with K_2O, U, Ba and Rb) do not hold for the most primitive central Gawler Craton samples (Appendix 1 Figure A1). Importantly for this discussion, there is not a positive correlation between LOI and enrichment indicators such as Th/Nb (Appendix 1 Figure A1).

Samples from the Barns Au deposit (central Gawler Craton) yield the most primitive Mg# (47–67) and highest values of elements such as Ni and Cr. These samples show a coherent fractional crystallisation trend between these elements and Mg#, consistent with the fractionation of olivine and clinopyroxene. To constrain the role of fractional crystallisation and assimilation we chose 3 samples from the Barns Au deposit (PDBN 321-02, 2465592 and 2465593) to represent parental magmas for modelling of the intrusive mafic component. An average composition of the Mesoarchean Cooyerdoo Granite (Fraser *et al.* 2010) was used as the assimilant. Fractional crystallisation (FC) and assimilation-fractional crystallisation (AFC) were stopped when SiO_2 reached ~55 and 59 wt% SiO_2 respectively, equivalent to 9% crystallisation, and an r value = 0.4. Figure 8 shows the modelled FC curves (Figure 8a, c and e) and AFC curves (Figure 8b, d and f) for SiO_2, Cr and Th versus MgO for samples PDBN 321-02, 2465592 and 2465593. A number of northern and eastern Gawler Craton samples fit the trace element FC and AFC curves of samples 2465592 and 2465593 (e.g. Fig. 8c and 8d). However, the SiO_2 values obtained for these FC-AFC models are all much higher than the measured values for the Hiltaba Suite samples suggesting that, in part at least, variation in sample compositions is a result of mantle source compositional variation. Similarly, samples from the south eastern Gawler Craton and low-Mg samples from the central Gawler Craton are not consistent with FC-AFC models from these starting compositions and are taken to indicate mantle source

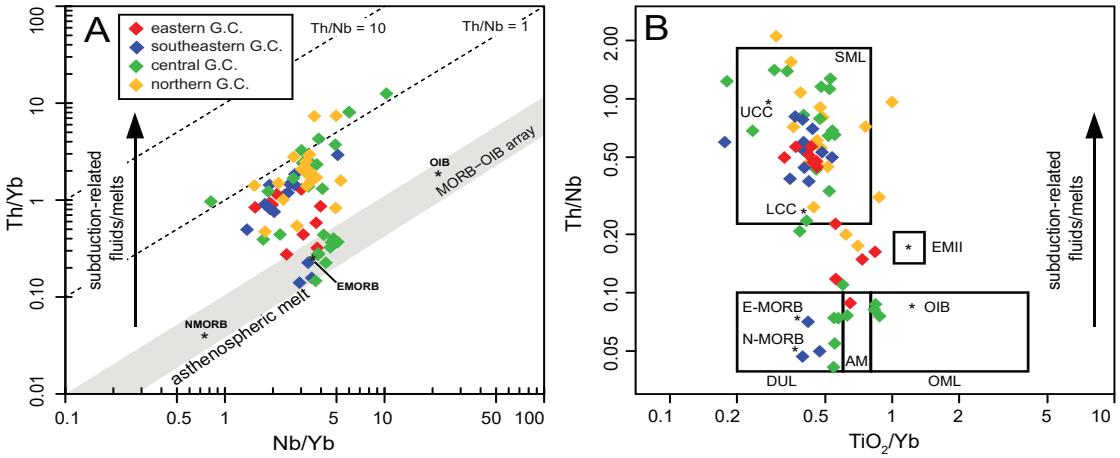

Figure 10: A) Th/Yb vs Nb/Yb plot of Pearce (2008) and B) Th/Nb vs TiO_2/Yb plot of Pearce et al. (2015), highlighting mantle source regions for the mafic Hiltaba Suite divided by lithology this study. E-MORB: enriched mid-ocean ridge basalt; N-MORB: normal mid-ocean ridge basalt; AM: asthenospheric mantle; OIB: oceanic island basalt; SML: subduction modified lithosphere; DUL: depleted unmodified lithosphere; OML: oceanic island basalt modified lithosphere. E G.C. = eastern Gawler Craton, SE G.C. = southeastern Gawler Craton, C G.C. = central Gawler Craton and N G.C. = norhtern Gawler Craton.

variation.

Compositions of gabbros and gabbronorites from the Hillside deposit and Curramulka, south eastern Gawler Craton, and samples Erd-01, Erd-02 and Erd-03 of central Gawler Craton samples appear to fit well with fractional crystallisation curves of E-MORB (Fig. 8c and 8e). However, even the mild enrichment in elements such as Th or Zr in the south eastern Gawler Craton gabbros and gabbronorites cannot be explained through normal fractional crystallisation of a mantle source composition such as E-MORB. Remaining samples from drillhole DDH7 in the central Gawler Craton with MgO between ~8–10 wt% cluster together and do not lie on fractionation curves shown on Figure 8.

The compositions of the Hiltaba Suite samples cannot be obtained by the calculated fractional crystallisation curves of the high-Mg samples without exceeding SiO_2. Moreover, lack of correlation between Mg# and $\varepsilon_{Nd(t)}$ and elements indicative of crustal contamination (e.g. SiO_2, Zr/Y and $(La/Sm)_{PM}$ (Fig. 9)) suggest crustal assimilation was minimal. Assimilation of the most evolved crustal component in the Gawler Craton, the Mesoarchaean Cooyerdoo Granite, cannot achieve the HFSE, REE and isotopic compositions of the Hiltaba Suite magmas, which suggests the assimilation of a crustal component and fractional crystallisation was minimal. Compositions observed appear to be more complicated than that generated by pure fractional crystallisation and AFC processes.

Composition of the mantle sources

From the above discussion it is concluded that crustal contamination was in most cases negligible and a significant component of the geochemical enrichment (e.g. Th and Nb) of the mafic rocks is source-derived. Th/Nb ratios are sensitive to fluid mobilisation of Th during subduction and extraction of continental crust (Condie and Shearer 2017), enriching Th in the mantle wedge by fluids released from descending plates. Therefore, these ratios can be used to trace potential crustal input either by subduction-related metasomatism in a mantle source or crustal contamination during magmatic differentiation (Pearce 2008, Pearce *et al.* 2015, Condie and Shearer 2017). As is it has been concluded that the latter was negligible, Th/Nb ratios may be used to identify subduction-related metasomatism as a contributor to the mafic component of the Hiltaba Suite.

The Th/Yb vs. Nb/Yb diagram of Pearce (2008) shows a small number of the mafic Hiltaba Suite plot within or close to the MORB-OIB array, clustering around E-MORB (Fig. 10a), suggesting a relatively depleted source component. Occurring predominantly in the central Gawler Craton (e.g. Earea Dam and drillhole DDH C7, Kimba), examples are also found in the south eastern (e.g. drillhole CUR D4, Curramulka) and eastern Gawler Craton (e.g. drillhole BLD 3). These samples have low Mg# (28–48), Th/Nb ratios < 0.10 and commonly low abundances of Ba, Th and U. Also characteristic are flat trace element patterns with an absence of negative Nb-Ta-Ti anomalies which closely resemble E-MORB ($(La/Yb)_N$ = 2.1–4.6), with the exception of three samples from drill hole CUR D4 which have higher REE abundance (Appendix 1 Table A1). The Nd isotopic composition is narrow with $\varepsilon_{Nd(t)}$ ranging from -1.3 to + 1.1. It is logical to infer a mid-ocean ridge basalt (MORB) mantle source with mild enrichment in Zr, Nb and Y and minor LREEs that is relatively isotopically homogeneous as a source component for these samples. A depleted lithospheric component (i.e. the MORB-OIB array) for these samples is also illustrated on the Th/Nb vs. TiO_2/Yb diagram of Pearce (2015; Fig. 10b). The lower Mg# in these samples may be indicative of minor olivine fractionation and magmatic differentiation, in addition to high degrees of partial melting of the mantle source or metasomatism caused by the infiltration of mafic melts, toward the base of a SCLM (Griffin *et al.* 2009). Alternatively, the mild trace

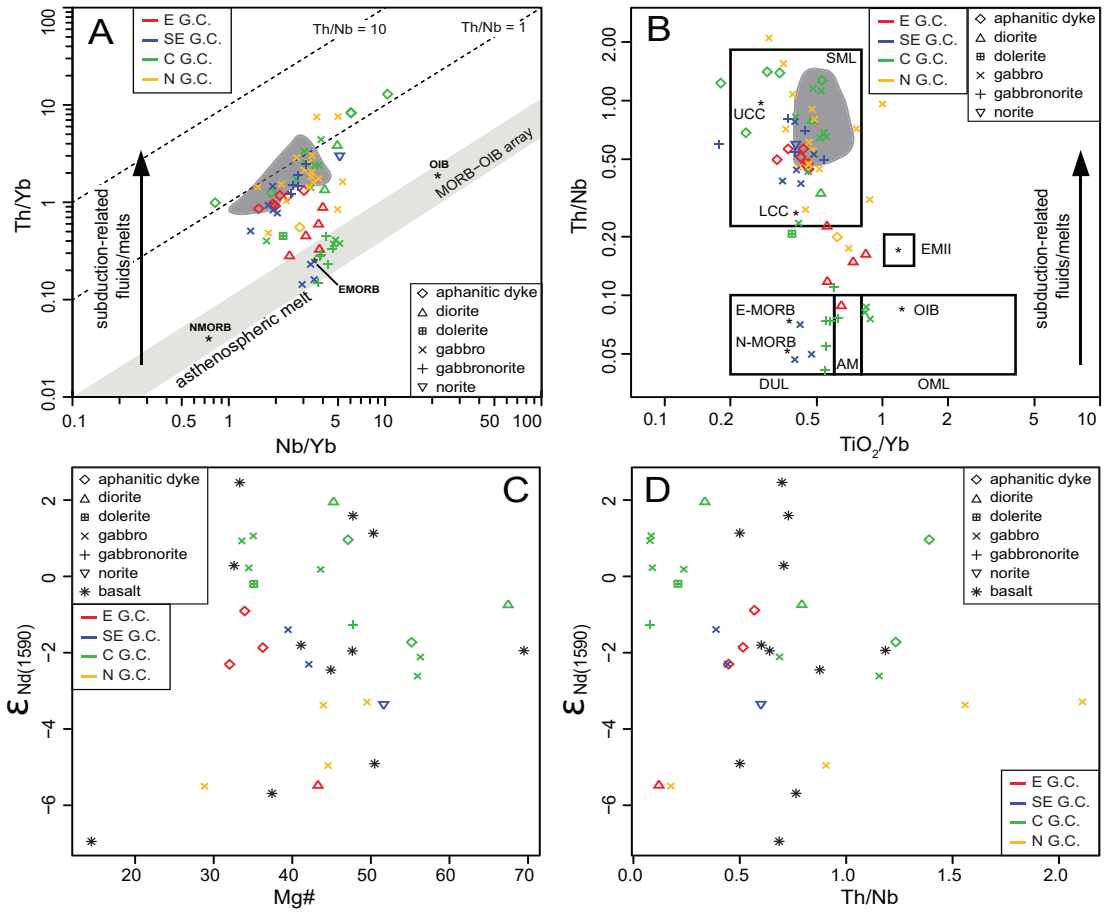

Figure 11: A) Th/Yb vs Nb/Yb plot of Pearce (2008), B) Th/Nb vs TiO_2/Yb plot of Pearce et al. (2015) C) $\varepsilon_{Nd(i)}$ vs Mg# and D) $\varepsilon_{Nd(i)}$ vs Th/Nb for the mafic Hiltaba Suite divided by lithology this study compared with basalts of the lower GRV. Data sources for mafic GRV: Giles (1980), Stewart (1994), Fricke (2005), Agangi (2011), Geoscience Australia (http://www.ga.gov.au/metadata-gateway/metadata/record/65464/ 2007, OZCHEM database and references therein) and Government of South Australia (https://map.sarig.sa.gov.au). E-MORB: enriched mid-ocean ridge basalt; N-MORB: normal mid-ocean ridge basalt; AM: asthenospheric mantle; OIB: oceanic island basalt; SML: subduction modified lithosphere; DUL: depleted unmodified lithosphere; OML: oceanic island basalt modified lithosphere. E G.C. = eastern Gawler Craton, SE G.C. = southeastern Gawler Craton, C G.C. = central Gawler Craton and N G.C. = norhtern Gawler Craton.

element enrichment could indicate enrichment occurred shortly before magma generation, i.e. upwelling of an asthenospheric mantle plume incorporating previously enriched lithospheric mantle. Due to mixing between a plume head and lithospheric mantle no primitive mantle reservoir is likely to have survived (Davaille *et al.* 2003). The Nd isotopic composition of these samples is not significantly juvenile, perhaps reflecting such mixing. However, their overall flat trace and REE patterns and low Th/Nb is more reflective of an uncontaminated mantle source similar to E-MORB and potentially a mantle plume.

This contrasts to the majority of the mafic Hiltaba Suite samples which plot well above the MORB-OIB array (Fig. 10a). Enrichment in crustal components (e.g. HFSE, REE) and high Th/Nb ratios (>0.25), in some cases greater than upper continental crust ratios

(>1.0), is consistent with an enriched and variably metasomatised source (e.g. Griffin *et al.* (2009), Cai *et al.* (2013), Callegaro *et al.* (2014) and Zhang *et al.* (2016)). Further evidence for a subduction-modified, metasomatised source is illustrated on the Th/Nb vs. TiO_2/Yb diagram of Pearce (2015; Fig. 10b). Additionally, the vertical trends from ~E-MORB are consistent with subduction zone enrichment (Kempton *et al.* 1991). This is particularly pertinent for the high-Mg and isotopically more juvenile samples from the central Gawler Craton. High ε_{Nd} samples from central Gawler Craton ($\varepsilon_{Nd(t)}$ = -0.8 and +1.0 for samples 321-02 and 2465593 respectively) with high $(La/Yb)_N$ (19.8 and 21.6 respectively) indicates a long-term LREE enrichment in their mantle source, along with potential long-term enrichments in HFSE such as Zr, Nb and Th. The data suggest primitive magmas already had variable isotopic and geochemical compositions before evolving into basaltic melts involved in the genesis of the Hiltaba Suite magmas.

Evidence from the high-Mg aphanitic dykes suggests that the crustal-like signatures in these rocks may be a result of partial melting of a metasomatised mantle. Similar incompatible element and isotopic signatures of mafic rocks from Archaean cratons such as the Wyoming craton, Greenland, the Baltic Shield, western Sao Francisco craton of Brazil and the southern Etendeka region of Namibia have been interpreted as deriving from an enriched lithospheric mantle that formed during the Archaean (Jahn *et al.* 1999, Cousens *et al.* 2001 and references therein). It is not unreasonable to consider a similar evolution for the Gawler Craton. The earliest known event in the Gawler Craton that could have produced an enriched lithospheric mantle may be related to ca. 2560–2520 Ma arc-like magmatism (Swain *et al.* 2005). Subsequent mantle plume activity at ca. 2520–2500 Ma (Swain *et al.* 2005), may have contributed to long-term stability of the lithospheric mantle (Arndt *et al.* 2009) and, together, possibly forming an enriched SCLM in the Gawler Craton. The implication here is the longevity of a SCLM (e.g. (Cousens *et al.* 2001, Griffin *et al.* 2003, Tang *et al.* 2013)) in the Gawler Craton that stabilised shortly after the Neoarchean.

Volcanic versus intrusive dichotomy

The GRV-HS SLIP is contains of a variety of subordinate mafic-ultramafic intrusions and basalts. Systematic differences, both spatially and compositionally, between the intrusive and extrusive 1590 Ma mafic rocks have been suggested by Skirrow *et al.* (2018). Hiltaba Suite intrusions and dykes are widespread across the Gawler Craton whereas the extrusive component is restricted to three cropping-out discrete volcanic centres. No known field relationships between the 1590 Ma extrusive and intrusive mafic rocks has been observed in the Gawler Craton in outcrop or in drill core, greatly hindered by scarcity of outcrop of intrusive phases and limited outcrop extent of basalts at Glyde Hill, Chitanilga and Roopena. Paramount to this is the extensive cover of the upper GRV felsic lavas, presumably obscuring the extent of the underlying mafic magmas. Well constrained magmatic crystallisation ages are also absent, preventing a comparative temporal evolution/distinction between possible phases related to the developmental and mature phases of the GRV. Despite this, geochemical and isotopic compositions of the extrusive and intrusive phases may provide insight into mantle fertility and composition.

Compositional differences identified between the extrusive and intrusive phases by Skirrow *et al*. (2018) were used to define differing mantle sources based on Th/Nb ratios and $\varepsilon_{Nd(t)}$ values. Extrusive phases were noted to have higher Th/Nb ratios (>0.53) and variable but lower $\varepsilon_{Nd(t)}$ values while intrusive phases of the Hiltaba Suite were low Th/Nb (<0.53) and high $\varepsilon_{Nd(t)}$, with the exception of a few

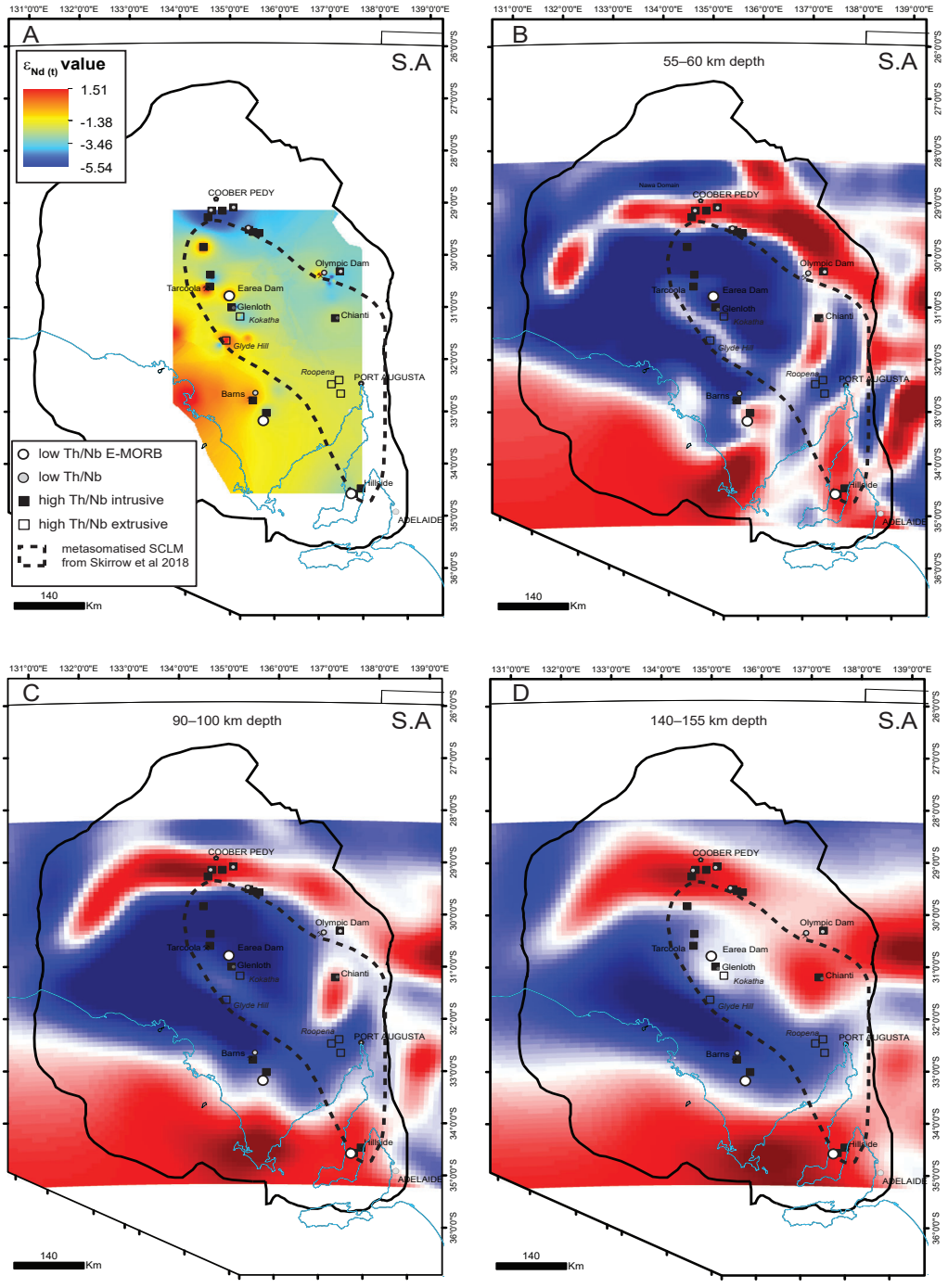

Figure 12: Maps of isotopic (A) and magnetotelluric data (B-D) of mafic rocks the study area in the Gawler Craton in relation to low and high Th/Nb mafic rocks and the metasomatised SCLM mantle domain of Skirrow et al. (2018). A) Isotopic map contoured for $\varepsilon_{Nd(i)}$ values for mafic rocks of the Hiltaba Suite and Gawler Range Volcanics; B) 55–60 km depth slice of magnetotelluric data for the Gawler Craton; C) 90–100 km depth slice of magnetotelluric data for the Gawler Craton; D) 140–155 km depth slice of magnetotelluric data for the Gawler Craton. Colour scale in figures B-D: blue colours are resistive and red colours are conductive. Data source for magnetotellurics data: Thiel *et al.* (2018).

high Th/Nb low $\varepsilon_{Nd(t)}$ samples (Skirrow *et al.* 2018). While low Th/Nb ratios (<0.25) are a feature unique to the intrusive phases, Figure 10 shows a large proportion of intrusive rocks have Th/Nb ratios >0.3. Indistinguishable trace element and REE patterns and similarly variable $\varepsilon_{Nd(t)}$ values in high Th/Nb extrusive and intrusive suites ($\varepsilon_{Nd(t)}$ =-7.0 to 2.5 and $\varepsilon_{Nd(t)}$ =-5.5 to 1.9 respectively; Fig. 11) suggests derivation from a similar or the same mantle source, i.e. metasomatised SCLM. The intrusive rocks with low Th/Nb ratios (≤0.25) are predominantly from the central Gawler Craton with $\varepsilon_{Nd(t)}$ values between -1.3 and 1.1 and have geochemical signatures consistent with relatively uncontaminated mafic melts of an enriched MORB mantle source.

The above compositional differences, that is compositional diversity in intrusive rocks not observed in volcanic rocks, is similar to the Permian Emeishan large igneous province, southwest China (Zhou *et al.* 2006) and mid-Neoproterozoic northern Zhejiang Province, South China (Li *et al.* 2008)). A feature common to large igneous provinces such as these are variable mantle sources and mantle plume-lithosphere interaction (Zhou *et al.* 2006, Li *et al.* 2008, Xu *et al.* 2017). In the GRV-HS SLIP, the role of an upwelling mantle plume may have been twofold: 1) involvement in the generation of the low Th/Nb intrusions of the Hiltaba Suite; and 2) providing sufficient heat to invoke substantial melting of the lithospheric mantle to produce the GRV basalts and high Th/Nb intrusions of the Hiltaba Suite.

SCLM heterogeneity and geochemical mapping

The composition and structure of the lithospheric mantle can become complex and heterogeneous as a result of multiple fluid (metasomatic) events affecting domains within the lithospheric mantle (O'reilly and Griffin 2013). Our results of geochemical modelling suggests samples of the Hiltaba Suite may be derived from an SCLM mantle source or domain that was isotopically and geochemically heterogeneous. Such small scale heterogeneities (i.e. enriched domains) in the mantle may allow for selective melting processes, whereby the more enriched portions melt preferentially (Zindler and Hart 1986). Mantle beneath the Gawler Craton contains multiple bodies, and perhaps large volumes of enriched mantle sampled by mafic rocks with varying geochemical and isotopic compositions (at the small scale). At the scale of the mantle beneath the Gawler Craton (440,000 km^2), the small scale heterogeneities, as observed between individual plutons, dykes or volcanic packages/ lavas, may appear as a largely homogeneous and metasomatised mantle (e.g. Zindler and Hart (1986).

Presence of extensive metasomatised SCLM beneath the Gawler Craton has been interpreted in seismic tomography and magnetotellurics, manifest by high conductivity and low velocity mantle domains within the middle lithospheric to deep lithospheric mantle (Thiel and Heinson 2013, Skirrow *et al.* 2018). Geochemical compositions of basalts and a large proportion of mafic Hiltaba Suite intrusives are consistent with a metasomatised SCLM source region (e.g. enriched HFSE, LREE, high Th/Nb ratios and variable $\varepsilon_{Nd(t)}$ values) and these samples largely coincide with the low velocity metasomatised SCLM of Skirrow *et al*. (2018). However, sparse distribution of mafic rocks in the GRV-HS SLIP limits the inferences that can be made about the composition of the SCLM beneath the Gawler Craton. Temporal relationships between extrusive and intrusive phases remain unresolved due to absence of field relationships, in both outcrop and drill core, and insufficient high precision geochronological data.

Our new Sm-Nd and geochemical data combined with pre-existing data for mafic intru-

sive phases allow for a review of the mantle domains and compositions proposed by Skirrow *et al*. (2018). Gridded $\varepsilon_{Nd(t)}$ values show more juvenile isotopic compositions in the southwest of the study area, while the northern and eastern portions of the Gawler Craton are largely more evolved (Fig. 12a). The more juvenile isotopic signatures broadly coincide with lower Th/Nb and E-MORB affinities. Distribution of the E-MORB-like rocks occur close to outer margins of the GRV-HS distribution and cross a number of S and P wave velocity gradients and resistive and conductive zones at various depths (Fig. 12b-d). Any correlations are treated cautiously, however, due limitations with combining high density point geochemical data with broad scale geophysical data to make interferences about mantle compositon and distribution.

SLIPs and cryptic crustal growth

A crucial component in the formation of SLIPs is the role of large volumes of mafic magmas underplating and causing partial melting of the crust (Ernst 2014). Mantle plumes impacting on the continental crust add material in the form of gabbroic underplates and mafic dyke swarms and have been attributed to formation of SLIPs. A feature of SLIPs are the paucity of mantle-derived rocks, due to poor exposure or concealment beneath low-density felsic magmas. Abundance of widespread mafic intrusive phases in the Gawler Craton suggests a large amount of unerupted mafic material in the crust. However, as with other SLIPs, a lack of mantle-derived rocks as coherent outcrops and lack of field relationships between mafic rocks complicates assessment of crustal growth during the petrogenesis of the GRV-HS SLIP. While both extrusive and intrusive components of mafic magmatism exist, a large proportion of the mafic magma added to the crust during the 1590 Ma SLIP event has Th/Nb greater than 0.2 and $\varepsilon_{Nd(t)}$ values in the range of 0 to -5 and is interpreted to be derived from a dominantly SCLM source. Such compositions are effectively indistinguishable from those considered to be consistent with Palaeoproterozoic reworking of Neoarchaean crust. Therefore, continental growth occurring during this event would not be detected by methods that are solely reliant on isotopic datasets (e.g. detrital zircons or bulk sediment compositions). Only a small proportion of the 1590 Ma mafic rocks studied here reflect a geochemically and isotopically distinguishable mantle-derived magma with a composition similar to E-MORB and may be representative of the mafic underplate related to a mantle plume. Mixing between a plume head and the lithospheric mantle will also obscure primitive mantle signatures and add to difficulty in distinguishing it from reworking of Neoarchaean crust. This further supports the conclusions of Couzinié *et al.* (2016) that potentially large volumes of crustal and continental growth are 'hidden' from the isotopic record.

CONCLUSIONS

Mafic rocks associated with the ca. 1590 Ma southern Australia SLIP are generally characterised by enrichment in HFSE and LREE, negative Nb-Ta-Ti anomalies, Th/Nb ratios greater than 0.25 and variable Nd isotopic compositions. Enriched geochemical signatures and lack of correlation with crustal proxy elements in the most primitive magmas (high Mg, Cr, Ni and $\varepsilon_{Nd(t)}$) suggest the enrichment is a primary source region characteristic. The mantle source for these magmas is interpreted to be dominantly SCLM with varying magma compositions interpreted to represent a heterogeneous SCLM.

A minor component of mafic rocks are characterised by only mild enrichment in HFSE and REE, absence of Nb-Ti-Ta anomalies, Th/Nb ratios less than 0.2 and have largely more juvenile Nd isotopic compositions and are attributed to an E-MORB type source magma.
Basaltic rocks coeval with the Hiltaba Suite

have geochemical affinity with the enriched intrusive rocks, thus implying a common source region from within the SCLM.

Compositional differences in the mafic rocks of the GRV-HS SLIP suggest multiple mantle sources, inferred by the geochemical compostions of the intrusive phases, and are similar to those observed in other large igneous provinces. The differences in type of intrusions and geochemical affinity suggest a variety of processes were involved in the formation of the SLIP.

Mantle plume-lithosphere interaction is a common feature in SLIPs and other large igneous provinces. An upwelling mantle plume may have been involved in the generation of the E-MORB-like mafic Hiltaba Suite intrusions. Heat provided by such a mantle plume would have allowed substantial melting of the SCLM, resulting in the formation of the GRV basalts and high Th/Nb mafic intrusives of the Hiltaba Suite.

Subduction modified metasomatised SCLM is the most prominent mantle composition and occurs across almost all of the Gawler Craton. Enrichment of the SCLM is considered to be related to metasomatism during earlier subduction events with the isotopic composition of the magmas suggesting it may have been as early as the Neoarchean. Previous subduction events may play a crucial role in formation of SLIPs by producing hydrous lower crust, primed to produce large volume crustal-derived melts related to high thermal input from the underlying mantle.

ACKNOWLEDGEMENTS

This study is a part of Ph.D. project (C. Wade), and was financially supported by Australian Research Council Linkage Project LP160100578, with the support of the Geological Survey of South Australia. David Bruce, University of Adelaide, is thanked for assistance with Sm–Nd isotope analysis. We acknowledge Greg Swain for providing several whole-rock and Sm-Nd isotope analyses from the central Gawler Craton. Jonathan Irvine, Geological Survey of South Australia, is thanked for assistance with gridding Sm-Nd data. We thank Derek Wyman and Roland Maas for their insightful comments and valuable suggestions. We thank Xian-Hua Li for his efficient editorial handling. CW and AR publish with permission of the Director, Geological Survey of South Australia, Department for Energy and Mining, South Australia.

REFERENCES

Agangi, A., Kamenetsky, M. and McPhie, J., 2012. Evolution and emplacement of high fluorine rhyolites in the Mesoproterozoic Gawler silicic large igneous province, South Australia. Precambrian Research, 208-211, 124-144. doi: https://doi.org/10.1016/j.precamres.2012.03.011

Allen, S. R., Simpson, C. J., McPhie, J. and Daly, S. J., 2003. Stratigraphy, distribution and geochemistry of widespread felsic volcanic units in the Mesoproterozoic Gawler Range Volcanics, South Australia. Australian Journal of Earth Sciences, 50, 97-112. doi: http://dx.doi.org/10.1046/j.1440-0952.2003.00980.x

Arndt, N. T., Coltice, N., Helmstaedt, H. and Gregoire, M., 2009. Origin of Archean subcontinental lithospheric mantle: Some petrological constraints. Lithos, 109, 61-71. doi: https://doi.org/10.1016/j.lithos.2008.10.019

Bleeker, W. and Ernst, R., 2006. Short-lived mantle generated magmatic events and their dyke swarms: The key unlocking Earth's paleogeographic record back to 2.6 Ga. In: Hanski, E., Mertanen, J., Rämö, T. and Vuollo, J. (Eds), Dyke Swarms - Time Markers of Crustal Evolution. Taylor and Francis/Balke-

ma, London, 3-26.

Blissett, A. H., Creaser, R. A., Daly, S., Flint, D. J. and Parker, A. J., 1993. Gawler Range Volcanics. In: Drexel, J. F., Preiss, W. V. and Parker, A. J. (Eds), The geology of South Australia. Volume 1, The Precambrian. Geological Survey of South Australia, Bulletin 54, 107-131. Available at: https://sarigbasis.pir.sa.gov.au/WebtopEw/ws/samref/sarig1/image/DDD/BULL054(V1).pdf

Brotodewo, A., Tiddy, C. J., Reid, A., Wade, C. and Conor, C., 2018. Relationships between magmatism and deformation in northern Yorke Peninsula and south-eastern Proterozoic Australia. Australian Journal of Earth Sciences, 65, 619-641. doi: https://doi.org/10.1080/08120099.2018.1470573

Budd, A. R. and Skirrow, R. G., 2007. The Nature and Origin of Gold Deposits of the Tarcoola Goldfield and Implications for the Central Gawler Gold Province, South Australia. Economic Geology, 102, 1541–1563. doi: https://doi.org/10.2113/gsecongeo.102.8.1541

Cai, Y.-C., Fan, H.-R., Santosh, M., Liu, X., Hu, F.-F., Yang, K.-F., Lan, T.-G., Yang, Y.-H. and Liu, Y., 2013. Evolution of the lithospheric mantle beneath the southeastern North China Craton: Constraints from mafic dikes in the Jiaobei terrain. Gondwana Research, 24, 601-621. doi: https://doi.org/10.1016/j.gr.2012.11.013

Callegaro, S., Rapaille, C., Marzoli, A., Bertrand, H., Chiaradia, M., Reisberg, L., Bellieni, G., Martins, L., Madeira, J., Mata, J., Youbi, N., De Min, A., Azevedo, M. R. and Bensalah, M. K., 2014. Enriched mantle source for the Central Atlantic magmatic province: New supporting evidence from southwestern Europe. Lithos, 188, 15-32. doi: https://doi.org/10.1016/j.lithos.2013.10.021

Cheng, T., Nebel, O., Sossi, P. A., Wu, J., Siebel, W., Chen, F. K. and Nebel-Jacobsen, Y. J., 2018. On the Sr-Nd-Pb-Hf isotope code of enriched, Dupal-type sub-continental lithospheric mantle underneath south-western China. Chemical Geology, 489, 46-60. doi: https://doi.org/10.1016/j.chemgeo.2018.05.018

Chesley, J. T. and Ruiz, J., 1998. Crust–mantle interaction in large igneous provinces: Implications from the Re–Os isotope systematics of the Columbia River flood basalts. Earth and Planetary Science Letters, 154, 1-11. doi: https://doi.org/10.1016/S0012-821X(97)00176-3

Condie, K. C. and Shearer, C. K., 2017. Tracking the evolution of mantle sources with incompatible element ratios in stagnant-lid and plate-tectonic planets. Geochimica et Cosmochimica Acta, 213, 47-62. doi: https://doi.org/10.1016/j.gca.2017.06.034

Cousens, B. L., Aspler, L. B., Chiarenzelli, J. R., Donaldson, J. A., Sandeman, H., Peterson, T. D. and LeCheminant, A. N., 2001. Enriched Archean lithospheric mantle beneath western Churchill Province tapped during Paleoproterozoic orogenesis. Geology, 29, 827-830. doi: https://doi.org/10.1130/0091-7613(2001)029<0827:EALMBW>2.0.CO;2

Couzinié, S., Laurent, O., Moyen, J.-F., Zeh, A., Bouilhol, P. and Villaros, A., 2016. Post-collisional magmatism: Crustal growth not identified by zircon Hf–O isotopes. Earth and Planetary Science Letters, 456, 182-195. doi: https://doi.org/10.1016/j.epsl.2016.09.033

Creaser, R. A., 1995. Neodymium isotopic constraints for the origin of Mesoproterozoic felsic magmatism, Gawler Craton, South Australia. Canadian Journal of Earth Sciences, 32, 460-471. doi: https://doi.org/10.1139/e95-

039

Curtis, S. and Thiel, S., 2019. Identifying lithospheric boundaries using magnetotellurics and Nd isotope geochemistry: An example from the Gawler Craton, Australia. Precambrian Research, 320, 403-423. doi: https://doi.org/10.1016/j.precamres.2018.11.013

Curtis, S., Wade, C. and Reid, A., 2018. Sedimentary basin formation associated with a silicic large igneous province: stratigraphy and provenance of the Mesoproterozoic Roopena Basin, Gawler Range Volcanics. Australian Journal of Earth Sciences, 65, 447–463. doi: https://doi.org/10.1080/08120099.2018.1460398

Davaille, A., Le Bars, M. and Carbonne, C., 2003. Thermal convection in a heterogeneous mantle. Comptes Rendus Geoscience, 335, 141-156. doi: https://doi.org/10.1016/S1631-0713(03)00003-8

Ernst, R. E., 2014. Large igneous provinces: Cambridge University Press, Cambridge, UK. https://doi.org/10.1017/CBO9781139025300

Ernst, R. E. and Buchan, K. L., 2001. Large mafic magmatic events through time and links to mantle-plume heads. In: Ernst, R. E. and K.L., B. (Eds), Mantle Plumes: Their Identification Through Time. Geological Society of America, Special Paper 352, 483-575. https://doi.org/10.1130/0-8137-2352-3.483

Fanning, C. M., Reid, A. and Teale, G. S., 2007. A geochronological framework for the Gawler Craton, South Australia: South Australia. Geological Survey, Bulletin 55, Available at: https://sarigbasis.pir.sa.gov.au/WebtopEw/ws/samref/sarig1/image/DDD/BULL055.pdf

Ferris, G. M. and Schwarz, M. P., 2003. Proterozoic gold province of the Central Gawler Craton. Minerals and Energy South Australia Journal, 30, 4-12. doi: Available at: https://sarigbasis.pir.sa.gov.au/WebtopEw/ws/samref/sarig1/image/DDD/MESAJ030004-012.pdf

Fraser, G. L., McAvaney, S., Neumann, N., Szpunar, M. and Reid, A., 2010. Discovery of early Mesoarchean crust in the eastern Gawler Craton, South Australia. Precambrian Research, 179, 1–21. doi: https://doi.org/10.1016/j.precamres.2010.02.008

Fraser, G. L., Reid, A. J. and Stern, R. J., 2012. Timing of deformation and exhumation across the Karari Shear Zone, north-western Gawler Craton, South Australia. Australian Journal of Earth Sciences, 59, 547–570. doi: https://doi.org/10.1080/08120099.2012.678586

Fricke, C., 2005. Source and origin of the Lower Gawler Range Volcanics (GRV), South Australia: geochemical constraints from mafic magmas. Monash University, Hons. thesis (unpublished).

Giles, C. W., 1988. Petrogenesis of the Proterozoic Gawler Range volcanics, South Australia. Precambrian Research, 40-41, 407-427. doi: https://doi.org/10.1016/0301-9268(88)90078-2

Green, D. H. and Falloon, T. J., 2015. Mantle-derived magmas: intraplate, hotspots and mid-ocean ridges. Science Bulletin, 60, 1873-1900. doi: https://doi.org/10.1007/s11434-015-0920-y

Griffin, W., O'Reilly, S. Y., Afonso, J. C. and Begg, G. C., 2009. The Composition and Evolution of Lithospheric Mantle: a Re-evaluation and its Tectonic Implications. Journal of Petrology, 50, 1185-1204. doi: https://doi.org/10.1093/petrology/egn033

Griffin, W. L., O'Reilly, S. Y., Abe, N., Aulbach, S., Davies, R. M., Pearson, N. J., Doyle, B. J. and Kivi, K., 2003. The origin and evolution of Archean lithospheric mantle. Precambrian Re-

search, 127, 19-41. doi: https://doi.org/10.1016/S0301-9268(03)00180-3

Halama, R., Marks, M., Brügmann, G., Siebel, W., Wenzel, T. and Markl, G., 2004. Crustal contamination of mafic magmas: evidence from a petrological, geochemical and Sr–Nd–Os–O isotopic study of the Proterozoic Isortoq dike swarm, South Greenland. Lithos, 74, 199-232. doi: https://doi.org/10.1016/j.lithos.2004.03.004

Hand, M., Reid, A., Szpunar, M., Direen, N. G., Wade, B., Payne, J. and Barovich, K., 2008. Crustal architecture during the early Mesoproterozoic Hiltaba-related mineralisation event: are the Gawler Range Volcanics a foreland basin fill? MESA Journal, 51, 19-24. Available at: https://sarigbasis.pir.sa.gov.au/WebtopEw/ws/samref/sarig1/image/DDD/MESAJ051019-024.pdf

Hou, B., Keeling, J., Reid, A. J., Warland, I., Belousova, E., Frakes, L., Hocking, R. and Fairclough, M., 2011. Heavy mineral sands in the Eucla Basin, Southern Australia: deposition and province-scale prospectivity. Economic Geology, 106, 687-712. doi:

Howard, K. E., Hand, M., Barovich, K. M., Payne, J. L. and Belousova, E. A., 2011. U-Pb, Lu-Hf and Sm-Nd isotopic constraints on provenance and depositional timing of metasedimentary rocks in the western Gawler Craton: Implications for Proterozoic reconstruction models. Precambrian Research, 184, 43–62. doi: https://doi.org/10.1016/j.precamres.2010.10.002

Huang, Q., Kamenetsky, V. S., Ehrig, K., McPhie, J., Kamenetsky, M., Cross, K., Meffre, S., Agangi, A., Chambefort, I., Direen, N. G., Maas, R. and Apukhtina, O., 2016. Olivine-phyric basalt in the Mesoproterozoic Gawler silicic large igneous province, South Australia: Examples at the Olympic Dam Iron Oxide Cu–U–Au–Ag deposit and other localities. Precambrian Research, 281, 185-199. doi: https://doi.org/10.1016/j.precamres.2016.05.019

Huppert, H. E., Stephen, R. and Sparks, J., 1985. Cooling and contamination of mafic and ultramafic magmas during ascent through continental crust. Earth and Planetary Science Letters, 74, 371-386. doi: https://doi.org/10.1016/S0012-821X(85)80009-1

Jagodzinski, E. A., Reid, A., Crowley, J., McAvaney, S. and Wade, C., 2016. Precise zircon U–Pb dating of a Mesoproterozoic silicic large igneous province: The Gawler Range Volcanics and Benagerie Volcanic Suite, South Australia. Hornsby, NSW: Geological Society of Australia. Geological Society of Australia Abstracts, No. 118.

Jagodzinski, E. A., Reid, A. J., Chalmers, N. C., Swain, G., Frew, R. A. and Foudoulis, C., 2007. Compilation of SHRIMP U-Pb geochronological data for the Gawler Craton, South Australia, 2007. South Australia. Department of Primary Industries and Resources, Report Book 2007/21, pp. 93. Available at: https://sarigbasis.pir.sa.gov.au/WebtopEw/ws/samref/sarig1/image/DDD/RB200700021.pdf

Jahn, B.-m., Wu, F., Lo, C.-H. and Tsai, C.-H., 1999. Crust–mantle interaction induced by deep subduction of the continental crust: geochemical and Sr–Nd isotopic evidence from post-collisional mafic–ultramafic intrusions of the northern Dabie complex, central China. Chemical Geology, 157, 119-146. doi: https://doi.org/10.1016/S0009-2541(98)00197-1

Johnson, J. P. and McCulloch, M. T., 1995. Sources of mineralising fluids for the Olympic Dam Deposit (South Australia); Sm-Nd isotopic constraints.

Chemical Geology, 121, 177-199. doi: https://doi.org/10.1016/0009-2541(94)00125-R

Kelemen, P. B., Shimizu, N. and Dunn, T., 1993. Relative depletion of niobium in some arc magmas and the continental crust: partitioning of K, Nb, La and Ce during melt/rock reaction in the upper mantle. Earth and Planetary Science Letters, 120, 111-134. doi: https://doi.org/10.1016/0012-821X(93)90234-Z

Kempton, P. D., Fitton, J. G., Hawkesworth, C. J. and Ormerod, D. S., 1991. Isotopic and trace element constraints on the composition and evolution of the lithosphere beneath the southwestern United States. Journal of Geophysical Research: Solid Earth, 96, 13713-13735. doi: https://doi.org/10.1029/91JB00373

Li, X.-H., Li, W.-X., Li, Z.-X. and Liu, Y., 2008. 850–790 Ma bimodal volcanic and intrusive rocks in northern Zhejiang, South China: A major episode of continental rift magmatism during the breakup of Rodinia. Lithos, 102, 341-357. doi: https://doi.org/10.1016/j.lithos.2007.04.007

Morrissey, L. J., Barovich, K. M., Hand, M., Howard, K. E. and Payne, J. L., 2019. Magmatism and metamorphism at ca. 1.45 Ga in the northern Gawler Craton: The Australian record of rifting within Nuna (Columbia). Geoscience Frontiers, 10, 175-194. doi: https://doi.org/10.1016/j.gsf.2018.07.006

Nicolson, B. E., Anderson, J. A. and Cross, K. C., 2017. Menninnie Dam Pb–Zn–Ag and Paris Ag–Pb deposits. In: Phillips, N. (Eds), Australian ore deposits. Australasian Institute of Mining and Metallurgy, Carlton, Victoria, 629-630.

O'Reilly, S. Y. and Griffin, W. L., 2013. Mantle Metasomatism. In: Harlov, D. and Austrheim, H. (Eds), Metasomatism and the Chemical Transformation of Rock: The Role of Fluids in Terrestrial and Extraterrestrial Processes. Springer Berlin Heidelberg, 471-533. https://doi.org/10.1007/978-3-642-28394-9_12

O'Reilly, S. Y. and Zhang, M., 1995. Geochemical characteristics of lava-field basalts from eastern Australia and inferred sources: Connections with the subcontinental lithospheric mantle? Contributions to Mineralogy and Petrology, 121, 148. doi: https://doi.org/10.1007/s004100050096

Pankhurst, M. J., Schaefer, B. F., Turner, S. P., Argles, T. and Wade, C. E., 2013. The source of A-type magmas in two contrasting settings: U–Pb, Lu–Hf and Re–Os isotopic constraints. Chemical Geology, 351, 175-194. doi: https://doi.org/10.1016/j.chemgeo.2013.05.010

Payne, J., Barovich, K. and Hand, M., 2006. Provenance of metasedimentary rocks in the northern Gawler Craton, Australia: Implications for Palaeoproterozoic reconstructions. Precambrian Research, 148, 275-291. doi: https://doi.org/10.1016/j.precamres.2006.05.002

Pearce, J. A., 2008. Geochemical fingerprinting of oceanic basalts with applications to ophiolite classification and the search for Archean oceanic crust. Lithos, 100, 14-48. doi: https://doi.org/10.1016/j.lithos.2007.06.016

Pearce, J. A., Ernst, R. E. and Peate, D. W., 2015. A Geochemical Proxy Approach to LIP Forensics. Abstracts - Geological Association of Canada 38, doi: https://doi.org/10.1130/abs/2017AM-301471

Peck, D. C. and Huminicki, M. A. E., 2016. Value of mineral deposits associated with mafic and ultramafic magmatism: Implications for exploration strategies. Ore Geology Reviews, 72, 269-298. doi: https://doi.org/10.1016/j.oregeorev.2015.06.004

Prouteau, G., Scaillet, B., Pichavant, M. and

Maury, R., 2001. Evidence for mantle metasomatism by hydrous silicic melts derived from subducted oceanic crust. Nature, 410, 197-200. doi: https://doi.org/10.1038/35065583

Reid, A., Hand, M., Jagodzinski, E., Kelsey, D. and Pearson, N. J., 2008. Palaeoproterozoic orogenesis within the southeastern Gawler Craton, South Australia Australian Journal of Earth Sciences, 55, 449-471. doi: https://doi.org/10.1080/08120090801888594

Reid, A. J. and Payne, J. L., 2017. Magmatic zircon Lu–Hf isotopic record of juvenile addition and crustal reworking in the Gawler Craton, Australia. Lithos, 292-293, 294-306. doi: https://doi.org/10.1016/j.lithos.2017.08.010

Rogers, C., Kamo, S. L., Söderlund, U., Hamilton, M. A., Ernst, R. E., Cousens, B., Harlan, S. S., Wade, C. E. and Thorkelson, D. J., 2018. Geochemistry and U-Pb geochronology of 1590 and 1550 Ma mafic dyke swarms of western Laurentia: Mantle plume magmatism shared with Australia. Lithos, 314-315, 216-235. doi: https://doi.org/10.1016/j.lithos.2018.06.002

Sharkov, E., Bogina, M. and Chistyakov, A., 2017. Magmatic systems of large continental igneous provinces. Geoscience Frontiers, 8, 621-640. doi: https://doi.org/10.1016/j.gsf.2016.03.006

Skirrow, R., van der Wielen, S. E., Champion, D. C., Czarnota, K. and Thiel, S., 2018. Lithospheric artchitecture and mantle metasomatism linked to iron-oxide Cu-Au ore formation: Multidiciplinary evidence from the Olympic Dam region, South Australia. Geochemistry, Geophysics, Geosystems, 19, doi: https://doi.org/10.1029/2018GC007561

Skirrow, R. G., Bastrakov, E., Barovich, K., Fraser, G., Fanning, C. M., Creaser, R. and Davidson, G., 2007. Timing of Iron Oxide Cu-Au-(U) Hydrothermal Activity and Nd Isotope Constraints on Metal Sources in the Gawler Craton, South Australia. Economic Geology, 102, 1441-1470. doi: https://doi.org/10.2113/gsecongeo.102.8.1441

Stewart, K., 1994. High temperature felsic volcanism and the role of mantle magmas in Proterozoic crustal growth : the Gawler Range volcanic province. University of Adelaide, PhD thesis (unpublished).

Stewart, K. P. and Foden, J., 2003. Mesoproterozoic granites of South Australia. South Australia. Department of Primary Industries and Resources. Report Book, 2003/15, pp. 142. Available at: https://sarigbasis.pir.sa.gov.au/WebtopEw/ws/samref/sarig1/image/DDD/RB200300015.pdf

Swain, G., Barovich, K., Hand, M., Ferris, G. and Schwarz, M., 2008. Petrogenesis of the St Peter Suite, southern Australia: arc magmatism and Proterozoic crustal growth of the South Australian Craton. Precambrian Research, 166, 283-296. doi: https://doi.org/10.1016/j.precamres.2007.07.028

Swain, G., Woodhouse, A., Hand, M., Barovich, K., Schwarz, M. and Fanning, C. M., 2005. Provenance and tectonic development of the late Archaean Gawler Craton, Australia; U-Pb zircon, geochemical and Sm-Nd isotopic implications. Precambrian Research, 141, 106-136. doi: https://doi.org/10.1016/j.precamres.2005.08.004

Szpunar, M., Hand, M., Barovich, K., Jagodzinski, E. and Belousova, E., 2011. Isotopic and geochemical constraints on the Paleoproterozoic Hutchison Group, southern Australia: Implications for Paleoproterozoic continental reconstructions. Precambrian Research, 187, 99-126. doi: https://doi.org/10.1016/j.precamres.2011.02.006

Tang, Y.-J., Zhang, H.-F., Ying, J.-F., Su, B.-

X., Chu, Z.-Y., Xiao, Y. and Zhao, X.-M., 2013. Highly heterogeneous lithospheric mantle beneath the Central Zone of the North China Craton evolved from Archean mantle through diverse melt refertilization. Gondwana Research, 23, 130-140. doi: https://doi.org/10.1016/j.gr.2012.01.006

Thiel, S. and Heinson, G., 2013. Electrical conductors in Archean mantle—Result of plume interaction? Geophysical Research Letters, 40, 2947–2952. doi: https://doi.org/10.1002/grl.50486

Vassallo, J. J. and Wilson, C. J. L., 2002. Palaeoproterozoic regional-scale non-coaxial deformation; an example from eastern Eyre Peninsula, South Australia. Journal of Structural Geology, 24, 1-24. doi: https://doi.org/10.1016/S0191-8141(01)00043-8

Wade, C. E., 2019. Original laboratory geochemical data for mafic Hiltaba Suite (including analysis of standards). Mendeley Data, doi:

Wade, C. E., Reid, A., Wingate, M. T. D., Jagodzinski, E. A. and Barovich, K., 2012. Geochemistry and geochronology of the c. 1585 Ma Benagerie Volcanic Suite, southern Australia: relationship to the Gawler Range Volcanics and implications for the petrogenesis of a Mesoproterozoic silicic large igneous province Precambrian Research, 206–207, 17–35. doi: https://doi.org/10.1016/j.precamres.2012.02.020

Wurst, A. T., 1994. Analyses of late stage, Mesoproterozoic, syn- and post-tectonic, magmatic events in the Moonta Subdomain: implications for Cu-Au mineralisation in the 'Copper Triangle' of South Australia. University of Adelaide, Honours thesis (unpublished).

Xia, L. and Li, X., 2019. Basalt geochemistry as a diagnostic indicator of tectonic setting. Gondwana Research, 65, 43-67. doi: https://doi.org/10.1016/j.gr.2018.08.006

Xu, W., Xu, X. and Zeng, G., 2017. Crustal contamination versus an enriched mantle source for intracontinental mafic rocks: Insights from early Paleozoic mafic rocks of the South China Block. Lithos, 286-287, 388-395. doi: https://doi.org/10.1016/j.lithos.2017.06.023

Zang, W., Fanning, C. M., Purvis, A. C., Raymond, O. L. and Both, R. A., 2007. Early Mesoproterozoic bimodal plutonism in the southeastern Gawler Craton, South Australia. Australian Journal of Earth Sciences, 54, 661-674. doi: https://doi.org/10.1080/08120090701305210

Zhang, S.-B., Zheng, Y.-F., Zhao, Z.-F. and Yuan, H.-L., 2016. The extremely enriched mantle beneath the Yangtze Craton in the Neoproterozoic: Constraints from the Qichun pyroxenite. Precambrian Research, 276, 194-210. doi: https://doi.org/10.1016/j.precamres.2016.02.002

Zhou, M.-F., Zhao, J.-H., Qi, L., Su, W. and Hu, R., 2006. Zircon U-Pb geochronology and elemental and Sr–Nd isotope geochemistry of Permian mafic rocks in the Funing area, SW China. Contributions to Mineralogy and Petrology, 151, 1-19. doi: https://doi.org/10.1007/s00410-005-0030-y

Zindler, A. and Hart, S., 1986. Chemical Geodynamics. Annual Review of Earth and Planetary Sciences, 14, 493-571. doi: https://doi.org/10.1146/annurev.ea.14.050186.002425

Chapter 3

This chapter is written for submission to Lithos as:
Wade, C., Payne, J., Barovich, K., and Reid, A. Subcontinental lithospheric mantle contribution to granites in a silicic-dominated large igneous province: Geochemistry and Nd isotopic constraints

Statement of Authorship

Title of Paper	Subcontinental lithospheric mantle contribution to granites in a silicic-dominated large igneous province: Geochemistry and Nd isotopic constraints
Publication Status	☐ Published ☐ Accepted for Publication ☐ Submitted for Publication ☑ Unpublished and Unsubmitted work written in manuscript style
Publication Details	Wade, C., Payne, J., Barovich, K., and Reid, A. Subcontinental lithospheric mantle contribution to granites in a silicic-dominated large igneous province: Geochemistry and Nd isotopic constraints

Principal Author

Name of Principal Author (Candidate)	Claire Wade		
Contribution to the Paper	Fieldwork, sample collection and drill core inspections Data collection, Data processing, Data curation Investigation, Conceptualisation, Visualisation, Methodology, Formal Analysis, Validation Writing original draft, editing and review		
Overall percentage (%)	70%		
Certification:	This paper reports on original research I conducted during the period of my Higher Degree by Research candidature and is not subject to any obligations or contractual agreements with a third party that would constrain its inclusion in this thesis. I am the primary author of this paper.		
Signature		Date	21/11/2020

Co-Author Contributions

By signing the Statement of Authorship, each author certifies that:

i. the candidate's stated contribution to the publication is accurate (as detailed above);

ii. permission is granted for the candidate in include the publication in the thesis; and

iii. the sum of all co-author contributions is equal to 100% less the candidate's stated contribution.

Name of Co-Author	Justin Payne		
Contribution to the Paper	Investigation, Conceptualisation, Visualisation, Methodology, Validation Writing, editing and review Supervision Fieldwork Funding acquisition		
Signature		Date	29/11/2020

Name of Co-Author	Karin Barovich		
Contribution to the Paper	Conceptualisation, Investigation, Visualisation Methodology, Formal analysis, Validation Supervision Editing and review		
Signature		Date	25/11/2020

Name of Co-Author	Anthony Reid		
Contribution to the Paper	Fieldwork Investigation, Validation Supervision Editing and review		
Signature		Date	25/11/2020

ABSTRACT

Mesoproterozoic Hiltaba Suite granitoids form the intrusive component of a silicic-dominated large igneous province, either outcropping or appearing in drillholes across an area of ~378 000 km² in southern Australia. The petrogenesis of the Hiltaba Suite is of particular importance due its proximity and interpreted genetic links to major iron oxide-copper-gold (IOCG) mineral deposits, including Olympic Dam, one of the world's most significant copper, gold, silver and uranium resources. The Hiltaba Suite has high Ga/Al*10000 ratios, and enriched high field strength element (HFSE) and rare earth element (REE) compositions. Felsic magmas of the Hiltaba Suite have trace and RE element patterns similar to their mafic counterparts, suggesting a common source region. The felsic magmas are distinguished from the mafic magmas geochemically by their large negative Ba, Sr, P, Eu and Ti anomalies on primitive mantle normalised trace element diagrams, which can be attributed to plagioclase, apatite and titanite fractionation. The isotopic compositions of Hiltaba Suite granitoids are reflective of their underlying basement rocks but the isotopic origins also extend down to their underlying mantle. Granitoid Nd isotopic compositions are similar to or only slightly more negative than the mafic Hiltaba Suite, suggesting an isotopically similar source region, coupled with crustal contamination. Mixing calculations suggest varying amounts of crustal material were incorporated into mantle-derived magmas to achieve the isotopic compositions in the granitic magmas. In the western Gawler Craton 4–15% crust is calcualted, moderate amounts of crustal assimilation (13–44%) were calculated for more centrally located plutons and plutons from the eastern Gawler Craton show the highest amounts of crustal material, ranging from 15–86% crust.

The petrogenesis of the Hiltaba Suite granitoids was likely a multistage process that involved a mantle plume, mafic underplating, mixing, and assimilation and fractional crystallisation in an intracontinental tectonic setting. The wide diversity of geochemical and isotopic compositions in the Hiltaba Suite granites that formed in the same tectonic setting may be explained by magma batches derived from heterogeneous lithospheric mantle-lower crust underplates and subsequently variably modified by differing degrees of crustal assimilation of heterogeneous crustal reservoirs.

INTRODUCTION

The composition of felsic intrusive rocks provides a pathway to understanding the composition of the continental crust and its lithospheric column. Granitoids can have a wide range of sources: from purely mantle-derived (asthenosphere or lithosphere) by the fractional crystallisation of a basaltic source magma; to purely crustal-derived (partial melting of the lower to upper crust); or a mixed origin of crust and mantle e.g. assimilation and fractional crystallisation (AFC) or magma, assimilation, segregation and homogenisation (MASH) processes (Pearce 1996, Barbarin 1999, Yang *et al.* 2004, Frost and Frost 2010). Thus, each granitic pluton possesses a unique signature which preserves a reflection of the history of the deeper levels of the crust and/or mantle at a particular location (e.g. Vielzeuf *et al.* 1990, Pearce 1996, Patiño Douce 1999). Where large amounts of crustal melting occur, usually in large igneous provinces (LIPs), a large thermal supply is required, and hence mantle plumes are often invoked as the driving mechanism for crustal melting. Plumbing systems of LIPs related to mantle plumes can be quite complex, influenced by the geometry, thickness and composition of lithospheric mantle on which they impinge (Ernst *et al.* 2019). Common features in LIPs include large volume magmas, high magmatic temperatures, bimodal compositions and spatial variation of the central volcanic province at the plume centre with intrusive magmatism

distal (Ernst *et al.* 2019). Variations in lithospheric thickness will also play a role in the distribution of extrusive vs intrusive magmas, as well as distribution of felsic vs mafic magmas (Ernst *et al.* 2019).

In southern Australia, a Mesoproterozoic silicic-dominated large igneous province (LIP) in the Gawler Craton and Curnamona Province contains ~ 110 000 km^3 of erupted volcanic rocks (Allen *et al.* 2003, McPhie *et al.* 2008, Pankhurst *et al.* 2011, Wade *et al.* 2012). Approximately 80 granitic plutons representing ~70 000 km^3 of unerupted magma over an area of ~378 000 km^2 in the Gawler Craton are also considered part of the LIP. The intrusive phases of the LIP in the Gawler Craton are collectively referred to as the Hiltaba Suite (Flint *et al.* 1993). The magmatic evolution and balance of mantle and crustal contributions to this Mesoproterozoic LIP is of particular importance because it hosts and is temporally coincident to the Olympic Dam deposit, one of the world's most significant copper, gold, silver and uranium resources.

The tectonic setting for the LIP magmatism is contentious. Mafic underplating and/or a mantle plume model in a continental back-arc setting has been invoked by many authors, as they satisfy the volume of magma produced as well as the high temperatures required for the largely felsic magmatism (Blissett *et al.* 1993, Flint *et al.* 1993, Stewart 1994, Stewart and Foden 2003, Zang *et al.* 2007, Wade *et al.* 2012, Wade *et al.* 2019). Plume models are also proposed to link the Gawler Craton to the Curnamona Province and Mt Isa Inlier (e.g. Betts *et al.* 2007), and western Laurentia (e.g. Rogers *et al.* 2018). More recently, models involving delamination and asthenospheric upwelling in a supra-subduction setting have been proposed for the generation of the Gawler LIP magmatism (e.g. Skirrow *et al.* 2018, Tiddy and Giles 2020). In any model, the age progression and the spatial distribution of mafic–felsic, and intrusive- extrusive magmatism, the largely felsic nature of the magmatism and the geochemical and isotopic attributes of the magmas need to be accounted for.

In this contribution, we present a geochemical model that can account for differing granitoid compositions formed in the same setting. Geochemical variation in the Hiltaba Suite granitoids provides insight into the composition of the lithospheric column and relative contributions of mantle and crustal sources in this Mesoproterozoic LIP. The results suggest while the isotopic compositions of the Hiltaba Suite granitoids reflect the underlying basement/crust in which they intrude, their trace and REE compositions reflect an overarching enriched SCLM source region. The data also suggest similar magmatic processes occurred across the region, regardless of the crustal column that was being partially melted. We propose a mantle plume can satisfy the temporal, spatial and compositional variation of the felsic intrusives associated with this LIP.

PRE-LIP BASEMENT GEOLOGY

Surficial basement units to the ca. 1590 Ma magmatic rocks range from well-exposed outcrops in the southern Gawler Craton, to partially covered or sparsely outcropping crystalline and metasedimentary units in the eastern, western and northern Gawler Craton (Fig. 1). Mesoarchean and Neoarchean granitic and volcanosedimentary units are preserved in the core of the craton and overlain by extensive Palaeoproterozoic metasedimentary and igneous packages (Fig. 2).

Mesoarchean granite and granite gneiss (ca. 3150 Ma; Fraser *et al.* 2010) is exposed in the southeast of the craton but inferred to extend westwards into the middle and lower crust (Curtis and Thiel 2019). The Mesoarchean granite is calc-alkaline, derived from partial melting of a tonalite-trondhjemite-granodiorite source (Fraser *et al.* 2010). Volcano-sedimentary sequences rocks ca. 2535–2410 Ma largely occupy the core of the Gawler Craton,

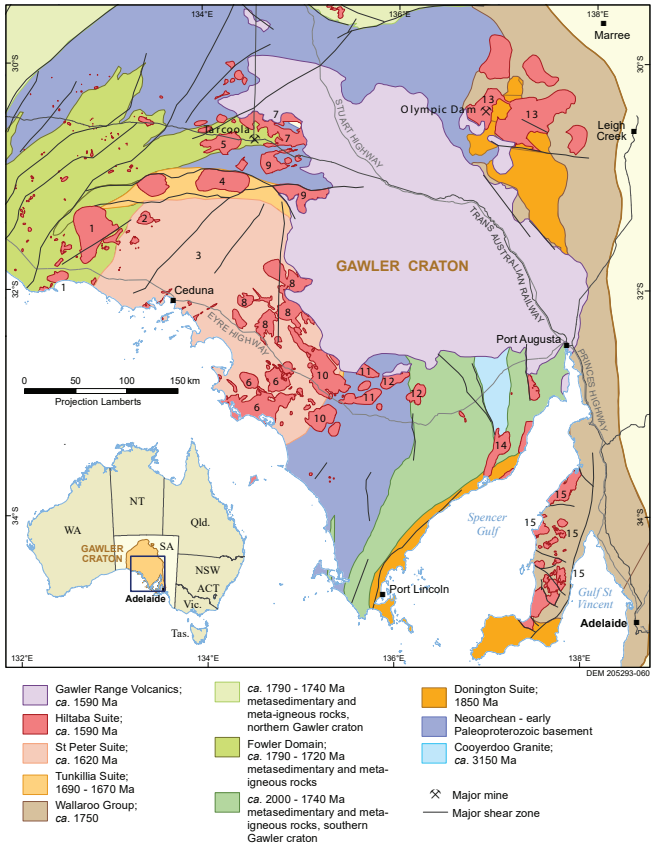

Figure 1: Simplified solid geology and location map of the study area, Gawler Craton. Plutons used in this study are grouped based on similar host rocks and proximity. Numbers correspond to the groups listed in Table 2.

now only exposed in the south as felsic volcanic and gneissic units and in the north as ultramafic and felsic volcanic sequences and gneisses. The ca. 2535–2410 Ma package is most likely part of a formerly contiguous basin system that has been dismembered by Proterozoic tectonism (Swain *et al.* 2005, Halpin and Reid 2016). Komatiitic rocks (2520 Ma) are linked to Neoarchean mantle plume activity (Hoatson *et al.* 2005), and felsic volcanic packages are considered to represent subduction-related magmatism deposited during active basin development in a back-arc or arc-rift setting (Swain et al 2005). The ca. 2470–2410 Ma Sleafordian Orogeny terminated the basin deposition and magmatism (Swain *et al.* 2005, Halpin and Reid 2016).

Prolonged basin formation and crustal growth over the period ca. 2000 to 1730 Ma occurred across the entire Gawler Craton (Payne *et al.* 2006, Fanning *et al.* 2007, Szpunar *et al.* 2011) with remnant packages now exposed in the northwest and eastern portions of the craton. Basin formation was punctuated by the Cornian Orogeny and syn-orogenic magmatism at ca. 1850 Ma (Reid *et al.* 2008) in the eastern Gawler Craton and ultimately terminated by the craton-wide ca. 1730–1690 Ma Kimban Orogeny (Vassallo and Wilson 2002, Hand *et al.* 2007), with associated widespread magmatism and localised sedimentation (Howard *et al.* 2011, Wade and McAvaney 2017). Post-tectonic magmatism (1690–1670 Ma; Payne *et al.* 2010) occurred in the central and western Gawler Craton, characterised by high-K, alkali-calcic and magnesian felsic granitoids. Localised sedimentation and volcanism from the period 1680–1650 Ma is preserved in the southern (ca. 1680 Ma) and

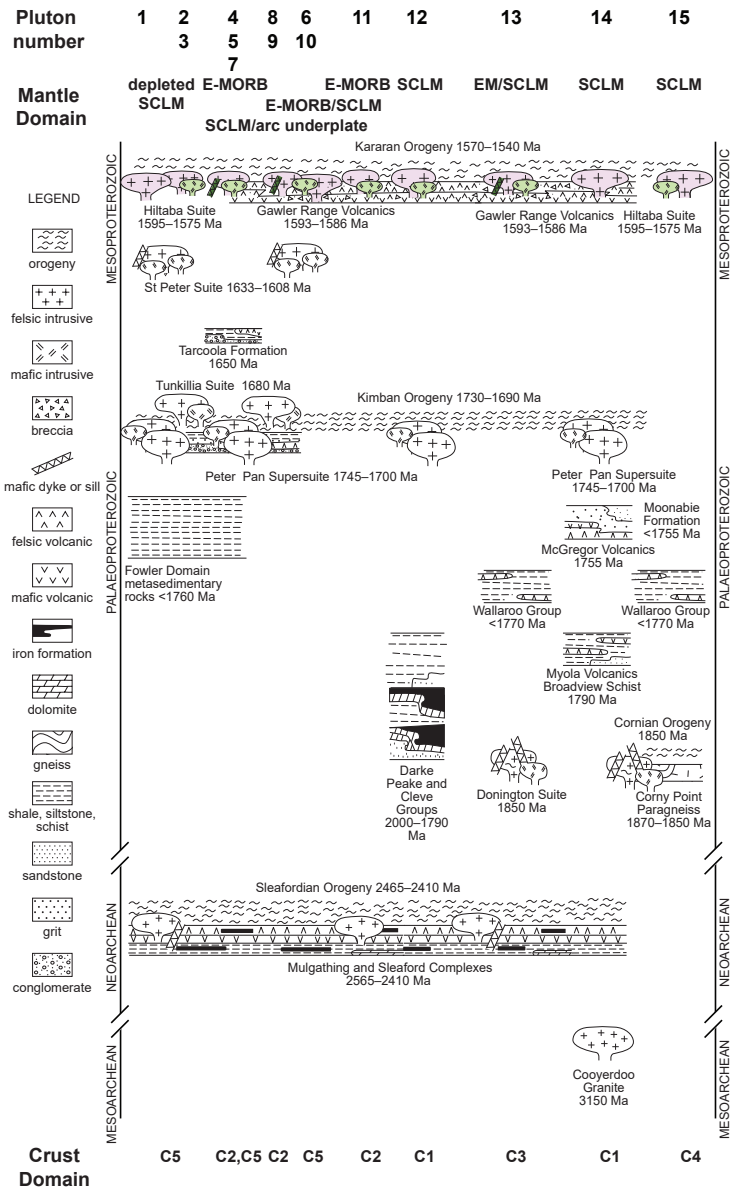

Figure 2: Time space plot for the Gawler Craton indicating the relative position of the pluton groups with their underlying basement rocks.

central Gawler Craton (ca. 1655 Ma; Fanning *et al.* 2007 and references therein).

The youngest basement to the ca. 1590 Ma magmatic rocks include comagmatic ca. 1633–1608 Ma quartz monzonite, granite, granodiorite, and diorite to gabbro of the St Peter Suite in the southwestern Gawler Craton (Swain *et al.* 2008, Reid *et al.* 2019). These magmatic rocks have geochemical signatures consistent with subduction-related settings, and have been variably interpreted as either an oceanic (Swain *et al.* 2008) or continental magmatic arc (Skirrow *et al.* 2018, Reid *et al.* 2019).

THE CA 1590 MA HILTABA SUITE GRANITOIDS

Hiltaba Suite granitoids occur as approximately 80 individual plutons distributed across the Gawler Craton (Fig. 1). Plutons range in size from 10 km to upward of 60 km in breadth

and are most commonly completely buried to partially exposed, and very rarely entirely exposed. Most plutons are elliptical or circular in shape and appear as relatively undeformed, highly magnetic features that appear to disrupt earlier magnetic and structural features on total magnetic imagery (TMI). They intrude the above-described basement units of the Gawler Craton (Fig. 2). Although commonly undeformed, Hiltaba Suite rocks have been affected by syn- to post-magmatic deformation at some localities (Conor 1995, Hand *et al.* 2008, Brotodewo *et al.* 2018).

Magmatism related to intrusive activity is constrained to ca. 1595–1575 Ma (Creaser and Cooper 1993, Creaser and Fanning 1993, Flint 1993, Reid and Dutch 2012, Cherry *et al.* 2018). The suite is commonly referred to as an "A-type" suite (Creaser *et al.* 1991, Budd 2006, Foden *et al.* 2015, Chapman *et al.* 2019), but it contains a number of plutons that are "I-type" in nature (Budd 2006). The "A-type" classification is a function of the high Ga/Al ratios, and rare earth element (REE) and high field strength element (HFSE) contents of the majority of the plutons (Collins *et al.* 1982, Creaser *et al.* 1991, Martin 2006). The "I-type" classification is a function of lower HFSE, Ga/Al ratios and Fe* (or higher Mg contents) in the plutons found in the central and west of the province. An apparent temporal relationship has been suggested by authors such as Budd (2006) and Tiddy and Giles (2020), where "A-type" granitoids in the eastern Gawler Craton are older than "I-type" granitoids in the central and western Gawler Craton. In general, older magmatic ages have been associated with felsic intrusive magmatism in the north east of the craton (e.g. Olympic Dam and Acropolis deposits ca. 1594–1590 Ma; Cherry *et al.* 2018, McPhie *et al.* 2020). Ages obtained by chemical abrasion thermal ionisation mass spectrometry (CA TIMS) geochronology for five granitoid samples indicate younger magmatic ages are recorded in the south east (1585.07 ± 0.83 Ma, 1583.50 ± 0.61 Ma and 1579.89 ± 0.53 Ma), central (1586.49 ± 0.49 Ma) and western Gawler Craton (1579.37 ± 0.73 Ma; Jagodzinski *et al.* in prep., Reid *et al.* in prep). However, the majority of geochronology of the Hiltaba Suite is based upon LA-ICP-MS or SHRIMP microbeam analysis techniques which do not have sufficient external precision to readily identify meaningful spatial trends in the age distribution of intrusions.

Overall, the Hiltaba Suite is granitic in composition, with lesser granodioritic to gabbroic phases. The granitoids are texturally variable, ranging from megacrystic to fine-grained sub-volcanic varieties (Flint *et al.* 1993, Stewart and Foden 2003), commonly composed of K-feldspar, plagioclase, quartz, biotite and hornblende. Granitic plutons range from being lithologically homogeneous to containing several facies of granitic to granodioritic composition, likely representing several phases of intrusive magmatism (Conor 1995, Stewart and Foden 2003, Budd 2006). Pervasive hematite alteration has affected Hiltaba Suite granitoids in the eastern parts of the central Gawler Craton, whereas granitoids in the western and some central areas are largely unaffected by such alteration.

Mafic intrusive rocks are less common in the Hiltaba Suite and are generally poorly exposed in the across most of the Gawler Craton (Budd and Skirrow 2007, Zang *et al.* 2007, Huang *et al.* 2016, Wade *et al.* 2019). Previous work has outlined a series of mantle source compositional domains using the isotopic and geochemical composition of mafic end-members of the Hiltaba Suite and their volcanic equivalents (Skirrow *et al.* 2018, Wade *et al.* 2019). These are outlined in Figure 1- 3, which highlights heterogeneous mantle source material identified as nine mantle types (M1–M9; Appendix Table A1). Crustal isotopic domains are also provided in Figures 2 and 3and are considered to represent the likely isotopic composition of crustal material that can be incorporated into

magmas in a given crustal column (C1–C5; Appendix Table A2 and A3). The areal extent of mantle domains identified by Skirrow *et al.* (2018) and Wade *et al.* (2019), are used as the basis for the grouping and discussion of the felsic Hiltaba Suite rocks (Table 1 and Figure 2). For the purpose of discussing the major, trace and rare earth element compositions, the plutons are assigned to six groups based upon their location in the identified mafic mantle domains which are simplified from the nine mantle types. The majority correspond to the SCLM mantle domain (which includes M5, M7, M8 and M9; Table 2 and Figure 3), the most prominent mantle type identified (see Fig. 11 in Skirrow *et al.* 2018, Wade *et al.* 2019). Other domains include:

- Depleted SCLM (M1), western Gawler Craton, after Skirrow *et al.* (2018)
- E-MORB (M2), central Gawler Craton, after Wade *et al.* (2019)
- E-MORB or SCLM (M3), after Wade *et al.* (2019)
- SCLM or preserved mafic underplate beneath an arc (arc underplate; M4) after Wade *et al.* (2019) and Skirrow

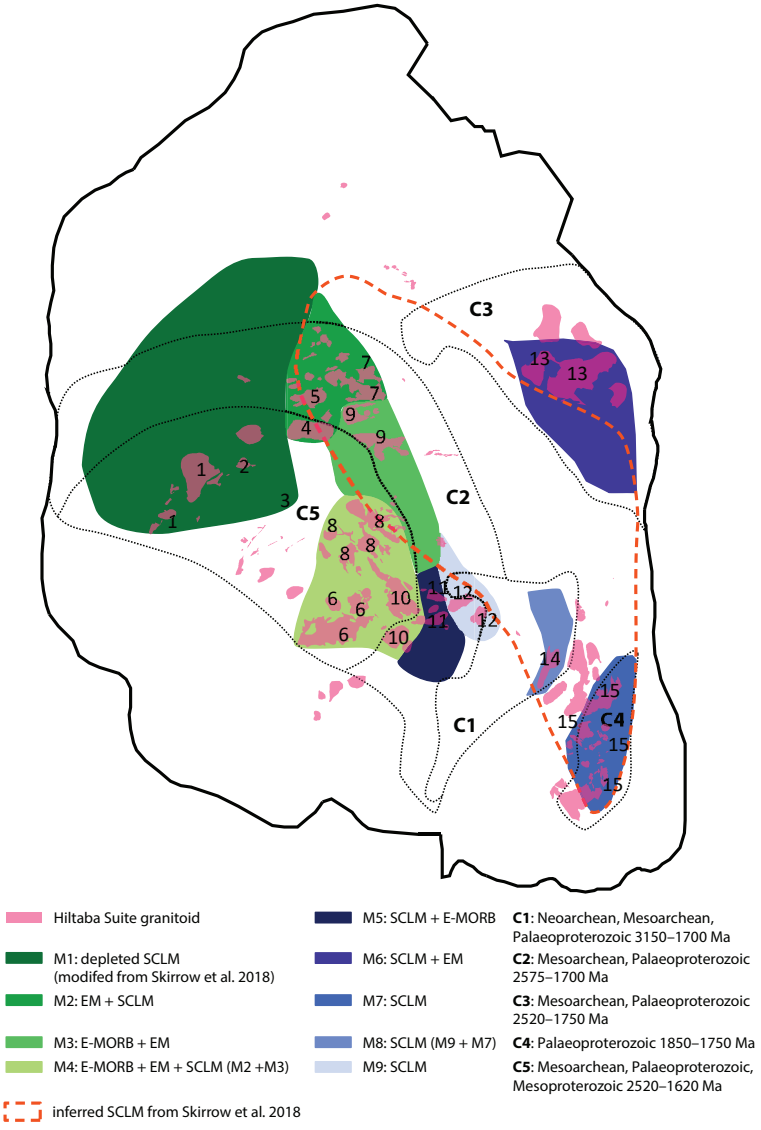

Figure 3: Location and inferred distribution of crustal and mantle domains used as the basis for mixing calculations. Numbers 1–15 correspond to Pluton Group in Table 1.

et al. (2018)

- Enriched mantle (EM) or SCLM (M6), north east Gawler Craton, after Wade *et al.* (2019).

METHODS

Analysed plutons are typical Hiltaba Suite granites considered to be of similar age, intruded during the ca. 1595–1570 Ma magmatic event. Samples with the prefix '1077-' were collected by K. Stewart, University of Adelaide (Stewart and Foden 2003). These samples have been re-analysed for whole rock geochemistry. Samples with the prefix 'SS-' were collected by Creaser (1989) and samples with the prefix '2001363' were collected by Budd (2006).

New samples were prepared and analysed for geochemistry by Bureau Veritas minerals laboratories in Perth (https://www.bureauveritas.com.au/home/about-us/our-business/commodities/exploration-and-mineral-labs). All weathered material was removed before being crushed, split and milled into a fine powder, with a quartz barren wash used between samples. The samples were cast using a 66:34 flux with 4% lithium nitrate added to form a glass bead. Major elements and chlorine were analysed using X-Ray Fluorescence (XRF) spectrometry. Trace elements were determined by laser ablation-inductively coupled plasma-mass spectrometry (LA-ICP-MS) and Au, Pt and Pd were analysed using fire assay ICP-MS. FeO was determined volumetrically and fluorine was determined using specific ion electrode.

Sm-Nd isotope analyses were undertaken at the University of Adelaide as per the method of Wade *et al.* (2019). Samples were loaded on 99.99% Re (standard grade) filaments. Sm and Nd isotopic measurements were collected on an Isotopx Phoenix thermal ionization mass spectrometer (TIMS) in a three-step dynamic peak hopping routine for Nd and a static rou-

Table 1: Hiltaba Suite plutons grouped based on similar host rocks and geographical proximity.

Group	Pluton	Host Rocks	Crust Type	Underlying mantle	Mantle Group	Mantle Group Number	Mantle Type
1	Boree, Mitcherie	7, 12, 14	C5	Depleted SCLM	Depleted SCLM	3	M1
2	Munjeela, Poondinga	14	C5	Depleted SCLM	Depleted SCLM	3	M1
3	Nicholls	14	C5	Depleted SCLM	Depleted SCLM	3	M1
4	Frogs Eyes, Jellabinna	3, 11, 12	C2	SCLM	SCLM	5	M2
5	Kychering, Pinding,	3, 7, 11, 13	C2	SCLM	SCLM	5	M2
6	Tyringa, Parla	14	C5	SCLM/E-MORB	SCLM/EM/E-MORB	8+5	M4
7	Birthday, Gibraltar, Coolading, Ambrosia, Peela, Partridge	3, 7, 11, 13	C2	E-MORB/SCLM	E-MORB, SCLM	5	M2
8	Childara, Kondoolka, Nunyah, Ilkina, Hiltaba, Wallala	12, 14	C5	SCLM/arc underplate	E-MORB/EM	8+5	M4
9	Kokatha, Acoordaby, Bulpara	3, 11, 12	C2	SCLM/E-MORB	E-MORB/EM	8	M3
10	Pheasant, Pordla, Minnipa, Wudina, Scrubby Peak	3, 14	C5	SCLM/E-MORB	E-MORB/EM/SCLM	8+5	M4
11	Waulkinna, Pennas, Corrobinnie	3	C2	SCLM/E-MORB	E-MORB	11	M5
12	Buckleboo, Cunyarie	2, 3, 4, 5	C2	SCLM	SCLM	12	M9
13	Roxby Downs, Andamooka	3, 6, 10	C3	EM/SCLM	EM/SCLM	13	M6
14	Charleston, Roopena	1, 2, 3, 4, 5, 11	C1	SCLM	SCLM	12+15	M8
15	Arthurton, Tickera, Hillside	6, 10	C4	SCLM	SCLM	15	M7

Underlying mantle composition is also listed, inferred from mantle domains/compositions identified by Skirrow *et al*., 2018 and Wade *et al.*, 2019. Average host rocks and mantle domains for each group were used in isotopic mixing calculations. Pluton group number refers to labels on Figure 1. Host Rocks: 1: 3150 Ma granitic gneiss; 2: 2575 Ma metasediments; 3: 2520–2410 Ma metagranite and gneiss; (felsic); 4: 2000 Ma metasediments; 5: 1865 Ma metasediments; 6: 1850 Ma metaigneous (felsic); 7: 1790-1720 Ma metasediments); 8: 1790 Ma volcanics (felsic); 9: 1760 Ma metasedimentary rocks; 10: 1750 Ma metasediments; 11: 1750–1700 Ma igneous (felsic); 12: 1690 Ma igneous (felsic); 13: 1650 Ma igneous (felsic); 14: 1620 Ma igneous (felsic).

tine for Sm. Nd isotope ratios are normalised to $^{146}Nd/^{144}Nd = 0.7219$, using exponential mass fractionation correction. Measured analytical blanks are on the order of 100 pg for Nd and 50 pg for Sm and are insignificant in this study. The mean value of measured $^{143}Nd/^{144}Nd$ ratios for the G2 standard granite material (granite, Rhode Island) is 0.512221 ± 0.000001 (2s, n= 2, within uncertainty of 0.512233 ± 0.00001 (GeoRem Preferred value)). Calculated concentrations for Nd and Sm are 54.3–54.6 ppm and 7.5–7.9 ppm, respectively, compared with the recommended United States Geological Survey values of 55 ± 6 ppm and 7.2 ± 0.7 ppm (https://crustal.usgs.gov/geochemical_reference_standards/granite.html) and GeoRem preferred values of 53.81 ± 0.67 ppm and 7.19 ± 0.1 ppm for Nd and Sm respectively.

RESULTS

Whole-rock geochemical data for 97 new analyses were collected and 145 pre-existing analyses with complete trace and rare earth element analysis were collated from Creaser (1989), Budd (2006), Wurst (1994) and the Geological Survey of South Australia's database SARIG (https://map.sarig.sa.gov.au/). All new whole-rock analyses are provided in Appendix Table A4. Sm-Nd isotope data for 19 analyses are provided in Table 2. Thirty-two previous Sm-Nd isotope analyses are compiled from Wurst (1994), Creaser (1989) and Stewart and Foden (2003).

GEOCHEMISTRY

Whole rock major, trace and rare earth element geochemistry

Approximately 87% of Hiltaba Suite samples are granitic in composition and the remaining 13% include quartz monzonite (8%), monzonite (2%), synenite (2%) and granodiorite (1%). Granites can be found in all mantle domains (Fig 4). Quartz monzonite and monzonite are mostly from the EM/SCLM and SCLM mantle domains (Fig. 4).

Table 2: Sm Nd isotopic composition for Hiltaba Suite samples

Sample	Pluton	Age (t)	Nd (ppm)	Sm (ppm)	$^{143}Nd/^{144}Nd$	2σ	$^{147}Sm/^{144}Nd$	$\varepsilon_{Nd(0)}$	$T_{(DM)}$	$\varepsilon_{Nd\ (t)}$
1077-27*	Pinding	1.59	22.63	7.02	0.512563	0.000002	0.1874	-1.5	3.3	0.4
1077-196	Charleston	1.59	62.90	9.17	0.511148	0.000001	0.0918	-29.1	2.5	-7.7
1077-175	Kondoolka	1.59	61.30	20.09	0.512035	0.000002	0.1464	-11.8	2.5	-1.5
1077-178	Kondoolka	1.59	20.68	3.35	0.511553	0.000002	0.0975	-21.2	2.1	-1.0
1077-229	Kondoolka	1.59	60.90	11.90	0.511867	0.000002	0.1177	-15.0	2.0	1.0
1077-193	Pennas	1.59	12.60	2.30	0.511533	0.000001	0.1116	-21.6	2.4	-4.2
1077-192	Pennas	1.59	12.00	1.91	0.511397	0.000002	0.0957	-24.2	2.3	-3.6
1834104	Poondinga	1.59	81.45	15.77	0.511841	0.000001	0.1177	-15.5	2.1	0.5
1834103	Poondinga	1.59	58.71	12.18	0.511943	0.000002	0.1250	-13.6	2.0	1.0
1834093	Poondinga	1.59	71.65	13.47	0.511818	0.000002	0.1175	-16.0	2.1	0.1
2705391	Arthurton	1.59	125.90	22.60	0.511528	0.000001	0.1085	-21.6	2.3	-3.7
2705398	Arthurton	1.59	89.30	14.59	0.511407	0.000002	0.0988	-24.0	2.3	-4.1
2696081	Birthday	1.59	33.60	6.50	0.511605	0.000001	0.1179	-20.2	2.4	-4.1
2696083	Birthday	1.59	63.80	9.17	0.511288	0.000002	0.0869	-26.3	2.2	-4.0
HDD393-01	Hillside	1.59	54.94	9.65	0.511489	0.000002	0.1060	-22.4	2.3	-4.0
HDD393-02	Hillside	1.59	69.55	12.07	0.511521	0.000002	0.1049	-21.8	2.3	-3.1
HDD396-01	Hillside	1.59	73.01	12.06	0.511504	0.000002	0.1071	-22.1	2.3	-3.9
HDD357-01	Hillside	1.59	79.04	15.55	0.511654	0.000002	0.1190	-19.2	2.4	-3.4
HDD357-03	Hillside	1.59	72.30	12.33	0.511517	0.000002	0.1030	-21.9	2.2	-2.8

Errors on $^{143}Nd/^{144}Nd$ measurements are 2σ (mean) and refer to the last significant figure(s).

Measured εNd values calculated with present-day CHUR $^{143}Nd/^{144}Nd$ and $^{147}Sm/^{144}Nd$ ratios of 0.512638 and 0.1966.

Depleted mantle Nd model ages calculated as in Goldstein et al. (1984).

*reanalysed pre-collected sample from Stewart and Foden 2003.

Harker diagrams illustrate coherent trends in major elements such as Al_2O3, CaO, Na_2O, P_2O_5, TiO_2, and FeO suggesting similar fractionating phases in the magmas. Distinguishable trends between groups are defined in some major elements, such as MgO and CaO contents, where depleted SCLM domain samples and SCLM/arc underplate domain samples and some E-MORB domain samples are clearly distinguished from SCLM domain samples (Fig. 4). In CaO and MgO plots, two trends are defined by samples from the SCLM domain, although less obvious in other elements such as P_2O_5 and FeOt (Fig. 4). Selected trace elements plotted against SiO_2 (Fig. 5) display high concentrations of Zr, Y, Ga and Th that are common to the Hiltaba Suite granitoids. Less variation is discernible in these trace element compositions between the domain groups. Hiltaba Suite samples have high concentrations of high field strength elements such as Zr, Ce, Nb and Y (Zr+Ce+Nb+Y typically >200 ppm), as well as high in Ga/Al/10000 ratios (>2) and high Th/Nb ratios (>0.5; Fig. 6). A subset of samples from the EM/SCLM and SCLM domains have very high Zr+Ce+Y+Nb (>780 ppm) and Ga*Al/10000 ratios <2.5 and define a separate group to the main data set (Fig. 6). Collectively, the EM domain samples have the highest HFSE contents (~420–900 ppm). The E-MORB affiliated domains (E-MORB and E-MORB/SCLM) have relatively high Zr+Ce+Nb+Y contents (~200–780 ppm).

Common features on primitive mantle normalised trace element diagrams include negative Nb-Ta-Ti anomalies, negative Ba, Sr and P anomalies, enriched Th and U signatures and flat heavy rare earth elements (HREEs; Fig. 7).

REE patterns normalised to chondrite are typically light REE (LREE) enriched with relatively flat HREE and variable negative Eu anomalies (Fig. 8). A subset of samples from the E-MORB, SCLM and SCLM/arc underplate domains have steep LREE and MREE depletions and steep HREE enrichments, creating convex shaped patterns (Fig. 8). The MREE-depleted samples are coupled with high $(La/Sm)_{CN}$ ratios (5.03–63.58). The MREE-depleted samples have lower Zr+Ce+Nb+Y abundances (~200 and less) and highly variable Ga*Al/10000 ratios (2.5–3.8) over their narrow range of HFSEs compared with the main data set. Four samples from the SCLM domain with $(Gd/Yb)_{CN} < 0.78$) have low $(La/Sm)_{CN}$ ratios (1.19–2.33).

Sm-Nd isotope data

New Sm-Nd isotope compositions for 18 Hiltaba Suite samples and one re-analysed pre-collected sample are provided in Table 2. Initial $\varepsilon_{Nd(i)}$ values are calculated at 1590 Ma. $^{147}Sm/^{144}Nd$ and $^{143}Nd/^{144}Nd$ ratios for the 19 new analyses are both within the range of pre-existing Hiltaba Suite samples. For samples collected in this study $^{147}Sm/^{144}Nd$ range between 0.0869 and 0.1874 and $^{143}Nd/^{144}Nd$ ratios range between 0.511148 and 0.512563 (Table 2). $\varepsilon_{Nd(i)}$ values for samples from this study range from -7.7 to +1.0 (Table 2). Model ages range from 2.0 to 2.5 Ga, with one model age 3.3 Ga (Table 2).

DISCUSSION

Compositional variation in the Hiltaba Suite

As illustrated in Figure 4, Hiltaba Suite samples are largely granitic in composition and display coherent trends in major elements such as Al_2O_3, CaO, Na_2O, P_2O_5, TiO_2, and FeO, suggesting similar fractionating phases such as K-feldspar, plagioclase, apatite and Ti-Fe phases were involved in magma evolution. Large negative anomalies in Sr, Ba and Eu, P and Ti on primitive mantle normalised trace elements diagrams also indicate fractionation of plagioclase, as well as fractionation of apatite and titanite, respectively. Low Gd/Yb_{CN} ratios in the E-MORB, SCLM and SCLM/arc underplate domains may be attributed to early crystallisation of titanite from the fraction-

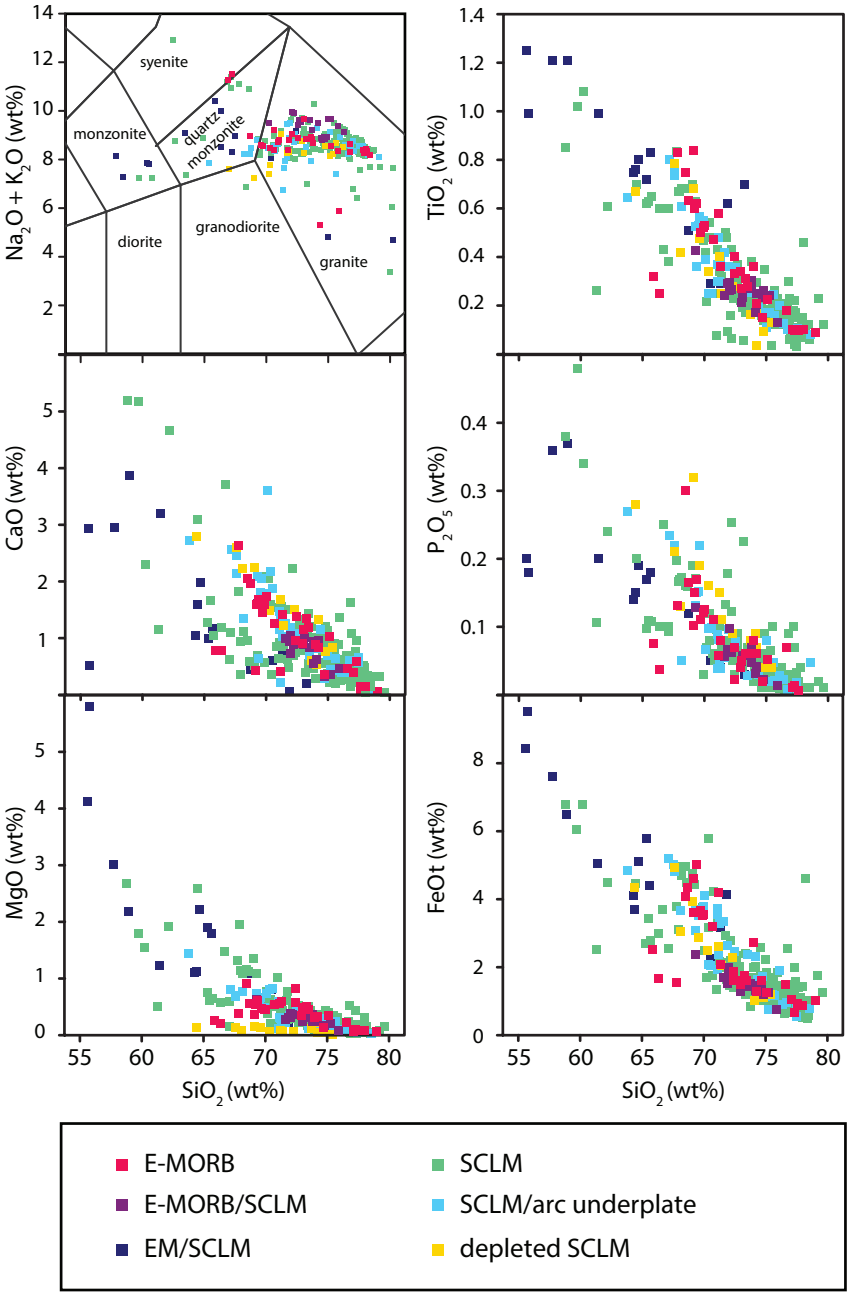

Figure 4: Selected major element variation plots for the Hiltaba Suite granitoids. Granites are grouped based on their underlying mantle domain as depicted on Figure 3.

ation of a more mafic magma, while high La/Sm_{CN} ratios may be attributed to late crystallisation of allanite (e.g. Budd 2006).

Aside from the high La/Sm_{CN} -low Gd/Yb_{CN} samples, there is little variation in the trace and rare earth element abundances of the Hiltaba Suite. An exception to this homogeneity is from the Depleted SCLM domain, with HREE depleted samples (Fig. 8). Compositional variation in the Depleted SCLM domain is not unsurprising, as this domain is largely separate from the prominent SCLM region beneath much of the Gawler Craton and is identified as a highly depleted lithosphere by Skirrow *et al.* (2018). The limited occurrence of mafic rocks in this region limits our understanding of the

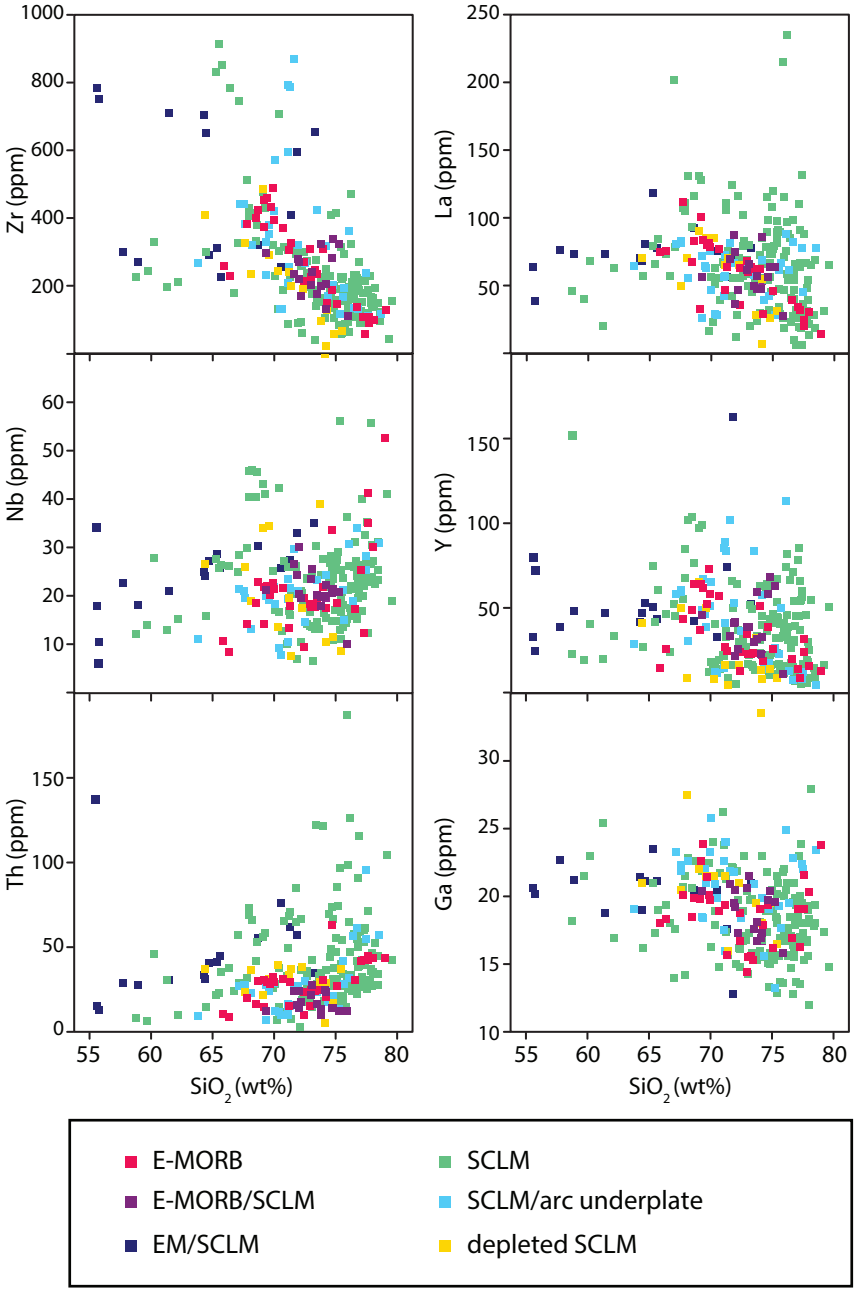

Figure 5: Selected trace element variation in the Hiltaba Suite granitoids, highlighting the high concentrations of high field strength elements such as Zr, Nb, Y and Th.

composition of the underlying mantle domain, but differences in some major and trace elements suggests a compositionally different source region for samples from the Depleted SCLM domain.

$\varepsilon_{Nd(i)}$ values for the felsic Hiltaba Suite are typically -5.2 to -2.1 (Fig. 9; Table 2). Samples from the depleted SCLM, SCLM/arc underplate and E-MORB/SCLM domains have relatively juvenile $\varepsilon_{Nd(i)}$ compositions ($\varepsilon_{Nd(i)}$ = -1.5 to 2.7). These more juvenile compositions are distinct from the majority of the suite (Fig. 9). Samples within the E-MORB/SCLM domain that are isotopically juvenile occur within close proximity to isotopically juvenile mafic

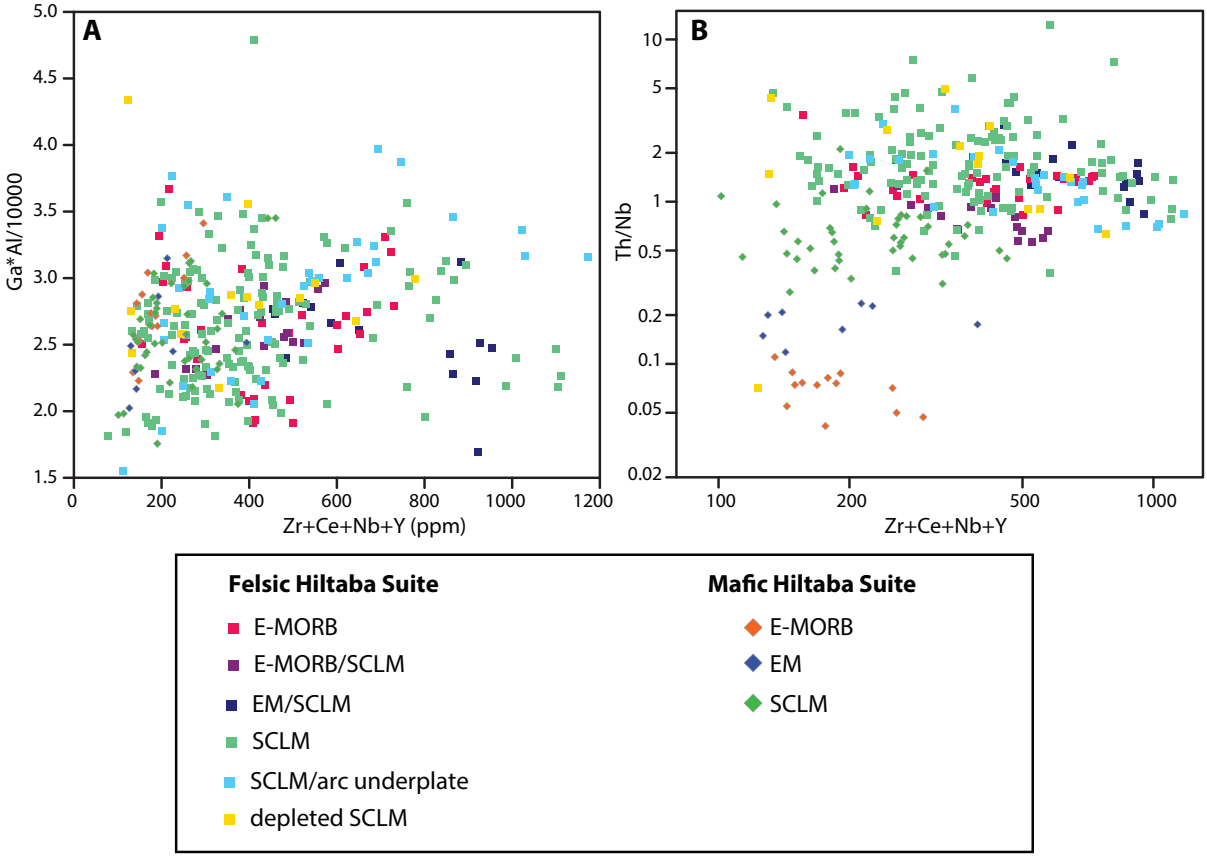

Figure 6: a) Ga/Al vs Zr+Ce+Nb+Y and b) Th/Nb vs Zr+Ce+Nb+Y for the granitic and mafic Hiltaba Suite.

rocks. In comparison, samples within the depleted SCLM and SCLM/arc underplate domains have no known associated mafic rocks and are therefore considered to either indicate the presence of buried mafic end-members and/or isotopically juvenile basement. A group of samples with evolved Nd signatures are from the EM/SCLM and SCLM domains with $\varepsilon_{Nd(i)}$ <-7 which likely reflects crustal contamination by Meso- to Neoarchean crust (e.g. Chapman *et al.* 2019). This will be explored in the following section.

The mafic and felsic connection of the Hiltaba Suite

The trace element and rare earth element compositions of mafic and felsic Hiltaba Suite samples are remarkable in their similarity. Figures 6, 7 and 8 display the overlap between the mafic and felsic Hiltaba Suite, most obvious in the SCLM domain samples. Overlap in Zr+Ce+Nb+Y between mafic and felsic samples (Fig. 6) shows the enriched nature of the source region for both end-members. E-MORB domain felsic samples are more enriched than the mafic samples in the incompatible elements, including Rb, Th, U and K abundances (Fig. 7). The magnitude of P, Ba, Eu and Ti anomalies are greater in the felsic samples. These differences can be attributed to fractionation of apatite, plagioclase and titanite or other Ti-bearing phases in the progression from mafic to felsic magmas.

Excluding the MREE-depleted samples, larger Eu anomalies in the felsic samples, driven by fractionation of plagioclase, are the main difference between REE patterns of the mafic and felsic Hiltaba Suite (Fig. 8). Felsic sam-

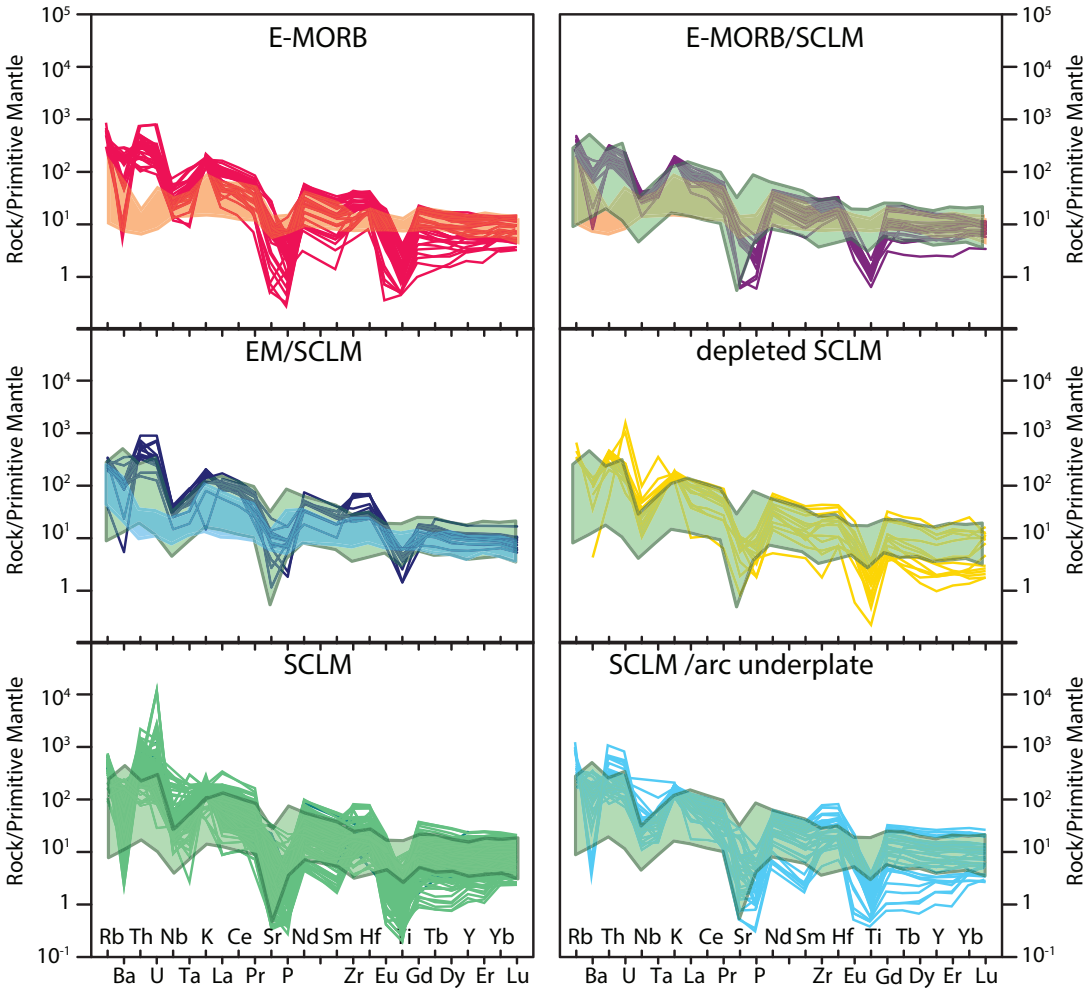

Figure 7: Primitive mantle normalised trace element diagrams for the Hiltaba Suite, divided by underlying mantle group. The shaded area on each plot corresponds to the trace-element pattern for the mafic Hiltaba Suite of each mantle group identified. Normalising values are from Sun and McDonough (1989). Data for mafic Hiltaba Suite is from Wade *et al.* (2019).

ples from the depleted SCLM domain have REE patterns that vary the most from the rest of the felsic Hiltaba Suite, as well as from the mafic samples in that domain. They are marked by lower REE abundances than the remainder of the felsic samples, and generally higher La/Yb ratios than the mafic samples in the depleted SCLM domain. Note that in the SCLM domain, felsic samples have no known proximal mafic rocks. Variation in the REE abundances of this group of felsic and mafic rocks suggests a source that differs to the main component of the Hiltaba Suite.

Many authors consider the mantle source that has provided the HFSE- and REE-enriched signature in the magmatic rocks to be a metasomatised SCLM (e.g. Huang *et al.* 2016, Rogers *et al.* 2018, Skirrow *et al.* 2018, Wade *et al.* 2019). The comagmatic GRV mafic magmas have the same SCLM source as the mafic Hiltaba Suite (Wade *et al.* 2019) and GRV rhyolites and dacites are equally as enriched in HFSE as the Hiltaba Suite granitoids (Fig. 6b).

With the exception of a number of highly negative $\varepsilon_{Nd(i)}$ samples, the isotopic composition of the felsic and mafic Hiltaba Suite also show overlap, regardless of the underlying mantle domain (Fig. 9). In many domains there is a

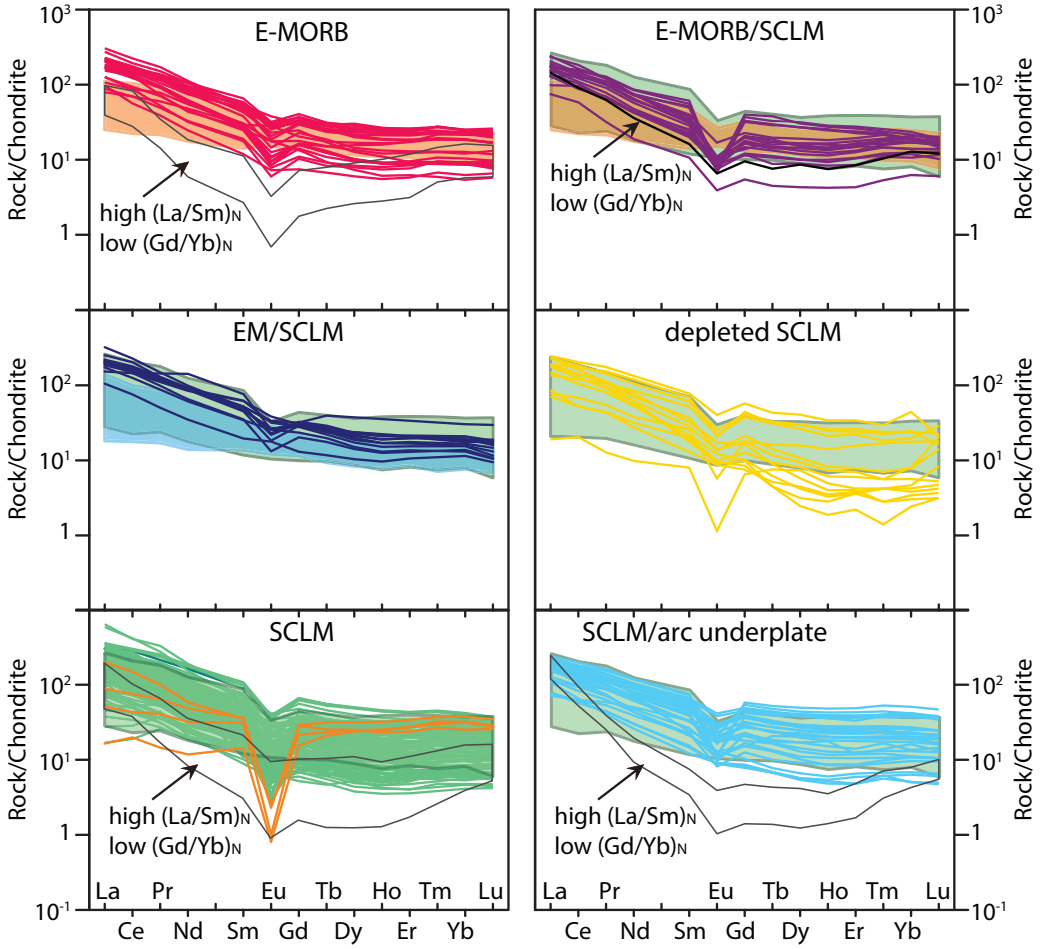

Figure 8: Chondrite-normalised rare earth element diagrams for the Hiltaba Suite REE diagrams divided by underlying mantle group. The shaded area on each plot corresponds to the rare earth element pattern for the mafic Hiltaba Suite of each mantle group identified. Orange = E-MORB, green = SCLM and blue = EM. The high $(La/Sm)_N$ and low $(Gd/Yb)_N$ granitoid samples are indicated by the black line or outline. Normalising values are from Taylor and McLennan (1985). Data for mafic Hiltaba Suite is from Wade *et al*. (2019).

near exact overlap between the mafic and felsic end-members (e.g. the SCLM domain granitoids $\varepsilon_{Nd(i)}$ = -5.2 to 2.3 and SCLM mafics $\varepsilon_{Nd(i)}$ = -5 to 1.9; E-MORB/SCLM domain granitoids $\varepsilon_{Nd(i)}$ = -0.3 to 0.5 and E-MORB mafics $\varepsilon_{Nd(i)}$ = -1.3 to 1.1), In contrast, granitoids in the E-MORB domain have much lower $\varepsilon_{Nd(i)}$ (-4.1 to -3.6) compared with the E-MORB mafics ($-\varepsilon_{Nd(i)}$ = 1.3 to 1.1).

A single mantle or crustal end-member composition cannot successfully be used to model the petrogenesis of the Hiltaba Suite (Skirrow *et al.* 2018, Wade *et al.* 2019). As outlined in section *The ca 1590 Ma Hiltaba Suite granitoids*, previous authors have suggested a wide range of crustal and mantle contributions to the Hiltaba Suite (Giles 1988, Creaser and White 1991, Stewart and Foden 2003, Huang *et al.* 2016, Skirrow *et al.* 2018, Chapman *et al.* 2019, Wade *et al.* 2019). As noted by Stewart and Foden (2003), the isotopic compositions of Hiltaba Suite granitoids are sympathetic to their underlying basement rocks but the influence on their isotopic composition is also due to the underlying mantle domain. In general, isotopically more juvenile mantle is interpreted to reside beneath the western and

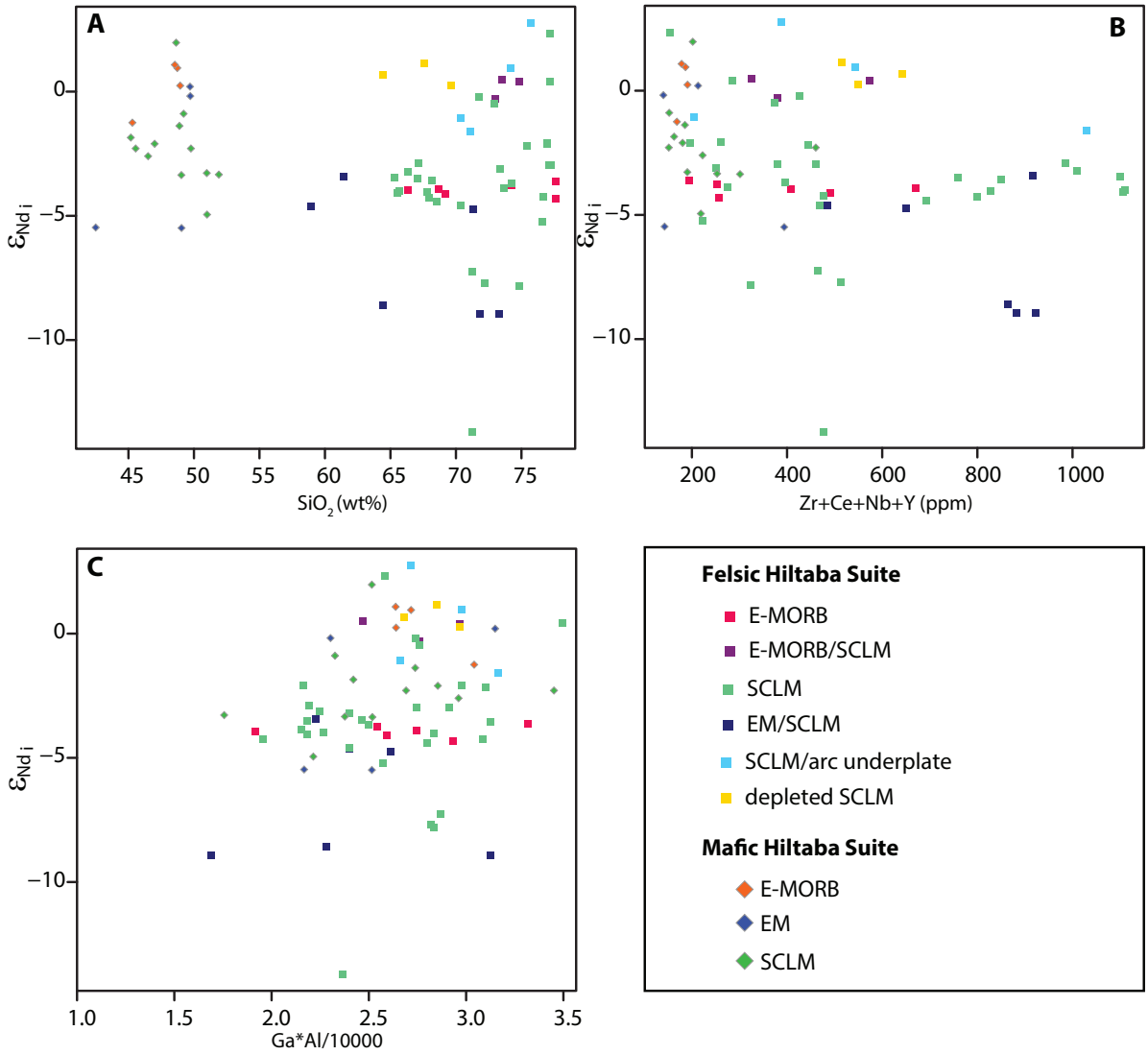

Figure 9: $\varepsilon_{Nd(i)}$ vs a) SiO_2, b) Zr+Ce+Nb+Y and c) Ga/Al x 10000 for the mafic and felsic Hiltaba Suite samples, highlighting the similar isotopic signatures between the two rock groups. Nd data for the mafic Hiltaba Suite is from Wade *et al*. (2019).

central Gawler Craton (Wade *et al.* 2019). The mantle in the eastern Gawler Craton is isotopically more evolved, and reflects an enriched and heterogeneous SCLM composition (Wade *et al.* 2019). Broadly similar crustal components that are 2570–1700 Ma extend across much of the central Gawler Craton, but the west and the east differ in that Mesoproterozoic rocks 1680–1610 Ma are located in the west and are absent in the east, and Neoarchean rocks 3150 Ma are located in the east and are absent in the western Gawler Craton (Fig. 2). In detail, at individual locations, the $\varepsilon_{Nd(i)}$ values of the felsic rocks are generally lower than the mafic rocks. As documented above, ,trace element and REE patterns in the mafic and felsic Hiltaba Suite show similar enrichments, with exceptions that can be attributed to fractionation in the granitoids (for example larger negative Eu Sr, Ba, P and Ti anomalies) which would not impact the isotopic composition. The assimilation of isotopically distinct crustal reservoirs would however affect the isotopic signature of the magmas. To quantify

the impact of crustal contributions to the felsic magmas in relation to the isotopic composition of mantle source domain, we have applied a two-component mixing calculation using the average isotopic compositions of the granitoids and their respective mantle and crustal domains that best represent the lithospheric columns they are sourced from, as identified on Figs 2 and 3 and Table 1. The mixing calculation used is as follows:

$$\% \, crust = \left[\frac{(MNd \; x \; M\varepsilon Nd(i)) - (G\varepsilon Nd(i) \; x \; MNd)}{(G\varepsilon Nd(i) \; x \; (CNd - MNd)) - (CNd \; x \; C\varepsilon Nd(i)) + (MNd \; x \; M\varepsilon Nd(i))}\right] x \; 100$$

where M = mantle type, G = Hiltaba Suite granitoid and C = crust type. Nd = average Nd concentration (ppm) and $\varepsilon_{Nd(i)}$ = average isotopic composition for each component. The isotopic compositions of the host rocks (crust), mantle rocks and granitoids used in the mixing calculation are listed in Appendix Tables A1–A3 and A5.

The mixing results are represented graphically on Figure 10. Lower amounts of crustal assimilation were calculated in granites from the western Gawler Craton, where 4–15% crust is estimated for granite groups 1, 2, 3, 6, 8 and 10 (Fig. 10). Moderate amounts of crustal assimilation were calculated for more centrally located plutons (groups 4, 5, 7 and 9), where 13–44% crust is estimated. Plutons from the eastern Gawler Craton show the highest amounts of crustal material, ranging from 15–86% crust in groups 11, 12, 13, 14, and 15 (Fig. 10). While it appears that lower amounts of crustal assimilation are more apparent for the western Gawler Craton plutons, the starting mantle composition is an important consideration. Although lower crustal additions are estimated for the western Gawler Craton, the mantle, as documented by mafic rocks, is more isotopically juvenile and with lower Nd concentrations ($\varepsilon_{Nd(i)}$ = 0.5 to 0.7 and Nd = 12–25 ppm). Therefore crustal additions, even if slight, have a greater effect on the resulting $\varepsilon_{Nd(i)}$ value. For example, 13–15% crust will change the $\varepsilon_{Nd(i)}$ from between 0.5–0.7 to -1.6 to -0.7, equivalent to 1.2–2.3 epsilon units (Appendix Table A5). Adding a similar amount of crust to the enrichmed mantle in the eastern Gawler Craton will result in a shift of only 1 epsilon unit (e.g. group 11 Fig. 10). As the crustal input increases to ~30%, the shift in $\varepsilon_{Nd(i)}$ value is far more significant when the mantle is juvenile (4.2–5.1 epsilon units compared with 1.4–2.1 for enriched mantle), but the end result is granitoids with similar $\varepsilon_{Nd(i)}$ values (-3.4 to -4.5). The greatest amounts of crustal assimilation are estimated in two groups from the eastern Gawler Craton where 81–86% crust is estimated and may be due to greater amounts of crustal melting in these regions, a suggestion supported by the significant amount of inherited ca 3150 Ma zircons in granitoids in these regions (Creaser and Fanning 1993).

The percentages of crustal input calculated in this study are consistent with previous estimates that produced widely varying numbers (>90%; Giles 1988, 15–40%; Creaser and White 1991, <30%; Stewart and Foden 2003, 3–30%; Chapman *et al.* 2019). Previous studies have produced widely varying estimates due to the localised nature of many of the studies. By taking into account spatial variation in crust and mantle source compositions this study has been able to resolve the apparent conflict between previous studies and demonstrate that in some instances, diverse isotopic signatures represent differing reservoir compositions as opposed to differing magmatic processes. However, the mixing calculations still demonstrate a wide range of crustal contribution amounts to the Hiltaba Suite.

Variable petrogenetic processes for the Hiltaba Suite

As observed in LIPs with silicic magmatism, many compositional and genetically different types of granites can be produced in the same tectonic setting (e.g. Emeishan LIP; Zhong *et*

al. 2007). The nature of the granite types depends on the melting conditions and the type and proportion of mantle and crustal material involved (Fyfe 1992, Zhong *et al.* 2007). Given the variation in the composition of the mantle source documented for the mafic end-members of the Hiltaba Suite (Wade *et al.* 2019), it is likely that the granitoids have a varied petrogenesis. Petrogenetic models appropriate for the Hiltaba Suite may include fractional crystallisation of a parent mafic magma or assimilation and fractionation crystallisation

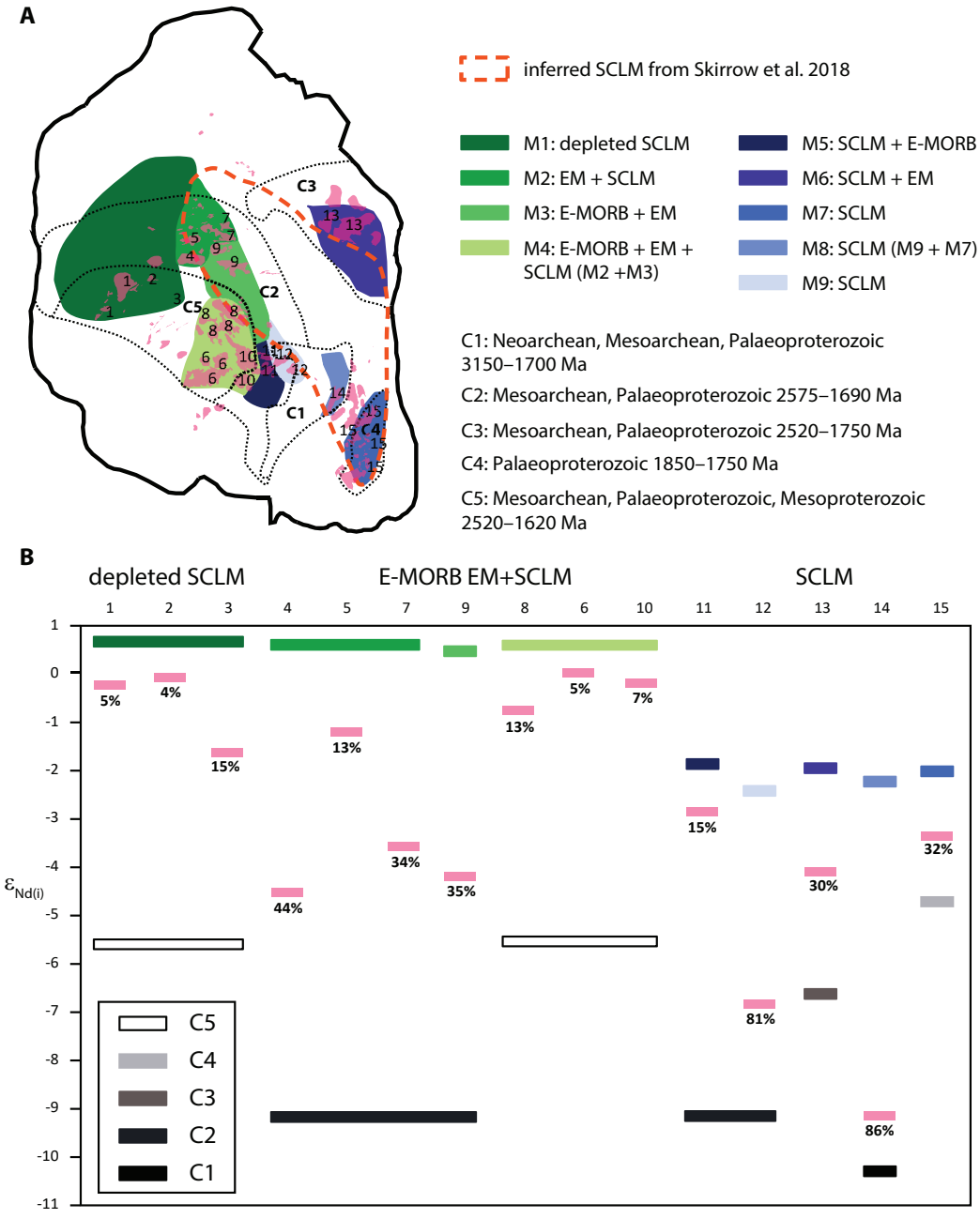

Figure 10: a) Location and inferred distribution of crustal and mantle domains (Figure 3) used as the basis for mixing calculations; and b) graphical representation of Nd isotopic mixing results between average Hiltaba Suite isotopic compositions from each group with their average underlying mantle isotopic composition from Wade *et al.* (2019). Average isotopic compositions for mantle, crust and granites used in the calculations are listed in Appendix Table A2–4.

processes (e.g. Loiselle and Wones 1979) or processes related to mafic underplating and partially melting or remelting of crustal or underplated rocks (e.g. Hildreth *et al.* 1991, Frost and Frost 1997).

Fractional crystallisation from a basaltic parent can provide a satisfactory explanation for depletions in compatible elements and enrichments in incompatible elements and where Nd isotopic compositions between felsic and mafic magmas overlap (Peccerillo *et al.* 2003). While it has been established that the mafic Hiltaba Suite have undergone some degree of fractionation (Wade *et al.* 2019), the absence or low abundance of intermediate magmas in the Hiltaba Suite argues against a purely fractional crystallisation model. The abundance of felsic compositions to low volume mafic magmas is also difficult to reconcile in a fractional crystallisation model. As fractional crystallisation to generate felsic magmas requires large volumes of mafic magma, large volumes of mafic and small volumes of differentiated rocks would be expected (e.g. Hawkesworth *et al.* 2000) and this is not observed in the Hiltaba Suite. Preserved mafic bodies in the subsurface amount to approximately 2500 km^3 of mafic rocks, in contrast to the 30 000 km^3 of felsic rocks. The generation of large volumes of felsic magma has been problematic for other petrogenetic models involving fractional crystallisation for the Gawler LIP as a whole (Giles 1988, Allen *et al.* 2008). Fractional crystallisation of a mafic parent will generate small magma batches, and may only account for small amounts of felsic magma in the Hiltaba Suite at the local scale, but as a sole model fails to explain the abundance of felsic magmas to the low volume mafic magmas in the Hiltaba Suite.

Petrogenetic models involving underplating and partial melting of mafic magmas generated from a plume may be a more satisfactory explanation for the formation of the felsic Hiltaba Suite. Large-scale plume-driven underplating at the base of the crust can create large volumes of crustal melting and provides a mechanism for magma contamination and mixing processes (Fyfe 1992). Mixing of mantle and crustal end-members can also produce coherent trends in major elements (e.g. Schiano *et al.* 2010) and would influence the Nd isotopic composition of the magmas, which can explain the variation in Nd isotopic compositions at any individual location. The lack of intermediate compositions could be explained by a continuous supply of magma, such as that derived from zones of melting at the plume-lithospheric mantle interface, where silicic melts at the top of the magma chamber suppress intermediate melts (Peccerillo *et al.* 2003).

The available geochemical and isotopic data does not unambiguously distinguish between a partial melting or a fractional crystallisation origin for the Hiltaba Suite (e.g. Schiano *et al.* 2010). It is probable that both processes were involved in the generation of the Hiltaba Suite, but a fractional crystallisation model alone cannot account for the relative volumes of mafic and felsic magma, lack of intermediate compositions and localities where the $\varepsilon_{Nd(i)}$ values of the felsic rocks is lower than the mafic rocks. A viable model therefore requires some amount of partial melting and mixing, like that related to mafic underplating, to generate the heterogeneity in the granites and large volumes of magma in the Gawler LIP.

A recipe for HFSE enrichment

The Hiltaba Suite is high in Zr, Nb and LREEs, low in Sr, Ba, P and CaO and has high Ga/Al*10000. The mafic Hiltaba Suite is equally as enriched in the incompatible HFSEs and REEs, a feature which has been attributed to source inheritance from an enriched SCLM (e.g. Wade et al 2019, Huang et al, Skirrow et al. 2018, Wade et al 2012). The remarkable similarity in the mafic and felsic compositions

and the Nd isotopic evidence indicates that all the Hiltaba Suite rocks share a common source region from within the SCLM, with varying fractional crystallisation and crustal contributions. Previous subduction-related processes are considered the cause for the SCLM enrichment, either by metasomatism-related enrichment processes during subduction itself (Plank 2005, Griffin *et al.* 2009, Pearce *et al.* 2017, Cheng *et al.* 2018) or by storing subducted ancient crustal components within the SCLM (Zhang *et al.* 2011, Cai *et al.* 2013). Melting of an enriched mantle source provides a mechanism to transfer that enrichment to mafic magmas emplaced within the crust but it is necessary to maintain that enrichment throughout the assimilation and fractional crystallisation processes in order to produce felsic magmas that are also enriched in HFSE and REE.

Incorporation of large volumes of pre-existing Gawler Craton crust with average compositions (Appendix Table A3) will likely lead to progressive dilution of any pre-existing HFSE-REE enrichment in the parent magmas. The production of HFSE-REE enriched crustal melts invariably requires the dissolution of accessory mineral phases that contain these elements such as zircon, titanite and apatite (Creaser *et al.* 1991, Vasyukova and Williams-Jones 2020). In a non-hydrous melting environment such as that envisioned for the Gawler LIP, high magmatic temperatures are required to cause the dissolution of refractory minerals, and is regarded as a mechanism to create HFSE and REE-enriched magmas (Collins *et al.* 1982, Creaser *et al.* 1991, Martin 2006). Reports of inverted pigeonite from the associated Gawler Range Volcanics highlight the high temperature (900–1100 °C) of the ca. 1590 Ma magmatism (Creaser *et al.* 1991, Pankhurst *et al.* 2011). As could be expected from high Zr content and a general lack of inherited zircon, the calculated Zr saturation temperatures for the majority of the suite are also high (average temperature of 781 ± 35 °C) and are likely to be an underestimate due to the paucity of inherited zircon in the plutons. Ti-in-zircon thermometry for a subset of Hiltaba Suite samples yield median temperatures between 719–937 °C, and are largely in agreement with whole rock Zr saturation temperatures on a per sample basis (Fig. 11a, b). Median Ti-in-zircon temperatures for a subset of GRV samples also yield high temperatures (810–846 °C for the lower GRV and 795–833 °C for the upper GRV). In this regard, the estimated magmatic temperatures of the Hiltaba Suite granitoids, based on both Ti-in-zircon thermometry and whole-rock zircon saturation temperatures, are comparable to the Gawler Range Volcanics and consistent with high temperature HFSE-enriched magmatism (e.g. Liu *et al.* 2019, Su *et al.* 2019). The maintenance of high temperature crystallisation paths suggests the Hiltaba Suite is unlikely to have incorporated extensive, low-temperature, hydrous mantle or crustal melts.

A mantle plume can account for melting of an enriched SCLM and maintenance of high magmatic temperatures throughout the evolution path of the Hiltaba Suite magmas by also providing a high temperature environment for crustal melting (due to high magma fluxes and increased mantle temperatures). High concentrations of HFSE may also be explained by an enriched plume source for the parental magmas (Vasyukova and Williams-Jones 2020). As a consequence, mantle plumes in intraplate settings have been linked to generating granites with HFSE enrichments (Eby 1992, Liu *et al.* 2019, Su *et al.* 2019).

The chemistry of the Hiltaba Suite magmas may also provide a mechanism to maintain high concentrations of HFSE. The solubility of accessory phases such as zircon and apatite is enhanced by high alkalinity of magmas, and can therefore contribute substantial HFSE to the melt, or fail to remove it early within the fractional crystallisation process as would

occur if zircon or apatite saturate early (Watson and Harrison 1984). The alkaline nature of granites from the Olympic Dam area has been reported elsewhere (e.g. Skirrow *et al.* 2018 and references therein). In our dataset, the group of samples with extreme HFSE enrichment (Zr+Ce+Nb+Y > 800; EM/SCLM and SCLM groups), are from the Olympic Dam and Moonta-Wallaroo areas, and may further support a high alkalinity and HFSE enrichment association. The Hiltaba Suite granites are also fluorine-enriched. Fluorine contents have been linked to enrichment in HFSE and REE (Collins *et al.* 1982, Creaser *et al.* 1991, Keppler 1993, Martin 2006, Agangi *et al.* 2010) by increasing the solubility of HFSE in

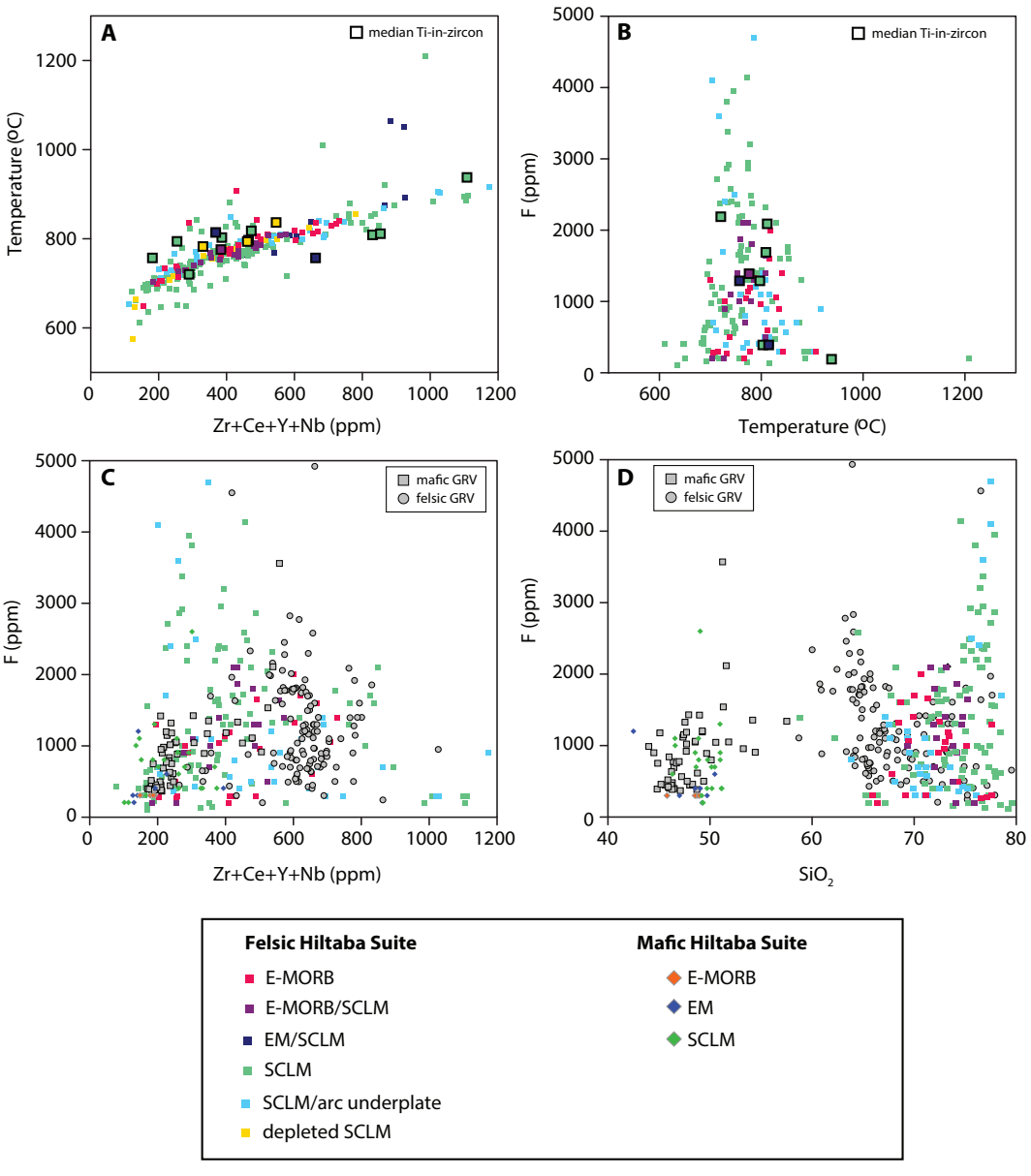

Figure 11: a) Temperature vs Zr+Ce+Nb+Y; b) F vs Temperature; c) F vs Zr+Ce+Nb+Y for the Hiltaba Suite and GRV; d) F vs SiO_2 for the Hiltaba Suite and felsic Gawler Range Volcanics (GRV) units. Data for the GRV compiled from Wade unpub. data (Chapter 4). Temperature calculated as zircon saturation temperature using method of Boehnke et al. 2013. Ti-in-zircon thermometer calculations from Ferry and Watson (2007), where $\alpha TiO_2 = 0.7$ and $\alpha SiO_2 = 1$.

magmas (Keppler 1993). High F content in the mafic to intermediate magmas may have contributed to increased HFSE in the residual melt by suppressing early crystallisation of accessory phases that host these elements, resulting in HFSEs behaving as incompatible elements during fractional crystallisation. A decrease in F and HFSE from the intermediate to felsic compositions suggests compatible behaviour of F and HFSE, prior to a final enrichment of F at high SiO_2 (Fig. 11d). This is consistent with the observations of Agangi *et al.* (2010) who attributed HFSE enrichment in the GRV to the late stage crystallisation of refractory minerals whose components were kept in the residual melts because of high F in the magmas. Some of the highest F contents (>2000 ppm) are high in SiO_2 (>74 wt%) samples which appear to be above the normal granite compositions, and probably reflect the effects of late stage fluids. It may be that a combination of HFSE-enriched sources magmas from the plume and SCLM, high F contents and high temperatures created multiple mechanisms by which to maintain HFSE-REE enrichment in the magmas.

A geodynamic setting for granites in a LIP

The Gawler LIP shares many features with intracontinental mafic LIPs with voluminous silicic magmatism (Pankhurst *et al.* 2011). In such a setting, a heat source related to a mantle plume and/or mafic underplating would be sufficient to facilitate the high temperature melting of old, refractory crust and maintain the high magmatic temperatures recorded in the Hiltaba Suite. The co-magmatic GRV in the Gawler LIP suggest a two-stage model in their petrogenesis, which is linked to constrained magmatic time intervals (Chapter 4). Volcanic rocks at ca. 1593–1590 Ma were derived from partial melting of the SCLM and fractional crystallisation processes relating basalts and rhyolites. This was followed by large-scale crustal melting ca. 1586 Ma, attributed to sustained thermal input from a mantle plume, which produced the voluminous silicic rocks of the Upper GRV. This intensive volcanic episode likely marks the onset of the waning phase of magmatism where silicic magmas ceased to erupt and may have instead been emplaced as shallow level intrusions. While the geochronological constraints are not as well defined for the Hiltaba Suite, a small number of magmatic ages overlap with the early phase of volcanism (1594–1590) but also extend to younger magmatic ages (1585–1579 Ma; Jagodzinski *et al.* 2020, Reid *et al.* 2020), which are consistent with the continuum of felsic plutonism during the waning phase (Bryan *et al.* 2002, Jerram and Widdowson 2005). The spatial and compositional overlap between the Hiltaba Suite and the GRV indicate they were formed in the same tectonic setting.

In an intracontinental tectonic setting involving a mantle plume, zones of melting at the plume-lithospheric mantle interface would produce mafic magmas that ascend and accumulate as underplates at the base of the lower crust (Fig. 12). Some mafic magmas derived from the lithospheric mantle underplates would generate the mafic Hiltaba Suite and GRV basalts distal to the plume head. This suggests the initial starting conditions of the mafic magmas were similar and then variably modified by differing crustal assimilation regimes with varying crustal reservoirs (e.g. Chapter 4). High temperatures associated with the plume and mafic underplating may have facilitated efficient melting and mixing between the lithospheric mantle underplated material and a variety of crustal rocks. Heterogeneity in the granites is a function of variations in both the lithospheric mantle material and the crustal composition at the site of partial melting and mixing. A continuous magma supply to chamber/s related to zones of melting in the plume-lithospheric mantle interface may explain the bimodal nature of the Hiltaba Suite (Peccerillo *et al.* 2003). The diversity of geochemical and isotopic compositions in the

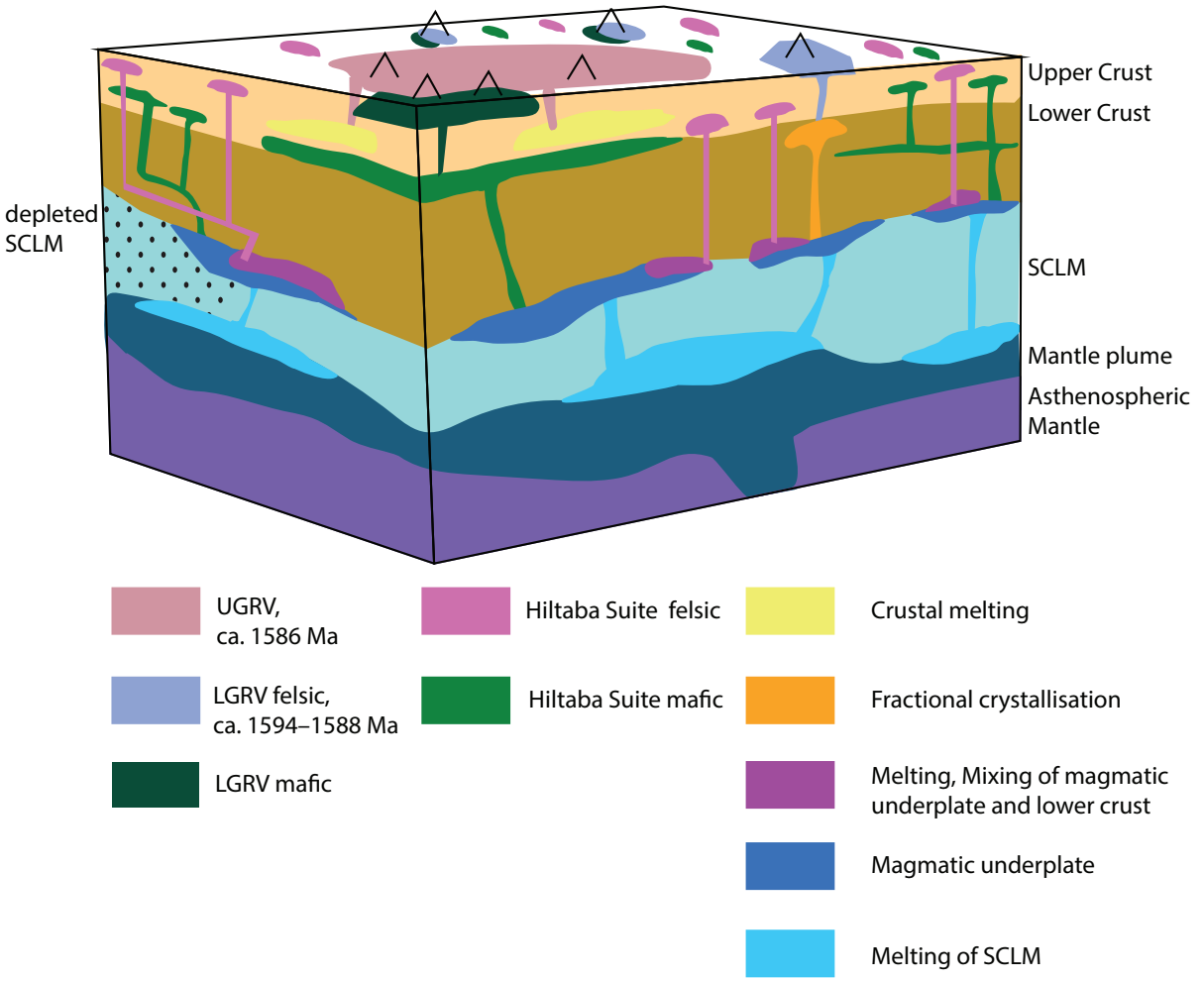

Figure 12: Conceptual model for the formation of the Hiltaba Suite granitoids in the Gawler LIP, showing the role of underplated mafic magmas derived from the subcontinental lithospheric mantle mixing with lower crust to produce Hiltaba Suite granites. UGRV = upper Gawler Range Volcanics; LGRV = lower Gawler Range Volcanics; SCLM = subcontinental lithospheric mantle.

Hiltaba Suite granites may be explained by magma batches derived from the SCLM-lower crust mafic underplates and crustal level magma chambers, where fractional crystallisation processes occurred at the later stages of shallow pluton emplacement (Fig. 12).

CONCLUSIONS

The Hiltaba Suite granitoids have significant enrichments in HFSE, REE and F. Similar trace and rare earth element compositions are shared between the mafic and felsic Hiltaba Suite rocks, suggest they were derived from common source regions, largely from within the SCLM. Two-component Nd isotopic mixing calculations show that the Hiltaba felsic rocks assimilated between 4–86% crustal material to achieve their final Nd isotopic compositions. Lower amounts of crustal additions (3–44%) are estimated for plutons in the western Gawler Craton where juvenile mantle compositions occur, while additions of 15–86% are estimated where enriched SCLM exists beneath the eastern Gawler Craton.

The Hiltaba Suite were formed in an intracontinental setting analogous to a mafic LIP which involved plume-generated melting of the SCLM forming mafic underplates of the lower crust, which caused melting an mixing with various crustal components of the low-

er crust, followed by fractional crystallisation and assimilation processes. Such a model allows for compositionally and genetically variable types of granites to be produced in the same tectonic setting.

ACKNOWLEDGEMENTS

This study is a part of Ph.D. project (C. Wade), and was financially supported by Australian Research Council Linkage Project LP160100578, with the support of the Geological Survey of South Australia. Martin Hand, University of Adelaide, is thanked for insightful discussions that generated many of the ideas explored in this manuscript. David Bruce, University of Adelaide, is thanked for assistance with Sm–Nd isotope analysis. Jessica Bonsell, Department for Energy and Mining, is thanked for drafting Figure 1. CW and AR publish with permission of the Director, Geological Survey of South Australia, Department for Energy and Mining, South Australia.

REFERENCES

Agangi, A., Kamenetsky, V. S. and McPhie, J., 2010. The role of fluorine in the concentration and transport of lithophile trace elements in felsic magmas: Insights from the Gawler Range Volcanics, South Australia. Chemical Geology, v. 273, p. 314-325. doi: https://doi.org/10.1016/j.chemgeo.2010.03.008

Allen, S. R., McPhie, J., Ferris, G. and Cadd, A. G., 2008. Evolution and architecture of a large felsic igneous province in western Laurentia: The 1.6 Ga Gawler Range Volcanics, South Australia. Journal of Volcanology and Geothermal Research, v. 172, p. 132-147. doi: https://doi.org/10.1016/j.jvolgeores.2005.09.027

Allen, S. R., Simpson, C. J., McPhie, J. and Daly, S. J., 2003. Stratigraphy, distribution and geochemistry of widespread felsic volcanic units in the Mesoproterozoic Gawler Range Volcanics, South Australia. Australian Journal of Earth Sciences, v. 50, p. 97-112. doi: http://dx.doi.org/10.1046/j.1440-0952.2003.00980.x

Barbarin, B., 1999. A review of the relationships between granitoid types, their origins and their geodynamic environments. Lithos, v. 46, p. 605–626. doi: https://doi.org/10.1016/S0024-4937(98)00085-1

Betts, P. G., Giles, D., Schaefer, B. F. and Mark, G., 2007. 1600–1500 Ma hotspot track in eastern Australia: implications for Mesoproterozoic continental reconstructions. Terra Nova, v. 19, p. 496–501. doi: https://doi.org/10.1111/j.1365-3121.2007.00778.x

Blissett, A. H., Creaser, R. A., Daly, S., Flint, D. J. and Parker, A. J., 1993. Gawler Range Volcanics. In: Drexel, J. F., Preiss, W. V. and Parker, A. J. (Eds), The geology of South Australia. Volume 1. The Precambrian. Geological Survey of South Australia, v. Bulletin 54, p. 107-131. Available at: https://sarigbasis.pir.sa.gov.au/WebtopEw/ws/samref/sarig1/image/DDD/BULL054(V1).pdf

Brotodewo, A., Tiddy, C. J., Reid, A., Wade, C. and Conor, C., 2018. Relationships between magmatism and deformation in northern Yorke Peninsula and southeastern Proterozoic Australia. Australian Journal of Earth Sciences, v. 65, p. 619-641. doi: https://doi.org/10.1080/08120099.2018.1470573

Bryan, S. E., Riley, T. R., Jerram, D. A., Stephens, C. J. and Leat, P. T., 2002. Silicic volcanism: an undervalued component of large igneous provinces and volcanic rifted margins. In: Menzies, M. A., Klemperer, S. I., Ebinger, C. J. and Baker, J. (Eds), Volcanic Rifted Margins. Geological Society of America, Special Paper, v. 362, p. 97–118. https://doi.org/10.1130/0-8137-2362-0.97

Budd, A., 2006. The Tarcoola Goldfield of the Central Gawler Gold Province, and the Hiltaba Association Granites, Gawler Craton, South Australia. Australian National

University, Department of Earth and Marine Sciences, PhD thesis (unpublished).

Budd, A. R. and Skirrow, R. G., 2007. The Nature and Origin of Gold Deposits of the Tarcoola Goldfield and Implications for the Central Gawler Gold Province, South Australia. Economic Geology, v. 102, p. 1541–1563. doi: https://doi.org/10.2113/gsecongeo.102.8.1541

Cai, Y.-C., Fan, H.-R., Santosh, M., Liu, X., Hu, F.-F., Yang, K.-F., Lan, T.-G., Yang, Y.-H. and Liu, Y., 2013. Evolution of the lithospheric mantle beneath the southeastern North China Craton: Constraints from mafic dikes in the Jiaobei terrain. Gondwana Research, v. 24, p. 601-621. doi: https://doi.org/10.1016/j.gr.2012.11.013

Chapman, N. D., Ferguson, M., Meffre, S. J., Stepanov, A., Maas, R. and Ehrig, K. J., 2019. Pb-isotopic constraints on the source of A-type Suites: Insights from the Hiltaba Suite - Gawler Range Volcanics Magmatic Event, Gawler Craton, South Australia. Lithos, v. 346-347, p. 105156. doi: https://doi.org/10.1016/j.lithos.2019.105156

Cheng, T., Nebel, O., Sossi, P. A., Wu, J., Siebel, W., Chen, F. K. and Nebel-Jacobsen, Y. J., 2018. On the Sr-Nd-Pb-Hf isotope code of enriched, Dupal-type sub-continental lithospheric mantle underneath south-western China. Chemical Geology, v. 489, p. 46-60. doi: https://doi.org/10.1016/j.chemgeo.2018.05.018

Cherry, A. R., Ehrig, K., Kamenetsky, V. S., McPhie, J., Crowley, J. L. and Kamenetsky, M. B., 2018. Precise geochronological constraints on the origin, setting and incorporation of ca. 1.59 Ga surficial facies into the Olympic Dam Breccia Complex, South Australia. Precambrian Research, v. 315, p. 162-178. doi: https://doi.org/10.1016/j.precamres.2018.07.012

Collins, W. J., Beams, S. D., White, A. J. R. and Chappell, B. W., 1982. Nature and origin of A-type granites with particular reference to southeastern Australia. Contributions to Mineralogy and Petrology, v. 80, p. 189-200. doi: https://doi.org/10.1007/bf00374895

Conor, C. H. H., 1995. Moonta-Wallaroo region - South Australian Exploration Initiative. Prospectivity re-assessment and GIS data package (compiled 1994-1995). South Australia. Department of Primary Industries and Resources, Adelaide. v. Open file Envelope, 8886, p. 537. availabie at: Available at: https://sarigbasis.pir.sa.gov.au/WebtopEw/ws/samref/sarig1/image/DDD/ENV08886.pdf

Creaser, R. A., 1989. The geology and petrology of middle Proterozoic felsic magmatism of the Stuart Shelf, South Australia. LaTrobe University, PhD thesis (unpublished).

Creaser, R. A. and Cooper, J. A., 1993. U-Pb geochronology of middle Proterozoic felsic magmatism surrounding the Olympic Dam Cu-U-Au-Ag and Moonta Cu-Au-Ag deposits, South Australia. Economic Geology and the Bulletin of the Society of Economic Geologists, v. 88, p. 186-197. doi: https://doi.org/10.2113/gsecongeo.88.1.186

Creaser, R. A. and Fanning, C. M., 1993. A U-Pb zircon study of the Mesoproterozoic Charleston Granite, Gawler Craton, South Australia. Australian Journal of Earth Sciences, v. 40, p. 519-526. doi: https://doi.org/10.1080/08120099308728101

Creaser, R. A., Price, R. C. and Wormald, R. J., 1991. A-type granites revisited: assessment of a residual-source model. Geology, v. 19, p. 163-166. doi: https://doi.org/10.1130/0091-7613(1991)019<0163:ATGRAO>2.3.CO;2

Creaser, R. A. and White, A. J. R., 1991. Yardea Dacite; large-volume, high-temperature felsic volcanism from the middle Proterozoic of South Australia. Geology, v. 19, p. 48-51. doi: https://doi.rg/10.1130/0091-7613(1991)019<0048:YDLVHT>2.3.CO;2

Curtis, S. and Thiel, S., 2019. Identifying lithospheric boundaries using magnetotellurics and Nd isotope geochemistry: An example from the Gawler Craton, Australia. Precambrian Research, v. 320, p. 403-423. doi: https://doi.org/10.1016/j.precamres.2018.11.013

Eby, G. N., 1992. Chemical subdivision of the A-type granitoids: Petrogenetic and tectonic implications. Geology, v. 20, p. 641-644. doi: https://doi.rg10.1130/0091-7613(1992)020<0641:Csotat>2.3.Co;2

Ernst, R. E., Liikane, D. A., Jowitt, S. M., Buchan, K. L. and Blanchard, J. A., 2019. A new plumbing system framework for mantle plume-related continental Large Igneous Provinces and their mafic-ultramafic intrusions. Journal of Volcanology and Geothermal Research, v. 384, p. 75-84. doi: https://doi.org/10.1016/j.jvolgeores.2019.07.007

Fanning, C. M., Reid, A. and Teale, G. S., 2007. A geochronological framework for the Gawler Craton, South Australia: South Australia. Geological Survey, v. Bulletin 55, p. availabie at: Available at: https://sarigbasis.pir.sa.gov.au/WebtopEw/ws/samref/sarig1/image/DDD/BULL055.pdf

Flint, R. B., 1993. Hiltaba Suite. In: Drexel, J. F., Preiss, W. V. and Parker, A. J. (Eds), The geology of South Australia. Volume 1. The Precambrian. Geological Survey of South Australia, v. Bulletin 54, p. 127-131. Available at: https://sarigbasis.pir.sa.gov.au/WebtopEw/ws/samref/sarig1/image/DDD/BULL054(V1).pdf

Flint, R. B., Blissett, A. H., Conor, C. H. H., Cowley, W. M., Cross, K. C., Creaser, R. A., Daly, S. J., Krieg, G. W., Major, R. B., Teale, G. S. and Parker, A. J., 1993. Mesoproterozoic. In: Drexel, J. F., Preiss, W. V. and Parker, A. J. (Eds), The geology of South Australia. Volume 1. The Precambrian. Geological Survey of South Australia, v. Bulletin 54, p. 106-169. Available at: https://sarigbasis.pir.sa.gov.au/WebtopEw/ws/samref/sarig1/image/DDD/BULL054(V1).pdf

Foden, J., Sossi, P. A. and Wawryk, C. M., 2015. Fe isotopes and the contrasting petrogenesis of A-, I- and S-type granite. Lithos, v. 212-215, p. 32-44. doi: https://doi.org/10.1016/j.lithos.2014.10.015

Fraser, G. L., McAvaney, S., Neumann, N., Szpunar, M. and Reid, A., 2010. Discovery of early Mesoarchean crust in the eastern Gawler Craton, South Australia. Precambrian Research, v. 179, p. 1–21. doi: https://doi.org/10.1016/j.precamres.2010.02.008

Frost, C. D. and Frost, B. R., 2010. On Ferroan (A-type) Granitoids: their Compositional Variability and Modes of Origin. Journal of Petrology, v. 52, p. 39-53. doi: https://doi.org.10.1093/petrology/egq070

Frost, C. D. and Frost, R. B., 1997. Reduced rapakivi-type granites: The tholeiite connection. Geology, v. 25, p. 647-650. doi: https://doi.rg/10.1130/0091-7613(1997)025<0647:Rrtgtt>2.3.Co;2

Fyfe, W. S., 1992. Magma underplating of continental crust. Journal of Volcanology and Geothermal Research, v. 50, p. 33-40. doi: https://doi.org/10.1016/0377-0273(92)90035-C

Giles, C. W., 1988. Petrogenesis of the Proterozoic Gawler Range volcanics, South Australia. Precambrian Research, v. 40-41, p. 407-427. doi: https://doi.org/10.1016/0301-9268(88)90078-2

Griffin, W., O'Reilly, S. Y., Afonso, J. C. and Begg, G. C., 2009. The Composition and Evolution of Lithospheric Mantle: a Re-evaluation and its Tectonic Implications. Journal of Petrology, v. 50, p. 1185-1204. doi: https://doi.org/10.1093/petrology/egn033

Halpin, J. A. and Reid, A. J., 2016. Earliest Paleoproterozoic high-grade metamorphism and orogenesis in the Gawler Craton, South Australia: The southern cousin in the Rae family? Precambrian Research, v. 276, p.

123–144. doi: https://doi.org/10.1016/j.precamres.2016.02.001

Hand, M., Reid, A. and Jagodzinski, E., 2007. Tectonic framework and evolution of the Gawler Craton, South Australia. Economic Geology, v. 102, p. 1377-1395. doi: https://doi.org/10.2113/gsecongeo.102.8.1377

Hand, M., Reid, A., Szpunar, M., Direen, N. G., Wade, B., Payne, J. and Barovich, K., 2008. Crustal architecture during the early Mesoproterozoic Hiltaba-related mineralisation event: are the Gawler Range Volcanics a foreland basin fill? MESA Journal, v. 51, p. 19-24. Available at: https://sarigbasis.pir.sa.gov.au/WebtopEw/ws/samref/sarig1/image/DDD/MESAJ051019-024.pdf

Hawkesworth, C. J., Blake, S., Evans, P., Hughes, R., Macdonald, R., Thomas, L. E., Turner, S. P. and Zellmer, G., 2000. Time Scales of Crystal Fractionation in Magma Chambers—Integrating Physical, Isotopic and Geochemical Perspectives. Journal of Petrology, v. 41, p. 991-1006. doi: 10.1093/petrology/41.7.991

Hildreth, W., Halliday, A. N. and Christiansen, R. L., 1991. Isotopic and Chemical Evidence Concerning the Genesis and Contamination of Basaltic and Rhyolitic Magma Beneath the Yellowstone Plateau Volcanic Field. Journal of Petrology, v. 32, p. 63-138. doi: https://doi.org/10.1093/petrology/32.1.63

Hoatson, D. M., Sun, S.-S., Duggan, M. B., Davies, M. B., Daly, S. J. and Purvis, A. C., 2005. Late Archaean Lake Harris Komatiite, central Gawler Craton, South Australia: geologic setting and geochemistry. Economic Geology, v. 100, p. 349-374. doi: https://doi.org/10.2113/gsecongeo.100.2.349

Howard, K. E., Hand, M., Barovich, K. M., Payne, J. L. and Belousova, E. A., 2011. U-Pb, Lu-Hf and Sm-Nd isotopic constraints on provenance and depositional timing of metasedimentary rocks in the western Gawler Craton: Implications for Proterozoic reconstruction models. Precambrian Research, v. 184, p. 43–62. doi: https://doi.org/10.1016/j.precamres.2010.10.002

Huang, Q., Kamenetsky, V. S., Ehrig, K., McPhie, J., Kamenetsky, M., Cross, K., Meffre, S., Agangi, A., Chambefort, I., Direen, N. G., Maas, R. and Apukhtina, O., 2016. Olivine-phyric basalt in the Mesoproterozoic Gawler silicic large igneous province, South Australia: Examples at the Olympic Dam Iron Oxide Cu–U–Au–Ag deposit and other localities. Precambrian Research, v. 281, p. 185-199. doi: https://doi.org/10.1016/j.precamres.2016.05.019

Jagodzinski, E. A., Crowley, J. L. and Reid, A. J., in prep. Precise zircon U-Pb dating of the Hiltaba Suite, Gawler Craton. Department for Energy and Mining, South Australia, Adelaide, v. Report Book 2021/00001

Jerram, D. A. and Widdowson, M., 2005. The anatomy of Continental Flood Basalt Provinces: geological constraints on the processes and products of flood volcanism. Lithos, v. 79, p. 385-405. doi: https://doi.org/10.1016/j.lithos.2004.09.009

Keppler, H., 1993. Influence of fluorine on the enrichment of high field strength trace elements in granitic rocks. Contributions to Mineralogy and Petrology, v. 114, p. 479-488. doi: 10.1007/BF00321752

Liu, H.-Q., Xu, Y.-G., Zhong, Y.-T., Luo, Z.-Y., Mundil, R., Riley, T. R., Zhang, L. and Xie, W., 2019. Crustal melting above a mantle plume: Insights from the Permian Tarim Large Igneous Province, NW China. Lithos, v. 326-327, p. 370-383. doi: https://doi.org/10.1016/j.lithos.2018.12.031

Loiselle, M. C. and Wones, D. R., 1979. Characteristics of Anorogenic Granites. Geological Society of America, v. Abstracts with Programs, 11, p. 468. doi:

Martin, R. F., 2006. A-type granites of crustal origin ultimately result from open-system fenitization-type reactions in an exten-

sional environment. Lithos, v. 91, p. 125-136. doi: https://doi.org/10.1016/j.lithos.2006.03.012

McPhie, J., DellaPasqua, F., Allen, S. R. and Lackie, M. A., 2008. Extreme effusive eruptions: Palaeoflow data on an extensive felsic lava in the Mesoproterozoic Gawler Range Volcanics. Journal of Volcanology and Geothermal Research, v. 172, p. 148-161. doi: https://doi.org/10.1016/j.jvolgeores.2006.11.011

McPhie, J., Ehrig, K. J., Kamenetsky, M. B., Crowley, J. L. and Kamenetsky, V. S., 2020. Geology of the Acropolis prospect, South Australia, constrained by high-precision CA-TIMS ages. Australian Journal of Earth Sciences, v. 67, p. 699-716. doi: https://doi.org/10.1080/08120099.2020.1717617

Pankhurst, M. P., Schaefer, B. F., Betts, P. G., Phillips, N. and Hand, M., 2011. A Mesoproterozoic continental flood rhyolite province, the Gawler Ranges, Australia: the end member example of the Large Igneous Province clan. Solid Earth, v. 2, p. 1-9. doi: https://doi.org/10.5194/se-2-25-2011

Patiño Douce, A. E., 1999. What do experiments tell us about the relative contributions of crust and mantle to the origin of granitic magmas? Geological Society, London, Special Publications, v. 168, p. 55-75. doi: https://doi.org/10.1144/gsl.Sp.1999.168.01.05

Payne, J., Barovich, K. and Hand, M., 2006. Provenance of metasedimentary rocks in the northern Gawler Craton, Australia: Implications for Palaeoproterozoic reconstructions. Precambrian Research, v. 148, p. 275-291. doi: https://doi.org/10.1016/j.precamres.2006.05.002

Payne, J. L., Ferris, G., Barovich, K. M. and Hand, M., 2010. Pitfalls of classifying ancient magmatic suites with tectonic discrimination diagrams: An example from the Paleoproterozoic Tunkillia Suite, southern Australia. Precambrian Research, v. 177, p. 227-240. doi: https://doi.org/10.1016/j.precamres.2009.12.005

Pearce, J., 1996. Sources and settings of granitic rocks. Episodes, v. 19, p. 120-125. doi: https://doi.org/10.4236/jssm.2008.11008

Pearce, J. A., Ernst, R. E., Rogers, C. and Peate, D. W., 2017. LIP Printing: A Geochemical Proxy Approach to LIP Forensics. Geological Society of America Annual Meeting, Seattle, Washington, USA. Geological Society of America Abstracts with Programs, v. 49, No. 6, p. doi: https://doi.org.10.1130/abs/2017AM-301471

Peccerillo, A., Barberio, M. R., Yirgu, G., Ayalew, D., Barbieri, M. and Wu, T. W., 2003. Relationships between Mafic and Peralkaline Silicic Magmatism in Continental Rift Settings: a Petrological, Geochemical and Isotopic Study of the Gedemsa Volcano, Central Ethiopian Rift. Journal of Petrology, v. 44, p. 2003-2032. doi: https://doi.org/10.1093/petrology/egg068

Plank, T., 2005. Constraints from Thorium/Lanthanum on Sediment Recycling at Subduction Zones and the Evolution of the Continents. Journal of Petrology, v. 46, p. 921-944. doi: https://doi.org/10.1093/petrology/egi005

Reid, A. and Dutch, R., 2012. Reconnaissance LA-ICPMS zircon U-Pb geochronology of crystalline basement outcrops on the FOWLER 1:250000 mapsheet. Department for Manufacturing, Innovation, Trade, Resources and Energy, v. Report Book 2012/00013, p. pp. 66. Available at: https://sarigbasis.pir.sa.gov.au/WebtopEw/ws/samref/sarig1/image/DDD/RB201200013.pdf

Reid, A., Hand, M., Jagodzinski, E., Kelsey, D. and Pearson, N. J., 2008. Palaeoproterozoic orogenesis within the southeastern Gawler Craton, South Australia Australian Journal of Earth Sciences, v. 55, p. 449-471. doi: https://doi.org/10.1080/08120090801888594

Reid, A. J., Pawley, M. J., Wade, C., Jagodzinski, E. A., Dutch, R. A. and Armstrong, R., 2019. Resolving tectonic settings of ancient magmatic suites using structural, geochemical and isotopic constraints: the example of the St Peter Suite, southern Australia. Australian Journal of Earth Sciences, v. p. 1-28. doi: https://10.1080/08120099.2019.1632224

Reid, A. J., Tiddy, C. J., Jagodzinski, E. A., Crowley, J. L., Conor, C., Brotodewo, A. and Wade, C., in prep.. Precise zircon U-Pb geochronology of Hiltaba Suite granites, Point Reilley, Yorke Peninsula. Department for Energy and Mining, South Australia, Adelaide, v. Report Book 2021/00002

Rogers, C., Kamo, S. L., Söderlund, U., Hamilton, M. A., Ernst, R. E., Cousens, B., Harlan, S. S., Wade, C. E. and Thorkelson, D. J., 2018. Geochemistry and U-Pb geochronology of 1590 and 1550 Ma mafic dyke swarms of western Laurentia: Mantle plume magmatism shared with Australia. Lithos, v. 314-315, p. 216-235. doi: https://doi.org/10.1016/j.lithos.2018.06.002

Schiano, P., Monzier, M., Eissen, J. P., Martin, H. and Koga, K. T., 2010. Simple mixing as the major control of the evolution of volcanic suites in the Ecuadorian Andes. Contributions to Mineralogy and Petrology, v. 160, p. 297-312. doi: https://doi.org/10.1007/s00410-009-0478-2

Skirrow, R., van der Wielen, S. E., Champion, D. C., Czarnota, K. and Thiel, S., 2018. Lithospheric artchitecture and mantle metasomatism linked to iron-oxide Cu-Au ore formation: Multidiciplinary evidence from the Olympic Dam region, South Australia. Geochemistry, Geophysics, Geosystems, v. 19, p. doi: https://doi.org/10.1029/2018GC007561

Stewart, K., 1994. High temperature felsic volcanism and the role of mantle magmas in Proterozoic crustal growth : the Gawler Range volcanic province. University of Adelaide, PhD thesis (unpublished).

Stewart, K. P. and Foden, J., 2003. Mesoproterozoic granites of South Australia. South Australia. Department of Primary Industries and Resources. Report Book, 2003/15, v. p. pp. 142. Available at: https://sarigbasis.pir.sa.gov.au/WebtopEw/ws/samref/sarig1/image/DDD/RB200300015.pdf

Su, Y., Zheng, J., Liang, L., Dai, H., Zhao, J., Chen, M., Ping, X., Liu, Z. and Wang, J., 2019. Derivation of A1-type granites by partial melting of newly underplated rocks related with the Tarim mantle plume. Geological Magazine, v. 156, p. 409-429. doi: https://10.1017/S0016756817000838

Swain, G., Barovich, K., Hand, M., Ferris, G. and Schwarz, M., 2008. Petrogenesis of the St Peter Suite, southern Australia: arc magmatism and Proterozoic crustal growth of the South Australian Craton. Precambrian Research, v. 166, p. 283-296. doi: https://doi.org/10.1016/j.precamres.2007.07.028

Swain, G., Woodhouse, A., Hand, M., Barovich, K., Schwarz, M. and Fanning, C. M., 2005. Provenance and tectonic development of the late Archaean Gawler Craton, Australia; U-Pb zircon, geochemical and Sm-Nd isotopic implications. Precambrian Research, v. 141, p. 106-136. doi: https://doi.org/10.1016/j.precamres.2005.08.004

Szpunar, M., Hand, M., Barovich, K., Jagodzinski, E. and Belousova, E., 2011. Isotopic and geochemical constraints on the Paleoproterozoic Hutchison Group, southern Australia: Implications for Paleoproterozoic continental reconstructions. Precambrian Research, v. 187, p. 99-126. doi: https://doi.org/10.1016/j.precamres.2011.02.006

Tiddy, C. J. and Giles, D., 2020. Supra-subduction zone model for metal endowment at 1.60-1.575 Ga in eastern Australia. Ore Geology Reviews, v. 122, p. doi: https://doi.org/10.1016/j.oregeorev.2020.103483

Vassallo, J. J. and Wilson, C. J. L., 2002. Pa-

laeoproterozoic regional-scale non-coaxial deformation; an example from eastern Eyre Peninsula, South Australia. Journal of Structural Geology, v. 24, p. 1-24. doi: https://doi.org/10.1016/S0191-8141(01)00043-8

Vasyukova, O. and Williams-Jones, A., 2020. Partial melting, fractional crystallisation, liquid immiscibility and hydrothermal mobilisation – A 'recipe' for the formation of economic A-type granite-hosted HFSE deposits. Lithos, v. 356-357, p. 105300. doi: https://doi.org/10.1016/j.lithos.2019.105300

Vielzeuf, D., Clemens, J. D., Pin, C. and Moinet, E., 1990. Granites, Granulites, and Crustal Differentiation: Granulites and Crustal Evolution. NATO ASI Series (Series C: Mathematical and Physical Sciences). Springer, Dordrecht. v. vol 311, p. availabie at: https://doi.org/10.1007/978-94-009-2055-2_5

Wade, C. E. and McAvaney, S., 2017. Stratigraphy and geochemistry of the 1745–1700 Ma Peter Pan Supersuite. v. RB 2016/00026, p. 71. Available at: https://sarigbasis.pir.sa.gov.au/WebtopEw/ws/samref/sarig1/wcir/Record?r=0&m=1&w=catno=2039428

Wade, C. E., Payne, J. L., Barovich, K. M. and Reid, A. J., 2019. Heterogeneity of the sub-continental lithospheric mantle and 'non-juvenile' mantle additions to a Proterozoic silicic large igneous province. Lithos, v. 340-341, p. 87-107. doi: https://doi.org/10.1016/j.lithos.2019.05.005

Wade, C. E., Reid, A., Wingate, M. T. D., Jagodzinski, E. A. and Barovich, K., 2012. Geochemistry and geochronology of the c. 1585 Ma Benagerie Volcanic Suite, southern Australia: relationship to the Gawler Range Volcanics and implications for the petrogenesis of a Mesoproterozoic silicic large igneous province Precambrian Research, v. 206–207, p. 17–35. doi: https://doi.org/10.1016/j.precamres.2012.02.020

Wurst, A. T., 1994. Analyses of late stage, Mesoproterozoic, syn- and post-tectonic, magmatic events in the Moonta Subdomain: implications for Cu-Au mineralisation in the 'Copper Triangle' of South Australia. University of Adelaide, Honours thesis (unpublished).

Yang, J.-H., Wu, F.-Y., Chung, S.-L., Wilde, S. A. and Chu, M.-F., 2004. Multiple sources for the origin of granites: Geochemical and Nd/Sr isotopic evidence from the Gudaoling granite and its mafic enclaves, northeast China. Geochimica et Cosmochimica Acta, v. 68, p. 4469-4483. doi: https://doi.org/10.1016/j.gca.2004.04.015

Zang, W., Fanning, C. M., Purvis, A. C., Raymond, O. L. and Both, R. A., 2007. Early Mesoproterozoic bimodal plutonism in the southeastern Gawler Craton, South Australia. Australian Journal of Earth Sciences, v. 54, p. 661-674. doi: https://doi.org/10.1080/08120090701305210

Zhang, Y.-L., Liu, C.-Z., Ge, W.-C., Wu, F.-Y. and Chu, Z.-Y., 2011. Ancient sub-continental lithospheric mantle (SCLM) beneath the eastern part of the Central Asian Orogenic Belt (CAOB): Implications for crust–mantle decoupling. Lithos, v. 126, p. 233-247. doi: https://doi.org/10.1016/j.lithos.2011.07.022

Zhong, H., Zhu, W.-G., Chu, Z.-Y., He, D.-F. and Song, X.-Y., 2007. Shrimp U–Pb zircon geochronology, geochemistry, and Nd–Sr isotopic study of contrasting granites in the Emeishan large igneous province, SW China. Chemical Geology, v. 236, p. 112-133. doi: https://doi.org/10.1016/j.chemgeo.2006.09.004

Chapter 4

This chapter is written for submission to Precambrian Research as: Wade, C., Payne, J., Barovich, K., Reid, A., Curtis, S., Jagodzinski, E. and Hill, J. in review. Temporal, geochemical and isotopic constraints on plume-driven felsic and mafic components in a large igneous province.

Statement of Authorship

Title of Paper	Temporal, geochemical and isotopic constraints on plume-driven felsic and mafic components in a large igneous province
Publication Status	☐ Published ☐ Accepted for Publication ☐ Submitted for Publication ☑ Unpublished and Unsubmitted work written in manuscript style
Publication Details	Wade, C.E., Payne, J. L, Barovich, K.M., Reid, A. J., Jagidzinski, E. A, S Curtis, S. and Hill, J. in prep. Temporal, geochemical and isotopic constraints on plume-driven felsic and mafic components in a large igneous province

Principal Author

Name of Principal Author (Candidate)	Claire Wade		
Contribution to the Paper	Fieldwork, sample collection and drill core inspections Data collection, Data processing, Data curation Conceptualisation, Investigation, Formal Analysis, Visualisation Methodology, Validation Writing original draft, editing and review		
Overall percentage (%)	75%		
Certification:	This paper reports on original research I conducted during the period of my Higher Degree by Research candidature and is not subject to any obligations or contractual agreements with a third party that would constrain its inclusion in this thesis. I am the primary author of this paper.		
Signature		Date	6/10/2020

Co-Author Contributions

By signing the Statement of Authorship, each author certifies that:

i. the candidate's stated contribution to the publication is accurate (as detailed above);

ii. permission is granted for the candidate in include the publication in the thesis; and

iii. the sum of all co-author contributions is equal to 100% less the candidate's stated contribution.

Name of Co-Author	Justin Payne		
Contribution to the Paper	Conceptualisation, Investigation, Validation, Supervision Writing, Editing and review Fieldwork Funding acquisition		
Signature		Date	

Name of Co-Author	Karin Barovich

20/11/2020

Contribution to the Paper	Conceptualisation, Investigation, Visualisation, Validation Supervision Writing, editing and review		
Signature		Date	15/11/2020

Name of Co-Author	Anthony Reid		
Contribution to the Paper	Validation Supervision Writing - Editing and review Fieldwork		
Signature		Date	16/11/2020

Name of Co-Author	Elizabeth Jagodzinski		
Contribution to the Paper	Manuscript editing Fieldwork		
Signature		Date	15/11/2020

Name of Co-Author	Stacey Curtis		
Contribution to the Paper	Data collection, Data Curation Writing - Editing and review		
Signature		Date	15/11/2020

Name of Co-Author	Jesse Hill		
Contribution to the Paper	Data collection, Data Curation Writing - Editing and review		
Signature		Date	23/11/2020

ABSTRACT
The Gawler Range Volcanics (GRV) form a Mesoproterozoic felsic large igneous province (LIP) extruded between 1593.61 and 1586.39 Ma. A revised detailed stratigraphy and regional correlation between units of the GRV provide an opportunity to study temporal changes in geochemistry, isotope geochemistry and magmatic temperatures during the 7 Myr duration of this magmatic event. Formation of the Gawler felsic LIP involved a mantle plume and mafic underplating underneath a metasomatised subcontinental lithospheric mantle (SCLM). Minor extrusive basalt to andesite rocks show the evolution of mantle composition during the initial stages of LIP formation (ca. 1593–1590 Ma). All basalt to andesite units are consistent with a subduction modified SCLM mantle origin, characterised by high Th/Nb ratios and variable $\varepsilon_{Nd(i)}$ values. The earliest basaltic magmatism has low Nb/Yb ratios, low $(La/Yb)_N$, and high $\varepsilon_{Nd(i)}$, representing a relatively depleted region from within the metasomatised SCLM. The more depleted composition and higher volume of this magmatism is consistent with early plume-head driven melts. These characteristics are indicative of an E-MORB-like source in SCLM. Subsequent basaltic magmatism shows increasing enrichment in the source, evidenced by increasing Nb/Yb and Th/Nb ratios and decreasing $\varepsilon_{Nd(i)}$, possibly related to longer crustal residence times. The final stage of basaltic magmatism is marked by a different isotopically juvenile E-MORB-like SCLM source characterised by lower Th/Nb ratios, possibly representing a rejuvenation of different mantle plume source composition entrained in the SCLM-derived melts.

Dacite to rhyolite rocks record fractional crystallisation processes related to basaltic units and the behaviour of crustal melting above a mantle plume. The older dacite to rhyolite units extruded between 1593.61 and 1588.47 Ma represent compositionally heterogeneous rocks that correlate temporally with the basaltic to andesitic units. The Nd isotopic record suggests an increasing SCLM component from the early to late stages of felsic magmatism, and occurred synchronously with increasing enrichment in basaltic magmas. The younger dacite to rhyolite units (1586.66–1586.39 Ma) have no associated mafic component, are geochemically and isotopically homogeneous and represent large volumes of felsic lava extruded in 300 Kyr. The final stage of felsic magmatism (1586.39 Ma) is marked by crystal-rich dacite, decreasing $\varepsilon_{Nd(i)}$ and lower Ti-in-zircon temperatures which together are interpreted to represent the waning phase of mantle plume and increasing crustal melting in the LIP. Paucity of mafic rocks after ca. 1588 Ma is likely the result of a "wet felsic blanket" inhibiting basaltic magmas from reaching the surface, although the thermal influence of a mafic underplate enabled the large-scale crustal melting.

The two phases of volcanism can be linked to changes in the melting regime, melt flux and plumbing systems, related to increasing and then decreasing thermal and compositional contribution of a mantle plume. This study provides a rare example of temporally constrained geochemical and isotopic compositions in mafic and felsic volcanism in a LIP. Our detailed petrogenetic work best demonstrates the generation of the Gawler LIP occurred in an intracontinental, plume setting analogous to a mafic LIP model.

INTRODUCTION
Silicic large igneous provinces (SLIPs) represent the silicic end-member of large igneous provinces (Bryan 2007). They are crustally-derived, large volume (>100,000 km^3) silicic-dominant (>65 wt% SiO_2) rocks with a significant aerial extent (>100,000 km^2), and eruption lifetimes not exceeding 50 Myr

(Bryan *et al.* 2002, Ewart *et al.* 2004, Bryan 2007). SLIPs may form in response to lithospheric extension associated with mantle or asthenospheric upwelling in intraplate tectonic settings, along palaeo- and active continental margins or in back-arc environments (e.g. Whitsunday Province, eastern Australia, Chon Aike SLIP of Patagonia and the Yellowstone-Snake River Plain SLIP; Bryan *et al.* 2002, Ernst 2014, Liu *et al.* 2019). Rapid large volume silicic magmas in SLIPs are associated with the sustained intrusion of hydrous melts into lower crust (Bryan *et al.* 2002, Pankhurst *et al.* 2011a, Ernst 2014). Intraplate and back-arc SLIPs occur exclusively in the Phanerozoic (Bryan *et al.* 2002, Pankhurst *et al.* 2011a). SLIPs are typically characterised by igneous pulses of short 1–5 Myr duration during which a large proportion of the total silicic igneous volume is emplaced (Bryan 2007).

Large volume silicic magmas as part of mafic large igneous provinces (LIPs) have occurred with remarkable frequency throughout the geological record from the Proterozoic (ca. 2.4 Ga) until the present (e.g. Pankhurst *et al.* 2011a and references therein). Large volume silicic magmatism in mafic LIPs is associated with high thermal input from hot underlying mantle as a plume e.g. 1.1 Ga Keweenan LIP, 132 Ma Parana-Etendeka LIP and 30 Ma Yemen-Ethiopia LIP (Ewart *et al.* 1998, Ayalew and Gibson 2009, Pankhurst *et al.* 2011a). The silicic magmas in mafic LIPs are high temperature, low aspect ratio rhyolites with high Ga/Al ratios, are F-rich and have low water contents (e.g. Pankhurst *et al.* 2011a). Silicic magmas in mafic LIPs are formed by processes of differentiation of a mafic parent involving fractional crystallisation and assimilation, are sourced from the convecting mantle, the lithosphere or both (Ewart *et al.* 1998).

Analysis of lithospheric melting above a mantle plume provides insight into melting dynamics, magma plumbing systems, compositional evolution of the source magma reservoirs and relative contributions and compositions of mantle and crustal components (Kirstein *et al.* 2000, Hoernle *et al.* 2015, Liu *et al.* 2019). Mantle components discussed in relation to LIP formation include plume, subcontinental lithospheric mantle (SCLM) and depleted mantle (e.g. Hawkesworth *et al.* 2000, Kirstein *et al.* 2000, Ewart *et al.* 2004). Mafic magmas associated with LIPs can therefore track the composition of mantle material entrained in the plume (e.g. Hoernle *et al.* 2015), while felsic magmas in LIPs provide insight into crustal melting dynamics above a plume (e.g. Liu *et al.* 2019).

Proterozoic southern Australia hosts a significant Mesoproterozoic silicic event named the Gawler SLIP. It contains a minimum volume of 70 000 km^3 erupted magma (McPhie *et al.* 2008). The SLIP extends under younger sediments and into the once adjacent Curnamona Province (Fig. 1), giving a total minimum extent of approximately 108 000 km^2 (McPhie *et al.* 2008, Wade *et al.* 2012). An estimated volume of 110 000 km^3 of magma (Allen *et al.* 2003, McPhie *et al.* 2008, Pankhurst *et al.* 2011b, Wade *et al.* 2012) was erupted in the once-contiguous province in approximately 7 Myr. (Jagodzinski *et al.* in prep.). Synchronous extrusive mafic rocks and broadly synchronous intrusive felsic and mafic rocks (Blissett *et al.* 1993, Allen *et al.* 2003, Allen *et al.* 2008) add an additional 30 000 km^3 of magma to the SLIP (Flint 1993, McPhie *et al.* 2008, Wade *et al.* 2019). The bulk of the felsic magma was erupted in ca. 300 kyr, representing >30 000 km^3 preserved felsic lava (Stewart 1994, Pankhurst *et al.* 2011b). At least three individual felsic units each represent up to 4000 km^3 of magma (Allen *et al.* 2003, Allen *et al.* 2008). The physio-chemical properties of the felsic magma, including high halogen content, high temperature and low viscosity, allowed such rapid and large volume emplacement (Pankhurst *et al.* 2011b). These features, in addition to differences in tectonic setting,

magma geochemical characteristics, magmatic temperatures and association with a mafic component (e.g. Giles 1988, Blissett *et al.* 1993), suggest the Gawler SLIP sits outside of the conceptual model established for SLIPs and is more akin to mafic LIP models with voluminous silicic magmatism (Pankhurst *et al.* 2011a, Pankhurst *et al.* 2011b). For this reason we adopt the nomenclature introduced by Pankhurst *et al.* (2011a) and herein refer to the province as the Gawler LIP.

The units comprising the Gawler LIP are the Gawler Range Volcanics (GRV) on the Gawler Craton (Fig. 1 and Fig. 2) and the Benagerie Volcanic Suite in the adjacent Curnamona Province (Fig. 1; Wade *et al.* 2012). The GRV are subdivided into a lower sequence

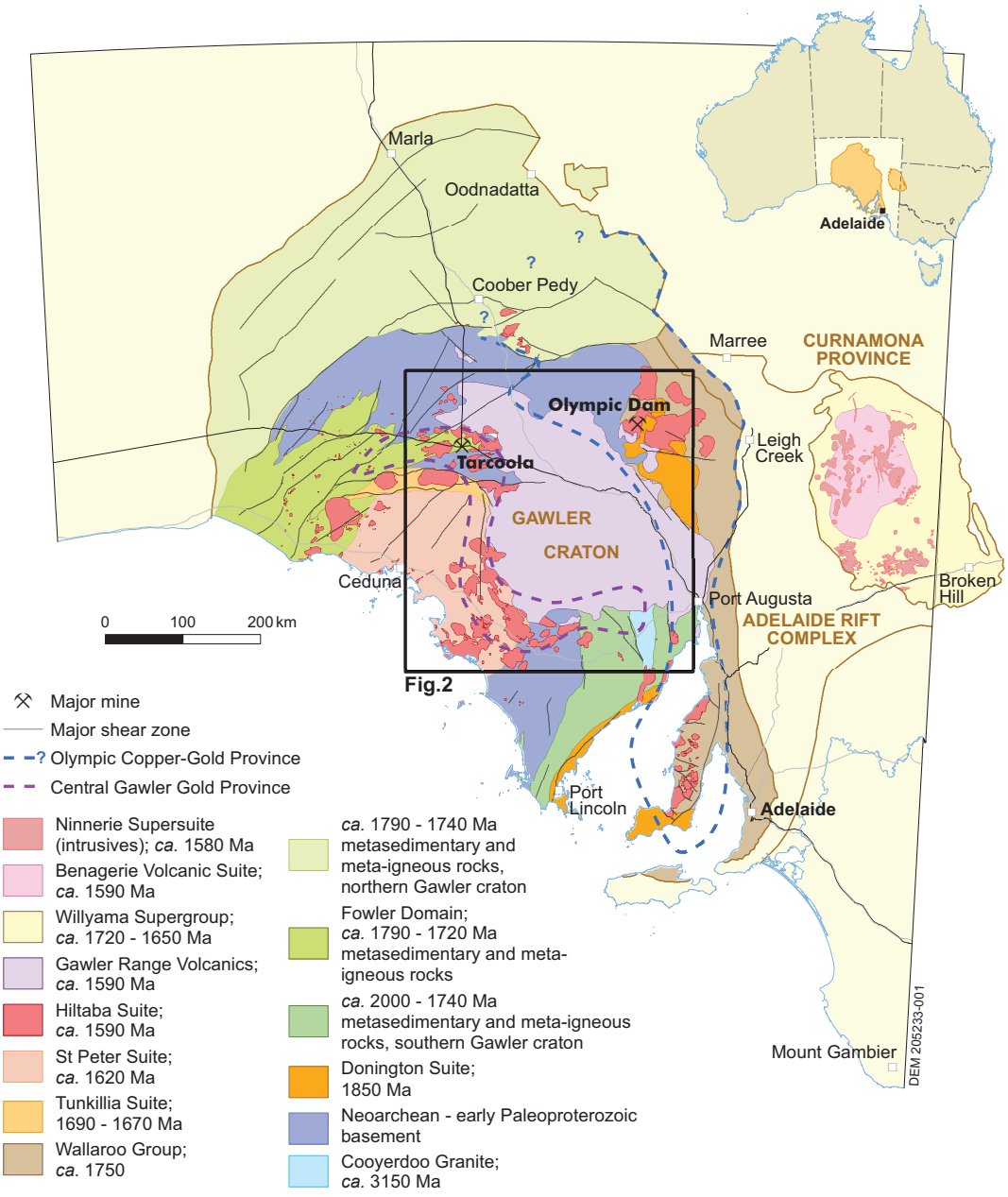

Figure 1: Simplified solid geology for the Gawler Craton, highlighting the spatial extent of the Gawler Range Volcanics within the Gawler Craton. The inset marked refers to Figure 2.

and upper sequence (Fig. 3), representing different styles of eruptive volcanism (Blissett *et al.* 1993, Allen *et al.* 2003, Allen *et al.* 2008). New high precision U-Pb zircon geochronology has helped refine the temporal evolution for the GRV, indicating the sequence erupted from ca. 1594–1586 Ma (Cherry *et al.* 2018, Courtney-Davies *et al.* 2019, Jagodzinski *et al.* in prep.). A comprehensive description of the geochronology is documented in Jagodzinski *et al.* (in prep.). This companion study has distinguished the lower (1593.61–1588.47 Ma) from the upper (1586.66–1586.39 Ma) sequences. In this contribution, we present new whole rock geochemical and Sm-Nd isotopic data for felsic and mafic extrusive rocks, combined with pre-existing data, to demonstrate the petrogenesis of the Gawler LIP can be attributed to upwelling and underplating of hot mantle in the form of a mantle plume. This model is analogous to a mafic LIP in a plume setting, in contrast to previous tectonic models involving subduction, slab-roll back and delamination.

GEOLOGICAL BACKGROUND AND UNIT DESCRIPTIONS

The oldest crystalline basement in the Gawler Craton includes ca. 3150 Ma granite and granite gneiss (Fraser *et al.* 2010). Subduction-related magmatism and sedimentation occurred during the Neoarchean (2520–2440 Ma), disrupted by an orogenic event ca. 2440–2410 Ma (Swain *et al.* 2005, Reid *et al.* 2009). Palaeoproterozoic sequences are dominated by metasedimentary rocks, and represent craton-wide sedimentation that occurred from approximately 2000–1650 Ma, disrupted by two orogenic events at ca. 1850 Ma in the southeast of the craton and a craton-wide event at 1750–1700 Ma (Payne *et al.* 2006, Hand *et al.* 2007, Howard *et al.* 2011a, Howard *et al.* 2011b, Szpunar *et al.* 2011). Post-tectonic magmatism (1690–1670 Ma; Payne *et al.* 2010) occurred in the central and western Gawler Craton, followed by a period of localised sedimentation and magmatism in the southern and central Gawler Craton ca. 1680–1650 Ma (Fanning *et al.* 2007 and references therein). In the late Palaeoproterozoic felsic volcanism around 1630 Ma and the intrusion of subduction-related gabbros and granites between 1635–1608 Ma occurred in the southwest Gawler Craton (Swain *et al.* 2008, Symington *et al.* 2014, Skirrow *et al.* 2018, Reid *et al.* 2019). During the Mesoproterozoic, contemporaneous mafic and felsic lavas known as the Gawler Range Volcanics (GRV) were extruded, accompanied by intrusive magmatism and local sedimentation (Daly 1993, Flint *et al.* 1993, Bull *et al.* 2015, McPhie *et al.* 2016, Curtis *et al.* 2018).

Basaltic to rhyolitic lavas of the GRV are subdivided into a lower and an upper phase (Fig. 2 and Fig. 3; Blissett *et al.* 1993, Allen *et al.* 2003, Allen *et al.* 2008). The lower phase represents a developmental period erupted from 1593.61–1588.47 Ma (Jagodzinski *et al.* in prep.). It comprises lithologically variable rocks from basaltic to rhyolitic assemblages, pyroclastic, volcaniclastic and explosive volcanic facies (Blissett *et al.* 1993, Allen *et al.* 2003, Allen *et al.* 2008). Lower GRV units are preserved in outcrop at the southern margin of the GRV, Roopena, Myall Creek, Kokatha, Glyde Hill and Tarcoola-Kingoonya, and in the subsurface (drill hole DDH RED 2) on the Stuart Shelf (Fig. 2 and Fig. 3; Giles 1980, Blissett *et al.* 1993, Stewart 1994, Allen *et al.* 2003, Ferris 2003, Allen *et al.* 2008, Agangi 2011, Huang *et al.* 2016, Curtis *et al.* 2018). Localised sedimentation accompanied mafic volcanism in these areas (Bull *et al.* 2015, McPhie *et al.* 2016, Curtis *et al.* 2018). Figure 3b provides simplified stratigraphic sections for each of the Lower GRV locations.

Lower GRV felsic rocks along the southern margin of the GRV, Roopena and Myall Creek area are largely felsic lavas and ignimbrites including porphyritic dacite that is locally amygdaloidal, porphyritic crystal-rich pyroclastic rocks (a tuff or ignimbrite), feldspar-phyric

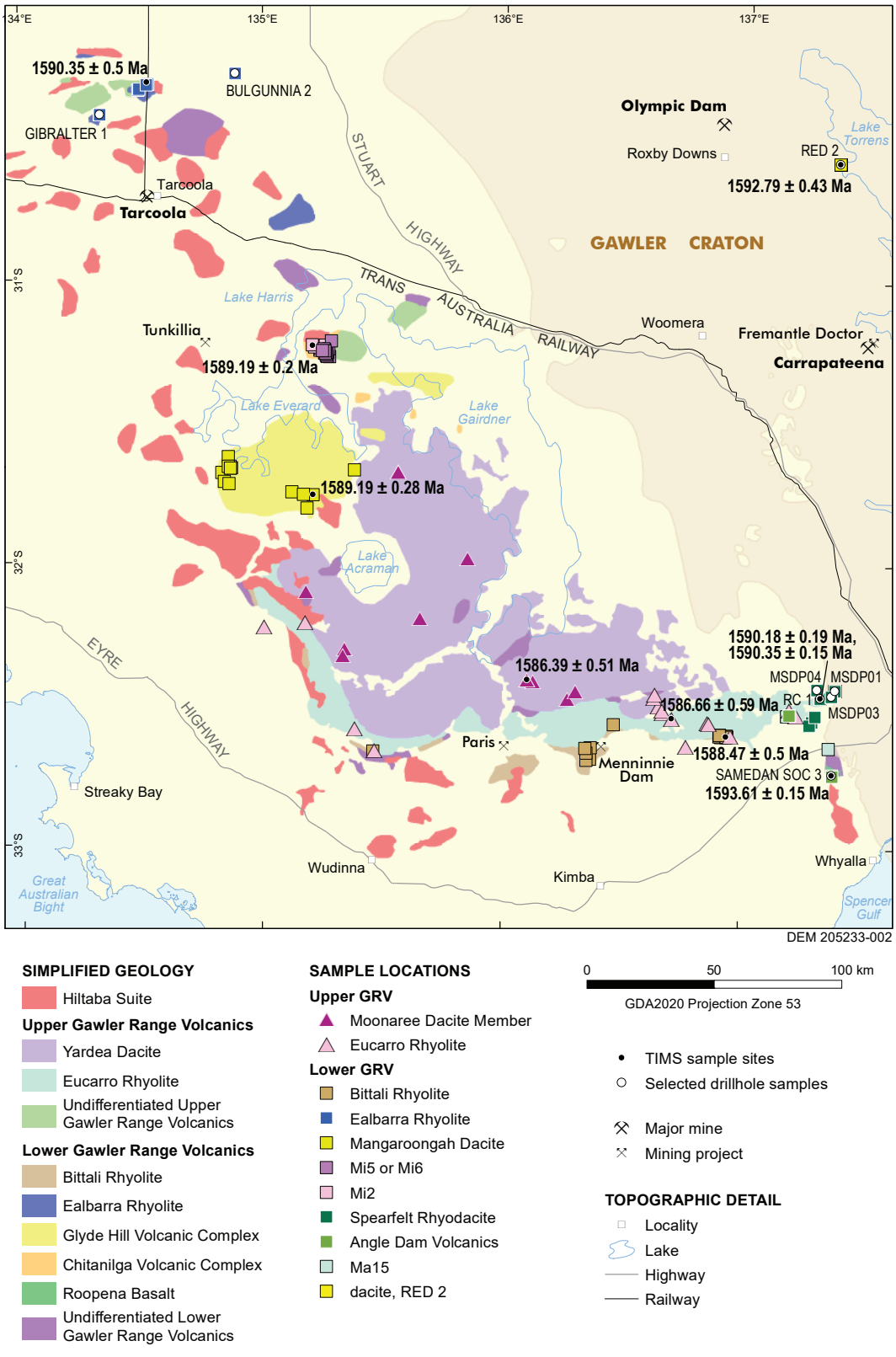

Figure 2: Simplified geological map of the Gawler Range Volcanics showing the distribution of volcanic units and sample locations used in this study. Ages for dated units are labelled.

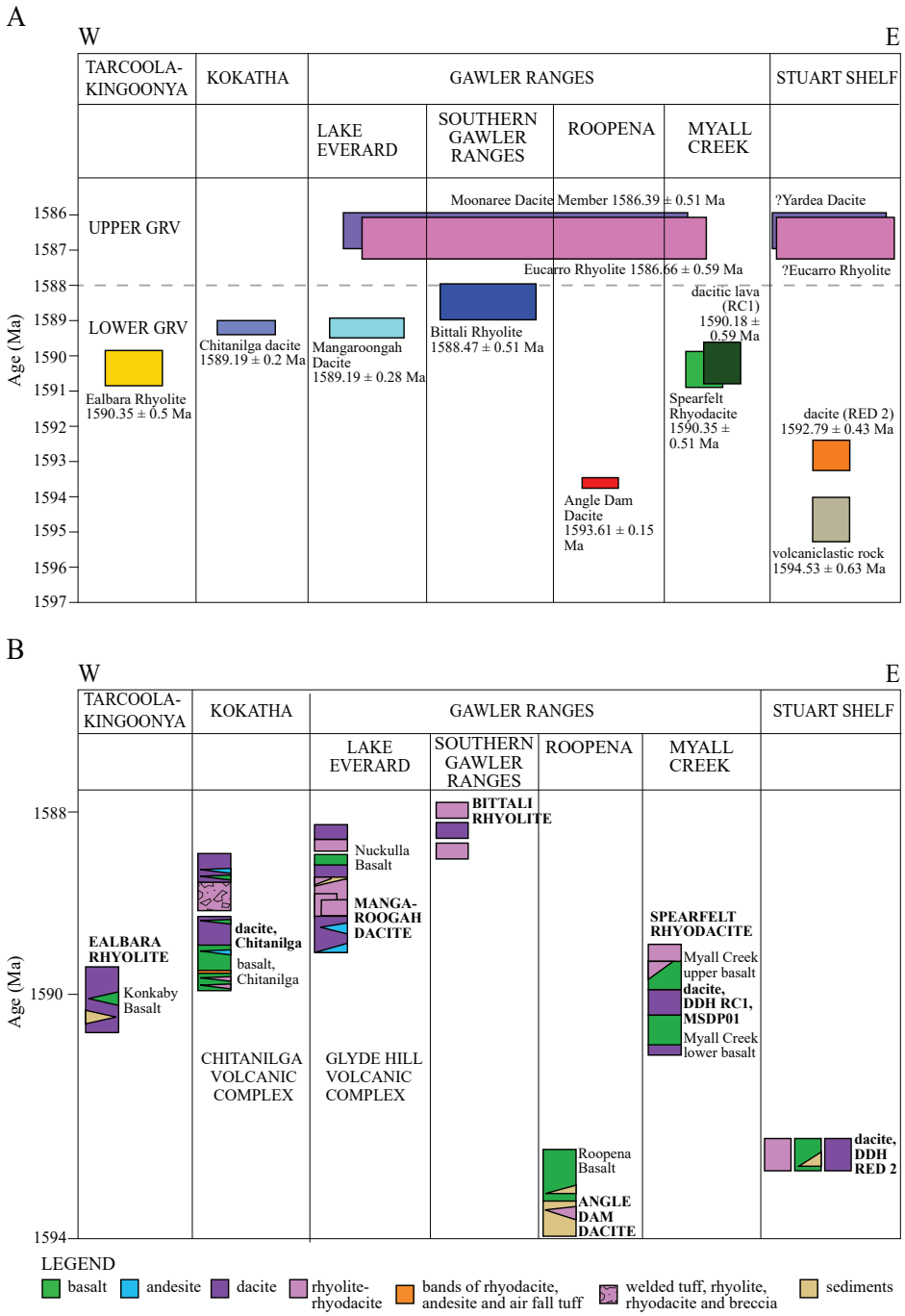

Figure 3: A) Time space plot of the Gawler Range Volcanics (GRV) felsic units used in this study. Height of respective boxes represent the age uncertainty for each unit. Width of respective boxes represent approximate spatial extent of each unit, highlighting the large extent of the Upper GRV units in comparison to the Lower GRV units; B) Simplified stratigraphic relationships for each of the volcanic centres within the Lower GRV, illustrating the relationship between the dated felsic units and the basalts in the sequence used in this study. In the Myall Creek area, lower basalt, is found in drill holes MSDP01 and MDSO04, upper basalt is found in drill holes MSDP01, MSDP03, MSDP04, RC1 and SAMEDON SOC 3. Stratigraphic sequences at Glyde Hill Volcanic Complex and Chitanilga Volcanic Complex are simplified from Figure 2 of Allen et al. (2008).

and quartz-phyric rhyodacite and flow banded rhyolite (Stewart 1994, McAvaney *et al.* 2016). At Roopena and Myall Creek, a syn-volcanic sedimentary basin (the Roopena Basin) containing the Angle Dam Dacite, several basaltic lava flows and immature sediments (Fig. 3b) is preserved in outcrop and in the subsurface (Curtis *et al.* 2018). In the Roopena area, the basaltic lava flows are part of the Roopena Basalt. Two basaltic units are found in the Myall Creek area, which include a lower basalt (drill holes RC1, MSDP01 and MSDP04), and an upper basalt (drillholes MSDP01, -03 and -04, RC1 and SAMEDAN SOC 6). They are herein referred to as Myall Creek lower basalt and Myall Creek upper basalt, respectively. In drill holes RC1 and MSDP01, the Myall Creek lower and upper basalt are separated by a dacite, herein referred to as RC1 dacite. The Spearfelt Rhyodacite overlies the Myall Creek upper basalt in drill holes RC1, MSDO01, -03 and -04 (Figs. 2 and 3b).

Lower GRV rhyolite to rhyodacite in the Kokatha area comprises six mappable units that include welded tuff, air fall tuff and breccia (Blissett *et al.* 1993). The Chitanilga Volcanic Complex at Kokatha also includes amygdaloidal basalt to andesite at the base and in the mid-upper level of the sequence (Fig. 3b). Successions at Glyde Hill Volcanic Complex, Lake Everard, grade from minor basaltic andesite to dacite and rhyolite, representing several lava flows (Fig. 3b). Felsic units include porphyritic and aphyric, massive and partly flow-banded dacite separated by epiclastic and pyroclastic layers, dacite containing hyaloclastite and peperite blocks, porphyritic and flow banded rhyolite and minor welded rhyolitic ignimbrite (Giles 1980, Ferris 2003). Rhyolite from the Tarcoola-Kingoonya area includes porphyritic rhyolite lava with in situ peperitic and porphyritic rhyolite breccias, spherulitic devitrification textures and complex flow banding (Beinke *et al.* 2012). The rhyolite is interlayered with porphyritic to amygdaloidal andesite-basalt and sedimentary rocks (Blissett *et al.* 1993; Fig. 3b). Fine-grained, porphyritic dacite is found in DDH RED 2 on the Stuart Shelf, herein referred to as RED 2 dacite.

The Upper GRV represents voluminous high-silica volcanism comprised of two individual units, the Eucarro Rhyolite and Yardea Dacite (Fig. 2 and Fig. 3; Stewart 1994, Allen and McPhie 2002, Allen *et al.* 2008). Volumes of lavas within the Eucarro Rhyolite and Yardea Dacite are interpreted to be 1000–4000 km^3 each and erupted in a 0.3 Myr time period (Jagodzinski *et al.* in prep.). The Eucarro Rhyolite is approximately 300 m thick with a strike distance of 225 km, and its north-south extent ranges from 4.5–14 km (Allen *et al.* 2003). It includes black-brown plagioclase rhyolite along the southern contacts, red-pink columnar jointed rhyolite in the central regions and vesicular rhyolite mingled with quartz-rich rhyolite on the northern margins (Allen *et al.* 2003). It is crystal-poor but relatively quartz-rich compared with the Yardea Dacite.
The uppermost unit of the Yardea Dacite is the Moonaree Dacite Member (Allen *et al.* 2003). It has an east-west spatial extent of 160 km and north-south extent of 100 km, with an exposed thickness of ~250 m (Allen *et al.* 2003). The Moonaree Dacite Member is either red dacite with a granophyric groundmass or brown, silica-rich quartz dacite, both of which are columnar jointed (Allen *et al.* 2003). The dacite is crystal-rich, richer in ferromagnesian phases and less silicic than the Eucarro Rhyolite (Allen *et al.* 2003).

ANALYTICAL METHODS

Thirty-one new samples collected from outcrop and drill core were analysed for whole-rock major and trace elements. Samples with the prefix '884-' and 'Y-' were collected by Stewart (1994). A subset of these were re-analysed for whole rock major and trace elements. Representative whole-rock geochemical anal-

yses are listed in Table 1 and the complete dataset is in [dataset Wade et al. 2020]. Additional samples are compiled from the Geological Survey of South Australia database (SARIG https://map.sarig.sa.gov.au/), Agangi (2011), Giles (1980) and Fricke (2005). Fourteen newly collected rhyolitic samples and six basaltic samples were analysed for whole rock Sm-Nd isotope geochemistry and are listed in Table 2.

New samples had all weathered material removed before being crushed, split and milled into a fine powder, with a quartz barren wash used between samples. Geochemical analyses were performed at Bureau Veritas minerals laboratories in Perth (https://www.bureauveritas.com.au/home/about-us/our-business/commodities/exploration-and-mineral-labs). The samples were cast using a 66:34 flux with 4% lithium nitrate added to form a glass bead. Major elements and chlorine, were analysed using X-Ray Fluorescence (XRF) spectrometry. Trace elements were determined by laser ablation-inductively coupled plasma-mass spectrometry (LA-ICP-MS) and Au, Pt and Pd were analysed using fire assay ICP-MS. FeO was determined volumetrically and fluorine was determined using specific ion electrode.
Sm-Nd analyses were undertaken at the University of Adelaide as per the method of Wade *et al.* (2019). Samples were loaded on 99.99% Re (standard grade) filaments. Sm and Nd isotopic abundance ratio measurements were collected on an Isotopx Phoenix thermal ionization mass spectrometer (TIMS) in a three-step dynamic hopping routine for Nd and a static routine for Sm. Nd isotopic ratio measurements are corrected for fractionation using $^{146}Nd/^{144}Nd = 0.7219$ and an exponential mass bias correction. Measured analytical blanks are on the order of 100 pg for Nd and 50 pg for Sm and are insignificant in this study. Average $^{143}Nd/^{144}Nd$ ratios for the G2 standard granite material (granite, Rhode Island) is 0.512216 ± 0.000002 (2σ, n= 3, slightly outside of uncertainty of the GeoRem Preferred value of 0.512233 ± 0.000010 (Jochum *et al.* 2005). Calculated concentrations for Nd and Sm in G2 are 53.7–54.6 ppm and 7.2–7.9 ppm, respectively, and are comparable to the recommended United States Geological Survey values of 55 ± 6 ppm and 7.2 ± 0.7 ppm and the GeoRem preferred values of 53.81 ± 0.67 ppm and 7.19 ± 0.1 ppm, respectively. $^{143}Nd/^{144}Nd$ ratios for the BCR-2 standard (basalt, Columbia River) is 0.512622 ± 0.000002 (n = 1), within uncertainty of the GeoRem preferred value (0.512635 ± 0.000029). Calculated concentrations for Nd and Sm in BCR-2 are 29.6 ppm and 6.7 ppm, respectively, and are comparable to the recommended United States Geological Survey values of 28 ± 2 ppm and 6.7 ± 0.3 ppm and the GeoRem preferred values of 28.26 ± 0.37 ppm and 6.547 ± 0.047 ppm, respectively.

RESULTS

Geochemistry

Major and minor elements

Lower GRV rocks range from basalt to rhyolite (Fig. 4a). On Fe* (FeOt/(FeOt/MgO) and modified alkali lime index (MALI) plots basalt to andesite rocks are largely magnesian and predominantly alkali-calcic to calc-alkalic (Fig. 4b and 4c respectively). Lower GRV dacite to rhyolite rocks are ferroan, with the exception of magnesian samples from the Mangaroongah Dacite, RC1 dacite and Spearfelt Rhyodacite (Fig. 4b). Lower GRV dacites and rhyolites are alkali to calcic in the MALI plot (Fig. 4c) and peraluminous (Fig. 4d). Upper GRV units are trachydacites to rhyolites, predominantly ferroan, alkali-calcic and peraluminous to weakly metaluminous (Fig. 4).

Lower GRV Roopena Basalt and Myall Creek lower and upper basalt have SiO_2 contents between 41.4 and 57.5 wt% SiO_2, moderate MgO contents (3.2–9.8 wt%) and high TiO_2 contents (Fig. 5). Samples from Chitanilga, Nuckulla and Konkaby have relatively high-

Table 1: Representative whole rock geochemical data for the Gawler Range Volcanics

Sample	884Bi5	2721825	884T30	18-TAR-07	2721839	884GH10	884GH5	2746487	884-K10	2729186	2729189
Lithology	rhyolite	rhyolite	rhyolite	rhyolite	dacite	dacite	dacite	rhyolite	rhyolite	dacite	dacite
Group	LGRV	LGRV	LGRV	LGRV	LGRV	LGRV	LGRV	LGRV	LGRV	LGRV	LGRV
Map Unit	Bittali Rhyolite	Bittali Rhyolite	Ealbara Rhyolite	Ealbara Rhyolite	Mangaroongah Dacite	Mangaroongah Dacite	Mangaroongah Dacite	Dacite, Chitanilga	Dacite, Chitanilga	RED 2 dacite	RED 2 dacite
Major elements (wt %)											
SiO_2	72.65	74.90	73.74	75.22	64.91	64.70	58.70	72.75	72.3	67.93	64.73
TiO_2	0.20	0.15	0.22	0.23	0.92	0.91	1.20	0.27	0.38	0.72	0.82
Al_2O_3	13.20	13.20	12.78	13.09	14.58	14.47	14.97	14.00	13.4	14.79	14.41
Fe_2O_3T	1.55	2.18	2.22	1.83	5.42	5.06	8.01	1.96	2.84	4.53	6.32
MnO	0.05	0.15	0.07	0.03	0.15	0.16	0.16	0.03	0.05	0.05	0.07
MgO	0.34	0.18	0.17	0.13	2.07	1.91	2.90	0.36	0.2	0.91	1.33
CaO	1.54	0.12	0.76	0.15	1.14	1.91	3.90	1.66	0.47	0.91	1.00
Na_2O	3.04	3.34	3.55	3.32	3.80	3.83	3.71	4.01	4.37	3.25	2.75
K_2O	5.40	5.03	5.27	5.51	4.65	4.83	3.81	4.22	5.08	5.60	6.79
P_2O_5	0.06	0.03	0.03	0.04	0.35	0.31	0.46	0.09	0.048	0.16	0.27
FeO	0.43	-0.10	1.18	0.74	1.99	2.64	3.83	0.65	0.33	1.77	2.47
LOI	1.92	0.97	0.83	0.56	1.67	1.30	1.80	0.55	0.55	1.18	1.40
Total	100.38	100.14	100.82	100.86	101.65	102.02	103.45	100.55	100.02	101.80	102.36
Trace elements (ppm)											
Sc	3.70	3.70	5.40	5.90	15.80	15.60	20.60	2.40	9.5	11.90	12.60
V	15.30	5.80	2.40	2.40	74.80	61.30	140.00	26.40	2.6	26.40	50.10
Cr	4	7	5	11	11	7	15	7	1	9	5
Co	77.80	13.80	76.80	41.30	24.50	35.60	40.30	41	75.4	25.30	27.80
Ni	4	6	8	10	14	12	24	6	4	12	4
Cu	4	2	16	10	8	20	26	8	-2	78	146
Zn	80	40	95	115	115	110	90	45	50	40	40
Ga	18.40	21.00	22.60	24.10	20.60	19.70	19.50	19.40	18.2	20.80	20.30
Rb	154	180	228	234	143	144	119	150	166	251	283
Sr	174	131	69.70	71.80	325	283	496	340	112	106	96.40
Y	19.20	21.50	56.50	57.00	44.60	44.10	40.60	16.00	43.2	62.50	53.60
Zr	167	139	396	421	416	508	314	151	318	438	364
Nb	11.20	14.00	24.50	24.60	15.90	15.70	12.20	12.20	15.8	26.60	23.10
Mo	1.20	1.00	2.20	2.20	0.40	0.40	0.60	1.00	0.6	2.00	4.00
Sn	2.00	2.00	4.00	4.00	2.40	2.60	2.40	1.40	3.2	4.80	7.40
Cs	1.09	1.12	1.96	1.74	4.91	1.94	3.57	2.95	1.26	1.48	1.02
Ba	646	668	276	305	2360	2990	1560	1020	1710	1080	1300
La	74.30	58	96.40	96.20	64.10	67.80	53.10	46.70	68.1	105	121
Ce	145	114	187	189	132	139	113	85.40	133	197	205
Pr	16.50	12.80	21	21.50	16	16.60	13.40	9.60	16.2	22	21.70
Nd	55.10	43.20	75	76.60	62.30	64.40	54.50	31.80	58.6	78.40	73.80
Sm	9.68	8.10	13.70	13.40	12.50	12.50	11.20	5.28	11	14.90	13.50
Eu	1.27	0.95	0.76	0.90	3.17	3.48	2.70	0.93	2.34	2.79	2.49
Gd	6.30	5.40	10.50	10.80	10.10	10.20	9.25	3.61	8.76	12.50	11.20
Tb	0.83	0.75	1.69	1.74	1.53	1.49	1.40	0.54	1.37	1.99	1.74
Dy	4.05	3.94	10.30	10.40	8.63	8.35	7.67	2.93	7.83	11.50	10.20
Ho	0.75	0.76	2.18	2.18	1.76	1.69	1.55	0.58	1.57	2.42	2.14
Er	1.92	2.14	6.30	6.41	4.90	4.82	4.34	1.69	4.57	7.28	5.71
Tm	0.28	0.27	0.95	0.94	0.69	0.67	0.62	0.27	0.67	1.08	0.84
Yb	1.70	1.91	6.28	6.48	4.29	4.25	3.92	1.78	4.54	6.94	5.26
Lu	0.24	0.27	0.92	0.90	0.63	0.63	0.57	0.27	0.64	1.03	0.81
Hf	4.99	4.72	11.20	11.70	10.50	12.20	7.95	4.44	8.98	12.10	10.00
Ta	1.05	1.12	1.94	1.72	1.00	1.00	0.86	1.02	1.29	2.15	1.94
Pb	23	16	42	54	20	46	28	29	20	12	10
Th	26.80	31.80	28.40	27.50	14.90	14.40	11.00	17.00	23.2	43.60	38.20
U	4.48	5.68	5.55	5.04	2.60	2.46	1.78	3.79	5.1	11.20	13.30
F	650	700	1600	300	800	1100	1100	450	200	500	2300
Cl	180							40	90		
Ga/Al*10000	2.63	3.01	3.34	3.48	2.67	2.57	2.46	2.62	2.57	2.66	2.66
Eu/Eu*	0.50	0.44	0.19	0.23	0.86	0.94	0.81	0.65	0.73	0.62	0.62
$(La/Yb)_{CN}$	31.35	21.78	11.01	10.65	10.72	11.44	9.72	18.82	10.76	10.85	16.50

er SiO_2 values (50.1–62.4 wt% SiO_2) and a broader range of major and minor element compositions (e.g. Chitanilga samples, MgO = 1.8–11.8 wt% and P_2O_5 = 0.2–1.4 wt%, Fig. 5). Chitanilga samples have both high TiO_2 (>1.5 wt%) and low TiO_2 (<1.2 wt%) samples, whereas Nuckulla and Konkaby basalts are low TiO_2 (<1.2 wt% TiO_2).

Lower GRV dacite to rhyolite samples have SiO_2 between 60 and 79.5 wt%, Al_2O_3 between 8.4–16.1 wt% and TiO_2 between 0.1–1.3 wt% (Fig. 5 and Table 1). Upper GRV dacites and rhyolites have narrower major element ranges e.g. SiO_2 = 65.9–73.3 wt%, Al_2O_3 = 12.5–14.8 wt% and TiO_2 = 0.3–0.8 wt%; Fig. 5 and Table 1).

Trace element variation

Basalt to andesite Lower GRV samples display a large variation in Zr, Nb and Th contents (Fig. 6). Rocks from Roopena Basalt and the lower and upper basalt from Myall Creek tend to cluster around the lower end of Zr, Nb, U and Th concentrations, although a few samples display relative enrichments in these

Table 1 cont: Representatite whole-rock geochemical data for the Gawler Range Volcanics

Sample	884-T6	884-T18	GCT86	GCT87	GCT13	GCT13A	884Eu2	2721816	2174053	2721820	2721829
Lithology	basalt	basalt	basalt	basalt	basalt	basalt	rhyolite	rhyolite	dacite	dacite	dacite
Group	LGRV	LGRV	LGRV	LGRV	LGRV	LGRV	UGRV	UGRV	UGRV	UGRV	UGRV
Map Unit	Konkaby Basalt	Konkaby Basalt	Konkaby Basalt	Konkaby Basalt	Nuckulla Basalt	Nuckulla Basalt	Eucarro Rhyolite	Eucarro Rhyolite	Moonaree Dacite	Moonaree Dacite	Moonaree Dacite
Major elements (wt%)											
SiO_2	54.43	53.26	60.10	61.40	50.60	50.90	71.09	71.93	68.10	66.61	68.54
TiO_2	0.97	0.76	0.80	0.71	1.16	1.15	0.42	0.39	0.66	0.80	0.60
Al_2O_3	16.5	14.3	17.60	17.10	16.80	16.80	13.24	13.36	14.29	13.84	13.81
Fe_2O_3T	9.14	9.06	6.37	4.58	9.92	9.92	3.77	3.52	4.77	5.67	4.40
MnO	0.15	0.19	0.11	0.09	0.16	0.16	0.09	0.03	0.10	0.14	0.09
MgO	4.27	6.91	1.63	1.48	5.06	5.09	0.30	0.17	0.75	1.25	1.30
CaO	8.16	8.65	4.53	3.99	7.20	7.22	1.33	0.17	2.31	1.93	0.86
Na_2O	3.1	2.45	2.85	3.96	3.45	3.47	3.18	2.64	3.45	3.19	3.24
K_2O	2.21	2.8	3.40	4.24	2.20	2.22	5.73	6.16	4.88	4.86	5.42
P_2O_5	0.421	0.334	0.44	0.31	0.24	0.22	0.07	0.07	0.18	0.23	0.15
FeO	4.11	4.82					1.83	0.46	3.10	3.55	2.50
LOI	0.47	0.87	0.90	0.92	2.61	2.60	0.44	1.31	0.60	1.32	1.30
Total	103.38	103.38	98.73	98.78	99.40	99.75	101.49	100.21	103.19	103.38	102.21
Trace elements (ppm)											
Sc	23	29.4	0.00	0.00	0.00	0.00	8.60	8.00	10.80	13.20	9.70
V	220	182	0.00	0.00	0.00	0.00	5.90	6.20	27.90	38.80	24.20
Cr	20	291	0.00	0.00	50	50	1	7	7	12	8
Co	49.6	63.9	34.50	34	46	46.50	57.10	12.40	22.40	18.70	14.70
Ni	30	66	0.00	7	88	88	4	10	10	14	6
Cu	28	70	16.50	22	120	60	6	18	8	12	8
Zn	80	90	86	78	82	86	95	85	90	105	100
Ga	18.1	16.8	21.50	21	21	20.50	24.80	24.50	22.40	22.30	22.70
Rb	61.6	82.9	135	120	84	84	260	292	214	207	236
Sr	762	707	550	550	460	460	105	117	217	207	129
Y	17.6	18.1	18	20	25.50	25.50	64.20	56.20	51.80	56.80	52.70
Zr	129	132	210	250	170	170	520	540	437	431	443
Nb	6.36	5.82	11.50	16	10	10	26	27	21.10	21.70	21.10
Mo	1	0.6	1.50	2.50	0.90	0.70	2.20	3.00	1.80	2.40	0.60
Sn	1.2	1.2	0.00	0.00	0.00	0.00	4.80	4.40	4.20	3.60	3.80
Cs	2.77	4.17	8.00	3.10	4.20	4.20	3.22	3.93	2.94	2.87	3.47
Ba	911	1040	800	1300	470	470	1340	1490	1560	1420	1470
La	30.1	26.5	35.50	50	28.00	27.50	98.90	49.80	80	84.20	80.70
Ce	61.3	55	64	88	52	52	193	105	154	162	155
Pr	7.73	7.18	8	10.50	7.00	7.00	21.60	11.70	17.60	18.80	17.40
Nd	30.5	28.5	29	36.50	26.50	26.50	80	42.90	63.50	69.80	63.10
Sm	5.72	5.51	5.50	6	6	6	15.20	9.28	12.10	13.50	11.80
Eu	1.57	1.45	1.60	1.80	1.65	1.65	2.39	1.73	2.40	2.50	2.15
Gd	4.5	4.37	4.10	4.40	4.70	4.90	12.80	8.39	9.99	11.50	9.94
Tb	0.65	0.66	0.59	0.65	0.75	0.76	2.06	1.63	1.63	1.82	1.64
Dy	3.56	3.59	3.50	3.70	4.90	4.80	11.80	10.50	9.39	10.60	9.59
Ho	0.66	0.67	0.63	0.68	0.92	0.91	2.57	2.23	2.01	2.14	1.97
Er	1.88	1.9	1.80	2.00	2.60	2.70	7.19	6.60	5.43	6.27	5.71
Tm	0.24	0.27	0.25	0.25	0.35	0.35	1.07	1.02	0.82	0.93	0.85
Yb	1.61	1.64	1.85	2.00	2.60	2.60	6.81	6.42	5.31	5.78	5.51
Lu	0.24	0.25	0.26	0.28	0.35	0.35	1.04	0.98	0.79	0.87	0.84
Hf	3.48	3.5	4.00	5.00	3.00	3.00	13.70	14.40	11.40	11.70	11.90
Ta	0.44	0.42	0.00	0.00	0.00	0.00	2.00	1.92	1.58	1.50	1.52
Pb	11	14	18.50	20.50	8.50	8.50	43	20	37	37	6
Th	4.69	4.05	7.50	14.50	5	5	35	34.50	27.80	28.10	30.10
U	0.96	0.75	1.85	2.90	0.83	0.70	7.64	7.55	5.82	5.75	6.43
F	900	950					1400	700	1300	1200	1200
Cl	120	100									
Ga/Al*10000	2.07	2.22					3.54	3.46	2.96	3.04	3.11
Eu/Eu*	0.95	0.90	1.03	1.07	0.95	0.93	0.52	0.60	0.67	0.61	0.61
$(La/Yb)_{CN}$	13.41	11.59	13.76	17.93	7.72	7.59	10.42	5.56	10.81	10.45	10.51

LGRV: Lower Gawler Range Volcanics; UGRV: Upper Gawler Range Volcanics
LOI: Loss on ignition
$Eu/Eu^* = (Eu/(Sm \times Gd)_{CN}^{0.5}$
CN: Condrite normalised
Normalising values from McDonough and Sun (1995)

elements (Fig. 6). Lower GRV samples from Konkaby Basalt, Chitanilga basaltic andesite and Nuckulla Basalt are far more variable in their trace element compositions, in particular Zr, Nb and Th (Fig. 6).

Significant trace element variation is present in Lower GRV dacite to rhyolite samples (Fig. 6). Mangaroongah Dacite is distinguished from the other Lower GRV felsic units by its high Zr, low U and Th contents (Fig. 6). The Spearfelt and RC1 dacites have high Nb and Th contents, while RED 2 dacite has high U (Fig. 6).

Upper GRV dacite and rhyolite units tend to cluster in their trace element abundances and display less variation compared with Lower GRV felsic units (Fig. 6). The Eucarro Rhyolite has higher Zr, Nb, U and Th than the Moonaree Dacite Member (Fig. 6). Zr, Nb and

Table 2: Sm-Nd isotopic composition for Gawler Range Volcanics samples collected in this study. Geological units dated by CA-TIMS U-Ob zircon geochronology are indicated by *.

Sample Number	Unit	Age (t)	Nd (ppm)	Sm (ppm)	$^{143}Nd/^{144}Nd$	2σ	$^{147}Sm/^{144}Nd$	$\varepsilon_{Nd(0)}$	$T_{(DM)}$	$\varepsilon_{Nd\,(t)}$
2721829*	Moonaree Dacite Member, Yardea Dacite	1586.39	59.39	10.75	0.511560	0.000001	0.1094	-21.0	2.31	-3.3
2018200	Eucarro Rhyolite	1586.66	72.74	13.06	0.511492	0.000007	0.1085	-22.4	2.39	-4.4
2721816*	Eucarro Rhyolite	1586.66	41.26	8.56	0.511542	0.000002	0.1254	-21.4	2.75	-6.9
2018616*	Bittali Rhyolite	1588.47	77.57	13.28	0.511550	0.000010	0.1035	-21.2	2.20	-2.3
2721825	Bittali Rhyolite	1588.47	41.05	7.25	0.511477	0.000002	0.1068	-22.7	2.37	-4.0
2721839*	Mangaroongah Dacite	1589.19	58.27	10.83	0.511761	0.000002	0.1124	-17.1	2.08	0.0
2746487*	dacite, Chitanilga	1589.19	31.00	4.80	0.511479	0.000003	0.0941	-22.6	2.12	-1.7
2472362*	RC1 dacite	1590.18	78.10	13.60	0.511444	0.000003	0.1051	-23.3	2.38	-4.6
2559255^	Myall Creek upper basalt	1590.00	30.92	6.44	0.511772	0.000002	0.1258	-16.9	2.37	-2.5
2559257^	Myall Creek upper basalt	1590.00	23.53	5.33	0.511914	0.000004	0.1369	-14.1	2.44	-2.0
2559258^	Myall Creek upper basalt	1590.00	37.23	7.13	0.511610	0.000002	0.1158	-20.0	2.38	-3.6
GCT86^	Konkaby Basalt	1590.35	45.29	7.83	0.511424	0.000016	0.1045	-23.7	2.39	-4.90
GCT87^	Konkaby Basalt	1590.35	41.91	6.88	0.511384	0.000012	0.0992	-24.5	2.34	-4.60
18-TAR-07*	Ealbara Rhyolite	1590.35	72.82	12.02	0.511542	0.000002	0.0998	-21.4	2.14	-1.6
2746361*	Spearfelt Rhyodacite	1590.35	71.60	12.60	0.511389	0.000002	0.1066	-24.4	2.49	-6.0
2559256^	Myall Creeklower basalt	1591.00	22.10	5.04	0.511931	0.000002	0.1378	-13.8	2.43	-1.8
2729186*	RED 2 dacite	1592.79	75.69	13.51	0.511531	0.000002	0.1079	-21.6	2.32	-3.5
2729189	RED 2 dacite	1592.79	64.99	11.90	0.511499	0.000002	0.1107	-22.2	2.43	-4.7
2017742*	Angle Dam Dacite	1593.61	70.40	12.90	.511364	0.000002	0.1106	-24.8	2.62	-7.3
2019330	Angle Dam Dacite	1593.61	73.71	12.05	0.511347	0.000002	0.0988	-25.2	2.38	-5.3

Errors on $^{143}Nd/^{144}Nd$ measurements are 2σ (mean).
Measured εNd values calculated with present-day CHUR $^{143}Nd/^{144}Nd$ and $^{147}Sm/^{144}Nd$ ratios of 0.512638 and 0.1966.
Depleted mantle Nd model ages calculated as in Goldstein et al. (1984).
*TIMS dated sample
^extrusion age of basalt are estimated based on stratigraphy summarised in Figure 3b.

Th contents in the Eucarro Rhyolite are similar in abundance to the Bittali Rhyolite and Spearfelt Rhyodacite of the Lower GRV. The Upper GRV Moonaree Dacite Member has similar Zr, Nb and U abundances to dacites of the Lower GRV, while its Th concentrations are lower (Fig. 6).

Primitive mantle-normalised trace element patterns for the basalt to andesite Lower GRV samples are characterised by variable large ion lithophile element (LILE), and flat rare earth element (REE) and high field strength element (HFSE) patterns (Fig. 7). Small to moderate negative anomalies in Nb, Ta, Ti and Sr are present in each of the units. The most prominent negative Sr anomalies are present in Myall Creek upper basalt. The Chitanilga basaltic andesite has the largest negative Ti anomalies (Fig. 7).

Primitive mantle-normalised trace element patterns in dacitic to rhyolitic Lower and Upper GRV units (Fig. 8) exhibit greater negative Nb, Ta, Ti, Ba, Sr and P anomalies compared to the mafic to intermediate suites. REE, Th, U, Zr and Hf are relatively enriched. The greatest variation in trace element abundance within a unit is seen in the Lower GRV Bittali Rhyolite, RED 2 dacite and Chitanilga dacite (Fig. 8a). Negative Sr, P and Ti anomalies are largest in RED 2 dacite, Ealbara Rhyolite, Bittali Rhyolite and RC1 dacite from the Lower GRV (Fig. 8a). Upper GRV Eucarro Rhyolite shows slightly more enrichment in trace elements and stronger negative anomalies in Sr, P and Ti compared with the Upper GRV Moonaree Dacite Member (Fig. 8b).

Rare earth element variation

Basaltic to andesitic Lower GRV REE patterns display variable light REE (LREE) enrichment relative to heavy REE (HREE; $(La/Yb)_N$ = 2.5–25.1). The higher $(La/Yb)_N$ ratios are seen in Myall Creek lower basalt, Myall Creek upper basalt and Konkaby Basalt. The ΣREE are mostly similar to global oceanic subducted sediment (GLOSS), although Myall Creek upper and lower basalts and Chitanilga basaltic andesite have sllightly higher REE abundances than GLOSS (Fig. 9). REE patterns in the Roopena Basalt and Myall Creek lower basalt are similar to E-MORB but enriched overall and with a slightly higher $(La/Yb)_N$ ratio (average = 4.63 and 5.9 respectively) than E-MORB (3.48; Klein 2004). Negative Eu anomalies are minor (Fig. 9), with Eu/Eu* values between 0.66–1.15. LREE/HREE ra-

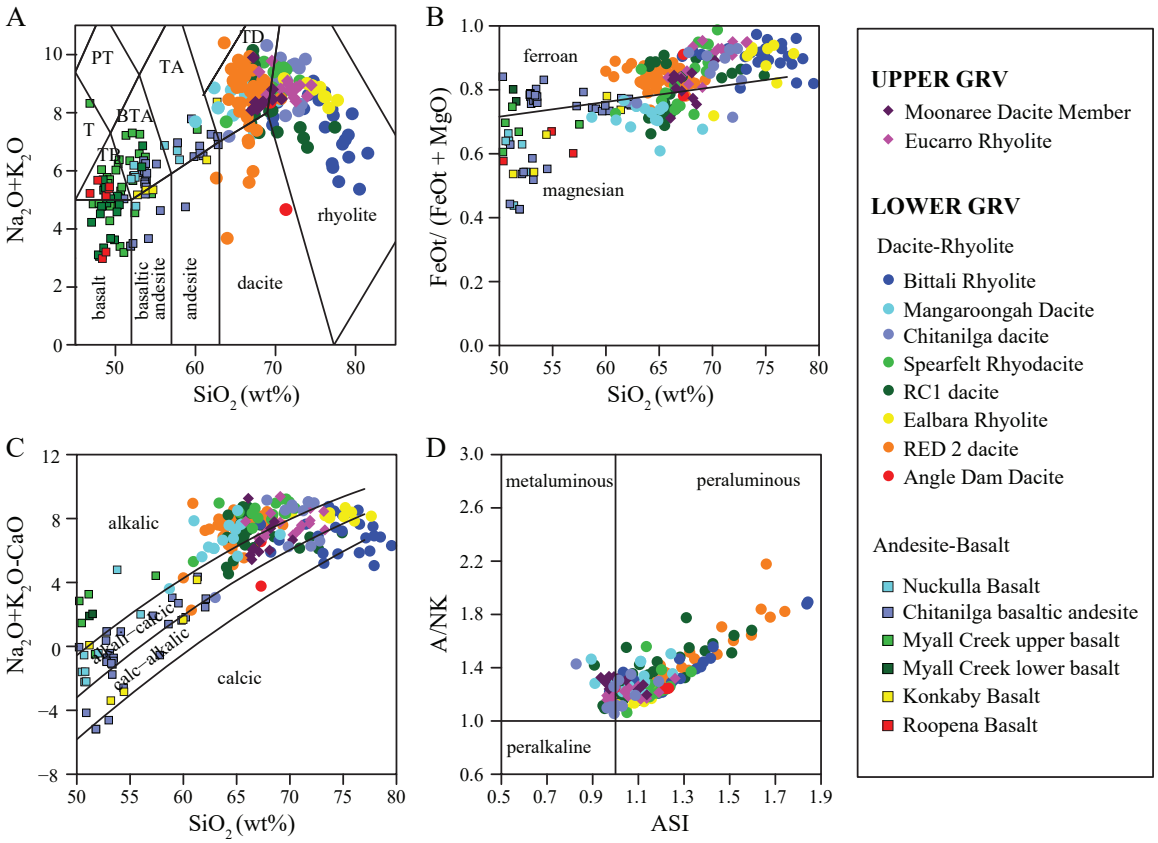

Figure 4: Classification diagrams after Middlemost (1994; A) and Frost et al. (2001; B-D). A) Total alkali silica (TAS) classification diagram for mafic and felsic units of the Gawler Range Volcanics (GRV) showing basalt-andesite compositions for mafic rocks and dacite-rhyolite compositions in the felsic units. Abbreviations: TB: trachybasalt, T: trachyte; BTA basaltic trachy andesite; TA trachyandesite; PT phono-tephrite; and TD: trachydacite. B) Fe* (FeOt/(FeOt/MgO) versus SiO_2 classification diagram for rhyolites and dacites of the GRV; C) Modified alkali lime index (MALI) diagram for rhyolite and dacite units of the GRV showing the alkalic to calc-alkalic compositions of the Lower GRV units and alkali-calcic compositions of the Upper GRV units and; D) $Al_2O_3/(Na_2O+K_2O)$ (A/NK) vs aluminium saturation index (ASI) for the rhyolite and dacite GRV units showing the predominantly peraluminous nature of the units. Basalt-andesite and rhyolite-dacite units occurring in the sample location/complex are denoted by having the same colour. Note: RED 2 dacite and Bittali Rhyolite are absent of any related basalt-andesite.

tios increase upward through the stratigraphy (Roopena Basalt $(La/Yb)_N$ = 2.5–5.9; Myall Creek lower basalt $(La/Yb)_N$ = 4.5–8.7; and Myall Creek upper basalt $(La/Yb)_N$ = 4.5–12.5). There is large variation in LREE/HREE ratios in the younger basalt to andesite units (Konkaby Basalt $(La/Yb)_N$ = 3.6–17.9; Chitanilga basaltic andesite $(La/Yb)_N$ = 6.7–25.1; while Nuckulla Basalt has moderate $(La/Yb)_N$ ratios (7.2–9.4).

Individual dacite to rhyolite Lower GRV units display parallel REE patterns typically enriched in LREE with flat HREE (Fig. 10a). Negative Eu anomalies are present in all Lower GRV units, although the size of the anomaly varies between units. The Ealbara and Bittali Rhyolites have the largest variation in Eu/Eu* ratios in the Lower GRV units (Eu/Eu* = 0.19–0.51 and 0.11–0.83 respectively), while the Mangaroongah Dacite has Eu/Eu* ratios between 0.59–0.94. Upper GRV REE patterns

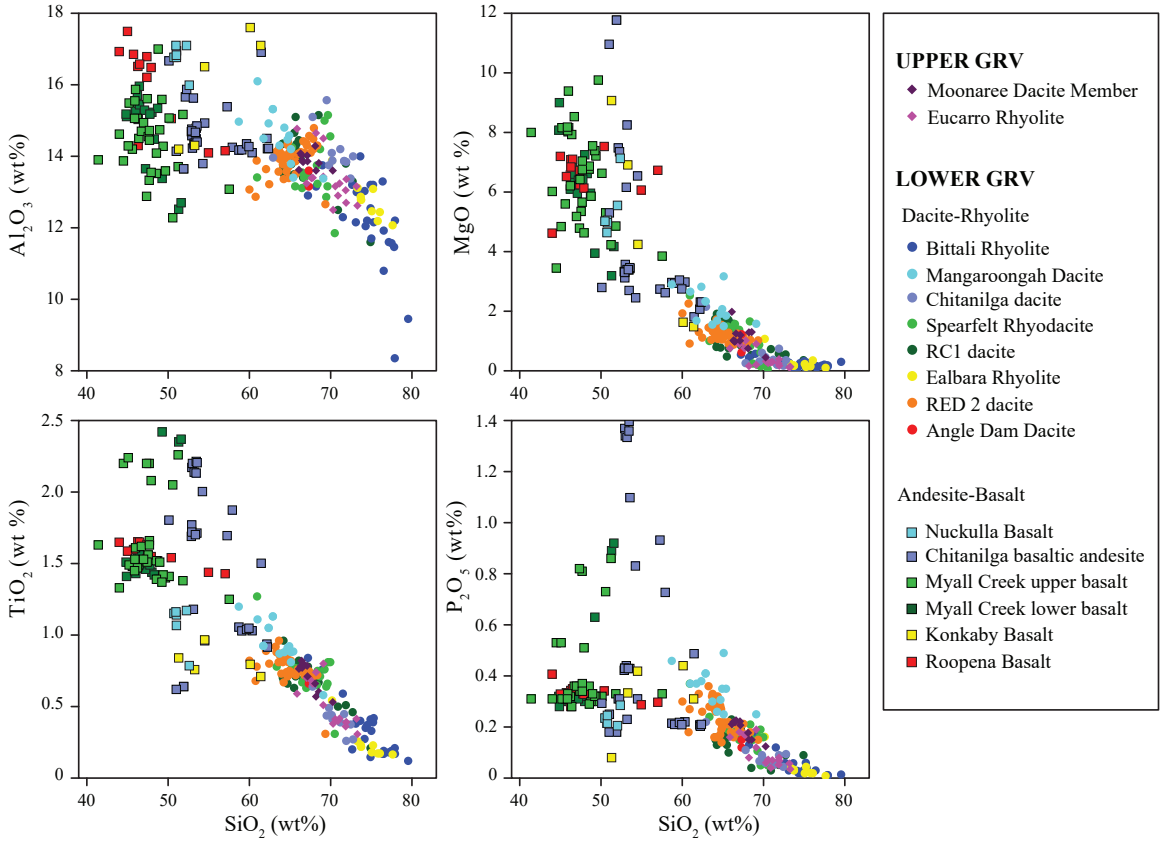

Figure 5: Selected major element plots versus SiO_2 for mafic and felsic units of the Gawler Range Volcanics. Note the TiO_2 variation in the mafic rocks illustrating high-TiO_2 (>1.5 wt%) and low-TiO_2 (<1 wt% TiO_2) types.

are also characterised by steep LREE and flat HREE patterns, with negative Eu anomalies. Eu/Eu* ratios in the Upper GRV Eucarro Rhyolite range from 0.36–0.91, while the Moonaree Dacite Member has more consistent Eu/Eu* ratios of 0.57–0.67. The Upper GRV Eucarro Rhyolite displays more variation in LREE, compared to the Upper GRV Moonaree Dacite Member (Fig. 10b).

Whole-rock Nd isotopes

A total of 20 samples, representing each stratigraphic rhyolitic and dacitic unit and selected basaltic units, were analysed for Sm-Nd isotopes in this study (Table 2; Fig. 11). $\varepsilon_{Nd(i)}$ were calculated at respective extrusion times based on the U-Pb zircon geochronology for each unit reported in the companion study of Jagodzinski *et al.* (in prep.). The ages of basaltic units are estimated based on stratigraphic relationships (see Fig. 3b).

$\varepsilon_{Nd(i)}$ values for the Konkaby Basalt, Myall Creek upper basalt and Myall Creek lower basalt are -4.6 and -4.9, -3.6 to -2 and -1.8, respectively (Table 2). Eleven dacite to rhyolite Lower GRV samples have $\varepsilon_{Nd(i)}$ values that range from -7.3 to 0.0 (samples 2018616, 2721825, 2721839, 2746487, 2472362, 18-TAR-07, 2746361, 2729186, 2729189, 2017742 and 2019330; Table 2). Two Eucarro Rhyolite samples (2018200 and 2721816) have $\varepsilon_{Nd(i)}$ = -4.4 and -6.9, respectively (Table 2). The Mangaroongah Dacite Member (2721829) has an $\varepsilon_{Nd(i)}$ value of -3.3 (Table 2).

DISCUSSION

Existing tectonic models for the Gawler LIP

Recent models for the generation of the Gawl-

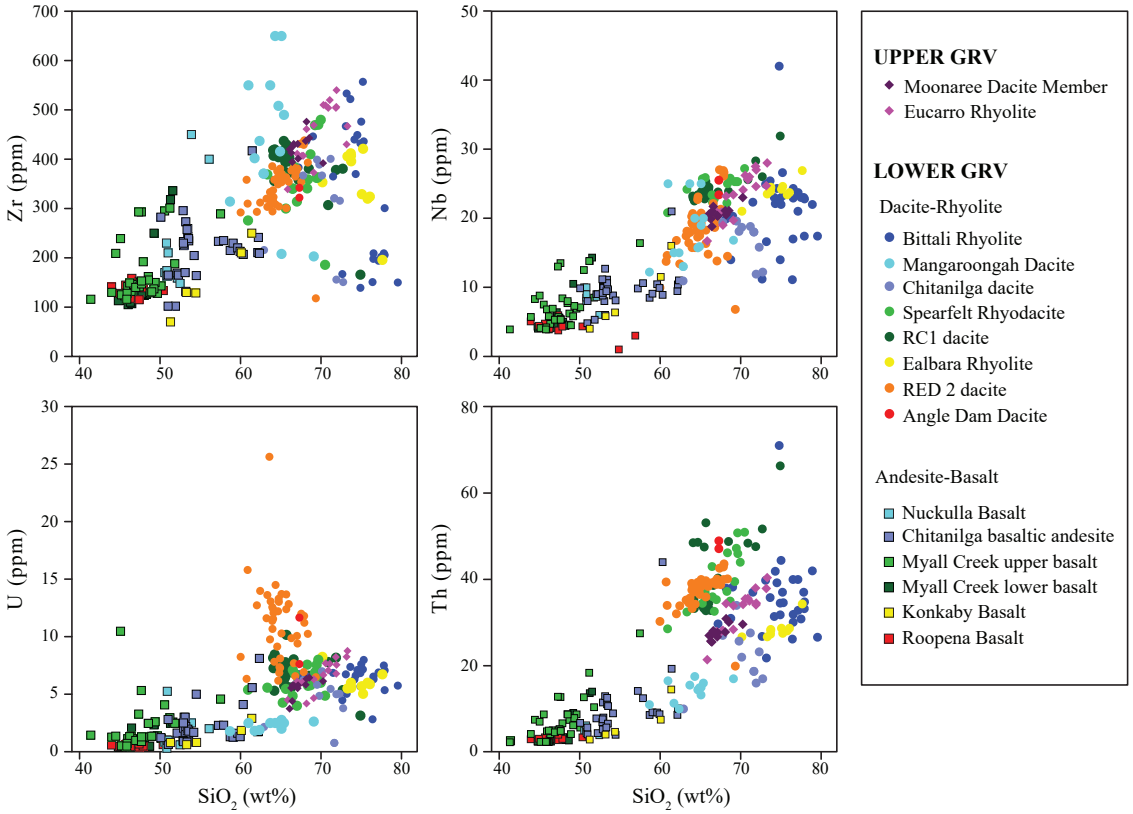

Figure 6: Selected trace element plots versus SiO_2 for mafic and felsic Gawler Range Volcanics, exhibiting elevated Zr and Nb in andesite-basalt and dacite-rhyolite units, and high Th in some basalt-andesite units.

er LIP have been developed for the purpose of explaining the generation of the IOCG deposits that are temporally associated with the LIP magmatism (e.g. Skirrow *et al.* 2018, Tiddy and Giles 2020). This previous work has not examined the cause of the melting event. A combination of factors play a critical role in the formation and preservation of a mineral system (e.g. Hagemann *et al.* 2016), and magmatic hydrothermal mineral deposit formation is generally a function of the latter stages of magmatic processes, including fractional crystallisation and evolution of oxidation state (e.g. Lee and Tang 2020).

Delamination and supra-subduction settings have been suggested as the drivers of IOCG mineralisation and the Gawler LIP magmatism (Skirrow *et al.* 2018, Tiddy and Giles 2020). Tiddy and Giles (2020) suggest a supra-subduction setting for this magmatic-hydrothermal event, likening the Gawler LIP magmatism to the Phanerozoic Sierra Madre Occidental in North America and mineralisation to the Cretaceous Coastal Cordillera of Chile. As noted by Pankhurst *et al.* (2011b) and Skirrow *et al.* (2018), a supra-subduction setting does not fully account for key geological and geochemical features observed in the Gawler LIP. These key features include: 1) the HFSE-enriched compositions of the GRV and Hiltaba Suite rocks are atypical of subduction-related magmatism; 2) Gawler LIP magmas are largely felsic and alkaline to alkali-calcic in composition, and the lack of intermediate calc-alkaline magmas and high K composition is inconsistent with a magmatic arc setting; 3) The geometry of the Gawler LIP is sub-circular and not a linear belt; 4) There is an absence of extensive basins, as would be

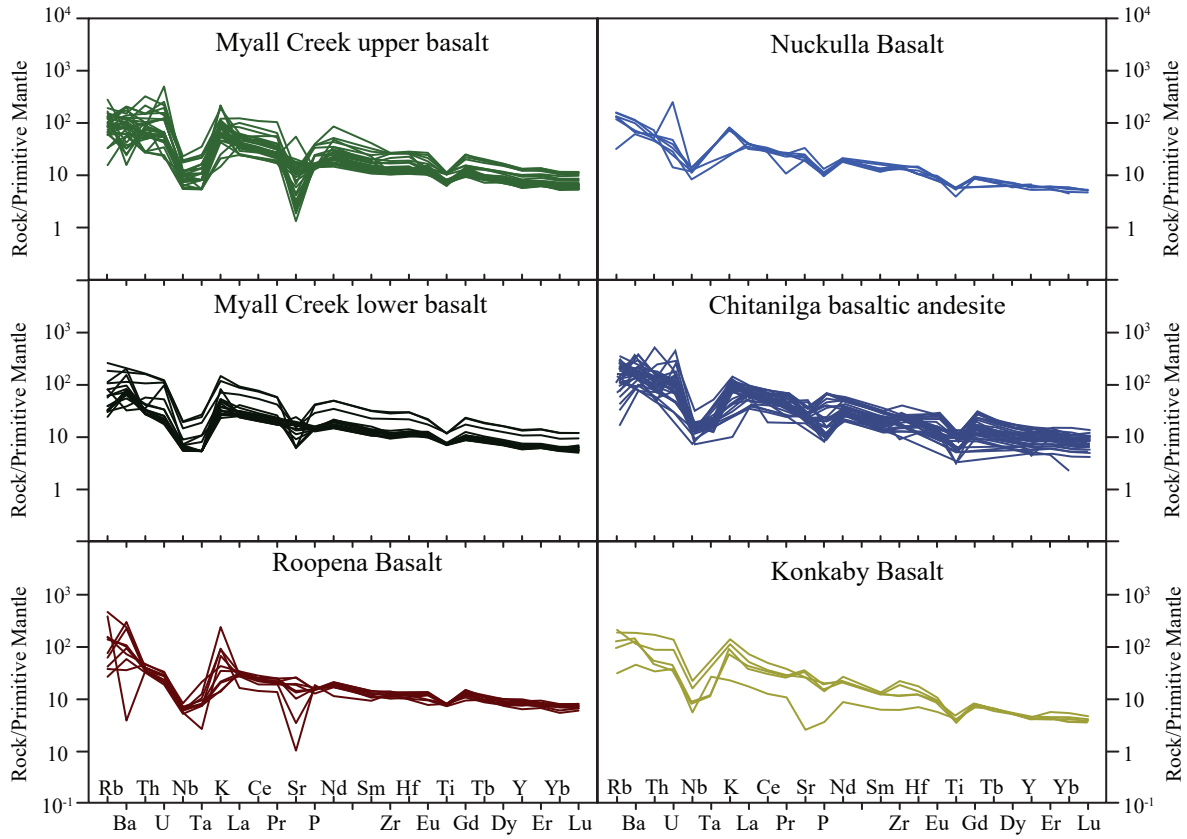

Figure 7: Primitive mantle-normalised trace element diagrams for basalts and andesites of the Lower Gawler Range Volcanics, divided by the stratigraphic unit. Normalising values are from Sun and McDonough (1989).

expected to develop in continental back-arc basins or intracontinental rift settings (Friedmann and Burbank 1995, Ferrari *et al.* 2013, Nakakuki and Mura 2013); 5) Magmatism of the GRV is largely anhydrous, associated with melting of a refractory, old crust, which is in contrast to partial melting of fertile, hydrous lower-crust with high H_2O contents in supra-subduction settings (Bryan *et al.* 2002); 6) Magmatic temperatures in the Gawler LIP are higher than supra-subduction settings. Magmatic temperatures in Sierra Madre Occidental rhyolites are low (zircon saturation temperature values of 734 to 771 °C; Cheng *et al.* 2020) compared with the Gawler SLIP (900 to 1100 °C; Creaser *et al.* 1991, Pankhurst *et al.* 2011b) and other felsic rocks in mafic LIPs e.g. 790–944 °C in the Tarim LIP; 900–1050 °C in Columbia River-Snake River Plain-Yellowstone; and 1000–1100°C in Keweenawan (Pankhurst *et al.* 2011a and references therein, Cheng *et al.* 2020); and 7) The duration of volcanism in the Gawler LIP is short-lived (7 Myr) compared with ~20 Myr of the Sierra Madre Occidental and up to 50 Myr of volcanism in active continental margins (Bryan 2007).

Tiddy and Giles (2020) invoke long-lived subduction in their model beginning with 1690 Ma Tunkillia Suite magmatism in the central and western Gawler Craton through to the GRV-Hiltaba Suite (1595–1575 Ma). Payne *et al.* (2010) demonstrated the Tunkillia Suite event is consistent with magmatism in a post-orogenic tectonic rather than an arc setting, contradicting a ca. 115 Ma subduction setting in the Tiddy and Giles model. Subduction-related magmatism preceding the Gawler LIP occurred at 1633–1610 Ma with magmat-

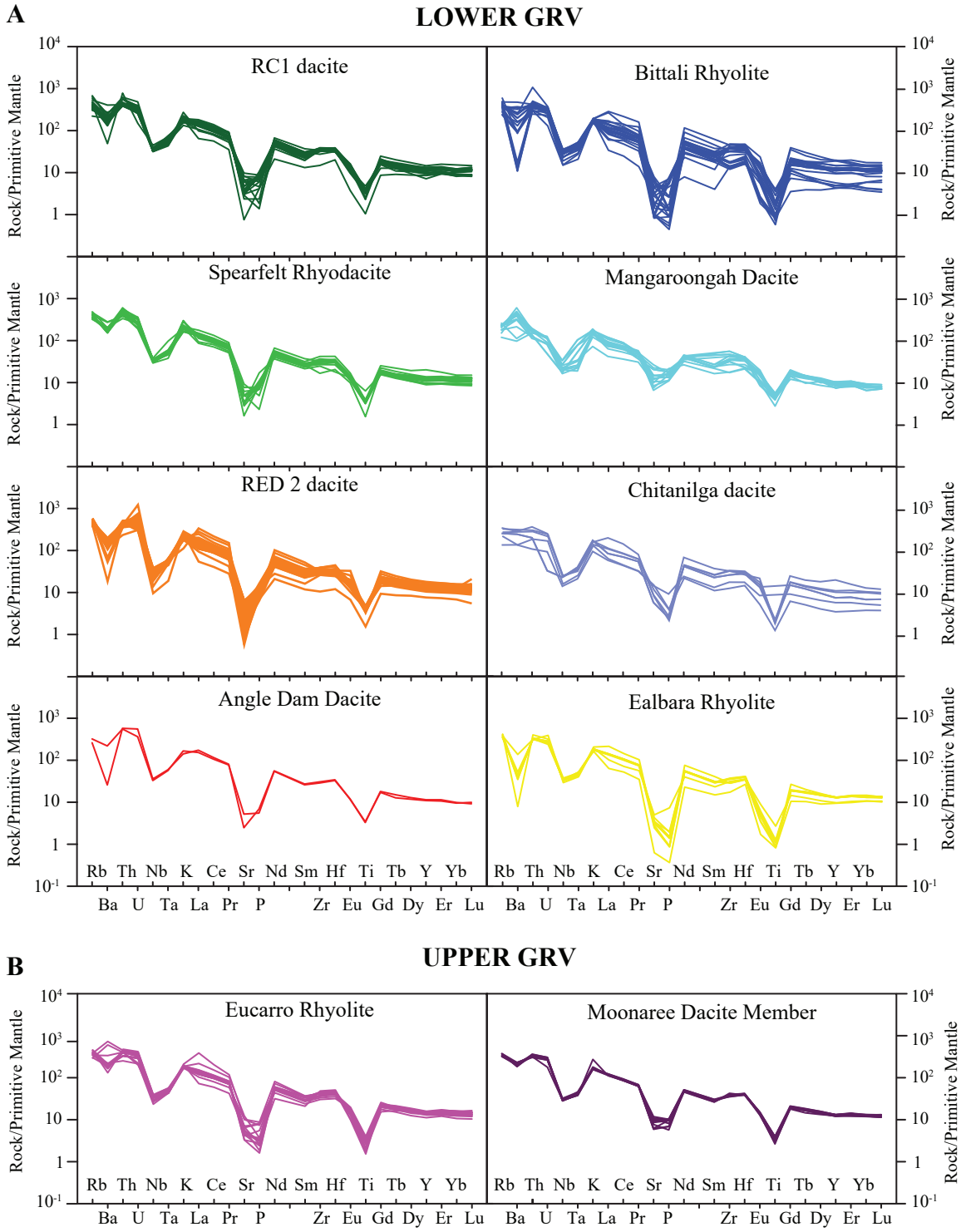

Figure 8: Primitive mantle-normalised trace element plots for dacite to rhyolite of the (A) Lower and (B) Upper Gawler Range Volcanics. Normalising values are from Sun and McDonough (1989).

ic geochemical signatures of the St Peter Suite consistent with an intraplate-oceanic (Swain *et al.* 2008) or a continental magmatic arc setting (Skirrow *et al.* 2018, Reid *et al.* 2019). The Tiddy and Giles model suggests a period of subduction roll-back during formation of the

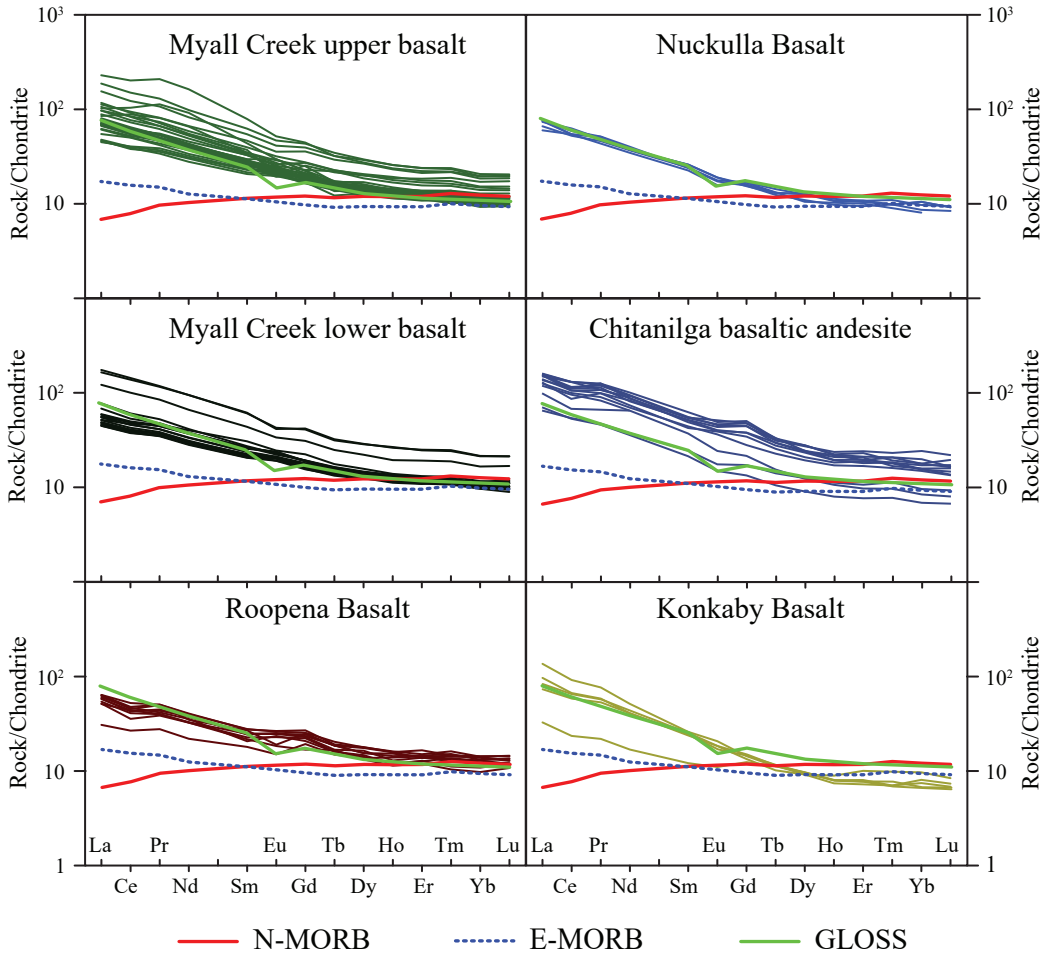

Figure 9: Chondrite-normalised rare earth element diagrams from basalt-andesite for the Lower Gawler Range Volcanics, divided by the stratigraphic unit. Normalising values are from Taylor and McLennan (1985). Data sources: N-MORB (normal mid ocean ridge basalt) Sun and McDonough (1989); E-MORB (enriched mid ocean ridge basalt) Klein (2004); GLOSS (global oceanic subducted sediment) Plank and Langmuir (1998).

St Peter Suite arc proceeding on to a switch to flat-slab subduction and compression, immediately prior to onset of the formation of the Gawler LIP. This switch from extension to compression is inconsistent with the published structural interpretation of the St Peter Suite which considers the suite to have been emplaced during east-west directed shortening with subsequent extension affecting post-1.6 Ga Hiltaba Suite intrusions (Reid *et al.* 2019). An outstepping of the arc to the present-day southwest of the Gawler Craton may have occurred during this period, but there is no evidence to indicate this correlates to a period of extensive rifting and extension on the Gawler Craton. Only localised and isolated basin formation has been documented in the eastern Gawler Craton (e.g. McPhie *et al.* 2016, Curtis *et al.* 2018). Sedimentation occurred from ca. 1590–1580, constrained by sediments in the Roopena Basin that overlie the Angle Dam Dacite (1593.61 ± 0.15 Ma; Fig. 3b) and have detrital spectra that range from 2560–1580 Ma (Johnson 1993, Curtis *et al.* 2018). A bedded clastic facies at Olympic Dam has a single detrital peak of 1590 Ma (McPhie *et al.* 2016). These systems are of limited areal extent, do not represent a continuous large basin and are not on the scale of substantial basin fill expected in an extensional setting (Fried-

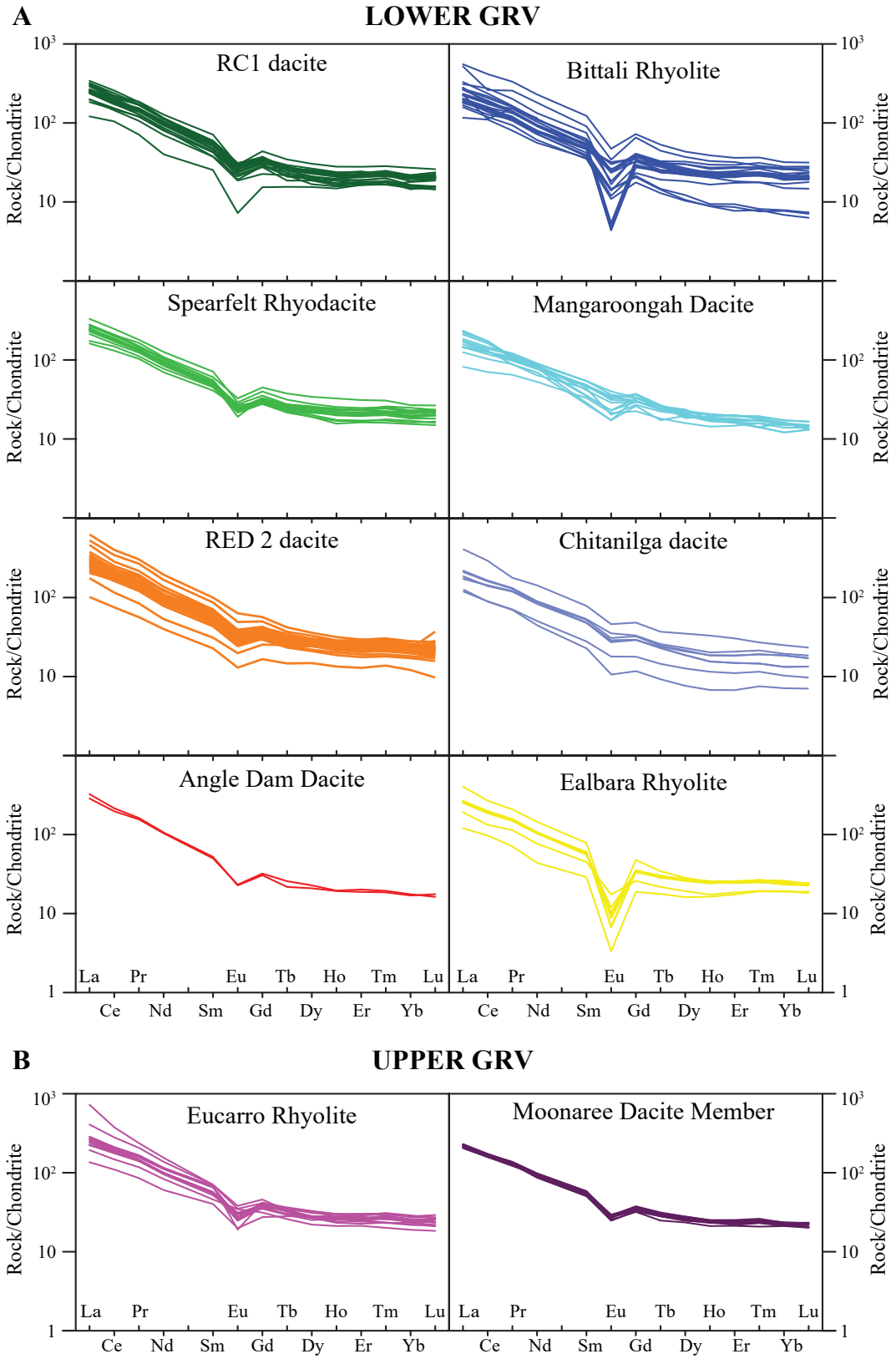

Figure 10: Chondrite-normalised rare earth element plots for rhyolite to dacite of the (A) Lower and (B) Upper Gawler Range Volcanics. Normalising values are from Taylor and McLennan (1985).

mann and Burbank 1995, Nakakuki and Mura 2013). In Tiddy and Giles, the magmatism of the Gawler LIP is suggested to be driven by slab roll-back and re-introduction of asthenospheric mantle to the base of the altered SCLM, metasomatised during the late Paleo- to Mesoproterozoic flat-slab subduction event. The isotopic signature of the St Peters Suite suggests subducted sedimentary material was not particularly isotopically evolved (Swain *et al.* 2008, Reid *et al.* 2019). Isotopic data from mafic components of the Gawler LIP indicate much earlier metasomatism of the SCLM (i.e. Archean or early Palaeoproterozoic; Wade *et al.* 2019 and this contribution). The enriched signature associated with Archean or early Palaeoproterozoic metasomatism is documented in mafic magmatic rocks throughout the late Archean, Palaeoproterozoic and Mesoproterozoic, as evidenced by consistently Archean Nd model ages (2.2–2.6 Ga; Wade 2012), further supporting that a long-lived metasomatised SCLM exists beneath the Gawler Craton (Wade et al. 2019). Evidence of ancient metasomatism is significant as late Palaeoproterozoic subduction and its associated recent metasomatism involving even ancient sediments cannot account for the isotopic compositions in mafic magmatic rocks throughout the late Archean to Mesoproterozoic.

The style and geochemical character of magmatism in the Gawler LIP is also inconsistent with a flat-slab roll-back model. Mesozoic South China has been nominated as flat-slab event with a 50 Myr time gap between arc shut-off and onset of slab foundering which is followed by ~100 Myr of slab retreat-related magmatism (Li and Li 2007, Dai *et al.* 2020). Such timelines are inconsistent with the evolution of the St Peter Suite and Gawler LIP. The South China flat slab melting event is dominated by I-type magmatism with subordinate A-type magmatism (Li and Li 2007 and references therein), whereas the Gawler LIP is dominated by A-type magmatism with subordinate I-type rocks. Similarly, the Sierra Madre Occidental SLIP includes magmatism that indicates lithospheric mantle melting for ~12 Myr prior to the 20 Myr period during which the voluminous SLIP magmatism forms (Ferrari *et al.* 2018). Coupled with the lower magmatic temperatures and linear nature of magmatism and basin formation associated with the Sierra Madre Occidental, we suggest the mantle and crustal thermal regimes of the Gawler LIP differed significantly from both the Mesozoic South China and Sierra Madre Occidental flat-slab subduction regimes.

As outlined above, we agree with Skirrow *et al.* (2018) that a supra-subduction setting does not fully account for key geological and geochemical features observed in the Gawler LIP. The delamination model as proposed by Skirrow *et al.* (2018) also does not fully account for key geological features observed in the Gawler LIP. While delamination can produce continental magmatism with a range of major and trace elements and volatile contents and may produce a heterogeneous upper mantle (e.g. Elkins-Tanton *et al.* 2005), there are topographic and melt production consequences of delamination (Li *et al.* 2016). Delamination models require rapid regional uplift and change in topography, and significant lithospheric thinning (Kay and Kay 1993, Wells and Hoisch 2008). The lithospheric thickness in the Gawler Craton is great, with the lithosphere-asthenosphere boundary reaching maximum thicknesses of 180–220 km (Kennett *et al.* 2012). Upwelling material cannot sufficiently depressurise beneath a continent, and ascending material is essentially blocked by the thick lithosphere (Elkins-Tanton *et al.* 2005). Magmas generated by rising asthenosphere replacing a delaminated lithospheric keel are typically adakitic and/or anorthositic (Xu *et al.* 2002, Gao *et al.* 2004, Zhang *et al.* 2007, Lee *et al.* 2014, Liu *et al.* 2018, Karsli *et al.* 2020). Neither compositions are recorded in the GRV. Therefore, it is difficult to recon-

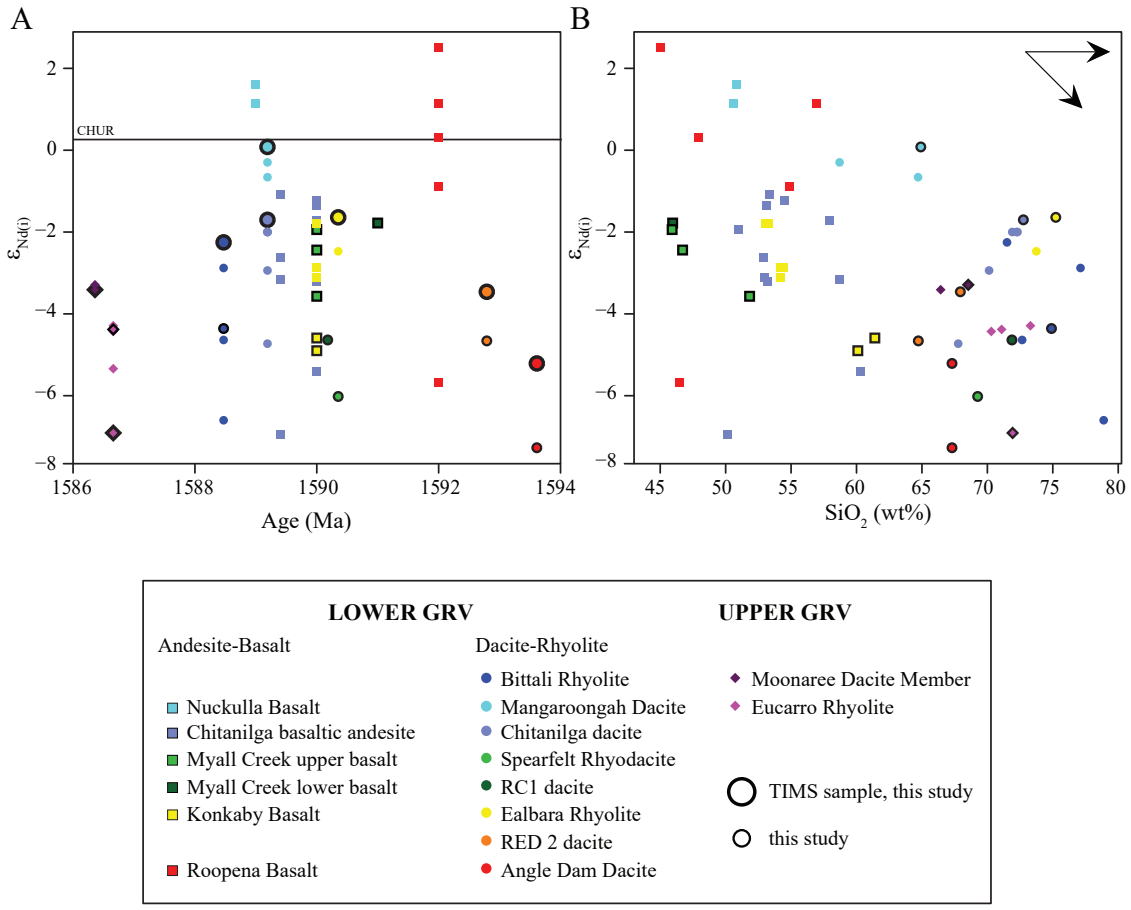

Figure 11: (A) $\varepsilon_{Nd(i)}$ versus age for the dacite-rhyolite units and related basalts (B) $\varepsilon_{Nd(i)}$ versus SiO_2 for the basalts, andesites, dacite and rhyolites. Horizontal arrow refers to partial melting and/or fractional crystallisation and the oblique arrow refers to assimilation and fractional crystallisation. Negative correlation between $\varepsilon_{Nd(i)}$ and SiO_2 in basalts is consistent with crustal contamination. Horizontal trends formed between related basalts and rhyolites suggests fractionation was a dominant process. Data collected in this study are denoted by black outlines. Additional Nd isotope data from Stewart (1994), Fricke (2005) and Ross (2015), are also shown and denoted by no outlines.

cile the magma compositions, the amount of crustal melting and the high temperature melts (1000 °C) required to melt a refractory crust to produce the volume of the GRV in a thinned lithosphere.

Skirrow *et al.* (2018) argue against a plume model primarily due to the lack of asthenospheric-derived tholeiitic mafic magmas as could be expected in hot-spot or plume magmatism in large igneous provinces. Not all plume-related magmatic rocks have asthenospheric signatures. Enriched Nd isotopic ratios and lithospheric trace elements such as high Ba, Pb and La are common in continental flood basalts, which reflect a contribution from the continental lithosphere (Baker *et al.* 2000). Geochemical composition of the basalts from the GRV are HFSE-enriched and have variable $\varepsilon_{Nd(i)}$ compositions, consistent with derivation from the sub-continental lithosphere (e.g. Wade *et al.* 2012, Huang *et al.* 2016, Wade *et al.* 2019). Continental flood basalt systems also contain significant volumes of silicic magma that occur throughout the eruptive history (e.g. Pankhurst *et al.* 1998, Pankhurst *et al.* 2000, Marsh *et al.* 2001). Magma compositions in continental flood basalts are related through differentiation processes

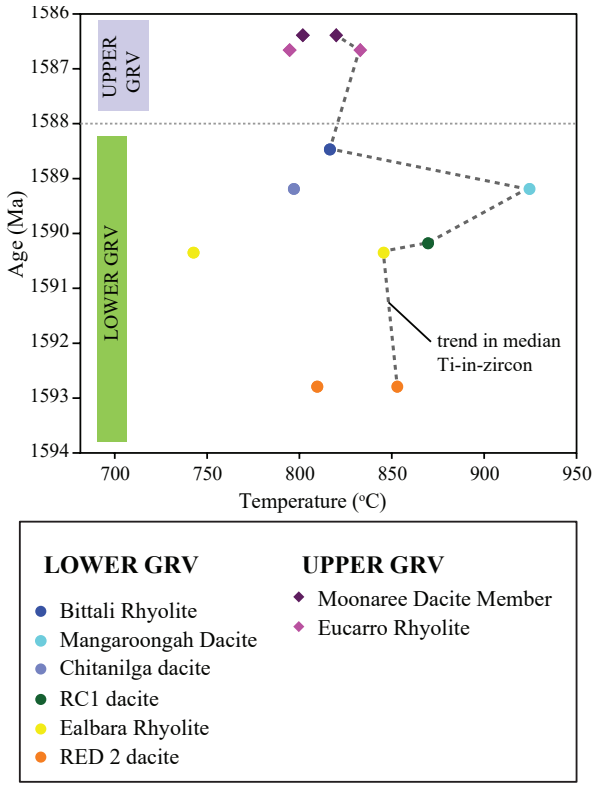

Figure 12: Calculated median Ti-in-zircon versus age for a subset of felsic Gawler Range Volcanics (data from Chapter 5) displaying the temporal variation in estimated magmatic temperature, calculated from the Ti-in-zircon thermometer (Ferry and Watson 2007), where $\alpha TiO_2 = 0.7$ and $\alpha SiO_2 = 1$.

where rhyolites are dominated by fractional crystallisation or assimilation and fractional crystallisation and crustal melting processes (e.g. Etendeka, Yemen and North Atlantic). The large volume of silicic magmas in continental flood basalts requires basaltic input in the magmas for both heat transfer and material addition (Ewart *et al.* 1998, Bryan 2007). The mantle plume model was developed to explain the large volumes of mafic magma produced over short periods (White and McKenzie 1989, Campbell and Griffiths 1990) in continental flood basalts, but also meets the temperature requirement needed to melt old, refractory crust in intracontinental settings. The Gawler LIP is represented by relatively short-lived volcanism in an intracontinental setting, where HFSE-enriched lavas were emplaced on an Archean to Palaeoproterozoic craton. Ti-in-zircon thermometry (Fig. 12) indicates the magmatic temperatures in the Gawler LIP (795–925 °C) are comparable to silicic rocks in LIPs (790–944 °C; Cheng *et al.* 2020), and consistent with high temperatures required to melt old, refractory crust. The Gawler LIP and continental flood basalt LIPs share similar attributes, including intraplate magmatism emplaced on, or adjacent to, Archean cratons, high magmatic temperatures associated with volcanism, enriched geochemical and isotopic signatures indicative of a continental lithosphere contribution and fractional crystallisation and assimilation processes to generate the felsic to intermediate magmas. These attributes can be explained by plume-driven magmatism. In these respect, the Gawler LIP shows more similarities to mantle plume-related continental flood basalts and mafic LIPs (e.g. Pankhurst *et al.* 2011b) than Phanerozoic active margin or continental break-up SLIPs.

Genesis and Evolution of Gawler LIP mafic magmatism

The earliest mafic magmatism in the Gawler LIP is in the Roopena area, southeast Gawler Craton (Fig. 2; Roopena Basalt, ca. 1592 Ma). The Roopena Basalt lavas are the most primitive of the GRV mafic-end members, with low SiO_2 and moderate MgO, Cr and Ni contents, lower $(La/Yb)_N$ and isotopically more juvenile. Source discrimination diagrams (Pearce 2008, Pearce *et al.* 2017) highlight that Nb, Th and Yb compositions of the Roopena Basalt are lower than the other GRV basalts. The Roopena Basalt samples plot within N-MORB transitional to E-MORB compositions (Fig. 13a), and within the metasomatised/subduction-modified lithospheric mantle array (Fig. 13b and 13c). Previous authors have also suggested these geochemical characteristics are linked to a metasomatised SCLM (Huang *et al.* 2016, Rogers *et al.* 2018, Skirrow *et al.* 2018, Wade *et al.* 2019). Comparatively primitive compositions of the Roopena Basalt, with

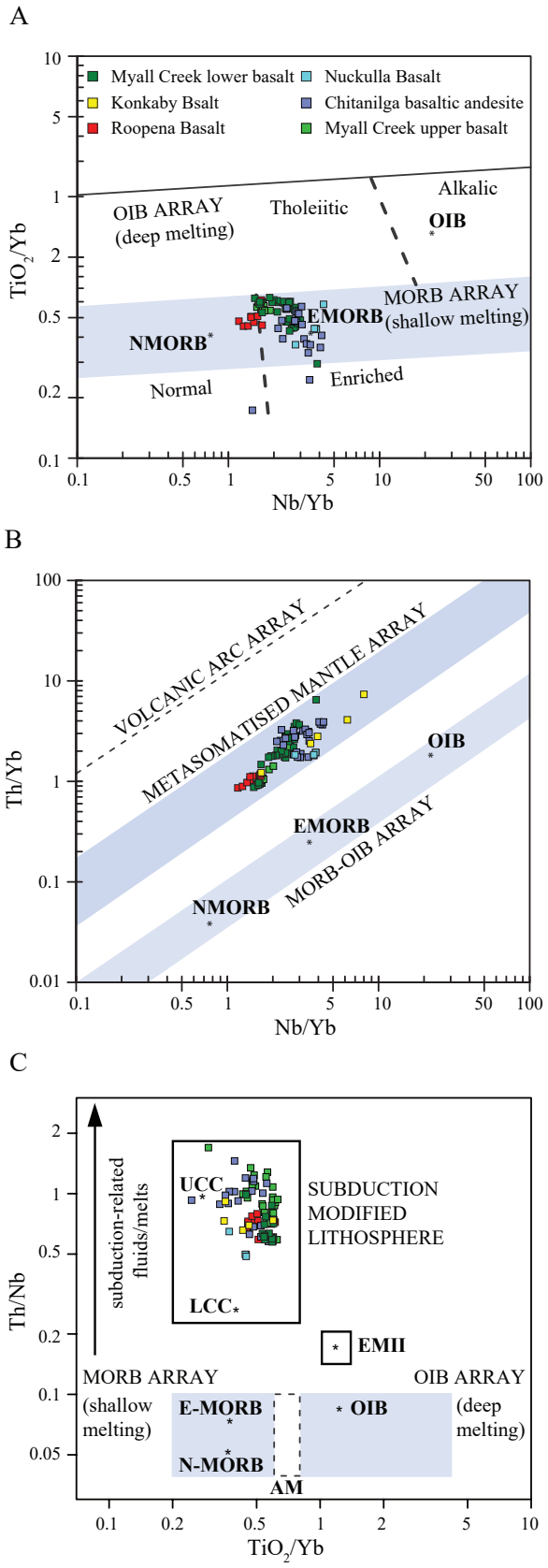

Figure 13: Basalt source discrimination diagrams after Pearce (2008) and Pearce et al. (2017). A) TiO_2/Yb vs Nb/Yb and B) Th/Yb vs Yb/Nb, modified after Pearce (2008) showing the enriched compositions of the GRV basalt-andesite. Metasomatised mantle array forms a trend parallel to the MORB array in (B); C) Th/Nb vs TiO2/Yb illustrating the high Th/Nb nature of the GRV basalts corresponding to subduction modified lithosphere, modified after Pearce et al. (2017). Abbreviations: OIB: oceanic island basalt; MORB: mid-ocean ridge basalt; AM: asthenospheric mantle: EMII: enriched mantle II (Workman et al. 2004); UCC: upper continental crust; LCC: lower continental crust.

higher degrees of partial melting, as indicated by lower $(La/Yb)_N$ ratios are consistent with early plume-head driven melts (Hoernle *et al.* 2015). Additionally, the larger volume of mafic volcanism associated with the Roopena basin system (Curtis *et al.* 2018) is also consistent with high flux and high volume magmas generated in early plume-head onset melting (White 1993, Jellinek and Manga 2004, Kumagai *et al.* 2008, Harrison *et al.* 2017).
Following the eruption of the Roopena Basalt, there was little to no mafic material erupted in the southeast region for approximately 3 Myr (1593–1590 Ma). Erupted basaltic lavas in the Myall Creek area, to the north of the Roopena Basalt (drillholes MSDP01, -03 and -04 and RC1, Fig. 2) evolved towards lower $\varepsilon_{Nd(i)}$ isotopic values (Fig. 12 and Fig.14a) and higher Nb/Yb and Th/Yb ratios (Fig. 13b). A similar evolution is seen in hot spot and plume-derived magmas in Samoa and Hawaii, and continental flood basalts (Bryan *et al.* 2002, Haase *et al.* 2019). Higher $(La/Yb)_N$ in the Myall Creek upper and lower basalts may be indicative of lower degrees of partial melting possibly related to lower heat flux from the plume tail (White 1993, Jellinek and Manga 2004, Kumagai *et al.* 2008).

Coincident with Myall Creek mafic volcanism in the southeast, Konkaby Basalt and Chitanil-

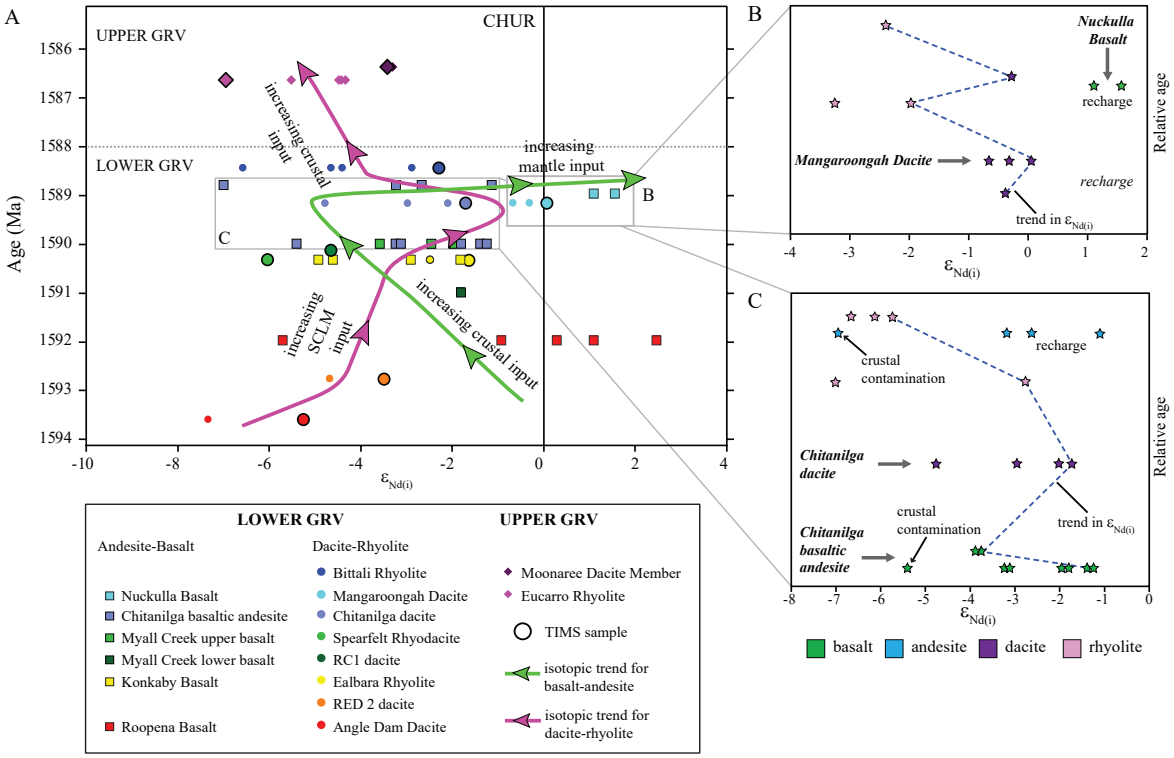

Figure 14: A) Isotopic evolution path for basalts and rhyolites of the GRV, highlighting opposing trends in mafic and felsic units. B) $\varepsilon_{Nd(i)}$ vs stratigraphy for Glyde Hill Volcanic Complex and C) Chitanilga Volcanic Complex, showing magmatic cycles involving recharge of fresh basaltic to andesitic magma at individual volcanic complexes. Stratigraphy for each volcanic complex is based on Fig. 3b, adapted from Figure 2 of Allen et al. (2008). Trend lines mark the maximum $\varepsilon_{Nd(i)}$ values. Recharge in italics for Glyde Hill Volcanic Complex denotes interpreted recharge where no isotopic data is available for mafic units in the sequence. Nd isotope data sources as per Figure 11.

ga basaltic andesite volcanism in the northwest of the LIP extends to higher SiO_2 values (Fig. 11b), increasing Nb/Yb (Fig. 12b) and $\varepsilon_{Nd(i)}$ values as low as -4.9 (Konkaby Basalt) and -7.0 (Chitanilga basaltic andesite; Fig. 11 and Fig. 14a). The style of volcanism switched from high volume mafic magmas in a basinal setting (e.g. Curtis *et al.* 2018) to smaller volume, discrete magmatic centres (e.g. Allen *et al.* 2008). Possibly linked to the downstream plume, volcanism at Tarcoola-Kingoonya and Kokatha have more intermediate compositions (e.g. Fig. 4a) which is likely a function of longer residence or storage times in the SCLM or crust, where they have undergone some degree of fractional crystallisation. The basaltic rocks at Tarcoola-Kingoonya and Kokatha also show evidence for crustal assimilation (e.g. Pankhurst *et al.* 2013, Rogers *et al.* 2018; Figs. 11b and 14, Appendix 1). The low-Ti compositions of the Konkaby Basalt and Chitanilga basaltic andesite (Fig. 5) may be linked to crustal contamination processes (Hawkesworth *et al.* 2000) or previous subduction events (Hawkesworth *et al.* 1988), but correlation between $\varepsilon_{Nd(i)}$ and SiO_2 (Fig. 11b) is further evidence for assimilation of crustal material (Appendix 1). Longevity of the overall thermal input distal to the plume head, combined with longer residence times, smaller magma chambers and waning plume activity is considered akin to decreasing magma flux and volume, and more intermediate magma compositions (e.g. Fig. 14a) downstream of plume heads in younger mantle plume magmas (Riciputi *et al.* 1995, Bryan *et al.* 2002,

Haase *et al.* 2019).

The youngest mafic event is represented by the Nuckulla Basalt that erupted sometime after 1589 Ma. The Nuckulla Basalt is significant as it marks a change in mantle melting with the production of relatively primitive, low SiO_2, small degree partial melts. Positive Nd isotopic values ($\varepsilon_{Nd(i)}$ = 1.1 to 1.6) indicate an isotopically juvenile source, while Nb/Yb ratios are similar to E-MORB (Fig. 13a and 13b), and Th/Nb ratios range to lower values compared with older basalts (Fig. 13c).
Extrusive mafic rocks show the lithospheric mantle isotopic evolution during the initial stages of LIP formation (ca. 1593–1590 Ma; Fig. 14a). Given the Roopena Basalt and Myall Creek basalts have similar Mg# and SiO_2 values, isotopic variation is likely at least in part representative of heterogeneous mantle source compositions (e.g. Wade *et al.* 2012, Huang *et al.* 2016, Wade *et al.* 2019). The earliest basaltic magmatism represents a relatively depleted region from within the metasomatised SCLM, which may have entrained or mixed components of plume-derived material during the onset of melting. Subsequent basaltic magmatism represent heterogeneous SCLM components, and magmatism becomes more enriched with time (Fig. 14a). The final stage of basaltic magmatism is marked by a relatively isotopically juvenile E-MORB-like SCLM source.

The heterogeneities recorded by the extrusive volcanism are largely from the SCLM and more subtle when compared to the greater mafic magmatic event at ca. 1590. The intrusive component represents greater compositional diversity reflective of multiple source components (e.g. plume and SCLM; Wade *et al.* 2019), whereas the extrusive component largely reflects a single source component, although heterogeneous, from within the SCLM. This association is observed in plume-related LIPs elsewhere (Zhou *et al.* 2006, Li *et al.* 2008, Xu *et al.* 2017). Our work on the basaltic volcanism in this LIP however, has the advantage of temporal constraints, and reflects a transition from relatively depleted and isotopically juvenile SCLM source components to enriched SCLM source components then back to isotopically juvenile E-MORB-like SCLM components from ca. 1594 to 1590 Ma. As well as possible entrainment or mixing of plume-derived material in the initial stages of volcanism, the isotopically juvenile compositions and slightly lower Th/Nb ratios in the Nuckulla Basalt (Fig. 13c) suggest additions of a MORB-like component with low Th/Nb, possibly representing a rejuvenation of different mantle plume source composition incorporated into the SCLM.

Silicic magmas and crustal melting above a mantle plume

Two main phases of silicic magmatism generated the Lower GRV from 1593.61–1588.47 Ma and the Upper GRV Ma from 1586.66–1586.39 Ma. These two phases document a change in the system from small volume, heterogeneous silicic lavas developed in discrete centres of the Lower GRV over a 5 Myr period to mature, high volume homogeneous silicic lavas of the Upper GRV erupted in 300 Kyr (Allen *et al.* 2003, Allen *et al.* 2008, Jagodzinski *et al.* in prep.). Lower GRV silicic volcanism was accompanied by mafic magmatism. Coherent trends in major and trace elements between Lower GRV basaltic to rhyolitic units (Fig. 5 and Fig. 6) indicate a relationship through fractionation. Such a relationship is observed in basalts and rhyolites in a number of LIPs (e.g. Chon Aike Province, North Atlantic Province, Karroo and San Juan volcanic field; Storey and Alabaster 1991, Pankhurst *et al.* 1998, Pankhurst *et al.* 2011a and references therein).

The Glyde Hill and Chiltanilga volcanic complexes demonstrate continued eruption of mantle-derived basaltic lavas involving re-

charge and fractional crystallisation and assimilation (Figs. 14b and c). Differences in evolution trends within individual volcanic centres likely reflects heterogeneous source components, varying partial melting percentages and changing magma dynamics (e.g. Hildreth and Moorbath 1988, Riciputi *et al.* 1995). A trend towards lower $\varepsilon_{Nd(i)}$ isotopic values in higher silica units (Fig. 11) is also consistent with assimilation and fractional crystallisation in the Lower GRV lavas. Lead isotopic constraints suggest the Lower GRV magmas have a mantle-dominant source region with small amounts of crustal contribution to the Lower GRV dacites and rhyolites (3–8 %; Chapman *et al.* 2019). The evolution in Nd isotopic compositions towards greater SCLM input in the Lower GRV dacites to rhyolites (Fig. 14a) supports the findings of Chapman *et al.* (2019). Contribution of mafic material to felsic magmas in the Glyde Hill Volcanic Complex evidenced by an increase in $\varepsilon_{Nd(i)}$ of the youngest felsic lavas is coincident with recharge by the Nuckulla Basalt (Fig. 14b).

The Upper GRV is solely silicic in composition. The consistency of negative Nb-Ta-Ti-Sr anomalies, enrichment in HFSE and LREE and low $\varepsilon_{Nd(i)}$ are consistent with crustal sources for the Upper GRV felsic magmas (Rudnick and Gao 2003). Up to 20% crustal material was incorporated in the Upper GRV (Chapman *et al.* 2019), substantially more than in the Lower GRV felsic magmas.

Larger magma chambers tend to average out isotopic heterogeneity of end-member compositions (Riciputi *et al.* 1995). The homogeneity of the Upper GRV magmas suggests larger, and well mixed, magma chamber/s (e.g. Allen *et al.* 2003, Pankhurst *et al.* 2011b). This indicates a change in the magma plumbing system, from small isolated chambers to a large and possibly centralised magma chamber(s). Large volume silicic magmas (>100 km^3) require high temperatures and long thermal histories (10000's–100000's years) prior to eruption (Huppert and Sparks 1988, Bachmann and Huber 2016). Felsic lava production can be very fast at the beginning, as much as 200 km^3 in 10 Kyr (Schöpa and Annen 2013, Bachmann and Huber 2016). Estimated volumes for three of the Upper GRV units range from 1000–4000 km^3 each (Allen *et al.* 2003, Allen *et al.* 2008), suggesting at least 3000–12000 km^3 silicic magma may have been erupted in 300 Kyr. The time required to create this volume of magma would be on the order of 150–600 Kyr, and possibly longer, as magma generation slows down after initial rapid growth (Liu and Lee 2020). As the silicic magma temperatures are high, this lava volume requires an elevated thermal anomaly such as a mantle plume to provide sustained high temperature mafic magma input able to facilitate the rapid production of large volumes of silicic magma (Bachmann and Bergantz 2009).

It is possible the change in mantle source component to a relatively primitive and isotopically juvenile source as documented by the Nuckulla Basalt ca. 1589 Ma (Fig. 14a) generated excessive heat which triggered the large volume silicic magmatism (Liu and Lee 2020). A 1.8 Myr hiatus in magmatic activity preceding the eruption of the Upper GRV Eucarro Rhyolite, and importantly the absence of mafic volcanism after ca. 1589 Ma, may be related to this change. Consequently, partially molten felsic magmas in the crust likely inhibited further mafic magma from erupting (Huppert and Sparks 1988, Pankhurst *et al.* 1998, Ernst 2014) but provided sustained high thermal input. An important feature of the Eucarro Rhyolite is its crystal-poor composition. Crystal-poor magmas are typically generated after periods of inactivity (Kaiser *et al.* 2017). The 1.8 Myr hiatus in magmatic activity from ca. 1588.47 to 1586.66 Ma is consistent with the crystal-poor character of the Eucarro Rhyolite.

The waning thermal effect of a mantle plume

is accompanied by a decrease in magmatic temperatures (e.g. Liu *et al.* 2019). Median Ti-in-zircon temperatures for a subset of felsic GRV rocks show that the maximum temperatures initially increase from 853 to 925 °C at ca. 1592.79 to 1589.19 Ma, and then steadily decline in the younger units (Fig. 12). The pattern of increasing temperatures to a peak and then decreasing in the younger units after such a peak is common in LIPs with associated silicic volcanism (e.g. Chon Aike, Snake River Plain and Tarim; Liu *et al.* 2019) and consistent with the waning effect of a plume. Decrease in temperature is often accompanied by increase in crystallisation in the magma (Liu and Lee 2020). The distinctive crystal-rich composition of the Moonaree Dacite Member is consistent with a decrease in magmatic temperatures (e.g. Liu *et al.* 2019). Median Ti-in-zircon temperatures for the Moonaree Dacite Member range from 802–820 °C, lower than the peak magmatic temperatures recorded by the Mangaroongah Dacite (925 °C; Fig. 12). The Moonaree Dacite Member contains abundant ferromagnesian phases, mafic enclaves and has SiO_2 contents on the lower end of dacite, suggesting recharge of mafic magma into the magma chamber (Bacon 1986, Wiebe 1993). Perturbation of temperature and/or intrusion of mafic magma into silicic magma may have triggered eruption (e.g. Wiebe 1993) in the final stages of the Gawler LIP development. No further volcanism is recorded after 1586.39 Ma, although intrusive magmatism continued until ca. 1570 Ma, also consistent with a waning phase of mantle plume activity (Jagodzinski *et al.* in prep.).

CONCLUSIONS

High precision geochronological data has allowed for a detailed geochemical and isotopic assessment of mafic and felsic extrusive magmas in a Mesoproterozoic LIP. Key features of the tectonic setting, chemistry and magmatic processes for the Gawler LIP include:

1) The 1594–1586 Ma Gawler magmatic event is more like mafic LIPs containing voluminous silicic magmas marked by the high magmatic temperatures associated with mantle plumes, with emplacement on or adjacent to Archean to Proterozoic crust. Its age fits with the range of Proterozoic to recent ages of LIPs. This contrasts to SLIPs (sensu stricto), which are Phanerozoic in age, formed in active margin or continental-rift related settings, nearly exclusively lower in temperature and derived from the melting of hydrous lower crust.
2) A plume model satisfies several key geological and geochemical features in the Gawler LIP:
   i. Melting of thick, old, refractory crust that requires high and sustained thermal input required to generate large volumes of silicic lavas in a short period of time.
   ii. HFSE and REE enriched compositions in felsic rocks inherited from such a crust.
   iii. Generation of mafic and felsic rocks in an intracontinental setting related via fractional crystallisation processes.
   iv. Relatively depleted mafic magmas followed by enriched compositions in the earlier stages of magmatism, related to sustained thermal input into the SCLM.
   v. An isotopically juvenile rejuvenation phase represented by the final stage of basaltic volcanism.
   vi. Changes in magmatic temperatures recorded in felsic units consistent with plume activity, from early high temperatures to decreasing temperatures marking the waning phase of a plume.
3) Changes in magmatic style coupled with geochemical and isotopic features, reflect the evolution of the Gawler LIP magmatic/plumbing system. Higher degrees of partial melting and the larger volume of mafic volcanism associated with the early Roopena Basin system is consistent with

high flux and high volume magmas generated in early plume-head onset melting. Subsequent volcanism developed as isolated, smaller scale melting, producing volcanic centres related through fractional crystallisation and assimilation processes. The final stage of volcanism is manifest as large-scale crustal melting and increased crustal input. The overall isotopic evolution of the Gawler LIP shows two opposing yet complementary trends involving increasing amounts of SCLM and crustal input into the magmas at the province scale, while a complex interplay of magma recharge and differentiation occurs at the individual volcanic centre scale.

ACKNOWLEDGEMENTS

This study is a part of Ph.D. project (C. Wade), and was financially supported by Australian Research Council Linkage Project LP160100578, with the support of the Geological Survey of South Australia. David Bruce, University of Adelaide, is thanked for assistance with Sm–Nd isotope analysis. We acknowledge Greg Swain for providing several whole-rock and Sm-Nd isotope analyses from the central Gawler Craton. Jess Bonsell, Department for Energy and Mining, is thanked for drafting Figure 1 and Figure 2. CW, SC, EJ and AR publish with permission of the Director, Geological Survey of South Australia, Department for Energy and Mining, South Australia.

REFERENCES

Agangi, A., 2011. Magmatic and volcanic evolution of a silicic large igneous province (SLIP): the Gawler Range Volcanics and Hiltaba Suite, South Australia. University of Tasmania, PhD thesis (unpublished).

Allen, S. R. and McPhie, J., 2002. The Eucarro Rhyolite, Gawler Range Volcanics, South Australia; a >675 km^3 compositionally zoned lava of Mesoproterozoic age. Geological Society of America Bulletin, v. 114, p. 1592-1609. doi: https://doi.org/10.1130/0016-7606(2002)114<1592:TERGRV>2.0.CO;2

Allen, S. R., McPhie, J., Ferris, G. and Cadd, A. G., 2008. Evolution and architecture of a large felsic igneous province in western Laurentia: The 1.6 Ga Gawler Range Volcanics, South Australia. Journal of Volcanology and Geothermal Research, v. 172, p. 132-147. doi: https://doi.org/10.1016/j.jvolgeores.2005.09.027

Allen, S. R., Simpson, C. J., McPhie, J. and Daly, S. J., 2003. Stratigraphy, distribution and geochemistry of widespread felsic volcanic units in the Mesoproterozoic Gawler Range Volcanics, South Australia. Australian Journal of Earth Sciences, v. 50, p. 97-112. doi: http://dx.doi.org/10.1046/j.1440-0952.2003.00980.x

Ayalew, D. and Gibson, S. A., 2009. Head-to-tail transition of the Afar mantle plume: Geochemical evidence from a Miocene bimodal basalt–rhyolite succession in the Ethiopian Large Igneous Province. Lithos, v. 112, p. 461-476. doi: https://doi.org/10.1016/j.lithos.2009.04.005

Bachmann, O. and Bergantz, G. W., 2009. Rhyolites and their Source Mushes across Tectonic Settings. Journal of Petrology, v. 49, p. 2277-2285. doi: https://doi.org/10.1093/petrology/egn068

Bachmann, O. and Huber, C., 2016. Silicic magma reservoirs in the Earth's crust. American Mineralogist, v. 101, p. 2377-2404. doi: https://doi.org/10.2138/am-2016-5675

Bacon, C. R., 1986. Magmatic inclusions in silicic and intermediate volcanic rocks. Journal of Geophysical Research: Solid Earth, v. 91, p. 6091-6112. doi: https://doi.org/10.1029/JB091iB06p06091

Baker, J. A., Macpherson, C. G., Menzies, M. A., Thrilwall, M. F., Al-Kasasi, M. and Mattey, D. P., 2000. Resolving Crustal and Mantle Contributions to Continental Flood Volcanism, Yemen; Constraints from Mineral Oxygen Isotope Data. Journal of Petrology, v. 41, p. 1805-1820. doi: https://doi.org/10.1093/petrology/41.12.1805

Beinke, L., Wright, J., McCarthy, A., Barnes, J., Rava, B. and Coopes, G. A., 2012. Data release - as updated [made at SA Director of Mines' discretion] : Bulgunnia. Annual reports to licence expiry/renewal, for the period 8/10/2007 to 7/10/2013. Department of State Development, Government of South Australia, v. ENV 11712, p. pp. 413. Available at: http://mer-env.s3.amazonaws.com/ENV11712.pdf

Blissett, A. H., Creaser, R. A., Daly, S., Flint, D. J. and Parker, A. J., 1993. Gawler Range Volcanics. In: Drexel, J. F., Preiss, W. V. and Parker, A. J. (Eds), The geology of South Australia. Volume 1. The Precambrian. Geological Survey of South Australia, v. Bulletin 54, p. 107-131. Available at: https://sarigbasis.pir.sa.gov.au/WebtopEw/ws/samref/sarig1/image/DDD/BULL054(V1).pdf

Bryan, S. E., 2007. Silicic Large Igneous Provinces. Episodes, v. 30, p. 20–31. doi: https://doi.org/10.18814/epiiugs/2007/v30i1/004

Bryan, S. E., Riley, T. R., Jerram, D. A., Stephens, C. J. and Leat, P. T., 2002. Silicic volcanism: an undervalued component of large igneous provinces and volcanic rifted margins. In: Menzies, M. A., Klemperer, S. I., Ebinger, C. J. and Baker, J. (Eds), Volcanic Rifted Margins. Geological Society of America, Special Paper, v. 362, p. 97–118. https://doi.org/10.1130/0-8137-2362-0.97

Bull, S., Meffre, S., Allen, M., Freeman, H., Tomkinson, M. and Williams, P., 2015. Volcanosedimentary and chronostratigraphic architecture of the host rock succession at Prominent Hill, South Australia. SEG 2015: World-class ore deposits: Discovery to recovery. Society of Economic Geologists, v. p. Available at: http://www.segweb.org/SEG/_Events/Conference_Archives/2015/Conference_Proceedings/files/pdf/Oral-Presentations/Abstracts/Bull.pdf

Campbell, I. H. and Griffiths, R. W., 1990. Implications of mantle plume structure for the evolution of flood basalts. Earth and Planetary Science Letters, v. 99, p. 79-93. doi: https://doi.org/10.1016/0012-821X(90)90072-6

Chapman, N. D., Ferguson, M., Meffre, S. J., Stepanov, A., Maas, R. and Ehrig, K. J., 2019. Pb-isotopic constraints on the source of A-type Suites: Insights from the Hiltaba Suite - Gawler Range Volcanics Magmatic Event, Gawler Craton, South Australia. Lithos, v. 346-347, p. 105156. doi: https://doi.org/10.1016/j.lithos.2019.105156

Cheng, Z., Zhang, Z., Wang, Z., Wang, F., Mao, Q., Xu, L., Ke, S., Yu, H. and Santosh, M., 2020. Petrogenesis of Transitional Large Igneous Province: Insights From Bimodal Volcanic Suite in the Tarim Large Igneous Province. Journal of Geophysical Research: Solid Earth, v. 125, p. e2019JB018382. doi: https://doi/org/10.1029/2019jb018382

Cherry, A. R., Ehrig, K., Kamenetsky, V. S., McPhie, J., Crowley, J. L. and Kamenetsky, M. B., 2018. Precise geochronological constraints on the origin, setting and incorporation of ca. 1.59 Ga surficial facies into the Olympic Dam Breccia Complex, South Australia. Precambrian Research, v. 315, p. 162-178. doi: https://doi.org/10.1016/j.pre-

camres.2018.07.012

Courtney-Davies, L., Tapster, S. R., Ciobanu, C. L., Cook, N. J., Verdugo-Ihl, M. R., Ehrig, K. J., Kennedy, A. K., Gilbert, S. E., Condon, D. J. and Wade, B. P., 2019. A multi-technique evaluation of hydrothermal hematite UPb isotope systematics: Implications for ore deposit geochronology. Chemical Geology, v. 513, p. 54-72. doi: https://doi.org/10.1016/j.chemgeo.2019.03.005

Creaser, R. A., Price, R. C. and Wormald, R. J., 1991. A-type granites revisited: assessment of a residual-source model. Geology, v. 19, p. 163-166. doi: https://doi.org/10.1130/0091-7613(1991)019<0163:ATGRAO>2.3.CO;2

Curtis, S., Wade, C. and Reid, A., 2018. Sedimentary basin formation associated with a silicic large igneous province: stratigraphy and provenance of the Mesoproterozoic Roopena Basin, Gawler Range Volcanics. Australian Journal of Earth Sciences, v. 65, p. 447–463. doi: https://doi.org/10.1080/08120099.2018.1460398

Dai, L., Wang, L., Lou, D., Li, Z.-H., Dong, H., Ma, F., Li, F., Li, S. and Yu, S., 2020. Slab Rollback Versus Delamination: Contrasting Fates of Flat-Slab Subduction and Implications for South China Evolution in the Mesozoic. Journal of Geophysical Research: Solid Earth, v. 125, p. e2019JB019164. doi: https://doi.org/10.1029/2019jb019164

Daly, S. J., 1993. Sediments associated with the Gawler Range Volcanics. In: Drexel, J. F., Preiss, W. V. and Parker, A. J. (Eds), The geology of South Australia. Volume 1. The Precambrian. South Australia. Geological Survey., v. Bulletin 54, p. 124-126. Available at: https://sarigbasis.pir.sa.gov.au/WebtopEw/ws/samref/sarig1/image/DDD/BULL054(V1).pdf

Elkins-Tanton, L. T., Foulger, G. R., Natland, J. H., Presnall, D. C. and Anderson, D. L., 2005. Continental magmatism caused by lithospheric delamination. In: (Eds), Plates, plumes and paradigms. Geological Society of America, v. 388, p. 0. https://doi.org/10.1130/0-8137-2388-4.449

Ernst, R. E., 2014. Large igneous provinces: Cambridge University Press, Cambridge, UK. v. p. availabie at: https://doi.org/10.1017/CBO9781139025300

Ewart, A., Marsh, J. S., Milner, S. C., Duncan, A. R., Kamber, B. S. and Armstrong, R. A., 2004. Petrology and Geochemistry of Early Cretaceous Bimodal Continental Flood Volcanism of the NW Etendeka, Namibia. Part 1: Introduction, Mafic Lavas and Re-evaluation of Mantle Source Components. Journal of Petrology, v. 45, p. 59-105. doi: https://doi.org/10.1093/petrology/egg083

Ewart, A., Milner, S. C., Armstrong, R. A. and Dungan, A. R., 1998. Etendeka Volcanism of the Goboboseb Mountains and Messum Igneous Complex, Namibia. Part I: Geochemical Evidence of Early Cretaceous Tristan Plume Melts and the Role of Crustal Contamination in the Paraná–Etendeka CFB. Journal of Petrology, v. 39, p. 191-225. doi: https://doi.org.10.1093/petroj/39.2.191

Fanning, C. M., Reid, A. and Teale, G. S., 2007. A geochronological framework for the Gawler Craton, South Australia: South Australia. Geological Survey, v. Bulletin 55, p. availabie at: Available at: https://sarigbasis.pir.sa.gov.au/WebtopEw/ws/samref/sarig1/image/DDD/BULL055.pdf

Ferrari, L., López-Martínez, M., Orozco-Esquivel, T., Bryan, S. E., Duque-Trujillo, J., Lonsdale, P. and Solari, L., 2013. Late Oligocene to Middle Miocene rifting and synextensional magmatism

in the southwestern Sierra Madre Occidental, Mexico: The beginning of the Gulf of California rift. Geosphere, v. 9, p. 1161-1200. doi: https://doi.org/10.1130/ges00925.1

Ferrari, L., Orozco-Esquivel, T., Bryan, S. E., López-Martínez, M. and Silva-Fragoso, A., 2018. Cenozoic magmatism and extension in western Mexico: Linking the Sierra Madre Occidental silicic large igneous province and the Comondú Group with the Gulf of California rift. Earth-Science Reviews, v. 183, p. 115-152. doi: https://doi.org/10.1016/j.earscirev.2017.04.006

Ferris, G., 2003. Volcanic textures within the Glyde Hill Volcanic Complex. MESA Journal, v. 29, p. 36–41. doi: Available at: https://sarigbasis.pir.sa.gov.au/WebtopEw/ws/samref/sarig1/image/DDD/MESAJ029036-041.pdf

Flint, R. B., 1993. Hiltaba Suite. In: Drexel, J. F., Preiss, W. V. and Parker, A. J. (Eds), The geology of South Australia. Volume 1. The Precambrian. Geological Survey of South Australia, v. Bulletin 54, p. 127-131. Available at: https://sarigbasis.pir.sa.gov.au/WebtopEw/ws/samref/sarig1/image/DDD/BULL054(V1).pdf

Flint, R. B., Blissett, A. H., Conor, C. H. H., Cowley, W. M., Cross, K. C., Creaser, R. A., Daly, S. J., Krieg, G. W., Major, R. B., Teale, G. S. and Parker, A. J., 1993. Mesoproterozoic. In: Drexel, J. F., Preiss, W. V. and Parker, A. J. (Eds), The geology of South Australia. Volume 1. The Precambrian. Geological Survey of South Australia, v. Bulletin 54, p. 106-169. Available at: https://sarigbasis.pir.sa.gov.au/WebtopEw/ws/samref/sarig1/image/DDD/BULL054(V1).pdf

Fraser, G. L., McAvaney, S., Neumann, N., Szpunar, M. and Reid, A., 2010. Discovery of early Mesoarchean crust in the eastern Gawler Craton, South Australia. Precambrian Research, v. 179, p. 1–21. doi: https://doi.org/10.1016/j.precamres.2010.02.008

Fricke, C., 2005. Source and origin of the Lower Gawler Range Volcanics (GRV), South Australia: geochemical constraints from mafic magmas. Monash University, Hons. thesis (unpublished).

Friedmann, S. J. and Burbank, D. W., 1995. Rift basins and supradetachment basins: intracontinental extensional end-members. Basin Research, v. 7, p. 109-127. doi: https://doi/org.10.1111/j.1365-2117.1995.tb00099.x

Gao, S., Rudnick, R. L., Yuan, H.-L., Liu, X.-M., Liu, Y.-S., Xu, W.-L., Ling, W.-L., Ayers, J., Wang, X.-C. and Wang, Q.-H., 2004. Recycling lower continental crust in the North China craton. Nature, v. 432, p. 892-897. doi: https://doi.org/10.1038/nature03162

Giles, C. W., 1980. A comparative study of Archaean and Proterozoic felsic volcanic associations in southern Australia. University of Adelaide, PhD thesis (unpublished).

Giles, C. W., 1988. Petrogenesis of the Proterozoic Gawler Range volcanics, South Australia. Precambrian Research, v. 40-41, p. 407-427. doi: https://doi.org/10.1016/0301-9268(88)90078-2

Haase, K. M., Beier, C. and Kemner, F., 2019. A Comparison of the Magmatic Evolution of Pacific Intraplate Volcanoes: Constraints on Melting in Mantle Plumes. Frontiers in Earth Science, v. 6, p. doi: https://doi.org/10.3389/feart.2018.00242

Hagemann, S. G., Lisitsin, V. A. and Huston, D. L., 2016. Mineral system analysis: Quo vadis. Ore Geology Reviews, v. 76, p. 504-522. doi: https://doi.org/10.1016/j.oregeorev.2015.12.012

Hand, M., Reid, A. and Jagodzinski, E., 2007. Tectonic framework and evolution of the Gawler Craton, South Australia. Economic Geology, v. 102, p. 1377-1395. doi: https://doi.org/10.2113/gsecongeo.102.8.1377

Harrison, L. N., Weis, D. and Garcia, M. O., 2017. The link between Hawaiian mantle plume composition, magmatic flux, and deep mantle geodynamics. Earth and Planetary Science Letters, v. 463, p. 298-309. doi: https://doi.org/10.1016/j.epsl.2017.01.027

Hawkesworth, C., Mantovani, M. and Peate, D., 1988. Lithosphere Remobilization during Paraná CFB Magmatism. Journal of Petrology, v. Special_Volume, p. 205-223. doi: https://doi.org/10.1093/petrology/Special_Volume.1.205

Hawkesworth, C. J., Gallagher, K., Kirstein, L., Mantovani, M. S. M., Peate, D. W. and Turner, S. P., 2000. Tectonic controls on magmatism associated with continental break-up: an example from the Paraná–Etendeka Province. Earth and Planetary Science Letters, v. 179, p. 335-349. doi: https://doi.org/10.1016/S0012-821X(00)00114-X

Hildreth, W. and Moorbath, S., 1988. Crustal contributions to arc magmatism in the Andes of Central Chile. Contributions to Mineralogy and Petrology, v. 98, p. 455-489. doi: https://doi.org/10.1007/BF00372365

Hoernle, K., Rohde, J., Hauff, F., Garbe-Schönberg, D., Homrighausen, S., Werner, R. and Morgan, J. P., 2015. How and when plume zonation appeared during the 132 Myr evolution of the Tristan Hotspot. Nature Communications, v. 6, p. 7799. doi: https://doi.org/10.1038/ncomms8799

Howard, K. E., Hand, M., Barovich, K. and Belousova, E., 2011a. Provenance of late Paleoproterozoic cover sequences in the central Gawler Craton: exploring stratigraphic correlations in eastern Proterozoic Australia using detrital zircon ages, Hf and Nd isotopic data. Australian Journal of Earth Sciences, v. 58, p. 475–500. doi: https://doi.org/10.1080/08120099.2011.577753

Howard, K. E., Hand, M., Barovich, K. M., Payne, J. L. and Belousova, E. A., 2011b. U-Pb, Lu-Hf and Sm-Nd isotopic constraints on provenance and depositional timing of metasedimentary rocks in the western Gawler Craton: Implications for Proterozoic reconstruction models. Precambrian Research, v. 184, p. 43–62. doi: https://doi.org/10.1016/j.precamres.2010.10.002

Huang, Q., Kamenetsky, V. S., Ehrig, K., McPhie, J., Kamenetsky, M., Cross, K., Meffre, S., Agangi, A., Chambefort, I., Direen, N. G., Maas, R. and Apukhtina, O., 2016. Olivine-phyric basalt in the Mesoproterozoic Gawler silicic large igneous province, South Australia: Examples at the Olympic Dam Iron Oxide Cu–U–Au–Ag deposit and other localities. Precambrian Research, v. 281, p. 185-199. doi: https://doi.org/10.1016/j.precamres.2016.05.019

Huppert, H. E. and Sparks, R. S. J., 1988. The Generation of Granitic Magmas by Intrusion of Basalt into Continental Crust. Journal of Petrology, v. 29, p. 599-624. doi: https://doi.org/10.1093/petrology/29.3.599

Jagodzinski, E. A., Reid, A. J., Crowley, J. L., McAvaney, S. and Wade, C. E., in prep. Precise zircon U-Pb dating of a Mesoproterozoic felsic large igneous province: the Gawler Range Volcanics and Benagerie Volcanic Suite, South Australia.

Jellinek, A. M. and Manga, M., 2004. Links between long-lived hot spots, mantle plumes, D", and plate tectonics. Reviews of Geophysics, v. 42, p. doi:

https://doi.org/10.1029/2003rg000144

Jochum, K. P., Nohl, U., Herwig, K., E, L., B, S. and Hofmann, A. W., 2005. GeoReM: A New Geochemical Database for Reference Materials and Isotopic Standards. Geostandards and Geoanalytical Research v. 29 p. 333-338. doi: https://doi.org.10.1111/j.1751-908X.2005.tb00904.x

Johnson, J. P., 1993. The geochronology and radiogenic isotope systematics of the Olympic Dam copper-uranium-gold-silver deposit, South Australia. Australian National University, PhD thesis (unpublished).

Kaiser, J. F., de Silva, S., Schmitt, A. K., Economos, R. and Sunagua, M., 2017. Million-year melt–presence in monotonous intermediate magma for a volcanic–plutonic assemblage in the Central Andes: Contrasting histories of crystal-rich and crystal-poor super-sized silicic magmas. Earth and Planetary Science Letters, v. 457, p. 73-86. doi: https://doi.org/10.1016/j.epsl.2016.09.048

Karsli, O., Caran, Ş., Çoban, H., Şengün, F., Tekkanat, O. and Andersen, T., 2020. Melting of the juvenile lower crust in a far-field response to roll-back of the southern Neotethyan oceanic lithosphere: the Oligocene adakitic dacites, NE Turkey. Lithos, v. 370-371, p. 105614. doi: https://doi.org/10.1016/j.lithos.2020.105614

Kay, R. W. and Kay, M., S. , 1993. Delamination and delamination magmatism. Tectonophysics, v. 219, p. 177-189. doi: https://doi.org/10.1016/0040-1951(93)90295-U

Kennett, B. L. N., Fichtner, A., Fishwick, S. and Yoshizawa, K., 2012. Australian Seismological Reference Model (AuSREM): mantle component. Geophysical Journal International, v. 192, p. 871-887. doi: https://doi.org/10.1093/gji/ggs065

Kirstein, L. A., Peate, D. W., Hawkesworth, C. J., Turner, S. P., Harris, C. and Mantovani, M. S. M., 2000. Early Cretaceous Basaltic and Rhyolitic Magmatism in Southern Uruguay Associated with the Opening of the South Atlantic. Journal of Petrology, v. 41, p. 1413-1438. doi: https://doi.org/10.1093/petrology/41.9.1413

Klein, E. M., 2004. Geochemistry of the Igneous Oceanic Crust. In: Holland, H. D. and Turekian, K. K. (Eds), In: Treatise on Geochemistry. Elsevier, v. 3, p. 433–463. https://.org/10.1016/B0-08-043751-6/03030-9

Kumagai, I., Davaille, A., Kurita, K. and Stutzmann, E., 2008. Mantle plumes: thin, fat, successful, or failing? Constraints to explain hot spot volcanism through time and space. Geophysical Research Letters, v. 35, p. doi: https://doi.org/10.1029/2008GL035079

Lee, C.-T. A. and Tang, M., 2020. How to make porphyry copper deposits. Earth and Planetary Science Letters, v. 529, p. 115868. doi: https://doi.org/10.1016/j.epsl.2019.115868

Lee, Y., Cho, M., Cheong, W. and Yi, K., 2014. A massif-type (~1.86 Ga) anorthosite complex in the Yeongnam Massif, Korea: late-orogenic emplacement associated with the mantle delamination in the North China Craton. Terra Nova, v. 26, p. 408-416. doi: https://doi.org/10.1111/ter.12115

Li, X.-H., Li, W.-X., Li, Z.-X. and Liu, Y., 2008. 850–790 Ma bimodal volcanic and intrusive rocks in northern Zhejiang, South China: A major episode of continental rift magmatism during the breakup of Rodinia. Lithos, v. 102, p. 341-357. doi: https://doi.org/10.1016/j.lithos.2007.04.007

Li, Z.-H., Liu, M. and Gerya, T., 2016. Lithosphere delamination in continental

collisional orogens: A systematic numerical study. Journal of Geophysical Research: Solid Earth, v. 121, p. 5186-5211. doi: https://doi.org/10.1002/2016jb013106

Li, Z.-X. and Li, X.-H., 2007. Formation of the 1300-km-wide intracontinental orogen and postorogenic magmatic province in Mesozoic South China: A flat-slab subduction model. Geology, v. 35, p. 179-182. doi: https://doi.org/10.1130/g23193a.1

Liu, B. and Lee, C.-T., 2020. Large Silicic Eruptions, Episodic Recharge, and the Transcrustal Magmatic System. Geochemistry, Geophysics, Geosystems, v. 21, p. e2020GC009220. doi: https://doi.org/10.1029/2020gc009220

Liu, H.-Q., Xu, Y.-G., Zhong, Y.-T., Luo, Z.-Y., Mundil, R., Riley, T. R., Zhang, L. and Xie, W., 2019. Crustal melting above a mantle plume: Insights from the Permian Tarim Large Igneous Province, NW China. Lithos, v. 326-327, p. 370-383. doi: https://doi.org/10.1016/j.lithos.2018.12.031

Liu, J.-H., Xie, C.-M., Li, C., Wang, M., Wu, H., Li, X.-K., Liu, Y.-M. and Zhang, T.-Y., 2018. Early Carboniferous adakite-like and I-type granites in central Qiangtang, northern Tibet: Implications for intra-oceanic subduction and back-arc basin formation within the Paleo-Tethys Ocean. Lithos, v. 296-299, p. 265-280. doi: https://doi.org/10.1016/j.lithos.2017.11.005

Marsh, J. S., Ewart, A., Milner, S. C., Duncan, A. R. and Miller, R. M., 2001. The Etendeka Igneous Province: magma types and their stratigraphic distribution with implications for the evolution of the Paraná-Etendeka flood basalt province. Bulletin of Volcanology, v. 62, p. 464-486. doi: https://doi.org/10.1007/s004450000115

McAvaney, S. O., Werner, M., Pawley , M. J., Krapf, C. B. E. and Nicolson, B. E., 2016. Geology of the Six Mile Hill 1:75 000 Map Sheet. Department of State Development, v. Report Book 2016/00014, p. pp. 245. Available at: Available at: https://sarigbasis.pir.sa.gov.au/WebtopEw/ws/samref/sarig1/image/DDD/RB201600014.pdf

McPhie, J., DellaPasqua, F., Allen, S. R. and Lackie, M. A., 2008. Extreme effusive eruptions: Palaeoflow data on an extensive felsic lava in the Mesoproterozoic Gawler Range Volcanics. Journal of Volcanology and Geothermal Research, v. 172, p. 148-161. doi: https://doi.org/10.1016/j.jvolgeores.2006.11.011

McPhie, J., Orth, K., Kamenetsky, V. S., Kamenetsky, M. and Ehrig, K., 2016. Characteristics, origin and significance of Mesoproterozoic bedded clastic facies at the Olympic Dam Cu-U-Au-Ag deposit, South Australia. Precambrian Research, v. 276, p. 85-100. doi: https://doi.org/10.1016/j.precamres.2016.01.029

Nakakuki, T. and Mura, E., 2013. Dynamics of slab rollback and induced back-arc basin formation. Earth and Planetary Science Letters, v. 361, p. 287-297. doi: https://doi.org/10.1016/j.epsl.2012.10.031

Pankhurst, M. J., Schaefer, B. F. and Betts, P. G., 2011a. Geodynamics of rapid voluminous felsic magmatism through time. Lithos, v. 123, p. 92-101. doi: https://doi.org/10.1016/j.lithos.2010.11.014

Pankhurst, M. J., Schaefer, B. F., Turner, S. P., Argles, T. and Wade, C. E., 2013. The source of A-type magmas in two contrasting settings: U–Pb, Lu–Hf and Re–Os isotopic constraints. Chemical Geology, v. 351, p. 175-194. doi: https://doi.org/10.1016/j.chemgeo.2013.05.010

Pankhurst, M. P., Schaefer, B. F., Betts, P. G., Phillips, N. and Hand, M., 2011b. A Mesoproterozoic continental flood rhyolite province, the Gawler Ranges, Australia: the end member example of the Large Igneous Province clan. Solid Earth, v. 2, p. 1-9. doi: https://doi.org/10.5194/se-2-25-2011

Pankhurst, R. J., Leat, P. T., Sruoga, P., Rapela, C. W., Márquez, M., Storey, B. C. and Riley, T. R., 1998. The Chon Aike province of Patagonia and related rocks in West Antarctica: A silicic large igneous province. Journal of Volcanology and Geothermal Research, v. 81, p. 113-136. doi: https://doi.org/10.1016/S0377-0273(97)00070-X

Pankhurst, R. J., Riley, T. R., Fanning, C. M. and Kelley, S. P., 2000. Episodic Silicic Volcanism in Patagonia and the Antarctic Peninsula: Chronology of Magmatism Associated with the Break-up of Gondwana. Journal of Petrology, v. 41, p. 605-625. doi: https://doi.org/10.1093/petrology/41.5.605

Payne, J., Barovich, K. and Hand, M., 2006. Provenance of metasedimentary rocks in the northern Gawler Craton, Australia: Implications for Palaeoproterozoic reconstructions. Precambrian Research, v. 148, p. 275-291. doi: https://doi.org/10.1016/j.precamres.2006.05.002

Payne, J. L., Ferris, G., Barovich, K. M. and Hand, M., 2010. Pitfalls of classifying ancient magmatic suites with tectonic discrimination diagrams: An example from the Paleoproterozoic Tunkillia Suite, southern Australia. Precambrian Research, v. 177, p. 227-240. doi: https://doi.org/10.1016/j.precamres.2009.12.005

Pearce, J. A., 2008. Geochemical fingerprinting of oceanic basalts with applications to ophiolite classification and the search for Archean oceanic crust. Lithos, v. 100, p. 14-48. doi: https://doi.org/10.1016/j.lithos.2007.06.016

Pearce, J. A., Ernst, R. E., Rogers, C. and Peate, D. W., 2017. LIP Printing: A Geochemical Proxy Approach to LIP Forensics. Geological Society of America Annual Meeting, Seattle, Washington, USA. Geological Society of America Abstracts with Programs, v. 49, No. 6, p. doi: https://doi.org.10.1130/abs/2017AM-301471

Reid, A., Fricke, C. E. and Cowley, W. M., 2009. Extent of the low-grade Archaean Devils Playground Volcanics in the north-eastern Gawler Craton: evidence from recent PACE drilling. MESA Journal, v. 54, p. 9-19. Available at: https://sarigbasis.pir.sa.gov.au/WebtopEw/ws/samref/sarig1/image/DDD/MESAJ054009-019.pdf

Reid, A. J., Pawley, M. J., Wade, C., Jagodzinski, E. A., Dutch, R. A. and Armstrong, R., 2019. Resolving tectonic settings of ancient magmatic suites using structural, geochemical and isotopic constraints: the example of the St Peter Suite, southern Australia. Australian Journal of Earth Sciences, v. p. 1-28. doi: https://10.1080/08120099.2019.1632224

Riciputi, L. R., Johnson, C. M., Sawyer, D. A. and Lipman, P. W., 1995. Crustal and magmatic evolution in a large multicyclic caldera complex: isotopic evidence from the central San Juan volcanic field. Journal of Volcanology and Geothermal Research, v. 67, p. 1-28. doi: https://doi.org/10.1016/0377-0273(94)00097-Z

Rogers, C., Kamo, S. L., Söderlund, U., Hamilton, M. A., Ernst, R. E., Cousens, B., Harlan, S. S., Wade, C. E. and Thorkelson, D. J., 2018. Geochemistry and U-Pb geochronology of 1590 and

1550 Ma mafic dyke swarms of western Laurentia: Mantle plume magmatism shared with Australia. Lithos, v. 314-315, p. 216-235. doi: https://doi.org/10.1016/j.lithos.2018.06.002

Rudnick, R. L. and Gao, S., 2003. Composition of the continental crust. In: Holland, H. D., Rudnick, R. L. and Turekian, K. K. (Eds), The Crust. Elsevier/Pergamon, Oxford, v. Treatise on Geochemistry, vol. 3, p. 1-64.

Schöpa, A. and Annen, C., 2013. The effects of magma flux variations on the formation and lifetime of large silicic magma chambers. Journal of Geophysical Research: Solid Earth, v. 118, p. 926-942. doi: https://doi.org/10.1002/jgrb.50127

Skirrow, R., van der Wielen, S. E., Champion, D. C., Czarnota, K. and Thiel, S., 2018. Lithospheric artchitecture and mantle metasomatism linked to iron-oxide Cu-Au ore formation: Multidiciplinary evidence from the Olympic Dam region, South Australia. Geochemistry, Geophysics, Geosystems, v. 19, p. doi: https://doi.org/10.1029/2018GC007561

Stewart, K., 1994. High temperature felsic volcanism and the role of mantle magmas in Proterozoic crustal growth : the Gawler Range volcanic province. University of Adelaide, PhD thesis (unpublished).

Storey, B. C. and Alabaster, T., 1991. Tectonomagmatic controls on Gondwana break-up models: Evidence from the Proto-Pacific Margin of Antarctica. Tectonics, v. 10, p. 1274-1288. doi: https://doi.org.10.1029/91tc01122

Swain, G., Barovich, K., Hand, M., Ferris, G. and Schwarz, M., 2008. Petrogenesis of the St Peter Suite, southern Australia: arc magmatism and Proterozoic crustal growth of the South Australian Craton. Precambrian Research, v. 166, p. 283-296. doi: https://doi.org/10.1016/j.precamres.2007.07.028

Swain, G., Woodhouse, A., Hand, M., Barovich, K., Schwarz, M. and Fanning, C. M., 2005. Provenance and tectonic development of the late Archaean Gawler Craton, Australia; U-Pb zircon, geochemical and Sm-Nd isotopic implications. Precambrian Research, v. 141, p. 106-136. doi: https://doi.org/10.1016/j.precamres.2005.08.004

Symington, N. J., Weinberg, R. F., Hasalová, P., Wolfram, L. C., Raveggi, M. and Armstrong, R. A., 2014. Multiple intrusions and remelting-remobilization events in a magmatic arc: The St Peter Suite, South Australia. GSA Bulletin, v. 126, p. 1200–1218. doi: https://doi.org/10.1130/B30975.1

Szpunar, M., Hand, M., Barovich, K., Jagodzinski, E. and Belousova, E., 2011. Isotopic and geochemical constraints on the Paleoproterozoic Hutchison Group, southern Australia: Implications for Paleoproterozoic continental reconstructions. Precambrian Research, v. 187, p. 99-126. doi: https://doi.org/10.1016/j.precamres.2011.02.006

Tiddy, C. J. and Giles, D., 2020. Supra-subduction zone model for metal endowment at 1.60-1.575 Ga in eastern Australia. Ore Geology Reviews, v. 122, p. doi: https://doi.org/10.1016/j.oregeorev.2020.103483

Wade, C. E., 2012. Geochemistry of pre-1570 Ma mafic magmatism within Southern Australia: implications for possible tectonic settings and of major mineralisation events in South Australia. Geological Survey of South Australia, v. Report Book 2012/00019, p. 270. Available at: https://sarigbasis.pir.sa.gov.au/WebtopEw/ws/samref/sarig1/image/DDD/RB201200019.pdf

Wade, C. E., Payne, J. L., Barovich, K. M. and Reid, A. J., 2019. Heterogeneity of the sub-continental lithospheric mantle and 'non-juvenile' mantle additions to a Proterozoic silicic large igneous province. Lithos, v. 340-341, p. 87-107. doi: https://doi.org/10.1016/j.lithos.2019.05.005

Wade, C. E., Reid, A., Wingate, M. T. D., Jagodzinski, E. A. and Barovich, K., 2012. Geochemistry and geochronology of the c. 1585 Ma Benagerie Volcanic Suite, southern Australia: relationship to the Gawler Range Volcanics and implications for the petrogenesis of a Mesoproterozoic silicic large igneous province Precambrian Research, v. 206–207, p. 17–35. doi: https://doi.org/10.1016/j.precamres.2012.02.020

Wells, M. L. and Hoisch, T. D., 2008. The role of mantle delamination in widespread Late Cretaceous extension and magmatism in the Cordilleran orogen, western United States. GSA Bulletin, v. 120, p. 515-530. doi: https://doi/org/10.1130/b26006.1

White, R. and McKenzie, D., 1989. Magmatism at rift zones: the generation of volcanic continental margins and flood basalts. Journal of Geophysical Research: Solid Earth, v. 94, p. 7685-7729. doi: https://doi.org/10.1029/JB094iB06p07685

White, R. S., 1993. Melt production rates in mantle plumes. Philosophical Transactions of the Royal Society of London. Series A: Physical and Engineering Sciences, v. 342, p. 137-153. doi: https://doi.org/10.1098/rsta.1993.0010

Wiebe, R. A., 1993. Basaltic injections into floored silicic magma chambers. Eos, Transactions American Geophysical Union, v. 74, p. 1-3. doi: https://doi.org/10.1029/93eo00161

Xu, J.-F., Shinjo, R., Defant, M. J., Wang, Q. and Rapp, R. P., 2002. Origin of Mesozoic adakitic intrusive rocks in the Ningzhen area of east China: Partial melting of delaminated lower continental crust? Geology, v. 30, p. 1111-1114. doi: https://doi.org/10.1130/0091-7613(2002)030<1111:Oomair>2.0.Co;2

Xu, W., Xu, X. and Zeng, G., 2017. Crustal contamination versus an enriched mantle source for intracontinental mafic rocks: Insights from early Paleozoic mafic rocks of the South China Block. Lithos, v. 286-287, p. 388-395. doi: https://doi.org/10.1016/j.lithos.2017.06.023

Zhang, H.-F., Parrish, R., Zhang, L., Xu, W.-C., Yuan, H.-L., Gao, S. and Crowley, Q. G., 2007. A-type granite and adakitic magmatism association in Songpan–Garze fold belt, eastern Tibetan Plateau: Implication for lithospheric delamination. Lithos, v. 97, p. 323-335. doi: https://doi.org/10.1016/j.lithos.2007.01.002

Zhou, M.-F., Zhao, J.-H., Qi, L., Su, W. and Hu, R., 2006. Zircon U-Pb geochronology and elemental and Sr–Nd isotope geochemistry of Permian mafic rocks in the Funing area, SW China. Contributions to Mineralogy and Petrology, v. 151, p. 1-19. doi: https://doi.org/10.1007/s00410-005-0030-y

Chapter 5

This chapter is written for submission to Economic Geology as: Wade, C., Payne, J., Barovich, K., Gilbert, S., Wade, B.P., Crowley, J. L., Reid, A. and Jagodzinski, E. A., in review. Zircon trace element geochemistry as an indicator of magma fertility in iron oxide-copper-gold terrains.

Statement of Authorship

Title of Paper	Zircon trace element geochemistry as an indicator of magma fertility in iron oxide-copper-gold terranes
Publication Status	☐ Published ☐ Accepted for Publication ☐ Submitted for Publication ☑ Unpublished and Unsubmitted work written in manuscript style
Publication Details	Wade, C.E., Payne, J.L, Barovich, K.M., Gilbert, S.E., Wade, B.P., Reid, A.J., Crowley, J.L., and Jagodzinski, E.A. Zircon trace element geochemistry as an indicator of magma fertility in iron oxide-copper-gold provinces.

Principal Author

Name of Principal Author (Candidate)	Claire Wade		
Contribution to the Paper	Sample collection and preparation Data collection, Data processing, Data curation Investigation, Conceptualisation, Formal Analysis, Visualisation, Methodology, Validation Writing original draft, editing and review		
Overall percentage (%)	65%		
Certification:	This paper reports on original research I conducted during the period of my Higher Degree by Research candidature and is not subject to any obligations or contractual agreements with a third party that would constrain its inclusion in this thesis. I am the primary author of this paper.		
Signature		Date	6/10/2020

Co-Author Contributions

By signing the Statement of Authorship, each author certifies that:

i. the candidate's stated contribution to the publication is accurate (as detailed above);

ii. permission is granted for the candidate in include the publication in the thesis; and

iii. the sum of all co-author contributions is equal to 100% less the candidate's stated contribution.

Name of Co-Author	Justin Payne		
Contribution to the Paper	Conceptualisation, Investigation, Visualisation, Methodology Data collection and processing, Formal analysis, Validation Supervision Writing, editing and review Funding acquisition		
Signature		Date	11/10/2020

Name of Co-Author	Karin Barovich		
Contribution to the Paper	Investigation, Conceptualisation, Validation Supervision Writing, editing and review		
Signature		Date	15/11/2020

Name of Co-Author	Sarah Gilbert
Contribution to the Paper	Data collection, Resources Validation Writing, editing
Signature	Date: 20/11/2020

Name of Co-Author	Ben Wade
Contribution to the Paper	Data collection and processing, Formal analysis, Resources Validation Writing, editing
Signature	Date: 17/11/2020

Name of Co-Author	Anthony Reid
Contribution to the Paper	Conceptualisation, Validation Sample collection Supervision Editing and review
Signature	Date: 16/11/2020

Name of Co-Author	James Crowley
Contribution to the Paper	Data collection, Data processing, Data curation Formal analysis, Validation Resources Editing and review
Signature	Date: 17/11/2020

Name of Co-Author	Elizabeth Jagodzinski
Contribution to the Paper	Sample collection, Data collection, Data processing, Data curation Editing and review
Signature	Date: 15/11/2020

ABSTRACT
Extrusive and intrusive felsic magmas occur throughout the evolution of silicic large igneous province (SLIP) magmatism that is temporally related to numerous economically significant IOCG deposits in southern Australia. We investigate zircon trace element signatures of such felsic magmas to assess whether zircon composition can be related to inferred fertility of the volcanic and intrusive suites within IOCG hosted mineral provinces. The rare earth element (REE) patterns of zircon sourced from both extrusive and intrusive magmatic rocks are characterized by light REE depletions, and a range of positive Ce and negative Eu anomalies, consistent with zircon formation in oxidizing magmatic conditions. Zircon in mineralization-related intrusives and extrusives are distinguished from zircon in mineralization-absent rocks by higher Eu/Eu*, Ce/Ce* and Ti values and separate magma evolution paths with respect to Hf. These zircon characteristics correspond to lower degrees of fractionation and/or crustal assimilation, more oxidizing magmatic conditions and higher magmatic temperatures, respectively, in magmas coeval with mineralization. In this respect, we consider higher oxidation state, lower degrees of fractionation and higher magmatic temperatures to be features of fertile magmas in southern Australian IOCG terrains. Similar zircon REE characteristics are shared between magmas associated with southern Australian IOCG and IOA rhyolites from the St Francois Mountains, Missouri, namely high Ce/Ce* and high Dy/Yb, indicative of oxidized and dry magmas, respectively. The dry and more fractionated nature of the IOCG and IOA associated magmas contrasts with the hydrous and unfractionated nature of fertile porphyry Cu deposit magmas. The oxidized nature, as indicated by high Ce/Ce* ratios, is considered a key element in magma fertility in IOCG-IOA terrains. In both IOCG and IOA terrains, the trace element compositions of zircon are able to broadly differentiate fertile from non-fertile magmatic rocks.

INTRODUCTION

Iron oxide-copper-gold (IOCG) and iron oxide-apatite (IOA) deposits are some of the world's most valuable ore resources, and contain appreciable amounts of critical metals including rare earth elements, U, F, P, Mo, Ag, Ba, Co, Ni and As (Groves *et al.* 2010, Barton 2014). IOCG and IOA deposits are associated with one another in some Phanerozoic and Proterozoic belts, suggesting that, at least in some instances, they represent a continuum of magmatic-hydrothermal deposits formed by related processes (Corriveau *et al.* 2016). The complexity of these deposits has led to ongoing debate about their origin, tectonic setting and source(s) of mineralizing hydrothermal fluids and metals for the IOCG-IOA systems (Hitzman 2000, Sillitoe 2003, Skirrow 2009, Groves *et al.* 2010). Investigations into IOCG-IOA origins are hindered by the Precambrian age of most deposits, although some are extremely well exposed and unmetamorphosed, many are concealed beneath younger sedimentary cover and have undergone subsequent reworking events (Hitzman 2000, Groves *et al.* 2010). IOCG and IOA end-members occur in the Olympic Cu-Au Province in southern Australia (Reid 2019 and references therein), the Chilean Iron Belt (e.g. Sillitoe 2003), Benavides *et al.* (2007), the Great Bear magmatic zone, Canada (Corriveau *et al.* 2016) and the St Francois Mountains, Missouri (Day *et al.* 2016).

The IOCG-IOA deposit family is interpreted to share some genetic attributes with porphyry Cu deposit, including subduction-modified magmatic sources and association with highly oxidized, calc-alkaline to mildly alkaline magmas (e.g. Richards and Mumin 2013). Porphyry Cu deposits are associated with felsic to intermediate, call-alkaline to alkaline, hydrous magmas centered on intrusions (e.g. Sillitoe 2010). In these systems, water content,

oxidation state and magma source are considered significant determinants of magma fertility (Cooke *et al.* 2005, Sillitoe 2010, Richards 2011, 2015, Sun *et al.* 2015) and this information is well preserved in zircon chemistry (Lu *et al.* 2016, Loader *et al.* 2017, Shu *et al.* 2019). Thus, zircon trace element signatures have recently been applied to Phanerozoic porphyry-related magmatic rocks and their mineralizing systems, as a means to assess potential magmatic suite fertility (e.g. Lu *et al.* 2016, Shu *et al.* 2019). IOCG-IOA mineralization is associated with discrete volcanic centers and coeval intrusions with mafic to felsic composition (Cross *et al.* 1993, Johnson and McCulloch 1995, Skirrow *et al.* 2018). IOCG-IOA mineralization in the Olympic Cu-Au Province and Great Bear Magmatic Zone is followed by large volume rhyolite volcanism and emplacement of barren intrusions (Montreuil *et al.* 2016, Reid 2019). IOCG-IOA affiliated magmas are enriched in rare earth elements and high field strength elements, consistent with high temperature, A-type affinity magmas (Hildebrand *et al.* 2010, Corriveau *et al.* 2016, Day *et al.* 2016, Montreuil *et al.* 2016). It is often the case that the Precambrian igneous rocks associated with IOCG-IOA deposits are extensively altered or deformed by younger events and/or highly weathered, making it exceedingly difficult to reconstruct their original magmatic character from whole rock chemistry. The demonstrated relationship between magma fertility and zircon chemistry in porphyry Cu deposits raises the possibility that the trace element signature of zircon in magmatic systems associated with IOCG and IOA systems could be used to assess the fertility of igneous rocks within mineral provinces, including regions with extensively overprinted whole rock chemistry.

Magmas with A-type affinity occur throughout the evolution of the c. 1590 Ma Gawler silicic large igneous province (SLIP) magmatism (e.g. Allen *et al.* 2008, Agangi *et al.* 2012) in the Olympic Cu-Au Province. Not all of these magmas show affiliation with mineralization. To test the relationship between magma fertility and zircon chemistry in IOCG and IOA systems, we use zircon from the Gawler SLIP located in the Gawler Craton, southern Australia. This SLIP is temporally related to numerous economically significant IOCG deposits, including the world-class type-deposit Olympic Dam (Skirrow *et al.* 2018). Our new zircon compositional data suggest that the trace element signature of zircon from mineralization-related magmatic rocks is distinct from those that are not mineralized raising the possibility that this approach is applicable to exploration for IOCG-IOA deposits in addition to porphyry Cu deposits.

BACKGROUND

A Mesoproterozoic SLIP and associated IOCG mineralization

The c. 1590 Ma SLIP consists of the Gawler Range Volcanics (GRV), which comprise rhyolite-dacite lavas, with lesser basalt-andesite lavas (Allen *et al.* 2008) and comagmatic felsic and lesser mafic and ultramafic intrusive rocks of the Hiltaba Suite (Wade *et al.* 2019). The total magmatic volume of the Gawler SLIP is estimated to be 110 000 km^3 (Allen *et al.* 2003, McPhie *et al.* 2008, Pankhurst *et al.* 2011, Wade *et al.* 2012). Precise, chemical abrasion thermal ionization mass spectrometer (CA-TIMS) U-Pb zircon dating shows GRV magmatism occurred in two phases, the first from 1593.6–1588.5 Ma (Lower GRV) and the second phase from 1586.7–1586.4 Ma (Upper GRV; Jagodzinski *et al.* 2016). Ages obtained for the Hiltaba Suite using LA-ICP-MS and SHRIMP U-Pb geochronology range from 1595–1570 Ma (Reid 2019 and references therein). As the external uncertainty of LA-ICP-MS and SHRIMP methods is typically ~1% (2SD, e.g. Allen and Campbell 2012, Horstwood *et al.* 2016) a precise duration and internal stratigraphy of the SLIP cannot be reliably established using data from these

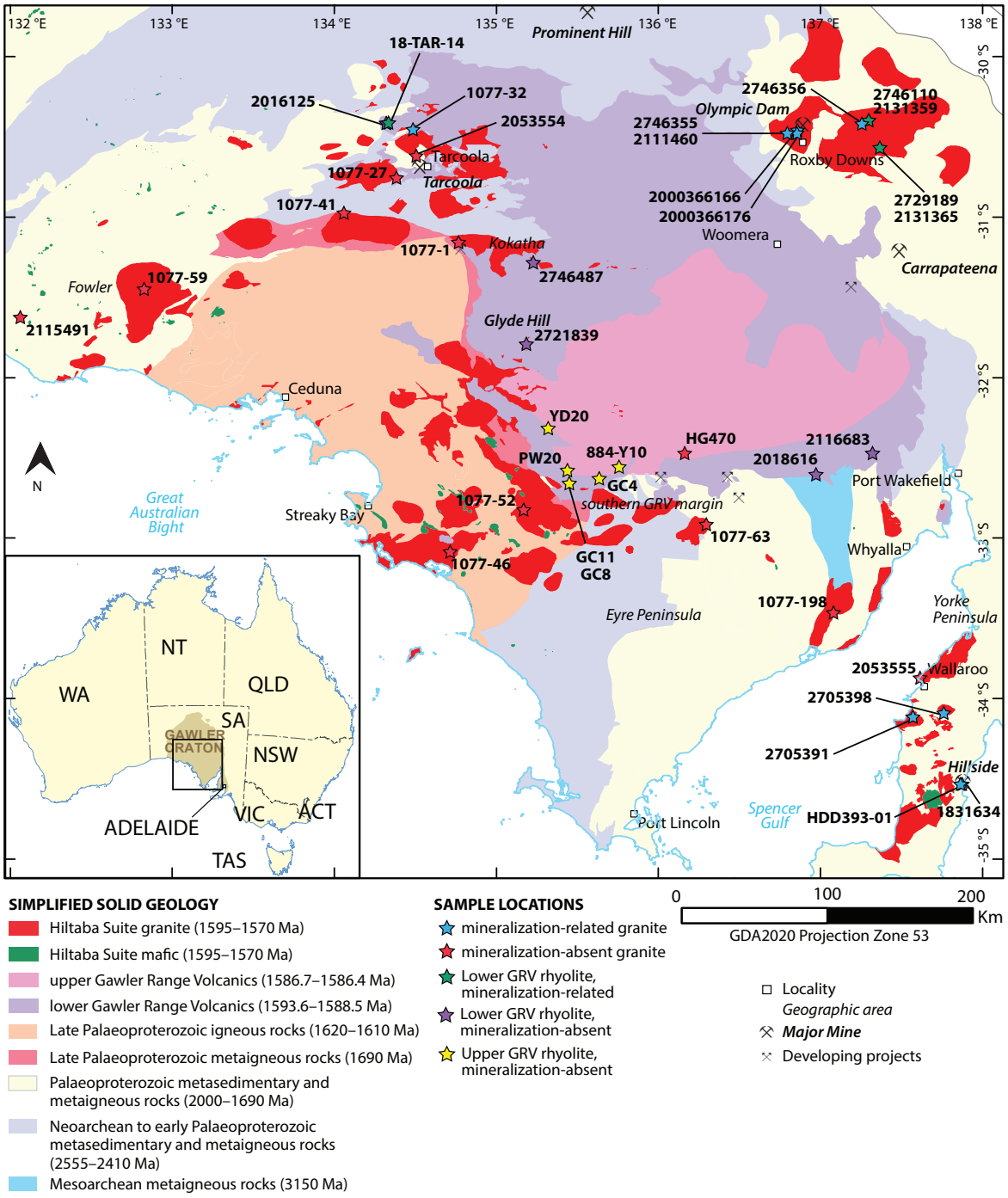

Figure 1. Regional diagram of the interpreted solid geology of the Gawler Craton and study area, displaying locations sampled for zircon trace element analysis.

microbeam analysis methods. As a result, the relative age of rocks is only referred to when constrained by volcanic stratigraphy or CA-TIMS high precision geochronology.

Magmatic rocks associated with the SLIP are predominantly trace and REE-enriched and are considered to be consistent with an A-type classification (Whalen *et al.* 1987, Creaser 1996). Significant mineralization developed between 1594 and 1590 Ma (Cherry *et al.* 2018, Courtney-Davies *et al.* 2019, Court-

ney-Davies *et al.* 2020, McPhie *et al.* 2020), during the early stages of the SLIP event, and produced a belt of IOCG-dominated deposits in the eastern Gawler Craton (Fig. 1; Skirrow *et al.* 2007, Reid 2019). The timing of this major phase of mineralization (as currently constrained) overlaps with the early part of the first phase of Lower GRV magmatism (1593.6–1590.4 Ma). The "mineralization-related" Lower GRV rhyolites display evidence for alteration and some mineralization, e.g. pervasive quartz-sericite-pyrite alteration, disseminated sulfides and elevated Cu (up to 1300 ppm Cu), whereas later magmas in the Lower GRV (1590.2–1588.5 Ma) are not mineralized (contain no visible sulfides and have low Cu contents, <30 ppm Cu). The second phase of volcanism (Upper GRV, 1586.7–1586.4 Ma) is absent of any evidence for mineralization and may be considered mineralization-absent extrusive magmatism. Intrusive felsic magmas of the Hiltaba Suite occur pre-, syn- and post-dating the main IOCG mineralizing event (1594–1590 Ma). Precise U-Pb zircon geochronology of the Roxby Downs Granite demonstrates this granite is synchronous with mineralization within the uncertainty of the CA-TIMS technique (1593.87 ± 0.21 Ma; Cherry *et al.* 2018; sample 2000366176 1593.06 ± 0.40 Ma, Jagodzinski *et al*. in prep.). In general, mineralization-related CA-TIMS age-constrained granitoids with evidence of some form of IOCG-related alteration and/or mineralization are older (ca. 1594–1592 Ma) than mineralization-absent granitoids (ca. 1587–1580 Ma, sample 2053554 1586.49 ± 0.49 Ma and sample 2115491 1579.37 ± 0.73 Ma, Jagodzinski *et al*. in prep.). Granitoids without precise CA-TIMS age constraints are divided based upon the presence or absence IOCG-style alteration and sulfide mineralization. The CA-TIMS age constrained, mineralization-related GRV and Hiltaba Suite plutons are combined with alteration/mineralization present Hiltaba Suite plutons and referred to as "mineralization-related" samples. The CA-TIMS age constrained, GRV and Hiltaba Suite plutons unrelated to mineralization are combined with alteration/mineralization-absent Hiltaba Suite plutons and referred to as "mineralization-absent" samples.

Magmas of the older, Lower GRV and younger, Upper GRV have been shown to have distinct compositional, geochemical and isotopic signatures attributed to variation in the source magmas (e.g. Agangi *et al.* 2012, Pankhurst *et al.* 2013, Chapman *et al.* 2019). Lower GRV magmas range from basalt to rhyolite, commonly forming as discrete volcanic centers throughout the province, and are geochemically and isotopically heterogeneous (Stewart 1994, Pankhurst *et al.* 2013, Chapman *et al.* 2019). Lower GRV magmas have considerably more SCLM input in their parent magmas and basalts and rhyolites are related through processes of fractional crystallization (e.g. Allen *et al.* 2008, Pankhurst *et al.* 2013, Chapman *et al.* 2019). This is in contrast to the Upper GRV magmas which are exclusively felsic (dacitic to rhyolitic) in composition and are relatively geochemically and isotopically homogeneous with predominantly crustal signatures (up to 20% crustal assimilation; Stewart 1994, Chapman *et al.* 2019). These whole-rock geochemical and isotopic features highlight a temporal compositional evolution in the Gawler SLIP magmatism.

METHODS AND RESULTS

Zircon trace element geochemistry

Samples used in this study are summarized in Table 1. Zircon grains were separated and analyzed from ten rhyolitic units of the Lower GRV that represent five mineralization-related (1593.6–1590.4 Ma) and five mineralization-absent (1590.2–1588.5 Ma) magmatic rocks. Twenty-two intrusive samples of the Hiltaba Suite were also analyzed. Five of these samples are taken from plutons that are age-constrained with CA-TIMS geochronology, three of which are mineralization-related.

Table 1: Summary of samples used in this study, including the CA-TIMS age and source where it exists. Ages are calculated using the preferred $^{238}U/^{235}U$ value of 137.8185 ± 0.045.

Sample	Unit	Location	Group	Zircon trace element analysis	Data Source	TIMS Age (Ma)	Error (Ma)	Geochronology Source
2131359	lower GRV	drill hole BRD1, Roxby Downs area	mineralization-related	Boise State University	This study	1592.62	0.52	Jagodzinski *et al*. 2020
2746110	lower GRV	drill hole BRD1, Roxby Downs area	mineralization-related	University of Adelaide	This study			
2131365	lower GRV	drill hole RED 2, Roxby Downs area	mineralization-related	Boise State University	This study	1592.79	0.43	Jagodzinski *et al.,* 2016
2729189	lower GRV	drill hole RED 2, Roxby Downs area	mineralization-related	University of Adelaide	This study	1592.79	0.43	Jagodzinski *et al.,* 2016
18-TAR-14	lower GRV	Birthday Quarry, Tarcoola	mineralization-related	University of Adelaide	This study	1590.35	0.50	Jagodzinski *et al.,* 2016
2016125	lower GRV	Birthday Quarry, Tarcoola	mineralization-absent	Boise State University	This study	1590.35	0.50	Jagodzinski *et al.,* 2016
2116683	lower GRV	southern GRV margin	mineralization-absent	Boise State University	This study	1590.18	0.29	Jagodzinski *et al.,* 2016
2746487	lower GRV	Kokatha	mineralization-absent	Boise State University	This study	1589.19	0.20	Jagodzinski *et al.,* 2016
2721839	lower GRV	Glyde Hill	mineralization-absent	Boise State University	This study	1589.19	0.28	Jagodzinski *et al.,* 2016
2018616	lower GRV	southern GRV margin	mineralization-absent	Boise State University	This study	1588.47	0.51	Jagodzinski *et al.,* 2016
2000366176	Hiltaba Suite	drill hole RD575, Roxby Downs	mineralization-related	Boise State University	This study	1593.06	0.40	Jagodzinski *et al*. in prep.
2111460	Hiltaba Suite	drill hole Blanche 1, Roxby Downs	mineralization-related	Boise State University	This study	1591.79	0.42	Jagodzinski *et al*. in prep.
2000366166	Hiltaba Suite	drill hole RU45, Roxby Downs	mineralization-related	Boise State University	This study	1590.50	0.54	Jagodzinski *et al*.in prep.
2746355	Hiltaba Suite	drill hole Blanche 1, Roxby Downs	mineralization-related	University of Adelaide	This study			
2746356^	Hiltaba Suite	drill hole BLD2, Roxby Downs	mineralization-related	University of Adelaide	This study			
1077-32	Hiltaba Suite	Tarcoola area	mineralization-related	University of Adelaide	This study			
2705391	Hiltaba Suite	Wallaroo, Yorke Peninsula	mineralization-related	University of Adelaide	This study			
2705398	Hiltaba Suite	Wallaroo, Yorke Peninsula	mineralization-related	University of Adelaide	This study			
HDD393-01	Hiltaba Suite	Hillside, Yorke Peninsula	mineralization-related	University of Adelaide	This study			
1831634	Hiltaba Suite	Hillside, Yorke Peninsula	mineralization-related	Boise State University	This study			
2053554	Hiltaba Suite	Tarcoola area	mineralization-absent	Boise State University	This study	1586.49	0.49	Jagodzinski *et al*. in prep.
2053555	Hiltaba Suite	Wallaroo, Yorke Peninsula	mineralization-absent	Boise State University	This study			
2115491	Hiltaba Suite	drill hole NDR 13, Fowler	mineralization-absent	Boise State University	This study	1579.37	0.73	Jagodzinski *et al*. in prep.
1077-1	Hiltaba Suite	Kokatha	mineralization-absent	University of Adelaide	This study			
1077-27	Hiltaba Suite	Tarcoola area	mineralization-absent	University of Adelaide	This study			
1077-41	Hiltaba Suite	Tarcoola area	mineralization-absent	University of Adelaide	This study			
1077-46	Hiltaba Suite	north western Eyre Peninsula	mineralization-absent	University of Adelaide	This study			
1077-52	Hiltaba Suite	north western Eyre Peninsula	mineralization-absent	University of Adelaide	This study			
1077-59	Hiltaba Suite	Fowler	mineralization-absent	University of Adelaide	This study			
1077-63	Hiltaba Suite	northern Eyre Peninsula	mineralization-absent	University of Adelaide	This study			
1077-198	Hiltaba Suite	Eyre Peninsula	mineralization-absent	University of Adelaide	This study			
HG470	Hiltaba Suite	southern GRV margin	mineralization-absent	University of Adelaide	This study			
PW20	upper GRV	southern GRV margin	mineralization-absent	University of Tasmania	Fergusson *et al.,* 2020	1586.66	0.59	Jagodzinski *et al.,* 2016
GC4	upper GRV	southern GRV margin	mineralization-absent	University of Tasmania	Fergusson *et al.,* 2020	1586.66	0.59	Jagodzinski *et al.,* 2016
GC8	upper GRV	southern GRV margin	mineralization-absent	University of Tasmania	Fergusson *et al.,* 2020	1586.66	0.59	Jagodzinski *et al.,* 2016
GC11	upper GRV	southern GRV margin	mineralization-absent	University of Tasmania	Fergusson *et al.,* 2020	1586.66	0.59	Jagodzinski *et al.,* 2016
YD20	upper GRV	southern GRV margin	mineralization-absent	University of Tasmania	Fergusson *et al.,* 2020	1586.39	0.51	Jagodzinski *et al.,* 2016
884-Y10	upper GRV	southern GRV margin	mineralization-absent	University of Tasmania	Fergusson *et al.,* 2020	1586.39	0.51	Jagodzinski *et al.,* 2016

^ entire sample eliminated based on data filtering criteria.

Of the remaining Hiltaba Suite samples, seven are mineralization-related and ten are mineralization-absent. Data for mineralization-absent Upper GRV samples are compiled from Fergusson *et al.* (2020).

Zircon analysis for this study was conducted at the University of Adelaide and Boise State University. Full analytical methods and metadata are provided in Appendix 4, Appendix 4 Table A1 and A2, respectively. Analysis at the University of Adelaide used a Resonetics 193nm Resolution Excimer laser coupled to a Agilent 7900 ICP-MS. Analysis at Boise State University used a New Wave UP-213 Nd-YAG 213nm laser coupled to a ThermoElectron X-Series II ICP- MS. Zircon analyzed at Boise State University were thermally annealed prior to analysis. In order to further improve the quality of trace element and age data (Keller *et al.* 2019, Widmann *et al.* 2019), the zircon grains analyzed at the University of Adelaide were chemically abraded prior to analysis (Fig. 2; Appendix 4). This approach has been used due to the high frequency of inclusions and metamict zones within Hiltaba/GRV zircons. Resultant data were filtered first using age criteria to eliminate inherited or >5% discordant grains, so that only grains representative of the ca. 1590 Ma Hiltaba Suite and GRV magmatic rocks were included for discussion, and second using a maximum threshold of 370 ppm P (Yang *et al.* 2016; Appendix 4 Figure A1; Appendix 4 Table A3–A6). As P concentration in zircon increases, the likelihood for erroneous incorporation of otherwise undetect-

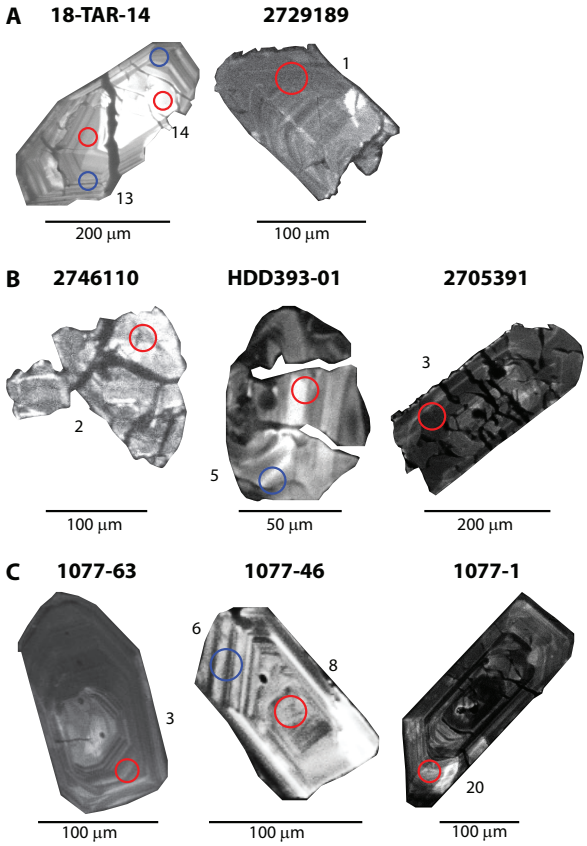

Figure 2. Representative cathodoluminescence images for zircon grains that have been chemically abraded for this study. A) mineralization-related rhyolite; B) mineralization-related granitoid; and C) mineralization-absent granitoid. Red circles and number indicate spot location and spot number for combined zircon trace element and U-Pb analysis. Blue circles indicate location for U-Pb analysis where collected separately. U-Pb data is in Appendix Table A4.

ed inclusions is higher. Coupled P and REE substitution into zircon through a xenotime substitution mechanism also means that modified zircon-melt partitioning relationships are likely to be recorded by high P-REE zones creating a biased record of melt composition (Yang *et al.* 2016). All analyses from one granitoid samples (2746356) were eliminated based on the data filtering criteria, leaving a total of 31 samples for discussion (Appendix 4 Figure A2 and A3). These filtering criteria were also applied to data compiled from Ferguson *et al.* (2020).

Zircon from both rhyolitic and granitic samples are characterized by heavy REE enrichments, light REE depletions and positive Ce and negative Eu anomalies relative to chondrite (Fig. 3). The zircon Th/U ratios are 0.07–5.3 (Appendix 4 Table A3 and A5), within the range of magmatic zircon (Kirkland *et al.* 2015). Zircon Ce/Ce* ratios (method from Loader *et al.* (2017)) are variable and show considerable overlap between the groups (Fig. 4 and Fig. 5).

Rhyolitic zircon compositions

Mineralization-related Lower GRV rhyolites (ca. 1593–1590 Ma) have total zircon REE contents of 285–1782 ppm (Appendix 4 Table A3 and A5). Zircon Eu/Eu* values are typically 0.2–0.59, although five values between 0.13 and 0.18 are present in the group (Appendix 4 Table A3 and A5, Fig. 4). Mineralization-absent Lower GRV rhyolites (1590.2–1588.5 Ma) have higher total zircon REE contents (431–3690 ppm) compared with the mineralization-related Lower GRV rhyolites. Zircon Eu/Eu* values show more variation, ranging between 0.01 and 0.84 Appendix 4 Table A3 and A5, Fig. 4). However, like the mineralization-related Lower GRV rhyolites, Eu/Eu* values between 0.2 and 0.6 are more common. The very low zircon Eu/Eu* values (0.01–0.06) are from sample 2016125 and the value of 0.84 is from sample 2746487. Mineralization-absent Upper GRV magmas (1586.7–1586.4 Ma) compiled from Ferguson *et al.* (2020) show less variation and lower values in their zircon chemistry compared with the Lower GRV magmas. Total zircon REE contents are 399–1118 ppm and Eu/Eu* are 0.04–0.13.

Granitoid zircon compositions

Mineralization-related granitoids (ca. 1594–1592 Ma) have total zircon REE between 245 and 2468 ppm (Appendix 4 Table A3 and A5).

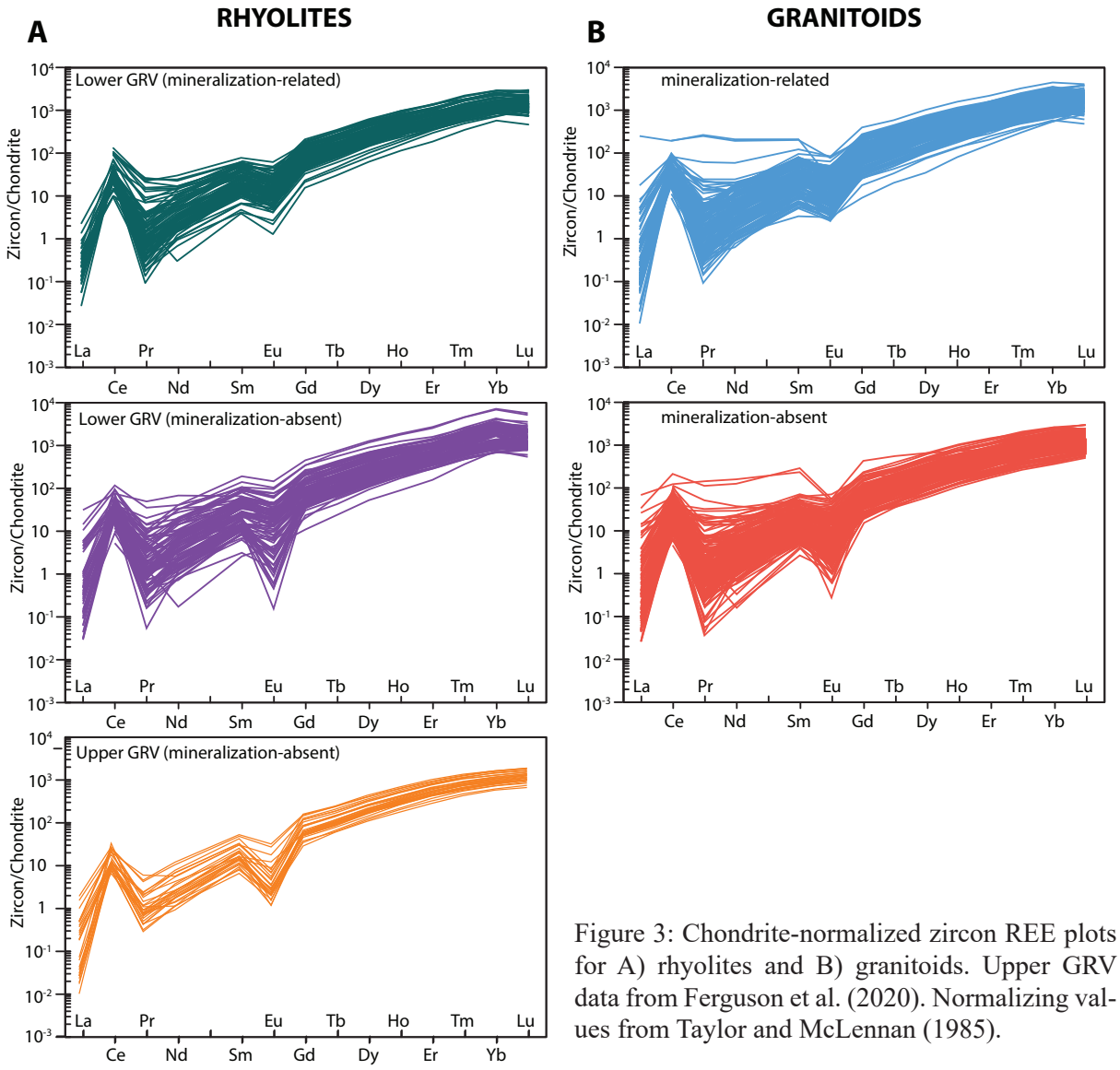

Figure 3: Chondrite-normalized zircon REE plots for A) rhyolites and B) granitoids. Upper GRV data from Ferguson et al. (2020). Normalizing values from Taylor and McLennan (1985).

The zircon Eu/Eu* values are 0.1–0.61, although values between 0.15 and 0.5 are more common. The Roxby Downs Granite itself (sample 2000366176) has zircon Eu/Eu* values of 0.12–0.61. Mineralization-absent granitoids (<1587 Ma) have total zircon total REE contents and Eu/Eu* that overlap with the mineralization-related granitoids (211–1698 ppm and 0.01–0.69 respectively). The mineralization-absent Hiltaba Suite granitoid (sample 2115491, 1580.21 ± 0.73 Ma, Jagodzinski *et al*., 2020) has very low zircon Eu/Eu* values (typically 0.01–0.14).

DISCUSSION

Geochemical variation of zircon in a SLIP and IOCG terrain

Zircon chemistry is seen to differ between magmatic rocks that are related to mineralization, either temporally (CA-TIMS constrained) or with the presence of mineralization in the intrusion, and those rocks that post-date mineralization or are unmineralized. Lower GRV and Upper GRV rhyolites show differing negative Eu/Eu* vs Hf correlations, (Fig. 4a) suggesting two separate magmatic paths. The same negative Eu/Eu* vs Hf correlations are observed in the Roxby Downs Granite (sam-

ple 2000366176) and mineralization-absent granitoid sample 2115491 (Fig. 4a). Mineralization-absent rhyolites of the Lower GRV show much more variation in zircon Eu/Eu* and Hf compared with the mineralization-related lower GRV zircon, and define another separate but parallel negative trend towards higher Hf values (Fig. 4b). Similar separate negative correlations are present for the mineralization-related and mineralization-absent granitoids (Fig. 4b). The Eu/Eu* ratios extend to lower values in the Upper GRV and mineralization-absent granitoids over the same Hf concentration range, suggesting greater degrees of fractionation compared with the Lower GRV and mineralization-related granitoid zircon (Fig. 4b). The presence of Eu/Eu* ratios < 1 is typically related to fractionation of phases such as plagioclase. All samples have Eu/Eu* ratios < 1, however lower Eu/Eu* ratios (< 0.2) in the Upper GRV and some mineralization-absent granitoids suggest higher degrees of plagioclase fractionation compared with the Lower GRV and mineralization-related granitoids (Fig. 4b). Loader *et al*. (2017) caution that steep/sharp increases in $(Yb/Gd)_N$ and Eu/Eu* may be caused by co-crystallization of even minute amounts of titanite with plagioclase, giving the appearance within zircon of a lack of a negative Eu anomaly (Fig. 4c). Such an effect also should be accompanied by correlation between high $(Yb/Gd)_N$ or Eu/Eu* and low Nb (Nb <1 ppm; Belousova *et al.* 2002) in the magmatic zircon, as Nb is enriched in titanite. Zircon from one mineralization-absent Lower GRV sample (2746487) shows a weak positive correlation between $(Yb/Gd)_N$ and Eu/Eu* (Fig. 4c) which may be interpreted as a consequence of titanite-co-crystallization in this magma. However, very few of our data have Nb <1 ppm, and lack of correlation between $(Yb/Gd)_N$ and Eu/Eu* (Fig. 4c) in the majority of the data suggest Eu/Eu* was not significantly impacted by titanite co-crystallization.

High magma water contents combined with oxidized conditions suppresses fractionation of plagioclase, also resulting in higher zircon Eu/Eu* values (e.g. Lu *et al.* 2016; Fig. 5a). Using zircon Dy/Yb ratios as a proxy for magmatic water, Lu *et al.* (2016) showed that values <0.3 correspond to high magma water contents. As zircon Dy/Yb ratios in the GRV and Hiltaba Suite samples are >0.2, magmatic water contents were low, suggesting that hornblende-driven or high-pressure fractional crystallization were not significant. Moreover, no correlation exists between increasing Dy/Yb and decreasing Eu/Eu* (as seen in the fertile and infertile porphyry samples) in the GRV and Hiltaba Suite samples. Therefore, suppression of plagioclase due to higher magma water contents or fractionation of plagioclase due to lower magmatic water contents is unlikely to be the sole reason for apparent differences between zircon from the two rock groups. The exception is sample 2746487 where, as noted above, zircon with higher $(Yb/Gd)_N$ and Eu/Eu* ratios also has Dy/Yb <0.2. Eu/Eu* ratios towards higher values coupled with low Dy/Yb ratios may be indicative of higher magma water in addition to titanite-co-crystallization in this particular sample.

The data broadly show two separate but roughly parallel, negative correlations between zircon Eu/Eu* and Ce/Ce* ratios, with the Upper GRV rhyolite and mineralization-absent granitoid zircon having lower Eu/Eu* values (Fig. 4d, 5b). Hf and Ti contents (the latter as a proxy for temperature) show consistent progressive fractional crystallization trends within each sample (Appendix 4 Figure A4). These zircon trends are repeated at the suite scale (Fig. 4e), an observation that is consistent with previous interpretations of Hf as a measure of fractional crystallization (e.g. Samperton *et al.* 2015). For equivalent levels of fractional crystallization, the Upper GRV rhyolites have lower Eu/Eu* (Fig. 4b) and lower Ce/Ce*(Fig. 4d), both consistent with a lower oxidation state. While

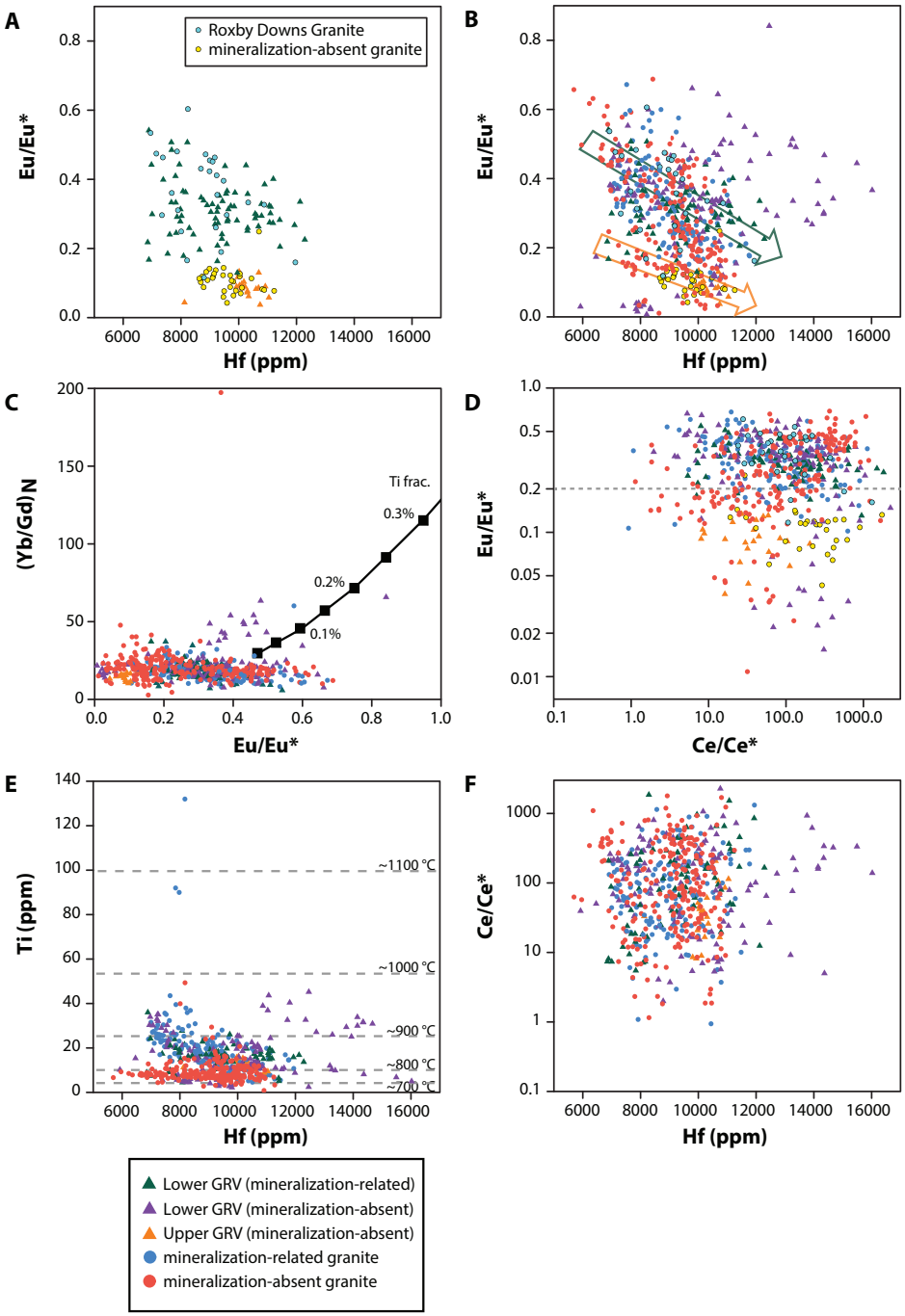

Figure 4. A) Eu/Eu* vs Hf for zircon in mineralization-related Lower GRV and mineralization-absent Upper GRV rhyolites, the Roxby Downs Granite (sample 2000366176) and a mineralization-absent granite (sample 2115491); B) Eu/Eu* vs Hf in zircon for all granitoids and rhyolites analyzed in this study. Green and yellow arrows represent the main trends in mineralization-related and mineralization-absent magmatic rocks, respectively; C) (Yb/Gd)N vs Eu/Eu* in zircon with modelled titanite fractionation curve (Ti frac.) from Loader et al. (2017); D) Eu/Eu* vs Ce/Ce* in zircon; E) Ti vs Eu/Eu* in zircon. Dashed lines represent estimated temperatures for a given Ti concentration calculated from the Ti-in-zircon thermometer (Ferry and Watson 2007), where $\alpha TiO_2 = 0.7$ and $\alpha SiO_2 = 1$ and F) Ce/Ce vs Hf for zircon analyzed in this study.

Eu/Eu* > 0.2 is mostly applicable to the Lower GRV and mineralization-related granitoids, Ce/Ce* does not as clearly define higher oxidation states at equivalent levels of fractional crystallization in the granitoids (Fig. 4d and f). This suggests that the lower Eu/Eu* values are not controlled solely by oxidation state of the magmas and a role for plagioclase is likely.

In a purely fractional crystallization model, lower Eu/Eu* values for equivalent levels of crystallization represent higher quantities of plagioclase removal with the signal potentially augmented by more reduced magmas. However, there is a discernible difference in "starting" or early temperatures for the evolving magmas, with the Upper GRV and mineralization-absent magmas having lower temperatures than the Lower GRV and mineralization-related granitoid samples (Fig. 4e). This is consistent with the lower Eu/Eu* values resulting from additional incorporation of low-temperature, crustally-derived melts into the magmas and where plagioclase acted as a residual phase during partial melting of the crust. This could explain variation seen in Lower GRV sample 2016125 with low zircon Eu/Eu*. These observations are consistent with isotopic constraints in the GRV, where up to 20% assimilation of crustal material was incorporated into the Upper GRV magmas, compared with 3-8% in Lower GRV magmas (Chapman *et al.* 2019). As in porphyry Cu systems, an oxidative fractional crystallization path has the benefit of retaining sulfur, and hence metals, within the magma (e.g. Richards 2015, Sun *et al.* 2015, Lee and Tang 2020). Crustal melts that have incorporated significant amounts of ancient crustal material are likely to have been reduced (e.g. Ishihara 1981) and this would also have been a mechanism for lowering the oxidation state of the magmas (e.g. Zhang *et al.* 2020). For the purposes of assessing suite prospectivity, crustal melt addition or reduced fractional crystallization paths are likely to have the same end-result for early S saturation and removal of metals.

Magma sources and processes

Links with partial melting of a subduction modified metasomatised mantle is considered integral in porphyry Cu formation (e.g. Xu *et al.* 2017) and more recently has been recognized as an important source of IOCG mineralization (Groves *et al.* 2010, Skirrow *et al.* 2018). Lower GRV magmas and Hiltaba Suite granitoids display a strong affinity to a metasomatised SCLM source region (Huang *et al.* 2016, Skirrow *et al.* 2018, Wade *et al.* 2019), with variable interactions with crustal material (Chapman *et al.* 2019). As discussed above, higher equivalent oxidation state in the mineralization-related lower GRV and mineralization-related granitoids and their higher starting magmatic temperatures, supports a potential link with oxidized basaltic parent magmas derived from a metasomatised SCLM source region. The coincidence of these magmas with mineralization/mineral occurrences further suggests a link with a metasomatised SCLM for IOCG mineralization.

While broadly similar starting magma conditions are observed in all Lower GRV magmas (Fig. 4), not all magmas are mineralized or associated with mineralization. Rhyolitic magmas that formed penecontemporaneously with mineralization can be distinguished in their zircon characteristics from mineralization-absent rhyolitic magmas, suggestive of differences in magmatic processes as magmatism in the SLIP evolved. Affinity between intrusive magma zircon composition with phases of the rhyolites suggests similar magmatic processes were recorded in the intrusive magmatism and, while temporal constraints are not as well defined, suggests similar magmatic processes were responsible for the formation of intrusive and extrusive magmas.

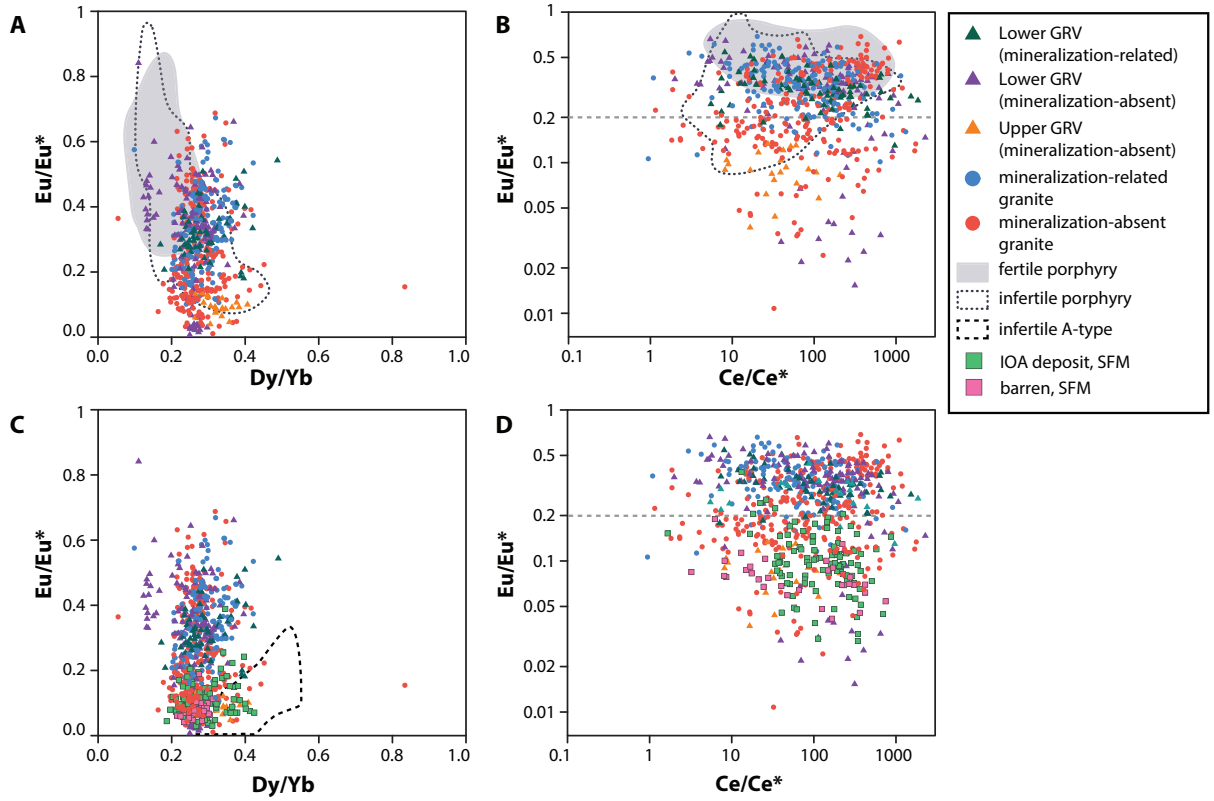

Figure 5. A) Eu/Eu* vs Dy/Yb* for zircon analyzed in this study compared with the fertile and infertile porphyry Cu magmatic rocks; B) Eu/Eu* vs Ce/Ce* for zircon analyzed in this study compared with fertile and infertile porphyry Cu magmatic rocks; C) Eu/Eu* vs Dy/Yb in zircon analyzed in this study compared with St Francois Mountains and infertile A-type granites, and D) Eu/Eu* vs Ce/Ce* for zircon analyzed in this study compared with St Francois Mountains. Fertile porphyry Cu data fields from Loader et al. (2017) and Zhong et al. (2019) screened for <0.2 ppm Ta, infertile porphyry Cu data fields from Zhong et al. (2019), St Francois Mountains (SFM) data compiled from Watts and Mercer (2020). IOA deposit SFM data from Pea Ridge and Bourbon; barren SFM data from Eminence. Infertile A-type data field from Lu et al. (2016).

A regional view for suite fertility - IOGC and IOA deposit examples

IOA deposits are mineralogically similar to early magnetite-rich alteration that evolve to and are commonly spatially and temporally associated to systems with IOCG deposits though they may not be proximal to such deposit types (e.g. Corriveau *et al.* 2016). Both deposit types share similarities including a magmatic-hydrothermal origin, and links to a metasomatised mantle and high temperature oxidized felsic to intermediate magmatism (e.g. Bilenker *et al.* 2016, Day *et al.* 2016, Velasco *et al.* 2016, Storey and Smith 2017, Skirrow *et al.* 2018, Watts and Mercer 2020). Hematite-dominant IOCG deposits are common in the Gawler Craton while in the St Francois Mountains, Missouri, IOA deposits dominate (Day *et al.* 2016). Both regions are typified by A-type silicic magmatic rocks rich in F, Zr and REEs, providing an opportunity to compare the two deposit types in broadly similar Mesoproterozoic igneous regimes.

Overall, the St Francois Pea Ridge and Bourbon IOA deposit zircon has low Eu/Eu* ratios (typically <0.3; Watts and Mercer 2020). These values are lower than in zircon associated with Gawler IOCG mineralization (Fig. 5c), suggesting that magmatic rocks associat-

ed with IOA deposits are typically more fractionated. As is the case for rhyolite samples in areas hosting IOCG deposits, fertile IOA deposit-related host rhyolites tend to have higher Eu/Eu* ratios compared to zircon from the barren IOA rocks (e.g. Eminence, Fig. 5c). Despite IOA deposit rhyolites having lower Eu/Eu* overall than IOCG-related rhyolites, Ce/Ce* are similar (Fig. 5d) and consistent with oxidized magmas.

A fundamental tenet of the use of zircon trace element data in porphyry Cu exploration is that fertile magmas are both oxidized and hydrous (Richards 2011, Sun *et al.* 2015). Using Eu/Eu* and Dy/Yb as proxies for magmatic water content, the magma for the Hiltaba Suite granitoids, GRV rhyolites and St Francois Mountains rhyolites had low water contents. Felsic rocks with A-type affinity are often used as the infertile suite in porphyry Cu deposit comparisons (e.g. Fig. 5c; Lu *et al.* 2016). While A-type magmas have no association with porphyry Cu deposits, they do show an affiliation with IOCG and IOA deposits. The magmas associated with IOA and IOCG deposits as presented here, can also be distinguished from other A-type granites (e.g. Fig. 5c). Therefore, while dry magmas and high magmatic temperatures typical of A-type magmas are features considered unfavorable for porphyry Cu deposits, they appear to have less bearing on a magma's fertility in IOCG and IOA deposits. In fact, zircon indicative of higher starting magmatic temperatures (e.g. Fig. 4e) shows a stronger affiliation with IOCG mineralization in the Olympic Cu-Au Province than zircon with lower starting magmatic temperatures. Comparison with zircon data from porphyry deposits highlights the fundamental differences in the two magmatic systems, despite Phanerozoic porphyry Cu deposits and Precambrian IOCG-IOA deposits sharing many attributes. The data from both regions highlight that the use of specific zircon trace element indicators for porphyry system fertility is not necessarily a robust indicator of magma fertility when considering a broader range of magmatic-related, hydrothermal mineralizing systems such as IOCG and IOA types. At the very least, consideration should be given to the characteristics of different deposit types that could be present in a terrain and a fertility assessment should be conducted on an intra-terrain basis. This is particularly true for regions hosting critical metal deposits such as the St Francois Mountains or southern Australia, for which the principal causative magmas are A-type.

CONCLUSIONS

Rhyolites and granitoids from a Mesoproterozoic SLIP in southern Australia host numerous major IOCG deposits. Zircon rare earth element signatures are consistent with igneous zircon formed in oxidizing magmatic conditions. Combined Hf, Eu/Eu*, Ce/Ce* and Dy/Yb plots differentiate mineralization-related rhyolites and granitoids from mineralization-absent rhyolites and granitoids.

Our data suggest zircon trace element geochemistry is an applicable method to assess magma fertility in non-porphyry Cu settings. A-type magmas are not associated with porphyry Cu deposits but that does not preclude them from being fertile magmas in other magmatic-hydrothermal systems such as IOCG-IOA systems. Similarities in zircon chemistry such as Eu/Eu*, Ce/Ce*, Hf and Ti between mineralization-related and mineralization-absent rhyolites suggests broadly similar starting magma conditions in the Lower GRV. These conditions differ to the younger Upper GRV magmas which are lower temperature and more fractionated. The mineralization-related Roxby Downs Granite and other mineralization-related granitoids can be clearly distinguished from mineralization-absent granitoids in their zircon chemistry. However, exceptions exist in mineralization-absent rhyolites and mineralization-absent granitoids that may be

attributed to source variation and magmatic processes (e.g. crustal assimilation). Lower degrees of plagioclase fractionation, higher oxidation state and higher magmatic temperatures, denoted by higher Eu/Eu*, Ce/Ce* and Ti, respectively, at equivalent degrees of fractionation are characteristic of the mineralization-related magmas. These features are considered to be indicative of fertile magmas in southern Australian IOCG and south-central USA IOA terrains. The oxidized nature of IOCG-IOA-related A-type magmas as indicated by high Ce/Ce* ratio is considered a key element in magma fertility in IOCG-IOA terrains. The study highlights the importance of understanding intra-terrain magmatic rock compositions before assessing the fertility of a magmatic system.

ACKNOWLEDGEMENTS

This study is a part of Ph.D. project (C. Wade), and was financially supported by Australian Research Council Linkage Project LP160100578, with the support of the Geological Survey of South Australia. David Bruce, Morgan Blades, Laura Morrissey, Naomi Tucker, Brandon Alessio and Aoife McFadden are thanked for assistance with sample preparation and analysis. Ken Cross is thanked for providing sample HG470. L. Corriveau provided very detailed and insightful comments on a previous version of this manuscript. CW and AR publish with permission of the Director, Geological Survey of South Australia, Department for Energy and Mining, South Australia.

REFERENCES

Agangi, A., Kamenetsky, M. and McPhie, J., 2012. Evolution and emplacement of high fluorine rhyolites in the Mesoproterozoic Gawler silicic large igneous province, South Australia. Precambrian Research, v. 208-211, p. 124-144. doi: https://doi.org/10.1016/j.precamres.2012.03.011

Allen, C. M. and Campbell, I. H., 2012. Identification and elimination of a matrix-induced systematic error in LA–ICP–MS 206Pb/238U dating of zircon. Chemical Geology, v. 332-333, p. 157-165. doi: https://doi.org/10.1016/j.chemgeo.2012.09.038

Allen, S. R., McPhie, J., Ferris, G. and Cadd, A. G., 2008. Evolution and architecture of a large felsic igneous province in western Laurentia: The 1.6 Ga Gawler Range Volcanics, South Australia. Journal of Volcanology and Geothermal Research, v. 172, p. 132-147. doi: https://doi.org/10.1016/j.jvolgeores.2005.09.027

Allen, S. R., Simpson, C. J., McPhie, J. and Daly, S. J., 2003. Stratigraphy, distribution and geochemistry of widespread felsic volcanic units in the Mesoproterozoic Gawler Range Volcanics, South Australia. Australian Journal of Earth Sciences, v. 50, p. 97-112. doi: http://dx.doi.org/10.1046/j.1440-0952.2003.00980.x

Barton, M. D., 2014. 13.20 - Iron Oxide(–Cu–Au–REE–P–Ag–U–Co) Systems. In: Holland, H. D. and Turekian, K. K. (Eds), Treatise on Geochemistry (Second Edition). Elsevier, v. p. 515-541. https://doi.org/10.1016/B978-0-08-095975-7.01123-2

Belousova, E. A., Griffin, W. L., O'Reilly, S. Y. and Fisher, N. I., 2002. Igneous zircon: trace element composition as an indicator of source rock type. Contributions to Mineralogy and Petrology, v. 143, p. 602–622. doi: https://doi.org/10.1007/s00410-002-0364-7

Benavides, J., Kyser, T. K., Clark, A. H., Oates, C. J., Zamora, R., Tarnovschi, R. l. and Castillo, B., 2007. The Mantoverde Iron Oxide-Copper-Gold District, III Región, Chile: The Role of Regionally Derived, Nonmagmatic Fluids in Chalcopyrite Mineralization.

Economic Geology, v. 102, p. 415-440. doi: https://doi.org/10.2113/gsecongeo.102.3.415

Bilenker, L. D., Simon, A. C., Reich, M., Lundstrom, C. C., Gajos, N., Bindeman, I., Barra, F. and Munizaga, R., 2016. Fe–O stable isotope pairs elucidate a high-temperature origin of Chilean iron oxide-apatite deposits. Geochimica et Cosmochimica Acta, v. 177, p. 94-104. doi: https://doi.org/10.1016/j.gca.2016.01.009

Chapman, N. D., Ferguson, M., Meffre, S. J., Stepanov, A., Maas, R. and Ehrig, K. J., 2019. Pb-isotopic constraints on the source of A-type Suites: Insights from the Hiltaba Suite - Gawler Range Volcanics Magmatic Event, Gawler Craton, South Australia. Lithos, v. 346-347, p. 105156. doi: https://doi.org/10.1016/j.lithos.2019.105156

Cherry, A. R., Ehrig, K., Kamenetsky, V. S., McPhie, J., Crowley, J. L. and Kamenetsky, M. B., 2018. Precise geochronological constraints on the origin, setting and incorporation of ca. 1.59 Ga surficial facies into the Olympic Dam Breccia Complex, South Australia. Precambrian Research, v. 315, p. 162-178. doi: https://doi.org/10.1016/j.precamres.2018.07.012

Cooke, D. R., Hollings, P. and Walshe, J. L., 2005. Giant Porphyry Deposits: Characteristics, Distribution, and Tectonic Controls. Economic Geology, v. 100, p. 801-818. doi: https://doi.org//10.2113/gsecongeo.100.5.801

Corriveau, L., Montreuil, J.-F. and Potter, E. G., 2016. Alteration Facies Linkages Among Iron Oxide Copper-Gold, Iron Oxide-Apatite, and Affiliated Deposits in the Great Bear Magmatic Zone, Northwest Territories, Canada. Economic Geology, v. 111, p. 2045-2072. doi: https://doi.org/10.2113/econgeo.111.8.2045

Courtney-Davies, L., Ciobanu, C. L., Tapster, S. R., Cook, N. J., Ehrig, K., Crowley, J. L., Verdugo-Ihl, M. R., Wade, B. P. and Condon, D. J., 2020. Opening the magmatic-hydrothermal window: High-precision U-Pb geochronology of the Mesoproterozoic Olympic Dam Cu-U-Au-Ag deposit, South Australia. Economic Geology, v. p. doi: https://doi.org/10.5382/econgeo.4772

Courtney-Davies, L., Tapster, S. R., Ciobanu, C. L., Cook, N. J., Verdugo-Ihl, M. R., Ehrig, K. J., Kennedy, A. K., Gilbert, S. E., Condon, D. J. and Wade, B. P., 2019. A multi-technique evaluation of hydrothermal hematite UPb isotope systematics: Implications for ore deposit geochronology. Chemical Geology, v. 513, p. 54-72. doi: https://doi.org/10.1016/j.chemgeo.2019.03.005

Creaser, R. A., 1996. Petrogenesis of a Mesoproterozoic quartz latite-granitoid suite from the Roxby Downs area, South Australia. Precambrian Research, v. 79, p. 371-394. doi: https://doi.org/10.1016/S0301-9268(96)00002-2

Cross, K. C., Daly, S. J. and Flint, R. B., 1993. Mineralisation associated with the Gawler Range Volcanics and Hiltaba Suite Granitoids. Olympic Dam Deposit. In: Drexel, J. F., Preiss, W. V. and Parker, A. J. (Eds), The geology of South Australia; Volume 1, The Precambrian. Geological Survey of South Australia, v. Bulletin 54, p. Available at: https://sarigbasis.pir.sa.gov.au/WebtopEw/ws/samref/sarig1/image/DDD/BULL054(V1).pdf

Day, W. C., Slack, J. F., Ayuso, R. A. and Seeger, C. M., 2016. Regional Geologic and Petrologic Framework for Iron Oxide ± Apatite ± Rare Earth Element and Iron Oxide Copper-Gold Deposits of the Mesoproterozoic St. Francois Mountains Terrane, Southeast Missouri, USA. Economic Geology,

v. 111, p. 1825-1858. doi: https://doi.org/10.2113/econgeo.111.8.1825

Ferguson, M. R. M., Ehrig, K., Meffre, S. and Cherry, A. R., 2020. Associations between zircon and Fe–Ti oxides in Hiltaba event magmatic rocks, South Australia: atomic- or pluton-scale processes? Australian Journal of Earth Sciences, v. 67, p. 201-220. doi: https://doi.org/10.1080/08120099.2019.1653990

Groves, D. I., Bierlein, F. P., Meinert, L. D. and Hitzman, M. W., 2010. Iron Oxide Copper-Gold (IOCG) Deposits through Earth History: Implications for Origin, Lithospheric Setting, and Distinction from Other Epigenetic Iron Oxide Deposits. Economic Geology, v. 105, p. 641-654. doi: https://doi.org/10.2113/gsecongeo.105.3.641

Hildebrand, R. S., Hoffman, P. F., Housh, T. and Bowring, S. A., 2010. The nature of volcano-plutonic relations and the shapes of epizonal plutons of continental arcs as revealed in the Great Bear magmatic zone, northwestern Canada. Geosphere, v. 6, p. 812-839. doi: https://doi.org/10.1130/ges00533.1

Hitzman, M. W., 2000. Iron oxide copper gold deposits: what, where, why and when? In: Porter, T. M. (Eds), Hydrothermal iron oxide copper-gold and related ore deposits: A global perspective. Australian Mineral Foundation, v. p. 3-25.

Horstwood, M. S. A., Košler, J., Gehrels, G., Jackson, S. E., McLean, N. M., Paton, C., Pearson, N. J., Sircombe, K., Sylvester, P., Vermeesch, P., Bowring, J. F., Condon, D. J. and Schoene, B., 2016. Community-Derived Standards for LA-ICP-MS U-(Th-)Pb Geochronology – Uncertainty Propagation, Age Interpretation and Data Reporting. Geostandards and Geoanalytical Research, v. 40, p. 311-332. doi: https://doi.org/10.1111/j.1751-908X.2016.00379.x

Huang, Q., Kamenetsky, V. S., Ehrig, K., McPhie, J., Kamenetsky, M., Cross, K., Meffre, S., Agangi, A., Chambefort, I., Direen, N. G., Maas, R. and Apukhtina, O., 2016. Olivine-phyric basalt in the Mesoproterozoic Gawler silicic large igneous province, South Australia: Examples at the Olympic Dam Iron Oxide Cu–U–Au–Ag deposit and other localities. Precambrian Research, v. 281, p. 185-199. doi: https://doi.org/10.1016/j.precamres.2016.05.019

Ishihara, S., 1981. The granitoid series and mineralization: Economic Geology. v. 75th Anniversay Volume, p. 458-484.

Jagodzinski, E. A., Crowley, J. L. and Reid, A. J., in prep. Precise zircon U-Pb dating of the Hiltaba Suite, Gawler Craton. Department for Energy and Mining, South Australia, Adelaide, v. Report Book 2021/00001

Jagodzinski, E. A., Reid, A., Crowley, J., McAvaney, S. and Wade, C., 2016. Precise zircon U–Pb dating of a Mesoproterozoic silicic large igneous province: The Gawler Range Volcanics and Benagerie Volcanic Suite, South Australia. Hornsby, NSW: Geological Society of Australia. Geological Society of Australia Abstracts, v. No. 118, p. doi: https://sarigbasis.pir.sa.gov.au/WebtopEw/ws/samref/sarig1/image/DDD/RB201600032.pdf

Johnson, J. P. and McCulloch, M. T., 1995. Sources of mineralising fluids for the Olympic Dam Deposit (South Australia); Sm-Nd isotopic constraints. Chemical Geology, v. 121, p. 177-199. doi: https://doi.org/10.1016/0009-2541(94)00125-R

Keller, C. B., Boehnke, P., Schoene, B. and Harrison, T. M., 2019. Stepwise chemical abrasion–isotope dilution–thermal ionization mass spectrometry with trace element analysis of microfrac-

tured Hadean zircon. Geochronology, v. 1, p. 85-97. doi: https://doi.org/10.5194/gchron-1-85-2019

Kirkland, C. L., Smithies, R. H., Taylor, R. J. M., Evans, N. and McDonald, B., 2015. Zircon Th/U ratios in magmatic environs. Lithos, v. 212-215, p. 397-414. doi: https://doi.org/10.1016/j.lithos.2014.11.021

Lee, C.-T. A. and Tang, M., 2020. How to make porphyry copper deposits. Earth and Planetary Science Letters, v. 529, p. 115868. doi: https://doi.org/10.1016/j.epsl.2019.115868

Loader, M. A., Wilkinson, J. J. and Armstrong, R. N., 2017. The effect of titanite crystallisation on Eu and Ce anomalies in zircon and its implications for the assessment of porphyry Cu deposit fertility. Earth and Planetary Science Letters, v. 472, p. 107-119. doi: https://doi.org/10.1016/j.epsl.2017.05.010

Lu, Y.-J., Loucks, R. R., Fiorentini, M., McCuaig, T. C., Evans, N. J., Yang, Z.-M., Hou, Z.-Q., Kirkland, C. L., Parra-Avila, L. A., Kobussen, A. and Richards, J. P., 2016. Zircon Compositions as a Pathfinder for Porphyry Cu ± Mo ± Au Deposits. In: (Eds), Tectonics and Metallogeny of the Tethyan Orogenic Belt. Society of Economic Geologists Special Publication, v. 19, Paper 13, p.

McPhie, J., DellaPasqua, F., Allen, S. R. and Lackie, M. A., 2008. Extreme effusive eruptions: Palaeoflow data on an extensive felsic lava in the Mesoproterozoic Gawler Range Volcanics. Journal of Volcanology and Geothermal Research, v. 172, p. 148-161. doi: https://doi.org/10.1016/j.jvolgeores.2006.11.011

McPhie, J., Ehrig, K. J., Kamenetsky, M. B., Crowley, J. L. and Kamenetsky, V. S., 2020. Geology of the Acropolis prospect, South Australia, constrained by high-precision CA-TIMS ages. Australian Journal of Earth Sciences, v. 67, p. 699-716. doi: https://doi.org/10.1080/08120099.2020.1717617

Montreuil, J.-F., Corriveau, L., Potter, E. G. and De Toni, A. F., 2016. On the Relationship Between Alteration Facies and Metal Endowment of Iron Oxide-Alkali-Altered Systems, Southern Great Bear Magmatic Zone (Canada). Economic Geology, v. 111, p. 2139-2168. doi: https://doi.org/10.2113/econgeo.111.8.2139

Pankhurst, M. J., Schaefer, B. F., Turner, S. P., Argles, T. and Wade, C. E., 2013. The source of A-type magmas in two contrasting settings: U–Pb, Lu–Hf and Re–Os isotopic constraints. Chemical Geology, v. 351, p. 175-194. doi: https://doi.org/10.1016/j.chemgeo.2013.05.010

Pankhurst, M. P., Schaefer, B. F., Betts, P. G., Phillips, N. and Hand, M., 2011. A Mesoproterozoic continental flood rhyolite province, the Gawler Ranges, Australia: the end member example of the Large Igneous Province clan. Solid Earth, v. 2, p. 1-9. doi: https://doi.org/10.5194/se-2-25-2011

Reid, A., 2019. The Olympic Cu-Au Province, Gawler Craton: A Review of the Lithospheric Architecture, Geodynamic Setting, Alteration Systems, Cover Successions and Prospectivity. Minerals, v. 9, p. 371. doi: https://www.mdpi.com/2075-163X/9/6/371

Richards, J. P., 2011. High Sr/Y arc magmas and porphyry Cu ± Mo ± Au deposits: Just add water. Economic Geology, v. 106, p. 1075-1081. doi: https://doi.org/10.2113/econgeo.106.7.1075

Richards, J. P., 2015. The oxidation state, and sulfur and Cu contents of arc magmas: implications for metallogeny. Lithos, v. 233, p. 27-45. doi: https://doi.org/10.1016/j.lithos.2014.12.011

Richards, J. P. and Mumin, A. H., 2013. Mag-

matic-hydrothermal processes within an evolving Earth: Iron oxide-copper-gold and porphyry Cu ± Mo ± Au deposits. Geology, v. 41, p. 767-770. doi: https://doi.org/10.1130/g34275.1

Samperton, K. M., Schoene, B., Cottle, J. M., Brenhin Keller, C., Crowley, J. L. and Schmitz, M. D., 2015. Magma emplacement, differentiation and cooling in the middle crust: Integrated zircon geochronological–geochemical constraints from the Bergell Intrusion, Central Alps. Chemical Geology, v. 417, p. 322-340. doi: https://doi.org/10.1016/j.chemgeo.2015.10.024

Shu, Q., Chang, Z., Lai, Y., Hu, X., Wu, H., Zhang, Y., Wang, P., Zhai, D. and Zhang, C., 2019. Zircon trace elements and magma fertility: insights from porphyry (-skarn) Mo deposits in NE China. Mineralium Deposita, v. 54, p. 645-656. doi: https://doi.org/10.1007/s00126-019-00867-7

Sillitoe, R., H., 2003. Iron oxide-copper-gold deposits; an Andean view. Mineralium Deposita, v. 38, p. 787-812. doi: https://doi.org/10.1007/s00126-003-0379-7

Sillitoe, R. H., 2010. Porphyry Copper Systems. Economic Geology, v. 105, p. 3-41. doi: https://doi.org/10.2113/gsecongeo.105.1.3

Skirrow, R., van der Wielen, S. E., Champion, D. C., Czarnota, K. and Thiel, S., 2018. Lithospheric artchitecture and mantle metasomatism linked to iron-oxide Cu-Au ore formation: Multidiciplinary evidence from the Olympic Dam region, South Australia. Geochemistry, Geophysics, Geosystems, v. 19, p. doi: https://doi.org/10.1029/2018GC007561

Skirrow, R. G., 2009. "Hematite-group" IOCG±U ore systems: tectonic settings, hydrothermal characteristics, and Cu-Au and U mineralizing processes. In: Corriveau, L. and Mumin, H. (Eds), Exploring for Iron Oxide Copper-Gold Deposits: Canada and global analogues: Geological Association of Canada. Short Course Notes, v. No. 20, p. p. 39-57. Available at: https://gac.ca/product/exploring-for-iron-oxide-copper-gold-deposits-canada-and-global-analogues/

Skirrow, R. G., Bastrakov, E., Barovich, K., Fraser, G., Fanning, C. M., Creaser, R. and Davidson, G., 2007. Timing of Iron Oxide Cu-Au-(U) Hydrothermal Activity and Nd Isotope Constraints on Metal Sources in the Gawler Craton, South Australia. Economic Geology, v. 102, p. 1441-1470. doi: https://doi.org/10.2113/gsecongeo.102.8.1441

Stewart, K., 1994. High temperature felsic volcanism and the role of mantle magmas in Proterozoic crustal growth : the Gawler Range volcanic province. University of Adelaide, PhD thesis (unpublished).

Storey, C. D. and Smith, M. P., 2017. Metal source and tectonic setting of iron oxide-copper-gold (IOCG) deposits: Evidence from an in situ Nd isotope study of titanite from Norrbotten, Sweden. Ore Geology Reviews, v. 81, p. 1287-1302. doi: https://doi.org/10.1016/j.oregeorev.2016.08.035

Sun, W., Huang, R.-f., Li, H., Hu, Y.-b., Zhang, C.-c., Sun, S.-j., Zhang, L.-p., Ding, X., Li, C.-y., Zartman, R. E. and Ling, M.-x., 2015. Porphyry deposits and oxidized magmas. Ore Geology Reviews, v. 65, p. 97-131. doi: https://doi.org/10.1016/j.oregeorev.2014.09.004

Taylor, S. R. and McLennan, S. M., 1985. The continental crust: Its composition and evolution: Blackwell Scientific Publications, v. p. 312. https://doi.org/10.1002/gj.3350210116

Velasco, F., Tornos, F. and Hanchar, J. M., 2016. Immiscible iron- and silica-rich

melts and magnetite geochemistry at the El Laco volcano (northern Chile): Evidence for a magmatic origin for the magnetite deposits. Ore Geology Reviews, v. 79, p. 346-366. doi: https://doi.org/10.1016/j.oregeorev.2016.06.007

Wade, C. E., Payne, J. L., Barovich, K. M. and Reid, A. J., 2019. Heterogeneity of the sub-continental lithospheric mantle and 'non-juvenile' mantle additions to a Proterozoic silicic large igneous province. Lithos, v. 340-341, p. 87-107. doi: https://doi.org/10.1016/j.lithos.2019.05.005

Wade, C. E., Reid, A., Wingate, M. T. D., Jagodzinski, E. A. and Barovich, K., 2012. Geochemistry and geochronology of the c. 1585 Ma Benagerie Volcanic Suite, southern Australia: relationship to the Gawler Range Volcanics and implications for the petrogenesis of a Mesoproterozoic silicic large igneous province Precambrian Research, v. 206–207, p. 17–35. doi: https://doi.org/10.1016/j.precamres.2012.02.020

Watts, K. E. and Mercer, C. N., 2020. Zircon-hosted melt inclusion record of silicic magmatism in the Mesoproterozoic St. Francois Mountains terrane, Missouri: Origin of the Pea Ridge iron oxide-apatite-rare earth element deposit and implications for regional crustal pathways of mineralization. Geochimica et Cosmochimica Acta, v. 272, p. 54-77. doi: https://doi.org/10.1016/j.gca.2019.12.032

Whalen, J. B., Currie, K. L. and Chappell, B. W., 1987. A-type granites: geochemical characteristics, discrimination and petrogenesis. Contributions to Mineralogy and Petrology, v. 95, p. 407-419. doi: https://doi.org/10.1007/BF00402202

Widmann, P., Davies, J. H. F. L. and Schaltegger, U., 2019. Calibrating chemical abrasion: Its effects on zircon crystal structure, chemical composition and UPb age. Chemical Geology, v. 511, p. 1-10. doi: https://doi.org/10.1016/j.chemgeo.2019.02.026

Xu, X.-W., Li, H., Peters, S. G., Qin, K.-Z., Mao, Q., Wu, Q., Hong, T., Wu, C., Liang, G.-L., Zhang, Z.-F. and Dong, L.-H., 2017. Cu-rich porphyry magmas produced by fractional crystallization of oxidized fertile basaltic magmas (Sangnan, East Junggar, PR China). Ore Geology Reviews, v. 91, p. 296-315. doi: https://doi.org/10.1016/j.oregeorev.2017.09.020

Yang, W., Lin, Y., Hao, J., Zhang, J., Hu, S. and Ni, H., 2016. Phosphorus-controlled trace element distribution in zircon revealed by NanoSIMS. Contributions to Mineralogy and Petrology, v. 171, p. 28. doi: https://doi.org/10.1007/s00410-016-1242-z

Zhang, X., Ni, P., Wang, G.-G., Jiang, Y.-H., Jiang, D.-S., Li, S.-N. and Fan, M.-S., 2020. Petrogenesis and oxidation state of granodiorite porphyry in the Jurassic Chuankeng skarn Cu deposit, South China: Implications for the Cu fertility and mineralization potential. Journal of Asian Earth Sciences, v. 191, p. 104184. doi: https://doi.org/10.1016/j.jseaes.2019.104184

Zhong, S., Seltmann, R., Qu, H. and Song, Y., 2019. Characterization of the zircon Ce anomaly for estimation of oxidation state of magmas: a revised Ce/Ce* method. Mineralogy and Petrology, v. 113, p. 755-763. doi: https://doi.org/10.1007/s00710-019-00682-y

Chapter 6

This chapter has not been published but has been prepared in manuscript style as:

Wade, C., Barovich, K., Grooby, C., Reid, A., Payne, J and Gilbert, S. Mapping hydrothermal systems in IOCG deposits using apatite geochronology and geochemsitry: An example from Vulcan Cu-Au prospect

Statement of Authorship

Title of Paper	Mapping hydrothermal systems in IOCG deposits using apatite geochronology and geochemistry: an example from Vulcan Cu-Au Prospect
Publication Status	☐ Published ☐ Accepted for Publication ☐ Submitted for Publication ☑ Unpublished and Unsubmitted work written in manuscript style
Publication Details	Wade, C.E., Barovich, K.M., Grooby, C., Reid, A.J., Payne, J.L. and Gilbert, S.E. Iron-oxide and rare earth element signatures in iron-oxide deposits: an example from Vulcan Cu-Au Prospect

Principal Author

Name of Principal Author (Candidate)	Claire Wade		
Contribution to the Paper	Data collection, Data processing, Data curation Conceptualisation, Investigation, Formal Analysis, Visualisation Methodology, Validation Writing original draft, editing and review		
Overall percentage (%)	70%		
Certification:	This paper reports on original research I conducted during the period of my Higher Degree by Research candidature and is not subject to any obligations or contractual agreements with a third party that would constrain its inclusion in this thesis. I am the primary author of this paper.		
Signature		Date	3/12/2020

Co-Author Contributions

By signing the Statement of Authorship, each author certifies that:

i. the candidate's stated contribution to the publication is accurate (as detailed above);

ii. permission is granted for the candidate in include the publication in the thesis; and

iii. the sum of all co-author contributions is equal to 100% less the candidate's stated contribution.

Name of Co-Author	Karin Barovich		
Contribution to the Paper	Conceptualisation, Investigation, Validation, Visualisation, Supervision Writing, Editing and review		
Signature		Date	3/12/2020

Name of Co-Author	Caelan Grooby
Contribution to the Paper	Conceptualisation, Investigation, Visualisation, Validation Data Collection, Data Cuation Writing, editing and review
Signature	Date 3/12/2020

Name of Co-Author	Anthony Reid
Contribution to the Paper	Conceptualisation, Investigation, Visualisation, Validation Supervision Writing, editing and review
Signature	Date 3/12/2020

Name of Co-Author	Justin Payne
Contribution to the Paper	Conceptualisation, Investigation, Visualisation, Validation Data Collection, Data Cuation Writing, editing and review Funding acquisition
Signature	Date 3/12/2020

Name of Co-Author	Sarah Gilbert
Contribution to the Paper	Data collection, Resources Validation Writing - editing and review
Signature	Date 4/12/2020

ABSTRACT

The Vulcan Prospect is a hematite breccia-hosted Cu-Au prospect located in the Olympic Cu-Au Province, Gawler Craton, southern Australia. U-Pb apatite geochronology indicates at least three stages of apatite growth or resetting occurred at the Vulcan Prospect. Each apatite stage has characteristic trace element and REY compositions that can be related to changes in hydrothermal activity and mineral assemblages. Trace element compositions of ca. 1600 Ma apatite are characterised by LREE enrichment and HREE depletions. This apatite is commonly associated with magnetite. Two phases of apatite are associated with hematite and record U-Pb ages of ca. 1100 Ma and ca. 450 Ma. Hematite-associated apatite is characterised by LREE depletions, and becomes increasingly depleted as age decreases. LREE depletions in hematite-associated apatite are attributed to breakdown of apatite in acidic fluid conditions accompanied by the new growth of the REE phosphate mineral florencite. The temporal constraints on the geochemistry of apatite show the changing fluid parameters and hydrothermal assemblages hosting the apatite. As such, the apatite geochemistry is able to fingerprint changes in individual assemblages and changes in the REY behaviour during the evolution of the Vulcan Prospect.

Trace element geochemistry of iron oxides at Vulcan also record variation in transition metal and high field strength element distributions. Magnetite is characterised by higher V and Ni, and lower Co, Mg, Mn, Cu, Nb, Y, Th, U, Mo+Sn+W and REY compared with hematite. U and Th are positively correlated with REY in magnetite and hematite suggesting partitioning of U, Th and REY into phases within the Fe-oxide.

Vulcan shares similar geochemical and geochronological features with Olympic Dam, including hematite-sericite-chlorite-carbonate dominated breccias with abundant phosphate accessory minerals similar apatite trace element evolution and a post-mineralisation history of hydrothermal fluid movement.

INTRODUCTION

The study of trace element compositions of minerals in ore deposits has advanced our understanding of their parent hydrothermal systems and fluid chemistries (Lowell and Guilbert 1970, Giggenbach 1997, Cooke *et al.* 2014, Wilkinson *et al.* 2015, Cook *et al.* 2016, Ahmed *et al.* 2019). Characterising the trace element chemistry of minerals is a useful tool in mineral exploration, as alteration minerals can provide critical information about the fluid chemistry, hydrothermal assemblages and conditions of ore formation (Reed 1997, Heinrich 2007). More specifically, observed changes in geochemistry may mark significant changes in the hydrothermal system and can be used as vectors towards mineralisation (Cooke *et al.* 2014).

Iron oxide-copper-gold (IOCG) deposits include a family of deposits ranging from magnetite to hematite end-members (Groves *et al.* 2010). As well as appreciable amounts of Cu and Au, IOCG deposits also contain considerable amounts of rare earth elements (REE) and uranium. REE-enrichment is commonly associated with iron oxide-apatite (IOA) deposits, which form at the magnetite-rich end of the IOCG family (Groves *et al.* 2010). Typically, magnetite-dominant deposits represent deeper level, higher temperature deposit formation compared with hematite-dominant deposits which are lower temperature and shallower level (Groves *et al.* 2010).

Trace element signatures in iron oxides in IOCG-IOA deposits may be linked to different stages of mineralisation (e.g. Verdugo-Ihl *et al.* 2019). Magnetite typically forms early in the magmatic-hydrothermal system, and may be overprinted by hematite (Apukhtina

et al. 2017, Reid 2019 and references therein). Differences in trace element compositions in magnetite and hematite may provide insight into the types of fluids present at various stages throughout mineral growth and the hydrothermal system as a whole, although the fluid evolution is likely to be continuous (e.g. Verdugo-Ihl *et al.* 2019). Accessory minerals such as apatite, monazite, xenotime, zircon, titanite and rutile are useful as geochronometers (e.g. Kirkland *et al.* 2018), where measureable amounts of U and Pb allow them to be dated by U-Pb methods. As repositories for a range of major, trace and rare earth elements, accessory minerals are an important indicator for the trace element distributions in rocks (e.g. Webster and Piccoli 2015). In particular, apatite can be used to address mid-temperature thermochronology questions, as diffusion experiments suggest closure temperatures in the range of 375–600 °C (Schoene and Bowring 2007, Cochrane *et al.* 2014). However, apatite can also undergo recrystallization and new growth processes during metasomatism (Kirkland *et al.* 2018). As a result, linking apatite chemistry to a U-Pb age is a powerful tool for tracking fluid-rock interaction (Kirkland *et al.* 2018).

Southern Proterozoic Australia hosts a large iron oxide-copper-gold (IOCG) province, related to ca 1590 Ma magmatic units (Cross *et al.* 1993, Skirrow *et al.* 2007) and large alteration systems (Skirrow *et al.* 2002). Located ~25 km to the northeast of the Olympic Dam Deposit, the Vulcan Prospect is characterised by a complex breccia system of magnetite-hematite-sericite-dolomite-chlorite (Reid *et al.* 2013). The prospect is particularly REE-enriched and represents a transitional prospect, where some magnetite is preserved, but also lower temperature alteration assemblages comprised of hematite, sericite and chlorite. These latter assemblages are not present in the magnetite-end member deposits. This study investigates trace element geochemistry and the evolution of apatite, florencite, hematite and magnetite of the Vulcan Prospect. Combined apatite trace element geochemistry and U-Pb apatite geochronology provides some constraints on the timing of mineral growth and variable fluid compositions of hydrothermal activity within the prospect.

THE OLYMPIC CU-AU PROVINCE

Significant mineralisation was developed in the Gawler Craton around 1590 Ma, producing a belt of IOCG-dominated deposits in the eastern Gawler Craton (Skirrow *et al.* 2007 and references therein). A hydrothermal-magmatic model is envisaged for the IOCG mineralisation e.g. (e.g. Haynes *et al.* 1995, Pollard 2006, Groves *et al.* 2010) related to the emplacement of a ca. 1590 Ma silicic-dominated large igneous province (LIP), and comagmatic felsic and mafic intrusive magmas (Johnson and McCulloch 1995, Wade *et al.* 2019). The LIP is comprised of the Gawler Range Volcanics (GRV), predominantly rhyolite-dacite lavas, with lesser basalt-andesite lava (Blissett *et al.* 1993, Allen *et al.* 2003, Allen *et al.* 2008). The GRV erupted as two sequences between 1593.6 and 1588.5 Ma and 1586.7–1586.4 Ma (Jagodzinski *et al.* 2016). The younger sequence is comprised entirely of dacite-rhyolite lavas which constitute the bulk of the LIP (Blissett *et al.* 1993, Allen and McPhie 2002, Allen *et al.* 2008). The intrusive component of the LIP is the Hiltaba Suite (1600–1575 Ma; Flint 1993 and references therein), comprised of felsic and mafic plutons that were emplaced pre-, syn- and post the GRV magmas. The Hiltaba Suite and GRV are intimately associated with the ca. 1590 Ma IOCG mineralisation (Haynes *et al.* 1995, Johnson and McCulloch 1995, Courtney-Davies *et al.* 2020). High precision geochronological data indicates hydrothermal alteration and IOCG mineralisation occurred between 1594 and 1590 Ma (Cherry *et al.* 2018a, Courtney-Davies *et al.* 2019b, Courtney-Davies *et al.* 2020, McPhie *et al.* 2020).

Host rocks to the IOCG deposits include 1850 Ma Donington Suite granitoids, 1780 Ma Wallaroo Group metasedimentary rocks and 1590 Ma GRV and Hiltaba Suite (Reid 2019). Host rocks at Vulcan include hematite-sericite-chlorite altered and brecciated granite which has a zircon U-Pb crystallisation age of ca. 1745 Ma (Reid *et al.* 2013), adding diversity to the host rocks at different deposits and prospects.

Corriveau *et al.* (2016) have identified five main alteration stages in IOCG-IOA deposits that reflect temperature decrease and increased oxygen fugacity in the system. The five stages are summarised below:

1) sodic alteration produces mostly albitite that will replace supracrustal rocks regardless of their composition. Albitites can be brecciated and contain fragments of weakly altered and albitised albitites;
2) calcic-iron alteration and IOA mineralisation is associated with high-temperature alteration comprising amphibole, magnetite and apatite rich assemblages, commonly as fine-grained veins to patchy zones and sometimes as in-fill breccias (e.g. apatite-dominant assemblages);
3) high temperature potassic-iron alteration consisting of K-feldspar-magnetite, biotite-magnetite and/or K-feldspar-biotite-magnetite assemblages;
4) low temperature and hydrolytic potassic-iron alteration is hematite-bearing and associated with chlorite or talc. Retrograde alteration of magnetite through replacement by hematite is the most common transition. Low temperature alteration facies are common in the hematite IOCG group e.g. Olympic Dam and;
5) low temperature hydrothermal and transitional epithermal alteration that includes quartz and carbonate veins. Epidote replacements and vein-type metasomatism and barite veins form during the late stages.

THE VULCAN PROSPECT

The Vulcan Prospect is located in the north-eastern Gawler Craton within the Olympic Cu-Au Province, approximately 25 km NE of Olympic Dam (Fig. 1). Tasman Resources discovered the Vulcan IOCG-U system in 2009 as part of their Lake Torrens project (Smith 2017). Eight holes diamond drilled by Tasman Resources in 2009–2011 intersected IOCG-U related mineralisation and alteration, including strong chalcopyrite/pyrite mineralisation, mineralised hematite-breccias and bornite-chalcopyrite-pyrite mineralisation (Reid *et al.* 2013). An additional nine diamond holes were completed from 2012–2014.

The Vulcan Prospect is defined as a gravity anomaly at approximately 850 m depth and has a hematite-magnetite footprint (~12 km^2) similar to Olympic Dam (Reid *et al.* 2013). The prospect is hosted within brecciated, ca. 1745 Ma granite (Reid *et al.* 2013). Molybdenite within hematite-rich brecciated granite has been dated via the Re-Os method and yielded a crystallization age of 1586 ± 8 Ma. (Fig. 2a; Reid *et al.* 2013). Mineralisation is associated with hematite-dominant breccias with clasts ranging in composition from purely hydrothermal minerals (Fig. 2b-d) to clasts of unaltered protolith rock (Reid *et al.* 2013). Mineralised hematite breccias have a fine-grained hematite-sericite-chlorite rich matrix enveloping angular to rounded aggregates of quartz, carbonate, sericite, chlorite, pyrite, chalcopyrite ± gold ± apatite ± molybdenite (Fig. 2e). Coarse-grained pyrite and chalcopyrite are associated with bladed hematite (Fig. 2f) and locally intergrown with molybdenite (Reid *et al.* 2013). Carbonate and apatite occur within hematite-rich sulphide aggregates (Fig. 2c). The Vulcan Prospect has a sulphide zonation pattern comprising bornite through chalcopyrite to pyrite + chalcopyrite (Solo-

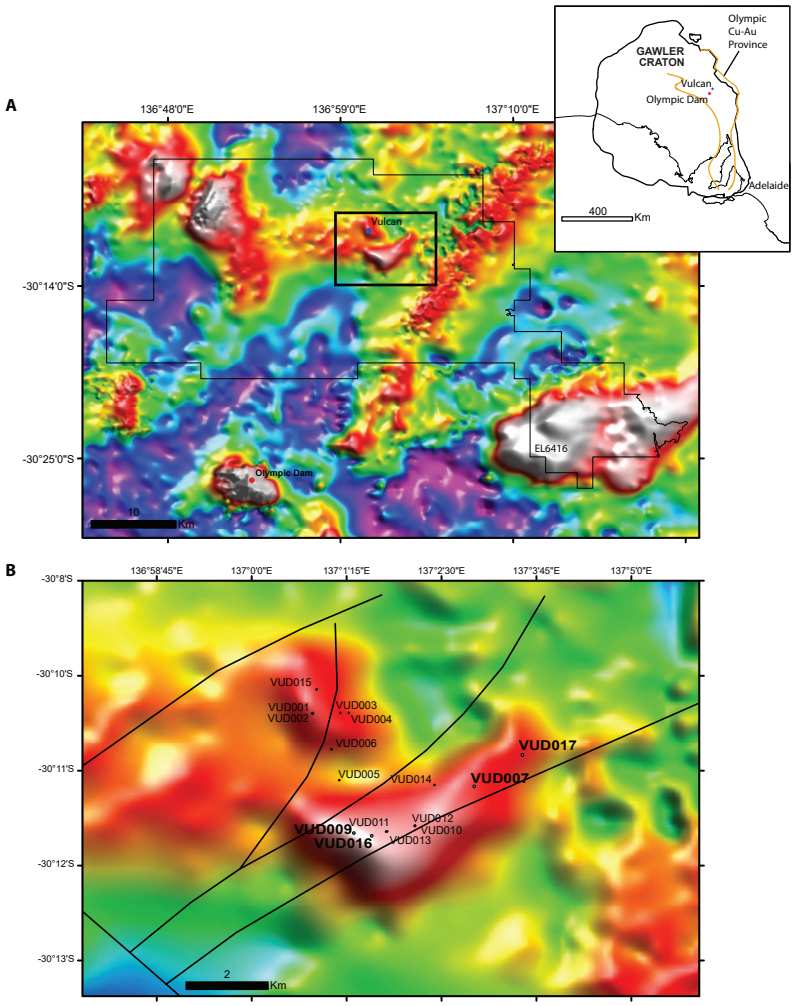

Figure 1: Location diagram of the Vulcan Prospect and drill holes analysed in this study. A) Gravity imagery for the north-eastern Gawler Craton indicating the location of the Vulcan Prospect with respect to Olympic Dam. EL6416, held by Fortescue Minerals Group and Tasman Resource is indicated by the solid black outline. B) Inset shown on A) showing the location of diamond drill holes into the Vulcan Prospect. Holes VUD007, VUD009, VUD016 and VUD 017 are highlighted in bold font and the focus holes of this study. Source for gravity images from https://map.sarig.sa.gov.au/.

mon and Smith 2011), similar to that observed at Olympic Dam (Reeve *et al.* 1990) 180 m of alteration and sulphide zoning and 150 m of mineralised hematite-breccias akin to Olympic Dam has been intersected in drilling. Significant intervals of hematite-rich alteration and Cu-Au mineralisation include 57 m @ 0.59% Cu and 163 m @ 0.23% Cu and 0.08 g/t. Higher grade zones are present within these intersections, including 0.75 m @ 4.44% Cu, 1.34 g/t Au, 0.58 kg/t U_3O_8,0.34 m @ 5.9% Cu and 2.23 g/t Au and 0.65 m @ 7.82% Cu and 2.41 g/t Au (Solomon and Smith 2011).

Composite hematite-magnetite grains are found within the prospect, where magnetite is altered to, and pseudomorphed by, hematite (Fig. 2g, h). These composite grains indicate that the alteration system at Vulcan was likely initially dominated by higher temperature minerals such as magnetite, and has subsequently been overprinted by lower temperature min-

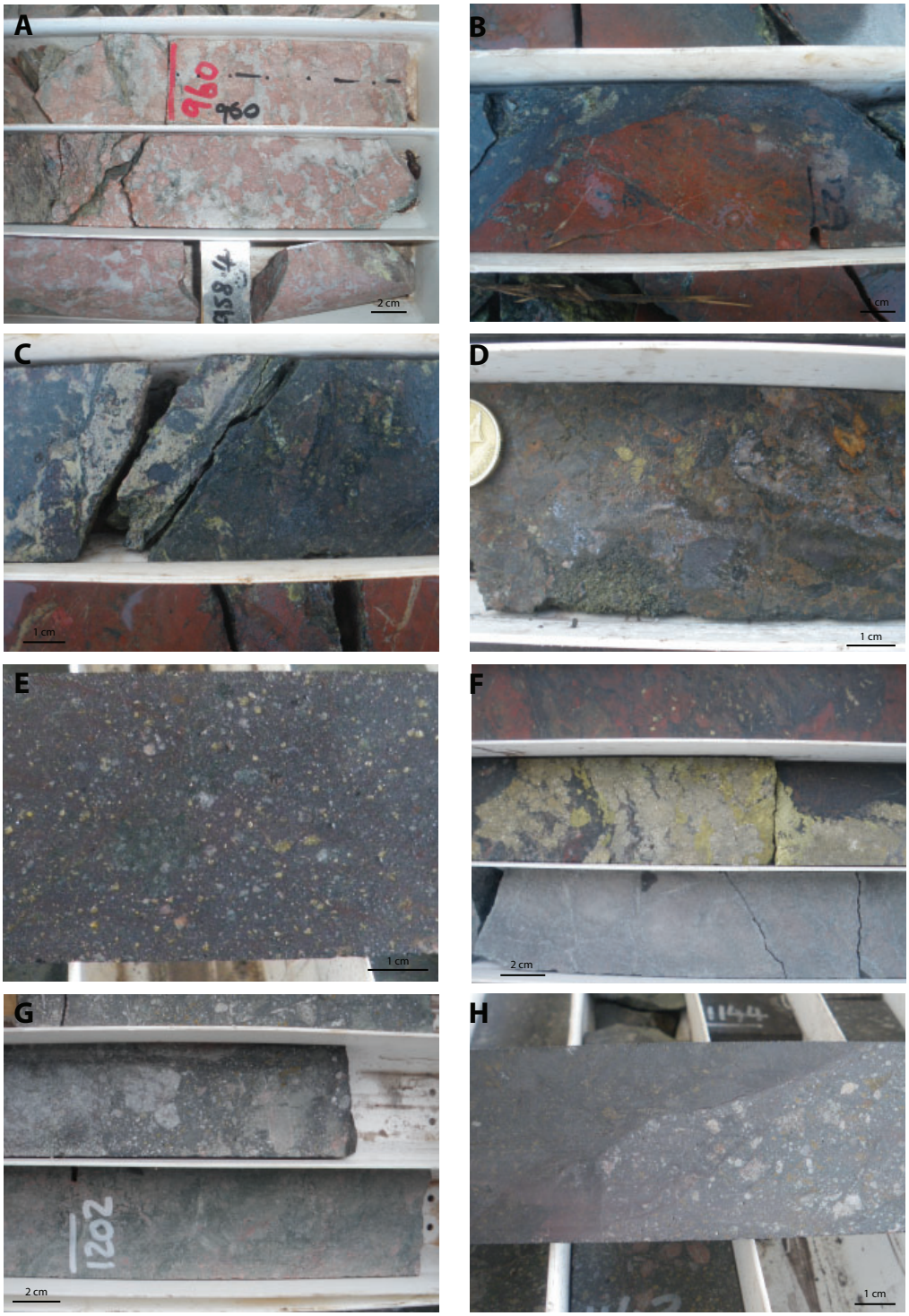

Figure 2: Lithologies and textures observed in drill core at Vulcan. A) coarse-grained host granite to the mineralisation, VUD 008 956.1–961.4 m; B) hematised clast within carbonate-pyrite altered host rock, VUD001 1026.8–1032.6 m; C) chlorite-sericite-carbonate altered breccia, VUD001 1026.8–1032.6 m; D) sericite-carbonate altered breccia, VUD003 870.8–877.11 m; E) hematite-dominated breccia, VUD 007, 1138 m; F) massive pyrite and chalcopyrite mineralisation over printing hematite alteration, VUD003, ~900.6–906.5 m; G) mineralised magnetite-rich breccia, VUD007, ~1202 m; H) mineralised magnetite-rich breccia in contact with mineralised hematite-rich breccia, VUD007, 1141.0–1147.1 m.

erals such as hematite, chlorite and sericite. Magnetite-rich assemblages are mainly located to the east of the prospect (e.g. VUD007 and VUD017; Fig 1, Fig. 2g, h), while hematite-dominated assemblages (Fig. 2e) are more abundant in to the western part of the prospect (e.g. VUD001, VUD003 and VUD009; Fig. 1). This progressive change in alteration from high temperature potassic-iron (magnetite dominant) alteration to low temperature potassic-iron (hematite dominant) alteration is also documented from Olympic Dam and is typical of the progression of alteration facies in other IOA-IOCG terranes (Corriveau *et al.* 2016).

METHODS

Representative samples were taken from both from the magnetite-dominant zone in the east and hematite-dominant zones in the central area at the Vulcan Prospect (Table 1). Eleven samples from four drill holes have been characterised using light microscopy supplemented by scanning electron microscopy using a mineral liberation analyser (MLA) system on a FEI Quanta 600 SEM with dual EDAX EDS detectors. Mineral Liberation Analysis (MLA) XBSE maps were collected with the FEI MLA Suite 3.0 software. The SEM and MLA settings used were 25kV, spot size 7.2, 10 mm working distance and resolution of 2.5um/pix. XBSE maps were collected with an individual frame resolution of 512 x 400 and X-Ray acquisition time of 20 ms.

Apatite, florencite, magnetite and hematite were analysed by *in-situ* single spot laser ablation analysis for age and trace elements by laser ablation inductively coupled plasma mass spectrometry (LA-ICP-MS; Table 1) in polished thin sections. Spot analyses were collected in 4 sessions at Adelaide Microscopy, University of Adelaide, Australia. Grains were ablated using a Resonetics 193 nm Resolution Excimer laser coupled to an Agilent 7900 ICP-MS.

Analysis of apatite for U-Pb and trace element analyses was undertaken using a 30 µm spot size at 5 Hz and 3.5 J/cm^2 laser fluence. Measured isotopes include ^{204}Pb, ^{206}Pb, ^{207}Pb, ^{208}Pb, ^{232}Th and ^{238}U (Appendix Table A1). Measured trace elements include: ^{29}Si, ^{31}P, ^{43}Ca, ^{51}V, ^{55}Mn, ^{57}Fe, ^{65}Cu, ^{75}As, ^{88}Sr, ^{89}Y, ^{90}Zr, ^{139}La, ^{140}Ce, ^{141}Pr, ^{146}Nd, ^{147}Sm, ^{153}Eu, ^{157}Gd, ^{159}Tb, ^{163}Dy, ^{165}Ho, ^{166}Er, ^{169}Tm, ^{172}Yb, ^{175}Lu, ^{178}Hf, ^{201}Hg, ^{204}Pb, ^{206}Pb, ^{207}Pb, ^{208}Pb, ^{232}Th and ^{238}U (Appendix Table 2). The glass reference material NIST-610 was used for trace element calibration and instrument drift correction. ^{43}Ca was used as the internal standard element assuming stoichiometric proportions in apatite. Madagascar apatite reference material was used for U-Pb geochronology calibration with 401 apatite and McClure Mountain apatite used as a secondary standard. Calculated ages for Madagascar apatite from the two analytical sessions are 476.1 ±9.4 Ma and 473.2 ±1.6 Ma (pooled ages for both analytical sessions are 473 ±1.5 Ma), in agreement with the reported age 473.5 ±0.7 Ma (Chew *et al.* 2014). Calculated ages for secondary standard material 401 are 526.5 ±7.3 Ma and 522.6 ±5.9 Ma (pooled age of 524.5 ±4.5 Ma), within uncertainty of the reported ages for 401 (530.3 ±1.5 Ma; Thompson *et al.* 2016). Calculated ages for secondary standard material McClure Mountain are 536 ±23 Ma and 528 ±21 Ma (pooled age of 530 ±15 Ma), within uncertainty of reported ages for McClure Mountain (523.51 ±1.4 Ma; Schoene and Bowring 2006).

Florencite trace element analyses were undertaken using a 13 µm spot size at 5 Hz and 3.5 J/cm^2 laser fluence. Trace elements include: ^{23}Na, ^{27}Al, ^{29}Si, ^{31}P, ^{43}Ca, ^{45}Sc, ^{55}Mn, ^{57}Fe, ^{65}Cu, ^{75}As, ^{88}Sr, ^{89}Y, ^{90}Zr, ^{93}Nb, ^{137}Ba, ^{139}La, ^{140}Ce, ^{141}Pr, ^{146}Nd, ^{147}Sm, ^{153}Eu, ^{157}Gd, ^{159}Tb, ^{163}Dy, ^{165}Ho, ^{166}Er, ^{169}Tm, ^{172}Yb, ^{175}Lu, ^{178}Hf, ^{181}Ta, ^{182}W, ^{204}Pb, ^{206}Pb, ^{207}Pb, ^{208}Pb, ^{209}Bi, ^{232}Th and ^{238}U (Appendix Table 4). The glass reference material NIST-610 was used

Table 1: List of drill holes, samples and intervals used in mineral spot analysis.

Drill Hole	Sample	Interval	Mineralogy	Alteration Assemblage	Analysis
VUD007	VUD007 1084	1084.50–1084.70	Mag ± hem, chl, dol, alb, ap, qtz, py, cpy	Chlorite, potassic	Apatite U-Pb geochronology, Apatite trace elements
VUD007	VUD007 1183	1183.0–1183.20	Mag ± hem, chl, dol, alb, ap, qtz, py, cpy	Chlorite, potassic	Apatite U-Pb geochronology, Apatite trace elements, Magnetite U-Pb geochronology*, Magnetite trace elements
VUD007	VUD007 1192	1192.05–1192.20	Mag ± hem, chl, dol, ap, qtz, py, cpy, ti	Chlorite, potassic	Magnetite trace elements
VUD009	VUD009 801	801.45–801.55	Hem, flor, alb, ap, qtz, py, cpy, zir	Sericite	Apatite U-Pb geochronology, Apatite trace elements, Florencite trace elements
VUD009	VUD009 852	852.0–852.10	Hem, flor, bar, ap, qtz, py, cpy	Sericite	Apatite U-Pb geochronology, Apatite trace elements, Florencite trace elements, Hematite U-Pb geochronology*, Hematite trace elements
VUD009	VUD009 973	973.50–973.60	Hem, flor, alb, ap, qtz, py, cpy, zir	Sericite	Apatite U-Pb geochronology, Apatite trace elements, Florencite trace elements, Hematite U-Pb geochronology*, Hematite trace elements
VUD009	VUD009 994	994.0–994.10	Hem, flor, alb, ap, qtz, py, cpy	Sericite	Hematite U-Pb geochronology*, Hematite trace elements
VUD016	VUD016 1488	1488.05–1488.15	Hem, flor, alb, ap, qtz, py, cpy	Sericite	Apatite U-Pb geochronology, Apatite trace elements
VUD017	VUD017 1210	1210.13–1210.25	Mag ± hem, chl, dol, alb, ap, qtz, py, cpy	Chlorite, potassic	Apatite U-Pb geochronology, Apatite trace elements
VUD017	VUD017 1259	1259.80–1259.95	Mag ± hem, chl, dol, alb, ap, qtz, py, cpy	Chlorite, potassic	Magnetite U-Pb geochronology*, Magnetite trace elements
VUD017	VUD 017 1268	1268.0–1268.35	Mag ± hem, chl, dol, ap, qtz, py, cpy	Chlorite, potassic	Magnetite U-Pb geochronology*, Magnetite trace elements

*U-Pb and trace elements were collected in single spot analyses, however U concentrations were too low for U-Pb geochronology. Mineral legend: alb: albite; ap: apatite; bar: barite; chl: chlorite; cpy: chalcopyrite; dol: dolomite; flor: florencite; hem: hematite; mag: magnetite; py: pyrite; qtz: quartz; ti: titanite; zir: zircon.

for calibration and drift correction. ^{27}Al was used as the internal standard element assuming stoichiometric compositions of florencite.

Magnetite and hematite were ablated using a 30 µm spot size at 5 Hz and 3.0 J/cm^2 laser fluence. Measured trace elements include: ^{24}Mg, ^{27}Al, ^{29}Si, ^{31}P, ^{43}Ca, ^{49}Ti, ^{51}V, ^{55}Mn, ^{57}Fe, ^{59}Co, ^{60}Ni, ^{65}Cu, ^{66}Zn, ^{75}As, ^{88}Sr, ^{89}Y, ^{90}Zr, ^{93}Nb, ^{95}Mo, ^{118}Sn, ^{137}Ba, ^{139}La, ^{140}Ce, ^{141}Pr, ^{146}Nd, ^{147}Sm, ^{153}Eu, ^{157}Gd, ^{159}Tb, ^{163}Dy, ^{165}Ho, ^{166}Er, ^{169}Tm, ^{172}Yb, ^{175}Lu, ^{178}Hf, ^{181}Ta, ^{182}W, ^{204}Pb, ^{206}Pb, ^{207}Pb, ^{208}Pb, ^{232}Th and ^{238}U (Appendix Table A3). The iron oxide reference material hydrated ferric oxide (HFO; Courtney-Davies *et al.* 2019b) was used in calibration and drift correction. ^{57}Fe was used as the internal standard element assuming stoichiometric compositions of 72 wt% in magnetite and 69 wt% in hematite.

The time-resolved ablation signal for each analysis was examined in detail and intervals in magnetite, hematite, apatite and florencite were selected based on high and consistent counts of the primary cation in each phase (^{43}Ca for apatite and ^{27}Al for florencite; and ^{57}Fe for magnetite and hematite). Apatite grains for U-Pb geochronology were also selected based on high and consistent ^{31}P, ^{238}U, ^{232}Th and Pb isotopes. Elevated counts of cations in any analyses that are not formula ions within the target phase were taken to represent mixing with other phases, including inclusions, and were avoided or the analyses were excluded all together.

The spot trace element data were reduced using data reduction scheme software LaDR (https://norsci.com/?p=ladr). The complete datasets, including excluded analyses, are provided in Appendix Table A1-A4.

RESULTS

Petrography

Thin sections were scanned using mineral liberation analysis (MLA) to aid in phase identification and to locate apatite and florencite for spot analysis. (Appendix Figure A1-A11).

Samples include magnetite-rich and hematite-rich breccias. Magnetite breccias are com-

prised of magnetite, albite, chlorite, apatite, dolomite, hematite, quartz and minor pyrite and chalcopyrite in a dolomite-chlorite-rich matrix. Magnetite occurs as fine-grained to large euhedral grains, with a mottled texture and fine-grained inclusions (Fig. 3a-c), including monazite and apatite. Some magnetite grains are brecciated and milled, with fracture zones commonly replaced by hematite (Fig. 3b) and in some instances by pyrite. Pyrite and chalcopyrite occur as fine-grained inclusions in magnetite (Fig. 3c and d), and in places along fractures and veins within magnetite. Locally, magnetite is intergrown with or replaced by pyrite and chalcopyrite (Fig.3e and 2f). Magnetite is almost completely replaced by hematite, or has hematite rims. In places, hematite veins cross cut magnetite or replace magnetite along fracture zones (Fig. 3a-c). Chlorite and potassic alteration are pervasive throughout the magnetite-rich breccias.

Hematite-rich breccias comprise massive hematite overprinting magnetite, hematite clasts associated with quartz and albite and bladed hematite, with apatite, barite, quartz, florencite, pyrite and chalcopyrite. Hematite is present as pseudomorphs after magnetite, as replacement of eudhedral or blebby magnetite. Hematite is intergrown with pyrite and chalcopyrite, where sulphide formation occurs along fractures and veins. Bladed hematite is observed as new generation mineral growth (Fig. 2d). Both new and pseudomorphed hematite has a mottled texture and contains inclusions such as florencite. In samples VUD009 973 and VUD016 1488, hematite and florencite are commonly in association with each other (Fig. 3k and 2l). Pervasive sericite alteration is observed in the hematite-rich breccia with minor potassic alteration.

At least two generations of pyrite are present. Pyrite occurs in the matrix with magnetite and hematite (Fig. 3g) and also as a replacement texture in the magnetite matrix (Fig 3h). Overgrowths of chalcopyrite occur along pyrite boundaries and fractures within pyrite (Fig 3h). Locally, pyrite is overprinted by hematite and second-generation chalcopyrite. Chalcopyrite is also present as rims on hematite associated with pyrite.

Three groups of apatite are identified based on their crystallisation and growth habits. The first apatite form is associated with magnetite-dominant sections and occurs as small subhedral grains or veins between dolomite crystals and clasts (Fig. 3i). Magnetite-associated apatite is found in samples VUD007 1183, VUD0007 1084 and VUD017 1210. The second form of apatite is associated with hematite as fine-grained veins in the host rock, between hematite grains, present in samples VUD009 852 and VUD009 973 (Fig. 3j), or within fractures of bladed hematite. This hematite-associated vein apatite is associated with barite, florencite and albite. The third apatite is also associated with hematite, present in samples VUD009 801 and VUD016 1488. This apatite occurs as coarse (mm scale), euhedral, hexagonal minerals within the hematite and quartz-dolomite breccia matrices (Fig. 3k and 3l) associated with quartz, sericite and/or albite. This texture was seen in samples VUD009 801 and VUD016 1488. Hematite-associated apatite appears to be partially replaced by hematite in sample VUD009 801 and VUD009 852 (Fig. 3k). Both types of Hematite-associated apatite are altered by sericite and contains inclusions (Fig. 3k) that are interpreted to be florencite and monazite. In samples VUD009 973 and VUD009 801, both vein and euhedral forms of hematite-associated apatite are associated with fine-grained florencite (Fig. 3m). Florencite and apatite inclusions are abundant in Fe-oxides in these samples. Florencite is very fine-grained and commonly intergrown in and around Fe-oxides (e.g. VUD009 994 and VUD016 1488; Fig. 3n). Florencite is also abundant as small inclusions or separate but fine-grained minerals in the breccias.

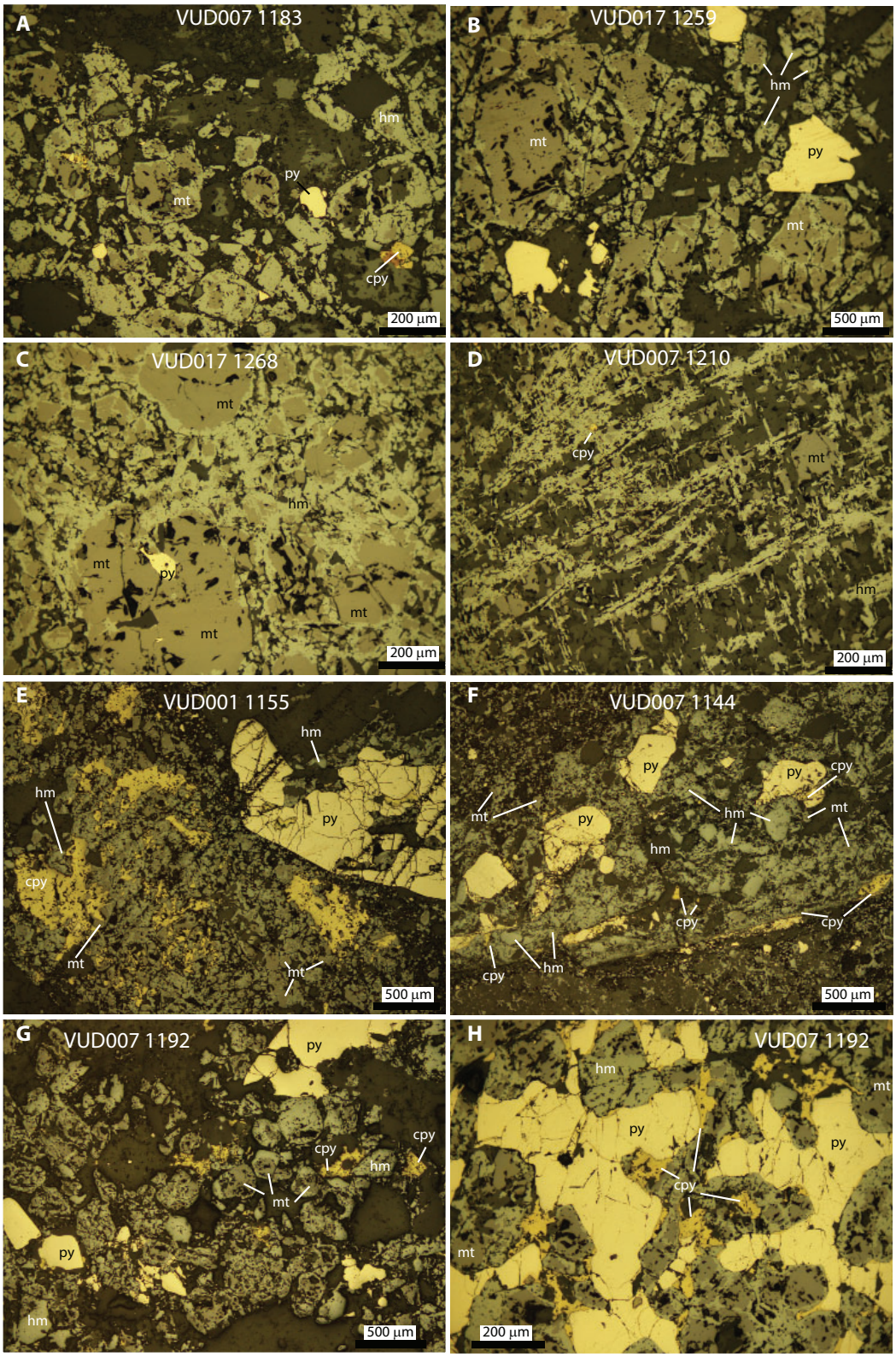
A
VUD007 1183
hm
py
mt
cpy
200 µm
B
VUD017 1259
hm
mt
py
mt
500 µm
C
VUD017 1268
mt
hm
mt
py
mt
mt
200 µm
D
VUD007 1210
cpy
mt
hm
200 µm
E
VUD001 1155
hm
hm
py
cpy
mt
mt
500 µm
F
VUD007 1144
py
py
cpy
mt
py
hm
mt
hm
cpy
cpy
cpy
hm
500 µm
G
VUD007 1192
py
cpy
cpy
hm
mt
py
hm
500 µm
H
VUD07 1192
hm
mt
py
py
cpy
mt
200 µm

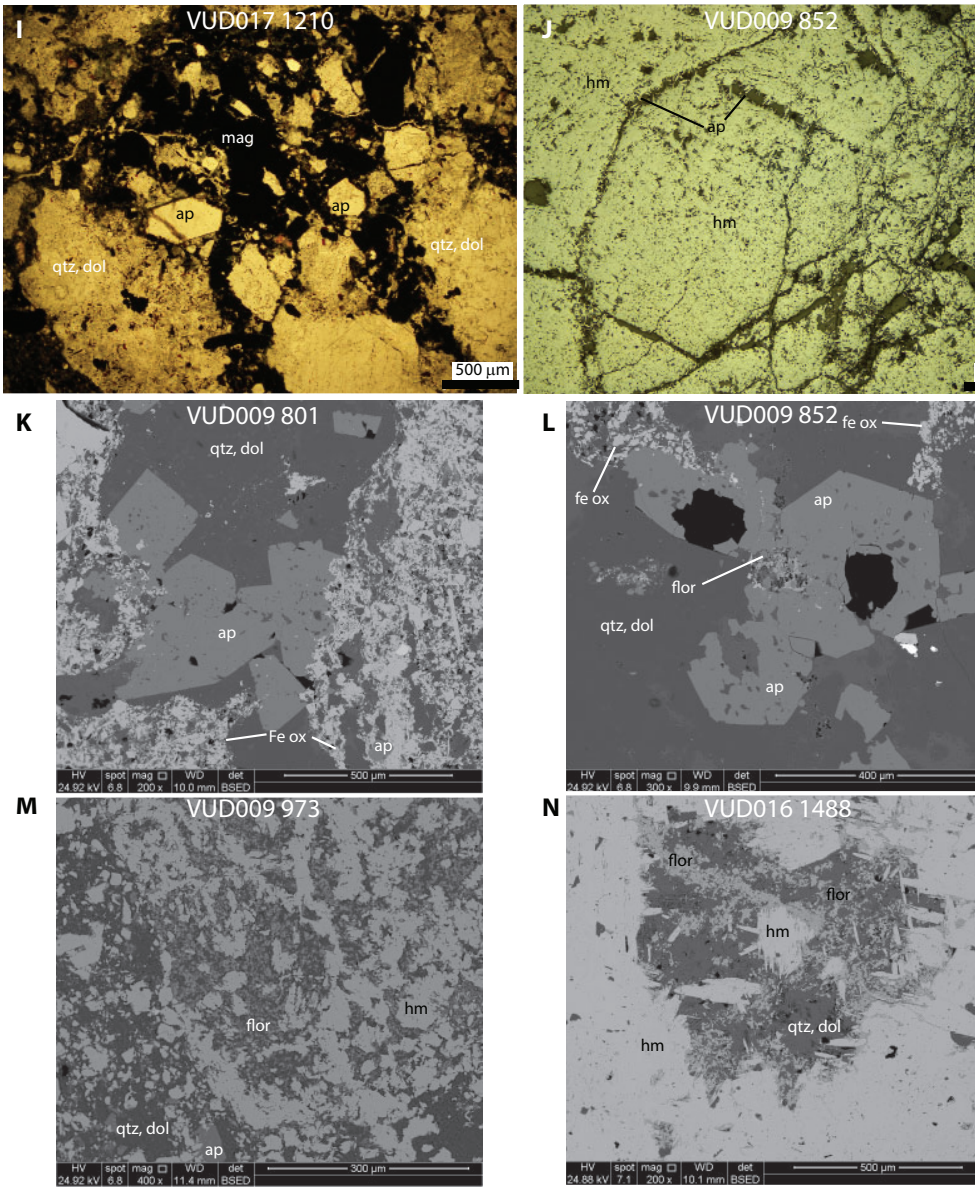

Figure 3: Reflected light microphotographs (a-h), plane-polarised light (PPL; i-j)) and back scatter electron (BSE) images (k-n) for representative sections of samples analysed in this study. a) Magnetite pseudomorphed by hematite and intergrown with pyrite and chalcopyrite in VUD 007 1183; b) magnetite with hematite rims from VUD017 1259. Note the mottled and fractured texture of magnetite grains and growth of hematite along fracture zones; c) magnetite with pyrite inclusions, rimmed by hematite in VUD017 1268; d) bladed hematite in VUD007 1210; e) chalcopyrite intergrown with magnetite partially replaced by hematite, sample VUD001 1155 m; f) pyrite and chalcopyrite intergrown with magnetite replaced by hematite. Chalcopyrite also occurs along fractures within pyrite, sample VUD007 1144 m; g) partially replaced magnetite by hematite, intergrown with chalcopyrite and pyrite, sample VUD007 1192 m; h) association of sulphides, pyrite and chalcopyrite, with iron oxides in sample VUD007 1192m; i) magnetite-assocaited apatite with quartz and dolomite clasts, sample VUD 017 1210; j) apatite veins replacing hematite, sample VUD 009 852; k) apatite intergrown with Fe-oxides in a quartz-dolomite matrix. Apatite also occurs within Fe-oxide matrix, sample VUD009 801; l) apatite intergrown with florencite in quartz-dolomite matrix, sample VUD009 852; m) florencite intergrown with Fe-oxide, sample VUD009 973; and n) florencite intergrown with bladed hematite, sample VUD016 1488. Fe-ox: Iron oxide; qtz: quartz; dol: dolomite, ap: apatite; flor: florencite; haem: hematite.

Apatite U-Pb geochronology

Data obtained from seven samples analysed for apatite U-Pb geochronology are presented in Figure 4 and Appendix Table A1. The time-resolved profiles for each analysis were filtered for inclusions, particularly REE-bearing inclusions, which were abundant in apatite. Likely mineral inclusions in the apatite are florencite, and to a lesser extent monazite, zircon and xenotime. Such inclusions compromise the U-Pb signals measured in the grain. Data that did not meet the following criteria were rejected:

- a minimum threshold of 1 ppm U,
- obvious outliers due to common Pb or low radiogenic Pb counts or Pb loss
- a maximum threshold of 10,000 ppm Fe. The application of 10,000 ppm Fe was used to eliminate potential inclusions within the apatite grains.

In addition, the majority of analyses from sample VUD009 852 were discarded due to low Ca counts in time-resolved profiles Such grains with low Ca were likely to be a phosphate mineral phase or a mixture of minerals phases that were not apatite. Representative time resolved profiles for grains included in the calculations and those containing inclusions are presented in Appendix Figure A2.

Magnetite-associated apatite

Three samples of apatite from magnetite-rich holes located in the east of the prospect were analysed for U-Pb geochronology. None of the samples yield data that define statistically robust isochron intercept ages. As the uncertainties on individual analyses are large (typically 3-15% for $^{206}Pb/^{238}U$ ratios and 5-20% for $^{207}Pb/^{235}U$ ratios) this is unlikely to represent an underestimate of analytical uncertainties and instead represents multiple populations that are likely to represent variable common Pb, Pb loss and age resetting. The ages obtained for magnetite-associated apatite are Mesoproterozoic in age (ca. 1586–1411 Ma) and within uncertainty of each other. Twenty-five analyses of apatite from VUD007 1084 define a regression that yields a lower intercept of 1539 ±43 Ma and an upper intercept of 3446 ± 280 Ma (MSWD = 2.4; Fig. 4a). Calculation of a weighted mean age using > 90% concordant data is 1595 ±66 Ma (MSWD 4.3, n = 7). Twenty-three analyses of apatite from VUD007 1183 yield a lower intercept of 1586 ±42 Ma and an upper intercept of 3474 ±280 Ma (MSWD = 2.1; Fig 4). Calculation of a weighted mean age using only concordant data (>90% concordant) is 1605 ±26 Ma (MSWD 0.88, n = 8). Twenty-nine analyses of apatite from VUD017 1210 yield a lower intercept of 1411 ±160 Ma and an upper intercept of 2349 ±280 Ma (MSWD = 3.9; Fig. 4c). An age is not assigned to this sample as analyses plot along concordia between ca. 2400 Ma and ca. 1600 Ma and it is therefore impossible to isolate a statistically meaningful group.

Hematite-associated apatite

Four samples of apatite from hematite-dominated drill holes in the central and east of the prospect were analysed for U-Pb geochronology. Two age populations were obtained in the hematite-associated apatite at ca. 1110 Ma and ca. 450 Ma. Twenty-five analyses from VUD009 973 yield a lower intercept of 1077 ±30 Ma and an upper intercept of 4364 ±480 Ma (MSWD = 5; Fig. 4d). Calculation of a weighted mean age using $^{206}Pb/^{238}U$ ages from the younger population (less than 1150 Ma) is 1105 ±16 Ma (MSWD 2.1, n = 18). Ten analyses of VUD009 852 apatite yield a lower intercept of 1069 ±51 Ma and an upper intercept of 4843 ± 470 Ma (MSWD = 4.0; Fig. 4e). Collectively these data are taken to be representative of apatite growth or recrystallization at ca. 1100 Ma.

Thirty-three analyses of apatite from VUD009 801 yield a lower intercept of 449 ±20 Ma and an upper intercept of 4092 ±240 Ma (MSWD = 3.1; Fig. 4f). Thirty-seven analyses of apa-

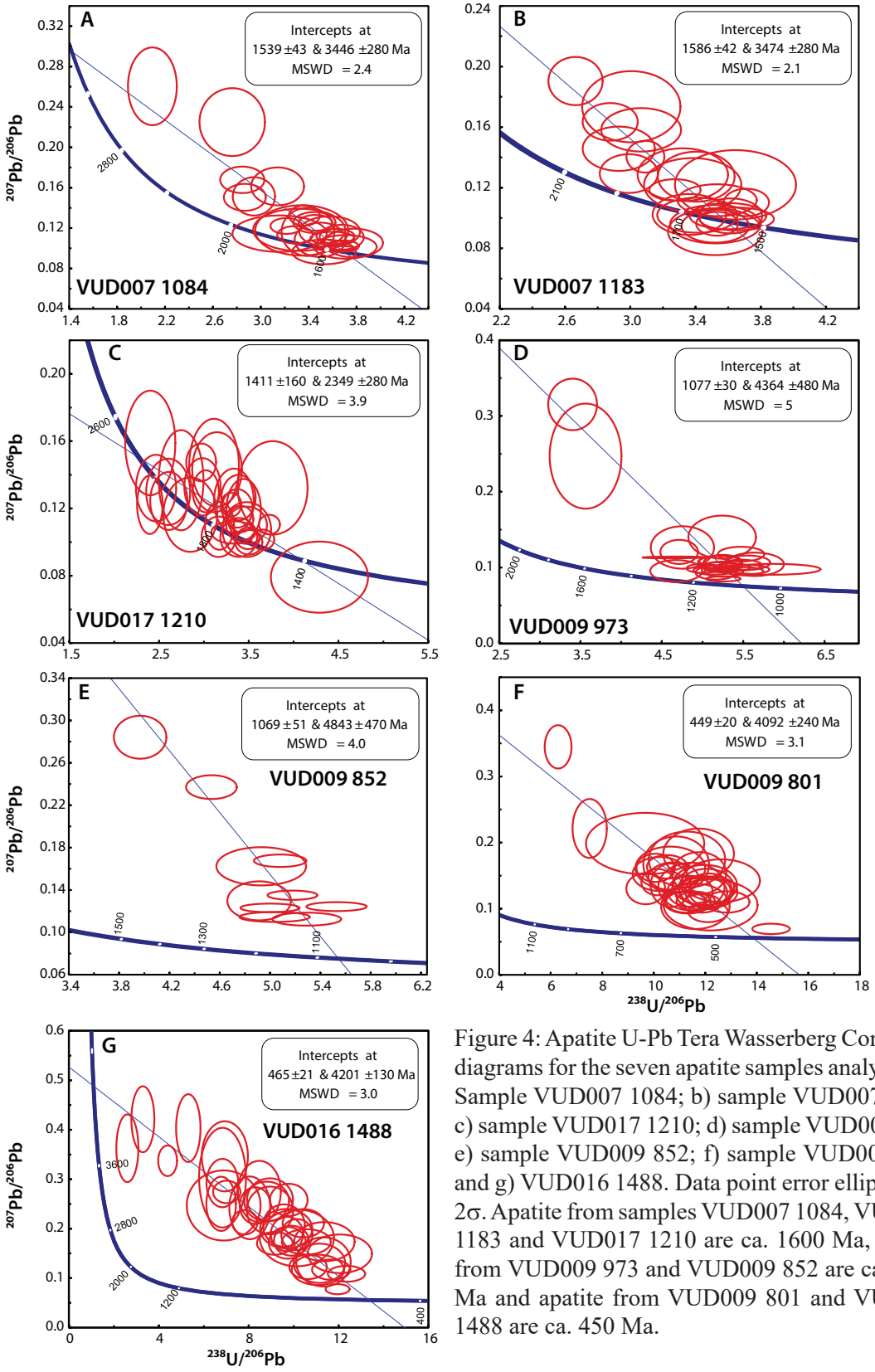

Figure 4: Apatite U-Pb Tera Wasserberg Concordia diagrams for the seven apatite samples analysed. a) Sample VUD007 1084; b) sample VUD007 1183; c) sample VUD017 1210; d) sample VUD009 973; e) sample VUD009 852; f) sample VUD009 801; and g) VUD016 1488. Data point error ellipses are 2σ. Apatite from samples VUD007 1084, VUD007 1183 and VUD017 1210 are ca. 1600 Ma, apatite from VUD009 973 and VUD009 852 are ca. 1100 Ma and apatite from VUD009 801 and VUD016 1488 are ca. 450 Ma.

tite from VUD016 1488 yield a lower intercept of 465 ±21 Ma and an upper intercept of 4201 ±140 Ma (MSWD = 3.0; Fig. 4g). Although neither of these ages are statistically valid, they are considered sufficiently robust to indicate apatite growth or recrystallization at ca. 450 Ma.

Mineral chemistry and compositional data

LA-ICP-MS data for apatite, florencite, magnetite and hematite are reported in Appendix Tables A2–A4. Representative time-resolved profiles for each element are presented in Appendix Figure A2.

Apatite trace element geochemistry

Magnetite-associated apatite grains (ca. 1600 Ma) have high total REY (627–8321 ppm), which distinguishes them from younger apatite populations (Fig. 5). These apatite grains have high Y/Y* (0.42–0.72) and low Eu/Eu* (0.13–0.67; Fig. 5b) ratios. U+Th contents in magnetite-associated apatite span a wide range of values (1-400 ppm) and form positive correlations with total REY (Fig 5c). La/Nd ratios are generally high (0.1 to 1) and U/Th are <10 (Fig. 5d). Trace element abundances in magnetite-associated apatite tend to cluster on scatter plots, with the exception of U and Th contents (e.g. Fig. 5c). Ce/Ce* values or ratios (calculated as Ce_{CN} /(La_{CN} x Pr_{CN})$^{0.5}$ in ca. 1600 Ma magnetite-associated apatite are restricted in their range and close to 1 (0.93–1.2; Appendix Table A2). Chondrite-normalised REY patterns for magnetite-associated apatite have LREE enrichment relative to HREE, most prominent in sample VUD007 1084. All magnetite-associated apatite have negative Eu anomalies and negative Y anomalies (Fig. 6a). The ca. 1100 Ma hematite-associated apatite have moderate Y/Y* and E/Eu* values of 0.36-0.61 and 0.26-0.54, and total REY (372–4663 ppm) compared with other apatite groups, but are separated from each other by their total ΣREY and Eu/Eu* (VUD009 852 ΣREY = 1132–4663 and Eu/Eu* = 0.26–0.31; VUD 009 973 ΣREY = 372–1759 and Eu/Eu* = 0.37–0.54). U+Th is generally high in the ca. 1100 Ma hematite-associated apatite and forms a separate but parallel trend to the magnetite-associated apatite (Fig. 5c). La/Nd ratios are typically high in VUD009 973 and U/Th ratios are similar (Fig. 5d). Ce/Ce* in variable (0.82–4.97; Appendix Table A2).

Chondrite-normalised REY of ca. 1100 Ma hematite-associated apatite have distinctive patterns attributed to large variations in LREE between the two samples (VUD009 852 ΣLREE (La to Sm) = 540–2037 ppm and VUD009 973 ΣLREE (La to Sm) = 24–335 ppm). Differences in $(La/Sm)_{CN}$ ratios are also significant (VUD009 852 = 0.031–0.1852 and VUD009 973 = 0.0026–1.6112), which correspond to a positively curved LREE profile in VUD009 852 and steep positive to flat LREE profiles in VUD009 973 (Fig. 6b). Another distinction between the ca. 1100 Ma hematite-associated apatite is the relative size of the Eu anomaly, where a larger negative anomaly is present in VUD009 852. Relative LREE/HREE depletions differ significantly, where VUD009 852 has relative uniform $(La/Yb)_{CN}$ values (0.19-0.88), while VUD009 973 has a wide range of $(La/Yb)_{CN}$ values (0.03-2.87).

The two ca. 450 Ma hematite-associated apatite samples are distinguished from the other apatite groups by their lower Y/Y* (0.18–0.43) and higher Eu/Eu* values (0.38–0.84). The two samples are distinguished from each other in their ΣREY and Eu/Eu* values. VUD009 801 has higher ΣREY and lower Eu/Eu* compared with VUD016 1488 (Fig. 5). VUD009 801 also plots separately from the other apatite populations on Figure 9b, having lower Y/Y* at higher Eu/Eu*. U+Th form positive correlations with ΣREY and each ca. 450 Ma apatite sample forms a separate trend. VUD009 801 forms a trend similar to the magnetite-associated apatite, whereas VUD016 1488 has lower ΣREY at similar U+Th and forms a separate group on Figure 5c. U/Th ratios are high in

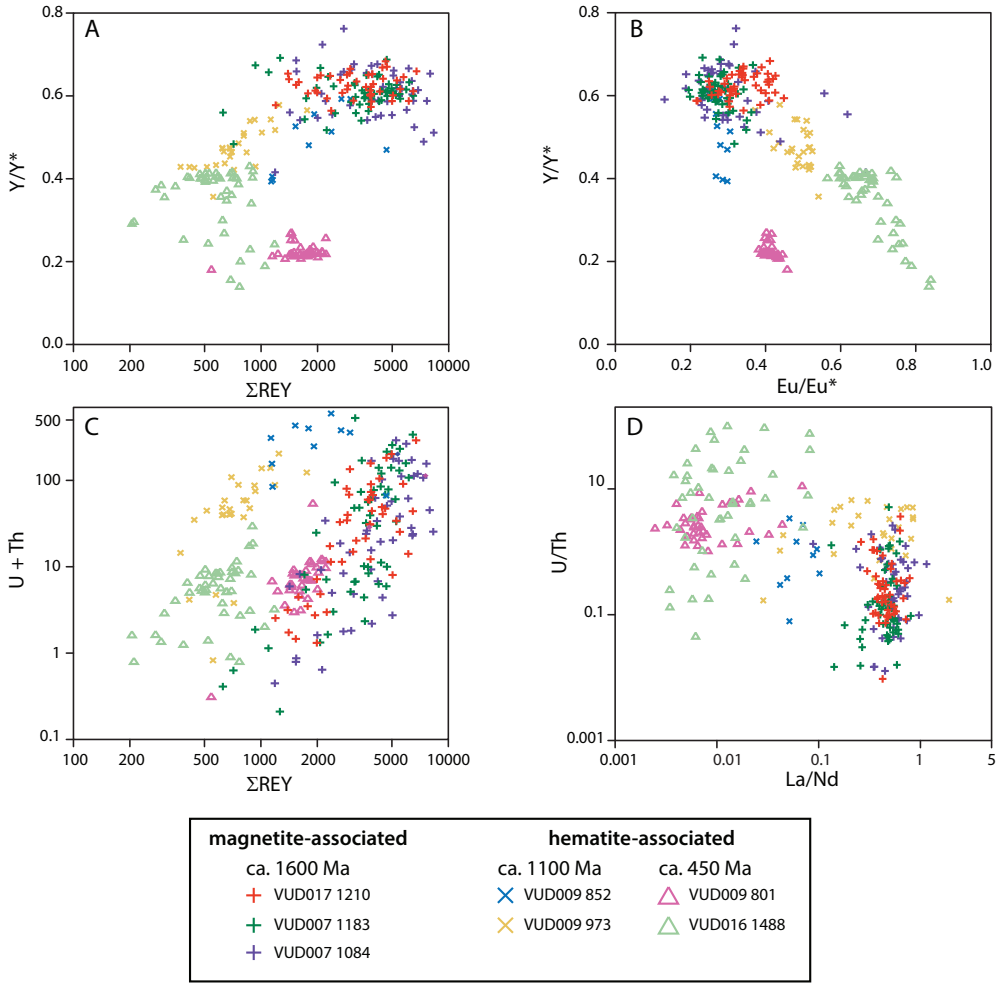

Figure 5: Selected scatter plots for apatite collected in this study. a) Y/Y* vs ΣREY where Y/Y* = [(Y_{CN}/(Dy_{CN}+Ho_{CN})/2)]; b) Y/Y* vs Eu/Eu* where Eu/Eu* = [(Eu_{CN}/(Sm_{CN}+Gd_{CN})/2)]; c) U+Th vs ΣREY; and d) U/Th vs La/Nd. Chondrite normalising values are from Sun and McDonough (1989).

ca. 460 Ma hematite-associated apatite (Fig. 9). Ce/Ce* in ca. 460 Ma hematite-associated apatite are variable (0.65–2.29; Appendix Table A2).

Chondrite-normalised REY patterns for the ca. 450 Ma hematite-associated apatite have similar patterns and are characterised by extremely low LREE concentrations (apatite $(La/Sm)_{CN}$ = 0.0003-0.0167) compared with the other apatite samples. The humped-shaped profiles are indicative of MREE enrichment relative to extreme LREE and HREE depletions (Fig. 5c). LREE/HREE depletions are marked by very low $(La/Yb)_{CN}$ ratios (0.001-0.016) in this apatite group.

Eu/Eu* values in apatite tend cluster for each age group, and increase as apatite becomes younger, forming a negative correlation between Y/Y* and Eu/Eu* (Fig. 5b). The exception is VUD009 801, where apatite forms a tight cluster on Y/Y* vs Eu/Eu*, and have higher Eu/Eu* values at similar Y/Y* values than VUD016 1488 (Fig. 5b).

Florencite trace element geochemistry

Florencite from three samples from one drill hole (VUD009) were analysed for trace ele-

ment concentrations. Results are listed in Appendix Table A3.

Concentrations of transition metals (e.g. Sc, Mn, Fe and Cu) in florencite are variable. Sc, Mn Fe and Cu are highest in sample VUD009 973, most likely attributed to the close proximity of Fe oxides with florencite (Fig. 3g) and fine-grained chalcopyrite and hematite in the ablated volume. VUD009 852 has low Sc and Fe but intermediate Mn and Cu relative to sample VUD009 801 and VUD009 973. Th concentrations are significantly higher and U concentrations are generally higher in sample VUD009 852 relative to the other florencite.

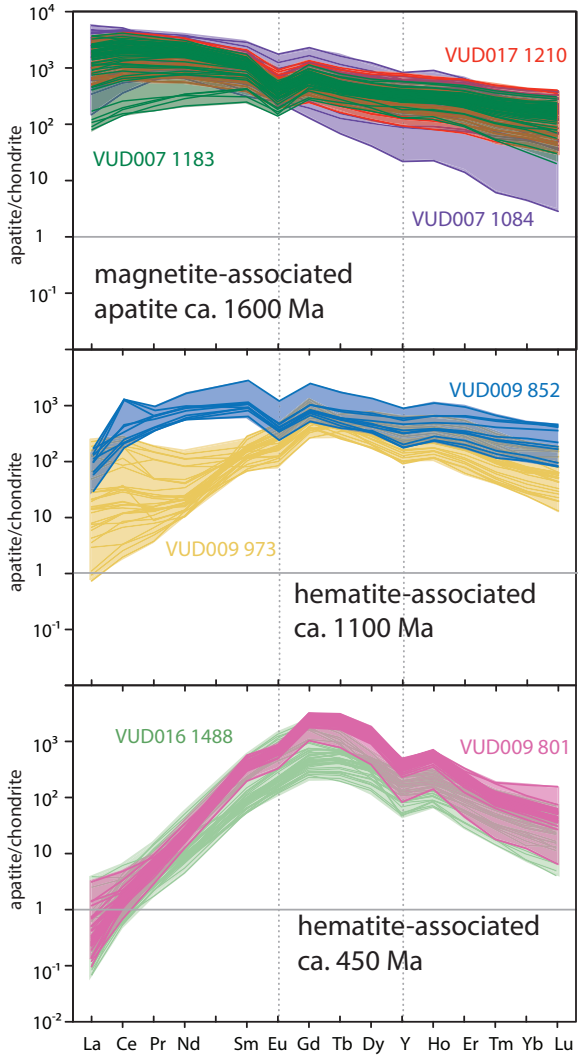

Figure 6: REY plots for apatite collected in this study, grouped by age and type. Apatite from VUD007 and VUD017 are ca. 1600 Ma apatite; VUD009 852 and VUD009 973 are ca. 1100 Ma hydrothermal apatite; and VUD009 801 and VUD016 1488 are ca. 450 Ma hydrothermal apatite. Chondrite normalising values are from Sun and McDonough (1989).

REY

Florencite have La/Ce <1, indicating the florencite from these samples is Ce-dominant ($CeAl_3(PO)_4(OH)_6$). La/Ce from each sample are relatively consistent on a per sample basis. Florencite from VUD009 973 has the highest La/Ce ratios (0.62–0.78), VUD009 852 has the lowest La/Ce ratios (0.35–0.50) and VUD009 801 have La/Ce transitional between the two (La/Ce = 0.41–0.67). Higher concentrations of Pr+Nd correlate with higher concentrations in Ce, seen in VUD009 852 and to a lesser extent in VUD009 801. ΣREY are highest in sample VUD009 852, and cover a relatively narrow range of high values (ΣREY = 10.85–16.36 wt %). Whereas ΣREY in sample VUD009 801 is 1.87–12.08 wt % and ΣREY = 2.51–16.65 wt % in sample VUD009 973 (Appendix Table A3).

Chondrite-normalised REY trends for florencite are characterised by extreme LREE enrichments and HREE depletions, creating a steep slope and slight flattening out of HREE, most apparent in sample VUD009 852 (Fig. 7). VUD009 852 shows little variation in LREE abundance, while HREE in this sample are variable. REY in the other two samples display greater variation, with one order of magnitude difference between some REY (Fig. 7). Eu/Eu* values in florencite are less than one corresponding to negative Eu anomalies on the REY plot.

All florencite samples have negative Y anomalies, although the size of the anomaly is small in samples VUD009 973 (Y/Y* = 0.38–1.12) and VUD009 852 (Y/Y* = 0.30–0.58) compared with Y/Y* = 0.24–2.53 in VUD009 801.

Magnetite trace element chemistry

Time-resolved LA-ICP-MS profiles typically show smooth profiles in magnetite, suggesting homogeneous element distributions within grains. However, some spots showed spikes in the profiles in elements such as LREE, Th and P and transition metals such as Co, Ni, Cu and Ti, suggesting inclusions are present within the magnetite grains and were ablated in the volume (Appendix Figure A2). High values of V and Al are present in all magnetite grains, while Mg concentrations are variable. As noted above, profiles consistent with inclusions such as monazite and apatite (high values of LREE, Th, P and Ca), most abundant in sample VUD 017 1269, were filtered from the dataset. Higher transition metal abundances in magnetite (e.g. Mn, Ti, Co, Cu and Ni) may be due to substitution for Fe in magnetite and do not appear to significantly affect the REE concentrations of magnetite (Appendix Figure A3). Mg-rich inclusions in magnetite are generally associated with lower REE abundance in the magnetite grains.

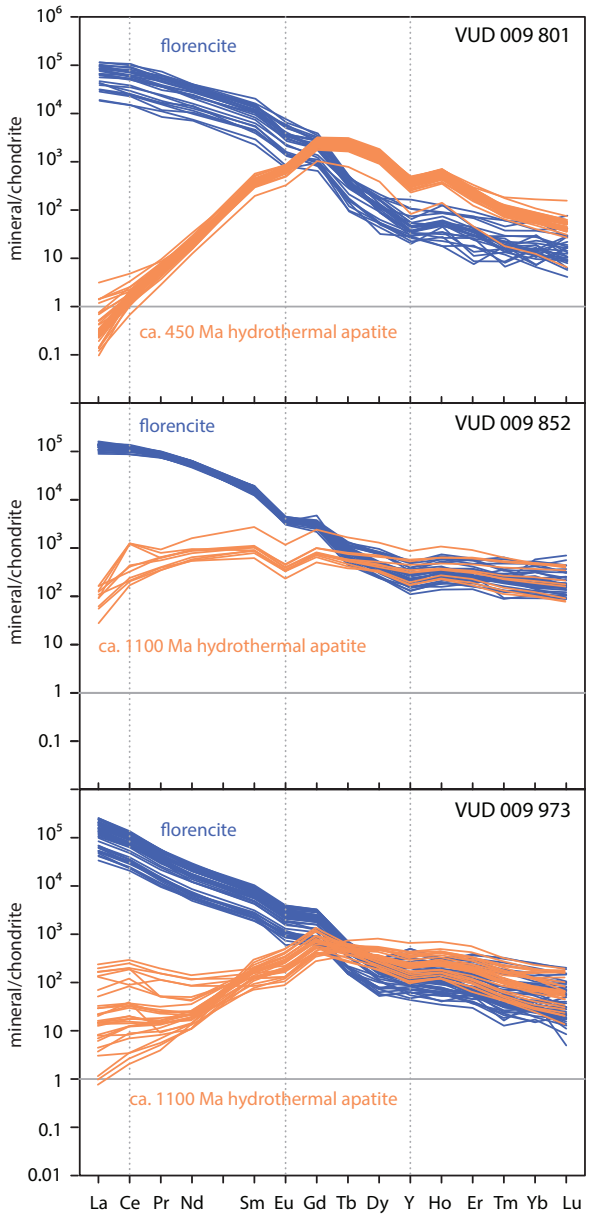

Figure 7: REY plots for florencite and apatite occurring in the same sample from drill hole VUD009. Chondrite normalising values are from Sun and McDonough (1989).

Magnetite grains from the studied samples are generally high Ti-V and low Mn-Cu (Fig. 8). Selected scatter plots for magnetite show that grains from individual drill holes have distinct trace element signatures. Magnetite from VUD007 display overlap in their trace element geochemistry, Similar ranges of transition metals are observed in VUD007 magnetite, although Co is slightly elevated and Zn is slightly lower in VUD007 1192 compared with VUD007 1183. VUD007 magnetite grains are typically high in V and Ni, low Mn and Zn and Cu is low to moderate (Fig. 8a-h). A small group of low Ti-V-Ni and high Mg magnetite analyses, mostly from sample VUD007 1192, plot separate from the main population. VUD007 form a weak positive correlation between V and Ti (Fig.8), while other transition metals do not exhibit any correlations (Fig. 8). In sample VUD007 1192, a weak positive correlation is seen between Zn and Mn (Fig. 8g).

Magnetite grains from VUD017 have distinguishable Ni and V contents from each other display overlap in other transition metals (Fig. 8). VUD017 magnetite grains have very restricted V concentrations over a range of Ti values, forming horizontal trends (Fig. 8a). VUD017 1259 is high in V and Ni compared with VUD017 1268 (Fig. 8a and b). Other

transition metals have similar concentrations between the two VUD0017 samples (Fig. 8a-h). No correlations are formed between any transition metals in VUD017 magnetite.

On a per sample basis, magnetite grains display variations in HFSE such as Th, Nb, Y and Ta and form positive correlations with other HFSE (Fig. 9a-e). Inter-sample variation is observed in magnetite grains from VUD017, where VUD017 1259 magnetite has lower Nb, Ta, and Th contents relative to VUD017 1268 magnetite (Fig. 9a, c, d). The range in HFSE concentrations is similar among VUD007 magnetite grains (Fig. 13). U and Th are low in magnetite grains but show positive correlations with total rare earth element yttrium (ΣREY) in all samples (Fig. 13e, f). The granitophile elements W, Sn, Mo and U are very low in magnetite from Vulcan (Fig. 9f, g). Uranium and Mo+Sn+W contents are <1.4 and <2 ppm, respectively; W and Mo are commonly below the detection limit. Despite the low values, a positive correlation between U and Mo+Sn+W is observed in all magnetite samples (Fig. 9g).

REY

Variation in ΣREY in magnetite range from 0.006–17.2 ppm. Many REY measurements are below detection limit, contributing to the low total concentrations. Magnetite from VUD007 display similar variation in ΣREY (0.01–13.58 ppm and 0.006–17.20 for VUD007 1183 and 1192 respectively), whereas magnetite from VUD017 have consistent and very low ΣREY contents (VUD017 1268 ΣREY = 0.10–2.93 ppm and VUD017 1259 ΣREY = 0.01–2.28 ppm; Fig. 9f and 9g).

Chondrite-normalised (CN) REY patterns in magnetite are variable in each sample (Fig. 10). REY patterns for magnetite grains with REY below detection limit are presented in Appendix Figure A3, as the shape of their REY profiles are not representative of the magnetite. Magnetite from VUD 007 has similar REY patterns, characterised by enrichments in some LREE, positive Ce anomalies, negative Eu anomalies and flat HREE (Fig. 10). Y/Y* (calculated as $[(Y_{CN})/(Dy_{CN}+Ho_{CN})/2)]$ are variable between and within magnetite samples, represented by both positive and negative anomalies (Fig. 10). Magnetite from VUD007 1192 has similar LREE contents, however HREE form two groups, one with relatively high HREE abundances (ΣHREE = 0.289–1.153 ppm) and one with relatively low HREE abundances (ΣHREE = 0.030–0.172 ppm). Magnetite from VUD007 1192 with higher HREE abundances also has higher Nb and Ta.

Magnetite from VUD017 has distinct REY patterns. VUD017 1259 grains display concave slopes with HREE enriched patterns and are less enriched in LREE compared with other magnetite (Fig. 11). Ce and Y anomalies range from weakly positive to positive and Eu anomalies range from negative to weakly positive. In contrast, chondrite-normalised REYs for magnetite from VUD017 1268 are characterised by slightly steeper negative patterns with LREE enrichments and HREE depletions. Weak positive Ce anomalies, strong negative Eu anomalies and positive to negative Y anomalies are present (Fig. 11).

Hematite trace element geochemistry

Time-resolved LA-ICP-MS profiles for hematite show both smooth and irregular downhole profiles. Smooth profiles suggest homogeneous element distributions within grains, whereas irregular profiles suggest inclusions within the grains or mixtures of phases in the ablated volume (Appendix Figure A2). Florencite was identified as the most abundant inclusion phase in hematite.

Trace element concentrations

Hematite grains were analysed from three samples at different intervals from one drill hole, VUD009. Hematite grains generally display a wide variation in trace element com-

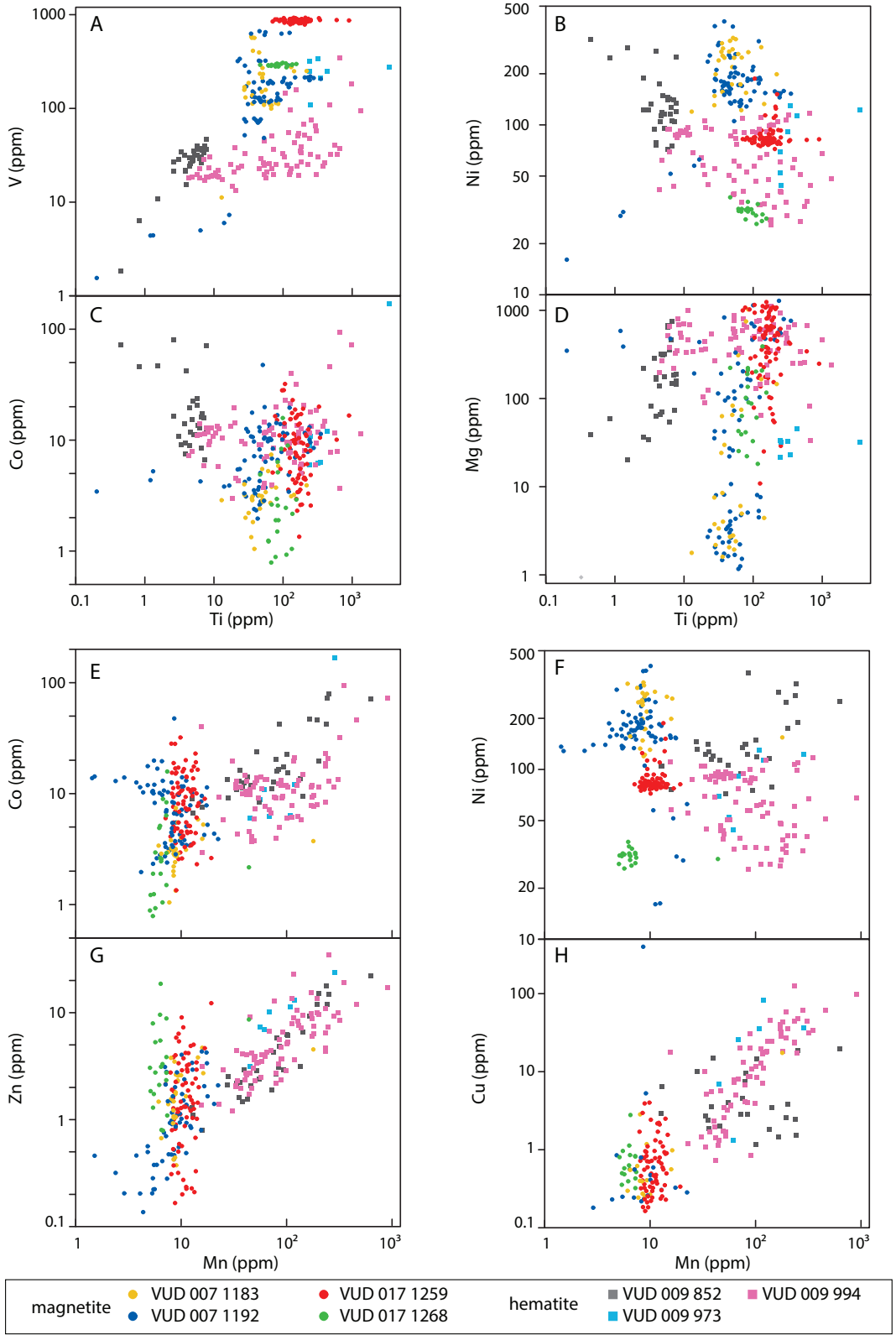

Figure 8: Selected transition metal scatter plots versus Ti (a-d) and Mn (e-h) for magnetite and hematite collected in this study. A) V vs Ti; b; Ni vs Ti; c) Co vs Ti; d) Mg vs Ti; e) Co vs Mn; f) Ni vs Mn; g) Zn vs Mn; and h) Cu vs Mn. Samples are divided by drillhole sample number.

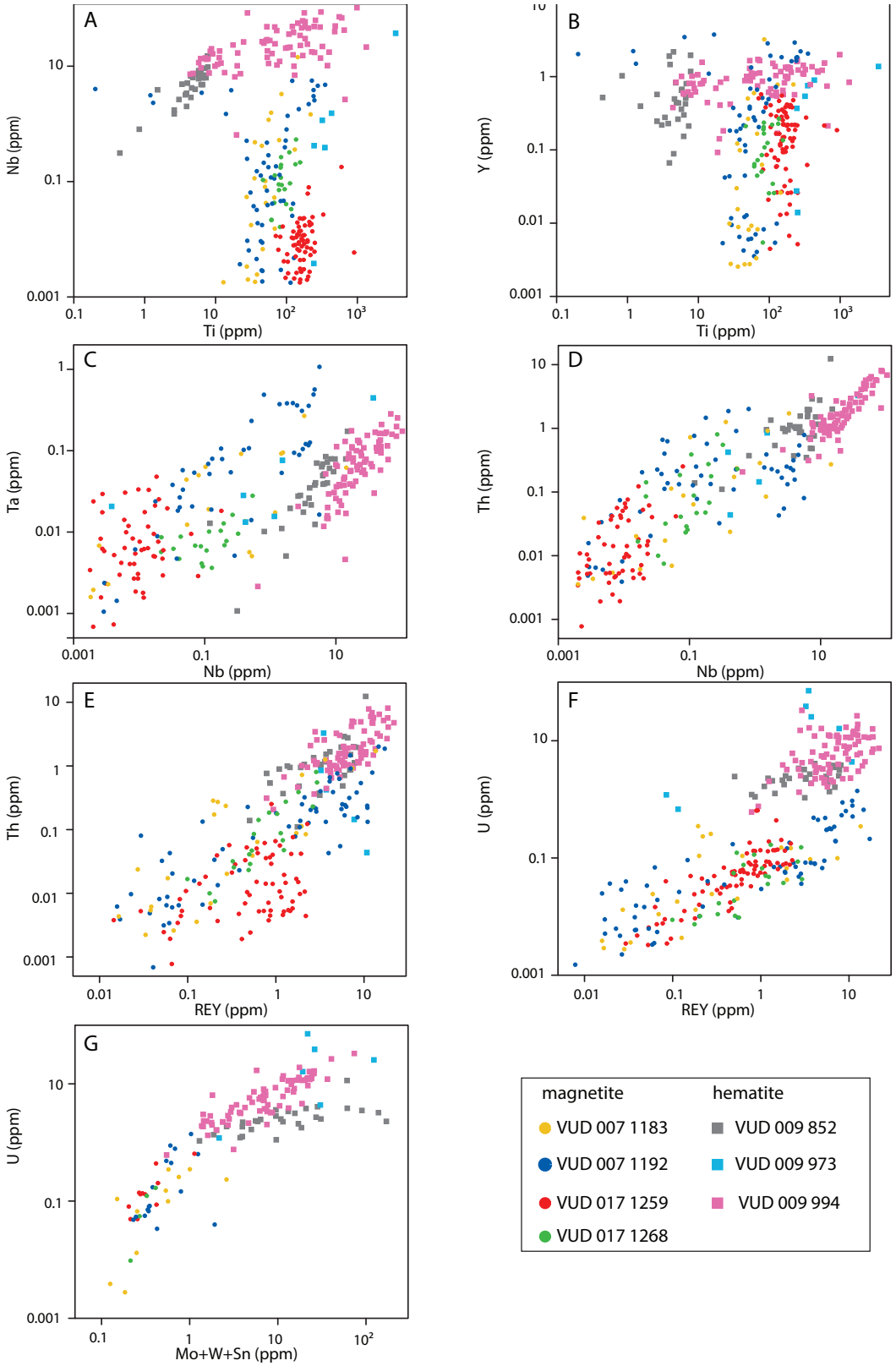

Figure 9: Selected scatter plots for high field strength elements (HFSE) and granitophile elements in magnetite and hematite collected in this study. A) Nb vs Ti; b) Y vs Ti; c) Ta vs Nb; d) Th vs Nb; e) U vs REY; f) Th vs REY; and g) U vs Mo+W+Sn.

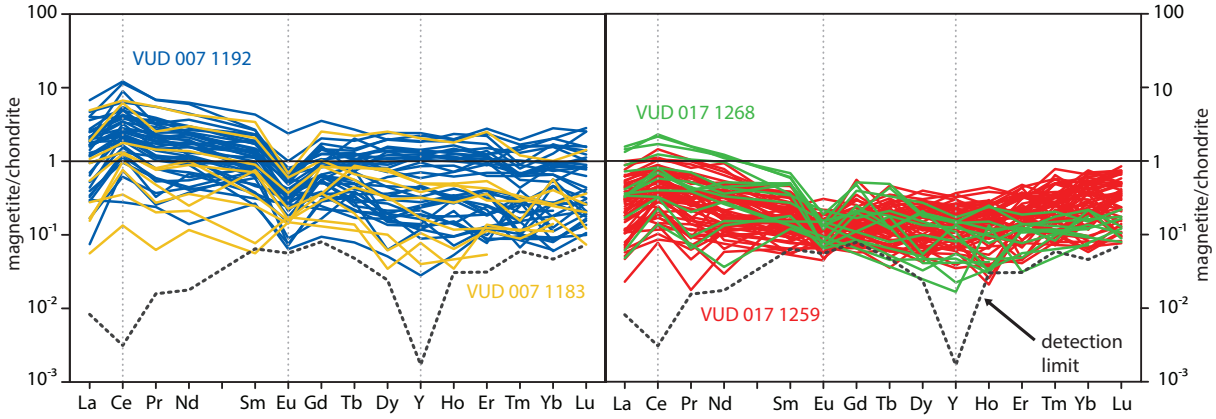

Figure 10: REY diagrams for magnetite collected in this study, grouped by drill hole. Dark grey dashed line represents the detection limit for each element. Shaded areas represent the data field for each sample. Vertical light grey dotted lines highlight where Ce, Eu and Y sit. Chondrite normalising values are from Sun and McDonough (1989).

positions (Fig. 8), and are characterised by higher Mg and Mn contents relative to magnetite (Fig.812d and e-h). Ti and V have a wide range of concentrations (0.4–3473 ppm and 1.8–346 ppm, respectively), and are lowest in sample VUD009 852 and highest in VUD009 973 (Fig. 8a). Positive correlations are formed between V and Ti in hematite. VUD009 852 hematite has higher Ni and Co and lower Ti relative to hematite from intervals 994 and 973, and forms negative correlations between Ni and Co with Ti. VUD009 852 also forms a positive correlation between Mg and Ti, while hematite from VUD007 973 and 994 show no correlations between Ni, Co, Mg and Ti. Co, Zn and Cu form positive correlations with Mn in hematite (Fig. 8e-h), whereas Ni contents show no correlations.

Nb, Y and Th concentrations are generally high in hematite and form positive correlations with other HFSE (Fig. 9a-d). Yttrium in hematite does not vary significantly with Ti (Fig. 9b). At equivalent concentrations of Nb, hematite has lower Ta and Th concentrations than magnetite, forming separate but parallel trends between Ta and Th with Nb (Fig. 9c and d). Uranium concentrations are higher in hematite relative to magnetite (Fig. 9e and g). Separate trends are formed between U and Mo+W+Sn in hematite from VUD 009 852 and hematite from VUD 009 973 and 994, where the former has lower U at similar Mo+W+Sn concentrations (Fig. 9g).

REY

Hematite ΣREY are variable and are generally higher when compared with magnetite (0.5–21.85 ppm). REY patterns in hematite differ between the samples. VUD009 852 generally has flat LREE and flat HREE with weak positive to no Ce anomalies, negative to positive Eu anomalies and variable Y anomalies (Fig. 11). VUD009 973 has a concave pattern characterised by steep LREE and enriched HREE concentrations, and two analyses below detection limit (Appendix Figure A3). Ce anomalies are weakly positive and Eu anomalies are generally negative. VUD009 994 has LREE enriched and flat to concave HREE patterns, weak positive Ce anomalies, negative Eu anomalies and Y/Y* in unity (Fig. 11). Many HREE in sample VUD009 994 are near detection limit, giving the appearance of spiky patterns that would otherwise be smooth (Fig. 11).

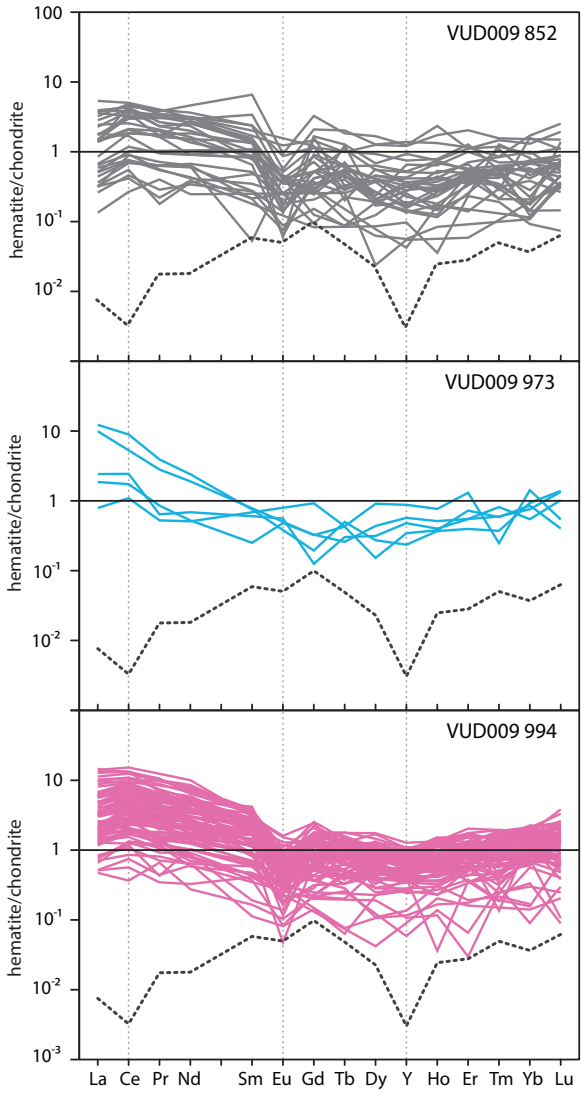

Figure 11: REY diagrams for hematite collected in this study, divided by sample. Dark grey dashed line represents the detection limit for each element. Vertical light grey dotted lines highlight where Ce, Eu and Y sit. Chondrite normalising values are from Sun and McDonough (1989).

DISCUSSION

Summary and significance of U-Pb apatite results

Apatite analysed from four drill holes at Vulcan yield ages that can be roughly grouped into three time periods: ca. 1600 Ma, ca. 1100 Ma and ca. 450 Ma (Table 2). Each of these ages corresponds to magmatic, hydrothermal and tectonic events recorded in southern Australia, and importantly, correspond to similar ages recorded at Olympic Dam and surrounding prospects (e.g. Fig. 12; Trueman *et al.* 1988. , Wawryk 1989, Johnson 1993, Meffre *et al.* 2010, Ciobanu *et al.* 2013, Diemar 2014, Jagodzinski 2014, Huang *et al.* 2015, Kamenetsky *et al.* 2015, Apukhtina 2016, Kirchenbaur *et al.* 2016, Apukhtina *et al.* 2017, Cherry *et al.* 2018b, Ehrig *et al.* 2018, Courtney-Davies *et al.* 2019a, Courtney-Davies *et al.* 2020, Maas *et al.* 2020). Hydrothermal alteration and IOCG mineralisation at Olympic Dam and the Acropolis Prospect in the Olympic Cu-Au Province occurred between 1594–1590 Ma (Cherry *et al.* 2018a, Courtney-Davies *et al.* 2019b, Courtney-Davies *et al.* 2020, McPhie *et al.* 2020). Mineralisation at Vulcan is interpreted to have occurred at 1586 ± 8 Ma (Reid *et al.* 2013), within the time bracket of mineralisation and original hydrothermal activity in the Olympic Cu-Au Province. Apatite growth at ca. 1600 Ma in the magnetite-associated samples at Vulcan broadly correlates with its mineralisation age (1586 ±8 Ma) and the 1594-1590 Ma hydrothermal-magmatic event recorded in the Olympic Cu-Au Province. While the apatite ages only partly overlap with mineralisation at Vulcan and hydrothermal alteration in the Olympic Cu-Au Province (due to large associated errors), lower uranium contents and moderate to significant amounts of non-radiogenic (common) lead present challenges for apatite geochronology and calculated ages rarely have the precision from those obtained by zircon. Nonetheless, apatite is likely recording the extent of the low-temperature processes associated with hydrothermal activity related to ca. 1586 Ma mineralisation at Vulcan.

Hematite-associated apatite with ca. 1100 Ma ages from Vulcan is similar to fluid events recorded at Olympic Dam (Fig. 12; Table 2) in which U was partly remobilised (e.g. Kirchenbaur *et al.* 2016, Reid *et al.* 2017, Maas *et al.* 2020) and Re-Os in sulphides was reset

(Oreskes and Einaudi 1992, McInnes *et al.* 2008). Re-Os isochron data for chalcopyrite and pyrite at Olympic Dam yield ages of 1258 ± 28 Ma which are attributed to resetting of the Re-Os system (McInnes *et al.* 2008). Apatite growth at ca. 1100 Ma is correlated with regional metamorphic and igneous activity recorded in the Musgrave Province, namely the Musgrave Orogeny (Smithies *et al.* 2011, Kirkland *et al.* 2013) and intrusion of the Alcurra Dykes and Giles Complex (Glikson *et al.* 1995). Similar tectonic and magmatic activity is observed to the west of the Gawler Craton (Wingate *et al.* 2004, Betts and Giles 2006, Dutch *et al.* 2018). Resetting ages from this time period are also obtained in the east-adjacent basement block Curnamona Province (Fig. 12; Lu *et al.* 1996). The ca. 1100 Ma apatite age is considered to be a resetting age as opposed to a cooling age.

The third age obtained by apatite U-Pb geochronology at Vulcan is ca. 450 Ma. Apatite

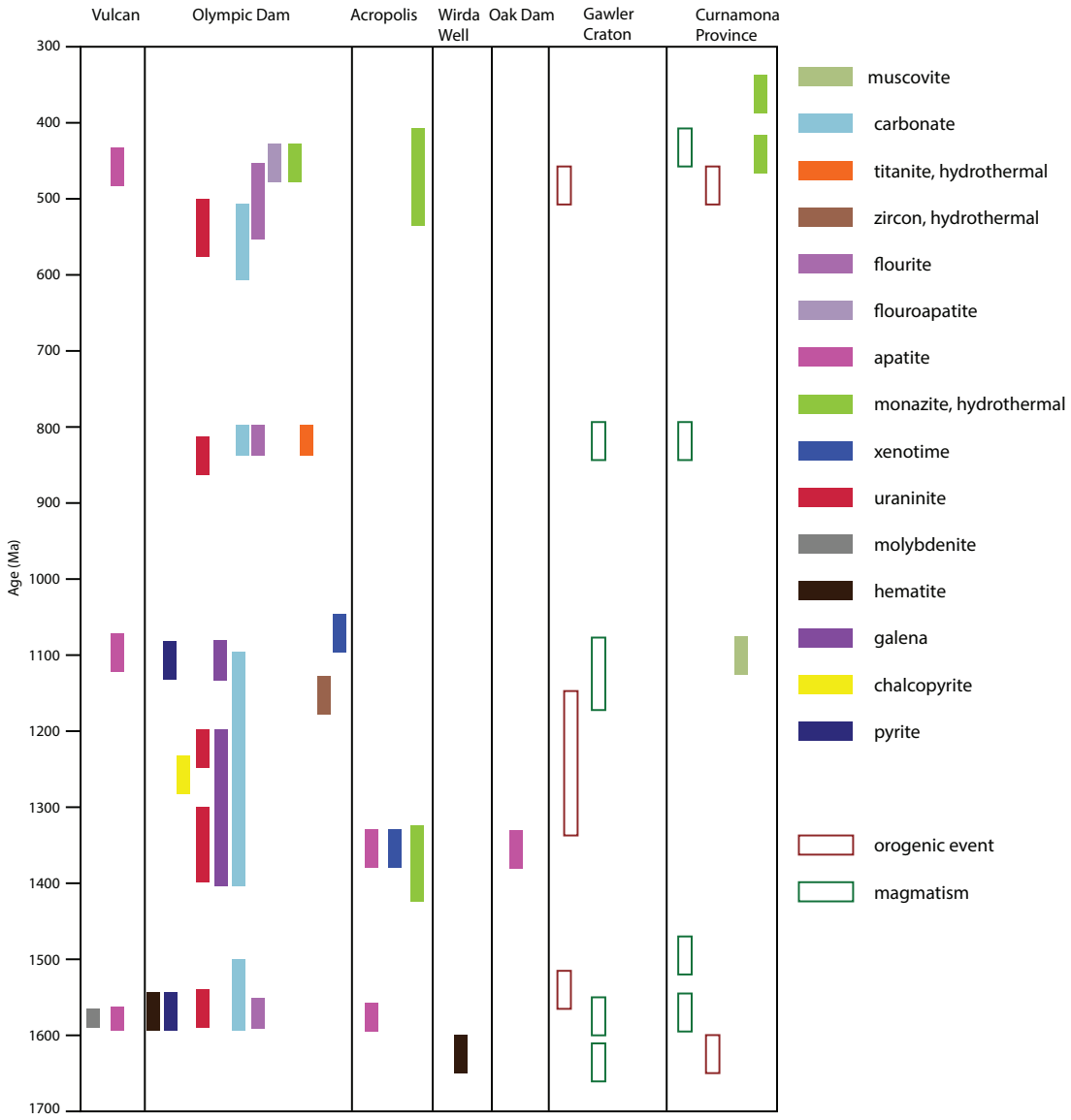

Figure 12: Time space plot showing the distribution of ages related to hydrothermal activity in the Olympic Cu-Au Province and tectonic and magmatic events in the surrounding Gawler Craton and Curnamona Province. Summary of ages and data sources are adapted from Figure 7 from Maas *et al.* 2020.

growth at ca. 450 Ma is broadly coincident with the Delamerian Orogeny (Foden *et al.* 2006) which affected much of southeastern Australia, including the Curnamona Province (Fig. 12; Rutherford *et al.* 2006). Hydrothermal activity at ca. 500 Ma has been documented at Olympic Dam (Oreskes and Einaudi 1992, Maas *et al.* 2011, Kamenetsky *et al.* 2015, Kirchenbaur *et al.* 2016, Maas *et al.* 2020), including the formation of hydrothermal carbonate ca. 490 Ma (Maas *et al.* 2020). This thermal event has been correlated with significant remobilisation and possibly introduction of U at Olympic Dam (Kamenetsky *et al.* 2015, Kirchenbaur *et al.* 2016). A magmatic-hydrothermal event in the Mount Painter Province (northern Curnamona Province) occurred between 460 and 440 Ma related to the intrusion of the British Empire Granite (Elburg *et al.* 2013). Hydrothermal activity and U-REE mineralisation related to iron-rich uranium ores is recorded to have peaked ca. 365 Ma in the Mount Painter Province (Elburg *et al.* 2013, Hore *et al.* 2020). This activity at ca. 460–440 Ma is also recorded in the Adelaide Fold Belt (435 ±5 Ma K-Ar age for willemite ore); and intrusion-related activity in the Harts Range to the northwest and the Alice Springs Orogeny (Elburg *et al.* 2013 and references therein). The timing of this 440–460 Ma magmatic-hydrothermal event more closely corresponds to the ca. 450 Ma apatite age obtained from Vulcan in this study and could represent a driver for the hydrothermal activity recorded at Vulcan. The hydrothermal events as recorded by apatite U-Pb geochronology at Vulcan correspond to similarly aged events within its host Olympic Cu-Au Province and points to a long-lived multistage hydrothermal history in the IOCG deposits of the Olympic Cu-Au Province (e.g. Ciobanu *et al.* 2013, Kamenetsky *et al.* 2015, Kirchenbaur *et al.* 2016, Cherry *et al.* 2017, Cherry *et al.* 2018b, Maas *et al.* 2020).

REE and the evolution of the hydrothermal system

Each age group of apatite at Vulcan has different REY abundances and profiles that show a progressive depletion in LREE with decreasing age. The ca. 1600 Ma magnetite-associated apatite is closest in age to the mineralisation age at Vulcan. As an early-stage apatite, this generation may represent the closest composition to initial REE abundances in apatite in the Vulcan system. Early apatite found in IOCG and IOA deposits is characterised by LREE enriched patterns and negative Eu anomalies (Mao *et al.* 2016, Krneta *et al.* 2017a). Magnetite-associated apatite is also LREE-enriched compared with the younger hematite-associated apatite at Vulcan (Fig. 7). Compared with IOCG magmatic apatite (Krneta *et al.* 2017a), total REY in 1600 Ma magnetite-associated apatite from Vulcan is lower, particularly Ce and La abundances (Fig. 13a), and is in the lower range of REY abundances of apatite from IOCG breccia and IOA deposits (Fig. 13a; Mao *et al.* 2016). The REY patterns and abundances for magnetite-associated apatite most closely resemble early hydrothermal apatite depleted in REY, -S and –Cl, found in altered zones in deep mineralisation from Olympic Dam (Fig. 13b; Krneta *et al.* 2017a). Depletion of LREEs in apatite has been documented in other IOCG and IOA deposits (Harlov *et al.* 2002, Krneta *et al.* 2017a, Krneta *et al.* 2017b).

Apatites are increasingly depleted in LREE as the their measured age decreases, represented by moderate depletions in the ca. 1100 Ma hematite-associated apatite and significant depletions in the ca. 450 Ma hematite-associated apatite. Krneta *et al.* (2017a), Krneta *et al.* (2017b) and Cherry *et al.* (2017) noted that REY-depleted apatite were more commonly associated with hematite-stable assemblages and related hydrothermal activity. Ca. 1100 Ma apatite at Vulcan occurs in assemblages where hematite is observed to pseudomorph magnetite and the samples display sericite

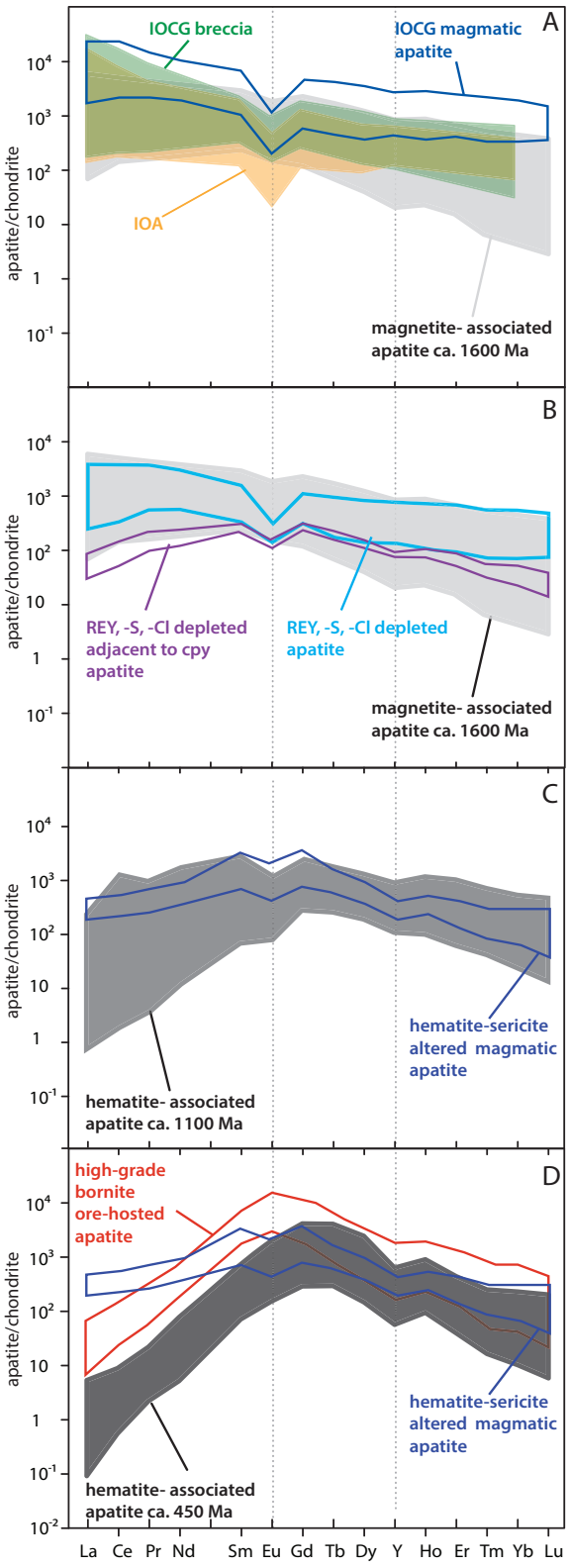

Figure 13: a) Comparison of 1600 Ma magnetite-associated apatite REY profiles from Vulcan with IOCG magmatic apatite, IOCG-breccia apatite and IOA apatite; b) 1600 Ma magnetite-associated apatite REY profiles compared with hydrothermal apatite from Olympic Dam; c) 1100 Ma hematite-associated apatite REY profiles compared with hydrothermal apatite from Olympic Dam; and d) 450 Ma hematite-associated apatite REY profiles compared with bornite-rich apatite from Olympic Dam. Fields for Olympic Dam hydrothermal apatite and IOCG magmatic apatite are from Krneta *et al.* (2017a) and fields for IOCG-breccia and IOA apatite is from Mao *et al.* (2016).

alteration and minor potassic alteration. The REY abundances of the ca. 1100 Ma apatite only partly overlap with hematite-sericite altered magmatic apatite from Olympic Dam (Fig. 13c). The most REY depleted apatite grains (ca. 450 Ma) occur in hematite-bearing assemblages with pervasive sericite alteration, but their REY profiles differ significantly to the hematite-sericite altered magmatic apatite from Olympic Dam and more closely resemble the high-grade bornite ore-related apatite (Fig. 13d). As the ca. 450 Ma hematite-associated apatite is not representative of a high-grade mineralised zone, another explanation for the LREE and HREE depletion is required. Acidic conditions can be produced by the replacement of K-feldspar to sericite. The destruction of apatite under acidic conditions releases P, Ca and LREE, which can be incorporated into new phosphate phases such as florencite. Figure 7 displays the association of florencite with apatite grains that appear to have undergone breakdown reactions, suggesting florencite is a product of that breakdown. Although florencite was not analysed in sample VUD016 1488, abundant florencite in close proximity to apatite and as inclusions within both apatite and hematite (Fig. 3n), is likely the explanation for the LREE-depletion in apatite in this sample. The appearance of florencite in ca. 1100 Ma and ca. 450 Ma samples is consistent with florencite scavenging LREE from the breakdown of apatite.

REE-bearing phases identified in the Olympic Dam IOCG deposit include bastnäsite ($(La,Ce)CO_3F$), synchisite ($CaCe(CO_3)_2F$), apatite and florencite ($LaAl_3(PO_4)_2(OH)_6$); Schmandt *et al.* 2019). At Vulcan, the most abundant LREE-bearing phase is florencite ($CeAl_3(PO_4)_2(OH)_6$). Florencite may be formed under hydrothermal and metamorphic conditions and has been related to the dissolution of apatite by acidic fluids (Stoffregen and Alpers 1987, Nazari-Dehkordi and Spandler 2019). The reason for the lack of other REE-bearing phases at Vulcan may be related to the fluid present was depleted in CO_2 and F, which impeded the growth of flurocarbonate minerals such as bastnäsite. At Olympic Dam, granite-derived fluids were the likely source of REE and F, and mafic to ultramafic rocks may have also been the source of CO_2 (Schmandt *et al.* 2017). The source of the hydrothermal fluids and REE at Vulcan is unknown, but the absence of flurocarbonates and presence of florencite at Vulcan can add constraints to the chemistry of the fluid associated with hydrothermal alteration and environment at Vulcan. The decrease in U+Th and REY from early magnetite-associated apatite to younger hematite-associated apatite suggests that the hydrothermal environment has a strong influence over the partitioning of trace elements in apatite (e.g. Krneta *et al.* 2017a). A change to acidic fluid conditions in the younger hydrothermal events at Vulcan may be the cause of redistribution of elements from apatite into florencite. The low pH hydrothermal fluids were potentially also rich in Cl, which facilitated the formation of REE-chloride complexes able to be transported under acidic conditions (Harlov *et al.* 2002, Migdisov and Williams-Jones 2014).

Verdugo-Ihl *et al.* (2019) showed differences in magnetite and hematite chemistry closer to the mineralisation shell in the Olympic Dam deposit. These differences highlighted transition in magnetite and hematite geochemistry throughout the deposit, attributed to the evolution of fluid chemistry. Magnetite and hematite at Vulcan show a transition in chemistry (Figs. 8–11), however the limited dataset makes correlations or changes between magnetite and hematite chemistry difficult to attribute to evolution of fluid chemistry. Magnetite and hematite both show similar chemical attributes to those observed at Olympic Dam, although trace and rare earth elements in magnetite at Vulcan are generally lower than Olympic Dam, and hematite trace and rare earth element concentrations are at the lower end of abundances at Olympic Dam (Verdugo-Ihl *et al.* 2019). The similar attributes in Fe-oxide chemistry between OD and Vulcan are encouraging, but, the true relationship of the similar geochemical attributes of Fe-oxides at Olympic Dam and Vulcan requires complete characterisation of Fe-oxide phases at Vulcan. This will help assess any compositional changes in magnetite and hematite across and throughout the Vulcan Prospect, and how this may relate to changes in the hydrothermal system such as those observed at Olympic Dam.

The apparent spatial segregation of the different apatite generations, as well as different mineral assemblages associated with them, suggests localised hydrothermal activity was more prevalent in the central parts of the prospect where hematite-rich assemblages are more common. However, it should be noted that the footprint of hydrothermal activity might be larger than what has been identified by the limited sample set in this study. Further work is required to quantify the association of LREE depleted apatite with hematite assemblages. As observed by Krneta *et al.* (2017b), lower concentrations of LREE and HREE and Y occur when hematite is the primary phase.

Redox state

As discussed by Cao *et al.* (2012), Eu and Ce anomalies in apatite may be used to infer the redox state of the magma. The crystal struc-

ture of apatite shows a strong preference for Eu^{3+} over Eu^{2+} and Ce^{3+} over Ce^{4+}. The Eu^{2+}/Eu^{3+} ratio is critical in controlling the Eu abundance and degree of Eu depletion in apatite. Low oxygen fugacity results in high Eu^{2+}/Eu^{3+}, Ce^{3+}/Ce^{4+}, low Eu^{3+} and high Ce^{3+} concentration in melts, resulting in a strong negative Eu and a positive Ce anomaly in apatite crystallised in low oxygen fugacity conditions (Sha and Chappell 1999, Cao *et al.* 2012). In magmatic apatite, Cao *et al.* (2012) showed that Ce enters apatite in the form of Ce^{3+} due to similar ionic radii at Ca^{2+} coordination sites, regardless of the oxygen fugacity. This leads to no distinct differences in the Ce/Ce* but obvious differences in the Eu/Eu*. Although not considered pristine magmatic apatite, the early magnetite-associated apatite at Vulcan has a limited range of Ce/Ce* ratios (0.93–1.2) and a wide range of Eu/Eu* ratios (0.13–0.67), similar to the ranges observed in magmatic-hydrothermal mineral deposit apatite (Fig. 14; Mao *et al.* 2016). Eu/Eu* ratios in magnetite-associated apatite from Vulcan are typically <0.45, which correspond to a moderately reduced oxidation path (Mukherjee *et al.*

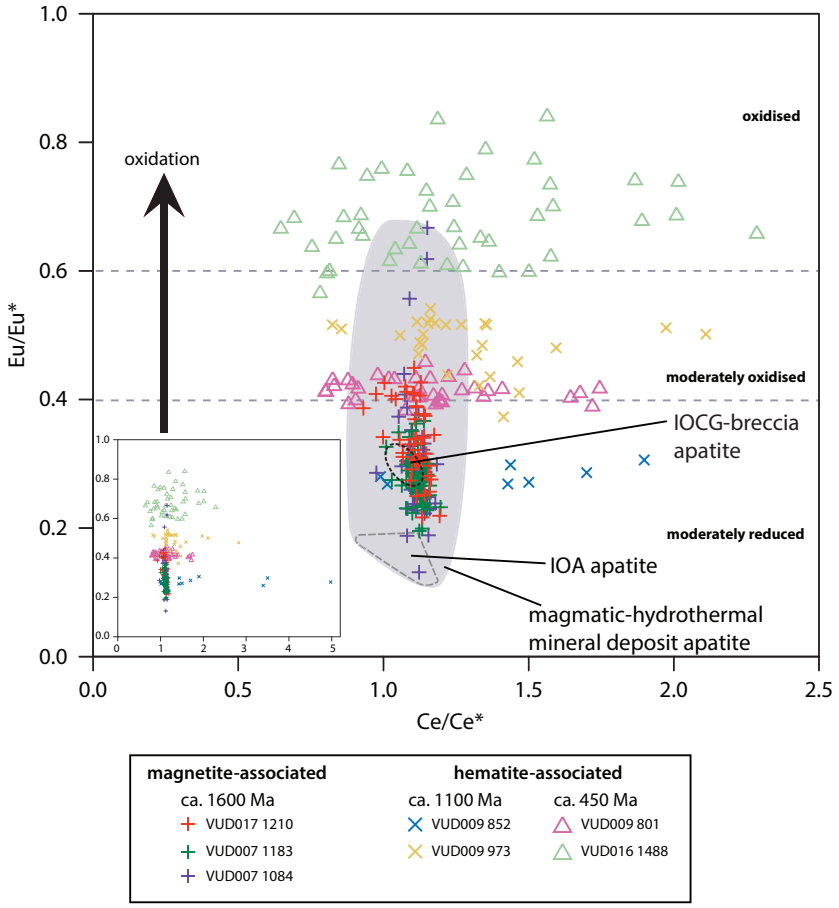

Figure 14: Apatite Eu/Eu* vs apatite Ce/Ce* indicating the increasing oxidising environments associated with hydrothermal apatite, as evidenced by higher Eu/Eu* values. Note the narrow range of Ce/Ce* in ca. 1600 Ma hydrothermal apatite compared with wide range in Ce/Ce* values in ca. 1100 Ma and ca. 450 Ma hydrothermal apatite. Dashed lines represent approximate evolutionary paths in oxidation after Mukherjee *et al*. (2017). Fields for magmatic-hydrothermal mineral deposit apatite, IOCG-breccia apatite and IOA apatite is from Mao *et al*. (2016). Magmatic-hydrothermal mineral deposit apatite includes IOCG, IOCG-breccia, Kiruna-type, alkalic porphyry Cu-Au, porphyry Cu-Au and porphyry replaced Cu-Au breccia compiled from Mao *et al*. (2016).

2017) and overlap with Eu/Eu* and Ce/Ce* in IOCG breccia apatite (Mao *et al.* 2016) and partially overlap with IOA apatite (Fig. 14; Mao *et al.* 2016). The Ce/Ce* ratios of younger hematite-associated apatite from Vulcan are similar in range regardless of the apparent age of the apatite (Ce/Ce* value in 1100 Ma apatite = 0.83–4.97 and Ce/Ce* value in 450 Ma apatite = 0.65–2.29). The total range in Eu/Eu* values in hematite-associated apatite are 0.26–0.84, which are comparable to the range in magnetite-associated apatite (Fig. 14), although the majority of the hematite-associated apatite values are >0.37. Eu/Eu* values show inter-sample variation where restricted Eu/Eu* values are observed in individual hematite-associated apatite samples (Eu/Eu* values in VUD009 852 = 0.26–0.31; VUD009 973 = 0.37–0.54; VUD009 801 = 0.38–0.46 and; VUD009 1488 = 0.56–0.84). Consistently higher Eu/Eu* values in the hematite-associated apatite correspond to moderately to strongly oxidised conditions (Mukherjee *et al.* 2017), and the dominance of hematite in these samples supports an environment that was oxidised. The presence of barite in the ca. 1100 Ma hematite-associated apatite is also suggestive of a more oxidised and/or low pH environment (Nazari-Dehkordi and Spandler 2019). In a hydrothermal environment, the influence of oxygen fugacity, bulk rock compositions and temperature on the Eu and Ce anomaly in apatite is less widely reported. Variance in Ce/Ce* values of 1100 Ma and 450 Ma hydrothermal apatite from Vulcan relative to magmatic apatite in IOCG and IOA deposits show that Ce partitioning into apatite in hydrothermal fluid conditions is somewhat different than in magmatic conditions.

CONCLUSIONS

The Vulcan Prospect is a hematite-dominated IOCG deposit hosted in ca. 1750 Ma granitoid rock. The prospect is comprised of magnetite- and hematite-rich breccias. Magnetite breccias are comprised of magnetite, albite, chlorite, apatite, dolomite, hematite, quartz and minor pyrite and chalcopyrite in a dolomite-chlorite-rich matrix. Hematite-rich breccias comprise massive hematite overprinting magnetite, hematite clasts associated with quartz and albite and bladed hematite, apatite, barite, quartz, florencite, pyrite and chalcopyrite. Hematite is present as pseudomorphs after magnetite, as replacement of eudhedral or blebby magnetite. Pyrite and chalcopyrite occur as inclusions in magnetite and are intergrown with hematite. Apatite is particularly abundant in the Vulcan Prospect and is associated with both magnetite-rich and hematite-rich breccias. U-Pb apatite dating indicates at least three generations of apatite are present within the Vulcan Prospect, at ca. 1600 Ma, ca. 1100 Ma and ca. 450 Ma. Each apatite phase has distinct chemical characteristics that display a transition from magnetite-associated to hematite-associated hydrothermal apatite. The oldest recorded apatite at Vulcan is ca. 1600 and has a REY profile characterised by LREE enrichment patterns, high Y/Y* values and low Eu/Eu* values. LREE become increasingly depleted with apparent decreasing age. The lower abundance of LREE in 1100 Ma and 450 Ma hematite-associated apatite can be attributed to the breakdown of apatite in acidic hydrothermal conditions where new growth of florencite incorporated the LREE. There is scope to further investigate the full extent of iron-oxide and accessory mineral compositions with detailed SEM work and additional U-Pb geochronology across the Vulcan Prospect. These will further refine the timing of events suggested by apatite geochronology and provide insight into the evolution of fluid chemistry at the Vulcan Prospect.

ACKNOWLEDGEMENTS

This study was financially supported by Australian Research Council Linkage Project LP160100578, with the support of the Geological Survey of South Australia and Fortescue Metals Group. Martin Hand, University

of Adelaide, is thanked for input into project generation, assistance with petrography and providing constructive discussion and ideas about the study. Ben Wade, Adelaide Microscopy, is thanked for assistance with analytical analysis and data processing. CW and AR publish with permission of the Director, Geological Survey of South Australia, Department for Energy and Mining, South Australia.

REFERENCES

Ahmed, A. D., Hood, S. B., Gazley, M. F., Cooke, D. R. and Orovan, E. A., 2019. Interpreting element addition and depletion at the Ann Mason porphyry-Cu deposit, Nevada, using mapped mass balance patterns. Journal of Geochemical Exploration, v. 196, p. 81-94. doi: https://doi.org/10.1016/j.gexplo.2018.09.009

Allen, S. R. and McPhie, J., 2002. The Eucarro Rhyolite, Gawler Range Volcanics, South Australia; a >675 km^3 compositionally zoned lava of Mesoproterozoic age. Geological Society of America Bulletin, v. 114, p. 1592-1609. doi: https://doi.org/10.1130/0016-7606(2002)114<1592:TERGRV>2.0.CO;2

Allen, S. R., McPhie, J., Ferris, G. and Cadd, A. G., 2008. Evolution and architecture of a large felsic igneous province in western Laurentia: The 1.6 Ga Gawler Range Volcanics, South Australia. Journal of Volcanology and Geothermal Research, v. 172, p. 132-147. doi: https://doi.org/10.1016/j.jvolgeores.2005.09.027

Allen, S. R., Simpson, C. J., McPhie, J. and Daly, S. J., 2003. Stratigraphy, distribution and geochemistry of widespread felsic volcanic units in the Mesoproterozoic Gawler Range Volcanics, South Australia. Australian Journal of Earth Sciences, v. 50, p. 97-112. doi: http://dx.doi.org/10.1046/j.1440-0952.2003.00980.x

Apukhtina, O. B., 2016. Distribution, petrology, geochemistry and geochronology of carbonate assemblages at the Olympic Dam deposit University of Tasmania, PhD thesis (unpublished).

Apukhtina, O. B., Kamenetsky, V. S., Ehrig, K., Kamenetsky, M. B., Maas, R., Thompson, J., McPhie, J., Ciobanu, C. L. and Cook, N. J., 2017. Early, deep magnetite-fluorapatite mineralization at the Olympic Dam Cu-U-Au-Ag deposit, South Australia. Economic Geology, v. 112, p. 1531-1542. doi: https://doi.org/10.5382/econgeo.2017.4520

Betts, P. G. and Giles, D., 2006. The 1800-1100 Ma tectonic evolution of Australia. Precambrian Research, v. 144, p. 92-125. doi: https://doi.org/10.1016/j.precamres.2005.11.006

Blissett, A. H., Creaser, R. A., Daly, S., Flint, D. J. and Parker, A. J., 1993. Gawler Range Volcanics. In: Drexel, J. F., Preiss, W. V. and Parker, A. J. (Eds), The geology of South Australia. Volume 1. The Precambrian. Geological Survey of South Australia, v. Bulletin 54, p. 107-131. Available at: https://sarigbasis.pir.sa.gov.au/WebtopEw/ws/samref/sarig1/image/DDD/BULL054(V1).pdf

Cao, M., Li, G., Qin, K., Seimuratova, E. Y. and Liu, Y., 2012. Major and trace element characteristics of apatites in granitoids from central Kazakhstan: Implications for petrogenesis and mineralization. Resource Geology, v. 62, p. 63-83. doi: https://doi.org/10.1111/j.1751-3928.2011.00180.x

Cherry, A. R., Ehrig, K., Kamenetsky, V. S., McPhie, J., Crowley, J. L. and Kamenetsky, M. B., 2018a. Precise geochronological constraints on the origin, setting and incorporation of ca. 1.59 Ga surficial facies into the Olympic Dam Breccia Complex, South Australia. Precambrian Research, v. 315, p. 162-

178. doi: https://doi.org/10.1016/j.precamres.2018.07.012

Cherry, A. R., Kamenetsky, V. S., McPhie, J., Thompson, J. M., Ehrig, K., Meffre, S., Kamenetsky, M. B. and Krneta, S., 2018b. Tectonothermal events in the Olympic IOCG Province constrained by apatite and REE-phosphate geochronology. Australian Journal of Earth Sciences, v. 65, p. 643-659. doi: https://doi.org/10.1080/08120099.2018.1465473

Cherry, A. R., McPhie, J., Kamenetsky, V. S., Ehrig, K., Keeling, J. L., Kamenetsky, M. B., Meffre, S. and Apukhtina, O. B., 2017. Linking Olympic Dam and the Cariewerloo Basin: Was a sedimentary basin involved in formation of the world's largest uranium deposit? Precambrian Research, v. 300, p. 168-180. doi: https://doi.org/10.1016/j.precamres.2017.08.002

Chew, D. M., Petrus, J. A. and Kamber, B. S., 2014. U–Pb LA–ICPMS dating using accessory mineral standards with variable common Pb. Chemical Geology, v. 363, p. 185-199. doi: https://doi.org/10.1016/j.chemgeo.2013.11.006

Ciobanu, C. L., Wade, B. P., Cook, N. J., Schmidt Mumm, A. and Giles, D., 2013. Uranium-bearing hematite from the Olympic Dam Cu–U–Au deposit, South Australia: A geochemical tracer and reconnaissance Pb–Pb geochronometer. Precambrian Research, v. 238, p. 129-147. doi: https://doi.org/10.1016/j.precamres.2013.10.007

Cochrane, R., Spikings, R. A., Chew, D., Wotzlaw, J. F., Chiaradia, M., Tyrrell, S., Schaltegger, U. and Van der Lelij, R., 2014. High temperature (>350°C) thermochronology and mechanisms of Pb loss in apatite. Geochimica et Cosmochimica Acta, v. 127, p. 39-56. doi: https://doi.org/10.1016/j.gca.2013.11.028

Cook, N., Ciobanu, C. L., George, L., Zhu, Z.-Y., Wade, B. and Ehrig, K., 2016. Trace Element Analysis of Minerals in Magmatic-Hydrothermal Ores by Laser Ablation Inductively-Coupled Plasma Mass Spectrometry: Approaches and Opportunities. Minerals v. 6, p. 111. doi: https://doi.org/10.3390/min6040111

Cooke, D. R., Baker, M., Hollings, P., Sweet, G., Chang, Z., Danyushevsky, L., Gilbert, S., Zhou, T., White, N. C., Gemmell, J. B., Inglis, S., Kelley, K. D. and Golden, H. C., 2014. New Advances in Detecting the Distal Geochemical Footprints of Porphyry Systems—Epidote Mineral Chemistry as a Tool for Vectoring and Fertility Assessments. In: (Eds), Building Exploration Capability for the 21st Century. Society of Economic Geologists, v. 18, p. 0. https://doi.org/10.5382/sp.18.07

Corriveau, L., Montreuil, J.-F. and Potter, E. G., 2016. Alteration Facies Linkages Among Iron Oxide Copper-Gold, Iron Oxide-Apatite, and Affiliated Deposits in the Great Bear Magmatic Zone, Northwest Territories, Canada. Economic Geology, v. 111, p. 2045-2072. doi: https://doi.org/10.2113/econgeo.111.8.2045

Courtney-Davies, L., Ciobanu C.L., Verdugo-Ihl M.R., Slattery A., Cook N.J., Dmitrijeva M., Keyser W., Wade B.P., Domnick U.I., Ehrig K., Xu J. and Kontonikas-Charos, A., 2019a. Zircon at the Nanoscale Records Metasomatic Processes Leading to Large Magmatic–Hydrothermal Ore Systems. Minerals, v. 9, p. 364. doi: https://doi.org/10.3390/min9060364

Courtney-Davies, L., Ciobanu, C. L., Tapster, S. R., Cook, N. J., Ehrig, K., Crowley, J. L., Verdugo-Ihl, M. R., Wade, B. P. and Condon, D. J., 2020. Opening the magmatic-hydrothermal window:

High-precision U-Pb geochronology of the Mesoproterozoic Olympic Dam Cu-U-Au-Ag deposit, South Australia. Economic Geology, v. p. doi: https://doi.org/10.5382/econgeo.4772

Courtney-Davies, L., Tapster, S. R., Ciobanu, C. L., Cook, N. J., Verdugo-Ihl, M. R., Ehrig, K. J., Kennedy, A. K., Gilbert, S. E., Condon, D. J. and Wade, B. P., 2019b. A multi-technique evaluation of hydrothermal hematite UPb isotope systematics: Implications for ore deposit geochronology. Chemical Geology, v. 513, p. 54-72. doi: https://doi.org/10.1016/j.chemgeo.2019.03.005

Cross, K. C., Daly, S. J. and Flint, R. B., 1993. Mineralisation associated with the Gawler Range Volcanics and Hiltaba Suite Granitoids. Olympic Dam Deposit. In: Drexel, J. F., Preiss, W. V. and Parker, A. J. (Eds), The geology of South Australia; Volume 1, The Precambrian. Geological Survey of South Australia, v. Bulletin 54, p. Available at: https://sarigbasis.pir.sa.gov.au/WebtopEw/ws/samref/sarig1/image/DDD/BULL054(V1).pdf

Diemar, G., 2014. The petrology of hydrothermal REE bearing minerals in the Olympic Dam IOCG deposit support a 1.3 Ga formation University of Tasmania, MSc thesis (unpublished).

Dutch, R. A., Wise, T. W., Pawley, M. J. and Petts, A. E., 2018. Coompana Drilling and Geochemistry Workshop, 2018. Extended abstracts. Government of South Australia. Department of the Premier and Cabinet, v. Report Book, 2018/00019, p. 171. Available at: https://sarigbasis.pir.sa.gov.au/WebtopEw/ws/samref/sarig1/image/DDD/RB201800019.pdf

Ehrig, K., McMillan, E., Kamenetsky, V. S., Kamenetsky, M., McPhie, J., Thompson, J., Ciobanu, C., Cook, N. and Maas, R., 2018. Uraninite age dating: multiple stages of uranium precipitation at Olympic Dam. AusIMM International Uranium Conference 2018, Adelaide. v. p. doi:

Elburg, M. A., Andersen, T., Bons, P. D., Simonsen, S. L. and Weisheit, A., 2013. New constraints on Phanerozoic magmatic and hydrothermal events in the Mt Painter Province, South Australia. Gondwana Research, v. 24, p. 700-712. doi: https://doi.org/10.1016/j.gr.2012.12.017

Flint, R. B., 1993. Hiltaba Suite. In: Drexel, J. F., Preiss, W. V. and Parker, A. J. (Eds), The geology of South Australia. Volume 1. The Precambrian. Geological Survey of South Australia, v. Bulletin 54, p. 127-131. Available at: https://sarigbasis.pir.sa.gov.au/WebtopEw/ws/samref/sarig1/image/DDD/BULL054(V1).pdf

Foden, J., Elburg, M. A., Dougherty-Page, J. and Burtt, A., 2006. The timing and duration of the Delamerian Orogeny: correlation with the Ross Orogen and implications for Gondwana assembly. The Journal of Geology, v. 114, p. 189-210. doi: https://doi.org/10.1086/499570

Giggenbach, W. F., 1997. The origin and evolution of fluids in magmatic-hydrothermal systems. In: Barnes, H. L. (Eds), Geochemistry of hydrothermal ore deposits. John Wiley & Sons, v. 3rd edition, p. 737–796.

Glikson, A. Y., Ballhaus, C. G., Clarke, G. L., Sheraton, J. W., Stewart, A. J. and Sun, S. S., 1995. Geological framework and crustal evolution of the Giles mafic-ultramafic complex and environs, western Musgrave Block, central Australia. AGSO Journal of Australian Geology and Geophysics, v. 16, p. 41-67. doi:

Groves, D. I., Bierlein, F. P., Meinert, L. D. and Hitzman, M. W., 2010. Iron Oxide Copper-Gold (IOCG) Deposits

through Earth History: Implications for Origin, Lithospheric Setting, and Distinction from Other Epigenetic Iron Oxide Deposits. Economic Geology, v. 105, p. 641-654. doi: https://doi.org/10.2113/gsecongeo.105.3.641

Harlov, D. E., Andersson, U. B., Förster, H.-J., Nyström, J. O., Dulski, P. and Broman, C., 2002. Apatite–monazite relations in the Kiirunavaara magnetite–apatite ore, northern Sweden. Chemical Geology, v. 191, p. 47-72. doi: https://doi.org/10.1016/S0009-2541(02)00148-1

Haynes, D. W., Cross, K. C., Bills, R. T. and Reed, M. H., 1995. Olympic Dam ore genesis; a fluid-mixing model. Economic Geology, v. 90, p. 281-307. doi: https://doi.org/10.2113/gsecongeo.90.2.281

Heinrich, C. A., 2007. Fluid-Fluid Interactions in Magmatic-Hydrothermal Ore Formation. Reviews in Mineralogy and Geochemistry, v. 65, p. 363-387. doi: https://doi.org/10.2138/rmg.2007.65.11

Hore, S. B., Hill, S. M., Reid, A., Wade, B., Alley, N. F. and Mason, D. R., 2020. U–Pb geochronology reveals evidence of a Late Devonian hydrothermal event, and protracted hydrothermal–epithermal system, within the Mount Painter Inlier, northern Flinders Ranges, South Australia. Australian Journal of Earth Sciences, v. 67, p. 1009-1044. doi: https://doi.org/10.1080/08120099.2020.1793383

Huang, Q., Kamenetsky, V. S., McPhie, J., Ehrig, K., Meffre, S., Maas, R., Thompson, J., Kamenetsky, M., Chambefort, I., Apukhtina, O. and Hu, Y., 2015. Neoproterozoic (ca. 820–830Ma) mafic dykes at Olympic Dam, South Australia: Links with the Gairdner Large Igneous Province. Precambrian Research, v. 271, p. 160-172. doi: https://doi.org/10.1016/j.precamres.2015.10.001

Jagodzinski, E. A., 2014. The age of magmatic and hydrothermal zircon at Olympic Dam. Australian Earth Sciences Convention (AESC), Newcastle. Geological Society of Australia, v. Abstracts, 260, p. doi: https://www.researchgate.net/publication/271387404_The_age_of_magmatic_and_hydrothermal_zircon_at_Olympic_Dam

Jagodzinski, E. A., Reid, A., Crowley, J., McAvaney, S. and Wade, C., 2016. Precise zircon U–Pb dating of a Mesoproterozoic silicic large igneous province: The Gawler Range Volcanics and Benagerie Volcanic Suite, South Australia. Hornsby, NSW: Geological Society of Australia. Geological Society of Australia Abstracts, v. No. 118, p. doi: https://sarigbasis.pir.sa.gov.au/WebtopEw/ws/samref/sarig1/image/DDD/RB201600032.pdf

Johnson, J. P., 1993. The geochronology and radiogenic isotope systematics of the Olympic Dam copper-uranium-gold-silver deposit, South Australia. Australian National University, PhD thesis (unpublished).

Johnson, J. P. and McCulloch, M. T., 1995. Sources of mineralising fluids for the Olympic Dam Deposit (South Australia); Sm-Nd isotopic constraints. Chemical Geology, v. 121, p. 177-199. doi: https://doi.org/10.1016/0009-2541(94)00125-R

Kamenetsky, V. S., Ehrig, K., Maas, R., Meffre, S., Kamenetsky, M., McPhie, J., Apukhtina, O., Huang, Q., Thompson, J., Ciobanu, C. L. and Cook, N. J., 2015. The supergiant Olympic Dam Cu–U–Au–Ag ore deposit: toward a new genetic model. Society of Economic Geologists, SEG 2015: World Class Ore Deposits: Discovery to Recovery, Hobart, Tasmania, Australia, v. 09/2015, p. doi:

Kirchenbaur, M., Maas, R., Ehrig, K., Kamenetsky, V. S., Strub, E., Ballhaus, C. and Münker, C., 2016. Uranium and Sm isotope studies of the supergiant Olympic Dam Cu–Au–U–Ag deposit, South Australia. Geochimica et Cosmochimica Acta, v. 180, p. 15-32. doi: https://doi.org/10.1016/j.gca.2016.01.035

Kirkland, C. L., Smithies, R. H., Woodhouse, A. J., Howard, H. M., Wingate, M. T. D., Belousova, E. A., Cliff, J. B., Murphy, R. C. and Spaggiari, C. V., 2013. Constraints and deception in the isotopic record; the crustal evolution of the west Musgrave Province, central Australia. Gondwana Research, v. 23, p. 759-781. doi: https://doi.org/10.1016/j.gr.2012.06.001

Kirkland, C. L., Yakymchuk, C., Szilas, K., Evans, N., Hollis, J., McDonald, B. and Gardiner, N. J., 2018. Apatite: a U-Pb thermochronometer or geochronometer? Lithos v. 318–319, p. 143–157. doi: https://doi.org/10.1016/j.lithos.2018.08.007

Krneta, S., Ciobanu, C. L., Cook, N. J., Ehrig, K. and Kontonikas-Charos, A., 2017a. Rare Earth Element Behaviour in Apatite from the Olympic Dam Cu–U–Au–Ag Deposit, South Australia. Minerals v. 7, p. 135. doi: https://doi.org/10.3390/min7080135

Krneta, S., Cook, N. J., Ciobanu, C. L., Ehrig, K. and Kontonikas-Charos, A., 2017b. The Wirrda Well and Acropolis prospects, Gawler Craton, South Australia: Insights into evolving fluid conditions through apatite chemistry. Journal of Geochemical Exploration, v. 181, p. 276-291. doi: https://doi.org/10.1016/j.gexplo.2017.08.004

Lowell, J. D. and Guilbert, J. M., 1970. Lateral and vertical alteration-mineralization zoning in porphyry ore deposits. Economic Geology, v. 65, p. 373-408. doi: https://doi.org/10.2113/gsecongeo.65.4.373

Lu, J., Plimer, I. R., Foster, D. A. and Lottermoser, B. G., 1996. Multiple Post-Orogenic Reactivation in the Olary Block, South Australia: Evidence from 40Ar/39Ar Dating of Pegmatitic Muscovite. International Geology Review, v. 38, p. 665-685. doi: https://doi/org/10.1080/00206819709465352

Maas, R., Apukhtina, O. B., Kamenetsky, V. S., Ehrig, K., Sprung, P. and Münker, C., 2020. Carbonates at the supergiant Olympic Dam Cu-U-Au-Ag deposit, South Australia part 2: Sm-Nd, Lu-Hf and Sr-Pb isotope constraints on the chronology of carbonate deposition. Ore Geology Reviews, v. p. 103745. doi: https://doi.org/10.1016/j.oregeorev.2020.103745

Maas, R., Kamenetsky, V., Ehrig, K., Meffre, S., McPhie, J. and Diemar, G., 2011. Olympic Dam U-Cu–Au deposit, Australia: new age constraints. Mineralogical Magazine, v. 75, p. 1375. doi:

Mao, M., Rukhlov, A. S., Rowins, S. M., Spence, J. and Coogan, L. A., 2016. Apatite Trace Element Compositions: A Robust New Tool for Mineral Exploration*. Economic Geology, v. 111, p. 1187-1222. doi: https://doi.org/10.2113/econgeo.111.5.1187

McInnes, B. I. A., Keays, R. R., Lambert, D. D., Hellstrom, J. and Allwood, J. S., 2008. Re–Os geochronology and isotope systematics of the Tanami, Tennant Creek and Olympic Dam Cu–Au deposits. Australian Journal of Earth Sciences, v. 55, p. 967-981. doi: https://doi.org/10.1080/08120090802097443

McPhie, J., Ehrig, K. J., Kamenetsky, M. B., Crowley, J. L. and Kamenetsky, V. S., 2020. Geology of the Acropolis prospect, South Australia, constrained by high-precision CA-TIMS ages. Australian Journal of Earth Sciences, v. 67,

p. 699-716. doi: https://doi.org/10.1080/08120099.2020.1717617

Meffre, S., Ehrig, K., Kamenetsky, V., Chambefort, I., Maas, R. and McPhie, J., 2010. Pb isotopes at Olympic Dam: constraining sulphide growth. In: 13th Quadrennial IAGOD Symposium, Giant Ore Deposits Down-Under, Adelaide, South Australia. PIRSA, v. p. 78–79. doi:

Migdisov, A. A. and Williams-Jones, A. E., 2014. Hydrothermal transport and deposition of the rare earth elements by fluorine-bearing aqueous liquids. Mineralium Deposita, v. 49, p. 987-997. doi: https://doi.org/10.1007/s00126-014-0554-z

Mukherjee, R., Venkatesh, A. S. and Fareeduddin, 2017. Chemistry of magnetite-apatite from albitite and carbonate-hosted Bhukia Gold Deposit, Rajasthan, western India – An IOCG-IOA analogue from Paleoproterozoic Aravalli Supergroup: Evidence from petrographic, LA-ICP-MS and EPMA studies. Ore Geology Reviews, v. 91, p. 509-529. doi: https://doi.org/10.1016/j.oregeorev.2017.09.005

Nazari-Dehkordi, T. and Spandler, C., 2019. Paragenesis and composition of xenotime-(Y) and florencite-(Ce) from unconformity-related heavy rare earth element mineralization of northern Western Australia. Mineralogy and Petrology, v. 113, p. 563-581. doi: https://doi.org/10.1007/s00710-019-00676-w

Oreskes, N. and Einaudi, M. T., 1992. Origin of hydrothermal fluids at Olympic Dam: preliminary results from fluid inclusions and stable isotopes. Economic Geology, v. 87, p. 64-90. doi: https://doi.org/10.2113/gsecongeo.87.1.64

Pollard, P. J., 2006. An intrusion-related origin for Cu–Au mineralization in iron oxide–copper–gold (IOCG) provinces. Mineralium Deposita, v. 41, p. 179. doi: https://doi.org/10.1007/s00126-006-0054-x

Reed, M. H., 1997. Hydrothermal alteration and its relationship to ore fluid composition. In: Barnes, H. L. (Eds), Geochemistry of hydrothermal ore deposits. John Wiley & Sons Inc., v. 3rd Edition, p. 303-365.

Reeve, J. S., Cross, K. C., Smith, R. N. and Oreskes, N., 1990. Olympic Dam copper-uranium-gold-silver deposit. In: Hughes, F. E. (Eds), Geology of the mineral deposits of Australia and Papua New Guinea. Australasian Institute of Mining and Metallurgy, v. Monograph 14, p. 1009-1035.

Reid, A., 2019. The Olympic Cu-Au Province, Gawler Craton: A Review of the Lithospheric Architecture, Geodynamic Setting, Alteration Systems, Cover Successions and Prospectivity. Minerals, v. 9, p. 371. doi: https://www.mdpi.com/2075-163X/9/6/371

Reid, A., Smith, R. N., Baker, T., Jagodzinski, E. A., Selby, D., Gregory, C. J. and Skirrow, R. G., 2013. Re-Os dating of molybdenite within hematite breccias from the Vulcan Cu-Au prospect, Olympic Cu-Au Province, South Australia. Economic Geology, v. 108, p. 883-894. doi: https://doi.org/10.2113/econgeo.108.4.883

Reid, A. J., Jourdan, F. and Jagodzinski, E. A., 2017. Mesoproterozoic fluid events affecting Archean crust in the northern Olympic Cu–Au Province, Gawler Craton: insights from $^{40}Ar/^{39}Ar$ thermochronology. Australian Journal of Earth Sciences v. 64, p. 103-119. doi: https://doi.org/10.1080/08120099.2017.1263806

Rutherford, L., Hand, M. and Mawby, J., 2006. Delamerian-aged metamorphism in the southern Curnamona Province, Australia: implications for the evolution of the Mesoproterozoic Olarian Orogeny.

Terra Nova, v. 18, p. 138-146. doi:

Schmandt, D. S., Cook, N. J., Ciobanu, C. L., Ehrig, K., Wade, B. P., Gilbert, S. and Kamenetsky, V. S., 2017. Rare Earth Element Fluorocarbonate Minerals from the Olympic Dam Cu-U-Au-Ag Deposit, South Australia. Minerals, v. 7, p. 202. doi: https://doi.org/10.3390/min7100202

Schmandt, D. S., Cook, N. J., Ciobanu, C. L., Ehrig, K., Wade, B. P., Gilbert, S. and Kamenetsky, V. S., 2019. Rare Earth Element Phosphate Minerals from the Olympic Dam Cu-U-Au-Ag Deposit, South Australia: Recognizing Temporal-Spatial Controls On Ree Mineralogy in an Evolved IOCG System. The Canadian Mineralogist, v. 57, p. 3-24. doi: https://doi.org/10.3749/canmin.1800043

Schoene, B. and Bowring, S. A., 2006. U–Pb systematics of the McClure Mountain syenite: thermochronological constraints on the age of the 40 Ar/39 Ar standard MMhb. Contributions to Mineralogy and Petrology, v. 151, p. 615. doi: https://doi.org/10.1007/s00410-006-0077-4

Schoene, B. and Bowring, S. A., 2007. Determining accurate temperature-time paths from U-Pb thermochronology: An example from the Kaapvaal craton, southern Africa. Geochimica et Cosmochimica Acta, v. 71, p. 165-185. doi: https://doi.org/10.1016/j.gca.2006.08.029

Sha, L.-K. and Chappell, B. W., 1999. Apatite chemical composition, determined by electron microprobe and laser-ablation inductively coupled plasma mass spectrometry, as a probe into granite petrogenesis. Geochimica et Cosmochimica Acta, v. 63, p. 3861-3881. doi: https://doi.org/10.1016/S0016-7037(99)00210-0

Skirrow, R. G., Bastrakov, E., Barovich, K., Fraser, G., Fanning, C. M., Creaser, R. and Davidson, G., 2007. Timing of Iron Oxide Cu-Au-(U) Hydrothermal Activity and Nd Isotope Constraints on Metal Sources in the Gawler Craton, South Australia. Economic Geology, v. 102, p. 1441-1470. doi: https://doi.org/10.2113/gsecongeo.102.8.1441

Skirrow, R. G., Bastrakov, E., Davidson, G., Raymond, O. L. and Heithersay, P., 2002. The geological framework, distribution and controls of Fe-oxide and related alteration, and Cu-Au mineralisation in the Gawler Craton, South Australia. Part II: Alteration and mineralisation. In: Porter, T. M. (Eds), Hydrothermal iron oxide copper-gold and related deposits: A global perspective. Porter Geoscience Consultancy Publishing, v. 2, p. 33-47.

Smith, R. N., 2017. Data release - as updated : The Lake Torrens JV Project. Joint annual reports, plus final report at the joint full surrender of two of the three remaining project licences, for the period 1/1/2012 to 9/3/2017. Tasman Resources Limited, Rio Tinto Exploration Pty Ltd, v. Open file Envelope, 11911, p. 212. Available at: https://sarigbasis.pir.sa.gov.au/WebtopEw/ws/samref/sarig1/image/DDD/ENV11911.pdf

Smithies, R. H., Howard, H. M., Evins, P. M., Kirkland, C. L., Kelsey, D. E., Hand, M., Wingate, M. T. D., Collins, A. S. and Belousova, E., 2011. High-Temperature Granite Magmatism, Crust–Mantle Interaction and the Mesoproterozoic Intracontinental Evolution of the Musgrave Province, Central Australia. Journal of Petrology, v. 52, p. 931-958. doi: https://doi.org/10.1093/petrology/egr010

Solomon, G. and Smith, R., 2011. The Vulcan Project The Product of Perseverance, Tasman Resources Ltd. Conference Name. doi: https://www.

tasmanresources.com.au/announcements/872150a06ce837502428e9e023adedef.pdf

Stoffregen, R. E. and Alpers, C. N., 1987. Woodhouseite and svanbergite in hydrothermal ore deposits; products of apatite destruction during advanced argillic alteration. The Canadian Mineralogist, v. 25, p. 201-211. doi:

Thompson, J., Meffre, S., Maas, R., Kamenetsky, V., Kamenetsky, M., Goemann, K., Ehrig, K. and Danyushevsky, L., 2016. Matrix effects in Pb/U measurements during LA-ICP-MS analysis of the mineral apatite. Journal of Analytical Atomic Spectrometry, v. 31, p. 1206-1215. doi: https://doi.org/10.1039/C6JA00048G

Trueman, N., Long, J., Reed, S. and Chinner, G., 1988. . The lead-uranium systematics, and rare earth element distributions of some Olympic Dam and Stuart Shelf mineralisation. v. Rep. K/3143, Western Mining Corp Adelaide, SA, p. Available at:

Verdugo-Ihl, M. R., Ciobanu, C. L., Cook, N. J., Ehrig, K. J. and Courtney-Davies, L., 2019. Defining early stages of IOCG systems: evidence from iron oxides in the outer shell of the Olympic Dam deposit, South Australia. Mineralium Deposita, v. p. doi: https://doi.org//10.1007/s00126-019-00896-2

Wade, C. E., Payne, J. L., Barovich, K. M. and Reid, A. J., 2019. Heterogeneity of the sub-continental lithospheric mantle and 'non-juvenile' mantle additions to a Proterozoic silicic large igneous province. Lithos, v. 340-341, p. 87-107. doi: https://doi.org/10.1016/j.lithos.2019.05.005

Wawryk, C., 1989. Strontium and rare earth element geochemistry of barite-fluorite mineralization at Olympic Dam, South Australia. B. Sc thesis, unpublished, (unpublished).

Webster, J. D. and Piccoli, P. M., 2015. Magmatic apatite: A powerful, yet deceptive, mineral. Elements, v. 11, p. 177-182. doi: https://doi.org/10.2113/gselements.11.3.177

Wilkinson, J. J., Chang, Z., Cooke, D. R., Baker, M. J., Wilkinson, C. C., Inglis, S., Chen, H. and Bruce Gemmell, J., 2015. The chlorite proximitor: A new tool for detecting porphyry ore deposits. Journal of Geochemical Exploration, v. 152, p. 10-26. doi: https://doi.org/10.1016/j.gexplo.2015.01.005

Wingate, M. T. D., Pirajno, F. and Morris, P. A., 2004. Warakurna large igneous province; a new Mesoproterozoic large igneous province in west-central Australia. Geology, v. 32, p. 105-108. doi: https://doi.org/10.1130/G20171.1

Chapter 7

Discussion and Conclusions

DISCUSSION

A metasomatised mantle source region is linked to a number of mineralisation styles globally, including post-subduction porphyry Cu-Au, iron oxide-copper gold (IOCG), iron oxide-apatite (IOA), gold deposits and Cu-Mo (e.g. Richards 2009, Groves *et al.* 2010, Lan *et al.* 2018, Groves *et al.* 2019, Holwell *et al.* 2019, Wang *et al.* 2019). Metasomatised mantle can be represented by a variety of compositions due to the competing or over-printing events of refertilisation due to interaction with melts and/or fluids and varying degrees of partial melt extraction (Ionov *et al.* 2002, Beyer *et al.* 2006, O'Reilly and Griffin 2013, Farmer *et al.* 2020). In subduction-induced mantle metasomatism the mantle wedge is considered to be modified by slab-derived fluids and/or subducted sediment melts and derived fluids (Kelemen *et al.* 1993, Prouteau *et al.* 2001, Cai *et al.* 2013, Cheng *et al.* 2018).

In the absence of samples of mantle material, trace elements of mantle-derived magmas are typically used to indicate the presence of an underlying metasomatised mantle. Incompatible trace elements such as Th, Nb, Ta and La are sensitive to fluid mobilisation during subduction. As Th is more incompatible than Nb and La during arc metasomatism, the mantle metasomatic process results in an increase in Th/Nb and Th/La ratios (Plank 2005, Pearce *et al.* 2017). Identification of high Th/Nb and high Th/La ratios and enrichments in high field strength elements (HFSE) in mafic rocks of the Gawler Range Volcanics (GRV) and Hiltaba Suite (Chapter 2) is a clear indication that the mantle lithosphere beneath the Gawler Craton is variably metasomatised. Metasomatism due to subduction could have occurred throughout the Neoarchean to Mesoproterozoic history of the Gawler Craton with clear evidence for subduction-related magmatism at ca. 2.5 Ga and ca. 1.62 Ga (Swain *et al.* 2005, Swain *et al.* 2008, Symington *et al.* 2014, Reid *et al.* 2019). Nd isotope data from the Hiltaba Suite and GRV indicate that the subduction-induced metasomatism is almost certainly Archean in age as the mafic rocks yield significantly more negative $\varepsilon_{Nd(i)}$ values than the preceding 1.62 Ma subduction event. The enriched signature associated with Archean or early Palaeoproterozoic metasomatism is documented in mafic magmatic rocks throughout the late Archean, Palaeoproterozoic and Mesoproterozoic, as evidenced by consistently Archean Nd model ages (2.2–2.6 Ga; Wade 2012), further supporting that a long-lived metasomatised SCLM exists beneath the Gawler Craton (Chapter 2; Wade *et al.* 2019).

Mantle metasomatism has been identified as a fundamental process in metal endowment in the Gawler Craton (Groves *et al.* 2010, Skirrow *et al.* 2018). Skirrow *et al.* (2018) correlated an Archean-Palaeoproterozoic metasomatised SCLM with the distribution of Cu-Au mineral despots in the Gawler Craton (Figure 1). Wade *et al.* (2019; Chapter 2) demonstrated that the presence of a metasomatised SCLM is linked to enriched geochemical signatures of mafic intrusive and extrusive rocks. An important difference between the mafic extrusive and intrusive rocks is that the latter record source diversity, a heterogeneous and enriched SCLM and a plume source, while the basaltic rocks have geochemical signatures consistent with a heterogeneous and enriched SCLM source. Chapter 4 demonstrates the basaltic rocks derived from the partial melting of a metasomatised SCLM were parent magmas to the felsic magmas of the GRV.

Recent models for the formation of the GRV and Hiltaba Suite have involved a complex history of subduction, slab-roll back and delamination (Skirrow *et al.* 2018, Tiddy and Giles 2020). Tiddy and Giles (2020) liken the GRV-Hiltaba Suite magmatism to the Phanerozoic Sierra Madre Occidental silicic large igneous province (SLIP). The work within this thesis demonstrates that the GRV-Hiltaba

Suite share more features with mafic LIPs accompanied by silicic volcanism than SLIPs sensu stricto. The traditional SLIP model includes formation in active margin or continental-rift related settings, where low magmatic temperatures (734–771 °C) are attributed to

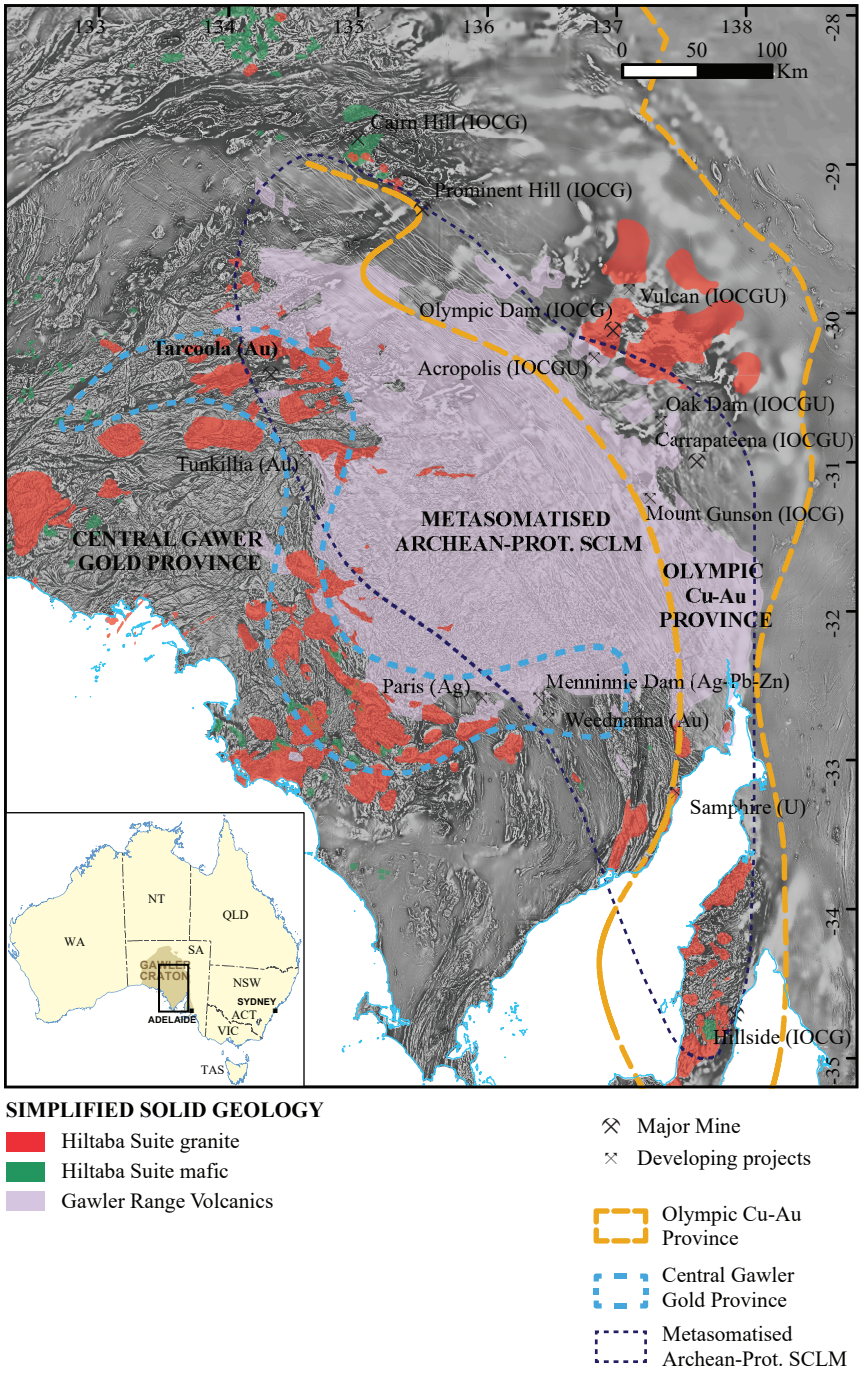

Figure 1: Simplified solid geology map of the Gawler Craton, highlighting the distribution of the ca. 1590 Ma magmatic rocks, the Gawler Range Volcanics and the Hiltaba Suite in relation to the two mineral provinces of the Gawler Craton, the IOCG Province and the Central Gawler Gold Province, overlain on total magnetic imagery (TMI). Also shown is the metasomatised Archean to Proterozoic subcontinental lithospheric mantle (SCLM) as identified by Skirrow et al. (2018) and mines and developing projects are indicated. Source for TMI: https://map.sarig.sa.gov.au/.

the melting of hydrous lower crust (Bryan 2007, Pankhurst *et al.* 2011b, Cheng *et al.* 2020). Magmas associated with SLIPs are intermediate, calc-alkaline and high-K, typical of magmatic arc settings. The volcanism is long-lived (20–50 Myr) and SLIPs typically formed in the Phanerozoic. These features are not observed in the GRV and Hiltaba Suite magmas.

Chapter 4 ascertains the petrogenesis of the Gawler LIP can be attributed to upwelling and underplating of hot mantle by a mantle plume. This model is analogous to an intraplate mafic LIP in a plume setting with voluminous silicic magmatism (e.g. Emeishan LIP, SW China; Tarim LIP, NW China; Keweenawan LIP, Canada; Yemen-Ethiopia LIP Nicholson and Shirey 1990, Ayalew and Gibson 2009, Hei *et al.* 2018, Liu *et al.* 2019). Similar to intraplate mafic LIPs, the GRV and Hiltaba Suite magmas were emplaced on/in Archean-Palaeoproterozoic crust. Melting of thick, old, refractory crust requires high and sustained thermal input to generate large volumes of silicic lavas in a short period of time. Ti-in-zircon thermometry indicate the temperatures in the felsic GRV magmas were high (802-925 °C) and correlate well with previous temperature estimates for the GRV (900–1100 °C; Creaser and White 1991, Pankhurst *et al.* 2011b), and other silicic magmas in LIPs (Pankhurst *et al.* 2011a, Cheng *et al.* 2020). Progressive changes from early high magmatic temperatures to lower magmatic temperatures in the younger silicic units are consistent with plume-LIP models, such as Chon Aike, Tarim LIP and Snake River Plain-Yellowstone Plateau volcanic province (Liu *et al.* 2019). Large-scale crustal melting is made possible by the high temperatures associated with the mantle plumes.

The felsic GRV and Hiltaba Suite rocks display enrichments in HFSE such as Zr, Nb, Th and Y, rare earth elements (REE), and halogens such as F and Cl (Creaser *et al.* 1991, Agangi *et al.* 2010, Pankhurst *et al.* 2011a, Pankhurst *et al.* 2011b). The enriched HFSE and REE compositions of the GRV and Hiltaba Suite rocks are inherited from a heterogeneous and enriched SCLM and partial melting of an ancient refractory crust. High field strength element and REE enrichment may be further enhanced by high F contents, as F will increase the solubility of zirconium and other HFSE (Keppler 1993). Positive correlations between F and HFSE may also be linked to differentiation processes (Keppler 1993). The F-HFSE correlation in the GRV and Hiltaba Suite rocks may be related to differentiation processes of magma or batches of magma derived from their common source region from within the heterogeneous and enriched SCLM.

Constraints on the timing of magmatism associated with the GRV rocks has provided insight into the relative contributions of SCLM and crust during this volcanic event. Lower GRV magmas (ca. 1594–1588 Ma) show an association with a SCLM source region, with only minimal crustal input in the felsic magmas (Chapter 4; Chapman *et al.* 2019). Basaltic rocks in the lower GRV track the transition of mantle compositions from N-MORB-like SCLM to E-MORB-like SCLM compositions throughout their evolution. In contrast, Upper GRV magmas (ca. 1586 Ma) display a strong affinity to crustal sources, with substantially more crustal contributions than the earlier magmas (Chapter 4; Chapman *et al.* 2019). Crustal contributions to the intrusive magmas are also variable, largely governed by the heterogeneous nature of the underlying mantle lithospheric components. The felsic Hiltaba Suite and mafic Hiltaba Suite rocks share many geochemical attributes that include enrichment in HFSE and REE (Chapter 3). Across the entire geographic region, the Nd isotopic compositions of the mafic and felsic intrusive rocks display a similar range, despite a large variation in SiO_2, suggesting a similar source region is shared among the intrusive rocks. In

detail, at individual locations, the $\varepsilon_{Nd(i)}$ values of the felsic rocks are generally lower than the mafic rocks. The mantle compositions in the west to central and the east of the Gawler Craton are isotopically distinct. In general, isotopically more juvenile mantle resides beneath the western and central Gawler Craton, and has been likened to E-MORB or OIB-like sources (Chapter 2; Wade *et al.* 2019). The mantle in the eastern Gawler Craton is isotopically more evolved, and reflects an enriched and heterogeneous SCLM composition (Chapter 2; Wade *et al.* 2019). The age, type and the isotopic composition of the crust also differs across the entire terrain, although broadly similar crustal components that are 2570–1700 Ma extend across much of the Gawler Craton. Nd isotopic mixing calculations demonstrate the felsic magmas of the Hiltaba Suite can be derived from basaltic magmas derived from the two mantle components mixing with the various crustal components in the Gawler Craton (Chapter 3 Figure 10). Similar inputs of crustal material, up to ~40%, are estimated across the Gawler Craton, however the effect on the isotopic composition is greater in the western Gawler Craton where the mantle is more juvenile, causing a greater shift in the $\varepsilon_{Nd(i)}$ values (Chapter 3 Figure 10). For instances where ~30–40% assimilated crust is estimated the resulting $\varepsilon_{Nd(i)}$ values in the granites are similar across the province ($\varepsilon_{Nd(i)}$ value $\approx$ -4.5 to -3.4), regardless of the starting mantle composition. In both instances, the granites are "mantle-derived" and have similar percentages of crustal additions (Chapter 3 Figure 10), but the relative amounts of crust overwhelm the mantle isotopic signature in the granites, giving the appearance of crustally-derived rocks where the mantle is juvenile. Substantial crustal assimilation is observed in two instances where 81–86% crust is estimated, suggesting greater amounts of crustal melting occurred in these localities. Large-scale plume-driven underplating at the base of the crust can provide a mechanism for crustal melting, magma contamination and mixing processes (Fyfe 1992). While the percentages of crust mixed with the mantle compositions from this study is in agreement with previous estimates (> 90%; Giles 1988, 15–40%; Creaser and White 1991, <30%; Stewart and Foden 2003, 3–30%; Chapman *et al.* 2019), an advancement in the understanding of the relative crustal contributions stems from the geochemical and isotopic characterisation of the mantle beneath the Gawler Craton. These results highlight the complexity and variability in the mixing processes within the Hiltaba Suite petrogenesis. Hiltaba Suite granites are widely distributed across the region and demonstrate the underlying mantle composition influences the isotopic composition of the granite regardless of the crustal composition, however crustal contributions of 30–40% will mask juvenile mantle isotopic signatures in the granites. The volcanic units on the other hand, show a change in melting dynamics that reflect the change from SCLM-derived melts and differentiation processes to large scale crustal melting in the Upper GRV. Compositional differences between the intrusive and extrusive phases highlight the complexity and diversity in the source regions and plumbing system of the Gawler LIP.

While the temporal constraints on intrusive magmatism are not as well defined as the extrusive counterparts, magmatic conditions, as constrained by zircon chemistry, indicate that early rhyolitic and granitic magmas (ca. 1594–1590 Ma) are more oxidised and higher temperature at equivalent degrees of fractionation. These magmas overlap in age with the main mineralisation event in the Olympic Cu-Au Province (Courtney-Davies *et al.* 2020, McPhie *et al.* 2020) and display alteration and textural features consistent with mineralisation. The younger magmas (<1580 Ma) generally lack mineralisation. The early and young magmas broadly define separate evolution paths in zircon chemistry, whole-rock chem-

istry and Nd isotope compositions, which are likely linked to the more dominant SCLM source region in the former and greater crustal input in the latter. Changes in the melting dynamics, from basalt-driven volcanism and fractional crystallisation processes to crustal melting may be related to the relative magma fertility. The granitic rocks display significantly greater overlap in their whole-rock and zircon chemistry. However, in general, the older granitic rocks tend to be associated with mineralisation and share similar zircon characteristics to the lower GRV magmas also associated with mineralisation, suggesting broadly similar magmatic conditions. Lower degrees of plagioclase fractionation, higher oxidation state and higher magmatic temperatures, denoted by higher Eu/Eu*, Ce/Ce* and Ti-in-zircon, respectively, at equivalent degrees of fractionation, are characteristic of the mineralisation-related magmatic rocks, and are considered to be features of fertile magmas in southern Australian IOCG terrains.

The relationship between oxidised magmas and magma fertility is well established, most notably in porphyry Cu systems (Ballard *et al.* 2002, Richards 2009, Trail *et al.* 2012, Richards and Mumin 2013, Richards 2015, Shen *et al.* 2015, Sun *et al.* 2015, Xu *et al.* 2017, Zhong *et al.* 2019, Zhang *et al.* 2020). The oxidation state and sulphur content of a magma influences the sulphur species that are stable in the magma (Jugo *et al.* 2005, Richards 2015, Sun *et al.* 2015) and, as the partitioning behaviour of Cu and Au is strongly controlled by the nature of the sulphide species, oxidation state can influence a magma's ability to carry significant Cu and Au concentrations. Solubility of Cu and Au in a silicate melt increase up to the FMQ+1 level, which is the sulphide/sulphate transition (Richards 2015). As sulphate proportions begin to rise above the FMQ buffer Cu solubility also increases, while Au precipitates will drop as sulphide is converted to sulphate (Richards 2015). While less oxidised magmas may not be able to carry as much Cu (Zhang *et al.* 2020), Au may be carried in the vapour phase, and deposited in shallow crustal levels.

Sulphur, H_2O and fO_2 all work together throughout subduction and arc magmatic processes to transport chaclcophile and siderophile metals from the mantle to the upper crust where they may be concentrated by hydrothermal processes and form ore deposits (Richards 2015). Remelting of subduction-modified lithosphere has been recognised as a potential model for porphyry Cu-Au and epithermal deposits, allowing the mobilisation of chalcophile and siderophile elements that were stored within the SCLM from previous subduction events (Richards 2009, Tassara *et al.* 2017, Holwell *et al.* 2019). Subduction-modified metasomatised mantle is also considered an important source for metals in the IOCG deposit class (Groves *et al.* 2010). The consistent spatial association of Hiltaba Suite rocks and a metasomatised SCLM with Au, IOCG and Ag deposits in the Gawler Craton (Figure 1; Skirrow *et al.* 2018) further supports the link between oxidised, SCLM-derived magmas and mineralisation (Richards 2009, Groves *et al.* 2010, Lan *et al.* 2018, Holwell *et al.* 2019, Wang *et al.* 2019). It is therefore the partial melting of a metasomatised SCLM that is a critical step in the formation of oxidised, fertile magmas (e.g. Xu *et al.* 2017) and the ensuing Cu-Au mineralisation.

As summarised in Figure 2, initial mantle metasomatism in the Gawler Craton was almost certainly Archean. The enriched signature associated with this metasomatism is documented in mafic magmatic rocks throughout the late Archean, Palaeoproterozoic and Mesoproterozoic supporting the notion that a long-lived metasomatised SCLM exists beneath the Gawler Craton (Chapter 2; Wade *et al.* 2019). Mantle melting events over almost 1 billion years may have further metasomatised and replenished the SCLM in volatiles, metals and

other elements (Lorand et al. 2013, O'Reilly and Griffin 2013). The favourable compositions of the basaltic GRV and Hiltaba Suite magmas may have facilitated the remobilisation of metals from within the SCLM, and it is possible that further enrichment in Cu and

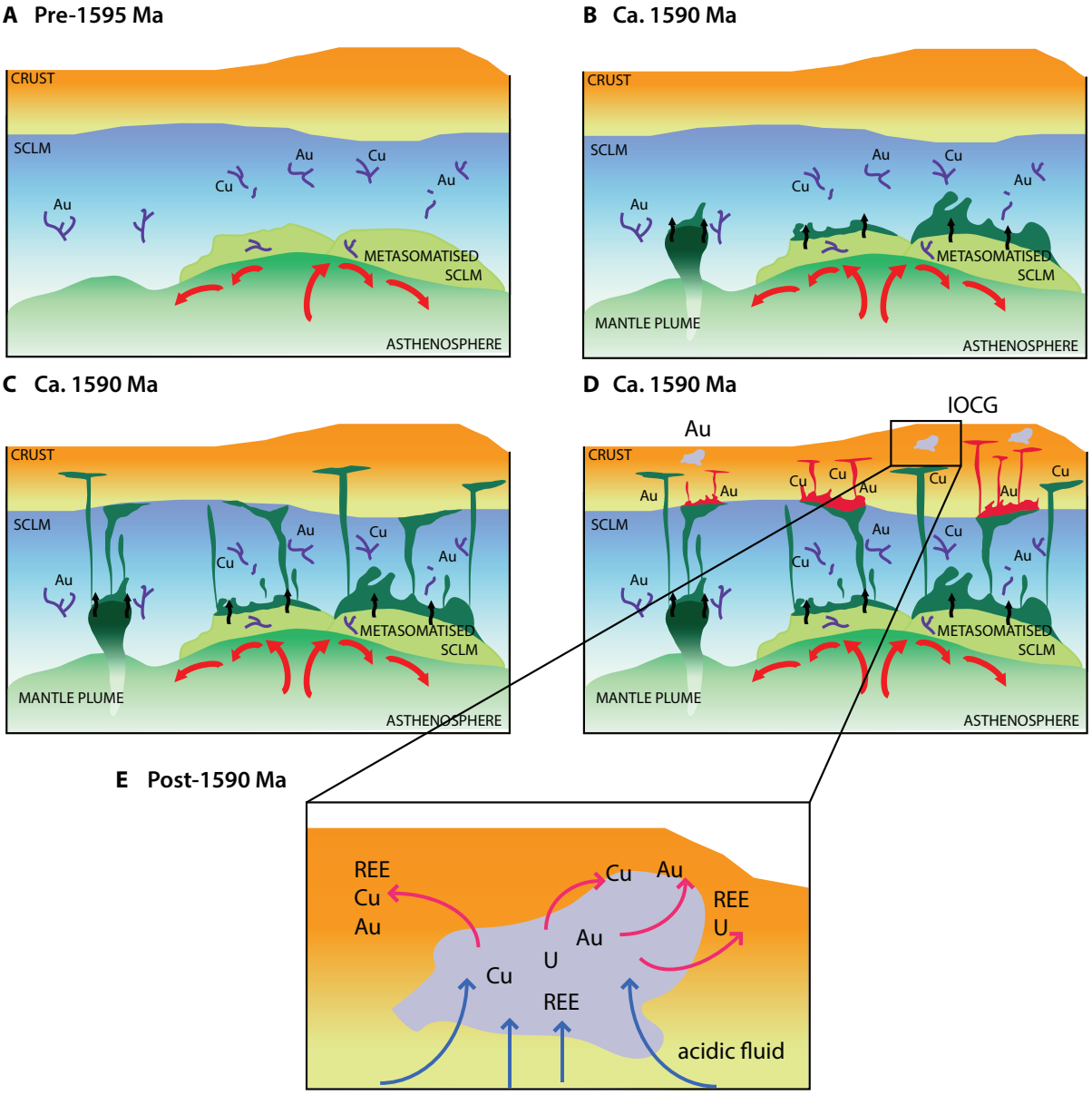

Figure 2: A conceptual model for the ca 1590 Ma mineral systems. A) Pre-1590 Ma. Multiple previous metasomatic events as a mechanism to create siderophile and chalcophile-rich zones or veins in the SCLM (e.g. Richards 2009, Groves et al. 2010, Corriveau et al. 2017, Xu et al. 2017); B) ca. 1590 Ma. Upwelling of asthenospheric mantle or mantle plume or invokes partial melting of metasomatised SCLM; C) ca. 1590 Ma. Hydrous and oxidised mafic magmas (mafic Hiltaba Suite) are produced by partial melting of the SCLM; D) ca. 1590 Ma. Oxidised felsic magmas produced by partial melting of the lower crust and fractional crystallisation of the mafic magmas. Au and Cu stored in the SCLM are remobilised by oxidised magmas of the Hiltaba Suite and form Au and IOCG mineral deposits in upper crust and E) Post-1590 Ma. Post-mineralisation hydrothermal fluid movement remobilises Cu, Au, REE and U in IOCG deposits.

Au was caused through fractional crystallisation processes (e.g. Sun et al. 2015, Xu et al. 2017). Evidence from other terrains suggests that Cu and Au, even in small concentrations, can survive within the SCLM on timescales of billions of years (Storey and Smith 2017, Wang et al. 2019). Therefore, it is reasonable to suggest that IOCG mineralisation in the Gawler Craton is linked to ancient metasomatic events in the lithospheric mantle.
The post-mineralisation history of hydrothermal fluid movement may have also been significant in the remobilisation of Cu, Au, REE and possibly U.

SUMMARY OF KEY OUTCOMES

This thesis has broadened our understanding of the role of magmatism in hydrothermal ore deposits by providing a comprehensive geochemical and isotopic framework for ca. 1590 Ma intrusive and extrusive rocks in the Gawler Craton. The ideas explored in this thesis build on pre-existing knowledge of our understanding of the composition of the lithospheric mantle and crust in the Gawler Craton and offers new insights into source compositions and magmatic conditions. The preceding chapters in this thesis provide a comprehensive assessment of the geochemical variation of ca. 1590 Ma magmatic rocks in the Gawler Craton, and use mineral chemistry to define conditions of magma formation and alteration related to the hydrothermal-magmatic event.

Chapter 2 identified the heterogeneous and enriched nature of the SCLM, as evidenced by enrichment in high field strength elements (HFSE), light rare earth elements (LREE), negative Nb-Ta-Ti anomalies and variable Nd isotopic compositions in mafic intrusive rocks. Enriched compositions are interpreted as primary source region characteristics due to insufficient evidence to support crustal contamination processes. Enrichment of the SCLM is linked to mantle metasomatism during earlier subduction events, which may have occurred as early as the Neoarchean.

SCLM composition as determined in Chapter 2 allowed for constraints in mantle source contributions to the felsic igneous rocks presented in Chapter 3. The felsic and mafic magmas of the Hiltaba Suite show geochemical affinity suggesting a common source region. Nd isotopic compositions in felsic magmas suggest mixing of 4–86% crust with SCLM-derived mafic magmas occurred, that was variable across the Gawler Craton. The mixing processes were enabled by large-scale mafic underplating and partial melting related to a plume.

Chapter 4 uses temporally constrained volcanism to evaluate LIP evolution and assess contributions from mantle and crust sources in its formation. Unlike the intrusive component, extensive outcrop and field relationships, in conjunction with high precision geochronological data, place accurate and precise time constraints on basaltic volcanism. The results show basalt-andesite units record increasing mantle enrichment from ca. 1594–1590 Ma followed by enriched juvenile mantle ca. 1590 Ma. By contrast, dacite-rhyolite units record increasing mantle input ca. 1594–1589 Ma followed by increasing crustal input ca. 1586.66–1586.39 Ma, which resulted in large scale crustal melting and produced the bulk of the silicic magmas in the province. The magmatic evolution can be related to mantle plume activity that is analogous to a mafic LIP model.

Chapter 5 and Chapter 6 focus on mineral chemistry to define conditions of magma formation and alteration respectively. The zircon trace element data in Chapter 5 reveal key indicators about magmatic composition for the GRV and Hiltaba Suite. All zircon compositions are characterised by depleted LREE, positive Ce anomalies and negative Eu anomalies. Such characteristics are consistent with

igneous zircon that formed in oxidising conditions. Zircon from rhyolites and granitoids associated with mineralisation are distinguished from other granitoids and rhyolites by their Ce/Ce*, Eu/Eu* and Ti compositions. The oxidised nature, as indicated by high Ce/Ce* ratios, is considered a key element in magma fertility in IOCG-IOA terrains. In both IOCG and IOA terrains, the trace element compositions of zircon are able to broadly differentiate fertile from non-fertile magmatic rocks.

The mineral study in Chapter 6 shows there are important attributes shared between the Vulcan Prospect mineralising fluids studied here and the Olympic Dam deposit. The local variation observed is most likely related to differences in host rock assemblage and probably fluid composition during hydrothermal activity. U-Pb apatite geochronology indicates there are at least three stages of apatite growth and/or resetting that correlate with known events in the Gawler Craton and most importantly at Olympic Dam. Each generation of apatite is characterised by different REY compositions, which are attributed to hydrothermal activity at ca. 1600 Ma, 1100 Ma and 450 Ma.

Further investigation into the hydrothermal activity in IOCG deposits such as Vulcan may include Sr-isotope studies on the different age populations of apatite, which may aid in identifying the source of hydrothermal fluids. Additionally, U-Pb studies on other accessory minerals such as florencite may help resolve the relationship between U+Th and REE concentrations in early magnetite-associated apatite to younger hematite-associated apatite. A comparative study of accessory minerals in other IOCG deposits from the Olympic Cu-Au Province will help define the hydrothermal activity in the Gawler Craton, and may be significant in the understanding of the formation of giant mineral deposits such as Olympic Dam.

Methodology for identifying magma fertility

There are a number of factors that are critical to the formation and preservation of a mineral system (e.g. Hagemann *et al.* 2016). This study is focussed on the role of magmatism and the chemical features of those magmas that may make them more favourable for ore deposit formation. The first critical step for a terrain to be favourable for Cu-Au mineralisation is the presence of a metasomatised SCLM. A metasomatised SCLM can be a repository for Cu and Au, in which the elements are introduced into the SCLM during previous subduction events (e.g. Richards 2009, Holwell *et al.* 2019). These metals are capable of being stored in the SCLM for long periods of time (Storey and Smith 2017, Wang *et al.* 2019). Partial melting of a metasomatised SCLM is critical in the formation of oxidised, fertile magmas which are capable of carrying significant amounts of Cu and Au. Further enrichment of Cu and Au may occur through fractional crystallisation processes of oxidised basaltic magmas (e.g. Sun et al. 2015, Xu et al. 2017). Therefore, comagmatic suites derived from a metasomatised SCLM through an oxidative crystallisation path are important in Cu-Au terrains.

Precambrian rocks associated with IOCG-IOA deposits are often extensively altered or deformed by younger events, making it exceedingly difficult to reconstruct their original magmatic character from whole-rock chemistry. To overcome regions with extensively overprinted whole-rock chemistry, zircon chemistry may be a reliable measure of oxidation state and other magmatic features. Features of zircon chemistry such as calculated higher magmatic temperature, and higher Ce/Ce* and Eu/Eu* values at lower degrees of fractionation may serve as fertility indicators in IOCG-IOA terranes. Reduced fractional crystallisation paths are likely to cause early S-saturation and removal of metals (e.g. Zhang *et al.* 2020). Therefore, identifying

crustal melts that have incorporated significant amounts of ancient crustal material or have a reduced crystallisation path is also important. These may present as very low whole-rock $\varepsilon_{Nd(i)}$ values, low zircon Eu/Eu* values (<0.2) and low zircon Ti concentrations.

A combination of whole-rock geochemistry, isotope geochemistry (e.g. Sm-Nd) and mineral chemistry is therefore required to adequately assess the magmatic rocks in terms of their fertility. Whole-rock geochemistry is essential to characterising the source regions to the magmatic rocks, identifying features that may point to a metasomatised mantle, and assessing magmatic processes such as fractional crystallisation; Sm-Nd isotope geochemistry can address mantle heterogeneities and crustal contamination and; mineral chemistry can be used to assess oxidation state and magmatic processes where whole-rock geochemistry may be unreliable due to extensive alteration, most applicable in Precambrian terrains.

As summarised above, each chapter builds on specific aspects that are key criteria for understanding the mineral system. Together, the outcomes of Chapter 2 to Chapter 5 point toward the importance of a previously metasomatised SCLM and oxidised magmas in Cu-Au prospective areas. Chapter 6 highlights the similarities between the Vulcan Cu-Au prospect and Olympic Dam. This chapter highlights the application of geochemical mineral mapping tools to understand the fluid evolution stages in a mineral prospect, and that similar protracted hydrothermal activity is recorded within the host Olympic Cu-Au Province.

Overall, the geological, geochemical and isotopic data collected in this study has better defined the geochemical composition of the mantle and the crust in the Gawler Craton at ca. 1590 Ma, and provided an assessment on magmatic and hydrothermal conditions during mineral deposit formation. This work has furthered our understanding on the role the mantle plays in IOCG mineral deposit formation. While the findings from Chapter 6 show promising results, further work is required to investigate the association of iron oxide and accessory mineral trace element compositions and prospective areas in the Gawler Craton in more detail. Likewise, links between IOCG and IOA deposits in the Gawler Craton require further investigation and offers an exciting mineral exploration platform for critical minerals in South Australia.

REFERENCES

Agangi, A., Kamenetsky, V. S. and McPhie, J., 2010. The role of fluorine in the concentration and transport of lithophile trace elements in felsic magmas: Insights from the Gawler Range Volcanics, South Australia. Chemical Geology, v. 273, p. 314-325. doi: https://doi.org/10.1016/j.chemgeo.2010.03.008

Ayalew, D. and Gibson, S. A., 2009. Head-to-tail transition of the Afar mantle plume: Geochemical evidence from a Miocene bimodal basalt–rhyolite succession in the Ethiopian Large Igneous Province. Lithos, v. 112, p. 461-476. doi: https://doi.org/10.1016/j.lithos.2009.04.005

Ballard, J. R., Palin, M. J. and Campbell, I. H., 2002. Relative oxidation states of magmas inferred from Ce(IV)/Ce(III) in zircon: application to porphyry copper deposits of northern Chile. Contributions to Mineralogy and Petrology, v. 144, p. 347-364. doi: https://doi.org/10.1007/s00410-002-0402-5

Beyer, E. E., Griffin, W. L. and O'Reilly, S. Y., 2006. Transformation of Archaean Lithospheric Mantle by Refertilization: Evidence from Exposed Peridotites in the Western Gneiss Region, Norway. Journal of Petrology, v. 47, p. 1611-1636. doi: https://doi.org/10.1093/petrology/egl022

Bryan, S. E., 2007. Silicic Large Igneous Provinces. Episodes, v. 30, p. 20–31. doi: https://doi.org/10.18814/epiiugs/2007/v30i1/004

Cai, Y.-C., Fan, H.-R., Santosh, M., Liu, X., Hu, F.-F., Yang, K.-F., Lan, T.-G., Yang, Y.-H. and Liu, Y., 2013. Evolution of the lithospheric mantle beneath the southeastern North China Craton: Constraints from mafic dikes in the Jiaobei terrain. Gondwana Research, v. 24, p. 601-621. doi: https://doi.org/10.1016/j.gr.2012.11.013

Chapman, N. D., Ferguson, M., Meffre, S. J., Stepanov, A., Maas, R. and Ehrig, K. J., 2019. Pb-isotopic constraints on the source of A-type Suites: Insights from the Hiltaba Suite - Gawler Range Volcanics Magmatic Event, Gawler Craton, South Australia. Lithos, v. 346-347, p. 105156. doi: https://doi.org/10.1016/j.lithos.2019.105156

Cheng, T., Nebel, O., Sossi, P. A., Wu, J., Siebel, W., Chen, F. K. and Nebel-Jacobsen, Y. J., 2018. On the Sr-Nd-Pb-Hf isotope code of enriched, Dupal-type sub-continental lithospheric mantle underneath south-western China. Chemical Geology, v. 489, p. 46-60. doi: https://doi.org/10.1016/j.chemgeo.2018.05.018

Cheng, Z., Zhang, Z., Wang, Z., Wang, F., Mao, Q., Xu, L., Ke, S., Yu, H. and Santosh, M., 2020. Petrogenesis of Transitional Large Igneous Province: Insights From Bimodal Volcanic Suite in the Tarim Large Igneous Province. Journal of Geophysical Research: Solid Earth, v. 125, p. e2019JB018382. doi: https://doi/org/10.1029/2019jb018382

Corriveau, L., C, Potter, E., G, Acosta-Gongora, P., A, Blein, O., Montreuil, J.-F., F, De Toni, A., A, Day, W., C, Slack, J., F, Ayuso, R., A and Hanes, R., 2017. Petrological Mapping and Chemical Discrimination of Alteration Facies as Vectors to IOA, IOCG, and Affiliated Deposits within Laurentia and Beyond. In: (Eds), SGA Québec 2017. v. p. Page. 408. doi: https://hal-brgm.archives-ouvertes.fr/hal-01488309/document

Courtney-Davies, L., Ciobanu, C. L., Tapster, S. R., Cook, N. J., Ehrig, K., Crowley, J. L., Verdugo-Ihl, M. R., Wade, B. P. and Condon, D. J., 2020. Opening the magmatic-hydrothermal window: High-precision U-Pb geochronology of the Mesoproterozoic Olympic Dam Cu-U-Au-Ag deposit, South Australia. Economic Geology, v. p. doi: https://doi.org/10.5382/econgeo.4772

Creaser, R. A., Price, R. C. and Wormald, R. J., 1991. A-type granites revisited: assessment of a residual-source model. Geology, v. 19, p. 163-166. doi: https://doi.org/10.1130/0091-7613(1991)019<0163:ATGRAO>2.3.CO;2

org/10.1130/0091-7613(1991)019<0048:YDLVHT>2.3.CO;2

Creaser, R. A. and White, A. J. R., 1991. Yardea Dacite; large-volume, high temperature felsic volcanism from the middle Proterozoic of South Australia. Geology, v. 19, p. 48-51. doi: https://doi.org/1.1130-0091-7613(1991)019<0048:YDLVHT>2.3.CO;2

Farmer, G. L., Fritz, D. E. and Glazner, A. F., 2020. Identifying Metasomatized Continental Lithospheric Mantle Involvement in Cenozoic Magmatism From Ta/Th Values, Southwestern North America. Geochemistry, Geophysics, Geosystems, v. 21, p. e2019GC008499. doi: https://doi.org/10.1029/2019gc008499

Fyfe, W. S., 1992. Magma underplating of continental crust. Journal of Volcanology and Geothermal Research, v. 50, p. 33-40. doi: https://doi.

org/10.1016/0377-0273(92)90035-C

Giles, C. W., 1988. Petrogenesis of the Proterozoic Gawler Range volcanics, South Australia. Precambrian Research, v. 40-41, p. 407-427. doi: https://doi.org/10.1016/0301-9268(88)90078-2

Groves, D. I., Bierlein, F. P., Meinert, L. D. and Hitzman, M. W., 2010. Iron Oxide Copper-Gold (IOCG) Deposits through Earth History: Implications for Origin, Lithospheric Setting, and Distinction from Other Epigenetic Iron Oxide Deposits. Economic Geology, v. 105, p. 641-654. doi: https://doi.org/10.2113/gsecongeo.105.3.641

Groves, D. I., Zhang, L. and Santosh, M., 2019. Subduction, mantle metasomatism, and gold: A dynamic and genetic conjunction. GSA Bulletin, v. 132, p. 1419-1426. doi: https://doi.org/10.1130/b35379.1

Hagemann, S. G., Lisitsin, V. A. and Huston, D. L., 2016. Mineral system analysis: Quo vadis. Ore Geology Reviews, v. 76, p. 504-522. doi: https://doi.org/10.1016/j.oregeorev.2015.12.012

Hei, H.-X., Su, S.-G., Wang, Y., Mo, X.-X., Luo, Z.-H. and Liu, W.-G., 2018. Rhyolites in the Emeishan large igneous province (SW China) with implications for plume-related felsic magmatism. Journal of Asian Earth Sciences, v. 164, p. 344-365. doi: https://doi.org/10.1016/j.jseaes.2018.05.032

Holwell, D. A., Fiorentini, M., McDonald, I., Lu, Y., Giuliani, A., Smith, D. J., Keith, M. and Locmelis, M., 2019. A metasomatized lithospheric mantle control on the metallogenic signature of post-subduction magmatism. Nature Communications, v. 10, p. 3511. doi: https://doi.org/10.1038/s41467-019-11065-4

Ionov, D. A., Bodinier, J.-L., Mukasa, S. B. and Zanetti, A., 2002. Mechanisms and Sources of Mantle Metasomatism: Major and Trace Element Compositions of Peridotite Xenoliths from Spitsbergen in the Context of Numerical Modelling. Journal of Petrology, v. 43, p. 2219-2259. doi: https://doi.org/10.1093/petrology/43.12.2219

Jugo, P. J., Luth, R. W. and Richards, J. P., 2005. Experimental data on the speciation of sulfur as a function of oxygen fugacity in basaltic melts. Geochimica et Cosmochimica Acta, v. 69, p. 497-503. doi: https://doi.org/10.1016/j.gca.2004.07.011

Kelemen, P. B., Shimizu, N. and Dunn, T., 1993. Relative depletion of niobium in some arc magmas and the continental crust: partitioning of K, Nb, La and Ce during melt/rock reaction in the upper mantle. Earth and Planetary Science Letters, v. 120, p. 111-134. doi: https://doi.org/10.1016/0012-821X(93)90234-Z

Keppler, H., 1993. Influence of fluorine on the enrichment of high field strength trace elements in granitic rocks. Contributions to Mineralogy and Petrology, v. 114, p. 479-488. doi: 10.1007/BF00321752

Lan, T.-G., Hu, R.-Z., Bi, X.-W., Mao, G.-J., Wen, B.-J., Liu, L. and Chen, Y.-H., 2018. Metasomatized asthenospheric mantle contributing to the generation of Cu-Mo deposits within an intracontinental setting: A case study of the ~128Ma Wangjiazhuang Cu-Mo deposit, eastern North China Craton. Journal of Asian Earth Sciences, v. 160, p. 460-489. doi: https://doi.org/10.1016/j.jseaes.2017.07.014

Liu, H.-Q., Xu, Y.-G., Zhong, Y.-T., Luo, Z.-Y., Mundil, R., Riley, T. R., Zhang, L. and Xie, W., 2019. Crustal melting above a mantle plume: Insights from the Permian Tarim Large Igneous Province, NW China. Lithos, v. 326-327, p.

370-383. doi: https://doi.org/10.1016/j.lithos.2018.12.031

Lorand, J.-P., Luguet, A. and Alard, O., 2013. Platinum-group element systematics and petrogenetic processing of the continental upper mantle: A review. Lithos, v. 164-167, p. 2-21. doi: https://doi.org/10.1016/j.lithos.2012.08.017

McPhie, J., Ehrig, K. J., Kamenetsky, M. B., Crowley, J. L. and Kamenetsky, V. S., 2020. Geology of the Acropolis prospect, South Australia, constrained by high-precision CA-TIMS ages. Australian Journal of Earth Sciences, v. 67, p. 699-716. doi: https://doi.org/10.1080/08120099.2020.1717617

Nicholson, S. W. and Shirey, S. B., 1990. Midcontinent rift volcanism in the Lake Superior Region: Sr, Nd, and Pb isotopic evidence for a mantle plume origin. Journal of Geophysical Research: Solid Earth, v. 95, p. 10851-10868. doi: https://doi.org/10.1029/JB095iB07p10851

O'Reilly, S. Y. and Griffin, W. L., 2013. Mantle Metasomatism. In: Harlov, D. and Austrheim, H. (Eds), Metasomatism and the Chemical Transformation of Rock: The Role of Fluids in Terrestrial and Extraterrestrial Processes. Springer Berlin Heidelberg, v. p. 471-533. https://doi.org/10.1007/978-3-642-28394-9_12

Pankhurst, M. J., Schaefer, B. F. and Betts, P. G., 2011a. Geodynamics of rapid voluminous felsic magmatism through time. Lithos, v. 123, p. 92-101. doi: https://doi.org/10.1016/j.lithos.2010.11.014

Pankhurst, M. P., Schaefer, B. F., Betts, P. G., Phillips, N. and Hand, M., 2011b. A Mesoproterozoic continental flood rhyolite province, the Gawler Ranges, Australia: the end member example of the Large Igneous Province clan. Solid Earth, v. 2, p. 1-9. doi: https://doi.org/10.5194/se-2-25-2011

Pearce, J. A., Ernst, R. E., Rogers, C. and Peate, D. W., 2017. LIP Printing: A Geochemical Proxy Approach to LIP Forensics. Geological Society of America Annual Meeting, Seattle, Washington, USA. Geological Society of America Abstracts with Programs, v. 49, No. 6, p. doi: https://doi.org.10.1130/abs/2017AM-301471

Plank, T., 2005. Constraints from Thorium/Lanthanum on Sediment Recycling at Subduction Zones and the Evolution of the Continents. Journal of Petrology, v. 46, p. 921-944. doi: https://doi.org/10.1093/petrology/egi005

Prouteau, G., Scaillet, B., Pichavant, M. and Maury, R., 2001. Evidence for mantle metasomatism by hydrous silicic melts derived from subducted oceanic crust. Nature, v. 410, p. 197-200. doi: https://doi.org/10.1038/35065583

Reid, A. J., Pawley, M. J., Wade, C., Jagodzinski, E. A., Dutch, R. A. and Armstrong, R., 2019. Resolving tectonic settings of ancient magmatic suites using structural, geochemical and isotopic constraints: the example of the St Peter Suite, southern Australia. Australian Journal of Earth Sciences, v. p. 1-28. doi: https://10.1080/08120099.2019.1632224

Richards, J. P., 2009. Postsubduction porphyry Cu-Au and epithermal Au deposits: Products of remelting of subduction-modified lithosphere. Geology, v. 37, p. 247-250. doi: https://doi.org/10.1130/G25451A.1

Richards, J. P., 2015. The oxidation state, and sulfur and Cu contents of arc magmas: implications for metallogeny. Lithos, v. 233, p. 27-45. doi: https://doi.org/10.1016/j.lithos.2014.12.011

Richards, J. P. and Mumin, A. H., 2013. Magmatic-hydrothermal processes within an

evolving Earth: Iron oxide-copper-gold and porphyry Cu ± Mo ± Au deposits. Geology, v. 41, p. 767-770. doi: https://doi.org/10.1130/g34275.1

Shen, P., Hattori, K., Pan, H., Jackson, S. and Seitmuratova, E., 2015. Oxidation Condition and Metal Fertility of Granitic Magmas: Zircon Trace-Element Data from Porphyry Cu Deposits in the Central Asian Orogenic Belt. Economic Geology, v. 110, p. 1861-1878. doi: https://doi.org/10.2113/econgeo.110.7.1861

Skirrow, R., van der Wielen, S. E., Champion, D. C., Czarnota, K. and Thiel, S., 2018. Lithospheric artchitecture and mantle metasomatism linked to iron-oxide Cu-Au ore formation: Multidiciplinary evidence from the Olympic Dam region, South Australia. Geochemistry, Geophysics, Geosystems, v. 19, p. doi: https://doi.org/10.1029/2018GC007561

Stewart, K. P. and Foden, J., 2003. Mesoproterozoic granites of South Australia. South Australia. Department of Primary Industries and Resources. Report Book, 2003/15, v. p. pp. 142. Available at: https://sarigbasis.pir.sa.gov.au/WebtopEw/ws/samref/sarig1/image/DDD/RB200300015.pdf

Storey, C. D. and Smith, M. P., 2017. Metal source and tectonic setting of iron oxide-copper-gold (IOCG) deposits: Evidence from an in situ Nd isotope study of titanite from Norrbotten, Sweden. Ore Geology Reviews, v. 81, p. 1287-1302. doi: https://doi.org/10.1016/j.oregeorev.2016.08.035

Sun, W., Huang, R.-f., Li, H., Hu, Y.-b., Zhang, C.-c., Sun, S.-j., Zhang, L.-p., Ding, X., Li, C.-y., Zartman, R. E. and Ling, M.-x., 2015. Porphyry deposits and oxidized magmas. Ore Geology Reviews, v. 65, p. 97-131. doi: https://doi.org/10.1016/j.oregeorev.2014.09.004

Swain, G., Barovich, K., Hand, M., Ferris, G. and Schwarz, M., 2008. Petrogenesis of the St Peter Suite, southern Australia: arc magmatism and Proterozoic crustal growth of the South Australian Craton. Precambrian Research, v. 166, p. 283-296. doi: https://doi.org/10.1016/j.precamres.2007.07.028

Swain, G., Woodhouse, A., Hand, M., Barovich, K., Schwarz, M. and Fanning, C. M., 2005. Provenance and tectonic development of the late Archaean Gawler Craton, Australia; U-Pb zircon, geochemical and Sm-Nd isotopic implications. Precambrian Research, v. 141, p. 106-136. doi: https://doi.org/10.1016/j.precamres.2005.08.004

Symington, N. J., Weinberg, R. F., Hasalová, P., Wolfram, L. C., Raveggi, M. and Armstrong, R. A., 2014. Multiple intrusions and remelting-remobilization events in a magmatic arc: The St Peter Suite, South Australia. GSA Bulletin, v. 126, p. 1200–1218. doi: https://doi.org/10.1130/B30975.1

Tassara, S., González-Jiménez, J. M., Reich, M., Schilling, M. E., Morata, D., Begg, G., Saunders, E., Griffin, W. L., O'Reilly, S. Y., Grégoire, M., Barra, F. and Corgne, A., 2017. Plume-subduction interaction forms large auriferous provinces. Nature communications, v. 8, p. 843-843. doi: https://doi.org/10.1038/s41467-017-00821-z

Tiddy, C. J. and Giles, D., 2020. Supra-subduction zone model for metal endowment at 1.60-1.575 Ga in eastern Australia. Ore Geology Reviews, v. 122, p. doi: https://doi.org/10.1016/j.oregeorev.2020.103483

Trail, D., Bruce Watson, E. and Tailby, N. D., 2012. Ce and Eu anomalies in zircon as proxies for the oxidation state of magmas. Geochimica et Cosmochimica

Acta, v. 97, p. 70-87. doi: https://doi.org/10.1016/j.gca.2012.08.032

Wade, C. E., 2012. Geochemistry of pre-1570 Ma mafic magmatism within Southern Australia: implications for possible tectonic settings and of major mineralisation events in South Australia. Geological Survey of South Australia, v. Report Book 2012/00019, p. 270. Available at: https://sarigbasis.pir.sa.gov.au/WebtopEw/ws/samref/sarig1/image/DDD/RB201200019.pdf

Wade, C. E., Payne, J. L., Barovich, K. M. and Reid, A. J., 2019. Heterogeneity of the sub-continental lithospheric mantle and 'non-juvenile' mantle additions to a Proterozoic silicic large igneous province. Lithos, v. 340-341, p. 87-107. doi: https://doi.org/10.1016/j.lithos.2019.05.005

Wang, Z., Cheng, H., Zong, K., Geng, X., Liu, Y., Yang, J., Wu, F., Becker, H., Foley, S. and Wang, C. Y., 2019. Metasomatized lithospheric mantle for Mesozoic giant gold deposits in the North China craton. Geology, v. 48, p. 169-173. doi: https://doi.org/10.1130/g46662.1

Xu, X.-W., Li, H., Peters, S. G., Qin, K.-Z., Mao, Q., Wu, Q., Hong, T., Wu, C., Liang, G.-L., Zhang, Z.-F. and Dong, L.-H., 2017. Cu-rich porphyry magmas produced by fractional crystallization of oxidized fertile basaltic magmas (Sangnan, East Junggar, PR China). Ore Geology Reviews, v. 91, p. 296-315. doi: https://doi.org/10.1016/j.oregeorev.2017.09.020

Zhang, X., Ni, P., Wang, G.-G., Jiang, Y.-H., Jiang, D.-S., Li, S.-N. and Fan, M.-S., 2020. Petrogenesis and oxidation state of granodiorite porphyry in the Jurassic Chuankeng skarn Cu deposit, South China: Implications for the Cu fertility and mineralization potential. Journal of Asian Earth Sciences, v. 191, p. 104184. doi: https://doi.org/10.1016/j.jseaes.2019.104184

Zhong, S., Seltmann, R., Qu, H. and Song, Y., 2019. Characterization of the zircon Ce anomaly for estimation of oxidation state of magmas: a revised Ce/Ce* method. Mineralogy and Petrology, v. 113, p. 755-763. doi: https://doi.org/10.1007/s00710-019-00682-y

Appendix 1

Supplementary material for: Heterogeneity of the sub-continental lithospheric mantle and "non-juvenile" mantle additions to a Proterozoic silicic large igneous province

Appendix 1 Supplementary material for Heterogeneity of the sub-continental lithospheric mantle and 'non-juvenile' mantle additions to a Proterozoic silicic large igneous province

Appendix 1 Table A1 Whole-rock geochemical composition for mafic Hiltaba Suite samples

Sample	**2465592**	**2465593**	**2435416**	**2435418**	**PDBN321-02**	**2435417**	**2448983**	**2450321**	**2450320**	**2450322**
Sample Type	pulp	pulp	drill core	drill core	drill core	drill core	drill core	drill core	drill core	drill core
Drill Hole	PDBN 134	PDBN 134	PDBN 135	PDBN 136	PDBN 321	PDBN 135	BLD 3	BLD 3	BLD 3	BLD 3
Depth From	53.8	139.49	141.5	150.25	102.4	161	977	927.2	936.53	893.14
Depth To	55.7	139.7	141.66	150.45	103.3	161.5	978	927.37	936.8	893.4
Data Source	This study	This study	This study	This study	This study	This study	This study	This study	This study	This study
Location	Barns	Barns	Barns	Barns	Barns	Barns	Bills Lookout	Bills Lookout	Bills Lookout	Bills Lookout
E	542274	542274	542368	542354	541914	542368	722947	722947	722947	722947
N	6366051	6366051	6366116	6366069	6366142	6366116	6637341	6637341	6637341	6637341
Zone	53	53	53	53	53	53	53	53	53	53
Lithology	ahpanitic dyke	ahpanitic dyke	ahpanitic dyke	ahpanitic dyke	diorite	ahpanitic dyke	diorite	diorite	diorite	diorite
Major elements (wt %)										
SiO_2	50.62	51.06	50.18	48.61	50.39	51.16	45.79	42.50	47.01	48.54
TiO_2	0.64	1.10	1.14	1.17	0.71	0.50	1.71	1.72	1.41	1.98
Al_2O_3	15.74	11.87	12.21	13.15	8.90	14.90	14.75	15.78	15.78	14.39
FeO	4.46	6.37	6.54	7.29	6.00	8.48	11.20	10.50	9.27	10.10
Fe_2O_3	9.55	11.80	8.59	9.78	8.54	10.80	15.00	14.10	13.20	15.90
MnO	0.20	0.69	0.20	0.29	0.20	0.32	0.22	0.18	0.20	0.22
MgO	8.98	8.46	12.80	15.00	15.80	12.70	8.18	9.91	7.99	5.76
CaO	6.34	3.04	5.67	2.08	8.33	0.72	9.04	6.44	8.41	7.96
Na_2O	2.20	0.98	2.31	1.20	0.69	0.95	1.64	1.58	2.04	2.10
K_2O	2.07	2.53	1.54	0.45	3.47	1.38	2.04	2.86	2.01	1.87
P_2O_5	0.20	1.11	1.12	1.11	0.30	0.23	0.28	0.25	0.24	0.28
LOI	3.09	6.94	3.90	6.71	2.01	6.13	1.31	4.47	1.69	0.82
F	0.06	0.19	0.19	0.21	0.20	0.11	0.03	0.12	0.03	0.04
Trace and rare earth elements (ppm)										
Ga	16.10	16.20	17.00	22.70	14.20	21.10	17.40	18.10	16.90	21.80
Cr	673.00	455.00	792.00	991.00	1510.00	998.00	303.00	356.00	165.00	139.00
Ni	265.00	260.00	425.00	640.00	625.00	290.00	185.00	215.00	170.00	205.00
Co	56.10	47.10	47.20	55.00	64.70	46.10	58.60	54.90	54.00	56.40
Sc	29.60	15.50	21.50	20.70	22.60	24.60	33.80	36.30	26.50	34.20
Ti			7300.00	7180.00	4300.00	2990.00	9940.00	10000.00	8040.00	11600.00
V	193.00	121.00	143.00	150.00	113.00	138.00	314.00	311.00	244.00	450.00
Cu	35.00	355.00	35.00	5.00	50.00	20.00	130.00	95.00	85.00	115.00
Zn	230.00	95.00	125.00	185.00	105.00	240.00	80.00	165.00	110.00	140.00
Y	37.60	31.80	30.20	47.50	15.50	19.20	25.90	27.50	18.00	23.60
Rb	131.00	151.00	49.70	36.00	212.00	87.40	92.10	146.00	96.20	85.00
Sr	379.00	299.00	785.00	211.00	138.00	68.00	147.00	128.00	171.00	209.00
Cs	2.90	4.43	0.94	1.07	9.36	3.14	3.17	9.76	2.90	2.83
Ba	699.00	1320.00	1730.00	121.00	628.00	351.00	301.00	439.00	393.00	531.00
Th	3.51	26.90	27.80	32.90	5.74	2.67	0.87	0.87	0.87	1.41
U	0.70	4.62	3.78	11.20	1.70	1.14	0.19	0.57	0.23	0.31
Pb	43.00	9.00	35.00	5.00	5.00	17.00	3.00	6.00	9.00	11.00
Zr	97.00	383.00	441.00	465.00	88.50	116.00	79.00	90.00	76.50	118.00
Hf	3.04	11.20	11.80	12.40	2.67	2.87	2.47	2.50	2.24	3.14
Nb	2.84	19.30	21.80	23.30	7.24	3.89	9.81	7.37	5.84	8.65
Ta	0.18	1.00	1.03	1.14	0.54	0.19	0.59	0.47	0.41	0.52
La	23.70	98.00	95.90	68.80	41.40	17.20	15.80	6.73	10.80	21.90
Ce	45.60	208.00	212.00	156.00	86.80	26.10	33.10	17.70	26.20	42.40
Pr	6.11	26.20	28.60	21.10	11.80	3.15	4.63	2.53	3.68	5.44
Nd	25.90	106.48	110.00	80.70	47.10	11.80	19.60	11.40	15.80	21.80
Sm	4.99	15.00	16.80	14.20	7.91	2.53	4.25	3.36	3.32	4.69
Eu	1.39	3.42	3.71	3.16	1.82	0.58	1.38	1.05	1.13	1.51
Gd	5.87	9.53	10.60	10.50	5.29	2.42	4.52	4.41	3.48	4.72
Tb	0.94	1.16	1.26	1.33	0.66	0.46	0.73	0.77	0.54	0.70
Dy	6.04	6.01	5.73	7.26	3.45	3.00	4.62	4.69	3.31	4.21
Ho	1.39	1.21	1.06	1.48	0.66	0.67	0.97	1.06	0.71	0.86
Er	4.03	3.35	2.78	4.27	1.63	2.04	3.00	3.23	2.14	2.60
Tm	0.55	0.50	0.35	0.60	0.25	0.30	0.40	0.45	0.25	0.35
Yb	3.54	3.26	2.16	3.96	1.50	2.12	2.64	3.08	1.92	2.36
Lu	0.52	0.48	0.28	0.59	0.17	0.27	0.38	0.44	0.26	0.35
Precious metals (ppb)										
Au	14.00	4880.00	2.00	4.00	12.00	33.00	2.00	2.00	4.00	-1.00
Pt	5.00	2.00	2.00	2.00	2.00	6.00	4.00	-1.00	-1.00	-1.00
Pd	4.00	4.00	2.00	2.00	3.00	7.00	6.00	-1.00	-1.00	-1.00
Eu/Eu*	0.79	0.87	0.85	0.79	0.86	0.72	0.96	0.83	1.02	0.98
$(La/Yb)_N$	4.80	21.56	31.85	12.46	19.80	5.82	4.29	1.57	4.03	6.66
Mg#	55	47	62	62	67	55	37	43	40	30
Total REE	130.57	482.60	491.23	373.95	210.44	72.64	96.02	60.90	73.54	113.89

$Eu/Eu^* = (Eu/(Sm \times Gd))_N^{0.5}$

Normalising values from Taylor and McLennon 1995

Mg# = (Mg/[Mg+Fe]x100)

Appendix 1 Supplementary material for Heterogeneity of the sub-continental lithospheric mantle and 'non-juvenile' mantle additions to a Proterozoic silicic large igneous province

Appendix 1 Table A1 Whole-rock geochemical composition for mafic Hiltaba Suite samples

Sample	**2448982**	**GCT 88B**	**2559254**	**2498051**	**2498052**	**2559253**	**2559247**	**2559249**	**2559248**	**2442088**
Sample Type	drill core	out crop	drill core	drill core	drill core	pulp	pulp	pulp	pulp	drill core
Drill Hole	BLD 3		MGD 35	MGD 45	MGD 45	MGD 34	MGD 45	MGD 46	MGD 45	CURD2
Depth From	873.6		412.45	768.73	744.43	593.05	767.05	740.65	800	98.8
Depth To	874.6		412.6	768.96	744.6	593.15	767.55	740.75	800.15	99.06
Data Source	This study	This study	This study	This study	This study	This study	This study	This study	This study	This study
Location	Bills Lookout	Bulgunnia	Chianti	Chianti	Chianti	Chianti	Chianti	Chianti	Chianti	Curramulka
E	722947	447953	714000	714464	714464	714250	714464	715052	714464	747769
N	6637341	6689418	6538775	6540377	6540377	6539800	6540377	6540987	6540377	6164961
Zone	53	53	53	53	53	53	53	53	53	53
Lithology	diorite	gabbro	ahpanitic dyke	ahpanitic dyke	ahpanitic dyke	ahpanitic dyke	ahpanitic dyke	ahpanitic dyke	ahpanitic dyke	gabbro
Major elements (wt %)										
SiO_2	50.47	49.70	49.21	49.51	49.19	46.79	45.18	45.55	47.43	48.55
TiO_2	1.47	1.69	1.23	1.66	1.25	1.55	1.35	3.26	2.78	1.64
Al_2O_3	15.12	14.40	13.81	13.22	14.16	13.41	14.13	14.89	14.13	14.89
FeO	8.38		11.80	8.09	5.94	10.40	9.31	10.20	13.70	7.14
Fe_2O_3	12.60	14.90	13.89	14.47	13.13	16.84	15.08	17.60	17.77	14.20
MnO	0.20	0.21	0.50	0.30	0.28	0.37	0.40	0.57	0.22	0.14
MgO	6.58	5.81	7.01	5.33	6.26	5.82	7.30	6.89	5.87	5.66
CaO	7.41	9.43	4.06	8.21	7.65	4.20	4.39	1.62	2.39	9.29
Na_2O	2.10	2.35	2.23	1.89	1.60	2.30	1.68	0.22	0.35	3.37
K_2O	2.14	0.40	2.56	1.61	2.31	1.25	2.75	3.10	2.30	1.23
P_2O_5	0.29	0.13	0.12	0.14	0.11	0.16	0.12	0.42	1.13	0.24
LOI	1.53	0.42	4.89	3.50	3.89	6.69	7.15	5.59	5.56	0.66
F	0.06									0.09
Trace and rare earth elements (ppm)										
Ga	19.60	24.00	17.00	19.40	17.50	17.80	18.10	27.20	25.80	21.50
Cr	184.00	60.00	231.00	77.00	245.00	122.00	195.00	105.00	100.00	61.00
Ni	115.00	76.00	100.00	70.00	90.00	90.00	80.00	60.00	55.00	100.00
Co	53.40	80.00	49.80	59.00	50.10	45.80	45.10	176.00	46.40	60.30
Sc	31.80		37.60	46.70	41.60	44.80	40.50	46.60	46.50	40.70
Ti	9060.00		7690.00	10400.00	7750.00	9800.00	8230.00	20200.00	17400.00	8810.00
V	261.00		318.00	437.00	341.00	397.00	346.00	491.00	184.00	344.00
Cu	130.00	195.00	50.00	265.00	165.00	60.00	330.00	310.00	585.00	110.00
Zn	105.00	120.00	195.00	165.00	120.00	325.00	390.00	825.00	520.00	90.00
Y	24.60	39.50	25.00	33.30	25.60	35.30	29.70	66.50	70.80	40.80
Rb	110.00	31.50	121.00	85.00	148.00	87.50	129.00	157.00	98.00	40.90
Sr	198.00	185.00	87.30	150.00	135.00	49.90	75.70	12.40	10.40	292.00
Cs	4.08	1.40	2.38	3.08	3.56	3.30	3.49	6.14	3.66	1.08
Ba	492.00	650.00	2030.00	873.00	1600.00	549.00	1720.00	547.00	233.00	588.00
Th	2.34	1.65	3.35	3.44	2.53	3.62	3.08	9.38	9.89	6.07
U	0.47	0.43	1.08	0.91	0.60	0.95	0.86	6.41	6.53	1.61
Pb	8.00	2.50	28.00	85.00	15.00	35.00	535.00	47.00	57.00	11.00
Zr	144.00	130.00	97.00	118.00	89.00	107.00	100.00	305.00	276.00	140.00
Hf	3.87	3.00	2.76	3.41	2.54	3.08	2.97	8.25	8.05	4.29
Nb	10.30	7.00	5.89	7.28	5.29	6.38	5.98	21.00	19.80	7.74
Ta	0.62	<2	0.41	0.46	0.38	0.44	0.42	1.42	1.33	0.55
La	24.30	19.00	11.20	14.00	11.00	17.90	12.70	32.70	35.20	35.00
Ce	47.10	36.50	24.40	30.30	23.70	35.70	26.90	67.90	76.00	70.50
Pr	6.05	5.50	3.35	4.29	3.21	4.65	3.74	8.91	10.80	9.56
Nd	23.40	21.50	14.70	18.50	14.00	19.30	14.90	37.70	44.80	38.40
Sm	4.94	6.00	3.72	4.90	3.79	4.95	3.89	9.80	10.50	7.64
Eu	1.48	1.95	0.93	1.46	0.99	1.34	0.98	2.32	1.93	2.07
Gd	4.69	6.00	3.97	5.69	4.14	5.58	4.26	11.50	11.30	7.26
Tb	0.72	1.05	0.71	0.97	0.75	0.97	0.80	2.04	1.90	1.16
Dy	4.34	7.50	4.54	6.00	4.57	6.11	5.13	12.40	12.40	7.18
Ho	0.94	1.45	1.02	1.33	0.98	1.37	1.18	2.71	2.83	1.48
Er	2.77	4.10	2.86	3.78	2.96	3.98	3.40	7.54	8.58	4.50
Tm	0.40	0.60	0.45	0.55	0.45	0.60	0.50	1.05	1.20	0.65
Yb	2.64	4.10	2.84	3.76	2.74	4.20	3.20	7.10	8.48	4.14
Lu	0.38	0.55	0.41	0.51	0.43	0.54	0.45	0.96	1.29	0.61
Precious metals (ppb)										
Au	1.00	<1	2.00	3.00	2.00	4.00	4.00	4.00	10.00	1.00
Pt	-1.00		2.00	3.00	3.00	2.00	3.00	6.00	3.00	-1.00
Pd	-1.00		2.00	2.00	2.00	1.00	3.00	5.00	2.00	-1.00
Eu/Eu*	0.94	0.99	0.74	0.85	0.76	0.78	0.74	0.67	0.54	0.85
$(La/Yb)_N$	6.60	3.32	2.83	2.67	2.88	3.06	2.85	3.30	2.98	6.06
Mg#	37	13	34	31	39	29	36	32	26	34
Total REE	124.15	115.80	75.10	96.04	73.71	107.19	82.03	204.63	227.21	190.15

$Eu/Eu^* = (Eu/(Sm \times Gd))_N^{0.5}$

Normalising values from Taylor and McLennon 1995

Mg# = (Mg/[Mg+Fe]x100)

Appendix 1 Supplementary material for Heterogeneity of the sub-continental lithospheric mantle and 'non-juvenile' mantle additions to a Proterozoic silicic large igneous province

Appendix 1 Table A1 Whole-rock geochemical composition for mafic Hiltaba Suite samples

Sample	**2492270**	**2492271**	**2492274**	**364685**	**364687**	**2492273**	**2442087**	**2492267**	**2492265**	**2492264**	**18ErD-02**
Sample Type	drill core	drill core	drill core	drill core	drill core	drill core	drill core	drill core	drill core	drill core	out crop
Drill Hole	CURD2	CURD2	CURD2	CUR D2	CUR D6	CURD2	CURD2	CURD4	CURD4	CURD4	
Depth From	64.53	71.59	92.15	58.2	60.4	91.47	89.1	93.04	89.92	88.23	
Depth To	64.98	71.8	92.43			91.77	89.5	93.26	90.17	88.46	
Data Source	This study	This study	This study	G. Swain	G. Swain	This study	This study	This study	This study	This study	This study
Location	Curramulka	Curramulka	Curramulka	Curramulka	Curramulka	Curramulka	Curramulka	Curramulka	Curramulka	Curramulka	Earea Dam
E	747769	747769	747769	747769	745809	747769	747769	744329	744329	744329	499735
N	6164961	6164961	6164961	6164961	6165691	6164961	6164961	6163731	6163731	6163731	6585307
Zone	53	53	53	53	53	53	53	53	53	53	53
Lithology	gabbronorite	gabbronorite	gabbronorite	norite	gabbronorite	gabbronorite	gabbro	gabbro	gabbro	gabbro	gabbro
Major elements (wt %)											
SiO_2	51.09	47.99	48.79	51.90	50.50	47.82	46.32	44.41	42.11	42.51	48.73
TiO_2	1.29	1.89	1.88	1.20	1.06	2.08	2.16	2.17	2.23	2.28	1.97
Al_2O_3	16.11	15.17	14.66	15.90	14.50	13.92	14.26	14.10	14.96	14.51	13.77
FeO	6.68	7.65	7.02			8.18	8.64	7.58	7.64	7.49	10.00
Fe_2O_3	10.99	15.42	14.37	11.30	13.40	16.25	17.00	16.33	17.05	17.59	14.60
MnO	0.16	0.18	0.16	0.16	0.15	0.18	0.18	0.18	0.13	0.18	0.21
MgO	6.16	5.43	5.42	6.07	6.90	5.32	5.21	6.53	7.35	6.89	6.57
CaO	8.05	8.50	9.03	7.63	6.29	8.53	9.20	9.39	7.72	8.56	10.81
Na_2O	3.32	3.44	3.28	3.12	3.19	3.01	3.21	2.77	3.10	2.96	2.32
K_2O	1.47	1.00	1.37	1.62	1.83	1.51	1.09	1.32	1.42	1.50	0.42
P_2O_5	0.27	0.66	0.29	0.29	0.14	0.33	0.54	0.24	0.28	0.29	0.21
LOI	0.61	0.16	0.85	0.95	1.58	0.84	0.67	2.67	3.17	2.60	0.31
F							0.06				0.03
Trace and rare earth elements (ppm)											
Ga	18.60	23.60	21.20	20.00	24.00	21.80	22.50	22.40	25.10	26.20	19.80
Cr	56.00	47.00	28.00	80.00	140.00	14.00	56.00	116.00	141.00	130.00	62.00
Ni	65.00	80.00	100.00	39.00	63.00	100.00	75.00	115.00	95.00	110.00	70.00
Co	56.70	66.30	69.50	27.00	24.00	68.10	62.40	66.90	60.50	64.20	54.10
Sc	31.00	32.00	40.50	30.00	50.00	39.30	40.50	43.00	44.30	45.30	35.70
Ti	8020.00	11300.00	11600.00			12800.00	11700.00	13200.00	13900.00	14000.00	12000.00
V	221.00	315.00	349.00	220.00	260.00	406.00	381.00	449.00	453.00	475.00	307.00
Cu	65.00	80.00	115.00	60.00	44.00	130.00	100.00	230.00	35.00	165.00	105.00
Zn	70.00	80.00	95.00	39.00	59.00	95.00	120.00	105.00	130.00	135.00	155.00
Y	34.80	36.20	43.40	29.00	52.00	44.00	48.00	47.60	42.80	54.50	23.80
Rb	56.90	22.40	44.50	52.00	110.00	57.70	32.40	42.90	38.70	34.10	14.80
Sr	279.00	524.00	293.00	280.00	160.00	273.00	323.00	159.00	143.00	147.00	218.00
Cs	1.09	0.58	0.96	<3	<3	1.23	0.96	0.96	1.04	0.52	1.91
Ba	541.00	634.00	592.00	550.00	310.00	620.00	663.00	146.00	144.00	121.00	85.00
Th	8.70	4.30	6.94	9.00	9.00	8.99	4.15	1.20	0.68	0.93	0.85
U	1.57	0.86	1.53	1.50	1.50	1.72	0.91	0.75	0.54	0.39	0.19
Pb	9.00	8.00	11.00	<3	48.00	11.00	9.00	5.00	7.00	8.00	8.00
Zr	140.00	105.00	195.00	140.00	130.00	154.00	120.00	123.00	143.00	127.00	124.00
Hf	3.71	2.84	5.21	6.00	6.00	4.54	3.96	3.48	4.12	3.66	3.61
Nb	10.70	8.59	12.70	15.00	15.00	12.80	7.80	16.90	13.60	19.80	11.20
Ta	0.68	0.57	0.80	2.00	2.00	0.86	0.51	0.94	0.88	1.33	0.67
La	42.30	50.90	41.50	38.00	35.00	44.30	43.20	26.50	23.20	37.30	11.60
Ce	85.10	102.00	87.30	69.00	70.00	92.50	85.90	63.80	57.30	94.30	27.50
Pr	10.20	13.10	11.20	8.00	9.00	12.20	12.30	8.83	7.92	12.40	4.04
Nd	37.80	50.10	43.50	42.50	55.00	46.60	49.20	35.10	32.00	48.70	18.60
Sm	7.21	9.32	8.52	6.00	10.00	9.44	10.10	8.24	7.62	10.10	4.91
Eu	1.69	2.30	2.04	1.50	2.00	2.12	2.53	1.90	1.99	2.22	1.77
Gd	6.51	7.97	8.08	6.00	10.00	8.61	9.48	8.13	7.58	9.89	5.27
Tb	1.05	1.24	1.32	1.00	1.50	1.37	1.46	1.40	1.31	1.63	0.79
Dy	6.35	7.09	8.19	6.00	11.50	8.07	8.92	8.68	7.73	9.89	4.67
Ho	1.38	1.43	1.75	1.00	2.00	1.72	1.84	1.79	1.64	2.06	0.97
Er	4.10	4.05	4.74	4.00	6.00	4.79	5.39	5.22	4.76	6.33	2.68
Tm	0.55	0.55	0.75		<1	0.70	0.70	0.80	0.70	0.90	0.35
Yb	3.52	3.52	4.72	3.00	6.00	4.74	4.46	5.18	4.72	5.76	2.24
Lu	0.50	0.48	0.62		1.00	0.64	0.63	0.70	0.69	0.85	0.30
Precious metals (ppb)											
Au	1.00	2.00	1.00	<1	1.00	1.00	-1.00	4.00	2.00	2.00	5.00
Pt	-1.00	-1.00	-1.00		<5	-1.00	-1.00	2.00	-1.00	2.00	-1.00
Pd	-1.00	2.00	-1.00		<1	-1.00	-1.00	2.00	-1.00	2.00	-1.00
Eu/Eu*	0.75	0.82	0.75	0.76	0.61	0.72	0.79	0.71	0.80	0.68	1.06
$(La/Yb)_N$	8.62	10.37	6.31	9.09	4.18	6.70	6.95	3.67	3.53	4.65	3.71
Mg#	40	31	33	52	50	29	28	34	36	35	34
Total REE	208.26	254.05	224.23	186.00	219.00	237.80	236.11	176.27	159.16	242.33	85.69

$Eu/Eu^* = (Eu/(Sm \times Gd))_N^{0.5}$

Normalising values from Taylor and McLennon 1995

Mg# = (Mg/[Mg+Fe]x100)

Appendix 1 Supplementary material for Heterogeneity of the sub-continental lithospheric mantle and 'non-juvenile' mantle additions to a Proterozoic silicic large igneous province

Appendix 1 Table A1 Whole-rock geochemical composition for mafic Hiltaba Suite samples

Sample	**18ErD-03**	**18ErD-01**	**18GL-05**	**HDD023-01**	**HDD023-02**	**2495985**	**2495986**	**2495988**	**2495989**	**2495990**
Sample Type	out crop	out crop	out crop	drill core	drill core	drill core	drill core	drill core	drill core	drill core
Drill Hole				HDD 023	HDD 023	DDH C7	DDH C7	DDH C7	DDH C7	DDH C7
Depth From				583	588.7	181.2	183.33	192.13	198.49	200.78
Depth To				583.6	589	181.45	183.57	192.39	200.58	200.9
Data Source	This study	This study	This study	This study	This study	This study	This study	This study	This study	This study
Location	Earea Dam	Earea Dam	Glenloth	Hillside	Hillside	Kimba	Kimba	Kimba	Kimba	Kimba
E	499735	499832	507194	763149.00	763149.00	568045	568045	568045	568045	568045
N	6585307	6585346	6560233	6174298.00	6174298.00	6319261	6319261	6319261	6319261	6319261
Zone	53	53	53	53	53	53	53	53	53	53
Lithology	gabbro	gabbro	dolerite	gabbro	gabbro	gabbronorite	gabbronorite	gabbronorite	gabbronorite	gabbronorite
Major elements (wt %)										
SiO_2	48.54	48.95	49.72	48.89	49.77	47.15	47.77	45.82	46.81	48.03
TiO_2	1.93	1.99	1.23	1.46	1.37	1.59	1.92	1.91	1.44	1.48
Al_2O_3	14.04	13.60	14.03	14.49	13.90	14.41	13.05	13.66	15.58	14.99
FeO	9.09	8.65	8.81	6.94	7.52	12.90	12.60	14.10	12.30	12.10
Fe_2O_3	14.30	14.40	14.00	12.50	12.20	15.82	15.49	17.51	15.30	14.89
MnO	0.21	0.21	0.26	0.13	0.15	0.24	0.25	0.24	0.22	0.21
MgO	6.65	6.38	6.50	6.65	7.54	6.75	6.54	6.66	6.72	6.85
CaO	10.59	10.56	9.45	5.60	6.04	10.00	11.70	10.03	10.05	9.84
Na_2O	2.33	2.50	2.47	4.41	4.21	2.66	2.49	2.47	2.66	2.60
K_2O	0.54	0.57	1.04	1.53	1.48	0.81	0.64	0.82	0.88	0.91
P_2O_5	0.20	0.22	0.14	0.14	0.12	0.17	0.18	0.17	0.15	0.16
LOI	0.72	0.44	0.99	3.78	3.14	0.00	-0.06	0.07	0.11	0.14
F	0.03	0.03	0.03	0.08	0.08					
Trace and rare earth elements (ppm)										
Ga	19.60	19.00	17.10	21.00	19.80	19.30	18.90	20.80	18.90	22.30
Cr	73.00	54.00	94.00	181.00	156.00	195.00	89.00	95.00	96.00	98.00
Ni	60.00	45.00	60.00	60.00	60.00	55.00	35.00	40.00	65.00	65.00
Co	54.20	46.90	48.60	50.40	48.70	70.20	59.30	73.10	69.40	68.10
Sc	36.50	36.40	46.50	42.40	38.70	49.30	63.10	51.30	36.80	40.90
Ti	11800.00	11800.00	7820.00	9200.00	8610.00	9800.00	11700.00	11500.00	9060.00	9520.00
V	308.00	308.00	297.00	361.00	345.00	315.00	389.00	334.00	270.00	277.00
Cu	145.00	135.00	150.00	90.00	225.00	140.00	-5.00	155.00	15.00	-5.00
Zn	140.00	120.00	165.00	45.00	70.00	105.00	90.00	115.00	120.00	140.00
Y	23.40	25.00	28.10	34.60	29.00	27.50	32.90	28.40	23.10	29.30
Rb	22.80	64.80	64.00	94.50	82.70	7.80	6.70	9.10	7.90	15.00
Sr	242.00	202.00	262.00	54.90	34.60	166.00	141.00	172.00	220.00	152.00
Cs	1.51	1.35	5.80	0.74	0.43	0.33	0.24	0.46	0.25	0.42
Ba	91.00	347.00	149.00	234.00	206.00	68.00	45.50	79.50	83.00	62.50
Th	0.87	0.97	1.45	3.26	2.83	0.81	0.53	0.88	1.08	0.62
U	0.22	0.24	0.22	1.69	2.67	0.46	0.15	0.24	0.38	0.71
Pb	10.00	7.00	20.00	2.00	2.00	7.00	5.00	4.00	7.00	7.00
Zr	118.00	127.00	86.00	118.00	92.50	89.00	105.00	93.00	81.50	75.50
Hf	3.47	3.43	2.61	3.46	2.80	2.55	2.92	2.75	2.29	2.16
Nb	10.60	11.10	6.97	8.40	6.39	10.90	12.80	11.50	9.80	11.30
Ta	0.63	0.68	0.41	0.57	0.55	0.69	0.74	0.64	0.59	0.82
La	11.10	11.30	8.22	11.00	11.00	9.99	10.50	10.30	9.31	10.70
Ce	26.40	27.70	19.00	24.40	23.60	22.40	25.40	22.90	20.30	27.50
Pr	3.88	4.15	2.77	3.40	3.15	3.24	3.70	3.32	2.90	4.13
Nd	17.40	18.60	12.30	15.50	14.10	14.30	16.70	14.90	12.80	18.30
Sm	4.68	4.78	3.28	4.32	4.00	4.00	4.77	4.26	3.24	5.30
Eu	1.59	1.75	1.20	1.06	1.13	1.37	1.72	1.45	1.23	1.59
Gd	4.69	5.03	4.12	4.66	4.67	4.63	5.43	4.87	3.96	5.73
Tb	0.85	0.83	0.73	0.81	0.80	0.77	0.91	0.81	0.74	0.97
Dy	4.86	4.96	4.97	6.22	5.64	5.21	5.81	5.18	4.48	5.63
Ho	0.94	1.02	1.14	1.30	1.17	1.06	1.36	1.15	0.94	1.13
Er	2.54	2.71	3.18	3.85	3.17	3.16	3.61	3.28	2.75	3.08
Tm	0.35	0.35	0.55	0.65	0.50	0.45	0.55	0.50	0.40	0.45
Yb	2.32	2.36	3.20	4.20	3.40	2.90	3.52	3.04	2.40	2.68
Lu	0.31	0.34	0.43	0.61	0.47	0.43	0.49	0.46	0.38	0.35
Precious metals (ppb)										
Au	6.00	6.00	6.00	5.00	15.00	2.00	2.00	1.00	2.00	2.00
Pt	-1.00	-1.00	-1.00	3.00	3.00	-1.00	-1.00	-1.00	-1.00	-1.00
Pd	1.00	-1.00	-1.00	4.00	3.00	-1.00	-1.00	-1.00	-1.00	-1.00
Eu/Eu*	1.04	1.09	1.00	0.72	0.80	0.97	1.03	0.97	1.05	0.88
$(La/Yb)_N$	3.43	3.43	1.84	1.88	2.32	2.47	2.14	2.43	2.78	2.86
Mg#	35	34	35	39	42	31	31	28	31	32
Total REE	81.91	85.88	65.09	81.98	76.80	73.91	84.47	76.42	65.83	87.54

$Eu/Eu^* = (Eu/(Sm \times Gd))_N^{0.5}$

Normalising values from Taylor and McLennon 1995

Mg# = (Mg/[Mg+Fe]x100)

Appendix 1 Supplementary material for Heterogeneity of the sub-continental lithospheric mantle and 'non-juvenile' mantle additions to a Proterozoic silicic large igneous province

Appendix 1 Table A1 Whole-rock geochemical composition for mafic Hiltaba Suite samples

Sample	**662450**	**2465598**	**2465599**	**2465634**	**2465633**	**2465596**	**2131954**	**2465620**	**2465618**	**2465621**
Sample Type	drill core	pulp	pulp	pulp	pulp	pulp	drill core	pulp	pulp	pulp
Drill Hole	DDH C7	CPN DD5	CPN DD5	CPN DD4	CPN DD4	DD87LR3	DD89LR 21	CPN DD5	CPN DD5	CPN DD5
Depth From	186.7	63.03	68.86	201.89	186.34	163.46	252.8	67.38	64.12	75.75
Depth To		63.71	69.3	202.04	186.9	163.86	253.8	67.82	64.6	76.4
Data Source	This study	This study	This study	This study	This study	This study	This study	This study	This study	This study
Location	Kimba	Leonard Rise	Leonard Rise	Leonard Rise	Leonard Rise	Leonard Rise	Leonard Rise	Leonard Rise	Leonard Rise	Leonard Rise
E	568045	480706	480706	485454	485454	462979	505329	480706	480706	480706
N	6319261	6765492	6765492	6765897	6765897	6768172	6773497	6765492	6765492	6765492
Zone	53	53	53	53	53	53	53	53	53	53
Lithology	gabbronorite	gabbro	gabbro	gabbro	gabbro	gabbro	gabbro	gabbro	gabbro	gabbro
Major elements (wt %)										
SiO_2	45.30	50.15	51.00	46.57	46.59	49.05	47.90	50.47	51.11	50.19
TiO_2	1.72	1.62	1.54	2.25	2.28	2.37	2.73	1.53	1.58	1.42
Al_2O_3	14.60	14.90	15.04	13.71	13.37	13.52	13.85	15.17	14.69	15.23
FeO		10.60	9.81	12.00	12.40	12.90	7.93	10.00	10.40	8.99
Fe_2O_3	16.60	12.70	12.20	15.80	16.20	16.10	12.08	12.40	12.40	12.20
MnO	0.22	0.24	0.23	0.28	0.26	0.29	0.19	0.23	0.23	0.23
MgO	7.62	5.86	5.73	5.50	5.65	6.24	5.31	5.93	6.00	5.77
CaO	10.40	9.09	8.83	10.22	10.17	7.74	10.76	9.20	9.16	8.87
Na_2O	2.30	2.44	2.52	2.43	2.24	1.81	3.27	2.57	2.46	2.48
K_2O	1.09	1.63	1.68	1.21	0.97	1.99	1.70	1.57	1.68	1.55
P_2O_5	0.18	0.57	0.50	1.63	1.43	0.69	1.35	0.57	0.48	0.38
LOI	1.76	0.50	0.53	0.11	0.86	-0.13	0.29	0.17	0.12	1.37
F		0.07	0.09	0.11	0.10	0.04		0.07	0.04	0.04
Trace and rare earth elements (ppm)										
Ga	23.50	19.40	19.00	18.70	18.20	18.00	19.20	18.60	18.00	19.00
Cr	80.00	150.00	149.00	62.00	137.00	233.00	64.00	126.00	136.00	120.00
Ni	70.00	45.00	45.00	20.00	20.00	50.00	45.00	45.00	45.00	40.00
Co	60.00	45.30	43.50	49.20	53.80	57.20	49.60	53.50	52.50	56.80
Sc	36.00	27.00	27.60	36.60	34.60	26.30	31.60	27.70	29.00	24.00
Ti		9390.00	9020.00	14100.00	13400.00	13700.00	16600.00	9160.00	9230.00	8480.00
V	310.00	179.00	177.00	173.00	179.00	214.00	255.00	166.00	171.00	154.00
Cu	17.00	20.00	15.00	15.00	10.00	50.00	55.00	15.00	15.00	10.00
Zn	115.00	100.00	95.00	115.00	115.00	145.00	70.00	100.00	105.00	105.00
Y	29.00	33.40	31.00	38.10	27.90	32.90	36.10	31.40	33.80	30.10
Rb	14.00	46.30	52.00	35.10	40.60	41.20	47.00	36.90	45.40	36.30
Sr	105.00	240.00	243.00	271.00	262.00	198.00	314.00	263.00	242.00	246.00
Cs	0.50	1.01	1.29	1.29	3.38	0.95	0.72	0.59	0.77	0.60
Ba	70.00	636.00	671.00	559.00	475.00	979.00	459.00	654.00	675.00	636.00
Th	1.00	7.18	8.05	4.54	3.30	2.87	5.08	4.27	5.50	5.43
U	0.85	1.08	1.09	0.60	1.77	0.66	0.81	0.53	0.85	0.99
Pb	5.50	12.00	11.00	9.00	9.00	22.00	9.00	19.00	23.00	19.00
Zr	100.00	220.00	166.00	114.00	39.00	250.00	97.00	158.00	193.00	209.00
Hf	3.00	5.96	4.43	3.00	1.26	6.37	2.72	4.12	5.22	5.39
Nb	13.50	11.70	10.00	6.30	3.42	16.40	16.30	9.54	11.70	11.40
Ta	<2	0.81	0.70	0.54	0.38	1.10	0.82	0.70	0.97	0.98
La	11.50	51.40	43.00	46.30	31.60	50.30	87.30	39.40	43.90	43.80
Ce	26.00	103.00	84.40	98.00	65.50	94.70	178.00	80.30	88.50	81.80
Pr	3.90	12.50	10.40	12.90	8.48	11.90	22.20	9.99	11.20	9.98
Nd	17.50	47.10	40.40	56.30	34.80	44.90	82.60	38.40	41.70	37.40
Sm	4.80	8.43	7.26	10.50	6.84	7.94	13.70	7.28	7.88	6.98
Eu	1.35	2.20	2.06	2.82	2.36	2.27	2.69	2.10	2.03	1.96
Gd	4.40	7.57	6.88	9.45	6.79	7.27	9.80	6.83	7.56	6.69
Tb	0.82	1.12	1.02	1.30	0.90	1.11	1.32	1.01	1.12	0.98
Dy	5.00	6.71	5.98	7.27	5.24	6.38	7.32	5.92	6.71	6.02
Ho	1.00	1.45	1.30	1.44	1.02	1.35	1.41	1.23	1.42	1.25
Er	3.10	3.76	3.61	3.77	2.80	3.86	3.75	3.36	3.95	3.43
Tm	0.40	0.55	0.50	0.50	0.35	0.50	0.50	0.45	0.55	0.50
Yb	3.00	3.52	3.16	2.96	2.28	3.38	3.12	2.98	3.44	3.10
Lu	0.41	0.50	0.44	0.42	0.31	0.50	0.44	0.41	0.52	0.45
Precious metals (ppb)										
Au	<1	6.00	3.00	4.00	6.00	7.00	2.00	11.00	4.00	4.00
Pt	2.40	-1.00	-1.00	-1.00	13.00	2.00	-1.00	5.00	-1.00	5.00
Pd	<0.2	-1.00	-1.00	-1.00	-1.00	1.00	-1.00	1.00	1.00	-1.00
Eu/Eu*	0.90	0.84	0.89	0.87	1.06	0.91	0.71	0.91	0.80	0.88
$(La/Yb)_N$	2.75	10.47	9.76	11.22	9.94	10.67	20.07	9.48	9.15	10.13
Mg#	48	32	33	27	27	29	33	33	33	34
Total REE	83.18	249.81	210.41	253.93	169.27	236.36	414.15	199.66	220.48	204.34

$Eu/Eu^* = (Eu/(Sm \times Gd))_N^{0.5}$

Normalising values from Taylor and McLennon 1995

Mg# = (Mg/[Mg+Fe]x100)

Appendix 1 Supplementary material for Heterogeneity of the sub-continental lithospheric mantle and 'non-juvenile' mantle additions to a Proterozoic silicic large igneous province

Appendix 1 Table A1 Whole-rock geochemical composition for mafic Hiltaba Suite samples

Sample	**2465619**	**2465597**	**2465617**	**2465616**	**2442108**	**2442106**	**2442105**	**18WPGTC-04**	**2442091**	**2442089**
Sample Type	pulp	pulp	pulp	pulp	drill core	drill core	drill core	out crop	drill core	drill core
Drill Hole	CPN DD5	DD87LR 3	DD87LR3	DD87LR3	DD86EN 46	RR DH 06 01	RR DH 06 01		99DD252	99DD254
Depth From	64.18	202.38	229.88	223.14	96.57	72.4	64.2		84.35	142.42
Depth To	66.3	202.78	230.28	223.54	96.87	73.35	64.85		84.75	142.7
Data Source	This study	This study	This study	This study	This study	This study	This study	This study	This study	This study
Location	Leonard Rise	Leonard Rise	Leonard Rise	Leonard Rise	Mt Brady	Robin Rise	Robin Rise	Tarcoola	White Hill	White Hill
E	480706	462979	462979	462979	508129	456993	456993	455149	561459	559079
N	6765492	6768172	6768172	6768172	6773722	6752788	6752788	6603235	6718232	6720282
Zone	53	53	53	53	53	53	53	53	53	53
Lithology	gabbro	gabbro	gabbro	gabbro	ahpanitic dyke	gabbro	gabbro	diorite	gabbro	gabbro
Major elements (wt %)										
SiO_2	51.16	48.88	49.27	49.32	49.23	49.71	51.00	48.64	49.04	50.98
TiO_2	1.60	1.50	0.93	0.86	1.34	1.21	1.15	1.20	0.92	0.56
Al_2O_3	14.74	13.20	15.06	15.52	14.11	16.74	14.42	12.92	11.03	13.77
FeO	10.50	14.10	10.40	9.50	8.69	7.88	8.57	5.18	8.65	5.42
Fe_2O_3	12.50	17.00	12.60	11.60	12.10	10.60	10.90	10.30	14.90	9.69
MnO	0.23	0.25	0.21	0.19	0.20	0.18	0.20	0.22	0.12	0.06
MgO	5.84	6.50	7.60	7.06	8.00	7.11	8.27	6.69	9.69	7.76
CaO	9.01	10.27	11.90	12.71	10.58	10.02	9.10	8.02	9.02	10.53
Na_2O	2.46	2.11	1.56	1.70	2.41	2.53	2.42	1.72	2.98	4.41
K_2O	1.57	0.49	0.69	0.67	0.67	1.30	1.65	1.70	0.90	0.79
P_2O_5	0.53	0.14	0.09	0.10	0.10	0.32	0.26	0.30	0.26	0.13
LOI	0.16	-0.31	-0.07	0.32	1.17	0.28	0.66	7.82	0.99	0.72
F	0.04	0.11	0.02	0.02	0.02	0.04	0.08	0.07	0.26	0.13
Trace and rare earth elements (ppm)										
Ga	18.70	17.60	15.80	16.20	18.60	18.20	16.90	17.20	14.70	12.80
Cr	169.00	96.00	144.00	203.00	363.00	265.00	387.00	412.00	133.00	302.00
Ni	45.00	55.00	60.00	60.00	160.00	140.00	150.00	90.00	210.00	155.00
Co	52.20	68.40	78.00	65.30	50.50	43.80	43.80	43.90	63.40	29.80
Sc	27.80	50.80	46.10	43.10	42.60	29.10	31.10	31.70	29.30	24.60
Ti	9260.00	8980.00	5520.00	5150.00	8310.00	6960.00	6910.00	7310.00	5160.00	2950.00
V	175.00	344.00	250.00	240.00	371.00	167.00	188.00	247.00	241.00	120.00
Cu	15.00	50.00	25.00	35.00	110.00	55.00	35.00	85.00	85.00	50.00
Zn	95.00	125.00	120.00	105.00	70.00	75.00	100.00	200.00	15.00	10.00
Y	32.10	28.90	20.20	19.30	24.50	32.20	25.80	23.10	26.40	17.50
Rb	38.10	5.75	24.80	27.10	26.30	53.10	107.00	41.60	32.30	34.90
Sr	238.00	128.00	148.00	164.00	182.00	176.00	155.00	326.00	596.00	421.00
Cs	0.78	0.34	0.47	1.66	1.11	2.35	7.57	1.67	0.88	2.39
Ba	635.00	98.00	132.00	88.00	190.00	413.00	224.00	519.00	254.00	100.00
Th	6.16	1.64	2.35	6.37	1.20	7.18	7.31	3.09	19.90	14.00
U	1.08	0.25	0.30	0.59	0.29	1.54	1.48	0.97	2.41	3.32
Pb	11.00	5.00	32.00	29.00	2.00	10.00	15.00	20.00	3.00	2.00
Zr	132.00	86.00	66.00	52.50	82.50	266.00	133.00	130.00	158.00	93.00
Hf	3.69	2.65	2.01	1.56	2.50	6.46	3.56	3.64	4.32	2.67
Nb	11.00	5.92	5.15	5.89	6.00	10.00	8.06	9.22	12.80	6.64
Ta	0.82	0.46	0.62	0.60	0.39	0.57	0.53	0.53	0.80	0.56
La	41.90	10.80	9.88	10.10	6.78	31.70	25.40	18.80	47.60	40.90
Ce	87.30	25.00	22.20	23.70	16.90	66.10	52.00	39.50	104.00	73.30
Pr	10.90	3.41	3.03	3.15	2.35	8.30	6.47	5.49	11.80	9.68
Nd	41.20	13.80	12.10	12.30	10.40	31.90	26.70	23.80	43.80	32.30
Sm	7.57	3.56	2.89	2.72	3.14	6.37	5.19	5.54	7.93	5.19
Eu	2.05	1.18	0.94	0.84	1.19	1.72	1.26	1.68	1.51	1.20
Gd	7.19	4.63	3.69	3.33	3.68	6.13	4.78	5.35	5.94	3.99
Tb	1.06	0.84	0.57	0.53	0.65	0.92	0.76	0.88	0.86	0.57
Dy	6.45	5.57	3.91	3.52	4.11	5.85	4.44	4.67	5.00	3.16
Ho	1.30	1.24	0.86	0.80	0.85	1.21	0.92	0.96	1.07	0.63
Er	3.48	3.53	2.54	2.33	2.50	3.65	2.74	2.38	2.96	1.92
Tm	0.50	0.55	0.35	0.35	0.35	0.50	0.40	0.40	0.45	0.25
Yb	3.34	3.38	2.26	2.22	2.16	3.36	2.42	2.30	2.62	1.86
Lu	0.47	0.49	0.32	0.30	0.31	0.47	0.36	0.35	0.38	0.23
Precious metals (ppb)										
Au	10.00	6.00	7.00	7.00	4.00	-1.00	-1.00	16.00	2.00	1.00
Pt	11.00	-1.00	6.00	5.00	6.00	-1.00	-1.00	8.00	1.00	1.00
Pd	1.00	-1.00	1.00	-1.00	17.00	-1.00	-1.00	9.00	2.00	4.00
Eu/Eu*	0.85	0.89	0.88	0.85	1.07	0.84	0.77	0.94	0.67	0.81
$(La/Yb)_N$	9.00	2.29	3.14	3.26	2.25	6.77	7.53	5.86	13.03	15.77
Mg#	32	28	38	39	42	42	45	45	44	49
Total REE	214.71	77.98	65.54	66.19	55.37	168.18	133.84	112.10	235.92	175.18

$Eu/Eu^* = (Eu/(Sm \times Gd))_N^{0.5}$

Normalising values from Taylor and McLennon 1995

Mg# = (Mg/[Mg+Fe]x100)

Appendix 1 Supplementary material for Heterogeneity of the sub-continental lithospheric mantle and 'non-juvenile' mantle additions to a Proterozoic silicic large igneous province

Appendix 1 Table A1 Whole-rock geochemical composition for mafic Hiltaba Suite samples

Sample	**2495984**	**2495983**	**698127**	**698128**	**698129**	**2495981**	**2495982**
Sample Type	drill core	drill core	drill core	drill core	drill core	drill core	drill core
Drill Hole	DD90WU25	DD90WU25	DD90WU25	DD90WU25	DD90WU25	DD90WU25	DD90WU25
Depth From	51.76	68.04	181.05	185.65	192.65	179.2	172.68
Depth To	52.2	68.39				179.4	177.9
Data Source	This study	This study	This study	This study	This study	This study	This study
Location	Wudinna	Wudinna	Wudinna	Wudinna	Wudinna	Wudinna	Wudinna
E	573929	573929	573929	573929	573929	573929	573929
N	6339271	6339271	6339271	6339271	6339271	6339271	6339271
Zone	53	53	53	53	53	53	53
Lithology	gabbro	gabbro	gabbro	gabbro	gabbro	gabbro	gabbro
Major elements (wt %)							
SiO_2	46.22	47.31	47.00	46.70	46.50	45.66	49.63
TiO_2	1.06	1.12	1.24	1.19	1.20	1.35	1.24
Al_2O_3	13.39	12.85	13.90	13.70	13.40	14.31	10.62
FeO	7.03	7.56				7.86	7.73
Fe_2O_3	12.60	13.50	13.00	13.50	13.60	13.32	15.01
MnO	0.26	0.27	0.22	0.23	0.25	0.23	0.21
MgO	9.22	9.02	8.42	8.45	8.68	8.37	8.92
CaO	10.03	9.14	8.93	9.47	9.10	8.63	8.72
Na_2O	2.00	2.02	2.07	2.10	2.05	1.65	1.44
K_2O	1.99	1.42	2.08	1.19	2.12	2.42	1.32
P_2O_5	0.82	0.42	0.54	0.53	0.44	0.65	0.46
LOI	1.68	2.18	2.75	2.80	2.58	2.93	2.08
F							
Trace and rare earth elements (ppm)							
Ga	18.00	18.00	21.00	22.00	21.00	21.30	17.50
Cr	134.00	152.00	160.00	150.00	160.00	144.00	121.00
Ni	75.00	80.00	68.00	68.00	72.00	70.00	70.00
Co	55.00	58.80	60.00	64.00	56.00	55.70	68.70
Sc	41.20	41.60				45.40	39.60
Ti	6460.00	6820.00				8080.00	7610.00
V	249.00	288.00				301.00	341.00
Cu	120.00	110.00	130.00	115.00	115.00	90.00	125.00
Zn	115.00	115.00	110.00	115.00	120.00	110.00	100.00
Y	21.70	24.80	28.50	28.00	29.00	37.00	41.10
Rb	64.00	48.40	74.00	40.50	82.00	113.00	60.70
Sr	560.00	454.00	600.00	550.00	600.00	539.00	440.00
Cs	0.39	0.30	0.40	0.20	0.50	0.84	0.68
Ba	865.00	461.00	600.00	260.00	700.00	760.00	3000.00
Th	3.31	7.16	5.50	5.50	11.00	4.20	7.80
U	1.52	1.77	1.25	1.50	2.80	1.80	1.67
Pb	6.00	5.00	17.00	11.50	13.50	12.00	7.00
Zr	66.50	83.50	80.00	80.00	110.00	66.00	84.50
Hf	2.06	2.84	2.00	3.00	3.00	2.69	2.88
Nb	5.06	6.35	8.00	8.50	9.50	9.69	9.42
Ta	0.34	0.40	<2	<2	<2	0.49	0.62
La	20.20	25.00	30.50	31.00	36.50	28.60	51.00
Ce	48.20	58.70	64.00	66.00	74.00	76.70	128.00
Pr	7.02	8.52	9.50	10.00	10.50	11.80	18.80
Nd	31.10	36.70	40.00	41.50	41.50	52.30	81.00
Sm	7.28	8.07	9.50	9.50	9.00	12.00	17.40
Eu	1.55	1.97	2.20	2.10	2.20	2.58	2.12
Gd	6.21	6.89	7.00	7.00	7.00	9.99	12.90
Tb	0.86	1.03	1.00	0.98	0.99	1.41	1.84
Dy	4.45	5.37	6.00	6.00	6.00	7.69	8.94
Ho	0.84	0.98	1.05	1.00	1.10	1.48	1.66
Er	2.22	2.62	2.80	2.70	2.80	3.74	4.25
Tm	0.30	0.35	0.35	0.35	0.35	0.50	0.55
Yb	1.92	2.14	2.30	2.30	2.50	2.96	3.10
Lu	0.25	0.29	0.30	0.29	0.34	0.41	0.39
Precious metals (ppb)							
Au	4.00	3.00	1.00	<1	2.00	3.00	3.00
Pt	1.00	1.00				1.00	1.00
Pd	1.00	2.00				1.00	1.00
Eu/Eu*	0.70	0.81	0.82	0.79	0.85	0.72	0.43
$(La/Yb)_N$	7.55	8.38	9.51	9.67	10.47	6.93	11.80
Mg#	47	45	56	55	56	43	43
Total REE	132.40	158.63	176.50	180.72	194.78	212.16	331.95

$Eu/Eu^* = (Eu/(Sm \times Gd))_N^{0.5}$

Normalising values from Taylor and McLennon 1995

Mg# = (Mg/[Mg+Fe]x100)

1 Figure A1 Selected major and trace elements versus LOI for the mafic Hiltaba Suite

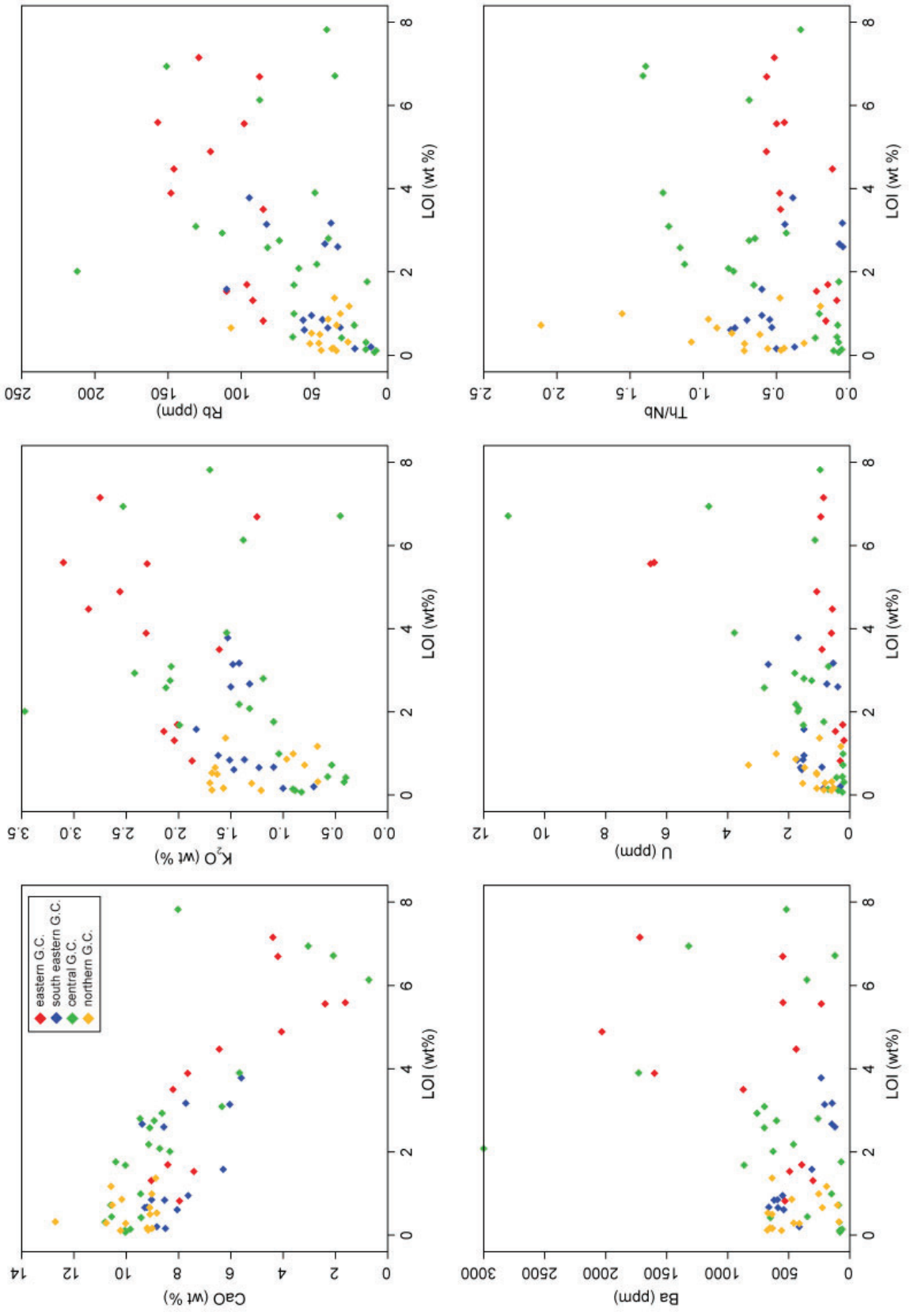

Appendix 2

Supplementary material for: Supplementary material for Subcontinental lithospheric mantle contribution to granites in a silicic large igneous province: Geochemistry and Nd isotopic constraints

Appendix 2 Supplementary material for Subcontinental lithospheric mantle contribution to granites in a silicic large igneous province: Geochemistry and Nd isotopic constraints

Appendix 2 Table A1 Mantle types identified and their average $\varepsilon_{Nd(1590\ Ma)}$ and Nd average compositions used in the mixing calculations

Mantle Type	Mantle Group Number	Mantle type	Average $\varepsilon_{Nd(1590\ Ma)}$	Average Nd (ppm)
M1	3	Depleted SCLM	0.7	11.87
M2	5	EM/SCLM	0.6	24.94
M3	8	E-MORB/EM	0.5	20.36
M4	8+5	E-MORB/EM + EM/SCLM	0.5	22.65
M5	11	SCLM/E-MORB	-1.9	39.81
M6	13	EM/SCLM	-2.0	22.34
M7	15	SCLM	-2.0	22.32
M8	12+15	SCLM	-2.2	42.57
M9	12	SCLM	-2.4	62.82

Mantle group number corresponds to closest granitoid pluton group as per Figure 1, Figure 10 and Table 2.

SCLM: subcontinental lithospheric mantle; EM: enriched mantle; E-MORB: enriched mid ocean ridge basalt.

Appendix 2 Supplementary material for Subcontinental lithospheric mantle contribution to granites in a silicic large igneous province: Geochemistry and Nd isotopic constraints

Appendix Table A2 Host rocks to the Hiltaba Suite granitoids and their average $\varepsilon_{Nd(1590\ Ma)}$ and average Nd compositions used in the mixing calculations

Host Rock	Age (Ma)	Average $\varepsilon_{Nd(1590\ Ma)}$	Average Nd (ppm)	Data Source
1	3150	-21.4	21.09	Fraser *et al.* (2010)
2	2575	-13.06	12.00	Szpunar *et al.* (2011)
3	2520-2400	-10.4	28.55	Swain *et al.* (2005)
4	2000	-10.9	29.40	Szpunar *et al.* (2011)
5	1865	-8.9	77.77	Szpunar *et al.* (2011)
6	1850	-4.8	57.74	Schaefer (1998)
7	1790-1720 (msed)	-6.3	35.18	Howard *et al.* (2011b)
8	1790	-7.3	77.07	Szpunar *et al.* (2011)
9	1760 (msed)	-5.2	49.54	Howard *et al.* (2011a)
10	1750(msed)	-4.7	35.60	Szpunar *et al.* (2011)
11	1750-1700	-9.3	58.72	Wade and McAvaney (2017)
12	1690	-3.5	36.91	Payne *et al.* (2010)
13	1650	-2.4	33.30	Wade (2012)
14	1620	-2.1	28.50	Swain *et al.* (2008), Reid *et al.* (2019)

All host rocks are igneous or metaigneous except for those denoted by msed (metasedimentary rock).

References

Fraser, G. L., McAvaney, S., Neumann, N., Szpunar, M. and Reid, A., 2010. Discovery of early Mesoarchean crust in the eastern Gawler Craton, South Australia. Precambrian Research, v. 179, p. 1–21. doi: https://doi.org/10.1016/j.precamres.2010.02.008

Howard, K. E., Hand, M., Barovich, K. and Belousova, E., 2011a. Provenance of late Paleoproterozoic cover sequences in the central Gawler Craton: exploring stratigraphic correlations in eastern Proterozoic Australia using detrital zircon ages, Hf and Nd isotopic data. Australian Journal of Earth Sciences, v. 58, p. 475–500. doi: https://doi.org/10.1080/08120099.2011.577753

Howard, K. E., Hand, M., Barovich, K. M., Payne, J. L. and Belousova, E. A., 2011b. U-Pb, Lu-Hf and Sm-Nd isotopic constraints on provenance and depositional timing of metasedimentary rocks in the western Gawler Craton: Implications for Proterozoic reconstruction models. Precambrian Research, v. 184, p. 43–62. doi: https://doi.org/10.1016/j.precamres.2010.10.002

Payne, J. L., Ferris, G., Barovich, K. M. and Hand, M., 2010. Pitfalls of classifying ancient magmatic suites with tectonic discrimination diagrams: An example from the Paleoproterozoic Tunkillia Suite, southern Australia. Precambrian Research, v. 177, p. 227-240. doi: https://doi.org/10.1016/j.precamres.2009.12.005

Reid, A. J., Pawley, M. J., Wade, C., Jagodzinski, E. A., Dutch, R. A. and Armstrong, R., 2019. Resolving tectonic settings of ancient magmatic suites using structural, geochemical and isotopic constraints: the example of the St Peter Suite, southern Australia. Australian Journal of Earth Sciences, v. p. 1-28. doi: https://10.1080/08120099.2019.1632224

Schaefer, B. F., 1998. Insights into Proterozoic tectonics from the southern Eyre Peninsula, South Australia. University of Adelaide, PhD thesis (unpublished).

Swain, G., Barovich, K., Hand, M., Ferris, G. and Schwarz, M., 2008. Petrogenesis of the St Peter Suite, southern Australia: arc magmatism and Proterozoic crustal growth of the South Australian Craton. Precambrian Research, v. 166, p. 283-296. doi: https://doi.org/10.1016/j.precamres.2007.07.028

Swain, G., Woodhouse, A., Hand, M., Barovich, K., Schwarz, M. and Fanning, C. M., 2005. Provenance and tectonic development of the late Archaean Gawler Craton, Australia; U-Pb zircon, geochemical and Sm-Nd isotopic implications. Precambrian Research, v. 141, p. 106-136. doi: https://doi.org/10.1016/j.precamres.2005.08.004

Szpunar, M., Hand, M., Barovich, K., Jagodzinski, E. and Belousova, E., 2011. Isotopic and geochemical constraints on the Paleoproterozoic Hutchison Group, southern Australia: Implications for Paleoproterozoic continental reconstructions. Precambrian Research, v. 187, p. 99-126. doi: https://doi.org/10.1016/j.precamres.2011.02.006

Wade, C. E., 2012. Geochemistry of pre-1570 Ma mafic magmatism within Southern Australia: implications for possible tectonic settings and of major mineralisation events in South Australia. Geological Survey of South Australia, v. Report Book 2012/00019, p. 270. Available at: https://sarigbasis.pir.sa.gov.au/WebtopEw/ws/samref/sarig1/image/DDD/RB201200019.pdf

Wade, C. E. and McAvaney, S., 2017. Stratigraphy and geochemistry of the 1745–1700 Ma Peter Pan Supersuite. v. RB 2016/00026, p. 71. Available at: https://sarigbasis.pir.sa.gov.au/WebtopEw/ws/samref/sarig1/wcir/Record?r=0&m=1&w=catno=2039428

Appendix 2 Supplementary material for Subcontinental lithospheric mantle contribution to granites in a silicic large igneous province: Geochemistry and Nd isotopic constraints

Appendix Table 2 A3: Host rock types to the Hiltaba Suite granitoids and their average $\varepsilon_{Nd(1590\ Ma)}$ and Nd average compositions used in the mixing calculations

Crust Type	Crust type	Crust age (Ma)	Host Rock number	Average $\varepsilon_{Nd(1590\ Ma)}$	Average Nd (ppm)
C1	Neoarchean, Mesoarchean, Palaeoproterozoic	3150–1700	1,2,3,4,5,7,8,9,11	-10.3	43.26
C2	Mesoarchean, Palaeoproterozoic	2575–1690	2,3,4,5,7,9,11,12	-9.0	41.59
C3	Mesoarchean, Palaeoproterozoic	2520–1750	3,6,10	-6.6	40.63
C4	Palaeoproterozoic	1850–1750	6,10	-4.7	46.67
C5	Mesoarchean, Palaeoproterozoic, Mesoproterozoic	2520–1620	3,7,9,11,12,13,14	-5.6	38.67

Crust type is the average of the host rocks listed. Host rock numbers refers to those listed in Appendix 2 Table A2.

Appendix 2 Table A4 New whole-rock geochemical data for Hiltaba Suite samples collected in this study

Sample	1834104	1834093	1834103	3687881	3687882	3687842	3687841	3687840	3687880	2696084	2696083	2696081
Other Sample Name				1077-30	1077-31	1077-29	1077-28	1077-26	1077-27			
Drill Hole										BUL 62	BUL 62	BUL 57
Depth From (m)										32.00	28.00	12.00
Depth To (m)										38.00	32.00	14.00
Easting	346846	345002	344412	438820	438820	441000	441000	440994	441001	455151	455151	454941
Northing	6524084	6527350	6520811	6597066	6597066	6596800	6596800	6597669	6596802	6652487	6652487	6644751
Zone	53	53	53	53	53	53	53	53	53	53	53.00	53
Longitude	133.3628	133.3700	133.3628			134.3835	134.3835	134.3835		134.5338	134.5338	134.5313
Latitude	31.4370	-31.3781	-31.4370			-30.7603	-30.7603	-30.7525		-30.2584	-30.2584	-30.3282
Datum	GDA94	GDA94	GDA94			GDA94	GDA94	GDA94		GDA94	GDA94	GDA94
Granite Group	2	2	2	5	5	5	5	5	5	7	7	7
Mantle Group	3	3	3	5	5	5	5	5	5	5	5	5
Major elements (wt %)												
SiO_2	64.40	69.60	67.60	72.94	76.93	77.45	77.35	72.67	77.18	65.88	66.37	69.16
TiO2	0.67	0.48	0.79	0.22	0.09	0.08	0.04	0.30	0.05	0.32	0.25	0.84
Al_2O_3	14.80	13.70	13.60	13.96	12.32	12.02	12.63	13.74	12.44	17.57	18.06	14.44
Fe_2O_{3t}	4.82	3.20	5.47	1.95	1.15	0.99	0.80	2.43	0.93	2.80	1.86	4.00
MnO	1.51	0.60	1.12	0.06	0.04	0.06	0.03	0.06	0.03	0.03	0.03	0.04
MgO	0.13	0.13	0.14	0.33	0.13	0.09	0.04	0.52	0.06	0.26	0.20	0.36
CaO	2.80	1.63	2.60	1.06	0.53	0.31	0.39	1.30	0.50	0.78	0.78	0.43
Na_2O	2.72	2.86	2.68	3.54	3.51	3.53	4.07	3.23	3.85	4.71	4.81	3.68
K_2O	4.63	5.21	4.45	5.40	4.82	4.76	4.29	5.06	4.36	6.45	6.61	5.40
P_2O_5	0.28	0.19	0.21	0.05	0.01	0.03	0.01	0.07	0.01	0.08	0.04	0.10
FeO	2.62	1.54	2.94	1.22	0.59	0.33	0.25	1.67	0.34	0.31	0.42	0.36
LOI	1.36	1.04	1.05	0.43	0.45	0.48	0.36	0.57	0.50	0.86	0.70	1.23
Total	100.74	100.18	102.65	101.16	100.57	100.13	100.26	101.62	100.25	100.05	99.71	99.68
Trace and rare earth elements (ppm)												
Sc	10.00	10.00	15.00	6.00	3.30	3.70	3.00	7.10	3.80	3.20	4.10	11.50
V	60.00	22.00	65.00	11.00	2.20	1.50	1.70	20.90	0.50	20.20	13.60	29.70
Cr	17.00	3.00	6.00	6.00	3.00	2.00	14.00	8.00	2.00	117.00	116.00	163.00
Co	11.50	4.80	11.50	37.10	54.20	55.30	40.50	44.50	32.90	4.20	3.50	4.10
Ni	19.00	5.00	11.00	8.00	-2.00	6.00	4.00	12.00	6.00	14.00	12.00	18.00
Cu	105.00	9.00	30.00	10.00	16.00	6.00	-2.00	24.00	-2.00	10.00	20.00	8.00
Zn	85.00	80.00	80.00	70.00	40.00	85.00	40.00	85.00	60.00	50.00	65.00	80.00
Ga	21.00	21.50	20.50	20.40	19.40	19.50	23.90	18.90	23.00	18.00	18.30	19.80
Rb	225.00	290.00	210.00	236.00	306.00	354.00	356.00	248.00	452.00	177.00	192.00	178.00
Sr	115.00	125.00	120.00	91.30	20.10	19.10	7.90	108.00	8.30	560.00	582.00	262.00
Y	41.00	50.00	50.00	37.10	45.10	56.30	54.60	30.30	85.10	14.70	25.50	36.80
Zr	410.00	290.00	325.00	200.00	123.00	117.00	92.00	238.00	118.00	258.00	229.00	373.00
Nb	26.50	34.50	26.00	16.60	23.50	26.60	32.50	14.10	40.10	10.60	8.45	14.10
Mo	1.10	0.40	1.00	1.20	2.60	15.00	0.80	2.20	0.80	1.00	1.20	2.20
Sn	0.00	0.00	0.00	3.80	3.00	4.80	6.60	5.60	7.00	1.20	1.60	2.80
Cs	5.50	10.00	7.00	7.93	8.01	5.58	9.21	14.00	12.20	1.82	1.91	2.26
Ba	745.00	740.00	780.00	585.00	95.50	80.00	66.00	601.00	37.50	1380.00	1440.00	1970.00
La	70.00	85.00	50.00	69.20	32.10	32.60	6.04	56.70	19.40	74.90	75.50	32.40
Ce	165.00	175.00	115.00	120.00	68.90	71.80	19.00	110.00	42.70	130.00	145.00	66.20
Pr	21.00	19.50	14.50	13.90	8.20	8.78	1.99	12.30	5.73	13.20	17.20	8.20
Nd	85.00	75.00	60.00	50.00	32.10	34.30	8.37	41.40	23.40	43.50	64.10	34.10
Sm	16.00	14.00	12.00	8.75	7.28	8.33	3.29	7.49	7.35	5.79	9.90	6.75
Eu	1.80	2.20	1.90	0.85	0.21	0.20	0.07	0.71	0.09	1.54	2.00	2.45
Gd	13.50	12.50	11.50	7.39	7.05	8.65	4.73	5.97	9.08	4.13	7.52	6.24
Tb	1.80	1.90	1.80	1.13	1.20	1.47	1.21	0.89	1.89	0.54	0.99	1.01
Dy	10.00	11.50	11.50	6.47	7.47	9.56	9.08	5.44	12.40	2.79	4.83	6.41
Ho	1.80	2.10	2.20	1.32	1.57	1.97	2.11	1.09	2.81	0.52	0.94	1.41
Er	5.50	6.00	6.50	3.65	4.79	5.89	6.77	3.47	8.74	1.55	2.32	4.28
Tm	0.65	0.80	0.85	0.56	0.77	0.95	1.07	0.48	1.36	0.21	0.33	0.67
Yb	4.90	6.00	6.00	3.82	4.98	6.24	7.72	3.24	9.60	1.34	2.20	4.59
Lu	1.10	0.62	0.86	0.55	0.72	0.98	1.06	0.43	1.36	0.22	0.29	0.65
Hf	11.00	7.00	9.00	6.02	5.04	5.32	5.19	6.84	6.32	5.60	5.21	9.05
Ta	0.00	0.00	0.00	1.94	2.79	3.42	3.38	1.60	3.62	0.33	0.37	1.00
Pb	26.00	35.00	25.00	39.00	49.00	63.00	68.00	41.00	53.00	17.00	17.00	21.00
Th	37.00	31.00	23.50	20.80	30.30	29.50	41.20	21.20	42.60	10.40	8.67	14.80
U	3.20	4.80	3.10	3.86	8.46	8.30	8.94	4.49	13.60	2.66	2.91	3.06
F	0.00	0.00	0.00	800.00	900.00	1000.00	700.00	1300.00	2200.00	300.00	200.00	300.00
Zr+Ce+Y+Nb	642.50	549.50	516.00	373.70	260.50	271.70	198.10	392.40	285.90	413.30	407.95	490.10
Ga/Al*10000	2.68	2.97	2.85	2.76	2.98	3.07	3.58	2.60	3.49	1.94	1.91	2.59
ASI	1.03	1.04	0.99	1.03	1.03	1.05	1.05	1.05	1.04	1.09	1.10	1.15
Eu/Eu*	0.37	0.51	0.49	0.32	0.09	0.07	0.05	0.32	0.03	0.96	0.71	1.15
$(La/Yb)_N$	10.25	10.16	5.98	12.99	4.62	3.75	0.56	12.55	1.45	40.09	24.62	5.06
$(La/Sm)_N$	2.82	3.92	2.69	5.11	2.85	2.53	1.19	4.89	1.70	8.35	4.92	3.10
$T_{Zr\ (°C)}$	825.87	799.32	796.65	760.10	720.45	718.82	695.28	782.23	718.08	777.58	766.29	843.04

Appendix 2 Supplementary material for Subcontinental lithospheric mantle contribution to granites in a silicic large igneous province: Geochemistry and Nd isotopic constraints

Appendix 2 Table A4 New whole-rock geochemical data for Hiltaba Suite samples collected in this study

Sample	2696080	2696079	2696082	3687838	3687879	3687796	3687813	3687830	3687807	3687801	3687816	3687826
Other Sample Name				1077-23	1077-21	1077-10	1077-16	1077-183	1077-15	1077-12	1077-17	1077-180
Drill Hole	BUL 57	BUL 56	BUL 58									
Depth From (m)	10.00	10.00	4.00									
Depth To (M)	12.00	12.00	6.00									
Easting	454941	454734	454984	469650	459210	501360	474243	477625	467610	484904	474490	490340
Northing	6644751	6640644	6645484	6539267	6502290	6452510	6467104	6470975	6471636	6470461	6465640	6463460
Zone	53	53	53	53	53	53	53	53	53	53	53	53
Longitude	134.5313	134.5289	134.5317	134.6812		135.0144	134.7275	134.7634	134.6575	134.8403	134.7301	134.8978
Latitude	-30.3282	-30.3653	-30.3216	-31.2805		-32.0636	-31.9317	-31.8968	-31.8906	-31.9016	-31.9449	-31.9648
Datum	GDA94	GDA94	GDA94	GDA94		GDA94	GDA94	GDA94	GDA94	GDA94	GDA94	GDA94
Granite Group	7	7	7	8	8	8	8	8	8	8	8	8
Mantle Group	5	5	5	8	8	8	8	8	8	8	8	8
Major elements (wt %)												
SiO_2	67.79	71.17	72.40	76.20	77.10	76.50	77.50	76.40	75.60	63.80	72.50	69.30
TiO2	0.83	0.58	0.40	0.18	0.09	0.13	0.11	0.13	0.25	0.64	0.36	0.53
Al_2O_3	14.72	13.76	13.62	12.40	12.00	12.10	12.30	12.60	12.60	16.20	13.70	13.90
Fe_2O_{3t}	1.73	4.65	1.79	1.48	1.22	1.38	0.62	1.00	1.32	5.38	2.74	4.12
MnO	0.01	0.04	0.01	0.03	0.04	0.02	0.03	0.04	0.09	0.10	0.07	0.11
MgO	0.39	0.56	0.83	0.12	0.07	0.13	0.07	0.10	0.24	1.44	0.48	0.74
CaO	2.64	0.41	0.96	0.48	0.52	0.40	0.57	0.40	0.64	2.73	1.08	2.08
Na_2O	2.96	1.56	1.79	3.10	3.07	3.13	3.69	3.42	3.41	4.30	3.45	3.37
K_2O	5.14	3.56	3.87	5.70	5.23	5.36	4.86	5.33	5.14	3.43	5.03	5.05
P_2O_5	0.13	0.06	0.02	0.02	0.01	0.01	0.01	0.02	0.05	0.27	0.08	0.13
FeO	0.29	0.39	0.20	0.61	0.69	0.65	0.13	0.41	0.36	2.60	1.81	2.10
LOI	3.45	3.30	3.68	0.39	0.41	0.54	0.40	0.38	0.41	1.24	0.50	0.42
Total	100.08	100.04	99.57	100.71	100.45	100.35	100.28	100.23	100.10	102.13	101.79	101.84
Trace and rare earth elements (ppm)												
Sc	11.60	9.60	6.80	0.20	-0.10	0.80	2.30	2.00	2.90	12.00	4.30	7.40
V	27.50	66.70	48.70	3.00	1.10	1.00	3.20	7.30	9.90	43.00	22.00	31.10
Cr	161.00	198.00	125.00	14.00	5.00	10.00	4.00	254.00	6.00	9.00	11.00	246.00
Co	1.20	5.10	1.90	56.90	70.90	58.20	55.20	2.30	59.50	45.70	51.80	7.20
Ni	14.00	26.00	14.00	10.00	4.00	4.00	4.00	10.00	4.00	8.00	8.00	16.00
Cu	6.00	16.00	36.00	2.00	10.00	6.00	-2.00	10.00	12.00	58.00	6.00	12.00
Zn	30.00	45.00	50.00	40.00	20.00	45.00	15.00	30.00	25.00	45.00	30.00	55.00
Ga	20.10	19.40	18.80	17.70	18.50	18.50	22.00	19.50	19.30	19.10	18.40	18.50
Rb	170.00	136.00	119.00	286.00	384.00	354.00	584.00	562.00	407.00	107.00	196.00	232.00
Sr	444.00	143.00	197.00	45.70	14.60	15.80	12.10	35.90	86.20	569.00	97.80	174.00
Y	43.50	27.00	12.60	81.90	78.00	66.60	12.00	12.50	22.90	28.90	36.40	48.70
Zr	382.00	306.00	214.00	323.00	152.00	173.00	108.00	133.00	168.00	267.00	267.00	329.00
Nb	14.20	13.40	9.36	17.40	24.80	21.40	28.20	18.90	21.20	11.00	14.60	20.00
Mo	1.80	2.80	1.20	1.40	1.80	2.20	3.20	5.20	0.80	1.40	3.40	3.40
Sn	2.80	2.80	2.00	3.20	6.60	5.20	3.00	3.00	2.80	1.60	5.00	4.60
Cs	2.37	2.64	2.48	3.14	7.01	4.83	14.50	11.90	10.00	4.42	3.82	6.39
Ba	2050.00	1060.00	1290.00	144.00	43.00	59.50	40.00	176.00	580.00	2470.00	668.00	1140.00
La	112.00	46.50	35.70	235.00	66.10	85.10	44.90	61.80	61.80	64.80	63.90	71.90
Ce	214.00	83.50	53.90	390.00	125.00	168.00	51.80	74.70	99.20	120.00	124.00	136.00
Pr	23.50	10.70	5.33	45.20	14.60	18.80	3.41	5.34	10.20	13.40	13.90	16.50
Nd	79.70	38.90	17.50	135.00	49.00	61.40	8.59	13.90	30.90	46.70	49.40	53.40
Sm	12.20	7.06	2.74	20.00	9.45	11.90	1.23	1.73	5.16	7.45	8.91	10.60
Eu	3.30	1.53	0.63	0.59	0.27	0.30	0.15	0.34	0.71	1.69	0.83	1.71
Gd	9.37	5.45	2.28	13.50	9.01	10.10	1.00	1.44	3.84	5.52	6.76	8.77
Tb	1.44	0.88	0.39	2.03	1.57	1.74	0.17	0.25	0.58	0.95	1.07	1.34
Dy	8.04	5.11	2.29	12.00	10.30	10.10	1.18	1.58	3.47	4.91	6.45	8.58
Ho	1.61	1.03	0.47	2.53	2.43	2.18	0.29	0.30	0.74	0.99	1.29	1.73
Er	4.51	3.06	1.44	7.58	7.04	6.65	1.07	1.20	2.16	2.94	3.49	4.82
Tm	0.69	0.45	0.24	1.14	1.11	1.07	0.25	0.23	0.35	0.43	0.59	0.69
Yb	4.67	2.99	1.55	8.03	7.69	6.82	1.93	1.97	2.67	2.76	3.35	4.67
Lu	0.63	0.50	0.25	1.21	1.10	0.98	0.39	0.35	0.40	0.40	0.55	0.65
Hf	9.12	7.46	5.39	12.00	6.34	6.73	5.35	5.14	5.89	6.92	7.56	9.33
Ta	1.00	0.96	0.63	2.81	2.83	2.81	2.31	1.05	2.31	0.87	1.74	1.37
Pb	29.00	25.00	24.00	54.00	31.00	26.00	38.00	80.00	45.00	17.00	33.00	32.00
Th	19.70	15.30	9.68	126.00	60.90	57.70	55.00	56.60	41.80	9.54	30.30	27.80
U	2.71	2.42	1.87	23.50	16.50	8.37	9.84	11.70	7.77	1.48	5.92	5.35
F	600.00	300.00	900.00	1000.00	2400.00	2100.00	4100.00	2400.00	2500.00	800.00	400.00	1200.00
Zr+Ce+Y+Nb	653.70	429.90	289.86	812.30	379.80	429.00	200.00	239.10	311.30	426.90	442.00	533.70
Ga/Al*10000	2.58	2.66	2.61	2.70	2.91	2.89	3.38	2.92	2.89	2.23	2.54	2.51
ASI	0.97	1.93	1.54	1.02	1.03	1.04	0.99	1.04	1.02	1.04	1.05	0.95
Eu/Eu*	0.94	0.75	0.77	0.11	0.09	0.08	0.41	0.66	0.49	0.81	0.33	0.54
$(La/Yb)_N$	17.20	11.16	16.52	20.99	6.17	8.95	16.69	22.50	16.60	16.84	13.68	11.04
$(La/Sm)_N$	5.93	4.25	8.41	7.59	4.52	4.62	23.57	23.06	7.73	5.62	4.63	4.38
$T_{Zr(°C)}$	812.85	907.72	835.22	821.25	742.61	755.91	702.99	728.39	747.96	768.32	794.80	789.06

Appendix 2 Table A4 New whole-rock geochemical data for Hiltaba Suite samples collected in this study

Sample	3687825	3687819	3687803	3687820	3687802	3687823	2696089	3687824	3687822	3687828	3687829	2696085	3687837
Other Sample Name	1077-18	1077-174	1077-14	1077-175	1077-13	1077-178	CHI 11	1077-179	1077-177	1077-182	1077-182B		1077-229
Drill Hole													
Depth From (m)													
Depth To (m)													
Easting	488360	464720	464311	464350	466193	484565	484694	488445	474400	488350	488350	463989	488640
Northing	6457269	6478715	6474316	6474035	6472254	6466590	6466762	6465465	6467130	6460220	6460220	6474629	6459770
Zone	53	53	53	53	53	53	53	53	53	53	53	53	53
Longitude	134.8767	134.6272	134.6227	134.6231	134.6425	134.8367	134.8381	134.8777	134.7292	134.8767	134.8767	134.6193	134.8797
Latitude	-32.0206	-31.8267	-31.8664	-31.8689	-31.8850	-31.9365	-31.9350	-31.9467	-31.9315	-31.9940	-31.9940	-31.8635	-31.9981
Datum	GDA94	GDA94	GDA94	GDA94	GDA94	GDA94		GDA94	GDA94	GDA94	GDA94		GDA94
Granite Group	8	8	8	8	8	8	8	8	8	8	8	8	8
Mantle Group	8	8	8	8	8	8	8	8	8	8	8	8	8
Major elements (wt %)													
SiO_2	67.60	73.50	71.30	71.10	71.60	70.37	70.54	78.56	76.72	71.09	77.47	68.15	74.18
TiO2	0.73	0.25	0.39	0.37	0.42	0.25	0.25	0.08	0.10	0.30	0.10	0.61	0.21
Al_2O_3	13.80	13.00	13.50	13.50	13.10	14.84	14.85	11.73	12.14	14.41	11.73	15.23	12.62
Fe_2O_{3t}	5.36	2.65	3.66	3.96	3.71	2.32	2.27	0.86	1.07	2.14	1.05	4.08	2.56
MnO	0.13	0.06	0.11	0.11	0.11	0.07	0.08	0.04	0.05	0.06	0.04	0.08	0.06
MgO	0.68	0.12	0.15	0.12	0.22	0.81	0.82	0.03	0.07	0.60	0.05	0.78	0.19
CaO	2.14	0.69	1.02	1.16	1.25	2.18	1.88	0.10	0.60	1.47	0.65	1.35	0.81
Na_2O	3.43	3.34	3.62	3.60	3.53	4.13	4.14	3.29	3.58	3.83	3.25	3.31	3.28
K_2O	4.94	5.92	5.83	5.82	5.49	3.74	3.88	4.81	4.94	4.80	4.91	5.39	5.61
P_2O_5	0.22	0.03	0.04	0.04	0.06	0.10	0.10	0.05	0.01	0.09	0.02	0.05	0.04
FeO	2.99	1.45	1.67	2.44	1.78	1.02	0.95	0.51	0.57	1.20	0.49	2.32	0.94
LOI	0.50	0.22	0.18	0.12	0.22	1.01	0.96	0.23	0.44	0.88	0.53	0.76	0.25
Total	102.52	101.23	101.46	99.90	101.48	100.84	100.72	100.29	100.29	100.87	100.29	102.11	100.75
Trace and rare earth elements (ppm)													
Sc	11.10	1.30	1.50	3.30	3.40	5.40	4.90	6.90	6.80	4.60	8.10	9.50	5.90
V	20.90	5.80	3.10	6.10	6.10	30.80	28.60	4.90	5.70	19.00	5.20	55.60	7.10
Cr	8.00	243.00	5.00	189.00	4.00	184.00	18.00	391.00	372.00	198.00	247.00	31.00	215.00
Co	43.50	1.50	44.20	1.30	59.90	5.20	4.60	1.70	1.80	3.60	1.80	10.80	2.10
Ni	4.00	8.00	10.00	12.00	6.00	16.00	20.00	12.00	12.00	10.00	8.00	16.00	10.00
Cu	14.00	6.00	40.00	8.00	6.00	4.00	8.00	6.00	4.00	10.00	8.00	148.00	6.00
Zn	90.00	70.00	120.00	150.00	125.00	65.00	65.00	15.00	25.00	50.00	30.00	95.00	85.00
Ga	21.90	20.90	24.00	22.60	21.90	20.90	19.90	23.40	22.80	17.50	22.40	22.60	19.90
Rb	199.00	257.00	158.00	157.00	217.00	173.00	179.00	818.00	664.00	223.00	631.00	247.00	307.00
Sr	166.00	26.20	35.60	31.20	45.30	591.00	607.00	39.90	11.40	357.00	16.90	159.00	66.70
Y	60.60	83.40	83.80	85.40	102.00	12.30	11.80	4.46	7.70	14.40	7.76	30.60	57.40
Zr	382.00	425.00	786.00	792.00	870.00	129.00	130.00	114.00	129.00	209.00	239.00	320.00	318.00
Nb	19.50	23.30	21.70	19.40	29.70	9.12	7.80	31.00	34.00	10.50	25.40	13.10	24.20
Mo	1.80	3.00	1.40	2.80	1.20	2.20	-0.20	5.60	4.80	3.20	4.80	1.20	3.00
Sn	3.80	4.60	3.20	3.60	5.80	2.40	2.00	4.20	4.40	2.60	3.40	8.40	4.00
Cs	3.16	9.07	4.22	4.52	6.20	5.92	6.22	10.80	11.90	6.83	13.00	8.44	6.75
Ba	1410.00	586.00	842.00	908.00	693.00	937.00	1000.00	25.50	52.50	1890.00	42.00	939.00	367.00
La	81.60	57.70	66.20	56.20	81.50	29.20	28.60	77.80	82.10	42.40	77.50	55.60	69.00
Ce	162.00	139.00	130.00	132.00	172.00	54.70	56.40	73.40	89.20	79.20	76.70	112.00	143.00
Pr	19.10	15.50	17.30	14.80	21.00	6.06	6.06	3.46	4.94	8.66	4.17	12.30	16.60
Nd	73.80	63.50	68.90	63.70	83.30	21.30	21.50	6.61	9.89	30.80	8.83	44.50	62.30
Sm	13.80	13.80	15.20	14.30	16.70	3.55	3.36	0.79	1.05	4.86	0.91	7.67	12.50
Eu	2.49	1.42	3.60	3.33	1.80	0.77	0.77	0.09	0.12	1.14	0.12	1.50	1.01
Gd	11.60	12.90	15.00	13.70	16.50	2.54	2.39	0.43	0.59	3.15	0.58	6.35	11.10
Tb	1.75	2.25	2.55	2.35	2.76	0.39	0.39	0.08	0.11	0.45	0.11	0.97	1.77
Dy	10.70	14.90	14.80	14.50	16.70	2.16	2.06	0.47	0.81	2.52	0.73	5.43	10.70
Ho	2.23	3.15	3.04	3.03	3.63	0.44	0.41	0.12	0.20	0.51	0.17	1.09	2.04
Er	6.52	9.03	8.25	9.21	10.70	1.20	1.19	0.42	0.75	1.63	0.80	3.13	5.86
Tm	0.89	1.43	1.37	1.31	1.57	0.22	0.20	0.11	0.18	0.24	0.17	0.47	0.84
Yb	5.49	10.40	9.72	9.13	10.30	1.24	1.26	1.06	1.77	1.69	1.72	3.22	5.75
Lu	0.82	1.39	1.30	1.36	1.45	0.19	0.18	0.21	0.38	0.25	0.38	0.48	0.80
Hf	11.50	12.60	19.70	19.20	23.10	3.89	3.86	5.69	5.98	5.00	9.88	8.74	9.88
Ta	1.71	1.53	1.69	1.00	2.25	0.74	0.64	1.65	1.74	0.56	1.37	0.82	1.72
Pb	30.00	33.00	26.00	27.00	33.00	32.00	33.00	55.00	51.00	26.00	47.00	52.00	44.00
Th	27.50	23.30	15.10	14.10	24.80	11.60	10.00	56.90	61.30	9.80	95.30	22.90	28.50
U	4.53	3.92	2.88	3.01	5.28	2.33	2.04	11.20	12.30	3.18	18.00	3.37	5.13
F	1100.00	700.00	300.00	300.00	900.00	700.00	600.00	1700.00	3600.00	1100.00	4700.00	500.00	500.00
Zr+Ce+Y+Nb	624.10	670.70	1021.50	1028.80	1173.70	205.12	206.00	222.86	259.90	313.10	348.86	475.70	542.60
Ga/Al*10000	3.00	3.04	3.36	3.16	3.16	2.66	2.53	3.77	3.55	2.29	3.61	2.80	2.98
ASI	0.94	0.99	0.96	0.94	0.94	1.01	1.03	1.09	0.99	1.02	0.99	1.11	0.98
Eu/Eu*	0.60	0.33	0.73	0.73	0.33	0.78	0.83	0.47	0.47	0.89	0.50	0.66	0.26
$(La/Yb)_N$	10.66	3.98	4.89	4.42	5.68	16.89	16.28	52.65	33.27	18.00	32.32	12.39	8.61
$(La/Sm)_N$	3.82	2.70	2.81	2.54	3.15	5.31	5.50	63.58	50.48	5.63	54.98	4.68	3.56
$T_{Zr\ (°C)}$	799.30	840.87	906.24	902.71	916.42	706.48	711.91	724.23	717.94	759.32	785.12	815.53	805.88

Appendix 2 Supplementary material for Subcontinental lithospheric mantle contribution to granites in a silicic large igneous province: Geochemistry and Nd isotopic constraints

Appendix 2 Table A4 New whole-rock geochemical data for Hiltaba Suite samples collected in this study

Sample	2696090	2696087	2696092	2696091	3687821	2696086	2696088	3687800	3687797	3687799	3687809	3687811	3687847
Other Sample Name	CHI 17		WIR 2	WIR 1	1077-176		CHI 2	1077-111	1077-109	1077-110	1077-153	1077-156	1077-53
Drill Hole													
Depth From (m)													
Depth To (M)													
Easting	490469	488442	488462	487609	465285	464122	463829	519540	521890	520630	520610	523250	523264
Northing	6463632	6463526	6457422	6459011	6472495	6474617	6474505	6541340	6541800	6542430	6375540	6366930	6366981
Zone	53	53	53	53	53	53	53	53	53	53	53	53	53
Longitude	134.8991	134.8777	134.8778	134.8688	134.6329	134.6207	134.6176	135.2052	135.2299	135.2167	135.2200	135.2484	135.2486
Latitude	-31.9633	-31.9642	-32.0193	-32.0049	-31.8828	-31.8636	-31.8646	-31.2620	-31.2578	-31.2522	-32.7578	-32.8354	-32.8350
Datum					GDA94			GDA94	GDA94	GDA94	GDA94	GDA94	GDA94
Granite Group	8	8	8	8	8	8	8	9	9	9	10	10	10
Mantle Group	8	8	8	8	8	8	8	8	8	8	11+3	11+3	11+3
Major elements (wt %)													
SiO_2	69.56	69.95	67.18	67.57	76.10	70.08	71.15	76.10	76.70	79.60	71.60	74.70	74.80
TiO2	0.53	0.55	0.80	0.76	0.20	0.39	0.48	0.12	0.14	0.12	0.24	0.23	0.26
Al_2O_3	13.85	13.47	13.57	13.51	11.86	12.60	13.10	12.30	12.00	10.50	14.60	13.20	13.00
Fe_2O_{3t}	3.98	4.20	5.78	5.59	2.12	4.58	4.15	1.50	1.60	1.38	1.90	1.52	1.34
MnO	0.10	0.09	0.14	0.13	0.05	0.11	0.09	0.03	0.03	0.01	0.08	0.12	0.10
MgO	0.65	0.49	0.81	0.70	0.07	0.74	0.32	0.09	0.14	0.15	0.27	0.15	0.17
CaO	1.81	1.78	2.57	2.45	0.39	3.60	1.33	0.46	0.43	0.08	1.00	0.32	0.36
Na_2O	3.18	3.41	3.31	3.33	3.02	1.81	3.11	3.35	3.00	2.39	4.06	4.37	4.31
K_2O	5.07	5.14	4.86	4.82	5.50	4.88	5.75	5.47	5.54	5.26	5.89	5.33	5.37
P_2O_5	0.15	0.12	0.23	0.22	0.03	0.07	0.08	0.01	0.02	0.01	0.06	0.02	0.02
FeO	1.50	1.50	3.71	3.61	0.90	1.04	1.56	0.51	1.00	0.35	1.09	0.54	0.44
LOI	0.78	0.46	0.57	0.58	0.34	0.94	0.29	0.51	0.50	0.34	0.28	0.20	0.14
Total	101.16	101.16	103.53	103.27	100.58	100.84	101.41	100.44	101.10	100.20	101.07	100.70	100.32
Trace and rare earth elements (ppm)													
Sc	10.10	10.70	13.80	13.40	3.10	5.40	7.10	-0.10	0.60	0.20	1.60	1.80	1.70
V	27.80	15.30	32.50	23.20	3.80	16.50	13.60	4.30	4.50	6.10	9.30	5.40	5.30
Cr	14.00	10.00	9.00	7.00	244.00	10.00	6.00	311.00	233.00	215.00	153.00	159.00	8.00
Co	5.50	3.60	6.40	5.10	2.20	3.80	3.10	2.00	2.60	2.00	3.00	1.20	35.50
Ni	12.00	8.00	6.00	4.00	12.00	6.00	8.00	8.00	10.00	6.00	18.00	20.00	6.00
Cu	14.00	38.00	10.00	8.00	6.00	28.00	4.00	10.00	20.00	6.00	22.00	18.00	2.00
Zn	85.00	65.00	110.00	110.00	105.00	95.00	110.00	40.00	90.00	35.00	40.00	65.00	85.00
Ga	22.00	23.30	23.30	22.30	24.90	25.80	24.00	20.50	19.60	14.80	20.90	19.70	20.40
Rb	253.00	218.00	209.00	204.00	278.00	204.00	213.00	460.00	353.00	320.00	307.00	159.00	158.00
Sr	183.00	148.00	177.00	172.00	16.00	177.00	76.20	24.00	24.70	39.70	117.00	12.80	13.70
Y	46.50	51.30	58.50	59.20	113.00	65.20	88.70	74.00	71.30	50.30	33.50	58.40	68.10
Zr	353.00	422.00	442.00	442.00	361.00	571.00	594.00	196.00	194.00	156.00	235.00	283.00	339.00
Nb	19.20	21.90	21.40	21.00	30.70	18.30	23.40	26.20	21.90	18.90	26.60	20.50	21.30
Mo	1.40	4.60	2.20	2.20	3.60	1.20	0.60	3.00	4.40	3.00	2.40	2.40	0.80
Sn	4.40	4.80	4.00	5.60	6.00	5.00	6.40	9.40	9.20	6.80	3.60	3.40	3.40
Cs	6.78	3.05	3.67	3.59	4.77	4.13	3.95	9.01	3.75	8.03	2.24	0.58	0.50
Ba	1200.00	1210.00	1360.00	1340.00	234.00	970.00	1010.00	97.50	139.00	407.00	737.00	57.00	64.00
La	64.70	75.70	80.90	82.80	88.30	46.80	72.70	75.80	98.50	65.10	69.50	56.40	64.00
Ce	141.00	151.00	163.00	168.00	189.00	92.40	158.00	146.00	189.00	126.00	129.00	123.00	145.00
Pr	15.20	17.30	18.80	19.00	22.30	12.00	19.10	14.20	21.60	14.10	13.90	15.00	17.50
Nd	56.00	63.10	71.10	72.50	84.60	49.60	74.10	42.80	71.80	44.80	46.20	51.50	61.20
Sm	10.30	11.90	13.40	13.10	17.50	11.40	15.30	8.36	13.20	8.81	7.16	11.90	14.10
Eu	1.81	2.02	2.66	2.64	0.93	2.38	2.20	0.22	0.42	0.41	0.91	0.59	0.61
Gd	8.28	9.74	11.70	11.90	17.70	11.30	14.50	6.80	10.40	7.08	5.18	9.76	11.30
Tb	1.40	1.59	1.80	1.92	3.02	1.81	2.49	1.39	1.85	1.28	0.85	1.67	1.90
Dy	7.99	9.27	10.90	11.00	18.80	11.20	15.50	9.79	10.80	7.75	5.01	10.30	12.00
Ho	1.70	1.91	2.23	2.38	4.09	2.37	3.34	2.21	2.27	1.64	1.05	2.09	2.42
Er	4.96	5.59	6.42	6.44	12.10	6.91	9.70	7.02	6.87	4.98	3.28	5.93	6.87
Tm	0.73	0.81	0.95	0.94	1.88	1.00	1.42	1.18	1.08	0.81	0.56	0.80	0.91
Yb	4.84	5.49	6.23	6.44	12.60	6.71	9.80	8.20	6.82	5.30	4.23	4.66	5.82
Lu	0.72	0.83	0.94	0.93	1.78	0.94	1.36	1.12	0.98	0.74	0.61	0.61	0.73
Hf	9.28	11.10	11.40	11.50	11.60	14.00	15.40	8.31	7.19	6.00	7.21	8.11	9.38
Ta	1.49	1.52	1.50	1.50	2.15	1.20	1.68	2.91	2.04	1.81	1.62	1.19	1.66
Pb	41.00	37.00	36.00	35.00	41.00	18.00	38.00	52.00	41.00	29.00	35.00	25.00	24.00
Th	28.20	28.90	27.30	27.70	31.60	12.50	16.50	65.10	55.10	42.50	24.30	14.30	14.00
U	5.37	5.78	5.28	5.40	5.94	3.19	3.40	9.92	10.30	3.15	4.21	2.16	1.77
F	900.00	400.00	1400.00	1300.00	300.00	300.00	700.00	2200.00	2100.00	200.00	2100.00	1300.00	1400.00
Zr+Ce+Y+Nb	559.70	646.20	684.90	690.20	693.70	746.90	864.10	442.20	476.20	351.20	424.10	484.90	573.40
Ga/Al*10000	3.00	3.27	3.24	3.12	3.97	3.87	3.46	3.15	3.09	2.66	2.70	2.82	2.96
ASI	1.00	0.94	0.89	0.90	1.02	0.85	0.96	1.00	1.03	1.08	0.98	0.98	0.96
Eu/Eu*	0.60	0.57	0.65	0.65	0.16	0.64	0.45	0.09	0.11	0.16	0.46	0.17	0.15
$(La/Yb)_N$	9.59	9.89	9.31	9.22	5.03	5.00	5.32	6.63	10.36	8.81	11.79	8.68	7.89
$(La/Sm)_N$	4.06	4.11	3.90	4.08	3.26	2.65	3.07	5.85	4.82	4.77	6.27	3.06	2.93
$T_{Zr(°C)}$	809.68	819.08	803.24	807.41	835.54	838.09	868.99	761.96	766.16	757.89	764.22	791.01	809.04

Appendix 2 Table A4 New whole-rock geochemical data for Hiltaba Suite samples collected in this study

Sample	3687845	3687812	3687846	3687860	3687810	3687805	3687836	3687861	3687808	3687817	3687806	3687862
Other Sample Name	1077-51	1077-157	1077-52	1077-91	1077-154	1077-146	1077-227	1077-92	1077-151	1077-170	1077-149	1077-94
Drill Hole												
Depth From (m)												
Depth To (m)												
Easting	514654	518770	516177	521420	520530	531490	516200	516267	511600	511150	520080	520414
Northing	6368788	6368990	6369897	6376162	6371060	6380996	6383020	6383066	6387800	6387250	6388790	6390498
Zone	53	53	53	53	53	53	53	53	53	53	53	53
Longitude	135.1565	135.2005	135.1728	135.2287	135.2193	135.3360	135.1728	135.1735	135.1237	135.1189	135.2141	135.2176
Latitude	-32.8188	-32.8169	-32.8088	-32.7522	-32.7982	-32.7083	-32.6904	-32.6900	-32.6474	-32.6523	-32.6383	-32.6229
Datum	GDA94	GDA94	GDA94	GDA94	GDA94	GDA94	GDA94	GDA94	GDA94	GDA94	GDA94	GDA94
Granite Group	10	10	10	10	10	10	10	10	10	10	10	10
Mantle Group	11+3	11+3	11+3	11+3	11+3	11+3	11+3	11+3	11+3	11+3	11+3	11+3
Major elements (wt %)												
SiO_2	71.90	72.00	73.00	73.10	74.10	73.80	74.20	75.90	69.30	72.00	72.20	73.80
TiO2	0.29	0.26	0.21	0.23	0.17	0.27	0.21	0.13	0.43	0.30	0.27	0.30
Al_2O_3	14.60	14.20	14.10	13.80	13.80	13.60	13.60	13.10	14.90	14.40	14.40	13.40
Fe_2O_{3t}	1.68	2.20	1.42	1.72	1.61	1.66	1.45	0.83	2.63	1.93	1.79	1.68
MnO	0.07	0.08	0.07	0.08	0.07	0.07	0.06	0.02	0.10	0.06	0.05	0.07
MgO	0.32	0.32	0.24	0.31	0.27	0.25	0.25	0.09	0.63	0.39	0.37	0.37
CaO	0.94	1.04	0.88	1.01	0.62	0.56	0.96	0.46	1.61	0.72	0.88	0.94
Na_2O	3.94	4.05	4.15	3.94	3.67	4.27	4.00	3.79	4.25	3.99	4.02	3.86
K_2O	5.99	5.35	5.45	5.24	5.23	5.24	4.83	5.34	5.18	5.62	5.49	4.93
P_2O_5	0.07	0.06	0.05	0.06	0.03	0.05	0.04	0.01	0.13	0.10	0.06	0.07
FeO	0.65	1.21	0.68	0.71	0.73	0.63	0.87	0.17	1.18	0.85	0.77	0.56
LOI	0.24	0.31	0.22	0.48	0.40	0.09	0.25	0.30	0.59	0.23	0.22	0.41
Total	100.69	101.09	100.47	100.68	100.70	100.49	100.71	100.15	100.92	100.58	100.52	100.39
Trace and rare earth elements (ppm)												
Sc	0.70	2.50	0.20	1.40	1.40	1.90	0.20	0.50	2.40	0.20	1.40	1.40
V	9.70	10.90	6.60	8.00	9.10	12.70	9.60	1.80	24.40	16.80	12.90	12.30
Cr	7.00	226.00	5.00	12.00	248.00	223.00	188.00	-1.00	194.00	193.00	213.00	8.00
Co	43.40	2.10	41.60	76.60	2.90	2.50	2.90	88.00	4.60	3.30	3.40	94.60
Ni	6.00	16.00	4.00	6.00	8.00	18.00	18.00	-2.00	10.00	14.00	14.00	6.00
Cu	6.00	2.00	6.00	6.00	-2.00	8.00	6.00	2.00	-2.00	10.00	-2.00	6.00
Zn	45.00	40.00	55.00	55.00	30.00	55.00	20.00	15.00	40.00	45.00	40.00	40.00
Ga	19.50	19.20	20.60	21.50	16.90	18.10	16.70	15.80	20.40	20.50	17.30	16.70
Rb	239.00	255.00	252.00	288.00	250.00	126.00	166.00	161.00	157.00	169.00	180.00	168.00
Sr	116.00	125.00	91.00	116.00	133.00	84.60	105.00	18.00	228.00	169.00	137.00	120.00
Y	40.90	41.60	38.50	38.70	22.80	59.60	22.00	10.90	46.00	21.30	25.90	31.80
Zr	278.00	270.00	202.00	242.00	130.00	324.00	149.00	108.00	296.00	219.00	171.00	198.00
Nb	24.20	30.00	23.40	25.50	19.90	17.90	19.50	10.10	21.10	20.40	19.50	19.80
Mo	0.60	3.00	0.80	0.80	2.40	2.40	2.40	0.60	2.80	2.40	2.60	0.80
Sn	3.00	4.40	3.40	3.40	2.60	3.40	2.60	1.20	2.80	2.60	2.60	2.60
Cs	1.34	1.97	1.49	1.68	3.08	1.32	1.63	0.83	1.32	1.17	1.40	1.32
Ba	645.00	757.00	475.00	660.00	624.00	427.00	462.00	142.00	1160.00	776.00	707.00	655.00
La	87.60	74.80	61.60	65.80	47.80	47.30	53.10	27.40	56.40	36.10	47.00	57.30
Ce	156.00	138.00	116.00	128.00	83.90	123.00	87.00	55.60	124.00	91.90	86.80	105.00
Pr	16.60	15.10	12.40	13.50	9.52	14.40	8.57	4.37	14.70	9.41	9.21	10.70
Nd	52.10	53.00	40.70	44.30	31.20	53.30	25.60	13.40	51.50	31.20	30.20	33.70
Sm	8.64	7.07	6.56	7.68	5.18	11.40	3.74	2.46	9.23	5.84	4.61	5.61
Eu	0.95	0.95	0.71	0.82	0.65	0.78	0.57	0.34	1.47	0.72	0.77	0.86
Gd	6.27	6.02	5.02	5.45	3.61	10.10	2.91	1.67	6.94	3.70	3.49	4.49
Tb	1.00	0.92	0.82	0.86	0.51	1.72	0.44	0.26	1.14	0.65	0.62	0.77
Dy	5.96	6.30	5.42	5.48	3.39	10.30	3.28	1.64	7.26	3.85	3.80	4.51
Ho	1.22	1.40	1.17	1.14	0.71	2.17	0.64	0.36	1.55	0.79	0.85	0.97
Er	4.11	4.41	3.67	3.72	2.12	5.62	2.10	1.07	4.82	2.59	2.63	3.14
Tm	0.63	0.68	0.63	0.66	0.39	0.77	0.37	0.19	0.76	0.41	0.43	0.52
Yb	4.87	5.14	4.20	4.58	2.64	4.73	3.18	1.55	4.76	2.95	3.09	3.46
Lu	0.65	0.77	0.61	0.67	0.44	0.56	0.46	0.23	0.60	0.39	0.48	0.53
Hf	7.92	7.90	6.44	7.34	4.55	8.14	4.78	3.97	8.32	6.51	5.26	5.73
Ta	2.01	1.79	2.00	2.03	1.79	1.23	1.40	1.27	1.42	1.30	1.39	1.93
Pb	31.00	32.00	34.00	46.00	41.00	24.00	27.00	28.00	23.00	26.00	27.00	25.00
Th	16.00	24.30	21.80	27.40	24.70	10.10	18.50	12.10	12.10	13.80	17.80	13.30
U	2.45	3.69	2.61	4.85	4.47	2.39	3.29	2.36	1.44	1.64	2.72	2.61
F	1300.00	1800.00	1400.00	2100.00	200.00	500.00	900.00	200.00	1000.00	700.00	1100.00	1000.00
Zr+Ce+Y+Nb	499.10	479.60	379.90	434.20	256.60	524.50	277.50	184.60	487.10	352.60	303.20	354.60
Ga/Al*10000	2.52	2.55	2.76	2.94	2.31	2.51	2.32	2.28	2.59	2.69	2.27	2.35
ASI	1.00	0.99	0.99	0.99	1.08	0.99	1.01	1.02	0.97	1.04	1.02	1.00
Eu/Eu*	0.39	0.45	0.38	0.39	0.46	0.22	0.53	0.51	0.56	0.47	0.59	0.52
$(La/Yb)_N$	12.90	10.44	10.52	10.31	12.99	7.17	11.98	12.68	8.50	8.78	10.91	11.88
$(La/Sm)_N$	6.55	6.83	6.06	5.53	5.96	2.68	9.17	7.19	3.94	3.99	6.58	6.59
$T_{Zr\ (°C)}$	785.70	782.66	752.57	773.17	726.09	807.72	728.36	703.22	779.42	767.50	739.54	756.52

Appendix 2 Supplementary material for Subcontinental lithospheric mantle contribution to granites in a silicic large igneous province: Geochemistry and Nd isotopic constraints

Appendix 2 Table A4 New whole-rock geochemical data for Hiltaba Suite samples collected in this study

Sample	3687853	3687834	3687835	3687855	3687859	3687856	3687858	3687857	3687854	3687872	3687873
Other Sample Name	1077-73	1077-192	1077-193	1077-76	1077-84	1077-81	1077-83	1077-82	1077-74	1077-197	1077-198
Drill Hole											
Depth From (m)											
Depth To (M)											
Easting	571856	557230	557545	570162	549339	551221	549511	551180	570476	691735	691876
Northing	6371298	6381290	6382735	6372705	6380510	6381063	6381767	6381443	6372220	6298280	6298910
Zone	53	53.00	53	53	53	53	53	53	53	53	53
Longitude	135.7674	135.6106	135.6139	135.7492	135.5265	135.5465	135.5282	135.5461	135.7526	137.0626	137.0639
Latitude	-32.7939	-32.7047	-32.6916	-32.7813	-32.7121	-32.7070	-32.7007	-32.7036	-32.7857	-33.4378	-33.4320
Datum	GDA94	GDA94	GDA94	GDA94	GDA94	GDA94	GDA94	GDA94	GDA94	GDA94	GDA94
Granite Group	11	11	11	11	11	11	11	11	11	14	14
Mantle Group	11	11	11	11	11	11	11	11	11	12+15	12+15
Major elements (wt %)											
SiO_2	77.30	77.60	77.60	75.10	68.70	69.90	70.00	70.70	74.25	74.50	74.70
TiO2	0.10	0.10	0.10	0.22	0.63	0.52	0.53	0.47	0.21	0.20	0.22
Al_2O_3	12.30	12.30	12.30	12.80	13.70	13.60	13.70	13.50	13.31	13.10	13.10
Fe_2O_{3t}	0.74	0.98	1.04	1.40	4.84	3.90	3.94	3.56	1.44	1.62	1.69
MnO	0.03	0.06	0.06	0.05	0.12	0.10	0.10	0.10	0.05	0.03	0.01
MgO	0.10	0.08	0.08	0.34	0.56	0.46	0.45	0.54	0.33	0.25	0.24
CaO	0.58	0.14	0.10	1.02	1.96	1.59	1.74	1.26	0.83	0.94	0.57
Na_2O	3.59	3.52	3.60	3.50	3.31	3.46	3.48	3.46	3.53	3.18	3.04
K_2O	4.65	4.80	4.82	4.83	5.17	5.25	5.18	5.27	4.97	5.47	5.66
P_2O_5	0.01	0.01	0.01	0.05	0.17	0.12	0.13	0.11	0.06	0.04	0.04
FeO	0.15	0.37	0.34	0.44	2.60	2.12	2.34	1.81	0.49	0.97	0.54
LOI	0.37	0.42	0.41	0.64	0.64	0.65	0.62	0.86	0.62	0.59	0.69
Total	99.92	100.00	100.12	100.40	102.40	101.67	102.20	101.65	100.09	100.89	100.51
Trace and rare earth elements (ppm)											
Sc	-0.10	0.50	2.00	0.60	9.40	11.10	7.40	6.10	3.30	1.60	2.20
V	3.60	4.40	7.30	11.40	14.70	19.40	14.50	11.80	12.20	8.40	11.40
Cr	5.00	337.00	328.00	8.00	7.00	19.00	6.00	9.00	2.00	7.00	206.00
Co	129.00	2.30	2.50	168.00	68.10	88.20	69.70	91.40	133.00	105.00	3.50
Ni	4.00	12.00	8.00	8.00	6.00	4.00	4.00	6.00	6.00	10.00	10.00
Cu	14.00	20.00	6.00	-2.00	4.00	24.00	4.00	-2.00	32.00	6.00	6.00
Zn	15.00	10.00	35.00	25.00	100.00	75.00	70.00	65.00	25.00	15.00	10.00
Ga	16.30	21.60	19.10	16.20	19.90	20.10	19.70	18.90	17.90	18.90	19.20
Rb	191.00	390.00	374.00	166.00	212.00	274.00	215.00	237.00	189.00	439.00	452.00
Sr	41.70	11.20	15.80	120.00	145.00	185.00	147.00	132.00	134.00	59.10	56.80
Y	8.60	23.80	31.40	25.80	63.90	72.70	58.40	56.80	18.70	61.00	59.20
Zr	55.50	89.50	106.00	146.00	423.00	488.00	395.00	372.00	149.00	192.00	195.00
Nb	12.30	35.10	41.20	18.50	22.90	22.70	21.50	21.60	17.40	23.70	25.20
Mo	1.20	4.40	5.20	1.20	2.00	0.80	1.80	1.80	1.00	1.20	5.60
Sn	1.20	4.80	3.20	2.00	4.60	5.60	4.40	5.80	4.40	2.60	2.80
Cs	1.31	2.22	1.91	1.21	4.89	6.00	4.74	3.85	1.20	5.07	4.54
Ba	76.50	65.00	73.50	448.00	1280.00	1560.00	1220.00	1130.00	501.00	329.00	356.00
La	32.30	24.70	20.20	46.10	83.10	81.60	78.60	77.00	29.10	78.80	98.30
Ce	79.90	46.00	79.10	89.50	160.00	147.00	147.00	151.00	66.80	143.00	182.00
Pr	4.13	4.61	4.75	9.65	18.80	17.40	18.40	17.40	6.74	16.60	20.10
Nd	10.30	12.20	13.10	32.40	74.00	61.40	68.30	62.90	23.30	54.00	67.10
Sm	1.42	2.29	2.59	5.70	12.80	12.10	13.40	11.70	4.36	10.00	11.70
Eu	0.22	0.15	0.12	0.74	2.57	2.36	2.20	1.79	0.68	0.75	0.94
Gd	1.00	1.80	2.19	4.29	10.30	11.40	10.10	9.30	3.36	8.24	9.52
Tb	0.16	0.34	0.46	0.63	1.77	1.70	1.61	1.42	0.53	1.35	1.47
Dy	1.03	2.42	3.44	3.62	10.90	11.50	9.67	8.83	3.17	8.85	9.06
Ho	0.24	0.62	0.86	0.76	2.10	2.27	2.04	1.94	0.68	1.91	1.88
Er	0.81	2.45	2.95	2.37	5.77	6.30	5.42	5.56	2.09	5.86	5.81
Tm	0.18	0.45	0.52	0.38	0.99	0.86	0.83	0.84	0.33	0.87	0.90
Yb	1.41	3.50	4.03	2.57	6.14	5.76	5.64	5.51	2.20	6.54	6.29
Lu	0.23	0.48	0.59	0.37	0.87	0.85	0.78	0.75	0.33	0.96	0.92
Hf	2.27	4.90	4.82	5.00	11.20	11.00	10.20	9.71	5.01	6.45	6.36
Ta	1.90	2.53	2.41	2.36	1.75	2.13	2.00	2.13	2.24	4.17	3.35
Pb	24.00	10.00	27.00	19.00	34.00	47.00	32.00	34.00	20.00	36.00	23.00
Th	42.30	42.70	44.50	27.10	30.20	32.50	29.60	31.10	20.50	69.40	73.60
U	3.63	6.37	6.73	3.31	6.16	5.00	5.01	7.19	4.00	16.20	15.00
F		1300.00	300.00	1000.00	1600.00	1400.00	1700.00	2000.00	500.00	1700.00	1300.00
Zr+Ce+Y+Nb	156.30	194.40	257.70	279.80	669.80	730.40	621.90	601.40	251.90	419.70	461.40
Ga/Al*10000	2.50	3.32	2.93	2.39	2.74	2.79	2.72	2.65	2.54	2.73	2.77
ASI	1.03	1.09	1.09	1.00	0.95	0.96	0.95	0.99	1.05	1.02	1.08
Eu/Eu*	0.56	0.23	0.15	0.46	0.68	0.61	0.58	0.52	0.54	0.25	0.27
$(La/Yb)_N$	16.43	5.06	3.60	12.87	9.71	10.16	10.00	10.02	9.49	8.64	11.21
$(La/Sm)_N$	14.68	6.96	5.03	5.22	4.19	4.35	3.79	4.25	4.31	5.09	5.42
$T_{Zr(°C)}$	648.39	699.87	714.72	728.54	816.76	841.11	813.47	817.87	737.17	758.98	770.69

Appendix 2 Table A4 New whole-rock geochemical data for Hiltaba Suite samples collected in this study

Sample	3687876	3687871		3687870	3687877	3687875	3687869					
Other Sample Name	1077-201A	1077-196	1077-116	1077-195	1077-201B	1077-200	1077-194	HDD393-01	HDD393-02	HDD396-01	HDD357-03	HDD357-01
Drill Hole								HDD 393	HDD 393	HDD 396	HDD 357	HDD 357
Depth From (m)												
Depth To (m)												
Easting	700235	703700	691129	703700	700235	698910	701030	763551	763551	763551	763551	763551
Northing	6311325	6314700	6305671	6314700	6311325	6305020	6311230	6174926	6174926	6174926	6174926	6174926
Zone	53	53	53	53	53	53	53	53	53	53	53	53
Longitude	137.1510	137.1875		137.1875	137.1510	137.1382	137.1596					
Latitude	-33.3186	-33.2875		-33.2875	-33.3186	-33.3757	-33.3193					
Datum	GDA94	GDA94		GDA94	GDA94	GDA94	GDA94					
Granite Group	14	14	14	14	14	14	14	15	15	15	15	15
Mantle Group	12+15	12+15	12+15	12+15	12+15	12+15	12+15	15	15	15	15	15
Major elements (wt %)												
SiO_2	75.00	72.20	71.25	71.74	75.38	74.80	75.90	65.52	66.36	65.71	67.13	65.29
TiO2	0.18	0.43	0.39	0.50	0.16	0.18	0.23	0.63	0.60	0.65	0.60	0.62
Al_2O_3	12.70	13.20	14.04	12.99	12.46	12.79	12.62	14.98	15.28	15.85	15.18	16.10
Fe_2O_{3t}	1.66	3.10	2.41	3.26	1.78	1.82	0.84	3.81	3.34	3.10	2.85	2.99
MnO	0.03	0.05	0.06	0.07	0.03	0.03	0.03	0.04	0.03	0.04	0.06	0.04
MgO	0.20	0.57	0.48	0.62	0.11	0.33	0.17	0.61	0.58	0.64	0.60	0.76
CaO	1.13	1.50	1.55	1.51	0.78	0.80	1.37	1.66	1.18	1.04	1.10	1.28
Na_2O	2.93	3.07	3.31	3.04	2.61	3.09	3.35	4.05	3.99	4.34	4.15	4.28
K_2O	5.47	5.12	5.55	5.13	6.19	5.50	4.61	6.66	6.92	6.85	6.57	6.69
P_2O_5	0.04	0.12	0.10	0.13	0.01	0.04	0.01	0.11	0.10	0.11	0.09	0.10
FeO	0.75	1.61	1.36	1.49	1.00	1.63	0.25	0.79	0.69	0.80	0.59	0.70
LOI	0.35	0.33	0.60	0.70	0.29	0.39	0.81	1.81	1.41	1.35	1.43	1.67
Total	100.44	99.70	101.10	101.18	100.80	101.40	100.19	100.67	100.48	100.48	100.35	100.52
Trace and rare earth elements (ppm)												
Sc	0.30	7.50	4.80	7.70	2.30	2.60	2.90	10.80	8.60	9.80	7.00	8.90
V	9.50	23.00	15.70	22.40	5.70	11.00	3.30	14.50	13.40	11.50	20.70	23.50
Cr	260.00	211.00	3.00	5.00	441.00	270.00	3.00	4.00	3.00	9.00	6.00	12.00
Co	3.10	6.40	64.90	64.20	2.80	4.00	81.80	94.10	65.80	249.00	149.00	141.00
Ni	10.00	12.00	4.00	6.00	16.00	9.00	6.00	-5.00	-5.00	-5.00	-5.00	-5.00
Cu	6.00	8.00	6.00	6.00	8.00	11.00	-2.00	90.00	25.00	25.00	35.00	20.00
Zn	20.00	20.00	50.00	60.00	35.00	24.00	25.00	20.00	10.00	15.00	15.00	15.00
Ga	18.90	19.70	21.30	22.20	20.20	19.20	21.80	17.30	19.40	19.00	17.60	21.00
Rb	386.00	334.00	339.00	334.00	424.00	405.57	308.00	207.00	221.00	207.00	188.00	242.00
Sr	111.00	134.00	165.00	133.00	58.60	53.63	74.90	14.80	15.10	15.20	14.60	36.20
Y	40.80	36.80	36.20	65.60	23.10	43.70	33.20	41.50	46.30	60.80	45.40	74.70
Zr	114.00	257.00	225.00	295.00	59.50	132.00	132.00	913.00	783.00	853.00	745.00	831.00
Nb	14.70	21.00	16.90	26.20	12.90	23.60	15.20	25.70	26.20	26.30	28.50	27.70
Mo	3.20	2.80	1.00	1.40	4.00	0.00	0.80	0.40	0.20	1.20	0.40	0.40
Sn	3.00	4.40	3.80	6.40	3.20	0.00	4.00	3.00	4.00	4.00	4.00	7.00
Cs	6.22	6.13	5.57	5.91	5.77	0.00	4.65	0.85	1.09	0.83	0.59	1.00
Ba	687.00	744.00	1000.00	777.00	191.00	193.00	224.00	356.00	371.00	386.00	353.00	518.00
La	73.10	116.00	106.00	124.00	89.20	67.00	215.00	65.90	73.10	84.00	78.80	79.40
Ce	121.00	199.00	186.00	232.00	185.00	124.00	397.00	125.00	154.00	171.00	166.00	167.00
Pr	12.90	20.50	18.60	24.80	14.60	0.00	37.70	15.70	19.20	20.40	20.20	22.30
Nd	40.60	65.50	59.00	82.90	42.50	38.18	109.00	57.50	71.60	78.80	78.70	89.30
Sm	7.06	9.03	9.17	14.00	6.12	6.34	14.30	10.30	12.60	14.00	13.90	17.60
Eu	1.22	1.51	1.75	1.75	0.72	0.00	1.00	2.31	2.61	3.05	2.44	3.59
Gd	5.67	6.73	6.78	11.40	4.21	0.00	8.31	9.35	10.30	11.30	9.54	14.60
Tb	0.97	1.06	1.07	1.86	0.72	0.00	1.16	1.27	1.50	1.81	1.47	2.36
Dy	5.80	6.35	6.38	11.10	4.31	0.00	6.13	6.93	8.76	11.20	9.08	13.20
Ho	1.28	1.20	1.28	2.39	0.87	0.00	1.18	1.57	1.81	2.36	1.90	2.75
Er	4.11	3.72	3.87	7.27	2.56	0.00	3.73	4.40	5.51	6.84	5.23	8.37
Tm	0.62	0.57	0.63	1.11	0.38	0.00	0.55	0.65	0.75	1.05	0.70	1.15
Yb	4.34	4.69	4.37	7.51	2.70	0.00	4.06	4.50	5.54	6.62	4.96	7.36
Lu	0.61	0.63	0.60	1.04	0.38	0.00	0.64	0.73	0.77	0.97	0.77	1.04
Hf	3.87	7.43	6.73	8.95	2.71	0.00	4.92	22.10	20.00	20.70	19.00	21.00
Ta	1.61	1.55	1.92	3.62	1.61	0.00	2.28	1.78	2.03	2.36	2.08	2.32
Pb	31.00	28.00	42.00	38.00	41.00	28.70	38.00	3.00	3.00	4.00	4.00	3.00
Th	55.30	66.50	68.50	84.90	97.00	66.80	187.00	23.10	37.40	35.60	29.00	21.80
U	8.61	12.70	11.70	7.79	14.30	25.50	28.70	5.91	6.74	11.00	4.76	3.80
F	1200.00	1800.00	1100.00	1400.00	400.00	0.00	200.00	200.00	300.00	300.00	200.00	300.00
Zr+Ce+Y+Nb	290.50	513.80	464.10	618.80	280.50	323.30	577.40	1105.20	1009.50	1111.10	984.90	1100.40
Ga/Al*10000	2.81	2.82	2.87	3.23	3.06	2.84	3.26	2.18	2.40	2.26	2.19	2.46
ASI	0.99	1.00	0.99	0.98	1.00	1.03	0.97	0.89	0.95	0.97	0.96	0.97
Eu/Eu*	0.59	0.59	0.68	0.42	0.43	#DIV/0!	0.28	0.72	0.70	0.74	0.65	0.68
$(La/Yb)_N$	12.08	17.74	17.40	11.84	23.70	#DIV/0!	37.99	10.50	9.46	9.10	11.40	7.74
$(La/Sm)_N$	6.68	8.29	7.46	5.72	9.41	6.82	9.71	4.13	3.75	3.87	3.66	2.91
$T_{Zr\ (°C)}$	704.33	780.65	761.73	792.87	648.81	722.56	716.60	885.56	884.03	897.58	1208.91	894.14

Appendix 2 Supplementary material for Subcontinental lithospheric mantle contribution to granites in a silicic large igneous province: Geochemistry and Nd isotopic constraints

Appendix 2 Table A4 New whole-rock geochemical data for Hiltaba Suite samples collected in this study

Sample	3687894	2705391	2705396	2705395	2705388	2705389	2705392	2705398	2705390	2705397	2705394	2705393
Other Sample Name	1077-173											
Drill Hole		DDH 33	DDH 103	DDH 103	DDH 33	DDH 33	DDH 33	DDH 221	DDH 33	DDH 103	DDH 103	DDH 103
Depth From (m)		230.19	210.77	188.65	85.04	97.01	250.65	85.15	151.07	219.39	181.69	167.11
Depth To (M)		230.74	211.21	189.14	85.53	97.48	251.23	85.87	151.57	219.73	182.31	167.33
Easting		737228	748299	748299	737228	737228	737228	754929	737228	748299	748299	748299
Northing		6222171	6214471	6214471	6222171	6222171	6222171	6224206	6222171	6214471	6214471	6214471
Zone		53	53	53	53	53	53	53	53	53	53	53
Longitude		137.5720	137.6941	137.6941	137.5720	137.5720	137.5720	137.7631	137.5720	137.6941	137.6941	137.6941
Latitude		-34.1158	-34.1812	-34.1812	-34.1158	-34.1158	-34.1158	-34.0919	-34.1158	-34.1812	-34.1812	-34.1812
Datum		GDA94	GDA94	GDA94	GDA94	GDA94	GDA94	GDA94	GDA94	GDA94	GDA94	GDA94
Granite Group	15	15	15	15	15	15	15	15	15	15	15	15
Mantle Group	15	15	15	15	15	15	15	15	15	15	15	15
Major elements (wt %)												
SiO_2	75.43	68.17	71.83	73.20	67.92	68.62	69.27	67.77	69.06	71.02	72.18	75.35
TiO2	0.24	0.68	0.09	0.06	0.67	0.68	0.63	0.83	0.70	0.08	0.07	0.04
Al_2O_3	12.27	13.78	14.09	13.35	13.82	14.02	13.56	13.80	13.54	16.25	13.71	13.57
Fe_2O_{3t}	1.89	5.22	1.83	1.45	5.51	5.00	4.94	4.20	5.30	1.51	2.43	0.93
MnO	0.07	0.02	0.02	0.01	0.03	0.02	0.02	0.03	0.02	0.02	0.02	0.02
MgO	0.18	1.09	0.78	0.48	1.96	1.12	1.09	1.32	1.36	1.02	0.52	0.21
CaO	0.61	1.12	0.48	0.40	0.36	0.58	0.69	1.82	0.52	0.64	0.69	0.25
Na_2O	3.40	3.68	3.29	2.08	2.77	4.06	3.27	3.04	3.71	6.63	3.66	4.20
K_2O	5.20	5.05	6.31	8.14	5.28	4.59	5.24	5.13	4.45	1.74	5.29	4.98
P_2O_5	0.04	0.17	0.18	0.23	0.17	0.16	0.17	0.20	0.19	0.10	0.25	0.07
FeO		1.98	1.15	0.49	1.36	2.22	1.53	1.99	1.55	0.88	1.34	0.51
LOI	0.62	0.73	0.92	0.54	1.41	1.01	0.97	1.60	1.06	1.03	1.08	0.45
Total	99.95	101.69	100.97	100.42	101.26	102.08	101.38	101.73	101.46	100.91	101.24	100.57
Trace and rare earth elements (ppm)												
Sc	4.80	11.70	5.80	3.20	11.30	12.10	11.50	10.90	12.40	4.90	4.40	2.50
V	6.80	42.50	19.70	7.70	41.60	35.90	42.60	45.80	46.90	9.10	13.60	4.00
Cr	205.00	9.00	4.00	5.00	11.00	11.00	13.00	15.00	12.00	6.00	7.00	8.00
Co	2.20	9.70	2.90	2.10	6.70	9.70	9.60	7.70	10.20	3.30	2.30	1.40
Ni	8.00	8.00	14.00	8.00	12.00	12.00	8.00	12.00	8.00	10.00	10.00	8.00
Cu	4.00	30.00	190.00	6.00	8.00	18.00	14.00	34.00	10.00	10.00	8.00	66.00
Zn	60.00	15.00	25.00	15.00	35.00	15.00	15.00	40.00	20.00	25.00	25.00	15.00
Ga	21.50	22.80	22.10	19.70	21.50	22.60	21.90	20.70	22.20	26.20	21.90	18.50
Rb	306.00	244.00	285.00	340.00	269.00	220.00	252.00	176.00	190.00	132.00	233.00	203.00
Sr	48.50	96.60	42.60	39.00	56.00	90.90	89.50	144.00	63.50	51.30	43.10	37.80
Y	67.20	102.00	49.90	51.80	67.80	76.30	99.20	55.10	97.40	22.30	64.30	32.50
Zr	313.00	414.00	89.00	37.50	430.00	378.00	430.00	513.00	478.00	85.00	58.00	57.00
Nb	25.40	46.00	6.99	6.58	45.80	45.50	41.10	29.90	43.20	10.00	10.40	56.10
Mo	3.80	1.40	0.60	0.40	0.80	1.80	2.40	1.00	1.40	1.00	0.80	0.60
Sn	5.40	5.20	0.60	0.40	4.80	6.20	4.60	4.00	5.00	0.60	0.20	0.40
Cs	4.57	1.42	1.35	0.99	2.12	1.04	0.89	1.03	0.62	1.38	2.00	0.70
Ba	359.00	973.00	654.00	764.00	853.00	927.00	1060.00	1570.00	830.00	170.00	486.00	527.00
La	81.60	131.00	55.60	20.20	105.00	116.00	128.00	107.00	131.00	67.60	28.40	63.90
Ce	164.00	288.00	107.00	47.70	220.00	266.00	268.00	229.00	275.00	116.00	73.00	110.00
Pr	18.00	34.60	10.80	4.90	25.20	33.20	32.20	27.10	32.90	11.40	7.31	10.80
Nd	63.00	130.00	37.50	20.50	93.50	124.00	118.00	101.00	126.00	36.70	28.90	35.30
Sm	11.70	24.60	7.31	5.60	16.10	22.60	22.90	17.00	24.90	6.18	7.94	5.38
Eu	0.73	3.05	1.08	0.92	2.24	3.23	3.01	2.87	3.39	0.83	1.16	0.83
Gd	9.73	19.90	6.43	5.92	11.90	17.10	19.00	13.20	20.40	4.24	7.94	4.43
Tb	1.72	3.21	1.32	1.43	1.95	2.65	3.05	1.97	3.20	0.67	1.73	0.90
Dy	11.20	19.10	8.87	9.73	12.30	15.20	18.40	10.80	18.70	4.23	11.40	6.36
Ho	2.40	3.89	2.00	2.19	2.67	3.10	3.75	2.10	3.76	0.88	2.60	1.47
Er	7.28	10.80	6.02	6.85	7.97	8.51	10.40	6.16	10.70	2.63	8.24	4.99
Tm	1.19	1.61	0.92	1.09	1.26	1.27	1.53	0.85	1.58	0.40	1.32	0.84
Yb	8.05	10.40	6.27	7.53	8.35	8.51	9.80	5.49	9.99	2.91	8.74	6.12
Lu	1.15	1.42	0.87	0.92	1.27	1.31	1.29	0.82	1.37	0.43	1.22	0.92
Hf	9.49	11.70	3.16	1.56	12.60	11.10	12.10	13.20	13.50	3.13	2.62	2.46
Ta	1.84	3.43	0.63	0.77	4.08	3.73	3.23	1.91	3.37	1.10	1.21	11.00
Pb	33.00	7.00	22.00	17.00	5.00	8.00	6.00	6.00	6.00	8.00	17.00	7.00
Th	27.30	65.80	26.10	25.20	68.90	53.20	58.20	31.50	56.00	33.10	36.80	20.90
U	4.93	15.40	249.00	40.90	5.61	19.10	18.50	5.61	14.10	42.20	243.00	58.90
F	1800.00	2100.00	400.00	400.00	1300.00	1600.00	1600.00	1700.00	700.00	600.00	400.00	200.00
Zr+Ce+Y+Nb	569.60	850.00	252.89	143.58	763.60	765.80	838.30	827.00	893.60	233.30	205.70	255.60
Ga/Al*10000	3.31	3.13	2.96	2.79	2.94	3.05	3.05	2.83	3.10	3.05	3.02	2.58
ASI	1.00	1.03	1.08	1.04	1.28	1.11	1.11	1.01	1.15	1.17	1.07	1.07
Eu/Eu*	0.21	0.42	0.48	0.49	0.49	0.50	0.44	0.59	0.46	0.50	0.45	0.52
$(La/Yb)_N$	7.27	9.04	6.36	1.92	9.02	9.78	9.37	13.98	9.41	16.66	2.33	7.49
$(La/Sm)_N$	4.50	3.44	4.91	2.33	4.21	3.31	3.61	4.06	3.40	7.06	2.31	7.67
$T_{Zr(°C)}$		829.23	686.11	610.95	878.44	836.03	854.66	851.93	874.32	688.25	647.34	650.80

Appendix 2 Supplementary material for Subcontinental lithospheric mantle contribution to granites in a silicic large igneous province: Geochemistry and Nd isotopic constraints

Appendix 2 Table A5 Hiltaba Suite granitoid groups and their average $\varepsilon_{Nd(1590\ Ma)}$ and Nd average compositions used in the mixing calculations

Pluton Group Number	Average $\varepsilon_{Nd(1590\ Ma)}$	Average Nd (ppm)	Average mantle $\varepsilon_{Nd(1590\ Ma)}$	Average mantle Nd (ppm)	Average host crust $\varepsilon_{Nd(1590\ Ma)}$	Average host crust Nd (ppm)	Crust Group
1	-0.2	41.15	0.7	11.87	-5.6	38.67	C5
2	-0.1	53.96	0.7	11.87	-5.6	38.67	C5
3	-1.6	14.12	0.7	11.87	-5.6	38.67	C5
4	-4.5	47.79	0.6	24.94	-5.6	38.67	C5
5	-1.2	22.38	0.6	24.94	-9.1	41.59	C2
6	0.0	58.69	0.5	22.65	-2.1	28.5	C5
7	-3.6	39.80	0.6	24.94	-9.1	41.59	C2
8	-0.7	41.21	0.5	20.36	-5.6	38.67	C5
9	-4.2	53.40	0.5	20.36	-9.1	41.59	C2
10	-0.2	40.30	0.5	22.65	-5.6	38.67	C5
11	-2.9	25.20	-1.9	39.81	-9.1	41.59	C2
12	-6.8	61.87	-2.4	62.82	-9.1	41.59	C2
13	-6.3	66.66	-2.0	22.34	-6.6	40.63	C3
14	-9.1	55.45	-2.2	42.57	-10.3	43.26	C1
15	-3.4	78.38	-2.0	22.32	-4.7	46.67	C4

Average mantle and crustal Nd compositions are listed for each pluton group, based on host rocks and mantle domains identified in Table 2 and on Figure 10.

Appendix 3

Supplementary material for: Temporal, geochemical and isotopic constraints on plume-driven felsic and mafic components in a large igneous province

Appendix 3 Table A1 Whole-rock geochemical composition for Gawler Range Volcanics samples

R number	Unit	2019333	2746362	2019334	2019336	2019337	2019339	2019340	2019342	2019343	2019345
Other Sample Number											
Drill_Hole		RC 1	RC1	RC 1	RC 1	RC 1	RC 1	RC 1	RC 1	RC 1	RC 1
Depth_From		117.77	118.59	169.45	223.08	267.82	340.63	364.88	410.55	496.95	545.25
Depth_To		118.14	119.1	169.75	223.52	268.36	341.32	365.46	411.20	497.84	546.16
Data Source		SARIG	Wade et al this study	SARIG	SARIG	SARIG	SARIG	SARIG	SARIG	SARIG	SARIG
Location		Myall Creek	Myall Creek	Myall Creek	Myall Creek	Myall Creek	Myall Creek	Myall Creek	Myall Creek	Myall Creek	Myall Creek
Suite		LGRV	LGRV	LGRV	LGRV	LGRV	LGRV	LGRV	LGRV	LGRV	LGRV
Formation											
Map Unit		Ma15	Ma15	Ma15	Ma15	Ma15	Ma15	Ma15	Ma15	Ma15	Ma15
Easting		718923.98	718923.98	718923.98	718923.98	718923.98	718923.98	718923.98	718923.98	718923.98	718923.98
Northing		6405394.45	6405394.45	6405394.45	6405394.45	6405394.45	6405394.45	6405394.45	6405394.45	6405394.45	6405394.45
Zone		53	53	53	53	53	53	53	53	53	53
Longitude		137.329366	137.329366	137.329366	137.329366	137.329366	137.329366	137.329366	137.329366	137.329366	137.329366
Latitude		-32.467133	137.329366	-32.467133	-32.467133	-32.467133	-32.467133	-32.467133	-32.467133	-32.467133	-32.467133
Datum		GDA94	GDA94	GDA94	GDA94	GDA94	GDA94	GDA94	GDA94	GDA94	GDA94
Age		1591.00	1591.00	1591.00	1591.00	1591.00	1591.00	1591.00	1591.00	1591.00	1591.00
Lithology		Ignimbrite	Rhyodacite	Ignimbrite	Rhyodacite	Rhyodacite	Rhyodacite	Rhyodacite	Rhyodacite	Ignimbrite	Ignimbrite
SiO_2	%	70.90	71.87	72.70	67.20	68.50	64.10	65.70	66.60	65.50	64.70
TiO_2	%	0.50	0.51	0.46	0.78	0.67	0.70	0.71	0.69	0.63	0.66
Al_2O_3	%	12.50	13.80	13.30	13.55	15.15	14.35	15.10	13.40	13.50	13.50
FeO	%	0.00	0.16	0.00	0.00	0.00	0.00	0.00	0.00	0.00	0.00
Fe_2O_3	%	4.13	3.59	3.83	4.94	5.13	7.58	6.21	4.36	5.19	6.74
MnO	%	0.05	0.05	0.06	0.11	0.07	0.09	0.13	0.26	0.07	0.10
MgO	%	0.73	0.57	0.55	0.85	0.53	1.00	0.76	1.38	0.48	0.78
CaO	%	0.73	0.52	0.56	0.90	0.29	0.49	0.99	1.54	1.04	1.60
Na_2O	%	1.82	1.90	2.12	4.48	2.27	1.48	2.09	2.70	2.90	0.14
K_2O	%	5.05	5.46	4.56	4.01	4.88	5.83	5.83	5.03	4.70	6.82
P_2O_5	%	0.03	0.05	0.09	0.19	0.04	0.15	0.10	0.17	0.13	0.17
LOI	%	1.85	1.88	1.87	1.22	1.67	1.90	2.05	2.44	1.68	2.71
Total	%	98.29	100.36	100.10	98.23	99.20	97.67	99.67	98.57	95.82	97.92
F	ppm	490.00	700.00	0.00	1820.00	0.00	0.00	0.00	1040.00	0.00	0.00
Ga	ppm	17.00	21.10	17.10	16.20	19.60	20.30	24.00	18.60	18.70	20.10
Cr	ppm	10.00	5.00	-10.00	10.00	-10.00	10.00	-10.00	10.00	-10.00	-10.00
Ni	ppm	9.00	4.00	1.00	8.00	9.00	8.00	6.00	9.00	5.00	6.00
Co	ppm	5.00	21.70	4.00	15.00	6.00	8.00	7.00	13.00	6.00	7.00
Sc	ppm	7.00	6.80	6.00	10.00	10.00	10.00	10.00	10.00	9.00	9.00
V	ppm	30.00	19.00	19.00	63.00	28.00	59.00	57.00	56.00	46.00	54.00
Cu	ppm	5.00	4.00	4.00	9.00	11.00	6.00	4.00	9.00	2.00	7.00
Zn	ppm	69.00	115.00	61.00	153.00	58.00	130.00	197.00	310.00	63.00	79.00
Y	ppm	57.40	62.70	45.80	42.60	30.70	42.50	41.30	42.70	39.70	41.90
Rb	ppm	242.00	288.00	261.00	140.50	248.00	372.00	404.00	311.00	297.00	431.00
Sr	ppm	61.00	49.70	64.40	205.00	141.50	100.00	135.00	169.50	174.00	70.70
Cs	ppm	4.41	5.45	5.16	4.88	7.27	18.45	15.55	11.60	7.90	14.85
Ba	ppm	908.00	992.00	932.00	1370.00	1220.00	1765.00	1700.00	1500.00	1255.00	1440.00
Th	ppm	48.40	47.60	51.70	40.30	48.80	48.50	53.10	38.60	47.50	48.60
U	ppm	7.80	8.17	5.35	6.19	6.61	7.26	10.15	8.03	6.93	8.00
Pb	ppm	17.00	17.00	12.00	13.00	16.00	31.00	23.00	16.00	14.00	17.00
Zr	ppm	307.00	378.00	381.00	358.00	381.00	407.00	430.00	373.00	402.00	404.00
Hf	ppm	9.00	10.60	9.00	9.40	9.30	8.90	9.80	8.80	9.00	8.80
Nb	ppm	25.60	28.30	26.00	23.80	23.90	22.90	25.30	22.90	23.10	23.40
Ta	ppm	2.50	2.62	2.80	2.00	2.20	2.10	2.40	1.70	2.20	2.10
La	ppm	106.00	117.00	117.50	72.90	72.70	125.00	97.90	90.30	87.60	94.90
Ce	ppm	196.00	212.00	228.00	147.00	138.00	246.00	195.50	174.50	165.50	192.00
Pr	ppm	23.40	25.50	23.60	16.35	14.55	25.10	20.30	17.65	17.65	20.10
Nd	ppm	81.20	90.60	79.70	57.20	49.90	82.20	67.30	61.70	58.80	66.80
Sm	ppm	13.50	16.40	12.55	9.77	8.62	13.30	11.05	10.05	8.69	10.65
Eu	ppm	2.21	2.56	2.05	1.67	1.62	2.69	2.14	1.92	1.83	2.06
Gd	ppm	11.45	13.40	10.85	8.65	6.92	11.35	9.28	8.71	8.45	9.16
Tb	ppm	1.55	2.00	1.33	1.27	1.26	1.44	1.24	1.37	1.08	1.21
Dy	ppm	9.67	11.60	8.00	7.25	6.38	8.03	7.72	7.30	7.11	7.53
Ho	ppm	1.99	2.38	1.67	1.45	1.34	1.57	1.66	1.59	1.38	1.47
Er	ppm	6.06	6.94	5.16	4.21	4.06	4.72	4.67	4.14	4.31	4.47
Tm	ppm	0.79	1.01	0.77	0.59	0.63	0.71	0.71	0.66	0.63	0.65
Yb	ppm	5.41	6.71	4.55	3.72	3.72	3.99	4.07	3.93	3.59	3.90
Lu	ppm	0.90	0.99	0.74	0.60	0.55	0.58	0.60	0.55	0.59	0.59
Eu/Eu*		0.54	0.53	0.54	0.56	0.64	0.67	0.65	0.63	0.65	0.64
$(La/Yb)_N$		14.05	12.51	18.52	14.06	14.02	22.47	17.25	16.48	17.50	17.45
Ga/Al		2.57	2.89	2.43	2.26	2.44	2.67	3.00	2.62	2.62	2.81
Temp	K	1123.00	1161.16	1167.52	1085.28	1177.48	1170.52	1154.78	1100.21	1127.19	1148.28
Temp upper error	K	1155.74	1194.46	1200.44	1123.40	1209.57	1204.42	1190.93	1137.94	1164.22	1183.81
Temp lower error	K	1091.88	1129.47	1136.16	1049.44	1146.85	1138.28	1120.56	1064.68	1092.22	1114.62
Temp	˚C	850.00	888.16	894.52	812.28	904.48	897.52	881.78	827.21	854.19	875.28
1 sigma error		31.93	32.49	32.14	36.98	31.36	33.07	35.18	36.63	36.00	34.59
Factor	M	1.11	1.04	1.01	1.52	0.94	1.04	1.19	1.44	1.32	1.18

$Eu/Eu^* = (Eu/(Sm \times Gd))_N^{0.5}$

Normalising values from Taylor and McLennon 1995

Appendix 3 Supplementary material for Temporal, geochemical and isotopic constraints on plume-driven felsic and mafic components in a large igneous province

Appendix 3 Table A1 Whole-rock geochemical composition for Gawler Range Volcanics samples

R number	2074199	2079420	2137570	2137571	2137572	2137574	2137575	2137576	2137577	2137599	2137600
Other Sample Number	SM2014-001										
Drill_Hole			MSDP01	MSDP01	MSDP01	MSDP01	MSDP01	MSDP01	MSDP01	MSDP01	MSDP01
Depth_From			390.00	569.00	589.00	607.00	630.00	650.00	663.00	411.00	431.00
Depth_To			391.00	570.00	590.00	608.00	631.00	651.00	664.00	412.00	432.00
Data Source	SARIG	SARIG	SARIG	SARIG	SARIG	SARIG	SARIG	SARIG	SARIG	SARIG	SARIG
Location	Myall Creek	Myall Creek	Myall Creek	Myall Creek	Myall Creek	Myall Creek	Myall Creek	Myall Creek	Myall Creek	Myall Creek	Myall Creek
Suite	LGRV	LGRV	LGRV	LGRV	LGRV	LGRV	LGRV	LGRV	LGRV	LGRV	LGRV
Formation											
Map Unit	Ma15	Ma15	Ma15	Ma15	Ma15	Ma15	Ma15	Ma15	Ma15	Ma15	Ma15
Easting	721997.73	705544.08	724657.89	724657.89	724657.89	724657.89	724657.89	724657.89	724657.89	724657.89	724657.89
Northing	6385710.85	6398501.84	6408347.76	6408347.76	6408347.76	6408347.76	6408347.76	6408347.76	6408347.76	6408347.76	6408347.76
Zone	53	53	53	53	53	53	53	53	53	53	53
Longitude	137.366701	137.188600	137.389625	137.389625	137.389625	137.389625	137.389625	137.389625	137.389625	137.389625	137.389625
Latitude	-32.643939	-32.531820	-32.439371	-32.439371	-32.439371	-32.439371	-32.439371	-32.439371	-32.439371	-32.439371	-32.439371
Datum	GDA94	GDA94	GDA94	GDA94	GDA94	GDA94	GDA94	GDA94	GDA94	GDA94	GDA94
Age	1591.00	1591.00	1591.00	1591.00	1591.00	1591.00	1591.00	1591.00	1591.00	1591.00	1591.00
Lithology	Dacite	Dacite	Rhyolite	Rhyolite	Rhyolite	Ignimbrite	Ignimbrite	Rhyolite	Ignimbrite	Rhyolite	Rhyolite
SiO_2	64.20	74.90	66.08	65.70	65.70	65.53	65.79	64.25	64.05	66.30	65.55
TiO_2	0.96	0.21	0.82	0.77	0.78	0.77	0.73	0.68	0.72	0.76	0.75
Al_2O_3	13.70	11.60	14.45	14.09	14.20	14.66	14.34	13.50	14.35	13.93	13.87
FeO	0.00	0.00	0.00	0.00	0.00	0.00	0.00	0.00	0.00	0.00	0.00
Fe_2O_3	6.89	2.16	4.48	4.80	4.62	4.92	4.39	4.13	4.73	4.91	4.93
MnO	0.05	0.02	0.10	0.13	0.11	0.10	0.11	0.16	0.10	0.13	0.12
MgO	0.80	0.36	1.55	1.60	1.70	1.45	1.53	1.91	1.74	1.58	1.42
CaO	0.11	0.14	1.21	1.27	1.53	1.37	1.73	3.04	2.56	1.14	1.35
Na_2O	0.11	1.62	2.75	3.33	2.91	2.46	2.35	2.34	2.00	3.34	3.51
K_2O	8.21	5.63	5.73	5.70	5.71	5.64	5.73	5.23	5.51	6.14	6.17
P_2O_5	0.15	0.09	0.23	0.18	0.20	0.19	0.18	0.13	0.16	0.17	0.17
LOI	1.76	1.06	3.12	2.69	3.16	3.43	3.49	4.98	4.47	2.26	2.58
Total	96.94	97.79	100.52	100.26	100.62	100.52	100.37	100.35	100.39	100.66	100.42
F	710.00	500.00	1112.00	636.00	746.00	965.00	967.00	926.00	850.00	496.00	570.00
Ga	20.70	18.10	20.00	17.40	18.40	19.90	19.30	17.80	18.20	18.70	17.80
Cr	10.00	10.00	0.00	0.00	0.00	0.00	0.00	0.00	0.00	0.00	0.00
Ni	6.00	0.00	3.00	1.00	0.00	0.00	0.00	0.00	1.00	3.00	3.00
Co	6.00	2.00	10.10	7.60	8.30	6.30	5.60	5.40	5.50	9.60	7.20
Sc	13.00	4.00	0.00	0.00	0.00	0.00	0.00	0.00	0.00	0.00	0.00
V	69.00	0.00	28.00	18.00	26.00	35.00	25.00	26.00	21.00	26.00	32.00
Cu	2.00	1.00	2.00	4.00	3.00	3.00	2.00	2.00	3.00	3.00	2.00
Zn	26.00	102.00	39.00	61.00	52.00	37.00	38.00	38.00	48.00	48.00	38.00
Y	48.90	36.60	56.40	49.40	50.90	47.40	48.30	51.70	47.50	51.10	49.20
Rb	339.00	269.00	210.70	201.30	198.70	228.30	230.20	211.90	240.30	219.40	206.30
Sr	124.50	15.90	59.90	84.80	71.50	69.60	72.80	67.60	140.60	82.70	72.50
Cs	5.07	2.19	4.48	2.11	2.72	5.30	4.34	4.66	8.78	1.38	1.36
Ba	2830.00	343.00	1191.50	1345.00	1420.50	1068.60	1292.70	1038.30	1346.90	1258.60	1179.40
Th	35.20	66.30	33.12	32.77	33.21	34.88	34.30	33.27	35.21	32.79	33.23
U	5.30	3.14	6.88	5.68	5.63	6.83	7.44	8.45	8.16	5.59	7.05
Pb	22.00	22.00	0.00	7.00	0.00	7.00	0.00	6.00	7.00	8.00	11.00
Zr	356.00	166.00	396.00	407.00	400.00	410.00	418.00	420.00	418.00	373.00	374.00
Hf	9.70	5.70	10.10	10.60	10.30	11.00	10.30	10.50	10.90	9.50	10.10
Nb	22.70	31.90	24.50	23.60	24.00	25.30	24.70	22.50	23.20	23.30	22.80
Ta	1.70	2.60	1.80	1.70	1.70	1.80	1.80	1.60	1.80	1.70	1.70
La	67.50	44.40	94.80	89.30	91.50	98.20	88.60	109.40	112.10	90.90	86.80
Ce	142.00	100.00	183.00	173.40	174.60	180.70	170.60	205.50	212.10	169.90	164.80
Pr	16.60	9.74	20.49	19.29	19.85	21.06	19.16	23.10	23.02	19.66	19.04
Nd	56.80	28.50	71.90	67.10	68.80	74.50	66.40	80.70	79.00	69.10	66.40
Sm	10.05	5.85	12.98	12.03	12.54	12.74	11.76	13.79	13.44	12.38	12.05
Eu	1.94	0.63	2.60	2.36	2.53	2.56	2.28	2.71	2.56	2.41	2.35
Gd	8.52	4.70	10.83	9.81	10.53	9.88	9.59	10.73	10.09	10.04	9.84
Tb	1.52	0.90	1.70	1.51	1.64	1.48	1.46	1.56	1.55	1.53	1.55
Dy	9.42	5.89	10.09	8.94	9.11	8.92	8.68	9.19	8.95	9.01	9.11
Ho	1.79	1.26	2.03	1.81	1.93	1.78	1.77	1.89	1.86	1.83	1.82
Er	5.62	4.08	5.80	5.22	5.35	5.16	5.08	5.36	5.34	5.19	5.23
Tm	0.79	0.59	0.88	0.78	0.80	0.75	0.78	0.81	0.81	0.77	0.84
Yb	5.03	4.44	5.40	4.81	5.04	4.93	5.01	5.20	5.06	5.06	4.89
Lu	0.80	0.71	0.89	0.76	0.79	0.77	0.76	0.82	0.80	0.75	0.76
Eu/Eu*	0.64	0.37	0.67	0.66	0.67	0.70	0.66	0.68	0.67	0.66	0.66
$(La/Yb)_N$	9.63	7.17	12.59	13.32	13.02	14.29	12.69	15.09	15.89	12.89	12.73
Ga/Al	2.85	2.95	2.62	2.33	2.45	2.56	2.54	2.49	2.40	2.54	2.42
Temp	1153.84	1059.29	1113.73	1093.47	1097.02	1124.89	1115.07	1072.21	1101.42	1077.05	1064.45
Temp upper error	1186.65	1087.46	1151.49	1133.11	1136.13	1162.44	1153.65	1113.76	1140.96	1116.39	1104.67
Temp lower error	1122.60	1032.38	1078.14	1056.29	1060.29	1089.48	1078.76	1033.42	1064.31	1040.15	1026.82
Temp	880.84	786.29	840.73	820.47	824.02	851.89	842.07	799.21	828.42	804.05	791.45
1 sigma error	32.03	27.54	36.67	38.41	37.92	36.48	37.45	40.17	38.33	38.12	38.92
Factor	1.04	1.05	1.40	1.57	1.53	1.35	1.44	1.75	1.53	1.61	1.71

$Eu/Eu^* = (Eu/(Sm \times Gd))_N^{0.5}$

Normalising values from Taylor and McLennon 1995

Appendix 3 Supplementary material for Temporal, geochemical and isotopic constraints on plume-driven felsic and mafic components in a large igneous province

Appendix 3 Table A1 Whole-rock geochemical composition for Gawler Range Volcanics samples

R number	2137601	2137602	2137603	2137604	2137605	2137606	2018596	2018616	1840802	
Other Sample Number							SM16	CW-PA-16	884Bi5	884BI2
Drill_Hole	MSDP01	MSDP01	MSDP01	MSDP01	MSDP01	MSDP01				
Depth_From	450.00	469.00	489.00	510.00	530.00	549.00				
Depth_To	451.00	470.00	490.00	511.00	531.00	550.00				
Data Source	SARIG	SARIG	SARIG	SARIG	SARIG	SARIG	SARIG	SARIG	Wade et al this study	Wade et al this study
Location	Myall Creek	Myall Creek	Myall Creek	Myall Creek	Myall Creek	Myall Creek	Southern GRV	Southern GRV	Southern GRV	Southern GRV
Suite	LGRV	LGRV	LGRV	LGRV	LGRV	LGRV	LGRV	LGRV	LGRV	LGRV
Formation							Bittali Rhyolite	Bittali Rhyolite	Bittali Rhyolite	Bittali Rhyolite
Map Unit	Ma15	Ma15	Ma15	Ma15	Ma15	Ma15	Mab	Mab	Mab	Mab
Easting	724657.89	724657.89	724657.89	724657.89	724657.89	724657.89	682252.57	681773.66	628250.00	628598.67
Northing	6408347.76	6408347.76	6408347.76	6408347.76	6408347.76	6408347.76	6390449.00	6390460.45	6381850.00	6386398.68
Zone	53	53	53	53	53	53	53	53	53	53
Longitude	137.389625	137.389625	137.389625	137.389625	137.389625	137.389625	136.942291	136.937187	136.368130	
Latitude	-32.439371	-32.439371	-32.439371	-32.439371	-32.439371	-32.439371	-32.608494	-32.608469	-32.693623	
Datum	GDA94	GDA94	GDA94	GDA94	GDA94	GDA94	GDA94	GDA94	GDA94	
Age	1591.00	1591.00	1591.00	1591.00	1591.00	1591.00	1589.30	1589.30	1589.30	1589.30
Lithology	Rhyolite	Rhyolite	Rhyolite	Rhyolite	Rhyolite	Rhyolite	Rhyodacite	Rhyolite	Rhyolite	Rhyolite
SiO_2	66.06	65.58	65.54	65.15	65.43	65.39	67.20	71.50	72.65	73.65
TiO_2	0.76	0.76	0.74	0.76	0.75	0.79	0.84	0.59	0.20	0.40
Al_2O_3	14.00	13.96	14.02	13.78	13.92	13.88	12.90	12.30	13.20	14.00
FeO	0.00	0.00	0.00	0.00	0.00	0.00	0.00	0.00	0.43	0.12
Fe_2O_3	5.16	4.74	4.24	4.94	5.08	4.77	5.60	4.23	1.55	1.19
MnO	0.10	0.12	0.12	0.12	0.10	0.13	0.08	0.02	0.05	-0.01
MgO	1.27	1.20	1.74	1.74	1.55	1.58	0.54	0.30	0.34	0.10
CaO	1.02	1.16	1.44	1.35	1.03	1.50	0.34	0.26	1.54	0.19
Na_2O	3.44	3.67	2.82	2.78	3.10	2.92	2.14	1.76	3.04	2.95
K_2O	6.30	6.23	5.97	5.88	6.10	6.26	5.85	6.15	5.40	6.00
P_2O_5	0.17	0.19	0.18	0.18	0.16	0.19	0.16	0.12	0.06	0.06
LOI	2.09	2.62	3.73	3.48	2.81	3.24	1.67	1.68	1.92	1.03
Total	100.37	100.23	100.54	100.16	100.03	100.65	97.32	98.91	100.38	99.68
F	638.00	425.00	678.00	811.00	711.00	737.00	0.00	500.00	650.00	950.00
Ga	18.10	17.90	19.50	18.80	19.10	19.30	22.40	18.80	18.40	25.00
Cr	0.00	0.00	0.00	0.00	0.00	0.00	-10.00	10.00	4.00	-1.00
Ni	2.00	1.00	2.00	3.00	1.00	4.00	2.00	4.00	4.00	-2.00
Co	7.20	5.90	8.30	9.50	7.50	7.90	4.00	3.00	77.80	64.60
Sc	0.00	0.00	0.00	0.00	0.00	0.00	12.00	9.00	3.70	7.90
V	22.00	27.00	24.00	30.00	27.00	32.00	11.00	6.00	15.30	3.70
Cu	0.00	4.00	3.00	6.00	2.00	5.00	3.00	3.00	4.00	6.00
Zn	45.00	34.00	46.00	49.00	53.00	62.00	118.00	57.00	80.00	25.00
Y	51.30	50.80	54.50	51.00	51.40	53.70	49.00	57.40	19.20	84.70
Rb	223.40	192.90	231.10	232.90	234.20	253.50	228.00	316.00	154.00	245.00
Sr	80.90	78.30	70.90	79.90	125.20	100.30	102.50	96.50	174.00	94.00
Cs	2.00	1.20	4.10	3.38	2.20	3.12	2.31	2.79	1.09	2.64
Ba	1263.40	1584.20	1173.60	1183.90	1533.00	1900.50	2680.00	3440.00	646.00	1440.00
Th	34.48	33.59	33.15	34.04	34.25	33.40	29.70	37.00	26.80	35.80
U	5.50	7.78	6.44	7.51	5.72	6.22	6.74	6.86	4.48	7.37
Pb	9.00	8.00	10.00	7.00	9.00	6.00	70.00	18.00	23.00	42.00
Zr	403.00	394.00	398.00	411.00	418.00	437.00	383.00	365.00	167.00	522.00
Hf	10.30	10.40	10.10	10.70	10.50	10.80	9.80	8.90	4.99	13.80
Nb	24.00	23.70	23.60	23.90	24.00	24.80	20.50	22.30	11.20	25.40
Ta	1.80	1.70	1.70	1.70	1.80	1.80	1.50	1.40	1.05	2.03
La	93.00	93.10	92.90	92.50	94.20	90.80	74.30	103.00	74.30	203.00
Ce	175.30	176.50	169.30	175.10	179.20	175.60	152.50	165.50	145.00	397.00
Pr	20.09	20.06	20.42	19.60	19.99	19.74	15.55	20.70	16.50	45.60
Nd	68.60	67.60	71.20	69.30	68.90	69.20	56.20	73.10	55.10	163.00
Sm	12.23	12.22	12.32	12.27	12.39	12.42	10.70	12.25	9.68	28.40
Eu	2.48	2.53	2.34	2.42	2.49	2.42	2.28	2.61	1.27	4.10
Gd	10.13	10.04	10.04	9.67	9.89	10.14	9.90	11.35	6.30	22.10
Tb	1.60	1.56	1.57	1.59	1.56	1.59	1.48	1.67	0.83	3.08
Dy	9.36	9.19	9.35	9.23	9.17	9.32	9.13	9.41	4.05	16.50
Ho	1.91	1.91	1.96	1.87	1.88	1.90	1.89	1.95	0.75	3.31
Er	5.52	5.33	5.51	5.44	5.30	5.38	5.29	5.28	1.92	9.01
Tm	0.81	0.80	0.88	0.79	0.81	0.83	0.76	0.80	0.28	1.30
Yb	5.12	5.09	5.22	5.24	5.06	5.22	4.98	5.11	1.70	7.90
Lu	0.79	0.82	0.82	0.85	0.77	0.80	0.83	0.75	0.24	1.20
Eu/Eu*	0.68	0.70	0.64	0.68	0.69	0.66	0.68	0.68	0.50	0.50
$(La/Yb)_N$	13.03	13.12	12.77	12.66	13.35	12.48	10.70	14.46	31.35	18.43
Ga/Al	2.44	2.42	2.63	2.58	2.59	2.63	3.28	2.89	2.63	3.37
Temp	1084.81	1072.45	1094.84	1099.72	1100.23	1093.02	1137.28	1138.54	1006.70	1180.99
Temp upper error	1124.87	1112.96	1134.02	1139.10	1139.85	1133.86	1172.71	1173.03	1039.18	1218.73
Temp lower error	1047.27	1034.54	1058.06	1062.76	1063.05	1054.80	1103.72	1105.82	976.01	1145.31
Temp	811.81	799.45	821.84	826.72	827.23	820.02	864.28	865.54	733.70	907.99
1 sigma error	38.80	39.21	37.98	38.17	38.40	39.53	34.49	33.60	31.58	36.71
Factor	1.62	1.70	1.54	1.53	1.54	1.63	1.21	1.16	1.49	1.19

$Eu/Eu^* = (Eu/(Sm \times Gd))_N^{0.5}$

Normalising values from Taylor and McLennon 1995

Appendix 3 Supplementary material for Temporal, geochemical and isotopic constraints on plume-driven felsic and mafic components in a large igneous province

Appendix 3 Table A1 Whole-rock geochemical composition for Gawler Range Volcanics samples

R number	2018624	2018599	2018210	2132375	884BI6	2721825	2721824	2746125	2746129
Other Sample Number	CW-22	SM19							
Drill_Hole								MSDP10	MSDP10
Depth_From								461.40	543.70
Depth_To								461.79	543.92
Data Source	SARIG	SARIG	SARIG	SARIG	SARIG	Wade et al this study	Wade et al this study	Wade et al this study	SARIG
Location	Southern GRV	Southern GRV	Southern GRV	Southern GRV	Southern GRV	Southern GRV	Southern GRV	Southern GRV	Southern GRV
Suite	LGRV	LGRV	LGRV	LGRV	LGRV	LGRV	LGRV	LGRV	LGRV
Formation	Bittali Rhyolite	Bittali Rhyolite	Bittali Rhyolite	Bittali Rhyolite	Bittali Rhyolite	Bittali Rhyolite	Bittali Rhyolite	Bittali Rhyolite	Bittali Rhyolite
Map Unit	Mab	Mab	Mab	Mab	Mab	Mab	Mab	Mab	Mab
Easting	679438.61	679451.47	679758.62	626910.26	543298.58	626926.10	626448.78	562243.79	562243.79
Northing	6390831.43	6390829.45	6390276.57	6381493.88	6385048.65	6384299.63	6386009.35	6386983.44	6386983.44
Zone	53	53	53	53	53	53	53	53	53
Longitude	136.912243	136.912381	136.915759	136.353890	0.000000	136.353677	136.348357	135.663717	135.663717
Latitude	-32.605506	-32.605522	-32.610457	-32.696990	0.000000	-32.671685	-32.656321	-32.653022	-32.653022
Datum	GDA94	GDA94	GDA94	GDA94		GDA94	GDA94	GDA94	GDA94
Age	1589.30	1589.30	1589.30	1589.30	1589.30	1589.30	1589.30	1589.30	1589.30
Lithology	Rhyolite	Rhyolite	Rhyolite	Rhyolite	Rhyolite	Rhyolite	Rhyolite	Rhyolite	Rhyolite
SiO_2	74.30	74.90	75.20	76.40	77.81	74.90	74.16	77.91	79.54
TiO_2	0.35	0.41	0.39	0.17	0.18	0.15	0.27	0.17	0.12
Al_2O_3	12.05	12.55	13.20	13.30	11.46	13.20	13.03	12.20	9.45
FeO	0.00	0.00	0.00	0.00	0.00	-0.10	-0.10	0.15	0.63
Fe_2O_3	1.54	2.62	1.94	1.34	0.00	2.18	2.26	0.71	1.50
MnO	0.01	0.01	0.02	0.01	0.06	0.15	0.10	0.02	0.05
MgO	0.18	0.24	0.08	0.16	0.18	0.18	0.06	0.14	0.30
CaO	0.15	0.14	0.31	0.21	0.28	0.12	0.07	0.20	0.13
Na_2O	1.63	1.68	3.16	3.08	2.72	3.34	2.64	1.34	1.48
K_2O	5.97	5.69	5.42	5.65	5.06	5.03	5.90	5.78	4.96
P_2O_5	0.02	0.03	0.06	0.03	0.01	0.03	0.03	0.01	0.01
LOI	1.34	1.52	0.85	0.70	0.41	0.97	0.95	1.09	0.94
Total	97.54	99.79	100.63	101.05	98.17	100.14	99.37	99.72	99.11
F	0.00	0.00	240.00	0.00	0.00	700.00	900.00	300.00	650.00
Ga	17.70	20.90	23.00	18.60	18.00	21.00	24.00	19.50	13.50
Cr	10.00	-10.00	30.00	10.00	-1.00	7.00	8.00	3.00	2.00
Ni	2.00	6.00	2.00	1.00	-1.00	6.00	4.00	-2.00	-2.00
Co	1.00	1.00	1.00	1.00	0.00	13.80	16.60	30.20	49.70
Sc	6.00	7.00	7.00	3.00	3.00	3.70	7.00	2.50	2.90
V	-5.00	-5.00	-5.00	9.00	-2.00	5.80	2.10	0.50	0.50
Cu	5.00	19.00	11.00	2.00	1.00	2.00	16.00	-2.00	4.00
Zn	32.00	53.00	74.00	26.00	23.00	40.00	110.00	20.00	300.00
Y	87.80	52.80	84.10	25.20	46.00	21.50	52.00	53.40	43.30
Rb	253.00	253.00	253.00	160.00	277.00	180.00	239.00	327.00	217.00
Sr	74.90	60.60	140.50	161.00	16.00	131.00	31.20	20.60	22.40
Cs	3.28	3.30	1.99	1.06	4.00	1.12	1.75	6.16	2.19
Ba	1735.00	2490.00	1880.00	1135.00	102.00	668.00	698.00	97.50	84.50
Th	41.90	34.50	37.00	26.20	37.00	31.80	31.40	34.80	26.60
U	6.62	6.83	7.16	2.82	7.50	5.68	6.28	7.06	5.74
Pb	11.00	11.00	29.00	35.00	48.00	16.00	23.00	25.00	158.00
Zr	370.00	432.00	557.00	151.00	209.00	139.00	440.00	206.00	150.00
Hf	10.50	11.60	13.80	4.70	7.00	4.72	12.00	7.20	5.40
Nb	22.10	22.90	26.60	11.10	23.00	14.00	23.00	22.80	17.40
Ta	1.80	1.70	1.90	0.80	0.00	1.12	1.51	1.72	1.36
La	190.50	96.20	99.40	70.80	84.00	58.00	114.00	74.60	61.60
Ce	250.00	183.50	198.00	131.50	107.00	114.00	262.00	151.00	122.00
Pr	35.10	19.35	21.60	14.60	21.00	12.80	27.60	18.20	15.20
Nd	128.50	66.80	77.70	51.20	82.00	43.20	94.70	65.20	53.90
Sm	20.90	12.65	14.55	9.05	0.00	8.10	17.30	12.60	11.40
Eu	2.98	1.59	2.20	1.24	0.00	0.95	1.45	0.47	0.40
Gd	20.00	11.40	12.50	6.53	0.00	5.40	12.10	10.50	9.92
Tb	2.58	1.78	1.90	0.85	0.00	0.75	1.86	1.66	1.61
Dy	14.15	9.80	12.35	4.65	0.00	3.94	10.20	9.45	8.85
Ho	2.80	1.96	2.52	0.80	0.00	0.76	1.98	2.06	1.74
Er	7.96	5.41	7.32	2.33	0.00	2.14	5.46	5.73	4.55
Tm	1.02	0.80	1.11	0.29	0.00	0.27	0.81	0.85	0.63
Yb	6.65	4.83	6.93	1.95	0.00	1.91	5.14	5.46	3.71
Lu	1.01	0.80	1.07	0.28	0.00	0.27	0.77	0.80	0.56
Eu/Eu*	0.45	0.40	0.50	0.49		0.44	0.31	0.12	0.11
$(La/Yb)_N$	20.55	14.29	10.29	26.04		21.78	15.91	9.80	11.91
Ga/Al	2.78	3.15	3.29	2.64	2.97	3.01	3.48	3.02	2.70
Temp	1154.59	1184.67	1181.90	1028.52	1063.57	1022.98	1161.03	1096.38	1043.64
Temp upper error	1188.04	1218.53	1220.80	1057.87	1094.88	1051.61	1197.12	1124.73	1071.63
Temp lower error	1122.78	1152.44	1145.18	1000.58	1033.81	995.70	1126.86	1069.26	1016.91
Temp	881.59	911.67	908.90	755.52	790.57	749.98	888.03	823.38	770.64
1 sigma error	32.63	33.04	37.81	28.64	30.53	27.96	35.13	27.73	27.36
Factor	1.06	1.01	1.24	1.22	1.22	1.19	1.17	0.96	1.09

$Eu/Eu^* = (Eu/(Sm \times Gd))_N^{0.5}$

Normalising values from Taylor and McLennon 1995

Appendix 3 Supplementary material for Temporal, geochemical and isotopic constraints on plume-driven felsic and mafic components in a large igneous province

Appendix 3 Table A1 Whole-rock geochemical composition for Gawler Range Volcanics samples

R number	2138004	2138002	2138000	2137999	2018597	2018612	2018614	2018615	2018625
Other Sample Number	2748522	2748521	2748520	2748519	SM17	CW-PA-12	CW-PA-14	CW-PA-15	CW-23
Drill_Hole	MSDP10	MSDP10	MSDP10	MSDP10					
Depth_From	468.9	481	492	500					
Depth_To	469.75	482	493	501					
Data Source	SARIG	SARIG	SARIG	SARIG	SARIG	SARIG	SARIG	SARIG	SARIG
Location	Southern GRV	Southern GRV	Southern GRV	Southern GRV	Southern GRV	Southern GRV	Southern GRV	Southern GRV	Southern GRV
Suite	LGRV	LGRV	LGRV	LGRV	LGRV	LGRV	LGRV	LGRV	LGRV
Formation	Bittali Rhyolite	Bittali Rhyolite	Bittali Rhyolite	Bittali Rhyolite	Bittali Rhyolite	Bittali Rhyolite	Bittali Rhyolite	Bittali Rhyolite	Bittali Rhyolite
Map Unit	Mab	Mab	Mab	Mab	Mab	Mab	Mab	Mab	Mab
Easting	562243.79	562243.79	562243.79	562243.79	682016.59	681946.80	681889.43	681879.27	679352.84
Northing	6386983.44	6386983.44	6386983.44	6386983.44	6390920.82	6390280.09	6390389.26	6390424.95	6391142.98
Zone	53	53	53	53	53	53	53	53	53
Longitude	135.663717	135.663717	135.663717	135.663717	136.939686	136.939067	136.938435	136.938319	136.911270
Latitude	-32.653022	-32.653022	-32.653022	-32.653022	-32.604279	-32.610067	-32.609092	-32.608772	-32.602711
Datum	GDA94	GDA94	GDA94	GDA94	GDA94	GDA94	GDA94	GDA94	GDA94
Age	1589.30	1589.30	1589.30	1589.30	1589.30	1589.30	1589.30	1589.30	1589.30
Lithology	Tuff	Ignimbrite	Ignimbrite	Tuff	Tuff	Tuff	Tuff	Tuff	Tuff
SiO_2	77.14	77.49	76.52	76.53	75.30	75.00	69.00	68.20	77.90
TiO_2	0.18	0.19	0.17	0.19	0.42	0.33	0.76	0.73	0.21
Al_2O_3	11.60	11.57	10.80	11.92	12.15	11.70	13.75	13.15	8.35
FeO	0.94	0.63	1.17	1.39	0.00	0.00	0.00	0.00	0.00
Fe_2O_3	1.76	1.70	2.26	2.01	2.56	4.55	6.33	5.62	4.78
MnO	0.07	0.03	0.07	0.07	0.01	0.02	0.12	0.10	0.01
MgO	0.17	0.21	0.16	0.11	0.28	0.32	0.57	0.44	0.18
CaO	0.13	0.37	0.90	0.41	0.01	0.03	0.86	1.79	0.13
Na_2O	1.51	1.04	1.80	2.06	-0.01	-0.01	2.25	2.35	0.10
K_2O	5.41	5.29	4.95	5.99	5.79	4.72	5.25	5.33	5.09
P_2O_5	<0.01	<0.01	<0.01	<0.01	0.04	0.02	0.17	0.13	0.01
LOI	1.14	1.78	1.35	0.95	1.84	2.09	2.27	2.39	1.16
Total	100.05	100.30	100.15	101.63	98.39	98.77	101.33	100.23	97.92
F	435.00	1964.00	4556.00	1634.00	0.00	0.00	0.00	0.00	0.00
Ga	18.00	20.80	15.20	16.60	18.40	18.80	22.50	20.90	12.50
Cr	-20.00	-20.00	-20.00	-20.00	-10.00	-10.00	-10.00	-10.00	10.00
Ni	-1.00	-1.00	-1.00	-1.00	1.00	1.00	3.00	1.00	1.00
Co	0.20	0.40	0.40	0.40	1.00	2.00	5.00	4.00	-1.00
Sc	-10.00	-10.00	-10.00	-10.00	6.00	6.00	12.00	11.00	4.00
V	-10.00	-10.00	-10.00	-10.00	-5.00	9.00	16.00	15.00	5.00
Cu	5.00	4.00	3.00	1.00	2.00	13.00	2.00	5.00	3.00
Zn	98.00	470.00	950.00	32.00	46.00	195.00	120.00	77.00	31.00
Y	52.60	50.90	53.80	52.40	56.40	56.20	52.30	49.40	41.80
Rb	300.50	306.90	248.10	296.30	277.00	391.00	237.00	236.00	190.50
Sr	21.70	19.20	21.90	33.70	18.20	18.00	67.80	73.00	21.40
Cs	4.66	5.39	3.55	3.54	3.72	3.64	2.36	4.53	1.58
Ba	91.10	102.90	78.40	127.90	1440.00	621.00	2320.00	1925.00	944.00
Th	32.83	30.84	30.06	31.89	34.60	44.40	38.20	38.00	33.20
U	6.88	6.85	6.53	6.30	7.97	7.59	6.64	6.57	5.36
Pb	65.00	104.00	413.00	22.00	11.00	14.00	8.00	27.00	14.00
Zr	194.00	202.00	198.00	209.00	436.00	476.00	446.00	437.00	301.00
Hf	6.00	6.60	6.40	6.50	11.50	11.10	9.90	10.00	8.10
Nb	23.70	23.00	22.90	24.30	23.30	22.00	20.30	19.90	17.40
Ta	1.90	1.80	1.80	2.00	1.80	2.00	1.70	1.70	1.30
La	67.00	70.10	66.90	67.00	121.00	42.70	85.90	82.00	65.60
Ce	142.20	143.80	145.50	143.50	226.00	105.50	177.50	167.00	138.00
Pr	15.77	15.71	16.17	16.06	22.50	10.95	18.70	18.85	14.95
Nd	56.20	54.70	56.50	56.90	80.00	39.80	64.70	64.70	51.40
Sm	11.13	10.69	10.97	11.06	13.45	8.32	10.90	11.00	8.70
Eu	0.39	0.39	0.38	0.44	2.05	1.21	2.77	2.77	1.04
Gd	9.03	8.40	8.84	8.76	12.30	8.74	10.70	10.80	7.10
Tb	1.45	1.42	1.38	1.43	1.71	1.40	1.45	1.36	1.11
Dy	8.64	8.36	8.53	8.86	9.79	9.15	9.22	8.66	7.00
Ho	1.83	1.74	1.77	1.80	2.03	2.01	1.97	1.89	1.41
Er	5.44	5.12	5.26	5.42	5.93	6.09	5.67	5.83	4.35
Tm	0.81	0.79	0.78	0.81	0.84	0.94	0.82	0.81	0.63
Yb	5.07	5.05	4.88	5.45	5.22	5.64	5.21	4.70	4.19
Lu	0.79	0.81	0.73	0.78	0.88	0.90	0.78	0.74	0.68
Eu/Eu*	0.12	0.13	0.12	0.14	0.49	0.43	0.78	0.78	0.40
$(La/Yb)_N$	9.48	9.96	9.83	8.82	16.63	5.43	11.83	12.51	11.23
Ga/Al	2.93	3.40	2.66	2.63	2.86	3.04	3.09	3.00	2.83
Temp		1099.11	1055.93						
Temp upper error		1126.90	1087.03						
Temp lower error		1072.49	1026.37						
Temp		826.11	782.93						
1 sigma error		27.21	30.33						
Factor		0.92	1.23						

$Eu/Eu^* = (Eu/(Sm \times Gd))_N^{0.5}$

Normalising values from Taylor and McLennon 1995

Appendix 3 Supplementary material for Temporal, geochemical and isotopic constraints on plume-driven felsic and mafic components in a large igneous province

Appendix 3 Table A1 Whole-rock geochemical composition for Gawler Range Volcanics samples

R number	2018626	2018627	2115406	1840815	88429	88428	88427	2729181	2729182
Other Sample Number	CW-24	CW-25		884T30	884T29	884T28	884T27		
Drill_Hole								6608	6608
Depth_From								113	151.28
Depth_To								113.25	151.46
Data Source	SARIG	SARIG	SARIG	Wade et al this study	Wade et al this study	Wade et al this study	Wade et al this study	Wade et al this study	Wade et al this study
Location	Southern GRV	Southern GRV	Southern GRV	Tarcoola-Kingoonya	Tarcoola-Kingoonya	Tarcoola-Kingoonya	Tarcoola-Kingoonya	Tarcoola-Kingoonya	Tarcoola-Kingoonya
Suite	LGRV	LGRV	LGRV	LGRV	LGRV	LGRV	LGRV	LGRV	LGRV
Formation	Bittali Rhyolite	Bittali Rhyolite	Bittali Rhyolite	Ealbara Rhyolite	Ealbara Rhyolite	Ealbara Rhyolite	Ealbara Rhyolite	Ealbara Rhyolite	Ealbara Rhyolite
Map Unit	Mab	Mab	Mab	Mae	Mae	Mae	Mae	Mae	Mae
Easting	679256.20	679256.20	637667.53	450998.24	451448.24	454948.24	454398.24	489170.64	489170.64
Northing	6391174.75	6391174.75	6395387.89	6644297.98	6644747.98	6646797.98	6646447.98	6650927.86	6650927.86
Zone	53	53	53	53	53	53	53	53	53
Longitude	136.910235	136.910235	136.466572	134.490250				134.887408	134.887408
Latitude	-32.602440	-32.602440	-32.570404	-30.332138				-30.273272	-30.273272
Datum	GDA94	GDA94	GDA94	GDA94				GDA94	GDA94
Age	1589.30	1589.30	1589.30	1591.20	1591.20	1591.20	1591.20	1591.20	1591.20
Lithology	Tuff	Tuff	Tuff	Rhyolite	Rhyolite	Rhyolite	Rhyolite	Rhyolite	Rhyolite
SiO_2	73.10	74.50	73.20	73.74	73.70	73.30	73.73	70.16	77.64
TiO_2	0.38	0.37	0.40	0.22	0.23	0.26	0.22	0.54	0.17
Al_2O_3	12.15	12.20	13.00	12.78	12.87	13.12	12.79	13.88	12.07
FeO	0.00	0.00	0.00	1.18	1.33	1.18	1.57	0.58	0.18
Fe_2O_3	2.86	3.16	1.74	2.22	2.28	2.43	2.56	3.02	1.15
MnO	0.01	0.01	0.00	0.07	0.08	0.08	0.16	0.10	0.02
MgO	0.28	0.26	0.25	0.17	0.18	0.23	0.17	1.07	0.10
CaO	0.10	0.11	0.08	0.76	0.80	0.74	0.32	0.68	0.27
Na_2O	0.11	0.11	0.15	3.55	3.52	3.63	3.36	3.20	3.47
K_2O	5.81	5.79	5.13	5.27	5.33	5.30	5.32	5.85	4.94
P_2O_5	0.03	0.02	0.00	0.03	0.03	0.04	0.03	0.16	0.01
LOI	1.86	1.98	2.62	0.83	0.82	0.68	0.92	1.43	0.38
Total	96.69	98.51	96.57	100.82	101.17	100.99	101.15	100.67	100.40
F	0.00	0.00	0.00	1600.00	1400.00	1300.00	1300.00	900.00	1700.00
Ga	19.60	19.90	18.70	22.60	22.50	23.00	23.40	23.20	22.30
Cr	-10.00	10.00	0.00	5.00	4.00	3.00	3.00	14.00	4.00
Ni	-1.00	-1.00	2.00	8.00	8.00	6.00	4.00	16.00	4.00
Co	1.00	1.00	2.00	76.80	71.00	97.60	80.30	24.90	29.40
Sc	7.00	7.00	5.00	5.40	5.20	6.00	6.00	7.90	2.40
V	8.00	8.00	22.00	2.40	2.40	4.20	2.60	18.90	1.60
Cu	3.00	3.00	2.00	16.00	6.00	12.00	18.00	22.00	4.00
Zn	77.00	68.00	43.00	95.00	85.00	95.00	105.00	180.00	50.00
Y	64.60	65.50	22.00	56.50	56.20	54.90	55.60	41.90	41.00
Rb	266.00	244.00	264.00	228.00	224.00	218.00	225.00	242.00	261.00
Sr	43.40	38.10	37.20	69.70	75.70	90.70	66.10	106.00	13.30
Cs	5.08	4.96	1.95	1.96	2.04	1.94	1.80	2.70	1.95
Ba	1905.00	1820.00	1190.00	276.00	288.00	367.00	296.00	964.00	55.50
Th	39.80	39.20	21.80	28.40	27.30	26.70	28.20	26.70	34.30
U	6.72	7.11	5.03	5.55	5.65	5.49	5.99	8.24	6.73
Pb	11.00	17.00	6.00	42.00	42.00	48.00	46.00	63.00	45.00
Zr	467.00	449.00	533.00	396.00	412.00	406.00	407.00	353.00	196.00
Hf	13.30	12.80	13.40	11.20	11.40	11.40	11.50	10.10	7.59
Nb	24.90	24.30	16.60	24.50	23.90	23.50	24.40	21.00	26.90
Ta	1.90	1.90	1.60	1.94	1.82	1.88	1.92	1.50	1.86
La	81.50	99.40	46.30	96.40	94.60	92.20	95.10	70.40	44.00
Ce	174.00	209.00	88.00	187.00	183.00	178.00	184.00	127.00	93.20
Pr	19.10	22.10	9.33	21.00	20.70	20.30	20.80	15.60	9.70
Nd	67.00	78.00	32.50	75.00	73.50	73.30	74.00	54.50	31.20
Sm	11.85	13.75	5.44	13.70	13.30	12.80	13.50	10.40	6.67
Eu	2.04	2.07	1.29	0.76	0.88	1.04	0.85	1.51	0.29
Gd	9.98	11.60	4.12	10.50	10.40	10.20	10.40	7.93	5.75
Tb	1.80	1.80	0.67	1.69	1.72	1.69	1.76	1.26	1.03
Dy	11.45	11.45	4.05	10.30	10.40	9.83	9.92	7.32	6.13
Ho	2.31	2.22	0.83	2.18	2.13	2.11	2.11	1.48	1.39
Er	6.88	6.68	2.44	6.30	6.09	6.18	6.27	4.60	4.34
Tm	0.98	0.97	0.39	0.95	0.94	0.90	0.94	0.69	0.68
Yb	6.40	6.46	2.68	6.28	6.11	5.79	5.98	4.77	4.70
Lu	1.03	0.94	0.41	0.92	0.91	0.91	0.88	0.69	0.72
Eu/Eu*	0.57	0.50	0.83	0.19	0.23	0.28	0.22	0.51	0.14
$(La/Yb)_N$	9.13	11.04	12.39	11.01	11.11	11.42	11.41	10.59	6.72
Ga/Al	3.05	3.08	2.72	3.34	3.30	3.31	3.46	3.16	3.49
Temp				1107.30	1111.67	1111.67	1128.71	1101.59	1044.66
Temp upper error				1145.52	1150.25	1150.00	1165.84	1138.31	1076.50
Temp lower error				1071.32	1075.37	1075.59	1093.65	1066.94	1014.46
Temp				834.30	838.67	838.67	855.71	828.59	771.66
1 sigma error				37.10	37.44	37.21	36.10	35.68	31.02
Factor				1.44	1.45	1.44	1.32	1.39	1.31

$Eu/Eu^* = (Eu/(Sm \times Gd))_N^{0.5}$

Normalising values from Taylor and McLennon 1995

Appendix 3 Supplementary material for Temporal, geochemical and isotopic constraints on plume-driven felsic and mafic components in a large igneous province

Appendix 3 Table A1 Whole-rock geochemical composition for Gawler Range Volcanics samples

R number	2729175	2729176	2729179		2079354	2079353	2079355	2079352	19574	2746361
Other Sample Number				18-TAR-07						
Drill_Hole	145202	145202	145202						20540	RC 1
Depth_From	27.3	37.96	63.45						13.19	16.2
Depth_To	27.77	38.2	63.65						13.3	16.77
Data Source	Wade et al this study	Wade et al this study	Wade et al this study	Wade et al this study	SARIG	SARIG	SARIG	SARIG	SARIG	Wade et al this study
Location	Tarcoola-Kingoonya	Tarcoola-Kingoonya	Tarcoola-Kingoonya	Tarcoola-Kingoonya	Myall Creek	Myall Creek	Myall Creek	Myall Creek	Myall Creek	Myall Creek
Suite	LGRV	LGRV	LGRV	LGRV	LGRV	LGRV	LGRV	LGRV	LGRV	LGRV
Formation	Ealbarra Rhyolite	Ealbarra Rhyolite	Ealbarra Rhyolite	Ealbarra Rhyolite	Spearfelt Rhyodacite	Spearfelt Rhyodacite	Spearfelt Rhyodacite	Spearfelt Rhyodacite	Spearfelt Rhyodacite	Spearfelt Rhyodacite
Map Unit	Mae	Mae	Mae	Mae	Mas	Mas	Mas	Mas	Mas	Mas
Easting	436081.57	436081.57	436081.57	436081.57	714446.47	715508.13	714460.26	716800.57	718923.98	718923.98
Northing	6634795.68	6634795.68	6634795.68	6634795.68	6394707.98	6396053.39	6394813.67	6398174.50	6405394.45	6405394.45
Zone	53	53	53	53	53	53	53	53	53	53
Longitude	134.334479	134.334479	134.334479	134.334479	137.284194	137.295186	137.284317	137.308451	137.329366	137.329366
Latitude	-30.417204	-30.417204	-30.417204	-30.417204	-32.564332	-32.551999	-32.563377	-32.532628	-32.467133	-32.467133
Datum	GDA94	GDA94	GDA94	GDA94	GDA94	GDA94	GDA94	GDA94	GDA94	GDA94
Age	1591.20	1591.20	1591.20	1591.20	1591.20	1591.20	1591.20	1591.20	1591.20	1591.20
Lithology	Rhyolite	Rhyolite	Rhyolite	Rhyolite	Rhyolite	Rhyolite	Rhyolite	Rhyolite	Rhyodacite	Rhyodacite
SiO_2	75.78	75.06	76.07	75.22	70.50	67.00	66.50	68.30	69.65	69.26
TiO_2	0.17	0.18	0.17	0.23	0.31	0.63	0.67	0.65	0.81	0.76
Al_2O_3	12.19	12.46	12.44	13.09	11.85	13.45	13.55	13.75	15.15	15.00
FeO	0.15	0.44	0.34	0.74					0.18	0.11
Fe_2O_3	2.49	1.76	1.77	1.83	4.81	4.55	4.86	4.77	2.70	3.69
MnO	0.03	0.14	0.04	0.03	0.02	0.08	0.21	0.32	0.01	0.01
MgO	0.15	0.23	0.35	0.13	0.06	1.38	1.57	1.66	0.15	0.20
CaO	0.07	0.33	0.25	0.15	0.12	0.47	0.81	0.64	0.13	0.21
Na_2O	2.23	2.81	2.56	3.32	2.94	3.66	3.26	3.46	3.80	3.55
K_2O	6.25	5.63	5.54	5.51	5.83	4.86	4.95	5.13	5.55	5.89
P_2O_5	0.02	0.02	0.02	0.04	0.05	0.15	0.17	0.17	0.05	0.11
LOI	0.56	0.85	0.76	0.56	0.24	1.22	1.29	1.33		1.07
Total	100.09	99.91	100.31	100.86	96.73	97.45	97.84	100.18	98.18	99.86
F	400.00	1800.00	700.00	300.00						500.00
Ga	20.10	22.40	21.20	24.10	10.60	20.40	21.50	21.30		24.50
Cr	3.00	4.00	3.00	11.00	10.00	10.00	10.00	10.00	5.00	6.00
Ni	4.00	4.00	6.00	10.00	2.00	8.00	8.00	7.00	5.00	14.00
Co	23.80	23.20	22.00	41.30	1.00	8.00	9.00	9.00	35.00	29.80
Sc	4.60	4.40	4.30	5.90	7.00	8.00	10.00	9.00		9.00
V	2.80	3.10	2.40	2.40	21.00	45.00	53.00	48.00	45.00	27.00
Cu	20.00	4.00	16.00	10.00	5.00	4.00	24.00	92.00	5.00	12.00
Zn	65.00	40.00	50.00	115.00	28.00	219.00	419.00	202.00	80.00	135.00
Y	56.00	55.90	55.50	57.00	56.90	38.20	40.90	41.50		86.50
Rb	266.00	249.00	249.00	234.00	308.00	210.00	229.00	223.00	230.00	229.00
Sr	55.90	60.70	52.10	71.80	108.50	99.70	161.00	106.00	170.00	195.00
Cs	3.83	2.38	3.10	1.74	2.61	1.46	2.33	1.58		1.44
Ba	279.00	252.00	244.00	305.00	1395.00	1295.00	1220.00	1295.00	1100.00	1410.00
Th	28.10	28.70	28.70	27.50	50.90	35.30	36.00	37.20	46.00	39.50
U	6.00	5.69	5.87	5.04	4.87	3.99	7.11	7.56	8.00	6.90
Pb	36.00	18.00	34.00	54.00	9.00	7.00	1040.00	38.00	20.00	14.00
Zr	320.00	329.00	324.00	421.00	186.00	314.00	341.00	341.00	470.00	469.00
Hf	9.73	10.10	9.90	11.70	5.80	8.40	9.20	9.20		11.90
Nb	23.40	24.20	23.70	24.60	27.20	21.20	22.30	22.20		25.30
Ta	1.56	1.64	1.62	1.72	3.60	1.80	1.80	1.80		1.85
La	148.00	97.50	97.60	96.20	86.90	90.40	88.40	90.40		103.00
Ce	257.00	189.00	189.00	189.00	170.00	164.50	167.00	171.00		198.00
Pr	28.50	21.30	21.10	21.50	17.80	17.85	17.70	18.20		22.50
Nd	103.00	74.90	74.30	76.60	64.80	64.00	63.00	64.50		77.40
Sm	18.10	13.70	13.90	13.40	11.65	10.45	10.85	10.60		14.00
Eu	0.81	0.60	0.58	0.90	1.66	1.87	1.97	1.99		2.84
Gd	14.60	10.40	10.40	10.80	9.97	8.47	8.72	8.71		13.70
Tb	1.99	1.64	1.74	1.74	1.58	1.25	1.31	1.36		2.18
Dy	10.80	9.99	9.86	10.40	9.27	7.24	7.23	7.65		13.00
Ho	2.15	2.09	2.05	2.18	1.98	1.33	1.44	1.48		2.77
Er	6.05	6.07	6.22	6.41	5.79	4.04	4.16	4.26		7.73
Tm	0.91	0.88	0.92	0.94	0.92	0.57	0.63	0.61		1.09
Yb	5.77	5.95	5.94	6.48	6.15	3.83	4.22	4.01		6.63
Lu	0.86	0.93	0.89	0.90	0.89	0.57	0.61	0.63		1.01
Eu/Eu*	0.15	0.15	0.15	0.23	0.47	0.61	0.62	0.63		0.63
$(La/Yb)_N$	18.40	11.75	11.79	10.65	10.14	16.93	15.03	16.17		11.14
Ga/Al	3.12	3.40	3.22	3.48	1.69	2.87	3.00	2.93	0.00	3.09
Temp	1116.27	1110.09	1119.85	1141.78	1030.05	1088.30	1097.37	1097.29	1158.73	1153.41
Temp upper error	1150.24	1145.01	1153.76	1178.53	1062.27	1124.09	1133.84	1133.77	1196.19	1191.23
Temp lower error	1084.05	1077.04	1087.69	1107.03	999.54	1054.51	1062.97	1062.89	1123.33	1117.70
Temp	843.27	837.09	846.85	868.78	757.05	815.30	824.37	824.29	885.73	880.41
1 sigma error	33.10	33.99	33.03	35.75	31.36	34.79	35.43	35.44	36.43	36.76
Factor	1.20	1.26	1.18	1.26	1.38	1.38	1.39	1.39	1.24	1.28

$Eu/Eu^* = (Eu/(Sm \times Gd))_N^{0.5}$

Normalising values from Taylor and McLennon 1995

Appendix 3 Supplementary material for Temporal, geochemical and isotopic constraints on plume-driven felsic and mafic components in a large igneous province

Appendix 3 Table A1 Whole-rock geochemical composition for Gawler Range Volcanics samples

R number	19575	2116182	2137549	2137550	2137659	2137660	2137662	2137792	2137791	2137790	2137788
Other Sample Number											
Drill_Hole	20540	20540	MSDP01	MSDP01	MSDP03	MSDP03	MSDP03	MSDP04	MSDP04	MSDP04	MSDP04
Depth_From	17.5	33	30.50	48	38	50	101	19	39	59	79
Depth_To	17.63	34	32.00	49	39	51	102	20	40	60	80
Data Source	SARIG	SARIG	SARIG	SARIG	SARIG	SARIG	SARIG	SARIG	SARIG	SARIG	SARIG
Location	Myall Creek	Myall Creek	Myall Creek	Myall Creek	Myall Creek	Myall Creek	Myall Creek	Myall Creek	Myall Creek	Myall Creek	Myall Creek
Suite	LGRV	LGRV	LGRV	LGRV	LGRV	LGRV	LGRV	LGRV	LGRV	LGRV	LGRV
Formation	Spearfelt Rhyodacite	Spearfelt Rhyodacite	Spearfelt Rhyodacite	Spearfelt Rhyodacite	Spearfelt Rhyodacite	Spearfelt Rhyodacite	Spearfelt Rhyodacite	Spearfelt Rhyodacite	Spearfelt Rhyodacite	Spearfelt Rhyodacite	Spearfelt Rhyodacite
Map Unit	Mas	Mas	Mas	Mas	Mas	Mas	Mas	Mas	Mas	Mas	Mas
Easting	718923.98	718923.98	724657.89	724657.89	723300.56	723300.56	723300.56	717634.69	717634.69	717634.69	717634.69
Northing	6405394.45	6405394.45	6408347.76	6408347.76	6406055.81	6406055.81	6406055.81	6408769.86	6408769.86	6408769.86	6408769.86
Zone	53	53	53	53	53	53	53	53	53	53	53
Longitude	137.329366	137.329366	137.389625	137.389625	137.375741	137.375741	137.375741	137.314878	137.314878	137.314878	137.314878
Latitude	-32.467133	-32.467133	-32.439371	-32.439371	-32.460302	-32.460302	-32.460302	-32.436961	-32.436961	-32.436961	-32.436961
Datum	GDA94	GDA94	GDA94	GDA94	GDA94	GDA94	GDA94	GDA94	GDA94	GDA94	GDA94
Age	1591.20	1591.20	1591.20	1591.20	1591.20	1591.20	1591.20	1591.20	1591.20	1591.20	1591.20
Lithology	Rhyodacite	Rhyodacite	Rhyolite	Rhyolite	Rhyolite	Rhyolite	Ignimbrite	Rhyolite	Rhyolite	Rhyolite	Rhyolite
SiO_2	69.96	68.69	60.94	65.62	63.35	65.25	66.73	69.61	68.38	66.47	69.47
TiO_2	0.81	0.71	1.27	0.77	0.78	0.77	0.69	0.66	0.75	0.78	0.64
Al_2O_3	14.56	14.20	13.41	13.16	14.07	14.25	13.40	13.16	13.23	13.11	12.86
FeO	0.22		0.00								
Fe_2O_3	2.79	4.83	7.38	6.17	7.01	4.77	4.57	5.26	5.98	6.96	5.77
MnO	0.02	0.02	0.18	0.09	0.08	0.09	0.07	0.07	0.08	0.09	0.12
MgO	0.25	0.24	2.53	1.49	1.00	1.32	1.34	0.62	0.83	1.44	0.87
CaO	0.26	0.29	2.02	0.93	0.32	0.80	0.82	0.22	0.34	0.40	0.31
Na_2O	3.55	3.58	1.19	0.23	0.38	2.16	0.45	2.18	2.29	1.84	2.40
K_2O	5.74	5.67	6.14	8.43	8.92	7.05	9.02	6.35	6.31	6.89	6.26
P_2O_5	0.16	0.15	0.37	0.19	0.24	0.21	0.19	0.19	0.21	0.22	0.16
LOI		0.91	4.90	3.26	2.90	2.20	2.95	1.77	1.83	1.86	1.37
Total	98.32	99.29	100.33	100.34	99.05	98.87	100.23	100.09	100.23	100.06	100.23
F		447.00	878.00	754.00	909.00	605.00	535.00	818.00	931.00	933.00	680.00
Ga		17.90	19.20	19.50	20.20	19.70	15.10	20.30	20.20	18.90	19.20
Cr	5.00	-20.00	0.00	-20.00	-20.00	-20.00	-20.00	-20.00	-20.00	-20.00	-20.00
Ni	5.00	-1.00	5.00	3.00	5.00	-1.00	2.00	3.00	-1.00	-1.00	-1.00
Co	55.00	7.00	13.10	10.50	9.50	8.70	5.00	10.50	7.00	10.50	5.70
Sc		8.00	16.00	10.00	-10.00	-10.00	-10.00	11.00	-10.00	10.00	-10.00
V	40.00	24.00	114.00	63.00	63.00	33.00	39.00	34.00	44.00	49.00	27.00
Cu	5.00	5.00	210.00	2.00	3.00	6.00	2.00	8.00	6.00	4.00	3.00
Zn	130.00	66.00	41.00	41.00	53.00	37.00	39.00	46.00	35.00	39.00	31.00
Y		57.30	46.10	47.80	57.10	48.60	47.40	59.00	52.00	50.00	54.10
Rb	230.00	216.30	202.80	259.10	295.70	230.20	255.80	264.70	277.00	255.70	250.60
Sr	170.00	129.80	65.80	34.10	71.00	102.50	69.60	68.50	67.60	66.10	58.60
Cs		1.77	4.69	3.89	8.14	2.06	4.04	3.21	3.08	2.86	1.73
Ba	840.00	1200.20	1422.20	1065.40	1944.00	1416.90	1893.30	1110.80	1075.40	1074.60	1068.10
Th	44.00	34.97	28.56	36.91	32.47	34.47	32.59	50.79	46.19	42.96	47.21
U	6.00	5.78	5.38	5.45	5.56	4.26	6.78	6.61	5.72	4.85	7.55
Pb	14.00	14.00	9.00	7.00	12.00	7.00	13.00	8.00	5.00	8.00	8.00
Zr	480.00	410.00	276.00	300.00	369.00	366.00	384.00	363.00	359.00	340.00	362.00
Hf		9.70	0.00	7.50	9.40	9.20	10.10	9.90	9.40	9.00	9.40
Nb		25.80	20.80	25.90	24.20	25.70	22.80	25.30	25.00	23.40	25.30
Ta		1.80	1.40	1.90	1.70	1.90	1.70	2.20	2.10	2.00	2.20
La		83.90	59.30	93.40	63.90	85.10	78.10	121.40	98.00	90.90	101.40
Ce		165.10	125.20	171.20	141.70	172.30	153.00	236.30	191.90	180.40	200.40
Pr		18.22	14.16	19.30	15.27	18.27	16.96	24.69	20.02	18.68	20.57
Nd		64.70	49.60	64.40	54.90	65.60	59.70	89.80	71.80	68.20	74.30
Sm		12.07	9.48	11.32	10.46	12.08	10.74	16.44	12.79	12.02	12.80
Eu		2.38	2.19	2.01	2.14	2.17	2.32	2.53	2.03	2.01	2.09
Gd		10.82	8.47	9.05	9.52	9.74	9.00	12.19	9.83	9.38	10.09
Tb		1.59	1.34	1.41	1.57	1.44	1.44	1.82	1.50	1.45	1.56
Dy		9.85	8.14	8.52	9.74	8.59	8.35	10.55	8.83	8.66	9.23
Ho		1.97	1.74	1.72	2.06	1.83	1.69	2.16	1.86	1.85	1.95
Er		5.80	4.88	4.98	5.82	5.09	4.84	6.13	5.42	5.26	5.74
Tm		0.89	0.71	0.74	0.86	0.78	0.75	0.90	0.79	0.77	0.80
Yb		5.47	4.51	4.81	5.50	4.81	4.67	5.69	5.21	4.92	5.40
Lu		0.83	0.69	0.75	0.87	0.76	0.75	0.89	0.84	0.80	0.85
Eu/Eu*		0.64	0.75	0.61	0.66	0.61	0.72	0.55	0.55	0.58	0.56
$(La/Yb)_N$		11.00	9.43	13.93	8.33	12.69	12.00	15.30	13.49	13.25	13.47
Ga/Al	0.00	2.38	2.71	2.80	2.71	2.61	2.13	2.91	2.88	2.72	2.82
Temp	1154.69	1125.93	1059.00	1093.25	1131.46	1105.48	1114.84	1128.48	1118.87	1106.16	1115.32
Temp upper error	1192.84	1163.40	1094.91	1127.93	1166.69	1142.52	1152.00	1163.65	1154.59	1141.93	1151.45
Temp lower error	1118.69	1090.59	1025.16	1060.43	1098.09	1070.55	1079.78	1095.16	1085.09	1072.36	1081.18
Temp	881.69	852.93	786.00	820.25	858.46	832.48	841.84	855.48	845.87	833.16	842.32
1 sigma error	37.07	36.41	34.87	33.75	34.30	35.98	36.11	34.25	34.75	34.78	35.13
Factor	1.29	1.34	1.49	1.31	1.22	1.39	1.36	1.22	1.28	1.32	1.31

$Eu/Eu^* = (Eu/(Sm \times Gd))_N^{0.5}$

Normalising values from Taylor and McLennon 1995

Appendix 3 Supplementary material for Temporal, geochemical and isotopic constraints on plume-driven felsic and mafic components in a large igneous province

Appendix 3 Table A1 Whole-rock geochemical composition for Gawler Range Volcanics samples

R number	2721839	884GH4	1840803	1840807				370985	370964
Other Sample Number			884GH10	884GH5	76	E747	9615		
Drill_Hole									
Depth_From									
Depth_To									
Data Source	Wade et al this study	Wade et al this study	Wade et al this study	Wade et al this study	Agangi, A. (2011)	Giles, C.W. (1980)	Giles, C.W. (1980)	SARIG	SARIG
Location	Lake Everard	Lake Everard	Lake Everard	Lake Everard	Lake Everard	Lake Everard	Lake Everard	Lake Everard	Lake Everard
Suite	LGRV	LGRV	LGRV	LGRV	LGRV	LGRV	LGRV	LGRV	LGRV
Formation	Mangaroongah Dacite	Mangaroongah Dacite	Mangaroongah Dacite	Mangaroongah Dacite	Mangaroongah Dacite	Mangaroongah Dacite	Mangaroongah Dacite	Mangaroongah Dacite	Mangaroongah Dacite
Map Unit	Mym	Mym	Mym	Mym	Mym	Mym	Mym	Mym	Mym
Easting	519800.14	517398.05	511500.00	536050.00	486560.00	483937.26	487810.67	485006.61	487318.62
Northing	6485620.49	6480448.22	6486850.00	6495350.00	6500658.00	6494357.44	6496261.57	6490951.59	6496781.58
Zone	53	53	53	53	53	53	53	53	53
Longitude	135.209092		135.121427	135.380332			134.871411	134.841749	134.866228
Latitude	-31.764750		-31.753771	-31.676573			-31.668851	-31.716725	-31.664154
Datum	GDA94		GDA94	GDA94			GDA94	GDA94	GDA94
Age	1589.80	1589.80	1589.80	1589.80	1589.80	1589.80	1589.80	1589.80	1589.80
Lithology	Dacite	Dacite	Dacite	Dacite	Dacite	Dacite	Rhyodacite	Dacite	Dacite
SiO_2	64.91	69.10	64.70	58.70	65.10	62.88	62.88	63.70	65.40
TiO_2	0.92	0.58	0.91	1.20	0.88	1.13	1.13	0.87	0.89
Al_2O_3	14.58	13.38	14.47	14.97	13.79	15.32	15.32	14.30	13.40
FeO	1.99	1.79	2.64	3.83		0.00	6.85	0.00	0.00
Fe_2O_3	5.42	3.65	5.06	8.01	5.44	7.61	7.61	4.89	6.01
MnO	0.15	0.14	0.16	0.16	0.18	0.17	0.17	0.13	0.09
MgO	2.07	1.58	1.91	2.90	3.17	2.33	2.33	1.55	1.85
CaO	1.14	1.27	1.91	3.90	1.40	2.04	2.04	2.04	1.06
Na_2O	3.80	3.60	3.83	3.71	4.77	3.11	3.11	3.20	2.75
K_2O	4.65	4.67	4.83	3.81	2.28	5.06	5.06	5.48	5.94
P_2O_5	0.35	0.25	0.31	0.46	0.49	0.41	0.41	0.30	0.35
LOI	1.67	1.31	1.30	1.80	2.25	1.57	1.57	0.00	0.00
Total	101.65	101.32	102.02	103.45	99.75	101.63	108.48	96.46	97.74
F	800.00	900.00	1100.00	1100.00	0.00	0.00	0.00	0.00	0.00
Ga	20.60	18.40	19.70	19.50	19.00	0.00	0.00	23.00	14.00
Cr	11.00	24.00	7.00	15.00	5.00	-1.00	0.50	10.00	10.00
Ni	14.00	38.00	12.00	24.00	8.00	25.00	25.00	10.00	10.00
Co	24.50	49.20	35.60	40.30	0.00	0.00	0.00	15.00	8.00
Sc	15.80	10.00	15.60	20.60	14.30	20.00	20.00	15.00	15.00
V	74.80	45.90	61.30	140.00	73.00	109.00	109.00	70.00	90.00
Cu	8.00	16.00	20.00	26.00	10.00	0.00	0.00	10.00	3.00
Zn	115.00	95.00	110.00	90.00	129.00	0.00	0.00	80.00	52.00
Y	44.60	41.00	44.10	40.60	34.20	47.00	47.00	41.00	33.00
Rb	143.00	172.00	144.00	119.00	79.30	155.00	155.00	150.00	135.00
Sr	325.00	231.00	283.00	496.00	217.60	453.00	453.00	330.00	165.00
Cs	4.91	2.46	1.94	3.57	1.27	0.00	0.00	1.50	1.50
Ba	2360.00	817.00	2990.00	1560.00	708.00	2830.00	2830.00	3150.00	4400.00
Th	14.90	17.00	14.40	11.00	13.40	0.00	0.00	15.50	16.00
U	2.60	2.62	2.46	1.78	2.77	0.00	0.00	2.50	2.50
Pb	20.00	39.00	46.00	28.00	6.00	0.00	0.00	8.00	4.00
Zr	416.00	203.00	508.00	314.00	208.00	371.00	371.00	550.00	490.00
Hf	10.50	6.26	12.20	7.95	6.47	0.00	0.00	12.00	11.00
Nb	15.90	16.80	15.70	12.20	19.00	13.00	13.00	25.00	20.00
Ta	1.00	1.24	1.00	0.86	1.33	0.00	0.00	4.00	3.00
La	64.10	45.90	67.80	53.10	30.10	53.00	53.30	81.00	62.00
Ce	132.00	98.10	139.00	113.00	67.30	122.00	122.00	165.00	125.00
Pr	16.00	12.10	16.60	13.40	8.87	0.00	0.00	15.00	12.00
Nd	62.30	45.50	64.40	54.50	37.50	55.00	55.40	57.00	49.50
Sm	12.50	10.10	12.50	11.20	7.61	11.00	10.70		
Eu	3.17	1.76	3.48	2.70	1.85	3.00	2.80	2.00	1.50
Gd	10.10	8.27	10.20	9.25	6.87	11.00	11.40	9.00	8.00
Tb	1.53	1.29	1.49	1.40	1.05	0.00	0.00	1.50	1.00
Dy	8.63	7.79	8.35	7.67	6.05	7.00	7.33	7.50	7.50
Ho	1.76	1.52	1.69	1.55	1.22	0.00	0.00	1.50	1.50
Er	4.90	4.28	4.82	4.34	3.66	5.00	4.50	4.00	4.00
Tm	0.69	0.62	0.67	0.62	0.56	0.00	0.00	0.50	0.50
Yb	4.29	3.80	4.25	3.92	3.69	4.00	3.90	3.00	3.00
Lu	0.63	0.56	0.63	0.57	0.57	0.00	0.00	0.50	0.50
Eu/Eu*	0.86	0.59	0.94	0.81	0.78	0.83	0.78		
$(La/Yb)_N$	10.72	8.66	11.44	9.72	5.85	9.50	9.80	19.37	14.82
Ga/Al	2.67	2.60	2.57	2.46	2.60	0.00	0.00	3.04	1.97
Temp	1109.05	1024.47	1104.64	1004.91	1027.94	1082.48	1082.48	1114.26	1123.21
Temp upper error	1147.98	1058.36	1147.22	1046.26	1061.93	1121.37	1121.37	1157.57	1163.95
Temp lower error	1072.45	992.49	1064.86	966.47	995.87	1045.97	1045.97	1073.83	1084.99
Temp	836.05	751.47	831.64	731.91	754.94	809.48	809.48	841.26	850.21
1 sigma error	37.76	32.94	41.18	39.89	33.03	37.70	37.70	41.87	39.48
Factor	1.47	1.50	1.68	2.05	1.50	1.57	1.57	1.68	1.52

$Eu/Eu^* = (Eu/(Sm \times Gd))_N^{0.5}$

Normalising values from Taylor and McLennon 1995

Appendix 3 Supplementary material for Temporal, geochemical and isotopic constraints on plume-driven felsic and mafic components in a large igneous province

Appendix 3 Table A1 Whole-rock geochemical composition for Gawler Range Volcanics samples

R number			370968	370983	370966	1969461	1969460	1969459	1969458	1969457
Other Sample Number	73	20								
Drill_Hole						20772	20772	20772	20772	20772
Depth_From						311.8	324.6	334.1	344.5	354.1
Depth_To						312.85	325.6	335.1	345.5	355.1
Data Source	Agangi, A. (2011)	Agangi, A. (2011)	SARIG	SARIG	SARIG	SARIG	SARIG	SARIG	SARIG	SARIG
Location	Lake Everard	Lake Everard	Lake Everard	Lake Everard	Lake Everard	Stuart Shelf	Stuart Shelf	Stuart Shelf	Stuart Shelf	Stuart Shelf
Suite	LGRV	LGRV	LGRV	LGRV	LGRV	LGRV	LGRV	LGRV	LGRV	LGRV
Formation	Mangaroongah Dacite	Mangaroongah Dacite	Mangaroongah Dacite	Mangaroongah Dacite	Mangaroongah Dacite	RED 2	RED 2	RED 2	RED 2	RED 2
Map Unit	Mym	Mym	Mym	Mym	Mym					
Easting	487389.00	516088.00	486528.60	486802.60	487378.63	727055.84	727055.84	727055.84	727055.84	727055.84
Northing	6496156.00	6485851.00	6496768.60	6489973.58	6496166.61	6615049.80	6615049.80	6615049.80	6615049.80	6615049.80
Zone	53	53	53	53	53	53	53	53	53	53
Longitude			134.857893	134.860692	134.866852	137.367642	137.367642	137.367642	137.367642	137.367642
Latitude			-31.664262	-31.725571	-31.669703	-30.575543	-30.575543	-30.575543	-30.575543	-30.575543
Datum			GDA94	GDA94	GDA94	GDA94	GDA94	GDA94	GDA94	GDA94
Age	1589.80	1589.80	1589.80	1589.80	1589.80	1593.60	1593.60	1593.60	1593.60	1593.60
Lithology	Dacite	Dacite	Dacite	Dacite	Dacite	Dacite	Dacite	Dacite	Dacite	Dacite
SiO_2	62.36	61.74	64.30	65.10	61.00	64.21	68.37	66.79	60.76	64.68
TiO_2	1.05	0.92	0.88	0.81	1.11	0.67	0.72	0.72	0.68	0.71
Al_2O_3	14.92	14.50	14.80	14.20	16.10	13.36	14.30	14.10	12.87	13.97
FeO			0.00	0.00	0.00					
Fe_2O_3	6.73	6.10	4.99	4.67	7.01	5.30	5.23	6.03	13.17	10.25
MnO	0.12	0.14	0.10	0.08	0.11	0.20	0.08	0.09	0.34	0.17
MgO	2.82	1.69	1.69	1.50	2.66	1.72	1.04	1.25	2.26	1.23
CaO	1.40	2.79	1.39	0.57	0.80	2.01	0.82	0.74	1.22	0.33
Na_2O	2.98	3.95	3.64	3.60	4.46	2.29	2.93	2.06	0.11	0.09
K_2O	4.64	4.45	5.33	5.48	4.20	6.09	6.02	6.47	3.38	5.34
P_2O_5	0.38	0.37	0.26	0.25	0.37	0.16	0.18	0.18	0.18	0.17
LOI	2.04	3.00	0.00	0.00	0.00					
Total	99.44	99.65	97.38	96.26	97.82	96.01	99.69	98.43	94.97	96.94
F	0.00	0.00	0.00	0.00	0.00	831.00	791.00	1199.00	1857.00	1759.00
Ga	17.90	19.20	22.00	23.00	21.00	20.10	21.10	21.40	20.90	21.50
Cr	9.00	9.00	10.00	10.00	10.00	-20.00	-20.00	-20.00	-20.00	-20.00
Ni	14.00	13.00	10.00	9.00	12.00	5.00	6.00	3.00	9.00	1.00
Co	0.00	0.00	11.00	7.00	14.00	9.50	10.10	12.80	42.70	34.60
Sc	17.20	15.90	15.00	10.00	15.00	10.00	10.00	10.00	11.00	9.00
V	82.00	80.00	70.00	60.00	90.00	32.00	28.00	28.00	33.00	35.00
Cu	23.00	11.00	9.00	2.00	9.00	348.00	110.00	39.00	44.00	63.00
Zn	91.00	89.00	88.00	88.00	98.00	49.00	49.00	46.00	123.00	104.00
Y	37.30	40.40	38.00	41.00	46.00	57.10	59.10	59.20	77.00	58.80
Rb	159.90	119.70	150.00	155.00	100.00	301.70	265.00	306.30	256.00	328.10
Sr	586.40	261.30	185.00	145.00	320.00	111.90	108.80	64.70	15.60	16.30
Cs	6.17	2.60	1.50	1.50	1.50	2.29	2.42	3.58	2.15	1.86
Ba	2363.00	2270.00	3250.00	3600.00	3500.00	1374.00	1138.00	1069.30	128.60	414.10
Th	10.00	11.30	17.50	15.00	16.50	37.06	40.14	39.50	39.38	39.29
U	1.89	1.81	2.50	2.00	2.50	7.81	10.24	6.57	6.33	6.18
Pb	26.00	18.00	8.00	6.00	6.00	81.00	11.00	7.00	-5.00	7.00
Zr	437.00	402.00	650.00	650.00	550.00	358.00	393.00	365.00	358.00	365.00
Hf	10.45	9.61	12.00	12.00	11.00	8.80	10.00	8.80	9.40	9.30
Nb	15.00	15.00	20.00	25.00	25.00	19.33	14.48	18.66	13.75	17.27
Ta	0.73	0.90	3.00	4.00	3.00	2.10	2.40	2.30	2.20	2.40
La	53.50	57.80	77.00	86.00	85.00	75.70	94.70	93.00	230.90	76.30
Ce	120.00	120.90	155.00	165.00	165.00	160.30	185.80	186.00	384.10	157.20
Pr	14.91	14.54	15.00	14.00	15.00	18.42	21.08	20.83	41.70	17.28
Nd	59.10	56.50	61.00	56.00	60.00	66.20	72.40	72.00	138.30	60.00
Sm	10.98	10.64				11.91	12.78	12.87	23.06	10.78
Eu	2.98	2.93	2.50	1.50	2.00	2.48	2.60	2.63	5.50	2.32
Gd	9.32	9.10	9.00	10.00	10.00	10.60	11.07	11.38	17.34	9.26
Tb	1.36	1.36	1.50	1.50	1.50	1.58	1.69	1.72	2.43	1.46
Dy	7.52	7.62	8.00	8.00	9.00	9.63	10.20	10.19	13.65	9.48
Ho	1.42	1.51	1.50	1.50	1.50	2.00	2.09	2.08	2.69	2.06
Er	4.01	4.16	4.00	4.00	4.00	5.59	5.86	5.86	7.31	5.83
Tm	0.56	0.61	0.50	0.50	0.50	0.83	0.89	0.89	1.07	0.88
Yb	3.44	3.75	4.00	4.00	4.00	5.40	5.68	5.79	6.88	5.65
Lu	0.53	0.55	0.50	0.50	0.50	0.79	0.94	0.86	1.05	0.82
Eu/Eu*	0.90	0.91				0.67	0.67	0.66	0.84	0.71
$(La/Yb)_N$	11.16	11.06	13.81	15.42	15.24	10.06	11.96	11.52	24.07	9.69
Ga/Al	2.27	2.50	2.81	3.06	2.46	2.84	2.79	2.87	3.07	2.91
Temp	1128.27	1050.28	1152.73	1172.64	1151.62	1066.82	1114.93	1119.47	1201.55	1209.02
Temp upper error	1166.67	1092.50	1196.53	1215.12	1192.45	1106.21	1152.48	1155.43	1230.37	1237.54
Temp lower error	1092.09	1010.95	1111.78	1132.80	1113.25	1029.92	1079.54	1085.47	1173.88	1181.61
Temp	855.27	777.28	879.73	899.64	878.62	793.82	841.93	846.47	928.55	936.02
1 sigma error	37.29	40.78	42.38	41.16	39.60	38.14	36.47	34.98	28.24	27.96
Factor	1.38	1.88	1.56	1.43	1.42	1.66	1.38	1.29	0.74	0.71

$Eu/Eu^* = (Eu/(Sm \times Gd))_N^{0.5}$

Normalising values from Taylor and McLennon 1995

Appendix 3 Supplementary material for Temporal, geochemical and isotopic constraints on plume-driven felsic and mafic components in a large igneous province

Appendix 3 Table A1 Whole-rock geochemical composition for Gawler Range Volcanics samples

R number	2131365	1969456	1969455	1969454	1969453	1969452	1969451	1969450	1969449	1969448	1969447
Other Sample Number											
Drill_Hole	20772	20772	20772	20772	20772	20772	20772	20772	20772	20772	20772
Depth_From	363.3	364.1	374.75	382.55	395.95	404.9	415	425	434	445	455.1
Depth_To	369	365	375.7	383.5	397	405.9	416	426	435	446	456.1
Data Source	SARIG	SARIG	SARIG	SARIG	SARIG	SARIG	SARIG	SARIG	SARIG	SARIG	SARIG
Location	Stuart Shelf	Stuart Shelf	Stuart Shelf	Stuart Shelf	Stuart Shelf	Stuart Shelf	Stuart Shelf	Stuart Shelf	Stuart Shelf	Stuart Shelf	Stuart Shelf
Suite	LGRV	LGRV	LGRV	LGRV	LGRV	LGRV	LGRV	LGRV	LGRV	LGRV	LGRV
Formation	RED 2	RED 2	RED 2	RED 2	RED 2	RED 2	RED 2	RED 2	RED 2	RED 2	RED 2
Map Unit											
Easting	727055.84	727055.84	727055.84	727055.84	727055.84	727055.84	727055.84	727055.84	727055.84	727055.84	727055.84
Northing	6615049.80	6615049.80	6615049.80	6615049.80	6615049.80	6615049.80	6615049.80	6615049.80	6615049.80	6615049.80	6615049.80
Zone	53	53	53	53	53	53	53	53	53	53	53
Longitude	137.367642	137.367642	137.367642	137.367642	137.367642	137.367642	137.367642	137.367642	137.367642	137.367642	137.367642
Latitude	-30.575543	-30.575543	-30.575543	-30.575543	-30.575543	-30.575543	-30.575543	-30.575543	-30.575543	-30.575543	-30.575543
Datum	GDA94	GDA94	GDA94	GDA94	GDA94	GDA94	GDA94	GDA94	GDA94	GDA94	GDA94
Age	1593.60	1593.60	1593.60	1593.60	1593.60	1593.60	1593.60	1593.60	1593.60	1593.60	1593.60
Lithology	Dacite	Dacite	Dacite	Dacite	Dacite	Dacite	Dacite	Dacite	Dacite	Dacite	Dacite
SiO_2	67.90	67.08	63.94	66.62	64.91	64.93	64.80	66.32	65.10	64.57	65.69
TiO_2	0.71	0.73	0.73	0.74	0.75	0.73	0.72	0.75	0.74	0.74	0.72
Al_2O_3	14.20	14.30	14.07	14.42	14.06	14.11	13.70	14.12	14.02	13.58	13.50
FeO											
Fe_2O_3	4.61	5.86	8.97	6.74	6.44	7.38	8.01	7.41	8.68	8.76	10.10
MnO	0.06	0.09	0.10	0.06	0.16	0.13	0.19	0.06	0.07	0.16	0.09
MgO	0.92	0.96	1.39	1.02	1.26	1.05	1.26	0.88	1.13	1.44	1.28
CaO	1.05	0.78	0.38	0.40	0.87	0.33	0.86	0.30	0.29	0.65	0.31
Na_2O	3.22	2.42	0.51	1.61	0.91	0.13	0.18	0.87	0.38	0.15	0.45
K_2O	5.57	6.25	7.34	7.21	7.19	6.96	7.14	7.38	7.30	6.59	5.39
P_2O_5	0.16	0.19	0.16	0.21	0.20	0.20	0.19	0.16	0.22	0.22	0.21
LOI	1.11										
Total	99.51	98.66	97.59	99.03	96.75	95.95	97.05	98.25	97.93	96.86	97.74
F		1224.00	4929.00	1162.00	1495.00	1821.00	1816.00	1560.00	1744.00	1708.00	1920.00
Ga	21.20	21.70	21.00	20.80	19.90	20.70	20.30	20.40	20.90	20.20	20.10
Cr	10.00	-20.00	-20.00	-20.00	-20.00	-20.00	-20.00	-20.00	-20.00	-20.00	-20.00
Ni	3.00	6.00	5.00	6.00	3.00	7.00	8.00	6.00	7.00	7.00	8.00
Co	8.00	12.30	40.50	23.50	19.80	32.40	23.10	28.90	30.00	36.00	31.60
Sc	11.00	11.00	10.00	11.00	10.00	11.00	11.00	11.00	11.00	11.00	10.00
V	31.00	29.00	32.00	25.00	31.00	27.00	34.00	35.00	30.00	30.00	29.00
Cu	121.00	87.00	537.00	64.00	55.00	113.00	50.00	1320.00	319.00	339.00	629.00
Zn	36.00	46.00	85.00	55.00	46.00	70.00	49.00	78.00	74.00	79.00	87.00
Y	59.80	63.10	62.70	64.60	60.50	62.90	57.80	58.50	57.80	65.50	72.50
Rb	262.00	297.50	339.70	327.50	341.00	361.30	368.80	362.10	370.00	354.60	335.80
Sr	137.00	62.90	50.40	66.70	45.90	21.20	24.90	50.60	42.50	31.00	27.30
Cs	1.59	1.71	4.04	3.70	3.58	1.79	2.77	3.02	3.61	3.02	2.36
Ba	1110.00	885.90	1129.80	1077.90	994.10	748.70	791.10	995.50	957.10	766.40	473.80
Th	40.00	40.06	39.08	39.18	38.97	36.51	37.32	39.15	38.31	37.70	35.94
U	11.80	9.40	11.37	7.69	8.09	7.27	6.86	9.87	10.29	9.13	12.39
Pb	12.00	11.00	28.00	9.00	11.00	7.00	-5.00	8.00	11.00	6.00	6.00
Zr	436.00	381.00	386.00	383.00	381.00	361.00	356.00	377.00	371.00	376.00	363.00
Hf	12.60	9.50	9.90	10.30	9.70	9.30	8.50	9.30	9.00	9.20	9.20
Nb	26.10	13.81	20.26	22.15	19.86	17.51	18.60	19.98	19.31	18.22	16.34
Ta	2.20	2.30	2.30	2.30	2.30	2.20	2.10	2.20	2.20	2.30	2.10
La	98.80	94.20	97.10	87.90	90.50	105.20	96.10	105.30	92.00	99.20	193.80
Ce	193.00	184.30	195.60	176.10	181.80	188.10	177.30	196.90	176.90	189.40	330.10
Pr	21.40	20.33	21.73	19.61	20.18	21.39	19.59	21.25	19.54	20.23	36.69
Nd	76.50	69.80	74.00	67.40	69.60	69.80	66.50	73.00	67.30	68.00	118.90
Sm	14.05	12.48	13.17	11.99	12.74	12.05	11.66	13.22	12.00	12.29	19.99
Eu	2.52	2.68	2.78	2.59	2.52	2.57	2.49	2.86	2.50	2.64	4.27
Gd	11.50	11.01	11.68	10.59	11.11	10.59	9.99	11.32	10.31	11.17	15.23
Tb	1.82	1.72	1.77	1.66	1.67	1.65	1.63	1.74	1.62	1.80	2.14
Dy	11.15	10.67	10.51	10.34	10.29	10.25	9.84	10.04	9.87	11.07	12.52
Ho	2.23	2.23	2.20	2.17	2.12	2.18	2.04	2.06	2.08	2.33	2.45
Er	6.53	6.23	6.24	6.13	5.97	6.25	5.70	5.97	5.84	6.49	6.63
Tm	1.03	0.94	0.91	0.90	0.88	0.90	0.87	0.87	0.87	0.95	0.96
Yb	6.12	6.04	5.77	5.75	5.86	5.61	5.54	5.60	5.58	6.16	6.08
Lu	0.98	0.91	0.87	0.87	0.88	0.83	0.98	0.84	1.06	0.94	0.90
Eu/Eu*	0.61	0.70	0.69	0.70	0.65	0.70	0.71	0.71	0.69	0.69	0.75
$(La/Yb)_N$	11.58	11.19	12.07	10.97	11.08	13.45	12.44	13.49	11.83	11.55	22.86
Ga/Al	2.82	2.87	2.82	2.73	2.67	2.77	2.80	2.73	2.82	2.81	2.81
Temp	1120.56	1120.76	1160.74	1137.81	1138.17	1176.88	1147.40	1153.99	1164.84	1171.39	1193.23
Temp upper error	1159.48	1157.36	1194.46	1173.20	1173.44	1208.02	1180.74	1187.82	1197.50	1203.75	1223.05
Temp lower error	1083.95	1086.20	1128.68	1104.29	1104.75	1147.12	1115.70	1121.83	1133.72	1140.53	1164.64
Temp	847.56	847.76	887.74	864.81	865.17	903.88	874.40	880.99	891.84	898.39	920.23
1 sigma error	37.76	35.58	32.89	34.46	34.34	30.45	32.52	33.00	31.89	31.61	29.20
Factor	1.43	1.32	1.06	1.20	1.20	0.90	1.08	1.08	1.00	0.97	0.80

$Eu/Eu^* = (Eu/(Sm \times Gd))_N^{0.5}$

Normalising values from Taylor and McLennon 1995

Appendix 3 Supplementary material for Temporal, geochemical and isotopic constraints on plume-driven felsic and mafic components in a large igneous province

Appendix 3 Table A1 Whole-rock geochemical composition for Gawler Range Volcanics samples

R number	1969446	1969445	1969444	1969442	1969441	1969440	1969439	1969438	1969437	1969436	1969435
Other Sample Number											
Drill_Hole	20772	20772	20772	20772	20772	20772	20772	20772	20772	20772	20772
Depth_From	465.1	475.3	484.5	493.7	504.7	514.1	524.4	535.3	544.05	554.1	565.3
Depth_To	466.1	476.3	485.5	494.8	505.75	515.1	525.4	536.3	545.05	555.1	566.3
Data Source	SARIG	SARIG	SARIG	SARIG	SARIG	SARIG	SARIG	SARIG	SARIG	SARIG	SARIG
Location	Stuart Shelf	Stuart Shelf	Stuart Shelf	Stuart Shelf	Stuart Shelf	Stuart Shelf	Stuart Shelf	Stuart Shelf	Stuart Shelf	Stuart Shelf	Stuart Shelf
Suite	LGRV	LGRV	LGRV	LGRV	LGRV	LGRV	LGRV	LGRV	LGRV	LGRV	LGRV
Formation	RED 2	RED 2	RED 2	RED 2	RED 2	RED 2	RED 2	RED 2	RED 2	RED 2	RED 2
Map Unit											
Easting	727055.84	727055.84	727055.84	727055.84	727055.84	727055.84	727055.84	727055.84	727055.84	727055.84	727055.84
Northing	6615049.80	6615049.80	6615049.80	6615049.80	6615049.80	6615049.80	6615049.80	6615049.80	6615049.80	6615049.80	6615049.80
Zone	53	53	53	53	53	53	53	53	53	53	53
Longitude	137.367642	137.367642	137.367642	137.367642	137.367642	137.367642	137.367642	137.367642	137.367642	137.367642	137.367642
Latitude	-30.575543	-30.575543	-30.575543	-30.575543	-30.575543	-30.575543	-30.575543	-30.575543	-30.575543	-30.575543	-30.575543
Datum	GDA94	GDA94	GDA94	GDA94	GDA94	GDA94	GDA94	GDA94	GDA94	GDA94	GDA94
Age	1593.60	1593.60	1593.60	1593.60	1593.60	1593.60	1593.60	1593.60	1593.60	1593.60	1593.60
Lithology	Dacite	Dacite	Dacite	Dacite	Dacite	Dacite	Dacite	Dacite	Dacite	Dacite	Dacite
SiO_2	64.84	67.00	64.36	62.04	63.73	63.98	60.01	63.24	63.66	65.98	64.04
TiO_2	0.73	0.76	0.86	0.89	0.86	0.87	0.82	0.92	0.96	0.76	0.84
Al_2O_3	13.39	14.37	13.93	13.64	13.93	13.97	13.07	13.98	14.22	14.07	13.96
FeO											
Fe_2O_3	9.41	6.92	7.62	9.32	7.43	8.07	12.78	7.49	7.30	5.77	6.66
MnO	0.12	0.07	0.08	0.07	0.09	0.07	0.19	0.08	0.06	0.07	0.05
MgO	1.54	0.97	1.07	1.30	1.32	1.31	1.93	1.45	1.49	1.12	1.33
CaO	0.35	0.62	0.91	0.91	1.22	0.84	1.23	1.30	1.40	1.01	1.32
Na_2O	0.17	1.90	1.53	2.16	1.93	2.11	0.07	2.67	3.23	2.64	2.97
K_2O	6.69	6.58	7.51	6.01	6.15	6.59	5.44	6.23	5.69	6.66	5.93
P_2O_5	0.14	0.19	0.32	0.33	0.33	0.32	0.30	0.36	0.32	0.18	0.28
LOI											
Total	97.38	99.38	98.19	96.67	96.99	98.13	95.84	97.72	98.33	98.26	97.38
F	1379.00	1282.00	1588.00	1755.00	1780.00	1638.00	2333.00	2775.00	2282.00	1803.00	2827.00
Ga	19.90	21.00	20.40	20.30	21.10	20.60	21.10	21.30	21.90	20.70	21.20
Cr	-20.00	-20.00	-20.00	-20.00	-20.00	-20.00	30.00	-20.00	-20.00	-20.00	-20.00
Ni	5.00	5.00	6.00	13.00	6.00	5.00	7.00	4.00	7.00	4.00	10.00
Co	33.60	16.00	17.50	78.00	20.00	14.40	28.30	11.10	11.10	7.10	9.70
Sc	10.00	10.00	12.00	14.00	12.00	12.00	11.00	13.00	13.00	10.00	12.00
V	37.00	34.00	45.00	51.00	46.00	55.00	50.00	51.00	51.00	34.00	43.00
Cu	66.00	166.00	309.00	793.00	235.00	221.00	68.00	167.00	82.00	85.00	88.00
Zn	108.00	60.00	46.00	36.00	42.00	40.00	91.00	29.00	50.00	26.00	30.00
Y	55.30	59.80	48.10	57.10	56.10	50.50	61.40	63.60	58.40	59.80	60.40
Rb	319.00	305.20	307.20	262.70	292.20	289.40	334.10	255.00	242.80	283.00	244.70
Sr	30.50	73.90	38.50	54.70	75.10	52.30	12.00	81.60	126.70	100.30	122.30
Cs	2.64	2.53	1.59	1.39	2.01	1.57	2.23	1.14	0.89	0.90	1.18
Ba	900.70	1025.10	884.10	774.00	853.00	972.70	368.00	1038.00	1108.30	1200.90	1072.50
Th	37.04	38.85	34.29	32.03	35.72	33.28	30.27	35.22	35.02	38.36	34.32
U	7.35	10.06	14.50	12.72	13.06	10.67	8.24	11.60	9.76	12.83	11.55
Pb	-5.00	15.00	13.00	9.00	9.00	7.00	-5.00	6.00	15.00	6.00	10.00
Zr	362.00	370.00	308.00	293.00	312.00	294.00	292.00	320.00	333.00	354.00	315.00
Hf	8.90	8.60	7.50	7.30	8.10	6.90	7.30	8.00	8.00	9.80	7.70
Nb	18.59	19.59	15.75	16.79	17.95	15.73	9.94	17.44	18.00	14.80	19.16
Ta	2.20	2.30	1.90	2.00	2.20	2.10	1.80	2.10	2.00	2.40	2.00
La	85.10	92.40	110.50	170.10	111.80	117.80	64.50	123.20	79.50	94.20	110.20
Ce	157.00	181.40	196.80	272.20	194.10	187.80	110.70	217.30	166.00	177.30	196.70
Pr	16.63	20.25	20.65	29.72	22.25	20.81	11.56	25.50	18.74	20.64	22.65
Nd	56.10	69.10	67.00	97.40	74.50	69.20	37.90	88.60	67.20	70.30	76.30
Sm	10.00	12.11	11.47	16.26	13.11	12.36	7.18	15.46	12.64	12.50	13.49
Eu	2.11	2.58	2.55	3.41	2.83	2.51	1.72	3.28	3.09	2.62	2.96
Gd	9.14	10.72	9.24	13.04	11.22	10.30	7.76	12.86	11.16	10.80	11.60
Tb	1.42	1.67	1.42	1.78	1.63	1.56	1.45	1.87	1.70	1.64	1.74
Dy	9.20	10.27	8.34	10.39	9.94	9.27	9.91	11.50	10.42	10.23	10.90
Ho	1.95	2.12	1.71	2.06	2.02	1.86	2.13	2.33	2.15	2.11	2.23
Er	5.59	6.05	4.73	5.63	5.57	5.13	6.13	6.61	5.88	6.05	6.12
Tm	0.84	0.89	0.68	0.82	0.81	0.74	0.91	0.97	0.87	0.89	0.91
Yb	5.26	5.72	4.49	5.18	5.60	4.90	5.79	6.22	5.53	5.81	5.71
Lu	0.79	1.08	0.65	0.76	1.41	0.74	0.83	0.90	0.76	0.86	0.87
Eu/Eu*	0.67	0.69	0.76	0.72	0.71	0.68	0.70	0.71	0.80	0.69	0.72
$(La/Yb)_N$	11.60	11.59	17.65	23.55	14.32	17.24	7.99	14.21	10.31	11.63	13.84
Ga/Al	2.81	2.76	2.77	2.81	2.86	2.79	3.05	2.88	2.91	2.78	2.87
Temp	1171.22	1130.03	1083.15	1078.88	1088.57	1079.34	1130.81	1065.62	1064.88	1086.61	1062.79
Temp upper error	1202.90	1165.42	1119.02	1114.27	1124.24	1114.75	1162.05	1103.34	1103.27	1124.46	1100.46
Temp lower error	1140.99	1096.53	1049.31	1045.47	1054.89	1045.91	1101.03	1030.18	1028.85	1051.01	1027.39
Temp	898.22	857.03	810.15	805.88	815.57	806.34	857.81	792.62	791.88	813.61	789.79
1 sigma error	30.95	34.45	34.85	34.40	34.68	34.42	30.51	36.58	37.21	36.72	36.53
Factor	0.94	1.23	1.40	1.39	1.37	1.39	1.02	1.57	1.61	1.50	1.58

$Eu/Eu^* = (Eu/(Sm \times Gd))_N^{0.5}$

Normalising values from Taylor and McLennon 1995

Appendix 3 Supplementary material for Temporal, geochemical and isotopic constraints on plume-driven felsic and mafic components in a large igneous province

Appendix 3 Table A1 Whole-rock geochemical composition for Gawler Range Volcanics samples

R number	1969434	1969433	1969432	1969430	1969429	1969428	1969427	1969426	1969425	1969424	1969423
Other Sample Number											
Drill_Hole	20772	20772	20772	20772	20772	20772	20772	20772	20772	20772	20772
Depth_From	575.3	584.3	594.7	614.8	624	633.6	642.8	655.1	665.2	674.1	686.2
Depth_To	576.3	585.3	595.65	615.8	625	634.7	643.8	656.1	666.2	675	686.9
Data Source	SARIG	SARIG	SARIG	SARIG	SARIG	SARIG	SARIG	SARIG	SARIG	SARIG	SARIG
Location	Stuart Shelf	Stuart Shelf	Stuart Shelf	Stuart Shelf	Stuart Shelf	Stuart Shelf	Stuart Shelf	Stuart Shelf	Stuart Shelf	Stuart Shelf	Stuart Shelf
Suite	LGRV	LGRV	LGRV	LGRV	LGRV	LGRV	LGRV	LGRV	LGRV	LGRV	LGRV
Formation	RED 2	RED 2	RED 2	RED 2	RED 2	RED 2	RED 2	RED 2	RED 2	RED 2	RED 2
Map Unit											
Easting	727055.84	727055.84	727055.84	727055.84	727055.84	727055.84	727055.84	727055.84	727055.84	727055.84	727055.84
Northing	6615049.80	6615049.80	6615049.80	6615049.80	6615049.80	6615049.80	6615049.80	6615049.80	6615049.80	6615049.80	6615049.80
Zone	53	53	53	53	53	53	53	53	53	53	53
Longitude	137.367642	137.367642	137.367642	137.367642	137.367642	137.367642	137.367642	137.367642	137.367642	137.367642	137.367642
Latitude	-30.575543	-30.575543	-30.575543	-30.575543	-30.575543	-30.575543	-30.575543	-30.575543	-30.575543	-30.575543	-30.575543
Datum	GDA94	GDA94	GDA94	GDA94	GDA94	GDA94	GDA94	GDA94	GDA94	GDA94	GDA94
Age	1593.60	1593.60	1593.60	1593.60	1593.60	1593.60	1593.60	1593.60	1593.60	1593.60	1593.60
Lithology	Dacite	Dacite	Dacite	Dacite	Dacite	Dacite	Dacite	Dacite	Dacite	Dacite	Dacite
SiO_2	64.11	62.44	64.05	60.90	63.58	63.96	63.34	65.10	69.34	64.78	65.69
TiO_2	0.81	0.80	0.87	0.78	0.81	0.83	0.88	0.82	0.31	0.81	0.73
Al_2O_3	13.77	13.22	14.02	13.88	13.57	14.02	14.13	14.20	12.66	14.05	13.86
FeO											
Fe_2O_3	7.63	9.11	6.75	7.97	7.99	6.23	7.38	6.39	5.50	5.81	6.08
MnO	0.06	0.06	0.04	0.06	0.08	0.05	0.05	0.07	0.08	0.05	0.04
MgO	1.20	1.11	1.21	0.91	1.04	1.50	1.45	1.20	1.02	1.30	0.90
CaO	0.86	0.62	1.57	1.01	1.01	1.72	1.36	1.26	0.73	1.30	1.04
Na_2O	2.47	0.70	3.13	1.35	0.80	3.15	2.66	2.76	0.47	2.65	2.45
K_2O	6.46	7.26	5.97	8.61	7.90	5.50	6.67	6.35	7.85	6.69	7.32
P_2O_5	0.26	0.26	0.30	0.27	0.28	0.27	0.28	0.21	0.15	0.27	0.22
LOI											
Total	97.63	95.58	97.91	95.74	97.06	97.23	98.20	98.36	98.11	97.71	98.33
F	2015.00	2060.00	2584.00	1771.00	1985.00	1778.00	2453.00	1928.00	1149.00	2164.00	1997.00
Ga	20.70	20.10	21.60	19.40	19.00	18.80	18.90	19.20	13.50	19.90	17.20
Cr	-20.00	-20.00	-20.00	-20.00	-20.00	-20.00	-20.00	-20.00	-20.00	-20.00	-20.00
Ni	7.00	6.00	6.00	10.00	8.00	5.00	8.00	5.00	4.00	5.00	8.00
Co	12.70	22.00	11.40	65.40	29.50	12.90	16.10	10.40	9.10	11.70	14.70
Sc	11.00	11.00	12.00	10.00	11.00	11.00	13.00	11.00	5.00	11.00	11.00
V	47.00	46.00	49.00	49.00	48.00	43.00	51.00	38.00	26.00	48.00	42.00
Cu	125.00	184.00	71.00	537.00	282.00	63.00	149.00	95.00	167.00	90.00	230.00
Zn	32.00	65.00	26.00	24.00	39.00	32.00	30.00	39.00	36.00	41.00	36.00
Y	55.80	60.00	60.60	44.90	57.90	52.30	51.60	56.40	32.70	56.00	49.20
Rb	260.50	323.70	246.30	321.80	350.30	243.20	275.50	267.00	328.00	269.80	284.40
Sr	74.50	32.30	130.50	60.60	29.50	136.30	97.50	102.00	36.60	110.70	90.00
Cs	1.21	1.15	1.06	1.05	1.13	1.41	1.31	1.43	1.42	1.17	1.01
Ba	986.20	859.90	1147.80	1289.20	1003.10	923.20	1106.60	1153.50	857.30	1101.30	1149.30
Th	34.20	33.90	38.29	33.99	34.54	37.57	35.16	39.98	19.91	38.36	39.68
U	12.07	13.97	12.40	15.80	25.64	12.56	13.62	13.71	6.48	13.03	13.68
Pb	6.00	-5.00	7.00	5.00	7.00	12.00	9.00	12.00	9.00	11.00	12.00
Zr	323.00	312.00	337.00	310.00	305.00	321.00	303.00	353.00	118.00	304.00	301.00
Hf	8.20	8.30	8.70	8.00	8.20	8.10	7.80	8.90	3.40	7.10	7.90
Nb	19.11	13.38	20.68	14.62	16.41	19.36	18.12	20.74	6.83	18.47	18.27
Ta	2.10	2.10	2.20	1.90	2.10	2.00	1.80	2.10	0.70	1.90	1.80
La	112.60	114.30	139.10	123.50	83.50	102.90	107.80	109.00	37.30	75.20	81.10
Ce	197.50	183.70	240.60	193.80	154.90	183.30	202.10	205.90	71.90	161.60	161.90
Pr	23.33	19.98	26.58	20.80	16.69	18.15	20.76	20.75	7.74	19.24	17.13
Nd	78.90	65.00	87.10	66.00	55.60	66.40	75.50	74.40	28.40	67.00	63.30
Sm	14.07	11.34	14.53	10.96	10.05	11.75	13.11	12.91	5.25	12.36	11.39
Eu	3.09	2.38	3.14	2.60	2.23	2.40	3.06	2.67	1.13	2.60	2.45
Gd	11.92	10.01	11.31	8.96	9.22	10.36	11.60	11.36	5.08	10.91	9.95
Tb	1.77	1.53	1.74	1.35	1.49	1.55	1.66	1.72	0.85	1.65	1.48
Dy	10.04	9.75	10.44	8.00	9.64	9.54	10.23	10.53	5.64	10.20	9.24
Ho	1.98	2.07	2.12	1.59	2.04	1.92	1.93	2.11	1.14	2.08	1.82
Er	5.41	5.85	5.85	4.39	5.83	5.28	5.35	5.82	3.21	5.87	5.08
Tm	0.78	0.86	0.88	0.64	0.83	0.79	0.78	0.87	0.49	0.85	0.77
Yb	5.01	5.44	5.69	4.24	5.23	5.07	4.92	5.36	3.00	5.38	4.88
Lu	0.74	0.81	0.85	0.60	0.80	0.71	0.67	0.77	0.37	0.75	0.71
Eu/Eu*	0.73	0.68	0.75	0.80	0.71	0.67	0.76	0.67	0.67	0.68	0.70
$(La/Yb)_N$	16.12	15.07	17.54	20.89	11.45	14.56	15.72	14.59	8.92	10.03	11.92
Ga/Al	2.84	2.87	2.91	2.64	2.65	2.53	2.53	2.55	2.01	2.68	2.34
Temp	1080.47	1111.58	1058.66	1060.50	1087.49	1056.96	1052.07	1080.62	1001.77	1057.73	1057.73
Temp upper error	1117.28	1145.50	1097.65	1098.08	1122.88	1095.32	1089.89	1118.84	1029.90	1095.21	1095.05
Temp lower error	1045.79	1079.42	1022.12	1025.18	1054.06	1020.97	1016.57	1044.71	974.98	1022.52	1022.65
Temp	807.47	838.58	785.66	787.50	814.49	783.96	779.07	807.62	728.77	784.73	784.73
1 sigma error	35.75	33.04	37.77	36.45	34.41	37.18	36.66	37.07	27.46	36.35	36.20
Factor	1.46	1.21	1.67	1.58	1.36	1.64	1.63	1.54	1.23	1.59	1.58

$Eu/Eu^* = (Eu/(Sm \times Gd))_N^{0.5}$

Normalising values from Taylor and McLennon 1995

Appendix 3 Supplementary material for Temporal, geochemical and isotopic constraints on plume-driven felsic and mafic components in a large igneous province

Appendix 3 Table A1 Whole-rock geochemical composition for Gawler Range Volcanics samples

R number	2729184	2729186	2729188	2729189	2729190	2729191	2019330	2017742		1840536
Other Sample Number									39	90847
Drill_Hole	20772	20772	20772	20772	20772	20772	140476			
Depth_From	331.34	366.74	456.32	558.1	637.85	668.88	87.62			
Depth_To	331.56	367.04	456.56	558.7	638.02	669.02	88			
Data Source	Wade et al this study	Wade et al this study	Wade et al this study	Wade et al this study	Wade et al this study	Wade et al this study	SARIG	SARIG	Agangi, A. (2011)	SARIG
Location	Stuart Shelf	Stuart Shelf	Stuart Shelf	Stuart Shelf	Stuart Shelf	Stuart Shelf	Roopena	Roopena	Kokatha	Kokatha
Suite	LGRV	LGRV	LGRV	LGRV	LGRV	LGRV	LGRV	LGRV	LGRV	LGRV
Formation	RED 2	RED 2	RED 2	RED 2	RED 2	RED 2	Angle Dam Volcanics	Angle Dam Volcanics		
Map Unit							Mag	Mag	Mi2	Mi2
Easting	727055.84	727055.84	727055.84	727055.84	727055.84	727055.84	723282.96	723318.72	525051.00	524111.00
Northing	6615049.80	6615049.80	6615049.80	6615049.80	6615049.80	6615049.80	6375206.41	6374758.29	6540439.00	6543713.00
Zone	53	53	53	53	53	53	53	53	53	53
Longitude	137.367642	137.367642	137.367642	137.367642	137.367642	137.367642	137.382908	137.383397		135.253198
Latitude	-30.575543	-30.575543	-30.575543	-30.575543	-30.575543	-30.575543	-32.738356	-32.742388		-31.240532
Datum	GDA94	GDA94	GDA94	GDA94	GDA94	GDA94	GDA94	GDA94		GDA94
Age	1593.60	1593.60	1593.60	1593.60	1593.60	1593.60	1594.40	1594.40	1590.00	1590.00
Lithology	Dacite	Dacite	Dacite	Dacite	Dacite	Dacite	Rhyolite	Rhyolite	Dacite	Dacite
SiO_2	67.86	67.93	67.38	64.73	64.67	67.54	67.30	67.30	62.92	67.78
TiO_2	0.71	0.72	0.75	0.82	0.87	0.68	0.69	0.66	0.00	0.64
Al_2O_3	14.49	14.79	14.57	14.41	14.32	14.10	13.60	13.15	13.96	15.10
FeO	1.85	1.77	1.85	2.47	2.71	1.90				0.00
Fe_2O_3	5.12	4.53	4.67	6.32	6.31	4.53	6.93	4.84	7.58	3.23
MnO	0.04	0.05	0.06	0.07	0.06	0.04	0.06	0.08	0.12	0.06
MgO	0.93	0.91	0.99	1.33	1.23	1.16	0.62	1.23	2.15	0.26
CaO	0.51	0.91	0.81	1.00	1.48	1.44	0.63	1.55	4.00	1.01
Na_2O	2.58	3.25	2.84	2.75	2.34	2.98	0.15	3.10	3.90	4.83
K_2O	6.37	5.60	6.14	6.79	7.36	6.02	4.25	5.01	3.14	5.31
P_2O_5	0.17	0.16	0.18	0.27	0.28	0.21	0.15	0.12	0.22	0.11
LOI	1.27	1.18	1.20	1.40	1.15	1.12	3.23	2.40	0.70	0.37
Total	101.90	101.80	101.44	102.36	102.78	101.72	97.61	99.44	98.69	98.70
F	1100.00	500.00	900.00	2300.00	1700.00	1800.00	690.00	850.00		
Ga	19.80	20.80	21.00	20.30	18.90	20.40	19.00	18.80	20.60	0.00
Cr	9.00	9.00	2.00	5.00	4.00	11.00	10.00	10.00	5.00	1.00
Ni	8.00	12.00	4.00	4.00	6.00	10.00	5.00	7.00	9.00	27.00
Co	26.90	25.30	30.40	27.80	40.90	24.10	6.00	8.00	0.00	0.00
Sc	11.70	11.90	11.60	12.60	14.40	11.10	7.00	9.00	17.40	10.70
V	28.60	26.40	27.70	50.10	55.00	38.00	55.00	57.00	160.00	10.00
Cu	44.00	78.00	226.00	146.00	108.00	64.00	3.00	26.00	11.00	0.00
Zn	30.00	40.00	45.00	40.00	30.00	40.00	81.00	218.00	91.00	0.00
Y	61.90	62.50	55.20	53.60	53.80	54.60	47.10	49.20	27.00	67.00
Rb	295.00	251.00	263.00	283.00	303.00	249.00	165.50	204.00	94.30	183.00
Sr	68.00	106.00	102.00	96.40	122.00	132.00	52.20	110.00	336.10	222.00
Cs	2.68	1.48	1.72	1.02	1.20	1.28	10.80	1.82	1.97	0.00
Ba	1060.00	1080.00	1120.00	1300.00	1380.00	1040.00	180.50	1530.00	1045.00	1946.00
Th	42.90	43.60	42.60	38.20	37.70	38.80	48.90	47.10	10.10	27.00
U	6.93	11.20	11.70	13.30	12.20	12.00	11.65	7.62	2.15	6.20
Pb	6.00	12.00	24.00	10.00	26.00	22.00	20.00	33.00	30.00	25.00
Zr	429.00	438.00	431.00	364.00	349.00	354.00	342.00	322.00	216.00	367.00
Hf	12.00	12.10	11.90	10.00	10.00	9.90	9.70	9.30	5.44	0.00
Nb	26.90	26.60	27.00	23.10	22.70	21.30	25.50	23.40	11.00	19.40
Ta	2.05	2.15	2.19	1.94	1.98	1.65	2.20	2.10	0.86	0.00
La	121.00	105.00	98.30	121.00	129.00	92.90	119.00	105.00	44.00	82.00
Ce	224.00	197.00	185.00	205.00	218.00	172.00	206.00	188.50	85.60	162.00
Pr	24.70	22.00	20.60	21.70	22.80	19.20	22.20	21.30	9.71	0.00
Nd	86.10	78.40	74.30	73.80	77.30	67.50	75.60	73.80	35.90	71.00
Sm	16.40	14.90	14.20	13.50	13.80	12.80	12.05	11.55	6.43	0.00
Eu	2.92	2.79	2.66	2.49	3.17	2.42	1.98	2.02	1.56	0.00
Gd	12.80	12.50	11.80	11.20	11.40	10.90	9.34	9.81	5.46	0.00
Tb	2.00	1.99	1.84	1.74	1.73	1.70	1.26	1.49	0.84	0.00
Dy	11.40	11.50	10.60	10.20	10.20	10.10	7.96	8.67	4.82	0.00
Ho	2.36	2.42	2.15	2.14	2.16	2.06	1.64	1.66	0.98	0.00
Er	6.91	7.28	6.39	5.71	6.00	6.13	4.68	5.01	2.75	0.00
Tm	1.01	1.08	0.97	0.84	0.87	0.90	0.66	0.69	0.41	0.00
Yb	6.43	6.94	6.07	5.26	5.69	5.67	4.20	4.35	2.55	0.00
Lu	0.92	1.03	0.93	0.81	0.83	0.85	0.67	0.62	0.37	0.00
Eu/Eu*	0.62	0.62	0.63	0.62	0.77	0.63	0.57	0.58	0.80	
$(La/Yb)_N$	13.50	10.85	11.62	16.50	16.26	11.75	20.32	17.31	12.38	
Ga/Al	2.58	2.66	2.72	2.66	2.49	2.73	2.64	2.70	2.79	0.00
Temp	1141.00	1131.02	1130.05	1085.67	1066.87	1080.25	1213.23	1068.73	971.08	1075.73
Temp upper error	1178.15	1169.27	1168.08	1124.03	1105.85	1118.55	1240.09	1106.33	1009.44	1114.90
Temp lower error	1105.91	1094.98	1094.19	1049.62	1030.32	1044.28	1187.35	1033.38	935.31	1038.99
Temp	868.00	858.02	857.05	812.67	793.87	807.25	940.23	795.73	698.08	802.73
1 sigma error	36.12	37.14	36.95	37.21	37.77	37.14	26.37	36.47	37.07	37.96
Factor	1.28	1.37	1.36	1.53	1.63	1.54	0.63	1.55	2.03	1.61

$Eu/Eu^* = (Eu/(Sm \times Gd))_N^{0.5}$

Normalising values from Taylor and McLennon 1995

Appendix 3 Supplementary material for Temporal, geochemical and isotopic constraints on plume-driven felsic and mafic components in a large igneous province

Appendix 3 Table A1 Whole-rock geochemical composition for Gawler Range Volcanics samples

R number	1840380	1840526	11350	1840193		1840523		2746487	1998164	1998165
Other Sample Number	CKO20	908137	5935/120	GH34	34	908122	884K10	CH-WPT264	GRV-7	GRV-8
Drill_Hole										
Depth_From										
Depth_To										
Data Source	SARIG	SARIG	SARIG	Agangi, A. (2011)	Agangi, A. (2011)	SARIG	SARIG	Wade et al this study	SARIG	SARIG
Location	Kokatha	Kokatha	Kokatha	Kokatha	Kokatha	Kokatha	Kokatha	Kokatha	Kokatha	Kokatha
Suite	LGRV	LGRV	LGRV	LGRV	LGRV	LGRV	LGRV	LGRV	LGRV	LGRV
Formation										
Map Unit	Mi2	Mi2	Mi2	Mi2	Mi2	Mi2	Mi2	Mi2	Mi2	Mi2
Easting	522574.69	522602.00	520423.11	523864.00	524277.00	519493.00	524698.05	519635.00	524303.71	524718.74
Northing	6542344.66	6543020.00	6543605.28	6543978.00	6543641.00	6544465.00	6544298.26	6544209.00	6543679.45	6545557.50
Zone	53	53	53	53	53	53	53		53	53
Longitude	135.237096	135.237368	135.214473	135.250598		135.204689			135.255223	135.259535
Latitude	-31.252909	-31.246815	-31.241574	-31.238146		-31.233833			-31.240830	-31.223876
Datum	GDA94	GDA94	GDA94	GDA94		GDA94				
Age	1590.00	1590.00	1590.00	1590.00	1590.00	1590.00	1590.00	1590.00	1590.00	1590.00
Lithology	Rhyolite	Rhyodacite	Rhyodacite	Rhyodacite	Rhyodacite	Rhyodacite	Rhyodacite	Rhyolite	Dacite	Dacite
SiO_2	69.50	70.13	70.22	71.65	71.65	71.91	72.24	72.75	69.80	71.20
TiO_2	0.44	0.44	0.41	0.45	0.00	0.26	0.38	0.27	0.49	0.39
Al_2O_3	15.57	14.09	13.88	13.87	13.87	13.84	13.36	14.00	13.75	14.20
FeO	0.00	0.00	1.42	0.00		0.00	0.00	0.65		
Fe_2O_3	3.42	3.22	0.00	2.98	2.98	2.07	0.00	1.96	3.86	3.70
MnO	0.14	0.12	0.10	0.03	0.03	0.07	0.04	0.03	0.12	0.13
MgO	0.32	0.41	0.46	0.21	0.21	0.74	0.21	0.36	0.60	0.37
CaO	0.61	0.99	0.73	0.55	0.55	1.70	0.47	1.66	1.51	0.63
Na_2O	3.89	4.02	4.22	3.84	3.84	3.61	4.39	4.01	3.27	3.75
K_2O	5.21	5.79	5.15	5.73	5.73	4.34	5.12	4.22	4.46	5.34
P_2O_5	0.07	0.07	0.06	0.06	0.06	0.09	0.03	0.09	0.09	0.05
LOI	0.79	0.47	0.00	0.36	0.36	0.67	0.53	0.55	1.19	0.52
Total	99.96	99.75	96.65	99.73	99.28	99.30	96.77	100.55	99.14	100.28
F								450.00	800.00	880.00
Ga	40.17	0.00	0.00	19.70	19.70	0.00	19.00	19.40	21.50	22.70
Cr	0.00	6.00	0.00	2.00	2.00	11.00	-1.00	7.00	20.00	20.00
Ni	4.00	22.00	-5.00	3.00	3.00	9.00	-1.00	6.00	3.00	2.00
Co	0.79	0.00	0.00	0.00	0.00	0.00	0.00	41.00	2.00	1.00
Sc	12.03	11.10	0.00	6.20	6.20	5.20	9.00	2.40	9.00	9.00
V	1.81	5.00	8.00	4.00	4.00	29.00	-2.00	26.40	16.00	8.00
Cu	2.58	0.00	8.00	3.00	3.00	0.00	1.00	8.00	5.00	4.00
Zn	96.64	0.00	92.00	55.00	55.00	0.00	44.00	45.00	91.00	110.00
Y	93.70	54.00	0.00	35.20	35.20	17.00	50.00	16.00	46.70	50.50
Rb	240.35	191.00	165.00	177.80	177.80	133.00	173.00	150.00	185.50	222.00
Sr	204.71	186.00	155.00	134.10	134.10	296.00	123.00	340.00	261.00	181.00
Cs	6.49	0.00	0.00	1.61	1.61	0.00	-3.00	2.95	2.81	3.89
Ba	2190.99	2251.00	2140.00	1871.00	1871.00	933.00	1728.00	1020.00		
Th	34.01	22.00	0.00	18.70	18.70	16.00	30.00	17.00	25.70	27.60
U	5.81	7.00	0.00	0.76	0.76	5.00	6.50	3.79	4.85	5.47
Pb	47.30	44.00	32.00	34.00	34.00	20.00	24.00	29.00	39.00	30.00
Zr	399.19	367.00	0.00	321.00	321.00	156.00	363.00	151.00	389.00	401.00
Hf	0.00	0.00	0.00	8.75	8.75	0.00	10.00	4.44	9.10	9.70
Nb	19.56	18.70	0.00	18.00	18.00	11.90	19.00	12.20	18.10	18.80
Ta	1.30	0.00	0.00	1.62	1.62	0.00	2.00	1.02	1.40	1.50
La	150.51	74.00	0.00	63.80	63.80	16.00	76.00	46.70	79.50	82.60
Ce	279.79	149.00	0.00	136.50	136.50	80.00	147.00	85.40	157.50	161.50
Pr	24.36	0.00	0.00	16.53	16.53	0.00	15.00	9.60	18.15	18.50
Nd	101.54	64.00	0.00	62.40	62.40	29.00	66.00	31.80	64.50	65.60
Sm	18.12	0.00	0.00	11.07	11.07	0.00	0.00	5.28	12.30	12.65
Eu	4.01	0.00	0.00	2.49	2.49	0.00	0.00	0.93	2.74	3.14
Gd	14.75	0.00	0.00	8.95	8.95	0.00	0.00	3.61	10.10	10.35
Tb	2.14	0.00	0.00	1.33	1.33	0.00	0.00	0.54	1.46	1.53
Dy	13.32	0.00	0.00	7.12	7.12	0.00	0.00	2.93	8.41	8.97
Ho	2.81	0.00	0.00	1.32	1.32	0.00	0.00	0.58	1.61	1.76
Er	7.58	0.00	0.00	3.70	3.70	0.00	0.00	1.69	4.67	5.27
Tm	0.96	0.00	0.00	0.52	0.52	0.00	0.00	0.27	0.70	0.78
Yb	6.19	0.00	0.00	3.29	3.29	0.00	0.00	1.78	4.69	4.93
Lu	0.89	0.00	0.00	0.51	0.51	0.00	0.00	0.27	0.67	0.72
Eu/Eu*	0.75			0.76	0.76			0.65	0.75	0.84
$(La/Yb)_N$	17.43			13.91	13.91			18.82	12.16	12.02
Ga/Al	4.87	0.00	0.00	2.68	2.68	0.00	2.69	2.62	2.95	3.02
Temp	1130.58	1079.72	#DIV/0!	1082.30	1082.92	1003.63	1093.42	997.26	1111.25	1118.42
Temp upper error	1167.24	1118.62	#DIV/0!	1118.89	1119.46	1035.40	1131.19	1029.07	1148.89	1156.05
Temp lower error	1095.94	1043.21	#DIV/0!	1047.82	1048.48	973.56	1057.87	967.17	1075.78	1082.93
Temp	857.58	806.72	#DIV/0!	809.30	809.92	730.63	820.42	724.26	838.25	845.42
1 sigma error	35.65	37.71	#DIV/0!	35.53	35.49	30.92	36.66	30.95	36.56	36.56
Factor	1.29	1.58	1.46	1.45	1.44	1.45	1.47	1.48	1.40	1.38

$Eu/Eu^* = (Eu/(Sm \times Gd))_N^{0.5}$

Normalising values from Taylor and McLennon 1995

Appendix 3 Supplementary material for Temporal, geochemical and isotopic constraints on plume-driven felsic and mafic components in a large igneous province

Appendix 3 Table A1 Whole-rock geochemical composition for Gawler Range Volcanics samples

R number	2018200	2018199	2018618	88432	88434	88433	88431	2132103	2132105	88430	2721812
Other Sample Number			CW-PA-18	884EU32	884EU34	884EU33	884EU31			884EU30	
Drill_Hole											
Depth_From											
Depth_To											
Data Source	SARIG	SARIG	SARIG	SARIG	SARIG	SARIG	SARIG	SARIG	SARIG	SARIG	SARIG
Location	Gawler Ranges	Gawler Ranges	Gawler Ranges	Gawler Ranges	Gawler Ranges	Gawler Ranges	Gawler Ranges	Gawler Ranges	Gawler Ranges	Gawler Ranges	Gawler Ranges
Suite	UGRV	UGRV	UGRV	UGRV	UGRV	UGRV	UGRV	UGRV	UGRV	UGRV	UGRV
Formation	Eucarro Rhyolite	Eucarro Rhyolite	Eucarro Rhyolite	Eucarro Rhyolite	Eucarro Rhyolite	Eucarro Rhyolite	Eucarro Rhyolite	Eucarro Rhyolite	Eucarro Rhyolite	Eucarro Rhyolite	Eucarro Rhyolite
Map Unit	Mau	Mau	Mau	Mau	Mau	Mau	Mau	Mau	Mau	Mau	Mau
Easting	674476.20	675033.85	683524.93	655301.58	656840.59	656593.59	653492.58	706629.08	709295.52	653785.58	665917.25
Northing	6395809.62	6395428.78	6390474.82	6402316.11	6399875.10	6400751.10	6405881.11	6400954.82	6398323.47	6407239.11	6386514.16
Zone	53	53	53	53	53	53	53	53	53	53	53
Longitude	136.858458	136.864466	136.955839					137.199607	137.228559		136.768444
Latitude	-32.561415	-32.564761	-32.608051					-32.509506	-32.532727		-32.619494
Datum	GDA94	GDA94	GDA94					GDA94	GDA94		GDA94
Age	1587.50	1587.50	1587.50	1587.50	1587.50	1587.50	1587.50	1587.50	1587.50	1587.50	1587.50
Lithology	Rhyolite	Rhyolite	Rhyolite	Rhyolite	Rhyolite	Rhyolite	Rhyolite	Rhyolite	Rhyolite	Rhyolite	Rhyolite
SiO_2	70.30	71.90	70.90	67.04	67.64	67.80	69.09	69.10	68.20	65.86	73.18
TiO_2	0.38	0.39	0.40	0.70	0.68	0.66	0.51	0.80	0.74	0.59	0.42
Al_2O_3	12.50	12.70	12.90	13.24	13.39	13.40	13.43	14.50	14.65	14.77	13.16
FeO	0.00	0.00	0.00	2.48	2.44	2.85	1.67	0.00	0.00	1.60	-0.10
Fe_2O_3	3.99	4.20	4.01	5.15	5.09	5.04	4.15	4.49	2.51	4.28	2.13
MnO	0.08	0.13	0.12	0.11	0.12	0.12	0.09	0.01	0.01	0.10	0.08
MgO	0.32	0.39	0.28	0.89	0.76	1.02	0.90	0.20	0.16	0.75	0.11
CaO	1.30	0.83	0.86	1.58	1.56	1.18	0.85	0.33	0.34	1.29	0.34
Na_2O	2.97	3.27	2.40	2.73	3.20	2.99	3.57	3.35	3.06	3.95	3.20
K_2O	5.31	5.44	5.80	5.64	5.22	5.37	5.05	6.36	5.61	5.16	5.59
P_2O_5	0.06	0.08	0.04	0.18	0.17	0.17	0.12	0.19	0.08	0.16	0.06
LOI	1.63	0.85	1.20	2.28	1.69	1.94	1.91	1.27	1.70	2.45	1.11
Total	98.84	100.18	98.91	102.02	101.96	102.54	101.34	100.60	97.06	100.96	99.27
F	1280.00	1390.00	1160.00								900.00
Ga	21.60	21.40	22.00	19.40	20.20	20.00	19.60	23.50	22.30	21.80	23.50
Cr	-10.00	10.00	10.00	3.00	3.00	4.00	3.00	10.00	10.00	2.00	7.00
Ni	2.00	1.00	1.00	1.50	1.50	1.50	1.00	3.00	1.00	1.00	10.00
Co	1.00	2.00	2.00	0.00	0.00	0.00	0.00	2.00	1.00	0.00	21.00
Sc	7.00	7.00	7.00	12.00	12.00	11.50	9.00	9.00	9.00	10.50	8.80
V	-5.00	-5.00	-5.00	17.00	16.00	16.00	12.00	31.00	26.00	15.00	4.60
Cu	4.00	5.00	4.00	3.00	5.00	4.00	7.00	5.00	3.00	4.00	6.00
Zn	70.00	109.00	179.00	123.00	134.00	117.00	117.00	58.00	14.00	101.00	80.00
Y	61.50	60.00	61.20	62.00	62.00	61.50	57.00	59.90	55.40	48.00	58.00
Rb	243.00	255.00	276.00	232.00	217.00	226.00	191.00	186.00	218.00	221.00	243.00
Sr	69.30	90.60	122.50	137.00	148.00	138.00	86.00	215.00	258.00	213.00	141.00
Cs	2.12	3.13	2.77	2.70	2.90	3.20	1.90	1.45	4.04	2.30	1.05
Ba	1205.00	1175.00	1305.00	1396.00	1355.00	1436.00	1314.00	4220.00	2350.00	1554.00	5090.00
Th	34.20	34.10	35.60	27.90	28.00	28.20	28.40	33.90	34.40	21.40	37.90
U	6.67	6.78	7.07	6.10	6.00	6.10	6.30	4.66	4.19	4.50	8.25
Pb	14.00	44.00	37.00	32.00	85.00	75.00	88.00	16.00	10.00	9.50	81.00
Zr	510.00	506.00	504.00	411.00	407.00	407.00	373.00	469.00	461.00	339.00	430.00
Hf	12.90	12.80	12.40	12.00	11.00	12.00	10.00	11.60	11.60	9.00	12.00
Nb	24.10	24.60	25.60	20.90	20.90	19.00	19.70	23.40	23.20	16.70	24.70
Ta	1.80	1.90	1.70	1.60	1.60	1.60	2.00	1.70	1.60	1.60	1.82
La	90.20	89.20	94.50	81.90	82.60	82.40	83.20	266.00	149.50	71.00	88.90
Ce	183.50	180.50	189.50	169.90	170.30	171.50	169.20	360.00	268.00	141.10	173.00
Pr	20.00	19.95	20.00	19.50	19.30	19.50	19.20	32.50	28.30	16.10	19.60
Nd	71.00	70.50	70.80	70.50	70.70	70.50	67.90	110.00	97.80	59.20	70.40
Sm	12.70	12.85	13.00	12.70	13.10	12.90	12.00	16.30	16.15	10.60	13.20
Eu	2.15	2.17	2.28	2.60	2.70	2.70	2.60	3.31	3.05	3.00	2.31
Gd	11.40	11.00	11.15	11.50	11.90	11.70	10.70	14.00	12.60	9.60	10.90
Tb	1.72	1.72	2.01	1.90	1.90	1.90	1.70	1.93	1.85	1.50	1.75
Dy	10.35	10.20	10.35	10.30	10.70	10.50	9.60	10.75	10.20	8.40	10.50
Ho	2.20	2.18	2.27	2.30	2.40	2.40	2.20	2.05	1.98	1.80	2.21
Er	6.35	6.48	6.01	6.90	6.80	6.80	6.20	6.03	5.63	5.30	6.24
Tm	0.96	0.95	0.99	0.00	0.00	0.00	0.00	0.82	0.83	0.00	0.93
Yb	6.05	5.83	6.13	6.00	6.10	6.10	5.50	5.80	5.41	4.70	6.04
Lu	0.99	0.96	0.90	0.90	0.90	0.90	0.80	0.83	0.83	0.70	0.89
Eu/Eu*	0.55	0.56	0.58	0.66	0.66	0.67	0.70	0.67	0.65	0.91	0.59
$(La/Yb)_N$	10.69	10.97	11.06	9.79	9.71	9.69	10.85	32.90	19.82	10.84	10.56
Ga/Al	3.26	3.18	3.22	2.77	2.85	2.82	2.76	3.06	2.88	2.79	3.37
Temp	1127.83	1134.04	1155.31	1096.20	1093.09	1107.83	1100.05	1139.58	1163.98	1076.21	1139.29
Temp upper error	1168.95	1174.60	1194.30	1135.82	1132.76	1146.47	1137.80	1178.41	1200.69	1114.10	1176.61
Temp lower error	1089.26	1095.95	1118.57	1059.03	1055.88	1071.48	1064.51	1103.00	1129.23	1040.60	1104.06
Temp	854.83	861.04	882.31	823.20	820.09	834.83	827.05	866.58	890.98	803.21	866.29
1 sigma error	39.84	39.32	37.87	38.39	38.44	37.50	36.64	37.70	35.73	36.75	36.28
Factor	1.52	1.47	1.33	1.56	1.57	1.46	1.44	1.37	1.19	1.54	1.29

$Eu/Eu^* = (Eu/(Sm \times Gd))_N^{0.5}$

Normalising values from Taylor and McLennon 1995

Appendix 3 Supplementary material for Temporal, geochemical and isotopic constraints on plume-driven felsic and mafic components in a large igneous province

Appendix 3 Table A1 Whole-rock geochemical composition for Gawler Range Volcanics samples

R number	2721816	1840817	8845	8843	1840818	1840825	2721843	2174053	2174054
Other Sample Number		Eu1	884EU5	884EU3	Eu2	Y49			
Drill_Hole									
Depth_From									
Depth_To									
Data Source	SARIG	Wade et al this study	Wade et al this study	Wade et al this study	Wade et al this study	SARIG	Wade et al this study	Wade et al this study	Wade et al this study
Location	Gawler Ranges	Gawler Ranges	Gawler Ranges	Gawler Ranges	Gawler Ranges	Gawler Ranges	Gawler Ranges	Gawler Ranges	Gawler Ranges
Suite	UGRV	UGRV	UGRV	UGRV	UGRV	UGRV	UGRV	UGRV	UGRV
Formation	Eucarro Rhyolite	Eucarro Rhyolite	Eucarro Rhyolite	Eucarro Rhyolite	Eucarro Rhyolite	Moonaree Dacite Member	Moonaree Dacite Member	Moonaree Dacite Member	Moonaree Dacite Member
Map Unit	Mau	Mau	Mau	Mau	Mau	Maym	Maym	Maym	Maym
Easting	660483.26	516750.00	543848.58	536048.57	500620.00	532150.00	580472.44	531434.99	517022.88
Northing	6397579.88	6435400.00	6385348.65	6393948.65	6433700.00	6425300.00	6460661.53	6422744.58	6447754.11
Zone	53	53	53	53	53	53	53	53	53
Longitude	136.709167	135.177754			135.006581	135.341521	135.851831	135.334010	135.180430
Latitude	-32.547568	-32.217877			-32.233339	-32.308657	-31.987242	-32.331730	-32.106420
Datum	GDA94	GDA94			GDA94	GDA94	GDA94	GDA94	GDA94
Age	1587.50	1587.50	1587.50	1587.50	1587.50	1587.20	1587.20	1587.20	1587.20
Lithology	Rhyolite	Rhyolite	Rhyolite	Rhyolite	Rhyolite	Dacite	Dacite	Dacite	Dacite
SiO_2	71.93	73.29	71.85	70.57	71.09	66.43	66.10	68.10	70.26
TiO_2	0.39	0.31	0.36	0.41	0.42	0.82	0.76	0.66	0.53
Al_2O_3	13.36	12.62	13.05	13.16	13.24	14.03	13.62	14.29	13.60
FeO	0.46	1.24	1.90	2.12	1.83	0.00	0.87	3.10	2.21
Fe_2O_3	3.52	2.92	3.44	3.71	3.77	5.89	5.38	4.77	4.05
MnO	0.03	0.07	0.09	0.09	0.09	0.12	0.05	0.10	0.10
MgO	0.17	0.14	0.25	0.26	0.30	0.98	1.98	0.75	0.45
CaO	0.17	1.19	1.10	1.50	1.33	2.58	0.47	2.31	1.75
Na_2O	2.64	2.75	3.25	3.09	3.18	3.40	1.52	3.45	3.32
K_2O	6.16	5.73	5.53	5.52	5.73	4.61	8.21	4.88	5.09
P_2O_5	0.07	0.04	0.05	0.07	0.07	0.22	0.21	0.18	0.12
LOI	1.31	0.58	0.54	1.28	0.44	0.93	1.18	0.60	0.34
Total	100.21	100.87	101.41	101.79	101.49	100.01	100.35	103.19	101.83
F	700.00	2100.00	1600.00	1400.00	1400.00		1500.00	1300.00	1300.00
Ga	24.50	25.70	25.20	24.70	24.80	22.00	21.50	22.40	23.10
Cr	7.00	2.00	4.00	4.00	1.00	0.00	10.00	7.00	8.00
Ni	10.00	4.00	4.00	8.00	4.00	0.00	14.00	10.00	6.00
Co	12.40	57.00	58.10	39.70	57.10	0.00	22.30	22.40	17.30
Sc	8.00	6.60	7.80	8.50	8.60	10.90	12.10	10.80	10.40
V	6.20	2.20	3.30	5.80	5.90	33.30	35.20	27.90	14.40
Cu	18.00	6.00	32.00	30.00	6.00	0.00	6.00	8.00	8.00
Zn	85.00	85.00	115.00	105.00	95.00	0.00	50.00	90.00	100.00
Y	56.20	68.30	66.10	65.20	64.20	54.60	56.40	51.80	56.20
Rb	292.00	282.00	249.00	250.00	260.00	182.80	238.00	214.00	233.00
Sr	117.00	69.60	92.40	111.00	105.00	208.30	131.00	217.00	162.00
Cs	3.93	2.20	2.90	3.09	3.22	0.00	3.30	2.94	2.99
Ba	1490.00	915.00	1140.00	1320.00	1340.00	1263.00	1610.00	1560.00	1280.00
Th	34.50	40.40	38.00	35.50	35.00	25.50	27.00	27.80	29.60
U	7.55	8.76	8.23	7.68	7.64	4.40	3.74	5.82	6.13
Pb	20.00	41.00	52.00	38.00	43.00	24.80	20.00	37.00	40.00
Zr	540.00	467.00	504.00	509.00	520.00	394.30	420.00	437.00	392.00
Hf	14.40	12.60	13.40	13.80	13.70	0.00	11.50	11.40	11.00
Nb	27.00	28.00	27.50	26.20	26.00	18.80	20.60	21.10	23.00
Ta	1.92	2.10	2.08	2.00	2.00	0.00	1.41	1.58	1.67
La	49.80	105.00	103.00	97.20	98.90	75.00	76.60	80.00	84.40
Ce	105.00	202.00	199.00	190.00	193.00	151.00	152.00	154.00	166.00
Pr	11.70	22.80	22.60	21.40	21.60	0.00	17.20	17.60	18.70
Nd	42.90	81.80	82.00	79.00	80.00	67.00	65.50	63.50	69.40
Sm	9.28	15.80	15.30	15.00	15.20	0.00	12.80	12.10	13.40
Eu	1.73	1.66	2.20	2.40	2.39	0.00	2.43	2.40	2.30
Gd	8.39	12.70	12.50	12.40	12.80	0.00	10.80	9.99	11.30
Tb	1.63	2.11	2.06	2.01	2.06	0.00	1.71	1.63	1.78
Dy	10.50	12.50	12.00	12.00	11.80	0.00	10.20	9.39	10.60
Ho	2.23	2.56	2.55	2.41	2.57	0.00	2.08	2.01	2.13
Er	6.60	7.53	7.29	7.27	7.19	0.00	6.16	5.43	6.06
Tm	1.02	1.08	1.10	1.06	1.07	0.00	0.87	0.82	0.90
Yb	6.42	6.95	7.15	6.99	6.81	0.00	5.56	5.31	5.85
Lu	0.98	1.11	1.02	1.02	1.04	0.00	0.84	0.79	0.88
Eu/Eu*	0.60	0.36	0.49	0.54	0.52		0.63	0.67	0.57
$(La/Yb)_N$	5.56	10.84	10.33	9.97	10.42		9.88	10.81	10.35
Ga/Al	3.46	3.85	3.65	3.55	3.54	2.96	2.98	2.96	3.21
Temp	1180.25	1125.50	1130.19	1123.57	1126.08	1069.87	1119.50	1091.43	1090.31
Temp upper error	1218.68	1165.25	1170.95	1164.95	1167.65	1110.57	1157.85	1132.37	1129.55
Temp lower error	1143.95	1088.14	1091.95	1084.80	1087.12	1031.81	1083.39	1053.11	1053.47
Temp	907.25	852.50	857.19	850.57	853.08	796.87	846.50	818.43	817.31
1 sigma error	37.37	38.55	39.50	40.07	40.27	39.38	37.23	39.63	38.04
Factor	1.23	1.46	1.49	1.55	1.55	1.72	1.41	1.64	1.56

$Eu/Eu^* = (Eu/(Sm \times Gd))_N^{0.5}$

Normalising values from Taylor and McLennon 1995

Appendix 3 Supplementary material for Temporal, geochemical and isotopic constraints on plume-driven felsic and mafic components in a large igneous province

Appendix 3 Table A1 Whole-rock geochemical composition for Gawler Range Volcanics samples

R number	2721818	2721820	2721826	2721829	2174047	2721832	1998160
Other Sample Number							GRV-3
Drill_Hole							
Depth_From							
Depth_To							
Data Source	Wade et al this study	Wade et al this study	Wade et al this study	Wade et al this study	Wade et al this study	Wade et al this study	SARIG
Location	Gawler Ranges	Gawler Ranges	Gawler Ranges	Gawler Ranges	Gawler Ranges	Gawler Ranges	Gawler Ranges
Suite	UGRV	UGRV	UGRV	UGRV	UGRV	UGRV	UGRV
Formation	Moonaree Dacite Member	Moonaree Dacite Member	Moonaree Dacite Member	Moonaree Dacite Member	Moonaree Dacite Member	Moonaree Dacite Member	Moonaree Dacite Member
Map Unit	Maym	Maym	Maym	Maym	Maym	Maym	Maym
Easting	619454.85	622665.91	605986.14	603753.59	553227.01	561780.69	603745.00
Northing	6405507.35	6408515.76	6412434.64	6413012.96	6494516.87	6437341.50	6413019.00
Zone	53	53	53	53	53	53	53
Longitude	136.271311	136.305086	136.127216	136.103412	135.561590	135.655485	136.103320
Latitude	-32.481252	-32.453770	-32.420138	-32.415132	-31.683421	-32.198788	-32.415078
Datum	GDA94	GDA94	GDA94	GDA94	GDA94	GDA94	GDA94
Age	1587.20	1587.20	1587.20	1587.20	1587.20	1587.20	1587.20
Lithology	Dacite	Dacite	Dacite	Dacite	Dacite	Dacite	Dacite
SiO_2	66.49	66.61	67.15	68.54	67.10	66.30	68.20
TiO_2	0.77	0.80	0.71	0.60	0.79	0.78	0.57
Al_2O_3	13.88	13.84	13.86	13.81	14.02	14.08	13.60
FeO	3.43	3.55	2.61	2.50	3.47	3.21	
Fe_2O_3	5.60	5.67	5.16	4.40	5.62	5.51	4.85
MnO	0.12	0.14	0.11	0.09	0.13	0.12	0.09
MgO	0.99	1.25	1.20	1.30	1.01	1.02	1.29
CaO	2.20	1.93	1.59	0.86	2.13	2.32	0.89
Na_2O	3.33	3.19	3.21	3.24	3.22	3.31	3.09
K_2O	4.90	4.86	4.94	5.42	4.83	4.72	5.19
P_2O_5	0.22	0.23	0.21	0.15	0.22	0.22	0.15
LOI	1.17	1.32	1.55	1.30	1.03	1.17	1.25
Total	103.10	103.38	102.30	102.21	103.56	102.76	99.17
F	1200.00	1200.00	1100.00	1200.00	1200.00	1200.00	1070.00
Ga	21.70	22.30	22.40	22.70	22.60	22.90	21.80
Cr	14.00	12.00	7.00	8.00	8.00	8.00	10.00
Ni	14.00	14.00	8.00	6.00	8.00	8.00	3.00
Co	19.00	18.70	13.50	14.70	18.80	18.10	6.00
Sc	13.10	13.20	12.20	9.70	12.30	12.10	8.00
V	36.60	38.80	33.80	24.20	36.30	37.60	28.00
Cu	14.00	12.00	14.00	8.00	14.00	26.00	5.00
Zn	100.00	105.00	100.00	100.00	100.00	100.00	90.00
Y	56.60	56.80	53.80	52.70	53.90	51.90	53.20
Rb	212.00	207.00	208.00	236.00	202.00	205.00	234.00
Sr	195.00	207.00	181.00	129.00	249.00	230.00	124.50
Cs	2.77	2.87	3.03	3.47	3.49	3.66	3.18
Ba	1560.00	1420.00	1370.00	1470.00	1420.00	1610.00	1305.00
Th	27.40	28.10	27.70	30.10	26.70	25.70	30.90
U	5.78	5.75	5.77	6.43	5.52	5.54	6.34
Pb	31.00	37.00	36.00	6.00	37.00	35.00	5.00
Zr	426.00	431.00	401.00	443.00	431.00	413.00	476.00
Hf	11.20	11.70	11.00	11.90	11.80	11.10	10.90
Nb	21.00	21.70	20.30	21.10	20.40	19.90	20.50
Ta	1.40	1.50	1.46	1.52	1.45	1.46	1.70
La	82.40	84.20	78.60	80.70	80.50	78.00	81.50
Ce	161.00	162.00	152.00	155.00	156.00	152.00	158.50
Pr	18.40	18.80	17.50	17.40	17.90	17.20	17.60
Nd	67.40	69.80	64.70	63.10	65.90	63.60	61.50
Sm	13.00	13.50	12.40	11.80	12.80	12.60	11.65
Eu	2.57	2.50	2.37	2.15	2.46	2.39	2.20
Gd	10.90	11.50	10.60	9.94	10.50	10.60	9.77
Tb	1.74	1.82	1.66	1.64	1.68	1.63	1.44
Dy	10.20	10.60	9.69	9.59	9.97	9.55	8.95
Ho	2.09	2.14	2.02	1.97	2.05	2.00	1.80
Er	6.00	6.27	5.79	5.71	6.10	5.67	5.30
Tm	0.89	0.93	0.86	0.85	0.86	0.83	0.74
Yb	5.63	5.78	5.63	5.51	5.67	5.36	5.24
Lu	0.86	0.87	0.79	0.84	0.89	0.77	0.77
Eu/Eu*	0.66	0.61	0.63	0.61	0.65	0.63	0.63
$(La/Yb)_N$	10.50	10.45	10.01	10.51	10.18	10.44	11.16
Ga/Al	2.95	3.04	3.05	3.11	3.05	3.07	3.03
Temp	1085.06	1098.16	1099.72	1125.97	1095.61	1084.39	1139.81
Temp upper error	1126.00	1138.42	1138.69	1164.78	1136.04	1124.88	1178.89
Temp lower error	1046.75	1060.41	1063.11	1089.45	1057.72	1046.49	1103.02
Temp	812.06	825.16	826.72	852.97	822.61	811.39	866.81
1 sigma error	39.62	39.01	37.79	37.66	39.16	39.20	37.93
Factor	1.67	1.58	1.51	1.41	1.60	1.65	1.38

$Eu/Eu^* = (Eu/(Sm \times Gd))_N^{0.5}$

Normalising values from Taylor and McLennon 1995

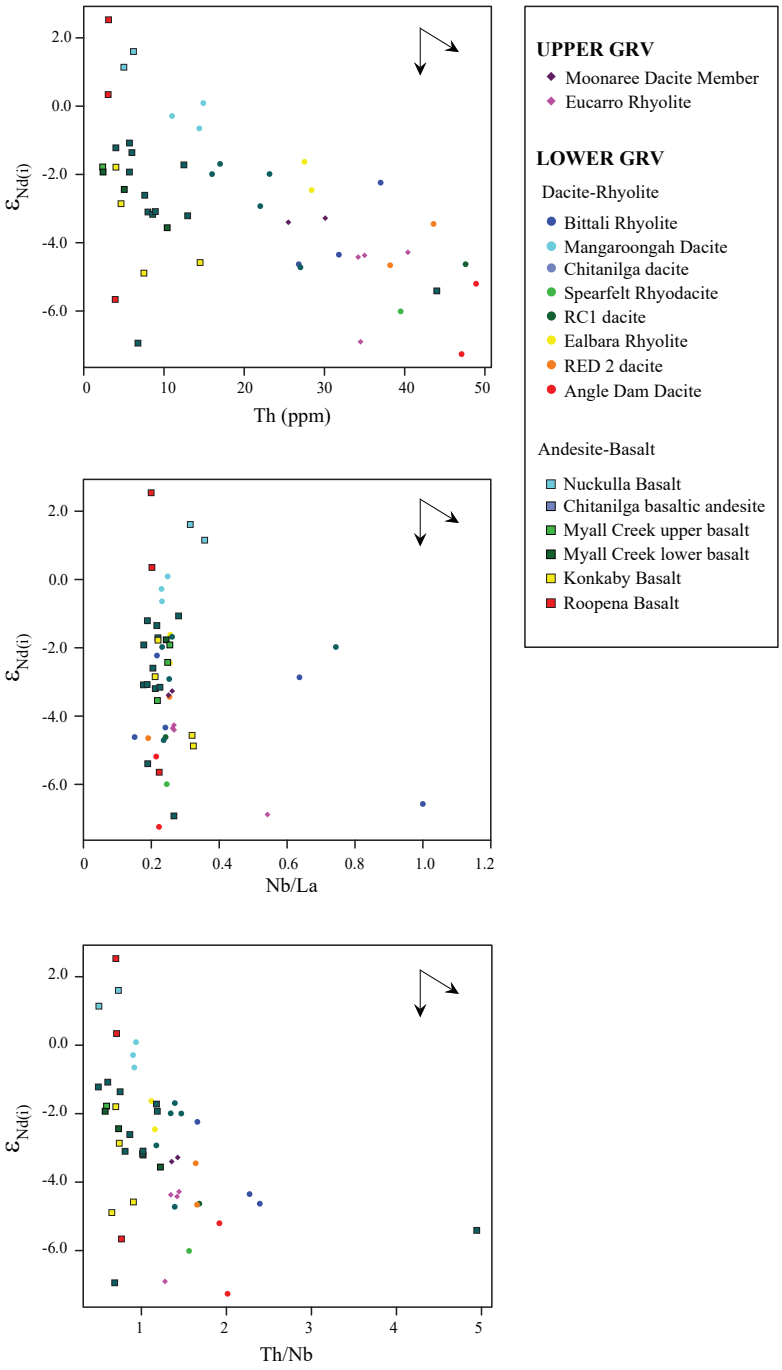

APPENDIX 3 FIGURE A1: $\varepsilon_{Nd(i)}$ vs Th, Nb/La and Th/Nb illustrating source composition variation in the SCLM and crustal assimilation traced via Th and decreasing $\varepsilon_{Nd(i)}$values. Vertical arrows correspond to source composition variation and oblique arrows show direction of expected crustal assimilation and fractional crystallisation. Nb/La and Th/Nb do not change significantly over large variations of $\varepsilon_{Nd(i)}$ values, interpreted to reflect source heterogeneity. Minor negative correlation between $\varepsilon_{Nd(i)}$ and Th can be traced in basalt and andesites from Nuckulla and Chitanilga, interpreted as evidence for crustal assimilation. An overall negative trend in the data suggests an increasing crustal input with increasing Th.

Appendix 4

Supplementary material for: Zircon trace element geochemistry as an indicator of magma fertility in iron oxide-copper-gold provinces

Appendix 4 Analytical Methods

University of Adelaide zircon analysis

Approximately 1 kg of fresh sample representative of each lithological unit were crushed and ground. Zircon grains were separated using standard panning and magnetic mineral separation techniques and handpicked under a binocular microscope. Zircon grains from nineteen samples were heat-treated for 48 hours at 900°C before being chemically abraded in HF/HNO_3 overnight at 160–180°C. Grains were mounted in epoxy and polished to expose grain interiors before being imaged by cathodoluminescence (CL) and back-scattered electron (BSE) using a Quanta 600 scanning electron microscope at Adelaide Microscopy, University of Adelaide. CL and BSE imaging provided crystal textures which aided selection of spots for analysis by LA-ICP-MS. Samples were analyzed in four analytical sessions between 2018 and 2020; the majority of the data were collected in two sessions in 2019.

U-Pb isotopes in zircons were analysed at Adelaide Microscopy, University of Adelaide, with a RESOlution-LR 193 nm ArF excimer laser ablation system with a S155 large format sample chamber. The laser was coupled to an Agilent 7900x ICP-MS. Samples were ablated at spots sizes of 29 micron with an fluence at the sample of ~2 J/cm^2 and a repetition rate of 5 Hz. Samples from analytical session 21/5/2020 were ablated at spot sizes of 19 micron at the same fluence and repetition rate, due to their smaller grain size. Samples were ablated in a He atmosphere (flow rate 0.35 L/min) and the aerosol mixed with Ar carrier gas (flow rate 1.01 L/min) for transport to the ICP-MS. An analysis consisted on 30 seconds of gas background collected while the laser was not firing followed by 50 seconds of ablated signal.

The GJ zircon (Jackson *et al.* 2004) was used as the primary standard to correct for down hole fractionation, instrument drift and mass bias. Zircons 91500 (Wiedenbeck *et al.* 1995) and Plesovice (Sláma *et al.* 2008) were used as secondary standards. NIST 610 was used as an external standard for trace element analysis (Pearce *et al.* 1997). The following isotopes were measured with counting times in brackets: ^{29}Si (5 ms), ^{31}P (5 ms), ^{49}Ti (5 ms), ^{89}Y (5 ms), ^{91}Zr (5 ms), ^{93}Nb (5 ms), ^{139}La (20 ms), ^{140}Ce (20 ms), ^{141}Pr (20 ms), ^{146}Nd (10 ms), ^{147}Sm (10 ms), ^{153}Eu (10 ms), ^{157}Gd (10 ms), ^{159}Tb (5 ms), ^{163}Dy (5 ms), ^{156}Ho (5 ms), ^{169}Tm (5 ms), ^{172}Yb (5 ms), ^{175}Lu (5 ms), ^{177}Hf (5 ms),, ^{202}Hg (20 ms), ^{204}Pb (10 ms), ^{206}Pb (30 ms), ^{207}Pb (60 ms), ^{208}Pb (10 ms), ^{232}Th (10 ms), and ^{238}U (30 ms), giving a total sweep time of ~0.378 seconds. Data was processed using iolite software and the VisualAge data reduction scheme (Paton *et al.* 2011, Petrus and Kamber 2012).

Boise State University zircon analysis

LA-ICPMS methods

Zircon grains were separated from rocks using standard techniques, annealed at 900°C for 60 hours in a muffle furnace and mounted in epoxy and polished until their centers were exposed. Cathodoluminescence (CL) images were obtained with a JEOL JSM-300 scanning electron microscope and Gatan MiniCL. Zircon was analyzed by laser ablation inductively coupled plasma mass spectrometry (LA-ICPMS) using a ThermoElectron X-Series II quadrupole ICPMS and New Wave Research UP-213 Nd:YAG UV (213 nm) laser ablation system. In-house analytical protocols, standard materials, and data reduction software were used for acquisition and calibration of U-Pb dates and a suite of high field strength elements (HFSE)

and rare earth elements (REE). Zircon was ablated with a laser spot of 25 μm wide using fluence and pulse rates of 5 J/cm^2 and 5 Hz, respectively, during a 45 second analysis (15 sec gas blank, 30 sec ablation) that excavated a pit ~25 μm deep. Ablated material was carried by a 1.2 L/min He gas stream to the nebulizer flow of the plasma. Dwell times were 5 ms for Si and Zr, 200 ms for ^{49}Ti and ^{207}Pb, 80 ms for ^{206}Pb, 40 ms for ^{202}Hg, ^{204}Pb, ^{208}Pb, ^{232}Th, and ^{238}U and 10 ms for all other HFSE and REE. Background count rates for each analyte were obtained prior to each spot analysis and subtracted from the raw count rate for each analyte. Ablations pits that appear to have intersected glass or mineral inclusions were identified based on Ti and P. U-Pb dates from these analyses are considered valid if the U-Pb ratios appear to have been unaffected by the inclusions. Analyses that appear contaminated by common Pb were rejected based on mass 204 being above baseline. For concentration calculations, background-subtracted count rates for each analyte were internally normalized to ^{29}Si and calibrated with respect to NIST SRM-610 and -612 glasses as the primary standards. Temperature was calculated from the Ti-in-zircon thermometer (Watson *et al.* 2006). Because there are no constraints on the activity of TiO_2, an average value in crustal rocks of 0.7 was used.

Data were collected in seven experiments in July 2014, October 2014, January 2016, and November 2019. For U-Pb and ^{207}Pb/^{206}Pb dates, instrumental fractionation of the background-subtracted ratios was corrected and dates were calibrated with respect to interspersed measurements of zircon standards and reference materials. The primary zircon standard used in most experiments was Plešovice (Sláma *et al.* 2008), which was used to monitor time-dependent instrumental fractionation based on two analyses for every 10 analyses of unknown zircon. FC1 (1098 Ma, unpublished data, Boise State University) was used in one experiment. A secondary correction to the ^{206}Pb/^{238}U dates was made based on results from 1-3 of the following zircon standards Seiland (531 Ma, unpublished data, Boise State University), Zirconia (327 Ma, unpublished data, Boise State University), 91500 (Wiedenbeck *et al.* 1995), FC1 (1098 Ma, unpublished data, Boise State University), and Orapa (92 Ma, unpublished data, Boise State University), which were treated as unknowns and measured once for every 10 analyses of unknown zircon. These results showed a linear age bias of several percent that is related to the ^{206}Pb count rate. The secondary correction is thought to mitigate matrix-dependent variations due to contrasting compositions and ablation characteristics between the Plešovice zircon and other standards (and unknowns).

Radiogenic isotope ratio and age error propagation for all analyses includes uncertainty contributions from counting statistics and background subtraction. The standard calibration uncertainty for U/Pb is the local standard deviation of the polynomial fit to the fractionation factor of the primary zircon standard versus time and for ^{207}Pb/^{206}Pb is the standard error of the mean of the fractionation factor of primary zircon standard. These uncertainties are 0.9-2.3% (2σ) for ^{206}Pb/^{238}U and 0.2-0.6% (2σ) for ^{207}Pb/^{206}Pb. Age interpretations are based on ^{207}Pb/^{206}Pb dates. Errors on the dates are at 2σ.

Appendix 4 Analytical Methods

REFERENCES

Jackson, S. E., Pearson, N. J., Griffin, W. L. and Belousova, E. A., 2004. The application of laser ablation-inductively coupled plasma-mass spectrometry to in situ U–Pb zircon geochronology. Chemical Geology, v. 211, p. 47-69. doi: https://doi.org/10.1016/j.chemgeo.2004.06.017

Paton, C., Hellstrom, J., Paul, B., Woodhead, J. and Hergt, J., 2011. Iolite: Freeware for the visualisation and processing of mass spectrometric data. Journal of Analytical Atomic Spectrometry, v. 26, p. 2508-2518. doi: https://doi.org/10.1039/c1ja10172b

Pearce, N. J. G., Perkins, W. T., Westgate, J. A., Gorton, M. P., Jackson, S. E., Neal, C. R. and Chenery, S. P., 1997. A Compilation of New and Published Major and Trace Element Data for NIST SRM 610 and NIST SRM 612 Glass Reference Materials. Geostandards Newsletter, v. 21, p. 115-144. doi: https://doi.org/10.1111/j.1751-908X.1997.tb00538.x

Petrus, J. A. and Kamber, B. S., 2012. VizualAge: A novel approach to Laser Ablation ICP-MS U-Pb geochronology data reduction. Geostandards and Geoanalytical Research, v. 36, p. 247-270. doi: https://doi.org/10.1111/j.1751-908X.2012.00158.x

Sláma, J., Kosler, J., Condon, D. J., Crowley, J. L., Gerdes, A., Hanchar, J. M., Horstwood, M. S. A., Morris, G. A., Nasdala, L., Norberg, N., Schaltegger, U., Schoene, B., Tubrett, M. N. and Whitehouse, M. J., 2008. Plešovice zircon - A new natural reference material for U-Pb and Hf isotopic microanalysis Chemical Geology v. 249, p. 1-35. doi: https://doi.org/10.1016/j.chemgeo.2007.11.005

Watson, E. B., Wark, D. A. and Thomas, J. B., 2006. Crystallization thermometers for zircon and rutile. Contributions to Mineralogy and Petrology, v. 151, p. 413. doi: https://doi.org10.1007/s00410-006-0068-5

Wiedenbeck, M., Alle, P., Corfu, F., W.L., G., Meier, M., Oberli, F., A., V., Roddick, J. C. and W., S., 1995. 3 Natural Zircon Standards for U-Th-Pb, Lu-Hf, Trace-Element and REE Analyses. Geostandards Newsletter, v. 19, p. 1-23. doi: https://doi.org/10.1111/j.1751-908X.1995.tb00147.x

Appendix 4 Table A1 Metadata for LA-ICP-MS U-Pb analyses, University of Adelaide

Laboratory and Sample Preparation	
Laboratory name	Adealide Microscopy, University of Adelaide
Sample type/mineral	Zircon
Sample preparation	Conventional mineral separation, 1 inch resin mount, 0.3 mm polish to finish
Imaging	CL, FEI Quanta600 SEM, 15kV, spot size 7, 15 mm working distance
Laser ablation system	
Make, Model and type	RESOlution-LR 193 nm ArF excimer
Ablation cell and volume	S155 large format cell (Laurin technic)
Laser wavelength (nm)	193 nm
Pulse width (ns)	20 ns
Fluence (J cm^{-2})	~2 J cm^{-2}
Repetition rate (Hz)	5 Hz
Ablation duration (s)	30 s
Ablation pit depth / ablation rate	~10um / ~0.67 um/pulse
Spot diameter (mm)	29 mm and 19 mm
Sampling mode / pattern	Static spot ablation
Carrier gas	100% He in the cell, Ar make-up gas added in the sample funnel immediately after ablation
Cell carrier gas flow (l min^{-1})	0.35 l/min He
ICP-MS Instrument	
Make, Model and type	Agilent 7900x
Sample introduction	Ablation aerosol transported through 2.5mm id nylon tubing, with Squid mixing device (Laurin Technic)
RF power (W)	1550 W
Make-up gas flow (l min^{-1})	1.01 l min^{-1} Ar
Detection system	single ion-counting SEM
Masses measured	29, 91 (5); 202–207, 235, 238
Masses measured and dwell times per peak (ms)	29,31,49,89,91,93(5);139,140,141(20);146,147,153,157(10);159,163,165,166,169,172,175, 177(5); 202(20);204(10);206(30);207(60);208,232(10);238(30)
Total integration time per output data point (s)	0.378 s
'Sensitivity' as useful yield (%, element)	~4000 cps/ppm U (NIST610, 51um, 5Hz) -
Dead time (ns)	36 ns
Data Processing	
Gas blank	30 s
Calibration strategy	GJ used as primary reference material. Plešovice & 91500 used as secondary reference materials.
Reference Material info	Plešovice (Slama et al., 2008) 91500 (Weidenbeck et al., 1995) GJ (Jackson et al., 2004)
Data processing package used	Iolite software
Mass discrimination	$^{207}Pb/^{206}Pb$, $^{206}Pb/^{238}U$ and $^{207}Pb/^{235}U$ normalized to reference material (^{235}U calcualted from ^{238}U)
Common-Pb correction, composition and uncertainty	No common Pb correction applied; ablation sweeps with mass 204 signals above background rejected.
Uncertainty level and propagation	Ages are quoted at 2 sigma absolute Fully propagated errors (calculated in LADR), includes within-run reference material reproducibility
Quality control / Validation	See accompanying data tables.

Appendix 4 Table A2 Metadata for LA-ICP-MS U-(Th-)Pb analyses, Boise State University

Laboratory and Sample Preparation	
Laboratory name	Boise State University Isotope Geology Laboratory
Sample type/mineral	Zircon
Sample preparation	Conventional mineral separation, 1 inch resin mount, 0.3 mm polish to finish
Imaging	CL, JEOL T300, 10 nA, 17 mm working distance
Laser ablation system	
Make, Model and type	ESI/New Wave Research, UP213
Ablation cell and volume	Standard ablation cell
Laser wavelength (nm)	213 nm
Pulse width (ns)	4 ns
Fluence (J cm^{-2})	~5 J cm^{-2}
Repetition rate (Hz)	5 Hz
Ablation duration (s)	30 s
Ablation pit depth / ablation rate	15 mm pit depth, measured using an optical microscope, equivalent to 0.05 mm/pulse
Spot diameter (mm)	25 mm
Sampling mode / pattern	Static spot ablation
Carrier gas	100% He in the cell, Ar make-up gas combined using a Y-piece 70 cm from the torch.
Cell carrier gas flow (l min^{-1})	1.15 l min^{-1}
ICP-MS Instrument	
Make, Model and type	ThermoElectron, X-series II, quadrupole
Sample introduction	Ablation aerosol transported through 90 cm long, 1.5 cm dia. tygon tubing coil
RF power (W)	1400 W
Make-up gas flow (l min^{-1})	0.74 l min^{-1} Ar
Detection system	single ion-counting SEM
Masses measured	29, 91 (5); 202–207, 235, 238
Masses measured and dwell times per peak (ms)	29,91(5); 31,89,93,139,140,141,146,147,153,157,159,163,165,166,169,172,175,177,181 (10); 202,204,208,232,238(40); 206(80); 49,207(200)
Total integration time per output data point (s)	~ 0.895 s
'Sensitivity' as useful yield (%, element)	0.01% U ((#ions detected/#atoms sampled)*100; Schaltegger et al. 2015)
IC Dead time (ns)	29 ns
Data Processing	
Gas blank	30 s on-peak zero subtracted
Calibration strategy	Plešovice or FC1 used as primary reference material. Seiland, Zirconia, FC1, 91500, Orapa used as secondary reference material.
Reference Material info	Plešovice (Slama et al., 2008) Seiland, Zirconia, Orapa, FC1 (Boise State University, unpublished data) 91500 (Weidenbeck et al., 1995)
Data processing package used / Correction for LIEF	ThermoElectron Plasmalab TRA software for integrated cps acquisition; in-house Microsoft VBA coded spreadsheet for data normalization, concentration calibration, uncertainty propagation and age calculation.
Mass discrimination	$^{207}Pb/^{206}Pb$ and $^{206}Pb/^{238}U$ normalized to reference material
Common-Pb correction, composition and uncertainty	No common Pb correction applied; ablation sweeps with mass 204 signals above background rejected.
Uncertainty level and propagation	Ages are quoted at 2 sigma absolute, propagation is by quadratic addition. Systematic errors based upon reproducibility of reference material are propagated where appropriate: 2% (2 sigma) for Pb/U and 1% (2 sigma) for Pb/Pb.
Quality control / Validation	See accompanying data tables.

Appendix 4 Table A3 Zircon trace element data for GRV and Hiltaba Suite samples analyzed at the University of Adelaide

Unit	Group	Sample	Spot Number	Zircon Treatment	Discordance	Other	Analytical Session
Included Data							
LGRV	mineralization-related	18-TAR-14	18-TAR-14 - 1	Chemical Abrasion			26/08/2018
LGRV	mineralization-related	18-TAR-14	18-TAR-14 - 2	Chemical Abrasion			26/08/2018
LGRV	mineralization-related	18-TAR-14	18-TAR-14 - 3	Chemical Abrasion			26/08/2018
LGRV	mineralization-related	18-TAR-14	18-TAR-14 - 4	Chemical Abrasion			26/08/2018
LGRV	mineralization-related	18-TAR-14	18-TAR-14 - 5	Chemical Abrasion			26/08/2018
LGRV	mineralization-related	18-TAR-14	18-TAR-14 - 6	Chemical Abrasion			26/08/2018
LGRV	mineralization-related	18-TAR-14	18-TAR-14 - 7	Chemical Abrasion			26/08/2018
LGRV	mineralization-related	18-TAR-14	18-TAR-14 - 8	Chemical Abrasion			26/08/2018
LGRV	mineralization-related	18-TAR-14	18-TAR-14 - 9	Chemical Abrasion			26/08/2018
LGRV	mineralization-related	18-TAR-14	18-TAR-14 - 13	Chemical Abrasion			27/08/2018
LGRV	mineralization-related	18-TAR-14	18-TAR-14 - 14	Chemical Abrasion			27/08/2018
LGRV	mineralization-related	2729189	189 - 1	Chemical Abrasion			11/11/2019
LGRV	mineralization-related	2729189	189 - 2	Chemical Abrasion			11/11/2019
LGRV	mineralization-related	2729189	189 - 3	Chemical Abrasion			11/11/2019
LGRV	mineralization-related	2729189	189 - 4	Chemical Abrasion			11/11/2019
LGRV	mineralization-related	2729189	189 - 5	Chemical Abrasion			11/11/2019
LGRV	mineralization-related	2729189	189 - 6	Chemical Abrasion			11/11/2019
LGRV	mineralization-related	2729189	189 - 7	Chemical Abrasion			11/11/2019
LGRV	mineralization-related	2729189	189 - 8	Chemical Abrasion			11/11/2019
LGRV	mineralization-related	2729189	189 - 9	Chemical Abrasion			11/11/2019
LGRV	mineralization-related	2729189	189 - 11	Chemical Abrasion			11/11/2019
Hiltaba Suite	mineralization-related	2705391	391-3	Chemical Abrasion			30/09/2019
Hiltaba Suite	mineralization-related	2705391	391-5	Chemical Abrasion			30/09/2019
Hiltaba Suite	mineralization-related	2705391	391-6	Chemical Abrasion			30/09/2019
Hiltaba Suite	mineralization-related	2705391	391-7	Chemical Abrasion			30/09/2019
Hiltaba Suite	mineralization-related	2705391	391-9	Chemical Abrasion			30/09/2019
Hiltaba Suite	mineralization-related	2705391	391-11	Chemical Abrasion			30/09/2019
Hiltaba Suite	mineralization-related	2705391	391-13	Chemical Abrasion			30/09/2019
Hiltaba Suite	mineralization-related	2705391	391-14	Chemical Abrasion			30/09/2019
Hiltaba Suite	mineralization-related	2705391	391-16	Chemical Abrasion			30/09/2019
Hiltaba Suite	mineralization-related	2705391	391-17	Chemical Abrasion			30/09/2019
Hiltaba Suite	mineralization-related	2705391	391-18	Chemical Abrasion			30/09/2019
Hiltaba Suite	mineralization-related	2705391	391-20	Chemical Abrasion			30/09/2019
Hiltaba Suite	mineralization-related	2705391	391-21	Chemical Abrasion			30/09/2019
Hiltaba Suite	mineralization-related	2705391	391-22	Chemical Abrasion			30/09/2019
Hiltaba Suite	mineralization-related	2705391	391-23	Chemical Abrasion			30/09/2019
Hiltaba Suite	mineralization-related	2705391	391-24	Chemical Abrasion			30/09/2019
Hiltaba Suite	mineralization-related	2705398	398-1	Chemical Abrasion			30/09/2019
Hiltaba Suite	mineralization-related	2705398	398-2	Chemical Abrasion			30/09/2019
Hiltaba Suite	mineralization-related	2705398	398-3	Chemical Abrasion			30/09/2019
Hiltaba Suite	mineralization-related	2705398	398-4	Chemical Abrasion			30/09/2019
Hiltaba Suite	mineralization-related	2705398	398-6	Chemical Abrasion			30/09/2019
Hiltaba Suite	mineralization-related	2705398	398-8	Chemical Abrasion			30/09/2019
Hiltaba Suite	mineralization-related	2705398	398-9	Chemical Abrasion			30/09/2019
Hiltaba Suite	mineralization-related	2705398	398-10	Chemical Abrasion			30/09/2019
Hiltaba Suite	mineralization-related	2705398	398-11	Chemical Abrasion			30/09/2019
Hiltaba Suite	mineralization-related	2705398	398-13	Chemical Abrasion			30/09/2019
Hiltaba Suite	mineralization-related	2705398	398-14	Chemical Abrasion			30/09/2019
Hiltaba Suite	mineralization-related	2705398	398-15	Chemical Abrasion			30/09/2019
Hiltaba Suite	mineralization-related	2705398	398-16	Chemical Abrasion			30/09/2019
Hiltaba Suite	mineralization-related	2705398	398-17	Chemical Abrasion			30/09/2019
Hiltaba Suite	mineralization-related	2705398	398-19	Chemical Abrasion			30/09/2019
Hiltaba Suite	mineralization-related	2746110	110-2	Chemical Abrasion			11/11/2019
Hiltaba Suite	mineralization-related	2746110	110-4	Chemical Abrasion			11/11/2019
Hiltaba Suite	mineralization-related	2746110	110-5	Chemical Abrasion			11/11/2019
Hiltaba Suite	mineralization-related	2746355	355-2	Chemical Abrasion			11/11/2019
Hiltaba Suite	mineralization-related	2746355	355-4	Chemical Abrasion			11/11/2019
Hiltaba Suite	mineralization-related	2746355	355-5	Chemical Abrasion			11/11/2019
Hiltaba Suite	mineralization-related	2746355	355-6	Chemical Abrasion			11/11/2019
Hiltaba Suite	mineralization-related	2746355	355-7	Chemical Abrasion			11/11/2019
Hiltaba Suite	mineralization-related	2746355	355-9	Chemical Abrasion			11/11/2019
Hiltaba Suite	mineralization-related	2746355	355-10	Chemical Abrasion			11/11/2019
Hiltaba Suite	mineralization-related	2746355	355-11	Chemical Abrasion			11/11/2019
Hiltaba Suite	mineralization-related	2746355	355-13	Chemical Abrasion			11/11/2019
Hiltaba Suite	mineralization-related	2746355	355-14	Chemical Abrasion			11/11/2019
Hiltaba Suite	mineralization-related	2746355	355-15	Chemical Abrasion			11/11/2019
Hiltaba Suite	mineralization-related	2746355	355-16	Chemical Abrasion			11/11/2019
Hiltaba Suite	mineralization-related	HDD-393-01	HDD393-01 - 1	Chemical Abrasion			27/08/2018
Hiltaba Suite	mineralization-related	HDD-393-01	HDD393-01 - 2	Chemical Abrasion			27/08/2018
Hiltaba Suite	mineralization-related	HDD-393-01	HDD393-01 - 5	Chemical Abrasion			27/08/2018
Hiltaba Suite	mineralization-related	HDD-393-01	HDD393-01 - 6	Chemical Abrasion			27/08/2018

Appendix 4 Table A3 Zircon trace element data for GRV and Hiltaba Suite samples analyzed at the University of Adelaide

Spot Number	P	Ti	Y	Nb	La	Ce	Pr	Nd	Sm	Eu	Gd	Tb	Dy	Ho
	ppm	ppm	ppm	ppm	ppm	ppm	ppm	ppm	ppm	ppm	ppm	ppm	ppm	ppm
18-TAR-14 - 1	87.3	6.6	898.00	1.63		106.60	2.96	12.30	11.30	2.49	30.60	8.68	91.70	29.68
18-TAR-14 - 2	152	17.4	958.00	1.26		97.00	3.70	16.40	14.30	2.94	35.50	10.40	106.10	33.20
18-TAR-14 - 3	116	23.9	1096.00	1.71		130.00	3.40	17.70	14.70	2.92	49.00	12.70	119.30	38.40
18-TAR-14 - 4	165	21.2	975.00	1.81		99.30	1.77	10.40	11.20	1.25	38.20	10.78	101.40	35.08
18-TAR-14 - 5	204	15.8	1036.00	2.55		48.90	0.16	2.77	5.33	0.83	31.40	9.72	109.30	37.36
18-TAR-14 - 6	96	10	1076.00	2.25		89.00	0.98	5.90	6.82	2.20	25.80	8.27	97.90	36.20
18-TAR-14 - 7	121	9.1	1105.00	1.00		96.60	2.18	12.10	12.00	3.40	38.30	10.98	111.10	38.50
18-TAR-14 - 8	125	36	1037.00	0.41		89.30	3.13	21.80	18.50	5.53	52.70	12.63	121.70	38.00
18-TAR-14 - 9	113.6	21.5	851.00	0.99		45.40	2.01	11.00	8.45	1.86	29.10	8.73	84.60	28.50
18-TAR-14 - 13	67.8	6.6	745.00	1.13		41.11	0.15	2.11	3.82	1.23	18.87	5.52	66.90	25.36
18-TAR-14 - 14	102	4.8	1424.00	0.59		61.40	1.11	11.00	14.10	4.35	48.80	13.87	146.20	51.00
189 - 1	265	14.2	803	5.06	b.d.l.	48.90	0.06	1.28	2.31	0.49	14.62	5.00	66.20	25.92
189 - 2	170	6.4	463	4.08	b.d.l.	33.90	0.02	0.67	0.97	0.23	6.61	2.45	31.80	13.80
189 - 3	333	15.7	936	2.61	b.d.l.	34.25	0.09	1.38	3.15	0.61	19.16	6.22	81.40	30.74
189 - 4	150	4.5	1376	1.83	0.172	14.50	0.56	6.37	8.57	1.07	39.40	12.24	133.20	48.60
189 - 5	331	17.1	1603	1.55	0.098	28.95	0.30	4.73	8.22	2.07	40.40	12.58	148.50	53.70
189 - 6	362	12.6	2290	2.13	0.23	70.50	0.45	7.11	11.88	2.55	54.60	18.70	209.00	77.90
189 - 7	233	10.7	695	4.4	0.083	44.98	0.10	1.16	2.15	0.41	11.82	4.23	56.70	22.21
189 - 8	254	12.1	765	5.23	0.061	49.94	0.12	1.43	2.51	0.56	12.99	4.64	61.30	24.66
189 - 9	204	8.3	575.2	3.28	0.01	32.43	0.05	0.72	1.54	0.37	10.30	3.61	45.60	18.47
189 - 11	137	5.1	532.2	6.56	b.d.l.	40.24	0.02	0.48	1.12	0.19	7.25	2.81	39.60	16.36
391-3	278.00	12.10	1619.00	7.13	0.05	54.80	0.32	4.81	7.86	1.37	34.50	11.18	141.70	52.00
391-5	333.00	7.00	916.00	7.63	0.20	42.70	0.22	1.73	3.00	0.44	15.10	5.28	72.50	30.00
391-6	236.00	14.00	689.20	5.73	0.32	32.49	0.13	1.07	2.18	0.40	12.30	4.25	57.80	22.03
391-7	303.00	14.20	1950.00	4.76	2.44	76.90	3.11	16.10	13.40	3.29	54.00	19.50	240.00	75.00
391-9	250.00	13.60	2367.00	4.41	0.17	51.30	0.72	9.43	12.03	2.23	54.70	17.48	211.10	78.00
391-11	344.00	15.70	547.00	3.61	0.03	25.40	0.06	0.94	1.64	0.33	9.80	3.39	45.90	17.86
391-13	192.00	10.10	726.00	5.98	b.d.l.	35.53	0.05	1.07	2.40	0.41	13.01	4.36	58.80	23.17
391-14	271.00	7.80	690.00	6.68	b.d.l.	36.50	0.05	0.90	2.08	0.32	10.78	3.99	52.10	21.07
391-16	245.00	10.60	638.80	3.93	b.d.l.	27.31	0.05	0.86	1.93	0.39	11.64	4.04	52.60	20.52
391-17	255.00	5.50	1019.00	8.52	1.75	66.00	1.73	8.50	4.73	0.75	19.50	6.30	78.70	31.10
391-18	212.00	16.00	1699.00	3.56	0.09	39.47	0.56	7.03	9.86	1.98	42.40	13.08	155.90	56.20
391-20	297.00	18.60	1691.00	13.58	0.55	86.00	0.66	4.88	7.30	1.19	35.20	11.46	163.00	57.30
391-21	353.00	10.90	1420.00	6.22	0.92	67.90	0.87	5.47	6.39	1.54	28.20	11.10	138.00	46.10
391-22	288.00	12.40	962.00	6.71	0.28	53.00	0.38	2.42	3.43	0.63	17.44	5.95	77.80	29.95
391-23	296.00	9.60	2060.00	7.58	1.78	87.10	1.78	9.20	10.10	2.48	40.70	16.10	218.00	72.70
391-24	283.00	9.30	1369.00	8.26	0.91	71.50	0.58	3.63	5.12	1.19	26.20	9.80	120.60	45.30
398-1	252.00	14.60	799.00	4.53	0.00	45.76	0.07	1.39	2.64	0.53	15.47	5.21	67.00	25.43
398-2	307.00	6.90	714.00	5.61	0.09	48.59	0.18	1.12	2.04	0.49	11.21	4.25	53.60	22.15
398-3	202.00	9.10	537.00	4.26	b.d.l.	37.23	0.04	0.75	1.55	0.28	8.31	2.99	41.50	16.75
398-4	224.00	16.20	577.00	3.26	b.d.l.	22.90	0.05	0.82	1.50	0.31	10.06	3.46	44.70	17.90
398-6	191.00	10.50	564.50	5.01	b.d.l.	41.22	0.04	0.71	1.40	0.31	8.95	3.25	41.90	17.35
398-8	198.00	11.50	452.70	2.66	0.00	24.15	0.04	0.59	1.21	0.24	7.64	2.64	35.60	13.96
398-9	194.00	15.50	1952.00	2.96	0.85	61.80	1.06	10.12	11.58	2.60	46.70	15.38	180.90	67.10
398-10	317.00	13.80	490.90	2.69	b.d.l.	23.96	0.03	0.61	1.35	0.23	8.62	3.16	40.40	15.70
398-11	184.00	7.80	330.90	2.84	0.01	24.17	0.02	0.59	1.10	0.21	5.05	1.81	26.20	10.46
398-13	258.00	7.60	501.50	5.29	0.17	38.93	0.19	1.62	1.37	0.37	7.47	2.73	40.00	15.93
398-14	165.00	13.00	580.00	4.08	b.d.l.	35.03	0.05	0.84	1.49	0.32	10.49	3.50	47.70	18.53
398-15	223.00	11.00	887.00	3.83	1.61	46.60	0.80	3.76	4.25	0.95	18.70	7.01	82.80	30.40
398-16	249.00	11.20	495.40	3.55	0.04	22.65	0.06	0.62	1.37	0.25	8.28	3.08	39.90	15.96
398-17	199.00	14.30	1036.00	5.75	0.01	55.35	0.11	2.16	4.13	0.79	23.71	7.39	91.50	34.10
398-19	231.00	7.00	1866.00	5.07	1.26	61.70	2.22	13.30	11.20	3.09	38.50	14.40	184.00	65.50
110-2	349.00	11.80	1475.00	2.87	6.00	73.60	7.80	38.90	26.20	6.80	57.70	15.90	162.00	51.00
110-4	310.00	12.40	833.70	3.43	b.d.l.	19.41	0.06	1.21	2.76	0.46	16.71	5.88	71.80	27.61
110-5	236.00	8.10	936.00	5.59	1.37	42.00	2.69	13.80	11.00	1.66	32.00	8.90	85.50	31.60
355-2	167.00	5.20	617.00	3.97	0.27	26.50	0.29	2.40	1.83	0.63	9.80	3.63	49.50	19.80
355-4	289.00	6.80	831.00	4.10	0.02	29.21	0.08	1.06	2.64	0.27	15.62	5.52	69.80	27.53
355-5	305.00	7.00	2160.00	7.80	85.00	171.00	33.70	138.00	45.00	2.02	75.00	17.40	209.00	69.80
355-6	177.00	6.00	1395.00	6.71	0.07	31.60	0.18	2.10	3.57	0.45	21.60	8.07	110.50	45.30
355-7	368.00	11.60	1358.00	4.57	0.27	42.31	0.38	3.45	5.59	0.81	28.50	9.34	118.80	44.80
355-9	262.00	4.90	1383.00	6.77	0.86	43.30	0.75	5.56	5.29	0.65	24.50	8.61	111.40	44.60
355-10	243.00	6.60	930.70	6.57	b.d.l.	27.70	0.04	0.72	2.08	0.21	15.82	5.72	76.60	30.80
355-11	270.00	6.40	908.00	7.32	2.80	38.40	1.47	9.20	3.53	0.27	15.50	5.25	75.10	29.48
355-13	364.00	13.30	1788.00	3.89	0.64	54.80	0.64	6.36	7.92	1.11	39.60	12.60	160.80	59.10
355-14	293.00	17.30	733.20	2.14	b.d.l.	25.52	0.07	1.29	3.17	0.78	16.86	5.38	65.60	23.86
355-15	347.00	10.70	1636.00	5.05	1.37	37.27	0.73	4.50	5.55	0.74	33.40	11.26	141.20	54.60
355-16	181.00	4.60	959.00	5.22	0.41	32.54	0.17	1.45	2.03	0.35	12.83	4.87	69.60	29.20
HDD393-01 - 1	114.00	10.40	1775.00	5.75		65.20	2.20	8.40	7.90	2.19	36.90	13.16	150.30	61.00
HDD393-01 - 2	25.20	26.00	213.00	0.87		14.39	0.12	0.80	0.72	0.26	2.57	1.09	12.30	6.36
HDD393-01 - 5	158.00	132.00	1819.00	3.07		39.40	1.85	12.10	13.50	4.09	54.90	16.82	180.50	66.60
HDD393-01 - 6	80.40	21.50	455.20	4.76		26.92	0.08	0.73	1.34	0.32	7.20	2.68	36.60	15.17

Appendix 4 Table A3 Zircon trace element data for GRV and Hiltaba Suite samples analyzed at the University of Adelaide

Spot Number	Er	Tm	Yb	Lu	Hf	Th	U	Eu/Eu*	Ce/Ce*	$(Yb/Gd)_N$	Ti-in-Zircon	Total REE	Th/U
	ppm	ppm	ppm	ppm	ppm	ppm	ppm						
18-TAR-14 - 1	127.30	27.30	242.20	48.80	7811.00	213.00	96.10	0.41	18.54	9.81	755	742	2.2
18-TAR-14 - 2	135.40	28.60	264.00	55.30	7387.00	458.00	108.90	0.40	12.01	9.22	857	803	4.2
18-TAR-14 - 3	159.60	32.70	282.00	61.20	7820.00	190.00	81.60	0.33	14.21	7.13	895	924	2.3
18-TAR-14 - 4	143.00	30.20	259.40	55.80	7541.00	187.70	87.30	0.18	23.95	8.42	880	798	2.2
18-TAR-14 - 5	156.90	30.70	279.00	58.60	8647.00	120.70	111.60	0.20	79.12	11.01	846	771	1.1
18-TAR-14 - 6	168.80	35.93	340.80	74.60	7668.00	147.00	108.20	0.51	40.61	16.37	796	893	1.4
18-TAR-14 - 7	156.20	32.50	294.00	62.00	7678.00	163.00	83.00	0.48	18.44	9.51	786	870	2.0
18-TAR-14 - 8	144.30	28.24	248.10	52.60	6890.00	162.90	30.94	0.54	8.10	5.83	947	837	5.3
18-TAR-14 - 9	119.80	24.84	233.90	47.60	8160.00	179.00	99.50	0.36	7.38	9.96	882	646	1.8
18-TAR-14 - 13	115.00	24.84	243.70	52.50	7946.00	93.80	76.30	0.44	82.16	16.00	755	601	1.2
18-TAR-14 - 14	207.90	41.50	366.00	72.60	8222.00	205.00	97.10	0.51	16.66	9.29	725	1040	2.1
189 - 1	129.60	27.13	260.10	52.80	10310.00	197.60	252.10	0.26	160.58	22.05	834	634	0.8
189 - 2	76.60	18.30	185.20	42.30	11420.00	165.60	313.90	0.28	170.61	34.72	752	413	0.5
189 - 3	149.10	30.73	280.00	56.51	9420.00	168.90	208.00	0.24	131.95	18.11	845	693	0.8
189 - 4	210.80	40.40	333.90	62.80	8090.00	197.80	275.70	0.18	7.13	10.50	719	913	0.7
189 - 5	249.10	48.26	420.80	81.90	8700.00	219.30	196.80	0.35	24.77	12.91	855	1100	1.1
189 - 6	363.00	68.60	605.00	120.00	9250.00	391.00	304.90	0.31	38.59	13.73	821	1610	1.3
189 - 7	115.60	24.91	238.80	50.17	10300.00	194.90	257.90	0.25	167.39	25.04	803	573	0.8
189 - 8	123.60	27.26	265.30	56.00	10570.00	226.70	299.00	0.30	142.77	25.31	816	630	0.8
189 - 9	92.60	20.59	192.00	40.50	9940.00	115.20	161.30	0.28	224.38	23.10	777	459	0.7
189 - 11	88.60	21.39	217.30	46.99	11430.00	210.70	438.30	0.20	455.60	37.14	731	482	0.5
391-3	257.30	55.70	527.60	108.60	9380.00	477.40	441.00	0.25	43.36	18.95	816	1258	1.08
391-5	152.20	35.35	346.20	72.50	10830.00	237.30	307.10	0.20	99.69	28.41	760	777	0.77
391-6	112.50	25.20	240.70	50.83	9820.00	173.10	213.20	0.23	144.09	24.25	832	562	0.81
391-7	310.00	64.30	569.00	100.00	9580.00	196.80	173.10	0.37	9.26	13.06	834	1547	1.14
391-9	365.80	73.90	677.00	135.70	9450.00	491.00	399.70	0.27	16.16	15.34	829	1690	1.23
391-11	89.70	20.05	187.30	39.51	9630.00	95.60	125.50	0.25	109.80	23.68	845	442	0.76
391-13	117.60	27.00	258.50	55.90	10210.00	204.00	263.50	0.22	173.47	24.62	797	598	0.77
391-14	114.40	25.90	256.40	55.10	11120.00	205.60	295.00	0.21	218.30	29.47	771	580	0.70
391-16	103.20	22.53	215.10	45.74	9540.00	128.20	164.00	0.25	165.99	22.90	802	506	0.78
391-17	167.50	38.80	376.00	80.40	11480.00	353.00	468.00	0.24	10.06	23.89	738	882	0.75
391-18	264.30	52.64	479.10	93.60	8950.00	293.10	248.70	0.30	18.34	14.00	847	1216	1.18
391-20	271.00	59.70	565.00	118.00	10560.00	472.70	429.00	0.23	61.40	19.89	864	1381	1.10
391-21	231.00	49.90	443.00	82.80	9430.00	283.60	310.10	0.35	33.77	19.47	805	1113	0.91
391-22	156.90	35.24	332.10	67.20	9480.00	284.10	323.70	0.25	72.30	23.60	819	783	0.88
391-23	364.00	80.30	731.00	135.00	9760.00	401.00	344.80	0.37	24.21	22.26	792	1770	1.16
391-24	215.90	44.50	437.00	86.50	9920.00	358.70	419.40	0.31	64.71	20.67	789	1069	0.86
398-1	127.60	26.95	248.20	49.90	9190.00	175.90	217.50	0.25	145.63	19.88	837	616	0.81
398-2	116.10	26.14	261.10	53.80	10100.00	228.30	352.00	0.31	184.05	28.86	759	601	0.65
398-3	87.90	20.10	200.10	42.05	10010.00	156.40	243.90	0.24	238.94	29.84	786	460	0.64
398-4	87.60	19.50	183.20	37.40	9640.00	79.30	128.20	0.24	118.98	22.57	848	429	0.62
398-6	90.20	20.31	201.50	43.40	9930.00	162.90	242.10	0.27	266.63	27.90	801	471	0.67
398-8	73.50	15.99	150.90	32.28	9200.00	85.30	138.50	0.24	195.52	24.48	811	359	0.62
398-9	306.00	62.50	508.00	103.90	8920.00	315.00	239.00	0.34	16.28	13.48	843	1378	1.32
398-10	78.80	16.67	158.20	33.60	9670.00	90.40	123.50	0.21	202.47	22.74	830	381	0.73
398-11	56.80	12.88	124.80	28.44	10210.00	75.40	148.00	0.28	177.89	30.63	771	293	0.51
398-13	88.10	19.92	194.10	42.71	11000.00	167.50	309.20	0.35	47.33	32.20	768	454	0.54
398-14	96.60	21.14	193.20	41.84	9400.00	146.40	209.70	0.24	172.29	22.82	824	471	0.70
398-15	143.50	29.50	288.00	56.90	9370.00	190.30	230.30	0.33	32.63	19.09	806	715	0.83
398-16	82.10	17.66	164.60	34.97	9650.00	90.00	157.30	0.22	188.02	24.64	808	392	0.57
398-17	169.80	35.13	310.00	64.40	9010.00	274.80	320.10	0.25	114.12	16.20	834	799	0.86
398-19	303.00	63.30	526.00	102.70	9660.00	328.00	309.00	0.45	9.10	16.93	760	1390	1.06
110-2	218.00	45.50	384.00	70.80	9240.00	438.00	200.00	0.53	2.97	8.25	813	1164	2.19
110-4	131.80	26.61	240.50	49.13	8770.00	116.10	193.30	0.21	85.22	17.84	819	594	0.60
110-5	145.00	29.70	265.20	51.70	10660.00	245.00	309.30	0.27	5.65	10.27	775	722	0.79
355-2	101.90	22.57	220.90	46.40	10370.00	136.80	262.00	0.45	19.61	27.93	732	506	0.52
355-4	134.80	28.36	251.00	52.40	10420.00	161.20	252.70	0.13	159.85	19.91	758	618	0.64
355-5	335.00	66.90	636.00	134.00	10440.00	481.00	611.00	0.11	0.94	10.51	760	2018	0.79
355-6	226.40	47.70	432.00	87.00	11280.00	332.00	592.00	0.16	59.58	24.78	746	1017	0.56
355-7	215.50	43.10	382.60	77.90	9800.00	324.80	374.20	0.20	46.28	16.64	812	973	0.87
355-9	222.00	45.10	413.00	83.70	9990.00	324.00	468.00	0.17	17.26	20.89	727	1009	0.69
355-10	151.40	32.12	285.00	56.66	10740.00	216.00	414.70	0.11	258.86	22.33	755	685	0.52
355-11	149.10	31.91	293.90	59.30	10790.00	186.80	376.00	0.11	3.73	23.50	752	715	0.50
355-13	281.20	55.89	485.20	96.50	10110.00	374.90	396.00	0.19	24.99	15.18	826	1262	0.95
355-14	113.30	22.99	207.50	40.57	8770.00	136.00	145.00	0.33	113.23	15.25	856	527	0.94
355-15	252.00	51.90	453.00	86.30	10170.00	312.00	424.00	0.17	23.79	16.81	803	1134	0.74
355-16	156.70	36.07	346.40	72.90	10510.00	275.90	487.10	0.21	73.18	33.46	721	766	0.57
HDD393-01 - 1	312.00	57.60	509.00	99.10	10500.00	378.00	353.00	0.39	17.00	17.09	800	1325	1.07
HDD393-01 - 2	36.20	9.91	124.80	35.47	9320.00	73.50	522.10	0.58	37.71	60.18	905	245	0.14
HDD393-01 - 5	269.90	51.40	462.00	91.40	8172.00	284.00	160.80	0.46	8.46	10.43	1152	1264	1.77
HDD393-01 - 6	74.70	16.84	170.90	35.07	8508.00	90.40	172.30	0.31	157.66	29.41	882	389	0.52

Ti-in-Zircon calculated using the method of Ferry and Watson (2007), assuming $\alpha TiO_2 = 0.7$ and $\alpha SiO_2 = 1$

Ferry, J. M. and Watson, E. B., 2007. New thermodynamic models and revised calibrations for the Ti-in-zircon and Zr-in-rutile thermometers. Contributions to Mineralogy and Petrology, 154, 429-437. doi: https://doi.org/10.1007/s00410-007-0201-0

Appendix 4 Table A3 Zircon trace element data for GRV and Hiltaba Suite samples analyzed at the University of Adelaide

Unit	Group	Sample	Spot Number	Zircon Treatment	Discordance	Other	Analytical Session
Included Data							
Hiltaba Suite	mineralization-related	HDD-393-01	HDD393-01 - 7	Chemical Abrasion			27/08/2018
Hiltaba Suite	mineralization-related	HDD-393-01	HDD393-01 - 8	Chemical Abrasion			27/08/2018
Hiltaba Suite	mineralization-related	HDD-393-01	HDD393-01 - 9	Chemical Abrasion			27/08/2018
Hiltaba Suite	mineralization-related	HDD-393-01	HDD393-01 - 10	Chemical Abrasion			27/08/2018
Hiltaba Suite	mineralization-related	HDD-393-01	HDD393-01 - 11	Chemical Abrasion			27/08/2018
Hiltaba Suite	mineralization-related	HDD-393-01	HDD393-01 - 12	Chemical Abrasion			27/08/2018
Hiltaba Suite	mineralization-related	HDD-393-01	HDD393-01 - 13	Chemical Abrasion			27/08/2018
Hiltaba Suite	mineralization-related	HDD-393-01	HDD393-01 - 15	Chemical Abrasion			27/08/2018
Hiltaba Suite	mineralization-related	1077-32	1077-32-1	Chemical Abrasion			26/08/2018
Hiltaba Suite	mineralization-related	1077-32	1077-32-2	Chemical Abrasion			26/08/2018
Hiltaba Suite	mineralization-related	1077-32	1077-32-3	Chemical Abrasion			26/08/2018
Hiltaba Suite	mineralization-related	1077-32	1077-32-4	Chemical Abrasion			26/08/2018
Hiltaba Suite	mineralization-absent	1077-01	1077-01-2	Chemical Abrasion			26/08/2018
Hiltaba Suite	mineralization-absent	1077-01	1077-01-3	Chemical Abrasion			26/08/2018
Hiltaba Suite	mineralization-absent	1077-01	1077-01-4	Chemical Abrasion			26/08/2018
Hiltaba Suite	mineralization-absent	1077-01	1077-01-6	Chemical Abrasion			26/08/2018
Hiltaba Suite	mineralization-absent	1077-01	1077-01-7	Chemical Abrasion			26/08/2018
Hiltaba Suite	mineralization-absent	1077-01	1077-01-8	Chemical Abrasion			26/08/2018
Hiltaba Suite	mineralization-absent	1077-01	1077-01-10	Chemical Abrasion			26/08/2018
Hiltaba Suite	mineralization-absent	1077-01	1077-01-13	Chemical Abrasion			27/08/2018
Hiltaba Suite	mineralization-absent	1077-01	1077-01-14	Chemical Abrasion			27/08/2018
Hiltaba Suite	mineralization-absent	1077-01	1077-01-15	Chemical Abrasion			27/08/2018
Hiltaba Suite	mineralization-absent	1077-01	1077-01-17	Chemical Abrasion			27/08/2018
Hiltaba Suite	mineralization-absent	1077-01	1077-01-19	Chemical Abrasion			27/08/2018
Hiltaba Suite	mineralization-absent	1077-01	1077-01-20	Chemical Abrasion			27/08/2018
Hiltaba Suite	mineralization-absent	1077-27	1077-27-1	Chemical Abrasion			30/09/2019
Hiltaba Suite	mineralization-absent	1077-27	1077-27-2	Chemical Abrasion			30/09/2019
Hiltaba Suite	mineralization-absent	1077-52	1077-52-2	Chemical Abrasion			26/08/2018
Hiltaba Suite	mineralization-absent	1077-52	1077-52-7	Chemical Abrasion			26/08/2018
Hiltaba Suite	mineralization-absent	1077-52	1077-52-9	Chemical Abrasion			26/08/2018
Hiltaba Suite	mineralization-absent	1077-52	1077-52-10	Chemical Abrasion			26/08/2018
Hiltaba Suite	mineralization-absent	1077-52	1077-52-11	Chemical Abrasion			26/08/2018
Hiltaba Suite	mineralization-absent	1077-52	1077-52-12	Chemical Abrasion			26/08/2018
Hiltaba Suite	mineralization-absent	HG470	HG-470 - 1	Chemical Abrasion			21/05/2020
Hiltaba Suite	mineralization-absent	HG470	HG-470 - 2	Chemical Abrasion			21/05/2020
Hiltaba Suite	mineralization-absent	HG470	HG-470 - 8	Chemical Abrasion			21/05/2020
Hiltaba Suite	mineralization-absent	HG470	HG-470 - 9	Chemical Abrasion			21/05/2020
Hiltaba Suite	mineralization-absent	HG470	HG-470 - 10	Chemical Abrasion			21/05/2020
Hiltaba Suite	mineralization-absent	HG470	HG-470 - 11	Chemical Abrasion			21/05/2020
Hiltaba Suite	mineralization-absent	HG470	HG-470 - 12	Chemical Abrasion			21/05/2020
Hiltaba Suite	mineralization-absent	HG470	HG-470 - 13	Chemical Abrasion			21/05/2020
Hiltaba Suite	mineralization-absent	1077-198	1077-198-5	Chemical Abrasion			30/09/2019
Hiltaba Suite	mineralization-absent	1077-198	1077-198-6	Chemical Abrasion			30/09/2019
Hiltaba Suite	mineralization-absent	1077-198	1077-198-8	Chemical Abrasion			30/09/2019
Hiltaba Suite	mineralization-absent	1077-41	1077-41 - 2	Chemical Abrasion			21/05/2020
Hiltaba Suite	mineralization-absent	1077-41	1077-41 - 6	Chemical Abrasion			21/05/2020
Hiltaba Suite	mineralization-absent	1077-41	1077-41 - 7	Chemical Abrasion			21/05/2020
Hiltaba Suite	mineralization-absent	1077-41	1077-41 - 8	Chemical Abrasion			21/05/2020
Hiltaba Suite	mineralization-absent	1077-41	1077-41 - 9	Chemical Abrasion			21/05/2020
Hiltaba Suite	mineralization-absent	1077-41	1077-41 - 11	Chemical Abrasion			21/05/2020
Hiltaba Suite	mineralization-absent	1077-41	1077-41 - 13	Chemical Abrasion			21/05/2020
Hiltaba Suite	mineralization-absent	1077-41	1077-41 - 15	Chemical Abrasion			21/05/2020
Hiltaba Suite	mineralization-absent	1077-41	1077-41 - 16	Chemical Abrasion			21/05/2020
Hiltaba Suite	mineralization-absent	1077-41	1077-41 - 17	Chemical Abrasion			21/05/2020
Hiltaba Suite	mineralization-absent	1077-41	1077-41 - 18	Chemical Abrasion			21/05/2020
Hiltaba Suite	mineralization-absent	1077-41	1077-41 - 20	Chemical Abrasion			21/05/2020
Hiltaba Suite	mineralization-absent	1077-41	1077-41 - 21	Chemical Abrasion			21/05/2020
Hiltaba Suite	mineralization-absent	1077-41	1077-41 - 25	Chemical Abrasion			21/05/2020
Hiltaba Suite	mineralization-absent	1077-41	1077-41 - 26	Chemical Abrasion			21/05/2020
Hiltaba Suite	mineralization-absent	1077-41	1077-41 - 27	Chemical Abrasion			21/05/2020
Hiltaba Suite	mineralization-absent	1077-41	1077-41 - 29	Chemical Abrasion			21/05/2020
Hiltaba Suite	mineralization-absent	1077-41	1077-41 - 30	Chemical Abrasion			21/05/2020
Hiltaba Suite	mineralization-absent	1077-41	1077-41 - 31	Chemical Abrasion			21/05/2020
Hiltaba Suite	mineralization-absent	1077-41	1077-41 - 32	Chemical Abrasion			21/05/2020
Hiltaba Suite	mineralization-absent	1077-41	1077-41 - 33	Chemical Abrasion			21/05/2020
Hiltaba Suite	mineralization-absent	1077-41	1077-41 - 36	Chemical Abrasion			21/05/2020
Hiltaba Suite	mineralization-absent	1077-41	1077-41 - 37	Chemical Abrasion			21/05/2020
Hiltaba Suite	mineralization-absent	1077-41	1077-41 - 38	Chemical Abrasion			21/05/2020
Hiltaba Suite	mineralization-absent	1077-46	1077-46 - 1	Chemical Abrasion			26/08/2018
Hiltaba Suite	mineralization-absent	1077-46	1077-46 - 2	Chemical Abrasion			26/08/2018
Hiltaba Suite	mineralization-absent	1077-46	1077-46 - 3	Chemical Abrasion			26/08/2018

Appendix 4 Table A3 Zircon trace element data for GRV and Hiltaba Suite samples analyzed at the University of Adelaide

Spot Number	P	Ti	Y	Nb	La	Ce	Pr	Nd	Sm	Eu	Gd	Tb	Dy	Ho
	ppm	ppm	ppm	ppm	ppm	ppm	ppm	ppm	ppm	ppm	ppm	ppm	ppm	ppm
HDD393-01 - 7	217.00	35.90	2026.00	5.46		48.70	0.69	9.90	13.32	2.68	56.40	17.14	194.40	71.10
HDD393-01 - 8	95.00	23.30	817.00	3.55		32.90	0.16	1.76	2.75	0.63	17.30	5.65	71.20	27.90
HDD393-01 - 9	151.00	30.90	1243.00	2.81		33.12	0.39	5.21	8.08	2.25	34.30	10.79	121.10	44.20
HDD393-01 - 10	160.00	90.00	1212.00	2.15		31.10	0.86	7.00	8.26	2.26	35.20	11.00	121.70	43.00
HDD393-01 - 11	177.00	92.00	1138.00	2.04		29.20	1.03	6.59	8.30	2.31	33.60	9.63	105.30	39.70
HDD393-01 - 12	227.00	43.50	1337.00	2.72		38.01	0.54	6.07	8.16	2.21	34.00	11.15	123.00	44.50
HDD393-01 - 13	195.00	39.50	1452.00	3.26		33.41	0.41	6.19	7.47	2.43	37.10	11.29	132.80	50.90
HDD393-01 - 15	165.00	21.10	1191.00	4.10		45.82	0.19	2.99	5.29	0.90	26.20	9.23	109.80	41.80
1077-32-1	108.00	6.90	758.00	1.14		46.00	0.45	4.30	4.82	1.46	19.10	6.05	67.40	25.38
1077-32-2	106.30	14.10	596.70	0.61		41.40	2.90	11.70	6.03	1.77	18.70	5.02	56.90	20.48
1077-32-3	92.00	13.30	787.00	1.01		33.10	0.33	3.85	4.42	1.84	19.90	6.43	69.50	25.74
1077-32-4	100.00	7.00	1370.00	2.30		174.00	31.70	127.00	43.30	6.20	62.00	13.50	136.00	48.30
1077-01-2	137.00	15.90	774.00	2.60		16.09	0.14	2.10	2.99	0.31	16.58	6.00	67.70	26.48
1077-01-3	149.00	12.20	866.30	3.32		22.69	0.09	1.46	3.01	0.44	16.23	6.12	74.90	29.70
1077-01-4	109.00	7.10	1211.00	3.18		31.10	2.79	14.40	8.48	1.39	28.20	9.46	107.50	41.87
1077-01-6	144.00	10.90	1011.00	3.54		26.60	1.06	5.50	4.18	0.42	20.10	6.53	84.30	33.60
1077-01-7	128.00	16.50	752.70	2.98		15.36	0.07	1.13	2.64	0.30	15.10	5.32	65.60	26.37
1077-01-8	112.00	13.70	1402.00	1.53		13.88	0.29	4.40	7.90	1.02	35.10	11.80	136.90	48.80
1077-01-10	127.00	10.40	962.00	4.49		39.80	4.37	24.30	11.90	1.85	28.80	8.25	92.60	33.58
1077-01-13	119.00	11.40	848.00	4.19		20.12	0.13	1.45	3.08	0.16	15.80	5.32	72.60	29.10
1077-01-14	110.00	14.10	590.40	2.02		11.85	0.07	0.80	1.86	0.21	11.29	3.61	51.70	19.88
1077-01-15	91.00	14.20	605.00	1.78		16.40	0.25	2.31	2.56	0.31	11.50	4.32	52.40	20.40
1077-01-17	109.00	11.90	835.00	3.35		22.20	0.78	5.20	4.01	0.47	17.30	5.78	72.70	27.69
1077-01-19	98.00	9.90	639.00	2.39		29.40	2.61	15.30	6.40	1.32	15.90	4.66	55.00	20.76
1077-01-20	119.50	18.40	692.50	1.55		13.39	0.18	2.09	3.12	0.44	14.32	5.01	59.20	23.18
1077-27-1	291.00	4.40	1517.00	1.28	0.14	16.14	0.61	7.43	10.85	1.57	49.70	13.68	157.30	52.90
1077-27-2	193.00	4.60	983.00	1.85	0.34	15.30	0.44	4.31	7.23	0.77	31.00	8.98	101.40	34.10
1077-52-2	147.00	5.40	1119.00	3.91		55.80	0.96	5.00	4.49	0.59	19.70	6.88	88.60	36.30
1077-52-7	174.00	7.50	1189.00	6.45		60.10	0.95	4.60	3.91	0.61	18.99	7.35	95.40	39.30
1077-52-9	196.00	24.00	1110.00	2.80		80.73	0.34	4.72	7.58	0.94	32.20	10.11	107.60	38.81
1077-52-10	170.00	39.90	1811.00	1.42		46.50	1.34	16.10	16.40	4.08	60.80	17.21	184.30	65.20
1077-52-11	187.00	5.50	2111.00	5.24		106.40	0.92	7.00	11.00	1.90	47.80	16.80	198.80	75.10
1077-52-12	236.00	8.80	1189.00	8.30		108.80	6.98	26.40	6.90	0.67	19.30	7.22	89.00	37.00
HG-470 - 1	186.00	9.90	684.00	2.45	b.d.l	17.89	0.07	1.41	2.99	0.34	16.30	5.31	63.40	23.32
HG-470 - 2	196.00	8.00	1800.00	1.78	12.20	204.00	15.30	89.00	67.00	4.76	132.00	32.40	251.00	62.10
HG-470 - 8	143.00	11.30	680.00	2.75	b.d.l	16.35	0.06	1.04	3.00	0.25	14.50	4.97	59.30	22.00
HG-470 - 9	159.00	15.20	375.00	1.02	b.d.l	5.72	0.04	0.71	1.47	0.17	7.93	2.76	34.20	12.78
HG-470 - 10	230.00	15.40	633.00	2.25	0.05	12.70	0.07	1.54	3.64	0.44	15.30	5.08	59.00	21.69
HG-470 - 11	159.00	9.20	640.00	1.58	3.20	47.00	2.16	11.50	7.70	0.92	22.20	6.21	63.50	21.20
HG-470 - 12	179.00	11.30	556.00	1.30	0.03	8.06	0.09	2.10	2.62	0.39	15.10	4.59	51.00	19.33
HG-470 - 13	162.00	4.70	587.00	1.87	b.d.l	15.29	0.04	0.90	2.05	0.24	12.20	4.46	51.50	20.12
1077-198-5	368.00	7.50	664.50	2.72	0.15	23.27	0.12	1.10	1.79	0.26	10.97	3.93	52.80	21.05
1077-198-6	217.00	15.00	885.00	2.15	4.99	54.00	1.82	9.70	8.90	0.81	22.40	8.50	81.50	28.50
1077-198-8	218.00	10.00	844.00	2.55	9.50	56.70	2.10	12.90	11.40	0.61	23.30	8.00	85.00	29.00
1077-41 - 2	168.00	9.70	410.00	0.83	0.05	10.15	0.14	1.61	1.70	0.34	9.50	3.08	37.20	13.74
1077-41 - 6	205.00	7.10	672.00	2.04	0.65	24.70	0.46	4.12	4.92	0.15	20.90	5.94	66.30	23.10
1077-41 - 7	104.00	13.20	276.00	0.98	0.07	5.75	0.09	1.56	1.11	0.13	7.33	2.04	22.70	9.16
1077-41 - 8	179.00	10.50	619.00	1.16	0.12	9.11	0.21	2.63	3.90	0.42	17.50	5.17	59.20	22.10
1077-41 - 9	165.00	11.60	560.00	1.19	4.50	29.90	3.90	20.60	11.10	0.69	20.10	4.26	49.30	19.10
1077-41 - 11	198.00	8.40	510.50	1.22	b.d.l	9.73	0.05	0.95	1.99	0.19	11.90	3.89	45.50	16.81
1077-41 - 13	180.00	10.10	392.00	1.16	0.02	8.21	0.06	0.66	1.78	0.22	8.28	2.80	32.80	13.17
1077-41 - 15	119.00	b.d.l	346.20	1.69	0.20	5.93	0.15	1.45	1.72	0.18	6.66	2.24	26.50	10.94
1077-41 - 16	226.00	8.20	600.00	2.79	0.14	11.86	0.12	1.59	2.96	0.02	14.40	4.46	54.70	20.90
1077-41 - 17	127.00	10.20	313.00	0.80	0.14	6.16	0.14	0.88	1.52	0.26	6.62	2.24	25.70	10.49
1077-41 - 18	191.00	6.00	580.20	1.90	0.10	17.25	0.13	1.52	3.65	0.09	17.60	4.76	55.60	20.32
1077-41 - 20	144.00	10.10	326.00	0.94	0.62	8.74	0.42	2.79	2.58	0.25	7.50	2.63	28.40	10.80
1077-41 - 21	209.00	9.80	1023.00	0.84	5.30	23.30	3.20	11.80	11.20	0.79	33.80	9.34	99.30	36.40
1077-41 - 25	141.00	9.70	423.00	1.18	3.25	21.80	2.16	11.90	6.50	0.42	12.50	3.80	38.90	14.43
1077-41 - 26	177.00	6.90	449.70	1.07	0.19	9.54	0.33	2.20	2.63	0.27	11.40	3.79	39.60	14.76
1077-41 - 27	188.00	10.70	532.00	1.07	b.d.l	7.82	0.11	1.54	2.61	0.30	14.70	4.14	47.40	18.60
1077-41 - 29	163.00	5.40	689.00	1.08	0.05	9.77	0.17	2.47	4.08	0.49	19.20	6.39	64.40	23.00
1077-41 - 30	180.00	14.60	929.00	0.96	25.00	117.00	19.60	113.00	54.10	4.16	60.10	11.00	100.70	31.20
1077-41 - 31	104.00	4.20	326.00	1.51	0.81	8.20	0.35	2.06	1.90	0.23	7.31	2.17	28.20	10.47
1077-41 - 32	178.00	7.90	550.00	1.82	0.77	17.40	0.78	4.80	4.43	0.33	15.80	5.07	52.90	19.70
1077-41 - 33	172.00	10.10	1065.00	0.92	3.50	22.00	2.39	16.40	12.20	1.04	39.80	10.08	111.50	36.80
1077-41 - 36	318.00	9.30	1061.00	1.61	0.02	17.14	0.30	5.26	8.43	0.27	35.10	9.60	108.60	37.80
1077-41 - 37	146.00	6.60	441.00	1.11	0.12	8.28	0.14	1.03	1.69	0.18	9.80	3.30	38.50	15.25
1077-41 - 38	172.00	8.30	375.00	0.56	b.d.l	4.31	0.04	0.77	1.30	0.36	8.00	2.55	32.90	13.00
1077-46 - 1	105.00	24.70	725.00	1.26		17.80	0.18	2.17	3.88	0.32	14.30	5.37	62.90	24.50
1077-46 - 2	168.00	49.30	872.00	0.91		13.76	0.17	2.35	3.76	0.50	19.60	6.78	77.50	30.02
1077-46 - 3	187.00	10.30	1156.00	4.06		31.91	0.21	2.26	2.72	0.15	20.30	7.90	101.70	39.74

Appendix 4 Table A3 Zircon trace element data for GRV and Hiltaba Suite samples analyzed at the University of Adelaide

Spot Number	Er	Tm	Yb	Lu	Hf	Th	U	Eu/Eu*	Ce/Ce*	$(Yb/Gd)_N$	Ti-in-Zircon	Total REE	Th/U
	ppm	ppm	ppm	ppm	ppm	ppm	ppm						
HDD393-01 - 7	299.10	59.20	534.90	105.80	8254.00	261.60	216.20	0.30	15.42	11.75	947	1413	1.21
HDD393-01 - 8	126.70	26.60	253.00	52.80	9970.00	118.80	170.60	0.28	68.03	18.12	891	619	0.70
HDD393-01 - 9	183.10	36.30	323.00	62.90	8527.00	138.00	103.70	0.41	22.96	11.67	927	865	1.33
HDD393-01 - 10	183.00	34.90	322.20	62.90	7978.00	160.00	91.30	0.41	12.21	11.34	1085	863	1.75
HDD393-01 - 11	166.70	33.40	304.00	60.00	7851.00	150.00	88.40	0.42	13.00	11.21	1088	800	1.70
HDD393-01 - 12	196.10	40.70	363.10	71.20	7660.00	247.90	189.80	0.41	19.61	13.23	973	939	1.31
HDD393-01 - 13	219.10	44.40	411.00	78.30	7860.00	162.30	139.60	0.45	15.17	13.73	960	1035	1.16
HDD393-01 - 15	184.30	38.25	352.90	68.20	9400.00	153.90	148.30	0.23	63.15	16.69	879	886	1.04
1077-32-1	114.30	24.10	236.60	53.90	8286.00	119.30	86.30	0.47	27.93	15.35	759	604	1.38
1077-32-2	88.50	18.53	174.30	38.16	7730.00	102.70	61.59	0.51	4.25	11.55	833	484	1.67
1077-32-3	116.50	25.77	239.00	52.79	8710.00	98.00	76.50	0.60	22.99	14.88	826	599	1.28
1077-32-4	202.00	44.80	401.00	86.10	7914.00	227.00	117.00	0.37	1.09	8.02	760	1376	1.94
1077-01-2	117.90	25.31	240.00	44.37	9592.00	104.50	156.00	0.14	25.41	17.94	846	566	0.67
1077-01-3	136.70	30.79	292.00	57.64	10020.00	113.20	160.00	0.19	74.63	22.30	817	672	0.71
1077-01-4	189.40	40.06	362.70	68.20	10430.00	180.70	267.00	0.27	2.96	15.94	762	906	0.68
1077-01-6	157.70	34.10	325.00	62.30	10640.00	189.00	299.00	0.14	8.56	20.04	805	761	0.63
1077-01-7	116.50	24.89	231.00	43.71	9537.00	103.50	155.90	0.15	73.97	18.96	851	548	0.66
1077-01-8	201.50	42.30	367.00	69.80	9310.00	138.40	151.40	0.19	13.19	12.96	830	941	0.91
1077-01-10	148.90	31.85	294.00	56.90	10460.00	168.30	233.50	0.31	1.87	12.65	800	777	0.72
1077-01-13	132.20	28.60	265.90	54.50	10180.00	144.60	228.90	0.07	68.65	20.86	810	629	0.63
1077-01-14	94.20	20.13	186.50	38.77	9461.00	68.90	111.00	0.14	80.21	20.47	833	441	0.62
1077-01-15	96.60	20.03	186.60	39.00	9800.00	70.60	117.90	0.17	18.33	20.11	834	453	0.60
1077-01-17	128.30	27.90	261.40	53.90	10337.00	138.50	210.90	0.17	7.67	18.72	814	628	0.66
1077-01-19	97.30	22.26	202.40	43.10	10240.00	95.70	157.70	0.40	1.87	15.77	795	516	0.61
1077-01-20	106.70	22.30	209.70	43.10	9214.00	79.20	105.30	0.20	22.28	18.15	863	503	0.75
1077-27-1	234.00	45.00	381.00	74.70	7240.00	132.80	142.40	0.21	7.39	9.50	717	1045	0.93
1077-27-2	149.40	27.48	229.20	47.00	7390.00	83.00	88.30	0.16	13.87	9.16	721	657	0.94
1077-52-2	177.40	40.40	410.00	81.30	10756.00	124.30	110.00	0.19	23.34	25.79	736	927	1.13
1077-52-7	192.20	43.27	439.70	84.20	9890.00	111.50	108.10	0.22	25.87	28.69	767	991	1.03
1077-52-9	167.40	34.51	321.20	60.50	8887.00	71.71	42.25	0.18	63.98	12.36	895	867	1.70
1077-52-10	266.30	51.40	462.00	85.10	8010.00	78.00	36.90	0.40	6.85	9.42	961	1277	2.11
1077-52-11	327.00	68.70	623.00	114.10	9640.00	168.50	99.40	0.25	55.63	16.15	738	1599	1.70
1077-52-12	187.80	45.40	447.10	91.00	10405.00	220.20	196.90	0.18	2.51	28.71	783	1074	1.12
HG-470 - 1	98.30	21.49	191.90	37.10	9070.00	122.90	198.10	0.15	62.67	14.59	795	480	0.6
HG-470 - 2	204.00	36.20	301.00	53.50	8240.00	141.50	120.10	0.15	4.02	2.83	773	1464	1.2
HG-470 - 8	103.10	20.60	182.00	36.60	9610.00	109.80	204.00	0.11	105.62	15.55	809	464	0.5
HG-470 - 9	56.10	11.33	105.80	20.70	8490.00	25.80	55.40	0.15	38.85	16.53	841	260	0.5
HG-470 - 10	91.50	19.31	165.90	33.20	8160.00	73.90	114.30	0.18	45.40	13.44	843	429	0.6
HG-470 - 11	90.00	17.78	161.70	32.10	8520.00	98.20	108.00	0.22	6.37	9.03	788	487	0.9
HG-470 - 12	80.70	15.94	149.50	29.10	7890.00	46.60	78.20	0.19	11.15	12.27	809	379	0.6
HG-470 - 13	91.10	19.40	170.50	33.70	9440.00	88.40	148.60	0.15	90.13	17.32	723	421	0.6
1077-198-5	109.50	23.09	223.70	45.39	9770.00	159.80	242.60	0.18	80.18	25.27	767	517	0.66
1077-198-6	127.80	27.30	236.00	44.80	9200.00	124.20	111.90	0.18	11.90	13.06	840	657	1.11
1077-198-8	124.00	26.00	244.00	46.90	10940.00	205.00	179.40	0.11	9.05	12.98	796	679	1.14
1077-41 - 2	65.50	13.32	124.20	26.40	7830.00	38.30	89.20	0.26	15.50	16.20	793	307	0.4
1077-41 - 6	100.30	20.35	181.00	38.20	8120.00	132.10	223.20	0.04	16.67	10.73	762	491	0.6
1077-41 - 7	43.00	9.47	89.50	19.30	8890.00	20.74	63.60	0.14	6.11	15.13	826	211	0.3
1077-41 - 8	90.10	18.80	171.40	35.70	7570.00	51.70	103.10	0.16	11.96	12.14	801	436	0.5
1077-41 - 9	82.00	16.70	154.90	33.00	8760.00	71.00	128.00	0.14	1.82	9.55	812	450	0.6
1077-41 - 11	79.40	16.51	152.40	31.50	7750.00	49.10	102.10	0.12	49.97	15.87	778	371	0.5
1077-41 - 13	60.50	12.32	124.20	24.80	8160.00	38.70	93.10	0.17	78.14	18.59	797	290	0.4
1077-41 - 15	56.70	12.42	119.30	25.20	10790.00	37.90	158.50	0.16	11.30	22.20		270	0.2
1077-41 - 16	94.00	19.22	175.30	35.70	8640.00	72.60	191.40	0.01	32.34	15.09	776	435	0.4
1077-41 - 17	47.10	10.34	95.60	21.00	7740.00	25.00	67.60	0.25	28.16	17.90	798	228	0.4
1077-41 - 18	91.00	17.52	168.80	33.20	7950.00	89.20	164.00	0.03	63.47	11.89	746	432	0.5
1077-41 - 20	50.30	10.99	101.00	21.70	7880.00	33.20	76.30	0.17	6.75	16.69	797	249	0.4
1077-41 - 21	149.90	29.80	262.00	51.70	7730.00	93.50	137.00	0.12	4.37	9.61	794	728	0.7
1077-41 - 25	63.40	13.52	126.20	26.50	8590.00	60.10	117.50	0.14	2.33	12.51	793	345	0.5
1077-41 - 26	69.60	14.81	133.30	26.74	7730.00	45.20	99.30	0.15	12.07	14.49	759	329	0.5
1077-41 - 27	82.00	17.17	153.10	31.90	7500.00	50.00	106.80	0.15	20.04	12.91	803	381	0.5
1077-41 - 29	99.60	20.70	188.00	38.60	7960.00	58.00	110.10	0.17	15.22	12.13	736	477	0.5
1077-41 - 30	124.90	25.00	223.00	45.60	8290.00	101.20	115.10	0.22	1.15	4.60	837	954	0.9
1077-41 - 31	51.90	10.75	112.20	22.97	9960.00	40.20	177.70	0.19	8.55	19.02	713	260	0.2
1077-41 - 32	82.40	17.90	162.00	33.00	8190.00	80.90	163.90	0.12	7.79	12.71	772	417	0.5
1077-41 - 33	155.60	30.60	271.00	52.70	7800.00	88.20	140.20	0.14	2.32	8.44	797	766	0.6
1077-41 - 36	160.20	32.30	288.30	56.60	8160.00	126.50	217.00	0.05	12.16	10.18	789	760	0.6
1077-41 - 37	67.70	14.20	135.70	28.40	7810.00	42.30	103.10	0.14	30.72	17.16	755	324	0.4
1077-41 - 38	56.80	12.47	115.10	24.20	7410.00	21.83	59.30	0.34	22.01	17.83	777	272	0.4
1077-46 - 1	112.80	25.30	222.70	53.40	9130.00	32.05	47.00	0.13	34.16	19.30	899	546	0.68
1077-46 - 2	132.10	28.41	258.10	60.50	8179.00	33.41	38.23	0.18	21.82	16.32	991	634	0.87
1077-46 - 3	186.40	41.01	385.60	92.00	10447.00	111.40	162.30	0.06	39.58	23.54	799	912	0.69

Ti-in-Zircon calculated using the method of Ferry and Watson (2007), assuming $\alpha TiO_2 = 0.7$ and $\alpha SiO_2 = 1$

Ferry, J. M. and Watson, E. B., 2007. New thermodynamic models and revised calibrations for the Ti-in-zircon and Zr-in-rutile thermometers. Contributions to Mineralogy and Petrology, 154, 429-437, doi: https://doi.org/10.1007/s00410-007-0201-0

Appendix 4 Table A3 Zircon trace element data for GRV and Hiltaba Suite samples analyzed at the University of Adelaide

Unit	Group	Sample	Spot Number	Zircon Treatment	Discordance	Other	Analytical Session
Included Data							
Hiltaba Suite	mineralization-absent	1077-46	1077-46 - 4	Chemical Abrasion			26/08/2018
Hiltaba Suite	mineralization-absent	1077-46	1077-46 - 6	Chemical Abrasion			26/08/2018
Hiltaba Suite	mineralization-absent	1077-46	1077-46 - 7	Chemical Abrasion			26/08/2018
Hiltaba Suite	mineralization-absent	1077-46	1077-46 - 9	Chemical Abrasion			26/08/2018
Hiltaba Suite	mineralization-absent	1077-46	1077-46 - 10	Chemical Abrasion			26/08/2018
Hiltaba Suite	mineralization-absent	1077-46	1077-46 - 11	Chemical Abrasion			26/08/2018
Hiltaba Suite	mineralization-absent	1077-46	1077-46 - 14	Chemical Abrasion			26/08/2018
Hiltaba Suite	mineralization-absent	1077-46	1077-46 - 15	Chemical Abrasion			26/08/2018
Hiltaba Suite	mineralization-absent	1077-46	1077-46 - 16	Chemical Abrasion			27/08/2018
Hiltaba Suite	mineralization-absent	1077-46	1077-46 - 19	Chemical Abrasion			27/08/2018
Hiltaba Suite	mineralization-absent	1077-46	1077-46 - 20	Chemical Abrasion			27/08/2018
Hiltaba Suite	mineralization-absent	1077-59	1077-59 - 2	Chemical Abrasion			21/05/2020
Hiltaba Suite	mineralization-absent	1077-59	1077-59 - 4	Chemical Abrasion			21/05/2020
Hiltaba Suite	mineralization-absent	1077-59	1077-59 - 5	Chemical Abrasion			21/05/2020
Hiltaba Suite	mineralization-absent	1077-59	1077-59 - 6	Chemical Abrasion			21/05/2020
Hiltaba Suite	mineralization-absent	1077-59	1077-59 - 8	Chemical Abrasion			21/05/2020
Hiltaba Suite	mineralization-absent	1077-59	1077-59 - 9	Chemical Abrasion			21/05/2020
Hiltaba Suite	mineralization-absent	1077-59	1077-59 - 10	Chemical Abrasion			21/05/2020
Hiltaba Suite	mineralization-absent	1077-59	1077-59 - 11	Chemical Abrasion			21/05/2020
Hiltaba Suite	mineralization-absent	1077-59	1077-59 - 13	Chemical Abrasion			21/05/2020
Hiltaba Suite	mineralization-absent	1077-59	1077-59 - 14	Chemical Abrasion			21/05/2020
Hiltaba Suite	mineralization-absent	1077-59	1077-59 - 15	Chemical Abrasion			21/05/2020
Hiltaba Suite	mineralization-absent	1077-59	1077-59 - 16	Chemical Abrasion			21/05/2020
Hiltaba Suite	mineralization-absent	1077-59	1077-59 - 20	Chemical Abrasion			21/05/2020
Hiltaba Suite	mineralization-absent	1077-59	1077-59 - 22	Chemical Abrasion			21/05/2020
Hiltaba Suite	mineralization-absent	1077-59	1077-59 - 23	Chemical Abrasion			21/05/2020
Hiltaba Suite	mineralization-absent	1077-59	1077-59 - 26	Chemical Abrasion			21/05/2020
Hiltaba Suite	mineralization-absent	1077-59	1077-59 - 30	Chemical Abrasion			21/05/2020
Hiltaba Suite	mineralization-absent	1077-59	1077-59 - 34	Chemical Abrasion			21/05/2020
Hiltaba Suite	mineralization-absent	1077-59	1077-59 - 35	Chemical Abrasion			21/05/2020
Hiltaba Suite	mineralization-absent	1077-59	1077-59 - 36	Chemical Abrasion			21/05/2020
Hiltaba Suite	mineralization-absent	1077-59	1077-59 - 37	Chemical Abrasion			21/05/2020
Hiltaba Suite	mineralization-absent	1077-59	1077-59 - 38	Chemical Abrasion			21/05/2020
Hiltaba Suite	mineralization-absent	1077-59	1077-59 - 39	Chemical Abrasion			21/05/2020
Hiltaba Suite	mineralization-absent	1077-59	1077-59 - 41	Chemical Abrasion			21/05/2020
Hiltaba Suite	mineralization-absent	1077-59	1077-59 - 43	Chemical Abrasion			21/05/2020
Hiltaba Suite	mineralization-absent	1077-59	1077-59 - 45	Chemical Abrasion			21/05/2020
Hiltaba Suite	mineralization-absent	1077-59	1077-59 - 47	Chemical Abrasion			21/05/2020
Hiltaba Suite	mineralization-absent	1077-59	1077-59 - 48	Chemical Abrasion			21/05/2020
Hiltaba Suite	mineralization-absent	1077-59	1077-59 - 49	Chemical Abrasion			21/05/2020
Hiltaba Suite	mineralization-absent	1077-59	1077-59 - 50	Chemical Abrasion			21/05/2020
Hiltaba Suite	mineralization-absent	1077-59	1077-59 - 52	Chemical Abrasion			21/05/2020
Hiltaba Suite	mineralization-absent	1077-59	1077-59 - 57	Chemical Abrasion			21/05/2020
Hiltaba Suite	mineralization-absent	1077-59	1077-59 - 58	Chemical Abrasion			21/05/2020
Hiltaba Suite	mineralization-absent	1077-59	1077-59 - 60	Chemical Abrasion			21/05/2020
Hiltaba Suite	mineralization-absent	1077-59	1077-59 - 61	Chemical Abrasion			21/05/2020
Hiltaba Suite	mineralization-absent	1077-63	1077-63 - 1	Chemical Abrasion			21/05/2020
Hiltaba Suite	mineralization-absent	1077-63	1077-63 - 2	Chemical Abrasion			21/05/2020
Hiltaba Suite	mineralization-absent	1077-63	1077-63 - 3	Chemical Abrasion			21/05/2020
Hiltaba Suite	mineralization-absent	1077-63	1077-63 - 4	Chemical Abrasion			21/05/2020
Hiltaba Suite	mineralization-absent	1077-63	1077-63 - 6	Chemical Abrasion			21/05/2020
Hiltaba Suite	mineralization-absent	1077-63	1077-63 - 7	Chemical Abrasion			21/05/2020
Hiltaba Suite	mineralization-absent	1077-63	1077-63 - 9	Chemical Abrasion			21/05/2020
Hiltaba Suite	mineralization-absent	1077-63	1077-63 - 10	Chemical Abrasion			21/05/2020
Hiltaba Suite	mineralization-absent	1077-63	1077-63 - 13	Chemical Abrasion			21/05/2020
Hiltaba Suite	mineralization-absent	1077-63	1077-63 - 17	Chemical Abrasion			21/05/2020
Hiltaba Suite	mineralization-absent	1077-63	1077-63 - 18	Chemical Abrasion			21/05/2020
Hiltaba Suite	mineralization-absent	1077-63	1077-63 - 19	Chemical Abrasion			21/05/2020
Hiltaba Suite	mineralization-absent	1077-63	1077-63 - 21	Chemical Abrasion			21/05/2020
Hiltaba Suite	mineralization-absent	1077-63	1077-63 - 22	Chemical Abrasion			21/05/2020
Hiltaba Suite	mineralization-absent	1077-63	1077-63 - 23	Chemical Abrasion			21/05/2020
Hiltaba Suite	mineralization-absent	1077-63	1077-63 - 24	Chemical Abrasion			21/05/2020
Hiltaba Suite	mineralization-absent	1077-63	1077-63 - 25	Chemical Abrasion			21/05/2020
Hiltaba Suite	mineralization-absent	1077-63	1077-63 - 27	Chemical Abrasion			21/05/2020
Hiltaba Suite	mineralization-absent	1077-63	1077-63 - 29	Chemical Abrasion			21/05/2020
Hiltaba Suite	mineralization-absent	1077-63	1077-63 - 32	Chemical Abrasion			21/05/2020
Hiltaba Suite	mineralization-absent	1077-63	1077-63 - 33	Chemical Abrasion			21/05/2020
Hiltaba Suite	mineralization-absent	1077-63	1077-63 - 34	Chemical Abrasion			21/05/2020
Hiltaba Suite	mineralization-absent	1077-63	1077-63 - 38	Chemical Abrasion			21/05/2020
Hiltaba Suite	mineralization-absent	1077-63	1077-63 - 39	Chemical Abrasion			21/05/2020
Hiltaba Suite	mineralization-absent	1077-63	1077-63 - 40	Chemical Abrasion			21/05/2020

Appendix 4 Table A3 Zircon trace element data for GRV and Hiltaba Suite samples analyzed at the University of Adelaide

Spot Number	P	Ti	Y	Nb	La	Ce	Pr	Nd	Sm	Eu	Gd	Tb	Dy	Ho
	ppm	ppm	ppm	ppm	ppm	ppm	ppm	ppm	ppm	ppm	ppm	ppm	ppm	ppm
1077-46 - 4	143.00	8.70	756.00	3.66		20.20	0.20	1.24	2.01	0.05	11.80	4.61	63.60	26.00
1077-46 - 6	158.00	11.90	984.00	3.62		23.53	0.08	1.10	2.84	0.06	17.56	6.38	84.50	33.97
1077-46 - 7	169.00	20.70	1116.00	3.38		35.30	0.22	2.16	3.92	0.11	23.30	8.14	99.60	38.10
1077-46 - 9	159.00	29.40	816.30	1.55		18.17	0.10	1.47	3.11	0.32	15.05	5.87	70.60	27.17
1077-46 - 10	201.00	15.20	1260.00	4.25		34.08	0.55	3.10	4.36	0.12	24.80	8.25	107.90	42.68
1077-46 - 11	183.00	16.10	1204.00	2.11		30.65	0.78	4.38	5.40	0.25	28.80	8.91	110.00	40.80
1077-46 - 14	227.00	11.30	1302.00	3.55		34.83	0.22	2.29	5.10	0.26	25.57	9.87	117.20	45.23
1077-46 - 15	142.00	13.80	686.60	1.59		45.13	0.09	1.19	2.42	0.51	13.92	4.80	60.30	23.26
1077-46 - 16	164.00	10.40	1288.00	4.17		97.30	2.03	9.60	6.72	0.20	25.60	8.73	115.80	43.80
1077-46 - 19	165.00	17.20	722.00	2.23		37.94	0.08	1.43	2.71	0.54	13.04	4.61	58.40	23.47
1077-46 - 20	151.00	11.10	1159.00	3.60		25.36	0.13	2.09	4.23	0.12	21.30	7.42	100.40	38.68
1077-59 - 2	229.00	5.70	772.00	3.34	b.d.l	27.12	0.02	0.41	1.82	0.29	10.70	4.46	62.30	25.70
1077-59 - 4	250.00	6.50	807.00	2.87	0.06	25.65	0.04	0.90	1.79	0.26	12.60	5.17	67.80	27.70
1077-59 - 5	190.00	6.30	474.50	2.74	0.01	14.00	0.00	0.13	0.60	0.10	5.70	2.60	33.80	14.28
1077-59 - 6	351.00	7.20	1056.00	2.66	0.04	24.70	0.10	1.13	3.19	0.48	18.10	6.52	85.90	35.40
1077-59 - 8	249.00	8.50	887.00	3.84	1.10	44.50	0.60	3.97	3.41	0.44	14.60	5.61	73.10	28.50
1077-59 - 9	172.00	6.00	658.00	2.89	0.02	19.95	0.04	0.65	1.26	0.24	9.47	3.74	50.90	21.26
1077-59 - 10	250.00	7.60	950.00	4.78	0.27	35.30	0.24	1.59	2.69	0.34	14.90	5.94	75.70	31.10
1077-59 - 11	252.00	8.90	1088.00	4.76	0.42	31.40	0.28	2.75	3.88	0.35	19.40	7.04	90.80	36.50
1077-59 - 13	291.00	6.90	858.00	4.62	b.d.l	23.67	0.04	0.52	1.45	0.16	10.90	4.93	67.30	28.40
1077-59 - 14	342.00	6.80	1038.00	5.78	2.43	37.40	0.73	3.66	3.20	0.36	16.90	6.31	84.80	34.30
1077-59 - 15	239.00	7.70	708.00	2.43	0.25	26.20	0.24	2.43	2.66	0.38	13.20	5.10	65.10	25.00
1077-59 - 16	328.00	15.30	955.00	2.65	0.03	33.70	0.11	1.52	2.92	0.64	17.20	6.58	82.60	33.00
1077-59 - 20	258.00	10.00	908.00	4.78	0.93	34.70	0.51	2.72	2.81	0.34	15.00	5.58	73.20	30.90
1077-59 - 22	337.00	7.50	1450.00	2.79	0.17	21.00	0.33	3.38	6.36	1.24	33.10	11.20	136.00	49.70
1077-59 - 23	233.00	11.90	677.00	3.71	0.73	26.20	0.43	2.70	2.88	0.32	12.10	4.43	55.30	22.51
1077-59 - 26	323.00	11.40	923.00	3.32	b.d.l	35.80	0.04	1.00	1.98	0.34	14.40	5.54	75.00	30.40
1077-59 - 30	287.00	10.50	1114.00	4.81	0.21	29.10	0.18	1.71	3.59	0.47	16.60	6.63	91.20	37.30
1077-59 - 34	344.00	10.00	1076.00	2.88	0.30	19.60	0.14	1.93	3.72	0.84	21.60	8.31	97.40	37.30
1077-59 - 35	327.00	8.00	897.00	2.99	0.45	33.76	0.24	1.77	2.82	0.45	15.80	6.06	73.30	29.80
1077-59 - 36	367.00	7.30	1122.00	3.49	0.53	31.95	0.36	2.88	3.71	0.60	21.60	7.50	94.40	37.50
1077-59 - 37	327.00	10.50	1010.00	3.61	1.38	49.90	0.55	3.10	3.77	0.43	17.50	7.04	83.90	33.30
1077-59 - 38	262.00	12.20	672.00	3.52	0.28	21.42	0.18	1.23	1.33	0.21	9.60	4.03	54.10	21.90
1077-59 - 39	247.00	9.60	739.00	2.63	0.06	19.82	0.04	0.69	1.67	0.26	10.70	4.19	58.50	24.70
1077-59 - 41	257.00	12.00	903.00	2.42	0.95	26.90	0.42	2.17	2.60	0.25	15.50	5.54	72.50	31.00
1077-59 - 43	220.00	9.80	590.00	2.76	0.04	19.35	0.05	0.51	1.15	0.14	8.47	3.30	44.40	19.45
1077-59 - 45	226.00	9.00	757.00	3.13	0.04	24.01	0.05	0.77	1.81	0.27	11.40	4.80	62.50	25.50
1077-59 - 47	261.00	14.10	811.00	2.96	0.02	25.68	0.03	1.26	2.17	0.43	13.44	4.69	66.10	27.70
1077-59 - 48	323.00	10.80	1140.00	2.81	0.77	28.00	0.44	3.63	5.10	0.45	21.30	7.98	98.00	38.70
1077-59 - 49	242.00	6.60	693.00	2.71	b.d.l	27.79	0.02	0.82	1.58	0.32	11.90	3.99	53.80	22.91
1077-59 - 50	273.00	10.60	768.00	2.87	0.04	31.59	0.07	0.88	2.20	0.34	13.06	4.84	66.70	25.73
1077-59 - 52	177.00	6.60	496.00	2.55	0.02	16.07	0.04	0.39	1.02	0.17	6.85	2.70	37.50	15.99
1077-59 - 57	297.00	b.d.l	1015.00	6.48	0.33	25.30	0.18	1.35	2.16	0.18	11.80	5.28	75.70	32.10
1077-59 - 58	281.00	8.00	1073.00	5.04	1.36	42.60	0.72	4.20	3.28	0.59	17.70	7.58	88.00	35.50
1077-59 - 60	208.00	15.70	768.00	1.23	b.d.l	14.79	0.07	0.98	2.32	0.30	14.80	5.19	64.20	25.57
1077-59 - 61	186.00	7.60	472.00	2.58	b.d.l	15.33	0.01	0.14	0.93	0.09	5.66	2.40	36.00	15.51
1077-63 - 1	195.00	6.60	881.00	3.55	b.d.l	42.10	0.05	1.09	3.11	0.82	15.70	6.08	77.30	30.90
1077-63 - 2	187.00	4.60	678.00	3.14	0.32	35.30	0.12	1.39	1.67	0.34	10.40	4.09	52.60	21.60
1077-63 - 3	240.00	3.20	852.00	3.55	b.d.l	37.60	0.04	1.16	2.59	0.56	17.70	6.22	78.10	29.80
1077-63 - 4	126.00	6.80	602.00	2.79	0.64	33.60	0.23	1.97	2.10	0.41	10.80	4.22	49.80	21.10
1077-63 - 6	132.00	3.70	398.70	2.77	0.02	22.13	0.05	0.48	1.20	0.20	6.12	2.46	32.60	13.22
1077-63 - 7	306.00	8.00	2460.00	3.04	0.03	83.50	0.53	9.00	15.20	4.22	71.50	23.00	250.00	89.30
1077-63 - 9	243.00	6.60	668.00	1.67	0.02	33.80	0.04	0.85	2.20	0.84	14.50	4.99	59.30	22.70
1077-63 - 10	153.00	3.60	1318.00	2.46	b.d.l	53.10	0.04	1.35	3.67	0.78	25.60	9.42	113.10	43.80
1077-63 - 13	190.00	8.90	1479.00	3.08	0.03	65.00	0.18	3.78	6.98	2.08	39.20	12.13	142.50	49.80
1077-63 - 17	213.00	7.50	909.00	4.34	b.d.l	50.30	0.05	1.27	3.25	0.59	18.40	6.41	78.40	30.40
1077-63 - 18	217.00	5.40	858.00	3.88	b.d.l	48.70	0.04	0.95	2.92	0.63	17.70	6.57	74.10	28.90
1077-63 - 19	160.00	3.20	870.00	4.91	b.d.l	44.70	0.04	1.11	3.15	0.52	15.60	6.14	72.00	29.00
1077-63 - 21	196.00	9.80	766.00	3.17	b.d.l	43.00	0.11	2.00	3.99	1.21	18.90	6.02	67.40	26.20
1077-63 - 22	108.00	b.d.l	536.00	3.16	b.d.l	27.70	0.01	0.28	1.13	0.27	6.35	2.74	39.80	17.09
1077-63 - 23	196.00	4.50	890.00	4.63	0.03	46.40	0.08	1.26	3.01	0.53	16.50	5.94	75.40	29.10
1077-63 - 24	221.00	b.d.l	976.00	4.84	b.d.l	44.50	0.07	1.42	2.98	0.70	17.60	6.39	82.70	33.10
1077-63 - 25	113.00	b.d.l	756.00	2.92	b.d.l	34.40	0.04	0.83	2.40	0.64	13.80	5.30	61.70	24.70
1077-63 - 27	183.00	4.60	736.00	3.98	0.72	40.10	0.21	1.93	2.30	0.43	12.70	4.98	58.80	23.89
1077-63 - 29	157.00	8.00	1255.00	1.34	b.d.l	50.00	0.25	4.36	8.30	2.03	38.50	11.05	123.20	43.60
1077-63 - 32	198.00	b.d.l	824.00	3.81	b.d.l	36.89	0.03	0.91	2.54	0.47	15.50	5.46	70.70	28.60
1077-63 - 33	195.00	14.20	654.00	1.66	0.02	50.20	0.13	2.70	4.10	1.74	19.70	6.02	60.10	22.60
1077-63 - 34	209.00	6.80	1472.00	1.90	0.40	59.60	0.28	4.10	7.80	1.86	37.60	12.70	138.30	50.80
1077-63 - 38	244.00	12.70	957.00	2.00	0.10	54.20	0.25	3.84	6.16	2.09	27.00	8.03	89.20	33.00
1077-63 - 39	141.00	b.d.l	950.00	4.88	b.d.l	47.80	0.04	1.07	2.98	0.76	18.10	6.33	78.70	31.20
1077-63 - 40	206.00	13.80	903.00	2.23	0.02	47.20	0.19	2.45	5.29	1.70	24.90	7.66	79.80	30.60

Appendix 4 Table A3 Zircon trace element data for GRV and Hiltaba Suite samples analyzed at the University of Adelaide

Spot Number	Er	Tm	Yb	Lu	Hf	Th	U	Eu/Eu*	Ce/Ce*	$(Yb/Gd)_N$	Ti-in-Zircon	Total REE	Th/U
	ppm	ppm	ppm	ppm	ppm	ppm	ppm						
1077-46 - 4	121.50	27.90	267.60	64.20	10668.00	56.95	119.10	0.03	61.50	28.10	782	611	0.48
1077-46 - 6	158.60	34.64	329.10	79.60	10230.00	84.50	140.50	0.02	128.63	23.23	814	772	0.60
1077-46 - 7	173.00	37.78	350.90	83.60	10070.00	92.40	124.20	0.04	69.08	18.66	877	856	0.74
1077-46 - 9	126.30	27.51	261.10	63.40	9097.00	51.03	64.00	0.14	60.91	21.50	921	620	0.80
1077-46 - 10	199.30	42.41	395.30	92.30	10238.00	119.90	175.70	0.03	36.01	19.75	841	955	0.68
1077-46 - 11	186.90	40.40	368.20	84.90	9590.00	77.60	94.20	0.06	20.09	15.84	848	910	0.82
1077-46 - 14	203.50	44.52	415.20	91.40	9879.00	126.50	154.40	0.07	78.89	20.12	809	995	0.82
1077-46 - 15	112.80	24.18	245.70	55.40	9306.00	53.76	42.54	0.27	179.63	21.87	830	590	1.26
1077-46 - 16	211.80	44.20	415.00	80.30	9945.00	118.40	122.60	0.05	16.52	20.09	800	1061	0.97
1077-46 - 19	116.40	25.99	255.40	54.80	9239.00	41.50	37.06	0.28	117.11	24.27	855	595	1.12
1077-46 - 20	183.20	38.12	356.40	73.30	9466.00	72.65	96.05	0.04	57.20	20.74	807	851	0.76
1077-59 - 2	128.20	28.60	268.70	55.60	10640.00	140.30	174.70	0.20	683.89	31.12	741	614	0.8
1077-59 - 4	126.70	28.70	277.30	56.30	9940.00	135.60	155.90	0.17	132.02	27.27	753	631	0.9
1077-59 - 5	80.40	19.03	190.60	40.90	10950.00	73.30	157.60	0.16	1232.34	41.44	750	402	0.5
1077-59 - 6	161.50	35.50	341.00	68.30	9810.00	156.00	169.10	0.19	143.72	23.35	763	782	0.9
1077-59 - 8	140.20	31.30	304.00	60.60	10020.00	199.70	234.00	0.19	22.42	25.80	780	712	0.9
1077-59 - 9	107.70	24.37	239.70	50.90	10580.00	98.80	158.20	0.22	138.57	31.37	746	530	0.6
1077-59 - 10	149.40	34.60	323.00	66.00	10060.00	220.00	274.00	0.16	87.48	26.86	768	741	0.8
1077-59 - 11	169.00	37.00	356.00	73.30	9470.00	196.00	188.50	0.12	37.52	22.74	784	828	1.0
1077-59 - 13	140.20	32.00	315.00	63.40	11250.00	141.00	214.00	0.12	295.63	35.81	759	688	0.7
1077-59 - 14	163.00	37.40	360.00	70.10	10230.00	241.70	310.00	0.15	20.81	26.40	758	821	0.8
1077-59 - 15	107.40	23.20	217.00	44.20	10010.00	113.00	84.20	0.20	27.49	20.37	770	532	1.3
1077-59 - 16	149.40	32.50	302.00	62.00	9950.00	137.20	105.90	0.28	99.20	21.76	842	724	1.3
1077-59 - 20	148.50	32.60	308.00	62.70	10000.00	198.10	238.80	0.16	30.70	25.45	796	718	0.8
1077-59 - 22	222.00	45.30	405.00	79.30	9280.00	88.70	83.70	0.26	27.23	15.16	767	1014	1.1
1077-59 - 23	109.00	25.07	247.10	50.10	10730.00	128.00	161.70	0.17	24.11	25.31	814	559	0.8
1077-59 - 26	149.50	33.00	314.50	62.30	10350.00	172.10	175.90	0.19	165.10	27.07	810	724	1.0
1077-59 - 30	178.70	39.90	373.00	78.20	9340.00	179.50	234.90	0.19	83.21	27.85	801	857	0.8
1077-59 - 34	168.00	34.80	317.00	64.60	9120.00	121.90	142.70	0.29	45.59	18.19	796	776	0.9
1077-59 - 35	138.00	31.60	305.00	60.80	9820.00	157.60	151.00	0.21	70.78	23.92	773	700	1.0
1077-59 - 36	179.00	38.40	367.50	73.80	9720.00	189.20	186.80	0.20	33.29	21.08	765	860	1.0
1077-59 - 37	163.60	35.50	340.00	68.70	10080.00	224.00	231.00	0.16	45.59	24.08	801	809	1.0
1077-59 - 38	109.30	24.60	240.00	49.60	10570.00	96.10	156.00	0.18	43.86	30.98	817	538	0.6
1077-59 - 39	119.10	27.60	271.20	56.10	10520.00	109.90	175.80	0.18	161.92	31.41	792	595	0.6
1077-59 - 41	143.40	32.50	312.00	64.00	10110.00	150.20	163.00	0.12	34.59	24.94	815	710	0.9
1077-59 - 43	95.30	21.91	219.70	44.80	10490.00	89.00	138.90	0.14	199.26	32.14	794	479	0.6
1077-59 - 45	120.50	27.00	279.00	57.00	10470.00	125.80	167.60	0.18	170.72	30.33	785	615	0.8
1077-59 - 47	128.90	28.50	271.70	57.10	9750.00	131.20	146.10	0.24	81.75	25.05	833	628	0.9
1077-59 - 48	174.00	38.40	345.00	71.90	9620.00	178.00	188.10	0.13	25.24	20.07	804	834	0.9
1077-59 - 49	110.00	24.65	237.50	49.50	9920.00	115.90	123.30	0.22	152.09	24.73	755	545	0.9
1077-59 - 50	123.30	27.93	263.90	53.90	10080.00	140.80	150.90	0.19	209.02	25.04	802	614	0.9
1077-59 - 52	77.30	18.30	180.90	37.40	10430.00	68.40	112.70	0.19	251.00	32.73	755	395	0.6
1077-59 - 57	165.70	38.80	383.00	76.90	10750.00	199.00	351.40	0.11	69.84	40.22		819	0.6
1077-59 - 58	169.40	38.40	370.00	74.40	10790.00	276.40	317.00	0.24	18.45	25.90	773	854	0.9
1077-59 - 60	116.90	26.06	239.70	49.50	9330.00	72.10	69.60	0.16	83.21	20.07	845	560	1.0
1077-59 - 61	78.70	18.26	184.10	38.70	10800.00	73.50	141.80	0.12	1694.18	40.31	768	396	0.5
1077-63 - 1	137.90	28.60	266.90	53.20	9120.00	117.70	106.60	0.36	256.67	21.07	755	664	1.1
1077-63 - 2	104.70	23.60	219.00	45.20	9770.00	100.10	104.00	0.25	71.06	26.10	721	520	1.0
1077-63 - 3	134.10	27.90	254.40	50.90	9230.00	86.90	85.70	0.25	168.56	17.81	690	641	1.0
1077-63 - 4	93.20	21.24	194.60	36.80	9670.00	80.50	82.20	0.26	42.35	22.33	758	471	1.0
1077-63 - 6	60.40	13.59	135.30	27.50	10130.00	47.90	64.80	0.23	268.45	27.40	702	315	0.7
1077-63 - 7	366.00	68.40	601.00	115.80	9150.00	335.00	162.00	0.39	36.50	10.42	773	1697	2.1
1077-63 - 9	103.00	21.00	195.00	39.60	9030.00	66.40	52.10	0.45	239.71	16.67	755	498	1.3
1077-63 - 10	197.40	40.90	360.00	70.40	9930.00	194.00	139.60	0.25	249.05	17.43	700	920	1.4
1077-63 - 13	219.10	43.50	392.80	74.30	9010.00	214.80	124.40	0.38	73.96	12.42	784	1051	1.7
1077-63 - 17	138.80	29.10	262.60	51.10	9400.00	158.70	135.70	0.23	236.07	17.69	767	671	1.2
1077-63 - 18	131.20	26.60	243.40	48.00	9350.00	172.50	145.00	0.27	366.99	17.04	736	630	1.2
1077-63 - 19	134.80	28.50	264.30	52.90	9550.00	161.40	153.10	0.22	266.17	21.00	690	653	1.1
1077-63 - 21	115.30	25.66	243.50	51.30	8370.00	87.90	81.40	0.43	99.90	15.97	794	605	1.1
1077-63 - 22	85.50	19.36	192.00	40.60	9950.00	83.40	96.00	0.30	929.89	37.47		433	0.9
1077-63 - 23	133.70	28.50	268.50	53.40	9520.00	191.70	169.60	0.23	204.90	20.17	719	662	1.1
1077-63 - 24	153.80	31.80	291.00	62.20	9530.00	125.30	122.20	0.30	153.18	20.49		728	1.0
1077-63 - 25	114.70	24.50	232.00	45.70	9520.00	93.10	87.90	0.34	279.13	20.83		561	1.1
1077-63 - 27	112.60	23.74	220.60	44.90	9470.00	139.90	128.70	0.24	57.67	21.53	721	548	1.1
1077-63 - 29	189.90	35.80	324.00	64.00	8520.00	143.70	80.40	0.35	50.85	10.43	773	895	1.8
1077-63 - 32	125.90	27.40	251.60	50.90	9140.00	105.30	102.00	0.23	263.54	20.12		617	1.0
1077-63 - 33	98.50	19.20	174.00	34.80	7670.00	99.90	47.50	0.59	65.76	10.95	834	494	2.1
1077-63 - 34	219.90	42.70	380.00	72.80	9190.00	211.00	127.10	0.33	64.41	12.52	758	1029	1.7
1077-63 - 38	143.10	29.30	266.00	56.30	7540.00	103.40	54.90	0.50	52.74	12.21	821	719	1.9
1077-63 - 39	144.80	31.01	300.60	60.50	8680.00	124.30	112.80	0.32	289.78	20.58		724	1.1
1077-63 - 40	136.80	28.00	272.30	57.10	7640.00	82.60	54.50	0.45	96.88	13.55	830	694	1.5

Ti-in-Zircon calculated using the method of Ferry and Watson (2007), assuming $\alpha TiO_2 = 0.7$ and $\alpha SiO_2 = 1$

Ferry, J. M. and Watson, E. B., 2007. New thermodynamic models and revised calibrations for the Ti-in-zircon and Zr-in-rutile thermometers. Contributions to Mineralogy and Petrology, 154, 429-437. doi: https://doi.org/10.1007/s00410-007-0201-0

Appendix 4 Table A3 Zircon trace element data for GRV and Hiltaba Suite samples analyzed at the University of Adelaide

Unit	Group	Sample	Spot Number	Zircon Treatment	Discordance	Other	Analytical Session
Rejected data							
LGRV	mineralization-related	18-TAR-14	18-TAR-14 - 10	Chemical Abrasion	>5%		26/08/2018
LGRV	mineralization-related	18-TAR-14	18-TAR-14 - 11	Chemical Abrasion	>5%		27/08/2018
LGRV	mineralization-related	18-TAR-14	18-TAR-14 - 12	Chemical Abrasion	>5%		27/08/2018
LGRV	mineralization-related	2729189	189 - 10	Chemical Abrasion	inherited		11/11/2019
LGRV	mineralization-related	2729189	189 - 12	Chemical Abrasion	inherited		11/11/2019
Hiltaba Suite	mineralization-related	2705391	391-1	Chemical Abrasion		>370 ppm P	30/09/2019
Hiltaba Suite	mineralization-related	2705391	391-2	Chemical Abrasion	>5%		30/09/2019
Hiltaba Suite	mineralization-related	2705391	391-4	Chemical Abrasion	>5%		30/09/2019
Hiltaba Suite	mineralization-related	2705391	391-8	Chemical Abrasion	>5%		30/09/2019
Hiltaba Suite	mineralization-related	2705391	391-10	Chemical Abrasion		> 370 ppm P	30/09/2019
Hiltaba Suite	mineralization-related	2705391	391-12	Chemical Abrasion	>5%		30/09/2019
Hiltaba Suite	mineralization-related	2705391	391-15	Chemical Abrasion	>5%		30/09/2019
Hiltaba Suite	mineralization-related	2705391	391-19	Chemical Abrasion	>5%		30/09/2019
Hiltaba Suite	mineralization-related	2705398	398-5	Chemical Abrasion	>5%		30/09/2019
Hiltaba Suite	mineralization-related	2705398	398-7	Chemical Abrasion	>5%		30/09/2019
Hiltaba Suite	mineralization-related	2705398	398-12	Chemical Abrasion	>5%		30/09/2019
Hiltaba Suite	mineralization-related	2705398	398-18	Chemical Abrasion		>370 ppm P	30/09/2019
Hiltaba Suite	mineralization-related	2705398	398-20	Chemical Abrasion	>5%		30/09/2019
Hiltaba Suite	mineralization-related	2746110	110-1	Chemical Abrasion	>5%		11/11/2019
Hiltaba Suite	mineralization-related	2746110	110-3	Chemical Abrasion	>5%		11/11/2019
Hiltaba Suite	mineralization-related	2746355	355-1	Chemical Abrasion		no data	11/11/2019
Hiltaba Suite	mineralization-related	2746355	355-3	Chemical Abrasion	>5%		11/11/2019
Hiltaba Suite	mineralization-related	2746355	355-8	Chemical Abrasion		inherited	11/11/2019
Hiltaba Suite	mineralization-related	2746355	355-12	Chemical Abrasion		inherited	11/11/2019
Hiltaba Suite	mineralization-related	2746355	355-17	Chemical Abrasion	>5%		11/11/2019
Hiltaba Suite	mineralization-related	2746355	355-18	Chemical Abrasion	>5%		11/11/2019
Hiltaba Suite	mineralization-related	2746356*	356-1	Chemical Abrasion	>5%		11/11/2019
Hiltaba Suite	mineralization-related	2746356*	356-2	Chemical Abrasion	>5%		11/11/2019
Hiltaba Suite	mineralization-related	2746356*	356-3	Chemical Abrasion	>5%		11/11/2019
Hiltaba Suite	mineralization-related	2746356*	356-4	Chemical Abrasion	>5%		11/11/2019
Hiltaba Suite	mineralization-related	2746356*	356-5	Chemical Abrasion	>5%		11/11/2019
Hiltaba Suite	mineralization-related	2746356*	356-6	Chemical Abrasion	>5%	> 370 ppm P	11/11/2019
Hiltaba Suite	mineralization-related	2746356*	356-7	Chemical Abrasion	>5%		11/11/2019
Hiltaba Suite	mineralization-related	2746356*	356-8	Chemical Abrasion	>5%		11/11/2019
Hiltaba Suite	mineralization-related	2746356*	356-9	Chemical Abrasion	>5%	> 370 ppm P	11/11/2019
Hiltaba Suite	mineralization-related	2746356*	356-10	Chemical Abrasion			11/11/2019
Hiltaba Suite	mineralization-related	2746356*	356-11	Chemical Abrasion	>5%	> 370 ppm P	11/11/2019
Hiltaba Suite	mineralization-related	HDD-393-01	HDD393-01 - 14	Chemical Abrasion	>5%		27/08/2018
Hiltaba Suite	mineralization-related	1077-32	1077-32-5	Chemical Abrasion		inherited	26/08/2018
Hiltaba Suite	mineralization-absent	1077-01	1077-01-1	Chemical Abrasion		inherited	26/08/2018
Hiltaba Suite	mineralization-absent	1077-01	1077-01-5	Chemical Abrasion	>5%		26/08/2018
Hiltaba Suite	mineralization-absent	1077-01	1077-01-9	Chemical Abrasion	>5%		26/08/2018
Hiltaba Suite	mineralization-absent	1077-01	1077-01-11	Chemical Abrasion	>5%		27/08/2018
Hiltaba Suite	mineralization-absent	1077-01	1077-01-12	Chemical Abrasion	>5%		27/08/2018
Hiltaba Suite	mineralization-absent	1077-01	1077-01-16	Chemical Abrasion	>5%		27/08/2018
Hiltaba Suite	mineralization-absent	1077-01	1077-01-18	Chemical Abrasion		inherited	27/08/2018
Hiltaba Suite	mineralization-absent	1077-27	1077-27-4	Chemical Abrasion	>5%		30/09/2019
Hiltaba Suite	mineralization-absent	1077-27	1077-27-5	Chemical Abrasion		contamination	30/09/2019
Hiltaba Suite	mineralization-absent	1077-27	1077-27-3	Chemical Abrasion	>5%		30/09/2019
Hiltaba Suite	mineralization-absent	1077-52	1077-52-3	Chemical Abrasion	>5%		26/08/2018
Hiltaba Suite	mineralization-absent	1077-52	1077-52-4	Chemical Abrasion	>5%		26/08/2018
Hiltaba Suite	mineralization-absent	1077-52	1077-52-5	Chemical Abrasion	>5%		26/08/2018
Hiltaba Suite	mineralization-absent	1077-52	1077-52-6	Chemical Abrasion	>5%		26/08/2018
Hiltaba Suite	mineralization-absent	1077-52	1077-52-8	Chemical Abrasion	>5%		26/08/2018
Hiltaba Suite	mineralization-absent	HG470	HG-470 - 3	Chemical Abrasion		inherited	21/05/2020
Hiltaba Suite	mineralization-absent	HG470	HG-470 - 4	Chemical Abrasion	> 5%	inherited	21/05/2020
Hiltaba Suite	mineralization-absent	HG470	HG-470 - 5	Chemical Abrasion	> 5%	inherited	21/05/2020
Hiltaba Suite	mineralization-absent	HG470	HG-470 - 6	Chemical Abrasion	> 5%		21/05/2020
Hiltaba Suite	mineralization-absent	HG470	HG-470 - 7	Chemical Abrasion	> 5%		21/05/2020
Hiltaba Suite	mineralization-absent	1077-198	1077-198-1	Chemical Abrasion	>5%	> 370 ppm P	30/09/2019
Hiltaba Suite	mineralization-absent	1077-198	1077-198-2	Chemical Abrasion	>5%	not zircon	30/09/2019
Hiltaba Suite	mineralization-absent	1077-198	1077-198-3	Chemical Abrasion	>5%	> 370 ppm P	30/09/2019
Hiltaba Suite	mineralization-absent	1077-198	1077-198-4	Chemical Abrasion	>5%	> 370 ppm P	30/09/2019
Hiltaba Suite	mineralization-absent	1077-198	1077-198-7	Chemical Abrasion	>5%		30/09/2019
Hiltaba Suite	mineralization-absent	1077-198	1077-198-9	Chemical Abrasion	>5%		30/09/2019
Hiltaba Suite	mineralization-absent	1077-198	1077-198-10	Chemical Abrasion	>5%		30/09/2019
Hiltaba Suite	mineralization-absent	1077-198	1077-198-11	Chemical Abrasion	>5%	> 370 ppm P	30/09/2019
Hiltaba Suite	mineralization-absent	1077-41	1077-41 - 1	Chemical Abrasion	> 5%		21/05/2020
Hiltaba Suite	mineralization-absent	1077-41	1077-41 - 3	Chemical Abrasion	> 5%		21/05/2020
Hiltaba Suite	mineralization-absent	1077-41	1077-41 - 4	Chemical Abrasion	> 5%		21/05/2020
Hiltaba Suite	mineralization-absent	1077-41	1077-41 - 5	Chemical Abrasion	> 5%		21/05/2020

Appendix 4 Table A3 Zircon trace element data for GRV and Hiltaba Suite samples analyzed at the University of Adelaide

Spot Number	P	Ti	Y	Nb	La	Ce	Pr	Nd	Sm	Eu	Gd	Tb	Dy	Ho
	ppm	ppm	ppm	ppm	ppm	ppm	ppm	ppm	ppm	ppm	ppm	ppm	ppm	ppm
18-TAR-14 - 10	134	3.62	2401.00	8.87		532.00	37.00	128.00	78.00	9.60	131.00	38.30	312.00	83.10
18-TAR-14 - 11	98.9	3.5	819.00	0.65		112.00	4.80	21.50	15.00	2.71	32.60	8.77	90.80	30.10
18-TAR-14 - 12	111	3.64	1624.00	1.69		333.00	19.60	74.00	43.20	6.12	70.70	20.53	188.90	57.40
189 - 10	479	13.7	1580	5.99	0.151	54.10	0.30	2.88	6.17	1.51	31.60	10.99	134.30	52.49
189 - 12	268	3.9	2240	2.29	1.23	41.30	1.63	11.90	15.50	5.14	63.40	21.80	259.00	76.90
391-1	371.00	7.40	546.00	4.44	0.13	33.70	0.17	1.21	1.74	0.43	9.41	3.35	43.70	17.33
391-2	233.00	13.20	1440.00	4.12	3.09	91.70	11.30	72.00	73.00	16.90	112.00	29.90	234.00	55.90
391-4	415.00	24.00	640.00	3.79	6.50	41.00	3.17	10.90	5.02	0.69	13.89	4.35	55.20	20.12
391-8	279.00	10.60	3680.00	4.81	3.94	170.00	7.80	39.40	41.30	6.50	102.00	35.60	406.00	119.00
391-10	446.00	15.40	875.00	4.30	b.d.l.	34.15	0.11	2.12	3.59	0.75	19.23	6.26	77.30	29.34
391-12	240.00	6.20	2490.00	6.77	2.82	129.30	4.48	22.80	22.60	4.23	55.10	25.00	296.00	92.10
391-15	239.00	8.20	2427.00	6.93	3.49	118.20	4.02	22.70	16.90	4.08	58.00	21.80	253.00	85.90
391-19	304.00	19.10	1230.00	5.14	0.31	36.40	0.45	4.50	7.20	1.58	35.10	11.40	119.00	41.40
398-5	229.00	17.70	402.00	1.92	0.03	8.93	0.08	0.72	1.19	0.33	8.10	2.69	33.90	13.22
398-7	212.00	16.00	3630.00	2.46	5.26	75.40	4.36	21.40	21.80	7.84	84.50	34.10	421.00	155.00
398-12	175.00	10.90	442.00	2.37	15.80	28.81	3.05	10.30	2.66	0.43	8.98	3.05	37.50	14.30
398-18	379.00	7.70	621.00	4.76	b.d.l.	40.80	0.06	0.93	1.91	0.30	10.86	3.64	47.60	19.36
398-20	467.00	8.90	3050.00	3.60	2.83	70.90	2.79	17.80	15.20	5.43	63.80	24.80	312.00	113.00
110-1	310.00	13.60	3480.00	2.62	10.10	294.00	26.60	172.00	124.00	27.90	252.00	68.00	490.00	143.00
110-3	302.00	4.80	1111.00	7.27	0.49	38.00	0.74	4.15	4.77	0.82	21.90	7.60	99.60	37.70
355-1	b.d.l.	b.d.l.	b.d.l.	0.00	b.d.l.	b.d.l.	b.d.l.	b.d.l.	b.d.l.	b.d.l.	0.00	b.d.l.	b.d.l.	1.10
355-3	260.00	3.60	1590.00	6.68	1.58	50.20	1.08	7.30	6.70	0.50	29.40	9.87	142.00	50.90
355-8	270.00	7.80	1307.00	4.98	3.40	57.20	5.34	31.50	16.10	2.45	40.30	11.70	122.20	42.60
355-12	169.00	17.80	319.00	0.78	0.04	4.90	0.07	0.87	1.28	0.29	6.62	2.12	28.50	10.30
355-17	244.00	12.40	688.00	2.28	0.67	19.74	0.20	2.76	2.98	0.85	15.75	4.90	59.70	22.48
355-18	320.00	6.80	1322.00	6.51	0.13	44.10	0.21	2.94	4.19	0.46	25.80	8.71	114.40	43.80
356-1	372.00	118.00	3400.00	11.83	12.84	160.50	13.70	77.10	67.50	26.20	189.00	47.60	418.00	115.10
356-2	442.00	23.10	2149.00	10.73	1.53	69.40	1.79	14.47	15.21	3.91	55.40	16.70	191.80	71.70
356-3	414.00	18.60	3077.00	5.10	2.17	48.96	0.78	9.77	14.05	2.39	75.10	23.45	280.70	102.30
356-4	369.00	269.00	3229.00	6.32	83.60	500.00	63.10	300.00	162.00	81.30	267.70	48.53	357.10	104.40
356-5	414.00	19.30	5430.00	2.55	12.00	181.00	15.70	111.00	136.00	61.80	539.00	133.00	960.00	208.00
356-6	3710.00	620.00	55500.00	3.71	201.00	1840.00	243.00	1630.00	1710.00	711.00	5250.00	1290.00	9100.00	1930.00
356-7	193.00	58.00	7620.00	3.08	36.10	328.00	38.40	234.00	222.00	87.30	755.00	190.00	1480.00	306.00
356-8	432.00	560.00	11900.00	7.20	53.60	475.00	54.00	319.00	277.00	121.00	880.00	220.00	1590.00	372.00
356-9	569.00	45.70	4646.00	9.89	75.00	334.60	44.90	119.20	35.40	7.84	136.50	40.05	451.60	159.60
356-10	412.00	30.00	1864.00	6.82	0.85	68.70	1.28	10.96	13.00	3.50	52.90	15.89	179.80	63.20
356-11	505.00	37.20	2508.00	13.76	114.80	618.00	83.40	262.00	70.00	36.20	88.50	21.28	234.00	82.60
HDD393-01 - 14	172.00	42.20	1078.00	3.27		30.71	0.52	4.49	5.96	1.55	26.10	8.74	99.00	37.20
1077-32-5	188.00	19.30	2860.00	2.05		363.00	138.00	730.00	144.00	20.50	226.00	39.30	422.00	106.50
1077-01-1	108.00	7.50	1090.00	2.13		130.00	20.20	67.90	25.90	5.16	59.10	12.00	104.00	39.70
1077-01-5	142.00	19.50	1037.00	1.81		31.70	0.98	6.31	5.81	0.78	24.40	8.98	94.80	36.10
1077-01-9	121.00	20.50	1114.00	2.09		25.50	2.71	17.40	8.83	1.65	31.10	9.70	105.50	38.90
1077-01-11	110.30	14.00	1111.00	1.50		67.90	9.17	48.60	20.60	3.00	40.80	9.49	104.10	36.45
1077-01-12	85.00	29.00	486.00	1.89		11.17	0.23	1.77	1.96	0.26	8.62	3.30	39.60	15.88
1077-01-16	122.50	9.90	1075.00	4.23		67.70	5.80	34.40	12.00	1.76	33.00	8.33	99.40	36.30
1077-01-18	122.00	16.60	1011.00	2.23		87.20	15.90	97.10	34.60	9.35	54.50	10.08	99.00	32.40
1077-27-4	288.00	1.64	385.00	0.95	0.10	10.60	0.13	1.22	2.18	0.29	10.00	2.98	36.70	12.80
1077-27-5	128.00	9.10	992.00	2.00	0.99	16.50	0.77	5.73	7.89	0.44	34.10	9.07	97.90	34.40
1077-27-3	139.00	2.22	829.00	3.95	0.05	9.41	0.21	3.18	4.95	0.43	24.33	7.53	84.30	28.35
1077-52-3	185.00	22.60	1012.10	2.39		54.66	0.22	2.69	4.71	1.20	25.00	8.34	95.10	35.54
1077-52-4	230.00	39.10	1241.00	1.94		49.19	2.95	13.70	10.80	2.17	35.40	10.90	122.10	43.80
1077-52-5	177.00	14.00	1106.00	4.81		83.50	3.96	16.10	9.40	1.14	24.70	8.40	97.20	37.10
1077-52-6	133.00	43.60	1065.00	1.17		44.10	0.43	4.35	6.42	1.81	29.70	9.61	102.40	37.91
1077-52-8	110.00	7.10	702.00	4.25		37.40	0.04	0.38	1.44	0.24	9.98	4.43	55.20	23.40
HG-470 - 3	143.00	13.60	544.00	1.49	3.10	30.80	1.45	12.50	7.30	0.54	19.20	5.71	49.60	18.60
HG-470 - 4	192.00	6.40	1540.00	3.28	14.70	216.00	23.70	148.00	85.00	4.50	140.00	32.90	201.00	50.20
HG-470 - 5	206.00	47.00	1620.00	1.98	7.90	125.00	10.00	58.00	64.00	2.83	85.00	22.20	187.00	55.00
HG-470 - 6	216.00	13.10	4200.00	1.76	24.00	620.00	42.00	250.00	230.00	10.70	360.00	77.00	600.00	137.00
HG-470 - 7	100.00	13.90	490.00	1.13	1.62	26.00	1.30	6.20	8.60	0.45	23.20	4.89	48.70	18.00
1077-198-1	8000.00	8.80	500.00	2.23	b.d.l.	23.10	0.03	0.56	1.21	0.25	8.63	3.02	40.30	16.18
1077-198-2	210.00	35.00	78000.00	1.42	313000.00	580000.00	73000.00	253000.00	38700.00	1950.00	26500.00	3310.00	19400.00	2980.00
1077-198-3	800.00	7.20	3816.00	3.56	11.10	77.10	4.54	25.00	23.60	3.38	94.80	31.10	353.00	127.10
1077-198-4	827.00	9.10	1220.00	2.52	6.30	65.90	2.22	10.80	9.40	0.91	29.90	9.72	114.90	39.30
1077-198-7	254.00	11.80	757.00	2.77	28.00	51.80	6.30	18.60	5.80	0.71	19.50	5.95	68.70	25.60
1077-198-9	251.00	8.20	1370.00	2.56	14.60	99.00	5.18	24.60	17.20	1.49	43.60	14.80	133.00	47.90
1077-198-10	233.00	b.d.l.	4630.00	4.63	45.80	414.00	23.70	149.00	100.00	8.10	197.00	56.00	540.00	134.00
1077-198-11	570.00	7.30	1180.00	2.54	7.50	66.90	3.21	17.70	12.50	1.16	37.40	12.10	142.00	41.70
1077-41 - 1	209.00	6.70	536.00	1.08	4.40	60.00	5.90	36.40	19.80	1.75	28.00	5.50	53.70	18.30
1077-41 - 3	186.00	9.90	566.00	1.67	5.26	31.30	3.78	19.80	11.30	0.89	20.70	5.19	55.80	18.47
1077-41 - 4	217.00	11.80	1006.00	3.67	19.80	104.00	9.80	55.00	27.80	2.88	55.00	10.00	109.00	36.10
1077-41 - 5	315.00	6.40	923.00	2.66	7.00	44.90	5.40	28.00	20.00	1.27	34.10	8.68	89.90	32.40

Appendix 4 Table A3 Zircon trace element data for GRV and Hiltaba Suite samples analyzed at the University of Adelaide

Spot Number	Er	Tm	Yb	Lu	Hf	Th	U	Eu/Eu*	Ce/Ce*	$(Yb/Gd)_N$	Ti-in-Zircon	Total REE	Th/U
	ppm	ppm	ppm	ppm	ppm	ppm	ppm						
18-TAR-14 - 10	322.00	71.80	541.00	104.70	8270.00	430.00	172.00	0.29	5.90	5.12	700	2389	2.50
18-TAR-14 - 11	117.90	23.15	199.10	38.40	7475.00	133.00	53.74	0.37	8.46	7.57	698	697	2.47
18-TAR-14 - 12	226.50	44.00	406.60	78.10	8035.00	379.00	132.50	0.34	6.12	7.13	701	1569	2.86
189 - 10	251.50	51.80	470.50	95.40	8970.00	276.50	321.00	0.33	93.73	18.45	830	1164	0.9
189 - 12	329.00	58.00	459.00	82.00	9970.00	301.00	322.80	0.50	10.53	8.97	707	1426	0.9
391-1	91.20	20.20	198.10	42.10	9590.00	121.80	176.30	0.32	93.28	26.09	766	463	0.69
391-2	210.00	41.60	336.00	61.90	9460.00	140.40	149.10	0.57	3.01	3.72	826	1349	0.94
391-4	100.40	21.98	206.50	42.90	9790.00	98.90	117.30	0.25	4.03	18.42	895	533	0.84
391-8	557.00	117.0	1030.0	167.00	9120.00	343.00	221.90	0.31	10.53	12.51	802	2803	1.55
391-10	138.20	29.23	282.50	57.71	9070.00	185.20	195.10	0.27	63.53	18.21	843	680	0.95
391-12	490.00	97.30	983.00	163.00	9970.00	422.00	307.80	0.37	13.09	22.11	749	2388	1.37
391-15	399.00	84.80	763.00	153.00	9990.00	390.00	330.70	0.40	9.03	16.30	776	1988	1.18
391-19	179.00	34.60	330.00	51.90	9980.00	79.30	82.60	0.30	30.14	11.65	868	853	0.96
398-5	62.30	13.24	121.30	24.94	9190.00	33.50	66.30	0.32	47.74	18.56	859	291	0.51
398-7	617.00	111.0	774.00	132.70	9800.00	310.00	106.90	0.56	8.36	11.35	847	2465	2.90
398-12	73.30	16.04	145.00	30.70	8670.00	76.60	99.90	0.27	1.68	20.01	805	390	0.77
398-18	103.50	23.27	214.30	46.40	9800.00	182.40	263.80	0.20	209.85	24.45	770	513	0.69
398-20	471.00	85.00	636.00	112.10	9790.00	317.00	179.00	0.53	7.92	12.35	784	1933	1.77
110-1	580.00	98.00	790.00	171.00	9090.00	1450.00	233.20	0.48	2.87	3.88	829	3247	6.22
110-3	178.80	37.50	329.90	65.20	10080.0	331.90	513.70	0.25	24.51	18.67	725	827	0.65
355-1	b.d.l.	0.00	b.d.l.	0.00	0.00	b.d.l.	b.d.l.						
355-3	246.00	50.60	447.00	91.00	11090.0	352.00	457.00	0.11	14.70	18.84	700	1134	0.77
355-8	198.30	44.20	378.00	80.00	9350.00	224.80	397.00	0.29	2.16	11.62	771	1033	0.57
355-12	50.20	10.35	90.70	20.40	8255.00	25.10	47.50	0.31	19.30	16.98	859	227	0.53
355-17	107.90	22.87	203.30	43.40	8020.00	138.00	174.00	0.38	17.99	16.00	819	508	0.79
355-18	212.80	43.40	392.00	78.40	9780.00	340.00	488.70	0.14	49.79	18.83	758	971	0.70
356-1	472.00	90.00	800.00	148.30	8890.00	848.00	685.00	0.71	4.24	5.25	1131	2638	1.24
356-2	337.00	69.30	636.00	126.40	8070.00	677.00	634.00	0.41	11.74	14.23	890	1611	1.07
356-3	482.80	95.60	856.00	164.40	9470.00	1244.00	862.00	0.22	16.78	14.12	864	2158	1.44
356-4	473.90	94.60	856.00	165.40	10120.0	1489.00	1014.0	1.19	2.10	3.96	1296	3558	1.47
356-5	583.00	89.50	681.00	108.10	7420.00	1000.00	250.50	0.70	4.65	1.57	869	3819	3.99
356-6	5590.0	830.0	5800.0	810.00	9260.00	10800.0	650.00	0.73	2.76	1.37	1507	36935	16.62
356-7	927.00	131.0	1070.0	157.00	9350.00	2160.00	333.70	0.65	3.10	1.76	1015	5962	6.47
356-8	1410.0	251.0	2000.0	333.00	9540.00	1750.00	766.00	0.75	3.01	2.82	1478	8356	2.28
356-9	715.00	138.2	1188.0	224.60	8530.00	1947.00	1101.0	0.34	1.94	10.79	980	3670	1.77
356-10	288.30	57.40	510.20	97.00	8570.00	799.00	538.10	0.41	17.32	11.95	923	1363	1.48
356-11	394.50	76.90	692.00	132.00	8830.00	1406.00	940.00	1.41	1.47	9.69	952	2906	1.50
HDD393-01 - 14	164.70	34.59	332.10	67.60	8733.00	151.80	172.90	0.38	21.15	15.77	969	813	0.88
1077-32-5	400.00	81.90	633.00	123.30	7612.00	1130.00	167.50	0.35	0.23	3.47	869	3428	6.75
1077-01-1	166.00	34.70	297.00	59.30	10240.0	147.00	184.00	0.40	1.70	6.23	767	1021	0.80
1077-01-5	158.20	32.70	289.50	54.90	9110.00	123.00	137.20	0.20	10.77	14.70	870	745	0.90
1077-01-9	170.00	34.20	326.00	62.10	9380.00	112.00	143.40	0.30	1.73	12.99	876	834	0.78
1077-01-11	159.90	32.50	289.10	59.10	9116.00	291.00	115.61	0.32	1.38	8.78	832	881	2.52
1077-01-12	76.30	16.00	160.30	32.64	9912.00	55.80	103.70	0.20	16.28	23.05	919	368	0.54
1077-01-16	163.00	35.60	328.10	67.20	10720.0	185.10	274.80	0.27	1.60	12.32	795	893	0.67
1077-01-18	143.20	27.83	253.90	52.70	9580.00	97.90	130.10	0.66	0.75	5.77	851	918	0.75
1077-27-4	58.40	11.20	94.00	18.10	8620.00	83.30	112.60	0.19	36.16	11.65	637	259	0.74
1077-27-5	154.10	30.60	269.10	54.50	8363.00	113.90	163.10	0.08	9.24	9.78	786	716	0.70
1077-27-3	125.10	23.20	189.50	36.24	8270.00	73.50	81.10	0.12	10.73	9.65	660	537	0.91
1077-52-3	157.80	33.47	311.50	59.00	8719.00	64.65	42.18	0.34	82.87	15.44	888	789	1.53
1077-52-4	188.00	39.10	362.80	71.30	7837.00	75.70	26.99	0.34	6.59	12.70	959	952	2.80
1077-52-5	165.50	40.00	368.00	68.20	9980.00	142.00	95.10	0.23	7.05	18.46	832	923	1.49
1077-52-6	160.80	32.61	308.40	58.70	8476.00	39.00	23.90	0.40	34.85	12.87	974	797	1.63
1077-52-8	112.70	25.59	253.00	49.40	10890.0	57.00	72.62	0.19	868.68	31.42	762	573	0.78
HG-470 - 3	74.90	14.68	130.80	25.50	8050.00	66.20	88.20	0.14	3.35	8.44	829	395	0.8
HG-470 - 4	177.00	31.20	228.00	42.30	10680.0	186.00	232.40	0.13	1.95	2.02	752	1395	0.8
HG-470 - 5	194.00	37.50	292.00	57.00	7520.00	147.00	118.70	0.12	5.54	4.26	984	1197	1.2
HG-470 - 6	450.00	70.00	570.00	124.00	8850.00	510.00	156.50	0.11	5.31	1.96	825	3565	3.3
HG-470 - 7	72.10	14.30	128.00	26.10	8870.00	60.50	64.60	0.10	13.55	6.84	831	379	0.9
1077-198-1	82.80	18.02	168.00	35.03	9730.00	124.00	180.90	0.24	207.59	24.12	783	397	0.69
1077-198-2	7900.0	1300.	9500.0	1460.0	6550.00	16800.0	345.00	0.19	0.82	0.44	944		48.70
1077-198-3	576.00	107.9	904.00	162.70	9260.00	258.10	255.00	0.22	6.78	11.82	763	2501	1.01
1077-198-4	189.60	38.00	346.00	68.40	9480.00	258.00	244.60	0.17	12.37	14.34	786	931	1.05
1077-198-7	123.30	25.07	229.80	46.50	9610.00	198.00	194.60	0.20	2.02	14.60	813	656	1.02
1077-198-9	193.00	40.90	349.00	74.00	9320.00	275.00	231.70	0.17	6.55	9.92	776	1058	1.19
1077-198-10	511.00	84.30	800.00	121.00	7600.00	425.00	390.00	0.18	4.34	5.03		3184	1.09
1077-198-11	173.80	36.60	310.00	59.50	10210.0	220.10	204.10	0.16	6.22	10.27	765	922	1.08
1077-41 - 1	78.00	16.29	147.00	30.30	7780.00	147.00	84.00	0.23	2.09	6.51	756	505	1.8
1077-41 - 3	82.30	17.60	150.90	30.90	8570.00	87.10	150.00	0.18	2.10	9.03	795	454	0.6
1077-41 - 4	149.10	29.30	259.00	54.20	10800.0	208.00	391.00	0.23	2.23	5.84	813	921	0.5
1077-41 - 5	138.90	27.94	260.90	52.00	9010.00	129.90	244.00	0.15	2.67	9.48	752	751	0.5

Ti-in-Zircon calculated using the method of Ferry and Watson (2007), assuming $\alpha TiO_2 = 0.7$ and $\alpha SiO_2 = 1$

Ferry, J. M. and Watson, E. B., 2007. New thermodynamic models and revised calibrations for the Ti-in-zircon and Zr-in-rutile thermometers. Contributions to Mineralogy and Petrology, 154, 429-437. doi: https://doi.org/10.1007/s00410-007-0201-0

Appendix 4 Table A3 Zircon trace element data for GRV and Hiltaba Suite samples analyzed at the University of Adelaide

Unit	Group	Sample	Spot Number	Zircon Treatment	Discordance	Other	Analytical Session
Rejected data							
Hiltaba Suite	mineralization-absent	1077-41	1077-41 - 10	Chemical Abrasion	> 5%		21/05/2020
Hiltaba Suite	mineralization-absent	1077-41	1077-41 - 12	Chemical Abrasion	> 5%		21/05/2020
Hiltaba Suite	mineralization-absent	1077-41	1077-41 - 14	Chemical Abrasion	> 5%		21/05/2020
Hiltaba Suite	mineralization-absent	1077-41	1077-41 - 19	Chemical Abrasion	> 5%	inherited	21/05/2020
Hiltaba Suite	mineralization-absent	1077-41	1077-41 - 22	Chemical Abrasion	> 5%		21/05/2020
Hiltaba Suite	mineralization-absent	1077-41	1077-41 - 23	Chemical Abrasion		discordant	21/05/2020
Hiltaba Suite	mineralization-absent	1077-41	1077-41 - 24	Chemical Abrasion		discordant	21/05/2020
Hiltaba Suite	mineralization-absent	1077-41	1077-41 - 28	Chemical Abrasion	> 5%		21/05/2020
Hiltaba Suite	mineralization-absent	1077-41	1077-41 - 34	Chemical Abrasion	> 5%		21/05/2020
Hiltaba Suite	mineralization-absent	1077-41	1077-41 - 35	Chemical Abrasion	> 5%	inherited	21/05/2020
Hiltaba Suite	mineralization-absent	1077-46	1077-46 - 8	Chemical Abrasion		inherited	26/08/2018
Hiltaba Suite	mineralization-absent	1077-46	1077-46 - 12	Chemical Abrasion		inherited	26/08/2018
Hiltaba Suite	mineralization-absent	1077-46	1077-46-18	Chemical Abrasion		inherited	27/08/2018
Hiltaba Suite	mineralization-absent	1077-46	1077-46 - 17	Chemical Abrasion	>5%		27/08/2018
Hiltaba Suite	mineralization-absent	1077-59	1077-59 - 1	Chemical Abrasion	> 5%		21/05/2020
Hiltaba Suite	mineralization-absent	1077-59	1077-59 - 3	Chemical Abrasion		discordant	21/05/2020
Hiltaba Suite	mineralization-absent	1077-59	1077-59 - 7	Chemical Abrasion	> 5%	inherited	21/05/2020
Hiltaba Suite	mineralization-absent	1077-59	1077-59 - 12	Chemical Abrasion	> 5%		21/05/2020
Hiltaba Suite	mineralization-absent	1077-59	1077-59 - 17	Chemical Abrasion		> 370 ppm P	21/05/2020
Hiltaba Suite	mineralization-absent	1077-59	1077-59 - 24	Chemical Abrasion	> 5%	> 370 ppm P	21/05/2020
Hiltaba Suite	mineralization-absent	1077-59	1077-59 - 25	Chemical Abrasion	> 5%		21/05/2020
Hiltaba Suite	mineralization-absent	1077-59	1077-59 - 27	Chemical Abrasion		>370 ppm P	21/05/2020
Hiltaba Suite	mineralization-absent	1077-59	1077-59 - 28	Chemical Abrasion		>370 ppm P	21/05/2020
Hiltaba Suite	mineralization-absent	1077-59	1077-59 - 29	Chemical Abrasion	> 5%		21/05/2020
Hiltaba Suite	mineralization-absent	1077-59	1077-59 - 31	Chemical Abrasion	> 5%		21/05/2020
Hiltaba Suite	mineralization-absent	1077-59	1077-59 - 32	Chemical Abrasion		discordant	21/05/2020
Hiltaba Suite	mineralization-absent	1077-59	1077-59 - 33	Chemical Abrasion		> 370 ppm P	21/05/2020
Hiltaba Suite	mineralization-absent	1077-59	1077-59 - 40	Chemical Abrasion		discordant	21/05/2020
Hiltaba Suite	mineralization-absent	1077-59	1077-59 - 42	Chemical Abrasion		reversely discordant	21/05/2020
Hiltaba Suite	mineralization-absent	1077-59	1077-59 - 44	Chemical Abrasion		discordant	21/05/2020
Hiltaba Suite	mineralization-absent	1077-59	1077-59 - 46	Chemical Abrasion		inherited	21/05/2020
Hiltaba Suite	mineralization-absent	1077-59	1077-59 - 51	Chemical Abrasion	> 5%	> 370 ppm P	21/05/2020
Hiltaba Suite	mineralization-absent	1077-59	1077-59 - 53	Chemical Abrasion	> 5%		21/05/2020
Hiltaba Suite	mineralization-absent	1077-59	1077-59 - 54	Chemical Abrasion		inherited	21/05/2020
Hiltaba Suite	mineralization-absent	1077-59	1077-59 - 55	Chemical Abrasion	> 5%		21/05/2020
Hiltaba Suite	mineralization-absent	1077-59	1077-59 - 56	Chemical Abrasion	> 5%		21/05/2020
Hiltaba Suite	mineralization-absent	1077-59	1077-59 - 59	Chemical Abrasion	> 5%		21/05/2020
Hiltaba Suite	mineralization-absent	1077-63	1077-63 - 5	Chemical Abrasion		inherited	21/05/2020
Hiltaba Suite	mineralization-absent	1077-63	1077-63 - 8	Chemical Abrasion		inherited	21/05/2020
Hiltaba Suite	mineralization-absent	1077-63	1077-63 - 11	Chemical Abrasion		inherited	21/05/2020
Hiltaba Suite	mineralization-absent	1077-63	1077-63 - 12	Chemical Abrasion		> 370 ppm P	21/05/2020
Hiltaba Suite	mineralization-absent	1077-63	1077-63 - 14	Chemical Abrasion		inherited	21/05/2020
Hiltaba Suite	mineralization-absent	1077-63	1077-63 - 15	Chemical Abrasion		inherited	21/05/2020
Hiltaba Suite	mineralization-absent	1077-63	1077-63 - 16	Chemical Abrasion		reversely discordant	21/05/2020
Hiltaba Suite	mineralization-absent	1077-63	1077-63 - 20	Chemical Abrasion		reversely discordant	21/05/2020
Hiltaba Suite	mineralization-absent	1077-63	1077-63 - 26	Chemical Abrasion		discordant	21/05/2020
Hiltaba Suite	mineralization-absent	1077-63	1077-63 - 28	Chemical Abrasion		inherited	21/05/2020
Hiltaba Suite	mineralization-absent	1077-63	1077-63 - 30	Chemical Abrasion		reversely discordant	21/05/2020
Hiltaba Suite	mineralization-absent	1077-63	1077-63 - 31	Chemical Abrasion		reversely discordant	21/05/2020
Hiltaba Suite	mineralization-absent	1077-63	1077-63 - 35	Chemical Abrasion	> 5%		21/05/2020
Hiltaba Suite	mineralization-absent	1077-63	1077-63 - 36	Chemical Abrasion		discordant	21/05/2020
Hiltaba Suite	mineralization-absent	1077-63	1077-63 - 37	Chemical Abrasion		inherited	21/05/2020

*entire sample eliminated

Appendix 4 Table A3 Zircon trace element data for GRV and Hiltaba Suite samples analyzed at the University of Adelaide

Spot Number	P	Ti	Y	Nb	La	Ce	Pr	Nd	Sm	Eu	Gd	Tb	Dy	Ho
	ppm	ppm	ppm	ppm	ppm	ppm	ppm	ppm	ppm	ppm	ppm	ppm	ppm	ppm
1077-41 - 10	143.00	12.00	738.00	1.26	10.10	68.40	7.60	40.90	19.20	2.12	35.60	7.11	73.70	25.60
1077-41 - 12	470.00	b.d.l	2370.00	3.26	227.00	670.00	124.00	670.00	211.00	15.10	234.00	30.80	257.00	72.00
1077-41 - 14	460.00	6.30	1061.00	4.32	2.22	20.80	1.25	6.00	6.40	0.31	23.90	7.92	94.80	35.40
1077-41 - 19	201.00	9.40	966.00	0.92	18.70	72.00	11.40	76.00	32.70	2.55	51.10	10.30	98.30	35.60
1077-41 - 22	135.00	b.d.l	515.00	1.65	7.20	32.50	3.20	16.40	7.10	0.52	18.60	4.65	48.80	20.30
1077-41 - 23	142.00	b.d.l	483.00	0.96	0.54	13.80	0.37	2.31	2.88	0.31	13.10	3.93	38.80	15.10
1077-41 - 24	212.00	11.50	814.00	0.87	1.14	31.00	1.12	9.00	9.60	1.07	28.80	7.59	80.70	27.90
1077-41 - 28	174.00	8.30	1296.00	0.88	0.19	14.48	0.39	5.70	10.40	0.67	41.10	11.62	125.40	45.10
1077-41 - 34	152.00	6.30	304.00	0.80	0.07	8.89	0.09	0.97	1.27	0.16	6.80	2.07	26.10	10.28
1077-41 - 35	166.00	2.70	350.00	0.33	b.d.l	2.98	0.02	0.28	1.27	0.69	6.84	2.25	28.00	10.46
1077-46 - 8	172.00	29.10	954.00	1.74		22.54	0.26	2.37	3.78	0.25	20.34	7.03	84.60	32.67
1077-46 - 12	140.00	18.10	1507.00	1.62		117.00	2.54	8.50	6.25	0.89	29.10	9.92	124.20	47.80
1077-46-18	128.00	7.60	1314.00	4.44		877.00	137.00	420.00	47.00	0.49	35.10	8.32	98.70	36.50
1077-46 - 17	177.00	18.20	1388.00	4.42		252.00	55.00	157.00	24.80	0.42	35.50	10.39	127.10	46.90
1077-59 - 1	255.00	14.40	849.00	2.76	0.21	33.30	0.13	1.41	2.52	0.45	15.60	5.20	72.60	28.20
1077-59 - 3	366.00	5.90	1280.00	4.63	0.23	29.60	0.09	1.62	2.86	0.42	19.60	7.70	102.50	42.00
1077-59 - 7	497.00	24.80	1591.00	3.80	0.51	54.70	0.43	5.60	7.53	1.67	36.10	12.12	141.20	54.20
1077-59 - 12	268.00	12.40	1060.00	4.47	0.32	56.00	0.37	2.45	4.40	0.40	16.40	7.25	89.60	35.70
1077-59 - 17	448.00	10.00	1740.00	3.16	0.07	24.20	0.26	4.93	7.90	1.22	41.80	13.90	163.00	60.40
1077-59 - 24	2140.00	15.40	1528.00	2.50	43.00	137.00	13.50	62.00	16.30	2.03	39.70	11.60	133.60	50.50
1077-59 - 25	255.00	19.20	891.00	2.30	0.05	20.91	0.09	1.21	3.23	0.48	16.50	6.32	77.30	29.00
1077-59 - 27	399.00	14.70	2970.00	4.03	9.30	58.00	2.68	15.20	12.80	1.30	61.40	21.50	264.00	98.80
1077-59 - 28	392.00	38.00	1559.00	2.10	0.13	22.17	0.24	3.56	6.23	1.10	33.90	12.10	144.30	52.60
1077-59 - 29	377.00	13.10	1380.00	1.47	1.09	26.30	0.69	5.30	6.50	1.08	32.80	10.00	119.00	46.80
1077-59 - 31	252.00	7.40	983.00	3.45	0.03	27.20	0.10	1.24	2.70	0.70	17.90	6.94	85.00	33.50
1077-59 - 32	388.00	20.80	1940.00	2.34	0.04	44.60	0.36	5.66	9.70	2.19	46.00	15.30	178.50	63.60
1077-59 - 33	1110.00	11.70	1304.00	3.51	12.70	74.50	4.22	20.30	8.50	1.16	27.30	9.26	114.90	42.90
1077-59 - 40	285.00	b.d.l	806.00	5.03	0.10	25.30	0.15	1.28	2.10	0.30	12.20	4.68	61.40	26.50
1077-59 - 42	289.00	8.60	617.00	3.77	0.24	20.14	0.10	0.76	1.16	0.19	9.58	3.59	48.30	19.80
1077-59 - 44	353.00	18.00	931.00	1.62	b.d.l	20.32	0.08	1.59	3.34	1.10	19.30	6.64	80.90	32.50
1077-59 - 46	330.00	7.90	1031.00	4.06	4.65	47.10	2.16	11.80	6.20	0.70	18.90	6.42	81.60	33.90
1077-59 - 51	3290.00	6.90	684.00	2.92	63.00	178.00	21.60	97.00	22.00	1.03	27.90	6.11	63.40	22.80
1077-59 - 53	252.00	7.00	918.00	2.88	58.00	84.00	7.40	25.10	8.40	0.69	22.00	6.59	81.70	30.90
1077-59 - 54	191.00	44.00	546.00	3.27	4.21	32.80	1.11	4.65	2.00	0.17	8.14	3.10	42.40	18.20
1077-59 - 55	261.00	7.20	908.00	3.78	1.09	30.00	0.57	3.50	3.56	0.33	15.90	5.79	73.70	30.80
1077-59 - 56	261.00	10.20	955.00	2.24	23.90	74.20	7.09	29.40	11.50	1.18	27.70	7.46	88.30	31.90
1077-59 - 59	411.00	15.40	1161.00	2.13	0.40	33.54	0.24	2.72	4.69	0.83	24.40	8.43	103.70	40.30
1077-63 - 5	178.00	8.00	797.00	3.14	0.01	49.40	0.04	1.16	3.59	0.80	19.70	5.85	71.60	28.20
1077-63 - 8	185.00	12.70	404.00	0.85	0.33	24.92	0.09	0.96	2.32	0.84	10.40	3.30	34.80	13.06
1077-63 - 11	207.00	4.70	750.00	4.49	b.d.l	41.30	0.06	0.95	2.34	0.52	13.80	5.11	63.60	25.40
1077-63 - 12	419.00	4.50	869.00	2.11	b.d.l	32.80	0.04	1.32	2.78	0.89	19.90	6.29	79.10	30.30
1077-63 - 14	196.00	10.10	827.00	3.49	0.14	56.00	0.20	2.56	3.95	0.86	17.90	6.78	78.30	28.90
1077-63 - 15	212.00	b.d.l	771.00	4.06	0.09	44.30	0.18	1.20	2.44	0.53	15.50	5.57	68.50	25.10
1077-63 - 16	370.00	5.70	528.00	1.77	4.10	35.30	0.81	3.20	1.63	0.38	8.70	3.20	41.50	17.40
1077-63 - 20	193.00	14.80	738.00	1.37	0.02	38.30	0.15	2.68	4.52	1.74	20.70	5.71	64.10	24.40
1077-63 - 26	163.00	14.60	1215.00	1.10	0.09	38.80	0.57	8.62	10.10	3.66	44.00	12.21	124.00	42.20
1077-63 - 28	278.00	7.60	1415.00	8.25	0.04	71.10	0.15	2.08	4.68	1.03	26.00	9.32	117.80	46.80
1077-63 - 30	226.00	5.20	1117.00	3.71	0.03	41.92	0.08	1.75	3.73	0.82	21.70	7.65	91.90	37.20
1077-63 - 31	147.00	8.80	688.00	2.99	0.40	41.40	0.11	1.23	2.12	0.63	14.90	5.41	59.30	23.60
1077-63 - 35	108.00	7.70	405.00	2.55	b.d.l	22.16	0.01	0.15	0.70	0.20	5.72	2.24	31.00	13.15
1077-63 - 36	168.00	11.60	800.00	1.60	b.d.l	34.10	0.16	2.46	4.55	1.34	21.40	6.80	74.10	27.20
1077-63 - 37	284.00	9.40	1490.00	3.44	15.30	157.00	9.40	44.40	18.00	3.10	44.70	11.90	126.00	47.30

Appendix 4 Table A3 Zircon trace element data for GRV and Hiltaba Suite samples analyzed at the University of Adelaide

Spot Number	Er	Tm	Yb	Lu	Hf	Th	U	Eu/Eu*	Ce/Ce*	$(Yb/Gd)_N$	Ti-in-Zircon	Total REE	Th/U
	ppm	ppm	ppm	ppm	ppm	ppm	ppm						
1077-41 - 10	107.10	21.40	189.30	40.10	8650.00	79.30	140.80	0.25	1.83	6.59	815	648	0.6
1077-41 - 12	302.00	49.90	407.00	88.80	8510.00	423.00	389.00	0.21	0.73	2.16		3359	1.1
1077-41 - 14	162.30	32.30	298.00	62.50	9410.00	129.00	345.00	0.08	8.61	15.45	750	754	0.4
1077-41 - 19	136.90	28.10	238.00	49.20	8850.00	116.00	145.00	0.19	0.95	5.77	790	861	0.8
1077-41 - 22	78.50	16.00	149.80	31.00	8210.00	95.00	146.20	0.14	2.00	9.98		435	0.6
1077-41 - 23	72.30	15.00	145.20	29.50	8550.00	49.10	110.80	0.15	17.35	13.74		353	0.4
1077-41 - 24	120.40	23.60	212.00	43.70	7690.00	64.70	115.00	0.20	8.56	9.12	811	598	0.6
1077-41 - 28	185.00	37.70	323.00	62.50	8680.00	117.50	195.50	0.10	10.80	9.74	777	863	0.6
1077-41 - 34	45.90	9.90	94.70	20.70	7860.00	29.20	81.90	0.16	27.95	17.26	750	228	0.4
1077-41 - 35	52.00	12.21	131.80	32.30	9330.00	7.81	47.30	0.72	112.43	23.88	676	281	0.2
1077-46 - 8	148.00	32.32	304.10	72.40	9590.00	61.00	78.40	0.09	35.33	18.53	919	731	0.78
1077-46 - 12	221.70	48.20	452.00	102.90	9716.00	116.60	58.17	0.20	23.57	19.25	861	1171	2.00
1077-46-18	180.00	36.30	358.00	69.60	10220.00	117.60	111.50	0.04	0.54	12.64	768	2304	1.05
1077-46 - 17	213.20	43.50	402.70	82.10	9544.00	126.20	131.30	0.04	0.59	14.06	862	1451	0.96
1077-59 - 1	131.80	29.30	275.90	57.50	10060.00	111.00	97.50	0.22	98.31	21.92	835	654	1.1
1077-59 - 3	202.70	46.50	435.00	87.00	10030.00	204.00	276.10	0.17	75.13	27.50	744	978	0.7
1077-59 - 7	244.10	52.70	489.00	96.30	8540.00	215.00	107.30	0.31	30.59	16.79	899	1196	2.0
1077-59 - 12	172.10	37.60	356.00	73.30	10760.00	227.00	246.00	0.14	95.61	26.90	819	852	0.9
1077-59 - 17	262.00	53.10	488.00	95.10	8890.00	228.00	132.00	0.21	18.32	14.47	796	1216	1.7
1077-59 - 24	232.90	47.90	443.00	87.00	10080.00	190.40	140.00	0.24	1.35	13.83	843	1320	1.4
1077-59 - 25	137.60	28.40	276.70	55.80	9430.00	109.60	103.60	0.20	107.44	20.78	868	654	1.1
1077-59 - 27	449.00	91.10	818.00	156.30	8580.00	499.00	319.10	0.14	7.48	16.51	837	2059	1.6
1077-59 - 28	234.30	49.10	443.00	87.50	9240.00	163.00	114.20	0.23	25.38	16.19	955	1090	1.4
1077-59 - 29	210.00	42.50	384.00	76.10	8810.00	145.00	102.00	0.23	14.17	14.51	825	962	1.4
1077-59 - 31	153.00	33.40	324.00	64.20	10310.00	140.00	161.60	0.31	111.24	22.43	766	750	0.9
1077-59 - 32	290.00	60.10	551.00	107.20	8920.00	229.30	112.10	0.32	31.45	14.84	878	1374	2.0
1077-59 - 33	205.40	42.80	418.00	82.70	9280.00	250.60	184.70	0.23	3.58	18.97	813	1065	1.4
1077-59 - 40	126.50	31.10	299.00	60.40	11400.00	127.20	222.00	0.18	75.53	30.37		651	0.6
1077-59 - 42	98.50	22.30	215.60	46.90	10260.00	100.00	155.10	0.18	94.21	27.89	781	487	0.6
1077-59 - 44	141.00	30.70	282.00	54.60	8490.00	46.50	28.90	0.42	62.53	18.11	861	674	1.6
1077-59 - 46	158.20	36.80	360.00	73.40	10000.00	204.70	235.40	0.20	4.88	23.60	772	842	0.9
1077-59 - 51	105.60	23.90	222.90	45.70	10460.00	98.60	139.20	0.13	0.97	9.90	759	901	0.7
1077-59 - 53	145.10	30.00	281.90	57.90	9180.00	161.30	136.80	0.16	2.61	15.88	760	840	1.2
1077-59 - 54	89.10	20.40	199.00	41.50	9440.00	90.10	127.20	0.13	7.07	30.30	975	467	0.7
1077-59 - 55	142.40	31.90	311.00	62.30	10250.00	145.70	170.60	0.13	20.31	24.24	763	713	0.9
1077-59 - 56	138.60	30.20	287.00	56.70	9100.00	210.00	130.10	0.20	2.30	12.84	798	815	1.6
1077-59 - 59	175.30	37.50	344.10	68.90	8720.00	121.70	54.22	0.24	49.52	17.48	843	845	2.2
1077-63 - 5	125.30	26.20	228.00	44.60	9220.00	140.10	112.20	0.29	306.97	14.34	773	604	1.2
1077-63 - 8	62.50	13.30	122.30	26.50	7650.00	35.90	27.40	0.52	146.11	14.57	821	316	1.3
1077-63 - 11	115.60	25.20	225.00	43.90	10150.00	155.00	133.60	0.28	249.41	20.20	723	563	1.2
1077-63 - 12	136.90	27.20	258.00	51.70	9160.00	83.80	79.30	0.37	121.89	16.07	719	647	1.1
1077-63 - 14	130.20	26.10	243.00	46.30	10080.00	150.80	125.10	0.31	78.61	16.82	797	641	1.2
1077-63 - 15	119.50	25.10	234.00	45.70	9950.00	159.90	134.70	0.26	174.83	18.71		588	1.2
1077-63 - 16	81.10	18.51	182.50	40.00	10150.00	85.20	83.60	0.31	13.09	26.00	741	438	1.0
1077-63 - 20	115.00	24.90	230.10	50.90	7220.00	62.40	43.40	0.55	56.14	13.78	838	583	1.4
1077-63 - 26	180.20	34.30	306.00	62.60	7340.00	126.40	49.10	0.53	12.28	8.62	837	867	2.6
1077-63 - 28	217.00	45.30	422.00	84.40	8580.00	204.00	182.00	0.29	179.13	20.11	768	1048	1.1
1077-63 - 30	168.70	35.70	324.90	64.00	9090.00	172.40	143.00	0.28	118.92	18.55	732	800	1.2
1077-63 - 31	103.10	22.40	204.00	39.20	9080.00	134.80	92.50	0.34	135.12	16.97	783	518	1.5
1077-63 - 35	62.30	14.25	137.40	27.60	9720.00	48.50	62.20	0.31	1605.74	29.77	770	317	0.8
1077-63 - 36	120.00	22.80	219.00	43.40	8400.00	64.00	45.90	0.42	59.72	12.68	812	577	1.4
1077-63 - 37	209.00	44.10	411.00	84.80	9440.00	264.00	168.30	0.33	3.34	11.39	790	1226	1.6

Ti-in-Zircon calculated using the method of Ferry and Watson (2007), assuming $\alpha TiO_2 = 0.7$ and $\alpha SiO_2 = 1$

Ferry, J. M. and Watson, E. B., 2007. New thermodynamic models and revised calibrations for the Ti-in-zircon and Zr-in-rutile thermometers. Contributions to Mineralogy and Petrology, 154, 429-437. doi: https://doi.org/10.1007/s00410-007-0201-0

Appendix Table A4 LA-ICP MS U-Pb data for GRV and Hiltaba Suite zircon analyzed at the University of Adelaide

Unit	Group	Sample	Spot Number	Zircon Treatment	Analytical Session	Radiogenic Ratios							Age (Ma)											
						$^{207}Pb/^{206}Pb$	2σ	$^{207}Pb/^{235}U$	2σ	$^{206}Pb/^{238}U$	2σ	$^{207}Pb/^{206}Pb$	2σ	$^{207}Pb/^{235}Pb$	2σ	$^{206}Pb/^{238}U$	2σ	$^{208}Pb/^{232}Th$	2σ	% Conc	Th ppm	U ppm
Included data																						
LGRV	mineralization-related	18-TAR-14	18-TAR-14 - 1	CA	26/08/2018	0.0985	0.0022	3.6830	0.0780	0.2723	0.0037	**1589**	**42**	1565	17	1552	19	1283	48	98	213.00	96.10
LGRV	mineralization-related	18-TAR-14	18-TAR-14 - 2	CA	26/08/2018	0.0998	0.0026	4.0700	0.1000	0.2929	0.0030	**1614**	**50**	1648	21	1656	15	750	130	103	458.00	108.90
LGRV	mineralization-related	18-TAR-14	18-TAR-14 - 3	CA	26/08/2018	0.0982	0.0025	3.8300	0.1000	0.2793	0.0039	**1589**	**48**	1596	22	1588	20	1348	49	100	190.00	81.60
LGRV	mineralization-related	18-TAR-14	18-TAR-14 - 4	CA	26/08/2018	0.1002	0.0019	3.9790	0.0860	0.2877	0.0030	**1628**	**37**	1629	18	1630	15	1308	56	100	187.70	87.30
LGRV	mineralization-related	18-TAR-14	18-TAR-14 - 5	CA	26/08/2018	0.0952	0.0021	3.7120	0.0790	0.2796	0.0032	**1531**	**42**	1571	17	1589	16	1615	47	104	120.70	111.60
LGRV	mineralization-related	18-TAR-14	18-TAR-14 - 6	CA	26/08/2018	0.0992	0.0018	3.7570	0.0670	0.2727	0.0026	**1601**	**35**	1584	14	1554	13	1504	50	97	147.00	108.20
LGRV	mineralization-related	18-TAR-14	18-TAR-14 - 7	CA	26/08/2018	0.0984	0.0026	3.9420	0.0950	0.2879	0.0034	**1578**	**49**	1619	20	1631	17	1482	52	103	163.00	83.00
LGRV	mineralization-related	18-TAR-14	18-TAR-14 - 8	CA	26/08/2018	0.1019	0.0040	3.9600	0.1300	0.2838	0.0053	**1641**	**74**	1626	25	1609	26	894	49	98	162.90	30.94
LGRV	mineralization-related	18-TAR-14	18-TAR-14 - 9	CA	26/08/2018	0.0997	0.0022	3.7690	0.0920	0.2713	0.0032	**1617**	**42**	1590	20	1549	16	1462	44	96	179.00	99.50
LGRV	mineralization-related	18-TAR-14	18-TAR-14 - 13	CA	27/08/2018	0.0994	0.0022	3.8110	0.0840	0.2830	0.0028	**1613**	**43**	1599	17	1606	14	1583	43	100	93.80	76.30
LGRV	mineralization-related	18-TAR-14	18-TAR-14 - 14	CA	27/08/2018	0.1024	0.0028	4.0660	0.1100	0.2871	0.0035	**1658**	**51**	1642	22	1627	17	1629	34	98	205.00	97.10
LGRV	mineralization-related	2729189	189 - 1	CA	11/11/2019	0.0980	0.0012	3.7800	0.0440	0.2772	0.0019	**1586**	**22**	1589	10	1577	10	1630	26	99	197.60	252.10
LGRV	mineralization-related	2729189	189 - 2	CA	11/11/2019	0.0976	0.0010	3.7720	0.0380	0.2775	0.0018	**1576**	**19**	1586	8	1579	9	1630	27	100	165.60	313.90
LGRV	mineralization-related	2729189	189 - 3	CA	11/11/2019	0.0990	0.0012	3.8320	0.0400	0.2782	0.0018	**1602**	**23**	1600	9	1583	9	1577	29	99	168.90	208.00
LGRV	mineralization-related	2729189	189 - 4	CA	11/11/2019	0.0995	0.0009	3.9310	0.0360	0.2833	0.0018	**1613**	**17**	1620	7	1609	9	1591	30	100	197.80	275.70
LGRV	mineralization-related	2729189	189 - 5	CA	11/11/2019	0.0988	0.0013	3.8670	0.0530	0.2782	0.0022	**1608**	**26**	1608	11	1583	11	1587	28	98	219.30	196.80
LGRV	mineralization-related	2729189	189 - 6	CA	11/11/2019	0.0991	0.0010	3.8360	0.0390	0.2779	0.0018	**1609**	**19**	1599	8	1582	9	1422	59	98	391.00	304.90
LGRV	mineralization-related	2729189	189 - 7	CA	11/11/2019	0.0993	0.0010	3.8590	0.0390	0.2794	0.0019	**1609**	**19**	1604	8	1588	9	1602	33	99	194.90	257.90
LGRV	mineralization-related	2729189	189 - 8	CA	11/11/2019	0.0986	0.0010	3.7760	0.0350	0.2753	0.0018	**1605**	**19**	1587	7	1567	9	1563	24	98	226.70	299.00
LGRV	mineralization-related	2729189	189 - 9	CA	11/11/2019	0.0980	0.0011	3.8230	0.0460	0.2786	0.0020	**1588**	**22**	1597	10	1584	10	1622	32	100	115.20	161.30
LGRV	mineralization-related	2729189	189 - 11	CA	11/11/2019	0.0985	0.0009	3.8150	0.0360	0.2777	0.0014	**1596**	**17**	1595	8	1579	7	1625	23	99	210.70	438.30
Hiltaba Suite	mineralization-related	2705391	391-3	CA	30/09/2019	0.0988	0.0008	3.9200	0.0300	0.2853	0.0015	**1600**	**16**	1617	6	1618	7	1598	26	101	477.40	441.00
Hiltaba Suite	mineralization-related	2705391	391-5	CA	30/09/2019	0.0992	0.0013	3.9270	0.0430	0.2849	0.0022	**1610**	**23**	1619	9	1616	11	1641	31	100	237.30	307.10
Hiltaba Suite	mineralization-related	2705391	391-6	CA	30/09/2019	0.0990	0.0010	3.8790	0.0400	0.2841	0.0020	**1604**	**18**	1608	8	1612	10	1632	28	100	173.10	213.20
Hiltaba Suite	mineralization-related	2705391	391-7	CA	30/09/2019	0.1004	0.0014	3.8820	0.0580	0.2797	0.0033	**1627**	**27**	1610	12	1589	17	1310	48	98	196.80	173.10
Hiltaba Suite	mineralization-related	2705391	391-9	CA	30/09/2019	0.0994	0.0010	3.8260	0.0380	0.2781	0.0020	**1611**	**19**	1599	8	1582	10	1582	24	98	491.00	399.70
Hiltaba Suite	mineralization-related	2705391	391-11	CA	30/09/2019	0.0981	0.0012	3.8610	0.0440	0.2845	0.0023	**1591**	**24**	1605	9	1615	12	1672	43	102	95.60	125.50
Hiltaba Suite	mineralization-related	2705391	391-13	CA	30/09/2019	0.0995	0.0009	3.8770	0.0430	0.2817	0.0020	**1611**	**17**	1609	9	1600	10	1668	27	99	204.00	263.50
Hiltaba Suite	mineralization-related	2705391	391-14	CA	30/09/2019	0.0986	0.0011	3.9020	0.0380	0.2852	0.0026	**1596**	**21**	1615	8	1617	13	1685	37	101	205.60	295.00
Hiltaba Suite	mineralization-related	2705391	391-16	CA	30/09/2019	0.0986	0.0010	3.9150	0.0420	0.2860	0.0022	**1597**	**20**	1617	9	1621	11	1667	27	102	128.20	164.00
Hiltaba Suite	mineralization-related	2705391	391-17	CA	30/09/2019	0.0989	0.0010	3.9590	0.0500	0.2887	0.0027	**1603**	**19**	1628	10	1635	14	1430	40	102	353.00	468.00
Hiltaba Suite	mineralization-related	2705391	391-18	CA	30/09/2019	0.0974	0.0010	3.7240	0.0400	0.2775	0.0019	**1573**	**20**	1576	9	1579	9	1588	23	100	293.10	248.70
Hiltaba Suite	mineralization-related	2705391	391-20	CA	30/09/2019	0.0988	0.0009	3.8720	0.0320	0.2848	0.0017	**1603**	**17**	1608	6	1615	8	1469	29	101	472.70	429.00
Hiltaba Suite	mineralization-related	2705391	391-21	CA	30/09/2019	0.0989	0.0008	4.0560	0.0420	0.2972	0.0022	**1604**	**15**	1645	8	1677	11	1497	32	105	283.60	310.10
Hiltaba Suite	mineralization-related	2705391	391-22	CA	30/09/2019	0.0988	0.0009	3.8500	0.0400	0.2826	0.0020	**1598**	**16**	1603	9	1604	10	1483	32	100	284.10	323.70
Hiltaba Suite	mineralization-related	2705391	391-23	CA	30/09/2019	0.0979	0.0008	3.8260	0.0340	0.2827	0.0020	**1585**	**17**	1599	7	1604	10	1179	62	101	401.00	344.80
Hiltaba Suite	mineralization-related	2705391	391-24	CA	30/09/2019	0.0981	0.0009	3.9380	0.0360	0.2917	0.0022	**1587**	**17**	1621	8	1650	11	1550	28	104	358.70	419.40
Hiltaba Suite	mineralization-related	2705398	398-1	CA	30/09/2019	0.0986	0.0009	3.7680	0.0340	0.2784	0.0018	**1596**	**16**	1585	7	1583	9	1636	25	99	175.90	217.50
Hiltaba Suite	mineralization-related	2705398	398-2	CA	30/09/2019	0.0990	0.0009	3.8390	0.0300	0.2821	0.0016	**1604**	**16**	1601	6	1602	8	1532	27	100	228.30	352.00
Hiltaba Suite	mineralization-related	2705398	398-3	CA	30/09/2019	0.0987	0.0009	3.8590	0.0360	0.2844	0.0020	**1596**	**18**	1605	8	1613	10	1675	29	101	156.40	243.90
Hiltaba Suite	mineralization-related	2705398	398-4	CA	30/09/2019	0.0992	0.0023	3.7990	0.0720	0.2792	0.0029	**1612**	**41**	1593	15	1587	15	1598	57	98	79.30	128.20
Hiltaba Suite	mineralization-related	2705398	398-6	CA	30/09/2019	0.0991	0.0009	3.8770	0.0360	0.2848	0.0016	**1608**	**17**	1608	8	1617	8	1662	29	101	162.90	242.10
Hiltaba Suite	mineralization-related	2705398	398-8	CA	30/09/2019	0.0970	0.0012	3.8150	0.0420	0.2848	0.0022	**1562**	**23**	1595	9	1616	11	1576	35	103	85.30	138.50
Hiltaba Suite	mineralization-related	2705398	398-9	CA	30/09/2019	0.0987	0.0013	3.8780	0.0490	0.2859	0.0020	**1599**	**24**	1610	10	1621	10	1390	28	101	315.00	239.00
Hiltaba Suite	mineralization-related	2705398	398-10	CA	30/09/2019	0.0996	0.0030	3.6890	0.0960	0.2729	0.0038	**1606**	**57**	1567	21	1555	19	1548	60	97	90.40	123.50
Hiltaba Suite	mineralization-related	2705398	398-11	CA	30/09/2019	0.0978	0.0011	3.8530	0.0480	0.2849	0.0020	**1583**	**22**	1603	10	1616	10	1637	38	102	75.40	148.00
Hiltaba Suite	mineralization-related	2705398	398-13	CA	30/09/2019	0.0980	0.0011	3.7970	0.0400	0.2810	0.0019	**1584**	**21**	1592	9	1597	10	1519	35	101	167.50	309.20
Hiltaba Suite	mineralization-related	2705398	398-14	CA	30/09/2019	0.0977	0.0011	3.8870	0.0380	0.2901	0.0020	**1586**	**21**	1610	8	1642	10	1703	35	104	146.40	209.70
Hiltaba Suite	mineralization-related	2705398	398-15	CA	30/09/2019	0.0978	0.0009	3.8130	0.0420	0.2810	0.0024	**1585**	**19**	1595	9	1596	12	1363	38	101	190.30	230.30
Hiltaba Suite	mineralization-related	2705398	398-16	CA	30/09/2019	0.0977	0.0013	3.7290	0.0520	0.2761	0.0027	**1576**	**26**	1578	11	1575	14	1572	43	100	90.00	157.30
Hiltaba Suite	mineralization-related	2705398	398-17	CA	30/09/2019	0.0981	0.0008	3.8320	0.0320	0.2829	0.0017	**1589**	**16**	1600	7	1606	9	1652	25	101	274.80	320.10
Hiltaba Suite	mineralization-related	2705398	398-19	CA	30/09/2019	0.0987	0.0011	3.8590	0.0670	0.2841	0.0044	**1596**	**21**	1602	14	1613	22	1444	38	101	328.00	309.00
Hiltaba Suite	mineralization-related	2746110	110-2	CA	11/11/2019	0.0988	0.0012	3.9280	0.0480	0.2877	0.0022	**1599**	**22**	1622	10	1630	11	686	55	102	438.00	200.00
Hiltaba Suite	mineralization-related	2746110	110-4	CA	11/11/2019	0.0982	0.0010	3.8560	0.0390	0.2819	0.0022	**1586**	**19**	1604	8	1601	11	1689	33	101	116.10	193.30
Hiltaba Suite	mineralization-related	2746110	110-5	CA	11/11/2019	0.0998	0.0013	3.8590	0.0580	0.2802	0.0024	**1627**	**25**	1604	12	1592	12	1195	84	98	245.00	309.30

Appendix Table A4 LA-ICP MS U-Pb data for GRV and Hiltaba Suite zircon analyzed at the University of Adelaide

Unit	Group	Sample	Spot Number	Zircon Treatment	Analytical Session	Radiogenic Ratios							Age (Ma)										
						$^{207}Pb/^{206}Pb$	2σ	$^{207}Pb/^{235}U$	2σ	$^{206}Pb/^{238}U$	2σ	$^{207}Pb/^{206}Pb$	2σ	$^{207}Pb/^{235}Pb$	2σ	$^{206}Pb/^{238}U$	2σ	$^{208}Pb/^{232}Th$	2σ	% Conc	Th ppm	U ppm
Included data																						
Hiltaba Suite	mineralization-related	2746355	355-2	CA	11/11/2019	0.0979	0.0011	3.8380	0.0400	0.2849	0.0022	**1584**	**21**	1601	8	1617	11	1669	58	102	136.80	262.00
Hiltaba Suite	mineralization-related	2746355	355-4	CA	11/11/2019	0.0991	0.0012	3.8560	0.0420	0.2830	0.0020	**1609**	**22**	1604	9	1606	10	1700	31	100	161.20	252.70
Hiltaba Suite	mineralization-related	2746355	355-5	CA	11/11/2019	0.0985	0.0010	3.6480	0.0990	0.2724	0.0062	**1594**	**20**	1557	22	1552	31	1707	79	97	481.00	611.00
Hiltaba Suite	mineralization-related	2746355	355-6	CA	11/11/2019	0.0979	0.0008	3.7270	0.0440	0.2757	0.0031	**1584**	**15**	1577	10	1572	16	1695	31	99	332.00	592.00
Hiltaba Suite	mineralization-related	2746355	355-7	CA	11/11/2019	0.0983	0.0010	3.7750	0.0440	0.2792	0.0029	**1590**	**18**	1586	9	1588	15	1531	29	100	324.80	374.20
Hiltaba Suite	mineralization-related	2746355	355-9	CA	11/11/2019	0.0971	0.0009	3.6300	0.1100	0.2702	0.0071	**1567**	**17**	1550	24	1539	36	1347	36	98	324.00	468.00
Hiltaba Suite	mineralization-related	2746355	355-10	CA	11/11/2019	0.0984	0.0009	3.8830	0.0330	0.2870	0.0017	**1592**	**16**	1610	7	1627	9	1854	27	102	216.00	414.70
Hiltaba Suite	mineralization-related	2746355	355-11	CA	11/11/2019	0.0997	0.0010	3.9080	0.0510	0.2856	0.0028	**1616**	**18**	1616	11	1619	14	1769	41	100	186.80	376.00
Hiltaba Suite	mineralization-related	2746355	355-13	CA	11/11/2019	0.0987	0.0008	3.8000	0.0370	0.2800	0.0020	**1599**	**15**	1593	8	1592	10	1571	35	100	374.90	396.00
Hiltaba Suite	mineralization-related	2746355	355-14	CA	11/11/2019	0.0985	0.0012	3.9250	0.0500	0.2888	0.0024	**1596**	**23**	1619	10	1635	12	1856	33	102	136.00	145.00
Hiltaba Suite	mineralization-related	2746355	355-15	CA	11/11/2019	0.0997	0.0009	3.9050	0.0430	0.2838	0.0021	**1622**	**17**	1614	9	1610	11	1774	28	99	312.00	424.00
Hiltaba Suite	mineralization-related	2746355	355-16	CA	11/11/2019	0.0976	0.0007	3.9040	0.0440	0.2915	0.0023	**1577**	**14**	1613	9	1649	11	1743	35	105	275.90	487.10
Hiltaba Suite	mineralization-related	HDD393-01	HDD393-01 - 1	CA	27/08/2018	0.0993	0.0022	3.7500	0.1100	0.2771	0.0051	**1606**	**41**	1579	23	1576	26	1245	66	98	378.00	353.00
Hiltaba Suite	mineralization-related	HDD-393-01	HDD393-01 - 2	CA	27/08/2018	0.0973	0.0010	3.7890	0.0390	0.2822	0.0020	**1569**	**20**	1590	8	1602	10	1490	66	102	73.50	522.10
Hiltaba Suite	mineralization-related	HDD-393-01	HDD393-01 - 5	CA	27/08/2018	0.0976	0.0016	3.6380	0.0640	0.2705	0.0030	**1576**	**31**	1558	14	1545	16	1134	51	98	284.00	160.80
Hiltaba Suite	mineralization-related	HDD-393-01	HDD393-01 - 6	CA	27/08/2018	0.0967	0.0017	3.6420	0.0580	0.2712	0.0029	**1562**	**32**	1557	13	1547	15	1490	64	99	90.40	172.30
Hiltaba Suite	mineralization-related	HDD-393-01	HDD393-01 - 7	CA	27/08/2018	0.0977	0.0016	3.7930	0.0550	0.2797	0.0023	**1574**	**31**	1590	12	1591	12	1612	31	101	261.60	216.20
Hiltaba Suite	mineralization-related	HDD-393-01	HDD393-01 - 8	CA	27/08/2018	0.0981	0.0018	3.8710	0.0760	0.2876	0.0034	**1590**	**34**	1608	15	1629	17	1574	52	102	118.80	170.60
Hiltaba Suite	mineralization-related	HDD-393-01	HDD393-01 - 9	CA	27/08/2018	0.0977	0.0023	3.6900	0.0840	0.2765	0.0038	**1571**	**45**	1573	18	1573	19	1411	66	100	138.00	103.70
Hiltaba Suite	mineralization-related	HDD-393-01	HDD393-01 - 10	CA	27/08/2018	0.0988	0.0027	3.7760	0.0880	0.2784	0.0041	**1611**	**49**	1586	19	1583	21	1372	67	98	160.00	91.30
Hiltaba Suite	mineralization-related	HDD-393-01	HDD393-01 - 11	CA	27/08/2018	0.0972	0.0025	3.6470	0.0900	0.2728	0.0030	**1568**	**48**	1562	20	1554	15	1293	73	99	150.00	88.40
Hiltaba Suite	mineralization-related	HDD-393-01	HDD393-01 - 12	CA	27/08/2018	0.0985	0.0018	3.7450	0.0590	0.2749	0.0031	**1595**	**35**	1580	13	1565	16	1520	42	98	247.90	189.80
Hiltaba Suite	mineralization-related	HDD-393-01	HDD393-01 - 13	CA	27/08/2018	0.0982	0.0018	3.7620	0.0730	0.2787	0.0026	**1586**	**34**	1584	16	1584	13	1646	32	100	162.30	139.60
Hiltaba Suite	mineralization-related	HDD-393-01	HDD393-01 - 15	CA	27/08/2018	0.0981	0.0017	3.8570	0.0700	0.2842	0.0028	**1580**	**33**	1603	15	1612	14	1583	45	102	153.90	148.30
Hiltaba Suite	mineralization-related	1077-32	1077-32-1	CA	26/08/2018	0.0993	0.0025	3.8810	0.0910	0.2825	0.0037	**1607**	**47**	1612	18	1603	19	1643	48	100	119.30	86.30
Hiltaba Suite	mineralization-related	1077-32	1077-32-2	CA	26/08/2018	0.0988	0.0027	3.8400	0.1000	0.2807	0.0037	**1590**	**51**	1604	22	1594	19	1635	59	100	102.70	61.59
Hiltaba Suite	mineralization-related	1077-32	1077-32-3	CA	26/08/2018	0.0985	0.0022	3.9260	0.0890	0.2841	0.0035	**1601**	**40**	1616	18	1612	18	1637	48	101	98.00	76.50
Hiltaba Suite	mineralization-absent	1077-32	1077-32-4	CA	26/08/2018	0.0997	0.0024	3.9050	0.0800	0.2859	0.0036	**1608**	**44**	1619	16	1621	18	1294	86	101	227.00	117.00
Hiltaba Suite	mineralization-absent	1077-01	1077-01-2	CA	26/08/2018	0.0985	0.0019	3.8440	0.0570	0.2815	0.0026	**1587**	**35**	1601	12	1599	13	1637	45	101	104.50	156.00
Hiltaba Suite	mineralization-absent	1077-01	1077-01-3	CA	26/08/2018	0.0982	0.0018	3.8890	0.0600	0.2861	0.0025	**1583**	**34**	1612	13	1622	12	1671	52	102	113.20	160.00
Hiltaba Suite	mineralization-absent	1077-01	1077-01-4	CA	26/08/2018	0.0990	0.0013	3.8130	0.0540	0.2801	0.0026	**1603**	**24**	1596	12	1591	13	1591	36	99	180.70	267.00
Hiltaba Suite	mineralization-absent	1077-01	1077-01-6	CA	26/08/2018	0.0970	0.0011	3.8030	0.0440	0.2847	0.0024	**1568**	**21**	1593	9	1615	12	1681	46	103	189.00	299.00
Hiltaba Suite	mineralization-absent	1077-01	1077-01-7	CA	26/08/2018	0.0975	0.0018	3.7400	0.0640	0.2766	0.0021	**1584**	**37**	1578	14	1574	11	1611	46	99	103.50	155.90
Hiltaba Suite	mineralization-absent	1077-01	1077-01-8	CA	26/08/2018	0.0966	0.0049	3.8900	0.1800	0.2852	0.0040	**1567**	**89**	1615	36	1617	20	1644	82	103	138.40	151.40
Hiltaba Suite	mineralization-absent	1077-01	1077-01-10	CA	26/08/2018	0.0972	0.0015	3.9490	0.0550	0.2923	0.0023	**1577**	**27**	1624	11	1653	11	1453	38	105	168.30	233.50
Hiltaba Suite	mineralization-absent	1077-01	1077-01-13	CA	27/08/2018	0.0988	0.0043	3.9100	0.1400	0.2832	0.0049	**1607**	**79**	1614	30	1607	25	1653	80	100	144.60	228.90
Hiltaba Suite	mineralization-absent	1077-01	1077-01-14	CA	27/08/2018	0.0988	0.0021	3.7640	0.0720	0.2774	0.0029	**1600**	**40**	1585	16	1578	14	1549	56	99	68.90	111.00
Hiltaba Suite	mineralization-absent	1077-01	1077-01-15	CA	27/08/2018	0.0986	0.0029	3.9500	0.1200	0.2883	0.0041	**1602**	**60**	1621	25	1633	21	1688	94	102	70.60	117.90
Hiltaba Suite	mineralization-absent	1077-01	1077-01-17	CA	27/08/2018	0.0991	0.0014	3.8650	0.0560	0.2852	0.0028	**1603**	**27**	1607	12	1617	14	1552	48	101	138.50	210.90
Hiltaba Suite	mineralization-absent	1077-01	1077-01-19	CA	27/08/2018	0.0977	0.0018	3.8280	0.0540	0.2845	0.0030	**1577**	**35**	1599	12	1614	15	1474	48	102	95.70	157.70
Hiltaba Suite	mineralization-absent	1077-01	1077-01-20	CA	27/08/2018	0.0984	0.0023	3.8320	0.0830	0.2826	0.0032	**1593**	**41**	1597	17	1606	16	1456	52	101	79.20	105.30
Hiltaba Suite	mineralization-absent	1077-27	1077-27-1	CA	30/09/2019	0.0985	0.0017	3.7320	0.0660	0.2753	0.0027	**1596**	**31**	1577	14	1568	14	1433	52	98	132.80	142.40
Hiltaba Suite	mineralization-absent	1077-27	1077-27-2	CA	30/09/2019	0.1009	0.0018	3.8500	0.0720	0.2768	0.0027	**1639**	**34**	1605	15	1577	14	1311	66	96	83.00	88.30
Hiltaba Suite	mineralization-absent	1077-52	1077-52-2	CA	26/08/2018	0.0980	0.0021	3.8810	0.0850	0.2812	0.0028	**1585**	**39**	1609	17	1597	14	1608	39	101	124.30	110.00
Hiltaba Suite	mineralization-absent	1077-52	1077-52-7	CA	26/08/2018	0.1000	0.0020	3.9080	0.0760	0.2842	0.0037	**1620**	**37**	1615	16	1615	18	1548	52	100	111.50	108.10
Hiltaba Suite	mineralization-absent	1077-52	1077-52-9	CA	26/08/2018	0.1011	0.0031	3.8800	0.1100	0.2779	0.0043	**1651**	**57**	1610	23	1583	21	1547	49	96	71.71	42.25
Hiltaba Suite	mineralization-absent	1077-52	1077-52-10	CA	26/08/2018	0.0994	0.0033	3.8300	0.1400	0.2742	0.0042	**1604**	**61**	1591	28	1561	21	1556	55	97	78.00	36.90
Hiltaba Suite	mineralization-absent	1077-52	1077-52-11	CA	26/08/2018	0.1005	0.0031	3.9800	0.1200	0.2856	0.0054	**1626**	**56**	1629	24	1619	27	1409	90	100	168.50	99.40
Hiltaba Suite	mineralization-absent	1077-52	1077-52-12	CA	26/08/2018	0.0985	0.0019	3.8890	0.0770	0.2855	0.0026	**1590**	**37**	1610	16	1621	13	1660	41	102	220.20	196.90
Hiltaba Suite	mineralization-absent	HG470	HG-470 - 1	CA	22/05/2020	0.0989	0.0019	3.7550	0.0670	0.2744	0.0032	**1602**	**23**	1581	14	1562	16	1764	76	98	122.90	198.10
Hiltaba Suite	mineralization-absent	HG470	HG-470 - 2	CA	22/05/2020	0.1008	0.0026	3.9200	0.1000	0.2817	0.0038	**1642**	**28**	1615	22	1599	19	1234	73	97	141.50	120.10
Hiltaba Suite	mineralization-absent	HG470	HG-470 - 8	CA	22/05/2020	0.0995	0.0026	3.8390	0.0980	0.2800	0.0041	**1614**	**25**	1598	21	1591	20	1502	90	99	109.80	204.00
Hiltaba Suite	mineralization-absent	HG470	HG-470 - 9	CA	22/05/2020	0.0995	0.0044	3.8700	0.1900	0.2779	0.0067	**1630**	**43**	1604	36	1580	34	1420	160	97	25.80	55.40

Appendix Table A4 LA-ICP MS U-Pb data for GRV and Hiltaba Suite zircon analyzed at the University of Adelaide

Unit	Group	Sample	Spot Number	Zircon Treatment	Analytical Session	Radiogenic Ratios							Age (Ma)												
						$^{207}Pb/^{206}Pb$	2σ	$^{207}Pb/^{235}U$	2σ	$^{206}Pb/^{238}U$	2σ	$^{207}Pb/^{206}Pb$	2σ	$^{207}Pb/^{235}Pb$	2σ	$^{206}Pb/^{238}U$	2σ	$^{208}Pb/^{232}Th$	2σ	% Conc	Th ppm	U ppm
Included data																						
Hiltaba Suite	mineralization-absent	HG470	HG-470 - 10	CA	22/05/2020	0.0977	0.0031	3.7300	0.1200	0.2760	0.0048	**1584**	**40**	1570	26	1570	24	1604	86	99	73.90	114.30
Hiltaba Suite	mineralization-absent	HG470	HG-470 - 11	CA	22/05/2020	0.0998	0.0031	3.8800	0.1200	0.2822	0.0042	**1614**	**36**	1602	25	1602	21	1311	77	99	98.20	108.00
Hiltaba Suite	mineralization-absent	HG470	HG-470 - 12	CA	22/05/2020	0.0962	0.0031	3.7400	0.1200	0.2792	0.0045	**1551**	**39**	1572	26	1587	23	1500	100	102	46.60	78.20
Hiltaba Suite	mineralization-absent	HG470	HG-470 - 13	CA	22/05/2020	0.0991	0.0024	3.8120	0.0940	0.2780	0.0041	**1603**	**25**	1591	20	1581	21	1514	90	99	88.40	148.60
Hiltaba Suite	mineralization-absent	1077-198	1077-198-5	CA	30/09/2019	0.0985	0.0011	3.8430	0.0440	0.2844	0.0023	**1593**	**21**	1604	9	1613	12	1619	40	101	159.80	242.60
Hiltaba Suite	mineralization-absent	1077-198	1077-198-6	CA	30/09/2019	0.1036	0.0023	4.0800	0.1100	0.2902	0.0045	**1690**	**39**	1650	21	1642	23	1364	66	97	124.20	111.90
Hiltaba Suite	mineralization-absent	1077-198	1077-198-8	CA	30/09/2019	0.0989	0.0023	3.8610	0.0740	0.2800	0.0031	**1597**	**44**	1604	16	1591	15	910	110	100	205.00	179.40
Hiltaba Suite	mineralization-absent	1077-41	1077-41 - 2	CA	22/05/2020	0.1000	0.0047	3.7900	0.1600	0.2748	0.0049	**1613**	**54**	1581	36	1564	25	1560	140	97	38.30	89.20
Hiltaba Suite	mineralization-absent	1077-41	1077-41 - 6	CA	22/05/2020	0.0977	0.0021	3.6400	0.0710	0.2692	0.0039	**1575**	**27**	1558	16	1536	20	1264	51	98	132.10	223.20
Hiltaba Suite	mineralization-absent	1077-41	1077-41 - 7	CA	22/05/2020	0.0988	0.0066	3.8000	0.2500	0.2796	0.0072	**1598**	**50**	1581	52	1588	36	990	120	99	20.74	63.60
Hiltaba Suite	mineralization-absent	1077-41	1077-41 - 8	CA	22/05/2020	0.0971	0.0029	3.7900	0.1100	0.2815	0.0043	**1569**	**29**	1586	23	1598	21	1189	77	102	51.70	103.10
Hiltaba Suite	mineralization-absent	1077-41	1077-41 - 9	CA	22/05/2020	0.0990	0.0042	3.6800	0.1500	0.2690	0.0055	**1608**	**31**	1561	34	1535	28	826	74	95	71.00	128.00
Hiltaba Suite	mineralization-absent	1077-41	1077-41 - 11	CA	22/05/2020	0.0970	0.0030	3.8200	0.1100	0.2821	0.0042	**1568**	**31**	1590	23	1601	21	1130	70	102	49.10	102.10
Hiltaba Suite	mineralization-absent	1077-41	1077-41 - 13	CA	22/05/2020	0.0987	0.0038	3.7700	0.1400	0.2763	0.0057	**1591**	**41**	1579	30	1572	29	885	70	99	38.70	93.10
Hiltaba Suite	mineralization-absent	1077-41	1077-41 - 15	CA	22/05/2020	0.1009	0.0031	3.8500	0.1300	0.2759	0.0054	**1635**	**34**	1601	27	1570	27	846	95	96	37.90	158.50
Hiltaba Suite	mineralization-absent	1077-41	1077-41 - 16	CA	22/05/2020	0.0978	0.0024	3.8620	0.0820	0.2855	0.0036	**1578**	**25**	1606	16	1619	18	962	54	103	72.60	191.40
Hiltaba Suite	mineralization-absent	1077-41	1077-41 - 17	CA	22/05/2020	0.0962	0.0036	3.6800	0.1400	0.2727	0.0052	**1552**	**44**	1556	30	1553	26	911	78	100	25.00	67.60
Hiltaba Suite	mineralization-absent	1077-41	1077-41 - 18	CA	22/05/2020	0.0975	0.0025	3.7430	0.0930	0.2758	0.0037	**1573**	**28**	1576	20	1569	19	960	51	100	89.20	164.00
Hiltaba Suite	mineralization-absent	1077-41	1077-41 - 20	CA	22/05/2020	0.0981	0.0038	3.7500	0.1400	0.2754	0.0049	**1561**	**42**	1572	30	1571	26	856	79	101	33.20	76.30
Hiltaba Suite	mineralization-absent	1077-41	1077-41 - 21	CA	22/05/2020	0.1006	0.0030	3.9500	0.1200	0.2827	0.0048	**1630**	**34**	1618	25	1604	24	879	71	98	93.50	137.00
Hiltaba Suite	mineralization-absent	1077-41	1077-41 - 25	CA	22/05/2020	0.0987	0.0029	3.7700	0.1200	0.2762	0.0051	**1590**	**30**	1580	25	1571	26	3670	270	99	60.10	117.50
Hiltaba Suite	mineralization-absent	1077-41	1077-41 - 26	CA	22/05/2020	0.0995	0.0033	3.7300	0.1300	0.2693	0.0044	**1604**	**37**	1569	27	1536	22	3970	280	96	45.20	99.30
Hiltaba Suite	mineralization-absent	1077-41	1077-41 - 27	CA	22/05/2020	0.0974	0.0026	3.7170	0.0980	0.2731	0.0038	**1582**	**27**	1570	21	1556	19	4070	230	98	50.00	106.80
Hiltaba Suite	mineralization-absent	1077-41	1077-41 - 29	CA	22/05/2020	0.0986	0.0031	3.7090	0.0910	0.2701	0.0040	**1593**	**34**	1569	20	1541	20	3750	210	97	58.00	110.10
Hiltaba Suite	mineralization-absent	1077-41	1077-41 - 30	CA	22/05/2020	0.0979	0.0028	3.8600	0.1100	0.2835	0.0038	**1589**	**35**	1604	25	1609	19	2060	140	101	101.20	115.10
Hiltaba Suite	mineralization-absent	1077-41	1077-41 - 31	CA	22/05/2020	0.0996	0.0023	3.9410	0.0840	0.2859	0.0039	**1610**	**26**	1622	18	1620	19	3600	260	101	40.20	177.70
Hiltaba Suite	mineralization-absent	1077-41	1077-41 - 32	CA	22/05/2020	0.0975	0.0026	3.8030	0.0970	0.2819	0.0040	**1572**	**28**	1591	21	1600	20	2900	170	102	80.90	163.90
Hiltaba Suite	mineralization-absent	1077-41	1077-41 - 33	CA	22/05/2020	0.0977	0.0026	3.8000	0.1100	0.2784	0.0043	**1579**	**34**	1586	23	1583	22	2900	170	100	88.20	140.20
Hiltaba Suite	mineralization-absent	1077-41	1077-41 - 36	CA	22/05/2020	0.0973	0.0020	3.7640	0.0710	0.2794	0.0033	**1569**	**23**	1585	16	1588	17	2382	96	101	126.50	217.00
Hiltaba Suite	mineralization-absent	1077-41	1077-41 - 37	CA	22/05/2020	0.0969	0.0029	3.8300	0.1100	0.2843	0.0045	**1561**	**29**	1594	23	1612	23	2320	160	103	42.30	103.10
Hiltaba Suite	mineralization-absent	1077-41	1077-41 - 38	CA	22/05/2020	0.0976	0.0040	3.6800	0.1400	0.2725	0.0046	**1572**	**43**	1556	30	1553	23	2110	170	99	21.83	59.30
Hiltaba Suite	mineralization-absent	1077-46	1077-46 - 1	CA	26/08/2018	0.1033	0.0041	3.9600	0.1300	0.2828	0.0047	**1667**	**74**	1629	30	1605	23	1716	97	96	32.05	47.00
Hiltaba Suite	mineralization-absent	1077-46	1077-46 - 2	CA	26/08/2018	0.0963	0.0027	3.6200	0.1100	0.2779	0.0037	**1542**	**55**	1558	24	1580	19	1696	90	102	33.41	38.23
Hiltaba Suite	mineralization-absent	1077-46	1077-46 - 3	CA	26/08/2018	0.0995	0.0016	3.8230	0.0550	0.2797	0.0023	**1615**	**29**	1598	12	1589	12	1654	39	98	111.40	162.30
Hiltaba Suite	mineralization-absent	1077-46	1077-46 - 4	CA	26/08/2018	0.0979	0.0020	3.7710	0.0720	0.2799	0.0033	**1575**	**37**	1589	14	1590	16	1673	65	101	56.95	119.10
Hiltaba Suite	mineralization-absent	1077-46	1077-46 - 6	CA	26/08/2018	0.0986	0.0019	3.8660	0.0710	0.2841	0.0025	**1594**	**36**	1605	15	1612	12	1740	55	101	84.50	140.50
Hiltaba Suite	mineralization-absent	1077-46	1077-46 - 7	CA	26/08/2018	0.0994	0.0029	3.8300	0.1100	0.2803	0.0036	**1602**	**53**	1596	23	1593	18	1727	61	99	92.40	124.20
Hiltaba Suite	mineralization-absent	1077-46	1077-46 - 9	CA	26/08/2018	0.0970	0.0029	3.8690	0.0940	0.2881	0.0050	**1568**	**55**	1606	20	1631	25	1790	78	104	51.03	64.00
Hiltaba Suite	mineralization-absent	1077-46	1077-46 - 10	CA	26/08/2018	0.0999	0.0016	3.9600	0.0590	0.2872	0.0027	**1629**	**29**	1625	12	1627	13	1668	44	100	119.90	175.70
Hiltaba Suite	mineralization-absent	1077-46	1077-46 - 11	CA	26/08/2018	0.1014	0.0024	3.8920	0.0870	0.2805	0.0037	**1644**	**44**	1612	18	1593	19	1751	58	97	77.60	94.20
Hiltaba Suite	mineralization-absent	1077-46	1077-46 - 14	CA	26/08/2018	0.0976	0.0017	3.7580	0.0640	0.2784	0.0028	**1578**	**33**	1582	14	1583	14	1600	40	100	126.50	154.40
Hiltaba Suite	mineralization-absent	1077-46	1077-46 - 15	CA	26/08/2018	0.0975	0.0039	3.7800	0.1400	0.2810	0.0056	**1584**	**73**	1580	30	1595	28	1684	67	101	53.76	42.54
Hiltaba Suite	mineralization-absent	1077-46	1077-46 - 16	CA	27/08/2018	0.1003	0.0019	3.8980	0.0740	0.2819	0.0023	**1631**	**36**	1611	15	1601	12	1266	47	98	118.40	122.60
Hiltaba Suite	mineralization-absent	1077-46	1077-46 - 19	CA	27/08/2018	0.0963	0.0039	3.8200	0.1500	0.2842	0.0051	**1584**	**79**	1597	31	1612	26	1628	83	102	41.50	37.06
Hiltaba Suite	mineralization-absent	1077-46	1077-46 - 20	CA	27/08/2018	0.0985	0.0020	3.8740	0.0760	0.2839	0.0028	**1605**	**39**	1606	16	1610	14	1581	53	100	72.65	96.05
Hiltaba Suite	mineralization-absent	1077-59	1077-59 - 2	CA	21/05/2020	0.0970	0.0034	3.6660	0.1200	0.2734	0.0047	**1561**	**42**	1558	25	1557	24	1586	92	100	140.30	174.70
Hiltaba Suite	mineralization-absent	1077-59	1077-59 - 4	CA	21/05/2020	0.0960	0.0023	3.6750	0.0800	0.2763	0.0037	**1548**	**24**	1562	17	1572	19	1591	68	102	135.60	155.90
Hiltaba Suite	mineralization-absent	1077-59	1077-59 - 5	CA	21/05/2020	0.0990	0.0024	3.8010	0.0920	0.2767	0.0031	**1600**	**27**	1589	19	1574	16	1501	86	98	73.30	157.60
Hiltaba Suite	mineralization-absent	1077-59	1077-59 - 6	CA	21/05/2020	0.0961	0.0025	3.7510	0.0960	0.2822	0.0049	**1542**	**29**	1578	21	1601	25	969	44	104	156.00	169.10
Hiltaba Suite	mineralization-absent	1077-59	1077-59 - 8	CA	21/05/2020	0.0969	0.0023	3.8470	0.0850	0.2890	0.0046	**1562**	**27**	1600	18	1636	23	809	39	105	199.70	234.00
Hiltaba Suite	mineralization-absent	1077-59	1077-59 - 9	CA	21/05/2020	0.0957	0.0028	3.6720	0.0870	0.2784	0.0038	**1534**	**30**	1561	19	1583	19	877	46	103	98.80	158.20
Hiltaba Suite	mineralization-absent	1077-59	1077-59 - 10	CA	21/05/2020	0.0968	0.0020	3.7250	0.0790	0.2784	0.0038	**1563**	**22**	1573	17	1583	19	824	32	101	220.00	274.00
Hiltaba Suite	mineralization-absent	1077-59	1077-59 - 11	CA	21/05/2020	0.0978	0.0021	3.8140	0.0880	0.2814	0.0043	**1578**	**22**	1592	19	1597	21	850	37	101	196.00	188.50

Appendix Table A4 LA-ICP MS U-Pb data for GRV and Hiltaba Suite zircon analyzed at the University of Adelaide

Unit	Group	Sample	Spot Number	Zircon Treatment	Analytical Session	Radiogenic Ratios						Age (Ma)									
Included data						$^{207}Pb/^{206}Pb$	2σ	$^{207}Pb/^{235}U$	2σ	$^{206}Pb/^{238}U$	2σ	**$^{207}Pb/^{206}Pb$**	**2σ**	$^{207}Pb/^{235}Pb$	2σ	$^{206}Pb/^{238}U$	2σ	$^{208}Pb/^{232}Th$	2σ	% Conc	Th ppm	U ppm
Hiltaba Suite	mineralization-absent	1077-59	1077-59 - 13	CA	21/05/2020	0.0973	0.0027	3.7630	0.0970	0.2805	0.0036	**1573**	**27**	1582	21	1594	18	717	39	101	141.00	214.00
Hiltaba Suite	mineralization-absent	1077-59	1077-59 - 14	CA	21/05/2020	0.0971	0.0019	3.7050	0.0760	0.2762	0.0037	**1565**	**19**	1569	16	1572	19	764	35	100	241.70	310.00
Hiltaba Suite	mineralization-absent	1077-59	1077-59 - 15	CA	21/05/2020	0.0997	0.0034	3.8900	0.1400	0.2823	0.0057	**1614**	**38**	1601	30	1601	29	675	36	99	113.00	84.20
Hiltaba Suite	mineralization-absent	1077-59	1077-59 - 16	CA	21/05/2020	0.0985	0.0043	3.7900	0.1400	0.2814	0.0064	**1591**	**44**	1585	30	1597	32	656	34	100	137.20	105.90
Hiltaba Suite	mineralization-absent	1077-59	1077-59 - 20	CA	21/05/2020	0.0976	0.0025	3.7190	0.0890	0.2756	0.0035	**1573**	**26**	1571	19	1568	18	759	26	100	198.10	238.80
Hiltaba Suite	mineralization-absent	1077-59	1077-59 - 22	CA	21/05/2020	0.0981	0.0033	3.7400	0.1300	0.2790	0.0059	**1572**	**35**	1572	28	1584	30	802	45	101	88.70	83.70
Hiltaba Suite	mineralization-absent	1077-59	1077-59 - 23	CA	21/05/2020	0.1003	0.0026	3.7800	0.1000	0.2735	0.0040	**1624**	**26**	1587	20	1558	20	922	55	96	128.00	161.70
Hiltaba Suite	mineralization-absent	1077-59	1077-59 - 26	CA	21/05/2020	0.0974	0.0029	3.6420	0.0980	0.2724	0.0048	**1566**	**31**	1554	22	1552	24	-41100	5900	99	172.10	175.90
Hiltaba Suite	mineralization-absent	1077-59	1077-59 - 30	CA	21/05/2020	0.0971	0.0023	3.7360	0.0960	0.2798	0.0052	**1567**	**27**	1575	21	1589	26	-73000	20000	101	179.50	234.90
Hiltaba Suite	mineralization-absent	1077-59	1077-59 - 34	CA	21/05/2020	0.0997	0.0024	3.8370	0.0870	0.2776	0.0038	**1605**	**27**	1597	18	1579	19	7980	310	98	121.90	142.70
Hiltaba Suite	mineralization-absent	1077-59	1077-59 - 35	CA	21/05/2020	0.0980	0.0028	3.8300	0.1000	0.2849	0.0050	**1573**	**27**	1596	23	1615	25	5830	250	103	157.60	151.00
Hiltaba Suite	mineralization-absent	1077-59	1077-59 - 36	CA	21/05/2020	0.0961	0.0022	3.7290	0.0880	0.2796	0.0034	**1545**	**23**	1573	19	1589	17	4290	150	103	189.20	186.80
Hiltaba Suite	mineralization-absent	1077-59	1077-59 - 37	CA	21/05/2020	0.0981	0.0021	3.7220	0.0880	0.2763	0.0042	**1592**	**22**	1575	20	1572	21	3490	140	99	224.00	231.00
Hiltaba Suite	mineralization-absent	1077-59	1077-59 - 39	CA	21/05/2020	0.0960	0.0021	3.7840	0.0890	0.2857	0.0047	**1548**	**26**	1588	18	1619	23	2710	130	105	109.90	175.80
Hiltaba Suite	mineralization-absent	1077-59	1077-59 - 38	CA	21/05/2020	0.0962	0.0025	3.7000	0.1000	0.2774	0.0040	**1570**	**25**	1565	22	1578	20	2950	140	101	96.10	156.00
Hiltaba Suite	mineralization-absent	1077-59	1077-59 - 41	CA	21/05/2020	0.0978	0.0024	3.7730	0.0900	0.2801	0.0036	**1580**	**28**	1586	19	1591	18	1918	83	101	150.20	163.00
Hiltaba Suite	mineralization-absent	1077-59	1077-59 - 43	CA	21/05/2020	0.0969	0.0025	3.7900	0.1000	0.2822	0.0042	**1566**	**28**	1586	22	1602	21	1707	95	102	89.00	138.90
Hiltaba Suite	mineralization-absent	1077-59	1077-59 - 45	CA	21/05/2020	0.0997	0.0027	3.8900	0.1000	0.2821	0.0038	**1608**	**33**	1607	21	1601	19	1463	75	100	125.80	167.60
Hiltaba Suite	mineralization-absent	1077-59	1077-59 - 47	CA	21/05/2020	0.0987	0.0025	3.6900	0.0870	0.2705	0.0034	**1600**	**30**	1568	20	1543	17	1515	57	96	131.20	146.10
Hiltaba Suite	mineralization-absent	1077-59	1077-59 - 48	CA	21/05/2020	0.0991	0.0025	3.8530	0.0900	0.2795	0.0039	**1608**	**27**	1601	18	1588	20	1500	60	99	178.00	188.10
Hiltaba Suite	mineralization-absent	1077-59	1077-59 - 49	CA	21/05/2020	0.0956	0.0024	3.7040	0.0780	0.2794	0.0043	**1542**	**27**	1572	18	1587	22	1692	79	103	115.90	123.30
Hiltaba Suite	mineralization-absent	1077-59	1077-59 - 50	CA	21/05/2020	0.0984	0.0025	3.8130	0.0920	0.2797	0.0042	**1590**	**25**	1591	19	1589	21	1721	79	100	140.80	150.90
Hiltaba Suite	mineralization-absent	1077-59	1077-59 - 52	CA	21/05/2020	0.0980	0.0034	3.8300	0.1200	0.2815	0.0042	**1583**	**34**	1591	27	1598	21	1980	120	101	68.40	112.70
Hiltaba Suite	mineralization-absent	1077-59	1077-59 - 57	CA	21/05/2020	0.0994	0.0018	3.8820	0.0680	0.2808	0.0029	**1607**	**20**	1608	14	1595	15	2224	96	99	199.00	351.40
Hiltaba Suite	mineralization-absent	1077-59	1077-59 - 58	CA	21/05/2020	0.0995	0.0024	3.8530	0.0750	0.2801	0.0040	**1612**	**27**	1602	16	1592	20	1904	76	99	276.40	317.00
Hiltaba Suite	mineralization-absent	1077-59	1077-59 - 60	CA	21/05/2020	0.0988	0.0039	3.8400	0.1400	0.2810	0.0055	**1585**	**44**	1591	30	1595	28	2430	130	101	72.10	69.60
Hiltaba Suite	mineralization-absent	1077-59	1077-59 - 61	CA	21/05/2020	0.0977	0.0026	3.9200	0.1100	0.2873	0.0032	**1572**	**30**	1615	22	1630	17	2170	100	104	73.50	141.80
Hiltaba Suite	mineralization-absent	1077-63	1077-63 - 1	CA	21/05/2020	0.0985	0.0026	3.9250	0.0990	0.2864	0.0043	**1592**	**29**	1614	20	1623	22	3250	160	102	117.70	106.60
Hiltaba Suite	mineralization-absent	1077-63	1077-63 - 2	CA	21/05/2020	0.0979	0.0033	3.7700	0.1100	0.2778	0.0046	**1573**	**35**	1580	22	1579	23	3440	170	100	100.10	104.00
Hiltaba Suite	mineralization-absent	1077-63	1077-63 - 3	CA	21/05/2020	0.0990	0.0034	3.8400	0.1100	0.2805	0.0045	**1606**	**38**	1598	24	1593	23	3970	210	99	86.90	85.70
Hiltaba Suite	mineralization-absent	1077-63	1077-63 - 4	CA	21/05/2020	0.0990	0.0031	3.8700	0.1100	0.2829	0.0047	**1610**	**33**	1601	22	1605	24	4500	230	100	80.50	82.20
Hiltaba Suite	mineralization-absent	1077-63	1077-63 - 6	CA	21/05/2020	0.0974	0.0037	3.8000	0.1400	0.2802	0.0054	**1580**	**38**	1586	30	1591	27	4880	310	101	47.90	64.80
Hiltaba Suite	mineralization-absent	1077-63	1077-63 - 7	CA	21/05/2020	0.0991	0.0037	3.8000	0.1300	0.2781	0.0056	**1600**	**41**	1590	27	1581	28	4860	220	99	335.00	162.00
Hiltaba Suite	mineralization-absent	1077-63	1077-63 - 9	CA	21/05/2020	0.0989	0.0049	3.8000	0.1800	0.2792	0.0062	**1589**	**51**	1582	39	1591	32	5950	340	100	66.40	52.10
Hiltaba Suite	mineralization-absent	1077-63	1077-63 - 10	CA	21/05/2020	0.0985	0.0026	3.8070	0.0980	0.2772	0.0038	**1596**	**25**	1590	21	1577	19	5330	160	99	194.00	139.60
Hiltaba Suite	mineralization-absent	1077-63	1077-63 - 13	CA	21/05/2020	0.0980	0.0030	3.7200	0.1100	0.2739	0.0041	**1580**	**33**	1570	23	1560	21	3910	130	99	214.80	124.40
Hiltaba Suite	mineralization-absent	1077-63	1077-63 - 17	CA	21/05/2020	0.0997	0.0029	3.9100	0.1100	0.2833	0.0047	**1613**	**31**	1610	23	1607	23	1990	82	100	158.70	135.70
Hiltaba Suite	mineralization-absent	1077-63	1077-63 - 18	CA	21/05/2020	0.0977	0.0025	3.7400	0.0870	0.2780	0.0040	**1577**	**27**	1576	19	1581	20	938	41	100	172.50	145.00
Hiltaba Suite	mineralization-absent	1077-63	1077-63 - 19	CA	21/05/2020	0.0991	0.0025	3.7890	0.0850	0.2766	0.0040	**1604**	**24**	1589	17	1573	20	945	35	98	161.40	153.10
Hiltaba Suite	mineralization-absent	1077-63	1077-63 - 21	CA	21/05/2020	0.0986	0.0035	3.7400	0.1400	0.2738	0.0047	**1593**	**39**	1568	31	1559	24	931	44	98	87.90	81.40
Hiltaba Suite	mineralization-absent	1077-63	1077-63 - 22	CA	21/05/2020	0.0979	0.0031	3.7500	0.1100	0.2798	0.0045	**1581**	**30**	1579	25	1590	22	997	62	101	83.40	96.00
Hiltaba Suite	mineralization-absent	1077-63	1077-63 - 23	CA	21/05/2020	0.0970	0.0021	3.8090	0.0820	0.2819	0.0037	**1580**	**24**	1594	18	1600	18	1019	38	101	191.70	169.60
Hiltaba Suite	mineralization-absent	1077-63	1077-63 - 24	CA	21/05/2020	0.0980	0.0032	3.7100	0.1000	0.2739	0.0054	**1586**	**26**	1571	22	1560	27	853	49	98	125.30	122.20
Hiltaba Suite	mineralization-absent	1077-63	1077-63 - 25	CA	21/05/2020	0.0987	0.0034	3.8400	0.1200	0.2801	0.0053	**1589**	**32**	1595	25	1591	27	1080	53	100	93.10	87.90
Hiltaba Suite	mineralization-absent	1077-63	1077-63 - 27	CA	21/05/2020	0.0985	0.0024	3.7890	0.0910	0.2782	0.0039	**1590**	**24**	1586	20	1582	20	1131	48	99	139.90	128.70
Hiltaba Suite	mineralization-absent	1077-63	1077-63 - 29	CA	21/05/2020	0.0981	0.0035	3.7600	0.1500	0.2756	0.0058	**1595**	**41**	1584	28	1568	29	1175	43	98	143.70	80.40
Hiltaba Suite	mineralization-absent	1077-63	1077-63 - 32	CA	21/05/2020	0.0983	0.0029	3.7400	0.1100	0.2752	0.0043	**1586**	**32**	1573	23	1566	22	1491	71	99	105.30	102.00
Hiltaba Suite	mineralization-absent	1077-63	1077-63 - 33	CA	21/05/2020	0.0973	0.0049	3.6800	0.1700	0.2756	0.0065	**1561**	**41**	1550	37	1567	33	1501	81	100	99.90	47.50
Hiltaba Suite	mineralization-absent	1077-63	1077-63 - 34	CA	21/05/2020	0.0979	0.0030	3.7400	0.1100	0.2780	0.0048	**1578**	**33**	1573	24	1580	24	1614	72	100	211.00	127.10
Hiltaba Suite	mineralization-absent	1077-63	1077-63 - 38	CA	21/05/2020	0.0997	0.0037	3.7500	0.1400	0.2726	0.0055	**1612**	**39**	1577	29	1553	28	1900	100	96	103.40	54.90
Hiltaba Suite	mineralization-absent	1077-63	1077-63 - 39	CA	21/05/2020	0.0996	0.0025	3.7450	0.0760	0.2726	0.0040	**1613**	**28**	1580	17	1553	20	1723	68	96	124.30	112.80
Hiltaba Suite	mineralization-absent	1077-63	1077-63 - 40	CA	21/05/2020	0.0964	0.0045	3.7700	0.1700	0.2837	0.0052	**1560**	**45**	1570	37	1609	26	1780	89	103	82.60	54.50

Appendix Table A4 LA-ICP MS U-Pb data for GRV and Hiltaba Suite zircon analyzed at the University of Adelaide

Unit	Group	Sample	Spot Number	Zircon Treatment	Disc.	Other	Analytical Session	Radiogenic Ratios								Age (Ma)										
								$^{207}Pb/^{206}Pb$	2σ	$^{207}Pb/^{235}U$	2σ	$^{206}Pb/^{238}U$	2σ	$^{207}Pb/^{206}Pb$	2σ	$^{207}Pb/^{235}Pb$	2σ	$^{206}Pb/^{238}U$	2σ	$^{208}Pb/^{232}Th$	2σ	% Conc	Th ppm	U ppm
Rejected data																								
LGRV	mineralization-related	18-TAR-14	18-TAR-14 - 10	CA	>5%		26/08/2018	0.1223	0.0029	4.5400	0.1000	0.2703	0.0032	1983	42	1736	18	1542	16	1127	44	78	430.00	172.00
LGRV	mineralization-related	18-TAR-14	18-TAR-14 - 11	CA	>5%		27/08/2018	0.1035	0.0030	3.9700	0.1100	0.2750	0.0036	1713	56	1623	23	1566	18	1126	89	91	133.00	53.74
LGRV	mineralization-related	18-TAR-14	18-TAR-14 - 12	CA	>5%		27/08/2018	0.1184	0.0027	4.2960	0.0820	0.2626	0.0033	1926	40	1694	15	1503	17	911	31	78	379.00	132.50
LGRV	mineralization-related	2729189	189 - 10	CA		inherited	11/11/2019	0.1005	0.0010	3.8880	0.0380	0.2771	0.0020	**1635**	**17**	1610	8	1577	10	1511	38	96	276.50	321.00
LGRV	mineralization-related	2729189	189 - 12	CA		inherited >370	11/11/2019	0.1126	0.0014	5.2520	0.0590	0.3371	0.0037	**1839**	**23**	1860	10	1875	17	1061	64	102	301.00	322.80
Hiltaba Suite	mineralization-related	2705391	391-1	CA		ppm P	30/09/2019	0.0989	0.0012	3.9410	0.0530	0.2878	0.0021	**1603**	**22**	1622	11	1630	10	1598	45	102	121.80	176.30
Hiltaba Suite	mineralization-related	2705391	391-2	CA	>5%		30/09/2019	0.0978	0.0011	4.2150	0.0630	0.3105	0.0032	**1582**	**22**	1677	13	1742	16	1535	41	110	140.40	149.10
Hiltaba Suite	mineralization-related	2705391	391-4	CA	>5%		30/09/2019	0.1006	0.0020	4.4340	0.0880	0.3180	0.0040	**1630**	**36**	1717	16	1780	20	1891	51	109	98.90	117.30
Hiltaba Suite	mineralization-related	2705391	391-8	CA	>5%		30/09/2019	0.0990	0.0010	4.1590	0.0640	0.3041	0.0043	**1603**	**19**	1665	13	1710	21	1170	66	107	343.00	221.90
Hiltaba Suite	mineralization-related	2705391	391-10	CA			30/09/2019	0.0993	0.0010	3.9310	0.0420	0.2854	0.0019	**1614**	**20**	1620	9	1618	10	1659	25	100	185.20	195.10
Hiltaba Suite	mineralization-related	2705391	391-12	CA	>5%		30/09/2019	0.0987	0.0010	4.1250	0.0410	0.3003	0.0023	**1599**	**18**	1660	8	1692	11	814	42	106	422.00	307.80
Hiltaba Suite	mineralization-related	2705391	391-15	CA	>5%		30/09/2019	0.0991	0.0012	4.1440	0.0440	0.3005	0.0023	**1607**	**22**	1662	9	1693	11	1057	27	105	390.00	330.70
Hiltaba Suite	mineralization-related	2705391	391-19	CA	>5%		30/09/2019	0.0973	0.0024	3.9200	0.1000	0.2904	0.0051	**1560**	**47**	1621	20	1643	25	1556	57	105	79.30	82.60
Hiltaba Suite	mineralization-related	2705398	398-5	CA	>5%		30/09/2019	0.0996	0.0021	3.6760	0.0770	0.2685	0.0033	**1618**	**42**	1565	17	1533	17	1529	59	95	33.50	66.30
Hiltaba Suite	mineralization-related	2705398	398-7	CA	>5%		30/09/2019	0.0967	0.0021	4.0020	0.0790	0.2990	0.0032	**1555**	**40**	1638	16	1686	16	418	29	108	310.00	106.90
Hiltaba Suite	mineralization-related	2705398	398-12	CA	>5%	>370 ppm P	30/09/2019	0.0979	0.0017	4.0510	0.0650	0.3019	0.0034	**1587**	**32**	1644	13	1700	17	1577	53	107	76.60	99.90
Hiltaba Suite	mineralization-related	2705398	398-18	CA			30/09/2019	0.0988	0.0010	3.9090	0.0420	0.2865	0.0017	**1601**	**18**	1616	9	1625	8	1713	32	101	182.40	263.80
Hiltaba Suite	mineralization-related	2705398	398-20	CA	>5%		30/09/2019	0.0956	0.0015	4.0160	0.0570	0.3064	0.0042	**1535**	**29**	1636	12	1722	21	774	52	112	317.00	179.00
Hiltaba Suite	mineralization-related	2746110	110-1	CA	>5%		11/11/2019	0.0980	0.0019	3.5400	0.0780	0.2585	0.0038	**1587**	**38**	1537	17	1482	19	356	71	93	1450.00	233.20
Hiltaba Suite	mineralization-related	2746110	110-3	CA	>5%		11/11/2019	0.0970	0.0009	3.2730	0.0320	0.2421	0.0015	**1566**	**17**	1474	8	1397	8	1358	43	89	331.90	513.70
Hiltaba Suite	mineralization-related	2746355	355-1	CA		no data	11/11/2019	NA	NA	NA	NA	NA	NA	**NA**	**NA**	NA	NA	NA	NA	NA	NA	NA	b.d.l.	b.d.l.
Hiltaba Suite	mineralization-related	2746355	355-3	CA	>5%		11/11/2019	0.0978	0.0015	3.4600	0.1400	0.2580	0.0089	**1578**	**29**	1515	33	1477	46	1325	78	94	352.00	457.00
Hiltaba Suite	mineralization-related	2746355	355-8	CA		inherited	11/11/2019	0.1021	0.0009	4.1920	0.0530	0.2995	0.0031	**1662**	**17**	1672	10	1690	15	2172	59	102	224.80	397.00
Hiltaba Suite	mineralization-related	2746355	355-12	CA		inherited	11/11/2019	0.1042	0.0027	4.3200	0.1100	0.3047	0.0035	**1684**	**46**	1695	20	1716	18	2041	93	102	25.10	47.50
Hiltaba Suite	mineralization-related	2746355	355-17	CA	>5%		11/11/2019	0.0978	0.0015	3.9780	0.0730	0.2977	0.0038	**1587**	**27**	1628	15	1679	19	1842	52	106	138.00	174.00
Hiltaba Suite	mineralization-related	2746355	355-18	CA	>5%		11/11/2019	0.0990	0.0008	4.0780	0.0490	0.3003	0.0031	**1603**	**15**	1650	10	1692	15	1693	50	106	340.00	488.70
Hiltaba Suite	mineralization-related	2746356*	356-1	CA	>5%		11/11/2019	0.0953	0.0009	2.0050	0.0320	0.1520	0.0020	**1530**	**18**	1116	11	912	11	736	20	60	848.00	685.00
Hiltaba Suite	mineralization-related	2746356*	356-2	CA	>5%		11/11/2019	0.0981	0.0015	2.3710	0.0550	0.1713	0.0031	**1586**	**27**	1235	16	1019	17	1076	28	64	677.00	634.00
Hiltaba Suite	mineralization-related	2746356*	356-3	CA	>5%		11/11/2019	0.0857	0.0009	1.0570	0.0140	0.0900	0.0007	**1338**	**21**	733	7	555	4	630	9	42	1244.00	862.00
Hiltaba Suite	mineralization-related	2746356*	356-4	CA	>5%		11/11/2019	0.0876	0.0010	0.7510	0.0100	0.0626	0.0006	**1369**	**21**	570	6	391	4	471	8	29	1489.00	
Hiltaba Suite	mineralization-related	2746356*	356-5	CA	>5%	> 370	11/11/2019	0.0992	0.0013	4.8060	0.0600	0.3472	0.0039	**1608**	**25**	1785	10	1921	19	703	55	119	1000.00	250.50
Hiltaba Suite	mineralization-related	2746356*	356-6	CA	>5%	ppm P	11/11/2019	0.0961	0.0009	4.1230	0.0560	0.3096	0.0039	**1550**	**17**	1657	11	1738	19	247	39	112	10800.0	650.0
Hiltaba Suite	mineralization-related	2746356*	356-7	CA	>5%		11/11/2019	0.0999	0.0009	4.3740	0.0490	0.3182	0.0032	**1624**	**17**	1708	9	1780	15	218	15	110	2160.00	333.70
Hiltaba Suite	mineralization-related	2746356*	356-8	CA	>5%	> 370	11/11/2019	0.0877	0.0012	1.1380	0.0480	0.0927	0.0032	**1386**	**27**	766	23	574	19	440	20	41	1750.00	766.00
Hiltaba Suite	mineralization-related	2746356*	356-9	CA	>5%	ppm P	11/11/2019	0.0820	0.0009	0.7422	0.0083	0.0653	0.0004	**1248**	**22**	563	5	408	3	464	7	33	1947.00	1101.0
Hiltaba Suite	mineralization-related	2746356*	356-10	CA		> 370	11/11/2019	0.0991	0.0008	3.8700	0.0390	0.2831	0.0020	**1609**	**15**	1608	8	1607	10	1608	18	100	799.00	538.10
Hiltaba Suite	mineralization-related	2746356*	356-11	CA	>5%	ppm P	11/11/2019	0.0877	0.0011	0.7910	0.0110	0.0653	0.0007	**1372**	**24**	592	6	408	4	483	7	30	1406.00	940.00
Hiltaba Suite	mineralization-related	2746356*	HDD-393-01 - 14	CA	>5%		27/08/2018	0.0965	0.0015	3.9330	0.0570	0.2935	0.0028	**1554**	**30**	1621	12	1660	14	1685	38	107	151.80	172.90
Hiltaba Suite	mineralization-related	1077-32	1077-32-5	CA		inherited	26/08/2018	0.1033	0.0028	4.1200	0.1300	0.2895	0.0063	**1678**	**51**	1656	27	1639	32	493	66	98	1130.00	167.50
Hiltaba Suite	mineralization-absent	1077-01	1077-01-1	CA		inherited	26/08/2018	0.1026	0.0026	4.3700	0.1000	0.3074	0.0045	**1667**	**46**	1710	18	1728	22	1449	86	104	147.00	184.00
Hiltaba Suite	mineralization-absent	1077-01	1077-01-5	CA	>5%		26/08/2018	0.0983	0.0019	4.0190	0.0710	0.2964	0.0031	**1588**	**36**	1640	14	1675	16	1669	49	105	123.00	137.20
Hiltaba Suite	mineralization-absent	1077-01	1077-01-9	CA	>5%		26/08/2018	0.0975	0.0020	3.9580	0.0820	0.2945	0.0038	**1574**	**40**	1626	16	1664	19	1696	59	106	112.00	143.40
Hiltaba Suite	mineralization-absent	1077-01	1077-01-11	CA	>5%		27/08/2018	0.0990	0.0020	4.2420	0.0940	0.3060	0.0042	**1602**	**38**	1679	18	1721	21	549	28	107	291.00	115.61
Hiltaba Suite	mineralization-absent	1077-01	1077-01-12	CA	>5%		27/08/2018	0.0951	0.0023	3.8560	0.0800	0.2901	0.0036	**1538**	**46**	1603	17	1641	18	1597	79	107	55.80	103.70
Hiltaba Suite	mineralization-absent	1077-01	1077-01-16	CA	>5%		27/08/2018	0.0976	0.0013	3.9710	0.0680	0.2947	0.0027	**1578**	**26**	1629	13	1667	13	1505	47	106	185.10	274.80
Hiltaba Suite	mineralization-absent	1077-01	1077-01-18	CA		inherited	27/08/2018	0.1030	0.0019	4.4420	0.0810	0.3115	0.0036	**1680**	**36**	1720	16	1748	18	1733	47	104	97.90	130.10

Appendix Table A4 LA-ICP MS U-Pb data for GRV and Hiltaba Suite zircon analyzed at the University of Adelaide

Unit	Group	Sample	Spot Number	Zircon Treatment	Disc.	Other	Analytical Session	Radiogenic Ratios								Age (Ma)									
								$^{207}Pb/^{206}Pb$	2σ	$^{207}Pb/^{235}U$	2σ	$^{206}Pb/^{238}U$	2σ	**$^{207}Pb/^{206}Pb$**	**2σ**	$^{207}Pb/^{235}Pb$	2σ	$^{206}Pb/^{238}U$	2σ	$^{208}Pb/^{232}Th$	2σ	% Conc	Th ppm	U ppm
Rejected data																									
Hiltaba Suite	mineralization-absent	1077-27	1077-27-4	CA	>5%		30/09/2019	0.1191	0.0018	4.3200	0.1000	0.2665	0.0051	**1940**	**26**	1694	20	1521	26	1380	50	78	83.30	112.60
						contami-nation																			
Hiltaba Suite	mineralization-absent	1077-27	1077-27-3	CA			30/09/2019	0.0788	0.0017	2.1580	0.0490	0.1992	0.0024	**1164**	**43**	1167	16	1171	13	1287	41	101	73.50	81.10
Hiltaba Suite	mineralization-absent	1077-27	1077-27-5	CA	>5%		30/09/2019	0.1015	0.0016	3.7600	0.0690	0.2676	0.0031	**1651**	**28**	1586	14	1530	16	1318	60	93	113.90	163.10
Hiltaba Suite	mineralization-absent	1077-52	1077-52-3	CA	>5%		26/08/2018	0.0989	0.0036	3.9600	0.1400	0.2920	0.0048	**1571**	**69**	1624	29	1650	24	1689	61	105	64.65	42.18
Hiltaba Suite	mineralization-absent	1077-52	1077-52-4	CA	>5%		26/08/2018	0.1294	0.0074	5.7700	0.3600	0.3291	0.0085	**2071**	**99**	1946	49	1832	41	1349	94	88	75.70	26.99
Hiltaba Suite	mineralization-absent	1077-52	1077-52-5	CA	>5%		26/08/2018	0.1248	0.0044	5.8500	0.2500	0.3373	0.0068	**2012**	**63**	1953	37	1879	34	1949	97	93	142.00	95.10
Hiltaba Suite	mineralization-absent	1077-52	1077-52-6	CA	>5%		26/08/2018	0.1080	0.0050	4.2500	0.2100	0.2873	0.0066	**1750**	**87**	1684	39	1626	33	1656	78	93	39.00	23.90
Hiltaba Suite	mineralization-absent	1077-52	1077-52-8	CA	>5%		26/08/2018	0.0962	0.0022	3.8300	0.1000	0.2875	0.0036	**1544**	**45**	1594	21	1628	18	1641	56	105	57.00	72.62
Hiltaba Suite	mineralization-absent	HG470	HG-470 - 3	CA		inherited	21/05/2020	0.1041	0.0044	4.4500	0.1900	0.3102	0.0068	**1695**	**42**	1709	35	1740	33	1750	160	103	66.20	88.20
Hiltaba Suite	mineralization-absent	HG470	HG-470 - 4	CA	> 5%	inherited	21/05/2020	0.1028	0.0019	3.9330	0.0660	0.2766	0.0030	**1673**	**21**	1618	14	1574	15	1073	93	94	186.00	232.40
Hiltaba Suite	mineralization-absent	HG470	HG-470 - 5	CA	> 5%	inherited	21/05/2020	0.1049	0.0034	4.1300	0.1300	0.2861	0.0045	**1710**	**37**	1656	27	1621	22	1300	120	95	147.00	118.70
Hiltaba Suite	mineralization-absent	HG470	HG-470 - 6	CA	> 5%		21/05/2020	0.1044	0.0038	3.9900	0.1400	0.2791	0.0048	**1697**	**41**	1631	30	1586	24	760	120	93	510.00	156.50
Hiltaba Suite	mineralization-absent	HG470	HG-470 - 7	CA	> 5%		21/05/2020	0.1031	0.0050	3.9000	0.2100	0.2754	0.0084	**1670**	**55**	1604	42	1586	34	1070	130	95	60.50	64.60
						> 370																			
Hiltaba Suite	mineralization-absent	1077-198	1077-198-1	CA	>5%	ppm P	30/09/2019	0.0989	0.0013	3.9550	0.0480	0.2892	0.0026	**1598**	**25**	1624	10	1639	13	1702	38	103	124.00	180.90
						not																			
Hiltaba Suite	mineralization-absent	1077-198	1077-198-2	CA	>5%	zircon	30/09/2019	0.2499	0.0044	209.00	36.000	5.7500	0.9700	**3176**	**29**	5050	220	10800	1000	2900	210	340	16800	345.00
						> 370																			
Hiltaba Suite	mineralization-absent	1077-198	1077-198-3	CA	>5%	ppm P	30/09/2019	0.2719	0.0015	23.5900	0.2000	0.6305	0.0051	**3316**	**8**	3251	8	3153	20	2311	70	95	258.10	255.00
						> 370																			
Hiltaba Suite	mineralization-absent	1077-198	1077-198-4	CA	>5%	ppm P	30/09/2019	0.0990	0.0009	3.8570	0.0340	0.2816	0.0022	**1606**	**17**	1605	7	1600	11	1373	29	100	258.00	244.60
Hiltaba Suite	mineralization-absent	1077-198	1077-198-7	CA	>5%		30/09/2019	0.0994	0.0012	3.6700	0.0460	0.2679	0.0022	**1615**	**22**	1567	10	1531	11	1292	52	95	198.00	194.60
Hiltaba Suite	mineralization-absent	1077-198	1077-198-9	CA	>5%		30/09/2019	0.0989	0.0014	3.4430	0.0550	0.2526	0.0031	**1602**	**26**	1514	13	1451	16	929	63	91	275.00	231.70
Hiltaba Suite	mineralization-absent	1077-198	1077-198-10	CA	>5%		30/09/2019	0.1110	0.0024	4.9500	0.9200	0.3320	0.0580	**1815**	**38**	1640	110	1660	220	1155	99	91	425.00	390.00
						> 370																			
Hiltaba Suite	mineralization-absent	1077-198	1077-198-11	CA	>5%	ppm P	30/09/2019	0.1005	0.0017	3.6920	0.0600	0.2668	0.0027	**1632**	**29**	1569	13	1526	14	992	46	94	220.10	204.10
Hiltaba Suite	mineralization-absent	1077-41	1077-41 - 1	CA	> 5%		21/05/2020	0.1004	0.0032	4.1800	0.1500	0.3010	0.0056	**1617**	**36**	1662	29	1700	26	990	140	105	147.00	84.00
Hiltaba Suite	mineralization-absent	1077-41	1077-41 - 3	CA	> 5%		21/05/2020	0.1009	0.0032	3.7400	0.1300	0.2677	0.0055	**1640**	**32**	1571	28	1528	28	1314	75	93	87.10	150.00
Hiltaba Suite	mineralization-absent	1077-41	1077-41 - 4	CA	> 5%		21/05/2020	0.0980	0.0041	3.4800	0.1400	0.2575	0.0055	**1588**	**39**	1519	31	1477	28	1028	57	93	208.00	391.00
Hiltaba Suite	mineralization-absent	1077-41	1077-41 - 5	CA	> 5%		21/05/2020	0.0990	0.0020	3.6170	0.0810	0.2617	0.0041	**1601**	**25**	1550	18	1498	21	1055	62	94	129.90	244.00
Hiltaba Suite	mineralization-absent	1077-41	1077-41 - 10	CA	> 5%		21/05/2020	0.0993	0.0036	3.0100	0.1100	0.2129	0.0042	**1613**	**33**	1401	29	1243	22	1276	94	77	79.30	140.80
Hiltaba Suite	mineralization-absent	1077-41	1077-41 - 12	CA	> 5%		21/05/2020	0.1036	0.0035	4.0660	0.1600	0.2841	0.0073	**1709**	**46**	1644	32	1611	37	411	59	94	423.00	389.00
Hiltaba Suite	mineralization-absent	1077-41	1077-41 - 14	CA	> 5%		21/05/2020	0.1002	0.0028	3.4810	0.0910	0.2509	0.0043	**1623**	**27**	1520	20	1442	22	815	47	89	129.00	345.00
Hiltaba Suite	mineralization-absent	1077-41	1077-41 - 19	CA	> 5%	inherited	21/05/2020	0.1032	0.0036	3.8100	0.1500	0.2685	0.0074	**1678**	**29**	1585	31	1531	38	595	48	91	116.00	145.00
Hiltaba Suite	mineralization-absent	1077-41	1077-41 - 22	CA	> 5%		21/05/2020	0.0963	0.0026	4.0800	0.1300	0.3038	0.0063	**1550**	**30**	1644	25	1708	31	964	54	110	95.00	146.20
						discor-dant																			
Hiltaba Suite	mineralization-absent	1077-41	1077-41 - 23	CA		discor-dant	21/05/2020	0.0957	0.0061	3.4900	0.2200	0.2650	0.0100	**1540**	**49**	1516	49	1513	53	968	84	98	49.10	110.80
Hiltaba Suite	mineralization-absent	1077-41	1077-41 - 24	CA			21/05/2020	0.0953	0.0034	3.7800	0.1200	0.2823	0.0048	**1531**	**41**	1580	26	1602	24	3920	220	105	64.70	115.00
Hiltaba Suite	mineralization-absent	1077-41	1077-41 - 28	CA	> 5%		21/05/2020	0.1017	0.0036	3.6600	0.1100	0.2613	0.0065	**1654**	**39**	1560	24	1496	33	3380	220	90	117.50	195.50
Hiltaba Suite	mineralization-absent	1077-41	1077-41 - 34	CA	> 5%		21/05/2020	0.0971	0.0037	3.9800	0.1400	0.2931	0.0055	**1559**	**43**	1621	28	1656	27	2700	240	106	29.20	81.90
Hiltaba Suite	mineralization-absent	1077-41	1077-41 - 35	CA	> 5%	inherited	21/05/2020	-0.0300	0.1400	0.0030	0.0280	0.0015	0.0005	**2800**	**700**	1	29	9	3	20	110	0	7.81	47.30
Hiltaba Suite	mineralization-absent	1077-46	1077-46 - 8	CA		inherited	26/08/2018	0.1032	0.0025	4.1500	0.1000	0.2933	0.0039	**1689**	**47**	1664	20	1657	20	1792	78	98	61.00	78.40
Hiltaba Suite	mineralization-absent	1077-46	1077-46 - 12	CA		inherited	26/08/2018	0.1074	0.0029	4.4000	0.1200	0.2996	0.0039	**1773**	**52**	1714	24	1689	20	1451	63	95	116.60	58.17
Hiltaba Suite	mineralization-absent	1077-46	1077-46 - 17	CA		inherited	27/08/2018	0.1039	0.0019	4.2100	0.1200	0.2939	0.0058	**1690**	**34**	1673	23	1660	29	1423	49	98	126.20	131.30
Hiltaba Suite	mineralization-absent	1077-46	1077-46-18	CA	>5%		27/08/2018	0.1282	0.0059	5.9400	0.3800	0.3317	0.0092	**2073**	**80**	1956	57	1845	45	1700	130	89	117.60	111.50
Hiltaba Suite	mineralization-absent	1077-59	1077-59 - 1	CA	> 5%		21/05/2020	0.0985	0.0042	3.4000	0.1300	0.2506	0.0063	**1576**	**48**	1493	30	1440	33	1670	100	91	111.00	97.50
						discor-dant																			
Hiltaba Suite	mineralization-absent	1077-59	1077-59 - 3	CA			21/05/2020	0.0967	0.0022	3.5440	0.0890	0.2637	0.0052	**1563**	**27**	1533	20	1508	27	1464	44	96	204.00	276.10
Hiltaba Suite	mineralization-absent	1077-59	1077-59 - 7	CA	> 5%	inherited	21/05/2020	0.1039	0.0032	4.0100	0.1100	0.2808	0.0055	**1686**	**35**	1639	21	1594	28	922	36	95	215.00	107.30
Hiltaba Suite	mineralization-absent	1077-59	1077-59 - 12	CA	> 5%		21/05/2020	0.0957	0.0046	4.0300	0.1900	0.3044	0.0081	**1532**	**56**	1633	37	1712	39	692	46	112	227.00	246.00
						> 370																			
Hiltaba Suite	mineralization-absent	1077-59	1077-59 - 18	CA	> 5%	ppm P	21/05/2020	0.0987	0.0033	4.0700	0.1500	0.2990	0.0055	**1594**	**41**	1644	29	1685	27	736	45	106	131.00	158.00
						> 370																			
Hiltaba Suite	mineralization-absent	1077-59	1077-59 - 17	CA		ppm P	21/05/2020	0.0995	0.0030	3.7800	0.1100	0.2765	0.0041	**1614**	**32**	1583	24	1573	20	766	32	97	228.00	132.00

Appendix Table A4 LA-ICP MS U-Pb data for GRV and Hiltaba Suite zircon analyzed at the University of Adelaide

Unit	Group	Sample	Spot Number	Zircon Treatment	Disc.	Other	Analytical Session	Radiogenic Ratios								Age (Ma)										
								$^{207}Pb/^{206}Pb$	2σ	$^{207}Pb/^{235}U$	2σ	$^{206}Pb/^{238}U$	2σ	**$^{207}Pb/^{206}Pb$**	**2σ**	$^{207}Pb/^{235}Pb$	2σ	$^{206}Pb/^{238}U$	2σ	$^{208}Pb/^{232}Th$	2σ	% Conc	Th ppm	U ppm
Rejected data																								
Hiltaba Suite	mineralization-absent	1077-59	1077-59 - 19	CA		discordant	21/05/2020	0.0992	0.0056	3.6600	0.1900	0.2705	0.0068	**1594**	**66**	1554	41	1542	34	752	51	97	80.30	78.70
Hiltaba Suite	mineralization-absent	1077-59	1077-59 - 21	CA	> 5%	> 370	21/05/2020	0.0958	0.0029	3.8000	0.1100	0.2888	0.0045	**1543**	**30**	1588	24	1635	22	888	50	106	135.10	141.90
Hiltaba Suite	mineralization-absent	1077-59	1077-59 - 24	CA	> 5%	ppm P	21/05/2020	0.0988	0.0037	3.0000	0.1100	0.2165	0.0057	**1590**	**44**	1402	28	1262	30	1748	70	79	190.40	140.00
Hiltaba Suite	mineralization-absent	1077-59	1077-59 - 25	CA	> 5%	>370 ppm P	21/05/2020	0.0987	0.0034	3.5800	0.1200	0.2624	0.0043	**1584**	**42**	1536	28	1501	22	1237	64	95	109.60	103.60
Hiltaba Suite	mineralization-absent	1077-59	1077-59 - 27	CA		>370 ppm P	21/05/2020	0.0993	0.0025	3.8310	0.0910	0.2810	0.0040	**1618**	**30**	1596	19	1596	20	-34900	2600	99	499.00	319.10
Hiltaba Suite	mineralization-absent	1077-59	1077-59 - 28	CA		ppm P	21/05/2020	0.0968	0.0032	3.6400	0.1100	0.2745	0.0050	**1554**	**33**	1553	25	1563	25	-38000	4400	101	163.00	114.20
Hiltaba Suite	mineralization-absent	1077-59	1077-59 - 29	CA	> 5%		21/05/2020	0.0976	0.0030	3.4000	0.1400	0.2449	0.0086	**1599**	**32**	1498	33	1410	44	-37000	15000	88	145.00	102.00
Hiltaba Suite	mineralization-absent	1077-59	1077-59 - 31	CA	> 5%		21/05/2020	0.1015	0.0028	3.7490	0.0980	0.2692	0.0048	**1644**	**32**	1578	21	1536	24	NA	NA	93	140.00	161.60
Hiltaba Suite	mineralization-absent	1077-59	1077-59 - 32	CA		discordant > 370	21/05/2020	0.0940	0.0033	3.4900	0.1100	0.2708	0.0049	**1504**	**39**	1525	22	1544	25	23620	500	103	229.30	112.10
Hiltaba Suite	mineralization-absent	1077-59	1077-59 - 33	CA		ppm P	21/05/2020	0.0976	0.0024	3.6330	0.0980	0.2721	0.0047	**1575**	**26**	1557	21	1550	24	11530	360	98	250.60	184.70
Hiltaba Suite	mineralization-absent	1077-59	1077-59 - 40	CA		discordant reversely	21/05/2020	0.0965	0.0031	3.4960	0.0930	0.2628	0.0055	**1548**	**29**	1523	21	1503	28	1970	100	97	127.20	222.00
Hiltaba Suite	mineralization-absent	1077-59	1077-59 - 42	CA		discordant	21/05/2020	0.0998	0.0024	4.0700	0.1000	0.2950	0.0040	**1619**	**25**	1644	20	1666	20	2110	130	103	100.00	155.10
Hiltaba Suite	mineralization-absent	1077-59	1077-59 - 44	CA		discordant	21/05/2020	0.0981	0.0073	3.7300	0.2500	0.2788	0.0089	**1545**	**79**	1549	56	1582	45	1520	110	102	46.50	28.90
Hiltaba Suite	mineralization-absent	1077-59	1077-59 - 46	CA		inherited > 370	21/05/2020	0.1004	0.0021	4.1030	0.0900	0.2947	0.0040	**1627**	**23**	1651	18	1664	20	1382	65	102	204.70	235.40
Hiltaba Suite	mineralization-absent	1077-59	1077-59 - 51	CA	> 5%	ppm P	21/05/2020	0.0968	0.0023	3.9010	0.0900	0.2908	0.0045	**1563**	**22**	1613	18	1644	22	1972	96	105	98.60	139.20
Hiltaba Suite	mineralization-absent	1077-59	1077-59 - 53	CA	> 5%		21/05/2020	0.0976	0.0029	4.1100	0.1400	0.3021	0.0058	**1575**	**33**	1648	27	1700	29	1724	85	108	161.30	136.80
Hiltaba Suite	mineralization-absent	1077-59	1077-59 - 54	CA		inherited	21/05/2020	0.1013	0.0031	4.0500	0.1100	0.2895	0.0047	**1663**	**29**	1640	21	1638	23	2010	140	98	90.10	127.20
Hiltaba Suite	mineralization-absent	1077-59	1077-59 - 55	CA	> 5%		21/05/2020	0.0973	0.0022	3.2960	0.0970	0.2379	0.0057	**1566**	**21**	1474	23	1374	30	3480	180	88	145.70	170.60
Hiltaba Suite	mineralization-absent	1077-59	1077-59 - 56	CA	> 5%		21/05/2020	0.1004	0.0027	4.4200	0.1300	0.3164	0.0049	**1629**	**29**	1709	24	1771	24	1648	77	109	210.00	130.10
Hiltaba Suite	mineralization-absent	1077-59	1077-59 - 59	CA	> 5%		21/05/2020	0.0990	0.0043	4.0500	0.1500	0.2970	0.0068	**1586**	**51**	1634	31	1674	34	2200	110	106	121.70	54.22
Hiltaba Suite	mineralization-absent	1077-63	1077-63 - 5	CA		inherited	21/05/2020	0.0999	0.0032	3.7600	0.1100	0.2709	0.0042	**1608**	**36**	1577	23	1545	21	4680	180	96	140.10	112.20
Hiltaba Suite	mineralization-absent	1077-63	1077-63 - 8	CA		inherited	21/05/2020	0.1008	0.0051	4.1800	0.2200	0.2993	0.0080	**1635**	**62**	1651	43	1685	40	6960	400	103	35.90	27.40
Hiltaba Suite	mineralization-absent	1077-63	1077-63 - 11	CA		inherited > 370	21/05/2020	0.1013	0.0030	3.9300	0.1000	0.2810	0.0043	**1639**	**32**	1617	21	1596	22	4520	250	97	155.00	133.60
Hiltaba Suite	mineralization-absent	1077-63	1077-63 - 12	CA		ppm P	21/05/2020	0.0996	0.0032	3.9300	0.1200	0.2846	0.0044	**1609**	**36**	1613	25	1614	22	4540	190	100	83.80	79.30
Hiltaba Suite	mineralization-absent	1077-63	1077-63 - 14	CA		inherited	21/05/2020	0.1012	0.0035	3.8300	0.1300	0.2746	0.0057	**1643**	**43**	1595	28	1564	29	2930	140	95	150.80	125.10
Hiltaba Suite	mineralization-absent	1077-63	1077-63 - 15	CA		inherited reversely	21/05/2020	0.1019	0.0026	3.9700	0.1000	0.2800	0.0035	**1653**	**25**	1623	21	1591	17	2770	100	96	159.90	134.70
Hiltaba Suite	mineralization-absent	1077-63	1077-63 - 16	CA		discordant reversely	21/05/2020	0.0983	0.0033	3.9600	0.1300	0.2903	0.0042	**1586**	**35**	1619	26	1642	21	2680	140	104	85.20	83.60
Hiltaba Suite	mineralization-absent	1077-63	1077-63 - 20	CA		discordant	21/05/2020	0.0975	0.0054	3.6300	0.1800	0.2710	0.0054	**1562**	**51**	1544	39	1544	27	932	51	99	62.40	43.40
Hiltaba Suite	mineralization-absent	1077-63	1077-63 - 26	CA		discordant	21/05/2020	0.0955	0.0039	3.7300	0.1500	0.2813	0.0061	**1542**	**41**	1572	31	1596	31	1074	55	104	126.40	49.10
Hiltaba Suite	mineralization-absent	1077-63	1077-63 - 28	CA		inherited reversely	21/05/2020	0.1002	0.0025	3.8910	0.0890	0.2812	0.0035	**1628**	**25**	1608	18	1597	17	1199	50	98	204.00	182.00
Hiltaba Suite	mineralization-absent	1077-63	1077-63 - 30	CA		discordant reversely	21/05/2020	0.0994	0.0023	4.0170	0.0920	0.2914	0.0036	**1610**	**24**	1634	18	1648	18	1400	63	102	172.40	143.00
Hiltaba Suite	mineralization-absent	1077-63	1077-63 - 31	CA		discordant	21/05/2020	0.0997	0.0033	3.9900	0.1200	0.2902	0.0051	**1611**	**34**	1625	25	1642	25	1408	71	102	134.80	92.50
Hiltaba Suite	mineralization-absent	1077-63	1077-63 - 35	CA	> 5%		21/05/2020	0.0935	0.0039	3.6200	0.1500	0.2804	0.0058	**1486**	**40**	1540	34	1592	29	1720	100	107	48.50	62.20
Hiltaba Suite	mineralization-absent	1077-63	1077-63 - 36	CA		discordant	21/05/2020	0.0982	0.0049	3.7700	0.1800	0.2773	0.0070	**1589**	**60**	1581	37	1581	34	1750	120	99	64.00	45.90
Hiltaba Suite	mineralization-absent	1077-63	1077-63 - 37	CA		inherited	21/05/2020	0.1012	0.0028	3.9800	0.1000	0.2846	0.0043	**1639**	**29**	1624	21	1614	22	1676	65	98	264.00	168.30

* entire sample eliminated
CA: Chemical Abrasion

Appendix 4 Table A5 Zircon trace element data for GRV and Hiltaba Suite samples analyzed at Boise State University

Unit	Group	Sample	Spot Number	Zircon Treatment	Discordance	Other	Analytical Session	Experiment number
Included Data								
Hiltaba Suite	mineralization-related	2000366176	2000366176 L 214	Thermally Annealed			8/01/2016	6
Hiltaba Suite	mineralization-related	2000366176	2000366176 M 237	Thermally Annealed			8/01/2016	6
Hiltaba Suite	mineralization-related	2000366176	2000366176 L 206	Thermally Annealed			8/01/2016	6
Hiltaba Suite	mineralization-related	2000366176	2000366176 M 228	Thermally Annealed			8/01/2016	6
Hiltaba Suite	mineralization-related	2000366176	2000366176 M 235	Thermally Annealed			8/01/2016	6
Hiltaba Suite	mineralization-related	2000366176	2000366176 L 204	Thermally Annealed			8/01/2016	6
Hiltaba Suite	mineralization-related	2000366176	2000366176 M 234	Thermally Annealed			8/01/2016	6
Hiltaba Suite	mineralization-related	2000366176	2000366176 M 229	Thermally Annealed			8/01/2016	6
Hiltaba Suite	mineralization-related	2000366176	2000366176 M 233	Thermally Annealed			8/01/2016	6
Hiltaba Suite	mineralization-related	2000366176	2000366176 M 227	Thermally Annealed			8/01/2016	6
Hiltaba Suite	mineralization-related	2000366176	2000366176 L 202	Thermally Annealed			8/01/2016	6
Hiltaba Suite	mineralization-related	2000366176	2000366176 L 200	Thermally Annealed			8/01/2016	6
Hiltaba Suite	mineralization-related	2000366176	2000366176 M 219	Thermally Annealed			8/01/2016	6
Hiltaba Suite	mineralization-related	2000366176	2000366176 L 205	Thermally Annealed			8/01/2016	6
Hiltaba Suite	mineralization-related	2000366176	2000366176 M 226	Thermally Annealed			8/01/2016	6
Hiltaba Suite	mineralization-related	2000366176	2000366176 M 220	Thermally Annealed			8/01/2016	6
Hiltaba Suite	mineralization-related	2000366176	2000366176 L 203	Thermally Annealed			8/01/2016	6
Hiltaba Suite	mineralization-related	2000366176	2000366176 L 211	Thermally Annealed			8/01/2016	6
Hiltaba Suite	mineralization-related	2000366176	2000366176 L 212	Thermally Annealed			8/01/2016	6
Hiltaba Suite	mineralization-related	2000366176	2000366176 L 207	Thermally Annealed			8/01/2016	6
Hiltaba Suite	mineralization-related	2000366176	2000366176 M 238	Thermally Annealed			8/01/2016	6
Hiltaba Suite	mineralization-related	2000366176	2000366176 L 201	Thermally Annealed			8/01/2016	6
Hiltaba Suite	mineralization-related	2000366176	2000366176 L 199	Thermally Annealed			8/01/2016	6
Hiltaba Suite	mineralization-related	2000366176	2000366176 M 224	Thermally Annealed			8/01/2016	6
Hiltaba Suite	mineralization-related	2000366176	2000366176 L 213	Thermally Annealed			8/01/2016	6
Hiltaba Suite	mineralization-related	2000366176	2000366176 L 208	Thermally Annealed			8/01/2016	6
Hiltaba Suite	mineralization-related	2000366166	2000366166 M 175	Thermally Annealed			8/01/2016	4
Hiltaba Suite	mineralization-related	2000366166	2000366166 M 174	Thermally Annealed			8/01/2016	4
Hiltaba Suite	mineralization-related	2000366166	2000366166 M 187	Thermally Annealed			8/01/2016	4
Hiltaba Suite	mineralization-related	2000366166	2000366166 M 184	Thermally Annealed			8/01/2016	4
Hiltaba Suite	mineralization-related	2000366166	2000366166 M 188	Thermally Annealed			8/01/2016	4
Hiltaba Suite	mineralization-related	2000366166	2000366166 M 177	Thermally Annealed			8/01/2016	4
Hiltaba Suite	mineralization-related	2000366166	2000366166 M 190	Thermally Annealed			8/01/2016	4
Hiltaba Suite	mineralization-related	2000366166	2000366166 M 185	Thermally Annealed			8/01/2016	4
Hiltaba Suite	mineralization-related	2000366166	2000366166 L 167	Thermally Annealed			8/01/2016	4
Hiltaba Suite	mineralization-related	2000366166	2000366166 L 166	Thermally Annealed			8/01/2016	4
Hiltaba Suite	mineralization-related	2000366166	2000366166 M 171	Thermally Annealed			8/01/2016	4
Hiltaba Suite	mineralization-related	2000366166	2000366166 L 168	Thermally Annealed			8/01/2016	4
Hiltaba Suite	mineralization-related	2000366166	2000366166 M 191	Thermally Annealed			8/01/2016	4
Hiltaba Suite	mineralization-related	2000366166	2000366166 L 165	Thermally Annealed			8/01/2016	4
Hiltaba Suite	mineralization-related	2000366166	2000366166 M 178	Thermally Annealed			8/01/2016	4
Hiltaba Suite	mineralization-related	2111460	2111460 M 276	Thermally Annealed			8/01/2016	4
Hiltaba Suite	mineralization-related	2111460	2111460 M 271	Thermally Annealed			8/01/2016	4
Hiltaba Suite	mineralization-related	2111460	2111460 M 279	Thermally Annealed			8/01/2016	4
Hiltaba Suite	mineralization-related	2111460	2111460 M 267	Thermally Annealed			8/01/2016	4
Hiltaba Suite	mineralization-related	2111460	2111460 L 245	Thermally Annealed			8/01/2016	4
Hiltaba Suite	mineralization-related	2111460	2111460 L 242	Thermally Annealed			8/01/2016	4
Hiltaba Suite	mineralization-related	2111460	2111460 M 265	Thermally Annealed			8/01/2016	4
Hiltaba Suite	mineralization-related	2111460	2111460 L 241	Thermally Annealed			8/01/2016	4
Hiltaba Suite	mineralization-related	2111460	2111460 L 251	Thermally Annealed			8/01/2016	4
Hiltaba Suite	mineralization-related	2111460	2111460 M 278	Thermally Annealed			8/01/2016	4
Hiltaba Suite	mineralization-related	2111460	2111460 M 262	Thermally Annealed			8/01/2016	4
Hiltaba Suite	mineralization-related	2111460	2111460 M 268	Thermally Annealed			8/01/2016	4
Hiltaba Suite	mineralization-related	2111460	2111460 L 252	Thermally Annealed			8/01/2016	4
Hiltaba Suite	mineralization-related	2111460	2111460 L 243	Thermally Annealed			8/01/2016	4
Hiltaba Suite	mineralization-related	2111460	2111460 M 269	Thermally Annealed			8/01/2016	4
Hiltaba Suite	mineralization-related	2111460	2111460 L 248	Thermally Annealed			8/01/2016	4
Hiltaba Suite	mineralization-related	2111460	2111460 M 264	Thermally Annealed			8/01/2016	4
Hiltaba Suite	mineralization-related	2111460	2111460 L 250	Thermally Annealed			8/01/2016	4
Hiltaba Suite	mineralization-related	2111460	2111460 L 247	Thermally Annealed			8/01/2016	4
Hiltaba Suite	mineralization-related	2111460	2111460 L 249	Thermally Annealed			8/01/2016	4
Hiltaba Suite	mineralization-related	2111460	2111460 M 266	Thermally Annealed			8/01/2016	4
Hiltaba Suite	mineralization-related	2111460	2111460 M 270	Thermally Annealed			8/01/2016	4
Hiltaba Suite	mineralization-related	2111460	2111460 L 258	Thermally Annealed			8/01/2016	4
Hiltaba Suite	mineralization-related	2111460	2111460 M 277	Thermally Annealed			8/01/2016	4
Hiltaba Suite	mineralization-related	2111460	2111460 M 272	Thermally Annealed			8/01/2016	4
Hiltaba Suite	mineralization-related	2111460	2111460 L 253	Thermally Annealed			8/01/2016	4
Hiltaba Suite	mineralization-related	2111460	2111460 L 246	Thermally Annealed			8/01/2016	4
Hiltaba Suite	mineralization-related	2111460	2111460 L 257	Thermally Annealed			8/01/2016	4
Hiltaba Suite	mineralization-related	2111460	2111460 L 244	Thermally Annealed			8/01/2016	4
Hiltaba Suite	mineralization-related	1831634	1831634 M 45	Thermally Annealed			7/01/2016	3

Appendix 4 Table A5 Zircon trace element data for GRV and Hiltaba Suite samples analyzed at Boise State University

Spot Number	P	Ti	Y	Nb	La	Ce	Pr	Nd	Sm	Eu	Gd	Tb	Dy	Ho
	ppm	ppm	ppm	ppm	ppm	ppm	ppm	ppm	ppm	ppm	ppm	ppm	ppm	ppm
2000366176 L 214	281.95	17.41	1645.86	5.46	0.03	29.51	0.26	4.03	7.49	1.46	39.10	13.04	155.00	57.52
2000366176 M 237	194.85	19.34	514.31	0.99		7.94	0.04	1.24	2.44	0.83	14.01	4.63	54.49	20.29
2000366176 L 206	215.93	14.78	1993.63	1.54		25.09	0.25	6.90	11.84	2.91	59.88	17.84	199.78	73.40
2000366176 M 228	289.41	12.64	981.02	3.63		28.78	0.05	1.29	3.54	0.55	22.22	7.59	100.81	35.91
2000366176 M 235	310.58	23.93	936.72	1.74		15.98	0.12	2.60	5.24	1.98	24.33	7.67	92.74	35.74
2000366176 L 204	232.75	22.41	2140.99	1.25	0.04	23.69	0.74	12.02	15.76	5.13	72.30	22.05	225.52	81.47
2000366176 M 234	262.60	22.61	718.49	1.30		17.78	0.08	1.89	3.93	1.39	21.34	7.08	76.64	27.31
2000366176 M 229	226.70	17.34	1170.58	3.89		25.88	0.19	2.51	4.64	1.15	27.54	9.31	115.29	41.49
2000366176 M 233	261.79	16.99	1849.37	1.94		20.68	0.55	9.71	17.08	3.30	67.39	19.74	213.58	71.05
2000366176 M 227	151.75	5.33	669.13	3.39		9.90	0.08	1.42	2.97	0.37	15.90	5.38	64.96	24.84
2000366176 L 202	256.20	12.67	979.59	2.79		19.37	0.05	1.29	2.11	0.68	19.18	7.24	86.81	34.34
2000366176 L 200	239.22	23.94	1034.64	1.94		18.53	0.14	3.29	7.45	2.25	28.36	9.10	98.82	36.05
2000366176 M 219	252.67	12.27	1850.23	4.82	0.08	78.98	0.39	9.78	17.44	1.32	69.40	20.44	224.86	78.35
2000366176 L 205	228.52	20.71	1753.79	1.26	0.09	20.56	0.50	9.71	15.06	3.93	60.75	18.01	186.37	65.69
2000366176 M 226	322.08	16.13	1145.84	2.62		24.15	0.13	3.67	5.96	1.10	30.21	9.83	115.25	42.21
2000366176 M 220	269.48	15.81	1335.20	3.07	0.03	24.58	0.16	3.47	7.68	1.99	36.63	11.61	141.24	49.58
2000366176 L 203	303.49	37.97	1601.66	1.31	0.05	15.47	0.33	6.45	8.12	4.05	51.47	14.13	163.18	55.83
2000366176 L 211	222.52	21.73	788.01	1.37		13.96	0.21	2.13	4.65	1.35	20.22	6.02	76.86	28.04
2000366176 L 212	218.27	23.16	740.76	0.99		12.95	0.07	2.05	3.62	1.25	19.49	6.50	71.83	26.55
2000366176 L 207	249.22	23.79	1240.22	2.65		23.15	0.20	3.67	6.09	2.14	34.11	10.44	115.88	44.13
2000366176 M 238	257.58	25.65	1271.62	1.53	0.02	18.47	0.46	6.27	10.96	3.63	48.20	13.61	152.56	50.90
2000366176 L 201	249.91	10.76	1014.51	3.82		25.95	0.02	1.02	2.51	0.37	19.81	7.42	93.79	36.32
2000366176 L 199	229.90	20.81	1935.85	1.21	0.02	23.83	0.64	10.28	14.84	3.65	65.93	19.01	199.01	71.66
2000366176 M 224	268.26	22.15	872.04	2.44	0.02	19.99	0.15	3.52	5.27	1.77	24.48	7.91	92.60	31.11
2000366176 L 213	253.71	17.43	2382.03	2.85	0.08	26.76	0.64	10.98	17.15	3.43	72.35	23.21	252.71	87.53
2000366176 L 208	265.36	24.65	1643.83	2.14	0.02	23.20	0.41	6.80	9.62	2.96	49.87	13.92	165.48	59.54
2000366166 M 175	225.80	22.40	740.17	1.32		15.74	0.07	2.55	3.19	1.56	20.46	6.51	77.03	27.28
2000366166 M 174	225.52	18.85	829.39	1.60		16.90	0.13	2.71	4.56	1.41	22.67	7.43	88.37	30.67
2000366166 M 187	220.99	16.36	923.50	2.48		20.60	0.07	1.59	3.46	0.68	20.81	7.64	90.67	33.37
2000366166 M 184	229.76	14.08	834.14	1.83		8.45	0.05	2.00	4.29	0.71	24.12	7.23	85.15	30.94
2000366166 M 188	216.88	36.66	562.56	0.87	0.10	13.47	0.11	1.70	2.88	1.12	14.25	4.61	57.85	19.84
2000366166 M 177	263.39	18.47	1632.77	1.63	0.03	22.79	0.29	4.92	9.33	1.83	45.43	14.84	173.98	58.35
2000366166 M 190	233.60	18.28	1887.60	2.12	0.04	31.36	0.52	10.87	14.94	3.98	58.59	18.55	212.03	68.93
2000366166 M 185	219.68	28.11	672.26	0.88		13.72	0.05	2.54	3.63	1.48	18.91	6.03	71.07	23.43
2000366166 L 167	276.72	34.84	638.28	0.87		13.87	0.11	2.67	4.44	2.14	21.43	5.83	69.45	23.08
2000366166 L 166	269.99	20.98	900.98	2.41		21.63	0.12	2.37	5.26	1.31	23.57	7.86	95.90	34.81
2000366166 M 171	207.28	25.08	721.99	0.99	0.03	13.10	0.09	1.77	3.50	1.20	20.40	6.35	72.82	26.58
2000366166 L 168	204.59	32.12	1117.16	0.57	0.02	15.02	0.37	7.61	9.92	3.95	41.19	11.62	127.55	41.11
2000366166 M 191	259.35	21.14	1461.77	1.62	0.01	26.15	0.47	7.26	12.31	3.40	47.55	14.23	162.98	56.61
2000366166 L 165	273.12	19.51	941.47	2.51		24.49	0.10	2.09	4.19	1.25	22.77	7.98	93.58	34.20
2000366166 M 178	225.02	26.48	742.36	1.44	0.02	17.09	0.11	2.49	4.26	1.35	21.41	6.66	76.70	26.99
2111460 M 276	144.24	17.16	296.42	0.98		13.84	0.01	0.51	1.16	0.36	7.39	2.30	27.56	10.84
2111460 M 271	262.69	11.61	969.99	4.80		32.31	0.07	1.52	4.64	0.64	25.85	8.11	104.84	37.27
2111460 M 279	346.19	11.30	1318.94	4.77		32.87	0.09	2.87	5.62	0.74	32.56	11.49	144.02	52.37
2111460 M 267	235.93	15.15	793.83	2.34		19.80	0.03	1.50	3.66	0.54	16.75	6.53	79.01	30.64
2111460 L 245	214.64	15.28	960.01	1.91		18.56	0.07	1.48	3.50	1.12	21.25	7.92	95.97	35.13
2111460 L 242	317.50	19.79	1389.99	3.72		30.86	0.18	3.35	7.19	1.60	37.18	13.13	150.48	54.03
2111460 M 265	257.25	17.29	1095.31	2.19		22.22	0.17	2.65	6.60	1.35	27.88	10.27	122.00	42.76
2111460 L 241	296.71	24.70	1222.52	2.67	0.03	28.42	0.15	3.81	7.85	1.90	34.72	11.16	129.88	46.18
2111460 L 251	290.25	20.69	1031.81	3.99	0.29	28.85	0.56	7.16	7.52	1.77	26.69	9.55	105.96	36.71
2111460 M 278	293.47	20.76	890.28	2.21		18.64	0.13	2.63	4.56	0.68	23.52	7.95	93.65	33.42
2111460 M 262	288.66	8.78	1085.11	6.10		32.39	0.04	1.73	3.96	0.49	24.41	9.04	112.16	39.60
2111460 M 268	248.66	7.89	1044.26	6.20		30.84	0.05	1.87	4.16	0.33	23.51	8.51	106.44	39.55
2111460 L 252	284.30	13.53	968.55	3.47		29.62	0.06	1.38	3.35	0.63	24.86	7.79	97.07	37.11
2111460 L 243	331.47	28.05	3253.90	3.90	0.07	29.05	0.59	10.53	20.46	6.64	112.56	31.52	360.19	124.63
2111460 M 269	321.33	16.51	1123.14	4.15		24.22	0.18	2.70	4.84	1.00	28.46	9.74	119.94	42.15
2111460 L 248	281.17	16.95	1183.72	2.98		27.11	0.09	1.69	4.48	0.73	24.75	9.56	114.98	43.69
2111460 M 264	363.87	16.57	1584.86	6.90	0.19	34.85	0.41	4.42	8.26	1.39	39.58	13.19	161.25	59.82
2111460 L 250	360.89	14.66	1545.96	4.54		38.52	0.20	3.41	6.65	0.88	35.24	12.22	152.43	57.48
2111460 L 247	270.17	19.85	1874.66	1.29	0.05	21.96	0.41	7.34	11.26	2.70	57.41	17.29	201.28	70.22
2111460 L 249	313.20	14.56	1423.72	4.92		40.63	0.13	2.44	6.04	0.81	32.01	11.64	139.45	53.04
2111460 M 266	228.58	15.75	875.05	3.63	0.17	19.41	0.22	2.78	4.39	0.84	24.89	8.29	97.91	33.89
2111460 M 270	334.64	12.79	2025.00	3.50		33.82	0.37	8.17	13.44	1.87	60.90	18.67	224.26	79.89
2111460 L 258	280.16	16.79	1904.22	1.97	0.20	29.00	0.42	6.39	13.32	2.82	59.65	19.32	216.72	74.47
2111460 M 277	285.77	12.03	1666.48	3.97	0.09	34.16	0.23	5.24	9.09	1.09	47.57	15.84	182.26	63.71
2111460 M 272	260.55	13.69	1041.35	3.04	0.11	19.44	0.23	2.64	4.49	0.58	23.59	8.23	105.31	37.86
2111460 L 253	231.53	18.26	721.34	1.48		15.24	0.08	1.55	3.97	0.95	17.42	5.88	74.37	26.98
2111460 L 246	286.54	17.82	1012.29	1.89		16.45	0.09	1.32	3.82	0.85	23.31	7.95	100.36	38.67
2111460 L 257	240.74	13.56	1026.52	3.69		37.07	0.07	1.82	5.70	1.08	23.63	9.04	105.87	38.46
2111460 L 244	292.11	21.62	1455.77	3.77		25.95	0.14	3.54	6.27	1.65	36.06	11.98	141.65	53.60
1831634 M 45	262.43	30.36	872.42	1.01		17.83	0.18	3.69	6.10	1.86	27.18	8.53	94.96	31.22

Appendix 4 Table A5 Zircon trace element data for GRV and Hiltaba Suite samples analyzed at Boise State University

Spot Number	Er	Tm	Yb	Lu	Hf	Th	U	Eu/Eu*	Ce/Ce*	$(Yb/Gd)_N$	Ti-in-Zircon	Total REE	Th/U
	ppm	ppm	ppm	ppm	ppm	ppm	ppm						
2000366176 L 214	252.75	59.37	570.66	90.57	9177.89	275.05	288.01	0.26	77.92	18.09	857	1281	1.0
2000366176 M 237	82.88	19.86	210.18	26.17	8661.05	49.97	60.97	0.43	187.45	18.59	869	445	0.8
2000366176 L 206	294.71	64.43	596.60	88.58	10301.87	281.42	196.96	0.33	97.88	12.35	838	1442	1.4
2000366176 M 228	149.18	37.08	391.88	50.79	9362.82	194.27	254.94	0.19	574.30	21.85	821	830	0.8
2000366176 M 235	152.41	38.87	421.84	53.65	6912.68	134.92	160.29	0.54	132.04	21.49	895	853	0.8
2000366176 L 204	317.20	68.69	599.62	89.12	9140.99	276.72	155.68	0.46	32.75	10.28	887	1533	1.8
2000366176 M 234	108.81	25.46	271.33	32.91	7335.52	110.78	106.73	0.46	221.62	15.75	888	596	1.0
2000366176 M 229	184.14	44.92	484.24	62.44	7863.25	171.84	217.27	0.31	134.28	21.79	856	1004	0.8
2000366176 M 233	273.86	63.74	634.05	73.35	7305.33	292.89	236.29	0.30	36.66	11.66	854	1468	1.2
2000366176 M 227	102.56	24.55	260.47	31.84	8181.85	131.35	237.71	0.17	117.15	20.30	735	545	0.6
2000366176 L 202	154.95	35.33	348.60	53.65	10856.67	150.90	142.80	0.33	379.65	22.52	821	764	1.1
2000366176 L 200	160.64	36.23	347.62	55.75	8824.03	118.92	112.16	0.47	127.68	15.19	895	804	1.1
2000366176 M 219	294.12	68.03	702.81	81.56	8767.85	417.31	243.12	0.12	108.27	12.55	818	1648	1.7
2000366176 L 205	257.45	55.32	497.67	77.18	9447.48	217.49	132.71	0.40	24.46	10.15	877	1268	1.6
2000366176 M 226	177.72	41.10	464.99	51.25	7974.31	208.10	223.52	0.25	176.76	19.08	848	968	0.9
2000366176 M 220	203.84	49.17	523.68	63.59	7648.19	203.40	218.94	0.36	86.56	17.72	846	1117	0.9
2000366176 L 203	232.10	50.60	474.58	71.88	8207.27	186.99	106.72	0.61	28.33	11.43	955	1148	1.8
2000366176 L 211	120.00	26.35	257.96	39.94	8960.88	115.33	83.33	0.42	64.81	15.81	883	598	1.4
2000366176 L 212	111.95	26.25	246.56	39.60	8968.79	89.49	71.45	0.46	181.29	15.68	891	569	1.3
2000366176 L 207	186.06	43.13	413.22	66.50	9066.34	156.75	142.70	0.45	114.15	15.01	894	949	1.1
2000366176 M 238	205.90	45.54	473.63	58.82	7833.29	194.10	138.65	0.48	47.18	12.18	903	1089	1.4
2000366176 L 201	160.51	36.41	374.28	59.83	11940.22	177.37	204.87	0.16	1318.11	23.41	804	818	0.9
2000366176 L 199	284.49	59.84	548.29	80.16	9227.24	244.20	141.58	0.36	49.97	10.30	878	1382	1.7
2000366176 M 224	135.50	32.66	347.77	45.38	7111.50	117.78	137.71	0.48	84.36	17.60	885	748	0.9
2000366176 L 213	355.24	78.40	726.11	103.57	9557.52	391.62	274.28	0.30	29.44	12.44	857	1758	1.4
2000366176 L 208	241.24	52.67	497.29	74.11	9208.65	208.94	147.19	0.41	59.42	12.36	898	1197	1.4
2000366166 M 175	111.64	26.52	260.11	34.59	8413.55	113.93	93.49	0.59	17.96	15.75	887	1348	1.2
2000366166 M 174	127.51	30.32	301.18	41.58	8676.98	115.63	102.69	0.42	24.47	16.46	866	1438	1.1
2000366166 M 187	144.67	34.19	357.59	46.26	9826.08	166.22	178.21	0.25	65.50	21.30	850	1532	0.9
2000366166 M 184	123.12	30.04	282.54	40.13	8817.72	95.64	118.62	0.21	21.12	14.52	833	1442	0.8
2000366166 M 188	87.53	19.36	203.38	27.52	8367.38	81.56	64.05	0.54	31.19	17.69	950	1171	1.3
2000366166 M 177	248.97	57.52	543.19	72.70	9447.35	217.88	176.96	0.27	20.43	14.82	864	2241	1.2
2000366166 M 190	283.38	62.36	580.83	76.16	8531.38	309.57	198.36	0.41	9.24	12.29	862	2496	1.6
2000366166 M 185	100.54	23.79	241.11	33.28	8096.36	75.75	68.17	0.55	17.95	15.80	915	1281	1.1
2000366166 L 167	90.62	21.88	218.16	27.74	7529.96	93.60	62.88	0.67	20.08	12.62	943	1247	1.5
2000366166 L 166	141.74	33.77	345.88	43.41	8610.20	172.03	171.57	0.36	47.22	18.19	879	1509	1.0
2000366166 M 171	111.10	25.59	250.38	33.80	8145.09	79.25	64.84	0.43	34.16	15.21	900	1330	1.2
2000366166 L 168	161.46	36.02	356.02	44.71	7641.48	113.12	68.99	0.60	5.98	10.71	932	1725	1.6
2000366166 M 191	217.21	50.01	476.12	62.77	8202.33	241.27	171.29	0.43	14.23	12.41	880	2070	1.4
2000366166 L 165	142.31	34.32	352.72	44.16	8913.20	195.72	194.37	0.39	54.91	19.20	870	1550	1.0
2000366166 M 178	112.62	26.88	266.24	35.37	8414.63	127.65	93.45	0.43	27.36	15.41	907	1351	1.4
2111460 M 276	47.42	11.84	133.78	17.02	8561.45	42.02	57.77	0.38	1142.43	22.44	855	274	0.7
2111460 M 271	165.66	41.17	445.43	52.81	9364.59	233.51	325.69	0.18	483.57	21.35	812	920	0.7
2111460 M 279	219.72	52.63	564.97	65.77	9897.23	279.13	320.15	0.17	351.97	21.50	809	1186	0.9
2111460 M 267	130.04	32.70	368.02	43.81	9261.54	137.14	167.62	0.21	585.76	27.23	841	733	0.8
2111460 L 245	152.55	35.73	343.94	55.26	11067.96	123.81	121.04	0.40	262.44	20.06	842	772	1.0
2111460 L 242	223.27	49.93	477.82	71.90	10488.81	302.84	232.72	0.30	169.66	15.93	872	1121	1.3
2111460 M 265	179.94	43.00	448.38	53.82	9029.67	157.29	170.13	0.30	131.15	19.93	856	961	0.9
2111460 L 241	192.31	43.30	412.85	61.69	9690.55	294.87	181.86	0.35	102.84	14.73	899	974	1.6
2111460 L 251	155.46	38.51	392.48	52.13	9107.00	252.42	239.65	0.38	17.48	18.22	877	864	1.1
2111460 M 278	142.43	34.72	372.46	46.41	8999.31	151.86	171.02	0.20	135.82	19.63	877	781	0.9
2111460 M 262	179.29	45.49	489.87	55.93	9680.39	292.98	440.86	0.15	889.94	24.87	783	994	0.7
2111460 M 268	176.45	43.52	443.63	57.17	9782.44	271.81	430.41	0.10	639.42	23.38	772	936	0.6
2111460 L 252	155.06	38.97	416.30	51.31	10084.25	188.52	242.59	0.21	514.73	20.75	828	863	0.8
2111460 L 243	501.28	106.71	1020.85	143.07	9456.90	550.76	324.43	0.42	36.10	11.24	915	2468	1.7
2111460 M 269	181.54	44.35	473.19	56.91	8437.49	164.06	218.08	0.26	130.66	20.60	851	989	0.8
2111460 L 248	192.30	45.08	446.20	66.94	11648.58	229.48	228.92	0.21	297.39	22.34	854	978	1.0
2111460 M 264	256.47	65.29	698.48	85.46	9128.17	270.33	356.44	0.23	30.17	21.87	851	1429	0.8
2111460 L 250	248.84	58.45	576.37	84.42	11773.01	410.28	393.96	0.18	187.71	20.27	837	1275	1.0
2111460 L 247	290.38	63.65	596.56	87.81	11000.80	281.54	208.41	0.32	36.04	12.88	872	1428	1.4
2111460 L 249	232.62	54.19	539.92	77.53	11758.09	342.80	356.47	0.18	298.60	20.90	836	1190	1.0
2111460 M 266	143.34	33.87	365.15	43.95	9103.95	202.37	238.03	0.24	24.21	18.18	845	779	0.9
2111460 M 270	337.34	76.88	796.37	91.43	8982.28	391.68	417.15	0.20	90.52	16.20	822	1743	0.9
2111460 L 258	296.58	66.84	672.65	79.72	9174.77	286.87	248.77	0.31	24.54	13.97	853	1538	1.2
2111460 M 277	261.33	62.96	647.90	77.25	10066.76	337.58	365.32	0.16	56.96	16.88	816	1409	0.9
2111460 M 272	164.92	39.79	404.72	54.26	8638.67	222.29	288.51	0.17	30.22	21.27	830	866	0.8
2111460 L 253	117.77	28.47	305.21	39.33	8694.15	91.24	114.42	0.35	195.53	21.71	862	637	0.8
2111460 L 246	164.14	38.73	381.08	55.53	11121.12	150.81	140.05	0.28	188.01	20.26	859	832	1.1
2111460 L 257	161.94	40.74	434.33	50.06	8774.28	249.37	271.58	0.28	525.41	22.78	829	910	0.9
2111460 L 244	247.24	54.95	542.35	87.56	10310.63	196.53	205.54	0.34	178.20	18.64	882	1213	1.0
1831634 M 45	127.12	29.04	308.24	37.46	7233.17	79.99	54.69	0.44	95.02	14.06	925	693	1.5

Appendix 4 Table A5 Zircon trace element data for GRV and Hiltaba Suite samples analyzed at Boise State University

Unit	Group	Sample	Spot Number	Zircon Treatment	Discordance	Other	Analytical Session	Experiment
Included Data								number
Hiltaba Suite	mineralization-related	1831634	1831634 M 47	Thermally Annealed			7/01/2016	3
Hiltaba Suite	mineralization-related	1831634	1831634 M 42	Thermally Annealed			7/01/2016	3
Hiltaba Suite	mineralization-related	1831634	1831634 L 9	Thermally Annealed			7/01/2016	3
Hiltaba Suite	mineralization-related	1831634	1831634 M 48	Thermally Annealed			7/01/2016	3
Hiltaba Suite	mineralization-related	1831634	1831634 M 41	Thermally Annealed			7/01/2016	3
Hiltaba Suite	mineralization-related	1831634	1831634 L 5	Thermally Annealed			7/01/2016	3
Hiltaba Suite	mineralization-related	1831634	1831634 L 23	Thermally Annealed			7/01/2016	3
Hiltaba Suite	mineralization-related	1831634	1831634 M 29	Thermally Annealed			7/01/2016	3
Hiltaba Suite	mineralization-related	1831634	1831634 L 25	Thermally Annealed			7/01/2016	3
Hiltaba Suite	mineralization-related	1831634	1831634 M 31	Thermally Annealed			7/01/2016	3
Hiltaba Suite	mineralization-related	1831634	1831634 L 13	Thermally Annealed			7/01/2016	3
Hiltaba Suite	mineralization-related	1831634	1831634 L 22	Thermally Annealed			7/01/2016	3
Hiltaba Suite	mineralization-related	1831634	1831634 M 34	Thermally Annealed			7/01/2016	3
Hiltaba Suite	mineralization-related	1831634	1831634 L 6	Thermally Annealed			7/01/2016	3
Hiltaba Suite	mineralization-related	1831634	1831634 L 3	Thermally Annealed			7/01/2016	3
Hiltaba Suite	mineralization-related	1831634	1831634 L 16	Thermally Annealed			7/01/2016	3
Hiltaba Suite	mineralization-related	1831634	1831634 M 38	Thermally Annealed			7/01/2016	3
Hiltaba Suite	mineralization-related	1831634	1831634 L 8	Thermally Annealed			7/01/2016	3
Hiltaba Suite	mineralization-related	1831634	1831634 M 35	Thermally Annealed			7/01/2016	3
Hiltaba Suite	mineralization-related	1831634	1831634 M 30	Thermally Annealed			7/01/2016	3
Hiltaba Suite	mineralization-related	1831634	1831634 M 36	Thermally Annealed			7/01/2016	3
Hiltaba Suite	mineralization-related	1831634	1831634 L 15	Thermally Annealed			7/01/2016	3
Hiltaba Suite	mineralization-related	1831634	1831634 L 21	Thermally Annealed			7/01/2016	3
Hiltaba Suite	mineralization-related	1831634	1831634 M 40	Thermally Annealed			7/01/2016	3
Hiltaba Suite	mineralization-related	1831634	1831634 L 10	Thermally Annealed			7/01/2016	3
Hiltaba Suite	mineralization-related	1831634	1831634 M 46	Thermally Annealed			7/01/2016	3
Hiltaba Suite	mineralization-related	1831634	1831634 L 11	Thermally Annealed			7/01/2016	3
Hiltaba Suite	mineralization-related	1831634	1831634 M 44	Thermally Annealed			7/01/2016	3
Hiltaba Suite	mineralization-related	1831634	1831634 L 20	Thermally Annealed			7/01/2016	3
Hiltaba Suite	mineralization-related	1831634	1831634 L 14	Thermally Annealed			7/01/2016	3
Hiltaba Suite	mineralization-related	1831634	1831634 L 2	Thermally Annealed			7/01/2016	3
Hiltaba Suite	mineralization-related	1831634	1831634 M 32	Thermally Annealed			7/01/2016	3
Hiltaba Suite	mineralization-related	1831634	1831634 L 19	Thermally Annealed			7/01/2016	3
Hiltaba Suite	mineralization-absent	2053554	2053554 L 196	Thermally Annealed			30/07/2014	1
Hiltaba Suite	mineralization-absent	2053554	2053554 M 79	Thermally Annealed			17/10/2014	2
Hiltaba Suite	mineralization-absent	2053554	2053554 M 107	Thermally Annealed			17/10/2014	2
Hiltaba Suite	mineralization-absent	2053554	2053554 M 227	Thermally Annealed			31/07/2014	1
Hiltaba Suite	mineralization-absent	2053554	2053554 M 92	Thermally Annealed			17/10/2014	2
Hiltaba Suite	mineralization-absent	2053554	2053554 L 213	Thermally Annealed			31/07/2014	1
Hiltaba Suite	mineralization-absent	2053554	2053554 L 222	Thermally Annealed			31/07/2014	1
Hiltaba Suite	mineralization-absent	2053554	2053554 M 125	Thermally Annealed			17/10/2014	2
Hiltaba Suite	mineralization-absent	2053554	2053554 M 232	Thermally Annealed			31/07/2014	1
Hiltaba Suite	mineralization-absent	2053554	2053554 M 82	Thermally Annealed			17/10/2014	2
Hiltaba Suite	mineralization-absent	2053554	2053554 L 206	Thermally Annealed			31/07/2014	1
Hiltaba Suite	mineralization-absent	2053554	2053554 L 214	Thermally Annealed			31/07/2014	1
Hiltaba Suite	mineralization-absent	2053554	2053554 M 93	Thermally Annealed			17/10/2014	2
Hiltaba Suite	mineralization-absent	2053554	2053554 L 208	Thermally Annealed			31/07/2014	1
Hiltaba Suite	mineralization-absent	2053554	2053554 M 83	Thermally Annealed			17/10/2014	2
Hiltaba Suite	mineralization-absent	2053554	2053554 M 81	Thermally Annealed			17/10/2014	2
Hiltaba Suite	mineralization-absent	2053554	2053554 M 229	Thermally Annealed			31/07/2014	1
Hiltaba Suite	mineralization-absent	2053554	2053554 M 115	Thermally Annealed			17/10/2014	2
Hiltaba Suite	mineralization-absent	2053554	2053554 L 221	Thermally Annealed			31/07/2014	1
Hiltaba Suite	mineralization-absent	2053554	2053554 M 106	Thermally Annealed			17/10/2014	2
Hiltaba Suite	mineralization-absent	2053554	2053554 M 85	Thermally Annealed			17/10/2014	2
Hiltaba Suite	mineralization-absent	2053554	2053554 L 207	Thermally Annealed			31/07/2014	1
Hiltaba Suite	mineralization-absent	2053554	2053554 M 118	Thermally Annealed			17/10/2014	2
Hiltaba Suite	mineralization-absent	2053554	2053554 L 202	Thermally Annealed			31/07/2014	1
Hiltaba Suite	mineralization-absent	2053554	2053554 L 198	Thermally Annealed			30/07/2014	1
Hiltaba Suite	mineralization-absent	2053554	2053554 L 212	Thermally Annealed			31/07/2014	1
Hiltaba Suite	mineralization-absent	2053554	2053554 L 215	Thermally Annealed			31/07/2014	1
Hiltaba Suite	mineralization-absent	2053554	2053554 L 209	Thermally Annealed			31/07/2014	1
Hiltaba Suite	mineralization-absent	2053554	2053554 M 94	Thermally Annealed			17/10/2014	2
Hiltaba Suite	mineralization-absent	2053554	2053554 M 110	Thermally Annealed			17/10/2014	2
Hiltaba Suite	mineralization-absent	2053554	2053554 L 224	Thermally Annealed			31/07/2014	1
Hiltaba Suite	mineralization-absent	2053554	2053554 M 130	Thermally Annealed			17/10/2014	2
Hiltaba Suite	mineralization-absent	2053554	2053554 M 126	Thermally Annealed			17/10/2014	2
Hiltaba Suite	mineralization-absent	2053554	2053554 L 217	Thermally Annealed			31/07/2014	1
Hiltaba Suite	mineralization-absent	2053554	2053554 L 225	Thermally Annealed			31/07/2014	1
Hiltaba Suite	mineralization-absent	2053554	2053554 M 137	Thermally Annealed			17/10/2014	2
Hiltaba Suite	mineralization-absent	2053554	2053554 M 135	Thermally Annealed			17/10/2014	2
Hiltaba Suite	mineralization-absent	2053554	2053554 M 88	Thermally Annealed			17/10/2014	2

Appendix 4 Table A5 Zircon trace element data for GRV and Hiltaba Suite samples analyzed at Boise State University

Spot Number	P	Ti	Y	Nb	La	Ce	Pr	Nd	Sm	Eu	Gd	Tb	Dy	Ho
	ppm	ppm	ppm	ppm	ppm	ppm	ppm	ppm	ppm	ppm	ppm	ppm	ppm	ppm
1831634 M 47	259.45	19.13	709.19	2.80	0.02	34.76	0.11	1.88	3.95	1.18	16.74	6.22	73.61	26.48
1831634 M 42	238.98	24.21	640.91	1.60		19.92	0.09	1.93	3.47	1.14	18.40	5.40	67.09	23.28
1831634 L 9	348.20	26.15	1115.57	3.33	0.04	37.70	0.22	4.06	6.67	1.85	32.73	9.95	117.06	41.39
1831634 M 48	181.71	20.01	427.93	1.22		17.65	0.05	0.42	2.05	0.56	8.69	3.63	41.23	15.32
1831634 M 41	357.62	23.28	1134.25	3.70		30.11	0.15	3.92	6.74	1.71	31.07	9.83	116.02	41.01
1831634 L 5	367.70	29.11	1047.99	2.37	0.03	33.63	0.26	3.96	6.46	1.46	31.58	9.39	113.70	39.89
1831634 L 23	236.64	13.91	690.05	2.94		34.19	0.08	1.30	1.81	0.55	15.60	4.86	68.61	24.59
1831634 M 29	286.82	26.56	834.35	2.58		31.95	0.10	3.25	4.69	1.23	24.22	7.25	84.49	29.77
1831634 L 25	347.76	24.17	1271.11	4.55	0.03	35.60	0.30	5.39	8.20	1.50	33.40	10.95	128.18	47.16
1831634 M 31	292.30	22.45	1913.49	1.93	0.04	35.83	0.56	11.64	15.94	3.67	59.48	19.25	216.31	71.58
1831634 L 13	307.44	25.63	1519.82	1.65	0.05	30.53	0.39	6.94	12.49	2.77	48.88	14.84	170.16	57.23
1831634 L 22	322.15	26.11	1059.11	3.12	0.03	28.51	0.19	4.23	7.38	1.87	31.52	9.47	111.63	40.25
1831634 M 34	340.11	27.45	869.96	1.93	0.01	26.06	0.20	4.33	6.73	1.63	24.84	8.12	92.70	33.07
1831634 L 6	308.98	20.60	1004.20	3.38		42.61	0.10	2.45	6.16	1.15	28.18	9.12	105.47	37.50
1831634 L 3	204.37	10.14	604.11	3.28		28.26	0.03	0.65	2.09	0.37	12.28	4.10	54.23	20.69
1831634 L 16	353.55	23.40	1601.04	3.03	0.05	34.58	0.37	7.53	12.31	2.56	46.68	15.02	176.73	60.68
1831634 M 38	184.88	19.39	549.67	1.58		20.64	0.03	1.62	2.33	0.80	12.42	4.43	53.44	18.50
1831634 L 8	345.89	30.42	1189.96	2.82		37.47	0.27	3.66	7.20	2.15	34.08	10.72	121.31	44.16
1831634 M 35	304.07	15.06	2174.24	2.92	0.04	42.04	0.55	9.41	14.20	3.42	63.04	20.85	238.38	80.94
1831634 M 30	254.76	35.68	644.86	1.05		17.23	0.09	1.92	4.42	1.73	18.38	5.86	66.65	23.26
1831634 M 36	276.45	17.49	1934.24	1.76	0.12	35.31	0.52	11.59	16.26	3.24	63.76	19.44	218.21	71.63
1831634 L 15	271.33	20.04	831.54	2.77		34.04	0.11	3.23	4.84	1.28	21.83	7.35	88.13	30.85
1831634 L 21	338.21	24.57	1209.48	3.88		32.65	0.21	4.40	6.46	1.83	33.53	10.34	127.44	44.16
1831634 M 40	382.76	27.09	1294.82	4.08		37.69	0.20	4.77	8.55	2.14	37.84	12.02	129.98	47.45
1831634 L 10	303.97	23.09	1759.10	1.83	0.03	36.82	0.50	9.75	14.40	2.87	56.52	16.23	196.78	66.14
1831634 M 46	256.98	31.56	1339.77	0.96	0.04	22.17	0.39	7.56	12.15	3.33	41.92	13.06	144.84	48.93
1831634 L 11	351.85	21.31	2361.90	2.38	0.06	39.68	0.78	12.08	15.49	3.80	78.44	24.17	265.83	90.90
1831634 M 44	311.90	25.78	2046.96	1.93	0.06	36.14	0.61	11.87	14.16	4.00	65.68	19.37	221.75	77.59
1831634 L 20	328.10	23.37	2003.61	2.18		37.27	0.63	11.54	14.00	3.08	62.76	19.54	218.57	74.25
1831634 L 14	365.27	26.52	1555.81	3.88	0.05	36.20	0.38	6.57	10.47	2.20	42.46	13.63	159.01	56.80
1831634 L 2	368.06	29.95	1294.66	2.83	0.23	33.19	0.46	6.29	10.64	4.05	44.76	12.99	139.58	47.59
1831634 M 32	367.20	28.87	1419.28	4.77	0.04	40.73	0.40	5.40	8.99	1.99	38.21	12.25	144.44	50.62
1831634 L 19	330.17	20.66	2019.16	2.09		41.74	0.67	11.88	16.49	3.57	64.90	20.35	222.50	76.70
2053554 L 196	333.84	8.35	1016.52	1.05		43.73	0.12	3.35	6.16	2.92	27.26	8.50	87.55	31.15
2053554 M 79	238.37	7.75	1170.56	5.04	1.30	61.14	0.76	6.30	5.36	1.45	24.12	9.05	112.09	41.70
2053554 M 107	304.70	8.48	1119.59	3.20	0.12	67.08	0.19	4.22	6.22	1.79	27.82	9.39	108.56	40.25
2053554 M 227	195.80	8.56	771.18	2.18		36.98	0.10	1.63	3.60	1.34	19.55	6.21	69.49	26.72
2053554 M 92	241.93	7.72	1049.53	2.69		51.07	0.13	2.18	4.93	1.43	23.69	7.63	95.07	34.58
2053554 L 213	202.56	9.29	1140.12	3.45	0.22	63.18	0.34	4.97	6.99	2.37	30.25	9.24	111.92	41.50
2053554 L 222	184.96	6.53	1138.02	5.64		64.88	0.05	1.91	4.21	1.00	22.47	7.49	100.58	38.69
2053554 M 125	242.75	8.55	1116.41	2.69		43.62	0.08	2.50	4.72	1.34	25.13	8.79	102.17	38.97
2053554 M 232	230.73	10.54	977.72	3.87	0.47	64.64	0.96	8.14	9.38	2.53	27.41	7.86	99.77	35.63
2053554 M 82	246.78	7.99	1094.75	3.20	0.02	65.29	0.19	2.84	6.81	2.09	26.39	9.08	102.37	38.02
2053554 L 206	196.07	7.94	796.66	2.21		50.63	0.09	2.54	4.98	1.48	20.62	6.65	76.44	28.05
2053554 L 214	216.84	8.26	908.30	2.99		70.17	0.12	2.50	6.10	1.43	23.54	7.52	94.31	32.61
2053554 M 93	246.20	12.76	964.45	2.97	0.45	39.33	0.90	7.66	5.87	1.57	22.31	7.61	88.95	31.54
2053554 L 208	199.17	8.38	947.27	2.67		36.91	0.11	2.97	5.41	1.67	23.41	7.21	92.51	33.75
2053554 M 83	234.18	8.00	1097.00	3.47	0.10	49.89	0.13	1.97	5.21	1.68	24.86	7.88	101.21	38.53
2053554 M 81	202.08	8.93	664.31	1.59	0.11	38.63	0.14	1.90	3.71	1.20	15.71	5.17	64.70	23.29
2053554 M 229	206.33	7.96	1287.60	3.73	0.07	58.66	0.19	3.48	7.30	2.31	35.62	10.62	125.64	44.06
2053554 M 115	280.09	6.59	1285.65	4.37		55.01	0.12	2.16	5.47	1.55	30.86	9.71	119.94	45.16
2053554 L 221	201.32	7.96	1044.62	3.12	0.12	47.97	0.09	2.99	6.01	1.64	25.54	7.92	95.08	35.37
2053554 M 106	304.15	8.16	1829.64	2.96	0.11	55.56	0.34	6.38	12.13	3.15	48.62	15.16	182.34	64.88
2053554 M 85	235.09	7.58	1040.75	3.51	0.05	50.96	0.12	2.68	5.21	1.75	23.91	8.30	99.08	36.78
2053554 L 207	274.30	7.06	1429.71	4.84	0.90	80.51	0.43	5.23	7.33	2.77	37.11	12.02	141.74	52.27
2053554 M 118	245.10	8.07	1818.94	3.17	0.02	61.10	0.34	6.38	10.09	3.55	46.48	15.14	174.41	63.65
2053554 L 202	190.23	7.73	821.16	1.99		53.08	0.13	2.09	4.91	1.52	21.10	7.19	82.25	29.24
2053554 L 198	334.69	8.21	1548.87	5.32	0.03	89.85	0.28	4.08	6.10	2.24	36.85	12.45	136.56	53.60
2053554 L 212	189.53	6.69	1458.40	1.29	0.08	52.46	0.55	8.86	14.39	6.12	56.36	16.23	163.84	54.31
2053554 L 215	210.57	7.84	858.13	1.55		36.69	0.17	2.98	6.18	2.25	22.76	7.99	87.48	31.28
2053554 L 209	217.51	7.87	934.58	2.59		40.52	0.04	1.93	4.73	2.16	23.00	7.49	85.38	31.69
2053554 M 94	228.16	9.28	961.50	2.51	0.14	34.92	0.10	2.42	3.88	0.90	23.25	6.65	86.76	32.98
2053554 M 110	229.39	6.75	1893.08	2.89		58.04	0.21	6.17	10.93	2.55	49.30	15.16	185.48	64.88
2053554 L 224	201.58	8.69	937.64	2.41		47.48	0.15	2.10	4.78	1.61	22.72	7.27	86.81	33.27
2053554 M 130	232.39	7.12	2412.47	2.22	0.88	59.99	0.83	11.09	15.11	4.73	67.86	19.96	234.37	84.93
2053554 M 126	200.56	7.15	1172.65	3.24		61.78	0.09	2.56	4.89	1.66	25.86	9.02	105.04	40.19
2053554 L 217	201.76	6.71	1057.26	4.37		56.45	0.13	1.80	5.03	1.97	23.14	7.62	98.16	37.62
2053554 L 225	226.53	6.88	1224.83	3.66		55.71	0.07	2.83	5.49	1.94	26.24	8.56	110.51	42.77
2053554 M 137	243.47	8.15	1149.38	3.00		60.00	0.14	2.14	5.08	1.72	28.67	8.62	101.80	38.78
2053554 M 135	225.35	7.91	1252.11	4.03		63.62	0.19	2.72	6.28	1.77	26.64	9.16	112.12	42.86
2053554 M 88	276.12	8.05	1255.80	3.37		60.90	0.14	2.62	5.26	1.64	29.83	8.70	112.33	41.83

Appendix 4 Table A5 Zircon trace element data for GRV and Hiltaba Suite samples analyzed at Boise State University

Spot Number	Er	Tm	Yb	Lu	Hf	Th	U	Eu/Eu*	Ce/Ce*	$(Yb/Gd)_N$	Ti-in-Zircon	Total REE	Th/U
	ppm	ppm	ppm	ppm	ppm	ppm	ppm						
1831634 M 47	104.58	26.59	282.89	33.78	8617.57	137.76	112.34	0.44	180.81	20.94	868	613	1.2
1831634 M 42	95.61	24.05	252.33	31.91	7285.88	64.29	56.03	0.44	211.53	16.99	896	545	1.1
1831634 L 9	171.89	40.65	426.34	53.19	7878.80	154.61	123.95	0.38	102.18	16.14	906	944	1.2
1831634 M 48	65.32	17.08	180.83	21.62	8298.82	41.17	47.64	0.40	342.52	25.78	873	374	0.9
1831634 M 41	174.84	42.69	437.33	56.90	7523.77	121.53	120.98	0.36	197.36	17.44	891	952	1.0
1831634 L 5	159.20	37.18	388.57	49.77	7953.00	163.90	122.26	0.31	97.71	15.25	919	875	1.3
1831634 L 23	109.87	27.92	303.28	38.80	9108.87	99.80	108.43	0.32	409.12	24.10	831	631	0.9
1831634 M 29	125.54	29.41	315.52	38.04	7700.76	124.38	104.32	0.35	301.58	16.14	908	695	1.2
1831634 L 25	196.96	47.53	518.74	66.50	7659.09	145.95	160.87	0.28	93.18	19.25	896	1100	0.9
1831634 M 31	291.08	66.74	614.41	75.21	7580.25	225.24	141.89	0.36	61.63	12.80	887	1482	1.6
1831634 L 13	226.46	52.06	530.22	65.03	7428.19	168.65	117.07	0.34	56.21	13.44	903	1218	1.4
1831634 L 22	169.88	40.26	433.21	55.25	7275.70	111.84	116.08	0.38	94.48	17.03	906	934	1.0
1831634 M 34	133.42	32.30	336.74	42.00	7090.89	106.59	90.09	0.39	143.33	16.80	912	742	1.2
1831634 L 6	158.29	38.91	402.70	50.90	8642.43	184.06	161.81	0.27	400.19	17.71	876	884	1.1
1831634 L 3	97.16	24.91	266.73	38.65	10299.09	93.97	119.44	0.23	908.75	26.93	798	550	0.8
1831634 L 16	244.62	57.59	601.87	68.85	7396.41	189.66	158.31	0.33	64.23	15.98	892	1329	1.2
1831634 M 38	82.93	20.63	224.48	28.76	8049.05	67.22	65.47	0.45	584.54	22.40	869	471	1.0
1831634 L 8	183.02	43.85	457.92	59.26	7429.42	225.24	169.98	0.42	135.41	16.65	925	1005	1.3
1831634 M 35	322.50	72.98	722.59	88.61	8232.56	289.58	189.46	0.35	73.13	14.20	840	1680	1.5
1831634 M 30	98.36	23.37	237.13	29.17	7476.49	64.24	49.01	0.59	192.12	15.99	946	528	1.3
1831634 M 36	294.94	63.61	637.92	77.27	7817.36	223.35	137.64	0.31	34.45	12.40	857	1514	1.6
1831634 L 15	128.58	31.78	335.43	39.57	8059.08	136.96	125.71	0.38	292.88	19.04	873	727	1.1
1831634 L 21	185.22	47.06	499.21	62.94	7188.46	136.77	152.83	0.38	155.22	18.45	898	1055	0.9
1831634 M 40	201.87	49.21	516.29	66.23	7048.41	161.33	151.90	0.36	189.25	16.91	910	1114	1.1
1831634 L 10	270.64	62.38	631.08	76.81	7976.90	215.25	151.69	0.31	74.51	13.84	890	1441	1.4
1831634 M 46	189.01	43.38	423.77	50.50	7000.00	121.99	75.37	0.45	44.00	12.53	930	1001	1.6
1831634 L 11	367.31	82.68	812.85	97.84	7861.56	321.19	204.56	0.33	44.76	12.84	881	1892	1.6
1831634 M 44	308.16	70.45	702.68	82.15	7345.04	240.37	157.61	0.40	45.95	13.26	904	1615	1.5
1831634 L 20	303.25	68.63	706.98	86.25	7403.89	243.00	169.53	0.32	57.63	13.96	892	1607	1.4
1831634 L 14	235.73	57.80	609.09	73.88	7177.73	182.09	176.11	0.32	63.65	17.78	907	1304	1.0
1831634 L 2	197.61	46.98	466.85	65.64	8302.85	201.08	137.54	0.57	25.33	12.93	923	1077	1.5
1831634 M 32	218.01	54.27	555.70	69.97	7194.21	181.50	169.14	0.33	81.05	18.02	918	1201	1.1
1831634 L 19	306.20	69.92	694.82	82.55	7468.47	261.52	179.96	0.33	61.20	13.27	877	1612	1.5
2053554 L 196	142.23	29.56	275.02	48.40	8429.51	102.97	55.31	0.69	371.89	12.50	778	706	1.9
2053554 M 79	180.93	45.49	487.64	68.50	7461.61	122.21	127.18	0.39	15.06	25.06	770	1046	1.0
2053554 M 107	171.95	40.20	387.58	57.12	8550.30	243.39	157.63	0.42	107.67	17.26	779	922	1.5
2053554 M 227	119.48	28.68	324.31	42.36	6644.20	99.39	90.33	0.49	380.78	20.56	780	680	1.1
2053554 M 92	159.72	35.67	330.47	56.71	9678.30	186.57	117.61	0.41	371.05	17.28	770	803	1.6
2053554 L 213	181.16	45.02	463.52	59.24	5962.06	145.60	124.18	0.50	57.51	18.99	789	1020	1.2
2053554 L 222	176.87	43.24	443.13	69.63	8878.64	214.69	188.11	0.31	1192.37	24.44	754	974	1.1
2053554 M 125	170.93	38.32	379.60	66.93	9120.77	161.50	113.01	0.38	567.92	18.72	780	883	1.4
2053554 M 232	149.82	36.41	361.09	46.85	7038.26	214.34	158.53	0.48	23.49	16.32	802	851	1.4
2053554 M 82	167.22	40.17	398.09	54.67	7235.57	172.17	126.82	0.48	270.33	18.69	773	913	1.4
2053554 L 206	116.60	28.43	296.32	38.08	6987.11	151.84	113.64	0.45	542.07	17.81	773	671	1.3
2053554 L 214	143.28	34.87	363.19	44.06	6974.28	245.18	177.08	0.36	573.23	19.12	777	824	1.4
2053554 M 93	144.48	31.91	309.82	55.03	9433.48	117.45	95.75	0.42	15.24	17.21	822	747	1.2
2053554 L 208	144.67	36.82	385.43	54.24	6686.19	97.48	95.92	0.45	331.02	20.41	778	825	1.0
2053554 M 83	166.56	42.81	457.57	64.52	7219.65	115.60	110.30	0.45	107.12	22.81	774	963	1.0
2053554 M 81	104.75	24.60	252.71	34.21	7313.06	103.44	81.70	0.48	74.76	19.94	785	571	1.3
2053554 M 229	196.29	44.51	463.45	62.40	6994.86	158.20	135.42	0.44	125.31	16.12	773	1055	1.2
2053554 M 115	204.26	47.83	481.87	79.39	8536.98	133.42	122.25	0.37	447.94	19.35	755	1083	1.1
2053554 L 221	159.58	39.07	412.58	58.19	7510.72	109.57	96.80	0.40	114.82	20.02	773	892	1.1
2053554 M 106	269.00	60.59	586.55	87.19	8671.90	222.61	139.31	0.40	69.59	14.95	775	1392	1.6
2053554 M 85	161.25	38.86	411.45	62.44	7336.54	117.53	103.79	0.48	153.69	21.32	768	903	1.1
2053554 L 207	220.21	53.49	550.15	73.72	7135.05	240.95	188.19	0.51	31.69	18.37	761	1238	1.3
2053554 M 118	263.61	61.09	602.17	94.00	8344.29	204.61	127.53	0.50	201.08	16.05	774	1402	1.6
2053554 L 202	127.54	29.86	309.50	41.28	7367.92	134.52	105.97	0.46	395.25	18.18	770	710	1.3
2053554 L 198	229.13	51.47	499.55	83.70	9940.64	243.28	174.60	0.46	232.62	16.80	776	1206	1.4
2053554 L 212	206.81	47.87	471.70	56.69	5695.17	112.19	66.96	0.66	62.81	10.37	756	1156	1.7
2053554 L 215	134.05	32.88	342.75	43.59	6742.05	113.39	98.68	0.58	211.10	18.66	772	751	1.1
2053554 L 209	146.11	36.26	397.17	52.17	6358.08	78.99	84.10	0.63	1095.15	21.40	772	829	0.9
2053554 M 94	151.04	33.19	331.04	57.44	9475.30	106.86	92.65	0.29	70.61	17.65	788	765	1.2
2053554 M 110	285.49	65.74	654.18	92.36	8385.89	247.06	160.27	0.34	276.16	16.44	757	1490	1.5
2053554 L 224	138.85	35.80	311.28	52.25	8878.71	163.26	112.94	0.47	302.75	16.98	782	744	1.4
2053554 M 130	349.57	74.29	660.25	113.67	9304.68	282.03	138.46	0.45	17.20	12.06	762	1698	2.0
2053554 M 126	177.94	38.52	355.16	63.27	9268.51	147.53	96.46	0.45	670.34	17.02	762	886	1.5
2053554 L 217	167.62	40.92	445.38	60.66	6867.76	104.91	109.29	0.56	434.36	23.85	756	947	1.0
2053554 L 225	190.04	43.03	429.51	77.07	8265.72	184.29	129.28	0.49	807.76	20.28	759	994	1.4
2053554 M 137	167.39	38.89	361.57	60.32	9530.04	242.60	141.26	0.44	433.39	15.63	775	875	1.7
2053554 M 135	191.67	42.20	398.44	70.53	9428.03	187.45	127.21	0.42	331.99	18.53	772	968	1.5
2053554 M 88	194.86	43.55	435.29	74.73	9135.35	215.05	143.58	0.40	420.07	18.08	774	1012	1.5

Appendix 4 Table A5 Zircon trace element data for GRV and Hiltaba Suite samples analyzed at Boise State University

Unit	Group	Sample	Spot Number	Zircon Treatment	Discordance	Other	Analytical Session	Experiment
Included Data								number
Hiltaba Suite	mineralization-absent	2053554	2053554 M 231	Thermally Annealed			31/07/2014	1
Hiltaba Suite	mineralization-absent	2053554	2053554 L 201	Thermally Annealed			31/07/2014	1
Hiltaba Suite	mineralization-absent	2053554	2053554 M 105	Thermally Annealed			17/10/2014	2
Hiltaba Suite	mineralization-absent	2053554	2053554 M 136	Thermally Annealed			17/10/2014	2
Hiltaba Suite	mineralization-absent	2053554	2053554 M 101	Thermally Annealed			17/10/2014	2
Hiltaba Suite	mineralization-absent	2053554	2053554 M 239	Thermally Annealed			31/07/2014	1
Hiltaba Suite	mineralization-absent	2053554	2053554 M 134	Thermally Annealed			17/10/2014	2
Hiltaba Suite	mineralization-absent	2053554	2053554 M 78	Thermally Annealed			17/10/2014	2
Hiltaba Suite	mineralization-absent	2053554	2053554 M 86	Thermally Annealed			17/10/2014	2
Hiltaba Suite	mineralization-absent	2053554	2053554 M 120	Thermally Annealed			17/10/2014	2
Hiltaba Suite	mineralization-absent	2053554	2053554 M 234	Thermally Annealed			31/07/2014	1
Hiltaba Suite	mineralization-absent	2053554	2053554 M 98	Thermally Annealed			17/10/2014	2
Hiltaba Suite	mineralization-absent	2053554	2053554 M 131	Thermally Annealed			17/10/2014	2
Hiltaba Suite	mineralization-absent	2053554	2053554 M 102	Thermally Annealed			17/10/2014	2
Hiltaba Suite	mineralization-absent	2053554	2053554 M 139	Thermally Annealed			17/10/2014	2
Hiltaba Suite	mineralization-absent	2053554	2053554 M 108	Thermally Annealed			17/10/2014	2
Hiltaba Suite	mineralization-absent	2053554	2053554 M 132	Thermally Annealed			17/10/2014	2
Hiltaba Suite	mineralization-absent	2053554	2053554 M 133	Thermally Annealed			17/10/2014	2
Hiltaba Suite	mineralization-absent	2053554	2053554 L 210	Thermally Annealed			31/07/2014	1
Hiltaba Suite	mineralization-absent	2053554	2053554 L 220	Thermally Annealed			31/07/2014	1
Hiltaba Suite	mineralization-absent	2053554	2053554 L 223	Thermally Annealed			31/07/2014	1
Hiltaba Suite	mineralization-absent	2053554	2053554 M 237	Thermally Annealed			31/07/2014	1
Hiltaba Suite	mineralization-absent	2053554	2053554 M 121	Thermally Annealed			17/10/2014	2
Hiltaba Suite	mineralization-absent	2053554	2053554 M 138	Thermally Annealed			17/10/2014	2
Hiltaba Suite	mineralization-absent	2053554	2053554 M 230	Thermally Annealed			31/07/2014	1
Hiltaba Suite	mineralization-absent	2053554	2053554 M 91	Thermally Annealed			17/10/2014	2
Hiltaba Suite	mineralization-absent	2053554	2053554 M 84	Thermally Annealed			17/10/2014	2
Hiltaba Suite	mineralization-absent	2053554	2053554 M 238	Thermally Annealed			31/07/2014	1
Hiltaba Suite	mineralization-absent	2053554	2053554 M 124	Thermally Annealed			17/10/2014	2
Hiltaba Suite	mineralization-absent	2053554	2053554 M 123	Thermally Annealed			17/10/2014	2
Hiltaba Suite	mineralization-absent	2053554	2053554 M 127	Thermally Annealed			17/10/2014	2
Hiltaba Suite	mineralization-absent	2053554	2053554 M 119	Thermally Annealed			17/10/2014	2
Hiltaba Suite	mineralization-absent	2053555	2053555 L 250	Thermally Annealed			31/07/2014	1
Hiltaba Suite	mineralization-absent	2053555	2053555 L 262	Thermally Annealed			31/07/2014	1
Hiltaba Suite	mineralization-absent	2053555	2053555 L 264	Thermally Annealed			31/07/2014	1
Hiltaba Suite	mineralization-absent	2053555	2053555 L 268	Thermally Annealed			31/07/2014	1
Hiltaba Suite	mineralization-absent	2053555	2053555 M 270	Thermally Annealed			31/07/2014	1
Hiltaba Suite	mineralization-absent	2053555	2053555 M 277	Thermally Annealed			31/07/2014	1
Hiltaba Suite	mineralization-absent	2053555	2053555 M 278	Thermally Annealed			31/07/2014	1
Hiltaba Suite	mineralization-absent	2053555	2053555 M 280	Thermally Annealed			31/07/2014	1
Hiltaba Suite	mineralization-absent	2053555	2053555 M 283	Thermally Annealed			31/07/2014	1
Hiltaba Suite	mineralization-absent	2053555	2053555 L 258	Thermally Annealed			31/07/2014	1
Hiltaba Suite	mineralization-absent	2115491	2115491 M 312	Thermally Annealed			8/01/2016	4
Hiltaba Suite	mineralization-absent	2115491	2115491 M 289	Thermally Annealed			8/01/2016	4
Hiltaba Suite	mineralization-absent	2115491	2115491 L 282	Thermally Annealed			8/01/2016	5
Hiltaba Suite	mineralization-absent	2115491	2115491 M 311	Thermally Annealed			8/01/2016	4
Hiltaba Suite	mineralization-absent	2115491	2115491 M 290	Thermally Annealed			8/01/2016	4
Hiltaba Suite	mineralization-absent	2115491	2115491 M 298	Thermally Annealed			8/01/2016	4
Hiltaba Suite	mineralization-absent	2115491	2115491 L 283	Thermally Annealed			8/01/2016	5
Hiltaba Suite	mineralization-absent	2115491	2115491 L 285	Thermally Annealed			8/01/2016	5
Hiltaba Suite	mineralization-absent	2115491	2115491 M 297	Thermally Annealed			8/01/2016	4
Hiltaba Suite	mineralization-absent	2115491	2115491 M 294	Thermally Annealed			8/01/2016	4
Hiltaba Suite	mineralization-absent	2115491	2115491 M 307	Thermally Annealed			8/01/2016	4
Hiltaba Suite	mineralization-absent	2115491	2115491 M 301	Thermally Annealed			8/01/2016	4
Hiltaba Suite	mineralization-absent	2115491	2115491 L 286	Thermally Annealed			8/01/2016	5
Hiltaba Suite	mineralization-absent	2115491	2115491 M 304	Thermally Annealed			8/01/2016	4
Hiltaba Suite	mineralization-absent	2115491	2115491 M 300	Thermally Annealed			8/01/2016	4
Hiltaba Suite	mineralization-absent	2115491	2115491 M 299	Thermally Annealed			8/01/2016	4
Hiltaba Suite	mineralization-absent	2115491	2115491 M 314	Thermally Annealed			8/01/2016	4
Hiltaba Suite	mineralization-absent	2115491	2115491 M 310	Thermally Annealed			8/01/2016	4
Hiltaba Suite	mineralization-absent	2115491	2115491 L 280	Thermally Annealed			8/01/2016	5
Hiltaba Suite	mineralization-absent	2115491	2115491 M 305	Thermally Annealed			8/01/2016	4
Hiltaba Suite	mineralization-absent	2115491	2115491 M 293	Thermally Annealed			8/01/2016	4
Hiltaba Suite	mineralization-absent	2115491	2115491 M 302	Thermally Annealed			8/01/2016	4
Hiltaba Suite	mineralization-absent	2115491	2115491 M 308	Thermally Annealed			8/01/2016	4
Hiltaba Suite	mineralization-absent	2115491	2115491 L 281	Thermally Annealed			8/01/2016	5
Hiltaba Suite	mineralization-absent	2115491	2115491 M 288	Thermally Annealed			8/01/2016	4
Hiltaba Suite	mineralization-absent	2115491	2115491 M 291	Thermally Annealed			8/01/2016	4
Hiltaba Suite	mineralization-absent	2115491	2115491 M 306	Thermally Annealed			8/01/2016	4
Hiltaba Suite	mineralization-absent	2115491	2115491 M 303	Thermally Annealed			8/01/2016	4
Hiltaba Suite	mineralization-absent	2115491	2115491 M 292	Thermally Annealed			8/01/2016	4

Appendix 4 Table A5 Zircon trace element data for GRV and Hiltaba Suite samples analyzed at Boise State University

Spot Number	P	Ti	Y	Nb	La	Ce	Pr	Nd	Sm	Eu	Gd	Tb	Dy	Ho
	ppm	ppm	ppm	ppm	ppm	ppm	ppm	ppm	ppm	ppm	ppm	ppm	ppm	ppm
2053554 M 231	201.99	7.66	982.75	3.42	0.04	52.00	0.10	2.12	4.36	1.50	23.52	7.85	92.97	34.48
2053554 L 201	194.12	6.38	1874.40	3.00	0.03	59.61	0.35	6.71	13.90	3.75	54.88	16.56	197.51	68.83
2053554 M 105	310.34	7.26	1237.92	4.86	2.79	76.38	0.89	5.38	6.66	1.47	27.20	9.04	114.83	41.88
2053554 M 136	227.49	7.52	1294.73	3.71	0.01	72.38	0.14	2.81	5.29	1.56	30.26	9.77	118.65	44.41
2053554 M 101	222.10	6.94	1469.46	5.13		81.33	0.18	3.05	5.81	1.95	32.59	11.16	133.12	49.37
2053554 M 239	224.89	8.55	949.89	2.22		62.65	0.18	3.05	5.22	2.37	26.30	8.69	98.95	33.68
2053554 M 134	242.85	7.62	1243.75	3.58		55.59	0.07	2.57	5.40	1.72	29.77	8.99	112.61	43.35
2053554 M 78	241.56	8.79	794.18	2.57		36.44	0.10	1.95	4.03	1.26	19.03	6.73	75.87	27.70
2053554 M 86	230.51	7.50	975.84	2.62	0.05	48.36	0.12	2.25	4.85	1.21	22.87	7.81	95.14	33.47
2053554 M 120	227.00	6.78	1348.89	4.93	1.36	81.09	1.32	11.26	9.87	2.26	34.22	9.82	124.99	45.79
2053554 M 234	199.33	7.90	1008.71	3.26		50.06	0.14	1.70	4.59	1.57	23.88	7.71	89.55	35.67
2053554 M 98	232.75	8.55	1456.36	5.09		62.33	0.09	2.93	6.17	2.09	31.56	10.45	133.47	49.65
2053554 M 131	216.58	8.25	1132.16	2.59	0.11	56.53	0.13	2.83	4.50	1.56	26.35	8.42	105.22	39.60
2053554 M 102	278.27	7.66	1296.35	4.40		59.65	0.12	2.85	4.87	1.21	27.39	9.06	120.75	43.89
2053554 M 139	268.82	7.07	1315.54	2.40		45.13	0.09	3.01	5.55	1.74	30.05	9.22	121.48	44.03
2053554 M 108	246.56	8.26	1053.08	3.16	0.04	51.11	0.17	2.80	6.15	1.62	23.66	8.08	97.42	36.67
2053554 M 132	240.16	6.27	1733.61	1.88		46.98	0.29	5.90	9.47	3.02	43.94	14.67	164.20	62.93
2053554 M 133	262.69	9.15	1250.04	2.89		48.40	0.11	2.29	5.76	2.06	27.52	9.14	112.32	42.38
2053554 L 210	242.92	7.93	933.80	2.91		65.06	0.15	3.23	5.11	1.84	24.96	7.82	94.66	35.04
2053554 L 220	368.46	6.50	855.91	2.25		39.60	0.05	0.96	3.45	1.57	19.91	6.89	80.86	30.83
2053554 L 223	220.24	8.24	1124.67	2.59		65.93	0.11	2.79	6.42	1.91	25.56	8.36	109.83	39.38
2053554 M 237	225.47	8.85	946.06	2.60		55.88	0.12	2.79	3.89	1.98	25.38	7.18	87.25	33.56
2053554 M 121	232.96	8.07	1198.75	3.26	0.14	63.20	0.34	2.80	6.10	1.68	28.82	8.99	109.93	41.62
2053554 M 138	248.93	8.47	1181.10	2.73		56.15	0.14	2.17	4.76	1.55	26.92	9.59	106.10	40.40
2053554 M 230	235.77	9.16	1197.51	2.35	0.04	42.47	0.22	4.54	8.65	1.88	33.02	9.83	116.29	42.12
2053554 M 91	212.99	8.97	1176.62	2.87		42.88	0.07	1.55	4.65	1.53	25.72	8.42	105.47	37.46
2053554 M 84	241.99	7.85	1128.95	4.91		52.44	0.06	2.03	4.17	1.20	20.98	7.95	97.25	36.89
2053554 M 238	316.39	8.29	879.87	2.24		37.78	0.10	2.28	4.91	1.21	20.81	6.68	84.49	33.28
2053554 M 124	237.51	7.59	1347.27	2.67		44.68	0.12	3.58	6.72	1.79	30.74	11.09	126.26	47.25
2053554 M 123	243.64	8.06	1199.27	3.37		46.27	0.12	2.19	4.83	1.91	26.42	8.73	105.59	42.76
2053554 M 127	229.55	6.81	1379.33	4.52		64.26	0.11	1.87	5.51	1.69	29.23	10.28	123.50	46.81
2053554 M 119	256.24	7.45	1358.24	5.51	0.93	58.86	0.86	7.10	7.89	1.80	30.74	9.71	123.90	47.52
2053555 L 250	271.65	14.24	1845.01	4.82		35.49	0.53	7.49	11.22	2.01	47.50	15.88	172.70	66.03
2053555 L 262	292.07	14.04	846.56	5.98	0.01	50.74	0.19	2.15	3.23	0.63	18.39	6.41	76.71	31.20
2053555 L 264	310.74	8.61	2158.27	5.18	0.03	22.55	0.43	5.05	13.15	2.38	58.41	19.43	227.91	78.20
2053555 L 268	299.66	15.97	2381.16	3.35	0.03	22.05	0.44	7.76	12.46	2.28	62.77	21.03	236.53	83.48
2053555 M 270	342.00	11.96	1114.32	5.74	0.38	57.15	1.06	7.43	7.52	1.56	27.65	9.06	110.03	39.56
2053555 M 277	325.34	13.62	811.76	5.80	0.61	46.90	0.16	2.29	3.92	0.92	16.49	5.99	79.11	29.67
2053555 M 278	290.66	12.81	1217.06	2.28		10.66	0.26	4.76	7.60	1.23	30.83	10.88	127.47	44.36
2053555 M 280	327.43	6.25	738.31	4.94		24.28		0.56	2.20	0.25	12.55	4.89	65.31	24.07
2053555 M 283	356.61	12.03	1656.76	7.82		31.32	0.27	4.62	8.05	1.38	38.99	13.35	154.94	59.87
2053555 L 258	66.05	0.85	205.47	4.10	0.07	12.31	0.08	0.76	0.26	0.07	1.20	0.66	10.66	5.48
2115491 M 312	257.87	8.71	915.46	3.73	0.03	13.66	0.10	1.97	3.98	0.19	22.32	7.88	98.26	33.43
2115491 M 289	178.93	7.48	648.60	3.90		13.98	0.03	0.53	2.21	0.13	11.71	4.45	62.67	24.22
2115491 L 282	225.33	11.06	645.53	2.91		11.66	0.09	0.86	2.85	0.30	16.15	5.54	71.94	25.76
2115491 M 311	235.84	9.40	786.26	3.43		12.09	0.03	1.23	3.73	0.33	19.42	6.83	84.82	29.68
2115491 M 290	186.17	6.35	612.47	3.07	0.11	10.75	0.17	1.51	3.56	0.29	13.67	5.31	57.23	20.97
2115491 M 298	179.12	7.10	614.50	3.67		12.90		0.24	2.06	0.13	11.64	4.75	55.60	22.65
2115491 L 283	196.36	2.80	811.41	2.55		10.87	0.07	1.79	3.41	0.33	21.89	7.38	89.76	32.07
2115491 L 285	182.02	5.75	584.15	4.68	0.01	13.91	0.03	0.88	1.80	0.17	11.14	4.43	56.32	21.88
2115491 M 297	214.56	7.52	774.19	4.02		14.51	0.04	0.89	3.04	0.16	15.59	5.84	75.62	28.80
2115491 M 294	231.42	9.01	804.06	2.94		10.08	0.04	1.49	3.61	0.33	20.20	6.54	82.40	29.72
2115491 M 307	191.95	6.78	811.28	3.57		10.37	0.02	1.68	3.66	0.25	19.96	6.72	81.41	30.75
2115491 M 301	207.65	6.93	707.07	4.52		14.65	0.06	0.63	2.52	0.22	13.64	5.72	72.52	25.11
2115491 L 286	178.39	6.28	511.15	3.52		10.33	0.02	0.54	1.27	0.15	10.32	3.96	54.74	19.04
2115491 M 304	128.46	3.37	347.87	3.03		8.16		0.12	0.92	0.05	4.76	2.13	29.95	11.82
2115491 M 300	266.79	7.12	1032.31	5.85	0.15	19.46	0.17	2.77	5.28	0.89	22.66	8.83	109.27	37.98
2115491 M 299	218.21	9.04	801.24	3.77		12.42	0.03	1.15	2.84	0.16	19.17	6.42	81.38	30.62
2115491 M 314	193.57	5.78	712.21	4.48		14.61	0.02	0.55	2.50	0.19	16.45	5.43	68.12	25.65
2115491 M 310	242.21	9.84	801.69	3.90		13.13	0.07	1.16	3.31	0.30	19.88	7.17	85.25	29.71
2115491 L 280	196.48	7.83	697.85	4.33		12.98	0.04	0.92	2.79	0.22	15.46	5.94	74.19	27.27
2115491 M 305	196.52	4.86	863.46	2.97		10.34	0.07	1.66	3.53	0.21	20.36	7.38	88.39	31.53
2115491 M 293	132.72	4.85	430.25	3.35	0.02	8.03		0.48	1.33	0.09	6.90	2.78	42.02	15.93
2115491 M 302	154.47	10.19	540.38	2.57		7.53	0.01	0.72	2.30	0.22	13.36	4.09	52.61	19.27
2115491 M 308	180.93	6.02	518.66	3.17		10.59		0.52	1.84	0.15	11.42	3.48	47.48	18.93
2115491 L 281	235.39	8.15	1167.06	1.87		11.05	0.08	3.25	6.76	0.73	36.20	12.13	133.87	46.92
2115491 M 288	207.33	6.44	1029.61	3.09	0.08	12.10	0.19	3.72	6.07	0.62	28.34	9.66	112.84	38.40
2115491 M 291	203.70	7.74	593.76	2.87		10.33	0.01	0.85	1.83	0.16	11.66	4.93	61.54	22.49
2115491 M 306	198.68	7.07	780.58	3.09		9.70	0.03	1.13	3.21	0.28	18.28	6.11	78.37	28.71
2115491 M 303	225.07	6.56	935.54	6.13		20.65	0.09	0.81	2.90	0.20	20.90	7.19	93.50	34.58
2115491 M 292	186.75	6.80	635.00	3.35		10.81	0.01	0.75	1.75	0.23	15.67	5.26	61.99	23.58

Appendix 4 Table A5 Zircon trace element data for GRV and Hiltaba Suite samples analyzed at Boise State University

Spot Number	Er	Tm	Yb	Lu	Hf	Th	U	Eu/Eu*	Ce/Ce*	$(Yb/Gd)_N$	Ti-in-Zircon	Total REE	Th/U
	ppm	ppm	ppm	ppm	ppm	ppm	ppm						
2053554 M 231	156.06	38.62	419.67	56.15	6670.40	92.60	100.62	0.45	203.93	22.12	769	889	0.9
2053554 L 201	288.88	66.49	635.85	88.67	7588.19	223.12	146.01	0.42	135.56	14.36	752	1502	1.5
2053554 M 105	186.23	44.17	440.09	67.08	9363.74	228.67	168.18	0.33	11.90	20.05	764	1024	1.4
2053554 M 136	199.35	43.18	418.23	71.80	10217.62	222.98	144.57	0.38	501.51	17.13	767	1018	1.5
2053554 M 101	222.01	48.68	470.85	77.71	9677.62	261.99	170.23	0.43	442.55	17.90	760	1138	1.5
2053554 M 239	144.01	33.87	343.49	42.07	6232.24	230.58	134.51	0.62	345.31	16.18	780	805	1.7
2053554 M 134	189.88	43.77	412.07	75.65	9431.80	146.21	112.85	0.41	795.24	17.15	769	981	1.3
2053554 M 78	120.45	28.87	318.78	42.64	6882.37	96.84	84.10	0.44	360.32	20.75	783	684	1.2
2053554 M 86	153.05	35.61	359.36	50.22	8079.08	137.23	109.46	0.35	154.83	19.47	767	814	1.3
2053554 M 120	199.80	44.29	436.45	68.60	9607.76	277.37	180.77	0.38	14.84	15.81	757	1071	1.5
2053554 M 234	167.62	39.33	412.79	56.70	6613.11	92.80	104.61	0.46	339.92	21.42	772	891	0.9
2053554 M 98	228.45	54.09	514.35	90.25	9013.04	159.03	124.28	0.46	684.07	20.20	780	1186	1.3
2053554 M 131	177.91	39.43	375.24	65.41	9847.76	177.13	113.74	0.44	113.90	17.65	777	903	1.6
2053554 M 102	204.08	46.34	437.24	73.70	9446.00	208.77	146.53	0.32	485.09	19.78	769	1031	1.4
2053554 M 139	195.89	43.76	429.43	72.51	8998.97	116.66	90.38	0.41	499.67	17.71	761	1002	1.3
2053554 M 108	158.42	37.40	386.13	57.11	8129.76	153.23	117.78	0.41	160.77	20.22	777	867	1.3
2053554 M 132	261.99	56.20	517.33	86.91	9468.01	180.47	101.40	0.45	158.06	14.59	750	1274	1.8
2053554 M 133	192.67	43.23	433.27	73.15	9018.62	155.66	105.10	0.50	436.06	19.51	787	992	1.5
2053554 L 210	140.76	33.63	353.20	46.63	6688.18	233.62	161.88	0.50	432.45	17.54	773	812	1.4
2053554 L 220	133.98	33.21	333.06	48.70	7364.62	83.24	84.05	0.58	724.07	20.73	753	733	1.0
2053554 L 223	173.83	38.67	361.92	57.90	8581.96	251.96	156.89	0.46	569.61	17.55	776	893	1.6
2053554 M 237	141.78	35.24	356.44	47.14	6851.46	165.65	130.62	0.61	444.28	17.41	784	799	1.3
2053554 M 121	183.20	41.30	395.93	65.11	9088.02	166.83	115.36	0.39	69.40	17.03	774	949	1.4
2053554 M 138	180.59	39.34	377.90	65.70	9412.04	181.28	116.39	0.42	388.60	17.40	779	911	1.6
2053554 M 230	181.12	44.21	447.04	58.16	7159.93	142.65	114.76	0.34	108.72	16.78	787	990	1.2
2053554 M 91	177.19	40.92	396.73	71.22	9527.80	137.43	102.57	0.43	625.90	19.11	785	914	1.3
2053554 M 84	176.96	42.90	450.48	67.84	8145.44	111.21	123.78	0.39	791.43	26.61	772	961	0.9
2053554 M 238	140.51	35.57	369.18	48.76	6973.96	93.75	99.44	0.37	384.55	21.98	777	786	0.9
2053554 M 124	203.96	47.31	462.10	79.74	9761.47	149.64	108.63	0.38	363.71	18.63	768	1065	1.4
2053554 M 123	187.18	43.87	411.03	74.43	9074.68	132.93	103.13	0.52	371.77	19.28	774	955	1.3
2053554 M 127	209.26	49.84	476.47	83.61	9037.30	139.68	110.99	0.41	588.85	20.20	758	1102	1.3
2053554 M 119	210.83	50.29	512.77	86.16	9391.92	149.20	144.86	0.35	16.15	20.67	767	1149	1.0
2053555 L 250	274.68	63.09	588.86	89.85	9522.35	322.05	203.12	0.27	65.72	15.36	834	1375	1.6
2053555 L 262	132.91	33.87	372.37	50.44	9028.96	248.22	299.73	0.25	272.37	25.09	832	779	0.8
2053555 L 264	315.52	72.51	697.29	94.99	8437.68	437.72	463.28	0.26	47.01	14.79	781	1608	0.9
2053555 L 268	355.06	80.69	696.03	107.51	9326.33	386.45	375.59	0.25	46.49	13.74	847	1688	1.0
2053555 M 270	175.25	44.39	451.25	57.44	9035.75	258.10	322.16	0.33	22.15	20.22	815	990	0.8
2053555 M 277	126.09	31.34	344.45	45.43	8023.75	200.76	268.11	0.35	36.24	25.88	829	733	0.7
2053555 M 278	184.34	43.11	440.03	53.15	6904.31	187.47	332.21	0.25	39.77	17.68	822	959	0.6
2053555 M 280	116.56	30.71	336.70	42.94	8898.63	230.88	335.19	0.15		33.25	750	661	0.7
2053555 M 283	259.39	61.97	682.76	87.11	8206.86	507.92	532.33	0.24	111.89	21.70	816	1404	1.0
2053555 L 258	36.24	13.27	196.37	36.61	10911.94	48.38	744.09	0.36	39.78	202.35	590	314	0.1
2115491 M 312	143.69	33.85	345.04	44.92	9516.25	106.94	158.71	0.06	60.75	19.16	782	749	0.7
2115491 M 289	104.50	26.04	269.18	34.92	9947.04	79.96	131.85	0.08	410.77	28.49	767	555	0.6
2115491 L 282	109.04	25.71	283.84	35.17	9248.17	71.83	117.17	0.14	133.49	21.78	807	589	0.6
2115491 M 311	126.84	31.19	312.83	41.21	9162.05	85.26	127.32	0.12	346.89	19.96	790	670	0.7
2115491 M 290	94.60	24.34	250.03	30.36	9196.75	59.02	100.32	0.13	19.17	22.67	751	513	0.6
2115491 M 298	98.26	24.65	248.77	35.52	10856.17	69.07	110.63	0.08		26.48	762	517	0.6
2115491 L 283	134.94	32.73	342.62	39.71	8812.90	71.41	115.15	0.12	154.01	19.40	679	718	0.6
2115491 L 285	94.49	24.87	271.48	32.66	10079.43	73.14	137.86	0.12	188.01	30.19	742	534	0.5
2115491 M 297	124.18	29.60	304.37	40.57	10111.62	91.90	134.42	0.07	343.63	24.19	767	643	0.7
2115491 M 294	126.52	31.22	313.18	38.94	8790.56	73.27	109.48	0.12	230.67	19.21	785	664	0.7
2115491 M 307	126.73	30.72	314.69	38.67	8836.60	80.53	123.22	0.09	445.42	19.53	757	666	0.7
2115491 M 301	114.98	28.21	286.22	36.93	10485.06	87.45	133.82	0.11	245.35	26.01	759	601	0.7
2115491 L 286	86.75	21.44	236.39	27.91	9752.53	57.12	110.92	0.12	433.65	28.39	750	473	0.5
2115491 M 304	57.11	15.86	183.25	26.36	11268.23	55.24	193.67	0.08		47.68	694	340	0.3
2115491 M 300	161.79	39.28	390.49	51.58	10743.86	136.31	193.48	0.25	29.41	21.36	762	851	0.7
2115491 M 299	125.49	30.58	299.54	38.90	9864.53	79.28	115.17	0.06	399.54	19.37	786	649	0.7
2115491 M 314	116.15	27.56	297.73	36.01	9751.85	86.49	142.40	0.09	616.87	22.44	742	611	0.6
2115491 M 310	128.22	31.32	313.46	39.31	9143.98	91.79	136.36	0.11	178.02	19.54	794	672	0.7
2115491 L 280	115.35	28.62	297.76	37.24	9862.16	81.79	132.48	0.10	332.81	23.87	771	619	0.6
2115491 M 305	130.74	32.17	321.33	41.63	9540.93	72.30	109.07	0.08	149.42	19.55	726	689	0.7
2115491 M 293	68.74	16.77	192.68	24.26	10155.26	47.82	114.88	0.09	98.34	34.58	726	380	0.4
2115491 M 302	83.73	20.19	213.52	29.38	9505.47	47.05	76.37	0.12	557.93	19.80	798	447	0.6
2115491 M 308	78.10	19.55	221.77	26.54	8736.04	57.05	100.36	0.10		24.07	746	440	0.6
2115491 L 281	189.00	44.15	450.83	53.35	9035.67	91.02	114.80	0.14	130.44	15.43	775	988	0.8
2115491 M 288	168.38	40.15	405.23	49.61	9523.17	96.91	132.27	0.14	23.55	17.72	752	875	0.7
2115491 M 291	94.71	23.85	252.97	31.15	8969.96	62.72	105.87	0.11	896.46	26.89	770	516	0.6
2115491 M 306	121.58	30.92	307.10	39.95	8683.47	66.58	102.68	0.11	273.62	20.82	761	645	0.6
2115491 M 303	148.42	35.45	379.76	48.21	10926.64	137.95	199.20	0.08	221.53	22.52	754	793	0.7
2115491 M 292	102.92	25.05	260.35	32.07	8917.39	68.05	109.67	0.13	1730.84	20.59	758	540	0.6

Appendix 4 Table A5 Zircon trace element data for GRV and Hiltaba Suite samples analyzed at Boise State University

Unit	Group	Sample	Spot Number	Zircon Treatment	Discordance	Other	Analytical Session	Experiment
Included Data								number
Hiltaba Suite	mineralization-absent	2115491	2115491 M 309	Thermally Annealed			8/01/2016	4
Hiltaba Suite	mineralization-absent	2115491	2115491 M 296	Thermally Annealed			8/01/2016	4
Hiltaba Suite	mineralization-absent	2115491	2115491 M 295	Thermally Annealed			8/01/2016	4
LGRV	mineralization-related	2131365	2131365 L 143	Thermally Annealed			7/01/2016	4
LGRV	mineralization-related	2131365	2131365 M 149	Thermally Annealed			7/01/2016	4
LGRV	mineralization-related	2131365	2131365 L 128	Thermally Annealed			7/01/2016	4
LGRV	mineralization-related	2131365	2131365 M 151	Thermally Annealed			7/01/2016	4
LGRV	mineralization-related	2131365	2131365 M 164	Thermally Annealed			7/01/2016	4
LGRV	mineralization-related	2131365	2131365 M 158	Thermally Annealed			7/01/2016	4
LGRV	mineralization-related	2131365	2131365 M 150	Thermally Annealed			7/01/2016	4
LGRV	mineralization-related	2131365	2131365 L 144	Thermally Annealed			7/01/2016	4
LGRV	mineralization-related	2131365	2131365 M 147	Thermally Annealed			7/01/2016	4
LGRV	mineralization-related	2131365	2131365 M 154	Thermally Annealed			7/01/2016	4
LGRV	mineralization-related	2131365	2131365 M 145	Thermally Annealed			7/01/2016	4
LGRV	mineralization-related	2131365	2131365 M 152	Thermally Annealed			7/01/2016	4
LGRV	mineralization-related	2131365	2131365 L 126	Thermally Annealed			7/01/2016	4
LGRV	mineralization-related	2131365	2131365 L 134	Thermally Annealed			7/01/2016	4
LGRV	mineralization-related	2131365	2131365 M 155	Thermally Annealed			7/01/2016	4
LGRV	mineralization-related	2131365	2131365 L 132	Thermally Annealed			7/01/2016	4
LGRV	mineralization-related	2131365	2131365 L 133	Thermally Annealed			7/01/2016	4
LGRV	mineralization-related	2131365	2131365 L 137	Thermally Annealed			7/01/2016	4
LGRV	mineralization-related	2131365	2131365 L 138	Thermally Annealed			7/01/2016	4
LGRV	mineralization-related	2131365	2131365 L 136	Thermally Annealed			7/01/2016	4
LGRV	mineralization-related	2131365	2131365 L 127	Thermally Annealed			7/01/2016	4
LGRV	mineralization-related	2131365	2131365 L 139	Thermally Annealed			7/01/2016	4
LGRV	mineralization-related	2131365	2131365 M 162	Thermally Annealed			8/01/2016	4
LGRV	mineralization-related	2131365	2131365 L 141	Thermally Annealed			7/01/2016	4
LGRV	mineralization-related	2131365	2131365 L 130	Thermally Annealed			7/01/2016	4
LGRV	mineralization-related	2131365	2131365 M 146	Thermally Annealed			7/01/2016	4
LGRV	mineralization-related	2131365	2131365 L 142	Thermally Annealed			7/01/2016	4
LGRV	mineralization-related	2131365	2131365 L 125	Thermally Annealed			7/01/2016	4
LGRV	mineralization-related	2131365	2131365 M 159	Thermally Annealed			7/01/2016	4
LGRV	mineralization-related	2131365	2131365 M 157	Thermally Annealed			7/01/2016	4
LGRV	mineralization-related	2131365	2131365 L 140	Thermally Annealed			7/01/2016	4
LGRV	mineralization-related	2131365	2131365 M 161	Thermally Annealed			7/01/2016	4
LGRV	mineralization-related	2131365	2131365 L 131	Thermally Annealed			7/01/2016	4
LGRV	mineralization-related	2131365	2131365 L 135	Thermally Annealed			7/01/2016	4
LGRV	mineralization-related	2131365	2131365 L 129	Thermally Annealed			7/01/2016	4
LGRV	mineralization-related	2131359	2131359 L 99	Thermally Annealed			7/01/2016	3
LGRV	mineralization-related	2131359	2131359 M 116	Thermally Annealed			7/01/2016	4
LGRV	mineralization-related	2131359	2131359 L 107	Thermally Annealed			7/01/2016	3
LGRV	mineralization-related	2131359	2131359 L 105	Thermally Annealed			7/01/2016	3
LGRV	mineralization-related	2131359	2131359 M 119	Thermally Annealed			7/01/2016	4
LGRV	mineralization-related	2131359	2131359 L 102	Thermally Annealed			7/01/2016	3
LGRV	mineralization-related	2131359	2131359 L 109	Thermally Annealed			7/01/2016	3
LGRV	mineralization-related	2131359	2131359 M 123	Thermally Annealed			7/01/2016	4
LGRV	mineralization-related	2131359	2131359 M 113	Thermally Annealed			7/01/2016	4
LGRV	mineralization-related	2131359	2131359 L 91	Thermally Annealed			7/01/2016	3
LGRV	mineralization-related	2131359	2131359 L 95	Thermally Annealed			7/01/2016	3
LGRV	mineralization-related	2131359	2131359 M 117	Thermally Annealed			7/01/2016	4
LGRV	mineralization-related	2131359	2131359 L 103	Thermally Annealed			7/01/2016	3
LGRV	mineralization-related	2131359	2131359 M 122	Thermally Annealed			7/01/2016	4
LGRV	mineralization-related	2131359	2131359 L 93	Thermally Annealed			7/01/2016	3
LGRV	mineralization-related	2131359	2131359 L 96	Thermally Annealed			7/01/2016	3
LGRV	mineralization-related	2131359	2131359 M 112	Thermally Annealed			7/01/2016	4
LGRV	mineralization-related	2131359	2131359 L 98	Thermally Annealed			7/01/2016	3
LGRV	mineralization-related	2131359	2131359 L 110	Thermally Annealed			7/01/2016	3
LGRV	mineralization-related	2131359	2131359 L 94	Thermally Annealed			7/01/2016	3
LGRV	mineralization-absent	2116683	2116683 M 80	Thermally Annealed			7/01/2016	3
LGRV	mineralization-absent	2116683	2116683 L 56	Thermally Annealed			7/01/2016	3
LGRV	mineralization-absent	2116683	2116683 L 49	Thermally Annealed			7/01/2016	3
LGRV	mineralization-absent	2116683	2116683 L 53	Thermally Annealed			7/01/2016	3
LGRV	mineralization-absent	2116683	2116683 L 68	Thermally Annealed			7/01/2016	3
LGRV	mineralization-absent	2116683	2116683 M 85	Thermally Annealed			7/01/2016	3
LGRV	mineralization-absent	2116683	2116683 L 63	Thermally Annealed			7/01/2016	3
LGRV	mineralization-absent	2116683	2116683 M 77	Thermally Annealed			7/01/2016	3
LGRV	mineralization-absent	2116683	2116683 L 64	Thermally Annealed			7/01/2016	3
LGRV	mineralization-absent	2116683	2116683 L 55	Thermally Annealed			7/01/2016	3
LGRV	mineralization-absent	2116683	2116683 L 57	Thermally Annealed			7/01/2016	3
LGRV	mineralization-absent	2116683	2116683 M 86	Thermally Annealed			7/01/2016	3
LGRV	mineralization-absent	2116683	2116683 L 60	Thermally Annealed			7/01/2016	3

Appendix 4 Table A5 Zircon trace element data for GRV and Hiltaba Suite samples analyzed at Boise State University

Spot Number	P	Ti	Y	Nb	La	Ce	Pr	Nd	Sm	Eu	Gd	Tb	Dy	Ho
	ppm	ppm	ppm	ppm	ppm	ppm	ppm	ppm	ppm	ppm	ppm	ppm	ppm	ppm
2115491 M 309	208.64	7.43	775.45	4.83		16.53	0.06	1.43	2.60	0.09	17.17	6.33	76.96	28.31
2115491 M 296	168.10	7.27	667.67	2.68	0.11	9.92	0.06	0.89	2.23	0.24	14.54	5.08	62.71	23.73
2115491 M 295	216.69	8.02	885.61	4.81	0.11	17.14	0.09	2.59	3.74	0.29	18.74	7.01	90.14	32.67
2131365 L 143	312.01	16.91	1079.49	2.83		27.41	0.10	1.91	3.71	1.01	25.36	9.22	107.59	38.51
2131365 M 149	303.28	16.86	1086.86	2.46		24.06	0.09	2.03	4.89	1.03	27.20	8.96	103.97	38.84
2131365 L 128	230.01	15.83	832.18	2.16		25.78	0.03	1.04	1.59	0.45	16.92	5.31	69.49	28.61
2131365 M 151	299.31	16.53	1298.21	3.14	0.04	28.86	0.17	3.07	5.70	1.59	32.27	10.79	129.46	45.50
2131365 M 164	249.51	19.69	916.89	1.91		23.30	0.12	1.54	3.69	1.05	21.91	7.25	92.07	34.13
2131365 M 158	238.90	15.94	855.87	2.14		26.50	0.04	1.38	2.95	0.67	16.63	6.47	81.65	31.00
2131365 M 150	246.52	18.36	891.46	1.90	0.10	25.66	0.09	1.37	3.58	0.94	18.46	7.31	82.30	32.43
2131365 L 144	205.18	15.06	662.41	1.80		20.02	0.03	0.74	1.54	0.58	13.54	4.98	61.52	23.84
2131365 M 147	302.85	19.25	1087.69	2.85		23.83	0.12	1.91	6.12	1.29	27.06	9.10	111.98	41.01
2131365 M 154	278.83	17.74	1019.41	2.02		23.37	0.06	1.44	3.73	1.01	24.36	7.60	95.29	36.13
2131365 M 145	290.06	16.16	1708.15	1.82	0.04	30.32	0.21	4.79	10.14	2.11	50.06	15.18	181.60	64.46
2131365 M 152	268.83	18.27	847.07	1.83	0.08	22.66	0.06	1.34	2.91	0.72	19.12	6.17	79.57	29.85
2131365 L 126	255.98	16.71	964.98	2.18		28.58	0.02	1.41	3.88	0.78	19.32	7.22	88.24	33.64
2131365 L 134	215.61	15.82	1424.46	1.38		26.07	0.15	2.54	6.81	1.70	40.29	12.72	154.68	55.30
2131365 M 155	290.85	14.91	1337.66	3.34	0.16	41.53	0.25	3.56	4.78	1.18	29.75	10.14	133.90	48.14
2131365 L 132	324.85	18.55	1444.46	3.69	0.09	39.94	0.47	4.65	7.30	2.07	34.25	12.16	140.75	52.16
2131365 L 133	317.27	21.54	2357.73	2.11	0.05	31.50	0.34	8.01	13.08	3.49	66.53	21.04	247.51	85.64
2131365 L 137	293.69	13.56	1774.77	1.97	0.03	38.92	0.20	4.00	10.50	1.49	43.87	15.07	188.19	67.52
2131365 L 138	293.62	16.65	1067.11	3.63	0.08	39.79	0.14	2.40	4.09	1.10	24.35	7.77	105.33	38.00
2131365 L 136	281.63	16.01	1867.19	2.05		35.35	0.24	5.43	10.12	2.04	49.76	16.69	190.86	69.87
2131365 L 127	318.40	26.08	1218.27	2.36	0.03	29.29	0.27	3.56	6.34	1.50	31.75	10.40	120.19	44.73
2131365 L 139	316.25	11.04	1724.54	2.58		40.60	0.19	3.45	9.07	1.82	46.80	15.94	184.17	65.71
2131365 M 162	301.90	14.59	1930.80	2.27	0.05	36.96	0.19	4.74	10.72	2.04	51.89	16.42	192.34	71.18
2131365 L 141	273.50	16.20	914.42	2.93		29.71	0.05	1.50	3.56	1.03	20.61	7.42	91.21	33.87
2131365 L 130	306.31	13.69	2373.57	2.01	0.02	44.04	0.21	4.34	13.42	2.06	58.34	19.80	233.10	86.65
2131365 M 146	266.84	17.49	798.81	2.08	0.12	25.27	0.50	3.89	4.57	1.41	21.20	6.87	86.88	31.09
2131365 L 142	262.97	18.29	841.81	2.19		26.82	0.06	1.86	3.47	0.54	17.91	6.43	87.82	31.20
2131365 L 125	277.17	15.29	1137.43	2.34		30.20	0.10	1.55	4.08	0.83	20.92	8.50	109.54	40.97
2131365 M 159	265.99	16.91	1041.76	2.84	0.51	32.48	0.32	3.30	4.33	1.07	22.87	8.40	101.45	37.83
2131365 M 157	275.72	19.85	972.01	2.41	0.02	26.14	0.08	1.37	2.87	1.15	22.10	7.49	94.33	35.81
2131365 L 140	369.63	27.71	1141.72	2.15	0.29	30.14	0.58	6.50	7.45	1.84	31.89	9.67	118.21	42.66
2131365 M 161	299.48	17.31	2312.56	2.26		35.45	0.29	7.08	14.30	2.77	60.66	19.41	232.53	83.38
2131365 L 131	239.85	19.60	987.88	2.29		25.72	0.08	1.45	3.86	0.95	21.39	7.50	98.06	35.76
2131365 L 135	262.93	19.71	821.55	1.91		24.38	0.05	1.82	3.80	0.76	17.45	6.93	79.29	29.53
2131365 L 129	346.23	16.83	1895.83	3.63	0.85	52.96	1.28	9.06	9.83	2.38	47.82	16.58	200.86	68.49
2131359 L 99	140.02	10.39	286.50	1.77		14.34		0.21	0.92	0.11	4.84	1.80	24.57	10.03
2131359 M 116	270.50	22.83	903.11	2.08		20.09	0.17	2.15	3.20	0.96	23.26	7.40	96.02	32.65
2131359 L 107	257.14	21.06	718.43	1.89		22.65	0.09	2.33	3.82	0.89	17.49	5.92	73.85	25.70
2131359 L 105	240.07	19.90	723.02	1.94		18.88	0.10	1.58	2.99	0.70	17.82	5.32	67.52	26.55
2131359 M 119	209.02	13.70	790.77	3.04	0.13	25.40	0.14	1.21	2.92	0.72	15.87	5.97	76.97	28.61
2131359 L 102	245.06	16.40	755.24	2.31		22.14	0.07	1.12	2.53	0.51	16.51	5.88	70.46	26.74
2131359 L 109	138.74	8.42	672.14	2.84		8.95	0.04	1.53	2.61	0.36	16.51	5.87	71.63	23.57
2131359 M 123	136.38	9.14	626.68	2.29	0.14	9.47	0.43	4.05	4.31	0.69	18.03	5.46	66.49	24.07
2131359 M 113	263.00	17.13	797.66	2.20		18.83	0.06	1.20	2.78	0.73	16.76	5.77	75.76	29.48
2131359 L 91	197.01	24.21	844.65	0.91		13.57	0.15	2.38	6.42	1.80	24.00	8.10	88.19	30.30
2131359 L 95	119.86	7.44	1034.11	2.08	0.17	9.52	0.58	5.03	7.17	1.44	30.09	9.74	115.46	38.95
2131359 M 117	204.24	14.27	747.43	2.36		20.32	0.04	1.10	2.91	0.56	19.38	5.41	75.75	26.82
2131359 L 103	210.04	14.79	743.74	2.39		28.82	0.10	2.32	3.46	0.76	18.00	5.86	70.23	26.38
2131359 M 122	272.64	17.03	1494.86	1.57	0.04	21.93	0.48	5.43	9.83	2.22	43.43	14.12	171.01	55.22
2131359 L 93	238.13	17.84	702.12	2.13		20.91	0.10	1.04	2.58	0.56	14.78	5.52	67.51	25.78
2131359 L 96	134.21	9.00	1524.23	2.67	0.22	9.80	0.48	6.80	11.91	1.66	45.79	14.70	169.11	56.79
2131359 M 112	233.28	7.91	1098.07	6.97		30.64	0.03	1.89	4.46	0.45	25.26	8.94	111.63	40.44
2131359 L 98	220.34	19.24	685.10	2.13	0.05	20.10	0.21	2.03	2.63	0.68	16.80	5.39	68.87	23.82
2131359 L 110	226.20	16.01	681.69	3.14		23.74	0.01	0.86	2.85	0.51	12.62	5.01	68.70	23.45
2131359 L 94	136.05	7.32	835.33	3.26	0.34	12.83	0.98	8.02	5.99	1.01	26.67	7.94	90.22	30.28
2116683 M 80	229.65	14.44	858.99	2.97	0.02	27.68	0.19	2.67	4.48	0.98	18.32	6.87	83.40	30.88
2116683 L 56	328.48	22.53	1179.48	3.16		34.96	0.16	2.99	5.72	1.45	30.22	9.16	110.46	40.34
2116683 L 49	294.18	18.57	912.22	3.70		29.08	0.08	1.85	3.49	0.95	19.30	6.82	86.81	30.66
2116683 L 53	261.27	20.64	1551.03	2.42		30.80	0.21	4.50	7.59	1.90	42.24	13.02	153.82	53.97
2116683 L 68	274.33	20.45	1032.11	2.99	0.06	32.83	0.19	3.46	6.16	1.33	23.53	8.07	103.41	35.65
2116683 M 85	228.14	15.27	616.76	3.07	0.04	33.60	0.04	1.24	2.95	0.58	11.97	4.68	57.91	21.23
2116683 L 63	207.42	15.21	631.91	3.16		24.80	0.04	0.53	1.47	0.44	12.44	4.02	56.06	21.76
2116683 M 77	260.23	20.44	1476.98	1.95		30.70	0.44	5.96	8.68	2.20	41.40	13.01	152.29	53.76
2116683 L 64	198.21	20.29	531.46	1.78		18.60	0.05	0.60	1.25	0.54	10.81	3.81	47.94	19.02
2116683 L 55	304.99	21.43	1165.13	3.06		26.70	0.12	2.24	5.49	1.20	30.05	9.80	110.91	40.60
2116683 L 57	256.36	18.21	831.29	2.51	1.00	29.03	0.30	2.77	3.35	0.85	17.79	6.34	78.60	28.45
2116683 M 86	232.70	19.45	718.02	2.81		26.88	0.07	1.18	2.14	0.55	17.12	5.96	67.07	26.72
2116683 L 60	314.77	20.73	1345.62	2.99	0.02	32.01	0.33	5.64	6.50	2.16	39.04	12.18	138.80	49.03

Appendix 4 Table A5 Zircon trace element data for GRV and Hiltaba Suite samples analyzed at Boise State University

Spot Number	Er	Tm	Yb	Lu	Hf	Th	U	Eu/Eu*	Ce/Ce*	$(Yb/Gd)_N$	Ti-in-Zircon	Total REE	Th/U
	ppm	ppm	ppm	ppm	ppm	ppm	ppm						
2115491 M 309	124.56	31.05	318.17	40.95	9641.81	99.10	157.79	0.04	292.40	22.96	766	664	0.6
2115491 M 296	104.53	25.58	275.55	36.80	10086.91	56.22	94.03	0.13	30.72	23.49	764	562	0.6
2115491 M 295	138.68	34.25	350.17	44.64	9800.84	112.17	160.70	0.11	41.14	23.15	774	740	0.7
2131365 L 143	167.74	41.29	419.17	55.89	9279.55	159.90	165.42	0.32	275.48	20.48	853	899	1.0
2131365 M 149	164.19	39.79	411.21	55.29	9285.42	151.43	144.75	0.27	271.77	18.74	853	882	1.0
2131365 L 128	131.56	31.53	308.90	48.50	11932.88	135.65	137.80	0.27	852.59	22.62	846	670	1.0
2131365 M 151	201.90	46.94	449.33	64.17	9562.28	196.39	185.35	0.36	85.96	17.26	851	1020	1.1
2131365 M 164	143.99	34.63	339.20	50.38	10310.28	136.60	133.31	0.36	186.43	19.18	871	753	1.0
2131365 M 158	134.60	32.28	325.98	46.45	10624.99	145.92	152.65	0.29	656.73	24.29	847	707	1.0
2131365 M 150	133.44	33.03	331.51	47.56	9327.24	150.00	155.59	0.35	66.70	22.26	863	718	1.0
2131365 L 144	110.28	26.22	259.62	38.57	10896.38	99.32	108.24	0.39	655.81	23.76	840	561	0.9
2131365 M 147	171.91	42.98	428.22	56.76	9036.99	150.33	159.22	0.31	200.93	19.61	868	922	0.9
2131365 M 154	157.90	36.18	362.62	57.46	11059.48	139.24	128.23	0.32	365.03	18.45	859	807	1.1
2131365 M 145	261.47	62.81	596.72	75.80	9198.31	256.95	202.64	0.29	82.62	14.77	848	1356	1.3
2131365 M 152	131.65	30.89	303.21	45.73	10791.65	124.58	125.97	0.29	79.51	19.66	862	674	1.0
2131365 L 126	153.85	35.76	355.90	53.50	11070.22	166.45	165.76	0.28	1523.75	22.83	852	782	1.0
2131365 L 134	224.83	51.76	516.88	67.14	9642.80	202.76	164.24	0.31	172.64	15.90	846	1161	1.2
2131365 M 155	210.76	50.31	491.69	74.08	11098.71	300.65	260.45	0.30	50.85	20.48	839	1100	1.2
2131365 L 132	224.15	52.84	508.59	73.48	11198.00	293.75	262.71	0.40	48.83	18.40	864	1153	1.1
2131365 L 133	347.92	79.73	746.20	101.64	9872.07	339.42	237.90	0.36	61.29	13.90	882	1753	1.4
2131365 L 137	280.73	65.45	670.20	82.49	9587.20	327.35	277.08	0.21	120.24	18.93	829	1469	1.2
2131365 L 138	164.98	42.29	436.67	56.85	9438.72	213.54	240.02	0.34	94.33	22.22	852	924	0.9
2131365 L 136	289.11	68.07	682.11	85.06	9606.75	313.78	255.73	0.28	145.26	16.99	847	1505	1.2
2131365 L 127	192.49	42.96	406.47	61.59	9726.43	227.51	196.46	0.32	75.13	15.86	905	952	1.2
2131365 L 139	263.84	66.19	669.97	78.97	9178.10	335.52	291.69	0.27	209.39	17.74	806	1447	1.2
2131365 M 162	292.92	66.30	645.94	91.61	10683.65	317.73	236.49	0.26	93.94	15.43	837	1483	1.3
2131365 L 141	143.66	36.45	389.35	50.07	9596.62	156.84	173.33	0.37	632.97	23.41	848	808	0.9
2131365 L 130	360.07	82.83	760.81	115.86	12287.78	433.64	282.65	0.23	166.00	16.16	830	1782	1.5
2131365 M 146	129.06	31.54	308.46	41.94	9527.02	131.26	142.25	0.44	25.11	18.03	857	693	0.9
2131365 L 142	135.65	33.17	353.10	45.05	9265.00	144.36	168.06	0.21	444.06	24.43	862	743	0.9
2131365 L 125	181.48	43.44	409.59	65.34	11186.97	208.14	189.41	0.27	282.32	24.27	842	917	1.1
2131365 M 159	162.29	39.03	384.63	57.03	10786.77	200.59	185.70	0.33	19.76	20.84	853	856	1.1
2131365 M 157	148.57	34.43	342.07	51.61	10253.41	152.78	148.37	0.44	159.38	19.18	872	768	1.0
2131365 L 140	166.66	41.60	417.06	54.27	8071.03	206.41	218.94	0.37	18.14	16.21	913	929	0.9
2131365 M 161	346.51	78.61	746.66	108.50	10570.67	368.14	268.58	0.29	118.10	15.25	856	1736	1.4
2131365 L 131	156.88	36.66	350.50	55.39	11111.01	159.05	148.14	0.32	306.60	20.31	871	794	1.1
2131365 L 135	128.77	31.17	323.32	44.82	9624.09	141.83	151.48	0.28	440.04	22.95	871	692	0.9
2131365 L 129	289.75	65.58	614.50	89.20	12124.45	386.58	312.81	0.34	12.47	15.93	853	1469	1.2
2131359 L 99	48.00	12.93	149.07	18.45	9259.60	70.38	101.62	0.16		38.13	800	285	0.7
2131359 M 116	136.63	32.86	324.22	42.78	8785.49	121.63	126.36	0.34	115.30	17.27	889	722	1.0
2131359 L 107	109.49	25.85	282.89	33.75	7668.41	139.39	140.75	0.33	258.03	20.04	879	605	1.0
2131359 L 105	111.47	28.47	303.74	36.29	7864.61	123.09	154.92	0.29	187.88	21.12	872	621	0.8
2131359 M 119	124.87	30.70	310.11	43.30	9843.18	137.94	169.60	0.32	46.49	24.22	830	667	0.8
2131359 L 102	115.86	29.76	307.38	38.30	8428.79	118.36	158.02	0.24	302.14	23.07	850	637	0.7
2131359 L 109	103.73	24.29	256.89	30.47	6891.25	141.59	225.28	0.17	208.69	19.28	779	546	0.6
2131359 M 123	94.67	22.77	237.64	29.48	7611.53	161.11	191.52	0.24	9.40	16.34	787	518	0.8
2131359 M 113	124.90	30.10	333.52	41.83	8905.95	131.01	149.28	0.33	292.31	24.66	855	682	0.9
2131359 L 91	124.58	29.44	294.70	34.60	6980.36	96.96	93.45	0.44	88.02	15.22	896	658	1.0
2131359 L 95	152.82	36.45	356.79	41.67	7003.28	155.90	191.92	0.30	7.36	14.69	766	806	0.8
2131359 M 117	120.07	28.47	284.98	40.40	9417.33	112.14	143.34	0.23	444.92	18.22	834	626	0.8
2131359 L 103	114.51	28.32	303.66	37.39	8021.98	194.56	204.39	0.29	274.72	20.91	838	640	1.0
2131359 M 122	226.41	54.11	530.78	68.41	9087.16	219.31	183.42	0.33	39.74	15.14	854	1203	1.2
2131359 L 93	109.74	28.07	299.96	35.06	7979.12	113.15	144.83	0.28	212.97	25.16	860	612	0.8
2131359 L 96	231.03	52.76	532.97	60.56	6849.43	205.35	305.05	0.22	7.39	14.42	785	1195	0.7
2131359 M 112	175.96	44.21	454.12	57.37	9952.97	269.35	430.90	0.13	964.42	22.28	772	955	0.6
2131359 L 98	105.34	26.25	286.26	35.11	7983.02	108.74	133.19	0.31	48.15	21.12	868	594	0.8
2131359 L 110	105.97	27.04	284.28	34.86	8287.29	116.25	171.44	0.26	1854.94	27.91	847	590	0.7
2131359 L 94	122.02	28.45	299.37	34.82	7835.58	164.24	227.10	0.24	5.49	13.91	765	669	0.7
2116683 M 80	132.48	32.17	344.55	42.95	8574.56	130.60	137.64	0.33	105.77	23.31	835	728	0.9
2116683 L 56	178.05	40.40	386.57	58.52	10489.77	201.71	154.81	0.34	215.05	15.85	887	899	1.3
2116683 L 49	135.82	32.49	322.14	47.31	10166.91	191.51	168.62	0.35	373.33	20.69	864	717	1.1
2116683 L 53	228.72	53.48	490.92	75.41	10563.86	189.21	134.55	0.33	144.38	14.40	877	1157	1.4
2116683 L 68	152.83	35.92	344.14	54.02	10601.67	155.82	129.32	0.34	77.63	18.12	876	802	1.2
2116683 M 85	95.84	23.48	259.91	33.79	9505.02	115.16	133.65	0.30	194.93	26.90	842	547	0.9
2116683 L 63	99.18	24.43	257.33	38.71	10435.59	106.87	120.67	0.31	620.02	25.63	841	541	0.9
2116683 M 77	221.27	50.88	521.31	64.26	7800.44	173.12	150.67	0.36	68.56	15.61	876	1166	1.1
2116683 L 64	81.44	19.46	200.90	29.55	10251.27	61.94	63.77	0.45	403.75	23.03	875	434	1.0
2116683 L 55	177.18	39.37	367.85	57.80	10071.17	150.16	113.08	0.29	219.64	15.17	881	869	1.3
2116683 L 57	124.88	29.33	293.07	45.51	10629.06	143.24	139.68	0.34	13.01	20.41	862	661	1.0
2116683 M 86	113.79	28.03	289.37	38.68	9159.07	118.43	137.32	0.28	379.02	20.94	870	618	0.9
2116683 L 60	201.03	46.72	471.60	65.08	8535.08	197.31	160.70	0.41	97.02	14.97	877	1070	1.2

Appendix 4 Table A5 Zircon trace element data for GRV and Hiltaba Suite samples analyzed at Boise State University

Unit	Group	Sample	Spot Number	Zircon Treatment	Discordance	Other	Analytical Session	Experiment number
Included Data								
LGRV	mineralization-absent	2116683	2116683 M 81	Thermally Annealed			7/01/2016	3
LGRV	mineralization-absent	2116683	2116683 L 50	Thermally Annealed			7/01/2016	3
LGRV	mineralization-absent	2116683	2116683 L 52	Thermally Annealed			7/01/2016	3
LGRV	mineralization-absent	2116683	2116683 M 79	Thermally Annealed			7/01/2016	3
LGRV	mineralization-absent	2116683	2116683 M 73	Thermally Annealed			7/01/2016	3
LGRV	mineralization-absent	2116683	2116683 M 69	Thermally Annealed			7/01/2016	3
LGRV	mineralization-absent	2116683	2116683 L 51	Thermally Annealed			7/01/2016	3
LGRV	mineralization-absent	2116683	2116683 M 70	Thermally Annealed			7/01/2016	3
LGRV	mineralization-absent	2116683	2116683 L 59	Thermally Annealed			7/01/2016	3
LGRV	mineralization-absent	2116683	2116683 L 54	Thermally Annealed			7/01/2016	3
LGRV	mineralization-absent	2116683	2116683 L 58	Thermally Annealed			7/01/2016	3
LGRV	mineralization-absent	2116683	2116683 L 66	Thermally Annealed			7/01/2016	3
LGRV	mineralization-absent	2116683	2116683 M 76	Thermally Annealed			7/01/2016	3
LGRV	mineralization-absent	2116683	2116683 M 84	Thermally Annealed			7/01/2016	3
LGRV	mineralization-absent	2116683	2116683 M 78	Thermally Annealed			7/01/2016	3
LGRV	mineralization-absent	2116683	2116683 L 67	Thermally Annealed			7/01/2016	3
LGRV	mineralization-absent	2018616	2018616 100	Thermally Annealed			31/07/2014	1
LGRV	mineralization-absent	2018616	2018616 101	Thermally Annealed			31/07/2014	1
LGRV	mineralization-absent	2018616	2018616 102	Thermally Annealed			31/07/2014	1
LGRV	mineralization-absent	2018616	2018616 103	Thermally Annealed			31/07/2014	1
LGRV	mineralization-absent	2018616	2018616 104	Thermally Annealed			31/07/2014	1
LGRV	mineralization-absent	2018616	2018616 105	Thermally Annealed			31/07/2014	1
LGRV	mineralization-absent	2018616	2018616 106	Thermally Annealed			31/07/2014	1
LGRV	mineralization-absent	2018616	2018616 107	Thermally Annealed			31/07/2014	1
LGRV	mineralization-absent	2018616	2018616 109	Thermally Annealed			31/07/2014	1
LGRV	mineralization-absent	2018616	2018616 110	Thermally Annealed			31/07/2014	1
LGRV	mineralization-absent	2018616	2018616 80	Thermally Annealed			30/07/2014	1
LGRV	mineralization-absent	2018616	2018616 82	Thermally Annealed			31/07/2014	1
LGRV	mineralization-absent	2018616	2018616 83	Thermally Annealed			31/07/2014	1
LGRV	mineralization-absent	2018616	2018616 84	Thermally Annealed			31/07/2014	1
LGRV	mineralization-absent	2018616	2018616 85	Thermally Annealed			31/07/2014	1
LGRV	mineralization-absent	2018616	2018616 89	Thermally Annealed			31/07/2014	1
LGRV	mineralization-absent	2018616	2018616 90	Thermally Annealed			31/07/2014	1
LGRV	mineralization-absent	2018616	2018616 91	Thermally Annealed			31/07/2014	1
LGRV	mineralization-absent	2018616	2018616 92	Thermally Annealed			31/07/2014	1
LGRV	mineralization-absent	2018616	2018616 93	Thermally Annealed			31/07/2014	1
LGRV	mineralization-absent	2018616	2018616 94	Thermally Annealed			31/07/2014	1
LGRV	mineralization-absent	2018616	2018616 95	Thermally Annealed			31/07/2014	1
LGRV	mineralization-absent	2018616	2018616 97	Thermally Annealed			31/07/2014	1
LGRV	mineralization-absent	2018616	2018616 98	Thermally Annealed			31/07/2014	1
LGRV	mineralization-absent	2016125	2016125 L 53	Thermally Annealed			30/07/2014	1
LGRV	mineralization-absent	2016125	2016125 L 54	Thermally Annealed			30/07/2014	1
LGRV	mineralization-absent	2016125	2016125 L 56	Thermally Annealed			30/07/2014	1
LGRV	mineralization-absent	2016125	2016125 L 57	Thermally Annealed			30/07/2014	1
LGRV	mineralization-absent	2016125	2016125 L 58	Thermally Annealed			30/07/2014	1
LGRV	mineralization-absent	2016125	2016125 L 59	Thermally Annealed			30/07/2014	1
LGRV	mineralization-absent	2016125	2016125 L 61	Thermally Annealed			30/07/2014	1
LGRV	mineralization-absent	2016125	2016125 M 62	Thermally Annealed			30/07/2014	1
LGRV	mineralization-absent	2016125	2016125 M 64	Thermally Annealed			30/07/2014	1
LGRV	mineralization-absent	2016125	2016125 M 65	Thermally Annealed			30/07/2014	1
LGRV	mineralization-absent	2016125	2016125 M 66	Thermally Annealed			30/07/2014	1
LGRV	mineralization-absent	2016125	2016125 M 70	Thermally Annealed			30/07/2014	1
LGRV	mineralization-absent	2016125	2016125 M 71	Thermally Annealed			30/07/2014	1
LGRV	mineralization-absent	2016125	2016125 M 73	Thermally Annealed			30/07/2014	1
LGRV	mineralization-absent	2016125	2016125 M 74	Thermally Annealed			30/07/2014	1
LGRV	mineralization-absent	2016125	2016125 M 76	Thermally Annealed			30/07/2014	1
LGRV	mineralization-absent	2721839	2721839 M 110	Thermally Annealed			27/11/2019	7
LGRV	mineralization-absent	2721839	2721839 M 115	Thermally Annealed			27/11/2019	7
LGRV	mineralization-absent	2721839	2721839 M 117	Thermally Annealed			27/11/2019	7
LGRV	mineralization-absent	2721839	2721839 S 133	Thermally Annealed			27/11/2019	7
LGRV	mineralization-absent	2721839	2721839 M 114	Thermally Annealed			27/11/2019	7
LGRV	mineralization-absent	2721839	2721839 M 109	Thermally Annealed			27/11/2019	7
LGRV	mineralization-absent	2721839	2721839 M 119	Thermally Annealed			27/11/2019	7
LGRV	mineralization-absent	2721839	2721839 M 121	Thermally Annealed			27/11/2019	7
LGRV	mineralization-absent	2721839	2721839 M 125	Thermally Annealed			27/11/2019	7
LGRV	mineralization-absent	2721839	2721839 M 111	Thermally Annealed			27/11/2019	7
LGRV	mineralization-absent	2721839	2721839 S 137	Thermally Annealed			27/11/2019	7
LGRV	mineralization-absent	2721839	2721839 S 139	Thermally Annealed			27/11/2019	7
LGRV	mineralization-absent	2721839	2721839 M 123	Thermally Annealed			27/11/2019	7
LGRV	mineralization-absent	2721839	2721839 M 126	Thermally Annealed			27/11/2019	7
LGRV	mineralization-absent	2721839	2721839 M 113	Thermally Annealed			27/11/2019	7

Appendix 4 Table A5 Zircon trace element data for GRV and Hiltaba Suite samples analyzed at Boise State University

Spot Number	P	Ti	Y	Nb	La	Ce	Pr	Nd	Sm	Eu	Gd	Tb	Dy	Ho
	ppm	ppm	ppm	ppm	ppm	ppm	ppm	ppm	ppm	ppm	ppm	ppm	ppm	ppm
2116683 M 81	219.94	18.53	622.67	2.46		23.11	0.03	1.30	1.92	0.67	14.38	4.62	56.39	21.78
2116683 L 50	295.92	22.96	1203.71	3.69		28.75	0.15	3.49	5.58	1.38	28.05	9.09	113.99	42.16
2116683 L 52	304.48	25.43	1197.39	3.34	0.02	31.15	0.20	3.04	5.57	1.40	32.24	9.51	117.26	40.86
2116683 M 79	303.81	20.84	1227.14	2.92		28.83	0.19	3.94	7.56	1.94	33.98	10.92	133.33	44.07
2116683 M 73	240.11	18.02	711.22	3.66		33.94	0.07	1.16	2.71	0.84	16.97	6.21	70.43	25.22
2116683 M 69	200.02	15.35	608.19	2.96	0.24	26.56	0.31	3.50	3.03	0.69	15.06	4.88	58.40	21.80
2116683 L 51	307.45	25.29	1161.07	2.99		30.76	0.12	3.18	7.32	1.60	28.03	9.28	110.87	40.79
2116683 M 70	233.44	15.34	655.44	2.92		28.30	0.06	1.49	2.36	0.65	13.79	5.06	62.39	21.64
2116683 L 59	207.22	13.32	738.35	4.05		30.80	0.03	1.35	2.59	0.50	14.78	5.14	67.27	26.10
2116683 L 54	249.20	20.22	1930.22	2.15		33.08	0.37	7.23	12.35	2.83	54.52	16.92	188.65	66.79
2116683 L 58	276.09	21.94	968.27	2.93		29.30	0.10	2.27	5.16	1.39	23.92	7.70	91.58	34.41
2116683 L 66	250.81	19.19	892.33	2.74		26.48	0.10	2.26	3.39	0.92	19.71	7.10	84.96	31.35
2116683 M 76	193.66	17.99	515.40	2.63	0.11	23.50	0.13	1.62	1.75	0.62	11.47	4.07	54.44	18.35
2116683 M 84	239.90	15.60	709.86	3.22		30.76	0.06	1.01	3.17	0.79	13.48	5.35	67.64	25.20
2116683 M 78	217.88	16.33	529.92	2.11		20.93	0.06	0.84	1.72	0.57	11.49	3.86	52.84	19.76
2116683 L 67	257.21	21.32	1037.04	2.59		26.44	0.11	2.79	5.39	1.06	23.72	7.55	95.80	35.13
2018616 100	200.54	13.25	641.43	2.88	0.01	20.04	0.04	1.06	2.26	0.22	14.22	4.59	58.26	22.58
2018616 101	198.54	12.03	576.58	2.77		15.40	0.06	0.51	2.06	0.14	10.22	4.02	48.54	19.04
2018616 102	176.55	11.17	456.23	2.17		14.21	0.05	0.85	1.43	0.14	9.12	3.16	39.87	16.05
2018616 103	175.15	8.20	788.63	2.69	1.41	22.42	1.55	10.04	10.77	1.95	29.50	7.84	82.05	29.42
2018616 104	230.91	21.78	737.10	1.81		13.38	0.04	1.67	2.99	0.53	16.51	5.72	67.36	26.33
2018616 105	228.51	19.59	719.51	1.75		12.94	0.10	0.93	2.64	0.46	15.16	5.81	68.16	24.95
2018616 106	190.97	11.86	712.04	2.73		17.30	0.01	0.82	2.50	0.30	15.31	5.32	61.28	24.47
2018616 107	198.84	13.33	601.49	2.07		17.61		0.69	2.03	0.33	10.64	4.47	53.87	21.30
2018616 109	318.14	10.99	913.23	3.00	5.18	108.88	4.73	28.31	21.80	6.58	42.48	11.26	99.36	32.20
2018616 110	174.30	11.51	506.95	2.85	0.22	21.92	0.18	1.23	1.57	0.29	11.04	3.83	46.92	19.28
2018616 80	195.09	13.60	615.78	2.25	2.12	36.30	1.33	11.96	9.44	2.31	23.57	5.80	62.17	20.85
2018616 82	213.17	13.74	731.06	3.58		21.85	0.04	1.17	2.86	0.32	16.08	5.22	65.71	26.36
2018616 83	219.52	12.36	669.83	3.14	1.60	20.76	0.24	1.55	2.67	0.25	14.89	4.72	60.40	22.79
2018616 84	192.09	11.73	582.74	3.14		20.27	0.02	0.55	2.01	0.19	11.82	4.20	53.27	20.08
2018616 85	256.48	15.91	1187.00	2.17	0.32	23.67	0.45	6.64	9.65	1.36	36.87	10.90	117.69	41.62
2018616 89	194.52	10.39	622.03	3.34	0.19	21.55	0.25	3.22	3.87	0.57	13.61	4.91	54.99	21.73
2018616 90	145.39	11.06	453.17	1.85		20.71	0.03	0.57	0.71	0.11	7.03	2.43	34.79	14.31
2018616 91	185.63	12.28	567.08	2.65	0.09	19.54	0.05	0.72	1.98	0.10	10.48	3.72	49.56	19.67
2018616 92	218.39	10.70	669.70	3.93	2.13	41.83	1.52	10.03	8.13	2.10	20.39	5.57	63.27	23.16
2018616 93	216.71	12.86	522.36	2.46	1.37	39.82	1.02	5.58	4.71	1.74	14.50	4.38	48.08	18.16
2018616 94	196.65	12.70	567.46	2.91	0.30	30.28	0.47	3.72	3.29	0.68	11.64	4.19	51.69	19.10
2018616 95	244.46	10.56	759.23	3.34	1.69	38.00	1.05	7.13	5.61	1.10	20.91	6.18	72.90	26.18
2018616 97	217.76	12.23	790.86	2.22	1.93	56.76	1.89	13.69	10.65	2.42	23.52	6.73	73.06	26.91
2018616 98	169.35	11.54	505.63	2.61	1.17	34.64	1.00	7.49	5.74	1.17	12.34	4.27	46.34	17.49
2016125 L 53	204.05	7.96	755.34	3.11		11.21	0.07	1.22	3.03	0.09	16.96	6.10	74.37	27.21
2016125 L 54	200.31	15.37	432.81	1.19		4.96	0.10	0.99	2.34	0.30	11.57	3.75	44.47	16.02
2016125 L 56	183.83	5.02	624.90	4.39		13.49	0.07	0.86	2.34		15.97	4.88	61.53	23.64
2016125 L 57	195.79	5.39	740.41	4.33		15.91		1.97	3.28	0.08	19.30	6.19	75.53	27.34
2016125 L 58	163.88	4.66	635.67	4.63		15.10		0.91	2.47	0.01	14.09	5.22	63.18	23.47
2016125 L 59	158.86	4.62	563.03	4.11		12.97	0.03	0.68	1.93	0.04	11.64	4.44	55.49	20.46
2016125 L 61	253.53	18.68	1678.42	1.08	0.08	87.44	1.15	22.32	24.19	5.36	79.92	19.09	200.17	65.97
2016125 M 62	177.92	7.19	711.30	3.56		12.95	0.05	1.18	2.49	0.05	20.29	6.55	71.33	26.47
2016125 M 64	187.40	6.04	761.94	4.63	0.05	16.23	0.07	1.01	2.80	0.05	17.93	6.69	76.75	27.69
2016125 M 65	201.38	4.92	791.45	4.59		16.38	0.06	1.09	4.11	0.10	19.33	6.51	80.11	29.42
2016125 M 66	219.42	7.26	734.57	3.48		13.07	0.07	1.60	3.56	0.10	18.66	6.61	73.13	27.72
2016125 M 70	200.67	5.51	757.91	4.43		15.25	0.13	1.50	4.55	0.10	20.85	6.18	71.85	27.81
2016125 M 71	213.14	5.64	818.49	4.63		16.25	0.05	1.37	3.13	0.04	21.08	7.03	80.63	28.06
2016125 M 73	240.41	10.19	707.98	2.30	0.04	8.48	0.06	1.69	4.49	0.10	21.88	7.02	74.71	26.62
2016125 M 74	208.93	5.97	794.96	3.89		14.95	0.02	1.86	4.04	0.10	21.57	6.94	82.64	30.25
2016125 M 76	228.09	5.63	887.49	4.52		17.05	0.08	1.47	4.51	0.19	20.97	7.13	87.10	32.77
2721839 M 110	289.74	35.07	853.40	1.90		32.91	0.12	3.54	7.68	2.06	26.92	9.40	105.61	32.39
2721839 M 115	284.58	30.31	744.34	1.65		28.80	0.11	2.61	6.62	1.49	21.62	7.97	88.94	28.98
2721839 M 117	288.30	18.93	1015.58	3.07	0.12	46.79	0.16	2.56	5.82	1.21	24.10	9.27	114.35	39.43
2721839 S 133	285.02	31.60	1723.66	2.98		52.71	0.15	5.05	13.18	2.42	45.62	16.09	188.87	63.56
2721839 M 114	345.18	33.99	972.19	1.94		35.07	0.16	4.31	8.41	1.96	29.51	11.66	123.54	38.23
2721839 M 109	333.45	26.83	1063.42	2.63	0.41	47.84	0.31	4.76	8.60	1.86	30.86	10.78	125.68	42.76
2721839 M 119	288.94	32.98	845.33	1.76		26.01	0.11	2.69	6.01	1.56	27.56	8.94	107.00	32.34
2721839 M 121	271.49	21.21	1008.73	3.38		55.21	0.13	3.54	6.41	1.24	27.22	10.48	124.62	39.99
2721839 M 125	278.94	35.05	1426.24	1.43	0.05	35.66	0.53	12.70	19.98	5.60	59.22	17.58	185.36	56.33
2721839 M 111	361.59	20.29	1000.52	2.62		33.02	0.19	3.14	6.11	1.47	27.05	9.48	113.05	38.49
2721839 S 137	269.80	25.07	1697.11	4.59		69.18	0.11	4.47	10.60	1.87	43.00	15.00	188.86	62.84
2721839 S 139	365.07	27.14	2130.37	2.47		48.59	0.35	7.24	14.35	2.91	64.76	21.19	236.47	78.18
2721839 M 123	308.31	27.71	1100.84	1.96	0.14	38.28	0.26	5.81	10.94	2.51	35.78	12.26	140.63	45.78
2721839 M 126	270.88	14.76	1183.41	5.53		54.69	0.12	2.33	5.29	0.68	26.25	10.62	127.80	46.42
2721839 M 113	246.86	30.13	836.57	1.56	0.01	33.28	0.12	4.22	7.60	2.08	25.07	8.69	100.11	31.37

Appendix 4 Table A5 Zircon trace element data for GRV and Hiltaba Suite samples analyzed at Boise State University

Spot Number	Er	Tm	Yb	Lu	Hf	Th	U	Eu/Eu*	Ce/Ce*	$(Yb/Gd)_N$	Ti-in-Zircon	Total REE	Th/U
	ppm	ppm	ppm	ppm	ppm	ppm	ppm						
2116683 M 81	97.14	24.40	249.95	33.24	8453.96	88.94	102.43	0.39	802.81	21.55	864	529	0.9
2116683 L 50	183.85	43.71	419.25	67.83	9822.50	169.97	161.09	0.34	188.04	18.52	890	947	1.1
2116683 L 52	175.82	39.85	384.11	62.36	9994.41	148.62	126.45	0.32	117.61	14.76	902	903	1.2
2116683 M 79	185.92	46.36	474.94	58.39	7586.85	173.58	172.71	0.37	151.19	17.32	878	1030	1.0
2116683 M 73	111.06	27.53	297.17	36.39	7988.51	166.25	185.49	0.38	460.23	21.70	861	630	0.9
2116683 M 69	90.78	23.70	250.82	31.66	8632.25	99.37	129.83	0.31	24.00	20.64	842	531	0.8
2116683 L 51	176.23	40.41	378.89	60.06	10052.99	144.96	126.30	0.34	252.92	16.75	902	888	1.1
2116683 M 70	99.59	25.43	271.25	34.72	8541.73	115.80	143.06	0.35	448.29	24.38	842	567	0.8
2116683 L 59	117.83	29.22	297.05	41.01	10165.64	115.35	143.16	0.25	1067.86	24.90	827	634	0.8
2116683 L 54	288.91	63.18	597.52	88.58	10751.25	245.11	161.25	0.33	88.07	13.58	874	1421	1.5
2116683 L 58	149.39	35.18	345.98	50.95	9502.38	157.42	152.23	0.38	296.62	17.93	884	777	1.0
2116683 L 66	133.80	30.49	300.88	48.24	10785.51	127.98	112.37	0.34	264.09	18.92	868	690	1.1
2116683 M 76	80.75	21.11	226.14	27.79	8019.66	82.83	101.13	0.43	48.02	24.44	860	472	0.8
2116683 M 84	109.90	26.51	284.76	37.44	8896.07	129.26	149.97	0.37	508.95	26.17	844	606	0.9
2116683 M 78	86.82	21.14	231.72	29.67	8283.65	55.80	77.30	0.39	340.41	25.00	849	481	0.7
2116683 L 67	156.61	35.81	347.15	54.26	10692.68	156.15	136.25	0.29	227.82	18.13	881	792	1.1
2018616 100	99.96	23.36	227.97	37.25	10572.83	124.16	141.07	0.12	230.04	19.87	826	512	0.9
2018616 101	87.06	20.50	189.00	34.24	10463.54	103.95	136.41	0.09	248.66	22.92	816	431	0.8
2018616 102	72.61	16.66	163.17	28.76	10528.87	85.24	119.41	0.12	304.17	22.16	808	366	0.7
2018616 103	120.69	25.03	220.97	37.87	9018.30	99.42	156.52	0.33	3.72	9.28	776	602	0.6
2018616 104	112.48	23.87	229.82	40.33	10014.61	81.54	82.25	0.23	309.00	17.25	883	541	1.0
2018616 105	104.50	23.94	222.27	39.00	9966.98	76.23	79.42	0.22	129.90	18.17	870	521	1.0
2018616 106	111.81	24.32	237.42	42.36	10761.78	93.03	108.52	0.15	2275.86	19.22	814	543	0.9
2018616 107	93.78	21.57	205.52	36.25	10720.86	75.05	93.75	0.22		23.93	827	468	0.8
2018616 109	125.38	29.30	269.56	40.94	9788.64	149.81	174.08	0.66	5.39	7.86	806	826	0.9
2018616 110	83.47	20.17	209.81	30.90	9178.94	118.46	151.98	0.21	27.23	23.55	811	451	0.8
2018616 80	93.26	21.61	219.04	36.41	10554.19	109.30	127.71	0.47	5.31	11.52	829	546	0.9
2018616 82	116.41	26.62	252.62	40.24	10630.76	130.39	158.74	0.14	500.32	19.47	830	575	0.8
2018616 83	102.99	23.87	233.79	39.52	10551.13	140.83	169.34	0.12	8.21	19.45	818	530	0.8
2018616 84	94.09	21.67	200.00	35.25	10859.39	103.60	127.61	0.12	909.57	20.96	813	463	0.8
2018616 85	172.54	36.35	334.11	55.71	10039.07	135.96	119.54	0.22	15.28	11.23	846	848	1.1
2018616 89	98.20	22.99	207.51	37.77	11528.51	141.47	177.10	0.24	24.13	18.90	800	491	0.8
2018616 90	69.87	16.58	168.58	32.97	11310.17	91.53	108.67	0.15	724.12	29.70	807	369	0.8
2018616 91	90.34	20.96	195.13	35.69	10726.70	129.88	144.70	0.07	67.42	23.08	818	448	0.9
2018616 92	99.13	21.72	216.53	36.68	10776.24	128.89	162.18	0.50	5.71	13.16	803	552	0.8
2018616 93	81.08	19.16	190.99	33.50	10681.00	104.69	122.88	0.64	8.28	16.32	823	464	0.9
2018616 94	89.70	21.39	212.33	36.28	10456.15	138.90	153.14	0.33	19.75	22.60	821	485	0.9
2018616 95	115.72	27.29	248.43	39.84	10139.68	171.53	211.45	0.31	6.98	14.72	802	612	0.8
2018616 97	120.76	28.03	276.63	47.43	10674.50	158.26	160.36	0.47	7.30	14.57	817	690	1.0
2018616 98	73.45	18.02	168.81	29.99	10797.02	126.70	153.63	0.43	7.85	16.96	811	422	0.8
2016125 L 53	113.45	27.05	284.92	36.36	7937.06	70.15	120.78	0.04	149.42	20.82	773	602	0.6
2016125 L 54	68.88	16.31	166.70	22.32	6462.53	28.20	48.77	0.17	50.23	17.86	842	359	0.6
2016125 L 56	101.70	24.12	254.92	30.89	8137.45	84.36	176.58	#VALUE!	190.07	19.78	729	534	0.5
2016125 L 57	116.47	28.64	289.92	36.21	7990.33	100.81	188.51	0.03		18.61	736	621	0.5
2016125 L 58	99.16	24.08	253.30	32.38	8215.05	86.82	179.33	0.01		22.27	722	533	0.5
2016125 L 59	87.51	21.31	222.07	28.40	8341.04	70.47	150.43	0.03	403.31	23.64	722	467	0.5
2016125 L 61	238.33	53.15	505.84	70.73	7046.05	142.58	65.52	0.37	68.75	7.84	865	1374	2.2
2016125 M 62	109.43	26.98	257.52	33.44	7842.14	78.24	146.04	0.02	259.97	15.73	763	569	0.5
2016125 M 64	122.37	28.75	289.60	37.19	8357.00	109.12	199.87	0.02	69.77	20.02	746	627	0.5
2016125 M 65	125.34	29.16	299.92	37.79	8109.58	111.80	201.12	0.03	289.67	19.22	728	649	0.6
2016125 M 66	114.01	26.73	271.79	35.27	7856.44	85.77	161.12	0.04	173.94	18.05	764	592	0.5
2016125 M 70	121.46	27.94	287.87	33.55	7398.63	106.91	199.24	0.03	113.43	17.11	738	619	0.5
2016125 M 71	127.82	31.13	295.24	36.64	7895.91	109.76	198.80	0.02	313.96	17.36	740	648	0.6
2016125 M 73	107.27	24.37	251.76	30.12	5922.97	67.02	116.36	0.03	39.54	14.26	798	559	0.6
2016125 M 74	129.52	30.41	321.02	39.29	7941.11	106.69	190.04	0.03	648.05	18.44	745	683	0.6
2016125 M 76	134.89	32.44	319.45	45.83	9280.01	117.69	197.75	0.06	222.26	18.87	740	704	0.6
2721839 M 110	127.06	34.20	423.47	32.95	7227.23	54.48	35.51	0.44	266.84	19.49	944	838	1.5
2721839 M 115	115.68	31.61	408.67	30.22	6945.37	51.67	39.83	0.38	260.20	23.42	925	773	1.3
2721839 M 117	156.01	43.71	547.58	44.12	8341.79	88.42	65.12	0.31	82.37	28.15	866	1035	1.4
2721839 S 133	253.66	60.96	650.46	77.16	14347.14	134.02	53.64	0.30	338.30	17.67	930	1430	2.5
2721839 M 114	145.99	38.15	475.09	36.86	6971.85	72.41	52.08	0.38	208.75	19.95	940	949	1.4
2721839 M 109	167.22	43.78	505.59	42.81	7773.64	87.78	62.00	0.35	32.92	20.30	909	1033	1.4
2721839 M 119	126.39	33.58	421.05	31.53	7206.26	59.62	48.02	0.37	222.38	18.94	936	825	1.2
2721839 M 121	159.13	43.53	521.67	43.65	8089.88	96.42	74.89	0.29	417.94	23.75	880	1037	1.3
2721839 M 125	207.17	52.58	595.10	46.05	7249.89	78.74	39.38	0.50	56.22	12.45	944	1294	2.0
2721839 M 111	158.91	43.29	541.13	42.60	7546.49	65.37	56.24	0.35	167.54	24.79	875	1018	1.2
2721839 S 137	259.63	62.74	682.86	75.13	13939.13	144.69	67.70	0.27	618.95	19.68	900	1476	2.1
2721839 S 139	316.38	74.19	796.79	87.05	12722.97	128.30	53.08	0.29	136.01	15.25	910	1748	2.4
2721839 M 123	161.29	43.72	542.83	42.38	7516.73	70.63	45.12	0.39	49.98	18.80	913	1083	1.6
2721839 M 126	186.57	51.35	624.42	52.07	9125.08	158.10	124.40	0.18	452.11	29.48	838	1189	1.3
2721839 M 113	128.61	34.70	439.57	34.15	7069.47	31.31	21.76	0.46	216.78	21.73	924	850	1.4

Appendix 4 Table A5 Zircon trace element data for GRV and Hiltaba Suite samples analyzed at Boise State University

Unit	Group	Sample	Spot Number	Zircon Treatment	Discordance	Other	Analytical Session	Experiment number
Included Data								
LGRV	mineralization-absent	2721839	2721839 S 136	Thermally Annealed			27/11/2019	7
LGRV	mineralization-absent	2721839	2721839 M 116	Thermally Annealed			27/11/2019	7
LGRV	mineralization-absent	2721839	2721839 M 120	Thermally Annealed			27/11/2019	7
LGRV	mineralization-absent	2721839	2721839 S 140	Thermally Annealed			27/11/2019	7
LGRV	mineralization-absent	2721839	2721839 M 112	Thermally Annealed			27/11/2019	7
LGRV	mineralization-absent	2721839	2721839 S 138	Thermally Annealed			27/11/2019	7
LGRV	mineralization-absent	2721839	2721839 S 128	Thermally Annealed			27/11/2019	7
LGRV	mineralization-absent	2721839	2721839 S 145	Thermally Annealed			27/11/2019	7
LGRV	mineralization-absent	2721839	2721839 S 147	Thermally Annealed			27/11/2019	7
LGRV	mineralization-absent	2721839	2721839 S 144	Thermally Annealed			27/11/2019	7
LGRV	mineralization-absent	2721839	2721839 S 135	Thermally Annealed			27/11/2019	7
LGRV	mineralization-absent	2721839	2721839 M 122	Thermally Annealed			27/11/2019	7
LGRV	mineralization-absent	2721839	2721839 M 106	Thermally Annealed			27/11/2019	7
LGRV	mineralization-absent	2721839	2721839 S 132	Thermally Annealed			27/11/2019	7
LGRV	mineralization-absent	2721839	2721839 S 131	Thermally Annealed			27/11/2019	7
LGRV	mineralization-absent	2721839	2721839 S 129	Thermally Annealed			27/11/2019	7
LGRV	mineralization-absent	2721839	2721839 S 143	Thermally Annealed			27/11/2019	7
LGRV	mineralization-absent	2721839	2721839 S 142	Thermally Annealed			27/11/2019	7
LGRV	mineralization-absent	2746487	2746487 S 86	Thermally Annealed			27/11/2019	7
LGRV	mineralization-absent	2746487	2746487 S 84	Thermally Annealed			27/11/2019	7
LGRV	mineralization-absent	2746487	2746487 S 81	Thermally Annealed			27/11/2019	7
LGRV	mineralization-absent	2746487	2746487 S 88	Thermally Annealed			27/11/2019	7
LGRV	mineralization-absent	2746487	2746487 S 92	Thermally Annealed			27/11/2019	7
LGRV	mineralization-absent	2746487	2746487 S 80	Thermally Annealed			27/11/2019	7
LGRV	mineralization-absent	2746487	2746487 S 79	Thermally Annealed			27/11/2019	7
LGRV	mineralization-absent	2746487	2746487 S 93	Thermally Annealed			27/11/2019	7
LGRV	mineralization-absent	2746487	2746487 M 65	Thermally Annealed			27/11/2019	7
LGRV	mineralization-absent	2746487	2746487 M 74	Thermally Annealed			27/11/2019	7
LGRV	mineralization-absent	2746487	2746487 M 76	Thermally Annealed			27/11/2019	7
LGRV	mineralization-absent	2746487	2746487 M 72	Thermally Annealed			27/11/2019	7
LGRV	mineralization-absent	2746487	2746487 M 78	Thermally Annealed			27/11/2019	7
LGRV	mineralization-absent	2746487	2746487 M 59	Thermally Annealed			27/11/2019	7
LGRV	mineralization-absent	2746487	2746487 M 71	Thermally Annealed			27/11/2019	7
LGRV	mineralization-absent	2746487	2746487 M 77	Thermally Annealed			27/11/2019	7
LGRV	mineralization-absent	2746487	2746487 M 75	Thermally Annealed			27/11/2019	7
LGRV	mineralization-absent	2746487	2746487 M 70	Thermally Annealed			27/11/2019	7
LGRV	mineralization-absent	2746487	2746487 M 42	Thermally Annealed			27/11/2019	7
LGRV	mineralization-absent	2746487	2746487 M 73	Thermally Annealed			27/11/2019	7
LGRV	mineralization-absent	2746487	2746487 M 56	Thermally Annealed			27/11/2019	7
LGRV	mineralization-absent	2746487	2746487 M 39	Thermally Annealed			27/11/2019	7
LGRV	mineralization-absent	2746487	2746487 S 82	Thermally Annealed			27/11/2019	7

Appendix 4 Table A5 Zircon trace element data for GRV and Hiltaba Suite samples analyzed at Boise State University

Spot Number	P	Ti	Y	Nb	La	Ce	Pr	Nd	Sm	Eu	Gd	Tb	Dy	Ho
	ppm	ppm	ppm	ppm	ppm	ppm	ppm	ppm	ppm	ppm	ppm	ppm	ppm	ppm
2721839 S 136	239.72	29.39	1213.44	2.28		37.30	0.04	2.64	5.99	1.18	27.92	10.36	124.01	44.62
2721839 M 116	286.89	30.29	1681.25	1.27	0.07	36.43	0.49	11.17	20.55	5.30	62.98	20.88	227.28	69.11
2721839 M 120	288.53	23.51	1578.06	1.58		43.23	0.16	4.81	14.46	3.80	51.87	18.73	201.62	62.83
2721839 S 140	243.12	40.40	1387.71	1.74	0.03	34.25	0.25	4.97	11.86	3.18	39.14	14.18	157.12	51.99
2721839 M 112	275.57	32.09	797.47	1.88		30.10	0.14	2.71	5.62	1.70	23.60	7.94	93.81	31.61
2721839 S 138	339.05	25.97	1696.75	2.97		44.28	0.19	4.31	8.68	2.14	44.03	15.00	183.47	62.52
2721839 S 128	183.47	33.89	1182.69	1.15		16.51	0.10	3.49	6.42	1.74	28.64	10.32	127.24	43.42
2721839 S 145	258.64	43.64	995.29	1.13	0.05	25.56	0.12	3.96	5.37	2.41	29.71	9.69	113.61	37.69
2721839 S 147	332.29	38.94	1457.40	1.73	0.25	33.63	0.36	6.07	11.12	3.53	40.02	15.55	170.39	54.90
2721839 S 144	295.06	36.91	1870.80	2.20	0.18	33.57	0.64	11.30	18.51	3.70	61.74	20.67	225.49	73.09
2721839 S 135	290.44	45.22	2681.71	1.49	0.15	45.73	1.21	22.29	31.54	8.79	103.28	31.52	330.92	103.05
2721839 M 122	308.01	28.98	942.72	2.41	0.02	42.15	0.14	3.63	9.30	1.86	29.99	10.21	114.71	35.96
2721839 M 106	250.90	21.93	1159.57	1.98		25.89	0.18	2.99	7.91	2.83	30.86	10.47	126.92	44.24
2721839 S 132	293.74	31.54	1929.06	2.71		49.01	0.21	5.37	11.63	2.39	51.81	18.33	212.37	70.95
2721839 S 131	273.08	29.97	1799.23	2.50	0.03	45.20	0.13	4.51	12.06	2.54	47.14	17.74	195.06	66.64
2721839 S 129	243.09	30.91	1591.31	3.23		52.23	0.16	4.39	8.20	2.00	38.92	15.55	171.17	58.62
2721839 S 143	266.61	32.59	2159.97	1.74	0.04	42.32	0.47	13.55	20.17	5.06	74.41	24.27	259.40	83.80
2721839 S 142	314.19	32.66	2174.86	2.79	0.10	60.09	0.50	9.77	18.15	3.57	69.01	22.75	254.91	82.47
2746487 S 86	169.88	8.15	1538.02	1.95	1.91	39.63	1.97	19.18	12.95	3.56	41.78	13.40	153.54	54.45
2746487 S 84	315.70	12.01	4221.92	4.74	3.77	86.36	1.41	28.38	42.90	12.33	134.16	42.05	467.33	155.38
2746487 S 81	145.85	6.80	1426.20	5.24		42.46	0.12	2.61	5.55	1.62	22.39	9.57	128.09	46.41
2746487 S 88	284.49	24.42	4074.23	5.49	0.39	87.07	0.73	13.48	23.90	8.12	102.50	38.35	433.00	146.78
2746487 S 92	194.02	8.80	1625.33	2.29	0.01	26.14	0.34	7.65	13.04	3.91	39.70	14.41	165.90	60.11
2746487 S 80	184.17	9.87	1347.08	1.26		24.55	0.16	4.55	9.54	2.82	32.31	11.27	129.61	46.83
2746487 S 79	205.98	10.31	1705.94	1.48	0.02	30.71	0.42	6.60	12.31	3.94	44.50	14.33	170.38	59.51
2746487 S 93	171.88	10.94	2255.01	1.99	0.36	32.17	0.91	14.47	19.70	6.47	65.78	22.25	247.17	83.78
2746487 M 65	249.18	5.74	751.64	3.11	2.03	39.10	2.72	23.49	10.19	1.46	17.78	5.66	71.81	26.32
2746487 M 74	289.23	4.24	810.05	3.57	0.18	27.91	0.19	1.65	3.20	0.95	14.22	6.28	78.08	29.70
2746487 M 76	91.22	2.45	236.40	0.92		9.70		0.12	0.59	0.38	3.29	1.36	19.69	7.48
2746487 M 72	207.06	4.19	847.83	4.73	1.63	41.76	0.85	6.50	5.04	0.94	14.89	6.66	79.00	30.95
2746487 M 78	208.20	4.81	751.10	2.02	0.13	24.08	0.07	1.53	3.33	1.13	14.49	5.64	72.44	27.20
2746487 M 59	291.20	10.30	906.41	5.88	11.23	70.00	6.61	47.12	14.79	2.09	21.39	7.03	88.99	32.03
2746487 M 71	219.78	2.74	1054.63	5.03	0.33	19.66	0.24	1.63	3.30	1.09	15.99	7.36	102.01	37.52
2746487 M 77	101.18	3.35	434.45	1.27		17.71		0.94	1.86	0.53	6.04	3.44	41.94	15.61
2746487 M 75	283.34	2.87	830.35	3.23	0.17	22.60	0.17	1.45	2.34	0.82	14.49	5.49	73.59	30.06
2746487 M 70	212.73	2.22	1356.53	4.55	0.35	21.17	0.28	2.53	6.29	1.53	24.69	10.02	136.83	48.62
2746487 M 42	250.63	7.43	978.48	3.13	0.02	26.05	0.11	2.33	4.88	2.07	22.78	8.11	98.86	35.71
2746487 M 73	175.50	4.23	886.28	4.53	0.11	36.69	0.07	2.02	3.18	0.86	14.12	6.04	81.79	31.37
2746487 M 56	165.71	4.06	954.25	4.45	0.17	30.78	0.18	2.71	3.22	1.13	16.98	6.62	91.35	33.27
2746487 M 39	131.87	3.61	604.94	2.25		22.28		0.88	1.93	0.62	12.98	4.69	57.22	21.81
2746487 S 82	165.98	5.01	1694.01	7.75	0.05	50.24	0.16	2.20	4.94	1.38	26.62	10.84	143.21	56.54

Appendix 4 Table A5 Zircon trace element data for GRV and Hiltaba Suite samples analyzed at Boise State University

Spot Number	Er	Tm	Yb	Lu	Hf	Th	U	Eu/Eu*	Ce/Ce*	$(Yb/Gd)_N$	Ti-in-Zircon	Total REE	Th/U
	ppm	ppm	ppm	ppm	ppm	ppm	ppm						
2721839 S 136	184.47	46.63	498.07	59.28	13762.07	95.82	42.38	0.28	930.88	22.10	921	1043	2.3
2721839 M 116	252.36	61.91	716.37	54.57	7559.43	109.57	61.99	0.45	47.29	14.09	924	1539	1.8
2721839 M 120	234.98	60.51	721.31	55.68	7601.78	109.52	61.69	0.42	261.41	17.23	892	1474	1.8
2721839 S 140	200.79	47.38	514.57	56.46	11802.79	69.45	28.26	0.45	92.48	16.29	963	1136	2.5
2721839 M 112	121.30	32.22	395.17	31.22	7241.21	60.59	50.52	0.45	207.25	20.75	932	777	1.2
2721839 S 138	250.61	64.42	686.91	76.92	13280.09	103.82	45.60	0.34	226.66	19.34	905	1443	2.3
2721839 S 128	175.88	41.82	431.92	51.76	14144.68	54.83	30.61	0.39	159.53	18.69	939	939	1.8
2721839 S 145	150.87	37.55	401.05	42.18	11075.21	43.26	19.07	0.58	78.97	16.73	974	860	2.3
2721839 S 147	212.09	51.88	554.97	58.89	10870.99	65.88	27.65	0.51	27.70	17.18	958	1214	2.4
2721839 S 144	271.28	65.45	692.33	71.16	11042.17	121.00	58.17	0.33	24.14	13.90	951	1549	2.1
2721839 S 135	381.89	84.92	860.19	95.86	12463.13	144.11	41.70	0.47	26.61	10.32	979	2101	3.5
2721839 M 122	144.12	38.76	461.68	37.23	7359.42	72.39	52.09	0.34	179.62	19.08	919	930	1.4
2721839 M 106	180.67	51.93	640.06	55.73	7563.18	78.22	44.82	0.55	143.52	25.70	884	1181	1.7
2721839 S 132	284.03	69.93	697.36	84.73	14338.99	113.60	43.03	0.30	228.03	16.68	930	1558	2.6
2721839 S 131	269.22	63.77	657.13	79.73	14146.01	109.34	41.52	0.33	170.36	17.28	923	1461	2.6
2721839 S 129	240.69	58.69	598.32	74.70	14668.48	112.99	46.86	0.34	323.34	19.05	927	1324	2.4
2721839 S 143	321.54	73.42	782.62	80.91	11722.37	129.65	47.29	0.40	77.68	13.03	934	1782	2.7
2721839 S 142	322.88	78.19	834.35	86.54	12353.04	171.79	67.41	0.31	64.95	14.98	934	1843	2.5
2746487 S 86	235.08	64.46	716.79	91.46	14366.23	191.62	108.55	0.47	5.01	21.26	775	1450	1.8
2746487 S 84	647.62	157.32	1703.40	207.11	13193.81	578.80	168.04	0.50	9.18	15.73	815	3690	3.4
2746487 S 81	225.29	63.80	769.15	104.95	15491.91	225.66	163.20	0.44	334.06	42.58	758	1422	1.4
2746487 S 88	607.88	154.50	1630.13	188.63	11131.12	609.32	228.86	0.50	40.21	19.71	897	3435	2.7
2746487 S 92	245.95	65.73	763.29	87.00	11983.54	196.73	122.11	0.53	100.86	23.83	783	1493	1.6
2746487 S 80	207.91	57.20	642.96	87.19	13377.84	128.76	72.61	0.49	152.90	24.66	795	1257	1.8
2746487 S 79	258.30	70.45	768.88	104.04	13259.61	180.67	87.43	0.51	76.29	21.41	799	1544	2.1
2746487 S 93	346.67	89.92	1019.81	114.68	11606.12	298.10	152.39	0.55	13.74	19.21	805	2064	2.0
2746487 M 65	120.05	37.01	529.88	46.47	8618.07	103.40	159.78	0.33	4.07	36.94	742	934	0.6
2746487 M 74	137.50	42.65	567.85	53.59	9362.59	122.47	189.58	0.43	37.22	49.49	714	964	0.6
2746487 M 76	38.13	12.52	178.83	20.01	12458.86	34.06	58.63	0.84		67.42	668	292	0.6
2746487 M 72	140.73	44.25	599.81	57.11	9410.10	131.30	166.12	0.33	8.70	49.93	713	1030	0.8
2746487 M 78	120.89	38.33	516.67	47.68	9500.32	115.00	124.46	0.50	63.53	44.20	725	874	0.9
2746487 M 59	151.00	47.47	668.54	62.62	8783.29	128.43	174.48	0.36	1.99	38.73	799	1231	0.7
2746487 M 71	175.83	53.09	715.86	63.10	9713.22	109.76	202.96	0.46	17.10	55.46	677	1197	0.5
2746487 M 77	71.02	22.85	316.81	30.38	9793.18	49.59	69.07	0.48		65.04	694	529	0.7
2746487 M 75	136.73	43.89	595.21	57.32	9339.91	118.31	197.82	0.43	32.34	50.92	681	984	0.6
2746487 M 70	222.06	64.62	865.26	75.99	9798.93	152.85	252.76	0.38	16.58	43.42	660	1480	0.6
2746487 M 42	155.31	48.22	648.18	56.76	8277.85	98.50	102.04	0.60	151.70	35.26	766	1109	1.0
2746487 M 73	146.34	45.37	630.45	58.74	9391.09	143.04	167.12	0.39	99.27	55.34	714	1057	0.9
2746487 M 56	155.34	48.64	694.28	65.26	9044.49	126.42	166.38	0.47	43.16	50.66	710	1150	0.8
2746487 M 39	99.95	30.83	425.71	41.87	9380.86	75.82	102.26	0.38		40.64	700	721	0.7
2746487 S 82	275.21	78.29	951.30	130.38	16022.33	232.75	177.85	0.37	138.95	44.29	729	1731	1.3

Appendix 4 Table A5 Zircon trace element data for GRV and Hiltaba Suite samples analyzed at Boise State University

	Group	Sample	Spot Number	Zircon Treatment	Discordance	Other	Analytical Session	Experiment number
Rejected Data								
Hiltaba Suite	mineralization-related	2000366176	2000366176 M 239	Thermally Annealed	>5%		8/01/2016	
Hiltaba Suite	mineralization-related	2000366176	2000366176 L 217	Thermally Annealed		Nb <0.9	8/01/2016	
Hiltaba Suite	mineralization-related	2000366176	2000366176 L 195	Thermally Annealed		Nb <0.9	8/01/2016	
Hiltaba Suite	mineralization-related	2000366176	2000366176 L 198	Thermally Annealed		Nb <0.9	8/01/2016	
Hiltaba Suite	mineralization-related	2000366176	2000366176 L 197	Thermally Annealed		Nb <0.9	8/01/2016	
Hiltaba Suite	mineralization-related	2111460	2111460 L 255	Thermally Annealed		Nb <0.9	8/01/2016	
Hiltaba Suite	mineralization-related	2111460	2111460 L 259	Thermally Annealed		Nb <0.9	8/01/2016	
Hiltaba Suite	mineralization-related	2111460	2111460 M 274	Thermally Annealed	>5%		8/01/2016	
Hiltaba Suite	mineralization-related	2111460	2111460 L 260	Thermally Annealed		Nb <0.9	8/01/2016	
Hiltaba Suite	mineralization-related	2111460	2111460 L 261	Thermally Annealed		>370 ppm P	8/01/2016	
Hiltaba Suite	mineralization-related	1831634	1831634 M 37	Thermally Annealed		>370 ppm P	7/01/2016	
Hiltaba Suite	mineralization-related	1831634	1831634 L 27	Thermally Annealed		>370 ppm P	7/01/2016	
Hiltaba Suite	mineralization-related	1831634	1831634 L 26	Thermally Annealed		>370 ppm P	7/01/2016	
Hiltaba Suite	mineralization-related	1831634	1831634 L 18	Thermally Annealed		Nb <0.9	7/01/2016	
Hiltaba Suite	mineralization-related	1831634	1831634 L 7	Thermally Annealed		>370 ppm P	7/01/2016	
Hiltaba Suite	mineralization-related	1831634	1831634 L 12	Thermally Annealed		>370 ppm P	7/01/2016	
Hiltaba Suite	mineralization-related	1831634	1831634 L 17	Thermally Annealed		>370 ppm P	7/01/2016	
Hiltaba Suite	mineralization-related	1831634	1831634 L 24	Thermally Annealed	>5%		7/01/2016	
Hiltaba Suite	mineralization-absent	2053554	2053554 M 111	Thermally Annealed	>5%		17/10/2014	
Hiltaba Suite	mineralization-absent	2053554	2053554 M 80	Thermally Annealed	>5%		17/10/2014	
Hiltaba Suite	mineralization-absent	2053554	2053554 L 203	Thermally Annealed	>5%		31/07/2014	
Hiltaba Suite	mineralization-absent	2053554	2053554 L 197	Thermally Annealed	>5%		30/07/2014	
Hiltaba Suite	mineralization-absent	2053554	2053554 M 228	Thermally Annealed	>5%		31/07/2014	
Hiltaba Suite	mineralization-absent	2053554	2053554 M 129	Thermally Annealed	>5%		17/10/2014	
Hiltaba Suite	mineralization-absent	2053554	2053554 M 112	Thermally Annealed	>5%		17/10/2014	
Hiltaba Suite	mineralization-absent	2053554	2053554 L 204	Thermally Annealed	>5%		31/07/2014	
Hiltaba Suite	mineralization-absent	2053554	2053554 L 216	Thermally Annealed	>5%		31/07/2014	
Hiltaba Suite	mineralization-absent	2053554	2053554 M 114	Thermally Annealed		>370 ppm P	17/10/2014	
Hiltaba Suite	mineralization-absent	2053554	2053554 M 233	Thermally Annealed	>5%		31/07/2014	
Hiltaba Suite	mineralization-absent	2053554	2053554 M 99	Thermally Annealed	>5%		17/10/2014	
Hiltaba Suite	mineralization-absent	2053554	2053554 L 205	Thermally Annealed	>5%		31/07/2014	
Hiltaba Suite	mineralization-absent	2053554	2053554 M 241	Thermally Annealed	>5%		31/07/2014	
Hiltaba Suite	mineralization-absent	2053554	2053554 M 236	Thermally Annealed	>5%		31/07/2014	
Hiltaba Suite	mineralization-absent	2053554	2053554 M 109	Thermally Annealed		>370 ppm P	17/10/2014	
Hiltaba Suite	mineralization-absent	2053554	2053554 M 113	Thermally Annealed	>5%		17/10/2014	
Hiltaba Suite	mineralization-absent	2053554	2053554 M 122	Thermally Annealed	>5%		17/10/2014	
Hiltaba Suite	mineralization-absent	2053555	2053555 L 249	Thermally Annealed	>5%		31/07/2014	
Hiltaba Suite	mineralization-absent	2053555	2053555 L 251	Thermally Annealed		>370 ppm P	31/07/2014	
Hiltaba Suite	mineralization-absent	2053555	2053555 L 256	Thermally Annealed	>5%		31/07/2014	
Hiltaba Suite	mineralization-absent	2053555	2053555 L 257	Thermally Annealed		>370 ppm P	31/07/2014	
Hiltaba Suite	mineralization-absent	2053555	2053555 L 260	Thermally Annealed	>5%		31/07/2014	
Hiltaba Suite	mineralization-absent	2053555	2053555 L 263	Thermally Annealed	>5%		31/07/2014	
Hiltaba Suite	mineralization-absent	2053555	2053555 L 265	Thermally Annealed	>5%		31/07/2014	
Hiltaba Suite	mineralization-absent	2053555	2053555 L 266	Thermally Annealed		>370 ppm P	31/07/2014	
Hiltaba Suite	mineralization-absent	2053555	2053555 M 269	Thermally Annealed	>5%		31/07/2014	
Hiltaba Suite	mineralization-absent	2053555	2053555 M 271	Thermally Annealed	>5%		31/07/2014	
Hiltaba Suite	mineralization-absent	2053555	2053555 M 274	Thermally Annealed	>5%		31/07/2014	
Hiltaba Suite	mineralization-absent	2053555	2053555 M 275	Thermally Annealed	>5%		31/07/2014	
Hiltaba Suite	mineralization-absent	2053555	2053555 M 276	Thermally Annealed	>5%		31/07/2014	
Hiltaba Suite	mineralization-absent	2053555	2053555 M 279	Thermally Annealed	>5%		31/07/2014	
Hiltaba Suite	mineralization-absent	2053555	2053555 M 281	Thermally Annealed	>5%		31/07/2014	
Hiltaba Suite	mineralization-absent	2053555	2053555 M 284	Thermally Annealed	>5%		31/07/2014	
LGRV	mineralization-absent	2018616	2018616 108	Thermally Annealed	>5%		31/07/2014	
LGRV	mineralization-absent	2018616	2018616 79	Thermally Annealed	>5%		31/07/2014	
LGRV	mineralization-absent	2018616	2018616 96	Thermally Annealed	>5%		31/07/2014	
LGRV	mineralization-absent	2016125	2016125 L51	Thermally Annealed	>5%		30/07/2014	
LGRV	mineralization-absent	2016125	2016125 L52	Thermally Annealed	>5%		30/07/2014	
LGRV	mineralization-absent	2016125	2016125 L55	Thermally Annealed	>5%		30/07/2014	
LGRV	mineralization-absent	2016125	2016125 M63	Thermally Annealed		Nb <0.9	30/07/2014	
LGRV	mineralization-absent	2016125	2016125 M69	Thermally Annealed	>5%		30/07/2014	
LGRV	mineralization-absent	2016125	2016125 M72	Thermally Annealed		Nb <0.9	30/07/2014	
LGRV	mineralization-absent	2016125	2016125 M75	Thermally Annealed	>5%		30/07/2014	
LGRV	mineralization-absent	2721839	22421839 M 124	Thermally Annealed		>370 ppm P	30/07/2014	
LGRV	mineralization-absent	2746487	2746487 M 50	Thermally Annealed		Nb <0.9	27/11/2019	
LGRV	mineralization-absent	2746487	2746487 S 94	Thermally Annealed	>5%		27/11/2019	
LGRV	mineralization-absent	2746487	2746487 M 61	Thermally Annealed		Nb <0.9	27/11/2019	

Appendix 4 Table A5 Zircon trace element data for GRV and Hiltaba Suite samples analyzed at Boise State University

Spot Number	P	Ti	Y	Nb	La	Ce	Pr	Nd	Sm	Eu	Gd	Tb	Dy	Ho
Rejected Data	ppm	ppm	ppm	ppm	ppm	ppm	ppm	ppm	ppm	ppm	ppm	ppm	ppm	ppm
2000366176 M 239	321.86	13.15	1031.69	3.65		21.43	0.11	2.70	5.24	0.62	26.71	8.97	111.61	40.81
2000366176 L 217	190.28	25.58	602.43	0.89		10.33	0.07	1.70	3.60	1.46	17.40	5.59	60.29	21.69
2000366176 L 195	174.90	28.75	615.61	0.61	0.02	11.29	0.10	1.72	2.41	1.14	16.07	4.94	59.07	21.79
2000366176 L 198	254.01	33.54	1628.91	0.72	0.12	12.16	0.53	9.39	13.97	5.37	58.23	17.40	174.25	60.01
2000366176 L 197	225.98	31.94	1257.06	0.46	0.08	11.12	0.44	6.80	10.48	4.81	47.71	13.20	141.39	45.74
2111460 L 255	209.02	30.73	478.12	0.76		11.31	0.13	2.28	3.42	1.28	13.04	4.49	50.44	18.00
2111460 L 259	285.41	45.95	494.15	0.60	0.01	10.15	0.17	1.83	3.82	2.32	16.92	5.00	56.26	19.60
2111460 M 274	238.87	9.28	1931.80	2.44		16.35	0.42	9.50	11.72	2.10	65.09	19.80	220.28	77.68
2111460 L 260	192.65	39.34	359.19	0.35		6.40	0.04	0.81	1.70	1.44	8.67	3.34	35.50	12.66
2111460 L 261	416.94	12.86	1774.39	2.02	5.71	40.76	1.73	10.82	10.66	1.44	50.54	16.65	189.01	67.81
1831634 M 37	371.89	24.99	1161.86	2.88		30.65	0.20	3.39	6.45	1.46	32.74	10.14	119.23	42.06
1831634 L 27	447.71	28.57	1396.93	3.44		43.65	0.26	6.36	9.15	2.10	38.39	12.18	145.18	50.48
1831634 L 26	424.43	29.36	1453.58	3.20	0.04	48.97	0.24	5.44	9.41	2.07	39.04	12.58	153.63	52.04
1831634 L 18	213.83	30.06	520.95	0.90		15.06	0.07	1.43	2.74	0.93	13.16	4.64	52.89	19.14
1831634 L 7	421.98	31.31	1202.36	2.81	0.18	36.59	0.38	5.85	9.61	3.32	39.49	11.75	128.70	45.65
1831634 L 12	419.19	32.48	1545.54	4.94	0.13	41.12	0.38	6.10	9.18	3.41	40.46	12.92	154.71	55.53
1831634 L 17	375.22	29.66	1060.24	2.58	0.03	36.37	0.25	4.32	6.86	2.02	33.47	9.49	114.18	38.64
1831634 L 24	368.52	37.63	1135.73	2.37	0.59	27.33	0.68	6.99	10.52	6.42	47.90	13.66	136.10	43.61
2053554 M 111	314.18	11.86	1468.63	2.77	0.71	72.91	0.60	8.26	9.06	3.76	36.77	11.28	132.65	49.92
2053554 M 80	244.21	8.10	975.64	3.02		63.76	0.14	1.91	5.20	1.68	22.55	8.47	93.52	35.90
2053554 L 203	192.02	7.60	1274.59	3.34		53.48	0.17	4.01	6.18	2.10	31.72	9.92	117.41	46.53
2053554 L 197	319.32	8.44	1583.17	4.54		91.53	0.19	2.80	6.20	1.99	36.39	11.53	129.02	50.28
2053554 M 228	229.95	9.32	1215.49	5.25	3.65	92.93	3.87	24.90	10.02	3.12	32.62	9.06	112.94	43.82
2053554 M 129	259.68	7.91	1340.93	4.26	3.68	73.93	1.89	13.06	7.72	1.55	32.16	9.84	115.18	44.82
2053554 M 112	345.57	9.58	1987.08	3.29	0.17	68.19	0.72	7.37	13.49	4.77	63.69	17.64	209.50	72.18
2053554 L 204	195.66	6.92	1894.73	1.59	0.02	55.14	0.54	9.09	14.42	5.09	66.23	18.83	204.73	69.36
2053554 L 216	210.90	6.12	1023.13	5.59	0.17	66.96	0.09	2.04	4.50	0.97	21.64	7.68	94.15	34.91
2053554 M 114	385.11	7.95	1197.01	1.40	1.09	45.74	0.39	5.28	7.99	2.94	32.72	9.89	116.44	40.30
2053554 M 233	173.90	5.66	836.85	4.89		59.19	0.03	1.21	2.81	0.91	15.11	5.49	72.73	27.71
2053554 M 99	239.89	8.51	1027.65	2.45	0.25	45.05	0.42	3.73	4.61	1.33	23.85	8.15	95.52	35.09
2053554 L 205	219.57	8.40	1202.84	5.14		67.97	0.06	3.78	5.46	1.74	29.36	9.44	114.40	42.34
2053554 M 241	200.38	6.82	890.71	2.57		60.48	0.11	2.52	4.96	1.73	23.10	8.00	91.44	32.31
2053554 M 236	215.72	7.80	889.52	3.58		61.73	0.12	2.30	4.02	1.23	22.56	7.56	89.46	30.94
2053554 M 109	428.62	6.03	1008.81	2.64		36.65	0.03	1.34	3.04	0.88	20.51	6.81	91.53	33.84
2053554 M 113	240.72	7.91	1280.84	3.25		59.74	0.11	2.61	6.57	2.42	32.22	9.58	116.89	44.67
2053554 M 122	280.93	8.97	1503.34	4.02	0.84	94.01	1.33	9.15	10.34	2.62	39.30	11.90	142.06	52.38
2053555 L 249	73.88	2.31	275.86	5.23	5.03	20.90	2.07	11.26	2.33	0.47	4.53	1.37	18.70	7.99
2053555 L 251	413.84	16.39	1615.67	9.96	3.35	80.36	3.05	20.07	12.13	2.39	42.72	13.82	162.80	57.55
2053555 L 256	59.11	0.45	207.69	3.95	0.12	13.65	0.20	1.28	0.41	0.09	1.80	0.67	11.04	5.72
2053555 L 257	440.50	6.35	1143.23	7.41		40.92	0.08	1.54	4.28	0.44	23.44	8.44	112.99	40.06
2053555 L 260	597.72	16.12	4127.45	18.09	2.44	46.36	2.28	23.11	24.37	3.83	106.28	34.97	417.15	147.14
2053555 L 263	92.92	4.59	242.64	2.52	0.89	20.28	1.54	9.49	3.99	0.63	4.89	1.57	19.15	7.09
2053555 L 265	355.70	15.64	1437.62	5.66	5.72	44.59	4.79	25.85	11.19	2.34	33.81	11.17	133.02	48.46
2053555 L 266	609.10	20.33	3639.35	16.43	0.06	79.18	0.59	9.02	18.04	3.62	97.43	31.16	372.19	133.88
2053555 M 269	428.05	17.83	1434.48	7.85	0.17	72.83	0.77	6.59	9.00	1.95	32.50	12.06	142.86	51.07
2053555 M 271	151.86	5.32	785.85	4.56	3.74	38.09	5.75	34.04	13.16	2.64	21.53	6.13	62.35	26.94
2053555 M 274	355.89	16.19	1485.95	6.51	2.65	120.56	4.92	35.32	21.82	4.77	46.37	14.80	164.66	54.81
2053555 M 275	360.82	12.19	798.31	4.17	2.00	78.79	4.88	36.57	14.17	2.21	23.75	6.92	78.54	28.19
2053555 M 276	201.45	7.25	986.31	9.67	5.70	97.56	9.07	58.06	20.56	4.20	32.91	9.69	105.16	35.62
2053555 M 279	166.18	5.32	557.29	3.85		11.95	0.06	0.51	2.70	0.18	10.64	4.09	50.62	19.62
2053555 M 281	346.06	4.86	735.76	4.26	0.11	24.22	0.17	1.91	2.54	0.35	13.84	4.81	66.85	25.32
2053555 M 284	114.34	3.16	341.31	4.72	0.16	15.63	0.42	3.10	1.92	0.45	5.20	1.91	25.76	11.04
2018616 108	549.71	14.74	1330.91	3.32	16.05	198.40	9.87	67.25	36.58	12.11	78.48	17.05	147.38	46.04
2018616 79	326.73	19.72	1050.97	3.67	14.61	143.25	9.55	64.35	58.48	14.94	92.23	18.83	136.98	35.57
2018616 96	232.43	13.95	690.50	3.03	4.76	66.59	2.81	21.80	14.28	3.54	31.37	7.40	75.82	23.50
2016125 L 51	275.70	27.83	338.34	0.46	0.87	4.36	0.27	1.77	1.86	0.41	9.34	2.83	33.85	12.19
2016125 L 52	182.57	9.80	634.42	1.62		5.83	0.05	1.59	4.42	0.10	16.87	5.97	66.85	24.29
2016125 L 55	228.90	13.98	651.75	1.12	0.51	5.85	0.27	2.59	5.38	0.29	21.59	6.57	68.20	24.01
2016125 M 63	237.04	20.94	544.01	0.70		3.60	0.07	1.31	3.82	0.26	14.68	4.81	55.39	19.07
2016125 M 69	229.35	5.60	834.19	5.14		16.73	0.06	1.76	4.51	0.09	22.06	7.07	90.51	30.94
2016125 M 72	189.41	25.14	373.75	0.59		2.31	0.05	0.81	1.71	0.34	10.91	3.21	38.33	13.14
2016125 M 75	222.65	7.22	822.06	3.45		16.64	0.05	1.73	2.95	0.23	18.33	6.05	81.74	29.78
2721839 M 124	371.50	30.71	1118.36	2.19	2.20	42.09	0.86	7.42	8.13	2.12	33.42	12.01	135.36	42.97
2746487 M 50	199.09	57.44	280.94	0.21		10.81	0.11	2.82	3.29	2.04	10.06	3.46	37.55	10.69
2746487 S 94	152.50	19.70	1389.82	6.98	17.06	86.43	9.95	59.77	25.37	4.23	35.98	10.30	128.35	45.55
2746487 M 61	170.14	10.58	503.47	0.81		13.06	0.07	1.07	2.22	1.14	10.30	3.51	47.89	17.79

Appendix 4 Table A5 Zircon trace element data for GRV and Hiltaba Suite samples analyzed at Boise State University

Spot Number	Er	Tm	Yb	Lu	Hf	Th	U	Eu/Eu*	Ce/Ce*	$(Yb/Gd)_N$	Ti-in-Zircon	Total REE	Th/U
Rejected Data	ppm	ppm	ppm	ppm	ppm	ppm	ppm						
2000366176 M 239	168.77	41.77	439.35	52.38	9293.84	268.16	347.51	0.16	182.72	20.38	825	920	0.8
2000366176 L 217	88.91	20.28	196.06	29.10	8250.47	81.71	65.92	0.56	149.11	13.97	903	456	1.2
2000366176 L 195	90.57	19.84	208.05	31.67	8203.50	62.94	49.33	0.56	58.11	16.04	918	469	1.3
2000366176 L 198	236.84	48.60	434.96	67.32	8611.14	139.30	76.20	0.58	11.67	9.26	938	1139	1.8
2000366176 L 197	179.94	37.20	344.64	50.72	8733.07	92.87	51.20	0.66	14.78	8.95	931	894	1.8
2111460 L 255	74.49	17.71	184.62	23.81	7382.67	72.24	64.24	0.59	88.41	17.54	926	405	1.1
2111460 L 259	77.64	17.95	183.62	23.77	7258.96	51.02	36.01	0.88	55.77	13.44	981	419	1.4
2111460 M 274	300.95	68.37	704.71	83.33	7904.75	463.40	506.28	0.23	37.74	13.42	788	1580	0.9
2111460 L 260	57.04	13.54	137.69	17.57	7492.51	26.95	21.22	1.15	144.78	19.68	959	296	1.3
2111460 L 261	273.71	64.48	655.20	82.38	10083.45	290.94	265.36	0.19	3.18	16.07	823	1471	1.1
1831634 M 37	182.87	42.43	445.24	58.30	7681.92	120.76	117.53	0.31	153.86	16.85	900	975	1.0
1831634 L 27	215.45	49.83	511.87	68.40	8015.01	321.47	235.86	0.34	163.25	16.52	917	1153	1.4
1831634 L 26	225.62	53.33	542.14	70.61	8221.35	273.23	208.03	0.33	124.00	17.21	920	1215	1.3
1831634 L 18	80.31	19.94	206.48	25.20	7132.45	47.78	42.15	0.48	211.56	19.44	924	442	1.1
1831634 L 7	186.19	44.52	444.04	56.61	7465.76	269.60	171.36	0.52	34.59	13.93	929	1013	1.6
1831634 L 12	239.23	59.41	620.24	79.96	7087.36	196.90	180.22	0.54	45.95	19.00	934	1323	1.1
1831634 L 17	164.68	39.11	418.41	49.09	7064.86	194.67	162.49	0.41	107.73	15.49	922	917	1.2
1831634 L 24	168.83	39.12	389.50	52.18	7125.95	232.91	97.16	0.87	10.59	10.08	953	943	2.4
2053554 M 111	219.22	49.70	504.57	74.08	6295.76	187.03	94.93	0.63	27.43	17.01	814	1173	2.0
2053554 M 80	152.59	34.57	359.10	46.80	7516.66	215.52	154.91	0.48	438.96	19.73	775	826	1.4
2053554 L 203	195.10	50.01	497.26	70.53	6675.15	144.03	131.18	0.46	316.63	19.43	768	1084	1.1
2053554 L 197	241.00	51.52	477.96	81.12	10669.58	265.71	184.49	0.41	478.22	16.28	779	1182	1.4
2053554 M 228	193.48	47.33	493.16	67.14	7402.04	163.00	172.09	0.53	6.06	18.74	789	1138	0.9
2053554 M 129	197.23	45.37	411.26	71.84	10163.54	212.71	145.79	0.30	6.87	15.85	772	1030	1.5
2053554 M 112	299.05	69.06	672.97	95.31	7604.00	225.01	137.45	0.50	47.71	13.09	792	1594	1.6
2053554 L 204	282.37	64.82	602.77	81.24	6794.86	205.23	121.26	0.50	127.43	11.28	759	1475	1.7
2053554 L 216	159.97	41.39	430.74	57.27	7122.96	156.19	164.74	0.30	137.03	24.67	748	922	0.9
2053554 M 114	173.80	40.31	402.52	55.68	6873.31	91.62	58.28	0.56	17.21	15.24	773	935	1.6
2053554 M 233	126.46	31.50	355.25	48.56	7985.97	194.52	182.91	0.43	1818.27	29.14	740	747	1.1
2053554 M 99	159.21	35.62	336.20	60.14	8800.63	145.99	103.48	0.39	33.80	17.47	780	809	1.4
2053554 L 205	187.02	45.82	487.45	67.15	6700.76	120.86	122.97	0.42	1153.65	20.58	778	1062	1.0
2053554 M 241	132.03	31.89	322.08	41.03	6513.60	163.09	119.31	0.49	522.76	17.28	758	752	1.4
2053554 M 236	137.28	33.16	345.63	42.00	6583.24	204.37	164.07	0.40	486.12	18.99	771	778	1.2
2053554 M 109	156.17	37.63	379.58	58.19	8773.71	110.85	111.51	0.34	1053.97	22.94	746	826	1.0
2053554 M 113	200.72	45.09	467.12	70.77	7156.18	95.29	76.01	0.51	517.58	17.97	772	1059	1.3
2053554 M 122	222.36	48.58	451.78	73.39	9124.00	355.10	168.82	0.40	21.71	14.24	785	1160	2.1
2053555 L 249	43.59	13.17	164.95	34.30	12546.16	96.36	567.32	0.44	1.59	45.10	663	331	0.2
2053555 L 251	247.31	58.88	605.80	85.71	8584.90	473.48	519.14	0.32	6.17	17.57	850	1396	0.9
2053555 L 256	34.92	12.19	186.02	37.15	11205.73	51.18	730.46	0.33	21.83	127.92	550	305	0.1
2053555 L 257	176.50	43.93	458.65	61.97	9951.18	408.84	386.52	0.14	492.63	24.25	751	973	1.1
2053555 L 260	609.39	147.29	1511.92	186.68	6952.76	1786.39	1235.10	0.23	4.82	17.63	848	3263	1.4
2053555 L 263	36.20	10.94	140.31	25.08	9757.65	135.15	526.55	0.43	4.24	35.55	721	282	0.3
2053555 L 265	204.25	49.53	471.36	77.19	9422.95	439.28	550.80	0.37	2.09	17.28	844	1123	0.8
2053555 L 266	553.68	121.23	1121.80	177.30	9877.45	1051.30	646.34	0.26	101.11	14.27	875	2719	1.6
2053555 M 269	219.02	55.08	564.32	73.52	7792.47	522.70	519.58	0.35	49.52	21.52	859	1242	1.0
2053555 M 271	120.50	30.99	370.26	45.33	9354.50	288.68	710.61	0.48	2.01	21.31	735	781	0.4
2053555 M 274	226.44	54.55	571.61	70.48	7880.50	498.72	327.30	0.46	8.18	15.28	848	1394	1.5
2053555 M 275	126.84	32.41	346.42	43.38	9296.18	357.98	284.16	0.37	6.17	18.08	817	825	1.3
2053555 M 276	146.66	37.53	424.30	55.14	8380.88	447.25	680.41	0.49	3.33	15.98	764	1042	0.7
2053555 M 279	89.93	23.65	252.86	34.42	8437.97	166.39	470.16	0.11	194.08	29.44	734	501	0.4
2053555 M 281	111.55	28.79	322.07	42.58	8615.42	235.03	288.57	0.18	42.84	28.84	726	645	0.8
2053555 M 284	54.74	16.55	202.21	30.26	10088.42	123.52	534.79	0.43	15.00	48.18	689	369	0.2
2018616 108	178.73	38.44	339.95	54.01	10721.40	186.45	186.43	0.69	3.87	5.37	838	1240	1.0
2018616 79	132.49	27.57	248.84	39.37	10062.26	161.17	179.55	0.62	2.97	3.34	871	1037	0.9
2018616 96	101.20	24.14	236.67	37.03	9858.63	127.29	152.61	0.51	4.46	9.35	832	651	0.8
2016125 L 51	52.51	12.57	122.08	16.88	6103.44	13.54	20.88	0.30	2.20	16.20	914	272	0.6
2016125 L 52	98.78	22.45	220.96	30.63	6613.78	38.88	65.29	0.04	114.65	16.23	794	499	0.6
2016125 L 55	100.12	22.48	233.04	28.93	5625.67	41.66	68.53	0.08	3.84	13.38	832	520	0.6
2016125 M 63	85.71	18.74	193.64	26.02	6084.88	26.58	39.74	0.11	53.05	16.35	878	427	0.7
2016125 M 69	130.04	32.29	345.28	40.03	7798.96	138.65	243.24	0.03	260.46	19.39	739	721	0.6
2016125 M 72	57.33	14.01	138.13	18.19	5361.33	15.00	24.34	0.24	41.31	15.69	901	298	0.6
2016125 M 75	122.71	28.93	288.08	40.42	8109.95	94.71	152.39	0.10	355.79	19.47	763	638	0.6
2721839 M 124	167.94	43.41	532.58	43.51	7754.99	73.77	47.74	0.39	7.53	19.75	926	1074	1.5
2746487 M 50	41.58	10.84	139.22	12.98	6006.84	22.08	10.98	1.08	99.29	17.15	1014	285	2.0
2746487 S 94	216.26	62.25	755.95	90.40	13260.27	235.73	198.47	0.43	1.63	26.03	871	1548	1.2
2746487 M 61	79.04	24.48	371.52	36.19	7218.80	51.40	59.16	0.73	177.73	44.70	802	608	0.9

Appendix Table A6 LA-ICP MS U-Pb data for GRV and Hiltaba Suite zircon analyzed at Boise state University

Unit	Group	Sample	Spot Number	Disc.	Other	Experiment Number	Radiogenic Ratios							Age (Ma)								
							$^{207}Pb/^{206}Pb$	2σ	$^{207}Pb/^{235}U$	2σ	$^{206}Pb/^{238}U$	2σ	$^{207}Pb/^{206}Pb$	2σ	$^{207}Pb/^{235}Pb$	2σ	$^{206}Pb/^{238}U$	2σ	% Conc	Th ppm	U ppm
Hiltaba Suite	mineralization-related	2000366176	2000366176 L 214			6	0.1016	2.2264	3.8814	3.4914	0.2770	2.6894	1654	41	1610	28	1576	38	95	275.05	288.01
Hiltaba Suite	mineralization-related	2000366176	2000366176 M 237			6	0.1010	3.5685	3.9517	5.9563	0.2839	4.7690	1642	66	1624	48	1611	68	98	49.97	60.97
Hiltaba Suite	mineralization-related	2000366176	2000366176 L 206			6	0.1007	1.6642	3.9410	3.7347	0.2837	3.3434	1638	31	1622	30	1610	48	98	281.42	196.96
Hiltaba Suite	mineralization-related	2000366176	2000366176 M 228			6	0.1003	1.3729	3.7946	3.4326	0.2744	3.1461	1630	26	1592	28	1563	44	96	194.27	254.94
Hiltaba Suite	mineralization-related	2000366176	2000366176 M 235			6	0.1002	1.7974	3.8180	3.6433	0.2763	3.1690	1628	33	1597	29	1573	44	97	134.92	160.29
Hiltaba Suite	mineralization-related	2000366176	2000366176 L 204			6	0.1000	1.4734	3.8103	3.2954	0.2763	2.9477	1625	27	1595	27	1573	41	97	276.72	155.68
Hiltaba Suite	mineralization-related	2000366176	2000366176 M 234			6	0.0999	1.7937	3.7917	3.7487	0.2752	3.2917	1623	33	1591	30	1567	46	97	110.78	106.73
Hiltaba Suite	mineralization-related	2000366176	2000366176 M 229			6	0.0992	1.6161	3.8097	4.4435	0.2786	4.1392	1609	30	1595	36	1584	58	98	171.84	217.27
Hiltaba Suite	mineralization-related	2000366176	2000366176 M 233			6	0.0991	1.0038	3.8073	3.0577	0.2786	2.8883	1608	19	1594	25	1584	41	99	292.89	236.29
Hiltaba Suite	mineralization-related	2000366176	2000366176 M 227			6	0.0991	1.7202	3.7687	3.5716	0.2759	3.1301	1607	32	1586	29	1571	44	98	131.35	237.71
Hiltaba Suite	mineralization-related	2000366176	2000366176 L 202			6	0.0991	1.7609	3.8219	3.1705	0.2798	2.6365	1607	33	1597	26	1590	37	99	150.90	142.80
Hiltaba Suite	mineralization-related	2000366176	2000366176 L 200			6	0.0988	2.2141	3.8574	4.4181	0.2833	3.8233	1601	41	1605	36	1608	54	100	118.92	112.16
Hiltaba Suite	mineralization-related	2000366176	2000366176 M 219			6	0.0987	1.3986	3.7107	4.2597	0.2726	4.0235	1600	26	1574	34	1554	56	97	417.31	243.12
Hiltaba Suite	mineralization-related	2000366176	2000366176 L 205			6	0.0987	1.7822	3.8191	4.0737	0.2806	3.6632	1600	33	1597	33	1594	52	100	217.49	132.71
Hiltaba Suite	mineralization-related	2000366176	2000366176 M 226			6	0.0987	1.3534	3.7322	3.1591	0.2743	2.8545	1600	25	1578	25	1562	40	98	208.10	223.52
Hiltaba Suite	mineralization-related	2000366176	2000366176 M 220			6	0.0984	1.7359	3.7391	4.7937	0.2757	4.4684	1593	32	1580	38	1570	62	99	203.40	218.94
Hiltaba Suite	mineralization-related	2000366176	2000366176 L 203			6	0.0980	2.3871	3.8207	3.9638	0.2827	3.1643	1587	45	1597	32	1605	45	101	186.99	106.72
Hiltaba Suite	mineralization-related	2000366176	2000366176 L 211			6	0.0979	2.7559	3.8522	4.3481	0.2852	3.3632	1585	52	1604	35	1618	48	102	115.33	83.33
Hiltaba Suite	mineralization-related	2000366176	2000366176 L 212			6	0.0979	2.6924	3.8671	3.9953	0.2866	2.9518	1584	50	1607	32	1625	42	103	89.49	71.45
Hiltaba Suite	mineralization-related	2000366176	2000366176 L 207			6	0.0977	1.9085	3.7840	3.5096	0.2809	2.9453	1581	36	1589	28	1596	42	101	156.75	142.70
Hiltaba Suite	mineralization-related	2000366176	2000366176 M 238			6	0.0976	1.6237	3.7482	3.9924	0.2785	3.6473	1579	30	1582	32	1584	51	100	194.10	138.65
Hiltaba Suite	mineralization-related	2000366176	2000366176 L 201			6	0.0974	1.6635	3.7796	3.3888	0.2814	2.9524	1575	31	1588	27	1599	42	102	177.37	204.87
Hiltaba Suite	mineralization-related	2000366176	2000366176 L 199			6	0.0973	1.3990	3.7432	3.2654	0.2790	2.9505	1573	26	1581	26	1586	41	101	244.20	141.58
Hiltaba Suite	mineralization-related	2000366176	2000366176 M 224			6	0.0969	2.1235	3.8320	4.3844	0.2869	3.8358	1564	40	1599	35	1626	55	104	117.78	137.71
Hiltaba Suite	mineralization-related	2000366176	2000366176 L 213			6	0.0968	1.3291	3.6308	2.9267	0.2722	2.6075	1562	25	1556	23	1552	36	99	391.62	274.28
Hiltaba Suite	mineralization-related	2000366176	2000366176 L 208			6	0.0964	2.2409	3.8002	4.2104	0.2859	3.5646	1555	42	1593	34	1621	51	104	208.94	147.19
Hiltaba Suite	mineralization-related	2111460	2111460 M 276			4	0.1011	1.9219	3.9614	5.3340	0.2842	4.9757	1645	36	1626	43	1612	71	98	42.02	57.77
Hiltaba Suite	mineralization-related	2111460	2111460 M 271			4	0.1011	1.0736	3.9379	3.5571	0.2825	3.3912	1644	20	1621	29	1604	48	98	233.51	325.69
Hiltaba Suite	mineralization-related	2111460	2111460 M 279			4	0.1007	1.3659	3.8432	3.5967	0.2768	3.3273	1637	25	1602	29	1575	47	96	279.13	320.15
Hiltaba Suite	mineralization-related	2111460	2111460 M 267			4	0.1003	1.9519	3.7805	3.9073	0.2734	3.3848	1629	36	1589	31	1558	47	96	137.14	167.62
Hiltaba Suite	mineralization-related	2111460	2111460 L 245			4	0.0998	1.6137	3.8973	3.3690	0.2832	2.9574	1620	30	1613	27	1608	42	99	123.81	121.04
Hiltaba Suite	mineralization-related	2111460	2111460 L 242			4	0.0998	1.6396	3.7696	3.3998	0.2741	2.9783	1620	31	1586	27	1561	41	96	302.84	232.72
Hiltaba Suite	mineralization-related	2111460	2111460 M 265			4	0.0997	2.1495	3.9394	5.3710	0.2865	4.9221	1619	40	1622	43	1624	71	100	157.29	170.13
Hiltaba Suite	mineralization-related	2111460	2111460 L 241			4	0.0997	1.8975	3.7944	3.3903	0.2760	2.8096	1619	35	1592	27	1571	39	97	294.87	181.86
Hiltaba Suite	mineralization-related	2111460	2111460 L 251			4	0.0997	1.8956	3.7612	5.5610	0.2737	5.2279	1618	35	1584	45	1560	72	96	252.42	239.65

Appendix Table A6 LA-ICP MS U-Pb data for GRV and Hiltaba Suite zircon analyzed at Boise state University

Unit	Group	Sample	Spot Number	Disc.	Other	Experiment Number	Radiogenic Ratios							Age (Ma)								
							$^{207}Pb/^{206}Pb$	2σ	$^{207}Pb/^{235}U$	2σ	$^{206}Pb/^{238}U$	2σ	$^{207}Pb/^{206}Pb$	2σ	$^{207}Pb/^{235}Pb$	2σ	$^{206}Pb/^{238}U$	2σ	% Conc	Th ppm	U ppm
Hiltaba Suite	mineralization-related	2111460	2111460 M 278			4	0.0996	2.1790	3.8154	3.9758	0.2779	3.3254	1616	41	1596	32	1581	47	98	151.86	171.02
Hiltaba Suite	mineralization-related	2111460	2111460 M 262			4	0.0996	1.4979	3.6944	4.5305	0.2691	4.2757	1616	28	1570	36	1536	58	95	292.98	440.86
Hiltaba Suite	mineralization-related	2111460	2111460 M 268			4	0.0993	1.0642	3.7700	3.1800	0.2754	2.9966	1611	20	1586	26	1568	42	97	271.81	430.41
Hiltaba Suite	mineralization-related	2111460	2111460 L 252			4	0.0992	1.1877	3.6937	3.9268	0.2700	3.7429	1609	22	1570	31	1541	51	96	188.52	242.59
Hiltaba Suite	mineralization-related	2111460	2111460 L 243			4	0.0992	1.3429	3.8446	3.4095	0.2812	3.1339	1608	25	1602	27	1597	44	99	550.76	324.43
Hiltaba Suite	mineralization-related	2111460	2111460 M 269			4	0.0991	1.7912	3.8784	4.2134	0.2839	3.8137	1607	33	1609	34	1611	54	100	164.06	218.08
Hiltaba Suite	mineralization-related	2111460	2111460 L 248			4	0.0990	1.3011	3.7993	3.3186	0.2783	3.0529	1606	24	1593	27	1583	43	99	229.48	228.92
Hiltaba Suite	mineralization-related	2111460	2111460 M 264			4	0.0990	1.4486	3.6468	4.2392	0.2672	3.9840	1605	27	1560	34	1526	54	95	270.33	356.44
Hiltaba Suite	mineralization-related	2111460	2111460 L 250			4	0.0990	1.1991	3.7456	4.0463	0.2745	3.8646	1605	22	1581	32	1564	54	97	410.28	393.96
Hiltaba Suite	mineralization-related	2111460	2111460 L 247			4	0.0990	1.7717	3.8336	3.1178	0.2810	2.5655	1605	33	1600	25	1596	36	99	281.54	208.41
Hiltaba Suite	mineralization-related	2111460	2111460 L 249			4	0.0989	1.3247	3.7257	3.6714	0.2733	3.4241	1603	25	1577	29	1557	47	97	342.80	356.47
Hiltaba Suite	mineralization-related	2111460	2111460 M 266			4	0.0989	1.1434	3.7755	5.1393	0.2770	5.0105	1603	21	1588	41	1576	70	98	202.37	238.03
Hiltaba Suite	mineralization-related	2111460	2111460 M 270			4	0.0985	0.9876	3.7148	3.8052	0.2736	3.6748	1595	18	1575	30	1559	51	98	391.68	417.15
Hiltaba Suite	mineralization-related	2111460	2111460 L 258			4	0.0984	1.7456	3.7637	3.8451	0.2774	3.4260	1594	33	1585	31	1578	48	99	286.87	248.77
Hiltaba Suite	mineralization-related	2111460	2111460 M 277			4	0.0983	1.5925	3.6490	4.0460	0.2692	3.7194	1592	30	1560	32	1537	51	97	337.58	365.32
Hiltaba Suite	mineralization-related	2111460	2111460 M 272			4	0.0982	1.1641	3.9783	6.1366	0.2939	6.0252	1590	22	1630	50	1661	88	104	222.29	288.51
Hiltaba Suite	mineralization-related	2111460	2111460 L 253			4	0.0981	2.0464	3.8461	4.3235	0.2843	3.8085	1589	38	1602	35	1613	54	102	91.24	114.42
Hiltaba Suite	mineralization-related	2111460	2111460 L 246			4	0.0980	1.3528	3.8152	2.5802	0.2822	2.1972	1587	25	1596	21	1603	31	101	150.81	140.05
Hiltaba Suite	mineralization-related	2111460	2111460 L 257			4	0.0972	1.2225	3.7664	3.6152	0.2810	3.4022	1571	23	1586	29	1596	48	102	249.37	271.58
Hiltaba Suite	mineralization-related	2111460	2111460 L 244			4	0.0971	1.3108	3.8525	3.1422	0.2878	2.8558	1569	25	1604	25	1630	41	104	196.53	205.54
Hiltaba Suite	mineralization-related	1831634	1831634 M 45			3	0.0977	2.9766	3.9184	4.7191	0.2910	3.6620	1580	56	1617	38	1647	53	104	79.99	54.69
Hiltaba Suite	mineralization-related	1831634	1831634 M 47			3	0.0976	2.0875	3.9058	5.9803	0.2902	5.6042	1579	39	1615	48	1642	81	104	137.76	112.34
Hiltaba Suite	mineralization-related	1831634	1831634 M 42			3	0.0963	2.5372	3.7791	4.9057	0.2846	4.1986	1554	48	1588	39	1615	60	104	64.29	56.03
Hiltaba Suite	mineralization-related	1831634	1831634 L 9			3	0.0977	1.8851	3.8019	4.8771	0.2821	4.4981	1582	35	1593	39	1602	64	101	154.61	123.95
Hiltaba Suite	mineralization-related	1831634	1831634 M 48			3	0.0955	3.8766	3.6919	5.8817	0.2804	4.4235	1538	73	1570	47	1593	62	104	41.17	47.64
Hiltaba Suite	mineralization-related	1831634	1831634 M 41			3	0.0978	2.1406	3.7807	4.0333	0.2804	3.4184	1583	40	1589	32	1593	48	101	121.53	120.98
Hiltaba Suite	mineralization-related	1831634	1831634 L 5			3	0.0979	1.4114	3.7751	3.5360	0.2796	3.2421	1585	26	1587	28	1589	46	100	163.90	122.26
Hiltaba Suite	mineralization-related	1831634	1831634 L 23			3	0.0966	2.1382	3.7222	4.5630	0.2795	4.0310	1559	40	1576	37	1589	57	102	99.80	108.43
Hiltaba Suite	mineralization-related	1831634	1831634 M 29			3	0.0983	2.0255	3.7727	5.0407	0.2785	4.6159	1591	38	1587	40	1584	65	100	124.38	104.32
Hiltaba Suite	mineralization-related	1831634	1831634 L 25			3	0.0983	1.8036	3.7599	4.1098	0.2775	3.6928	1591	34	1584	33	1579	52	99	145.95	160.87
Hiltaba Suite	mineralization-related	1831634	1831634 M 31			3	0.0976	1.4479	3.7320	3.6231	0.2773	3.3212	1579	27	1578	29	1578	46	100	225.24	141.89
Hiltaba Suite	mineralization-related	1831634	1831634 L 13			3	0.0991	2.0240	3.7830	4.7665	0.2770	4.3154	1606	38	1589	38	1576	60	98	168.65	117.07
Hiltaba Suite	mineralization-related	1831634	1831634 L 22			3	0.0983	1.4770	3.7453	3.7219	0.2763	3.4162	1592	28	1581	30	1573	48	99	111.84	116.08
Hiltaba Suite	mineralization-related	1831634	1831634 M 34			3	0.0985	1.8150	3.7488	3.6119	0.2759	3.1228	1597	34	1582	29	1571	44	98	106.59	90.09

Appendix Table A6 LA-ICP MS U-Pb data for GRV and Hiltaba Suite zircon analyzed at Boise state University

Unit	Group	Sample	Spot Number	Disc.	Other	Experiment Number	Radiogenic Ratios							Age (Ma)							
							$^{207}Pb/^{206}Pb$	2σ	$^{207}Pb/^{235}U$	2σ	$^{206}Pb/^{238}U$	2σ	$^{207}Pb/^{206}Pb$	2σ	$^{207}Pb/^{235}Pb$	2σ	$^{206}Pb/^{238}U$	2σ	% Conc	Th ppm	U ppm
Hiltaba Suite	mineralization-related	1831634	1831634 L 6			3	0.0988	1.8011	3.7512	4.5705	0.2753	4.2006	1602	34	1582	37	1568	58	98	184.06	161.81
Hiltaba Suite	mineralization-related	1831634	1831634 L 3			3	0.0970	1.9889	3.6792	4.4044	0.2752	3.9298	1566	37	1567	35	1567	55	100	93.97	119.44
Hiltaba Suite	mineralization-related	1831634	1831634 L 16			3	0.0984	1.3698	3.7335	3.8918	0.2752	3.6428	1594	26	1579	31	1567	51	98	189.66	158.31
Hiltaba Suite	mineralization-related	1831634	1831634 M 38			3	0.0970	2.0569	3.6789	3.2620	0.2751	2.5318	1567	39	1567	26	1567	35	100	67.22	65.47
Hiltaba Suite	mineralization-related	1831634	1831634 L 8			3	0.0976	1.2605	3.6927	4.1208	0.2745	3.9233	1578	24	1570	33	1564	54	99	225.24	169.98
Hiltaba Suite	mineralization-related	1831634	1831634 M 35			3	0.0996	1.4271	3.7662	5.3730	0.2742	5.1800	1617	27	1586	43	1562	72	97	289.58	189.46
Hiltaba Suite	mineralization-related	1831634	1831634 M 30			3	0.0987	3.4232	3.7306	5.2668	0.2742	4.0026	1599	64	1578	42	1562	56	98	64.24	49.01
Hiltaba Suite	mineralization-related	1831634	1831634 M 36			3	0.0998	1.3203	3.7712	4.4048	0.2740	4.2023	1621	25	1587	35	1561	58	96	223.35	137.64
Hiltaba Suite	mineralization-related	1831634	1831634 L 15			3	0.0970	1.6560	3.6585	4.5115	0.2735	4.1965	1567	31	1562	36	1559	58	99	136.96	125.71
Hiltaba Suite	mineralization-related	1831634	1831634 L 21			3	0.0989	1.3950	3.7278	4.2018	0.2732	3.9635	1604	26	1577	34	1557	55	97	136.77	152.83
Hiltaba Suite	mineralization-related	1831634	1831634 M 40			3	0.0984	1.7480	3.6945	3.2522	0.2722	2.7425	1595	33	1570	26	1552	38	97	161.33	151.90
Hiltaba Suite	mineralization-related	1831634	1831634 L 10			3	0.0991	1.6420	3.7056	3.5270	0.2713	3.1214	1606	31	1573	28	1548	43	96	215.25	151.69
Hiltaba Suite	mineralization-related	1831634	1831634 M 46			3	0.0967	2.2018	3.6055	4.4223	0.2705	3.8352	1561	41	1551	35	1543	53	99	121.99	75.37
Hiltaba Suite	mineralization-related	1831634	1831634 L 11			3	0.0978	1.3537	3.6469	4.1584	0.2703	3.9318	1583	25	1560	33	1543	54	97	321.19	204.56
Hiltaba Suite	mineralization-related	1831634	1831634 M 44			3	0.0987	1.6937	3.6455	3.4719	0.2679	3.0307	1599	32	1560	28	1530	41	96	240.37	157.61
Hiltaba Suite	mineralization-related	1831634	1831634 L 20			3	0.0987	1.2384	3.6407	3.5644	0.2675	3.3424	1600	23	1558	28	1528	45	96	243.00	169.53
Hiltaba Suite	mineralization-related	1831634	1831634 L 14			3	0.0986	1.3112	3.6271	4.2187	0.2667	4.0097	1599	24	1555	34	1524	54	95	182.09	176.11
Hiltaba Suite	mineralization-related	1831634	1831634 L 2			3	0.0977	1.5701	3.5885	3.6780	0.2663	3.3260	1581	29	1547	29	1522	45	96	201.08	137.54
Hiltaba Suite	mineralization-related	1831634	1831634 M 32			3	0.0987	1.5870	3.6217	3.0274	0.2661	2.5781	1600	30	1554	24	1521	35	95	181.50	169.14
Hiltaba Suite	mineralization-related	1831634	1831634 L 19			3	0.0979	1.5510	3.5889	3.9775	0.2658	3.6627	1585	29	1547	32	1519	50	96	261.52	179.96
Hiltaba Suite	mineralization-absent	2053554	2053554 L 196			1	0.1024	2.9414	3.9662	4.9961	0.2808	4.0385	1669	54	1627	41	1595	57	96	102.97	55.31
Hiltaba Suite	mineralization-absent	2053554	2053554 M 79			2	0.1022	3.1362	3.9460	5.5497	0.2799	4.5785	1665	58	1623	45	1591	65	96	122.21	127.18
Hiltaba Suite	mineralization-absent	2053554	2053554 M 107			2	0.1010	2.1616	3.8271	5.4086	0.2747	4.9578	1643	40	1598	44	1565	69	95	243.39	157.63
Hiltaba Suite	mineralization-absent	2053554	2053554 M 227			1	0.1003	2.3064	3.8307	5.4283	0.2769	4.9140	1630	43	1599	44	1576	69	97	99.39	90.33
Hiltaba Suite	mineralization-absent	2053554	2053554 M 92			2	0.1002	1.9200	3.8875	4.9378	0.2813	4.5493	1628	36	1611	40	1598	64	98	186.57	117.61
Hiltaba Suite	mineralization-absent	2053554	2053554 L 213			1	0.1002	3.5409	3.8275	7.4063	0.2770	6.5051	1628	66	1599	60	1576	91	97	145.60	124.18
Hiltaba Suite	mineralization-absent	2053554	2053554 L 222			1	0.1002	2.3091	3.7974	4.6699	0.2750	4.0590	1627	43	1592	38	1566	56	96	214.69	188.11
Hiltaba Suite	mineralization-absent	2053554	2053554 M 125			2	0.0999	2.8186	3.8829	5.4710	0.2819	4.6890	1622	52	1610	44	1601	66	99	161.50	113.01
Hiltaba Suite	mineralization-absent	2053554	2053554 M 232			1	0.0998	3.2117	3.8282	7.4496	0.2782	6.7217	1621	60	1599	60	1582	94	98	214.34	158.53
Hiltaba Suite	mineralization-absent	2053554	2053554 M 82			2	0.0998	2.5488	3.8232	4.7983	0.2779	4.0654	1620	47	1598	39	1581	57	98	172.17	126.82
Hiltaba Suite	mineralization-absent	2053554	2053554 L 206			1	0.0997	2.2673	3.7331	4.9445	0.2716	4.3940	1619	42	1578	40	1549	60	96	151.84	113.64
Hiltaba Suite	mineralization-absent	2053554	2053554 L 214			1	0.0997	2.0143	3.8040	4.7514	0.2768	4.3033	1618	37	1594	38	1575	60	97	245.18	177.08
Hiltaba Suite	mineralization-absent	2053554	2053554 M 93			2	0.0996	2.1277	3.8389	4.4742	0.2795	3.9359	1617	40	1601	36	1589	55	98	117.45	95.75
Hiltaba Suite	mineralization-absent	2053554	2053554 L 208			1	0.0996	3.0787	3.7757	4.4860	0.2750	3.2628	1616	57	1588	36	1566	45	97	97.48	95.92
Hiltaba Suite	mineralization-absent	2053554	2053554 M 83			2	0.0996	2.7246	3.7637	6.3815	0.2742	5.7706	1616	51	1585	51	1562	80	97	115.60	110.30

Appendix Table A6 LA-ICP MS U-Pb data for GRV and Hiltaba Suite zircon analyzed at Boise state University

Unit	Group	Sample	Spot Number	Disc.	Other	Experiment Number	Radiogenic Ratios						Age (Ma)								
							$^{207}Pb/^{206}Pb$	2σ	$^{207}Pb/^{235}U$	2σ	$^{206}Pb/^{238}U$	2σ	$^{207}Pb/^{206}Pb$	2σ	$^{207}Pb/^{235}Pb$	2σ	$^{206}Pb/^{238}U$	2σ	% Conc	Th ppm	U ppm
Hiltaba Suite	mineralization-absent	2053554	2053554 M 81			2	0.0995	2.0286	4.0170	6.4532	0.2929	6.1260	1614	38	1638	52	1656	89	103	103.44	81.70
Hiltaba Suite	mineralization-absent	2053554	2053554 M 229			1	0.0995	2.8441	3.7867	6.3244	0.2761	5.6489	1614	53	1590	51	1572	79	97	158.20	135.42
Hiltaba Suite	mineralization-absent	2053554	2053554 M 115			2	0.0994	2.1142	3.7004	4.6871	0.2701	4.1832	1612	39	1571	37	1541	57	96	133.42	122.25
Hiltaba Suite	mineralization-absent	2053554	2053554 L 221			1	0.0993	3.4677	3.7987	5.0537	0.2774	3.6763	1611	65	1592	41	1578	51	98	109.57	96.80
Hiltaba Suite	mineralization-absent	2053554	2053554 M 106			2	0.0992	2.3067	3.6962	4.3088	0.2702	3.6394	1610	43	1571	34	1542	50	96	222.61	139.31
Hiltaba Suite	mineralization-absent	2053554	2053554 M 85			2	0.0992	3.0591	3.9215	7.2827	0.2867	6.6091	1609	57	1618	59	1625	95	101	117.53	103.79
Hiltaba Suite	mineralization-absent	2053554	2053554 L 207			1	0.0990	2.4381	3.8398	4.5000	0.2814	3.7822	1604	45	1601	36	1599	54	100	240.95	188.19
Hiltaba Suite	mineralization-absent	2053554	2053554 M 118			2	0.0989	2.3437	3.7029	5.5137	0.2714	4.9908	1604	44	1572	44	1548	69	96	204.61	127.53
Hiltaba Suite	mineralization-absent	2053554	2053554 L 202			1	0.0989	2.5221	3.8795	4.4974	0.2844	3.7236	1604	47	1609	36	1614	53	101	134.52	105.97
Hiltaba Suite	mineralization-absent	2053554	2053554 L 198			1	0.0989	2.7318	3.7314	5.1248	0.2736	4.3360	1604	51	1578	41	1559	60	97	243.28	174.60
Hiltaba Suite	mineralization-absent	2053554	2053554 L 212			1	0.0989	2.4506	3.7113	4.8305	0.2722	4.1628	1603	46	1574	39	1552	57	97	112.19	66.96
Hiltaba Suite	mineralization-absent	2053554	2053554 L 215			1	0.0988	2.4968	3.7208	4.8690	0.2730	4.1801	1602	47	1576	39	1556	58	97	113.39	98.68
Hiltaba Suite	mineralization-absent	2053554	2053554 L 209			1	0.0988	2.8001	3.9136	5.0661	0.2873	4.2219	1601	52	1616	41	1628	61	102	78.99	84.10
Hiltaba Suite	mineralization-absent	2053554	2053554 M 94			2	0.0988	2.1860	3.7974	4.4840	0.2789	3.9150	1601	41	1592	36	1586	55	99	106.86	92.65
Hiltaba Suite	mineralization-absent	2053554	2053554 M 110			2	0.0987	1.9468	3.7720	5.7631	0.2771	5.4244	1601	36	1587	46	1577	76	99	247.06	160.27
Hiltaba Suite	mineralization-absent	2053554	2053554 L 224			1	0.0987	2.1267	3.6747	4.9678	0.2699	4.4895	1600	40	1566	40	1540	62	96	163.26	112.94
Hiltaba Suite	mineralization-absent	2053554	2053554 M 130			2	0.0987	2.6267	3.8672	5.8223	0.2841	5.1961	1600	49	1607	47	1612	74	101	282.03	138.46
Hiltaba Suite	mineralization-absent	2053554	2053554 M 126			2	0.0987	2.3647	3.9096	5.1532	0.2874	4.5786	1599	44	1616	42	1629	66	102	147.53	96.46
Hiltaba Suite	mineralization-absent	2053554	2053554 L 217			1	0.0987	2.7303	3.7906	5.3087	0.2787	4.5528	1599	51	1591	43	1585	64	99	104.91	109.29
Hiltaba Suite	mineralization-absent	2053554	2053554 L 225			1	0.0984	2.4979	3.7558	5.4169	0.2769	4.8066	1594	47	1583	43	1576	67	99	184.29	129.28
Hiltaba Suite	mineralization-absent	2053554	2053554 M 137			2	0.0983	1.6756	3.6508	4.2923	0.2694	3.9518	1592	31	1561	34	1538	54	97	242.60	141.26
Hiltaba Suite	mineralization-absent	2053554	2053554 M 135			2	0.0982	2.4437	3.7037	4.7172	0.2736	4.0349	1590	46	1572	38	1559	56	98	187.45	127.21
Hiltaba Suite	mineralization-absent	2053554	2053554 M 88			2	0.0981	2.1221	3.8151	5.2730	0.2820	4.8272	1589	40	1596	42	1601	68	101	215.05	143.58
Hiltaba Suite	mineralization-absent	2053554	2053554 M 231			1	0.0981	2.8105	3.6672	5.7762	0.2711	5.0464	1589	53	1564	46	1546	69	97	92.60	100.62
Hiltaba Suite	mineralization-absent	2053554	2053554 L 201			1	0.0981	2.8795	3.7469	4.5019	0.2770	3.4605	1589	54	1581	36	1576	48	99	223.12	146.01
Hiltaba Suite	mineralization-absent	2053554	2053554 M 105			2	0.0981	1.4561	3.7013	6.3910	0.2737	6.2230	1588	27	1572	51	1560	86	98	228.67	168.18
Hiltaba Suite	mineralization-absent	2053554	2053554 M 136			2	0.0980	2.1284	3.8706	4.7177	0.2863	4.2103	1587	40	1608	38	1623	60	102	222.98	144.57
Hiltaba Suite	mineralization-absent	2053554	2053554 M 101			2	0.0980	2.2087	3.6921	5.3726	0.2732	4.8975	1587	41	1570	43	1557	68	98	261.99	170.23
Hiltaba Suite	mineralization-absent	2053554	2053554 M 239			1	0.0980	3.3236	3.7428	6.2780	0.2770	5.3261	1586	62	1581	50	1576	74	99	230.58	134.51
Hiltaba Suite	mineralization-absent	2053554	2053554 M 134			2	0.0979	2.4171	3.7545	4.2232	0.2781	3.4631	1584	45	1583	34	1582	49	100	146.21	112.85
Hiltaba Suite	mineralization-absent	2053554	2053554 M 78			2	0.0979	2.2749	3.6716	5.8356	0.2720	5.3739	1584	43	1565	47	1551	74	98	96.84	84.10
Hiltaba Suite	mineralization-absent	2053554	2053554 M 86			2	0.0978	3.0448	3.6088	6.4635	0.2675	5.7014	1583	57	1551	51	1528	78	96	137.23	109.46
Hiltaba Suite	mineralization-absent	2053554	2053554 M 120			2	0.0978	1.9777	3.6897	4.3920	0.2735	3.9216	1583	37	1569	35	1559	54	98	277.37	180.77
Hiltaba Suite	mineralization-absent	2053554	2053554 M 234			1	0.0978	3.9040	3.6948	6.6004	0.2739	5.3220	1583	73	1570	53	1561	74	99	92.80	104.61
Hiltaba Suite	mineralization-absent	2053554	2053554 M 98			2	0.0977	3.0254	3.8682	5.6484	0.2871	4.7698	1581	57	1607	46	1627	69	103	159.03	124.28

Appendix Table A6 LA-ICP MS U-Pb data for GRV and Hiltaba Suite zircon analyzed at Boise state University

Unit	Group	Sample	Spot Number	Disc.	Other	Experiment Number	Radiogenic Ratios							Age (Ma)								
							$^{207}Pb/^{206}Pb$	2σ	$^{207}Pb/^{235}U$	2σ	$^{206}Pb/^{238}U$	2σ	$^{207}Pb/^{206}Pb$	2σ	$^{207}Pb/^{235}Pb$	2σ	$^{206}Pb/^{238}U$	2σ	% Conc	Th ppm	U ppm
Hiltaba Suite	mineralization-absent	2053554	2053554 M 131			2	0.0977	2.1854	3.7621	5.1448	0.2794	4.6576	1580	41	1585	41	1588	66	101	177.13	113.74
Hiltaba Suite	mineralization-absent	2053554	2053554 M 102			2	0.0975	2.1649	3.6706	5.1948	0.2729	4.7222	1578	41	1565	41	1556	65	99	208.77	146.53
Hiltaba Suite	mineralization-absent	2053554	2053554 M 139			2	0.0975	2.6222	3.8164	5.0000	0.2839	4.2572	1577	49	1596	40	1611	61	102	116.66	90.38
Hiltaba Suite	mineralization-absent	2053554	2053554 M 108			2	0.0975	2.1305	3.8072	5.3952	0.2833	4.9567	1576	40	1594	43	1608	71	102	153.23	117.78
Hiltaba Suite	mineralization-absent	2053554	2053554 M 132			2	0.0973	3.1840	3.9605	5.7060	0.2952	4.7350	1573	60	1626	46	1667	70	106	180.47	101.40
Hiltaba Suite	mineralization-absent	2053554	2053554 M 133			2	0.0972	2.8333	3.8982	5.8693	0.2908	5.1402	1572	53	1613	47	1645	75	105	155.66	105.10
Hiltaba Suite	mineralization-absent	2053554	2053554 L 210			1	0.0971	2.1055	3.7834	4.8590	0.2825	4.3791	1570	39	1589	39	1604	62	102	233.62	161.88
Hiltaba Suite	mineralization-absent	2053554	2053554 L 220			1	0.0970	3.1230	3.8247	4.7856	0.2861	3.6262	1566	59	1598	39	1622	52	104	83.24	84.05
Hiltaba Suite	mineralization-absent	2053554	2053554 L 223			1	0.0969	2.1462	3.6757	4.4797	0.2750	3.9322	1566	40	1566	36	1566	55	100	251.96	156.89
Hiltaba Suite	mineralization-absent	2053554	2053554 M 237			1	0.0969	2.3402	3.7432	5.3917	0.2803	4.8574	1565	44	1581	43	1593	69	102	165.65	130.62
Hiltaba Suite	mineralization-absent	2053554	2053554 M 121			2	0.0964	2.1929	3.8378	7.4104	0.2888	7.0785	1555	41	1601	60	1636	102	105	166.83	115.36
Hiltaba Suite	mineralization-absent	2053554	2053554 M 138			2	0.0964	2.4462	3.5841	5.6442	0.2697	5.0865	1555	46	1546	45	1540	70	99	181.28	116.39
Hiltaba Suite	mineralization-absent	2053554	2053554 M 230			1	0.0963	2.8580	3.6839	5.3838	0.2775	4.5626	1553	54	1568	43	1579	64	102	142.65	114.76
Hiltaba Suite	mineralization-absent	2053554	2053554 M 91			2	0.0962	2.6095	3.7880	4.9169	0.2856	4.1673	1552	49	1590	39	1619	60	104	137.43	102.57
Hiltaba Suite	mineralization-absent	2053554	2053554 M 84			2	0.0959	3.5457	3.7144	7.3052	0.2809	6.3870	1546	67	1574	58	1596	90	103	111.21	123.78
Hiltaba Suite	mineralization-absent	2053554	2053554 M 238			1	0.0959	3.7975	3.7237	7.1355	0.2817	6.0410	1546	71	1576	57	1600	86	104	93.75	99.44
Hiltaba Suite	mineralization-absent	2053554	2053554 M 124			2	0.0954	2.0716	3.7252	4.6698	0.2833	4.1851	1535	39	1577	37	1608	60	105	149.64	108.63
Hiltaba Suite	mineralization-absent	2053554	2053554 M 123			2	0.0953	3.3711	3.8109	5.9213	0.2901	4.8681	1533	63	1595	48	1642	71	107	132.93	103.13
Hiltaba Suite	mineralization-absent	2053554	2053554 M 127			2	0.0948	1.9384	3.8365	5.3943	0.2934	5.0340	1525	37	1600	43	1658	74	109	139.68	110.99
Hiltaba Suite	mineralization-absent	2053554	2053554 M 119			2	0.0940	2.4716	3.6351	6.2467	0.2803	5.7369	1509	47	1557	50	1593	81	106	149.20	144.86
Hiltaba Suite	mineralization-absent	2053555	2053555 L 250			1	0.0979	1.5854	3.9025	3.7120	0.2890	3.3564	1585	30	1614	30	1637	49	103	322.05	203.12
Hiltaba Suite	mineralization-absent	2053555	2053555 L 262			1	0.0988	1.7433	3.7257	4.7112	0.2735	4.3767	1602	33	1577	38	1558	61	97	48.38	744.09
Hiltaba Suite	mineralization-absent	2053555	2053555 L 264			1	0.0968	2.2376	3.7178	4.2611	0.2785	3.6263	1564	42	1575	34	1584	51	101	248.22	299.73
Hiltaba Suite	mineralization-absent	2053555	2053555 L 268			1	0.0986	1.9189	3.7472	3.6640	0.2757	3.1213	1598	36	1582	29	1569	43	98	437.72	463.28
Hiltaba Suite	mineralization-absent	2053555	2053555 M 270			1	0.0984	2.0373	3.7560	4.5599	0.2768	4.0795	1594	38	1583	37	1575	57	99	386.45	375.59
Hiltaba Suite	mineralization-absent	2053555	2053555 M 277			1	0.0993	2.0000	3.6993	3.9968	0.2703	3.4604	1610	37	1571	32	1542	47	96	258.10	322.16
Hiltaba Suite	mineralization-absent	2053555	2053555 M 278			1	0.0992	2.3825	3.7659	5.1148	0.2753	4.5260	1609	44	1586	41	1568	63	97	200.76	268.11
Hiltaba Suite	mineralization-absent	2053555	2053555 M 280			1	0.0994	3.0148	3.7905	4.8728	0.2765	3.8282	1613	56	1591	39	1574	53	98	187.47	332.21
Hiltaba Suite	mineralization-absent	2053555	2053555 M 283			1	0.1012	3.0988	3.8744	6.1382	0.2778	5.2985	1645	57	1608	50	1580	74	96	230.88	335.19
Hiltaba Suite	mineralization-absent	2053555	2053555 L 258			1	0.0989	3.1036	3.7051	6.5583	0.2717	5.7774	1603	58	1572	52	1550	80	97	507.92	532.33
Hiltaba Suite	mineralization-absent	2115491	2115491 M 312			4	0.1041	1.5495	4.1353	4.2276	0.2880	3.9334	1699	29	1661	35	1632	57	96	106.94	158.71
Hiltaba Suite	mineralization-absent	2115491	2115491 M 289			4	0.1016	1.6572	3.9427	4.0896	0.2814	3.7388	1654	31	1623	33	1599	53	97	79.96	131.85
Hiltaba Suite	mineralization-absent	2115491	2115491 L 282			5	0.1005	2.3286	3.8194	4.9090	0.2755	4.3216	1634	43	1597	40	1569	60	96	71.83	117.17
Hiltaba Suite	mineralization-absent	2115491	2115491 M 311			4	0.1000	1.6285	3.9710	4.0832	0.2879	3.7444	1625	30	1628	33	1631	54	100	85.26	127.32
Hiltaba Suite	mineralization-absent	2115491	2115491 M 290			4	0.0998	2.3693	4.0816	5.3040	0.2968	4.7454	1619	44	1651	43	1675	70	103	59.02	100.32

Appendix Table A6 LA-ICP MS U-Pb data for GRV and Hiltaba Suite zircon analyzed at Boise state University

Unit	Group	Sample	Spot Number	Disc.	Other	Experiment Number	Radiogenic Ratios						Age (Ma)								
							$^{207}Pb/^{206}Pb$	2σ	$^{207}Pb/^{235}U$	2σ	$^{206}Pb/^{238}U$	2σ	$^{207}Pb/^{206}Pb$	2σ	$^{207}Pb/^{235}Pb$	2σ	$^{206}Pb/^{238}U$	2σ	% Conc	Th ppm	U ppm
Hiltaba Suite	mineralization-absent	2115491	2115491 M 298			4	0.0996	1.9341	3.8921	4.6294	0.2835	4.2060	1616	36	1612	37	1609	60	100	69.07	110.63
Hiltaba Suite	mineralization-absent	2115491	2115491 L 283			5	0.0994	1.3493	3.7341	3.7280	0.2725	3.4752	1613	25	1579	30	1553	48	96	71.41	115.15
Hiltaba Suite	mineralization-absent	2115491	2115491 L 285			5	0.0994	1.8765	3.8448	4.8186	0.2806	4.4382	1612	35	1602	39	1594	63	99	73.14	137.86
Hiltaba Suite	mineralization-absent	2115491	2115491 M 297			4	0.0991	1.7120	3.9578	4.0888	0.2895	3.7131	1608	32	1626	33	1639	54	102	91.90	134.42
Hiltaba Suite	mineralization-absent	2115491	2115491 M 294			4	0.0988	2.0612	3.8992	4.0679	0.2862	3.5071	1602	38	1614	33	1622	50	101	73.27	109.48
Hiltaba Suite	mineralization-absent	2115491	2115491 M 307			4	0.0987	1.7275	3.9407	4.0476	0.2895	3.6604	1600	32	1622	33	1639	53	102	80.53	123.22
Hiltaba Suite	mineralization-absent	2115491	2115491 M 301			4	0.0987	1.7559	3.8921	4.2684	0.2859	3.8905	1600	33	1612	34	1621	56	101	87.45	133.82
Hiltaba Suite	mineralization-absent	2115491	2115491 L 286			5	0.0986	1.7742	3.8122	4.5231	0.2805	4.1606	1597	33	1595	36	1594	59	100	57.12	110.92
Hiltaba Suite	mineralization-absent	2115491	2115491 M 304			4	0.0985	1.5105	3.7569	3.8526	0.2765	3.5442	1597	28	1584	31	1574	49	99	55.24	193.67
Hiltaba Suite	mineralization-absent	2115491	2115491 M 300			4	0.0984	1.2092	3.7924	3.4438	0.2795	3.2246	1594	23	1591	28	1589	45	100	136.31	193.48
Hiltaba Suite	mineralization-absent	2115491	2115491 M 299			4	0.0984	2.2367	3.7555	5.1554	0.2768	4.6449	1594	42	1583	41	1575	65	99	79.28	115.17
Hiltaba Suite	mineralization-absent	2115491	2115491 M 314			4	0.0983	1.5169	3.9578	4.2040	0.2919	3.9208	1593	28	1626	34	1651	57	104	86.49	142.40
Hiltaba Suite	mineralization-absent	2115491	2115491 M 310			4	0.0982	1.3694	3.8401	3.8676	0.2835	3.6170	1591	26	1601	31	1609	52	101	91.79	136.36
Hiltaba Suite	mineralization-absent	2115491	2115491 L 280			5	0.0979	2.5019	3.6291	4.3622	0.2688	3.5734	1585	47	1556	35	1535	49	97	81.79	132.48
Hiltaba Suite	mineralization-absent	2115491	2115491 M 305			4	0.0979	2.6292	3.8885	5.3192	0.2882	4.6240	1584	49	1611	43	1632	67	103	72.30	109.07
Hiltaba Suite	mineralization-absent	2115491	2115491 M 293			4	0.0979	2.3879	3.8777	3.7102	0.2874	2.8397	1584	45	1609	30	1628	41	103	47.82	114.88
Hiltaba Suite	mineralization-absent	2115491	2115491 M 302			4	0.0978	2.0799	3.8249	3.8847	0.2837	3.2809	1582	39	1598	31	1610	47	102	47.05	76.37
Hiltaba Suite	mineralization-absent	2115491	2115491 M 308			4	0.0977	2.0174	4.0480	3.5220	0.3004	2.8869	1581	38	1644	29	1693	43	107	57.05	100.36
Hiltaba Suite	mineralization-absent	2115491	2115491 L 281			5	0.0977	1.8668	3.7460	4.2293	0.2781	3.7951	1580	35	1581	34	1582	53	100	91.02	114.80
Hiltaba Suite	mineralization-absent	2115491	2115491 M 288			4	0.0975	2.1894	3.7782	4.8041	0.2809	4.2762	1578	41	1588	39	1596	60	101	96.91	132.27
Hiltaba Suite	mineralization-absent	2115491	2115491 M 291			4	0.0975	1.9860	3.8699	4.3662	0.2878	3.8884	1578	37	1607	35	1630	56	103	62.72	105.87
Hiltaba Suite	mineralization-absent	2115491	2115491 M 306			4	0.0974	2.2939	3.9674	4.2970	0.2955	3.6334	1574	43	1628	35	1669	53	106	66.58	102.68
Hiltaba Suite	mineralization-absent	2115491	2115491 M 303			4	0.0973	1.2411	3.7444	3.6633	0.2790	3.4466	1574	23	1581	29	1586	48	101	137.95	199.20
Hiltaba Suite	mineralization-absent	2115491	2115491 M 292			4	0.0972	2.0053	3.9822	4.1204	0.2972	3.5995	1571	38	1631	33	1677	53	107	68.05	109.67
Hiltaba Suite	mineralization-absent	2115491	2115491 M 309			4	0.0969	2.0614	3.8225	3.7403	0.2861	3.1209	1565	39	1597	30	1622	45	104	99.10	157.79
Hiltaba Suite	mineralization-absent	2115491	2115491 M 296			4	0.0968	2.0789	3.8867	6.8122	0.2913	6.4872	1563	39	1611	55	1648	94	105	56.22	94.03
Hiltaba Suite	mineralization-absent	2115491	2115491 M 295			4	0.0963	1.4433	3.7320	4.1666	0.2811	3.9086	1553	27	1578	33	1597	55	103	112.17	160.70
LGRV	mineralization-related	2131365	2131365 L 143			4	0.0976	1.6549	3.9217	4.6669	0.2915	4.3637	1578	31	1618	38	1649	63	104	159.90	165.42
LGRV	mineralization-related	2131365	2131365 M 149			4	0.0984	1.7273	3.9424	4.5590	0.2904	4.2190	1595	32	1622	37	1644	61	103	151.43	144.75
LGRV	mineralization-related	2131365	2131365 L 128			4	0.0975	1.5731	3.9018	3.5706	0.2903	3.2053	1576	29	1614	29	1643	46	104	135.65	137.80
LGRV	mineralization-related	2131365	2131365 M 151			4	0.0981	1.7207	3.9124	3.2748	0.2893	2.7863	1588	32	1616	26	1638	40	103	196.39	185.35
LGRV	mineralization-related	2131365	2131365 M 164			4	0.0977	1.4341	3.8915	3.1675	0.2889	2.8243	1580	27	1612	26	1636	41	104	136.60	133.31
LGRV	mineralization-related	2131365	2131365 M 158			4	0.0979	1.7385	3.8979	4.0234	0.2887	3.6284	1585	33	1613	33	1635	52	103	145.92	152.65
LGRV	mineralization-related	2131365	2131365 M 150			4	0.0975	1.6357	3.8666	3.3519	0.2877	2.9257	1576	31	1607	27	1630	42	103	150.00	155.59
LGRV	mineralization-related	2131365	2131365 L 144			4	0.0978	1.7049	3.8703	3.6848	0.2869	3.2667	1583	32	1608	30	1626	47	103	99.32	108.24

Appendix Table A6 LA-ICP MS U-Pb data for GRV and Hiltaba Suite zircon analyzed at Boise state University

Unit	Group	Sample	Spot Number	Disc.	Other	Experiment Number	Radiogenic Ratios							Age (Ma)								
							$^{207}Pb/^{206}Pb$	2σ	$^{207}Pb/^{235}U$	2σ	$^{206}Pb/^{238}U$	2σ	$^{207}Pb/^{206}Pb$	2σ	$^{207}Pb/^{235}Pb$	2σ	$^{206}Pb/^{238}U$	2σ	% Conc	Th ppm	U ppm
LGRV	mineralization-related	2131365	2131365 M 147			4	0.0990	1.1476	3.8968	4.2149	0.2856	4.0557	1605	21	1613	34	1619	58	101	150.33	159.22
LGRV	mineralization-related	2131365	2131365 M 154			4	0.0993	1.9354	3.8994	3.8367	0.2849	3.3128	1610	36	1614	31	1616	47	100	139.24	128.23
LGRV	mineralization-related	2131365	2131365 M 145			4	0.0967	1.2295	3.7976	4.0335	0.2848	3.8416	1561	23	1592	32	1616	55	103	256.95	202.64
LGRV	mineralization-related	2131365	2131365 M 152			4	0.0972	1.6360	3.8127	3.8699	0.2844	3.5071	1572	31	1595	31	1614	50	103	124.58	125.97
LGRV	mineralization-related	2131365	2131365 L 126			4	0.0974	1.4578	3.7987	4.0033	0.2828	3.7285	1575	27	1592	32	1605	53	102	166.45	165.76
LGRV	mineralization-related	2131365	2131365 L 134			4	0.0986	1.9027	3.8405	4.7755	0.2826	4.3801	1597	36	1601	38	1604	62	100	202.76	164.24
LGRV	mineralization-related	2131365	2131365 M 155			4	0.1013	1.3298	3.9398	4.3679	0.2820	4.1605	1648	25	1622	35	1602	59	97	300.65	260.45
LGRV	mineralization-related	2131365	2131365 L 132			4	0.0986	1.5398	3.8311	3.8560	0.2819	3.5352	1597	29	1599	31	1601	50	100	293.75	262.71
LGRV	mineralization-related	2131365	2131365 L 133			4	0.0987	1.2915	3.8333	3.9396	0.2817	3.7219	1599	24	1600	32	1600	53	100	339.42	237.90
LGRV	mineralization-related	2131365	2131365 L 137			4	0.0998	1.9794	3.8759	4.2563	0.2816	3.7680	1621	37	1609	34	1599	53	99	327.35	277.08
LGRV	mineralization-related	2131365	2131365 L 138			4	0.1009	1.6740	3.9044	4.7465	0.2805	4.4415	1641	31	1615	38	1594	63	97	213.54	240.02
LGRV	mineralization-related	2131365	2131365 L 136			4	0.0987	1.2295	3.8066	3.8648	0.2797	3.6640	1600	23	1594	31	1590	52	99	313.78	255.73
LGRV	mineralization-related	2131365	2131365 L 127			4	0.0993	1.3274	3.8221	3.6698	0.2791	3.4213	1611	25	1597	30	1587	48	98	227.51	196.46
LGRV	mineralization-related	2131365	2131365 L 139			4	0.0981	1.2039	3.7639	4.3506	0.2783	4.1807	1588	23	1585	35	1583	59	100	335.52	291.69
LGRV	mineralization-related	2131365	2131365 M 162			4	0.0984	1.4292	3.7742	3.0596	0.2781	2.7052	1595	27	1587	25	1582	38	99	317.73	236.49
LGRV	mineralization-related	2131365	2131365 L 141			4	0.1009	1.3254	3.8608	4.5562	0.2776	4.3591	1640	25	1606	37	1579	61	96	156.84	173.33
LGRV	mineralization-related	2131365	2131365 L 130			4	0.0984	1.0058	3.7644	2.9032	0.2776	2.7234	1593	19	1585	23	1579	38	99	433.64	282.65
LGRV	mineralization-related	2131365	2131365 M 146			4	0.0967	1.5163	3.6936	5.0557	0.2771	4.8230	1561	28	1570	40	1576	67	101	131.26	142.25
LGRV	mineralization-related	2131365	2131365 L 142			4	0.0987	1.6738	3.7575	4.1946	0.2761	3.8461	1600	31	1584	34	1571	54	98	144.36	168.06
LGRV	mineralization-related	2131365	2131365 L 125			4	0.0974	1.5747	3.7001	3.7368	0.2756	3.3888	1574	29	1571	30	1569	47	100	208.14	189.41
LGRV	mineralization-related	2131365	2131365 M 159			4	0.0990	1.4962	3.7553	5.1771	0.2752	4.9561	1605	28	1583	42	1567	69	98	200.59	185.70
LGRV	mineralization-related	2131365	2131365 M 157			4	0.0968	1.6978	3.6712	3.7322	0.2751	3.3236	1563	32	1565	30	1567	46	100	152.78	148.37
LGRV	mineralization-related	2131365	2131365 L 140			4	0.0990	1.4922	3.7247	4.9579	0.2729	4.7280	1605	28	1577	40	1555	65	97	206.41	218.94
LGRV	mineralization-related	2131365	2131365 M 161			4	0.0984	1.1955	3.6998	3.3855	0.2728	3.1674	1593	22	1571	27	1555	44	98	368.14	268.58
LGRV	mineralization-related	2131365	2131365 L 131			4	0.0987	2.0409	3.6984	3.3272	0.2719	2.6277	1599	38	1571	27	1550	36	97	159.05	148.14
LGRV	mineralization-related	2131365	2131365 L 135			4	0.0986	1.6530	3.6534	3.4272	0.2686	3.0022	1599	31	1561	27	1534	41	96	141.83	151.48
LGRV	mineralization-related	2131365	2131365 L 129			4	0.0979	1.2655	3.6147	4.4828	0.2677	4.3005	1585	24	1553	36	1529	59	96	386.58	312.81
LGRV	mineralization-related	2131359	2131359 L 99			3	0.0964	2.2450	3.8532	4.3406	0.2899	3.7149	1556	42	1604	35	1641	54	105	70.38	101.62
LGRV	mineralization-related	2131359	2131359 M 116			4	0.0993	2.4377	3.9505	5.0084	0.2884	4.3751	1612	45	1624	41	1634	63	101	121.63	126.36
LGRV	mineralization-related	2131359	2131359 L 107			3	0.0991	1.9762	3.9262	3.5016	0.2872	2.8906	1608	37	1619	28	1628	42	101	139.39	140.75
LGRV	mineralization-related	2131359	2131359 L 105			3	0.0985	1.0318	3.8864	3.5590	0.2860	3.4061	1597	19	1611	29	1622	49	102	123.09	154.92
LGRV	mineralization-related	2131359	2131359 M 119			4	0.0998	1.7704	3.9224	4.4818	0.2852	4.1173	1620	33	1618	36	1617	59	100	137.94	169.60
LGRV	mineralization-related	2131359	2131359 L 102			3	0.0981	1.6657	3.8466	4.9521	0.2843	4.6635	1589	31	1603	40	1613	67	102	118.36	158.02
LGRV	mineralization-related	2131359	2131359 L 109			3	0.0967	1.8106	3.7740	3.0447	0.2830	2.4478	1562	34	1587	24	1607	35	103	141.59	225.28
LGRV	mineralization-related	2131359	2131359 M 123			4	0.0994	1.7592	3.8619	3.8979	0.2817	3.4783	1613	33	1606	31	1600	49	99	161.11	191.52

Appendix Table A6 LA-ICP MS U-Pb data for GRV and Hiltaba Suite zircon analyzed at Boise state University

Unit	Group	Sample	Spot Number	Disc.	Other	Experiment Number	Radiogenic Ratios							Age (Ma)								
							$^{207}Pb/^{206}Pb$	2σ	$^{207}Pb/^{235}U$	2σ	$^{206}Pb/^{238}U$	2σ	$^{207}Pb/^{206}Pb$	2σ	$^{207}Pb/^{235}Pb$	2σ	$^{206}Pb/^{238}U$	2σ	% Conc	Th ppm	U ppm
LGRV	mineralization-related	2131359	2131359 M 113			4	0.0997	1.8310	3.8737	3.3884	0.2817	2.8511	1619	34	1608	27	1600	40	99	131.01	149.28
LGRV	mineralization-related	2131359	2131359 L 91			3	0.0956	2.0054	3.6748	3.5676	0.2788	2.9507	1540	38	1566	28	1585	41	103	96.96	93.45
LGRV	mineralization-related	2131359	2131359 L 95			3	0.0992	2.2669	3.8052	3.7515	0.2783	2.9891	1609	42	1594	30	1583	42	98	155.90	191.92
LGRV	mineralization-related	2131359	2131359 M 117			4	0.0976	1.6968	3.7454	3.9712	0.2782	3.5905	1579	32	1581	32	1582	50	100	112.14	143.34
LGRV	mineralization-related	2131359	2131359 L 103			3	0.0970	1.5271	3.7158	3.5465	0.2779	3.2009	1567	29	1575	28	1581	45	101	194.56	204.39
LGRV	mineralization-related	2131359	2131359 M 122			4	0.0990	1.5274	3.7923	4.2125	0.2777	3.9258	1606	28	1591	34	1580	55	98	219.31	183.42
LGRV	mineralization-related	2131359	2131359 L 93			3	0.0991	2.0575	3.7892	4.2093	0.2774	3.6722	1607	38	1590	34	1578	51	98	113.15	144.83
LGRV	mineralization-related	2131359	2131359 L 96			3	0.0986	1.0690	3.7561	3.3987	0.2762	3.2262	1598	20	1583	27	1572	45	98	205.35	305.05
LGRV	mineralization-related	2131359	2131359 M 112			4	0.0997	0.8770	3.7918	3.4133	0.2758	3.2987	1619	16	1591	27	1570	46	97	269.35	430.90
LGRV	mineralization-related	2131359	2131359 L 98			3	0.0995	2.1064	3.7770	4.1403	0.2752	3.5644	1615	39	1588	33	1567	50	97	108.74	133.19
LGRV	mineralization-related	2131359	2131359 L 110			3	0.0982	1.5071	3.7103	3.2672	0.2742	2.8988	1589	28	1574	26	1562	40	98	116.25	171.44
LGRV	mineralization-related	2131359	2131359 L 94			3	0.0972	1.7211	3.6710	3.0599	0.2739	2.5300	1571	32	1565	24	1561	35	99	164.24	227.10
LGRV	mineralization-absent	2116683	2116683 M 80			3	0.0999	2.6557	3.8754	5.5352	0.2814	4.8564	1622	49	1609	45	1598	69	99	130.60	137.64
LGRV	mineralization-absent	2116683	2116683 L 56			3	0.0999	1.9542	3.8600	3.7727	0.2803	3.2271	1622	36	1605	30	1593	46	98	201.71	154.81
LGRV	mineralization-absent	2116683	2116683 L 49			3	0.0997	1.5825	3.8668	3.9429	0.2813	3.6114	1619	29	1607	32	1598	51	99	191.51	168.62
LGRV	mineralization-absent	2116683	2116683 L 53			3	0.0996	1.8173	3.9039	4.2499	0.2841	3.8417	1618	34	1614	34	1612	55	100	189.21	134.55
LGRV	mineralization-absent	2116683	2116683 L 68			3	0.0996	1.8258	3.8411	4.2491	0.2797	3.8368	1617	34	1601	34	1590	54	98	155.82	129.32
LGRV	mineralization-absent	2116683	2116683 M 85			3	0.0995	2.1634	3.8054	4.3111	0.2773	3.7290	1616	40	1594	35	1578	52	98	115.16	133.65
LGRV	mineralization-absent	2116683	2116683 L 63			3	0.0995	1.4837	3.8056	3.5007	0.2774	3.1707	1615	28	1594	28	1578	44	98	106.87	120.67
LGRV	mineralization-absent	2116683	2116683 M 77			3	0.0989	1.7505	3.7954	3.3760	0.2782	2.8867	1604	33	1592	27	1582	41	99	173.12	150.67
LGRV	mineralization-absent	2116683	2116683 L 64			3	0.0988	3.0332	3.8526	5.0356	0.2828	4.0196	1602	57	1604	41	1605	57	100	61.94	63.77
LGRV	mineralization-absent	2116683	2116683 L 55			3	0.0987	1.6643	3.8756	3.9472	0.2847	3.5791	1600	31	1609	32	1615	51	101	150.16	113.08
LGRV	mineralization-absent	2116683	2116683 L 57			3	0.0986	1.9461	3.7119	4.1743	0.2730	3.6929	1598	36	1574	33	1556	51	97	143.24	139.68
LGRV	mineralization-absent	2116683	2116683 M 86			3	0.0984	1.7867	3.7508	4.0621	0.2766	3.6481	1593	33	1582	33	1574	51	99	118.43	137.32
LGRV	mineralization-absent	2116683	2116683 L 60			3	0.0983	1.3391	3.8154	3.8333	0.2815	3.5918	1592	25	1596	31	1599	51	100	197.31	160.70
LGRV	mineralization-absent	2116683	2116683 M 81			3	0.0982	1.9326	3.8188	3.6565	0.2821	3.1040	1590	36	1597	29	1602	44	101	88.94	102.43
LGRV	mineralization-absent	2116683	2116683 L 50			3	0.0981	1.5913	3.8592	4.4181	0.2854	4.1216	1588	30	1605	36	1618	59	102	169.97	161.09
LGRV	mineralization-absent	2116683	2116683 L 52			3	0.0979	1.9669	3.8545	4.3369	0.2855	3.8653	1585	37	1604	35	1619	55	102	148.62	126.45
LGRV	mineralization-absent	2116683	2116683 M 79			3	0.0979	1.7802	3.7776	3.8755	0.2799	3.4424	1584	33	1588	31	1591	49	100	173.58	172.71
LGRV	mineralization-absent	2116683	2116683 M 73			3	0.0978	1.9735	3.7657	4.7039	0.2792	4.2699	1583	37	1585	38	1588	60	100	166.25	185.49
LGRV	mineralization-absent	2116683	2116683 M 69			3	0.0977	2.1110	3.7652	5.0537	0.2796	4.5918	1580	39	1585	41	1590	65	101	99.37	129.83
LGRV	mineralization-absent	2116683	2116683 L 51			3	0.0975	1.5303	3.8167	3.7096	0.2838	3.3793	1577	29	1596	30	1611	48	102	144.96	126.30
LGRV	mineralization-absent	2116683	2116683 M 70			3	0.0974	1.4710	3.7815	4.2004	0.2817	3.9344	1574	28	1589	34	1600	56	102	115.80	143.06
LGRV	mineralization-absent	2116683	2116683 L 59			3	0.0973	1.9788	3.8048	4.4580	0.2836	3.9948	1573	37	1594	36	1609	57	102	115.35	143.16
LGRV	mineralization-absent	2116683	2116683 L 54			3	0.0971	2.1540	3.8231	4.3650	0.2856	3.7966	1569	40	1598	35	1619	54	103	245.11	161.25

Appendix Table A6 LA-ICP MS U-Pb data for GRV and Hiltaba Suite zircon analyzed at Boise state University

Unit	Group	Sample	Spot Number	Disc.	Other	Experiment Number	Radiogenic Ratios							Age (Ma)								
							$^{207}Pb/^{206}Pb$	2σ	$^{207}Pb/^{235}U$	2σ	$^{206}Pb/^{238}U$	2σ	$^{207}Pb/^{206}Pb$	2σ	$^{207}Pb/^{235}Pb$	2σ	$^{206}Pb/^{238}U$	2σ	% Conc	Th ppm	U ppm
LGRV	mineralization-absent	2116683	2116683 L 58			3	0.0971	1.9987	3.7734	4.1956	0.2819	3.6889	1569	37	1587	34	1601	52	102	157.42	152.23
LGRV	mineralization-absent	2116683	2116683 L 66			3	0.0969	2.3940	3.8232	4.7621	0.2863	4.1166	1565	45	1598	38	1623	59	104	127.98	112.37
LGRV	mineralization-absent	2116683	2116683 M 76			3	0.0964	2.1320	3.7509	4.1039	0.2823	3.5066	1555	40	1582	33	1603	50	103	82.83	101.13
LGRV	mineralization-absent	2116683	2116683 M 84			3	0.0963	1.5174	3.6984	3.6031	0.2787	3.2680	1553	28	1571	29	1585	46	102	129.26	149.97
LGRV	mineralization-absent	2116683	2116683 M 78			3	0.0962	2.4586	3.8047	4.4762	0.2867	3.7406	1552	46	1594	36	1625	54	105	55.80	77.30
LGRV	mineralization-absent	2116683	2116683 L 67			3	0.0961	2.0116	3.7448	4.3750	0.2827	3.8851	1549	38	1581	35	1605	55	104	156.15	136.25
LGRV	mineralization-absent	2018616	2018616 100			1	0.0995	2.0880	3.9197	3.8725	0.2858	3.2614	1614	39	1618	31	1620	47	100	124.16	141.07
LGRV	mineralization-absent	2018616	2018616 101			1	0.0994	2.1857	4.0305	5.3223	0.2942	4.8528	1612	41	1640	43	1662	71	103	103.95	136.41
LGRV	mineralization-absent	2018616	2018616 102			1	0.0972	5.1252	3.8798	8.7124	0.2895	7.0454	1571	96	1609	70	1639	102	104	85.24	119.41
LGRV	mineralization-absent	2018616	2018616 103			1	0.0985	2.0011	3.6691	3.8908	0.2702	3.3367	1596	37	1565	31	1542	46	97	99.42	156.52
LGRV	mineralization-absent	2018616	2018616 104			1	0.0997	3.1059	3.8873	5.8262	0.2828	4.9294	1618	58	1611	47	1606	70	99	81.54	82.25
LGRV	mineralization-absent	2018616	2018616 105			1	0.0998	2.4739	3.8909	3.8390	0.2829	2.9357	1620	46	1612	31	1606	42	99	76.23	79.42
LGRV	mineralization-absent	2018616	2018616 106			1	0.0973	2.6599	3.8172	4.2283	0.2845	3.2868	1573	50	1596	34	1614	47	103	93.03	108.52
LGRV	mineralization-absent	2018616	2018616 107			1	0.0970	3.0022	3.7933	5.0493	0.2838	4.0598	1566	56	1591	41	1610	58	103	75.05	93.75
LGRV	mineralization-absent	2018616	2018616 109			1	0.1023	2.5174	3.9543	4.7777	0.2803	4.0607	1666	47	1625	39	1593	57	96	149.81	174.08
LGRV	mineralization-absent	2018616	2018616 110			1	0.1009	1.8098	3.9978	4.1404	0.2873	3.7239	1641	34	1634	34	1628	54	99	118.46	151.98
LGRV	mineralization-absent	2018616	2018616 80			1	0.0977	2.7680	3.6669	5.0193	0.2723	4.1870	1580	52	1564	40	1552	58	98	109.30	127.71
LGRV	mineralization-absent	2018616	2018616 82			1	0.0991	2.5410	3.8848	5.1374	0.2842	4.4650	1608	47	1611	41	1612	64	100	130.39	158.74
LGRV	mineralization-absent	2018616	2018616 83			1	0.1004	1.9638	3.9370	4.1230	0.2844	3.6253	1632	36	1621	33	1613	52	99	140.83	169.34
LGRV	mineralization-absent	2018616	2018616 84			1	0.0999	1.8835	3.8449	4.0577	0.2790	3.5941	1623	35	1602	33	1586	51	98	103.60	127.61
LGRV	mineralization-absent	2018616	2018616 85			1	0.1003	2.4886	3.9102	4.3241	0.2826	3.5361	1630	46	1616	35	1605	50	98	135.96	119.54
LGRV	mineralization-absent	2018616	2018616 89			1	0.0982	2.4907	3.9097	4.4372	0.2887	3.6722	1590	47	1616	36	1635	53	103	141.47	177.10
LGRV	mineralization-absent	2018616	2018616 90			1	0.0989	2.8299	3.8434	4.4751	0.2820	3.4667	1603	53	1602	36	1601	49	100	91.53	108.67
LGRV	mineralization-absent	2018616	2018616 91			1	0.1003	2.0405	3.9325	3.5644	0.2842	2.9226	1630	38	1620	29	1613	42	99	129.88	144.70
LGRV	mineralization-absent	2018616	2018616 92			1	0.0977	2.2988	3.8814	4.0194	0.2882	3.2971	1580	43	1610	32	1633	48	103	128.89	162.18
LGRV	mineralization-absent	2018616	2018616 93			1	0.0996	3.6221	3.8714	5.6746	0.2820	4.3683	1616	67	1608	46	1601	62	99	104.69	122.88
LGRV	mineralization-absent	2018616	2018616 94			1	0.0993	2.0966	3.7710	4.4851	0.2756	3.9649	1610	39	1587	36	1569	55	97	138.90	153.14
LGRV	mineralization-absent	2018616	2018616 95			1	0.0987	2.2681	3.7698	4.3644	0.2771	3.7288	1599	42	1586	35	1577	52	99	171.53	211.45
LGRV	mineralization-absent	2018616	2018616 97			1	0.1008	2.7077	3.8774	5.6306	0.2789	4.9368	1640	50	1609	45	1586	69	97	158.26	160.36
LGRV	mineralization-absent	2018616	2018616 98			1	0.0987	2.0853	3.6579	3.5189	0.2687	2.8344	1600	39	1562	28	1534	39	96	126.70	153.63
LGRV	mineralization-absent	2016125	2016125 L 53			1	0.0999	1.9788	3.7557	5.2792	0.2726	4.8943	1623	37	1583	42	1554	68	96	70.15	120.78
LGRV	mineralization-absent	2016125	2016125 L 54			1	0.1012	3.1855	3.8952	6.4470	0.2791	5.6050	1647	59	1613	52	1587	79	96	28.20	48.77
LGRV	mineralization-absent	2016125	2016125 L 56			1	0.0962	1.6497	3.7378	4.3941	0.2818	4.0726	1551	31	1580	35	1601	58	103	84.36	176.58
LGRV	mineralization-absent	2016125	2016125 L 57			1	0.0987	2.2548	3.7832	4.6008	0.2780	4.0104	1600	42	1589	37	1581	56	99	100.81	188.51
LGRV	mineralization-absent	2016125	2016125 L 58			1	0.0986	1.6083	3.7878	4.3069	0.2787	3.9953	1597	30	1590	35	1585	56	99	86.82	179.33

Appendix Table A6 LA-ICP MS U-Pb data for GRV and Hiltaba Suite zircon analyzed at Boise state University

Unit	Group	Sample	Spot Number	Disc.	Other	Experiment Number	Radiogenic Ratios						Age (Ma)								
							$^{207}Pb/^{206}Pb$	2σ	$^{207}Pb/^{235}U$	2σ	$^{206}Pb/^{238}U$	2σ	$^{207}Pb/^{206}Pb$	2σ	$^{207}Pb/^{235}Pb$	2σ	$^{206}Pb/^{238}U$	2σ	% Conc	Th ppm	U ppm
LGRV	mineralization-absent	2016125	2016125 L 59			1	0.0964	2.2756	3.7239	4.2986	0.2801	3.6468	1556	43	1577	34	1592	51	102	70.47	150.43
LGRV	mineralization-absent	2016125	2016125 L 61			1	0.0986	3.0836	3.7713	6.1222	0.2775	5.2890	1597	58	1587	49	1579	74	99	142.58	65.52
LGRV	mineralization-absent	2016125	2016125 M 62			1	0.0985	2.2830	3.8731	5.3477	0.2851	4.8359	1596	43	1608	43	1617	69	101	78.24	146.04
LGRV	mineralization-absent	2016125	2016125 M 64			1	0.0997	2.2455	3.7887	5.1776	0.2755	4.6654	1619	42	1590	42	1569	65	97	109.12	199.87
LGRV	mineralization-absent	2016125	2016125 M 65			1	0.0972	3.0933	3.7145	5.7983	0.2771	4.9042	1572	58	1574	46	1577	69	100	111.80	201.12
LGRV	mineralization-absent	2016125	2016125 M 66			1	0.0989	1.6203	3.8793	4.3965	0.2845	4.0871	1604	30	1609	35	1614	58	101	85.77	161.12
LGRV	mineralization-absent	2016125	2016125 M 70			1	0.0998	3.3046	3.8033	5.5627	0.2764	4.4748	1620	61	1593	45	1573	62	97	106.91	199.24
LGRV	mineralization-absent	2016125	2016125 M 71			1	0.0993	2.7117	3.9674	5.6960	0.2897	5.0090	1612	51	1628	46	1640	73	102	109.76	198.80
LGRV	mineralization-absent	2016125	2016125 M 73			1	0.0986	4.0762	3.8686	8.2582	0.2846	7.1821	1597	76	1607	67	1615	103	101	67.02	116.36
LGRV	mineralization-absent	2016125	2016125 M 74			1	0.0977	3.1821	3.8351	5.4577	0.2846	4.4340	1581	60	1600	44	1614	63	102	106.69	190.04
LGRV	mineralization-absent	2016125	2016125 M 76			1	0.0977	3.4969	3.8808	6.8692	0.2882	5.9125	1580	65	1610	55	1632	85	103	117.69	197.75
LGRV	mineralization-absent	2721839	2721839 M 110			7	0.1008	3.0158	3.9274	4.1822	0.2825	2.8975	1639	56	1619	34	1604	41	98	54.48	35.51
LGRV	mineralization-absent	2721839	2721839 M 115			7	0.1007	1.2383	3.9003	2.6209	0.2810	2.3100	1637	23	1614	21	1596	33	98	51.67	39.83
LGRV	mineralization-absent	2721839	2721839 M 117			7	0.1006	1.7536	3.8239	3.0611	0.2757	2.5090	1635	33	1598	25	1570	35	96	88.42	65.12
LGRV	mineralization-absent	2721839	2721839 S 133			7	0.1003	2.3336	3.8677	3.0571	0.2798	1.9749	1629	43	1607	25	1590	28	98	134.02	53.64
LGRV	mineralization-absent	2721839	2721839 M 114			7	0.1000	1.7420	3.8981	3.1923	0.2826	2.6751	1625	32	1613	26	1605	38	99	72.41	52.08
LGRV	mineralization-absent	2721839	2721839 M 109			7	0.0999	1.7768	3.8670	2.5037	0.2808	1.7640	1622	33	1607	20	1596	25	98	87.78	62.00
LGRV	mineralization-absent	2721839	2721839 M 119			7	0.0998	2.6831	3.9088	3.2186	0.2841	1.7777	1620	50	1615	26	1612	25	100	59.62	48.02
LGRV	mineralization-absent	2721839	2721839 M 121			7	0.0995	1.8381	3.8070	2.8640	0.2774	2.1963	1615	34	1594	23	1578	31	98	96.42	74.89
LGRV	mineralization-absent	2721839	2721839 M 125			7	0.0990	2.7951	3.8758	3.7737	0.2838	2.5355	1606	52	1609	30	1611	36	100	78.74	39.38
LGRV	mineralization-absent	2721839	2721839 M 111			7	0.0990	2.3306	3.8068	3.3625	0.2788	2.4238	1606	43	1594	27	1585	34	99	65.37	56.24
LGRV	mineralization-absent	2721839	2721839 S 137			7	0.0990	1.8022	3.7290	2.4273	0.2732	1.6261	1605	34	1578	19	1557	22	97	144.69	67.70
LGRV	mineralization-absent	2721839	2721839 S 139			7	0.0987	2.2490	3.7851	3.2976	0.2782	2.4117	1599	42	1590	26	1582	34	99	128.30	53.08
LGRV	mineralization-absent	2721839	2721839 M 123			7	0.0987	3.6739	3.8540	4.1935	0.2833	2.0220	1599	69	1604	34	1608	29	101	70.63	45.12
LGRV	mineralization-absent	2721839	2721839 M 126			7	0.0987	2.0335	3.8468	2.5630	0.2828	1.5600	1599	38	1603	21	1605	22	100	158.10	124.40
LGRV	mineralization-absent	2721839	2721839 M 113			7	0.0985	3.2435	3.8353	3.8109	0.2824	2.0006	1596	61	1600	31	1603	28	100	31.31	21.76
LGRV	mineralization-absent	2721839	2721839 S 136			7	0.0985	2.6734	3.7647	3.6312	0.2772	2.4574	1596	50	1585	29	1577	34	99	95.82	42.38
LGRV	mineralization-absent	2721839	2721839 M 116			7	0.0985	2.0507	3.8257	3.0485	0.2817	2.2557	1596	38	1598	25	1600	32	100	109.57	61.99
LGRV	mineralization-absent	2721839	2721839 M 120			7	0.0983	2.4645	3.7653	3.3154	0.2778	2.2177	1592	46	1585	27	1580	31	99	109.52	61.69
LGRV	mineralization-absent	2721839	2721839 S 140			7	0.0979	3.7781	3.7462	4.3781	0.2774	2.2121	1585	71	1581	35	1578	31	100	69.45	28.26
LGRV	mineralization-absent	2721839	2721839 M 112			7	0.0979	2.1947	3.7821	2.9923	0.2802	2.0340	1584	41	1589	24	1593	29	101	60.59	50.52
LGRV	mineralization-absent	2721839	2721839 S 138			7	0.0977	2.5639	3.7651	3.5165	0.2795	2.4067	1581	48	1585	28	1589	34	101	103.82	45.60
LGRV	mineralization-absent	2721839	2721839 S 128			7	0.0976	3.1850	3.7779	3.7568	0.2806	1.9924	1580	60	1588	30	1594	28	101	54.83	30.61
LGRV	mineralization-absent	2721839	2721839 S 145			7	0.0974	4.1302	3.8549	5.3477	0.2869	3.3970	1576	77	1604	43	1626	49	103	43.26	19.07
LGRV	mineralization-absent	2721839	2721839 S 147			7	0.0974	3.8730	3.8192	4.6202	0.2845	2.5192	1574	73	1597	37	1614	36	103	65.88	27.65

Appendix Table A6 LA-ICP MS U-Pb data for GRV and Hiltaba Suite zircon analyzed at Boise state University

Unit	Group	Sample	Spot Number	Disc.	Other	Experiment Number	Radiogenic Ratios								Age (Ma)									
							$^{207}Pb/^{206}Pb$	2σ	$^{207}Pb/^{235}U$	2σ	$^{206}Pb/^{238}U$	2σ	$^{207}Pb/^{206}Pb$	2σ	$^{207}Pb/^{235}Pb$	2σ	$^{206}Pb/^{238}U$	2σ	% Conc	Th ppm	U ppm
LGRV	mineralization-absent	2721839	2721839 S 144			7	0.0973	1.9012	3.7184	2.3783	0.2771	1.4289	1574	36	1575	19	1577	20	100	121.00	58.17
LGRV	mineralization-absent	2721839	2721839 S 135			7	0.0971	3.1353	3.6628	4.2683	0.2736	2.8963	1569	59	1563	34	1559	40	99	144.11	41.70
LGRV	mineralization-absent	2721839	2721839 M 122			7	0.0970	2.6850	3.8014	3.9212	0.2844	2.8578	1566	50	1593	32	1613	41	103	72.39	52.09
LGRV	mineralization-absent	2721839	2721839 M 106			7	0.0968	2.7016	3.7682	3.1717	0.2825	1.6616	1562	51	1586	25	1604	24	103	78.22	44.82
LGRV	mineralization-absent	2721839	2721839 S 132			7	0.0965	2.7881	3.6736	3.3709	0.2760	1.8946	1558	52	1566	27	1571	26	101	113.60	43.03
LGRV	mineralization-absent	2721839	2721839 S 131			7	0.0965	3.1617	3.6969	4.1280	0.2778	2.6540	1558	59	1571	33	1580	37	101	109.34	41.52
LGRV	mineralization-absent	2721839	2721839 S 129			7	0.0965	2.2138	3.7506	3.5537	0.2819	2.7799	1557	42	1582	28	1601	39	103	112.99	46.86
LGRV	mineralization-absent	2721839	2721839 S 143			7	0.0959	2.2530	3.5985	3.0650	0.2721	2.0780	1546	42	1549	24	1551	29	100	129.65	47.29
LGRV	mineralization-absent	2721839	2721839 S 142			7	0.0958	2.6887	3.6382	3.7428	0.2755	2.6037	1543	51	1558	30	1569	36	102	171.79	67.41
LGRV	mineralization-absent	2746487	2746487 S 86			7	0.1003	1.7776	3.7715	2.3128	0.2727	1.4795	1630	33	1587	19	1554	20		103.40	159.78
LGRV	mineralization-absent	2746487	2746487 S 84			7	0.1003	1.7302	3.7612	3.0419	0.2720	2.5019	1630	32	1584	24	1551	34		191.62	108.55
LGRV	mineralization-absent	2746487	2746487 S 81			7	0.1002	1.3570	3.9585	2.2550	0.2864	1.8010	1629	25	1626	18	1624	26		122.47	189.58
LGRV	mineralization-absent	2746487	2746487 S 88			7	0.1001	2.4444	3.9202	3.2432	0.2839	2.1314	1627	45	1618	26	1611	30		34.06	58.63
LGRV	mineralization-absent	2746487	2746487 S 92			7	0.0997	1.6542	3.7555	3.0934	0.2731	2.6140	1619	31	1583	25	1556	36		131.30	166.12
LGRV	mineralization-absent	2746487	2746487 S 80			7	0.0996	1.5905	3.7796	2.3929	0.2752	1.7878	1617	30	1588	19	1567	25		578.80	168.04
LGRV	mineralization-absent	2746487	2746487 S 79			7	0.0995	1.4582	3.7942	2.2519	0.2764	1.7161	1616	27	1592	18	1573	24		225.66	163.20
LGRV	mineralization-absent	2746487	2746487 S 93			7	0.0990	1.7517	3.8216	2.5710	0.2799	1.8819	1606	33	1597	21	1591	27		115.00	124.46
LGRV	mineralization-absent	2746487	2746487 M 65			7	0.0990	1.5734	3.7966	2.8597	0.2782	2.3879	1605	29	1592	23	1582	34		128.43	174.48
LGRV	mineralization-absent	2746487	2746487 M 74			7	0.0990	1.2411	3.7056	2.5492	0.2716	2.2267	1604	23	1573	20	1549	31		609.32	228.86
LGRV	mineralization-absent	2746487	2746487 M 76			7	0.0989	1.0780	3.8304	2.1913	0.2808	1.9078	1604	20	1599	18	1595	27		109.76	202.96
LGRV	mineralization-absent	2746487	2746487 M 72			7	0.0989	2.2561	3.8228	3.4323	0.2804	2.5866	1603	42	1598	28	1593	37		49.59	69.07
LGRV	mineralization-absent	2746487	2746487 M 78			7	0.0989	1.3019	3.8379	2.6377	0.2815	2.2940	1603	24	1601	21	1599	32		118.31	197.82
LGRV	mineralization-absent	2746487	2746487 M 59			7	0.0989	1.3454	3.6916	2.2343	0.2708	1.7838	1603	25	1570	18	1545	25		152.85	252.76
LGRV	mineralization-absent	2746487	2746487 M 71			7	0.0987	2.0357	3.8465	2.8169	0.2827	1.9470	1600	38	1603	23	1605	28		98.50	102.04
LGRV	mineralization-absent	2746487	2746487 M 77			7	0.0980	1.2936	3.8237	2.4768	0.2831	2.1122	1586	24	1598	20	1607	30		143.04	167.12
LGRV	mineralization-absent	2746487	2746487 M 75			7	0.0978	1.6462	3.7923	2.4034	0.2813	1.7511	1582	31	1591	19	1598	25		196.73	122.11
LGRV	mineralization-absent	2746487	2746487 M 70			7	0.0977	1.5559	3.7479	2.2861	0.2782	1.6749	1581	29	1582	18	1582	24		126.42	166.38
LGRV	mineralization-absent	2746487	2746487 M 42			7	0.0976	1.9053	3.9233	3.5805	0.2917	3.0315	1578	36	1618	29	1650	44		75.82	102.26
LGRV	mineralization-absent	2746487	2746487 M 73			7	0.0974	2.2023	3.6961	2.9548	0.2753	1.9699	1574	41	1571	24	1568	27		128.76	72.61
LGRV	mineralization-absent	2746487	2746487 M 56			7	0.0972	2.5061	3.7464	3.3065	0.2794	2.1570	1572	47	1581	27	1589	30		180.67	87.43
LGRV	mineralization-absent	2746487	2746487 M 39			7	0.0972	1.8872	3.6905	2.6072	0.2754	1.7989	1571	35	1569	21	1568	25		298.10	152.39
LGRV	mineralization-absent	2746487	2746487 S 82			7	0.0966	1.6772	3.7777	3.4140	0.2835	2.9737	1560	31	1588	27	1609	42		232.75	177.85

Appendix Table A6 LA-ICP MS U-Pb data for GRV and Hiltaba Suite zircon analyzed at Boise state University

Unit	Group	Sample	Spot Number	Disc.	Other	Experiment Number	Radiogenic Ratios						Age (Ma)							
							$^{207}Pb/^{206}Pb$	2σ	$^{207}Pb/^{235}U$	2σ	$^{206}Pb/^{238}U$	2σ	$^{207}Pb/^{206}Pb$	2σ	$^{207}Pb/^{235}Pb$	2σ	$^{206}Pb/^{238}U$	2σ	% Conc	Th ppm	U ppm
Rejected data																					
Hiltaba Suite	mineralization-related	2000366176	2000366176 M 239	>5%			0.0999	1.2430	3.7056	3.9474	0.2691	3.7466	1622	23	1573	32	1536	51	95	268.16	347.51
Hiltaba Suite	mineralization-related	2000366176	2000366176 L 217		Nb <0.9		0.0978	2.8362	3.7362	4.0642	0.2770	2.9109	1583	53	1579	33	1576	41	100	81.71	65.92
Hiltaba Suite	mineralization-related	2000366176	2000366176 L 195		Nb <0.9		0.0978	2.7983	3.6742	4.1398	0.2724	3.0508	1583	52	1566	33	1553	42	98	62.94	49.33
Hiltaba Suite	mineralization-related	2000366176	2000366176 L 198		Nb <0.9		0.0978	2.2497	3.6236	2.9280	0.2688	1.8741	1582	42	1555	23	1535	26	97	139.30	76.20
Hiltaba Suite	mineralization-related	2000366176	2000366176 L 197		Nb <0.9		0.0963	3.6512	3.7191	4.8758	0.2800	3.2315	1554	69	1575	39	1592	46	102	92.87	51.20
Hiltaba Suite	mineralization-related	2111460	2111460 L 255		Nb <0.9		0.1006	2.7268	3.9749	4.5084	0.2866	3.5902	1635	51	1629	37	1624	52	99	72.24	64.24
Hiltaba Suite	mineralization-related	2111460	2111460 L 259		Nb <0.9		0.1004	3.9986	3.8087	4.9139	0.2751	2.8561	1632	74	1595	40	1566	40	96	51.02	36.01
Hiltaba Suite	mineralization-related	2111460	2111460 M 274	>5%			0.1002	1.2743	3.7408	4.4003	0.2708	4.2117	1627	24	1580	35	1545	58	95	463.40	506.28
Hiltaba Suite	mineralization-related	2111460	2111460 L 260		Nb <0.9		0.0984	4.5082	3.7593	6.4783	0.2772	4.6524	1593	84	1584	52	1577	65	99	26.95	21.22
Hiltaba Suite	mineralization-related	2111460	2111460 L 261		>370 ppm P		0.0983	1.4752	3.7878	3.9033	0.2794	3.6138	1593	28	1590	31	1588	51	100	290.94	265.36
Hiltaba Suite	mineralization-related	1831634	1831634 M 37		>370 ppm P		0.0999	2.1383	3.8163	4.9186	0.2772	4.4295	1621	40	1596	40	1577	62	97	120.76	117.53
Hiltaba Suite	mineralization-related	1831634	1831634 L 27		>370 ppm P		0.0987	1.3117	3.7623	4.2662	0.2765	4.0596	1599	24	1585	34	1574	57	98	321.47	235.86
Hiltaba Suite	mineralization-related	1831634	1831634 L 26		>370 ppm P		0.0985	2.0238	3.7321	4.5088	0.2747	4.0291	1597	38	1578	36	1564	56	98	273.23	208.03
Hiltaba Suite	mineralization-related	1831634	1831634 L 18		Nb <0.9		0.1003	2.4314	3.7909	4.5119	0.2742	3.8007	1629	45	1591	36	1562	53	96	47.78	42.15
Hiltaba Suite	mineralization-related	1831634	1831634 L 7		>370 ppm P		0.0977	2.1045	3.6699	4.4342	0.2724	3.9030	1581	39	1565	35	1553	54	98	269.60	171.36
Hiltaba Suite	mineralization-related	1831634	1831634 L 12		>370 ppm P		0.0979	1.4380	3.6012	3.9744	0.2668	3.7051	1584	27	1550	32	1525	50	96	196.90	180.22
Hiltaba Suite	mineralization-related	1831634	1831634 L 17		>370 ppm P		0.0981	1.5905	3.6079	4.2241	0.2666	3.9132	1589	30	1551	34	1524	53	96	194.67	162.49
Hiltaba Suite	mineralization-related	1831634	1831634 L 24	>5%			0.0975	2.8153	3.4593	5.3944	0.2574	4.6014	1576	53	1518	42	1476	61	94	232.91	97.16
Hiltaba Suite	mineralization-absent	2053554	2053554 M 111	>5%			0.1021	3.7505	3.7698	6.3874	0.2677	5.1703	1663	69	1586	51	1529	70	92	187.03	94.93
Hiltaba Suite	mineralization-absent	2053554	2053554 M 80	>5%			0.1018	2.5754	3.7849	4.6947	0.2695	3.9253	1658	48	1590	38	1539	54	93	215.52	154.91
Hiltaba Suite	mineralization-absent	2053554	2053554 L 203	>5%			0.1017	2.3178	3.7126	4.1673	0.2649	3.4632	1655	43	1574	33	1515	47	92	144.03	131.18
Hiltaba Suite	mineralization-absent	2053554	2053554 L 197	>5%			0.1016	1.8980	3.7428	3.7816	0.2672	3.2708	1654	35	1581	30	1526	44	92	265.71	184.49
Hiltaba Suite	mineralization-absent	2053554	2053554 M 228	>5%			0.1011	2.1522	3.6895	4.9876	0.2648	4.4994	1644	40	1569	40	1514	61	92	163.00	172.09
Hiltaba Suite	mineralization-absent	2053554	2053554 M 129	>5%			0.1008	1.7528	3.7416	4.3984	0.2691	4.0341	1639	33	1580	35	1536	55	94	212.71	145.79
Hiltaba Suite	mineralization-absent	2053554	2053554 M 112	>5%			0.1008	2.5609	3.6028	4.4212	0.2592	3.6040	1639	48	1550	35	1486	48	91	225.01	137.45

Appendix Table A6 LA-ICP MS U-Pb data for GRV and Hiltaba Suite zircon analyzed at Boise state University

Unit	Group	Sample	Spot Number	Disc.	Other	Experiment Number	Radiogenic Ratios							Age (Ma)								
							$^{207}Pb/^{206}Pb$	2σ	$^{207}Pb/^{235}U$	2σ	$^{206}Pb/^{238}U$	2σ	$^{207}Pb/^{206}Pb$	2σ	$^{207}Pb/^{235}Pb$	2σ	$^{206}Pb/^{238}U$	2σ	% Conc	Th ppm	U ppm
Hiltaba Suite	mineralization-absent	2053554	2053554 L 204	>5%			0.1007	2.8152	3.6618	5.4377	0.2637	4.6523	1637	52	1563	43	1509	63	92	205.23	121.26
Hiltaba Suite	mineralization-absent	2053554	2053554 L 216	>5%	>370 ppm P		0.1000	2.0208	3.6738	4.3508	0.2664	3.8530	1625	38	1566	35	1522	52	94	156.19	164.74
Hiltaba Suite	mineralization-absent	2053554	2053554 M 114				0.1000	2.9818	3.9040	5.8477	0.2833	5.0304	1623	55	1615	47	1608	72	99	91.62	58.28
Hiltaba Suite	mineralization-absent	2053554	2053554 M 233	>5%			0.0994	2.8821	3.5951	5.5628	0.2623	4.7579	1613	54	1548	44	1502	64	93	194.52	182.91
Hiltaba Suite	mineralization-absent	2053554	2053554 M 99	>5%			0.0994	2.7022	3.6727	5.4947	0.2681	4.7844	1612	50	1565	44	1531	65	95	145.99	103.48
Hiltaba Suite	mineralization-absent	2053554	2053554 L 205	>5%			0.0993	2.9843	3.5921	6.1575	0.2625	5.3860	1610	56	1548	49	1503	72	93	120.86	122.97
Hiltaba Suite	mineralization-absent	2053554	2053554 M 241	>5%			0.0991	3.6813	3.6648	5.6320	0.2681	4.2623	1608	69	1564	45	1531	58	95	163.09	119.31
Hiltaba Suite	mineralization-absent	2053554	2053554 M 236	>5%	>370 ppm P		0.0989	3.6884	3.6516	6.0607	0.2678	4.8092	1603	69	1561	48	1530	65	95	204.37	164.07
Hiltaba Suite	mineralization-absent	2053554	2053554 M 109				0.0986	2.7377	3.7626	5.5539	0.2766	4.8322	1599	51	1585	45	1574	67	98	110.85	111.51
Hiltaba Suite	mineralization-absent	2053554	2053554 M 113	>5%			0.0986	2.2149	3.6063	4.9955	0.2653	4.4776	1597	41	1551	40	1517	61	95	95.29	76.01
Hiltaba Suite	mineralization-absent	2053554	2053554 M 122	>5%			0.0975	1.7959	3.4926	4.5477	0.2597	4.1780	1577	34	1526	36	1488	56	94	355.10	168.82
Hiltaba Suite	mineralization-absent	2053555	2053555 L 249	>5%	>370 ppm P		0.1004	1.2824	3.6230	4.4437	0.2618	4.2547	1631	24	1555	35	1499	57	92	96.36	567.32
Hiltaba Suite	mineralization-absent	2053555	2053555 L 251				0.1012	1.2177	3.6561	4.1576	0.2621	3.9753	1645	23	1562	33	1501	53	91	473.48	519.14
Hiltaba Suite	mineralization-absent	2053555	2053555 L 256	>5%	>370 ppm P		0.1006	1.9560	3.7464	4.5844	0.2701	4.1461	1635	36	1581	37	1541	57	94	51.18	730.46
Hiltaba Suite	mineralization-absent	2053555	2053555 L 257				0.1000	1.5018	3.8463	4.5960	0.2789	4.3437	1624	28	1603	37	1586	61	98	408.84	386.52
Hiltaba Suite	mineralization-absent	2053555	2053555 L 260	>5%			0.0991	1.6276	3.3812	5.7780	0.2475	5.5440	1607	30	1500	45	1426	71	89	1786.39	1235.10
Hiltaba Suite	mineralization-absent	2053555	2053555 L 263	>5%			0.1000	1.7204	3.6956	3.2956	0.2680	2.8109	1624	32	1570	26	1531	38	94	135.15	526.55
Hiltaba Suite	mineralization-absent	2053555	2053555 L 265	>5%	>370 ppm P		0.1011	1.9545	3.7680	3.0476	0.2704	2.3383	1644	36	1586	24	1543	32	94	439.28	550.80
Hiltaba Suite	mineralization-absent	2053555	2053555 L 266				0.0986	1.4125	3.7836	4.0944	0.2783	3.8430	1598	26	1589	33	1583	54	99	1051.30	646.34
Hiltaba Suite	mineralization-absent	2053555	2053555 M 269	>5%			0.0995	1.5308	3.6484	4.1106	0.2659	3.8150	1615	29	1560	33	1520	52	94	522.70	519.58
Hiltaba Suite	mineralization-absent	2053555	2053555 M 271	>5%			0.0992	2.2038	3.5637	6.3662	0.2605	5.9726	1609	41	1541	50	1492	80	93	288.68	710.61
Hiltaba Suite	mineralization-absent	2053555	2053555 M 274	>5%			0.1010	2.9665	3.2770	5.0666	0.2354	4.1073	1642	55	1476	39	1363	50	83	498.72	327.30
Hiltaba Suite	mineralization-absent	2053555	2053555 M 275	>5%			0.1004	3.3272	3.7010	7.5778	0.2673	6.8083	1632	62	1572	61	1527	93	94	357.98	284.16
Hiltaba Suite	mineralization-absent	2053555	2053555 M 276	>5%			0.0994	2.5641	3.2815	7.4489	0.2393	6.9937	1614	48	1477	58	1383	87	86	447.25	680.41
Hiltaba Suite	mineralization-absent	2053555	2053555 M 279	>5%			0.0986	2.7000	3.6262	5.3364	0.2667	4.6030	1598	50	1555	42	1524	62	95	166.39	470.16
Hiltaba Suite	mineralization-absent	2053555	2053555 M 281	>5%			0.0993	2.5106	3.5934	4.3719	0.2624	3.5792	1611	47	1548	35	1502	48	93	235.03	288.57
Hiltaba Suite	mineralization-absent	2053555	2053555 M 284	>5%			0.1004	2.1946	3.7531	5.3195	0.2712	4.8457	1631	41	1583	43	1547	67	95	123.52	534.79
LGRV	mineralization-absent	2018616	2018616 108	>5%			0.1050	1.8590	3.9860	4.1287	0.2753	3.6865	1714	34	1631	34	1568	51	91	186.45	186.43
LGRV	mineralization-absent	2018616	2018616 79	>5%			0.0985	2.9341	3.2855	4.9668	0.2420	4.0076	1595	55	1478	39	1397	50	88	161.17	179.55
LGRV	mineralization-absent	2018616	2018616 96	>5%			0.0984	2.7236	3.5991	4.9317	0.2652	4.1114	1595	51	1549	39	1516	56	95	127.29	152.61
LGRV	mineralization-absent	2016125	2016125 L 51	>5%			0.0994	6.4237	3.6382	9.2252	0.2656	6.6211	1612	120	1558	73	1518	90	94	13.54	20.88
LGRV	mineralization-absent	2016125	2016125 L 52	>5%			0.1020	3.0297	3.7706	5.4515	0.2680	4.5321	1661	56	1587	44	1531	62	92	38.88	65.29
LGRV	mineralization-absent	2016125	2016125 L 55	>5%			0.1005	2.4973	3.7208	3.8998	0.2686	2.9954	1633	46	1576	31	1533	41	94	41.66	68.53
LGRV	mineralization-absent	2016125	2016125 M 63		Nb <0.9		0.0964	4.2838	3.6735	6.2135	0.2763	4.5007	1556	80	1566	50	1572	63	101	26.58	39.74
LGRV	mineralization-absent	2016125	2016125 M 69	>5%			0.0938	2.8894	3.6729	5.9278	0.2840	5.1758	1504	55	1566	47	1611	74	107	138.65	243.24

Appendix Table A6 LA-ICP MS U-Pb data for GRV and Hiltaba Suite zircon analyzed at Boise state University

Unit	Group	Sample	Spot Number	Disc.	Other	Experiment Number	Radiogenic Ratios						Age (Ma)							
							$^{207}Pb/^{206}Pb$	2σ	$^{207}Pb/^{235}U$	2σ	$^{206}Pb/^{238}U$	2σ	$^{207}Pb/^{206}Pb$	2σ	$^{207}Pb/^{235}Pb$	2σ	$^{206}Pb/^{238}U$	2σ	% Conc	Th ppm	U ppm
LGRV	mineralization-absent	2016125	2016125 M 72		Nb <0.9		0.0965	5.5235	3.7824	8.9219	0.2843	7.0065	1557	104	1589	72	1613	100	104	15.00	24.34
LGRV	mineralization-absent	2016125	2016125 M 75	>5%	>370 ppm P		0.0953	3.9013	3.7999	7.5949	0.2893	6.5163	1533	73	1593	61	1638	94	107	94.71	152.39
LGRV	mineralization-absent	2721839	2721839 M 124				0.0988	2.7569	3.8452	3.5523	0.2822	2.2402	1602	51	1602	29	1603	32	100	73.77	47.74
LGRV	mineralization-absent	2746487	2746487 M 50		Nb <0.9		0.1005	6.0044	4.0024	6.7543	0.2888	3.0931	1634	112	1635	55	1635	45		22.08	10.98
LGRV	mineralization-absent	2746487	2746487 S 94	>5%			0.0996	1.3580	3.6010	1.9573	0.2622	1.4096	1616	25	1550	16	1501	19		235.73	198.47
LGRV	mineralization-absent	2746487	2746487 M 61		Nb <0.9		0.0990	2.4077	3.8257	3.2436	0.2801	2.1734	1606	45	1598	26	1592	31		51.40	59.16

Appendix 4 Table A7: LA-ICP MS U-Pb data for standard zircon analyzed at the University of Adelaide

Standard	Spot Number	Zircon Treatment	Analytical Session	$^{207}Pb/^{206}Pb$	2σ	$^{207}Pb/^{235}U$	2σ	$^{206}Pb/^{238}U$	2σ	$^{207}Pb/^{206}Pb$	2σ	$^{207}Pb/^{235}Pb$	2σ	$^{206}Pb/^{238}U$	2σ	$^{208}Pb/^{232}Th$	2σ	% Conc	Th ppm	U ppm
Ples_1	CA_ples - 1	CA	26/08/2018 (1)	0.0531	0.0018	0.406	0.013	0.05601	0.00058	**333**	**75**	345.9	9.5	351.3	3.5	383	32	105	51.4	541
Ples_2	CA_ples - 2	CA	26/08/2018 (1)	0.054	0.0019	0.422	0.013	0.05644	0.00063	**361**	**78**	358.1	9.2	353.9	3.8	318	35	98	55	493
Ples_3	CA_ples - 3	CA	26/08/2018 (1)	0.0538	0.0015	0.398	0.011	0.05354	0.00063	**340**	**64**	339.8	8.3	336.2	3.9	362	42	99	41.5	462
Ples_4	CA_ples - 4	CA	26/08/2018 (1)	0.0541	0.0015	0.404	0.012	0.05347	0.00045	**368**	**64**	344.7	8.4	335.8	2.7	350	37	91	47.5	517
Ples_5	CA_ples - 5	CA	26/08/2018 (1)	0.0537	0.0015	0.409	0.011	0.05449	0.00058	**367**	**66**	348.4	7.7	342	3.6	343	34	93	48.2	524
Ples_6	CA_ples - 6	CA	26/08/2018 (1)	0.0534	0.0015	0.4053	0.0099	0.05441	0.00058	**334**	**63**	345.9	7.3	341.5	3.6	339	29	102	48.6	536
Ples_7	CA_ples - 7	CA	27/08/2018 (2)	0.0525	0.0016	0.401	0.011	0.05452	0.00063	**301**	**64**	342.6	8	342.2	3.9	347	31	114	45.8	509
Ples_8	CA_ples - 8	CA	27/08/2018 (2)	0.0548	0.0015	0.402	0.011	0.05358	0.0005	**391**	**61**	343.7	8	336.5	3	370	36	86	45.3	491
Ples_9	CA_ples - 9	CA	27/08/2018 (2)	0.0534	0.0014	0.401	0.01	0.0547	0.00058	**343**	**60**	342.8	7.4	343.3	3.6	306	36	100	41.8	441
Ples_10	CA_ples - 10	CA	27/08/2018 (2)	0.0518	0.0012	0.3966	0.0088	0.05547	0.00051	**262**	**52**	338.8	6.4	348	3.1	370	27	133	67.8	710
Ples_11	CA_ples - 11	CA	27/08/2018 (2)	0.0539	0.0019	0.403	0.013	0.05406	0.00058	**349**	**78**	342.9	9.7	339.4	3.6	358	33	97	42.9	468
Ples_12	CA_ples - 12	CA	27/08/2018 (2)	0.0519	0.0017	0.391	0.012	0.05377	0.00064	**281**	**75**	335.7	9.2	337.6	3.9	336	37	120	36.3	427
Z_GJ1_1	HTGJ - 1	TA	26/08/2018 (1)	0.0606	0.0017	0.825	0.021	0.0991	0.001	**611**	**59**	610	11	608.9	5.9	526	91	100	9.28	287.2
Z_GJ1_2	HTGJ - 2	TA	26/08/2018 (1)	0.06	0.0014	0.802	0.018	0.0971	0.0011	**596**	**50**	598	10	597.4	6.3	715	96	100	9.43	286.1
Z_GJ1_3	HTGJ - 3	TA	26/08/2018 (1)	0.0602	0.0017	0.801	0.02	0.09633	0.00087	**604**	**59**	596	11	592.9	5.1	620	110	98	9.81	287.7
Z_GJ1_4	HTGJ - 4	TA	26/08/2018 (1)	0.0615	0.0016	0.809	0.022	0.0967	0.001	**641**	**59**	605	13	595	5.9	568	88	93	9.78	287
Z_GJ1_5	HTGJ - 5	TA	26/08/2018 (1)	0.0596	0.0016	0.818	0.021	0.09868	0.00094	**591**	**57**	607	12	606.7	5.5	623	88	103	9.44	287.1
Z_GJ1_6	HTGJ - 6	TA	26/08/2018 (1)	0.059	0.0012	0.809	0.017	0.0984	0.0011	**572**	**46**	603.3	9.8	604.8	6.4	570	100	106	9.29	286.2
Z_GJ1_7	HTGJ - 7	TA	26/08/2018 (1)	0.0601	0.0016	0.811	0.021	0.0981	0.0011	**602**	**60**	603	12	603.3	6.7	720	100	100	9.5	288
Z_GJ1_8	HTGJ - 8	TA	26/08/2018 (1)	0.0618	0.0016	0.828	0.02	0.0972	0.001	**655**	**57**	613	11	598	5.9	592	99	91	9.35	287.1
Z_GJ1_9	HTGJ - 9	TA	26/08/2018 (1)	0.06	0.0015	0.798	0.019	0.0976	0.00092	**591**	**56**	596	11	600.3	5.4	582	92	102	9.75	286.8
Z_GJ1_10	HTGJ - 10	TA	26/08/2018 (1)	0.0594	0.0018	0.802	0.021	0.0978	0.0011	**578**	**67**	598	12	601.3	6.6	613	97	104	9.77	287.1
Z_GJ1_11	HTGJ - 11	TA	26/08/2018 (1)	0.0617	0.0015	0.839	0.02	0.0985	0.001	**652**	**53**	619	11	605.3	6.1	656	92	93	9.59	287.7
Z_GJ1_12	HTGJ - 12	TA	27/08/2018 (2)	0.0592	0.0014	0.794	0.019	0.09742	0.00098	**564**	**50**	595	11	599.2	5.8	580	110	106	9.37	286.1
Z_GJ1_13	HTGJ - 13	TA	27/08/2018 (2)	0.0598	0.0014	0.809	0.019	0.09795	0.00086	**598**	**56**	601	11	602.3	5	549	87	101	9.24	285.9
Z_GJ1_14	HTGJ - 14	TA	27/08/2018 (2)	0.0592	0.0016	0.787	0.02	0.0966	0.001	**584**	**57**	590	11	595	6.3	618	94	102	9.53	288.1
Z_GJ1_15	HTGJ - 15	TA	27/08/2018 (2)	0.06	0.0019	0.787	0.024	0.09642	0.00098	**592**	**70**	591	14	593.4	5.8	619	96	100	9.58	287.4
Z_GJ1_16	HTGJ - 16	TA	27/08/2018 (2)	0.0601	0.0016	0.807	0.02	0.0975	0.001	**607**	**56**	601	11	599.7	5.9	536	88	99	9.51	286.5
Z_GJ1_17	HTGJ - 17	TA	27/08/2018 (2)	0.0612	0.0015	0.824	0.02	0.0973	0.00079	**634**	**53**	609	11	598.5	4.7	638	88	94	9.47	285.6
Z_GJ1_18	HTGJ - 18	TA	27/08/2018 (2)	0.0613	0.0018	0.823	0.024	0.09798	0.0009	**643**	**62**	610	13	602.5	5.3	597	91	94	9.72	289.5
Z_GJ1_19	HTGJ - 19	TA	27/08/2018 (2)	0.0591	0.0015	0.809	0.021	0.0986	0.001	**574**	**59**	602	12	606.4	6.1	672	91	106	9.37	285.3
GJ1	N_GJ_1	N	30/09/2019 (2)	0.0595	0.0011	0.825	0.016	0.09952	0.00077	**593**	**42**	611.2	8.4	611.6	4.5	569	63	103	9.9	279.0
GJ1	N_GJ_2	N	30/09/2019 (2)	0.0607	0.0011	0.849	0.015	0.09984	0.00074	**641**	**38**	623.2	8.1	613.4	4.3	642	71	96	10.3	281.0
GJ1	N_GJ_3	N	30/09/2019 (2)	0.0597	0.0012	0.829	0.017	0.10075	0.00092	**593**	**43**	613.6	9.5	618.7	5.4	686	74	104	9.9	268.0
GJ1	N_GJ_4	N	30/09/2019 (2)	0.0606	0.0011	0.836	0.016	0.09989	0.00077	**623**	**39**	615.6	8.9	613.7	4.5	660	84	99	9.7	265.0
GJ1	N_GJ_5	N	30/09/2019 (2)	0.061	0.0013	0.85	0.018	0.10145	0.00093	**631**	**44**	623.4	9.7	622.9	5.5	505	63	99	9.9	270.0
GJ1	N_GJ_6	N	30/09/2019 (2)	0.0597	0.0011	0.833	0.015	0.10066	0.00085	**584**	**39**	614.5	8.2	618.2	5	585	73	106	9.9	272.0
GJ1	N_GJ_7	N	30/09/2019 (2)	0.0609	0.0013	0.839	0.017	0.10017	0.00086	**635**	**47**	620.2	9.2	615.4	5.1	556	73	97	9.9	270.0
GJ1	N_GJ_8	N	30/09/2019 (2)	0.0616	0.0013	0.848	0.016	0.10019	0.00083	**659**	**44**	622.6	9	615.5	4.9	652	70	93	9.8	264.0
GJ1	N_GJ_9	N	30/09/2019 (2)	0.0602	0.0013	0.82	0.018	0.09907	0.00081	**596**	**49**	608	10	608.9	4.8	610	73	102	9.7	272.0
GJ1	N_GJ_10	N	30/09/2019 (2)	0.0588	0.0013	0.802	0.016	0.09903	0.00085	**539**	**47**	598	8.9	608.6	5	610	65	113	9.8	274.0
GJ1	N_GJ_11	N	30/09/2019 (2)	0.0603	0.0012	0.852	0.017	0.10073	0.00086	**616**	**44**	625.6	9.5	618.6	5	691	79	100	9.6	264.0
GJ1	N_GJ_12	N	30/09/2019 (2)	0.0592	0.0011	0.821	0.015	0.10036	0.00079	**567**	**39**	609.6	8.1	616.5	4.6	569	70	109	10.0	271.0
GJ1	N_GJ_13	N	30/09/2019 (2)	0.0587	0.0011	0.817	0.015	0.10002	0.00084	**564**	**40**	607.4	8.5	614.5	4.9	671	80	109	9.8	272.0
GJ1	N_GJ_14	N	30/09/2019 (2)	0.0589	0.001	0.818	0.014	0.09917	0.00086	**572**	**38**	606.2	7.7	609.5	5	616	67	107	10.1	276.0
GJ1	N_GJ_15	N	30/09/2019 (2)	0.0598	0.0012	0.832	0.016	0.0992	0.0008	**597**	**43**	616.1	8.8	610.1	4.6	681	75	102	9.9	270.0
GJ1	N_GJ_16	N	30/09/2019 (2)	0.0581	0.0015	0.821	0.019	0.10148	0.00097	**549**	**54**	608	10	623	5.7	618	73	113	9.6	266.0
GJ1	HT_GJ-1_ - 1.d	TA	30/09/2019 (2)	0.0597	0.0011	0.813	0.015	0.09829	0.00072	**582**	**40**	603.3	8.3	604.3	4.2	0.0307	0.0037	104	7.9	268.8
GJ1	HT_GJ-1_ - 2.d	TA	30/09/2019 (2)	0.0612	0.0013	0.834	0.017	0.09759	0.00074	**651**	**46**	615.4	9	600.2	4.3	0.0303	0.0035	92	7.9	274.9
GJ1	HT_GJ-1_ - 3.d	TA	30/09/2019 (2)	0.0604	0.0011	0.815	0.015	0.09736	0.00084	**635**	**39**	605.8	8	598.8	5	0.0344	0.0042	94	7.9	269.9

CA: Chemical Abrasion; TA: Thermally Annealed; N: Normal

Appendix 4 Table A7: LA-ICP MS U-Pb data for standard zircon analyzed at the University of Adelaide

Standard	Spot Number	Zircon Treatment	Analytical Session	$^{207}Pb/^{206}Pb$	2σ	$^{207}Pb/^{235}U$	2σ	$^{206}Pb/^{238}U$	2σ	$^{207}Pb/^{206}Pb$	2σ	$^{207}Pb/^{235}Pb$	2σ	$^{206}Pb/^{238}U$	2σ	$^{208}Pb/^{232}Th$	2σ	% Conc	Th	U
																			ppm	ppm
GJ1	HT_GJ-1_ - 4.d	TA	30/09/2019 (2)	0.0593	0.0012	0.802	0.014	0.09821	0.0008	**580**	**42**	599.5	8	603.8	4.7	0.0321	0.0035	104	7.9	274.5
GJ1	HT_GJ-1_ - 5.d	TA	30/09/2019 (2)	0.0603	0.0011	0.817	0.015	0.0979	0.00077	**617**	**41**	605.3	8.7	602.1	4.5	0.0296	0.0037	98	7.8	273.8
GJ1	HT_GJ-1_ - 6.d	TA	30/09/2019 (2)	0.0602	0.001	0.81	0.015	0.09744	0.00067	**597**	**37**	602.3	8.2	599.3	3.9	0.0281	0.0035	100	8.1	277.5
GJ1	HT_GJ-1_ - 7.d	TA	30/09/2019 (2)	0.06033	0.00097	0.823	0.013	0.09868	0.00076	**608**	**35**	608.9	7.2	606.6	4.5	0.0307	0.0031	100	7.9	272.7
GJ1	HT_GJ-1_ - 8.d	TA	30/09/2019 (2)	0.0597	0.0011	0.807	0.015	0.09768	0.0008	**581**	**39**	600	8.5	600.7	4.7	0.0317	0.0038	103	7.9	275.2
GJ1	HT_GJ-1_ - 9.d	TA	30/09/2019 (2)	0.0606	0.0012	0.816	0.014	0.09726	0.00082	**623**	**43**	604.7	7.7	598.3	4.8	0.0316	0.0036	96	8.0	279.2
GJ1	HT_GJ-1_ - 10.d	TA	30/09/2019 (2)	0.0602	0.0013	0.812	0.016	0.0974	0.00082	**601**	**46**	604	9.4	599.1	4.8	0.029	0.0035	100	8.0	277.4
GJ1	HT_GJ-1_ - 11.d	TA	30/09/2019 (2)	0.0596	0.0011	0.812	0.014	0.09851	0.0008	**591**	**37**	602.7	7.9	605.6	4.7	0.0321	0.0039	102	8.1	277.4
GJ1	HT_GJ-1_ - 12.d	TA	30/09/2019 (2)	0.0595	0.0012	0.813	0.016	0.09792	0.00074	**586**	**47**	603.3	8.7	602.2	4.3	0.028	0.0038	103	8.0	273.7
GJ1	HT_GJ-1_ - 13.d	TA	30/09/2019 (2)	0.0617	0.0012	0.832	0.016	0.09785	0.00092	**656**	**41**	615.2	9.1	601.7	5.4	0.0314	0.0039	92	7.9	269.4
GJ1	HT_GJ-1_ - 14.d	TA	30/09/2019 (2)	0.0595	0.0012	0.81	0.015	0.09803	0.00069	**595**	**42**	601.7	8.3	602.8	4	0.0299	0.0036	101	7.8	267.4
GJ1	HT_GJ-1_ - 15.d	TA	30/09/2019 (2)	0.0597	0.0012	0.817	0.015	0.09846	0.00072	**598**	**43**	605.5	8.6	605.3	4.2	0.0311	0.0038	101	8.1	275.9
GJ1	HT_GJ-1_ - 16.d	TA	30/09/2019 (2)	0.0605	0.0012	0.811	0.014	0.09696	0.00074	**619**	**41**	604	8.1	596.5	4.3	0.0325	0.0038	96	8.4	278.4
Plesovice	ples_ - 1.d	N	30/09/2019 (2)	0.0547	0.0011	0.4092	0.0069	0.05376	0.00035	**396**	**44**	349.1	5.2	337.5	2.1	0.01743	0.00094	85	58.0	597.2
Plesovice	ples_ - 2.d	N	30/09/2019 (2)	0.05251	0.00097	0.3949	0.0074	0.05383	0.00038	**312**	**43**	337.5	5.4	338	2.4	0.0175	0.0011	108	58.6	601.4
Plesovice	ples_ - 3.d	N	30/09/2019 (2)	0.05422	0.00096	0.4026	0.0062	0.05371	0.00035	**379**	**39**	344.2	4.5	337.5	2.2	0.01705	0.00088	89	59.7	604.0
Plesovice	ples_ - 4.d	N	30/09/2019 (2)	0.0538	0.0012	0.395	0.007	0.05322	0.00043	**344**	**48**	338.2	5.2	334.2	2.6	0.01727	0.00092	97	59.9	608.5
Plesovice	ples_ - 5.d	N	30/09/2019 (2)	0.05408	0.00097	0.4021	0.0073	0.05397	0.00037	**365**	**41**	342.8	5.3	338.9	2.2	0.01703	0.00097	93	61.2	605.8
Plesovice	ples_ - 6.d	N	30/09/2019 (2)	0.0532	0.00084	0.3993	0.0066	0.0544	0.00038	**342**	**38**	340.8	4.8	341.5	2.3	0.01646	0.00081	100	85.9	722.0
Plesovice	ples_ - 7.d	N	30/09/2019 (2)	0.05315	0.00093	0.3969	0.0065	0.0545	0.00039	**327**	**40**	339.5	4.8	342.1	2.4	0.0167	0.00085	105	65.3	625.1
Plesovice	ples_ - 8.d	N	30/09/2019 (2)	0.05281	0.00088	0.3971	0.0071	0.05454	0.00038	**318**	**39**	340.2	5	342.3	2.3	0.01762	0.00091	108	65.8	629.9
Plesovice	ples_ - 9.d	N	30/09/2019 (2)	0.0532	0.001	0.3986	0.0077	0.0541	0.0004	**330**	**44**	340.1	5.6	339.6	2.5	0.01796	0.00098	103	63.5	626.0
Plesovice	ples_ - 10.d	N	30/09/2019 (2)	0.05222	0.0009	0.3873	0.0065	0.05355	0.00041	**289**	**39**	332.6	4.7	336.2	2.5	0.01694	0.00094	116	61.3	638.8
Plesovice	ples_ - 11.d	N	30/09/2019 (2)	0.05312	0.00089	0.4015	0.0064	0.05395	0.00037	**342**	**39**	342.4	4.6	338.7	2.3	0.01771	0.00097	99	59.4	613.0
Plesovice	ples_ - 12.d	N	30/09/2019 (2)	0.05433	0.0009	0.4091	0.0059	0.05424	0.00044	**382**	**36**	348	4.3	340.5	2.7	0.018	0.0011	89	62.6	620.3
Plesovice	ples_ - 13.d	N	30/09/2019 (2)	0.05278	0.00083	0.3966	0.006	0.05407	0.00037	**320**	**37**	339.3	4.5	339.4	2.3	0.01768	0.00082	106	100.6	769.0
Plesovice	ples_ - 14.d	N	30/09/2019 (2)	0.05297	0.00083	0.3957	0.0058	0.05372	0.00034	**325**	**35**	338.7	4.1	337.3	2.1	0.0179	0.001	104	63.0	676.9
Plesovice	ples_ - 15.d	N	30/09/2019 (2)	0.05349	0.00093	0.3996	0.0063	0.054	0.00037	**345**	**39**	341.1	4.6	339.1	2.3	0.01773	0.00093	98	63.5	677.4
Plesovice	ples_ - 16.d	N	30/09/2019 (2)	0.05328	0.00092	0.4013	0.0064	0.0545	0.00037	**335**	**40**	342.8	4.6	342.3	2.3	0.0184	0.0011	102	64.3	678.4
91500	95100_ - 1.d	N	30/09/2019 (2)	0.0769	0.002	1.932	0.051	0.1792	0.0023	**1121**	**55**	1094	19	1062	13	0.0542	0.0031	95	17.2	52.2
91500	95100_ - 2.d	N	30/09/2019 (2)	0.0762	0.0023	1.916	0.054	0.1784	0.0019	**1104**	**62**	1087	19	1058	11	0.0545	0.0035	96	17.1	52.3
91500	95100_ - 3.d	N	30/09/2019 (2)	0.0769	0.0024	1.893	0.056	0.1816	0.0022	**1111**	**62**	1085	20	1076	12	0.0549	0.003	97	17.2	52.5
91500	95100_ - 4.d	N	30/09/2019 (2)	0.0756	0.0019	1.868	0.044	0.1793	0.0022	**1087**	**53**	1071	15	1064	12	0.0549	0.0032	98	17.3	53.3
91500	95100_ - 5.d	N	30/09/2019 (2)	0.0757	0.0021	1.899	0.049	0.1817	0.0021	**1080**	**58**	1080	17	1076	11	0.0568	0.0033	100	17.1	53.1
91500	95100_ - 6.d	N	30/09/2019 (2)	0.0737	0.002	1.824	0.043	0.1793	0.0022	**1038**	**55**	1051	15	1063	12	0.0581	0.0033	102	17.3	53.2
91500	95100_ - 7.d	N	30/09/2019 (2)	0.0723	0.0019	1.801	0.045	0.1808	0.0021	**982**	**52**	1042	16	1071	11	0.0574	0.0033	109	17.4	52.7
91500	95100_ - 8.d	N	30/09/2019 (2)	0.079	0.003	1.992	0.069	0.1825	0.0023	**1169**	**72**	1108	24	1080	12	0.0613	0.0048	92	17.1	54.0
91500	95100_ - 9.d	N	30/09/2019 (2)	0.076	0.0023	1.874	0.056	0.1785	0.0022	**1071**	**62**	1066	20	1060	12	0.0587	0.0033	99	14.6	48.7
91500	95100_ - 10.d	N	30/09/2019 (2)	0.0772	0.0023	1.884	0.05	0.1779	0.0024	**1124**	**55**	1078	18	1057	13	0.053	0.0036	94	15.1	49.1
91500	95100_ - 11.d	N	30/09/2019 (2)	0.0742	0.0022	1.886	0.056	0.1827	0.0023	**1050**	**61**	1074	20	1081	12	0.0551	0.0033	103	14.5	48.1
91500	95100_ - 12.d	N	30/09/2019 (2)	0.0751	0.0027	1.863	0.055	0.1812	0.0025	**1065**	**70**	1068	20	1073	13	0.056	0.0038	101	14.0	47.4
91500	95100_ - 13.d	N	30/09/2019 (2)	0.0756	0.0024	1.889	0.06	0.1783	0.0022	**1080**	**67**	1077	21	1057	12	0.0608	0.0041	98	13.0	44.2
91500	95100_ - 14.d	N	30/09/2019 (2)	0.0724	0.0024	1.796	0.054	0.1794	0.0021	**983**	**66**	1043	19	1065	12	0.0579	0.0038	108	13.9	46.1
91500	95100_ - 15.d	N	30/09/2019 (2)	0.0718	0.0022	1.796	0.056	0.1808	0.0025	**976**	**62**	1044	20	1074	14	0.0604	0.0036	110	15.4	48.3
91500	95100_ - 16.d	N	30/09/2019 (2)	0.0729	0.0023	1.797	0.054	0.1796	0.0023	**994**	**64**	1049	20	1067	13	0.0568	0.0043	107	13.5	45.1
GJ1	N_GJ_ - 1.d	N	11/11/2019 (2)	0.0633	0.0013	0.869	0.017	0.09934	0.00078	**717**	**45**	634.6	9.4	610.5	4.6	0.0299	0.0034	85	8.9	269.0
GJ1	N_GJ_ - 2.d	N	11/11/2019 (2)	0.0602	0.0012	0.849	0.018	0.10112	0.00088	**615**	**45**	622.5	9.8	621.5	5.1	0.0348	0.0035	101	8.9	267.2
GJ1	N_GJ_ - 3.d	N	11/11/2019 (2)	0.0605	0.0011	0.832	0.016	0.099	0.00067	**623**	**40**	614.3	8.9	608.5	3.9	0.0281	0.0037	98	8.8	267.2
GJ1	N_GJ_ - 4.d	N	11/11/2019 (2)	0.0608	0.0012	0.828	0.016	0.09897	0.00075	**633**	**43**	613.3	8.8	608.3	4.4	0.0291	0.0032	96	8.9	266.3
GJ1	N_GJ_ - 5.d	N	11/11/2019 (2)	0.0612	0.0012	0.835	0.015	0.09811	0.00083	**633**	**44**	615.5	8.5	603.8	4.8	0.0258	0.003	95	9.1	265.6
GJ1	N_GJ_ - 6.d	N	11/11/2019 (2)	0.0596	0.0012	0.819	0.017	0.0985	0.00082	**590**	**45**	607.3	9.4	605.5	4.8	0.03	0.0037	103	9.0	265.7

CA: Chemical Abrasion; TA: Thermally Annealed; N: Normal

Appendix 4 Table A7: LA-ICP MS U-Pb data for standard zircon analyzed at the University of Adelaide

Standard	Spot Number	Zircon Treatment	Analytical Session	$^{207}Pb/^{206}Pb$	2σ	$^{207}Pb/^{235}U$	2σ	$^{206}Pb/^{238}U$	2σ	$^{207}Pb/^{206}Pb$	2σ	$^{207}Pb/^{235}Pb$	σ	$^{206}Pb/^{238}U$	2σ	$^{208}Pb/^{232}Th$	2σ	% Conc	Th ppm	U ppm
GJ1	N_GJ_ - 7.d	N	11/11/2019 (2)	0.0611	0.0013	0.834	0.018	0.09887	0.00074	**638**	**45**	615.4	9.6	607.8	4.3	0.0376	0.0047	95	8.8	265.6
GJ1	N_GJ_ - 8.d	N	11/11/2019 (2)	0.0598	0.0013	0.824	0.018	0.09993	0.0008	**603**	**46**	609.7	9.8	614.5	4.8	0.0307	0.0044	102	9.0	260.6
GJ1	N_GJ_ - 9.d	N	11/11/2019 (2)	0.0603	0.0014	0.83	0.019	0.1003	0.00095	**596**	**53**	613	11	616.1	5.6	0.0322	0.0046	103	8.7	259.4
GJ1	N_GJ_ - 10.d	N	11/11/2019 (2)	0.0611	0.0013	0.821	0.016	0.09838	0.0009	**640**	**46**	610.4	9.3	604.9	5.3	0.032	0.0038	95	8.6	258.2
GJ1	N_GJ_ - 11.d	N	11/11/2019 (2)	0.0597	0.0013	0.815	0.018	0.09982	0.00088	**594**	**47**	605	10	613.3	5.2	0.0338	0.0044	103	8.6	253.7
GJ1	N_GJ_ - 12.d	N	11/11/2019 (2)	0.0603	0.0012	0.823	0.016	0.09963	0.00083	**616**	**43**	609.3	8.9	612.2	4.9	0.0328	0.0036	99	8.7	253.3
GJ1	N_GJ_ - 13.d	N	11/11/2019 (2)	0.0595	0.0014	0.812	0.018	0.09929	0.00085	**572**	**52**	601.8	9.9	610.2	5	0.0331	0.0042	107	8.6	251.7
GJ1	N_GJ_ - 14.d	N	11/11/2019 (2)	0.0605	0.0015	0.826	0.019	0.0995	0.00083	**605**	**56**	613	11	611.4	4.8	0.0309	0.0046	101	8.7	254.3
GJ1	N_GJ_ - 15.d	N	11/11/2019 (2)	0.0602	0.0014	0.834	0.018	0.09962	0.0008	**611**	**52**	616	10	612.2	4.7	0.0347	0.0042	100	8.4	250.4
GJ1	N_GJ_ - 16.d	N	11/11/2019 (2)	0.0603	0.0013	0.813	0.017	0.0976	0.00079	**614**	**47**	604.9	9.1	600.3	4.6	0.033	0.0037	98	8.4	253.9
GJ1	N_GJ_ - 17.d	N	11/11/2019 (2)	0.0608	0.0013	0.835	0.018	0.09862	0.00078	**625**	**47**	616	10	606.2	4.6	0.0355	0.0039	97	8.5	249.5
GJ1	N_GJ_ - 18.d	N	11/11/2019 (2)	0.0609	0.0013	0.827	0.016	0.09796	0.00081	**623**	**45**	611.6	8.8	602.4	4.8	0.0349	0.0045	97	8.7	258.5
GJ1	N_GJ_ - 19.d	N	11/11/2019 (2)	0.0588	0.0014	0.807	0.019	0.09839	0.00087	**556**	**53**	600	11	604.9	5.1	0.0316	0.004	109	8.9	262.4
GJ1	N_GJ_ - 20.d	N	11/11/2019 (2)	0.0593	0.0015	0.804	0.019	0.0978	0.00086	**573**	**54**	601	11	602	5.1	0.0349	0.0042	105	8.9	265.5
GJ1	N_GJ_ - 21.d	N	12/11/2019 (3)	0.0606	0.0011	0.83	0.016	0.09908	0.00087	**616**	**38**	612.2	8.9	609	5.1	0.0333	0.0042	99	9.1	263.6
GJ1	N_GJ_ - 22.d	N	12/11/2019 (3)	0.0604	0.0012	0.827	0.017	0.09894	0.00091	**642**	**42**	613.4	8.8	608.1	5.4	0.0353	0.0042	95	8.9	265.8
Plesovice	N_Ples_ - 1.d	N	11/11/2019 (2)	0.0575	0.001	0.4466	0.0079	0.05618	0.00042	**502**	**39**	375	5.6	352.3	2.6	0.0229	0.0011	70	68.7	678.0
Plesovice	N_Ples_ - 2.d	N	11/11/2019 (2)	0.0594	0.0013	0.466	0.01	0.05705	0.00057	**583**	**49**	387.8	7.1	357.6	3.5	0.0213	0.0014	61	53.4	508.8
Plesovice	N_Ples_ - 3.d	N	11/11/2019 (2)	0.0558	0.0011	0.4335	0.0088	0.05629	0.0005	**437**	**44**	365.7	6.2	353	3	0.0221	0.0013	81	51.9	540.4
Plesovice	N_Ples_ - 4.d	N	11/11/2019 (2)	0.0564	0.0012	0.4258	0.0091	0.05486	0.00041	**461**	**48**	359.6	6.5	344.3	2.5	0.0203	0.0012	75	48.8	534.9
Plesovice	N_Ples_ - 5.d	N	11/11/2019 (2)	0.0564	0.0011	0.4238	0.0081	0.05388	0.00042	**471**	**44**	358.3	5.8	338.3	2.5	0.0209	0.0013	72	51.9	551.3
Plesovice	N_Ples_ - 6.d	N	11/11/2019 (2)	0.054	0.001	0.4103	0.0079	0.0547	0.00052	**372**	**44**	349.2	5.8	343.3	3.2	0.0173	0.0014	92	41.2	462.9
Plesovice	N_Ples_ - 7.d	N	11/11/2019 (2)	0.0538	0.0013	0.3989	0.0099	0.05422	0.00041	**359**	**55**	341.6	7.2	340.4	2.5	0.0164	0.0012	95	44.5	497.6
Plesovice	N_Ples_ - 8.d	N	11/11/2019 (2)	0.0528	0.0013	0.4016	0.0096	0.05524	0.00045	**311**	**55**	342.1	7	346.6	2.8	0.0192	0.0015	111	37.9	436.4
Plesovice	N_Ples_ - 9.d	N	11/11/2019 (2)	0.0611	0.0014	0.462	0.01	0.05496	0.00048	**636**	**51**	384.6	7.2	344.9	2.9	0.0284	0.0016	54	37.9	414.0
Plesovice	N_Ples_ - 10.d	N	11/11/2019 (2)	0.0546	0.0013	0.4025	0.0092	0.05411	0.00049	**374**	**54**	342.8	6.7	340.1	3.1	0.0194	0.0015	91	40.8	462.8
Plesovice	N_Ples_ - 11.d	N	11/11/2019 (2)	0.0541	0.0012	0.407	0.0089	0.0549	0.00041	**374**	**52**	347.3	6.5	344.5	2.5	0.0171	0.0013	92	46.6	517.7
Plesovice	N_Ples_ - 12.d	N	11/11/2019 (2)	0.0546	0.0013	0.4125	0.0094	0.05499	0.00037	**375**	**52**	350	6.7	345.1	2.3	0.0195	0.0012	92	43.1	489.7
Plesovice	N_Ples_ - 13.d	N	11/11/2019 (2)	0.0519	0.0012	0.3946	0.0091	0.05507	0.00046	**271**	**52**	337.8	6.7	345.6	2.8	0.0196	0.0014	128	46.6	516.3
Plesovice	N_Ples_ - 14.d	N	11/11/2019 (2)	0.0544	0.0011	0.4086	0.0078	0.05449	0.00042	**388**	**43**	348	5.7	342	2.6	0.0183	0.0012	88	52.6	568.4
Plesovice	N_Ples_ - 15.d	N	11/11/2019 (2)	0.05384	0.00086	0.4088	0.0063	0.05444	0.0004	**353**	**36**	347.7	4.5	341.7	2.5	0.0211	0.0013	97	72.5	725.8
Plesovice	N_Ples_ - 16.d	N	11/11/2019 (2)	0.0536	0.0011	0.4102	0.008	0.05521	0.00044	**359**	**44**	349.2	5.8	346.4	2.7	0.0195	0.0013	96	63.6	649.6
Plesovice	N_Ples_ - 17.d	N	11/11/2019 (2)	0.0528	0.0014	0.3977	0.0097	0.05432	0.0004	**298**	**56**	340	6.9	341	2.5	0.0205	0.0015	114	43.0	480.9
Plesovice	N_Ples_ - 18.d	N	11/11/2019 (2)	0.0529	0.0014	0.4015	0.0098	0.05456	0.00051	**316**	**58**	344.1	7	342.5	3.1	0.0198	0.0016	108	41.7	472.9
Plesovice	N_Ples_ - 19.d	N	11/11/2019 (2)	0.0516	0.0012	0.3876	0.0083	0.05404	0.00049	**255**	**49**	332.7	6.1	339.2	3	0.018	0.0013	133	41.6	470.8
Plesovice	N_Ples_ - 20.d	N	11/11/2019 (2)	0.053	0.001	0.4045	0.0077	0.05458	0.00044	**325**	**42**	345	5.5	342.6	2.7	0.0179	0.0014	105	45.4	508.7
Plesovice	N_Ples_ - 21.d	N	12/11/2019 (3)	0.0516	0.0015	0.391	0.01	0.05444	0.00047	**255**	**61**	335.3	7.2	341.7	2.9	0.0187	0.0014	134	36.2	415.1
Plesovice	N_Ples_ - 22.d	N	12/11/2019 (3)	0.0532	0.0014	0.404	0.01	0.05476	0.00054	**329**	**57**	343.5	7.4	343.6	3.3	0.0177	0.0016	104	30.2	366.2
91500	N_91500_ - 1.d	N	11/11/2019 (2)	0.0749	0.0023	1.883	0.055	0.1822	0.002	**1040**	**64**	1075	19	1079	11	0.0593	0.0033	104	21.9	62.4
91500	N_91500_ - 2.d	N	11/11/2019 (2)	0.076	0.0022	1.932	0.055	0.1839	0.0023	**1084**	**57**	1089	19	1088	13	0.0562	0.0031	100	21.5	61.6
91500	N_91500_ - 3.d	N	11/11/2019 (2)	0.0746	0.002	1.898	0.048	0.1821	0.0021	**1059**	**57**	1078	17	1078	11	0.0568	0.0032	102	22.2	62.9
91500	N_91500_ - 4.d	N	11/11/2019 (2)	0.0747	0.002	1.847	0.049	0.1787	0.0023	**1053**	**54**	1064	17	1059	13	0.0579	0.0035	101	22.4	63.0
91500	N_91500_ - 5.d	N	11/11/2019 (2)	0.0747	0.0022	1.853	0.058	0.1775	0.0025	**1062**	**62**	1060	21	1053	14	0.0508	0.003	99	22.6	63.6
91500	N_91500_ - 6.d	N	11/11/2019 (2)	0.0759	0.0023	1.885	0.053	0.1771	0.0023	**1098**	**61**	1071	19	1051	12	0.0544	0.0028	96	22.9	64.7
91500	N_91500_ - 7.d	N	11/11/2019 (2)	0.0756	0.0023	1.843	0.052	0.1799	0.0023	**1059**	**64**	1058	19	1066	12	0.059	0.0035	101	22.7	63.7
91500	N_91500_ - 8.d	N	11/11/2019 (2)	0.0757	0.0023	1.853	0.059	0.1794	0.0024	**1078**	**60**	1060	21	1063	13	0.0589	0.0037	99	22.6	63.3
91500	N_91500_ - 9.d	N	11/11/2019 (2)	0.0744	0.0019	1.85	0.049	0.1793	0.0021	**1059**	**55**	1062	17	1063	11	0.061	0.0036	100	22.3	63.7
91500	N_91500_ - 10.d	N	11/11/2019 (2)	0.0726	0.0021	1.848	0.052	0.1856	0.0023	**982**	**61**	1058	19	1097	13	0.0624	0.0036	112	22.3	63.7
91500	N_91500_ - 11.d	N	11/11/2019 (2)	0.0751	0.0021	1.853	0.051	0.1801	0.0022	**1082**	**58**	1071	18	1068	12	0.0581	0.0036	99	22.3	63.4
91500	N_91500_ - 12.d	N	11/11/2019 (2)	0.0748	0.0024	1.865	0.057	0.1804	0.0021	**1043**	**63**	1064	20	1072	12	0.0599	0.0036	103	22.5	63.4
91500	N_91500_ - 13.d	N	11/11/2019 (2)	0.077	0.0023	1.864	0.053	0.1764	0.0024	**1124**	**57**	1070	18	1047	13	0.0574	0.0034	93	21.7	62.3
91500	N_91500_ - 14.d	N	11/11/2019 (2)	0.0752	0.0023	1.865	0.055	0.1794	0.0025	**1064**	**62**	1067	19	1063	14	0.0567	0.0037	100	21.3	61.8

CA: Chemical Abrasion; TA: Thermally Annealed; N: Normal

Appendix 4 Table A7: LA-ICP MS U-Pb data for standard zircon analyzed at the University of Adelaide

Standard	Spot Number	Zircon Treatment	Analytical Session	$^{207}Pb/^{206}Pb$	2σ	$^{207}Pb/^{235}U$	2σ	$^{206}Pb/^{238}U$	2σ	$^{207}Pb/^{206}Pb$	2σ	$^{207}Pb/^{235}Pb$	2σ	$^{206}Pb/^{238}U$	σ	$^{208}Pb/^{232}Th$	2σ	% Conc	Th ppm	U ppm
91500	N_91500_ - 15.d	N	11/11/2019 (2)	0.0746	0.0022	1.854	0.05	0.179	0.0024	**1083**	**59**	1064	18	1061	13	0.0599	0.0037	98	22.1	62.4
91500	N_91500_ - 16.d	N	11/11/2019 (2)	0.0745	0.0024	1.879	0.057	0.1806	0.0022	**1068**	**66**	1076	21	1071	12	0.0636	0.0034	100	22.4	63.1
91500	N_91500_ - 17.d	N	11/11/2019 (2)	0.0755	0.0023	1.898	0.052	0.1794	0.002	**1122**	**58**	1084	19	1063	11	0.0617	0.0039	95	22.5	63.0
91500	N_91500_ - 18.d	N	11/11/2019 (2)	0.0738	0.0024	1.863	0.054	0.1809	0.0025	**1063**	**66**	1068	20	1074	13	0.061	0.004	101	22.3	63.5
91500	N_91500_ - 19.d	N	11/11/2019 (2)	0.0737	0.0022	1.834	0.053	0.1788	0.0023	**1033**	**61**	1056	19	1060	13	0.0595	0.0035	103	22.0	62.9
91500	N_91500_ - 20.d	N	11/11/2019 (2)	0.0737	0.002	1.806	0.053	0.1764	0.0022	**1043**	**58**	1052	18	1048	12	0.0577	0.0037	100	21.4	62.1
91500	N_91500_ - 21.d	N	12/11/2019 (3)	0.0748	0.0021	1.848	0.045	0.1761	0.0019	**1064**	**54**	1067	15	1046	11	0.0582	0.0033	98	21.4	62.2
91500	N_91500_ - 22.d	N	12/11/2019 (3)	0.0743	0.0023	1.847	0.055	0.1803	0.0023	**1031**	**63**	1061	19	1068	13	0.0601	0.0033	104	21.4	61.9
GJ1	HT_GJ_ - 1.d	TA	11/11/2019 (2)	0.0601	0.0011	0.829	0.015	0.09861	0.00082	**611**	**41**	612.1	8.3	606.2	4.8	0.0302	0.0041	99	285	9.5
GJ1	HT_GJ_ - 2.d	TA	11/11/2019 (2)	0.0589	0.0012	0.798	0.016	0.09717	0.00083	**563**	**46**	595.2	9.3	597.8	4.9	0.0304	0.0039	106	289	9.47
GJ1	HT_GJ_ - 3.d	TA	11/11/2019 (2)	0.0622	0.0015	0.838	0.02	0.09765	0.00071	**681**	**52**	617	11	600.6	4.1	0.0319	0.004	88	286.4	9.6
GJ1	HT_GJ_ - 4.d	TA	11/11/2019 (2)	0.0605	0.0011	0.822	0.015	0.09773	0.00079	**633**	**39**	607.8	8.6	601.6	4.5	0.0302	0.0038	95	287.6	9.51
GJ1	HT_GJ_ - 5.d	TA	11/11/2019 (2)	0.0591	0.0013	0.813	0.016	0.09793	0.00083	**565**	**46**	604	9.1	602.2	4.9	0.0325	0.004	107	287.3	9.7
GJ1	HT_GJ_ - 6.d	TA	11/11/2019 (2)	0.0601	0.0012	0.816	0.016	0.09846	0.00088	**588**	**44**	604.7	9.2	605.3	5.2	0.0308	0.0038	103	287	9.3
GJ1	HT_GJ_ - 7.d	TA	11/11/2019 (2)	0.0607	0.0011	0.819	0.017	0.09767	0.00077	**631**	**43**	608.1	9.2	600.7	4.5	0.0305	0.0039	95	287	9.37
GJ1	HT_GJ_ - 8.d	TA	11/11/2019 (2)	0.06	0.0013	0.808	0.017	0.09756	0.00088	**600**	**45**	602	9.6	600	5.2	0.0299	0.0044	100	287	9.65
GJ1	HT_GJ_ - 9.d	TA	11/11/2019 (2)	0.0599	0.0012	0.802	0.014	0.09759	0.00077	**582**	**42**	598.1	7.9	600.2	4.5	0.0304	0.0043	103	288	9.64
GJ1	HT_GJ_ - 10.d	TA	11/11/2019 (2)	0.0595	0.0012	0.803	0.016	0.09828	0.00071	**603**	**44**	599.3	9	604.3	4.2	0.0294	0.0038	100	286	9.46
GJ1	HT_GJ_ - 11.d	TA	11/11/2019 (2)	0.061	0.0013	0.81	0.017	0.09793	0.00084	**634**	**47**	603.2	9.2	602.2	4.9	0.0328	0.0044	95	286.8	9.49
GJ1	HT_GJ_ - 12.d	TA	11/11/2019 (2)	0.0605	0.0014	0.813	0.018	0.09768	0.0008	**601**	**51**	603	10	600.7	4.7	0.0299	0.0043	100	287	9.58
GJ1	HT_GJ_ - 13.d	TA	11/11/2019 (2)	0.0604	0.0014	0.821	0.018	0.09864	0.00092	**628**	**51**	607.2	9.9	606.4	5.4	0.0323	0.0045	97	289.3	9.62
GJ1	HT_GJ_ - 14.d	TA	11/11/2019 (2)	0.0611	0.0011	0.816	0.015	0.09696	0.00088	**643**	**42**	605.9	8.4	596.5	5.2	0.0313	0.0037	93	284.8	9.26
GJ1	HT_GJ_ - 15.d	TA	11/11/2019 (2)	0.0603	0.0011	0.821	0.014	0.09843	0.00087	**610**	**40**	607.8	8	605.1	5.1	0.03	0.0044	99	286.8	9.64
GJ1	HT_GJ_ - 16.d	TA	11/11/2019 (2)	0.0594	0.0011	0.801	0.014	0.09767	0.00084	**584**	**41**	597.1	8.3	600.7	4.9	0.0296	0.004	103	287.4	9.56
GJ1	HT_GJ_ - 17.d	TA	11/11/2019 (2)	0.0605	0.0014	0.818	0.018	0.09751	0.00085	**613**	**53**	606.5	9.8	599.7	5	0.0269	0.0039	98	286.1	9.43
GJ1	HT_GJ_ - 18.d	TA	11/11/2019 (2)	0.0607	0.0012	0.822	0.015	0.09781	0.00095	**620**	**42**	608.3	8.6	601.5	5.6	0.0349	0.0045	97	288	9.53
GJ1	HT_GJ_ - 19.d	TA	11/11/2019 (2)	0.0586	0.0012	0.809	0.017	0.09858	0.00086	**554**	**42**	602.7	9.3	606	5	0.0335	0.0043	109	286.8	9.7
GJ1	HT_GJ_ - 20.d	TA	11/11/2019 (2)	0.0605	0.0015	0.83	0.019	0.09748	0.00077	**624**	**54**	614	11	599.6	4.5	0.0301	0.0042	96	287	9.27
GJ1	HT_GJ_ - 21.d	TA	12/11/2019 (3)	0.0605	0.0012	0.821	0.016	0.09806	0.00074	**604**	**41**	608.4	8.9	603	4.4	0.0292	0.0037	100	287	9.69
GJ1	HT_GJ_ - 22.d	TA	12/11/2019 (3)	0.0598	0.0011	0.812	0.016	0.09753	0.00081	**595**	**41**	603.6	8.8	599.9	4.8	0.0317	0.004	101	287	9.36
91500	HT_91500_ - 1.d	TA	11/11/2019 (2)	0.0769	0.002	1.925	0.048	0.181	0.0023	**1097**	**53**	1089	16	1072	13	0.0634	0.003	98	79.1	31.7
91500	HT_91500_ - 2.d	TA	11/11/2019 (2)	0.0755	0.0021	1.887	0.05	0.1798	0.0019	**1070**	**57**	1076	17	1067	10	0.0586	0.0029	100	79.1	31.9
91500	HT_91500_ - 3.d	TA	11/11/2019 (2)	0.0754	0.002	1.881	0.048	0.1794	0.0019	**1081**	**53**	1076	17	1066	11	0.0537	0.0026	99	83.7	31.3
91500	HT_91500_ - 4.d	TA	11/11/2019 (2)	0.0765	0.0019	1.872	0.048	0.1776	0.002	**1100**	**52**	1074	17	1054	11	0.055	0.0026	96	82.6	31.2
91500	HT_91500_ - 5.d	TA	11/11/2019 (2)	0.0769	0.0021	1.908	0.05	0.1784	0.002	**1126**	**55**	1083	17	1058	11	0.0544	0.0027	94	79.3	29.7
91500	HT_91500_ - 6.d	TA	11/11/2019 (2)	0.0762	0.0019	1.873	0.046	0.1767	0.0019	**1112**	**50**	1070	17	1049	11	0.0523	0.0031	94	79.9	29.9
91500	HT_91500_ - 7.d	TA	11/11/2019 (2)	0.0754	0.0022	1.865	0.049	0.181	0.0022	**1071**	**58**	1068	18	1072	12	0.0569	0.0031	100	79.8	30.19
91500	HT_91500_ - 8.d	TA	11/11/2019 (2)	0.074	0.0017	1.854	0.047	0.1824	0.0019	**1043**	**48**	1062	17	1080	10	0.0567	0.0029	104	77.5	29.7
91500	HT_91500_ - 9.d	TA	11/11/2019 (2)	0.0744	0.0021	1.863	0.05	0.1831	0.0024	**1047**	**56**	1069	17	1085	13	0.0583	0.0033	104	77.3	28.6
91500	HT_91500_ - 10.d	TA	11/11/2019 (2)	0.0755	0.0022	1.886	0.05	0.1805	0.0023	**1092**	**60**	1072	18	1070	12	0.0588	0.0034	98	80.4	29
91500	HT_91500_ - 11.d	TA	11/11/2019 (2)	0.0768	0.002	1.909	0.051	0.1811	0.0019	**1123**	**51**	1080	18	1073	10	0.0606	0.0031	96	78	30.3
91500	HT_91500_ - 12.d	TA	11/11/2019 (2)	0.0746	0.0024	1.863	0.053	0.1798	0.0023	**1054**	**66**	1065	19	1066	13	0.0607	0.0031	101	77.7	30.4
91500	HT_91500_ - 13.d	TA	11/11/2019 (2)	0.075	0.002	1.873	0.049	0.1828	0.002	**1057**	**56**	1073	18	1082	11	0.0618	0.0034	102	82.8	29.4
91500	HT_91500_ - 14.d	TA	11/11/2019 (2)	0.0729	0.0019	1.804	0.043	0.1805	0.0021	**999**	**53**	1047	16	1070	11	0.0572	0.0032	107	85.3	29.3
91500	HT_91500_ - 15.d	TA	11/11/2019 (2)	0.0743	0.0018	1.865	0.043	0.1822	0.0021	**1047**	**51**	1072	15	1079	11	0.0633	0.0033	103	76.9	29.16
91500	HT_91500_ - 16.d	TA	11/11/2019 (2)	0.0757	0.002	1.898	0.054	0.1807	0.002	**1091**	**53**	1081	19	1070	11	0.064	0.0033	98	74.4	28.6
91500	HT_91500_ - 17.d	TA	11/11/2019 (2)	0.0732	0.0019	1.834	0.047	0.1814	0.0021	**1027**	**54**	1055	17	1074	12	0.0616	0.0029	105	82	31.2
91500	HT_91500_ - 18.d	TA	11/11/2019 (2)	0.0739	0.002	1.893	0.044	0.1834	0.0023	**1040**	**53**	1077	16	1086	12	0.0637	0.0032	104	79.3	30.7
91500	HT_91500_ - 19.d	TA	11/11/2019 (2)	0.0735	0.0018	1.835	0.046	0.1789	0.0018	**1024**	**52**	1057	17	1062	10	0.056	0.0033	104	81.2	30
91500	HT_91500_ - 20.d	TA	11/11/2019 (2)	0.0766	0.0022	1.874	0.05	0.1764	0.0019	**1092**	**56**	1074	18	1047	11	0.0584	0.0033	96	80.6	30.5
91500	HT_91500_ - 21.d	TA	12/11/2019 (3)	0.0737	0.002	1.816	0.045	0.1797	0.002	**1015**	**55**	1056	17	1065	11	0.0585	0.0032	105	80	29.73
91500	HT_91500_ - 22.d	TA	12/11/2019 (3)	0.0756	0.0018	1.935	0.05	0.1825	0.0023	**1084**	**50**	1091	17	1080	12	0.0574	0.0031	100	80.7	30.7

CA: Chemical Abrasion; TA: Thermally Annealed; N: Normal

Appendix 4 Table A7: LA-ICP MS U-Pb data for standard zircon analyzed at the University of Adelaide

Standard	Spot Number	Zircon Treatment	Analytical Session	$^{207}Pb/^{206}Pb$	2σ	$^{207}Pb/^{235}U$	2σ	$^{206}Pb/^{238}U$	2σ	**$^{207}Pb/^{206}Pb$**	2σ	$^{207}Pb/^{235}Pb$	2σ	$^{206}Pb/^{238}U$	2σ	$^{208}Pb/^{232}Th$	2σ	% Conc	Th ppm	U ppm
Plesovice	HT_Plesovice_ - 1.d	TA	11/11/2019 (2)	0.0537	0.0017	0.399	0.013	0.05396	0.00058	**352**	**70**	340.4	9.6	338.7	3.5	0.0179	0.0018	96	267.9	22.14
Plesovice	HT_Plesovice_ - 2.d	TA	11/11/2019 (2)	0.0531	0.0017	0.411	0.013	0.05535	0.0006	**330**	**70**	351.4	9.5	347.3	3.6	0.017	0.0023	105	265.4	21.36
Plesovice	HT_Plesovice_ - 3.d	TA	11/11/2019 (2)	0.0535	0.0019	0.4	0.013	0.05419	0.00063	**334**	**75**	343.1	9.7	340.2	3.9	0.0171	0.0021	102	249.4	20.98
Plesovice	HT_Plesovice_ - 4.d	TA	11/11/2019 (2)	0.0552	0.0014	0.409	0.01	0.05405	0.00054	**396**	**58**	348	7.6	339.7	3.3	0.0157	0.0015	86	385	33.63
Plesovice	HT_Plesovice_ - 5.d	TA	11/11/2019 (2)	0.0532	0.0013	0.3939	0.0082	0.05304	0.0005	**334**	**52**	336.7	6	333.2	3	0.0165	0.0015	100	420	37
Plesovice	HT_Plesovice_ - 6.d	TA	11/11/2019 (2)	0.0532	0.0014	0.4	0.01	0.05322	0.0005	**330**	**59**	341.6	7.4	334.3	3	0.019	0.0015	101	416	38.5
Plesovice	HT_Plesovice_ - 7.d	TA	11/11/2019 (2)	0.0531	0.0014	0.3953	0.0095	0.05434	0.00051	**327**	**58**	338.2	7	341.1	3.1	0.0184	0.0013	104	459	39.3
Plesovice	HT_Plesovice_ - 8.d	TA	11/11/2019 (2)	0.0541	0.0016	0.398	0.011	0.05389	0.00049	**348**	**63**	340.9	8	338.3	3	0.02	0.0015	97	424	35.7
Plesovice	HT_Plesovice_ - 9.d	TA	11/11/2019 (2)	0.0528	0.0013	0.4011	0.0097	0.05464	0.00048	**315**	**51**	342.4	7.1	342.9	2.9	0.0188	0.0016	109	408	37.8
Plesovice	HT_Plesovice_ - 10.d	TA	11/11/2019 (2)	0.0527	0.0014	0.389	0.01	0.05357	0.0005	**318**	**58**	333.9	7.3	336.4	3	0.0174	0.0016	106	398	33.9
Plesovice	HT_Plesovice_ - 11.d	TA	11/11/2019 (2)	0.053	0.0013	0.3969	0.0092	0.05464	0.00055	**309**	**54**	338.8	6.7	342.9	3.3	0.0199	0.0014	111	421	35
Plesovice	HT_Plesovice_ - 12.d	TA	11/11/2019 (2)	0.0512	0.0016	0.382	0.011	0.05406	0.00065	**248**	**64**	327.7	7.7	339.4	4	0.0195	0.0022	137	257.7	20.93
Plesovice	HT_Plesovice_ - 13.d	TA	11/11/2019 (2)	0.0539	0.0021	0.397	0.014	0.05385	0.00067	**338**	**81**	338	10	338.5	4	0.0172	0.0021	100	234.2	20.49
Plesovice	HT_Plesovice_ - 14.d	TA	11/11/2019 (2)	0.0523	0.002	0.382	0.014	0.0537	0.00068	**287**	**79**	329	10	337.1	4.2	0.0167	0.002	117	232.1	19.39
Plesovice	HT_Plesovice_ - 15.d	TA	11/11/2019 (2)	0.0522	0.0016	0.392	0.011	0.0539	0.00065	**287**	**63**	334.7	7.9	338.4	4	0.0182	0.0021	118	261.4	21.55
Plesovice	HT_Plesovice_ - 16.d	TA	11/11/2019 (2)	0.0526	0.0017	0.388	0.012	0.05338	0.00056	**309**	**69**	332.6	8.9	335.2	3.4	0.0172	0.0019	108	271.1	23.04
Plesovice	HT_Plesovice_ - 17.d	TA	11/11/2019 (2)	0.0533	0.0018	0.4	0.012	0.05448	0.00071	**320**	**73**	340.8	8.8	341.9	4.4	0.0194	0.0022	107	273.2	23.01
Plesovice	HT_Plesovice_ - 18.d	TA	11/11/2019 (2)	0.0543	0.0017	0.402	0.013	0.05389	0.00067	**363**	**69**	344.2	9.4	338.7	4	0.0179	0.0021	93	252.6	21.39
Plesovice	HT_Plesovice_ - 19.d	TA	11/11/2019 (2)	0.0537	0.0018	0.406	0.013	0.05452	0.00056	**343**	**73**	347	9.1	342.2	3.4	0.0152	0.0019	100	259.2	21.48
Plesovice	HT_Plesovice_ - 20.d	TA	11/11/2019 (2)	0.0549	0.0017	0.409	0.012	0.05299	0.00063	**394**	**67**	347.1	9	332.8	3.8	0.0174	0.0018	84	251.6	21.23
Plesovice	HT_Plesovice_ - 21.d	TA	12/11/2019 (3)	0.0538	0.0017	0.399	0.011	0.05379	0.00063	**340**	**67**	341.1	8.4	338.1	3.8	0.0173	0.0021	99	271	25.5
Plesovice	HT_Plesovice_ - 22.d	TA	12/11/2019 (3)	0.055	0.0016	0.414	0.012	0.05376	0.00061	**389**	**61**	351.4	8.5	337.5	3.7	0.0196	0.0019	87	323.4	26.94

CA: Chemical Abrasion; TA: Thermally Annealed; N: Normal

Appendix 4 Table A7: LA-ICP MS U-Pb data for standard zircon analyzed at the University of Adelaide

Standard	Spot Number	Zircon Treatment	Analytical Session	P	Ti	Y	Nb	La	Ce	Pr	Nd	Sm	Eu	Gd	Tb	Dy	Ho	Er	Tm	Yb	Lu	Hf
				ppm	ppm	ppm	ppm	ppm	ppm	ppm	ppm	ppm	ppm	ppm	ppm	ppm	ppm	ppm	ppm	ppm	ppm	ppm
GJ1	HT_GJ-1_ - 1.d	TA	30/09/2019 (2)	49	3.3	214.5	1.46	b.d.l	13.53	0.0236	0.515	1.27	0.911	5.9	1.594	17.63	5.75	27	5.72	52.5	11.29	6234
GJ1	HT_GJ-1_ - 2.d	TA	30/09/2019 (2)	71	2.37	225.6	1.41	b.d.l	13.92	0.0203	0.469	1.23	0.805	6.14	1.7	18.47	6.12	27.84	5.7	55.4	11.38	6436
GJ1	HT_GJ-1_ - 3.d	TA	30/09/2019 (2)	36	2.44	221.7	1.62	b.d.l	13.75	0.0201	0.422	1.07	0.84	5.82	1.524	17.62	5.93	26.19	5.61	52.5	11.08	6612
GJ1	HT_GJ-1_ - 4.d	TA	30/09/2019 (2)	36	3.2	225	1.5	b.d.l	14.14	0.0219	0.463	1.1	0.808	5.99	1.579	17.47	6.12	27.22	5.83	54.1	11.58	6627
GJ1	HT_GJ-1_ - 5.d	TA	30/09/2019 (2)	41	2.9	226.7	1.56	b.d.l	14.21	0.0182	0.414	0.98	0.886	5.92	1.67	17.77	6.17	27.59	5.53	55.8	11.35	6406
GJ1	HT_GJ-1_ - 6.d	TA	30/09/2019 (2)	15	3.7	229.6	1.4	b.d.l	14.23	0.021	0.389	1.21	0.834	6.14	1.673	17.94	5.96	28.08	5.75	55.5	11.85	6375
GJ1	HT_GJ-1_ - 7.d	TA	30/09/2019 (2)	71	3.5	223.5	1.4	b.d.l	13.91	0.0218	0.525	1.04	0.886	6.29	1.484	18.03	5.92	28.38	5.76	53.7	11.31	6337
GJ1	HT_GJ-1_ - 8.d	TA	30/09/2019 (2)	49	1.96	222.4	1.32	b.d.l	14.06	0.0103	0.366	1.16	0.841	6.07	1.71	17.19	5.96	27.59	5.62	54.6	11.39	6327
GJ1	HT_GJ-1_ - 9.d	TA	30/09/2019 (2)	b.d.l	2.37	234.9	1.5	b.d.l	14.5	0.0232	0.438	1.17	0.806	6.12	1.702	17.84	6.12	27.96	5.63	55.9	11.56	6642
GJ1	HT_GJ-1_ - 10.d	TA	30/09/2019 (2)	38	3.1	233.5	1.46	b.d.l	14.43	0.0177	0.446	1.05	0.793	6.37	1.547	18	6.04	27.9	5.78	55.4	11.69	6610
GJ1	HT_GJ-1_ - 11.d	TA	30/09/2019 (2)	25	2.8	226.4	1.41	b.d.l	14.32	0.0158	0.482	1.14	0.854	6.07	1.802	18.55	5.91	27.98	5.8	54.4	11.52	6506
GJ1	HT_GJ-1_ - 12.d	TA	30/09/2019 (2)	64	2.8	223.8	1.25	b.d.l	13.94	0.024	0.546	1.11	0.855	6.08	1.576	17.92	5.87	27.66	5.71	54.2	11.59	6468
GJ1	HT_GJ-1_ - 13.d	TA	30/09/2019 (2)	34	2.33	225.9	1.34	b.d.l	13.6	0.0223	0.399	1.13	0.857	6.5	1.62	17.8	6.03	26.25	5.94	52.5	11.22	6421
GJ1	HT_GJ-1_ - 14.d	TA	30/09/2019 (2)	24	2.9	220.7	1.34	b.d.l	13.7	0.0238	0.392	1.17	0.798	5.79	1.7	16.43	5.91	26.7	5.61	51.7	11.06	6383
GJ1	HT_GJ-1_ - 15.d	TA	30/09/2019 (2)	b.d.l	2.39	228	1.47	b.d.l	14.29	0.0184	0.484	1.28	0.782	5.92	1.68	18.49	6.01	28.48	5.6	56.3	11.75	6464
GJ1	HT_GJ-1_ - 16.d	TA	30/09/2019 (2)	34	2.6	230.7	1.57	b.d.l	14.35	0.0325	0.52	1.13	0.775	6.13	1.77	18.21	6.02	29.82	5.77	57.8	11.67	6378
Plesovice	ples_ - 1.d	N	30/09/2019 (2)	358	66.1	374.4	5.07	0.0062	1.932	0.088	1.03	2.33	0.577	9.34	3.71	40.8	11.07	40.22	6.68	43.7	6.11	10320
Plesovice	ples_ - 2.d	N	30/09/2019 (2)	344	67.2	373.5	5.04	0.0104	1.888	0.089	1.01	2.13	0.632	9.64	3.76	39.46	10.71	41.4	6.67	46	6.1	10300
Plesovice	ples_ - 3.d	N	30/09/2019 (2)	358	67.6	368.2	5.03	0.0047	1.936	0.091	1.1	2.11	0.646	10.02	3.71	40.21	10.59	39.99	6.5	43.6	6.22	10470
Plesovice	ples_ - 4.d	N	30/09/2019 (2)	341	61.3	371.6	5.05	0.005	1.935	0.098	1.23	2.4	0.652	10.28	3.74	40.4	11.1	39.52	6.28	45.4	5.98	10480
Plesovice	ples_ - 5.d	N	30/09/2019 (2)	374	63.2	377.6	5.12	0.0099	1.899	0.076	1.2	2.2	0.667	9.88	3.74	40.7	11.05	39.79	6.59	46	6.24	10350
Plesovice	ples_ - 6.d	N	30/09/2019 (2)	422	65.8	445	5.01	0.0099	2.283	0.162	2.06	3.75	0.859	14.09	4.82	49.9	13.62	47.5	7.43	50.5	6.99	10340
Plesovice	ples_ - 7.d	N	30/09/2019 (2)	393	65.6	387.4	5.31	0.0124	2.021	0.084	1.24	2.36	0.699	11.32	3.89	42.3	11.39	42.2	6.7	45.7	6.48	10050
Plesovice	ples_ - 8.d	N	30/09/2019 (2)	394	60.2	389.9	5.39	0.014	2.092	0.106	1.36	2.49	0.704	11.23	3.95	43.6	11.6	43.6	6.84	47.1	6.48	10130
Plesovice	ples_ - 9.d	N	30/09/2019 (2)	380	64.6	390.5	5.16	0.013	1.981	0.097	1.33	2.36	0.599	10.9	3.94	42.5	11.67	41.4	6.94	47.7	6.49	10410
Plesovice	ples_ - 10.d	N	30/09/2019 (2)	450	73.9	445	4.56	0.0117	1.935	0.099	1.4	2.74	0.721	11.88	4.36	48.1	12.94	47.6	7.83	53.6	7.64	10500
Plesovice	ples_ - 11.d	N	30/09/2019 (2)	380	72.4	393	4.92	0.0088	1.925	0.096	1.2	2.61	0.615	10.77	3.73	41.9	11.63	42.5	7.01	49	6.52	10220
Plesovice	ples_ - 12.d	N	30/09/2019 (2)	411	73.9	385.3	5.26	0.0137	1.978	0.102	1.24	2.61	0.673	10.53	3.94	42.8	11.49	42.4	6.75	47.1	6.46	10220
Plesovice	ples_ - 13.d	N	30/09/2019 (2)	457	66.2	508.1	4.95	0.0252	2.573	0.241	2.69	4.93	1.186	16.89	5.38	56.4	15.33	53.3	8.58	56.7	7.83	10120
Plesovice	ples_ - 14.d	N	30/09/2019 (2)	523	74.5	513.3	4.3	0.0143	2.031	0.151	1.66	3.3	0.889	13.67	4.88	54.9	15.32	55.1	9.18	63.3	9.27	10510
Plesovice	ples_ - 15.d	N	30/09/2019 (2)	495	75.2	521	4.5	0.0173	2.058	0.129	1.7	3.17	0.864	14.1	5.18	55	15.19	58.8	9.45	66.3	9.2	10550
Plesovice	ples_ - 16.d	N	30/09/2019 (2)	529	73.4	522.5	4.54	0.0169	2.028	0.147	1.69	3.22	0.864	13.43	5.06	56.3	15.24	57.7	9.2	66.3	9.22	10510
91500	95100_ - 1.d	N	30/09/2019 (2)	28	3.7	127	0.516	b.d.l	1.819	0.009	0.163	0.189	0.148	1.81	0.699	9.53	4.16	23.27	5.49	58.9	12.08	5240
91500	95100_ - 2.d	N	30/09/2019 (2)	30	3.4	125.7	0.499	b.d.l	1.851	0.0082	0.1	0.32	0.141	1.97	0.696	9.72	4.02	23.8	5.66	58.9	12.06	5216
91500	95100_ - 3.d	N	30/09/2019 (2)	b.d.l	3.8	124	0.587	b.d.l	1.829	0.0049	0.155	0.332	0.158	1.86	0.63	9.69	4.02	22.29	5.52	58	11.93	5301
91500	95100_ - 4.d	N	30/09/2019 (2)	b.d.l	2.8	128.2	0.456	b.d.l	1.828	0.007	0.101	0.293	0.15	1.92	0.758	9.93	4.14	23.83	5.41	58.7	12.39	5380
91500	95100_ - 5.d	N	30/09/2019 (2)	37	4.2	130.4	0.41	b.d.l	1.851	0.0075	0.154	0.334	0.149	1.84	0.717	10.2	4.18	23.13	5.75	60.1	12.21	5256
91500	95100_ - 6.d	N	30/09/2019 (2)	b.d.l	3.5	131	0.49	b.d.l	1.811	0.0071	0.079	0.286	0.221	1.78	0.717	10.15	4.18	24.1	5.7	62	12.51	5202
91500	95100_ - 7.d	N	30/09/2019 (2)	16	2.41	126.1	0.457	b.d.l	1.864	0.008	0.15	0.256	0.152	1.91	0.746	10.07	4.24	23.56	5.88	57.9	12.53	5195
91500	95100_ - 8.d	N	30/09/2019 (2)	b.d.l	3	122.3	0.554	0.0126	1.804	0.0108	0.16	0.278	0.168	1.79	0.686	9.93	4	22.72	5.51	56.1	11.89	5208
91500	95100_ - 9.d	N	30/09/2019 (2)	b.d.l	4.8	104.4	0.426	b.d.l	1.75	b.d.l	0.079	0.23	0.168	1.41	0.548	8.15	3.44	18.89	4.7	49.3	10.52	5276
91500	95100_ - 10.d	N	30/09/2019 (2)	28	4	104.5	0.521	b.d.l	1.737	0.0041	0.058	0.252	0.131	1.43	0.506	7.83	3.22	18.17	4.64	50.4	10.34	5292
91500	95100_ - 11.d	N	30/09/2019 (2)	25	3.8	99.1	0.502	b.d.l	1.73	b.d.l	0.035	0.284	0.116	1.44	0.44	7.67	3.06	17.81	4.34	48.1	10.04	5200
91500	95100_ - 12.d	N	30/09/2019 (2)	b.d.l	3.2	93.3	0.396	b.d.l	1.645	0.0022	0.102	0.131	0.111	1.3	0.501	6.99	3.04	17.14	4.33	46.5	9.39	5193
91500	95100_ - 13.d	N	30/09/2019 (2)	21	4.1	85.2	0.458	b.d.l	1.585	0.0033	0.088	0.182	0.107	1.23	0.472	6.41	2.72	15.91	3.89	41.1	8.67	5131
91500	95100_ - 14.d	N	30/09/2019 (2)	31	3.5	99.1	0.451	b.d.l	1.631	0.0042	0.066	0.267	0.123	1.25	0.474	7.37	3.03	18.08	4.37	44.3	9.69	5312
91500	95100_ - 15.d	N	30/09/2019 (2)	27	3.2	109.6	0.411	b.d.l	1.724	b.d.l	0.034	0.192	0.122	1.56	0.654	8.24	3.47	20.66	4.83	55.4	10.83	5340
91500	95100_ - 16.d	N	30/09/2019 (2)	32	2.6	90.8	0.431	b.d.l	1.639	b.d.l	0.083	0.175	0.135	1.43	0.499	6.92	2.92	17.7	4.04	45	9.11	5244
GJ1	N_GJ_ - 1.d	N	11/11/2019 (2)	38	2.37	217.9	1.38	0	14.27	0.0219	0.46	0.99	0.892	5.96	1.62	18.02	5.81	27.46	5.56	53	10.97	6461
GJ1	N_GJ_ - 2.d	N	11/11/2019 (2)	40	2.6	217.3	1.46	0	14.22	0.0233	0.427	1.03	0.797	6.19	1.55	17.92	5.97	26.47	5.63	52.8	11.36	6515
GJ1	N_GJ_ - 3.d	N	11/11/2019 (2)	33	1.02	212.7	1.45	0	14.19	0.0289	0.54	1.14	0.851	6.1	1.616	17.95	5.65	26.65	5.38	52.1	10.95	6422

CA: Chemical Abrasion; TA: Thermally Annealed; N: Normal

Appendix 4 Table A7: LA-ICP MS U-Pb data for standard zircon analyzed at the University of Adelaide

Standard	Spot Number	Zircon Treatment	Analytical Session	P	Ti	Y	Nb	La	Ce	Pr	Nd	Sm	Eu	Gd	Tb	Dy	Ho	Er	Tm	Yb	Lu	Hf
				ppm	ppm	ppm	ppm	ppm	ppm	ppm	ppm	ppm	ppm	ppm	ppm	ppm	ppm	ppm	ppm	ppm	ppm	ppm
GJ1	N_GJ_ - 4.d	N	11/11/2019 (2)	37	2.27	211.3	1.46	0	14.1	0.0231	0.473	1.2	0.782	6.13	1.57	17.83	5.79	26.25	5.48	51.5	11.05	6388
GJ1	N_GJ_ - 5.d	N	11/11/2019 (2)	18	2.9	218.2	1.32	0	14.35	0.0194	0.44	1.2	0.68	5.92	1.57	17.21	6	26.18	5.35	51.1	11.25	6416
GJ1	N_GJ_ - 6.d	N	11/11/2019 (2)	33	2.8	216.3	1.18	0	14.37	0.0223	0.399	1.29	0.775	5.92	1.76	17.72	5.78	27.06	5.31	52	11.45	6534
GJ1	N_GJ_ - 7.d	N	11/11/2019 (2)	-4	3	216.3	1.24	0	14.46	0.0243	0.353	1.28	0.855	5.8	1.61	17.55	5.83	26.23	5.53	52.5	10.87	6433
GJ1	N_GJ_ - 8.d	N	11/11/2019 (2)	41	2.5	216.4	1.49	0	14.27	0.027	0.39	1.11	0.853	5.66	1.51	17.17	5.67	26.87	5.43	50.1	10.87	6482
GJ1	N_GJ_ - 9.d	N	11/11/2019 (2)	53	2.3	210.6	1.5	0	14.17	0.0226	0.42	1.08	0.813	5.77	1.57	16.88	5.87	26.44	5.4	50.6	11.26	6478
GJ1	N_GJ_ - 10.d	N	11/11/2019 (2)	37	3.3	209.1	1.35	0	14.24	0.0167	0.328	1.05	0.79	6	1.51	16.8	5.64	25.88	5.25	49.7	10.76	6512
GJ1	N_GJ_ - 11.d	N	11/11/2019 (2)	51	0.48	209.1	1.37	0	14.05	0.02	0.41	1.02	0.79	5.89	1.578	16.86	5.6	25.98	5.32	50	10.36	6440
GJ1	N_GJ_ - 12.d	N	11/11/2019 (2)	44	3.6	207.9	1.24	0	14.32	0.0203	0.377	1.21	0.795	5.65	1.595	16.1	5.61	25.36	5.35	51.2	10.65	6401
GJ1	N_GJ_ - 13.d	N	11/11/2019 (2)	57	1.19	203.7	1.25	0	13.8	0.0183	0.354	1.22	0.695	5.17	1.57	15.94	5.43	25.7	5.3	50.6	10.5	6325
GJ1	N_GJ_ - 14.d	N	11/11/2019 (2)	36	1.32	203.4	1.36	0	13.91	0.0244	0.347	1.29	0.759	5.87	1.52	16.41	5.73	25.75	5.42	49.1	10.55	6383
GJ1	N_GJ_ - 15.d	N	11/11/2019 (2)	66	2.7	202.9	1.33	0	13.88	0.022	0.362	1.21	0.871	5.41	1.58	15.21	5.44	25.96	5.14	50.8	10.29	6297
GJ1	N_GJ_ - 16.d	N	11/11/2019 (2)	27	1.84	209.3	1.2	0	14.17	0.0206	0.57	0.98	0.786	5.59	1.51	16.45	5.55	25.54	5.32	51.4	10.75	6445
GJ1	N_GJ_ - 17.d	N	11/11/2019 (2)	31	2.06	201.4	1.44	0	13.91	0.0227	0.429	1.16	0.769	5.42	1.513	16	5.73	25.11	5.21	49.9	10.67	6248
GJ1	N_GJ_ - 18.d	N	11/11/2019 (2)	44	2.21	211	1.36	0	13.96	0.02	0.404	1.21	0.807	5.78	1.68	16.82	5.61	25.27	5.2	51.7	11.26	6391
GJ1	N_GJ_ - 19.d	N	11/11/2019 (2)	36	2.4	213.7	1.23	0	14.32	0.0185	0.35	1.27	0.836	5.76	1.56	17.77	5.63	25.95	5.39	52.7	11.12	6355
GJ1	N_GJ_ - 20.d	N	11/11/2019 (2)	34	1.02	213.3	1.38	0	14.21	0.019	0.44	1.25	0.797	6.07	1.6	16.78	5.98	26.93	5.3	52.2	10.91	6358
GJ1	N_GJ_ - 21.d	N	12/11/2019 (3)	47	2.6	212.7	1.37	0	14.12	0.0179	0.458	1.17	0.804	5.79	1.59	16.1	5.84	25.63	5.28	53.4	10.72	6392
GJ1	N_GJ_ - 22.d	N	12/11/2019 (3)	43	2.6	212.6	1.29	0	14.34	0.0212	0.446	1.03	0.842	5.85	1.6	17.28	5.78	26.38	5.51	52.4	10.8	6415
Plesovice	N_Ples_ - 1.d	N	11/11/2019 (2)	587	73.9	583.4	4.36	0.205	3.04	0.353	3.27	4.07	1.29	16.16	5.69	64	17.38	65	10.83	80.1	11.13	10430
Plesovice	N_Ples_ - 2.d	N	11/11/2019 (2)	440	59.8	431.1	3.74	0.395	4.46	0.84	5.56	3.93	1.36	11.95	4.29	44.9	13.04	48.6	8.16	59.6	8.59	10680
Plesovice	N_Ples_ - 3.d	N	11/11/2019 (2)	411	63.4	441.3	3.48	0.128	2.238	0.28	2.31	2.81	0.965	11.68	4.21	45.7	13.74	51.2	8.51	62.7	9.01	10600
Plesovice	N_Ples_ - 4.d	N	11/11/2019 (2)	439	60.7	427.4	3.63	0.059	1.761	0.15	1.71	2.53	0.771	11.23	4.08	45.5	12.68	49.9	8.27	60.6	8.85	10670
Plesovice	N_Ples_ - 5.d	N	11/11/2019 (2)	450	61.6	456.1	3.79	0.102	2.199	0.235	2.14	3.17	0.898	11.85	4.3	46.3	13.44	50.1	8.72	62.3	8.97	10670
Plesovice	N_Ples_ - 6.d	N	11/11/2019 (2)	358	55.7	366.4	3.13	0.0086	1.494	0.075	1.11	1.89	0.491	8.53	3.3	38.6	10.62	41.9	7.16	50.8	7.47	10930
Plesovice	N_Ples_ - 7.d	N	11/11/2019 (2)	369	58.3	401.5	3.33	0.0091	1.57	0.096	1.35	2.16	0.599	9.44	3.55	41.3	11.79	44.8	7.53	54.6	7.98	10850
Plesovice	N_Ples_ - 8.d	N	11/11/2019 (2)	299	47.5	310.3	3.02	0.0012	1.35	0.053	0.79	1.79	0.415	7.47	2.78	32	9.37	35.4	5.95	43.3	6.09	11030
Plesovice	N_Ples_ - 9.d	N	11/11/2019 (2)	308	45	287.6	2.91	0.189	2.436	0.354	2.48	1.95	0.725	7.27	2.63	30.61	8.32	31.54	5.46	39.7	5.59	10940
Plesovice	N_Ples_ - 10.d	N	11/11/2019 (2)	331	51.7	365.6	3.29	0.0038	1.498	0.088	1.16	2	0.57	8.95	3.15	36.9	10.8	42.5	7.13	50.8	7.46	10960
Plesovice	N_Ples_ - 11.d	N	11/11/2019 (2)	385	62.8	420.4	3.39	0.0055	1.651	0.108	1.19	2.06	0.627	9.61	3.83	44.5	12.15	47.49	8.12	59.4	8.18	10690
Plesovice	N_Ples_ - 12.d	N	11/11/2019 (2)	365	58.1	394.8	3.43	0.0092	1.58	0.089	0.99	2.03	0.655	9.37	3.6	40.28	11.39	44.2	7.69	56	7.99	10860
Plesovice	N_Ples_ - 13.d	N	11/11/2019 (2)	392	61.5	421.3	3.6	0.0139	1.729	0.108	1.3	2.37	0.627	10.37	3.63	43.4	12.48	47.1	8.28	59.3	8.7	10580
Plesovice	N_Ples_ - 14.d	N	11/11/2019 (2)	454	68.1	464.7	3.63	0.0104	1.703	0.119	1.25	2.88	0.718	11.41	4.25	47.9	13.48	51.8	8.98	63.1	9.07	10610
Plesovice	N_Ples_ - 15.d	N	11/11/2019 (2)	666	82.1	616.7	4.37	0.047	2.44	0.229	2.13	3.93	0.99	16.54	5.95	64	18.65	68.9	11.85	83.1	11.84	10420
Plesovice	N_Ples_ - 16.d	N	11/11/2019 (2)	571	69.6	548.3	3.99	0.048	2.25	0.194	2.22	3.4	0.985	14.45	5.33	59.5	16.28	61.6	10.41	73.5	10.9	10540
Plesovice	N_Ples_ - 17.d	N	11/11/2019 (2)	356	59.5	384.5	3.31	0.0075	1.523	0.108	1.19	2.13	0.581	9.33	3.33	40.6	11.41	42.9	7.5	53.2	7.96	10740
Plesovice	N_Ples_ - 18.d	N	11/11/2019 (2)	335	63.2	374.5	3.29	0.009	1.524	0.081	1.09	2.01	0.51	9.23	3.36	38.2	10.87	41.6	7.5	52.7	7.45	10760
Plesovice	N_Ples_ - 19.d	N	11/11/2019 (2)	313	56.4	366	3.24	0.0006	1.479	0.081	1.03	1.89	0.495	8.89	3.22	37.8	11.01	42.26	7.26	52.1	7.56	10850
Plesovice	N_Ples_ - 20.d	N	11/11/2019 (2)	334	63.4	406.8	3.59	0.0109	1.632	0.1	1.13	2.28	0.618	9.7	3.7	41.8	11.94	46.5	7.8	57.5	8.08	10810
Plesovice	N_Ples_ - 21.d	N	12/11/2019 (3)	288	49.4	311.5	2.84	0.0072	1.38	0.063	0.74	1.44	0.455	6.99	2.85	31.65	9.09	35.15	6.2	44.5	6.57	10930
Plesovice	N_Ples_ - 22.d	N	12/11/2019 (3)	229	39.7	229.4	2.28	0	1.222	0.0415	0.468	1.13	0.285	4.82	1.96	23.16	6.52	25.89	4.4	31.2	4.71	10920
91500	N_91500_ - 1.d	N	11/11/2019 (2)	36	4.5	111.7	0.77	0.0014	2.197	0.01	0.163	0.138	0.146	1.62	0.577	8.69	3.52	20.94	5.04	52.8	10.59	5644
91500	N_91500_ - 2.d	N	11/11/2019 (2)	36	3.3	110.6	0.75	0	2.088	0.0051	0.094	0.278	0.177	1.58	0.548	8.71	3.5	20.47	4.91	52.9	10.9	5564
91500	N_91500_ - 3.d	N	11/11/2019 (2)	24	2.3	112.8	0.632	0	2.187	0	0.047	0.172	0.143	1.71	0.58	8.75	3.65	20.77	5.09	53.4	10.88	5606
91500	N_91500_ - 4.d	N	11/11/2019 (2)	5	5.4	110.5	0.67	0	2.193	0	0.095	0.254	0.156	1.62	0.581	9.08	3.6	20.61	5.12	52.2	10.45	5581
91500	N_91500_ - 5.d	N	11/11/2019 (2)	17	3.4	113.5	0.59	0	2.283	0.0026	0.14	0.223	0.162	1.63	0.634	8.4	3.97	21.06	5.09	53.6	10.68	5566
91500	N_91500_ - 6.d	N	11/11/2019 (2)	8	3.3	115.5	0.75	0	2.243	0.0101	0.131	0.182	0.139	1.81	0.57	9.38	3.79	20.89	5.15	53	11.04	5657
91500	N_91500_ - 7.d	N	11/11/2019 (2)	35	3.9	114.6	0.7	0	2.173	0.0043	0.075	0.285	0.16	1.71	0.619	9.39	3.81	21.51	5.16	52.3	10.77	5614
91500	N_91500_ - 8.d	N	11/11/2019 (2)	25	4.2	113.8	0.71	0	2.147	0.0033	0.1	0.267	0.169	1.69	0.642	8.91	3.84	21.1	5.08	52.1	11.13	5566
91500	N_91500_ - 9.d	N	11/11/2019 (2)	-1	3.8	113.9	0.66	0	2.227	0	0.104	0.156	0.148	1.71	0.643	8.89	3.65	20.6	5.28	52.9	10.38	5546
91500	N_91500_ - 10.d	N	11/11/2019 (2)	7	2.8	113.5	0.631	0	2.141	0.001	0.085	0.226	0.151	1.64	0.639	9.11	3.81	21.32	5.23	51.7	11.38	5564
91500	N_91500_ - 11.d	N	11/11/2019 (2)	21	3.4	112.6	0.609	0	2.193	0.0021	0.101	0.352	0.136	1.71	0.572	8.54	3.57	20.98	5.24	51.2	10.98	5514

CA: Chemical Abrasion; TA: Thermally Annealed; N: Normal

Appendix 4 Table A7: LA-ICP MS U-Pb data for standard zircon analyzed at the University of Adelaide

Standard	Spot Number	Zircon Treatment	Analytical Session	P	Ti	Y	Nb	La	Ce	Pr	Nd	Sm	Eu	Gd	Tb	Dy	Ho	Er	Tm	Yb	Lu	Hf
				ppm	ppm	ppm	ppm	ppm	ppm	ppm	ppm	ppm	ppm	ppm	ppm	ppm	ppm	ppm	ppm	ppm	ppm	ppm
91500	N_91500_-12.d	N	11/11/2019 (2)	6	3.2	113.8	0.67	0	2.212	0.0026	0.106	0.311	0.158	1.86	0.619	9.16	3.66	20.85	5.01	52	10.74	5572
91500	N_91500_-13.d	N	11/11/2019 (2)	5	2.9	111.3	0.7	0	2.136	0.0032	0.102	0.28	0.139	1.56	0.588	8.46	3.62	19.86	5.04	51.4	10.66	5540
91500	N_91500_-14.d	N	11/11/2019 (2)	26	3.1	110.8	0.68	0	2.092	0.0021	0.076	0.319	0.159	1.49	0.646	8.91	3.62	19.71	5.17	52.1	10.44	5583
91500	N_91500_-15.d	N	11/11/2019 (2)	6	3.6	110.9	0.72	0	2.206	0	0.086	0.124	0.146	1.5	0.517	8.53	3.77	21.28	4.9	52.4	10.55	5491
91500	N_91500_-16.d	N	11/11/2019 (2)	14	3.3	113.6	0.613	0	2.188	0.0031	0.125	0.219	0.144	1.75	0.605	8.28	3.77	20.72	5.03	51.3	10.67	5583
91500	N_91500_-17.d	N	11/11/2019 (2)	-4	3.7	111.9	0.567	0	2.092	0.0045	0.046	0.242	0.167	1.6	0.655	8.64	3.6	19.8	5.05	51.8	10.93	5439
91500	N_91500_-18.d	N	11/11/2019 (2)	33	2.3	114	0.614	0	2.162	0.015	0.106	0.204	0.176	1.76	0.611	8.88	3.78	20.4	4.96	52.2	10.59	5493
91500	N_91500_-19.d	N	11/11/2019 (2)	21	2.6	113.3	0.61	0	2.161	0.0043	0.036	0.206	0.148	1.58	0.58	8.91	3.67	20.67	4.83	51	10.56	5509
91500	N_91500_-20.d	N	11/11/2019 (2)	24	3.4	109.2	0.535	0	2.077	0.00049	0.129	0.247	0.118	1.57	0.642	8.59	3.48	20.17	4.97	51.8	10.51	5517
91500	N_91500_-21.d	N	12/11/2019 (3)	28	3.1	110.1	0.71	0	2.173	0.0092	0.169	0.154	0.161	1.44	0.58	8.48	3.57	20.46	5.13	51.4	10.37	5519
91500	N_91500_-22.d	N	12/11/2019 (3)	12	4	108.1	0.75	0	2.116	0.0016	0.046	0.327	0.154	1.52	0.596	8.45	3.53	19.4	5.04	50.6	10.65	5494

CA: Chemical Abrasion; TA: Thermally Annealed; N: Normal

Appendix Table A8 LA-ICPMS isotopic U-Pb and trace element concentration data analyzed at Boise State University

	CA-TIMS	U	Th	Pb*	Th/U	$^{207}Pb/^{235}U$	±2s	$^{206}Pb/^{238}U$	±2s	error	$^{238}U/^{206}Pb$	±2s	$^{207}Pb/^{206}Pb$	±2s	$^{208}Pb/^{232}Th$	±2s	$^{207}Pb/^{206}Pb$	±2s	$^{207}Pb/^{235}U$	±2s	$^{206}Pb/^{238}U$	±2s	%
Analysis	label	ppm	ppm	ppm			(%)		(%)	corr.		(%)				(Ma)		(Ma)		(Ma)		(Ma)	disc
Plesovice - Primary zircon standard																						
PL 289 7/30/2014 10:45:24 PM (Run: 1)	std	657.93	65.89	37.39	0.10	0.38432	5.67	0.05229	4.74	0.84	19.12	4.74	0.05331	3.11	350	30	342	70	330	16	329	15	4
PL 290 7/30/2014 10:47:05 PM (Run: 1)	std	657.62	67.10	38.03	0.10	0.39103	5.24	0.05320	4.08	0.78	18.80	4.08	0.05330	3.28	351	28	342	74	335	15	334	13	2
PL 291 7/30/2014 10:48:46 PM (Run: 1)	std	665.40	68.87	38.86	0.10	0.40077	6.73	0.05376	5.81	0.86	18.60	5.81	0.05406	3.40	336	30	374	76	342	20	338	19	10
PL 292 7/30/2014 10:50:27 PM (Run: 1)	std	612.21	63.81	36.58	0.10	0.39877	6.28	0.05518	4.95	0.79	18.12	4.95	0.05241	3.86	323	24	303	88	341	18	346	17	15
PL 295 7/30/2014 11:12:35 PM (Run: 1)	std	658.27	67.45	38.12	0.10	0.38990	4.36	0.05340	3.05	0.70	18.73	3.05	0.05295	3.11	328	26	327	71	334	12	335	10	3
PL 296 7/30/2014 11:14:16 PM (Run: 1)	std	740.60	83.94	44.21	0.11	0.40881	5.37	0.05493	4.39	0.82	18.21	4.39	0.05398	3.10	318	29	370	70	348	16	345	15	7
PL 299 7/30/2014 11:33:04 PM (Run: 1)	std	894.54	141.59	53.63	0.16	0.40147	3.96	0.05424	3.46	0.87	18.44	3.46	0.05368	1.93	355	25	358	44	343	12	341	11	5
PL 300 7/30/2014 11:34:45 PM (Run: 1)	std	801.43	91.66	46.18	0.11	0.38674	4.00	0.05288	3.34	0.84	18.91	3.34	0.05304	2.19	341	26	331	50	332	11	332	11	0
PL 303 7/30/2014 11:57:00 PM (Run: 1)	std	760.06	84.26	43.81	0.11	0.37433	4.61	0.05303	3.19	0.69	18.86	3.19	0.05120	3.33	342	20	250	77	323	13	333	10	34
PL 304 7/30/2014 11:58:40 PM (Run: 1)	std	914.14	150.22	54.51	0.16	0.39407	5.13	0.05383	4.18	0.81	18.58	4.18	0.05309	2.97	358	21	333	67	337	15	338	14	2
PL 307 7/31/2014 12:17:30 AM (Run: 1)	std	755.97	87.62	43.91	0.12	0.39255	3.66	0.05337	2.65	0.72	18.74	2.65	0.05334	2.53	323	25	343	57	336	10	335	9	2
PL 308 7/31/2014 12:19:11 AM (Run: 1)	std	744.70	87.25	43.14	0.12	0.38834	4.13	0.05334	3.23	0.78	18.75	3.23	0.05280	2.58	303	25	320	59	333	12	335	11	5
PL 311 7/31/2014 12:41:28 AM (Run: 1)	std	740.21	84.98	43.73	0.11	0.40141	4.05	0.05423	2.99	0.74	18.44	2.99	0.05369	2.72	339	21	358	62	343	12	340	10	5
PL 312 7/31/2014 12:43:09 AM (Run: 1)	std	739.53	84.16	43.36	0.11	0.40146	4.00	0.05386	2.80	0.70	18.57	2.80	0.05406	2.86	328	25	373	64	343	12	338	9	10
PL 315 7/31/2014 1:02:00 AM (Run: 1)	std	704.76	77.51	41.15	0.11	0.39756	3.68	0.05345	2.86	0.78	18.71	2.86	0.05395	2.32	375	32	369	52	340	11	336	9	9
PL 316 7/31/2014 1:03:41 AM (Run: 1)	std	760.27	88.14	44.06	0.12	0.37751	4.45	0.05310	3.17	0.71	18.83	3.17	0.05156	3.12	364	32	266	72	325	12	334	10	26
PL 319 7/31/2014 1:25:52 AM (Run: 1)	std	754.33	87.66	43.58	0.12	0.39879	4.16	0.05297	3.33	0.80	18.88	3.33	0.05460	2.49	329	20	396	56	341	12	333	11	16
PL 320 7/31/2014 1:27:33 AM (Run: 1)	std	776.85	98.15	45.91	0.13	0.40594	3.35	0.05414	2.01	0.60	18.47	2.01	0.05438	2.68	320	25	387	60	346	10	340	7	12
PL 323 7/31/2014 1:46:18 AM (Run: 1)	std	700.04	77.36	41.19	0.11	0.40377	4.45	0.05398	3.13	0.70	18.52	3.13	0.05425	3.15	350	31	381	71	344	13	339	10	11
PL 324 7/31/2014 1:47:59 AM (Run: 1)	std	722.92	81.56	42.73	0.11	0.40400	4.19	0.05433	2.89	0.69	18.41	2.89	0.05393	3.03	329	19	368	68	345	12	341	10	8
PL 327 7/31/2014 2:10:13 AM (Run: 1)	std	478.10	49.36	28.68	0.10	0.39547	8.87	0.05543	7.00	0.79	18.04	7.00	0.05174	5.46	327	28	274	125	338	26	348	24	28
PL 328 7/31/2014 2:11:53 AM (Run: 1)	high $^{206}Pb/^{238}U$ variance	461.77	46.19	26.36	0.10	0.38049	9.87	0.05269	8.81	0.89	18.98	8.81	0.05237	4.44	326	38	302	101	327	28	331	28	10
PL 331 7/31/2014 2:30:37 AM (Run: 1)	std	510.17	51.53	29.31	0.10	0.38513	7.17	0.05290	6.29	0.88	18.90	6.29	0.05280	3.43	349	29	320	78	331	20	332	20	4
PL 335 7/31/2014 2:54:32 AM (Run: 1)	std	550.95	56.22	31.70	0.10	0.38475	6.65	0.05311	5.64	0.85	18.83	5.64	0.05254	3.53	321	37	309	80	331	19	334	18	8
PL 336 7/31/2014 2:56:13 AM (Run: 1)	std	499.50	51.44	29.43	0.10	0.39693	7.84	0.05414	6.08	0.78	18.47	6.08	0.05318	4.96	370	45	336	112	339	23	340	20	1
PL 340 7/31/2014 3:16:38 AM (Run: 1)	std	557.03	57.75	32.29	0.10	0.39203	7.11	0.05334	6.20	0.87	18.75	6.20	0.05331	3.49	347	25	342	79	336	20	335	20	2
PL 343 7/31/2014 3:38:54 AM (Run: 1)	std	552.05	57.76	31.55	0.10	0.39188	8.40	0.05270	7.44	0.89	18.98	7.44	0.05393	3.90	308	46	368	88	336	24	331	24	10
PL 344 7/31/2014 3:40:35 AM (Run: 1)	std	531.99	55.37	31.36	0.10	0.39589	8.18	0.05437	6.91	0.85	18.39	6.91	0.05281	4.37	329	38	320	99	339	24	341	23	7
PL 347 7/31/2014 3:57:36 AM (Run: 1)	std	645.32	71.41	38.41	0.11	0.39602	5.46	0.05468	4.93	0.90	18.29	4.93	0.05252	2.35	357	21	308	54	339	16	343	16	12
PL 348 7/31/2014 3:59:17 AM (Run: 1)	std	593.84	62.47	34.29	0.11	0.39736	6.18	0.05309	5.02	0.81	18.84	5.02	0.05429	3.60	337	25	383	81	340	18	333	16	13

Experiment 1 on July 31, 2014
Isotope ratio and date errors do not include systematic calibration errors of 0.60% ($^{207}Pb/^{206}Pb$) and 1.68% ($^{206}Pb/^{238}U$) (2 sigma).
Trace element concentrations were deleted from analyses known to have intersected inclusions of other minerals based on P and Ti.
Ablation used a laser spot size of 25 microns and a laser firing repetition rate of 5 Hz.
Activity of TiO_2 for Ti-in-Zircon temperature calculation is 0.8.

Appendix Table A8 LA-ICPMS isotopic U-Pb and trace element concentration data analyzed at Boise State University

Analysis	P	Ti	Y	Zr	Nb	La	Ce	Pr	Nd	Sm	Eu	Gd	Tb	Dy	Ho	Er	Tm	Yb	Lu	Hf	Ta	Th	U
	ppm	ppm	ppm	ppm	ppm	ppm	ppm	ppm	ppm	ppm	ppm	ppm	ppm	ppm	ppm	ppm	ppm	ppm	ppm	ppm	ppm	ppm	ppm
Plesovice - Primary zircon standard																							
PL 289 7/30/2014 10:45:24 PM (Run: 1)	387.67	79.18	546.99	545081.66	4.16		2.15	0.11	1.38	3.22	0.97	13.47	5.58	62.59	17.70	58.41	11.28	78.89	9.30	11524.56	2.70	65.89	657.93
PL 290 7/30/2014 10:47:05 PM (Run: 1)	414.80	79.20	561.56	555755.13	4.62		2.08	0.11	1.84	3.23	1.07	16.73	5.88	61.52	17.09	59.82	11.45	83.90	9.08	10701.37	3.03	67.10	657.62
PL 291 7/30/2014 10:48:46 PM (Run: 1)	416.66	79.65	553.00	508076.73	4.75		2.08	0.09	1.88	4.68	0.89	16.65	6.17	65.95	18.48	56.70	11.98	90.13	10.12	10524.77	2.50	68.87	665.40
PL 292 7/30/2014 10:50:27 PM (Run: 1)	379.09	73.35	494.31	517303.43	3.85		1.74	0.11	1.55	2.97	0.88	13.90	5.45	56.94	15.49	54.99	10.69	81.00	8.91	10643.65	3.02	63.81	612.21
PL 295 7/30/2014 11:12:35 PM (Run: 1)	409.68	83.75	568.64	561655.95	4.54		1.75	0.11	2.09	3.59	1.02	16.86	5.70	60.32	18.29	61.99	11.48	85.43	9.59	11588.98	2.96	67.45	658.27
PL 296 7/30/2014 11:14:16 PM (Run: 1)	545.62	87.82	654.30	544603.50	4.83		2.39	0.21	3.02	4.47	1.03	19.39	7.06	72.69	21.69	71.53	14.23	102.51	11.06	11467.96	3.04	83.94	740.60
PL 299 7/30/2014 11:33:04 PM (Run: 1)	477.66	71.06	700.94	544111.94	4.05	0.06	3.46	0.55	5.67	6.71	1.47	25.63	8.57	79.22	22.35	76.31	14.12	103.85	11.61	10551.04	3.60	141.59	894.54
PL 300 7/30/2014 11:34:45 PM (Run: 1)	599.30	95.81	720.88	531141.98	4.75		2.30	0.17	2.72	5.16	1.16	18.60	7.72	82.58	23.53	76.85	14.29	106.38	12.06	11096.96	2.94	91.66	801.43
PL 303 7/30/2014 11:57:00 PM (Run: 1)	537.33	92.44	685.64	539779.82	4.81	0.05	2.15	0.25	2.70	4.94	0.98	17.83	7.33	75.87	22.18	74.24	14.31	106.22	11.11	10613.08	2.93	84.26	760.06
PL 304 7/30/2014 11:58:40 PM (Run: 1)	440.80	66.41	678.51	513811.16	4.48	0.06	3.24	0.41	5.99	7.15	1.88	24.38	8.10	85.20	22.54	72.15	12.82	101.10	10.62	10380.19	3.45	150.22	914.14
PL 307 7/31/2014 12:17:30 AM (Run: 1)	551.10	91.30	713.36	544998.26	4.66		2.32	0.15	2.91	3.39	1.20	20.85	7.62	80.03	21.75	76.36	13.58	98.38	12.35	11661.18	3.02	87.62	755.97
PL 308 7/31/2014 12:19:11 AM (Run: 1)	552.92	91.40	707.85	551123.22	4.75		1.92	0.19	2.25	5.11	1.33	19.54	7.22	79.34	22.01	76.02	15.30	103.04	12.65	11627.17	3.07	87.25	744.70
PL 311 7/31/2014 12:41:28 AM (Run: 1)	529.75	89.42	706.71	555092.53	4.38		2.18	0.20	2.81	5.34	1.42	19.56	7.77	76.24	21.81	75.78	13.79	103.03	12.17	11616.39	2.94	84.98	740.21
PL 312 7/31/2014 12:43:09 AM (Run: 1)	507.31	90.08	694.61	551587.50	4.51		2.28	0.21	2.60	3.92	1.02	19.53	7.05	77.81	20.97	74.56	13.66	98.69	12.19	11833.16	2.74	84.16	739.53
PL 315 7/31/2014 1:02:00 AM (Run: 1)	479.82	83.70	638.94	551120.16	4.65		1.90	0.15	3.03	4.77	0.99	17.77	6.46	69.29	20.32	65.78	12.61	91.98	11.82	11773.28	2.88	77.51	704.76
PL 316 7/31/2014 1:03:41 AM (Run: 1)	562.38	93.32	720.16	553705.46	4.61		2.45	0.20	3.39	5.46	1.16	21.83	7.73	79.91	22.72	77.04	14.41	102.91	12.40	11587.49	2.87	88.14	760.27
PL 319 7/31/2014 1:25:52 AM (Run: 1)	528.50	92.95	702.34	559150.36	4.68		2.42	0.21	2.53	5.55	1.27	18.02	7.45	79.84	22.51	77.02	14.30	99.98	11.91	11859.70	2.91	87.66	754.33
PL 320 7/31/2014 1:27:33 AM (Run: 1)	533.81	86.13	721.92	547952.46	4.46	0.03	2.48	0.19	2.71	4.14	1.26	20.42	7.52	77.82	22.36	79.02	13.46	103.55	12.07	11425.73	3.10	98.15	776.85
PL 323 7/31/2014 1:46:18 AM (Run: 1)	494.78	83.32	630.67	553979.11	4.21		2.18	0.23	2.81	4.35	1.02	16.88	6.51	69.62	20.26	66.90	12.80	90.96	9.96	11773.43	2.90	77.36	700.04
PL 324 7/31/2014 1:47:59 AM (Run: 1)	503.41	87.75	659.80	543411.67	4.29		2.17	0.14	2.24	4.45	1.22	18.47	6.94	70.86	20.63	71.69	12.90	95.38	11.11	11699.06	2.84	81.56	722.92
PL 327 7/31/2014 2:10:13 AM (Run: 1)	301.42	61.35	410.26	531371.22	3.74		1.47	0.09	1.26	2.40	0.59	10.69	4.04	44.16	12.60	42.79	8.29	64.00	7.07	11131.62	2.46	49.36	478.10
PL 328 7/31/2014 2:11:53 AM (Run: 1)	265.61	61.16	362.43	546948.55	3.29		1.34	0.06	1.20	2.25	0.62	9.47	3.94	43.05	11.46	38.28	7.38	55.45	6.61	11223.38	1.70	46.19	461.77
PL 331 7/31/2014 2:30:37 AM (Run: 1)	255.30	62.65	398.26	553666.74	4.09		1.79	0.08	0.93	1.97	0.58	9.87	4.02	44.67	11.83	41.14	8.39	55.51	6.12	11622.22	2.59	51.53	510.17
PL 335 7/31/2014 2:54:32 AM (Run: 1)	337.63	69.14	489.28	529739.55	4.12		1.58	0.06	1.27	3.05	0.80	13.02	4.99	51.62	15.56	51.42	9.41	68.28	8.53	12468.93	2.71	56.22	550.95
PL 336 7/31/2014 2:56:13 AM (Run: 1)	282.25	64.57	423.20	538482.42	3.47		1.63	0.06	0.84	2.17	0.88	11.66	4.46	53.91	14.48	47.68	8.53	65.81	7.98	12292.47	2.54	51.44	499.50
PL 340 7/31/2014 3:16:38 AM (Run: 1)	344.61	71.06	497.22	548169.59	4.11		1.82	0.15	1.35	3.73	0.86	12.55	4.84	59.62	15.07	52.68	10.08	71.39	8.86	11659.03	2.63	57.75	557.03
PL 343 7/31/2014 3:38:54 AM (Run: 1)	348.02	68.25	473.10	514956.60	3.75		1.76	0.04	1.54	3.19	0.77	13.37	4.88	57.25	15.24	51.54	9.44	68.35	8.29	12045.25	2.61	57.76	552.05
PL 344 7/31/2014 3:40:35 AM (Run: 1)	321.69	68.10	462.06	552374.17	3.83		1.73	0.16	1.48	2.83	0.66	13.13	4.94	51.33	14.42	50.44	9.58	68.98	8.66	11867.98	2.59	55.37	531.99
PL 347 7/31/2014 3:57:36 AM (Run: 1)	296.87	69.99	407.88	559669.89	4.70		1.86	0.12	1.20	2.93	0.74	13.05	4.82	46.46	14.03	43.06	7.84	56.01	6.35	11461.66	3.34	71.41	645.32
PL 348 7/31/2014 3:59:17 AM (Run: 1)	266.90	64.80	383.38	566335.17	5.48		1.78	0.07	0.81	2.29	0.72	10.77	4.34	42.63	12.06	38.14	7.54	53.28	5.67	10895.86	2.83	62.47	593.84

Experiment 1 on July 31, 2014
Isotope ratio and date errors do not include systematic calibration errors of 0.60% ($^{207}Pb/^{206}Pb$) and 1.68% ($^{206}Pb/^{238}U$) (2 sigma).
Trace element concentrations were deleted from analyses known to have intersected inclusions of other minerals based on P and Ti.
Ablation used a laser spot size of 25 microns and a laser firing repetition rate of 5 Hz.
Activity of TiO_2 for Ti-in-Zircon temperature calculation is 0.8.

Appendix Table A8 LA-ICPMS isotopic U-Pb and trace element concentration data analyzed at Boise State University

Analysis	CA-TIMS label	U ppm	Th ppm	Pb* ppm	Th/U	$^{207}Pb/^{235}U$	±2s (%)	$^{206}Pb/^{238}U$	±2s (%)	error corr.	$^{238}U/^{206}Pb$	±2s (%)	$^{207}Pb/^{206}Pb$	±2s (%)	$^{208}Pb/^{232}Th$	±2s (Ma)	$^{207}Pb/^{206}Pb$	±2s (Ma)	$^{207}Pb/^{235}U$	±2s (Ma)	$^{206}Pb/^{238}U$	±2s (Ma)	% disc
FC1 - Secondary reference zircon																							
FC1 357 7/30/2014 10:52:10 PM (Run: 1)		301.66	187.42	69.83	0.62	1.93360	4.72	0.18547	3.59	0.76	5.39	3.59	0.07561	3.06	1015	39	1085	61	1093	32	1097	36	1
FC1 358 7/30/2014 10:53:50 PM (Run: 1)	high U signal variance	324.28	227.79	77.98	0.70	1.99955	5.27	0.18894	4.88	0.92	5.29	4.88	0.07676	2.01	1038	55	1115	40	1115	36	1116	50	0
FC1 361 7/30/2014 11:36:27 PM (Run: 1)		325.85	225.47	77.62	0.69	1.97773	4.91	0.18676	4.20	0.86	5.35	4.20	0.07680	2.54	1056	39	1116	51	1108	33	1104	43	1
FC1 362 7/30/2014 11:38:07 PM (Run: 1)		336.10	234.43	79.76	0.70	1.93820	4.51	0.18530	4.02	0.89	5.40	4.02	0.07586	2.04	1071	39	1091	41	1094	30	1096	41	0
FC1 365 7/31/2014 12:20:55 AM (Run: 1)		153.16	82.71	35.75	0.54	1.96844	4.53	0.18991	3.27	0.72	5.27	3.27	0.07517	3.13	1065	31	1073	63	1105	30	1121	34	5
FC1 366 7/31/2014 12:22:36 AM (Run: 1)		158.86	87.57	36.16	0.55	1.90256	4.02	0.18377	3.15	0.78	5.44	3.15	0.07509	2.50	1073	41	1071	50	1082	27	1088	31	2
FC1 369 7/31/2014 1:05:24 AM (Run: 1)		161.08	96.93	37.80	0.60	1.94792	3.58	0.18756	2.81	0.78	5.33	2.81	0.07532	2.23	1079	55	1077	45	1098	24	1108	29	3
FC1 370 7/31/2014 1:07:05 AM (Run: 1)		150.28	80.36	34.61	0.53	1.92655	3.93	0.18601	2.69	0.68	5.38	2.69	0.07512	2.86	1114	49	1072	58	1090	26	1100	27	3
FC1 373 7/31/2014 1:49:42 AM (Run: 1)		159.15	84.97	36.32	0.53	1.97473	4.10	0.18284	3.23	0.79	5.47	3.23	0.07833	2.53	1142	35	1155	50	1107	28	1082	32	7
FC1 374 7/31/2014 1:51:23 AM (Run: 1)		174.59	92.21	39.63	0.53	1.93940	3.70	0.18240	3.23	0.88	5.48	3.23	0.07711	1.79	1136	43	1124	36	1095	25	1080	32	4
FC1 377 7/31/2014 2:34:02 AM (Run: 1)		247.07	171.97	59.09	0.70	1.94086	5.24	0.18461	4.37	0.83	5.42	4.37	0.07625	2.88	1143	32	1102	58	1095	35	1092	44	1
FC1 378 7/31/2014 2:35:43 AM (Run: 1)		246.77	172.97	59.28	0.70	2.00484	4.59	0.18466	3.83	0.84	5.42	3.83	0.07874	2.52	1150	37	1166	50	1117	31	1092	38	7
FC1 381 7/31/2014 3:18:22 AM (Run: 1)		249.58	171.04	58.84	0.69	1.94338	3.59	0.18188	2.54	0.71	5.50	2.54	0.07750	2.53	1140	46	1134	50	1096	24	1077	25	5
FC1 382 7/31/2014 3:20:03 AM (Run: 1)		243.95	166.58	55.48	0.68	1.88052	4.70	0.17559	3.34	0.71	5.69	3.34	0.07767	3.30	1101	32	1138	66	1074	31	1043	32	9
FC1 385 7/31/2014 4:01:01 AM (Run: 1)		281.59	154.41	64.61	0.55	1.91948	3.18	0.18191	2.29	0.72	5.50	2.29	0.07653	2.20	1202	37	1109	44	1088	21	1077	23	3
FC1 386 7/31/2014 4:02:42 AM (Run: 1)		292.11	175.83	68.17	0.60	1.90778	3.09	0.18394	2.24	0.73	5.44	2.24	0.07522	2.12	1161	34	1074	43	1084	21	1088	22	1
Orapa - Secondary reference zircon																							
Orapa 399 7/30/2014 10:38:39 PM (Run: 1)	high $^{206}Pb/^{238}U$ variance	7.61	1.89	0.10	0.25	0.59536	177.60	0.01165	22.54	0.13	85.87	22.54	0.37078	176.17	-255	-110	3795	2668	474	673	75	17	99
Orapa 400 7/30/2014 10:40:20 PM (Run: 1)	high $^{206}Pb/^{238}U$ variance	7.69	2.04	0.13	0.27	0.28099	65.38	0.01457	23.84	0.36	68.65	23.84	0.13991	60.88	31	163	2226	1054	251	146	93	22	96
Orapa 401 7/30/2014 10:42:01 PM (Run: 1)	high $^{206}Pb/^{238}U$ variance	7.76	2.02	0.18	0.26	0.14255	75.69	0.01832	19.28	0.25	54.58	19.28	0.05643	73.20	315	184	469	1620	135	96	117	22	76
Orapa 402 7/30/2014 10:43:42 PM (Run: 1)	high $^{206}Pb/^{238}U$ variance	7.52	1.89	0.12	0.25	0.67915	156.86	0.01250	26.32	0.17	80.00	26.32	0.39406	154.64	-145	-208	3887	2328	526	644	80	21	98

Experiment 1 on July 31, 2014
Isotope ratio and date errors do not include systematic calibration errors of 0.60% ($^{207}Pb/^{206}Pb$) and 1.68% ($^{206}Pb/^{238}U$) (2 sigma).
Trace element concentrations were deleted from analyses known to have intersected inclusions of other minerals based on P and Ti.
Ablation used a laser spot size of 25 microns and a laser firing repetition rate of 5 Hz.
Activity of TiO_2 for Ti-in-Zircon temperature calculation is 0.8.

Appendix Table A8 LA-ICPMS isotopic U-Pb and trace element concentration data analyzed at Boise State University

Analysis	P	Ti	Y	Zr	Nb	La	Ce	Pr	Nd	Sm	Eu	Gd	Tb	Dy	Ho	Er	Tm	Yb	Lu	Hf	Ta	Th	U
	ppm	ppm	ppm	ppm	ppm	ppm	ppm	ppm	ppm	ppm	ppm	ppm	ppm	ppm	ppm	ppm	ppm	ppm	ppm	ppm	ppm	ppm	ppm
FC1 - Secondary reference zircon																							
FC1 357 7/30/2014 10:52:10 PM (Run: 1)	218.86	12.48	1606.27	554255.63	1.17		8.05		1.12	3.71	0.16	28.71	11.00	143.82	55.35	245.96	52.71	457.65	74.63	11229.81	0.97	187.42	301.66
FC1 358 7/30/2014 10:53:50 PM (Run: 1)	232.16	11.96	1979.59	519659.43	0.92	0.02	8.89	0.09	2.73	7.53	0.30	48.46	16.86	200.18	70.18	287.74	61.48	520.19	82.99	10127.44	1.01	227.79	324.28
FC1 361 7/30/2014 11:36:27 PM (Run: 1)	245.03	15.80	2109.14	535692.84	1.15		8.46	0.25	7.05	13.00	0.49	58.41	19.76	215.97	77.91	313.57	64.22	576.63	89.76	10045.72	1.08	225.47	325.85
FC1 362 7/30/2014 11:38:07 PM (Run: 1)	236.17	17.50	2199.64	563763.51	1.22		8.40	0.25	5.95	11.15	0.46	62.26	20.03	221.40	78.60	328.70	69.54	574.57	88.69	10214.02	0.84	234.43	336.10
FC1 365 7/31/2014 12:20:55 AM (Run: 1)	265.10	17.35	991.58	566488.45	1.69		6.10	0.05	1.13	2.85	0.08	18.19	7.13	90.01	34.38	152.46	34.88	309.97	49.39	9725.63	1.05	82.71	153.16
FC1 366 7/31/2014 12:22:36 AM (Run: 1)	259.34	18.64	1028.90	545215.08	1.77		6.08	0.03	0.82	3.27	0.09	21.75	7.77	102.50	36.36	156.55	34.12	311.89	49.74	9597.24	1.32	87.57	158.86
FC1 369 7/31/2014 1:05:24 AM (Run: 1)	278.34	19.07	1094.67	544427.73	1.81		6.90	0.08	1.15	3.54	0.12	25.21	7.96	105.51	39.81	169.74	36.48	328.68	50.78	9115.10	1.14	96.93	161.08
FC1 370 7/31/2014 1:07:05 AM (Run: 1)	254.55	17.69	921.48	541401.21	1.57		6.10	0.05	1.12	2.53	0.10	19.77	6.45	90.62	33.14	144.06	32.43	290.26	46.99	9539.58	0.87	80.36	150.28
FC1 373 7/31/2014 1:49:42 AM (Run: 1)	248.94	17.65	968.80	545566.94	1.51		6.63	0.03	0.99	2.30	0.07	20.17	6.98	92.94	34.38	149.41	32.92	301.23	48.11	9551.40	1.11	84.97	159.15
FC1 374 7/31/2014 1:51:23 AM (Run: 1)	261.52	15.35	989.55	526739.13	1.66	0.02	6.85	0.05	0.99	1.98	0.11	22.43	7.55	94.20	35.19	155.61	34.05	317.22	50.29	9088.85	1.15	92.21	174.59
FC1 377 7/31/2014 2:34:02 AM (Run: 1)	250.14	19.51	1923.86	544760.43	1.13		7.08	0.26	4.63	8.62	0.34	54.49	17.92	202.06	70.69	282.05	59.87	527.99	77.70	8304.23	0.84	171.97	247.07
FC1 378 7/31/2014 2:35:43 AM (Run: 1)	246.06	18.84	1913.41	538383.96	0.88		7.50	0.16	3.88	9.59	0.27	52.53	17.32	197.29	70.36	277.19	60.81	520.94	77.47	8511.75	0.64	172.97	246.77
FC1 381 7/31/2014 3:18:22 AM (Run: 1)	254.51	18.88	1863.25	545037.60	0.79		7.25	0.04	2.96	7.21	0.27	47.33	16.16	190.85	67.52	272.04	58.01	508.33	75.26	8464.31	0.66	171.04	249.58
FC1 382 7/31/2014 3:20:03 AM (Run: 1)	244.62	18.71	1855.97	534778.22	1.09		6.81	0.17	4.07	8.94	0.34	51.51	16.33	187.15	67.17	274.75	56.82	501.20	75.39	8126.83	0.63	166.58	243.95
FC1 385 7/31/2014 4:01:01 AM (Run: 1)	230.62	16.72	1461.80	526274.54	0.98		6.57	0.01	1.31	3.97	0.07	30.53	11.35	143.23	52.70	215.31	47.59	410.10	57.46	9812.79	0.74	154.41	281.59
FC1 386 7/31/2014 4:02:42 AM (Run: 1)	269.41	16.97	1698.94	534911.39	0.88		7.56	0.11	1.65	6.44	0.24	42.04	14.35	167.38	61.60	248.08	52.72	439.97	63.64	9898.80	0.62	175.83	292.11
Orapa - Secondary reference zircon																							
Orapa 399 7/30/2014 10:38:39 PM (Run: 1)	65.44	7.93	23.63	533680.73	1.00		0.39			0.14	0.06	0.96	0.29	3.17	0.89	3.21	0.62	4.70	0.74	11896.26	1.88	1.89	7.61
Orapa 400 7/30/2014 10:40:20 PM (Run: 1)	62.01	8.76	23.10	577867.19	1.24		0.29		0.13		0.10	0.77	0.24	2.54	0.89	2.98	0.60	4.98	0.84	11845.12	1.86	2.04	7.69
Orapa 401 7/30/2014 10:42:01 PM (Run: 1)	66.68	9.19	24.15	565426.96	1.27		0.34			0.16	0.10	0.53	0.20	2.99	0.92	3.29	0.59	5.45	0.78	12635.10	1.83	2.02	7.76
Orapa 402 7/30/2014 10:43:42 PM (Run: 1)	58.74	8.93	23.80	569309.46	1.25		0.35				0.11	0.88	0.24	3.04	0.93	3.19	0.71	5.39	0.67	12870.44	1.95	1.89	7.52

Experiment 1 on July 31, 2014
Isotope ratio and date errors do not include systematic calibration errors of 0.60% ($^{207}Pb/^{206}Pb$) and 1.68% ($^{206}Pb/^{238}U$) (2 sigma).
Trace element concentrations were deleted from analyses known to have intersected inclusions of other minerals based on P and Ti.
Ablation used a laser spot size of 25 microns and a laser firing repetition rate of 5 Hz.
Activity of TiO_2 for Ti-in-Zircon temperature calculation is 0.8.

Appendix Table A8 LA-ICPMS isotopic U-Pb and trace element concentration data analyzed at Boise State University

Analysis	CA-TIMS label	U ppm	Th ppm	Pb* ppm	Th/U	$^{207}Pb/^{235}U$	±2s (%)	$^{206}Pb/^{238}U$	±2s (%)	error corr.	$^{238}U/^{206}Pb$	±2s (%)	$^{207}Pb/^{206}Pb$	±2s (%)	$^{208}Pb/^{232}Th$	±2s (Ma)	$^{207}Pb/^{206}Pb$	±2s (Ma)	$^{207}Pb/^{235}U$	±2s (Ma)	$^{206}Pb/^{238}U$	±2s (Ma)	% disc
Plesovice - Primary zircon standard																							
PL 140 10/17/2014 9:32:39 AM (Run: 1)	std	419.36	40.51	24.62	0.10	0.39605	4.88	0.05415	3.70	0.76	18.47	3.70	0.05305	3.18	348	31	331	72	339	14	340	12	3
PL 141 10/17/2014 9:34:20 AM (Run: 1)	std	453.21	44.59	26.79	0.10	0.40098	5.85	0.05460	3.94	0.67	18.32	3.94	0.05326	4.32	328	36	340	98	342	17	343	13	1
PL 142 10/17/2014 9:36:01 AM (Run: 1)	std	468.18	47.92	27.82	0.10	0.40716	5.31	0.05475	4.20	0.79	18.26	4.20	0.05394	3.25	337	26	368	73	347	16	344	14	7
PL 143 10/17/2014 9:37:42 AM (Run: 1)	std	506.89	51.99	29.34	0.10	0.39123	6.92	0.05329	5.33	0.77	18.76	5.33	0.05324	4.42	345	24	339	100	335	20	335	17	1
PL 144 10/17/2014 9:59:54 AM (Run: 1)	std	532.97	53.97	30.37	0.10	0.38555	5.29	0.05236	4.02	0.76	19.10	4.02	0.05340	3.44	362	29	346	78	331	15	329	13	5
PL 146 10/17/2014 10:20:29 AM (Run: 1)	std	574.98	57.15	32.73	0.10	0.38811	5.87	0.05248	4.81	0.82	19.06	4.81	0.05364	3.37	330	32	356	76	333	17	330	15	8
PL 147 10/17/2014 10:22:10 AM (Run: 1)	std	597.80	61.13	34.19	0.10	0.37791	6.20	0.05285	5.31	0.86	18.92	5.31	0.05186	3.20	314	25	279	73	325	17	332	17	19
PL 148 10/17/2014 10:44:23 AM (Run: 1)	std	605.80	61.69	35.52	0.10	0.39772	5.51	0.05392	4.49	0.81	18.55	4.49	0.05349	3.20	359	27	350	72	340	16	339	15	3
PL 149 10/17/2014 10:46:04 AM (Run: 1)	std	600.43	62.46	34.51	0.10	0.39004	7.07	0.05302	6.23	0.88	18.86	6.23	0.05336	3.35	314	30	344	76	334	20	333	20	3
PL 150 10/17/2014 11:04:55 AM (Run: 1)	std	535.96	52.93	32.28	0.10	0.40963	6.40	0.05545	5.67	0.89	18.03	5.67	0.05358	2.97	368	31	353	67	349	19	348	19	2
PL 151 10/17/2014 11:06:36 AM (Run: 1)	std	418.89	38.80	24.12	0.09	0.38269	5.45	0.05343	4.19	0.77	18.71	4.19	0.05194	3.48	299	30	283	80	329	15	336	14	19
PL 152 10/17/2014 11:28:48 AM (Run: 1)	std	480.77	45.94	27.80	0.10	0.40240	4.84	0.05329	3.60	0.75	18.76	3.60	0.05476	3.23	338	34	403	72	343	14	335	12	17
PL 153 10/17/2014 11:30:29 AM (Run: 1)	std	498.50	48.65	28.89	0.10	0.38837	5.01	0.05344	4.40	0.88	18.71	4.40	0.05271	2.40	347	40	316	55	333	14	336	14	6
PL 154 10/17/2014 11:49:18 AM (Run: 1)	std	546.76	55.08	31.76	0.10	0.39240	4.83	0.05355	3.83	0.79	18.67	3.83	0.05314	2.94	334	23	335	67	336	14	336	13	0
PL 155 10/17/2014 11:50:59 AM (Run: 1)	std	560.34	56.62	32.50	0.10	0.39185	6.40	0.05350	5.08	0.79	18.69	5.08	0.05312	3.88	328	22	334	88	336	18	336	17	1
PL 156 10/17/2014 12:13:12 PM (Run: 1)	std	594.03	60.38	34.32	0.10	0.39036	6.11	0.05323	5.14	0.84	18.79	5.14	0.05319	3.29	336	30	337	75	335	17	334	17	1
PL 157 10/17/2014 12:14:54 PM (Run: 1)	std	590.69	59.06	34.62	0.10	0.39933	5.50	0.05408	4.48	0.81	18.49	4.48	0.05356	3.19	329	25	352	72	341	16	340	15	4
PL 158 10/17/2014 12:33:52 PM (Run: 1)	std	585.00	60.37	35.09	0.10	0.39794	5.97	0.05541	4.77	0.80	18.05	4.77	0.05209	3.60	329	26	289	82	340	17	348	16	21
PL 159 10/17/2014 12:35:33 PM (Run: 1)	std	518.41	50.35	29.72	0.10	0.38206	5.17	0.05280	3.12	0.60	18.94	3.12	0.05248	4.13	365	39	307	94	329	15	332	10	8
PL 160 10/17/2014 12:57:55 PM (Run: 1)	std	519.76	51.10	29.99	0.10	0.39053	6.33	0.05320	5.13	0.81	18.80	5.13	0.05324	3.71	342	31	339	84	335	18	334	17	2
PL 161 10/17/2014 12:59:36 PM (Run: 1)	std	578.73	57.38	33.51	0.10	0.39904	5.45	0.05336	4.51	0.83	18.74	4.51	0.05423	3.06	333	27	381	69	341	16	335	15	12
PL 162 10/17/2014 1:18:33 PM (Run: 1)	std	573.25	59.33	34.73	0.10	0.40532	4.71	0.05585	3.41	0.72	17.91	3.41	0.05264	3.25	349	32	313	74	346	14	350	12	12
PL 163 10/17/2014 1:20:14 PM (Run: 1)	std	603.48	63.03	35.88	0.10	0.40596	6.32	0.05476	5.21	0.82	18.26	5.21	0.05377	3.58	335	25	361	81	346	19	344	17	5
PL 164 10/17/2014 1:42:34 PM (Run: 1)	std	959.69	117.40	55.10	0.12	0.39821	5.53	0.05253	4.18	0.76	19.04	4.18	0.05498	3.62	328	19	412	81	340	16	330	13	20
PL 165 10/17/2014 1:44:15 PM (Run: 1)	std	946.22	115.80	55.20	0.12	0.40129	5.54	0.05333	4.51	0.81	18.75	4.51	0.05457	3.22	343	16	395	72	343	16	335	15	16
PL 166 10/17/2014 2:03:12 PM (Run: 1)	std	891.54	105.66	50.78	0.12	0.38030	7.19	0.05217	6.06	0.84	19.17	6.06	0.05287	3.87	343	21	323	88	327	20	328	19	1
PL 167 10/17/2014 2:04:53 PM (Run: 1)	std	812.65	99.43	47.82	0.12	0.38554	5.62	0.05401	4.80	0.85	18.51	4.80	0.05177	2.92	334	24	275	67	331	16	339	16	24
PL 168 10/17/2014 2:27:13 PM (Run: 1)	std	804.05	98.14	48.55	0.12	0.39798	4.69	0.05527	3.45	0.74	18.09	3.45	0.05222	3.17	364	15	295	72	340	14	347	12	18
PL 169 10/17/2014 2:28:54 PM (Run: 1)	std	859.78	101.73	49.07	0.12	0.38575	4.89	0.05225	4.18	0.86	19.14	4.18	0.05355	2.53	343	25	352	57	331	14	328	13	7
PL 170 10/17/2014 2:46:11 PM (Run: 1)	std	839.77	97.54	49.50	0.12	0.39993	6.60	0.05418	5.63	0.85	18.46	5.63	0.05354	3.44	322	22	352	78	342	19	340	19	3
PL 171 10/17/2014 2:47:52 PM (Run: 1)	std	842.19	96.35	48.84	0.11	0.39060	4.12	0.05334	3.03	0.74	18.75	3.03	0.05311	2.80	318	21	333	63	335	12	335	10	0

Experiment 2 on October 17, 2014
Isotope ratio and date errors do not include systematic calibration errors of 0.64% ($^{207}Pb/^{206}Pb$) and 2.31% ($^{206}Pb/^{238}U$) (2 sigma).
Trace element concentrations were deleted from analyses known to have intersected inclusions of other minerals based on P and Ti.

Ablation used a laser spot size of 25 microns and a laser firing repetition rate of 5 Hz.
Activity of TiO_2 for Ti-in-Zircon temperature calculation is 0.8.

Appendix Table A8 LA-ICPMS isotopic U-Pb and trace element concentration data analyzed at Boise State University

Analysis	P	Ti	Y	Zr	Nb	La	Ce	Pr	Nd	Sm	Eu	Gd	Tb	Dy	Ho	Er	Tm	Yb	Lu	Hf	Ta	Th	U
	ppm	ppm	ppm	ppm	ppm	ppm	ppm	ppm	ppm	ppm	ppm	ppm	ppm	ppm	ppm	ppm	ppm	ppm	ppm	ppm	ppm	ppm	ppm
Plesovice - Primary zircon standard																							
PL 140 10/17/2014 9:32:39 AM (Run: 1)	238.87	26.56	275.69	774479.97	2.70	0.02	2.03	0.08	0.97	1.85	0.49	5.74	2.56	33.57	9.11	33.16	7.80	69.86	8.08	9726.82	2.14	40.51	419.36
PL 141 10/17/2014 9:34:20 AM (Run: 1)	296.89	50.24	355.24	800382.35	3.36		1.76	0.13	1.30	2.54	0.53	10.43	3.61	43.42	11.55	37.38	7.90	63.79	6.32	10786.31	2.35	44.59	453.21
PL 142 10/17/2014 9:36:01 AM (Run: 1)	304.36	47.56	375.42	791630.36	3.49	0.01	1.78	0.07	1.34	2.54	0.72	10.92	3.86	45.41	12.25	40.80	7.57	60.40	6.28	10563.32	2.23	47.92	468.18
PL 143 10/17/2014 9:37:42 AM (Run: 1)	354.20	50.20	425.56	834913.06	3.89	0.03	2.11	0.14	1.85	3.33	0.69	10.84	4.57	44.31	13.05	42.52	8.50	64.37	6.26	11281.74	2.67	51.99	506.89
PL 144 10/17/2014 9:59:54 AM (Run: 1)	355.80	52.26	423.12	793409.29	3.56		1.99	0.16	1.49	3.35	0.88	11.25	4.50	51.49	14.42	47.36	8.53	66.29	6.90	10884.05	2.53	53.97	532.97
PL 146 10/17/2014 10:20:29 AM (Run: 1)	382.05	47.66	457.18	800529.71	3.59	0.04	2.49	0.18	2.12	3.73	0.77	13.40	4.80	51.64	14.85	46.63	8.85	72.18	7.40	10731.25	2.68	57.15	574.98
PL 147 10/17/2014 10:22:10 AM (Run: 1)	395.86	48.70	478.79	813451.10	3.69	0.19	2.88	0.28	2.03	2.79	0.74	14.31	4.84	56.62	15.30	51.30	9.98	71.32	7.44	10874.80	2.62	61.13	597.80
PL 148 10/17/2014 10:44:23 AM (Run: 1)	396.58	46.68	485.30	827258.66	4.10	0.30	2.65	0.31	1.99	3.52	0.86	13.81	4.77	54.91	14.91	51.02	9.87	70.83	7.33	10594.46	2.88	61.69	605.80
PL 149 10/17/2014 10:46:04 AM (Run: 1)	347.11	44.78	477.98	823782.50	4.24	0.04	2.46	0.27	2.10	3.29	0.77	12.03	4.86	55.91	15.80	49.69	10.09	70.51	7.79	11056.31	2.80	62.46	600.43
PL 150 10/17/2014 11:04:55 AM (Run: 1)	365.16	45.50	428.96	853607.24	3.46	0.08	2.30	0.20	1.98	3.42	0.73	11.40	4.80	47.52	12.70	46.44	9.19	66.44	6.93	10770.10	2.45	52.93	535.96
PL 151 10/17/2014 11:06:36 AM (Run: 1)	240.21	23.38	247.36	784696.62	2.30	0.01	2.02	0.07	1.15	2.23	0.40	7.24	2.28	26.91	7.83	30.84	6.69	61.98	7.81	10223.89	1.81	38.80	418.89
PL 152 10/17/2014 11:28:48 AM (Run: 1)	296.81	53.08	368.61	776431.38	2.96	0.03	1.73	0.13	1.09	1.92	0.53	10.76	4.15	43.15	12.03	39.37	7.35	63.03	5.43	10156.96	2.28	45.94	480.77
PL 153 10/17/2014 11:30:29 AM (Run: 1)	315.55	54.19	391.71	824887.08	3.70	0.01	1.79	0.11	1.70	2.74	0.67	10.40	4.13	47.61	12.19	44.34	7.74	64.33	6.36	11075.49	2.21	48.65	498.50
PL 154 10/17/2014 11:49:18 AM (Run: 1)	344.15	53.51	457.28	875601.11	4.07	0.05	2.05	0.11	2.02	3.05	0.93	11.31	4.79	53.03	14.34	45.97	8.75	67.84	6.69	11545.97	2.60	55.08	546.76
PL 155 10/17/2014 11:50:59 AM (Run: 1)	376.88	54.36	464.59	861611.97	3.99	0.47	2.63	0.36	1.80	3.07	0.63	12.11	5.02	54.09	13.75	46.81	9.15	70.93	7.48	10991.69	2.65	56.62	560.34
PL 156 10/17/2014 12:13:12 PM (Run: 1)	385.95	55.67	477.14	846327.92	3.65	0.04	2.33	0.15	2.16	2.93	0.98	12.39	4.91	55.00	15.67	49.97	10.03	72.19	7.93	11246.14	2.90	60.38	594.03
PL 157 10/17/2014 12:14:54 PM (Run: 1)	356.73	49.11	468.64	831651.79	3.60	0.13	2.69	0.22	2.81	4.16	0.95	12.96	5.28	54.35	15.61	49.80	9.24	74.41	7.29	10240.05	2.93	59.06	590.69
PL 158 10/17/2014 12:33:52 PM (Run: 1)	397.59	47.65	482.90	870432.51	3.73	0.53	3.43	0.25	3.07	3.78	0.89	12.84	5.62	55.09	14.43	52.13	9.58	75.69	7.97	10423.45	3.20	60.37	585.00
PL 159 10/17/2014 12:35:33 PM (Run: 1)	329.08	56.14	406.43	803744.27	3.79		1.88	0.15	1.86	2.33	0.75	11.78	4.41	47.38	13.44	41.48	8.86	65.67	7.31	10797.39	2.38	50.35	518.41
PL 160 10/17/2014 12:57:55 PM (Run: 1)	337.37	55.17	412.91	796726.21	3.91	0.04	1.82	0.15	2.00	2.85	0.76	11.60	4.04	49.75	13.15	43.74	8.54	68.26	7.13	10689.13	2.62	51.10	519.76
PL 161 10/17/2014 12:59:36 PM (Run: 1)	392.41	55.36	467.32	840425.63	3.81	0.06	2.11	0.15	2.52	3.07	0.79	13.47	4.68	54.75	14.25	49.35	9.41	72.83	7.54	11074.98	2.51	57.38	578.73
PL 162 10/17/2014 1:18:33 PM (Run: 1)	367.82	51.36	465.05	825873.79	3.85	0.22	2.46	0.20	2.32	3.35	0.88	11.24	5.43	56.60	14.69	48.89	9.49	75.26	7.91	10847.11	2.50	59.33	573.25
PL 163 10/17/2014 1:20:14 PM (Run: 1)	394.39	52.08	491.72	841502.41	3.85	0.19	2.69	0.23	2.60	4.19	0.82	13.93	4.61	54.91	16.27	51.49	9.71	74.97	7.70	11232.56	2.78	63.03	603.48
PL 164 10/17/2014 1:42:34 PM (Run: 1)	823.53	114.58	935.85	837584.66	5.47	0.04	2.65	0.29	4.02	6.55	1.88	27.87	10.18	105.84	29.70	102.02	20.48	154.00	15.03	10110.07	3.48	117.40	959.69
PL 165 10/17/2014 1:44:15 PM (Run: 1)	794.48	114.35	890.27	846522.97	5.27	0.03	2.91	0.28	3.59	6.11	1.78	25.63	9.59	106.88	28.65	95.73	19.06	142.55	14.86	10256.75	3.20	115.80	946.22
PL 166 10/17/2014 2:03:12 PM (Run: 1)	770.04	107.90	842.40	801921.54	5.09		2.53	0.26	3.74	7.04	1.57	23.63	9.01	96.60	26.46	90.81	17.79	145.39	15.05	9997.37	3.04	105.66	891.54
PL 167 10/17/2014 2:04:53 PM (Run: 1)	739.17	104.82	787.06	857611.13	5.40	0.01	2.13	0.26	3.12	5.91	1.53	23.17	8.98	90.60	24.87	84.10	15.86	125.95	13.30	10279.13	2.87	99.43	812.65
PL 168 10/17/2014 2:27:13 PM (Run: 1)	686.27	103.45	763.99	841633.96	4.86		2.55	0.22	3.48	5.44	1.30	21.64	8.19	89.26	23.48	83.31	15.46	120.25	12.45	10333.98	3.05	98.14	804.05
PL 169 10/17/2014 2:28:54 PM (Run: 1)	732.43	101.96	764.88	805595.63	4.48		2.52	0.24	3.01	6.22	1.62	22.26	8.85	93.88	24.53	82.20	16.30	130.15	13.44	9776.21	2.88	101.73	859.78
PL 170 10/17/2014 2:46:11 PM (Run: 1)	695.24	100.71	766.78	831814.57	5.19	0.03	2.47	0.20	3.70	5.83	1.44	22.61	8.41	87.97	24.87	77.92	15.90	120.46	13.56	10072.46	3.04	97.54	839.77
PL 171 10/17/2014 2:47:52 PM (Run: 1)	705.19	103.42	801.97	849543.47	4.85		2.61	0.25	2.56	7.36	1.58	22.02	8.97	97.34	25.38	83.81	16.17	128.84	12.76	10573.55	3.28	96.35	842.19

Experiment 2 on October 17, 2014
Isotope ratio and date errors do not include systematic calibration errors of 0.64% ($^{207}Pb/^{206}Pb$) and 2.31% ($^{206}Pb/^{238}U$) (2 sigma).
Trace element concentrations were deleted from analyses known to have intersected inclusions of other minerals based on P and Ti.

Ablation used a laser spot size of 25 microns and a laser firing repetition rate of 5 Hz.
Activity of TiO_2 for Ti-in-Zircon temperature calculation is 0.8.

Appendix Table A8 LA-ICPMS isotopic U-Pb and trace element concentration data analyzed at Boise State University

Analysis	CA-TIMS label	U ppm	Th ppm	Pb* ppm	Th/U	$^{207}Pb/^{235}U$	±2s (%)	$^{206}Pb/^{238}U$	±2s (%)	error corr.	$^{238}U/^{206}Pb$	±2s (%)	$^{207}Pb/^{206}Pb$	±2s (%)	$^{208}Pb/^{232}Th$	±2s (Ma)	$^{207}Pb/^{206}Pb$	±2s (Ma)	$^{207}Pb/^{235}U$	±2s (Ma)	$^{206}Pb/^{238}U$	±2s (Ma)	% disc
FC1 - Secondary reference zircon																							
FC1 198 10/17/2014 9:39:24 AM (Run: 1)		348.30	264.08	86.94	0.76	2.00140	7.57	0.19171	6.80	0.90	5.22	6.80	0.07572	3.32	1125	91	1088	67	1116	51	1131	71	-4
FC1 199 10/17/2014 9:41:05 AM (Run: 1)		370.08	280.44	92.92	0.76	1.99613	5.09	0.19351	4.48	0.88	5.17	4.48	0.07482	2.40	1118	94	1064	48	1114	34	1140	47	-7
FC1 200 10/17/2014 11:08:17 AM (Run: 1)		302.81	210.14	73.21	0.69	2.01932	6.82	0.18641	6.00	0.88	5.36	6.00	0.07857	3.24	1153	104	1161	64	1122	46	1102	61	5
FC1 201 10/17/2014 11:09:58 AM (Run: 1)		352.68	252.49	83.58	0.72	1.94776	6.72	0.18135	5.86	0.87	5.51	5.86	0.07789	3.29	1139	98	1144	65	1098	45	1074	58	6
FC1 202 10/17/2014 12:37:15 PM (Run: 1)		331.33	241.54	83.79	0.73	2.04830	5.98	0.19543	5.17	0.86	5.12	5.17	0.07601	3.01	1148	62	1095	60	1132	41	1151	55	-5
FC1 203 10/17/2014 12:38:56 PM (Run: 1)		394.18	301.68	101.85	0.77	2.05664	7.67	0.19908	7.20	0.94	5.02	7.20	0.07493	2.65	1140	59	1066	53	1135	52	1170	77	-10
FC1 204 10/17/2014 2:06:36 PM (Run: 1)		450.51	339.80	109.35	0.75	1.94564	7.09	0.18473	6.32	0.89	5.41	6.32	0.07639	3.23	1143	96	1105	65	1097	48	1093	63	1
FC1 205 10/17/2014 2:08:17 PM (Run: 1)		393.62	290.57	98.93	0.74	2.05019	5.76	0.19300	5.24	0.91	5.18	5.24	0.07704	2.38	1156	58	1122	48	1132	39	1138	55	-1
Orapa - Secondary reference zircon																							
Orapa 210 10/17/2014 9:25:53 AM (Run: 1)	high $^{206}Pb/^{238}U$ variance	5.86	1.45	0.07	0.25	0.23651	58.86	0.01331	20.33	0.35	75.13	20.33	0.12887	55.24	-195	-172	2083	972	216	114	85	17	97
Orapa 211 10/17/2014 9:27:34 AM (Run: 1)	high $^{206}Pb/^{238}U$ variance	5.94	1.48	0.12	0.25	0.57186	227.26	0.01272	18.65	0.08	78.63	18.65	0.32613	226.49	321	221	3599	3476	459	840	81	15	98
Orapa 212 10/17/2014 9:29:15 AM (Run: 1)	high $^{206}Pb/^{238}U$ variance	6.67	1.54	0.12	0.23	0.37047	121.37	0.01694	14.22	0.12	59.03	14.22	0.15860	120.53	-79	-156	2441	2041	320	333	108	15	96
Orapa 213 10/17/2014 9:30:56 AM (Run: 1)	high $^{206}Pb/^{238}U$ variance	6.51	1.55	0.11	0.24	0.20057	59.37	0.01360	19.85	0.33	73.51	19.85	0.10693	55.95	201	172	1748	1025	186	101	87	17	96
Seiland - Secondary reference zircon																							
Seiland 186 10/17/2014 10:23:53 AM (Run: 1)		46.92	41.41	5.21	0.88	0.69830	8.84	0.08236	5.21	0.59	12.14	5.21	0.06150	7.14	534	38	657	153	538	37	510	26	23
Seiland 187 10/17/2014 10:25:34 AM (Run: 1)		45.58	40.98	5.13	0.90	0.70432	8.34	0.08459	6.08	0.73	11.82	6.08	0.06039	5.70	506	27	618	123	541	35	523	31	16
Seiland 188 10/17/2014 11:52:42 AM (Run: 1)		47.60	42.91	5.29	0.90	0.69921	7.20	0.08305	5.20	0.72	12.04	5.20	0.06106	4.98	511	42	641	107	538	30	514	26	21
Seiland 189 10/17/2014 11:54:23 AM (Run: 1)		46.57	42.92	5.27	0.92	0.63649	13.85	0.08301	5.51	0.40	12.05	5.51	0.05561	12.71	553	50	437	283	500	55	514	27	18
Seiland 190 10/17/2014 1:21:57 PM (Run: 1)		47.93	42.80	5.29	0.89	0.65685	10.13	0.08264	6.16	0.61	12.10	6.16	0.05765	8.04	511	39	516	176	513	41	512	30	1
Seiland 191 10/17/2014 1:23:38 PM (Run: 1)		47.78	43.18	5.35	0.90	0.65911	9.26	0.08160	5.98	0.65	12.26	5.98	0.05859	7.06	563	46	552	154	514	37	506	29	9
Seiland 192 10/17/2014 2:49:35 PM (Run: 1)		47.11	42.81	5.17	0.91	0.61166	10.03	0.08189	5.73	0.57	12.21	5.73	0.05417	8.24	515	37	378	185	485	39	507	28	36
Seiland 193 10/17/2014 2:51:17 PM (Run: 1)		48.37	42.51	5.38	0.88	0.66506	10.35	0.08350	5.36	0.52	11.98	5.36	0.05777	8.85	519	25	521	194	518	42	517	27	1

Experiment 2 on October 17, 2014
Isotope ratio and date errors do not include systematic calibration errors of 0.64% ($^{207}Pb/^{206}Pb$) and 2.31% ($^{206}Pb/^{238}U$) (2 sigma).
Trace element concentrations were deleted from analyses known to have intersected inclusions of other minerals based on P and Ti.
Ablation used a laser spot size of 25 microns and a laser firing repetition rate of 5 Hz.
Activity of TiO_2 for Ti-in-Zircon temperature calculation is 0.8.

Appendix Table A8 LA-ICPMS isotopic U-Pb and trace element concentration data analyzed at Boise State University

Analysis	P	Ti	Y	Zr	Nb	La	Ce	Pr	Nd	Sm	Eu	Gd	Tb	Dy	Ho	Er	Tm	Yb	Lu	Hf	Ta	Th	U
	ppm	ppm	ppm	ppm	ppm	ppm	ppm	ppm	ppm	ppm	ppm	ppm	ppm	ppm	ppm	ppm	ppm	ppm	ppm	ppm	ppm	ppm	ppm
FC1 - Secondary reference zircon																							
FC1 198 10/17/2014 9:39:24 AM (Run: 1)	301.98	17.94	2110.39	700980.89	1.13	0.03	7.52	0.44	6.39	10.28	0.49	52.62	18.59	219.51	78.94	300.23	66.01	580.72	83.36	7495.22	0.99	264.08	348.30
FC1 199 10/17/2014 9:41:05 AM (Run: 1)	322.38	19.60	2601.14	829028.99	1.13	0.06	8.88	0.48	7.61	13.55	0.58	69.89	22.28	261.56	90.64	368.59	79.58	690.83	92.35	8304.14	0.86	280.44	370.08
FC1 200 10/17/2014 11:08:17 AM (Run: 1)	300.44	21.33	2096.12	853893.00	1.04	0.05	8.28	0.37	6.95	11.04	0.48	56.96	17.75	214.66	70.14	294.19	64.77	569.61	78.37	8167.10	0.92	210.14	302.81
FC1 201 10/17/2014 11:09:58 AM (Run: 1)	283.17	22.32	2241.34	799182.74	1.09	0.05	7.79	0.45	6.27	10.21	0.36	54.77	19.34	226.13	77.96	329.42	69.89	633.41	86.12	7967.43	0.89	252.49	352.68
FC1 202 10/17/2014 12:37:15 PM (Run: 1)	254.64	24.20	2312.17	928642.42	1.02	0.29	9.16	0.70	9.27	13.45	0.56	61.73	20.64	231.77	77.71	316.42	71.80	596.17	81.70	8196.61	0.84	241.54	331.33
FC1 203 10/17/2014 12:38:56 PM (Run: 1)	323.07	20.58	2485.60	779421.21	1.28	0.10	8.50	0.52	8.16	13.02	0.47	66.87	22.11	269.99	93.49	363.15	77.28	714.60	93.72	7476.49	1.15	301.68	394.18
FC1 204 10/17/2014 2:06:36 PM (Run: 1)	372.18	23.38	2863.03	825749.79	1.37	0.10	9.27	0.45	7.65	13.63	0.68	74.39	24.39	291.44	106.18	415.33	86.84	794.15	107.98	7945.44	1.07	339.80	450.51
FC1 205 10/17/2014 2:08:17 PM (Run: 1)	314.76	26.89	2531.71	873729.85	1.25	0.04	8.40	0.57	7.48	14.17	0.46	69.63	24.77	271.10	92.97	373.33	83.21	723.42	95.51	8041.67	0.93	290.57	393.62
Orapa - Secondary reference zircon																							
Orapa 210 10/17/2014 9:25:53 AM (Run: 1)	44.61	7.94	18.39	772858.68	1.17		0.19				0.09	0.49	0.19	2.26	0.64	2.70	0.45	4.63	0.58	10246.28	1.51	1.45	5.86
Orapa 211 10/17/2014 9:27:34 AM (Run: 1)	58.65	8.23	18.16	825202.72	0.75		0.30		0.07		0.19	0.23	0.25	2.29	0.72	2.28	0.52	4.39	0.64	11099.43	1.56	1.48	5.94
Orapa 212 10/17/2014 9:29:15 AM (Run: 1)	50.40	9.30	19.25	828155.77	1.10		0.30				0.06	0.51	0.22	2.71	0.72	2.66	0.60	4.96	0.60	11059.49	1.89	1.54	6.67
Orapa 213 10/17/2014 9:30:56 AM (Run: 1)	52.75	8.71	19.99	886566.06	1.13		0.26		0.04		0.12	0.61	0.19	2.67	0.72	2.80	0.47	4.79	0.80	12223.24	1.96	1.55	6.51
Seiland - Secondary reference zircon																							
Seiland 186 10/17/2014 10:23:53 AM (Run: 1)	46.69	1.85	194.47	836266.59	1.07		2.56		0.16	0.20	0.39	2.47	1.24	20.35	7.19	34.69	9.24	104.18	14.58	4667.79	0.75	41.41	46.92
Seiland 187 10/17/2014 10:25:34 AM (Run: 1)	72.19	2.18	200.97	837466.70	1.15		2.57	0.03	0.10	0.39	0.43	3.29	1.32	19.54	7.54	35.67	8.99	103.88	15.47	4797.40	0.83	40.98	45.58
Seiland 188 10/17/2014 11:52:42 AM (Run: 1)	66.82	2.01	207.56	860160.33	0.89		2.54		0.11	0.63	0.42	2.64	1.40	19.29	7.35	36.62	9.37	107.42	15.39	4931.45	0.74	42.91	47.60
Seiland 189 10/17/2014 11:54:23 AM (Run: 1)	80.42	2.01	201.24	848088.40	1.06		2.32		0.35	0.62	0.49	2.78	1.26	19.03	7.42	35.47	8.97	103.39	14.92	4714.18	0.66	42.92	46.57
Seiland 190 10/17/2014 1:21:57 PM (Run: 1)	55.67	1.76	202.02	857188.01	1.03		2.63		0.28	0.31	0.43	2.95	1.45	19.44	7.47	35.54	9.48	105.66	14.40	4783.17	0.74	42.80	47.93
Seiland 191 10/17/2014 1:23:38 PM (Run: 1)	75.09	1.67	209.93	875436.65	0.90		2.46			0.61	0.53	3.01	1.34	20.83	8.02	36.65	9.73	107.75	15.17	5105.44	0.77	43.18	47.78
Seiland 192 10/17/2014 2:49:35 PM (Run: 1)	56.70	2.49	204.66	864176.44	0.94		2.45	0.01	0.22	0.26	0.50	3.31	1.31	18.39	7.40	34.18	9.13	103.05	14.38	4795.14	0.61	42.81	47.11
Seiland 193 10/17/2014 2:51:17 PM (Run: 1)	71.87	1.90	209.85	868940.27	0.93		2.61		0.11	0.22	0.50	3.33	1.41	19.20	7.50	36.94	9.15	101.36	15.62	4822.06	0.86	42.51	48.37

Experiment 2 on October 17, 2014
Isotope ratio and date errors do not include systematic calibration errors of 0.64% ($^{207}Pb/^{206}Pb$) and 2.31% ($^{206}Pb/^{238}U$) (2 sigma).
Trace element concentrations were deleted from analyses known to have intersected inclusions of other minerals based on P and Ti.
Ablation used a laser spot size of 25 microns and a laser firing repetition rate of 5 Hz.
Activity of TiO_2 for Ti-in-Zircon temperature calculation is 0.8.

Appendix Table A8 LA-ICPMS isotopic U-Pb and trace element concentration data analyzed at Boise State University

Analysis	CA-TIMS label	U ppm	Th ppm	Pb* ppm	Th/U	$^{207}Pb/^{235}U$	±2s (%)	$^{206}Pb/^{238}U$	±2s (%)	error corr.	$^{238}U/^{206}Pb$	±2s (%)	$^{207}Pb/^{206}Pb$	±2s (%)	$^{208}Pb/^{232}Th$	±2s (Ma)	$^{207}Pb/^{206}Pb$	±2s (Ma)	$^{207}Pb/^{235}U$	±2s (Ma)	$^{206}Pb/^{238}U$	±2s (Ma)	% disc
Ptesovice - Primary zircon standard																							
PL 445 1/7/2016 5:07:41 PM (Run: 1)	std	672.61	83.97	39.61	0.12	0.39291	3.61	0.05388	2.96	0.81	18.56	2.96	0.05289	2.06	333	18	324	47	336	10	338	10	-4
PL 446 1/7/2016 5:09:24 PM (Run: 1)	std	622.13	75.14	36.23	0.12	0.39507	3.85	0.05336	3.20	0.82	18.74	3.20	0.05370	2.14	332	16	359	48	338	11	335	10	7
PL 447 1/7/2016 5:11:08 PM (Run: 1)	std	563.14	64.75	32.33	0.11	0.38257	3.17	0.05275	1.90	0.58	18.96	1.90	0.05260	2.53	336	20	311	58	329	9	331	6	-6
PL 448 1/7/2016 5:12:52 PM (Run: 1)	std	559.37	64.55	32.31	0.12	0.39150	3.20	0.05302	2.20	0.67	18.86	2.20	0.05355	2.32	342	22	352	52	335	9	333	7	5
PL 461 1/7/2016 5:35:33 PM (Run: 1)	std	604.04	78.29	35.94	0.13	0.39633	3.55	0.05445	2.67	0.74	18.37	2.67	0.05279	2.34	334	18	320	53	339	10	342	9	-7
PL 462 1/7/2016 5:37:17 PM (Run: 1)	std	585.94	77.06	34.77	0.13	0.40061	3.58	0.05423	2.88	0.79	18.44	2.88	0.05357	2.13	343	25	353	48	342	10	340	10	4
PL 469 1/7/2016 5:59:57 PM (Run: 1)	std	560.28	73.32	33.28	0.13	0.40254	3.22	0.05435	2.08	0.63	18.40	2.08	0.05371	2.46	338	16	359	55	343	9	341	7	5
PL 470 1/7/2016 6:01:41 PM (Run: 1)	std	599.14	85.11	35.45	0.14	0.39901	4.49	0.05404	3.14	0.69	18.50	3.14	0.05355	3.22	325	21	352	73	341	13	339	10	4
PL 477 1/7/2016 6:24:29 PM (Run: 1)	high U signal variance	540.46	53.57	32.22	0.10	0.39829	4.11	0.05480	1.95	0.46	18.25	1.95	0.05272	3.62	408	42	317	82	340	12	344	7	-9
PL 478 1/7/2016 6:26:12 PM (Run: 1)	std	586.31	67.70	33.58	0.12	0.38811	3.25	0.05269	2.27	0.68	18.98	2.27	0.05342	2.33	321	20	347	53	333	9	331	7	5
PL 485 1/7/2016 6:48:54 PM (Run: 1)	std	723.96	89.79	42.18	0.12	0.39107	3.13	0.05337	2.58	0.81	18.74	2.58	0.05314	1.77	322	17	335	40	335	9	335	8	0
PL 486 1/7/2016 6:50:37 PM (Run: 1)	std	675.88	80.62	39.46	0.12	0.39674	4.13	0.05369	3.30	0.79	18.63	3.30	0.05359	2.50	307	18	354	56	339	12	337	11	5
PL 493 1/7/2016 7:13:24 PM (Run: 1)	std	585.59	60.16	34.62	0.10	0.40387	3.86	0.05438	3.25	0.83	18.39	3.25	0.05386	2.09	367	23	365	47	344	11	341	11	7
PL 494 1/7/2016 7:15:08 PM (Run: 1)	std	664.51	78.10	38.14	0.12	0.38299	3.93	0.05269	2.94	0.74	18.98	2.94	0.05272	2.60	336	23	317	59	329	11	331	9	-4
PL 501 1/7/2016 7:37:47 PM (Run: 1)	std	713.30	88.68	42.01	0.12	0.39577	3.95	0.05392	2.55	0.63	18.55	2.55	0.05324	3.02	336	21	339	68	339	11	339	8	0
PL 502 1/7/2016 7:39:31 PM (Run: 1)	std	662.41	80.02	39.12	0.12	0.39254	3.62	0.05421	2.90	0.79	18.45	2.90	0.05252	2.17	338	16	308	49	336	10	340	10	-10
PL 509 1/7/2016 8:02:17 PM (Run: 1)	std	723.52	96.25	42.46	0.13	0.39699	3.12	0.05367	2.26	0.71	18.63	2.26	0.05365	2.14	327	18	356	48	339	9	337	7	5
PL 517 1/7/2016 8:26:42 PM (Run: 1)	std	654.86	78.00	38.30	0.12	0.38471	3.37	0.05370	2.67	0.78	18.62	2.67	0.05196	2.06	355	21	284	47	330	10	337	9	-19
PL 518 1/7/2016 8:28:25 PM (Run: 1)	std	671.84	81.00	38.81	0.12	0.38170	3.61	0.05312	2.60	0.71	18.83	2.60	0.05212	2.51	332	18	291	57	328	10	334	8	-15
PL 525 1/7/2016 8:51:13 PM (Run: 1)	std	658.62	77.63	38.34	0.12	0.39678	3.45	0.05351	2.63	0.75	18.69	2.63	0.05378	2.23	327	29	362	50	339	10	336	9	7
PL 526 1/7/2016 8:52:56 PM (Run: 1)	std	607.29	69.85	35.26	0.12	0.40400	4.12	0.05337	3.26	0.78	18.74	3.26	0.05490	2.52	334	20	408	56	345	12	335	11	18
PL 533 1/7/2016 9:15:35 PM (Run: 1)	std	747.42	100.08	43.57	0.13	0.39345	3.87	0.05307	3.02	0.77	18.84	3.02	0.05377	2.42	359	16	361	55	337	11	333	10	8
PL 534 1/7/2016 9:17:19 PM (Run: 1)	std	712.53	87.23	41.60	0.12	0.39864	4.08	0.05364	3.26	0.79	18.64	3.26	0.05390	2.46	315	17	367	55	341	12	337	11	8
PL 541 1/7/2016 9:38:16 PM (Run: 1)	std	722.53	79.77	42.60	0.11	0.39594	3.56	0.05428	3.02	0.84	18.42	3.02	0.05290	1.88	343	22	325	43	339	10	341	10	-5
PL 542 1/7/2016 9:40:00 PM (Run: 1)	std	586.45	63.42	34.63	0.11	0.39377	3.50	0.05456	2.58	0.72	18.33	2.58	0.05235	2.37	338	23	301	54	337	10	342	9	-14

Experiment 3 on January 7, 2016
Isotope ratio and date errors do not include systematic calibration errors of 0.48% ($^{207}Pb/^{206}Pb$) and 0.92% ($^{206}Pb/^{238}U$) (2 sigma).
Trace element concentrations were deleted from analyses known to have intersected inclusions of other minerals based on P and Ti.
Ablation used a laser spot size of 25 microns and a laser firing repetition rate of 5 Hz.
Activity of TiO_2 for Ti-in-Zircon temperature calculation is 0.8.

Appendix Table A8 LA-ICPMS isotopic U-Pb and trace element concentration data analyzed at Boise State University

Analysis	P	Ti	Y	Zr	Nb	La	Ce	Pr	Nd	Sm	Eu	Gd	Tb	Dy	Ho	Er	Tm	Yb	Lu	Hf	Ta	Th	U
	ppm	ppm	ppm	ppm	ppm	ppm	ppm	ppm	ppm	ppm	ppm	ppm	ppm	ppm	ppm	ppm	ppm	ppm	ppm	ppm	ppm	ppm	ppm
Plesovice - Primary zircon standard																							
PL 445 1/7/2016 5:07:41 PM (Run: 1)	482.53	85.73	703.04	551434.42	4.39		1.88	0.19	2.56	5.68	1.27	19.51	7.95	85.31	23.14	78.93	15.34	121.49	12.11	11081.81	3.33	83.97	672.61
PL 446 1/7/2016 5:09:24 PM (Run: 1)	419.52	84.25	638.31	561763.83	4.60		1.84	0.14	2.35	4.42	1.23	16.48	6.39	77.44	20.83	70.65	14.37	108.39	11.19	11592.49	3.28	75.14	622.13
PL 447 1/7/2016 5:11:08 PM (Run: 1)	344.33	78.53	563.98	557638.86	4.25		1.54	0.15	1.60	3.59	0.86	15.93	6.24	67.46	17.98	63.02	12.46	100.86	9.71	11629.14	3.35	64.75	563.14
PL 448 1/7/2016 5:12:52 PM (Run: 1)	360.73	78.02	562.17	566434.53	4.20	0.03	1.85	0.13	2.35	3.03	0.83	15.73	5.89	67.08	17.31	63.44	12.58	98.06	9.63	11701.53	3.29	64.55	559.37
PL 461 1/7/2016 5:35:33 PM (Run: 1)	313.35	73.68	455.35	559176.88	5.43		2.14	0.06	1.76	2.93	0.89	13.98	5.26	54.97	15.10	51.83	9.40	76.01	7.47	11041.87	3.44	78.29	604.04
PL 462 1/7/2016 5:37:17 PM (Run: 1)	294.43	75.33	450.88	563219.03	5.32		1.90	0.10	1.17	3.12	0.69	12.88	5.29	56.58	14.86	49.84	9.82	72.19	7.43	11452.33	3.10	77.06	585.94
PL 469 1/7/2016 5:59:57 PM (Run: 1)	264.44	72.52	427.49	551918.69	5.18		1.91	0.15	1.39	3.41	0.86	12.93	5.05	50.69	14.62	47.06	9.08	69.87	6.66	11051.76	3.27	73.32	560.28
PL 470 1/7/2016 6:01:41 PM (Run: 1)	292.92	77.58	469.02	570494.14	5.43		1.87	0.11	1.47	3.32	0.95	13.54	5.38	57.03	15.59	49.84	9.25	74.82	6.82	11234.34	3.23	85.11	599.14
PL 477 1/7/2016 6:24:29 PM (Run: 1)	332.38	68.59	436.01	555598.28	3.80		1.72	0.13	1.69	2.51	0.78	12.00	4.82	51.58	14.09	51.27	9.44	78.38	7.78	11571.10	2.83	53.57	540.46
PL 478 1/7/2016 6:26:12 PM (Run: 1)	384.22	81.04	559.62	564984.88	4.23		1.76	0.11	2.10	4.24	1.02	15.55	5.93	64.37	17.53	61.64	12.76	96.87	9.57	11541.12	3.09	67.70	586.31
PL 485 1/7/2016 6:48:54 PM (Run: 1)	506.34	97.84	717.61	569736.85	4.80	0.01	1.95	0.19	2.59	5.50	1.66	20.14	8.05	84.40	22.88	76.71	15.29	124.03	12.29	11461.96	3.46	89.79	723.96
PL 486 1/7/2016 6:50:37 PM (Run: 1)	460.46	93.40	653.33	569428.75	4.76		1.76	0.15	2.44	4.69	0.99	18.46	6.97	79.44	20.96	69.66	14.28	110.98	11.13	11620.16	3.32	80.62	675.88
PL 493 1/7/2016 7:13:24 PM (Run: 1)	354.62	76.60	494.02	551259.79	4.30		1.69	0.09	2.21	3.56	0.77	15.81	5.30	58.53	15.95	56.69	10.78	86.58	8.86	11154.78	2.91	60.16	585.59
PL 494 1/7/2016 7:15:08 PM (Run: 1)	434.86	89.90	643.54	580028.29	4.16	0.03	1.78	0.16	3.13	4.95	1.29	17.43	7.14	76.42	19.58	66.90	13.95	106.01	10.76	11577.21	3.22	78.10	664.51
PL 501 1/7/2016 7:37:47 PM (Run: 1)	505.67	100.85	731.95	572786.47	4.76	0.05	2.38	0.20	2.99	5.01	1.31	20.93	7.88	86.54	22.28	78.66	14.84	121.28	12.16	11563.47	3.41	88.68	713.30
PL 502 1/7/2016 7:39:31 PM (Run: 1)	471.68	94.34	645.17	576336.93	4.86		1.88	0.13	2.28	5.04	1.27	17.94	7.28	72.79	20.81	72.64	13.46	106.78	11.28	11759.87	3.43	80.02	662.41
PL 509 1/7/2016 8:02:17 PM (Run: 1)	463.98	94.17	684.63	586557.91	4.85		2.30	0.20	3.49	6.35	1.21	21.20	7.68	82.32	23.07	75.93	13.97	110.11	10.85	12032.07	3.30	96.25	723.52
PL 517 1/7/2016 8:26:42 PM (Run: 1)	428.36	90.55	631.50	592376.62	4.89		2.12	0.20	1.92	4.33	1.00	17.46	6.91	73.63	19.63	66.23	12.90	98.07	10.19	11979.28	3.43	78.00	654.86
PL 518 1/7/2016 8:28:25 PM (Run: 1)	432.61	94.73	672.43	594889.15	4.78		2.04	0.17	2.63	4.66	1.12	18.15	6.82	77.82	20.20	68.05	13.38	104.31	10.78	12276.99	3.59	81.00	671.84
PL 525 1/7/2016 8:51:13 PM (Run: 1)	451.31	91.69	629.41	582273.15	4.49		1.93	0.14	3.25	5.19	1.00	16.57	6.80	73.13	20.41	65.07	13.14	101.76	9.92	11695.66	3.24	77.63	658.62
PL 526 1/7/2016 8:52:56 PM (Run: 1)	351.04	80.83	555.04	586729.30	4.37		1.88	0.14	2.09	3.97	1.03	14.61	6.00	64.12	17.80	57.91	11.13	87.30	8.87	11930.86	3.39	69.85	607.29
PL 533 1/7/2016 9:15:35 PM (Run: 1)	498.31	106.20	735.93	604175.51	5.19		2.15	0.21	2.83	5.21	1.50	21.90	7.71	84.71	23.23	80.97	15.83	120.95	11.40	12025.10	3.36	100.08	747.42
PL 534 1/7/2016 9:17:19 PM (Run: 1)	510.91	102.07	708.58	591692.26	5.32	0.04	2.09	0.21	2.66	4.79	1.24	19.30	7.58	82.73	23.01	77.44	15.52	111.87	11.38	11998.58	3.44	87.23	712.53
PL 541 1/7/2016 9:38:16 PM (Run: 1)	349.96	38.86	422.68	595517.77	5.14	0.21	2.85	0.25	2.10	3.16	0.65	11.87	4.23	49.58	13.50	43.43	8.69	65.37	6.67	11727.79	3.45	79.77	722.53
PL 542 1/7/2016 9:40:00 PM (Run: 1)	308.57	36.96	351.59	584057.10	4.31	0.09	1.94	0.09	1.77	2.25	0.63	8.35	3.52	41.43	11.19	36.69	7.32	59.37	5.82	11761.84	3.17	63.42	586.45

Experiment 3 on January 7, 2016
Isotope ratio and date errors do not include systematic calibration errors of 0.48% ($^{207}Pb/^{206}Pb$) and 0.92% ($^{206}Pb/^{238}U$) (2 sigma).
Trace element concentrations were deleted from analyses known to have intersected inclusions of other minerals based on P and Ti.
Ablation used a laser spot size of 25 microns and a laser firing repetition rate of 5 Hz.
Activity of TiO_2 for Ti-in-Zircon temperature calculation is 0.8.

Appendix Table A8 LA-ICPMS isotopic U-Pb and trace element concentration data analyzed at Boise State University

Analysis	CA-TIMS label	U ppm	Th ppm	Pb* ppm	Th/U	$^{207}Pb/^{235}U$	±2s (%)	$^{206}Pb/^{238}U$	±2s (%)	error corr.	$^{238}U/^{206}Pb$	±2s (%)	$^{207}Pb/^{206}Pb$	±2s (%)	$^{208}Pb/^{232}Th$	±2s (Ma)	$^{207}Pb/^{206}Pb$	±2s (Ma)	$^{207}Pb/^{235}U$	±2s (Ma)	$^{206}Pb/^{238}U$	±2s (Ma)	% disc
Seiland - Secondary reference zircon																							
Seiland 565 1/7/2016 5:14:37 PM (Run: 1)		53.01	52.82	6.10	1.00	0.62798	7.06	0.08478	4.14	0.58	11.79	4.14	0.05372	5.72	536	34	359	129	495	28	525	21	-46
Seiland 566 1/7/2016 5:16:21 PM (Run: 1)		44.21	43.13	5.15	0.98	0.72539	7.34	0.08546	3.22	0.43	11.70	3.22	0.06156	6.60	548	44	659	141	554	31	529	16	20
Seiland 573 1/7/2016 6:03:27 PM (Run: 1)		57.81	58.90	6.90	1.02	0.76209	7.17	0.08567	3.62	0.50	11.67	3.62	0.06452	6.18	569	41	759	130	575	31	530	18	30
Seiland 574 1/7/2016 6:05:10 PM (Run: 1)		57.18	58.21	6.66	1.02	0.72864	6.16	0.08501	3.19	0.51	11.76	3.19	0.06216	5.27	531	33	680	113	556	26	526	16	23
Seiland 581 1/7/2016 6:52:23 PM (Run: 1)		51.11	50.50	5.97	0.99	0.70358	7.72	0.08535	3.90	0.50	11.72	3.90	0.05979	6.66	552	46	596	144	541	32	528	20	11
Seiland 582 1/7/2016 6:54:07 PM (Run: 1)		54.86	54.52	6.37	0.99	0.71996	6.96	0.08654	3.28	0.47	11.56	3.28	0.06034	6.13	508	31	616	132	551	30	535	17	13
Seiland 589 1/7/2016 7:41:16 PM (Run: 1)		53.78	52.88	6.21	0.98	0.69758	7.36	0.08561	3.62	0.49	11.68	3.62	0.05910	6.41	524	20	571	139	537	31	530	18	7
Seiland 590 1/7/2016 7:43:00 PM (Run: 1)		56.63	56.31	6.71	0.99	0.65766	7.69	0.08742	3.66	0.47	11.44	3.66	0.05456	6.76	547	40	394	152	513	31	540	19	-37
Seiland 597 1/7/2016 8:30:12 PM (Run: 1)		56.49	55.48	6.63	0.98	0.67914	5.89	0.08602	3.16	0.53	11.63	3.16	0.05726	4.97	557	30	502	109	526	24	532	16	-6
Seiland 598 1/7/2016 8:31:55 PM (Run: 1)		45.84	45.55	5.34	0.99	0.67061	8.40	0.08643	4.09	0.48	11.57	4.09	0.05627	7.33	528	25	463	162	521	34	534	21	-15
Zirconia - Secondary reference zircon																							
Zirconia 605 1/7/2016 5:39:02 PM (Run: 1)		364.53	1778.95	46.40	4.88	0.37411	4.27	0.05138	3.53	0.82	19.46	3.53	0.05281	2.41	302	9	321	55	323	12	323	11	-1
Zirconia 606 1/7/2016 5:40:45 PM (Run: 1)		564.82	4512.98	94.71	7.99	0.38190	3.66	0.05087	2.85	0.77	19.66	2.85	0.05445	2.29	287	5	390	51	328	10	320	9	18
Zirconia 615 1/7/2016 6:27:57 PM (Run: 1)	high U signal variance	501.61	3812.83	84.30	7.60	0.39904	4.25	0.05310	3.41	0.80	18.83	3.41	0.05450	2.53	296	9	392	57	341	12	334	11	15
Zirconia 616 1/7/2016 6:29:41 PM (Run: 1)		462.18	3379.40	73.13	7.31	0.37117	3.82	0.05137	2.29	0.59	19.47	2.29	0.05240	3.06	287	4	303	70	321	11	323	7	-7
Zirconia 623 1/7/2016 7:16:53 PM (Run: 1)		350.46	1814.73	45.80	5.18	0.39165	4.46	0.05243	3.56	0.79	19.07	3.56	0.05418	2.68	294	8	378	60	336	13	329	11	13
Zirconia 624 1/7/2016 7:18:37 PM (Run: 1)		292.92	1304.57	36.12	4.45	0.38420	5.21	0.05392	2.38	0.45	18.55	2.38	0.05168	4.63	302	6	271	106	330	15	339	8	-25
Zirconia 631 1/7/2016 8:05:46 PM (Run: 1)		343.96	1563.46	42.10	4.55	0.37985	5.09	0.05127	2.57	0.50	19.51	2.57	0.05374	4.39	304	6	360	99	327	14	322	8	10
Zirconia 632 1/7/2016 8:07:29 PM (Run: 1)		325.21	1391.77	37.60	4.28	0.37541	4.71	0.05143	2.97	0.62	19.45	2.97	0.05294	3.66	290	5	326	83	324	13	323	9	1
Zirconia 639 1/7/2016 8:54:42 PM (Run: 1)		297.33	1200.19	34.35	4.04	0.37553	4.69	0.05203	2.82	0.59	19.22	2.82	0.05235	3.74	304	7	301	85	324	13	327	9	-9
Zirconia 640 1/7/2016 8:56:25 PM (Run: 1)		364.59	1719.26	45.35	4.72	0.37634	3.89	0.05084	2.17	0.54	19.67	2.17	0.05369	3.23	303	5	358	73	324	11	320	7	11

Experiment 3 on January 7, 2016
Isotope ratio and date errors do not include systematic calibration errors of 0.48% ($^{207}Pb/^{206}Pb$) and 0.92% ($^{206}Pb/^{238}U$) (2 sigma).
Trace element concentrations were deleted from analyses known to have intersected inclusions of other minerals based on P and Ti.
Ablation used a laser spot size of 25 microns and a laser firing repetition rate of 5 Hz.
Activity of TiO_2 for Ti-in-Zircon temperature calculation is 0.8.

Appendix Table A8 LA-ICPMS isotopic U-Pb and trace element concentration data analyzed at Boise State University

Analysis	P	Ti	Y	Zr	Nb	La	Ce	Pr	Nd	Sm	Eu	Gd	Tb	Dy	Ho	Er	Tm	Yb	Lu	Hf	Ta	Th	U
	ppm	ppm	ppm	ppm	ppm	ppm	ppm	ppm	ppm	ppm	ppm	ppm	ppm	ppm	ppm	ppm	ppm	ppm	ppm	ppm	ppm	ppm	ppm
Seiland - Secondary reference zircon																							
Seiland 565 1/7/2016 5:14:37 PM (Run: 1)	40.02	1.76	226.19	548471.82	1.26		2.53			0.61	0.51	3.78	1.72	23.01	8.26	40.49	10.82	123.97	16.08	4824.95	0.92	52.82	53.01
Seiland 566 1/7/2016 5:16:21 PM (Run: 1)	51.02	1.75	200.89	549017.35	0.99		2.46			0.41	0.71	4.39	1.34	20.70	7.52	34.92	10.02	112.44	14.75	4958.11	0.92	43.13	44.21
Seiland 573 1/7/2016 6:03:27 PM (Run: 1)	69.06	1.89	231.97	563691.18	1.11		2.85		0.20	0.81	0.49	4.06	1.61	23.49	9.10	42.48	12.05	129.21	17.05	4981.75	0.95	58.90	57.81
Seiland 574 1/7/2016 6:05:10 PM (Run: 1)	89.07	2.06	234.69	563108.25	1.29	0.02	2.88	0.04	0.12	0.60	0.54	3.30	1.80	21.91	9.22	40.66	11.34	126.47	16.82	4890.91	0.89	58.21	57.18
Seiland 581 1/7/2016 6:52:23 PM (Run: 1)	54.80	1.95	214.04	561481.67	1.11		2.49	0.02	0.11	0.47	0.53	3.35	1.29	20.49	7.58	39.25	10.59	119.61	15.87	4939.78	0.85	50.50	51.11
Seiland 582 1/7/2016 6:54:07 PM (Run: 1)	57.92	1.85	229.10	561099.66	1.18	0.03	2.59	0.02		0.52	0.71	4.22	1.80	22.22	8.56	40.63	11.11	125.18	16.38	4948.78	0.89	54.52	54.86
Seiland 589 1/7/2016 7:41:16 PM (Run: 1)	46.47	1.62	226.61	565439.16	0.97		2.52	0.02		0.73	0.54	4.56	1.67	22.29	8.89	39.08	10.82	118.03	16.73	4896.23	0.98	52.88	53.78
Seiland 590 1/7/2016 7:43:00 PM (Run: 1)	51.05	2.09	234.52	565208.57	1.07		2.71		0.27	0.47	0.80	2.85	1.59	23.13	8.42	39.70	11.53	124.51	16.16	4983.53	0.97	56.31	56.63
Seiland 597 1/7/2016 8:30:12 PM (Run: 1)	58.64	2.21	229.35	559748.21	1.42		2.51	0.02		0.58	0.70	4.12	2.06	22.37	8.85	40.13	10.91	123.26	15.69	4888.14	1.18	55.48	56.49
Seiland 598 1/7/2016 8:31:55 PM (Run: 1)	56.87	1.98	205.71	555217.25	0.83		2.28			0.36	0.52	3.26	1.21	19.40	7.76	36.98	9.82	111.29	15.26	4926.57	0.94	45.55	45.84
Zirconia - Secondary reference zircon																							
Zirconia 605 1/7/2016 5:39:02 PM (Run: 1)	64.33	18.81	1743.07	606541.60	2.21	0.43	152.96	3.48	56.35	67.41	32.94	189.04	39.92	298.76	69.27	198.44	35.15	257.13	30.58	8623.40	0.68	1778.95	364.53
Zirconia 606 1/7/2016 5:40:45 PM (Run: 1)	60.20	24.46	1757.49	597747.81	3.14	0.83	227.51	5.63	80.49	93.46	41.36	229.27	44.97	316.04	69.45	194.66	32.41	241.08	28.91	8837.82	0.81	4512.98	564.82
Zirconia 615 1/7/2016 6:27:57 PM (Run: 1)	92.18	21.92	1547.88	598533.55	2.72	0.70	193.66	4.21	67.51	77.31	33.94	189.19	37.13	263.89	59.66	168.74	28.95	218.15	26.09	8593.72	0.75	3812.83	501.61
Zirconia 616 1/7/2016 6:29:41 PM (Run: 1)	50.81	20.09	1439.03	599615.74	2.37	0.73	170.46	3.56	53.56	62.83	30.93	164.63	33.19	245.87	55.97	161.54	27.55	201.96	24.00	8687.49	0.61	3379.40	462.18
Zirconia 623 1/7/2016 7:16:53 PM (Run: 1)	83.21	18.07	1665.28	625419.77	1.69	0.37	144.61	2.91	51.94	64.50	31.24	171.93	36.21	281.54	64.04	188.97	31.94	242.86	30.29	8904.63	0.51	1814.73	350.46
Zirconia 624 1/7/2016 7:18:37 PM (Run: 1)	91.14	14.60	1560.36	620040.44	1.53	0.22	122.09	2.59	40.58	52.50	26.76	147.89	33.55	256.85	60.89	174.72	29.89	228.33	28.49	8843.39	0.37	1304.57	292.92
Zirconia 631 1/7/2016 8:05:46 PM (Run: 1)	64.12	17.18	1686.74	616497.86	1.76	0.14	145.65	2.96	48.04	64.62	31.22	178.25	36.63	279.60	64.39	187.01	33.11	248.97	29.10	8501.20	0.54	1563.46	343.96
Zirconia 632 1/7/2016 8:07:29 PM (Run: 1)	81.21	13.92	1653.29	622507.47	1.79	0.14	135.15	2.48	39.75	56.77	28.33	159.69	35.00	270.63	63.54	190.98	32.85	253.03	31.05	8687.53	0.65	1391.77	325.21
Zirconia 639 1/7/2016 8:54:42 PM (Run: 1)	73.77	14.59	1511.68	607954.58	1.54	0.13	120.01	2.36	37.57	48.30	25.61	154.51	31.13	244.05	56.77	176.30	30.59	237.48	27.47	8298.41	0.38	1200.19	297.33
Zirconia 640 1/7/2016 8:56:25 PM (Run: 1)	82.12	17.56	1757.14	609366.78	2.12	0.18	157.11	3.54	52.50	67.51	33.97	187.15	39.99	298.07	69.46	200.01	35.40	268.29	29.52	8439.60	0.63	1719.26	364.59

Experiment 3 on January 7, 2016
Isotope ratio and date errors do not include systematic calibration errors of 0.48% ($^{207}Pb/^{206}Pb$) and 0.92% ($^{206}Pb/^{238}U$) (2 sigma).
Trace element concentrations were deleted from analyses known to have intersected inclusions of other minerals based on P and Ti.
Ablation used a laser spot size of 25 microns and a laser firing repetition rate of 5 Hz.
Activity of TiO_2 for Ti-in-Zircon temperature calculation is 0.8.

Appendix Table A8 LA-ICPMS isotopic U-Pb and trace element concentration data analyzed at Boise State University

Analysis	CA-TIMS label	U ppm	Th ppm	Pb* ppm	Th/U	$^{207}Pb/^{235}U$	±2s (%)	$^{206}Pb/^{238}U$	±2s (%)	error corr.	$^{238}U/^{206}Pb$	±2s (%)	$^{207}Pb/^{206}Pb$	±2s (%)	$^{208}Pb/^{232}Th$	±2s (Ma)	$^{207}Pb/^{206}Pb$	±2s (Ma)	$^{207}Pb/^{235}U$	±2s (Ma)	$^{206}Pb/^{238}U$	±2s (Ma)	% disc
Plesovice - Primary zircon standard																							
PL 453 1/8/2016 2:40:25 AM (Run: 1)	std	607.29	95.86	36.58	0.16	0.42319	4.64	0.05444	2.98	0.63	18.37	2.98	0.05638	3.56	354	33	467	79	358	14	342	10	27
PL 454 1/8/2016 2:42:08 AM (Run: 1)	std	605.66	72.96	35.19	0.12	0.38981	3.14	0.05334	2.22	0.69	18.75	2.22	0.05300	2.22	337	23	329	50	334	9	335	7	-2
PL 455 1/8/2016 2:43:52 AM (Run: 1)	std	566.35	64.85	33.04	0.11	0.37790	3.31	0.05383	2.30	0.68	18.58	2.30	0.05092	2.37	330	32	237	55	325	9	338	8	-43
PL 456 1/8/2016 2:45:36 AM (Run: 1)	std	572.76	67.19	33.56	0.12	0.39989	3.60	0.05381	2.33	0.63	18.59	2.33	0.05390	2.74	343	26	367	62	342	10	338	8	8
PL 465 1/8/2016 3:08:17 AM (Run: 1)	std	578.30	78.64	33.73	0.14	0.38683	3.56	0.05353	1.82	0.49	18.68	1.82	0.05241	3.06	314	21	303	70	332	10	336	6	-11
PL 466 1/8/2016 3:10:00 AM (Run: 1)	std	544.53	70.25	31.95	0.13	0.39594	3.91	0.05390	2.60	0.65	18.55	2.60	0.05328	2.92	321	21	341	66	339	11	338	9	1
PL 473 1/8/2016 3:32:41 AM (Run: 1)	std	555.00	73.08	32.37	0.13	0.38353	3.05	0.05354	1.93	0.61	18.68	1.93	0.05195	2.36	329	19	283	54	330	9	336	6	-19
PL 474 1/8/2016 3:34:25 AM (Run: 1)	std	565.98	74.76	33.09	0.13	0.39276	3.75	0.05352	2.25	0.58	18.68	2.25	0.05322	3.00	342	30	338	68	336	11	336	7	1
PL 481 1/8/2016 3:57:10 AM (Run: 1)	high U signal variance	592.03	68.88	34.93	0.12	0.40098	4.85	0.05408	3.57	0.73	18.49	3.57	0.05378	3.28	369	22	362	74	342	14	340	12	6
PL 482 1/8/2016 3:58:54 AM (Run: 1)	std	532.65	58.90	30.75	0.11	0.38460	3.70	0.05324	2.63	0.70	18.78	2.63	0.05239	2.60	341	29	302	59	330	10	334	9	-11
PL 489 1/8/2016 4:21:35 AM (Run: 1)	std	733.61	94.51	42.83	0.13	0.39460	3.31	0.05334	2.55	0.75	18.75	2.55	0.05366	2.10	333	22	357	48	338	9	335	8	6
PL 490 1/8/2016 4:23:18 AM (Run: 1)	std	721.80	91.40	42.12	0.13	0.39096	2.91	0.05333	2.61	0.88	18.75	2.61	0.05317	1.28	341	26	336	29	335	8	335	9	0
PL 497 1/8/2016 4:46:05 AM (Run: 1)	std	715.26	86.30	42.58	0.12	0.40653	3.64	0.05438	2.51	0.67	18.39	2.51	0.05422	2.64	346	21	380	59	346	11	341	8	10
PL 498 1/8/2016 4:47:49 AM (Run: 1)	std	606.00	70.20	35.85	0.12	0.39333	3.66	0.05429	2.63	0.70	18.42	2.63	0.05254	2.54	348	26	309	58	337	10	341	9	-10
PL 505 1/8/2016 5:10:28 AM (Run: 1)	std	632.08	73.08	37.36	0.12	0.40039	3.81	0.05421	2.43	0.62	18.45	2.43	0.05357	2.94	344	19	353	66	342	11	340	8	4
PL 506 1/8/2016 5:12:12 AM (Run: 1)	std	721.66	89.29	42.37	0.12	0.39635	3.95	0.05363	2.81	0.70	18.65	2.81	0.05360	2.77	349	19	354	63	339	11	337	9	5
PL 513 1/8/2016 5:35:00 AM (Run: 1)	std	728.46	90.05	42.60	0.12	0.38600	3.29	0.05361	2.48	0.74	18.65	2.48	0.05222	2.16	323	20	295	49	331	9	337	8	-14
PL 514 1/8/2016 5:36:43 AM (Run: 1)	std	738.03	91.80	42.87	0.12	0.39191	3.66	0.05322	2.09	0.55	18.79	2.09	0.05340	3.01	312	19	346	68	336	10	334	7	3
PL 521 1/8/2016 5:59:25 AM (Run: 1)	std	718.80	86.96	41.76	0.12	0.39381	3.85	0.05321	3.29	0.84	18.79	3.29	0.05368	2.00	325	26	358	45	337	11	334	11	7
PL 522 1/8/2016 6:01:08 AM (Run: 1)	std	747.88	93.29	43.66	0.12	0.39466	3.52	0.05331	2.74	0.76	18.76	2.74	0.05369	2.21	338	14	358	50	338	10	335	9	7
PL 529 1/8/2016 6:23:58 AM (Run: 1)	std	645.18	73.96	37.63	0.11	0.38851	3.54	0.05367	2.45	0.68	18.63	2.45	0.05250	2.55	329	23	307	58	333	10	337	8	-10
PL 530 1/8/2016 6:25:41 AM (Run: 1)	std	657.23	76.92	38.32	0.12	0.39812	3.18	0.05347	2.38	0.73	18.70	2.38	0.05400	2.11	338	28	371	47	340	9	336	8	10
PL 537 1/8/2016 6:48:28 AM (Run: 1)	std	671.68	73.53	39.32	0.11	0.39789	3.20	0.05376	2.61	0.80	18.60	2.61	0.05368	1.86	352	24	357	42	340	9	338	9	6
PL 538 1/8/2016 6:50:11 AM (Run: 1)	std	762.40	85.80	44.70	0.11	0.39827	3.39	0.05383	2.44	0.70	18.58	2.44	0.05366	2.36	329	27	357	53	340	10	338	8	5
PL 545 1/8/2016 7:07:41 AM (Run: 1)	std	658.45	72.01	38.33	0.11	0.38990	3.81	0.05352	2.61	0.67	18.68	2.61	0.05283	2.78	350	29	322	63	334	11	336	9	-4
PL 546 1/8/2016 7:09:25 AM (Run: 1)	std	703.16	77.61	41.14	0.11	0.38969	3.65	0.05385	2.31	0.62	18.57	2.31	0.05248	2.82	335	29	306	64	334	10	338	8	-10

Experiment 4 on January 8, 2016
Isotope ratio and date errors do not include systematic calibration errors of 0.52% ($^{207}Pb/^{206}Pb$) and 1.28% ($^{206}Pb/^{238}U$) (2 sigma).
Trace element concentrations were deleted from analyses known to have intersected inclusions of other minerals based on P and Ti.
Ablation used a laser spot size of 25 microns and a laser firing repetition rate of 5 Hz.
Activity of TiO_2 for Ti-in-Zircon temperature calculation is 0.8.

Appendix Table A8 LA-ICPMS isotopic U-Pb and trace element concentration data analyzed at Boise State University

Analysis	P	Ti	Y	Zr	Nb	La	Ce	Pr	Nd	Sm	Eu	Gd	Tb	Dy	Ho	Er	Tm	Yb	Lu	Hf	Ta	Th	U
	ppm	ppm	ppm	ppm	ppm	ppm	ppm	ppm	ppm	ppm	ppm	ppm	ppm	ppm	ppm	ppm	ppm	ppm	ppm	ppm	ppm	ppm	ppm
Plesovice - Primary zircon standard																							
PL 453 1/8/2016 2:40:25 AM (Run: 1)	338.69	77.32	529.23	577902.39	5.37	0.11	2.69	0.29	3.91	4.87	1.49	17.58	6.32	64.76	17.73	58.07	11.50	91.55	9.62	10911.01	3.63	95.86	607.29
PL 454 1/8/2016 2:42:08 AM (Run: 1)	389.46	81.72	594.92	573052.95	4.94		1.83	0.14	1.62	4.01	1.04	17.02	6.55	67.27	19.55	66.61	12.97	105.23	10.16	11640.51	3.36	72.96	605.66
PL 455 1/8/2016 2:43:52 AM (Run: 1)	387.49	79.30	562.35	570858.13	3.99		1.74	0.14	1.70	3.69	0.95	14.83	5.87	63.12	18.30	59.69	12.24	99.00	9.94	11503.59	3.04	64.85	566.35
PL 456 1/8/2016 2:45:36 AM (Run: 1)	378.03	80.38	574.49	576652.34	4.14		1.70	0.12	2.16	2.83	1.00	16.69	5.93	69.12	18.36	60.32	12.68	97.18	10.43	11613.50	3.03	67.19	572.76
PL 465 1/8/2016 3:08:17 AM (Run: 1)	310.50	69.30	455.88	575316.58	5.54	0.05	1.70	0.10	1.21	3.41	0.72	13.02	5.46	53.18	14.82	47.82	9.54	76.00	7.07	11261.03	3.36	78.64	578.30
PL 466 1/8/2016 3:10:00 AM (Run: 1)	302.89	66.90	453.73	571332.75	4.82		1.76	0.09	1.51	3.31	0.63	14.34	5.05	54.36	15.08	49.42	10.15	78.80	8.06	11319.93	3.10	70.25	544.53
PL 473 1/8/2016 3:32:41 AM (Run: 1)	289.26	66.45	432.54	578153.17	4.77		1.89	0.12	1.66	3.59	0.86	11.66	5.13	54.10	14.39	47.90	9.70	75.45	7.17	11444.47	3.16	73.08	555.00
PL 474 1/8/2016 3:34:25 AM (Run: 1)	315.24	71.40	456.94	575649.60	5.01		1.92	0.14	1.93	3.79	0.67	13.18	5.19	53.76	15.09	50.32	9.74	76.84	7.57	11597.87	3.16	74.76	565.98
PL 481 1/8/2016 3:57:10 AM (Run: 1)	418.40	78.45	566.42	574042.87	4.23		1.97	0.12	2.19	3.10	1.02	14.79	5.66	65.74	17.51	63.21	12.26	96.76	9.32	11791.99	2.79	68.88	592.03
PL 482 1/8/2016 3:58:54 AM (Run: 1)	360.85	71.75	503.36	576414.96	3.65		1.53	0.15	1.79	3.05	0.83	15.09	5.31	59.25	16.39	54.82	10.71	87.30	8.60	12067.91	2.80	58.90	532.65
PL 489 1/8/2016 4:21:35 AM (Run: 1)	533.09	96.45	744.15	585124.31	5.61		2.11	0.17	2.83	4.99	1.49	25.20	8.20	89.44	23.66	83.65	16.18	123.43	11.74	11727.65	3.54	94.51	733.61
PL 490 1/8/2016 4:23:18 AM (Run: 1)	514.63	95.23	728.47	581985.55	5.14		2.21	0.16	2.84	5.30	1.30	23.23	7.81	88.02	24.50	80.85	15.82	124.68	12.19	11771.52	3.87	91.40	721.80
PL 497 1/8/2016 4:46:05 AM (Run: 1)	430.85	86.20	662.52	588609.46	4.47		2.08	0.09	2.90	3.47	1.14	18.79	7.83	80.55	23.49	75.04	14.65	119.22	11.90	12989.14	3.78	86.30	715.26
PL 498 1/8/2016 4:47:49 AM (Run: 1)	363.62	75.75	541.01	574975.72	4.65		1.85	0.13	2.06	3.23	0.89	15.31	6.19	65.48	17.96	62.49	11.57	99.42	9.65	12886.39	3.15	70.20	606.00
PL 505 1/8/2016 5:10:28 AM (Run: 1)	395.39	77.63	575.37	576462.46	3.97		1.74	0.10	2.40	4.20	0.99	16.88	6.62	68.04	19.64	65.62	13.08	101.15	9.53	12347.95	3.43	73.08	632.08
PL 506 1/8/2016 5:12:12 AM (Run: 1)	482.19	89.48	669.01	596978.89	5.37	0.02	1.92	0.16	2.30	4.92	1.12	19.17	7.85	83.44	21.77	75.84	14.19	111.84	11.50	12857.47	3.82	89.29	721.66
PL 513 1/8/2016 5:35:00 AM (Run: 1)	437.87	90.31	691.16	593307.33	4.97		2.09	0.11	2.70	5.61	1.27	18.49	7.70	80.57	22.51	76.52	14.90	115.75	11.77	12908.07	3.58	90.05	728.46
PL 514 1/8/2016 5:36:43 AM (Run: 1)	461.46	90.74	696.65	590745.43	4.59	0.06	2.09	0.21	2.82	5.18	1.40	19.82	8.43	83.41	23.21	75.52	15.00	117.68	11.99	12878.11	3.63	91.80	738.03
PL 521 1/8/2016 5:59:25 AM (Run: 1)	434.91	82.37	638.10	585645.43	4.70	0.03	2.18	0.14	1.76	4.23	1.19	21.44	7.05	80.56	21.75	73.18	13.84	108.49	11.11	13195.00	3.81	86.96	718.80
PL 522 1/8/2016 6:01:08 AM (Run: 1)	468.56	89.36	693.04	597708.79	4.62		2.20	0.17	2.25	4.72	1.14	21.11	8.27	86.02	23.82	78.17	15.57	117.81	11.46	13038.40	3.88	93.29	747.88
PL 529 1/8/2016 6:23:58 AM (Run: 1)	333.83	78.77	557.45	598635.21	4.67		1.97	0.13	1.87	4.24	1.11	16.63	6.65	68.69	18.30	65.54	11.97	94.49	9.36	13329.14	3.77	73.96	645.18
PL 530 1/8/2016 6:25:41 AM (Run: 1)	400.11	79.58	582.65	595175.75	4.78		2.00	0.10	1.79	4.16	0.95	18.08	6.60	69.11	19.23	63.45	12.90	96.85	9.70	13029.60	3.57	76.92	657.23
PL 537 1/8/2016 6:48:28 AM (Run: 1)	309.84	30.76	378.92	587776.96	4.43	0.24	2.62	0.22	2.01	1.38	0.66	11.93	4.13	45.76	12.31	41.96	8.16	63.32	6.32	12684.60	3.76	73.53	671.68
PL 538 1/8/2016 6:50:11 AM (Run: 1)	356.44	34.24	423.97	589722.23	4.92	0.18	2.41	0.22	2.24	2.75	0.83	11.15	4.57	49.54	14.03	47.33	9.79	73.83	7.70	12460.25	3.42	85.80	762.40
PL 545 1/8/2016 7:07:41 AM (Run: 1)	345.36	35.93	383.22	597289.87	4.35	0.37	2.63	0.22	1.86	2.33	0.61	8.88	4.40	44.64	12.46	45.12	8.55	69.05	6.43	12576.71	3.63	72.01	658.45
PL 546 1/8/2016 7:09:25 AM (Run: 1)	335.49	33.36	421.73	602124.28	4.43	0.37	2.40	0.23	1.85	2.39	0.73	10.91	4.45	47.65	14.17	44.87	9.52	69.86	7.48	12585.28	3.83	77.61	703.16

Experiment 4 on January 8, 2016
Isotope ratio and date errors do not include systematic calibration errors of 0.52% ($^{207}Pb/^{206}Pb$) and 1.28% ($^{206}Pb/^{238}U$) (2 sigma).
Trace element concentrations were deleted from analyses known to have intersected inclusions of other minerals based on P and Ti.
Ablation used a laser spot size of 25 microns and a laser firing repetition rate of 5 Hz.
Activity of TiO_2 for Ti-in-Zircon temperature calculation is 0.8.

Appendix Table A8 LA-ICPMS isotopic U-Pb and trace element concentration data analyzed at Boise State University

Analysis	CA-TIMS label	U ppm	Th ppm	Pb* ppm	Th/U	$^{207}Pb/^{235}U$	±2s (%)	$^{206}Pb/^{238}U$	±2s (%)	error corr.	$^{238}U/^{206}Pb$	±2s (%)	$^{207}Pb/^{206}Pb$	±2s (%)	$^{208}Pb/^{232}Th$	±2s (Ma)	$^{207}Pb/^{206}Pb$	±2s (Ma)	$^{207}Pb/^{235}U$	±2s (Ma)	$^{206}Pb/^{238}U$	±2s (Ma)	% disc
Seiland - Secondary reference zircon																							
Seiland 569 1/8/2016 2:47:21 AM (Run: 1)		49.55	50.17	5.78	1.01	0.68880	6.70	0.08567	3.36	0.49	11.67	3.36	0.05832	5.80	536	39	542	127	532	28	530	17	2
Seiland 570 1/8/2016 2:49:05 AM (Run: 1)		53.74	54.83	6.25	1.02	0.69516	6.89	0.08505	3.76	0.54	11.76	3.76	0.05928	5.77	534	29	577	125	536	29	526	19	9
Seiland 577 1/8/2016 3:36:10 AM (Run: 1)		48.99	48.56	5.71	0.99	0.66640	6.17	0.08507	2.97	0.47	11.75	2.97	0.05681	5.41	559	35	484	119	519	25	526	15	-9
Seiland 578 1/8/2016 3:37:53 AM (Run: 1)		43.46	42.12	5.08	0.97	0.73023	7.88	0.08773	4.19	0.53	11.40	4.19	0.06037	6.67	517	38	617	144	557	34	542	22	12
Seiland 585 1/8/2016 4:25:04 AM (Run: 1)		55.40	55.60	6.60	1.00	0.68813	6.62	0.08615	3.50	0.52	11.61	3.50	0.05793	5.62	579	49	527	123	532	27	533	18	-1
Seiland 586 1/8/2016 4:26:48 AM (Run: 1)		50.76	50.90	5.87	1.00	0.63932	10.20	0.08480	4.73	0.46	11.79	4.73	0.05468	9.04	545	49	399	203	502	40	525	24	-31
Seiland 593 1/8/2016 5:13:58 AM (Run: 1)		46.44	44.28	5.49	0.95	0.71143	8.18	0.08693	3.42	0.41	11.50	3.42	0.05936	7.42	572	44	580	161	546	35	537	18	7
Seiland 594 1/8/2016 5:15:42 AM (Run: 1)		47.36	46.52	5.47	0.98	0.66457	10.17	0.08587	4.19	0.41	11.65	4.19	0.05613	9.27	529	38	458	206	517	41	531	21	-16
Seiland 601 1/8/2016 6:02:54 AM (Run: 1)		51.48	50.49	6.17	0.98	0.68643	7.83	0.08568	3.70	0.47	11.67	3.70	0.05811	6.89	615	48	534	151	531	32	530	19	1
Seiland 602 1/8/2016 6:04:38 AM (Run: 1)		62.36	61.63	7.40	0.99	0.71348	8.20	0.08590	3.54	0.43	11.64	3.54	0.06024	7.39	578	46	612	160	547	35	531	18	13
Zirconia - Secondary reference zircon																							
Zirconia 609 1/8/2016 3:11:45 AM (Run: 1)		516.02	4133.81	90.28	8.01	0.37875	3.93	0.05233	3.08	0.77	19.11	3.08	0.05249	2.45	301	7	307	56	326	11	329	10	-7
Zirconia 611 1/8/2016 3:13:29 AM (Run: 1)		486.57	3723.68	84.32	7.65	0.37646	3.29	0.05237	2.36	0.70	19.10	2.36	0.05214	2.28	310	3	291	52	324	9	329	8	-13
Zirconia 619 1/8/2016 4:00:39 AM (Run: 1)		534.12	4326.56	94.73	8.10	0.37177	3.95	0.05167	2.88	0.72	19.35	2.88	0.05218	2.71	305	7	293	62	321	11	325	9	-11
Zirconia 620 1/8/2016 4:02:23 AM (Run: 1)		545.88	4415.82	97.11	8.09	0.37450	3.61	0.05188	2.39	0.64	19.27	2.39	0.05235	2.71	306	4	301	62	323	10	326	8	-8
Zirconia 627 1/8/2016 4:49:34 AM (Run: 1)		346.20	1479.99	41.01	4.28	0.38579	4.17	0.05157	2.38	0.56	19.39	2.38	0.05425	3.43	303	4	382	77	331	12	324	8	15
Zirconia 628 1/8/2016 4:51:17 AM (Run: 1)		350.44	1554.47	43.01	4.44	0.38309	4.76	0.05200	2.59	0.53	19.23	2.59	0.05343	4.00	309	5	347	90	329	13	327	8	6
Zirconia 635 1/8/2016 5:38:29 AM (Run: 1)		425.58	2118.57	55.58	4.98	0.36835	3.96	0.05135	2.20	0.54	19.47	2.20	0.05202	3.30	310	4	286	75	318	11	323	7	-13
Zirconia 636 1/8/2016 5:40:12 AM (Run: 1)		321.50	1352.84	39.05	4.21	0.38634	3.91	0.05233	2.52	0.63	19.11	2.52	0.05354	2.99	318	8	352	68	332	11	329	8	7
Zirconia 643 1/8/2016 6:27:27 AM (Run: 1)		245.15	851.81	26.68	3.47	0.38079	4.34	0.05212	1.93	0.43	19.19	1.93	0.05298	3.89	314	8	328	88	328	12	328	6	0
Zirconia 644 1/8/2016 6:29:10 AM (Run: 1)		309.12	1298.08	36.37	4.20	0.36684	4.22	0.05113	2.23	0.51	19.56	2.23	0.05204	3.59	307	6	287	82	317	12	321	7	-12

Experiment 4 on January 8, 2016
Isotope ratio and date errors do not include systematic calibration errors of 0.52% ($^{207}Pb/^{206}Pb$) and 1.28% ($^{206}Pb/^{238}U$) (2 sigma).
Trace element concentrations were deleted from analyses known to have intersected inclusions of other minerals based on P and Ti.
Ablation used a laser spot size of 25 microns and a laser firing repetition rate of 5 Hz.
Activity of TiO_2 for Ti-in-Zircon temperature calculation is 0.8.

Appendix Table A8 LA-ICPMS isotopic U-Pb and trace element concentration data analyzed at Boise State University

Analysis	P	Ti	Y	Zr	Nb	La	Ce	Pr	Nd	Sm	Eu	Gd	Tb	Dy	Ho	Er	Tm	Yb	Lu	Hf	Ta	Th	U
	ppm	ppm	ppm	ppm	ppm	ppm	ppm	ppm	ppm	ppm	ppm	ppm	ppm	ppm	ppm	ppm	ppm	ppm	ppm	ppm	ppm	ppm	ppm
Seiland - Secondary reference zircon																							
Seiland 569 1/8/2016 2:47:21 AM (Run: 1)	65.44	2.05	222.82	549981.38	0.77		2.20			0.21	0.66	3.55	1.57	20.00	8.81	38.87	10.79	119.04	15.27	4971.45	0.80	50.17	49.55
Seiland 570 1/8/2016 2:49:05 AM (Run: 1)	69.63	1.45	227.94	558204.37	1.14		2.64	0.01		0.35	0.64	3.91	1.56	20.87	8.47	40.48	11.57	125.37	16.64	4956.72	0.92	54.83	53.74
Seiland 577 1/8/2016 3:36:10 AM (Run: 1)	66.27	1.95	213.52	572984.56	0.97		2.45		0.13	0.70	0.53	3.86	1.45	20.96	7.88	38.25	11.17	121.23	16.30	5093.52	0.79	48.56	48.99
Seiland 578 1/8/2016 3:37:53 AM (Run: 1)	55.90	1.70	201.55	570118.98	1.06		2.09			0.38	0.40	3.07	1.56	19.12	7.83	38.19	10.14	111.73	14.95	5141.48	0.77	42.12	43.46
Seiland 585 1/8/2016 4:25:04 AM (Run: 1)	64.17	1.81	239.84	564466.83	1.22		2.70		0.21	0.84	0.83	2.90	1.58	24.31	8.21	41.74	11.76	129.35	17.14	4963.47	1.07	55.60	55.40
Seiland 586 1/8/2016 4:26:48 AM (Run: 1)	38.26	1.50	218.61	559274.47	1.05		2.26	0.01	0.17	0.31	0.58	3.65	1.65	20.57	8.23	40.54	10.87	123.73	16.08	4973.28	0.94	50.90	50.76
Seiland 593 1/8/2016 5:13:58 AM (Run: 1)	76.93	1.61	206.53	563939.50	1.01		2.35		0.16	0.57	0.61	2.98	1.60	19.93	7.40	38.03	10.44	116.67	16.06	5351.50	0.86	44.28	46.44
Seiland 594 1/8/2016 5:15:42 AM (Run: 1)	61.62	1.83	211.09	567644.75	1.14		2.46		0.13	0.10	0.45	2.59	1.54	19.13	7.53	37.61	10.99	119.74	14.45	5294.95	0.75	46.52	47.36
Seiland 601 1/8/2016 6:02:54 AM (Run: 1)	56.66	1.87	211.66	558145.98	0.98		2.66	0.01		0.58	0.58	3.25	1.41	22.91	8.61	40.60	10.46	124.54	17.73	5392.36	1.03	50.49	51.48
Seiland 602 1/8/2016 6:04:38 AM (Run: 1)	72.55	1.99	241.99	558836.00	1.18		3.00	0.02	0.15	0.88	0.72	4.00	1.82	24.78	9.25	46.14	12.33	143.10	18.28	5436.68	1.02	61.63	62.36
Zirconia - Secondary reference zircon																							
Zirconia 609 1/8/2016 3:11:45 AM (Run: 1)	76.72	23.45	1622.89	601413.17	2.45	0.73	204.59	5.06	74.67	83.19	37.22	201.12	40.27	285.05	63.81	181.68	29.14	226.98	26.44	8488.90	0.73	4133.81	516.02
Zirconia 611 1/8/2016 3:13:29 AM (Run: 1)	78.68	20.61	1494.49	586621.78	2.30	0.69	182.83	4.43	65.42	73.90	35.36	185.86	36.75	258.97	57.95	163.63	27.28	206.77	24.03	8179.19	0.64	3723.68	486.57
Zirconia 619 1/8/2016 4:00:39 AM (Run: 1)	77.09	23.96	1700.00	594183.99	2.66	0.71	218.44	5.57	83.61	89.67	40.53	216.50	43.47	303.03	65.92	185.66	30.20	226.08	26.41	8473.51	0.70	4326.56	534.12
Zirconia 620 1/8/2016 4:02:23 AM (Run: 1)	54.82	25.03	1693.92	606390.19	2.98	0.89	223.12	5.83	86.59	94.64	42.06	222.43	42.92	300.96	65.48	185.53	31.34	232.12	27.04	8521.39	0.89	4415.82	545.88
Zirconia 627 1/8/2016 4:49:34 AM (Run: 1)	71.47	13.28	1705.17	621599.39	1.53	0.15	133.93	2.56	40.63	60.84	29.10	163.94	38.38	289.44	69.76	206.69	36.22	278.63	33.11	9767.34	0.59	1479.99	346.20
Zirconia 628 1/8/2016 4:51:17 AM (Run: 1)	65.16	14.17	1685.66	612989.02	1.75	0.29	140.57	2.77	41.29	59.70	30.15	178.61	38.28	295.62	69.89	201.88	36.33	265.43	32.93	9564.87	0.54	1554.47	350.44
Zirconia 635 1/8/2016 5:38:29 AM (Run: 1)	71.28	18.06	1957.26	620231.62	2.30	0.50	182.28	4.05	65.46	79.66	39.92	218.35	47.89	342.80	81.49	231.64	39.07	307.51	34.89	9094.99	0.68	2118.57	425.58
Zirconia 636 1/8/2016 5:40:12 AM (Run: 1)	88.85	14.76	1547.06	608642.66	1.34	0.21	123.02	2.40	40.84	55.66	27.93	159.97	36.38	269.09	62.69	189.95	33.22	261.31	29.44	9035.31	0.63	1352.84	321.50
Zirconia 643 1/8/2016 6:27:27 AM (Run: 1)	87.74	10.34	1252.01	620913.43	0.85	0.16	87.28	1.33	19.90	33.53	18.34	108.30	25.59	200.67	51.44	149.53	27.68	219.31	26.64	9734.83	0.42	851.81	245.15
Zirconia 644 1/8/2016 6:29:10 AM (Run: 1)	64.99	11.94	1377.91	631884.64	1.28	0.10	107.91	2.08	30.17	41.46	21.53	125.55	29.12	226.05	56.45	169.21	29.77	233.19	28.45	9578.20	0.51	1298.08	309.12

Experiment 4 on January 8, 2016
Isotope ratio and date errors do not include systematic calibration errors of 0.52% ($^{207}Pb/^{206}Pb$) and 1.28% ($^{206}Pb/^{238}U$) (2 sigma).
Trace element concentrations were deleted from analyses known to have intersected inclusions of other minerals based on P and Ti.
Ablation used a laser spot size of 25 microns and a laser firing repetition rate of 5 Hz.
Activity of TiO_2 for Ti-in-Zircon temperature calculation is 0.8.

Appendix Table A8 LA-ICPMS isotopic U-Pb and trace element concentration data analyzed at Boise State University

Analysis	CA-TIMS label	U ppm	Th ppm	Pb* ppm	Th/U	$^{207}Pb/^{235}U$	±2s (%)	$^{206}Pb/^{238}U$	±2s (%)	error corr.	$^{238}U/^{206}Pb$	±2s (%)	$^{207}Pb/^{206}Pb$	±2s (%)	$^{208}Pb/^{232}Th$	±2s (Ma)	$^{207}Pb/^{206}Pb$	±2s (Ma)	$^{207}Pb/^{235}U$	±2s (Ma)	$^{206}Pb/^{238}U$	±2s (Ma)	% disc
Plesovice - Primary zircon standard																							
PL 450 1/7/2016 9:57:25 PM (Run: 1)	std	646.63	79.16	38.09	0.12	0.39559	3.54	0.05389	2.42	0.67	18.56	2.42	0.05324	2.58	352	21	339	58	338	10	338	8	0
PL 451 1/7/2016 9:59:09 PM (Run: 1)	std	587.90	70.11	34.18	0.12	0.38783	4.68	0.05340	2.80	0.59	18.73	2.80	0.05267	3.75	326	24	315	85	333	13	335	9	-7
PL 452 1/7/2016 10:00:52 PM (Run: 1)	std	564.60	66.06	32.83	0.12	0.38922	3.75	0.05347	2.74	0.72	18.70	2.74	0.05280	2.55	325	25	320	58	334	11	336	9	-5
PL 463 1/7/2016 10:23:33 PM (Run: 1)	std	591.34	77.70	34.75	0.13	0.40453	3.34	0.05374	2.66	0.78	18.61	2.66	0.05459	2.02	326	17	396	45	345	10	337	9	15
PL 464 1/7/2016 10:25:17 PM (Run: 1)	std	646.28	81.39	37.45	0.13	0.39293	3.48	0.05291	2.43	0.68	18.90	2.43	0.05386	2.49	348	27	365	56	337	10	332	8	9
PL 471 1/7/2016 10:48:01 PM (Run: 1)	std	545.06	72.71	32.89	0.13	0.40090	3.50	0.05536	2.52	0.71	18.06	2.52	0.05253	2.43	320	23	308	55	342	10	347	9	-13
PL 472 1/7/2016 10:49:44 PM (Run: 1)	std	596.11	84.85	35.81	0.14	0.39118	4.01	0.05467	3.01	0.74	18.29	3.01	0.05189	2.66	363	23	281	61	335	11	343	10	-22
PL 479 1/7/2016 11:12:25 PM (Run: 1)	std	714.87	90.63	41.21	0.13	0.39550	4.02	0.05249	2.92	0.72	19.05	2.92	0.05464	2.76	359	16	398	62	338	12	330	9	17
PL 480 1/7/2016 11:14:09 PM (Run: 1)	std	708.42	87.56	40.93	0.12	0.38857	4.47	0.05288	3.30	0.73	18.91	3.30	0.05329	3.01	334	18	341	68	333	13	332	11	3
PL 487 1/7/2016 11:36:53 PM (Run: 1)	std	538.22	60.38	31.73	0.11	0.39854	3.50	0.05426	2.86	0.80	18.43	2.86	0.05328	2.02	334	23	341	46	341	10	341	9	0
PL 488 1/7/2016 11:38:37 PM (Run: 1)	std	621.72	75.37	36.10	0.12	0.39165	3.65	0.05326	3.12	0.84	18.78	3.12	0.05334	1.90	331	23	343	43	336	10	334	10	3
PL 495 1/8/2016 12:01:19 AM (Run: 1)	std	751.69	99.01	43.81	0.13	0.39379	4.03	0.05326	3.39	0.83	18.78	3.39	0.05362	2.17	325	18	355	49	337	12	335	11	6
PL 496 1/8/2016 12:03:03 AM (Run: 1)	std	739.09	94.64	43.56	0.13	0.39293	3.28	0.05385	2.76	0.83	18.57	2.76	0.05292	1.77	345	21	326	40	337	9	338	9	-4
PL 503 1/8/2016 12:25:50 AM (Run: 1)	std	653.32	77.02	38.78	0.12	0.39665	3.46	0.05435	2.91	0.83	18.40	2.91	0.05293	1.86	362	23	326	42	339	10	341	10	-5
PL 504 1/8/2016 12:27:34 AM (Run: 1)	std	668.67	79.42	39.46	0.12	0.39498	3.98	0.05408	3.19	0.79	18.49	3.19	0.05297	2.38	346	17	327	54	338	11	340	11	-4
PL 511 1/8/2016 12:50:18 AM (Run: 1)	std	745.57	110.96	44.29	0.15	0.40221	3.51	0.05407	2.74	0.77	18.49	2.74	0.05395	2.18	323	17	369	49	343	10	339	9	8
PL 512 1/8/2016 12:52:02 AM (Run: 1)	std	646.00	78.93	37.22	0.12	0.38318	3.71	0.05298	2.62	0.69	18.87	2.62	0.05245	2.63	309	20	305	60	329	10	333	9	-9
PL 519 1/8/2016 1:14:44 AM (Run: 1)	std	675.65	83.45	39.26	0.12	0.39201	3.60	0.05322	2.80	0.76	18.79	2.80	0.05342	2.26	335	21	347	51	336	10	334	9	4
PL 520 1/8/2016 1:16:27 AM (Run: 1)	std	626.78	73.72	36.43	0.12	0.39089	3.64	0.05334	2.09	0.56	18.75	2.09	0.05315	2.99	337	28	335	68	335	10	335	7	0
PL 527 1/8/2016 1:39:15 AM (Run: 1)	std	623.11	72.02	36.11	0.12	0.39073	4.01	0.05328	2.55	0.62	18.77	2.55	0.05319	3.10	325	23	337	70	335	11	335	8	1
PL 528 1/8/2016 1:40:59 AM (Run: 1)	std	627.07	75.18	36.95	0.12	0.39064	3.74	0.05404	2.62	0.69	18.50	2.62	0.05243	2.67	350	27	304	61	335	11	339	9	-12
PL 535 1/8/2016 2:03:43 AM (Run: 1)	std	638.68	68.80	37.63	0.11	0.40300	3.48	0.05423	2.73	0.77	18.44	2.73	0.05390	2.16	334	20	367	49	344	10	340	9	7
PL 536 1/8/2016 2:05:27 AM (Run: 1)	std	629.14	68.48	36.71	0.11	0.39483	3.25	0.05356	2.53	0.76	18.67	2.53	0.05347	2.03	364	22	349	46	338	9	336	8	4
PL 543 1/8/2016 2:22:59 AM (Run: 1)	std	647.68	70.15	37.68	0.11	0.38941	3.53	0.05359	2.73	0.76	18.66	2.73	0.05271	2.24	335	22	316	51	334	10	336	9	-6
PL 544 1/8/2016 2:24:43 AM (Run: 1)	std	622.63	68.76	36.42	0.11	0.39840	3.60	0.05384	2.52	0.69	18.57	2.52	0.05367	2.56	329	21	357	58	340	10	338	8	5

Experiment 5 on January 8, 2016
Isotope ratio and date errors do not include systematic calibration errors of 0.50% ($^{207}Pb/^{206}Pb$) and 1.03% ($^{206}Pb/^{238}U$) (2 sigma).
Trace element concentrations were deleted from analyses known to have intersected inclusions of other minerals based on P and Ti.
Ablation used a laser spot size of 25 microns and a laser firing repetition rate of 5 Hz.
Activity of TiO_2 for Ti-in-Zircon temperature calculation is 0.8.

Appendix Table A8 LA-ICPMS isotopic U-Pb and trace element concentration data analyzed at Boise State University

Analysis	P	Ti	Y	Zr	Nb	La	Ce	Pr	Nd	Sm	Eu	Gd	Tb	Dy	Ho	Er	Tm	Yb	Lu	Hf	Ta	Th	U
	ppm	ppm	ppm	ppm	ppm	ppm	ppm	ppm	ppm	ppm	ppm	ppm	ppm	ppm	ppm	ppm	ppm	ppm	ppm	ppm	ppm	ppm	ppm
Plesovice - Primary zircon standard																							
PL 450 1/7/2016 9:57:25 PM (Run: 1)	458.25	89.59	690.03	578494.57	4.67	0.03	2.08	0.18	2.59	4.83	1.25	18.88	6.75	81.29	22.41	73.57	15.17	115.83	11.61	11667.48	3.39	79.16	646.63
PL 451 1/7/2016 9:59:09 PM (Run: 1)	357.91	80.79	583.81	574887.50	4.40		1.73	0.10	2.23	3.29	1.10	17.06	6.33	70.68	19.52	63.74	13.53	102.15	10.40	11949.54	3.40	70.11	587.90
PL 452 1/7/2016 10:00:52 PM (Run: 1)	365.58	79.78	592.22	578550.29	4.45		1.76	0.13	1.82	4.53	1.04	15.98	6.01	68.18	18.50	63.25	12.62	103.47	9.82	11776.04	3.28	66.06	564.60
PL 463 1/7/2016 10:23:33 PM (Run: 1)	329.47	75.33	517.55	590540.01	5.16		2.17	0.13	1.78	3.50	0.78	14.78	5.28	59.15	16.47	54.84	11.57	91.46	8.92	11761.88	3.33	77.70	591.34
PL 464 1/7/2016 10:25:17 PM (Run: 1)	393.68	85.27	618.66	575271.10	5.21		2.10	0.15	2.28	5.21	1.34	17.46	6.54	73.55	20.30	65.35	13.29	105.04	9.83	11779.33	3.53	81.39	646.28
PL 471 1/7/2016 10:48:01 PM (Run: 1)	277.28	72.10	454.74	585680.41	4.94		1.84	0.06	1.80	3.08	0.73	13.27	5.06	54.15	14.60	48.90	9.95	74.80	7.33	11852.06	3.40	72.71	545.06
PL 472 1/7/2016 10:49:44 PM (Run: 1)	308.08	73.09	472.14	591046.51	5.78		1.96	0.04	1.50	3.59	0.93	14.47	5.61	60.02	15.72	49.83	9.72	74.26	7.17	11731.58	3.39	84.85	596.11
PL 479 1/7/2016 11:12:25 PM (Run: 1)	487.31	92.54	711.07	589026.33	4.87	0.03	2.05	0.14	2.95	4.74	1.21	20.97	7.88	85.76	23.82	79.99	16.19	122.79	12.25	12073.33	3.76	90.63	714.87
PL 480 1/7/2016 11:14:09 PM (Run: 1)	485.73	93.36	708.85	592405.52	5.02	0.03	2.25	0.12	3.17	5.28	1.40	21.33	7.81	85.20	24.27	79.19	15.92	119.67	12.21	12257.78	3.53	87.56	708.42
PL 487 1/7/2016 11:36:53 PM (Run: 1)	324.90	73.55	506.51	595394.32	4.42		1.63	0.11	2.21	3.58	0.86	13.91	5.70	60.08	16.15	55.80	11.45	90.91	8.79	12524.68	2.92	60.38	538.22
PL 488 1/7/2016 11:38:37 PM (Run: 1)	404.19	86.49	623.83	590172.72	4.53	0.03	2.08	0.20	2.51	3.89	1.21	16.00	6.42	71.75	20.34	67.79	13.69	107.27	10.68	12303.70	3.21	75.37	621.72
PL 495 1/8/2016 12:01:19 AM (Run: 1)	515.89	100.07	788.64	588814.53	5.02	0.04	2.16	0.10	2.29	6.45	1.22	24.15	8.68	91.70	25.75	83.39	16.31	129.08	13.29	12138.70	3.67	99.01	751.69
PL 496 1/8/2016 12:03:03 AM (Run: 1)	505.71	97.73	760.51	601472.60	4.57		2.04	0.19	3.04	5.77	1.11	22.10	8.74	90.81	24.82	83.99	16.13	127.90	12.33	12532.58	3.59	94.64	739.09
PL 503 1/8/2016 12:25:50 AM (Run: 1)	417.72	85.95	648.73	592847.88	4.14	0.04	2.04	0.13	2.57	5.60	1.17	18.24	6.93	77.48	20.87	69.58	13.73	110.47	10.75	12030.27	3.50	77.02	653.32
PL 504 1/8/2016 12:27:34 AM (Run: 1)	426.83	87.52	652.46	574687.89	4.38	0.05	2.07	0.13	2.10	4.60	0.95	19.91	7.04	78.34	21.20	71.38	14.63	112.22	11.21	11816.18	3.44	79.42	668.67
PL 511 1/8/2016 12:50:18 AM (Run: 1)	410.64	93.09	719.55	594329.55	4.42	0.04	2.78	0.27	3.74	6.00	1.36	24.25	8.08	88.40	23.10	77.86	14.51	116.61	10.49	12133.15	3.64	110.96	745.57
PL 512 1/8/2016 12:52:02 AM (Run: 1)	428.07	86.02	621.89	598510.68	4.69		2.02	0.18	1.61	4.29	1.21	18.46	6.93	72.05	19.55	66.76	13.00	102.32	10.03	12595.02	3.49	78.93	646.00
PL 519 1/8/2016 1:14:44 AM (Run: 1)	439.65	93.13	681.60	593274.61	4.53		2.13	0.14	2.60	5.72	1.27	19.38	7.74	79.96	22.11	73.81	14.10	110.02	10.77	12304.93	3.29	83.45	675.65
PL 520 1/8/2016 1:16:27 AM (Run: 1)	408.38	83.16	580.71	602539.91	4.14		1.73	0.16	2.21	3.86	1.24	15.64	6.55	70.80	18.88	64.79	12.25	90.34	9.16	12561.95	3.22	73.72	626.78
PL 527 1/8/2016 1:39:15 AM (Run: 1)	370.84	80.98	575.15	596886.91	4.59		1.86	0.12	1.94	3.15	1.08	15.87	6.38	67.25	18.38	61.52	12.19	91.14	9.09	12397.98	3.17	72.02	623.11
PL 528 1/8/2016 1:40:59 AM (Run: 1)	389.87	83.28	597.60	599573.80	4.62		1.84	0.12	2.06	3.88	1.04	16.37	6.94	68.87	18.68	65.53	12.33	91.71	9.06	12547.31	3.35	75.18	627.07
PL 535 1/8/2016 2:03:43 AM (Run: 1)	293.12	36.08	379.31	579491.00	4.48	0.28	2.44	0.11	1.23	2.09	0.47	10.73	4.16	43.24	11.85	40.93	8.14	61.95	6.44	11720.54	3.38	68.80	638.68
PL 536 1/8/2016 2:05:27 AM (Run: 1)	321.79	35.04	372.56	594888.53	4.51	0.23	2.17	0.18	1.39	1.94	0.64	10.72	3.95	42.32	11.80	40.74	8.06	62.72	5.95	12104.01	3.24	68.48	629.14
PL 543 1/8/2016 2:22:59 AM (Run: 1)	332.41	38.73	389.02	599918.65	4.68	0.09	2.06	0.13	1.07	2.75	0.53	11.57	4.11	45.91	12.78	44.35	8.00	62.96	6.86	12061.63	3.60	70.15	647.68
PL 544 1/8/2016 2:24:43 AM (Run: 1)	324.64	39.40	387.07	600264.49	4.73	0.10	2.41	0.14	1.51	2.42	0.52	10.16	4.07	43.33	12.11	41.40	8.42	65.20	6.01	12113.72	3.35	68.76	622.63

Experiment 5 on January 8, 2016
Isotope ratio and date errors do not include systematic calibration errors of 0.50% ($^{207}Pb/^{206}Pb$) and 1.03% ($^{206}Pb/^{238}U$) (2 sigma).
Trace element concentrations were deleted from analyses known to have intersected inclusions of other minerals based on P and Ti.
Ablation used a laser spot size of 25 microns and a laser firing repetition rate of 5 Hz.
Activity of TiO_2 for Ti-in-Zircon temperature calculation is 0.8.

Appendix Table A8 LA-ICPMS isotopic U-Pb and trace element concentration data analyzed at Boise State University

Analysis	CA-TIMS label	U ppm	Th ppm	Pb* ppm	Th/U	$^{207}Pb/^{235}U$	±2s (%)	$^{206}Pb/^{238}U$	±2s (%)	error corr.	$^{238}U/^{206}Pb$	±2s (%)	$^{207}Pb/^{206}Pb$	±2s (%)	$^{208}Pb/^{232}Th$	±2s (Ma)	$^{207}Pb/^{206}Pb$	±2s (Ma)	$^{207}Pb/^{235}U$	±2s (Ma)	$^{206}Pb/^{238}U$	±2s (Ma)	% disc
Seiland - Secondary reference zircon																							
Seiland 567 1/7/2016 10:02:38 PM (Run: 1)		43.35	41.60	5.06	0.96	0.70116	7.89	0.08594	2.92	0.36	11.64	2.92	0.05917	7.33	544	39	574	159	539	33	531	15	7
Seiland 568 1/7/2016 10:04:22 PM (Run: 1)		44.63	43.42	5.14	0.97	0.70893	7.96	0.08377	3.07	0.38	11.94	3.07	0.06138	7.35	548	35	653	158	544	34	519	15	21
Seiland 575 1/7/2016 10:51:29 PM (Run: 1)		54.56	55.28	6.37	1.01	0.68043	8.10	0.08436	3.68	0.45	11.85	3.68	0.05850	7.22	549	32	549	158	527	33	522	18	5
Seiland 576 1/7/2016 10:53:13 PM (Run: 1)		56.83	58.51	6.80	1.03	0.68176	5.93	0.08749	2.67	0.44	11.43	2.67	0.05651	5.29	535	31	473	117	528	24	541	14	-14
Seiland 583 1/7/2016 11:40:23 PM (Run: 1)		56.91	57.67	6.79	1.01	0.71534	7.09	0.08677	2.64	0.36	11.52	2.64	0.05979	6.59	547	34	596	143	548	30	536	14	10
Seiland 584 1/7/2016 11:42:06 PM (Run: 1)		58.02	58.02	6.89	1.00	0.68461	8.41	0.08581	3.74	0.44	11.65	3.74	0.05786	7.53	566	34	525	165	530	35	531	19	-1
Seiland 591 1/8/2016 12:29:19 AM (Run: 1)		55.36	55.29	6.51	1.00	0.67387	7.97	0.08462	3.14	0.39	11.82	3.14	0.05775	7.33	568	37	520	161	523	33	524	16	-1
Seiland 592 1/8/2016 12:31:03 AM (Run: 1)	high U signal variance	47.63	45.09	5.66	0.95	0.74288	6.95	0.08695	3.79	0.54	11.50	3.79	0.06197	5.83	568	42	673	125	564	30	537	20	20
Seiland 599 1/8/2016 1:18:13 AM (Run: 1)		44.53	41.76	5.24	0.94	0.65211	6.80	0.08603	4.29	0.63	11.62	4.29	0.05498	5.28	582	42	411	118	510	27	532	22	-29
Seiland 600 1/8/2016 1:19:57 AM (Run: 1)		43.85	42.15	5.26	0.96	0.66943	7.20	0.08642	3.13	0.43	11.57	3.13	0.05618	6.48	603	53	460	144	520	29	534	16	-16
Zirconia - Secondary reference zircon																							
Zirconia 607 1/7/2016 10:27:02 PM (Run: 1)		449.85	3247.33	71.81	7.22	0.37448	4.09	0.05194	2.59	0.62	19.25	2.59	0.05230	3.16	292	4	298	72	323	11	326	8	-9
Zirconia 608 1/7/2016 10:28:45 PM (Run: 1)		499.45	3882.69	84.46	7.77	0.36921	3.86	0.05100	3.14	0.80	19.61	3.14	0.05250	2.26	298	8	307	51	319	11	321	10	-4
Zirconia 617 1/7/2016 11:15:54 PM (Run: 1)	high U signal variance	457.38	3299.24	78.54	7.21	0.38370	5.11	0.05328	3.73	0.72	18.77	3.73	0.05223	3.50	322	8	295	80	330	14	335	12	-13
Zirconia 618 1/7/2016 11:17:38 PM (Run: 1)		496.27	3744.80	86.73	7.55	0.38239	3.76	0.05231	2.94	0.77	19.12	2.94	0.05301	2.34	318	7	329	53	329	11	329	9	0
Zirconia 625 1/8/2016 12:04:48 AM (Run: 1)		513.27	3999.56	89.30	7.79	0.36658	3.08	0.05181	1.75	0.54	19.30	1.75	0.05131	2.54	308	4	255	58	317	8	326	6	-28
Zirconia 626 1/8/2016 12:06:32 AM (Run: 1)		431.94	2972.33	70.45	6.88	0.38757	3.54	0.05315	2.22	0.61	18.81	2.22	0.05288	2.75	313	4	324	63	333	10	334	7	-3
Zirconia 633 1/8/2016 12:53:47 AM (Run: 1)		316.44	1330.92	37.81	4.21	0.36991	5.00	0.05112	2.54	0.50	19.56	2.54	0.05248	4.31	314	8	306	98	320	14	321	8	-5
Zirconia 634 1/8/2016 12:55:30 AM (Run: 1)		314.11	1359.00	38.95	4.33	0.38330	3.81	0.05231	2.41	0.62	19.12	2.41	0.05315	2.95	320	5	335	67	329	11	329	8	2
Zirconia 641 1/8/2016 1:42:44 AM (Run: 1)		355.51	1671.44	45.29	4.70	0.37638	4.49	0.05088	2.91	0.64	19.65	2.91	0.05365	3.41	315	5	356	77	324	12	320	9	10
Zirconia 642 1/8/2016 1:44:27 AM (Run: 1)		297.64	1238.91	36.93	4.16	0.38177	5.46	0.05190	3.29	0.60	19.27	3.29	0.05335	4.35	335	5	344	98	328	15	326	10	5

Experiment 5 on January 8, 2016
Isotope ratio and date errors do not include systematic calibration errors of 0.50% ($^{207}Pb/^{206}Pb$) and 1.03% ($^{206}Pb/^{238}U$) (2 sigma).
Trace element concentrations were deleted from analyses known to have intersected inclusions of other minerals based on P and Ti.
Ablation used a laser spot size of 25 microns and a laser firing repetition rate of 5 Hz.
Activity of TiO_2 for Ti-in-Zircon temperature calculation is 0.8.

Appendix Table A8 LA-ICPMS isotopic U-Pb and trace element concentration data analyzed at Boise State University

Analysis	P	Ti	Y	Zr	Nb	La	Ce	Pr	Nd	Sm	Eu	Gd	Tb	Dy	Ho	Er	Tm	Yb	Lu	Hf	Ta	Th	U
	ppm	ppm	ppm	ppm	ppm	ppm	ppm	ppm	ppm	ppm	ppm	ppm	ppm	ppm	ppm	ppm	ppm	ppm	ppm	ppm	ppm	ppm	ppm
Seiland - Secondary reference zircon																							
Seiland 567 1/7/2016 10:02:38 PM (Run: 1)	57.91	1.48	199.60	563540.06	1.02		2.48		0.15	0.37	0.48	3.83	1.25	19.68	7.95	37.42	9.61	111.90	14.97	5060.33	0.77	41.60	43.35
Seiland 568 1/7/2016 10:04:22 PM (Run: 1)	62.38	1.79	205.86	568880.13	0.96		2.20	0.03		0.42	0.40	4.13	1.37	20.52	8.00	37.41	9.88	111.43	14.73	5115.44	0.89	43.42	44.63
Seiland 575 1/7/2016 10:51:29 PM (Run: 1)	59.55	1.79	230.16	573239.38	1.24		2.40			0.63	0.51	3.75	1.63	22.39	8.47	43.09	11.51	129.00	16.82	5084.82	1.14	55.28	54.56
Seiland 576 1/7/2016 10:53:13 PM (Run: 1)	72.92	1.85	238.20	581918.17	0.85		2.92		0.24	0.81	0.53	3.71	1.61	24.41	8.81	42.45	11.64	126.24	16.65	5204.43	0.85	58.51	56.83
Seiland 583 1/7/2016 11:40:23 PM (Run: 1)	67.83	1.97	228.18	565853.12	0.96		2.71		0.16	0.66	0.61	3.39	1.36	23.33	9.02	41.30	11.27	127.60	16.58	5014.93	1.20	57.67	56.91
Seiland 584 1/7/2016 11:42:06 PM (Run: 1)	50.09	2.02	238.18	566431.93	1.00		2.73		0.24	0.34	0.73	4.20	1.77	22.12	8.91	40.52	11.65	128.30	16.22	4946.47	0.98	58.02	58.02
Seiland 591 1/8/2016 12:29:19 AM (Run: 1)	67.08	1.92	228.63	575734.31	1.10		2.68	0.02	0.24	0.78	0.50	4.81	1.71	23.40	8.50	41.64	11.64	127.07	16.62	5174.67	0.94	55.29	55.36
Seiland 592 1/8/2016 12:31:03 AM (Run: 1)	55.99	2.11	212.13	579444.30	1.00		2.53		0.27	0.25	0.50	3.88	1.29	22.24	7.87	36.90	10.53	119.16	16.15	5262.40	0.86	45.09	47.63
Seiland 599 1/8/2016 1:18:13 AM (Run: 1)	57.43	1.60	202.14	562720.43	0.93		2.32			0.57	0.45	3.59	1.53	20.73	7.95	34.89	10.14	108.05	14.84	5063.25	0.84	41.76	44.53
Seiland 600 1/8/2016 1:19:57 AM (Run: 1)	85.53	1.64	206.12	577030.99	1.04		2.41	0.01	0.23	0.53	0.50	2.91	1.42	19.11	7.59	37.38	9.79	110.96	14.75	5137.52	0.78	42.15	43.85
Zirconia - Secondary reference zircon																							
Zirconia 607 1/7/2016 10:27:02 PM (Run: 1)	65.30	18.23	1395.40	615993.47	1.76	0.86	157.64	3.46	49.78	61.40	26.62	158.58	31.52	233.46	55.42	154.98	27.28	197.79	24.33	8951.34	0.58	3247.33	449.85
Zirconia 608 1/7/2016 10:28:45 PM (Run: 1)	78.02	20.93	1605.46	611449.77	2.67	0.68	190.07	4.43	66.96	80.97	34.38	196.68	38.81	273.53	62.95	170.74	29.45	213.93	26.50	8796.19	0.60	3882.69	499.45
Zirconia 617 1/7/2016 11:15:54 PM (Run: 1)	63.78	19.57	1412.68	610652.17	2.08	0.45	162.88	3.41	53.79	64.45	29.99	165.41	34.37	244.86	56.29	156.23	26.44	200.53	23.80	8807.41	0.55	3299.24	457.38
Zirconia 618 1/7/2016 11:17:38 PM (Run: 1)	54.89	21.44	1528.73	608136.02	2.18	0.58	186.83	4.34	63.74	73.86	35.18	186.80	37.75	267.43	60.28	170.70	28.92	213.48	25.60	8765.56	0.55	3744.80	496.27
Zirconia 625 1/8/2016 12:04:48 AM (Run: 1)	62.14	20.91	1621.06	616547.12	2.62	0.55	200.35	4.72	69.85	83.46	36.38	195.87	38.07	284.55	62.73	179.49	29.52	226.84	26.61	8909.15	0.75	3999.56	513.27
Zirconia 626 1/8/2016 12:06:32 AM (Run: 1)	60.89	16.89	1307.18	617711.40	1.84	0.82	141.90	3.08	43.19	54.00	26.84	146.71	29.55	225.68	51.09	149.04	25.14	191.64	23.54	8926.40	0.45	2972.33	431.94
Zirconia 633 1/8/2016 12:53:47 AM (Run: 1)	72.80	14.16	1594.48	622111.32	1.47	0.13	127.25	2.31	42.18	52.24	27.01	160.20	33.72	263.46	63.67	189.32	32.48	252.73	31.11	8894.10	0.52	1330.92	316.44
Zirconia 634 1/8/2016 12:55:30 AM (Run: 1)	65.02	13.53	1570.65	614971.80	1.71	0.17	128.34	2.38	41.14	59.73	28.33	155.85	34.56	270.88	62.41	181.61	31.92	249.97	29.78	8772.88	0.50	1359.00	314.11
Zirconia 641 1/8/2016 1:42:44 AM (Run: 1)	68.55	17.30	1750.08	609702.34	1.85	0.32	150.52	3.38	52.80	64.80	33.71	179.66	39.55	299.72	68.79	199.17	33.80	270.24	30.82	8446.09	0.74	1671.44	355.51
Zirconia 642 1/8/2016 1:44:27 AM (Run: 1)	66.03	14.26	1477.28	608562.26	1.39	0.21	119.95	2.59	41.06	53.64	26.85	147.38	32.57	244.76	57.50	170.31	30.32	239.54	26.66	8328.39	0.51	1238.91	297.64

Experiment 5 on January 8, 2016
Isotope ratio and date errors do not include systematic calibration errors of 0.50% ($^{207}Pb/^{206}Pb$) and 1.03% ($^{206}Pb/^{238}U$) (2 sigma).
Trace element concentrations were deleted from analyses known to have intersected inclusions of other minerals based on P and Ti.
Ablation used a laser spot size of 25 microns and a laser firing repetition rate of 5 Hz.
Activity of TiO_2 for Ti-in-Zircon temperature calculation is 0.8.

Appendix Table A8 LA-ICPMS isotopic U-Pb and trace element concentration data analyzed at Boise State University

Analysis	CA-TIMS label	U ppm	Th ppm	Pb* ppm	Th/U	$^{207}Pb/^{235}U$	±2s (%)	$^{206}Pb/^{238}U$	±2s (%)	error corr.	$^{238}U/^{206}Pb$	±2s (%)	$^{207}Pb/^{206}Pb$	±2s (%)	$^{208}Pb/^{232}Th$	±2s (Ma)	$^{207}Pb/^{206}Pb$	±2s (Ma)	$^{207}Pb/^{235}U$	±2s (Ma)	$^{206}Pb/^{238}U$	±2s (Ma)	% disc
Plesovice - Primary zircon standard																							
PL 453 1/8/2016 2:40:25 AM (Run: 1)	std	607.29	95.86	36.58	0.16	0.42319	4.64	0.05444	2.98	0.63	18.37	2.98	0.05638	3.56	354	33	467	79	358	14	342	10	27
PL 454 1/8/2016 2:42:08 AM (Run: 1)	std	605.66	72.96	35.19	0.12	0.38981	3.14	0.05334	2.22	0.69	18.75	2.22	0.05300	2.22	337	23	329	50	334	9	335	7	-2
PL 455 1/8/2016 2:43:52 AM (Run: 1)	std	566.35	64.85	33.04	0.11	0.37790	3.31	0.05383	2.30	0.68	18.58	2.30	0.05092	2.37	330	32	237	55	325	9	338	8	-43
PL 456 1/8/2016 2:45:36 AM (Run: 1)	std	572.76	67.19	33.56	0.12	0.39989	3.60	0.05381	2.33	0.63	18.59	2.33	0.05390	2.74	343	26	367	62	342	10	338	8	8
PL 465 1/8/2016 3:08:17 AM (Run: 1)	std	578.30	78.64	33.73	0.14	0.38683	3.56	0.05353	1.82	0.49	18.68	1.82	0.05241	3.06	314	21	303	70	332	10	336	6	-11
PL 466 1/8/2016 3:10:00 AM (Run: 1)	std	544.53	70.25	31.95	0.13	0.39594	3.91	0.05390	2.60	0.65	18.55	2.60	0.05328	2.92	321	21	341	66	339	11	338	9	1
PL 473 1/8/2016 3:32:41 AM (Run: 1)	std	555.00	73.08	32.37	0.13	0.38353	3.05	0.05354	1.93	0.61	18.68	1.93	0.05195	2.36	329	19	283	54	330	9	336	6	-19
PL 474 1/8/2016 3:34:25 AM (Run: 1)	std	565.98	74.76	33.09	0.13	0.39276	3.75	0.05352	2.25	0.58	18.68	2.25	0.05322	3.00	342	30	338	68	336	11	336	7	1
PL 481 1/8/2016 3:57:10 AM (Run: 1)	high U signal variance	592.03	68.88	34.93	0.12	0.40098	4.85	0.05408	3.57	0.73	18.49	3.57	0.05378	3.28	369	22	362	74	342	14	340	12	6
PL 482 1/8/2016 3:58:54 AM (Run: 1)	std	532.65	58.90	30.75	0.11	0.38460	3.70	0.05324	2.63	0.70	18.78	2.63	0.05239	2.60	341	29	302	59	330	10	334	9	-11
PL 489 1/8/2016 4:21:35 AM (Run: 1)	std	733.61	94.51	42.83	0.13	0.39460	3.31	0.05334	2.55	0.75	18.75	2.55	0.05366	2.10	333	22	357	48	338	9	335	8	6
PL 490 1/8/2016 4:23:18 AM (Run: 1)	std	721.80	91.40	42.12	0.13	0.39096	2.91	0.05333	2.61	0.88	18.75	2.61	0.05317	1.28	341	26	336	29	335	8	335	9	0
PL 497 1/8/2016 4:46:05 AM (Run: 1)	std	715.26	86.30	42.58	0.12	0.40653	3.64	0.05438	2.51	0.67	18.39	2.51	0.05422	2.64	346	21	380	59	346	11	341	8	10
PL 498 1/8/2016 4:47:49 AM (Run: 1)	std	606.00	70.20	35.85	0.12	0.39333	3.66	0.05429	2.63	0.70	18.42	2.63	0.05254	2.54	348	26	309	58	337	10	341	9	-10
PL 505 1/8/2016 5:10:28 AM (Run: 1)	std	632.08	73.08	37.36	0.12	0.40039	3.81	0.05421	2.43	0.62	18.45	2.43	0.05357	2.94	344	19	353	66	342	11	340	8	4
PL 506 1/8/2016 5:12:12 AM (Run: 1)	std	721.66	89.29	42.37	0.12	0.39635	3.95	0.05363	2.81	0.70	18.65	2.81	0.05360	2.77	349	19	354	63	339	11	337	9	5
PL 513 1/8/2016 5:35:00 AM (Run: 1)	std	728.46	90.05	42.60	0.12	0.38600	3.29	0.05361	2.48	0.74	18.65	2.48	0.05222	2.16	323	20	295	49	331	9	337	8	-14
PL 514 1/8/2016 5:36:43 AM (Run: 1)	std	738.03	91.80	42.87	0.12	0.39191	3.66	0.05322	2.09	0.55	18.79	2.09	0.05340	3.01	312	19	346	68	336	10	334	7	3
PL 521 1/8/2016 5:59:25 AM (Run: 1)	std	718.80	86.96	41.76	0.12	0.39381	3.85	0.05321	3.29	0.84	18.79	3.29	0.05368	2.00	325	26	358	45	337	11	334	11	7
PL 522 1/8/2016 6:01:08 AM (Run: 1)	std	747.88	93.29	43.66	0.12	0.39466	3.52	0.05331	2.74	0.76	18.76	2.74	0.05369	2.21	338	14	358	50	338	10	335	9	7
PL 529 1/8/2016 6:23:58 AM (Run: 1)	std	645.18	73.96	37.63	0.11	0.38851	3.54	0.05367	2.45	0.68	18.63	2.45	0.05250	2.55	329	23	307	58	333	10	337	8	-10
PL 530 1/8/2016 6:25:41 AM (Run: 1)	std	657.23	76.92	38.32	0.12	0.39812	3.18	0.05347	2.38	0.73	18.70	2.38	0.05400	2.11	338	28	371	47	340	9	336	8	10
PL 537 1/8/2016 6:48:28 AM (Run: 1)	std	671.68	73.53	39.32	0.11	0.39789	3.20	0.05376	2.61	0.80	18.60	2.61	0.05368	1.86	352	24	357	42	340	9	338	9	6
PL 538 1/8/2016 6:50:11 AM (Run: 1)	std	762.40	85.80	44.70	0.11	0.39827	3.39	0.05383	2.44	0.70	18.58	2.44	0.05366	2.36	329	27	357	53	340	10	338	8	5
PL 545 1/8/2016 7:07:41 AM (Run: 1)	std	658.45	72.01	38.33	0.11	0.38990	3.81	0.05352	2.61	0.67	18.68	2.61	0.05283	2.78	350	29	322	63	334	11	336	9	-4
PL 546 1/8/2016 7:09:25 AM (Run: 1)	std	703.16	77.61	41.14	0.11	0.38969	3.65	0.05385	2.31	0.62	18.57	2.31	0.05248	2.82	335	29	306	64	334	10	338	8	-10

Experiment 6 on January 8, 2016
Isotope ratio and date errors do not include systematic calibration errors of 0.52% ($^{207}Pb/^{206}Pb$) and 1.28% ($^{206}Pb/^{238}U$) (2 sigma).
Trace element concentrations were deleted from analyses known to have intersected inclusions of other minerals based on P and Ti.
Ablation used a laser spot size of 25 microns and a laser firing repetition rate of 5 Hz.
Activity of TiO_2 for Ti-in-Zircon temperature calculation is 0.8.

Appendix Table A8 LA-ICPMS isotopic U-Pb and trace element concentration data analyzed at Boise State University

Analysis	P	Ti	Y	Zr	Nb	La	Ce	Pr	Nd	Sm	Eu	Gd	Tb	Dy	Ho	Er	Tm	Yb	Lu	Hf	Ta	Th	U
	ppm	ppm	ppm	ppm	ppm	ppm	ppm	ppm	ppm	ppm	ppm	ppm	ppm	ppm	ppm	ppm	ppm	ppm	ppm	ppm	ppm	ppm	ppm
Plesovice - Primary zircon standard																							
PL 453 1/8/2016 2:40:25 AM (Run: 1)	338.69	77.32	529.23	577902.39	5.37	0.11	2.69	0.29	3.91	4.87	1.49	17.58	6.32	64.76	17.73	58.07	11.50	91.55	9.62	10911.01	3.63	95.86	607.29
PL 454 1/8/2016 2:42:08 AM (Run: 1)	389.46	81.72	594.92	573052.95	4.94		1.83	0.14	1.62	4.01	1.04	17.02	6.55	67.27	19.55	66.61	12.97	105.23	10.16	11640.51	3.36	72.96	605.66
PL 455 1/8/2016 2:43:52 AM (Run: 1)	387.49	79.30	562.35	570858.13	3.99		1.74	0.14	1.70	3.69	0.95	14.83	5.87	63.12	18.30	59.69	12.24	99.00	9.94	11503.59	3.04	64.85	566.35
PL 456 1/8/2016 2:45:36 AM (Run: 1)	378.03	80.38	574.49	576652.34	4.14		1.70	0.12	2.16	2.83	1.00	16.69	5.93	69.12	18.36	60.32	12.68	97.18	10.43	11613.50	3.03	67.19	572.76
PL 465 1/8/2016 3:08:17 AM (Run: 1)	310.50	69.30	455.88	575316.58	5.54	0.05	1.70	0.10	1.21	3.41	0.72	13.02	5.46	53.18	14.82	47.82	9.54	76.00	7.07	11261.03	3.36	78.64	578.30
PL 466 1/8/2016 3:10:00 AM (Run: 1)	302.89	66.90	453.73	571332.75	4.82		1.76	0.09	1.51	3.31	0.63	14.34	5.05	54.36	15.08	49.42	10.15	78.80	8.06	11319.93	3.10	70.25	544.53
PL 473 1/8/2016 3:32:41 AM (Run: 1)	289.26	66.45	432.54	578153.17	4.77		1.89	0.12	1.66	3.59	0.86	11.66	5.13	54.10	14.39	47.90	9.70	75.45	7.17	11444.47	3.16	73.08	555.00
PL 474 1/8/2016 3:34:25 AM (Run: 1)	315.24	71.40	456.94	575649.60	5.01		1.92	0.14	1.93	3.79	0.67	13.18	5.19	53.76	15.09	50.32	9.74	76.84	7.57	11597.87	3.16	74.76	565.98
PL 481 1/8/2016 3:57:10 AM (Run: 1)	418.40	78.45	566.42	574042.87	4.23		1.97	0.12	2.19	3.10	1.02	14.79	5.66	65.74	17.51	63.21	12.26	96.76	9.32	11791.99	2.79	68.88	592.03
PL 482 1/8/2016 3:58:54 AM (Run: 1)	360.85	71.75	503.36	576414.96	3.65		1.53	0.15	1.79	3.05	0.83	15.09	5.31	59.25	16.39	54.82	10.71	87.30	8.60	12067.91	2.80	58.90	532.65
PL 489 1/8/2016 4:21:35 AM (Run: 1)	533.09	96.45	744.15	585124.31	5.61		2.11	0.17	2.83	4.99	1.49	25.20	8.20	89.44	23.66	83.65	16.18	123.43	11.74	11727.65	3.54	94.51	733.61
PL 490 1/8/2016 4:23:18 AM (Run: 1)	514.63	95.23	728.47	581985.55	5.14		2.21	0.16	2.84	5.30	1.30	23.23	7.81	88.02	24.50	80.85	15.82	124.68	12.19	11771.52	3.87	91.40	721.80
PL 497 1/8/2016 4:46:05 AM (Run: 1)	430.85	86.20	662.52	588609.46	4.47		2.08	0.09	2.90	3.47	1.14	18.79	7.83	80.55	23.49	75.04	14.65	119.22	11.90	12989.14	3.78	86.30	715.26
PL 498 1/8/2016 4:47:49 AM (Run: 1)	363.62	75.75	541.01	574975.72	4.65		1.85	0.13	2.06	3.23	0.89	15.31	6.19	65.48	17.96	62.49	11.57	99.42	9.65	12886.39	3.15	70.20	606.00
PL 505 1/8/2016 5:10:28 AM (Run: 1)	395.39	77.63	575.37	576462.46	3.97		1.74	0.10	2.40	4.20	0.99	16.88	6.62	68.04	19.64	65.62	13.08	101.15	9.53	12347.95	3.43	73.08	632.08
PL 506 1/8/2016 5:12:12 AM (Run: 1)	482.19	89.48	669.01	596978.89	5.37	0.02	1.92	0.16	2.30	4.92	1.12	19.17	7.85	83.44	21.77	75.84	14.19	111.84	11.50	12857.47	3.82	89.29	721.66
PL 513 1/8/2016 5:35:00 AM (Run: 1)	437.87	90.31	691.16	593307.33	4.97		2.09	0.11	2.70	5.61	1.27	18.49	7.70	80.57	22.51	76.52	14.90	115.75	11.77	12908.07	3.58	90.05	728.46
PL 514 1/8/2016 5:36:43 AM (Run: 1)	461.46	90.74	696.65	590745.43	4.59	0.06	2.09	0.21	2.82	5.18	1.40	19.82	8.43	83.41	23.21	75.52	15.00	117.68	11.99	12878.11	3.63	91.80	738.03
PL 521 1/8/2016 5:59:25 AM (Run: 1)	434.91	82.37	638.10	585645.43	4.70	0.03	2.18	0.14	1.76	4.23	1.19	21.44	7.05	80.56	21.75	73.18	13.84	108.49	11.11	13195.00	3.81	86.96	718.80
PL 522 1/8/2016 6:01:08 AM (Run: 1)	468.56	89.36	693.04	597708.79	4.62		2.20	0.17	2.25	4.72	1.14	21.11	8.27	86.02	23.82	78.17	15.57	117.81	11.46	13038.40	3.88	93.29	747.88
PL 529 1/8/2016 6:23:58 AM (Run: 1)	333.83	78.77	557.45	598635.21	4.67		1.97	0.13	1.87	4.24	1.11	16.63	6.65	68.69	18.30	65.54	11.97	94.49	9.36	13329.14	3.77	73.96	645.18
PL 530 1/8/2016 6:25:41 AM (Run: 1)	400.11	79.58	582.65	595175.75	4.78		2.00	0.10	1.79	4.16	0.95	18.08	6.60	69.11	19.23	63.45	12.90	96.85	9.70	13029.60	3.57	76.92	657.23
PL 537 1/8/2016 6:48:28 AM (Run: 1)	309.84	30.76	378.92	587776.96	4.43	0.24	2.62	0.22	2.01	1.38	0.66	11.93	4.13	45.76	12.31	41.96	8.16	63.32	6.32	12684.60	3.76	73.53	671.68
PL 538 1/8/2016 6:50:11 AM (Run: 1)	356.44	34.24	423.97	589722.23	4.92	0.18	2.41	0.22	2.24	2.75	0.83	11.15	4.57	49.54	14.03	47.33	9.79	73.83	7.70	12460.25	3.42	85.80	762.40
PL 545 1/8/2016 7:07:41 AM (Run: 1)	345.36	35.93	383.22	597289.87	4.35	0.37	2.63	0.22	1.86	2.33	0.61	8.88	4.40	44.64	12.46	45.12	8.55	69.05	6.43	12576.71	3.63	72.01	658.45
PL 546 1/8/2016 7:09:25 AM (Run: 1)	335.49	33.36	421.73	602124.28	4.43	0.37	2.40	0.23	1.85	2.39	0.73	10.91	4.45	47.65	14.17	44.87	9.52	69.86	7.48	12585.28	3.83	77.61	703.16

Experiment 6 on January 8, 2016
Isotope ratio and date errors do not include systematic calibration errors of 0.52% ($^{207}Pb/^{206}Pb$) and 1.28% ($^{206}Pb/^{238}U$) (2 sigma).
Trace element concentrations were deleted from analyses known to have intersected inclusions of other minerals based on P and Ti.
Ablation used a laser spot size of 25 microns and a laser firing repetition rate of 5 Hz.
Activity of TiO_2 for Ti-in-Zircon temperature calculation is 0.8.

Appendix Table A8 LA-ICPMS isotopic U-Pb and trace element concentration data analyzed at Boise State University

Analysis	CA-TIMS label	U ppm	Th ppm	Pb* ppm	Th/U	$^{207}Pb/^{235}U$	±2s (%)	$^{206}Pb/^{238}U$	±2s (%)	error corr.	$^{238}U/^{206}Pb$	±2s (%)	$^{207}Pb/^{206}Pb$	±2s (%)	$^{208}Pb/^{232}Th$	±2s (Ma)	$^{207}Pb/^{206}Pb$	±2s (Ma)	$^{207}Pb/^{235}U$	±2s (Ma)	$^{206}Pb/^{238}U$	±2s (Ma)	% disc
Seiland - Secondary reference zircon																							
Seiland 569 1/8/2016 2:47:21 AM (Run: 1)		49.55	50.17	5.78	1.01	0.68880	6.70	0.08567	3.36	0.49	11.67	3.36	0.05832	5.80	536	39	542	127	532	28	530	17	2
Seiland 570 1/8/2016 2:49:05 AM (Run: 1)		53.74	54.83	6.25	1.02	0.69516	6.89	0.08505	3.76	0.54	11.76	3.76	0.05928	5.77	534	29	577	125	536	29	526	19	9
Seiland 577 1/8/2016 3:36:10 AM (Run: 1)		48.99	48.56	5.71	0.99	0.66640	6.17	0.08507	2.97	0.47	11.75	2.97	0.05681	5.41	559	35	484	119	519	25	526	15	-9
Seiland 578 1/8/2016 3:37:53 AM (Run: 1)		43.46	42.12	5.08	0.97	0.73023	7.88	0.08773	4.19	0.53	11.40	4.19	0.06037	6.67	517	38	617	144	557	34	542	22	12
Seiland 585 1/8/2016 4:25:04 AM (Run: 1)		55.40	55.60	6.60	1.00	0.68813	6.62	0.08615	3.50	0.52	11.61	3.50	0.05793	5.62	579	49	527	123	532	27	533	18	-1
Seiland 586 1/8/2016 4:26:48 AM (Run: 1)		50.76	50.90	5.87	1.00	0.63932	10.20	0.08480	4.73	0.46	11.79	4.73	0.05468	9.04	545	49	399	203	502	40	525	24	-31
Seiland 593 1/8/2016 5:13:58 AM (Run: 1)		46.44	44.28	5.49	0.95	0.71143	8.18	0.08693	3.42	0.41	11.50	3.42	0.05936	7.42	572	44	580	161	546	35	537	18	7
Seiland 594 1/8/2016 5:15:42 AM (Run: 1)		47.36	46.52	5.47	0.98	0.66457	10.17	0.08587	4.19	0.41	11.65	4.19	0.05613	9.27	529	38	458	206	517	41	531	21	-16
Seiland 601 1/8/2016 6:02:54 AM (Run: 1)		51.48	50.49	6.17	0.98	0.68643	7.83	0.08568	3.70	0.47	11.67	3.70	0.05811	6.89	615	48	534	151	531	32	530	19	1
Seiland 602 1/8/2016 6:04:38 AM (Run: 1)		62.36	61.63	7.40	0.99	0.71348	8.20	0.08590	3.54	0.43	11.64	3.54	0.06024	7.39	578	46	612	160	547	35	531	18	13
Zirconia - Secondary reference zircon																							
Zirconia 609 1/8/2016 3:11:45 AM (Run: 1)		516.02	4133.81	90.28	8.01	0.37875	3.93	0.05233	3.08	0.77	19.11	3.08	0.05249	2.45	301	7	307	56	326	11	329	10	-7
Zirconia 611 1/8/2016 3:13:29 AM (Run: 1)		486.57	3723.68	84.32	7.65	0.37646	3.29	0.05237	2.36	0.70	19.10	2.36	0.05214	2.28	310	3	291	52	324	9	329	8	-13
Zirconia 619 1/8/2016 4:00:39 AM (Run: 1)		534.12	4326.56	94.73	8.10	0.37177	3.95	0.05167	2.88	0.72	19.35	2.88	0.05218	2.71	305	7	293	62	321	11	325	9	-11
Zirconia 620 1/8/2016 4:02:23 AM (Run: 1)		545.88	4415.82	97.11	8.09	0.37450	3.61	0.05188	2.39	0.64	19.27	2.39	0.05235	2.71	306	4	301	62	323	10	326	8	-8
Zirconia 627 1/8/2016 4:49:34 AM (Run: 1)		346.20	1479.99	41.01	4.28	0.38579	4.17	0.05157	2.38	0.56	19.39	2.38	0.05425	3.43	303	4	382	77	331	12	324	8	15
Zirconia 628 1/8/2016 4:51:17 AM (Run: 1)		350.44	1554.47	43.01	4.44	0.38309	4.76	0.05200	2.59	0.53	19.23	2.59	0.05343	4.00	309	5	347	90	329	13	327	8	6
Zirconia 635 1/8/2016 5:38:29 AM (Run: 1)		425.58	2118.57	55.58	4.98	0.36835	3.96	0.05135	2.20	0.54	19.47	2.20	0.05202	3.30	310	4	286	75	318	11	323	7	-13
Zirconia 636 1/8/2016 5:40:12 AM (Run: 1)		321.50	1352.84	39.05	4.21	0.38634	3.91	0.05233	2.52	0.63	19.11	2.52	0.05354	2.99	318	8	352	68	332	11	329	8	7
Zirconia 643 1/8/2016 6:27:27 AM (Run: 1)		245.15	851.81	26.68	3.47	0.38079	4.34	0.05212	1.93	0.43	19.19	1.93	0.05298	3.89	314	8	328	88	328	12	328	6	0
Zirconia 644 1/8/2016 6:29:10 AM (Run: 1)		309.12	1298.08	36.37	4.20	0.36684	4.22	0.05113	2.23	0.51	19.56	2.23	0.05204	3.59	307	6	287	82	317	12	321	7	-12

Experiment 6 on January 8, 2016
Isotope ratio and date errors do not include systematic calibration errors of 0.52% ($^{207}Pb/^{206}Pb$) and 1.28% ($^{206}Pb/^{238}U$) (2 sigma).
Trace element concentrations were deleted from analyses known to have intersected inclusions of other minerals based on P and Ti.
Ablation used a laser spot size of 25 microns and a laser firing repetition rate of 5 Hz.
Activity of TiO_2 for Ti-in-Zircon temperature calculation is 0.8.

Appendix Table A8 LA-ICPMS isotopic U-Pb and trace element concentration data analyzed at Boise State University

Analysis	P	Ti	Y	Zr	Nb	La	Ce	Pr	Nd	Sm	Eu	Gd	Tb	Dy	Ho	Er	Tm	Yb	Lu	Hf	Ta	Th	U
	ppm	ppm	ppm	ppm	ppm	ppm	ppm	ppm	ppm	ppm	ppm	ppm	ppm	ppm	ppm	ppm	ppm	ppm	ppm	ppm	ppm	ppm	ppm
Seiland - Secondary reference zircon																							
Seiland 569 1/8/2016 2:47:21 AM (Run: 1)	65.44	2.05	222.82	549981.38	0.77		2.20			0.21	0.66	3.55	1.57	20.00	8.81	38.87	10.79	119.04	15.27	4971.45	0.80	50.17	49.55
Seiland 570 1/8/2016 2:49:05 AM (Run: 1)	69.63	1.45	227.94	558204.37	1.14		2.64	0.01		0.35	0.64	3.91	1.56	20.87	8.47	40.48	11.57	125.37	16.64	4956.72	0.92	54.83	53.74
Seiland 577 1/8/2016 3:36:10 AM (Run: 1)	66.27	1.95	213.52	572984.56	0.97		2.45		0.13	0.70	0.53	3.86	1.45	20.96	7.88	38.25	11.17	121.23	16.30	5093.52	0.79	48.56	48.99
Seiland 578 1/8/2016 3:37:53 AM (Run: 1)	55.90	1.70	201.55	570118.98	1.06		2.09			0.38	0.40	3.07	1.56	19.12	7.83	38.19	10.14	111.73	14.95	5141.48	0.77	42.12	43.46
Seiland 585 1/8/2016 4:25:04 AM (Run: 1)	64.17	1.81	239.84	564466.83	1.22		2.70		0.21	0.84	0.83	2.90	1.58	24.31	8.21	41.74	11.76	129.35	17.14	4963.47	1.07	55.60	55.40
Seiland 586 1/8/2016 4:26:48 AM (Run: 1)	38.26	1.50	218.61	559274.47	1.05		2.26	0.01	0.17	0.31	0.58	3.65	1.65	20.57	8.23	40.54	10.87	123.73	16.08	4973.28	0.94	50.90	50.76
Seiland 593 1/8/2016 5:13:58 AM (Run: 1)	76.93	1.61	206.53	563939.50	1.01		2.35		0.16	0.57	0.61	2.98	1.60	19.93	7.40	38.03	10.44	116.67	16.06	5351.50	0.86	44.28	46.44
Seiland 594 1/8/2016 5:15:42 AM (Run: 1)	61.62	1.83	211.09	567644.75	1.14		2.46		0.13	0.10	0.45	2.59	1.54	19.13	7.53	37.61	10.99	119.74	14.45	5294.95	0.75	46.52	47.36
Seiland 601 1/8/2016 6:02:54 AM (Run: 1)	56.66	1.87	211.66	558145.98	0.98		2.66	0.01		0.58	0.58	3.25	1.41	22.91	8.61	40.60	10.46	124.54	17.73	5392.36	1.03	50.49	51.48
Seiland 602 1/8/2016 6:04:38 AM (Run: 1)	72.55	1.99	241.99	558836.00	1.18		3.00	0.02	0.15	0.88	0.72	4.00	1.82	24.78	9.25	46.14	12.33	143.10	18.28	5436.68	1.02	61.63	62.36
Zirconia - Secondary reference zircon																							
Zirconia 609 1/8/2016 3:11:45 AM (Run: 1)	76.72	23.45	1622.89	601413.17	2.45	0.73	204.59	5.06	74.67	83.19	37.22	201.12	40.27	285.05	63.81	181.68	29.14	226.98	26.44	8488.90	0.73	4133.81	516.02
Zirconia 611 1/8/2016 3:13:29 AM (Run: 1)	78.68	20.61	1494.49	586621.78	2.30	0.69	182.83	4.43	65.42	73.90	35.36	185.86	36.75	258.97	57.95	163.63	27.28	206.77	24.03	8179.19	0.64	3723.68	486.57
Zirconia 619 1/8/2016 4:00:39 AM (Run: 1)	77.09	23.96	1700.00	594183.99	2.66	0.71	218.44	5.57	83.61	89.67	40.53	216.50	43.47	303.03	65.92	185.66	30.20	226.08	26.41	8473.51	0.70	4326.56	534.12
Zirconia 620 1/8/2016 4:02:23 AM (Run: 1)	54.82	25.03	1693.92	606390.19	2.98	0.89	223.12	5.83	86.59	94.64	42.06	222.43	42.92	300.96	65.48	185.53	31.34	232.12	27.04	8521.39	0.89	4415.82	545.88
Zirconia 627 1/8/2016 4:49:34 AM (Run: 1)	71.47	13.28	1705.17	621599.39	1.53	0.15	133.93	2.56	40.63	60.84	29.10	163.94	38.38	289.44	69.76	206.69	36.22	278.63	33.11	9767.34	0.59	1479.99	346.20
Zirconia 628 1/8/2016 4:51:17 AM (Run: 1)	65.16	14.17	1685.66	612989.02	1.75	0.29	140.57	2.77	41.29	59.70	30.15	178.61	38.28	295.62	69.89	201.88	36.33	265.43	32.93	9564.87	0.54	1554.47	350.44
Zirconia 635 1/8/2016 5:38:29 AM (Run: 1)	71.28	18.06	1957.26	620231.62	2.30	0.50	182.28	4.05	65.46	79.66	39.92	218.35	47.89	342.80	81.49	231.64	39.07	307.51	34.89	9094.99	0.68	2118.57	425.58
Zirconia 636 1/8/2016 5:40:12 AM (Run: 1)	88.85	14.76	1547.06	608642.66	1.34	0.21	123.02	2.40	40.84	55.66	27.93	159.97	36.38	269.09	62.69	189.95	33.22	261.31	29.44	9035.31	0.63	1352.84	321.50
Zirconia 643 1/8/2016 6:27:27 AM (Run: 1)	87.74	10.34	1252.01	620913.43	0.85	0.16	87.28	1.33	19.90	33.53	18.34	108.30	25.59	200.67	51.44	149.53	27.68	219.31	26.64	9734.83	0.42	851.81	245.15
Zirconia 644 1/8/2016 6:29:10 AM (Run: 1)	64.99	11.94	1377.91	631884.64	1.28	0.10	107.91	2.08	30.17	41.46	21.53	125.55	29.12	226.05	56.45	169.21	29.77	233.19	28.45	9578.20	0.51	1298.08	309.12

Experiment 6 on January 8, 2016
Isotope ratio and date errors do not include systematic calibration errors of 0.52% ($^{207}Pb/^{206}Pb$) and 1.28% ($^{206}Pb/^{238}U$) (2 sigma).
Trace element concentrations were deleted from analyses known to have intersected inclusions of other minerals based on P and Ti.
Ablation used a laser spot size of 25 microns and a laser firing repetition rate of 5 Hz.
Activity of TiO_2 for Ti-in-Zircon temperature calculation is 0.8.

Appendix Table A8 LA-ICPMS isotopic U-Pb and trace element concentration data analyzed at Boise State University

Analysis	CA-TIMS label	U ppm	Th ppm	Pb* ppm	Th/U	$^{207}Pb/^{235}U$	±2s (%)	$^{206}Pb/^{238}U$	±2s (%)	error corr.	$^{238}U/^{206}Pb$	±2s (%)	$^{207}Pb/^{206}Pb$	±2s (%)	$^{208}Pb/^{232}Th$	±2s (Ma)	$^{207}Pb/^{206}Pb$	±2s (Ma)	$^{207}Pb/^{235}U$	±2s (Ma)	$^{206}Pb/^{238}U$	±2s (Ma)	% disc
FC1 - Primary zircon standard																							
FC1 151 11/27/2019 12:06:48 PM (Run: 1)	std	373.88	268.41	88.35	0.72	1.90880	2.01	0.18014	1.78	0.88	5.55	1.78	0.07685	0.92	1105	28	1117	18	1084	13	1068	18	4
FC1 152 11/27/2019 12:08:46 PM (Run: 1)	std	364.21	254.57	86.13	0.70	1.90337	1.83	0.18243	1.51	0.82	5.48	1.51	0.07567	1.04	1085	10	1086	21	1082	12	1080	15	1
FC1 153 11/27/2019 12:10:44 PM (Run: 1)	std	353.04	240.56	83.45	0.68	1.92178	1.81	0.18306	1.48	0.81	5.46	1.48	0.07614	1.04	1090	28	1099	21	1089	12	1084	15	1
FC1 154 11/27/2019 12:12:42 PM (Run: 1)	std	342.48	227.84	81.10	0.67	1.94735	2.08	0.18482	1.53	0.73	5.41	1.53	0.07642	1.41	1082	19	1106	28	1098	14	1093	15	1
FC1 155 11/27/2019 12:38:33 PM (Run: 1)	std	355.54	258.27	87.44	0.73	1.97184	2.26	0.18877	1.92	0.85	5.30	1.92	0.07576	1.19	1116	29	1089	24	1106	15	1115	20	-2
FC1 156 11/27/2019 12:40:31 PM (Run: 1)	std	385.53	275.18	93.05	0.71	1.93761	1.72	0.18595	1.38	0.80	5.38	1.38	0.07558	1.03	1080	17	1084	21	1094	12	1099	14	-1
FC1 157 11/27/2019 1:06:24 PM (Run: 1)	std	394.35	294.46	96.00	0.75	1.95349	1.85	0.18564	1.58	0.85	5.39	1.58	0.07632	0.96	1088	20	1103	19	1100	12	1098	16	1
FC1 158 11/27/2019 1:08:21 PM (Run: 1)	std	410.18	301.92	98.73	0.74	1.91810	1.84	0.18331	1.44	0.78	5.46	1.44	0.07589	1.14	1099	24	1092	23	1087	12	1085	14	1
FC1 159 11/27/2019 1:34:14 PM (Run: 1)	std	202.77	132.07	47.43	0.65	1.94313	2.30	0.18567	1.91	0.83	5.39	1.91	0.07590	1.27	1075	26	1092	25	1096	15	1098	19	0
FC1 160 11/27/2019 1:36:11 PM (Run: 1)	std	161.93	92.41	37.01	0.57	1.93333	2.48	0.18447	1.75	0.70	5.42	1.75	0.07601	1.75	1111	24	1095	35	1093	17	1091	18	0
FC1 161 11/27/2019 2:02:09 PM (Run: 1)	std	191.42	124.45	44.66	0.65	1.95232	2.63	0.18510	1.47	0.55	5.40	1.47	0.07650	2.19	1083	24	1108	44	1099	18	1095	15	1
FC1 162 11/27/2019 2:04:06 PM (Run: 1)	std	175.91	111.67	40.91	0.63	1.91092	2.48	0.18400	1.69	0.68	5.43	1.69	0.07532	1.82	1135	22	1077	37	1085	17	1089	17	-1
FC1 163 11/27/2019 2:29:53 PM (Run: 1)	std	219.80	154.32	52.47	0.70	1.98020	2.46	0.18619	1.95	0.79	5.37	1.95	0.07713	1.50	1102	31	1125	30	1109	17	1101	20	2
FC1 164 11/27/2019 2:31:51 PM (Run: 1)	std	231.48	163.33	55.96	0.71	1.97761	2.08	0.18794	1.44	0.69	5.32	1.44	0.07632	1.51	1127	29	1103	30	1108	14	1110	15	-1
FC1 165 11/27/2019 2:57:39 PM (Run: 1)	std	235.53	155.89	55.45	0.66	1.91218	1.88	0.18435	1.02	0.54	5.42	1.02	0.07523	1.57	1138	37	1075	32	1085	13	1091	10	-1
FC1 166 11/27/2019 2:59:36 PM (Run: 1)	std	237.88	160.19	57.09	0.67	1.99060	1.99	0.18824	1.47	0.73	5.31	1.47	0.07670	1.34	1117	31	1113	27	1112	13	1112	15	0
FC1 167 11/27/2019 3:25:24 PM (Run: 1)	std	283.57	221.06	67.19	0.78	1.94601	2.82	0.18223	2.26	0.80	5.49	2.26	0.07745	1.67	1038	24	1133	33	1097	19	1079	23	5
FC1 168 11/27/2019 3:27:21 PM (Run: 1)	std	299.24	226.88	72.29	0.76	1.94708	2.21	0.18638	1.69	0.76	5.37	1.69	0.07577	1.43	1074	19	1089	29	1097	15	1102	17	-1
FC1 169 11/27/2019 3:53:20 PM (Run: 1)	std	293.94	221.78	70.41	0.75	1.91677	2.50	0.18458	2.00	0.80	5.42	2.00	0.07532	1.49	1075	22	1077	30	1087	17	1092	20	-1
FC1 170 11/27/2019 3:55:18 PM (Run: 1)	std	294.88	222.98	71.92	0.76	1.98593	1.97	0.18770	1.29	0.65	5.33	1.29	0.07673	1.49	1088	19	1114	30	1111	13	1109	13	0
FC1 171 11/27/2019 4:17:02 PM (Run: 1)	std	290.62	220.19	71.00	0.76	1.98752	2.15	0.18771	1.33	0.61	5.33	1.33	0.07679	1.69	1097	23	1116	34	1111	15	1109	14	1
FC1 172 11/27/2019 4:19:00 PM (Run: 1)	std	303.19	229.10	73.46	0.76	1.95956	1.85	0.18630	1.29	0.69	5.37	1.29	0.07629	1.33	1086	26	1103	27	1102	12	1101	13	0
FC1 175 11/27/2019 4:40:51 PM (Run: 1)	std	282.81	230.50	68.79	0.82	1.92317	2.36	0.18327	2.02	0.85	5.46	2.02	0.07611	1.23	1123	27	1098	25	1089	16	1085	20	1
FC1 176 11/27/2019 4:42:49 PM (Run: 1)	std	287.74	237.65	70.29	0.83	1.95321	2.06	0.18492	1.43	0.69	5.41	1.43	0.07660	1.48	1082	26	1111	30	1100	14	1094	14	2
FC1 177 11/27/2019 5:04:40 PM (Run: 1)	std	291.56	236.89	71.45	0.81	1.93759	2.15	0.18626	1.51	0.70	5.37	1.51	0.07545	1.53	1090	25	1080	31	1094	14	1101	15	-2
FC1 178 11/27/2019 5:06:37 PM (Run: 1)	std	303.26	242.01	72.53	0.80	1.90306	1.68	0.18259	1.40	0.83	5.48	1.40	0.07559	0.92	1059	20	1084	19	1082	11	1081	14	0
FC1 179 11/27/2019 5:28:30 PM (Run: 1)	std	294.98	233.34	71.90	0.79	1.91880	2.48	0.18633	1.65	0.66	5.37	1.65	0.07469	1.86	1086	29	1060	37	1088	17	1101	17	-4
FC1 180 11/27/2019 5:30:27 PM (Run: 1)	std	279.78	229.02	69.55	0.82	1.96325	2.23	0.18783	1.59	0.71	5.32	1.59	0.07581	1.57	1122	23	1090	31	1103	15	1110	16	-2
FC1 181 11/27/2019 5:52:12 PM (Run: 1)	std	280.71	234.83	70.90	0.84	1.98863	1.72	0.19056	1.24	0.72	5.25	1.24	0.07569	1.18	1125	25	1087	24	1112	12	1124	13	-3
FC1 182 11/27/2019 5:54:10 PM (Run: 1)	std	283.73	237.91	69.97	0.84	1.93383	1.81	0.18561	1.48	0.81	5.39	1.48	0.07556	1.04	1112	27	1084	21	1093	12	1098	15	-1
FC1 183 11/27/2019 6:15:55 PM (Run: 1)	std	111.36	52.40	24.63	0.47	1.99032	2.88	0.18510	2.29	0.79	5.40	2.29	0.07798	1.75	1038	42	1146	35	1112	19	1095	23	5
FC1 184 11/27/2019 6:17:52 PM (Run: 1)	std	122.20	60.07	27.59	0.49	1.95778	2.20	0.18599	1.48	0.67	5.38	1.48	0.07635	1.63	1142	42	1104	33	1101	15	1100	15	0

Experiment 7 on November 27, 2019
Isotope ratio and date errors do not include systematic calibration errors of 0.18% ($^{207}Pb/^{206}Pb$) and 1.52% ($^{206}Pb/^{238}U$) (2 sigma).
Trace element concentrations were deleted from analyses known to have intersected inclusions of other minerals based on P and Ti.

Ablation used a laser spot size of 25 microns and a laser firing repetition rate of 5 Hz.
Activity of TiO_2 for Ti-in-Zircon temperature calculation is 0.8.

Appendix Table A8 LA-ICPMS isotopic U-Pb and trace element concentration data analyzed at Boise State University

Analysis	P	Ti	Y	Zr	Nb	La	Ce	Pr	Nd	Sm	Eu	Gd	Tb	Dy	Ho	Er	Tm	Yb	Lu	Hf	Ta	Th	U
	ppm	ppm	ppm	ppm	ppm	ppm	ppm	ppm	ppm	ppm	ppm	ppm	ppm	ppm	ppm	ppm	ppm	ppm	ppm	ppm	ppm	ppm	ppm
FC1 - Primary zircon standard																							
FC1 151 11/27/2019 12:06:48 PM (Run: 1)	179.23	16.03	1641.83	324632.78	1.23		7.01	0.07	1.12	4.15	0.17	30.61	12.96	168.73	59.95	254.77	63.15	669.07	62.03	11020.32	1.15	268.41	373.88
FC1 152 11/27/2019 12:08:46 PM (Run: 1)	166.93	15.17	1568.77	324163.10	1.04		6.25	0.03	1.47	4.10	0.17	27.95	12.42	158.36	57.52	242.35	61.32	663.82	60.80	11086.56	0.83	254.57	364.21
FC1 153 11/27/2019 12:10:44 PM (Run: 1)	168.56	14.10	1445.37	320439.25	1.15		6.18	0.04	0.88	3.45	0.17	25.06	10.67	139.90	52.30	215.11	55.74	621.22	56.89	11004.55	0.88	240.56	353.04
FC1 154 11/27/2019 12:12:42 PM (Run: 1)	141.51	13.52	1343.98	320159.19	1.25	0.02	6.16	0.05	0.98	3.63	0.13	24.26	10.25	135.73	49.58	202.90	51.86	593.03	56.14	11109.80	0.96	227.84	342.48
FC1 155 11/27/2019 12:38:33 PM (Run: 1)	166.26	11.24	1320.99	318698.01	1.10	0.10	6.80	0.06	1.30	3.27	0.11	23.81	9.73	131.80	48.96	197.23	50.83	571.04	53.48	11124.74	0.96	258.27	355.54
FC1 156 11/27/2019 12:40:31 PM (Run: 1)	179.24	13.68	1617.33	319753.21	1.16		6.46	0.02	1.09	4.82	0.17	30.80	12.02	166.51	57.07	247.52	63.22	671.65	62.40	11172.33	0.95	275.18	385.53
FC1 157 11/27/2019 1:06:24 PM (Run: 1)	185.46	15.32	1716.00	319306.55	1.17		6.83	0.04	1.52	4.93	0.24	31.45	13.36	176.48	63.25	257.82	65.59	696.17	64.24	10943.29	0.90	294.46	394.35
FC1 158 11/27/2019 1:08:21 PM (Run: 1)	188.89	15.01	1756.26	321211.75	1.10		7.47	0.04	1.35	5.42	0.25	34.34	13.77	182.11	64.20	262.49	68.14	719.71	66.22	11133.03	0.93	301.92	410.18
FC1 159 11/27/2019 1:34:14 PM (Run: 1)	154.07	21.29	1160.81	316580.15	0.82	0.17	4.98	0.06	0.64	4.14	0.18	21.61	9.42	123.36	42.81	170.33	42.63	474.37	42.35	10177.79	0.63	132.07	202.77
FC1 160 11/27/2019 1:36:11 PM (Run: 1)	143.58	22.67	806.38	310298.99	0.97	0.06	4.52	0.03	0.81	2.87	0.15	16.91	6.88	83.97	30.85	125.48	32.18	369.28	35.69	9930.05	0.72	92.41	161.93
FC1 161 11/27/2019 2:02:09 PM (Run: 1)	157.81	20.65	1048.70	314552.34	1.01	0.03	5.06	0.08	1.40	3.90	0.16	20.49	8.40	111.34	38.27	154.47	40.64	439.57	40.07	10003.78	0.87	124.45	191.42
FC1 162 11/27/2019 2:04:06 PM (Run: 1)	152.03	21.12	945.15	311833.73	0.95	0.02	5.27	0.05	1.19	3.86	0.13	20.74	8.23	98.45	35.39	141.32	36.83	409.94	37.06	9959.76	0.84	111.67	175.91
FC1 163 11/27/2019 2:29:53 PM (Run: 1)	154.28	19.59	1189.51	310432.68	0.97		5.32	0.02	1.11	3.88	0.29	26.05	10.17	124.21	44.50	180.58	45.84	498.47	44.35	9821.19	1.06	154.32	219.80
FC1 164 11/27/2019 2:31:51 PM (Run: 1)	178.57	19.84	1331.40	315489.31	0.96		5.69	0.07	1.50	4.27	0.18	28.68	11.53	143.60	48.93	196.56	49.38	540.16	48.07	9985.86	0.93	163.33	231.48
FC1 165 11/27/2019 2:57:39 PM (Run: 1)	174.33	19.79	1287.97	308811.57	0.98		5.16	0.03	1.18	4.63	0.27	27.60	10.38	143.37	48.51	197.64	50.37	541.20	46.85	9765.36	0.77	155.89	235.53
FC1 166 11/27/2019 2:59:36 PM (Run: 1)	183.13	19.56	1305.33	312603.25	1.11		5.10	0.06	1.34	4.35	0.16	26.81	10.85	140.44	47.71	196.77	48.26	534.82	49.17	9854.38	0.86	160.19	237.88
FC1 167 11/27/2019 3:25:24 PM (Run: 1)	215.63	26.17	2463.80	323214.50	1.41	0.10	9.01	0.68	12.69	22.20	0.78	73.66	28.49	306.58	96.68	378.96	92.79	977.65	87.05	10455.31	1.66	221.06	283.57
FC1 168 11/27/2019 3:27:21 PM (Run: 1)	241.75	29.29	2558.27	329129.17	1.59	0.08	9.15	0.71	11.82	21.34	0.74	76.17	28.08	319.16	103.13	389.60	96.04	984.84	91.56	10529.80	2.20	226.88	299.24
FC1 169 11/27/2019 3:53:20 PM (Run: 1)	248.15	28.81	2529.12	315733.79	1.45	0.09	8.96	0.63	12.15	21.31	0.61	71.18	27.35	300.99	101.81	385.64	95.21	998.79	90.83	10204.43	2.19	221.78	293.94
FC1 170 11/27/2019 3:55:18 PM (Run: 1)	214.32	29.32	2606.32	323869.98	1.37	0.07	9.11	0.67	12.30	18.87	0.64	77.94	27.93	314.67	102.40	390.84	95.11	991.73	91.21	10403.90	2.19	222.98	294.88
FC1 171 11/27/2019 4:17:02 PM (Run: 1)	241.89	28.86	2555.66	318265.55	1.58	0.11	8.27	0.68	12.79	19.89	0.79	74.39	26.48	308.75	97.57	386.56	95.36	996.65	91.42	10167.68	2.05	220.19	290.62
FC1 172 11/27/2019 4:19:00 PM (Run: 1)	260.58	30.51	2643.72	324661.80	1.64	0.09	8.90	0.72	13.33	21.00	0.71	79.79	27.94	318.93	102.52	400.31	98.07	1047.88	95.77	10698.23	2.29	229.10	303.19
FC1 175 11/27/2019 4:40:51 PM (Run: 1)	241.88	23.97	2514.05	317475.52	1.44		9.34	0.42	9.05	20.94	0.48	73.90	28.19	300.09	99.89	376.05	92.25	974.53	86.53	11725.96	1.49	230.50	282.81
FC1 176 11/27/2019 4:42:49 PM (Run: 1)	229.32	25.96	2557.07	315574.70	1.76	0.03	9.60	0.44	9.81	19.18	0.69	72.53	27.77	308.00	99.88	382.06	94.28	972.76	87.19	11286.59	1.53	237.65	287.74
FC1 177 11/27/2019 5:04:40 PM (Run: 1)	234.72	28.28	2594.07	320925.05	1.52		8.98	0.53	11.94	20.05	0.73	79.24	27.79	319.59	100.61	386.23	94.78	1015.66	89.78	10809.98	1.68	236.89	291.56
FC1 178 11/27/2019 5:06:37 PM (Run: 1)	244.24	28.02	2643.31	318670.88	1.73	0.03	9.14	0.58	11.72	21.15	0.69	74.32	27.62	316.35	101.99	390.27	98.04	1043.75	93.58	10296.48	1.87	242.01	303.26
FC1 179 11/27/2019 5:28:30 PM (Run: 1)	225.39	27.85	2623.21	324731.90	2.04	0.03	9.67	0.50	11.09	20.78	0.76	78.97	26.64	315.89	102.44	391.13	97.11	1014.84	93.27	10596.90	1.58	233.34	294.98
FC1 180 11/27/2019 5:30:27 PM (Run: 1)	235.34	24.41	2501.05	317403.94	1.82	0.02	8.91	0.44	10.30	18.50	0.83	72.71	27.13	304.64	97.40	377.64	92.11	980.85	86.96	11062.33	1.88	229.02	279.78
FC1 181 11/27/2019 5:52:12 PM (Run: 1)	232.40	24.03	2514.78	322837.95	1.35		9.13	0.37	8.26	16.79	0.57	76.30	26.94	302.46	98.72	374.65	92.73	986.70	84.53	11589.28	1.37	234.83	280.71
FC1 182 11/27/2019 5:54:10 PM (Run: 1)	225.17	25.65	2548.82	319781.25	1.91	0.04	9.12	0.36	7.03	18.52	0.68	72.65	27.29	309.60	97.65	389.03	93.92	990.99	86.29	11699.65	1.62	237.91	283.73
FC1 183 11/27/2019 6:15:55 PM (Run: 1)	143.12	23.54	578.47	321857.32	0.69		3.30	0.03	0.51	1.62	0.11	11.19	4.74	57.49	21.43	89.84	23.83	295.44	27.59	10868.92	0.91	52.40	111.36
FC1 184 11/27/2019 6:17:52 PM (Run: 1)	150.79	23.47	715.81	313700.82	0.66		3.81	0.04	1.15	2.90	0.07	13.77	5.33	73.67	25.67	106.98	29.28	342.85	33.03	10479.93	0.67	60.07	122.20

Experiment 7 on November 27, 2019
Isotope ratio and date errors do not include systematic calibration errors of 0.18% ($^{207}Pb/^{206}Pb$) and 1.52% ($^{206}Pb/^{238}U$) (2 sigma).
Trace element concentrations were deleted from analyses known to have intersected inclusions of other minerals based on P and Ti.

Ablation used a laser spot size of 25 microns and a laser firing repetition rate of 5 Hz.
Activity of TiO_2 for Ti-in-Zircon temperature calculation is 0.8.

Appendix Table A8 LA-ICPMS isotopic U-Pb and trace element concentration data analyzed at Boise State University

Analysis	CA-TIMS label	U ppm	Th ppm	Pb* ppm	Th/U	$^{207}Pb/^{235}U$	±2s (%)	$^{206}Pb/^{238}U$	±2s (%)	error corr.	$^{238}U/^{206}Pb$	±2s (%)	$^{207}Pb/^{206}Pb$	±2s (%)	$^{208}Pb/^{232}Th$	±2s (Ma)	$^{207}Pb/^{206}Pb$	±2s (Ma)	$^{207}Pb/^{235}U$	±2s (Ma)	$^{206}Pb/^{238}U$	±2s (Ma)	% disc
91500 - Secondary reference zircon																							
91500 204 11/27/2019 3:03:34 PM (Run: 1)		83.84	46.77	18.47	0.56	1.94212	3.49	0.18423	1.80	0.51	5.43	1.80	0.07646	2.99	900	49	1107	60	1096	23	1090	18	2
91500 193 11/27/2019 12:42:31 PM (Run: 1)		87.26	49.42	18.63	0.57	1.84642	2.80	0.17539	1.38	0.49	5.70	1.38	0.07635	2.44	972	49	1104	49	1062	18	1042	13	6
91500 200 11/27/2019 2:08:04 PM (Run: 1)		81.69	46.02	17.22	0.56	1.85142	2.76	0.17595	1.33	0.48	5.68	1.33	0.07632	2.42	873	40	1103	48	1064	18	1045	13	5
91500 205 11/27/2019 3:29:21 PM (Run: 1)		82.07	45.39	17.84	0.55	1.89390	3.23	0.18139	2.02	0.62	5.51	2.02	0.07573	2.52	919	47	1088	51	1079	21	1075	20	1
91500 198 11/27/2019 1:40:09 PM (Run: 1)		81.87	44.92	17.65	0.55	1.87048	2.67	0.17963	1.46	0.54	5.57	1.46	0.07552	2.23	931	33	1082	45	1071	18	1065	14	2
91500 195 11/27/2019 1:10:21 PM (Run: 1)		83.10	46.16	17.31	0.56	1.79307	3.93	0.17376	1.47	0.37	5.76	1.47	0.07484	3.65	885	33	1064	73	1043	26	1033	14	3
91500 197 11/27/2019 1:38:12 PM (Run: 1)		85.14	47.46	18.41	0.56	1.85358	2.60	0.17968	1.35	0.51	5.57	1.35	0.07482	2.22	937	45	1064	45	1065	17	1065	13	0
91500 202 11/27/2019 2:35:49 PM (Run: 1)		82.48	46.07	17.30	0.56	1.81908	3.06	0.17649	1.35	0.44	5.67	1.35	0.07475	2.75	834	37	1062	55	1052	20	1048	13	1
91500 201 11/27/2019 2:33:51 PM (Run: 1)	reverse fractionation	80.67	46.23	17.44	0.57	1.85609	3.31	0.18063	1.35	0.40	5.54	1.35	0.07453	3.03	883	40	1056	61	1066	22	1070	13	-1
91500 192 11/27/2019 12:16:39 PM (Run: 1)		86.95	50.36	18.72	0.58	1.83819	3.40	0.17904	1.63	0.48	5.59	1.63	0.07446	2.99	889	43	1054	60	1059	22	1062	16	-1
91500 191 11/27/2019 12:14:41 PM (Run: 1)		90.02	51.60	19.40	0.57	1.81964	2.46	0.17742	2.10	0.85	5.64	2.10	0.07438	1.28	966	43	1052	26	1053	16	1053	20	0
91500 196 11/27/2019 1:12:19 PM (Run: 1)		84.28	48.64	17.80	0.58	1.79368	2.25	0.17551	1.32	0.58	5.70	1.32	0.07412	1.83	888	35	1045	37	1043	15	1042	13	0
91500 206 11/27/2019 3:31:19 PM (Run: 1)		80.53	45.36	17.85	0.56	1.87006	3.64	0.18430	1.64	0.45	5.43	1.64	0.07359	3.25	955	43	1030	66	1071	24	1090	16	-6

Experiment 7 on November 27, 2019
Isotope ratio and date errors do not include systematic calibration errors of 0.18% ($^{207}Pb/^{206}Pb$) and 1.52% ($^{206}Pb/^{238}U$) (2 sigma).
Trace element concentrations were deleted from analyses known to have intersected inclusions of other minerals based on P and Ti.
Ablation used a laser spot size of 25 microns and a laser firing repetition rate of 5 Hz.
Activity of TiO_2 for Ti-in-Zircon temperature calculation is 0.8.

Appendix Table A8 LA-ICPMS isotopic U-Pb and trace element concentration data analyzed at Boise State University

Analysis	P	Ti	Y	Zr	Nb	La	Ce	Pr	Nd	Sm	Eu	Gd	Tb	Dy	Ho	Er	Tm	Yb	Lu	Hf	Ta	Th	U
	ppm	ppm	ppm	ppm	ppm	ppm	ppm	ppm	ppm	ppm	ppm	ppm	ppm	ppm	ppm	ppm	ppm	ppm	ppm	ppm	ppm	ppm	ppm
91500 - Secondary reference zircon																							
91500 204 11/27/2019 3:03:34 PM (Run: 1)	46.89	6.15	208.69	359063.02	1.10		2.74	0.01	0.22	0.79	0.41	3.48	1.53	19.79	7.31	34.08	11.10	141.90	16.32	7335.01	0.94	46.77	83.84
91500 193 11/27/2019 12:42:31 PM (Run: 1)	44.71	6.42	215.92	362862.17	1.06		2.79		0.24	0.92	0.40	3.00	1.58	20.74	8.06	38.10	11.98	149.83	16.72	6966.50	1.20	49.42	87.26
91500 200 11/27/2019 2:08:04 PM (Run: 1)	43.03	5.88	207.38	367432.99	0.99		3.12		0.17	0.70	0.42	2.86	1.30	21.14	7.21	34.68	11.20	140.91	15.41	7303.32	0.91	46.02	81.69
91500 205 11/27/2019 3:29:21 PM (Run: 1)	45.23	6.65	207.39	358991.87	1.07		2.57	0.03	0.18	0.78	0.31	2.88	1.39	20.48	6.83	36.37	11.35	139.94	15.44	7197.33	0.89	45.39	82.07
91500 198 11/27/2019 1:40:09 PM (Run: 1)	42.44	6.50	200.63	358458.70	1.00		2.60		0.19	0.65	0.35	3.06	1.43	18.35	7.23	35.30	10.76	138.15	15.49	7217.92	0.83	44.92	81.87
91500 195 11/27/2019 1:10:21 PM (Run: 1)	34.66	6.49	201.24	362872.06	1.05		2.65	0.02	0.35	0.84	0.37	2.87	1.44	19.73	7.46	36.93	12.09	141.88	16.57	7210.80	0.73	46.16	83.10
91500 197 11/27/2019 1:38:12 PM (Run: 1)	33.80	6.69	211.10	363651.27	1.28		2.88		0.53	1.03	0.33	2.41	1.58	18.58	7.40	37.50	11.60	146.78	15.73	7190.40	0.74	47.46	85.14
91500 202 11/27/2019 2:35:49 PM (Run: 1)	38.22	6.86	204.88	362273.07	0.78		2.63	0.03	0.29	0.91	0.40	3.77	1.19	19.83	7.66	36.53	10.74	145.10	15.68	7161.75	0.87	46.07	82.48
91500 201 11/27/2019 2:33:51 PM (Run: 1)	34.36	6.50	206.48	365568.75	1.03		2.70		0.37	0.48	0.38	3.90	1.31	20.96	6.81	36.08	11.24	147.19	15.77	7296.84	0.98	46.23	80.67
91500 192 11/27/2019 12:16:39 PM (Run: 1)	50.19	6.74	213.00	359356.39	1.05		2.76		0.11	1.06	0.45	3.83	1.45	20.35	7.81	38.60	11.76	150.81	16.24	6994.26	0.90	50.36	86.95
91500 191 11/27/2019 12:14:41 PM (Run: 1)	45.49	5.91	219.16	363058.07	1.30		2.95	0.02	0.44	0.74	0.47	3.10	1.44	21.83	8.20	36.80	12.60	154.81	17.11	6906.38	1.00	51.60	90.02
91500 196 11/27/2019 1:12:19 PM (Run: 1)	37.64	6.84	210.88	367516.50	1.10		2.90		0.19	0.65	0.32	3.36	1.55	18.06	7.49	37.94	12.22	145.97	15.85	7272.56	0.96	48.64	84.28
91500 206 11/27/2019 3:31:19 PM (Run: 1)	35.88	6.23	197.43	350671.97	1.00		2.75		0.33	0.48	0.33	3.75	1.48	19.72	7.56	36.06	10.81	135.42	15.69	7083.41	0.92	45.36	80.53

Experiment 7 on November 27, 2019
Isotope ratio and date errors do not include systematic calibration errors of 0.18% ($^{207}Pb/^{206}Pb$) and 1.52% ($^{206}Pb/^{238}U$) (2 sigma).
Trace element concentrations were deleted from analyses known to have intersected inclusions of other minerals based on P and Ti.
Ablation used a laser spot size of 25 microns and a laser firing repetition rate of 5 Hz.
Activity of TiO_2 for Ti-in-Zircon temperature calculation is 0.8.

Appendix 4 Table A9 Standard calibration uncertainties, Boise State University

Experiment 1 on July 31, 2014

Isotope ratio and date errors do not include systematic calibration errors of 0.60% ($^{207}Pb/^{206}Pb$) and 1.68% ($^{206}Pb/^{238}U$) (2 sigma).

Experiment 2 on October 17, 2014

Isotope ratio and date errors do not include systematic calibration errors of 0.64% ($^{207}Pb/^{206}Pb$) and 2.31% ($^{206}Pb/^{238}U$) (2 sigma).

Experiment 3 on January 7, 2016

Isotope ratio and date errors do not include systematic calibration errors of 0.48% ($^{207}Pb/^{206}Pb$) and 0.92% ($^{206}Pb/^{238}U$) (2 sigma).

Experiment 4 on January 8, 2016

Isotope ratio and date errors do not include systematic calibration errors of 0.52% ($^{207}Pb/^{206}Pb$) and 0.88% ($^{206}Pb/^{238}U$) (2 sigma).

Experiment 5 on January 8, 2016

Isotope ratio and date errors do not include systematic calibration errors of 0.50% ($^{207}Pb/^{206}Pb$) and 1.03% ($^{206}Pb/^{238}U$) (2 sigma).

Experiment 6 on January 8, 2016

Isotope ratio and date errors do not include systematic calibration errors of 0.52% ($^{207}Pb/^{206}Pb$) and 1.28% ($^{206}Pb/^{238}U$) (2 sigma).

Experiment 7 on November 27, 2019

Isotope ratio and date errors do not include systematic calibration errors of 0.18% ($^{207}Pb/^{206}Pb$) and 1.52% ($^{206}Pb/^{238}U$) (2 sigma).

Appendix 4 Figure A1

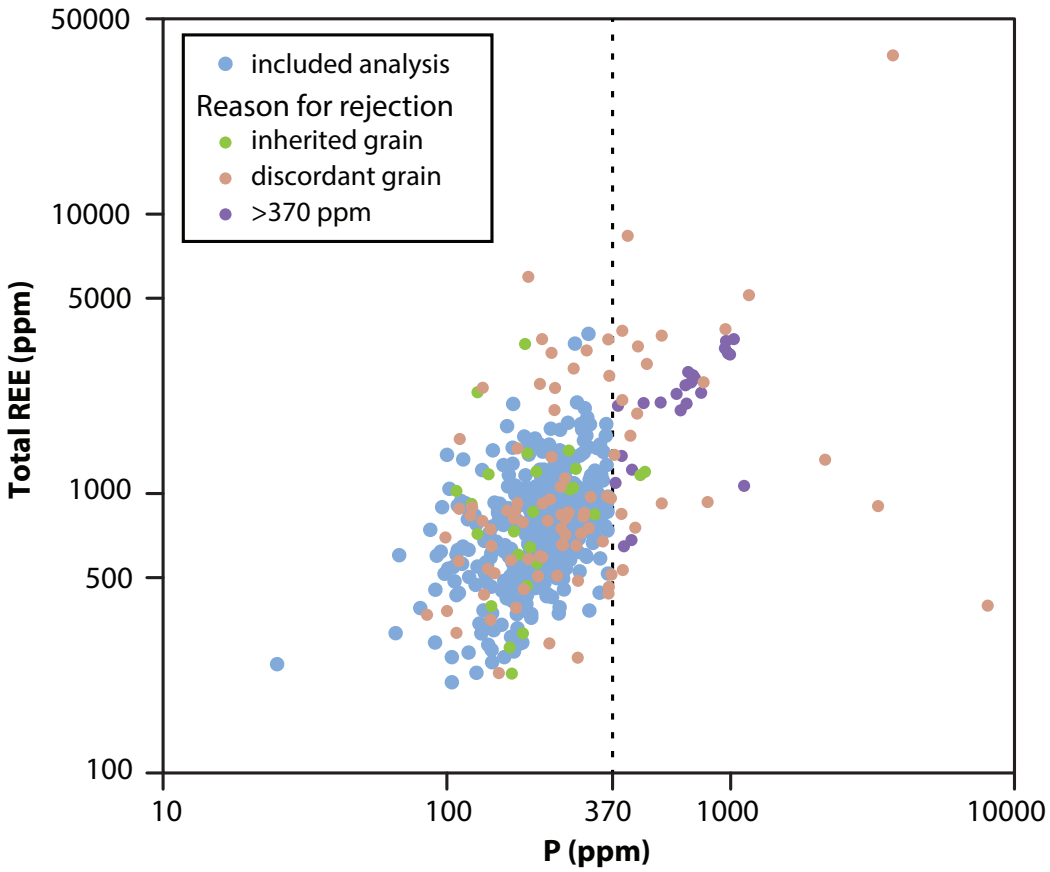

Appendix Figure A1 - Total rare earth elements (REE) vs P concentrations for the data indicating inherited and discordant grains, and 370 ppm P (dashed line), above which we have filtered the dataset to avoid bias towards data containing trace element signatures influenced by inclusions (e.g. Yang *et al*., 2016).

Appendix 4 Figure A2

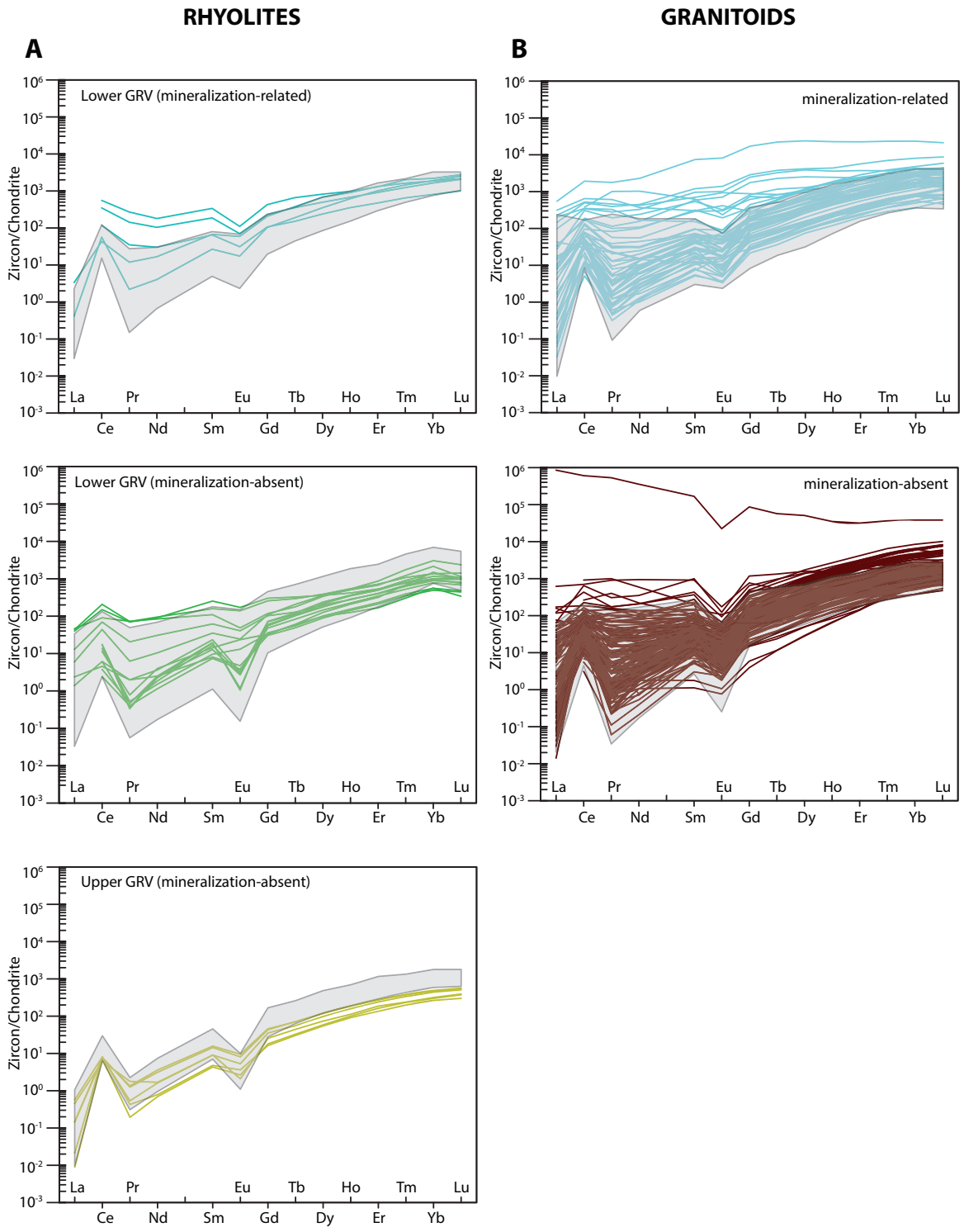

Appendix Figure A2 A) Rhyolite zircon rare earth element plots for zircon data used in this study (shaded area) and data excluded from this study (lines). **B)** Granitoid zircon rare earth element plots for zircon data used in this study (shaded areas) and data excluded from this study (lines). These pre-filtered data plots are presented to demonstrate that our conclusions are not biased by the removal of data that could be considered representative of magmatic zircon. Upper GRV data from Ferguson *et al.*, (2020).

Appendix 4 Figure A3

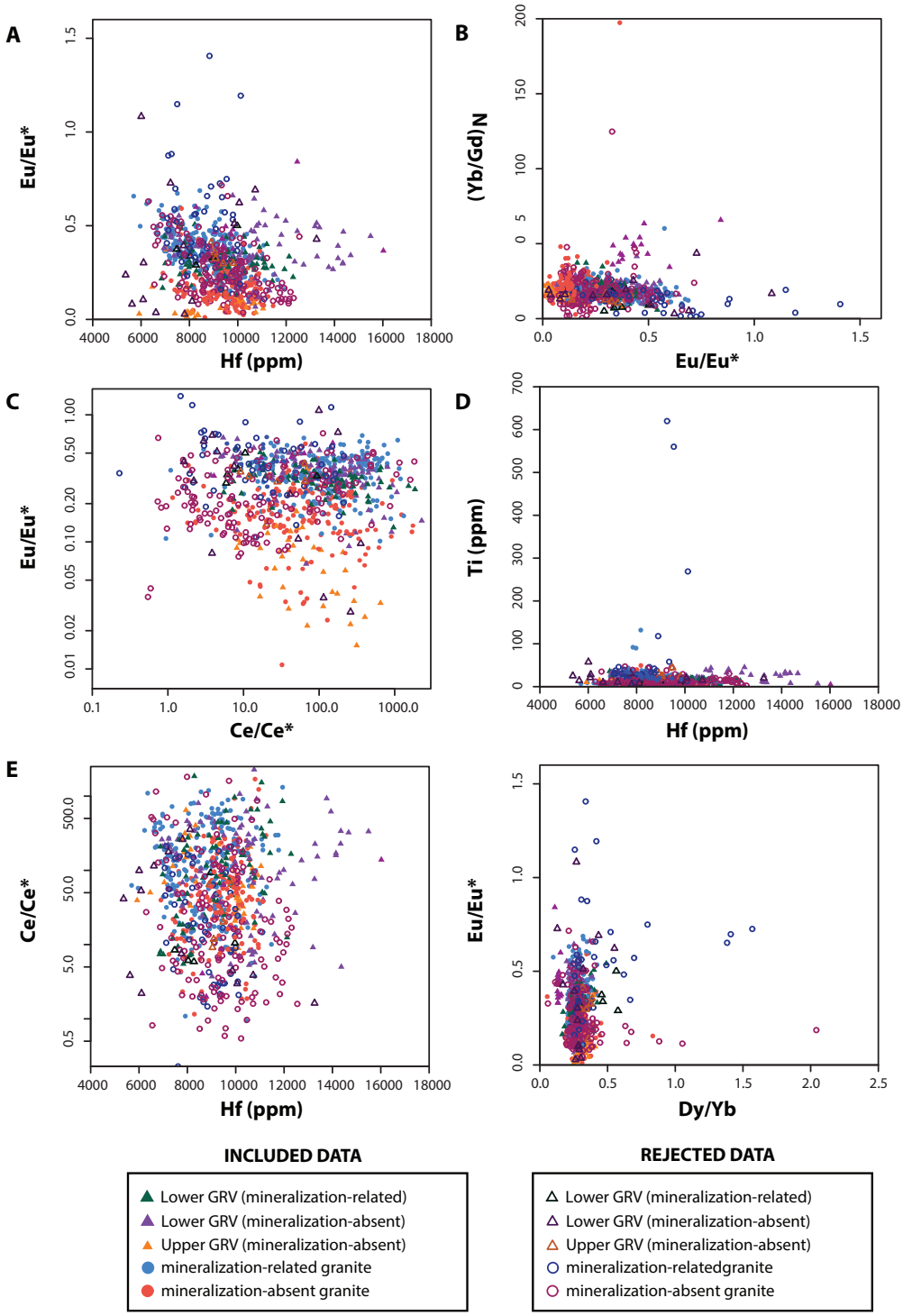

Appendix Figure A3 - Plots used in this study duplicated to include data that was excluded on the basis of discordance >5% and P > 370 ppm. These pre-filtered data plots are presented to demonstrate that our conclusions are not biased by the removal of data that could be considered representative of magmatic zircon. **A**) Eu/Eu* vs Hf; **B**) $(Yb/Gd)_N$ vs Eu/Eu*; **C**) Eu/Eu* vs Ce/Ce*; **D**) Ti vs Hf; **E**) Ce/Ce* vs Hf; and **F**) Eu/Eu* vs Dy/Yb. Upper GRV data from Ferguson *et al.*, (2020).

Appendix 4 Figure A4

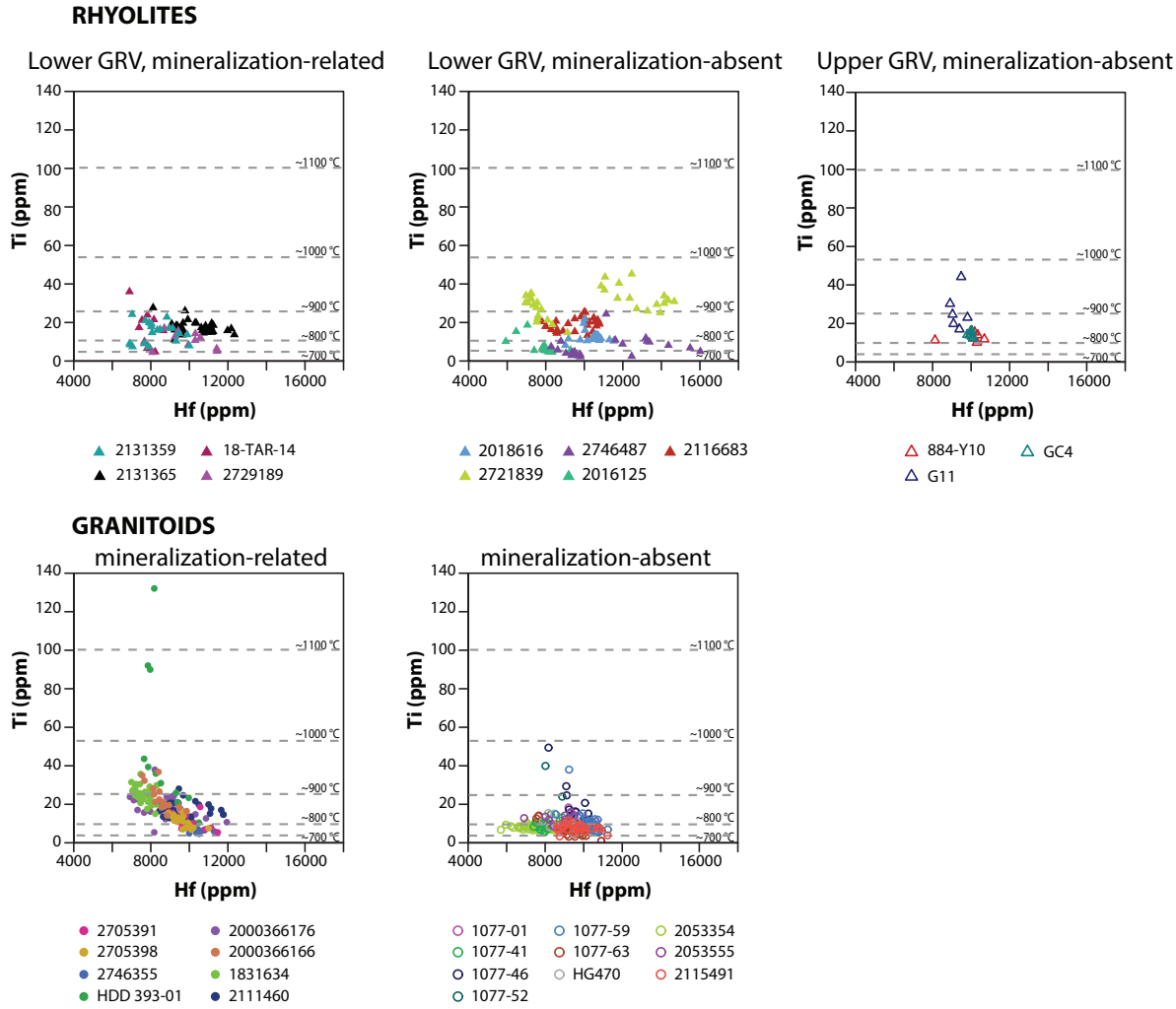

Appendix Figure A4: Ti vs Hf for individual samples with ≥5 analyses for rhyolites and granitoids. Dashed lines represent estimated temperatures for a given Ti concentration, calculated from the Ti-in-zircon thermometer (Ferry and Watson 2007), where $\alpha TiO_2 = 0.7$ and $\alpha SiO_2 = 1$. GRV = Gawler Range Volcanics. Upper GRV data from Ferguson *et al*., (2020).

Appendix 5

Supplementary material for: Mapping hydrothermal systems in IOCG deposits using apatite geochronology and geochemsitry: An example from Vulcan Cu-Au prospect

Appendix 5 Table A1 LA-ICP-MS U-Pb apatite data collected in this study

Included Data																													
Sample	Analytical Session	^{206}Pb ppm	^{207}Pb ppm	^{208}Pb ppm	U ppm	Th ppm	^{207}Pb/^{235}U (calc)	±2SE	^{206}Pb/^{238}U	±2SE	RHO	^{208}Pb/^{206}Pb	±2SE	^{238}U/^{206}Pb	±2SE	^{207}Pb/^{206}Pb	±2SE	^{207}Pb/^{235}U (calc) Age (Ma)	±2SE	^{206}Pb/^{238}U Age (Ma)	±2SE	^{207}Pb/^{206}Pb Age (Ma)	±2SE	^{238}U/^{206}Pb Age (Ma)	±2SE				
1084 - 13	2	2.6719	0.4442	3.0092	8.74	37.02	8.1310	0.6729	0.3514	0.0186	0.6405	1.1133	0.0932	2.8601	0.1593	0.1660	0.0121	2245.69	185.84	1941.45	102.90	2517.29	183.32	1932.84	107.66				
1084 - 15	2	10.2030	1.0299	4.7361	44.45	69.72	3.8142	0.2019	0.2709	0.0076	0.5318	0.4600	0.0290	3.6902	0.1065	0.1004	0.0044	1595.75	84.47	1545.36	43.50	1631.20	71.36	1545.82	44.60				
1084 - 16	2	2.3897	0.2644	10.8735	10.06	161.02	4.1605	0.4164	0.2721	0.0111	0.4093	4.5296	0.1830	3.6880	0.1564	0.1096	0.0092	1666.28	166.76	1551.31	63.54	1791.63	150.70	1546.62	65.59				
1084 - 18	2	3.0880	0.3430	3.4471	12.80	49.66	4.2576	0.2736	0.2760	0.0099	0.5580	1.1072	0.0699	3.6323	0.1390	0.1106	0.0063	1685.20	108.28	1570.93	56.32	1808.01	102.61	1567.67	59.99				
1084 - 2	2	0.9472	0.1496	1.9425	3.39	25.06	7.0837	0.7859	0.3185	0.0183	0.5176	2.0433	0.1797	3.1385	0.1825	0.1583	0.0155	2121.99	235.42	1782.25	102.34	2436.37	238.47	1782.99	103.70				
1084 - 22	2	0.9992	0.1060	6.7954	4.41	99.47	3.8459	0.4672	0.2649	0.0141	0.4368	6.6455	0.5300	3.7666	0.2008	0.1039	0.0127	1602.42	194.65	1514.90	80.37	1694.33	207.21	1517.88	80.91				
1084 - 25	2	6.3534	0.7436	10.8284	26.57	153.83	4.4921	0.5432	0.2797	0.0162	0.4795	1.6786	0.0356	3.5715	0.1319	0.1157	0.0116	1729.52	182.17	1589.75	89.63	1889.41	188.37	1591.32	89.47				
1084 - 27	2	4.9221	0.5976	6.9996	18.56	94.29	5.2372	0.3271	0.3112	0.0105	0.5394	1.4096	0.0693	3.2272	0.1083	0.1209	0.0063	1858.69	116.09	1746.40	58.84	1969.00	103.34	1740.04	58.41				
1084 - 28	2	0.5182	0.0595	0.2824	1.92	2.95	5.0030	0.8202	0.3168	0.0323	0.6211	0.5448	0.1259	3.1709	0.3370	0.1135	0.0181	1819.84	298.36	1773.98	180.64	1855.97	296.30	1767.05	187.79				
1084 - 29	2	1.1140	0.1685	0.6134	3.76	5.53	7.0945	0.8057	0.3398	0.0166	0.4311	0.5426	0.0777	2.9393	0.1413	0.1501	0.0157	2123.35	241.15	1885.83	92.32	2346.58	245.17	1887.73	90.73				
1084 - 3	2	2.8030	0.3157	1.7871	10.52	24.03	4.7565	0.3423	0.3043	0.0112	0.5136	0.6292	0.0486	3.2931	0.1267	0.1118	0.0075	1777.26	127.89	1712.55	63.29	1827.30	122.22	1709.46	65.77				
1084 - 33	2	6.5006	0.8598	7.1427	25.77	94.89	5.4283	0.3735	0.2973	0.0093	0.4528	1.0840	0.0602	3.3706	0.1057	0.1317	0.0071	1889.33	129.99	1677.75	52.27	2119.39	113.73	1674.82	52.54				
1084 - 34	2	6.3806	0.7938	2.9694	25.86	37.40	4.9946	0.3061	0.2893	0.0096	0.5431	0.4642	0.0557	3.4615	0.1239	0.1244	0.0065	1818.40	111.44	1637.92	54.52	2020.13	104.88	1636.00	58.57				
1084 - 37	2	2.7523	0.3411	18.1694	10.86	258.85	5.0211	0.3979	0.2901	0.0121	0.5273	6.5834	0.7499	3.4456	0.1385	0.1244	0.0088	1822.89	144.45	1641.88	68.61	2019.87	143.50	1642.65	66.04				
1084 - 38	2	3.2330	0.4828	1.6489	10.23	16.30	7.2357	0.6360	0.3488	0.0174	0.5671	0.5131	0.0681	2.8896	0.1440	0.1503	0.0121	2140.92	188.19	1928.83	96.14	2348.09	189.70	1915.78	95.44				
1084 - 39	2	0.5697	0.0679	1.1986	2.20	16.62	4.8583	0.9575	0.2992	0.0284	0.4817	2.0480	0.3101	3.3484	0.3143	0.1173	0.0235	1795.05	353.77	1687.38	160.18	1914.89	383.28	1684.63	158.13				
1084 - 46	2	0.5554	0.1255	0.4296	1.78	3.24	11.2324	1.6438	0.3621	0.0293	0.5527	0.7635	0.1306	2.7647	0.2474	0.2245	0.0250	2542.61	372.09	1992.16	161.14	3012.86	335.44	1990.21	178.11				
1084 - 5	2	1.0625	0.1126	1.3047	4.20	16.27	4.2761	0.5877	0.2861	0.0142	0.3619	1.2234	0.1138	3.4829	0.1727	0.1064	0.0137	1688.78	232.11	1621.89	80.67	1737.72	224.14	1627.10	80.68				
1084 - 53	2	4.7213	0.5209	18.9071	19.80	276.15	4.2146	0.2644	0.2779	0.0116	0.6634	3.9615	0.1457	3.6067	0.1462	0.1098	0.0060	1676.87	105.18	1580.96	65.79	1795.26	97.93	1577.56	63.93				
1084 - 54	2	1.2229	0.3166	0.8072	3.03	3.82	17.1394	2.4803	0.4773	0.0380	0.5499	0.6624	0.1114	2.1128	0.1813	0.2615	0.0316	2942.67	425.84	2515.54	200.16	3255.26	392.96	2498.05	214.42				
1084 - 55	2	22.0987	2.2033	5.4629	94.59	76.35	3.8001	0.1619	0.2757	0.0105	0.8935	0.2450	0.0145	3.6286	0.1335	0.0994	0.0030	1592.76	67.88	1569.68	59.77	1611.93	49.11	1569.10	57.73				
1084 - 56	2	2.1033	0.2450	1.2687	8.40	15.86	4.7253	0.8308	0.2946	0.0157	0.3027	0.5981	0.0711	3.4017	0.1855	0.1161	0.0177	1771.73	311.52	1664.62	88.58	1895.91	288.42	1661.32	90.58				
1084 - 57	2	1.1972	0.1217	1.1863	4.93	14.75	3.7721	0.4167	0.2698	0.0155	0.5213	0.9775	0.1129	3.7036	0.2104	0.1010	0.0107	1586.83	175.30	1539.66	88.66	1641.23	173.96	1540.85	87.55				
1084 - 58	2	0.9942	0.1169	1.0313	3.92	11.76	4.9111	0.8469	0.3012	0.0285	0.5485	1.0319	0.1648	3.3135	0.3214	0.1178	0.0200	1804.17	311.13	1697.11	160.52	1921.80	326.73	1700.20	164.93				
1084 - 59	2	1.5889	0.1535	0.6196	6.31	8.43	3.7673	0.4543	0.2834	0.0175	0.5119	0.3871	0.0824	3.5594	0.2158	0.0959	0.0110	1585.81	191.25	1608.36	99.30	1545.06	177.45	1596.14	96.79				
1084 - 54	2	3.8078	0.4133	23.1101	16.29	328.11	4.0954	0.3013	0.2694	0.0082	0.4151	6.0069	0.2137	3.7167	0.1250	0.1080	0.0072	1653.39	121.65	1537.98	46.97	1765.17	117.09	1536.02	51.66				
1183 - 16	2	2.1328	0.2125	15.7119	9.03	226.44	3.7512	0.3008	0.2738	0.0140	0.6368	7.2898	0.2521	3.6608	0.1827	0.0991	0.0073	1582.37	126.90	1560.18	79.68	1606.56	117.97	1556.84	77.71				
1183 - 2	2	0.5944	0.0726	0.4584	2.49	7.75	4.6110	0.8044	0.2744	0.0228	0.4769	0.7664	0.1834	3.6709	0.3035	0.1219	0.0207	1751.26	305.53	1562.85	130.04	1984.08	336.75	1553.02	128.38				
1183 - 46	2	1.1847	0.1194	0.3227	4.90	5.18	3.8679	0.3973	0.2766	0.0121	0.4253	0.2693	0.0480	3.6299	0.1570	0.1002	0.0098	1607.01	165.08	1574.35	68.77	1627.22	158.49	1568.60	67.84				
1183 - 32	2	3.2265	0.3273	7.7571	13.79	107.90	3.8778	0.3411	0.2779	0.0148	0.6055	2.3808	0.1259	3.6263	0.1674	0.1010	0.0086	1609.07	141.52	1580.83	84.19	1641.41	139.46	1569.99	72.47				
1183 - 14	2	2.1023	0.2363	10.1723	8.74	151.42	4.3630	0.4156	0.2831	0.0159	0.5895	4.8092	0.2403	3.5639	0.1908	0.1123	0.0108	1705.36	162.46	1606.85	90.25	1835.92	176.23	1594.35	85.34				
1183 - 49	2	3.5672	0.3391	13.9097	14.49	203.80	3.7544	0.2739	0.2831	0.0084	0.4064	3.8731	0.2652	3.5472	0.1046	0.0950	0.0060	1583.06	115.47	1607.16	47.64	1528.14	96.38	1600.97	47.20				
1183 - 5	2	1.1684	0.1124	2.6753	4.86	35.01	3.7558	0.4709	0.2840	0.0183	0.5135	2.2655	0.1898	3.5320	0.2277	0.0957	0.0116	1583.35	198.51	1611.25	103.73	1540.77	187.09	1607.07	103.58				
1183 - 37	2	4.1301	0.3902	16.3214	17.72	242.98	3.7082	0.3918	0.2840	0.0136	0.4540	3.9166	0.2324	3.5345	0.1750	0.0941	0.0110	1573.13	166.23	1611.60	77.31	1509.41	176.83	1606.07	79.52				
1183 - 4	2	1.2446	0.1129	0.1099	5.01	0.98	3.5622	0.5487	0.2840	0.0191	0.4365	0.0876	0.0341	3.5215	0.2296	0.0905	0.0137	1541.16	237.40	1611.64	108.35	1434.61	216.85	1611.31	105.07				
1183 - 13	2	1.3890	0.1418	4.6614	5.53	63.68	4.1172	0.4527	0.2932	0.0173	0.5353	3.3210	0.1982	3.4167	0.1977	0.1016	0.0099	1657.72	182.27	1657.53	97.56	1652.07	161.17	1654.91	95.77				
1183 - 40	2	3.2278	0.4100	3.6954	13.51	47.75	5.1550	0.6189	0.2937	0.0166	0.4707	1.1315	0.1180	3.4144	0.1904	0.1263	0.0139	1845.22	221.52	1660.21	93.82	2046.74	225.50	1655.88	92.34				
1183 - 1	2	0.6653	0.0807	0.4055	2.59	4.13	4.9678	0.6895	0.2957	0.0213	0.5197	0.6077	0.1067	3.3836	0.2450	0.1215	0.0169	1813.86	251.76	1669.76	120.44	1977.96	274.86	1669.16	120.87				
1183 - 33	2	1.0428	0.1072	2.0095	4.08	26.00	4.1965	0.5074	0.2974	0.0163	0.4530	1.8953	0.5580	3.3749	0.1821	0.1019	0.0118	1673.33	202.33	1678.47	91.93	1658.42	191.32	1672.94	90.29				
1183 - 12	2	0.9740	0.1256	0.2487	3.76	2.58	5.3386	0.6924	0.3011	0.0205	0.5257	0.2532	0.0550	3.3386	0.2383	0.1285	0.0145	1875.06	243.19	1696.53	115.68	2076.54	234.92	1688.95	120.56				
1183 - 35	2	3.8523	0.4559	9.2070	14.58	127.63	4.9912	0.3128	0.3055	0.0120	0.6257	2.3681	0.1994	3.2761	0.1263	0.1178	0.0061	1817.84	113.91	1718.30	67.37	1922.99	99.73	1717.24	66.20				
1183 - 54	2	3.3703	0.4656	14.3122	11.99	192.87	6.2635	0.4281	0.3233	0.0099	0.4492	4.2276	0.1503	3.0917	0.0943	0.1380	0.0079	2013.36	137.60	1806.06	55.45	2201.34	126.68	1806.52	55.08				
1183 - 17	2	0.8209	0.1299	0.3182	2.85	2.31	7.1136	0.7026	0.3261	0.0213	0.6605	0.3837	0.0711	3.0777	0.1997	0.1575	0.0146	2125.74	209.97	1819.50	118.70	2427.85	224.36	1813.71	117.66				
1183 - 26	2	0.3959	0.0685	1.9811	1.37	23.64	7.9561	1.0952	0.3326	0.0272	0.5947	4.9931	0.5745	3.0226	0.2471	0.1730	0.0256	2226.06	306.43	1851.16	151.54	2586.43	382.79	1842.45	150.61				
1183 - 30	2	1.6348	0.2107	4.0893	5.60	55.97	5.9614	0.5616	0.3343	0.0163	0.5165	2.4858	0.4957	2.9920	0.1521	0.1286	0.0114	1970.23	185.59	1859.38	90.47	2078.16	184.81	1858.81	94.52				
1183 - 9	2	1.5433	0.2265	5.2290	5.34	74.30	6.8586	0.7038	0.3414	0.0211	0.6015	3.3606	0.2161	2.9506	0.1820	0.1462	0.0152	2093.32	214.79	1893.32	116.86	2301.08	239.90	1881.41	116.02				
1183 - 27	2	1.8946	0.3102	12.2209	6.30	166.14	7.8346	0.6138	0.3476	0.0167	0.6126	6.3838	0.2732	2.8660	0.1369	0.1629	0.0117	2212.19	173.32	1923.09	92.30	2485.28	177.96	1929.44	92.13				
1183 - 68	2	1.9496	0.3647	9.9163	6.07	135.96	9.8544	0.8390	0.3754	0.0191	0.5982	5.0552	0.2685	2.6669	0.1352	0.1867	0.0144	2421.25	206.16	2054.71	104.65	2712.29	209.49	2052.69	104.04				
801 - 51	1	0.3241	0.0406	0.1242	4.49	2.56	1.4084	0.2290	0.0813	0.0051	0.3841	0.3785	0.0947	12.3106	0.7783	0.1243	0.0206	892.47	145.09	503.64	31.45	2018.54	334.93	503.47	31.83				
801 - 31	1	0.4822	0.0530	0.0961	7.03	2.70	1.1831	0.1556	0.0778	0.0043	0.4193	0.1982	0.0587	12.8889	0.7205	0.1098	0.0146	792.75	104.26	483.16	26.64	1794.48	239.07	481.70	26.93				
801 - 44	1	0.2235	0.0316	0.1172	3.13	2.37	1.5574	0.3258	0.0793	0.0078	0.4678	0.5191	0.1640	12.5546	1.1310	0.1402	0.0377	953.43	199.45	491.93	48.14	2229.21	599.71	494.04	44.51				
801 - 3	1	0.5662	0.0737	0.1577	6.43	0.70	1.8555	0.2974	0.1032	0.0066	0.3963	0.2754	0.0802	9.7265	0.6191	0.1296	0.0203	1065.39	170.78	633.13	40.22	2092.09	328.15	630.87	40.16				
801 - 21	1	0.2024	0.0274	0.0944	2.82	1.45	1.5638	0.3151	0.0835	0.0071	0.4241	0.4674	0.1554	12.1306	1.0394	0.1350	0.0279	955.98	192.64	516.70	44.16	2163.36	447.83	510.65	43.75				

Appendix 5 Table A1 LA-ICP-MS U-Pb apatite data collected in this study

Included Data																														
Sample	Analytical Session	^{206}Pb ppm	^{207}Pb ppm	^{208}Pb ppm	U ppm	Th ppm	^{207}Pb/^{235}U (calc)	±2SE	^{206}Pb/^{238}U	±2SE	RHO	^{208}Pb/^{206}Pb	±2SE	^{238}U/^{206}Pb	±2SE	^{207}Pb/^{206}Pb	±2SE	^{207}Pb/^{235}U (calc) Age (Ma)	±2SE	^{206}Pb/^{238}U Age (Ma)	±2SE	^{207}Pb/^{206}Pb Age (Ma)	±2SE	^{238}U/^{206}Pb Age (Ma)	±2SE
801 - 15	1	0.2935	0.0390	0.0894	3.97	0.65	1.6055	0.3831	0.0872	0.0080	0.3841	0.3008	0.1285	11.4559	1.0209	0.1324	0.0319	972.34	232.02	539.08	49.41	2129.92	513.28	539.49	48.08
801 - 23	1	0.6874	0.0928	0.1901	8.49	0.77	1.7523	0.3633	0.0939	0.0055	0.2848	0.2736	0.0677	10.6634	0.5959	0.1343	0.0236	1027.99	213.14	578.50	34.15	2154.81	379.00	577.84	32.29
801 - 10	1	0.4969	0.0627	0.1639	6.60	3.27	1.5260	0.2498	0.0877	0.0055	0.3825	0.3241	0.0872	11.3837	0.7137	0.1251	0.0187	940.90	154.01	541.68	33.92	2029.83	303.22	542.78	34.03
801 - 43	1	0.3564	0.0590	0.1260	4.46	1.83	2.1193	0.4815	0.0920	0.0088	0.4221	0.3579	0.1100	11.0317	0.8013	0.1646	0.0259	1155.11	262.44	567.32	54.40	2502.51	393.15	559.36	40.63
801 - 30	1	0.4573	0.0599	0.1446	6.47	1.77	1.5017	0.2935	0.0830	0.0060	0.3718	0.3132	0.1044	12.0612	0.8796	0.1302	0.0271	931.10	181.99	513.94	37.35	2099.99	436.53	513.47	37.45
801 - 9	1	0.3742	0.0472	0.1147	5.19	3.41	1.4365	0.2645	0.0824	0.0051	0.3332	0.3019	0.0824	12.1531	0.7570	0.1254	0.0243	904.26	166.53	510.38	31.32	2033.02	394.79	509.74	31.75
801 - 28	1	0.7337	0.0697	0.1498	10.27	1.52	1.0834	0.1541	0.0826	0.0043	0.3632	0.2020	0.0528	12.1381	0.6296	0.0945	0.0122	745.28	106.03	511.33	26.42	1517.28	195.71	510.34	26.47
801 - 42	1	0.2548	0.0465	0.1445	3.49	2.62	2.1503	0.4185	0.0852	0.0081	0.4909	0.5606	0.1864	11.6999	1.0859	0.1814	0.0367	1165.15	226.79	526.87	50.34	2665.23	539.25	528.70	49.07
801 - 14	1	0.3828	0.0400	0.1859	5.63	2.70	1.1931	0.3842	0.0819	0.0100	0.3792	0.4836	0.2183	12.2172	1.3922	0.1052	0.0352	797.40	256.78	507.69	61.99	1717.70	574.89	507.17	57.79
801 - 38	1	0.3998	0.0436	0.0931	5.08	2.27	1.3394	0.1915	0.0884	0.0058	0.4576	0.2335	0.0696	11.3935	0.6859	0.1099	0.0165	862.98	123.37	545.87	35.71	1797.16	270.33	542.33	32.65
801 - 11	1	1.1524	0.3972	0.9238	8.51	1.73	7.5600	0.7780	0.1591	0.0107	0.6561	0.7979	0.1106	6.3440	0.4284	0.3452	0.0232	2180.13	224.37	951.55	64.25	3685.18	247.49	943.59	63.72
801 - 36	1	0.6349	0.0705	0.1488	8.38	2.41	1.3207	0.1550	0.0860	0.0045	0.4449	0.2327	0.0564	11.6506	0.6044	0.1106	0.0128	854.81	100.32	531.83	27.77	1807.86	209.28	530.84	27.54
801 - 47	1	0.4598	0.0477	0.1417	6.33	2.70	1.2315	0.3528	0.0861	0.0080	0.3261	0.3050	0.1368	11.6821	1.0905	0.1031	0.0277	815.00	233.52	532.39	49.74	1679.64	451.05	529.47	49.42
801 - 37	1	0.6339	0.0683	0.1576	8.44	3.20	1.2561	0.1468	0.0843	0.0043	0.4360	0.2459	0.0568	11.8302	0.6050	0.1070	0.0123	826.17	96.57	521.84	26.59	1748.07	201.28	523.10	26.75
801 - 50	1	0.3351	0.0581	0.0976	4.45	0.77	2.1303	0.4800	0.0886	0.0095	0.4768	0.2905	0.1557	11.3195	1.2206	0.1730	0.0406	1158.67	261.08	547.23	58.79	2585.75	606.56	545.73	58.85
801 - 5	1	0.3822	0.0560	0.1369	4.73	1.44	1.8819	0.2794	0.0929	0.0068	0.4958	0.3540	0.1006	10.7026	0.7398	0.1460	0.0220	1074.72	159.57	572.91	42.17	2299.25	346.09	575.82	39.80
801 - 19	1	0.3147	0.0482	0.0826	4.29	1.59	1.8031	0.3313	0.0850	0.0062	0.3980	0.2599	0.0932	11.7373	0.8458	0.1520	0.0323	1046.57	192.28	526.16	38.47	2368.33	502.50	527.08	37.98
801 - 7	1	0.3331	0.0529	0.0927	4.16	1.21	2.0909	0.4066	0.0939	0.0098	0.5341	0.2688	0.1173	10.3379	0.9052	0.1561	0.0312	1145.83	222.84	578.82	60.13	2412.61	482.81	595.22	52.12
801 - 35	1	0.7071	0.0985	0.2052	8.13	3.28	1.9049	0.2411	0.0985	0.0050	0.4002	0.2883	0.0609	10.1531	0.5218	0.1388	0.0156	1082.81	137.07	605.81	30.69	2211.30	248.13	605.56	31.12
801 - 55	1	2.6413	0.1818	0.2580	44.14	10.19	0.6584	0.0667	0.0687	0.0028	0.4029	0.0975	0.0244	14.5279	0.5977	0.0688	0.0067	513.64	52.02	428.46	17.48	892.09	86.66	429.12	17.65
801 - 32	1	0.6323	0.0784	0.1476	8.86	3.50	1.4446	0.2592	0.0844	0.0058	0.3857	0.2314	0.0842	11.9035	0.8272	0.1234	0.0229	907.62	162.88	522.30	36.15	2004.68	371.68	520.01	36.14
801 - 34	1	0.3876	0.0591	0.1575	4.57	2.44	2.0552	0.3311	0.0977	0.0082	0.5218	0.4030	0.1103	10.2769	0.7171	0.1518	0.0231	1134.02	182.71	600.93	50.52	2365.29	360.47	598.60	41.77
801 - 4	1	0.4561	0.0743	0.1643	5.41	2.56	2.1419	0.2305	0.0951	0.0058	0.5661	0.3568	0.0753	10.5286	0.5781	0.1624	0.0181	1162.45	125.10	585.46	35.67	2480.16	276.72	584.92	32.12
801 - 6	1	0.4064	0.0656	0.1716	4.67	1.64	2.2157	0.2734	0.0993	0.0060	0.4864	0.4165	0.0908	10.0557	0.5979	0.1603	0.0195	1186.01	146.35	610.23	36.63	2458.03	299.61	611.16	36.34
801 - 17	1	0.3695	0.0726	0.1307	4.25	2.57	2.8314	0.7704	0.1034	0.0201	0.7127	0.3496	0.1909	9.5637	1.8691	0.1956	0.0490	1363.89	371.11	634.53	123.05	2789.14	698.84	641.09	125.29
801 - 20	1	0.8630	0.1902	0.5426	7.14	1.27	4.0627	0.7297	0.1331	0.0096	0.4023	0.6219	0.1284	7.5228	0.5296	0.2195	0.0280	1646.84	295.78	805.55	58.21	2976.67	379.60	804.55	56.64
801 - 33	1	0.6921	0.0762	0.1708	9.04	2.63	1.3482	0.1779	0.0888	0.0050	0.4305	0.2447	0.0624	11.3132	0.6454	0.1095	0.0148	866.80	114.37	548.19	31.14	1790.16	241.36	546.02	31.15
801 - 18	1	0.4441	0.0562	0.0782	6.22	0.72	1.4624	0.2288	0.0835	0.0058	0.4405	0.1754	0.0711	12.0728	0.8208	0.1265	0.0201	915.01	143.13	516.88	35.62	2049.54	325.07	513.00	34.88
852 - 10	1	31.1716	3.8268	7.3151	183.11	68.52	3.3936	0.1595	0.2000	0.0077	0.8183	0.2314	0.0160	4.9932	0.2137	0.1218	0.0034	1502.93	70.62	1175.40	45.20	1982.16	54.94	1176.78	50.37
852 - 2	1	2.6340	0.4245	3.0637	15.52	52.11	4.5413	0.4917	0.2028	0.0120	0.5457	1.1514	0.1386	4.9215	0.2915	0.1604	0.0167	1738.57	188.26	1190.59	70.35	2459.04	256.25	1192.43	70.63
852 - 27	1	60.0342	6.8482	19.7374	358.24	247.12	3.1357	0.1762	0.1986	0.0090	0.8059	0.3251	0.0097	5.0196	0.2286	0.1133	0.0033	1441.50	81.02	1167.56	52.88	1852.45	54.08	1171.12	53.33
852 - 28	1	8.7466	1.1287	2.9880	50.69	34.68	3.6403	0.4497	0.2035	0.0086	0.3406	0.3401	0.0423	4.9268	0.2081	0.1287	0.0120	1558.39	192.53	1194.31	50.25	2080.14	193.59	1191.26	50.31
852 - 37	1	4.9742	1.4095	16.8107	22.96	291.92	9.8798	0.7152	0.2521	0.0108	0.5936	3.3505	0.1964	3.9699	0.1729	0.2820	0.0137	2423.62	175.44	1449.15	62.27	3373.29	163.70	1448.24	63.06
852 - 40	1	47.2582	6.3640	11.3964	281.07	82.76	3.5959	0.1467	0.1931	0.0060	0.7642	0.2386	0.0074	5.1754	0.1635	0.1339	0.0023	1548.63	63.20	1138.32	35.50	2148.43	36.36	1138.81	35.97
852 - 47	1	9.2842	2.1976	8.6937	49.32	108.94	7.2104	0.3829	0.2206	0.0080	0.6839	0.9260	0.0532	4.5323	0.1668	0.2355	0.0066	2137.79	113.53	1284.82	46.66	3088.97	86.75	1285.25	47.29
973 - 43	1	1.9079	0.2237	1.6245	12.31	32.81	2.9650	0.2348	0.1827	0.0078	0.5370	0.8434	0.1048	5.4925	0.2339	0.1168	0.0083	1398.70	110.76	1081.48	45.99	1907.65	135.79	1078.26	45.91
973 - 44	1	8.9503	0.9163	2.9822	58.18	52.29	2.5999	0.1751	0.1827	0.0069	0.5647	0.3308	0.0506	5.4765	0.2086	0.1021	0.0060	1300.61	87.58	1081.54	41.13	1661.29	98.15	1081.16	41.19
973 - 31	1	10.4919	1.0429	3.9442	65.70	75.36	2.5738	0.1348	0.1862	0.0064	0.6514	0.3761	0.0605	5.3561	0.1887	0.0991	0.0039	1293.21	67.74	1101.02	37.57	1605.67	62.44	1103.49	38.87
973 - 57	1	15.3407	1.4271	2.6181	97.99	47.89	2.4644	0.1615	0.1901	0.0070	0.5606	0.1673	0.0309	5.2457	0.1999	0.0928	0.0052	1261.64	82.68	1121.95	41.22	1481.96	82.56	1124.80	42.87
973 - 33	1	28.0789	2.3295	2.1490	173.37	33.91	2.2292	0.1027	0.1902	0.0062	0.7123	0.0769	0.0100	5.2561	0.1743	0.0839	0.0026	1190.28	54.82	1122.51	36.83	1289.21	40.55	1122.75	37.23
973 - 13	1	4.6664	0.4901	0.9254	28.89	11.79	2.7873	0.2491	0.1904	0.0071	0.4158	0.1946	0.0289	5.2578	0.1962	0.1047	0.0079	1352.15	120.84	1123.77	41.76	1708.46	128.70	1122.42	41.89
973 - 45	1	0.4009	0.0559	0.1643	2.43	2.33	3.6847	0.6555	0.1907	0.0124	0.3642	0.4047	0.0874	5.2438	0.3338	0.1386	0.0234	1568.05	278.97	1125.41	72.91	2208.45	373.63	1125.17	71.62
973 - 16	1	9.5947	0.9606	2.0392	59.76	30.18	2.6531	0.1775	0.1910	0.0069	0.5395	0.2104	0.0351	5.2517	0.1886	0.0996	0.0056	1315.51	88.04	1126.82	40.69	1615.92	90.90	1123.61	40.34
973 - 12	1	7.1146	0.7183	1.2203	42.82	16.40	2.6861	0.1485	0.1915	0.0066	0.6264	0.1722	0.0171	5.2378	0.1825	0.1003	0.0043	1324.64	73.24	1129.57	39.12	1628.15	69.66	1126.35	39.25
973 - 28	1	5.9739	0.6383	0.7731	34.85	6.76	2.8597	0.1855	0.1916	0.0078	0.6259	0.1288	0.0125	5.2176	0.2128	0.1069	0.0045	1371.36	88.95	1129.96	45.87	1746.86	73.65	1130.36	46.10
973 - 41	1	4.8565	0.5124	0.7681	30.39	10.50	2.8311	0.2238	0.1917	0.0081	0.5366	0.1589	0.0282	5.2515	0.2202	0.1068	0.0077	1363.82	107.83	1130.67	47.97	1744.15	125.90	1123.65	47.12
973 - 7	1	5.7527	0.5302	0.6097	35.07	5.44	2.4928	0.2239	0.1938	0.0075	0.4330	0.1051	0.0309	5.1574	0.2020	0.0918	0.0070	1269.94	114.08	1141.87	44.42	1462.72	111.32	1142.44	44.74
973 - 18	1	7.9041	0.7562	0.8681	46.43	13.11	2.5854	0.1635	0.1944	0.0079	0.6414	0.1087	0.0142	5.1537	0.2072	0.0952	0.0046	1296.51	81.99	1145.28	46.45	1531.31	73.86	1143.20	45.97
973 - 30	1	11.4984	1.1329	1.6337	67.90	20.49	2.7234	0.1630	0.1996	0.0066	0.5550	0.1399	0.0136	5.0106	0.1678	0.0977	0.0047	1334.86	79.90	1173.39	38.98	1580.19	75.49	1173.05	39.29
973 - 32	1	1.8721	0.2439	0.3173	11.20	3.40	3.6696	0.7080	0.2104	0.0141	0.3467	0.1598	0.0433	4.8013	0.3908	0.1256	0.0216	1564.79	301.92	1231.04	82.35	2036.88	350.06	1219.63	99.26
973 - 23	1	5.8882	0.7014	2.9110	32.08	43.98	3.5292	0.4045	0.2122	0.0085	0.3492	0.4922	0.0775	4.7070	0.2328	0.1190	0.0097	1533.78	175.79	1240.32	49.64	1940.60	158.60	1241.86	61.41
973 - 36	1	3.6701	0.3580	0.9020	21.88	13.39	2.8141	0.3807	0.2138	0.0119	0.4125	0.2330	0.0639	4.6938	0.2554	0.0944	0.0105	1359.30	183.87	1249.09	69.70	1514.96	168.52	1245.04	67.76
973 - 4	1	7.6484	0.8562	1.0643	41.20	7.94	3.3654	0.2244	0.2154	0.0145	0.9927	0.1396	0.0213	4.7028	0.2600	0.1124	0.0084	1496.38	99.76	1257.40	84.44	1837.25	137.08	1242.87	68.70

Appendix 5 Table A1 LA-ICP-MS U-Pb apatite data collected in this study

Included Data																											
Sample	Analytical Session	^{206}Pb ppm	^{207}Pb ppm	^{208}Pb ppm	U ppm	Th ppm	^{207}Pb/^{235}U (calc)	±2SE	^{206}Pb/^{238}U	±2SE	RHO	^{208}Pb/^{206}Pb	±2SE	^{238}U/^{206}Pb	±2SE	^{207}Pb/^{206}Pb	±2SE	^{207}Pb/^{235}U (calc) Age (Ma)	±2SE	^{206}Pb/^{238}U Age (Ma)	±2SE	^{207}Pb/^{206}Pb Age (Ma)	±2SE	^{238}U/^{206}Pb Age (Ma)	±2SE
973 - 25	1	3.1648	0.7608	4.8671	13.17	76.45	9.5575	2.3970	0.2807	0.0284	0.4040	1.5997	0.1535	3.6326	0.3738	0.2472	0.0438	2393.09	600.18	1594.98	161.60	3165.98	560.69	1567.56	161.29
973 - 42	1	0.6458	0.2115	0.4932	2.71	1.47	12.7703	1.4515	0.2939	0.0212	0.6335	0.7450	0.1327	3.4797	0.2813	0.3202	0.0372	2662.86	302.66	1660.84	119.58	3570.16	415.31	1628.41	131.66
1488 - 10	2	0.3658	0.0653	0.0725	4.49	0.62	2.4672	0.7134	0.0986	0.0131	0.4589	0.1919	0.1572	9.8975	1.3105	0.1739	0.0525	1262.48	365.07	606.37	80.47	2594.64	783.59	620.47	82.15
1488 - 11	2	0.4112	0.1223	0.3091	3.26	0.54	6.1073	1.8206	0.1464	0.0183	0.4182	0.7417	0.1605	6.7993	0.8347	0.2953	0.0646	1991.29	593.62	880.81	109.82	3445.11	753.14	884.54	108.59
1488 - 13	2	0.3258	0.1344	0.3773	1.24	1.98	17.6206	3.1909	0.3043	0.0387	0.7015	1.1594	0.3999	3.2865	0.4452	0.4136	0.0594	2969.25	537.70	1712.84	217.58	3958.46	568.18	1712.46	231.98
1488 - 14	2	0.4975	0.1168	0.3311	5.16	0.49	3.6475	0.6948	0.1118	0.0105	0.4934	0.6517	0.1438	8.8267	0.6248	0.2330	0.0318	1559.97	297.15	683.30	64.22	3072.02	419.88	691.84	48.97
1488 - 17	2	0.6872	0.1186	0.2518	7.98	0.41	2.4481	0.3766	0.1011	0.0065	0.4166	0.3629	0.1052	9.8685	0.6473	0.1725	0.0247	1256.86	193.36	620.71	39.78	2581.19	370.36	622.21	40.81
1488 - 19	2	0.5857	0.2311	0.5530	3.39	0.23	10.4462	1.6896	0.1884	0.0158	0.5189	0.9404	0.1938	5.3131	0.4220	0.3959	0.0499	2475.16	400.35	1112.85	93.41	3892.93	490.28	1111.69	88.29
1488 - 2	2	0.5350	0.1363	0.3830	5.60	0.07	3.9847	0.6536	0.1118	0.0104	0.5686	0.7206	0.2128	8.9977	0.8410	0.2542	0.0410	1631.08	267.53	683.38	63.74	3210.52	517.63	679.36	63.50
1488 - 23	2	0.7856	0.1468	0.3039	8.90	0.21	2.6903	0.4342	0.1031	0.0062	0.3753	0.3828	0.0985	9.6617	0.5987	0.1858	0.0282	1325.79	213.96	632.72	38.33	2704.87	410.00	634.90	39.34
1488 - 27	2	0.3141	0.0787	0.1817	3.12	0.93	3.9927	0.6295	0.1137	0.0105	0.5881	0.5741	0.1854	8.8763	0.8147	0.2487	0.0408	1632.71	257.44	694.21	64.37	3176.05	521.01	688.17	63.17
1488 - 28	2	0.6034	0.1029	0.1518	7.46	0.18	2.2644	0.3315	0.0947	0.0080	0.5749	0.2511	0.0922	10.7179	0.7929	0.1705	0.0286	1201.26	175.85	583.22	49.08	2561.99	429.95	575.03	42.54
1488 - 29	2	0.4500	0.0931	0.2196	5.24	0.21	2.7888	0.3667	0.0959	0.0069	0.5497	0.4835	0.1259	10.4654	0.7067	0.2059	0.0312	1352.54	177.82	590.38	42.67	2872.65	435.90	588.29	39.73
1488 - 3	2	1.0932	0.2961	1.1156	9.03	20.66	5.3794	0.5253	0.1425	0.0101	0.7239	1.0106	0.1501	6.9949	0.4569	0.2697	0.0251	1881.58	183.74	858.73	60.70	3303.41	307.59	861.38	56.26
1488 - 30	2	1.1562	0.0886	0.1371	15.43	2.13	0.9033	0.1006	0.0837	0.0031	0.3284	0.1174	0.0318	11.9551	0.4349	0.0762	0.0084	653.51	72.76	518.00	18.94	1099.79	120.87	517.85	18.84
1488 - 31	2	0.7092	0.1795	0.4196	7.64	0.88	3.6339	0.4518	0.1023	0.0072	0.5637	0.5834	0.1429	9.7937	0.6828	0.2511	0.0323	1556.99	193.59	627.75	44.00	3191.25	409.98	626.74	43.70
1488 - 32	2	0.5836	0.0624	0.0929	7.98	0.50	1.2192	0.1606	0.0810	0.0045	0.4172	0.1579	0.0453	12.3435	0.5349	0.1064	0.0130	809.39	106.63	502.02	27.59	1738.01	212.33	502.17	21.76
1488 - 34	2	0.2011	0.0689	0.1610	1.61	0.02	6.8710	1.4154	0.1443	0.0175	0.5878	0.7849	0.2870	6.9549	0.8633	0.3367	0.0702	2094.92	431.55	868.79	105.20	3647.39	760.14	866.02	107.50
1488 - 35	2	0.7061	0.0815	0.1253	9.62	0.12	1.3897	0.2133	0.0857	0.0051	0.3879	0.1756	0.0669	11.7438	0.7151	0.1147	0.0179	884.58	135.78	530.12	31.56	1874.80	292.58	526.80	32.08
1488 - 36	2	0.1638	0.0395	0.1196	1.34	0.01	4.9414	1.5034	0.1454	0.0284	0.6411	0.7441	0.3999	7.0340	1.2329	0.2485	0.0868	1809.36	550.49	874.87	170.64	3174.55	1108.45	856.90	150.20
1488 - 37	2	0.6703	0.0881	0.1417	8.64	0.14	1.6223	0.5115	0.0883	0.0077	0.2776	0.2093	0.1087	11.4201	0.9977	0.1308	0.0371	978.90	308.61	545.64	47.75	2107.51	597.77	541.12	47.28
1488 - 38	2	0.4842	0.1315	0.3629	4.87	0.29	4.4718	0.9179	0.1181	0.0109	0.4510	0.7321	0.1919	8.4175	0.9172	0.2664	0.0453	1725.76	354.24	719.63	66.61	3284.49	558.89	723.65	78.85
1488 - 41	2	0.5926	0.1434	0.2777	5.75	0.43	4.0988	0.5734	0.1207	0.0082	0.4841	0.4633	0.1202	8.2832	0.5576	0.2409	0.0365	1654.06	231.41	734.59	49.76	3125.41	473.06	734.74	49.46
1488 - 43	2	1.1660	0.3935	1.0431	5.83	0.74	10.5772	1.1398	0.2280	0.0178	0.7236	0.8761	0.2580	4.4141	0.3241	0.3314	0.0347	2486.71	267.97	1324.00	103.23	3623.06	379.84	1316.36	96.65
1488 - 44	2	0.7260	0.1346	0.2264	8.24	0.40	2.5556	0.3741	0.0986	0.0055	0.3837	0.3078	0.0816	10.1248	0.5642	0.1841	0.0246	1288.05	188.53	606.33	34.05	2689.24	360.06	607.18	33.83
1488 - 45	2	0.5376	0.0917	0.1124	6.97	1.21	2.1091	0.4402	0.0880	0.0085	0.4638	0.2066	0.1200	11.2303	1.0864	0.1695	0.0368	1151.79	240.39	543.69	52.63	2552.13	554.19	549.88	53.19
1488 - 5	2	0.7248	0.1801	0.5248	5.83	3.50	5.0891	0.9920	0.1477	0.0117	0.4075	0.7250	0.2786	6.7852	0.5628	0.2464	0.0445	1834.29	357.56	888.08	70.54	3161.36	570.28	886.25	73.51
1488 - 51	2	0.6999	0.1182	0.2056	7.41	0.44	2.5660	0.3353	0.1092	0.0078	0.5433	0.2905	0.0871	9.1344	0.6041	0.1679	0.0223	1291.00	168.71	668.08	47.43	2535.73	336.93	669.71	44.29
1488 - 52	2	0.2819	0.0813	0.2119	2.21	0.68	5.8948	0.9446	0.1466	0.0124	0.5283	0.7471	0.1888	6.8235	0.5775	0.2877	0.0463	1960.47	314.14	881.90	74.66	3404.40	547.74	881.61	74.61
1488 - 54	2	0.4638	0.0540	0.1085	6.15	0.29	1.4587	0.3354	0.0903	0.0077	0.3728	0.2304	0.1303	11.0809	0.9867	0.1149	0.0284	913.48	210.02	557.30	47.77	1876.83	464.47	556.99	49.60
1488 - 56	2	0.4146	0.0819	0.2070	4.60	0.65	2.8519	0.5384	0.1035	0.0101	0.5192	0.4956	0.1232	9.6361	0.9070	0.1969	0.0296	1369.32	258.53	634.86	62.23	2800.27	421.03	636.50	59.91
1488 - 57	2	0.6700	0.1138	0.2424	7.11	0.17	2.4335	0.4057	0.1029	0.0071	0.4160	0.3578	0.1060	9.7526	0.6555	0.1694	0.0256	1252.57	208.84	631.53	43.81	2550.57	385.71	629.26	42.29
1488 - 63	2	0.6687	0.2414	0.6070	2.07	0.86	19.2106	4.1855	0.3853	0.0595	0.7088	0.9017	0.1836	2.6395	0.3592	0.3602	0.0410	3052.45	665.05	2100.82	324.41	3749.86	426.87	2070.97	281.83
1488 - 65	2	0.6850	0.1446	0.3505	6.24	1.66	3.7504	0.4153	0.1279	0.0075	0.5323	0.5060	0.1566	7.8112	0.4572	0.2100	0.0235	1582.19	175.19	775.90	45.73	2904.54	324.47	776.57	45.45
1488 - 66	2	0.4354	0.0531	0.1327	5.12	0.18	1.5970	0.2790	0.0940	0.0060	0.3675	0.2992	0.0922	10.5311	0.6685	0.1212	0.0201	969.03	169.29	579.19	37.18	1972.49	326.65	584.78	37.12
1488 - 69	2	0.8751	0.1131	0.3549	11.76	7.01	1.6139	0.4207	0.0897	0.0075	0.3216	0.3995	0.1625	11.1412	0.9437	0.1276	0.0273	975.61	254.32	554.02	46.45	2064.71	442.47	554.10	46.93
1488 - 70	2	0.3558	0.0726	0.2006	3.93	1.14	2.9724	0.5538	0.1045	0.0083	0.4257	0.5599	0.1768	9.5369	0.7220	0.2035	0.0346	1400.59	260.95	640.95	50.84	2853.86	485.31	642.80	48.66
1488 - 8	2	0.6873	0.1025	0.1550	10.00	1.61	1.7094	0.3983	0.0830	0.0080	0.4151	0.2235	0.1092	11.9071	1.0748	0.1485	0.0370	1012.07	235.80	513.91	49.70	2328.15	580.13	519.86	46.93
1488 - 9	2	0.4422	0.1067	0.2515	4.29	0.74	4.1458	0.9610	0.1243	0.0115	0.3979	0.5624	0.2208	8.1300	0.7483	0.2401	0.0553	1663.37	385.57	755.34	69.67	3119.87	718.48	747.82	68.83
1210 - 12	2	1.4901	0.1608	2.0920	6.33	34.79	4.2622	0.5936	0.2876	0.0184	0.4582	1.3832	0.1672	3.4803	0.2213	0.1070	0.0145	1686.09	234.83	1629.35	103.98	1748.19	237.24	1628.16	103.53
1210 - 69	2	0.2181	0.0171	0.0350	1.07	0.67	2.5461	0.6143	0.2332	0.0241	0.4279	0.1597	0.0825	4.3097	0.4724	0.0782	0.0188	1285.33	310.10	1351.26	139.49	1151.22	276.55	1345.14	147.45
1210 - 66	2	0.4276	0.0680	0.5430	1.20	6.03	9.1278	1.6970	0.4165	0.0397	0.5126	1.2542	0.2208	2.4116	0.2346	0.1573	0.0260	2350.90	437.07	2244.48	213.88	2425.86	401.37	2236.23	217.52
1210 - 42	2	0.6866	0.0915	1.2674	3.05	17.21	4.8425	0.9257	0.2655	0.0224	0.4416	1.8492	0.3200	3.7564	0.3118	0.1333	0.0279	1792.31	342.63	1517.96	128.14	2140.66	448.00	1521.55	126.29
1210 - 71	2	1.7470	0.2151	4.4220	6.72	62.48	5.1500	0.7048	0.2999	0.0162	0.3955	2.4988	0.1617	3.3327	0.1895	0.1225	0.0127	1844.40	252.41	1690.92	91.51	1992.40	206.93	1691.58	96.21
1210 - 26	2	2.0494	0.2462	0.7868	8.14	9.35	4.7848	0.6320	0.2905	0.0133	0.3468	0.3795	0.0557	3.4328	0.1560	0.1193	0.0146	1782.23	235.39	1643.91	75.29	1945.20	238.69	1648.05	74.87
1210 - 67	2	5.9410	0.5975	11.0063	25.11	159.82	3.8264	0.2141	0.2735	0.0079	0.5134	1.8305	0.0648	3.6608	0.1038	0.1000	0.0049	1598.32	89.42	1558.47	44.77	1623.08	79.82	1556.83	44.14
1210 - 54	2	5.4758	0.5504	1.6325	22.72	22.10	3.9353	0.2737	0.2856	0.0100	0.5043	0.2942	0.0328	3.5091	0.1228	0.0997	0.0062	1620.96	112.73	1619.61	56.80	1618.03	101.36	1616.36	56.57
1210 - 60	2	4.1644	0.4703	2.6250	16.42	33.29	4.5954	0.2992	0.2930	0.0097	0.5101	0.6289	0.0506	3.4132	0.1136	0.1129	0.0060	1748.44	113.84	1656.69	55.02	1845.82	98.89	1656.38	55.12
1210 - 13	2	0.5620	0.0806	0.5346	2.05	6.04	6.2793	0.9102	0.3179	0.0228	0.4941	0.9401	0.1478	3.1366	0.2244	0.1425	0.0186	2015.57	292.18	1779.46	127.46	2257.40	294.90	1783.93	127.62
1210 - 72	2	0.3498	0.0404	0.2886	1.14	3.70	5.6318	0.9995	0.3512	0.0302	0.4850	0.8191	0.1593	2.8651	0.2536	0.1150	0.0191	1920.99	340.92	1940.12	166.99	1879.73	312.57	1929.97	170.82
1210 - 70	2	0.5401	0.0777	14.3852	1.93	202.78	6.4464	1.1081	0.3212	0.0234	0.4233	26.4070	1.5787	3.1094	0.2345	0.1433	0.0200	2038.62	350.43	1795.70	130.66	2266.94	316.45	1797.55	135.57
1210 - 65	2	1.7165	0.2253	4.3319	5.86	62.60	6.1402	0.7281	0.3352	0.0186	0.4671	2.5160	0.4722	2.9761	0.1578	0.1313	0.0118	1995.97	236.67	1863.36	103.20	2114.06	190.47	1867.43	99.01
1210 - 73	2	3.0971	0.3370	8.3392	12.82	123.85	4.3668	0.4270	0.2877	0.0154	0.5460	2.6719	0.1859	3.4791	0.1752	0.1085	0.0102	1706.09	166.81	1630.00	87.02	1773.38	167.41	1628.69	82.00

Appendix 5 Table A1 LA-ICP-MS U-Pb apatite data collected in this study

Included Data																									
Sample	Analytical Session	^{206}Pb ppm	^{207}Pb ppm	^{208}Pb ppm	U ppm	Th ppm	^{207}Pb/^{235}U (calc)	±2SE	^{206}Pb/^{238}U	±2SE	RHO	^{208}Pb/^{206}Pb	±2SE	^{238}U/^{206}Pb	±2SE	^{207}Pb/^{206}Pb	±2SE	^{207}Pb/^{235}U (calc) Age (Ma)	±2SE	^{206}Pb/^{238}U Age (Ma)	±2SE	^{207}Pb/^{206}Pb Age (Ma)	±2SE	^{238}U/^{206}Pb Age (Ma)	±2SE
1210 - 48	2	1.9086	0.1980	5.5930	7.60	83.95	4.1844	0.4364	0.2952	0.0146	0.4738	2.9039	0.1861	3.4010	0.1681	0.1031	0.0103	1670.97	174.27	1667.32	82.38	1680.18	167.04	1661.62	82.12
1210 - 10	2	2.3638	0.2598	4.4481	8.82	65.54	4.7671	0.5429	0.3151	0.0131	0.3648	1.8654	0.1107	3.1860	0.1333	0.1095	0.0104	1779.12	202.60	1765.65	73.34	1789.53	170.01	1759.72	73.62
1210 - 38	2	6.7844	0.7194	0.7786	27.00	7.42	4.3816	0.3459	0.3004	0.0180	0.7604	0.1099	0.0350	3.3089	0.1850	0.1062	0.0077	1708.87	134.90	1693.39	101.65	1734.45	125.97	1702.28	95.16
1210 - 16	2	1.1393	0.1579	0.8883	3.69	10.54	6.8696	1.3227	0.3642	0.0270	0.3851	0.7574	0.1278	2.7227	0.1789	0.1348	0.0243	2094.74	403.32	2002.01	148.46	2161.26	388.83	2016.60	132.53
1210 - 20	2	1.2296	0.1537	1.1062	3.65	11.41	6.5799	0.8567	0.3834	0.0249	0.4992	0.8864	0.1212	2.5955	0.1684	0.1239	0.0146	2056.66	267.78	2091.96	135.98	2013.02	236.96	2100.89	136.32
1210 - 52	2	0.9909	0.1299	2.2631	3.10	31.70	6.8837	1.0044	0.3844	0.0296	0.5276	2.2421	0.2543	2.5997	0.1996	0.1296	0.0181	2096.57	305.92	2096.66	161.40	2091.28	291.56	2098.02	161.08
1210 - 74	2	1.6735	0.2437	4.2250	5.68	54.21	6.8457	0.5281	0.3368	0.0154	0.5941	2.5122	0.1494	2.9734	0.1370	0.1454	0.0102	2091.65	161.35	1871.23	85.76	2292.28	160.08	1868.94	86.14
1210 - 39	2	1.8812	0.2403	6.9310	7.34	99.08	5.1481	0.5090	0.2954	0.0136	0.4656	3.6582	0.3191	3.4003	0.1560	0.1271	0.0116	1844.07	182.32	1668.30	76.80	2057.24	188.55	1661.92	76.25
1210 - 6	2	2.9383	0.3814	2.4362	10.24	30.04	5.9453	0.5213	0.3311	0.0131	0.4511	0.8171	0.0915	3.0191	0.1243	0.1288	0.0097	1967.88	172.56	1843.78	72.94	2081.37	156.79	1844.33	75.94
1210 - 59	2	1.1966	0.1232	1.7870	4.38	26.97	4.4967	0.4811	0.3161	0.0155	0.4585	1.4789	0.1365	3.1618	0.1552	0.1025	0.0114	1730.36	185.13	1770.43	86.84	1668.23	184.88	1771.52	86.96
1210 - 21	2	8.1748	0.8387	1.2646	32.65	15.04	4.0357	0.2370	0.2866	0.0087	0.5149	0.1532	0.0261	3.4884	0.1060	0.1022	0.0051	1641.43	96.41	1624.26	49.12	1663.42	83.82	1624.83	49.36
1210 - 5	2	10.8371	1.1915	16.5022	46.94	248.56	4.0820	0.2042	0.2681	0.0069	0.5111	1.5049	0.0544	3.7229	0.0909	0.1093	0.0048	1650.71	82.59	1530.95	39.15	1787.03	78.60	1533.72	37.46
1210 - 14	2	2.2660	0.2727	1.2672	8.93	16.67	4.9092	0.4332	0.2967	0.0123	0.4716	0.5525	0.0711	3.3696	0.1369	0.1195	0.0100	1803.84	159.18	1674.78	69.69	1947.32	162.76	1675.28	68.07
1210 - 62	2	9.5071	1.1577	4.5126	36.23	55.96	5.1021	0.2796	0.3027	0.0085	0.5147	0.4722	0.0332	3.2938	0.0930	0.1213	0.0047	1836.45	100.63	1704.67	48.07	1974.11	77.06	1709.15	48.27
1210 - 8	2	2.6825	0.3282	2.2321	7.59	25.66	7.0316	0.8859	0.4172	0.0202	0.3849	0.8227	0.0672	2.3981	0.1052	0.1217	0.0121	2115.44	266.52	2247.64	108.99	1979.78	197.56	2246.84	98.58

Appendix 5 Table A1 LA-ICP-MS U-Pb apatite data collected in this study

Rejected Data Sample	Analytical Session	^{206}Pb ppm	^{207}Pb ppm	^{208}Pb ppm	U ppm	Th ppm	^{207}Pb/^{235}U (calc)	±2SE	^{206}Pb/^{238}U	±2SE	RHO	^{208}Pb/^{206}Pb	±2SE	^{238}U/^{206}Pb	±2SE	^{207}Pb/^{206}Pb	±2SE	^{207}Pb/^{235}U (calc) Age (Ma)	±2SE	^{206}Pb/^{238}U Age (Ma)	±2SE	^{207}Pb/^{206}Pb Age (Ma)	±2SE	^{238}U/^{206}Pb Age (Ma)	±2SE
1084 - 1	2	0.1548	0.0306	0.0591	0.42	0.38	11.4962	2.3368	0.4190	0.0669	0.7855	0.3784	0.1562	2.3961	0.3067	0.1960	0.0375	2564.27	521.24	2255.74	360.16	2792.08	534.49	2248.40	287.83
1084 - 10	2	2.6334	0.5065	1.4071	1.71	10.42	50.7009	8.4270	1.9164	0.2641	0.8292	0.5291	0.0752	0.5483	0.1036	0.1907	0.0159	4006.17	665.86	6899.91	950.99	2747.19	229.29	6691.78	1264.16
1084 - 11	2	29.2784	5.8995	18.7838	35.02	274.03	26.8270	2.5134	0.9650	0.0701	0.7750	0.6257	0.0320	1.0345	0.0934	0.1984	0.0059	3377.17	316.40	4354.61	316.19	2812.57	84.13	4359.91	393.55
1084 - 12	2	0.7796	0.1370	0.7280	0.34	8.11	65.3479	15.1145	2.6585	0.4238	0.6893	0.9252	0.1612	0.3726	0.0598	0.1748	0.0228	4259.44	985.18	8361.23	1333.00	2603.52	339.56	8405.46	1348.09
1084 - 14	2	1.9531	1.1387	3.0339	0.93	0.69	NA	NA	NA	NA	NA	1.5431	0.1126	NA	NA	0.5800	0.0260	0.00	0.00	0.00	0.00	4458.05	199.52	#NUM!	0.00
1084 - 17	2	0.2876	0.0637	0.1552	0.98	0.84	10.3652	1.6171	0.3365	0.0336	0.6409	0.5339	0.1502	2.9692	0.2919	0.2197	0.0328	2467.95	385.02	1869.81	186.95	2978.09	444.28	1871.21	183.97
1084 - 19	2	0.1062	0.0099	<0.020	0.42	0.22	3.7394	1.2675	0.2902	0.0416	0.4232	< DL	0.0948	3.4395	0.4849	0.0927	0.0311	1579.85	535.52	1642.51	235.60	1481.07	497.59	1645.20	231.94
1084 - 20	2	0.9353	0.1577	1.4344	3.57	19.54	NA	NA	NA	NA	NA	1.5194	0.1384	NA	NA	0.1677	0.0171	0.00	0.00	0.00	0.00	2533.86	258.12	#NUM!	0.00
1084 - 21	2	2.1756	0.2529	2.3407	4.73	33.90	8.6739	0.8269	0.5411	0.0287	0.5565	1.0615	0.1005	1.8413	0.0997	0.1154	0.0099	2304.34	219.68	2787.97	147.92	1885.32	162.37	2796.39	151.41
1084 - 26	2	0.8386	0.1723	0.4428	1.44	2.99	19.6392	0.2610	0.6882	0.0083	0.9046	0.5260	0.1042	1.4492	0.1028	0.2050	0.0054	3073.76	100.48	3375.68	47.02	2865.32	88.48	3382.74	45.81
1084 - 30	2	0.6316	0.1985	0.5834	0.33	5.63	97.3079	21.8520	2.2653	0.3802	0.7473	0.9221	0.1789	0.4484	0.0991	0.3159	0.0389	4658.68	1046.18	7628.30	1280.23	3549.28	437.17	7558.61	1671.30
1084 - 31	2	0.0898	0.0162	0.0308	0.32	0.12	8.1157	2.5217	0.3256	0.0580	0.5736	0.3368	0.2206	3.0552	0.5426	0.1789	0.0544	2244.00	697.25	1816.79	323.78	2642.40	803.09	1825.35	324.18
1084 - 35	2	0.9963	0.1828	0.3826	1.91	0.85	15.5555	2.0198	0.6126	0.0564	0.7092	0.3817	0.0817	1.6362	0.1459	0.1832	0.0191	2849.89	370.04	3080.45	283.67	2681.34	279.45	3074.69	274.18
1084 - 36	2	3.9971	0.4989	10.4926	12.03	146.34	6.4405	0.4662	0.3726	0.0222	0.8243	2.6039	0.1314	2.6748	0.1586	0.1244	0.0093	2037.81	147.50	2041.39	121.80	2020.02	151.66	2047.53	121.41
1084 - 4	2	1.5385	0.1875	2.1150	4.82	29.38	6.2247	0.6470	0.3639	0.0176	0.4657	1.3658	0.1139	2.7406	0.1342	0.1218	0.0117	2007.93	208.69	2000.58	96.83	1981.36	190.26	2005.30	98.18
1084 - 40	2	3.8858	0.7905	1.7718	2.10	23.65	60.7211	4.5624	2.1701	0.1814	0.8990	0.4494	0.0413	0.4609	0.0444	0.2020	0.0107	4186.04	314.53	7437.71	621.61	2841.87	150.12	7436.85	716.91
1084 - 41	2	18.7335	3.7040	13.0872	3.50	151.36	165.1502	10.0587	6.0719	0.3535	0.9560	0.6910	0.0264	0.1646	0.0107	0.1968	0.0053	5191.54	316.20	12609.94	734.22	2798.95	76.09	12612.34	822.44
1084 - 42	2	0.5313	0.1209	0.2729	0.78	1.01	24.3620	3.0639	0.7787	0.0791	0.8082	0.5092	0.0938	1.2881	0.1329	0.2267	0.0214	3282.99	412.89	3712.36	377.32	3028.45	285.27	3703.70	382.17
1084 - 44	2	3.8530	0.3672	2.8835	0.76	50.89	76.0131	9.8471	5.7971	0.6328	0.8426	0.7466	0.0820	0.1733	0.0241	0.0945	0.0057	4410.80	571.39	12354.47	1348.52	1517.22	91.17	12330.17	1716.88
1084 - 47	2	3.1301	1.4475	8.3870	0.58	73.06	394.0184	87.7006	6.1501	1.0659	0.7786	2.6554	0.1764	0.1608	0.0243	0.4608	0.0314	6070.91	1351.26	12680.89	2197.71	4119.73	281.14	12744.19	1927.37
1084 - 48	2	0.6525	0.1068	0.2036	1.16	1.05	14.1570	2.5784	0.6163	0.0757	0.6748	0.3120	0.1105	1.5964	0.1974	0.1648	0.0270	2760.28	502.72	3095.31	380.40	2504.81	410.38	3135.39	387.63
1084 - 49	2	1.1352	0.2797	0.7734	1.09	8.29	42.1397	5.0528	1.2472	0.1241	0.8296	0.6714	0.1053	0.8039	0.0795	0.2446	0.0217	3822.35	458.32	5219.61	519.22	3149.70	279.46	5209.98	515.25
1084 - 50	2	5.3133	1.2668	7.9480	1.58	107.02	125.3127	20.1299	3.8399	0.5372	0.8709	1.4778	0.0787	0.2627	0.0560	0.2371	0.0092	4913.20	789.24	10165.32	1422.05	3099.75	119.84	10121.42	2156.83
1084 - 51	2	0.1314	0.0293	0.1182	0.32	0.56	14.8955	4.8818	0.4881	0.0834	0.5215	0.8974	0.2963	2.0958	0.6167	0.2233	0.0754	2808.59	920.47	2562.37	437.95	3004.06	1014.91	2514.77	739.93
1084 - 6	2	4.7642	0.5881	10.8082	15.65	159.22	6.3414	0.5866	0.3672	0.0157	0.4631	2.2151	0.1652	2.7192	0.1222	0.1236	0.0094	2024.19	187.24	2016.37	86.38	2007.78	153.20	2018.80	90.75
1084 - 60	2	2.1462	0.4477	3.4187	4.33	53.56	17.2818	3.2141	0.6028	0.0737	0.6570	1.5579	0.1536	1.6445	0.1760	0.2060	0.0230	2950.61	548.76	3041.19	371.58	2873.99	320.29	3062.35	327.70
1084 - 7	2	0.4730	0.1128	0.5638	0.10	8.18	170.4925	55.5533	5.1597	1.5608	0.9284	1.1872	0.2454	0.1858	0.0554	0.2380	0.0417	5223.68	1702.08	11719.72	3545.16	3105.93	543.58	11947.36	3561.04
1084 - 8	2	1.8633	0.2072	2.2285	5.06	30.80	6.7234	1.0668	0.4347	0.0260	0.3770	1.1773	0.1257	2.2883	0.1456	0.1102	0.0139	2075.70	329.36	2326.93	139.20	1801.36	227.56	2337.19	148.70
1084 - 9	2	2.0629	0.3210	1.3416	4.22	19.93	12.6578	1.6925	0.5874	0.0843	0.9315	0.6497	0.0974	1.7121	0.2682	0.1556	0.0157	2654.53	354.95	2978.77	427.62	2407.62	242.45	2965.39	464.50
1083 - 31	2	6.3679	0.6349	24.3404	40.63	496.28	2.4428	0.2535	0.1787	0.0131	0.7048	3.7390	0.2004	5.5913	0.4807	0.0985	0.0069	1255.29	130.28	1059.98	77.53	1594.73	112.33	1060.69	91.19
1183 - 15	2	0.1992	0.0309	0.0882	0.86	0.79	5.7069	1.4998	0.2671	0.0345	0.4915	0.4459	0.1922	3.8081	0.5210	0.1572	0.0385	1932.42	507.86	1526.03	197.14	2424.89	593.74	1503.13	205.67
1183 - 24	2	0.9177	0.0901	1.9870	3.53	28.92	4.2997	0.9258	0.3175	0.0284	0.4159	2.1477	0.3466	3.1643	0.2827	0.0978	0.0189	1693.30	364.59	1777.32	159.17	1581.61	305.12	1770.30	158.13
1183 - 11	2	3.0063	0.3106	5.4486	10.43	75.58	4.6443	0.4317	0.3257	0.0174	0.5734	1.7943	0.1013	3.0705	0.1595	0.1027	0.0080	1757.27	163.36	1817.61	96.88	1673.20	130.11	1817.39	94.40
1183 - 64	2	0.2014	0.0338	0.3598	0.69	4.78	7.8573	2.0207	0.3361	0.0496	0.5738	1.7631	0.4303	3.0109	0.5441	0.1667	0.0416	2214.79	569.60	1868.00	275.66	2523.85	630.61	1848.67	334.09
1183 - 20	2	0.2116	0.0237	0.0574	0.70	0.63	5.2352	1.3618	0.3423	0.0445	0.4997	0.2682	0.1337	2.9442	0.3794	0.1114	0.0300	1858.37	483.39	1897.77	246.66	1821.43	490.70	1884.99	242.94
1183 - 36	2	1.8995	0.2362	5.2751	6.17	72.03	6.1024	0.5017	0.3566	0.0181	0.6172	2.7422	0.1439	2.8159	0.1463	0.1236	0.0086	1990.59	163.65	1965.88	99.74	2007.94	140.37	1959.05	101.79
1183 - 59	2	0.0415	0.0091	0.0380	0.12	0.09	11.9179	5.4745	0.3839	0.1127	0.6393	0.9059	0.5820	2.5433	0.7529	0.2173	0.0951	2597.97	1193.38	2094.45	615.05	2959.79	1295.38	2137.58	632.82
1183 - 34	2	2.2972	0.2480	3.2758	6.67	42.13	5.8717	0.4317	0.3937	0.0172	0.5959	1.4118	0.0803	2.5380	0.1115	0.1075	0.0069	1957.06	143.90	2139.95	93.76	1755.90	112.05	2141.42	94.08
1183 - 71	2	4.2462	0.4916	9.1443	11.53	120.38	6.9429	0.4602	0.4292	0.0150	0.5279	2.1298	0.2030	2.3259	0.0852	0.1152	0.0066	2104.16	139.48	2302.15	80.56	1881.56	107.93	2305.46	84.44
1183 - 19	2	1.5430	0.2053	5.5249	3.98	70.47	8.1171	0.8298	0.4443	0.0287	0.6328	3.5358	0.2163	2.2562	0.1439	0.1321	0.0121	2244.15	229.42	2369.74	153.29	2125.92	194.12	2365.09	150.85
1183 - 61	2	0.9841	0.3512	0.7306	2.49	1.96	23.0208	4.3654	0.4567	0.0415	0.4788	0.7443	0.1530	2.1576	0.1870	0.3581	0.0525	3227.82	612.08	2424.84	220.17	3741.06	548.29	2454.88	212.74
1183 - 67	2	0.9748	0.1543	0.7848	2.26	7.77	11.0425	1.2183	0.4987	0.0327	0.5948	0.7945	0.1082	2.0030	0.1309	0.1572	0.0157	2526.72	278.77	2608.30	171.17	2424.84	242.83	2610.55	170.54
1183 - 3	2	0.1796	0.0628	0.3431	0.39	1.96	26.2681	8.4055	0.5460	0.0973	0.5570	1.9012	0.4445	1.8453	0.3102	0.3491	0.0670	3356.57	1074.07	2808.42	500.58	3702.30	710.70	2791.49	469.33
1183 - 53	2	0.5052	0.0916	0.2927	1.03	2.00	14.1578	2.0328	0.5552	0.0485	0.6086	0.5742	0.1203	1.7858	0.1588	0.1807	0.0225	2760.33	396.33	2846.69	248.74	2658.34	331.04	2866.45	254.85
1183 - 29	2	1.2347	0.1521	4.2122	2.56	54.13	9.4820	1.1204	0.5590	0.0339	0.5138	3.3736	0.2486	1.7934	0.1078	0.1225	0.0110	2385.81	281.92	2862.63	173.81	1992.01	179.08	2856.68	171.73
1183 - 52	2	0.8062	0.1292	6.6254	1.51	94.44	13.1917	1.9323	0.5868	0.0500	0.5822	8.1849	0.5539	1.6852	0.1446	0.1608	0.0216	2693.46	394.53	2976.38	253.81	2463.45	330.64	3003.15	257.69
1183 - 47	2	3.4448	0.3810	3.7817	6.78	41.73	9.0426	0.8098	0.5889	0.0280	0.5316	1.0858	0.0690	1.7065	0.0853	0.1100	0.0070	2342.32	209.75	2985.09	142.10	1798.95	114.98	2973.22	148.69
1183 - 55	2	0.7070	0.1468	1.7246	1.38	9.90	17.1653	3.5088	0.5913	0.0774	0.6402	2.3963	0.2455	1.6802	0.1941	0.2056	0.0219	2944.12	601.81	2994.50	391.88	2870.37	305.35	3010.36	347.79
1183 - 28	2	1.3824	0.1745	2.3472	2.51	31.24	11.2189	1.9398	0.6444	0.0866	0.7772	1.6935	0.2715	1.5663	0.2511	0.1262	0.0121	2541.49	439.44	3206.41	430.87	2045.51	196.45	3182.92	510.31
1183 - 6	2	1.2910	0.1572	0.7838	2.29	6.15	10.9288	1.1620	0.6550	0.0489	0.7028	0.6008	0.0793	1.5408	0.1186	0.1212	0.0102	2517.09	267.62	3247.71	242.68	1972.70	166.51	3224.30	248.19
1183 - 7	2	0.8327	0.1158	0.5818	0.96	5.84	19.0372	2.5655	0.9960	0.0906	0.6752	0.6884	0.1051	1.0018	0.1050	0.1380	0.0156	3043.70	410.18	4455.37	405.38	2201.25	248.40	4462.64	467.69
1183 - 65	2	0.4741	0.0795	0.6212	0.32	7.82	41.0537	11.8740	1.6726	0.3518	0.7272	1.3238	0.3167	0.5925	0.1347	0.1713	0.0367	3796.46	1098.06	6337.26	1332.92	2569.45	550.60	6373.29	1448.38
1183 - 44	2	0.1239	0.0441	0.2613	0.06	1.82	121.8435	38.6805	2.4789	1.1419	0.6892	2.0738	0.4406	0.3905	0.1138	0.3556	0.0624	4884.92	1550.77	8036.87	3701.99	3730.41	654.90	8187.28	2385.59

Appendix 5 Table A1 LA-ICP-MS U-Pb apatite data collected in this study

Rejected Data																													
Sample	Analytical Session	^{206}Pb ppm	^{207}Pb ppm	^{208}Pb ppm	U ppm	Th ppm	^{207}Pb/^{235}U (calc)	±2SE	^{206}Pb/^{238}U	±2SE	RHO	^{208}Pb/^{232}Th	±2SE	^{238}U/^{206}Pb	±2SE	^{207}Pb/^{206}Pb	±2SE	^{207}Pb/^{235}U (calc) Age (Ma)	±2SE	^{206}Pb/^{238}U Age (Ma)	±2SE	^{207}Pb/^{206}Pb Age (Ma)	±2SE	^{238}U/^{206}Pb Age (Ma)	±2SE
1183 - 10	2	0.1549	0.0357	0.0540	0.07	1.07	85.3488	42.3536	2.6549	1.1448	0.8689	0.3439	0.2482	0.3874	0.1874	0.2287	0.0698	4526.98	2246.48	8354.91	3602.66	3042.22	928.10	8224.18	3977.70
1183 - 18	2	1.1960	0.1889	0.8099	0.36	6.81	82.1306	12.9238	3.7564	0.4969	0.8406	0.6711	0.0948	0.2642	0.0506	0.1573	0.0140	4488.41	706.28	10053.04	1329.77	2426.08	215.65	10092.36	1931.60
1183 - 38	2	0.0487	0.0230	0.1268	0.01	0.62	382.8105	320.5587	5.5570	4.4254	0.9510	2.5808	0.9689	0.1621	0.1361	0.4710	0.1590	6041.68	5059.20	12122.68	9653.94	4152.34	1401.40	12698.75	10662.92
1183 - 43	2	16.2834	13.3012	32.8745	7.24	101.73	930.3214	0.3367	8.2050	0.0109	0.2723	2.0037	0.1812	0.1223	0.1330	0.8145	0.0087	6941.77	140.11	14309.35	61.90	4946.64	140.63	14291.41	59.72
1183 - 58	2	0.0615	0.0213	0.1333	0.01	0.40	552.9381	603.2928	11.4272	12.2068	0.9791	2.1332	0.8119	0.0873	0.0933	0.3427	0.1082	6414.23	6998.36	16244.20	17352.34	3674.01	1160.18	16256.78	17361.18
801 - 48	1	0.2509	0.0424	<0.028	2.55	0.44	2.8121	1.2095	0.1193	0.0203	0.3955	< DL	0.0875	8.2875	1.2535	0.1714	0.0543	1358.77	584.43	726.56	123.61	2570.74	814.36	734.38	111.08
801 - 54	1	0.1565	0.0254	0.0815	1.98	1.60	2.0430	0.5475	0.0912	0.0112	0.4573	0.5188	0.2329	10.9077	1.2997	0.1610	0.0482	1129.96	302.83	562.85	68.98	2465.10	737.67	565.46	67.38
801 - 16	1	0.1025	0.0221	0.0928	1.59	1.55	2.2329	0.5092	0.0747	0.0108	0.6359	0.9006	0.3185	13.4233	1.6021	0.2154	0.0520	1191.43	271.72	464.38	67.34	2945.67	710.61	463.19	55.28
801 - 25	1	0.0352	0.0138	0.0353	0.17	0.14	13.0172	5.3111	0.2347	0.0772	0.8059	0.9940	0.5982	4.2226	1.5252	0.3921	0.1512	2680.90	1093.83	1358.93	446.84	3878.53	1495.19	1370.15	494.91
801 - 26	1	0.5941	0.1304	0.3579	6.14	1.81	3.4714	1.6140	0.1146	0.0225	0.4232	0.5965	0.2196	8.8110	1.4936	0.2159	0.0673	1520.75	707.05	699.37	137.62	2949.78	918.78	693.01	117.47
801 - 27	1	2.2262	0.9746	2.8760	9.45	3.89	16.6083	2.7692	0.2791	0.0388	0.8347	1.2134	0.3514	3.4650	0.4425	0.4101	0.0244	2912.49	485.62	1586.63	220.82	3945.77	234.62	1634.54	208.73
801 - 24	1	0.7787	0.2668	0.7222	4.07	1.28	10.8053	2.1039	0.2249	0.0221	0.5040	0.9247	0.2129	4.4437	0.4488	0.3429	0.0512	2506.52	488.04	1307.69	128.32	3675.22	548.31	1308.42	132.14
801 - 12	1	0.2562	0.0715	0.2473	1.96	1.63	5.9750	1.1020	0.1549	0.0197	0.6892	0.9590	0.2881	6.5094	0.8060	0.2787	0.0530	1972.21	363.75	928.31	118.00	3354.98	638.32	921.25	114.07
801 - 13	1	0.2552	0.0619	0.1315	3.41	1.82	3.0267	0.9377	0.0899	0.0183	0.6573	0.5048	0.2893	10.9971	1.4938	0.2428	0.0762	1414.37	438.18	554.70	112.95	3138.00	984.20	561.05	76.21
801 - 2	1	0.5280	0.0979	0.2612	5.28	3.24	2.8128	0.4365	0.1097	0.0109	0.6377	0.4891	0.1105	9.1394	0.8092	0.1843	0.0228	1358.97	210.91	670.93	66.40	2691.39	332.29	669.36	59.26
801 - 53	1	0.6991	0.1408	0.3835	5.32	1.14	4.3371	0.6360	0.1557	0.0123	0.5399	0.5392	0.1595	6.3801	0.5048	0.1994	0.0286	1700.43	249.36	932.79	73.86	2820.25	405.29	938.62	74.27
801 - 52	1	1.3922	0.3344	0.9794	9.05	17.16	6.0787	0.8873	0.1839	0.0201	0.7507	0.7012	0.1266	5.5255	0.5159	0.2409	0.0253	1987.20	290.07	1087.98	119.23	3124.99	328.55	1072.32	100.12
852 - 25	1	2.6448	0.3303	39.7688	16.45	901.87	3.2979	0.2728	0.1911	0.0097	0.6166	14.7502	1.4346	5.1816	0.2830	0.1234	0.0093	1480.55	122.48	1127.52	57.51	2005.11	151.11	1137.55	62.13
852 - 26	1	80.8431	8.6295	22.2453	506.76	261.28	2.8225	0.1265	0.1914	0.0066	0.7733	0.2727	0.0199	5.2326	0.1856	0.1060	0.0024	1361.54	61.03	1128.80	39.13	1731.67	39.29	1127.39	39.98
852 - 6	1	35.7178	4.0285	7.3713	233.49	71.47	2.8829	0.2060	0.1842	0.0068	0.5163	0.2037	0.0276	5.4030	0.1941	0.1117	0.0059	1377.46	98.45	1089.66	40.21	1826.76	96.06	1094.68	39.33
852 - 51	1	81.0913	8.4380	21.7169	567.00	334.36	2.4999	0.1345	0.1725	0.0066	0.7123	0.2651	0.0120	5.8035	0.2405	0.1038	0.0029	1272.01	68.43	1026.02	39.32	1692.10	46.97	1024.81	42.46
852 - 24	1	16.4587	3.2765	35.5758	111.12	684.50	4.8363	0.2598	0.1755	0.0063	0.6636	2.1455	0.0616	5.7071	0.2092	0.1982	0.0064	1791.24	96.21	1042.47	37.16	2810.77	91.18	1040.81	38.15
852 - 31	1	57.5860	6.5871	13.8992	427.37	1087.49	2.5645	0.2098	0.1603	0.0111	0.8438	0.2403	0.0246	6.1645	0.4548	0.1141	0.0032	1290.58	105.56	958.26	66.13	1865.55	52.44	969.09	71.50
852 - 63	1	60.7228	7.6461	14.6238	336.37	126.65	3.7433	0.2588	0.2148	0.0090	0.6092	0.2370	0.0106	4.6344	0.2029	0.1250	0.0044	1580.69	109.28	1254.25	52.83	2028.63	71.36	1259.51	55.14
852 - 12	1	24.1614	3.2681	16.3290	141.02	266.49	3.6781	0.2542	0.1971	0.0083	0.6093	0.6635	0.0373	5.0565	0.2183	0.1338	0.0038	1566.63	108.28	1159.80	48.84	2147.95	60.86	1163.30	50.23
852 - 56	1	49.4217	8.5127	18.8939	287.45	133.69	4.9685	0.2237	0.2078	0.0074	0.7919	0.3787	0.0181	4.8117	0.1688	0.1716	0.0047	1813.97	81.69	1217.08	43.40	2572.23	70.60	1217.24	42.71
852 - 1	1	1.2652	0.2149	12.0774	7.12	274.42	4.9000	0.6124	0.2076	0.0128	0.4920	9.5050	1.1641	4.8320	0.2896	0.1697	0.0218	1802.26	225.24	1216.14	74.78	2554.02	328.80	1212.57	72.67
852 - 8	1	21.7618	2.3484	7.8870	141.13	135.72	2.7769	0.1577	0.1860	0.0066	0.6202	0.3566	0.0336	5.3628	0.1903	0.1069	0.0046	1349.35	76.64	1099.62	38.74	1747.11	75.45	1102.21	39.10
852 - 45	1	18.9247	2.2947	4.6063	115.64	53.14	3.3148	0.1968	0.1975	0.0072	0.6164	0.2417	0.0226	5.0782	0.1822	0.1205	0.0058	1484.54	88.13	1161.82	42.51	1963.54	94.51	1158.75	41.56
852 - 5	1	30.2142	5.3850	12.3971	165.06	185.90	5.2324	0.2151	0.2121	0.0071	0.8115	0.4057	0.0336	4.7191	0.1588	0.1772	0.0032	1857.91	76.36	1240.04	41.36	2626.41	47.48	1238.96	41.68
852 - 53	1	96.6714	11.0670	19.8166	592.74	209.81	2.9573	0.1122	0.1866	0.0060	0.8423	0.2029	0.0066	5.3569	0.1732	0.1140	0.0012	1396.71	52.98	1103.09	35.25	1862.93	20.33	1103.34	35.67
852 - 4	1	38.8758	4.8379	13.3553	232.36	177.00	3.0999	0.1342	0.1921	0.0061	0.7838	0.3393	0.0157	5.2013	0.1670	0.1237	0.0023	1483.38	60.13	1132.99	36.00	2008.87	37.23	1133.61	36.39
852 - 19	1	30.2665	3.3754	17.0973	196.10	313.24	2.8006	0.1304	0.1825	0.0060	0.7012	0.5574	0.0290	5.4860	0.1801	0.1104	0.0028	1355.70	63.11	1080.83	35.28	1804.76	45.25	1079.43	35.45
852 - 61	1	40.3422	4.7942	7.2647	240.74	57.48	3.2321	0.1335	0.1966	0.0062	0.7661	0.1779	0.0120	5.0895	0.1626	0.1183	0.0023	1464.89	60.52	1157.14	36.63	1930.03	36.97	1156.40	36.95
852 - 54	1	47.2392	5.9720	10.2840	289.71	84.46	3.3790	0.1414	0.1932	0.0062	0.7677	0.2153	0.0106	5.1754	0.1678	0.1258	0.0025	1499.55	62.74	1138.72	36.58	2039.07	40.43	1138.80	36.92
852 - 49	1	40.3963	3.9789	8.9556	258.92	155.23	2.5400	0.1157	0.1867	0.0064	0.7536	0.2179	0.0180	5.3411	0.1832	0.0979	0.0028	1283.57	58.47	1103.56	37.88	1584.09	44.81	1106.33	37.96
852 - 21	1	12.3578	1.8905	23.8670	71.93	520.50	4.4222	0.2610	0.2118	0.0077	0.6161	1.8733	0.4031	4.7259	0.1682	0.1500	0.0084	1716.50	101.31	1238.26	45.03	2345.68	131.29	1237.34	44.03
852 - 15	1	25.4657	3.1146	4.8522	148.67	49.35	3.3571	0.1586	0.1977	0.0065	0.6950	0.1894	0.0147	5.0547	0.1669	0.1219	0.0033	1494.44	70.58	1162.95	38.17	1984.14	53.53	1163.68	38.42
852 - 17	1	23.3676	2.8977	21.4759	132.98	353.33	3.5149	0.1679	0.2046	0.0072	0.7408	0.9111	0.0385	4.8837	0.1728	0.1234	0.0040	1530.56	73.12	1199.87	42.46	2005.60	64.34	1200.86	42.48
852 - 34	1	45.6508	6.6293	10.3922	259.90	52.55	4.1068	0.1585	0.2047	0.0064	0.8125	0.2253	0.0086	4.8913	0.1549	0.1444	0.0024	1655.67	63.92	1200.44	37.65	2279.41	37.54	1199.15	37.98
852 - 50	1	36.2224	4.2505	5.3732	215.46	40.36	3.2731	0.1507	0.2009	0.0071	0.7662	0.1471	0.0123	4.9637	0.1831	0.1169	0.0034	1474.69	67.91	1180.22	41.65	1908.68	55.52	1183.17	43.65
825 - 3	1	49.1900	4.7836	6.0580	296.31	129.27	2.5962	0.1110	0.1927	0.0062	0.7524	0.1219	0.0107	5.1887	0.1686	0.0967	0.0017	1299.57	55.55	1135.90	36.53	1561.42	27.89	1136.11	36.91
852 - 22	1	59.2011	6.8524	24.1823	363.85	398.59	3.1005	0.1231	0.1935	0.0062	0.8034	0.4034	0.0131	5.1674	0.1669	0.1152	0.0019	1432.81	56.89	1140.48	36.38	1882.24	31.69	1140.42	36.84
852 - 11	1	29.1930	3.8206	5.7066	176.40	44.88	3.6018	0.1661	0.1996	0.0067	0.7230	0.1921	0.0137	5.0142	0.1707	0.1296	0.0038	1549.93	71.48	1172.99	39.11	2091.42	61.05	1172.28	39.92
852 - 16	1	32.3783	4.7163	24.1073	191.61	333.44	3.9753	0.1936	0.1977	0.0065	0.6766	0.7349	0.0690	5.0655	0.1706	0.1446	0.0040	1629.17	79.34	1162.85	38.31	2282.04	63.19	1161.40	39.11
852 - 57	1	105.6062	10.1148	7.0971	630.34	53.01	2.5763	0.0976	0.1958	0.0061	0.8282	0.0662	0.0026	5.1178	0.1619	0.0948	0.0012	1293.92	49.00	1152.86	36.16	1524.09	18.72	1150.53	36.39
852 - 14	1	57.5422	6.8884	11.4482	347.03	99.96	3.2281	0.1322	0.1948	0.0063	0.7894	0.1971	0.0083	5.1407	0.1690	0.1193	0.0020	1463.94	59.97	1147.26	37.10	1944.65	33.01	1145.85	37.66
852 - 32	1	115.9403	10.4437	11.5913	705.59	132.65	2.4297	0.0967	0.1946	0.0062	0.8045	0.0992	0.0073	5.1412	0.1656	0.0897	0.0013	1251.44	49.79	1146.23	36.68	1419.17	21.26	1145.73	36.89
852 - 20	1	33.8288	4.9086	22.6601	215.84	371.13	3.7652	0.1743	0.1878	0.0074	0.8468	0.6593	0.0275	5.3063	0.2263	0.1437	0.0042	1585.36	73.39	1109.63	43.50	2271.84	66.95	1113.00	47.47
852 - 39	1	26.1661	3.2106	8.6860	140.42	115.61	3.5270	0.1468	0.2075	0.0068	0.7852	0.3297	0.0148	4.8262	0.1593	0.1223	0.0027	1533.30	63.80	1215.55	39.72	1988.62	43.26	1213.89	40.06
852 - 59	1	21.1379	2.8665	8.2624	125.00	106.59	3.7721	0.1844	0.2028	0.0074	0.7422	0.3838	0.0249	4.9288	0.1768	0.1336	0.0039	1586.82	77.57	1190.25	43.18	2144.77	62.89	1190.81	42.71
852 - 43	1	45.2802	7.1494	11.7738	237.42	59.47	4.8567	0.1950	0.2222	0.0073	0.8129	0.2578	0.0087	4.5002	0.1475	0.1572	0.0024	1794.78	72.08	1293.43	42.22	2425.30	36.47	1293.56	42.40
852 - 36	1	53.1987	6.1566	20.1444	316.52	305.73	3.2477	0.1502	0.2024	0.0069	0.7391	0.3752	0.0235	4.9292	0.1729	0.1150	0.0036	1468.63	67.94	1188.01	40.62	1879.73	59.29	1190.74	41.78

Appendix 5 Table A1 LA-ICP-MS U-Pb apatite data collected in this study

Rejected Data																												
Sample	Analytical Session	^{206}Pb ppm	^{207}Pb ppm	^{208}Pb ppm	U ppm	Th ppm	^{207}Pb/^{235}U (calc)	±2SE	^{206}Pb/^{238}U	±2SE	RHO	^{208}Pb/^{206}Pb	±2SE	^{238}U/^{206}Pb	±2SE	^{207}Pb/^{206}Pb	±2SE	^{207}Pb/^{235}U (calc) Age (Ma)	±2SE	^{206}Pb/^{238}U Age (Ma)	±2SE	^{207}Pb/^{206}Pb Age (Ma)	±2SE	^{238}U/^{206}Pb Age (Ma)	±2SE			
852 - 18	1	18.4397	2.5909	29.9134	102.24	556.99	4.0392	0.2424	0.2081	0.0071	0.5648	1.6015	0.1583	4.8071	0.1641	0.1395	0.0052	1642.12	98.56	1218.91	41.32	2219.82	82.88	1218.29	41.59			
852 - 23	1	6.4250	1.4941	36.4554	31.43	764.53	7.7774	0.7134	0.2401	0.0100	0.4529	5.6316	0.4468	4.1489	0.1691	0.2316	0.0161	2205.60	202.32	1387.05	57.62	3062.28	212.69	1392.02	56.73			
852 - 55	1	35.8658	4.8489	13.6721	208.95	167.95	3.6772	0.1427	0.1970	0.0063	0.8181	0.3785	0.0125	5.0747	0.1651	0.1343	0.0020	1566.43	60.79	1159.15	36.80	2153.91	32.78	1159.48	37.73			
852 - 46	1	21.0917	3.1016	13.1341	134.14	200.79	3.8090	0.2302	0.1883	0.0075	0.6604	0.6102	0.0557	5.3010	0.2124	0.1454	0.0053	1594.65	96.36	1112.07	44.38	2291.35	83.39	1114.01	44.63			
852 - 13	1	32.5626	4.7541	13.6334	194.27	146.83	4.0991	0.2704	0.2024	0.0071	0.5326	0.4118	0.0305	4.9213	0.1768	0.1455	0.0065	1654.12	109.11	1188.19	41.74	2292.68	102.18	1192.47	42.85			
852 - 38	1	50.8943	5.9937	26.3674	304.64	462.93	3.1921	0.1278	0.1961	0.0062	0.7948	0.5133	0.0182	5.1022	0.1643	0.1172	0.0021	1455.24	58.24	1154.37	36.72	1912.83	34.60	1153.76	37.15			
852 - 33	1	102.3743	9.9819	8.0073	647.48	70.55	2.5472	0.1310	0.1896	0.0079	0.8090	0.0773	0.0040	5.2995	0.2502	0.0968	0.0016	1285.63	66.13	1119.28	46.58	1562.54	26.19	1114.30	52.62			
852 - 30	1	60.8750	6.8320	20.0073	353.09	302.37	3.1483	0.1765	0.2027	0.0066	0.5800	0.3266	0.0333	4.9444	0.1630	0.1119	0.0040	1444.59	80.99	1190.00	38.69	1829.88	65.14	1187.39	39.15			
852 - 44	1	26.8001	4.5194	14.7029	151.90	176.41	4.9351	0.4825	0.2101	0.0109	0.5296	0.5454	0.0371	4.7308	0.2482	0.1682	0.0091	1808.27	176.79	1229.32	63.65	2539.36	136.63	1236.17	64.85			
852 - 9	1	21.3644	3.2387	7.7485	122.47	73.11	4.1913	0.2533	0.2002	0.0073	0.6015	0.3577	0.0161	4.9998	0.1848	0.1505	0.0051	1672.32	101.05	1176.23	42.75	2350.33	79.04	1175.35	43.45			
852 - 58	1	60.9237	8.0144	21.1095	328.85	188.98	3.9429	0.1661	0.2167	0.0069	0.7579	0.3425	0.0175	4.6159	0.1489	0.1309	0.0035	1622.53	68.36	1264.58	40.38	2109.55	57.19	1264.12	40.77			
852 - 58	1	61.5297	9.6845	25.2621	330.25	215.02	4.8304	0.2879	0.2217	0.0112	0.8504	0.4088	0.0164	4.5352	0.2121	0.1565	0.0054	1790.21	106.71	1290.61	65.42	2417.14	82.76	1284.49	60.07			
973 - 52	1	0.1613	0.0219	0.0658	1.83	1.99	1.9122	1.1564	0.1036	0.0171	0.2725	0.4075	0.3051	9.5418	1.6790	0.1324	0.0860	1085.35	656.38	635.57	104.73	2129.09	1382.47	642.48	113.05			
973 - 14	1	3.9150	0.3330	0.4684	41.87	6.30	1.3059	0.1942	0.1115	0.0077	0.4647	0.1183	0.0288	9.0076	0.6524	0.0843	0.0088	848.34	126.14	681.38	47.08	1299.00	134.96	678.65	49.16			
973 - 46	1	2.9341	0.6416	1.4122	30.92	5.63	3.4653	0.3583	0.1182	0.0107	0.8793	0.4640	0.0890	8.4939	0.9011	0.2111	0.0151	1519.34	157.12	720.20	65.49	2913.48	208.76	717.49	76.12			
973 - 3	1	4.0711	0.5154	0.9055	31.30	6.54	2.6414	0.6236	0.1474	0.0171	0.4901	0.2242	0.0459	6.7295	0.8593	0.1275	0.0169	1312.24	309.82	886.50	102.58	2062.56	273.73	893.11	114.04			
973 - 39	1	2.4288	0.4956	1.0201	17.43	6.67	5.0908	2.0674	0.1552	0.0472	0.7494	0.4499	0.1477	6.2999	2.5387	0.2242	0.0277	1834.57	745.03	929.79	282.98	3010.67	371.97	949.72	382.71			
973 - 58	1	2.7920	0.3699	0.9157	19.47	12.79	3.1879	0.5831	0.1727	0.0225	0.7110	0.3227	0.0897	5.7818	0.7446	0.1334	0.0145	1454.23	266.00	1027.16	133.59	2141.92	233.31	1028.38	132.43			
973 - 40	1	7.6967	0.6498	0.6917	42.63	5.45	2.3167	0.1574	0.1924	0.0101	0.7717	0.0913	0.0158	5.2129	0.2866	0.0862	0.0046	1217.41	82.71	1134.53	59.48	1340.80	71.25	1131.29	62.19			
973 - 1	1	12.6910	1.1348	0.7220	79.28	6.00	2.4135	0.1662	0.1942	0.0088	0.6579	0.0549	0.0101	5.1468	0.2373	0.0886	0.0041	1246.62	85.87	1144.17	51.85	1395.26	64.28	1144.59	52.77			
973 - 24	1	12.2433	1.3582	2.2197	73.54	26.72	3.0208	0.1906	0.1963	0.0070	0.5635	0.1789	0.0161	5.0972	0.1881	0.1102	0.0046	1412.89	89.14	1155.25	41.07	1801.76	74.90	1154.80	42.62			
973 - 35	1	12.1916	1.1581	1.2430	75.24	16.88	2.5219	0.3277	0.1967	0.0154	0.6039	0.0985	0.0286	5.0396	0.5107	0.0910	0.0099	1278.38	166.13	1157.79	90.87	1446.61	157.00	1166.86	118.25			
973 - 10	1	8.0870	1.9301	3.7738	48.56	15.51	6.6902	2.8207	0.1969	0.0668	0.8040	0.4694	0.0642	5.1533	1.6265	0.2368	0.0246	2071.32	873.32	1158.88	392.84	3098.17	322.11	1143.28	360.86			
973 - 17	1	8.9795	1.0204	3.6822	53.36	58.72	3.1371	0.2233	0.1975	0.0072	0.5088	0.4092	0.0317	5.0773	0.1854	0.1137	0.0074	1441.84	102.62	1162.10	42.08	1858.27	120.83	1158.94	42.31			
973 - 6	1	6.6492	0.9585	1.3536	38.16	4.23	4.0800	0.6186	0.2033	0.0095	0.3090	0.2016	0.0439	4.9245	0.2280	0.1435	0.0168	1650.32	250.23	1193.11	55.89	2268.77	265.24	1191.76	55.18			
973 - 21	1	15.5450	1.5194	2.8826	87.78	40.46	2.7882	0.1378	0.2055	0.0069	0.6797	0.1867	0.0213	4.8674	0.1674	0.0971	0.0036	1352.37	66.85	1204.79	40.48	1568.91	58.00	1204.53	41.42			
973 - 20	1	7.5647	0.9092	1.3655	41.36	8.79	3.5531	0.2491	0.2104	0.0092	0.6264	0.1815	0.0208	4.7570	0.2207	0.1208	0.0057	1539.13	107.92	1230.83	54.06	1967.80	92.54	1229.97	57.07			
973 - 49	1	0.7266	0.2271	0.5396	3.86	1.55	9.5194	4.0585	0.2131	0.0534	0.5874	0.7486	0.2416	4.5308	1.3183	0.3147	0.0664	2389.42	1018.70	1245.44	311.88	3543.23	747.17	1285.63	374.08			
973 - 15	1	15.8981	3.7544	7.8978	83.72	75.82	7.1718	0.9327	0.2155	0.0274	0.9775	0.4890	0.0259	4.4970	1.0232	0.2342	0.0064	2133.00	277.39	1257.86	159.90	3080.08	83.69	1294.39	294.51			
973 - 48	1	18.6051	2.2943	3.5209	82.69	41.87	4.1356	0.4935	0.2402	0.0128	0.4461	0.1885	0.0261	4.1293	0.2371	0.1235	0.0091	1661.37	198.24	1387.69	73.86	2006.02	147.73	1397.97	80.28			
973 - 8	1	13.5666	2.0379	2.9621	65.85	16.63	5.1426	1.2638	0.2437	0.0297	0.4958	0.2153	0.0524	4.1510	0.4420	0.1497	0.0178	1843.17	452.96	1405.65	171.27	2341.46	278.22	1391.41	148.15			
973 - 5	1	3.5628	0.4760	0.6794	16.83	4.82	4.6505	1.3430	0.2524	0.0581	0.7968	0.1981	0.0871	4.1387	0.6088	0.1405	0.0200	1758.39	507.80	1451.05	333.88	2232.72	317.89	1395.12	205.21			
973 - 56	1	11.7156	1.2862	2.1207	47.16	20.39	3.8915	0.3441	0.2603	0.0120	0.5209	0.1811	0.0404	3.8418	0.1727	0.1073	0.0089	1611.92	142.52	1491.62	68.70	1753.86	144.69	1491.33	67.03			
973 - 60	1	35.0991	4.7494	6.9025	135.84	108.97	5.7556	0.4447	0.3094	0.0188	0.7853	0.1916	0.0112	3.2454	0.1954	0.1338	0.0032	1939.77	149.88	1737.59	105.43	2148.20	51.95	1731.47	104.23			
973 - 38	1	0.9417	0.1948	0.7599	3.54	10.32	9.0225	1.4083	0.3128	0.0265	0.5436	0.7990	0.1191	3.1719	0.2368	0.2058	0.0234	2340.29	365.29	1754.37	148.86	2872.33	326.25	1766.57	131.86			
973 - 53	1	11.6992	1.9817	3.8433	42.57	44.50	7.8933	1.1307	0.3349	0.0263	0.5490	0.3305	0.0598	3.0431	0.1918	0.1678	0.0144	2218.92	317.84	1862.22	146.46	2535.27	217.11	1831.62	115.46			
973 - 50	1	20.5691	3.8802	7.6747	61.37	61.89	10.3164	1.1101	0.3932	0.0346	0.8176	0.3643	0.0280	2.5124	0.2432	0.1851	0.0074	2463.58	265.09	2137.46	188.05	2698.61	108.16	2159.92	209.06			
973 - 37	1	0.0350	0.0294	0.0431	0.12	0.71	49.7597	46.5026	0.4116	0.3255	0.8460	1.2075	1.5063	2.5586	2.1320	0.8300	0.5059	3987.51	3726.51	2222.41	1757.15	4973.56	3031.55	2126.68	1772.10			
973 - 2	1	18.4584	3.5829	6.0571	48.99	37.89	11.4224	1.7184	0.4194	0.0477	0.7564	0.3247	0.0158	2.3654	0.2859	0.1934	0.0088	2558.26	384.86	2257.95	256.93	2770.50	126.64	2273.00	274.75			
973 - 29	1	13.3371	4.5054	10.5926	32.59	31.64	22.6818	1.7388	0.4869	0.0394	0.9462	0.7707	0.0675	2.0326	0.1684	0.3319	0.0173	3213.39	246.35	2557.09	207.19	3625.26	189.23	2579.24	213.70			
973 - 19	1	27.5576	6.8285	13.2543	43.46	121.32	26.0391	2.3284	0.7568	0.0639	0.9448	0.4703	0.0339	1.3085	0.1072	0.2447	0.0059	3348.00	299.38	3632.58	306.90	3149.85	75.33	3659.78	299.77			
973 - 59	1	0.8336	0.3256	0.7528	0.83	10.28	64.3078	15.5863	1.2437	0.2603	0.8636	0.9089	0.2702	0.8239	0.1505	0.3720	0.0448	4243.40	1028.47	5209.63	1090.47	3798.94	457.05	5122.95	935.99			
1488 - 1	2	17.6218	9.8464	30.4926	79.90	286.12	19.3352	5.3289	0.2497	0.0605	0.8788	1.7111	0.0965	4.0314	0.6129	0.5559	0.0192	3058.69	843.00	1436.94	348.03	4396.02	151.63	1428.42	217.17			
1488 - 12	2	4.2479	2.6845	7.2214	8.29	29.14	52.3828	7.6354	0.5970	0.0645	0.7413	1.6917	0.1086	1.6948	0.2030	0.6310	0.0268	4038.68	588.68	3017.73	326.06	4580.34	194.87	2989.51	358.07			
1488 - 15	2	1.1192	0.6277	1.5771	1.56	6.29	65.5442	12.0855	0.8273	0.0980	0.6427	1.4019	0.1830	1.1870	0.1322	0.5598	0.0506	4262.44	785.94	3885.99	460.50	4406.44	398.17	3939.40	438.86			
1488 - 16	2	0.5311	0.2681	0.6640	2.61	1.57	17.2038	4.1663	0.2429	0.0426	0.7237	1.2276	0.3384	4.1360	0.6543	0.5138	0.0815	2946.26	713.50	1401.56	245.62	4280.52	679.26	1395.94	220.83			
1488 - 18	2	0.1109	0.0738	0.2326	0.31	1.71	39.8151	9.8201	0.4321	0.0972	0.9122	2.0762	0.6922	2.3556	0.5276	0.6621	0.2013	3766.11	928.88	2315.31	520.92	4649.86	1413.89	2281.00	510.87			
1488 - 20	2	2.3151	1.3090	3.6363	8.75	15.93	24.1533	2.3182	0.3069	0.0215	0.7314	1.5399	0.1068	3.2485	0.2301	0.5589	0.0233	3274.60	314.29	1725.40	121.12	4404.09	183.70	1730.05	122.56			
1488 - 21	2	0.1510	0.0843	0.2356	0.40	0.39	32.6717	5.5496	0.4208	0.0736	0.9709	1.5530	0.3808	2.4245	0.4098	0.5574	0.0837	3570.75	606.53	2264.22	396.12	4400.03	660.77	2226.17	376.30			
1488 - 22	2	0.2499	0.1394	0.2809	0.44	1.17	51.3226	8.3297	0.6601	0.0957	0.8935	1.1076	0.2676	1.5191	0.2198	0.5532	0.0708	4018.31	652.18	3267.47	473.82	4388.99	561.77	3260.54	471.71			
1488 - 24	2	3.4602	2.3146	5.8725	7.09	20.52	53.1132	3.8858	0.5676	0.0269	0.6485	1.6720	0.1123	1.7581	0.0868	0.6633	0.0312	4052.47	296.48	2897.76	137.49	4652.45	218.85	2902.84	143.39			

Appendix 5 Table A1 LA-ICP-MS U-Pb apatite data collected in this study

Receted Data																													
Sample	Analytical Session	^{206}Pb ppm	^{207}Pb ppm	^{208}Pb ppm	U ppm	Th ppm	^{207}Pb/^{235}U (calc)	±2SE	^{206}Pb/^{238}U	±2SE	RHO	^{208}Pb/^{206}Pb	±2SE	^{238}U/^{206}Pb	±2SE	^{207}Pb/^{206}Pb	±2SE	^{207}Pb/^{235}U (calc) Age (Ma)	±2SE	^{206}Pb/^{238}U Age (Ma)	±2SE	^{207}Pb/^{206}Pb Age (Ma)	±2SE	^{238}U/^{206}Pb Age (Ma)	±2SE				
1488 - 33	2	1.1772	0.3443	1.0069	8.61	6.43	6.1905	0.8760	0.1511	0.0112	0.5222	0.8413	0.1247	6.5061	0.4785	0.2918	0.0319	2003.11	283.46	906.85	67.02	3426.80	375.01	921.67	67.78				
1488 - 4	2	0.0590	0.0389	0.0779	0.10	0.79	71.9525	37.5244	0.7857	0.3843	0.9379	1.3204	0.9622	1.4562	0.7242	0.6600	0.2601	4355.80	2271.62	3737.65	1828.16	4645.46	1830.81	3370.06	1675.93				
1488 - 40	2	3.9829	3.0214	8.2004	8.01	54.21	61.6932	7.2174	0.5793	0.0630	0.9297	2.0253	0.1052	1.7068	0.1880	0.7514	0.0298	4201.91	491.57	2945.73	320.37	4831.59	191.62	2972.69	327.35				
1488 - 42	2	0.2859	0.2179	0.4860	0.25	2.53	142.1062	34.7163	1.3539	0.3140	0.9494	1.5893	0.3691	0.7059	0.2260	0.7484	0.0948	5039.94	1231.25	5518.67	1279.96	4826.02	611.35	5688.31	1821.04				
1488 - 46	2	0.1903	0.0767	0.1884	0.99	0.41	12.2807	3.2006	0.2203	0.0357	0.6223	0.9795	0.3062	4.6324	1.0082	0.4009	0.0750	2626.10	684.41	1283.61	208.19	3911.73	731.37	1260.02	274.24				
1488 - 47	2	1.6915	0.4933	1.2431	13.20	4.61	6.0844	0.5712	0.1493	0.0067	0.4796	0.7287	0.0818	6.7185	0.3150	0.2909	0.0178	1988.02	186.63	896.79	40.38	3421.93	209.42	894.48	41.93				
1488 - 48	2	46.5184	40.9795	97.0114	6.62	23.10	954.8429	117.9363	7.7176	0.9107	0.9554	2.0953	0.0377	0.1306	0.0288	0.8846	0.0098	6968.16	860.66	13958.63	1647.14	5063.78	56.26	1913.85	3069.89				
1488 - 49	2	1.6635	0.9002	2.2003	10.28	1.04	14.2174	2.7270	0.1883	0.0201	0.5571	1.3082	0.1689	5.3060	0.6217	0.5379	0.0619	2764.32	530.22	1112.38	118.87	4347.94	500.15	1113.06	130.41				
1488 - 53	2	5.2255	3.3205	9.7142	17.63	81.47	30.0118	5.8645	0.3311	0.0546	0.8440	1.8608	0.1482	2.9138	0.7122	0.6367	0.0400	3487.20	681.42	1843.58	304.06	4593.53	288.78	1902.00	464.87				
1488 - 55	2	1.5568	0.9942	3.4405	3.67	33.24	43.4646	6.4262	0.4878	0.0527	0.7314	2.2043	0.1503	2.0387	0.2125	0.6385	0.0334	3853.07	569.67	2561.05	276.92	4597.60	240.48	2572.87	268.20				
1488 - 6	2	4.8261	2.7081	7.6122	7.83	51.46	56.8678	5.4609	0.7289	0.0566	0.8087	1.5750	0.1014	1.3876	0.1052	0.5618	0.0200	4120.59	395.70	3529.26	274.08	4411.45	157.07	3498.58	265.16				
1488 - 64	2	0.2843	0.1169	0.6077	0.62	2.49	31.0923	7.7861	0.5447	0.0805	0.5900	2.1060	0.4242	1.8279	0.2700	0.4079	0.0751	3521.97	881.97	2802.88	414.09	3937.80	724.80	2813.04	415.59				
1488 - 67	2	0.0529	0.0242	0.0899	0.03	0.76	111.1482	45.9312	1.7642	0.6801	0.9329	1.6875	0.6049	0.5783	0.2219	0.4560	0.1110	4792.43	1980.44	6554.27	2526.63	4104.18	998.98	6472.48	2483.54				
1488 - 68	2	1.4840	0.5045	1.5802	10.85	24.17	7.3298	0.5564	0.1551	0.0074	0.6312	1.0570	0.0915	6.4573	0.3192	0.3390	0.0167	2152.45	163.40	929.44	44.54	3657.43	180.53	928.16	45.88				
1488 - 7	2	0.2166	0.1046	0.2941	0.41	2.32	43.1320	12.6071	0.6407	0.1622	0.8659	1.3637	0.5475	1.5849	0.4040	0.4853	0.1177	3845.45	1123.99	3191.61	807.82	4196.50	1018.15	3153.30	803.84				
1488 - 71	2	0.8603	0.4379	1.0454	6.45	2.99	10.9062	3.5057	0.1546	0.0315	0.6335	1.2134	0.2530	6.5632	1.5121	0.5095	0.0618	2515.17	808.48	926.85	188.73	4268.42	517.97	914.20	210.61				
1488 - 72	2	1.6101	0.9154	2.2003	6.18	5.52	23.6171	3.1603	0.2979	0.0255	0.6396	1.3557	0.1454	3.3370	0.2663	0.5668	0.0399	3252.72	435.25	1680.92	143.87	4424.36	311.49	1689.65	134.85				
1488 - 73	2	1.1879	0.4734	1.0427	10.01	2.47	7.7380	0.9172	0.1399	0.0078	0.4688	0.8681	0.1226	7.1434	0.4057	0.3965	0.0358	2201.02	260.88	843.85	46.89	3895.14	351.61	844.60	47.97				
1488 - 74	2	0.2984	0.1583	0.4501	0.45	0.80	57.7638	17.6385	0.7727	0.1944	0.8237	1.5379	0.4944	1.3067	0.3113	0.5382	0.1064	4136.19	1263.01	3690.62	928.31	4348.70	859.78	3663.54	872.90				
1210 - 23	2	0.1251	0.0134	0.2212	0.50	2.66	4.2164	2.2148	0.2961	0.0704	0.4527	1.7009	0.7086	3.4402	0.8003	0.1042	0.0543	1677.22	881.03	1672.02	397.61	1698.86	884.82	1644.93	382.66				
1210 - 18	2	0.6319	0.0635	1.3985	2.27	19.18	4.4701	2.0859	0.3199	0.0293	0.1964	2.2265	0.2512	3.1211	0.2561	0.1010	0.0267	1725.43	805.15	1789.01	163.94	1642.54	434.77	1791.67	147.01				
1210 - 75	2	0.5294	0.0525	0.2008	0.20	2.36	39.0180	11.3075	2.7563	0.5571	0.6974	0.3769	0.1177	0.3410	0.1290	0.0988	0.0229	3746.08	1085.63	8531.46	1724.32	1600.33	371.16	8826.52	3338.61				
1210 - 61	2	0.3384	0.0660	0.1556	0.78	0.54	13.8724	2.2432	0.5135	0.0526	0.6340	0.4561	0.1271	1.9708	0.2046	0.1942	0.0291	2741.03	443.24	2671.54	273.87	2777.65	416.79	2645.60	274.67				
1210 - 47	2	1.9168	0.3763	5.8009	5.56	75.63	10.8196	4.7462	0.4034	0.0911	0.5146	2.9662	0.3330	2.4539	0.3201	0.1931	0.0331	2507.76	1100.06	2184.60	493.13	2767.73	474.92	2203.58	287.44				
1210 - 9	2	0.4071	0.0557	0.2713	0.94	3.55	9.8295	2.3359	0.5206	0.0696	0.5628	0.6632	0.2316	1.9309	0.2592	0.1366	0.0311	2418.92	574.83	2701.54	361.34	2183.37	497.05	2690.26	361.09				
1210 - 25	2	0.6004	0.0805	0.1886	1.42	1.34	8.9690	1.6846	0.4869	0.0461	0.5043	0.3098	0.0976	2.0350	0.1929	0.1330	0.0305	2334.85	438.54	2557.36	242.21	2136.59	489.99	2576.68	244.29				
1210 - 58	2	1.8041	0.2138	3.4042	4.02	40.45	7.9713	2.4492	0.4966	0.1158	0.7589	1.8812	0.3615	2.0137	0.5179	0.1184	0.0152	2227.78	684.49	2599.27	606.07	1931.56	248.29	2599.15	668.41				
1210 - 24	2	0.3909	0.0514	0.2595	0.81	2.70	9.9142	6.8409	0.5512	0.1713	0.4504	0.6627	0.2731	1.8469	0.6576	0.1316	0.0465	2426.83	1674.55	2830.01	879.45	2118.07	748.79	2789.53	993.26				
1210 - 28	2	0.8541	0.1142	0.8084	2.51	9.82	7.3862	1.0578	0.4054	0.0301	0.5187	0.9376	0.1490	2.4754	0.1953	0.1329	0.0181	2159.30	309.25	2193.85	162.96	2135.70	290.79	2187.31	172.55				
1210 - 46	2	1.0042	0.1519	1.1113	1.17	10.30	20.7969	3.0530	1.0084	0.1147	0.7750	1.1168	0.1400	1.0138	0.1141	0.1500	0.0160	3129.17	459.37	4495.38	511.46	2344.79	250.14	4424.34	497.82				
1210 - 45	2	2.3987	0.6029	4.9419	7.66	52.99	13.2495	2.0480	0.3870	0.0397	0.6634	2.0390	0.4225	2.5866	0.2500	0.2495	0.0399	2697.59	416.96	2109.10	216.26	3180.62	508.39	2107.07	203.64				
1210 - 17	2	0.5094	0.0707	0.2423	0.87	2.13	12.9487	2.3264	0.6779	0.0690	0.5666	0.4738	0.1142	1.4921	0.1509	0.1379	0.0227	2675.93	480.76	3336.47	339.66	2199.89	362.52	3306.54	334.34				
1210 - 33	2	1.3883	0.1664	0.8179	3.17	8.32	8.5110	1.7896	0.5280	0.0515	0.4635	0.5770	0.0884	1.9262	0.1904	0.1182	0.0184	2287.10	480.91	2732.98	266.35	1928.83	300.83	2695.60	266.49				
1210 - 3	2	0.3383	0.0865	0.2386	0.76	0.71	19.2143	5.3182	0.5418	0.0806	0.5376	0.6994	0.2337	1.8595	0.2766	0.2546	0.0610	3052.64	844.93	2791.07	415.34	3213.07	769.83	2774.11	412.66				
1210 - 68	2	2.7788	0.2982	10.1836	14.10	145.74	3.4076	0.2750	0.2279	0.0080	0.4347	3.6265	0.1677	4.3886	0.1547	0.1068	0.0077	1506.16	121.56	1323.58	46.44	1745.03	125.39	1323.28	46.63				
1210 - 76	2	2.4634	0.2779	2.6625	5.36	25.82	8.5314	0.9406	0.5421	0.0318	0.5326	1.0725	0.1026	1.8438	0.1090	0.1125	0.0146	2289.27	252.39	2792.19	163.96	1839.33	238.55	2793.27	165.10				
1210 - 7	2	2.0027	0.3934	0.9209	1.95	3.54	32.6326	3.5062	1.2005	0.0820	0.6356	0.4569	0.0606	0.8318	0.0580	0.1959	0.0148	3569.58	383.54	5084.11	347.22	2791.94	210.74	5089.24	354.78				
1210 - 2	2	3.3237	0.7180	1.9427	7.24	2.48	16.6656	2.1337	0.5519	0.0432	0.6120	0.5815	0.1229	1.8087	0.1459	0.2152	0.0206	2915.80	373.32	2833.19	222.01	2944.51	281.91	2837.08	228.81				
1488 - 74	2	0.2984	0.1583	0.4501	0.45	0.80	57.7638	17.6385	0.7727	0.1944	0.8237	1.5379	0.4944	1.3067	0.3113	0.5382	0.1064	4136.19	1263.01	3690.62	928.31	4348.70	859.78	3663.54	872.90				
1210 - 23	2	0.1251	0.0134	0.2212	0.50	2.66	4.2164	2.2148	0.2961	0.0704	0.4527	1.7009	0.7086	3.4402	0.8003	0.1042	0.0543	1677.22	881.03	1672.02	397.61	1698.86	884.82	1644.93	382.66				
1210 - 18	2	0.6319	0.0635	1.3985	2.27	19.18	4.4701	2.0859	0.3199	0.0293	0.1964	2.2265	0.2512	3.1211	0.2561	0.1010	0.0267	1725.43	805.15	1789.01	163.94	1642.54	434.77	1791.67	147.01				
1210 - 75	2	0.5294	0.0525	0.2008	0.20	2.36	39.0180	11.3075	2.7563	0.5571	0.6974	0.3769	0.1177	0.3410	0.1290	0.0988	0.0229	3746.08	1085.63	8531.46	1724.32	1600.33	371.16	8826.52	3338.61				
1210 - 61	2	0.3384	0.0660	0.1556	0.78	0.54	13.8724	2.2432	0.5135	0.0526	0.6340	0.4561	0.1271	1.9708	0.2046	0.1942	0.0291	2741.03	443.24	2671.54	273.87	2777.65	416.79	2645.60	274.67				
1210 - 47	2	1.9168	0.3763	5.8009	5.56	75.63	10.8196	4.7462	0.4034	0.0911	0.5146	2.9662	0.3330	2.4539	0.3201	0.1931	0.0331	2507.76	1100.06	2184.60	493.13	2767.73	474.92	2203.58	287.44				
1210 - 9	2	0.4071	0.0557	0.2713	0.94	3.55	9.8295	2.3359	0.5206	0.0696	0.5628	0.6632	0.2316	1.9309	0.2592	0.1366	0.0311	2418.92	574.83	2701.54	361.34	2183.37	497.05	2690.26	361.09				
1210 - 25	2	0.6004	0.0805	0.1886	1.42	1.34	8.9690	1.6846	0.4869	0.0461	0.5043	0.3098	0.0976	2.0350	0.1929	0.1330	0.0305	2334.85	438.54	2557.36	242.21	2136.59	489.99	2576.68	244.29				
1210 - 58	2	1.8041	0.2138	3.4042	4.02	40.45	7.9713	2.4492	0.4966	0.1158	0.7589	1.8812	0.3615	2.0137	0.5179	0.1184	0.0152	2227.78	684.49	2599.27	606.07	1931.56	248.29	2599.15	668.41				
1210 - 24	2	0.3909	0.0514	0.2595	0.81	2.70	9.9142	6.8409	0.5512	0.1713	0.4504	0.6627	0.2731	1.8469	0.6576	0.1316	0.0465	2426.83	1674.55	2830.01	879.45	2118.07	748.79	2789.53	993.26				
1210 - 28	2	0.8541	0.1142	0.8084	2.51	9.82	7.3862	1.0578	0.4054	0.0301	0.5187	0.9376	0.1490	2.4754	0.1953	0.1329	0.0181	2159.30	309.25	2193.85	162.96	2135.70	290.79	2187.31	172.55				
1210 - 46	2	1.0042	0.1519	1.1113	1.17	10.30	20.7969	3.0530	1.0084	0.1147	0.7750	1.1168	0.1400	1.0138	0.1141	0.1500	0.0160	3129.17	459.37	4495.38	511.46	2344.79	250.14	4424.34	497.82				

Appendix 5 Table A1 LA-ICP-MS U-Pb apatite data collected in this study

Rejected Data Sample	Analytical Session	^{206}Pb ppm	^{207}Pb ppm	^{208}Pb ppm	U ppm	Th ppm	^{207}Pb/^{235}U (calc)	±2SE	^{206}Pb/^{238}U	±2SE	RHO	^{208}Pb/^{206}Pb	±2SE	^{238}U/^{206}Pb	±2SE	^{207}Pb/^{206}Pb	±2SE	^{207}Pb/^{235}U (calc) Age (Ma)	±2SE	^{206}Pb/^{238}U Age (Ma)	±2SE	^{207}Pb/^{206}Pb Age (Ma)	±2SE	^{238}U/^{206}Pb Age (Ma)	±2SE
1210 - 45	2	2.3987	0.6029	4.9419	7.66	52.99	13.2495	2.0480	0.3870	0.0397	0.6634	2.0390	0.4225	2.5866	0.2500	0.2495	0.0399	2697.59	416.96	2109.10	216.26	3180.62	508.39	2107.07	203.64
1210 - 17	2	0.5094	0.0707	0.2423	0.87	2.13	12.9487	2.3264	0.6779	0.0690	0.5666	0.4738	0.1142	1.4921	0.1509	0.1379	0.0227	2675.93	480.76	3336.47	339.66	2199.89	362.52	3306.54	334.34
1210 - 33	2	1.3883	0.1664	0.8179	3.17	8.32	8.5110	1.7896	0.5280	0.0515	0.4635	0.5770	0.0884	1.9262	0.1904	0.1182	0.0184	2287.10	480.91	2732.98	266.35	1928.83	300.83	2695.60	266.49
1210 - 3	2	0.3383	0.0865	0.2386	0.76	0.71	19.2143	5.3182	0.5418	0.0806	0.5376	0.6994	0.2337	1.8595	0.2766	0.2546	0.0610	3052.64	844.93	2791.07	415.34	3213.07	769.83	2774.11	412.66
1210 - 68	2	2.7788	0.2982	10.1836	14.10	145.74	3.4076	0.2750	0.2279	0.0080	0.4347	3.6265	0.1677	4.3886	0.1547	0.1068	0.0077	1506.16	121.56	1323.58	46.44	1745.03	125.39	1323.28	46.63
1210 - 76	2	2.4634	0.2779	2.6625	5.36	25.82	8.5314	0.9406	0.5421	0.0318	0.5326	1.0725	0.1026	1.8438	0.1090	0.1125	0.0146	2289.27	252.39	2792.19	163.96	1839.33	238.55	2793.27	165.10
1210 - 7	2	2.0027	0.3934	0.9209	1.95	3.54	32.6326	3.5062	1.2005	0.0820	0.6356	0.4569	0.0606	0.8318	0.0580	0.1959	0.0148	3569.58	383.54	5084.11	347.22	2791.94	210.74	5089.24	354.78
1210 - 2	2	3.3237	0.7180	1.9427	7.24	2.48	16.6656	2.1337	0.5519	0.0432	0.6120	0.5815	0.1229	1.8087	0.1459	0.2152	0.0206	2915.80	373.32	2833.19	222.01	2944.51	281.91	2837.08	228.81

Appendix 5 Table A1 LA-ICP-MS U-Pb apatite data collected in this study

Apatite U-Pb Standard reference materials																											
Sample	Analytical Session	^{206}Pb ppm	^{207}Pb ppm	^{208}Pb ppm	U ppm	Th ppm	^{207}Pb/^{235}U (calc)	±2SE	^{206}Pb/^{238}U	±2SE	^{208}Pb/^{206}Pb	±2SE	^{238}U/^{206}Pb	±2SE	^{207}Pb/^{206}Pb	±2SE	^{207}Pb/^{235}U (calc) Age (Ma)	±2SE	^{206}Pb/^{238}U Age (Ma)	±2SE	^{207}Pb/^{206}Pb Age (Ma)	±2SE	^{238}U/^{206}Pb Age (Ma)	±2SE			
401 - 1	1	1.0601	0.0683	2.4583	13.60	108.34	0.7792	0.0837	0.0867	0.0036	2.3002	0.1354	11.5314	0.4874	0.0642	0.0066	585.0088	62.8267	535.7135	22.3970	747.6332	77.2819	536.1051	22.6595			
401 - 10	1	1.0813	0.0707	2.6736	13.82	115.98	0.7979	0.0856	0.0879	0.0037	2.4535	0.1415	11.3616	0.4821	0.0652	0.0067	595.6339	63.9084	543.2112	22.8028	779.5275	80.5152	543.7883	23.0740			
401 - 11	1	1.0433	0.0892	2.5857	13.43	112.26	1.0335	0.1063	0.0873	0.0037	2.4579	0.1417	11.4433	0.4853	0.0851	0.0082	720.6549	74.1074	539.8143	22.6491	1317.8727	126.8538	540.0669	22.9051			
401 - 12	1	1.1893	0.1577	2.9573	13.62	112.76	1.8009	0.3928	0.0981	0.0058	2.4807	0.1349	10.2383	0.5527	0.1329	0.0222	1045.7744	228.1171	603.4486	35.5786	2135.6469	356.3276	600.7513	32.4283			
401 - 13	1	1.0285	0.0859	2.6267	13.49	110.47	0.9893	0.0968	0.0854	0.0036	2.5276	0.1463	11.6925	0.4990	0.0832	0.0078	698.3839	68.3414	528.4138	22.3078	1274.0791	119.1923	529.0148	22.5747			
401 - 14	1	1.0262	0.0656	2.6559	13.57	108.01	0.7514	0.0822	0.0848	0.0036	2.5569	0.1697	11.7649	0.5007	0.0636	0.0069	569.0096	62.2394	524.5834	22.0922	727.7464	79.2674	525.8905	22.3824			
401 - 15	1	1.0195	0.0669	2.5996	13.52	108.37	0.7687	0.0836	0.0845	0.0036	2.5207	0.1455	11.8001	0.5022	0.0653	0.0068	579.0179	65.2279	523.1737	22.0262	783.4408	81.7138	524.3827	22.3181			
401 - 16	1	1.0415	0.0685	2.7058	13.38	109.80	0.7951	0.0873	0.0874	0.0037	2.5761	0.1466	11.4702	0.4877	0.0657	0.0068	594.0848	65.2279	540.3775	22.7185	794.5416	82.2058	538.8516	22.9115			
401 - 17	1	1.0305	0.0698	2.6481	13.33	109.55	0.8039	0.0909	0.0858	0.0037	2.5474	0.1461	11.6450	0.4955	0.0673	0.0074	599.0283	67.7629	530.5593	22.9232	846.6630	92.6894	531.0872	22.5998			
401 - 18	1	1.0261	0.0695	2.4566	13.52	110.04	0.7893	0.0915	0.0842	0.0038	2.3788	0.1646	11.8946	0.5057	0.0676	0.0074	590.7469	68.4924	521.0038	23.5298	853.8714	94.0897	520.3781	22.1235			
401 - 19	1	1.0760	0.0700	2.6276	13.43	111.89	0.8001	0.0857	0.0888	0.0037	2.4247	0.1400	11.2799	0.4782	0.0649	0.0067	596.8780	63.9699	548.2633	22.9900	770.5315	79.4776	547.5640	23.2149			
401 - 2	1	1.0398	0.0679	2.5758	13.37	107.72	0.7877	0.0842	0.0865	0.0036	2.4582	0.1436	11.5741	0.4896	0.0650	0.0067	589.8798	63.0779	534.6988	22.3745	775.0086	79.7470	534.2093	22.5984			
401 - 20	1	1.0499	0.0705	2.5703	13.47	110.00	0.8034	0.0897	0.0863	0.0038	2.4310	0.1417	11.5951	0.4934	0.0670	0.0074	598.7487	66.8754	533.6696	23.6761	836.5560	92.6468	533.2795	22.6917			
401 - 3	1	1.0556	0.0722	2.5216	13.66	109.11	0.8214	0.1068	0.0860	0.0037	2.3697	0.1384	11.6035	0.4914	0.0682	0.0086	608.8273	79.1356	531.8995	22.9757	874.5887	110.2073	532.9111	22.5689			
401 - 4	1	1.0576	0.0690	2.8068	13.40	111.58	0.8009	0.0857	0.0881	0.0039	2.6313	0.1471	11.3435	0.4775	0.0650	0.0067	597.3157	63.9515	544.2612	23.9826	773.7090	79.7088	544.6202	22.9244			
401 - 5	1	1.0332	0.0659	2.6003	13.67	112.01	0.7600	0.0828	0.0856	0.0036	2.4949	0.1554	11.6751	0.4959	0.0636	0.0067	574.0337	62.5391	529.4359	22.2402	728.3570	76.5124	529.7732	22.5023			
401 - 6	1	1.0421	0.0728	2.6325	13.90	111.64	0.8245	0.1158	0.0849	0.0036	2.5017	0.1440	11.7615	0.4995	0.0695	0.0090	610.5733	85.7144	525.4683	22.0805	913.4459	117.7909	526.0342	22.3419			
401 - 7	1	1.0467	0.0747	2.6870	13.66	110.42	0.8486	0.0886	0.0857	0.0036	2.5446	0.1547	11.6728	0.4957	0.0711	0.0072	623.9042	65.1073	529.9336	22.3973	960.2546	96.8481	529.8700	22.5017			
401 - 8	1	1.0679	0.0723	2.4980	13.67	109.17	0.8196	0.0919	0.0873	0.0036	2.3141	0.1444	11.4434	0.4830	0.0673	0.0076	607.8279	68.1701	539.7691	22.5357	846.4435	95.8942	540.0627	22.7958			
401 - 9	1	1.1051	0.0768	2.7366	13.88	113.59	0.8615	0.0924	0.0895	0.0037	2.4566	0.1553	11.1706	0.4715	0.0692	0.0071	630.9628	67.7061	552.4085	23.0647	904.6115	92.9251	552.6993	23.3271			
MAD	1	1.7375	0.1812	13.0678	23.88	614.52	0.6055	0.0183	0.0763	0.0023	7.7960	0.2700	13.1137	0.3943	0.0566	0.0050	480.7010	14.5612	473.9943	14.0696	476.5591	41.6879	473.7357	14.2449			
MAD	1	1.7705	0.2120	13.0716	24.25	624.52	0.5939	0.0180	0.0749	0.0022	7.7657	0.2408	13.3542	0.4016	0.0566	0.0050	473.3375	14.3381	465.6840	13.8229	475.5523	41.6510	465.5061	13.9975			
MAD	1	1.7942	0.1982	13.2048	24.37	628.52	0.6095	0.0185	0.0770	0.0023	7.6497	0.2534	12.9625	0.3898	0.0566	0.0049	483.2757	14.6392	478.1087	14.1917	474.1643	41.1599	479.0603	14.4050			
MAD	1	1.8223	0.2028	13.6614	24.50	637.22	0.6105	0.0185	0.0773	0.0023	7.8331	0.2729	12.9433	0.3892	0.0566	0.0049	483.8901	14.6578	480.1134	14.2512	474.6320	41.2606	479.7444	14.4256			
MAD	1	1.7799	0.1972	13.7446	25.08	641.46	0.5923	0.0179	0.0749	0.0022	8.0432	0.2456	13.3308	0.4008	0.0566	0.0049	472.3387	14.3079	465.5807	13.8198	475.6075	41.4419	466.2916	14.0211			
MAD	1	1.8261	0.2225	13.7719	25.03	641.96	0.6031	0.0183	0.0761	0.0023	7.9222	0.2421	13.1299	0.3948	0.0567	0.0049	479.2035	14.5158	472.6238	14.0289	478.7257	41.5324	473.1709	14.2279			
MAD	1	1.8241	0.1992	13.5890	25.33	649.68	0.5947	0.0180	0.0755	0.0022	7.7492	0.2384	13.2663	0.3989	0.0566	0.0049	473.8335	14.3532	469.2923	13.9300	476.3970	41.3799	468.4798	14.0869			
MAD	1	1.8568	0.2010	14.0696	25.21	645.42	0.6099	0.0185	0.0772	0.0023	7.8659	0.2386	12.9467	0.3893	0.0567	0.0049	483.4956	14.6458	479.2253	14.2249	477.5684	41.0539	479.6241	14.4220			
MAD	1	1.8181	0.2020	13.8036	24.73	632.20	0.6046	0.0183	0.0770	0.0023	7.9430	0.2479	13.0078	0.3911	0.0566	0.0050	480.1334	14.5440	478.3578	14.1991	474.1985	42.1180	477.4537	14.3567			
MAD	1	1.8001	0.1923	13.2784	24.40	632.09	0.6122	0.0185	0.0778	0.0023	7.6620	0.2698	12.8489	0.3864	0.0566	0.0050	484.9270	14.6892	483.1676	14.3419	474.6503	41.5766	483.1408	14.5277			
MAD	1	1.7875	0.2103	13.1772	24.16	627.25	0.6061	0.0184	0.0769	0.0023	7.7338	0.2415	12.9832	0.3904	0.0566	0.0050	481.0884	14.5729	477.5721	14.1758	475.5581	41.9221	478.3249	14.3829			
MAD	1	1.8017	0.1800	13.5066	24.94	643.11	0.6042	0.0183	0.0769	0.0023	7.7476	0.2501	13.0146	0.3913	0.0566	0.0049	479.8897	14.5366	477.5336	14.1746	474.7403	41.3742	477.2143	14.3495			
MAD	1	1.7683	0.1967	13.4218	24.98	639.94	0.5826	0.0176	0.0741	0.0022	7.9134	0.2485	13.5084	0.4062	0.0566	0.0050	466.1013	14.1189	460.9110	13.6812	476.0806	42.4541	460.3756	13.8432			
MAD	1	1.8223	0.2051	13.8990	24.97	645.21	0.6025	0.0182	0.0764	0.0023	7.9230	0.2617	13.0640	0.3928	0.0566	0.0050	478.8015	14.5036	474.3949	14.0815	476.5066	41.7287	475.4724	14.2971			
MAD	1	1.6673	0.1638	13.0729	23.74	613.78	0.5896	0.0179	0.0750	0.0022	8.0527	0.2538	13.3526	0.4015	0.0566	0.0051	470.5900	14.2549	465.9455	13.8307	476.8040	42.8591	465.5578	13.9990			
MAD	1	1.8156	0.2336	13.4591	24.49	628.81	0.5962	0.0181	0.0758	0.0023	7.8408	0.2473	13.1763	0.3962	0.0566	0.0049	474.8134	14.3828	471.0566	13.9824	474.2217	41.1884	471.5657	14.1797			
MAD	1	1.7153	0.1843	13.2159	23.87	617.45	0.5903	0.0179	0.0749	0.0022	7.9991	0.2589	13.3356	0.4010	0.0566	0.0050	471.0466	14.2687	465.6135	13.8208	476.0879	42.0735	466.1308	14.0162			
MAD	1	1.7438	0.1887	13.1464	23.72	613.59	0.6022	0.0182	0.0764	0.0023	7.8421	0.2426	13.0739	0.3931	0.0566	0.0050	478.6457	14.4989	474.7511	14.0920	476.4359	41.7213	475.1256	14.2867			
MAD	1	1.8312	0.2143	13.7269	24.75	636.34	0.5969	0.0181	0.0759	0.0023	7.8657	0.3217	13.1819	0.3964	0.0566	0.0049	475.2503	14.3961	471.5779	13.9979	474.7920	41.5233	471.3735	14.1739			
MAD	1	1.8378	0.1870	13.5354	24.48	632.46	0.6194	0.0188	0.0785	0.0023	7.6087	0.2338	12.7293	0.3828	0.0567	0.0049	489.4940	14.8275	487.4007	14.4675	477.2165	41.1701	487.5142	14.6592			
McClure -1	1	0.9775	0.2693	1.1500	9.31	24.67	4.4846	0.3025	0.1167	0.0051	1.1689	0.0955	8.5824	0.3775	0.2751	0.0156	1728.1167	116.5530	711.8124	31.0848	3334.6200	189.5667	710.4867	31.2523			
McClure -10	1	1.4140	0.3447	2.0022	13.75	54.25	3.9107	0.2309	0.1155	0.0046	1.4044	0.0936	8.6333	0.3481	0.2427	0.0121	1615.8989	95.4086	704.4483	28.0982	3136.9447	156.8470	706.5189	28.4839			
McClure -11	1	1.7056	0.2420	1.9690	19.60	64.27	1.9201	0.1341	0.0976	0.0037	1.1478	0.0729	10.2450	0.3934	0.1416	0.0091	1088.0904	75.9809	600.6128	22.8139	2245.9738	143.7335	600.3786	23.0570			
McClure -12	1	2.0576	0.6055	2.2697	11.22	33.45	8.3934	3.0278	0.2065	0.0482	1.0900	0.6104	4.8330	1.1485	0.2923	0.1075	2274.4644	820.4919	1209.9429	282.4999	3429.0057	1260.9610	1212.3245	288.0845			
McClure -13	1	1.3891	0.2643	1.7367	15.05	53.12	2.7340	0.1924	0.1033	0.0041	1.2426	0.0829	9.6898	0.3891	0.1907	0.0107	1337.7566	94.1621	633.7165	25.1552	2747.0530	153.6593	633.1394	25.4232			
McClure -14	1	1.5255	0.2359	1.6203	17.14	53.87	2.1373	0.1415	0.0999	0.0039	1.0517	0.0733	10.0203	0.3948	0.1543	0.0090	1160.9609	76.8447	613.7367	23.9233	2393.1222	139.2299	613.2224	24.1631			

MAD: Madagascar; McClure: McClure Mountains

Appendix 5 Table A1 LA-ICP-MS U-Pb apatite data collected in this study

Apatite U-Pb Standard reference materials																									
Sample	Analytical Session	^{206}Pb ppm	^{207}Pb ppm	^{208}Pb ppm	U ppm	Th ppm	^{207}Pb/^{235}U (calc)	±2SE	^{206}Pb/^{238}U	±2SE	^{208}Pb/^{206}Pb	±2SE	^{238}U/^{206}Pb	±2SE	^{207}Pb/^{206}Pb	±2SE	^{207}Pb/^{235}U (calc) Age (Ma)	±2SE	^{206}Pb/^{238}U Age (Ma)	±2SE	^{207}Pb/^{206}Pb Age (Ma)	±2SE	^{238}U/^{206}Pb Age (Ma)	±2SE
McClure - 15	1	< DL	< DL	< DL	< DL	< DL	NA	NA	NA	NA	2.1538	1.3669	NA	NA	0.6242	0.2677	0.0000	0.0000	0.0000	0.0000	4564.7201	1958.0327	#NUM!	0.0000
McClure - 16	1	0.8193	0.2078	0.8932	8.29	20.91	3.8926	0.3068	0.1107	0.0050	1.0794	0.0999	9.0251	0.4149	0.2527	0.0163	1612.1460	127.0823	676.6687	30.7699	3201.0100	206.3374	677.4037	31.1398
McClure - 17	1	2.1605	0.3867	1.9329	23.13	53.24	2.5750	1.3000	0.1040	0.0395	0.8880	0.0679	9.6210	1.3412	0.1782	0.0160	1293.5693	653.0655	637.5356	242.1453	2635.6129	236.5201	637.4505	88.8636
McClure - 18	1	< DL	< DL	< DL	< DL	< DL	NA	NA	NA	NA	< DL	0.0136	NA	NA	< DL	0.0075	0.0000	0.0000	0.0000	0.0000	< DL	0.0000	#NUM!	0.0000
McClure - 19	1	1.8349	0.2646	1.9762	21.29	62.14	1.9083	0.1353	0.0956	0.0036	1.0663	0.0714	10.4586	0.3987	0.1435	0.0093	1083.9810	76.8664	588.4562	22.1972	2268.6364	147.1012	588.6579	22.4430
McClure - 2	1	1.1235	0.2976	1.3662	11.54	33.25	3.9971	0.2558	0.1081	0.0045	1.2074	0.0940	9.2612	0.3896	0.2643	0.0152	1633.6171	104.5357	661.7937	27.5412	3271.9195	187.9704	660.9887	27.8091
McClure - 20	1	1.4901	0.4650	1.9635	13.44	40.77	5.3199	0.3235	0.1227	0.0049	1.3118	0.0829	8.1701	0.3276	0.3127	0.0146	1872.0664	113.8471	746.3234	30.0730	3533.4798	164.9687	744.3479	29.8468
McClure - 3	1	1.0280	0.2020	1.1039	10.91	31.32	2.8814	0.2012	0.1049	0.0045	1.0694	0.0881	9.5460	0.4101	0.1967	0.0124	1377.0655	96.1721	642.7764	27.2937	2798.4360	176.7913	642.2191	27.5909
McClure - 4	1	1.7598	0.3990	2.2227	18.37	62.09	3.3757	0.9697	0.1068	0.0139	1.2525	0.1194	9.3492	0.6962	0.2260	0.0264	1498.7644	430.5385	654.3489	84.9457	3022.9401	352.5570	655.0755	48.7831
McClure - 5	1	1.5251	0.2369	1.6862	17.93	59.54	2.0845	0.1448	0.0966	0.0037	1.0935	0.0814	10.3365	0.4039	0.1545	0.0100	1143.7132	79.4479	594.3499	22.9825	2395.7751	155.4894	595.3022	23.2627
McClure - 6	1	1.3171	0.2440	1.4462	14.36	44.29	2.6789	0.2014	0.1040	0.0042	1.0882	0.0898	9.6052	0.3878	0.1846	0.0125	1322.6384	99.4331	637.6689	25.4696	2693.4874	182.6338	638.4497	25.7791
McClure - 7	1	0.8008	0.1860	0.8979	8.31	20.56	3.4733	0.2656	0.1078	0.0049	1.1112	0.1087	9.2891	0.4294	0.2317	0.0156	1521.1837	116.3223	659.6930	30.1573	3063.0979	206.8867	659.1015	30.4672
McClure - 8	1	1.2842	0.3033	1.5324	12.74	38.45	3.6840	0.2541	0.1123	0.0046	1.1824	0.0908	8.8968	0.3669	0.2353	0.0139	1567.9128	108.1610	686.3206	27.9889	3088.0120	182.4614	686.6700	28.3217
McClure - 9	1	0.8304	0.2458	0.9312	7.83	18.68	4.8947	0.3587	0.1191	0.0055	1.1138	0.1103	8.3893	0.3889	0.2952	0.0199	1801.3422	132.0135	725.1172	33.2361	3444.6482	231.9546	725.9496	33.6515
401 - 1	2	1.0684	0.0715	2.7241	13.80	114.29	0.8035	0.0974	0.0862	0.0039	2.5193	0.1479	11.5819	0.5439	0.0664	0.0074	598.8163	72.6067	533.2681	24.2809	819.0833	90.9750	533.8611	25.0718
401 - 10	2	1.0093	0.0684	2.2716	13.42	102.01	0.7932	0.0987	0.0850	0.0043	2.2267	0.1619	11.7538	0.5852	0.0674	0.0085	592.9743	73.7951	525.8627	26.7898	848.3077	106.4080	526.3661	26.2085
401 - 11	2	1.0544	0.0687	2.6369	13.65	110.32	0.7824	0.0949	0.0869	0.0038	2.4729	0.1481	11.5002	0.4875	0.0648	0.0077	586.8337	71.2128	537.3685	23.2308	766.7250	91.0909	537.5012	22.7845
401 - 12	2	1.1112	0.0954	2.8261	13.61	114.83	1.0887	0.2258	0.0918	0.0046	2.5212	0.1480	10.9215	0.5000	0.0855	0.0141	747.8723	155.0995	566.0271	28.2991	1326.2757	218.9900	564.7689	25.8538
401 - 13	2	1.0564	0.0705	2.8143	13.75	110.30	0.7969	0.1064	0.0848	0.0030	2.6397	0.1570	11.8160	0.3927	0.0664	0.0087	595.0517	79.4834	524.5737	18.4423	819.6411	107.0700	523.7025	17.4053
401 - 14	2	1.0569	0.0777	2.4898	13.44	105.87	0.8987	0.1152	0.0867	0.0031	2.3344	0.1658	11.5486	0.3861	0.0732	0.0093	651.0379	83.4621	535.8001	18.8897	1019.1946	129.6525	535.3407	17.8959
401 - 15	2	0.9957	0.0599	2.3912	13.51	102.43	0.6980	0.1089	0.0838	0.0031	2.3777	0.1726	11.9249	0.4280	0.0599	0.0090	537.5925	83.8836	518.8619	18.8960	598.7598	90.4154	519.1101	18.6319
401 - 16	2	1.0535	0.0673	2.6360	13.45	108.90	0.7875	0.0978	0.0891	0.0032	2.4739	0.1609	11.1964	0.3952	0.0636	0.0072	589.7669	73.2648	550.1999	19.7213	726.0333	82.6039	551.4796	19.4668
401 - 17	2	1.0472	0.0988	2.6116	13.62	108.69	1.1210	0.1202	0.0868	0.0033	2.4659	0.1621	11.5064	0.4255	0.0937	0.0091	763.4312	81.8870	536.4523	20.3016	1501.2449	146.5720	537.2252	19.8641
401 - 18	2	1.2133	0.1783	2.9148	13.44	109.90	2.0515	0.6232	0.1020	0.0073	2.3805	0.1833	9.8208	0.5578	0.1462	0.0290	1132.8016	344.1131	626.1685	44.7799	2300.8927	456.7521	625.0918	35.5036
401 - 19	2	1.0522	0.0680	2.5431	13.71	111.24	0.7716	0.1037	0.0876	0.0032	2.3926	0.1505	11.4106	0.4166	0.0641	0.0083	580.6931	78.0719	541.3824	19.9092	745.1701	96.5303	541.5487	19.7701
401 - 2	2	1.0699	0.0658	2.7388	13.95	116.00	0.7306	0.0966	0.0852	0.0041	2.5322	0.1481	11.7230	0.5551	0.0611	0.0082	556.8761	73.5993	527.2934	25.4451	642.5054	86.4516	527.6933	24.9853
401 - 20	2	1.0601	0.0672	2.5402	13.74	112.70	0.7615	0.0963	0.0882	0.0032	2.3717	0.1450	11.3414	0.4137	0.0629	0.0079	574.8626	72.6744	544.8027	20.0231	703.9574	88.9090	544.7198	19.8689
401 - 21	2	1.0428	0.0646	2.5576	13.87	111.91	0.7285	0.0827	0.0844	0.0033	2.4289	0.1770	11.8224	0.4513	0.0617	0.0069	555.6744	63.1153	522.5947	20.5523	661.0689	73.9013	523.4314	19.9794
401 - 22	2	1.0650	0.0703	2.7357	13.66	111.33	0.8052	0.0878	0.0876	0.0034	2.5429	0.1509	11.4072	0.4334	0.0657	0.0070	599.7789	65.3930	541.1559	21.0041	795.4140	85.1559	541.7027	20.5791
401 - 23	2	1.0427	0.0771	2.5891	13.68	111.01	0.8806	0.1117	0.0858	0.0032	2.4552	0.1495	11.6509	0.4365	0.0735	0.0096	641.3231	81.3703	530.7274	20.0170	1028.0899	134.2815	530.8285	19.8877
401 - 24	2	1.0435	0.0727	2.6663	13.54	112.51	0.8378	0.0948	0.0866	0.0033	2.5268	0.1512	11.5225	0.4304	0.0693	0.0080	617.9250	69.9151	535.5097	20.1397	905.7510	104.2002	536.5027	20.0394
401 - 25	2	1.0188	0.0698	2.6311	13.52	109.07	0.8048	0.1125	0.0834	0.0030	2.5559	0.1679	11.9949	0.4217	0.0681	0.0087	599.5560	83.7788	516.5935	18.4367	871.7660	111.4834	516.1975	18.1469
401 - 26	2	1.0465	0.0683	2.5646	13.77	110.63	0.7736	0.0959	0.0841	0.0030	2.4258	0.1485	11.9033	0.4148	0.0649	0.0079	581.8467	72.1498	520.7717	18.4235	771.1438	93.2346	520.0145	18.1222
401 - 27	2	1.0289	0.0752	2.6454	13.76	113.57	0.8560	0.0950	0.0841	0.0029	2.5446	0.1657	11.8925	0.4078	0.0727	0.0078	627.9610	69.6926	520.4002	18.1697	1004.0010	107.8445	520.4675	17.8475
401 - 28	2	1.0643	0.0692	2.6963	13.46	111.92	0.8045	0.0883	0.0889	0.0031	2.5058	0.1604	11.2374	0.3789	0.0646	0.0070	599.3788	65.7951	549.0289	18.8641	760.3153	81.9549	549.5488	18.5290
401 - 29	2	1.0536	0.0700	2.7908	13.88	114.49	0.7866	0.0870	0.0853	0.0033	2.6199	0.1639	11.7095	0.4044	0.0661	0.0072	589.2321	65.1841	527.7264	20.5352	809.0655	88.0237	528.2791	18.2437
401 - 3	2	1.0195	0.0716	2.5195	13.83	106.94	0.8026	0.0862	0.0823	0.0031	2.4469	0.1791	12.1469	0.4614	0.0699	0.0074	598.3217	64.2650	509.5615	19.0803	923.4644	97.4541	509.9865	19.3729
401 - 30	2	1.0580	0.0656	2.6408	13.86	113.88	0.7382	0.0841	0.0859	0.0030	2.4687	0.1559	11.6340	0.4010	0.0617	0.0069	561.3570	63.9199	530.9989	18.6573	661.2654	74.1082	531.5688	18.3219
401 - 4	2	1.0438	0.0676	2.5676	13.56	106.84	0.7729	0.0888	0.0859	0.0033	2.4357	0.1550	11.6400	0.4495	0.0644	0.0070	581.4045	66.7897	531.4691	20.6921	755.0995	82.3002	531.3045	20.5194
401 - 5	2	1.0331	0.0725	2.5103	13.66	106.95	0.8177	0.0876	0.0846	0.0032	2.4062	0.1475	11.8292	0.4449	0.0699	0.0074	606.7475	65.0306	523.6839	19.9705	923.4089	97.2058	523.1443	19.6740
401 - 6	2	1.0618	0.0741	2.5252	13.51	112.67	0.8467	0.1110	0.0881	0.0033	2.3563	0.1573	11.3807	0.4257	0.0696	0.0095	622.8138	81.6363	544.3739	20.6493	914.5319	125.5522	542.9156	20.3094
401 - 7	2	1.0548	0.0732	2.7927	13.96	115.51	0.8146	0.0975	0.0853	0.0041	2.6196	0.1791	11.7354	0.5313	0.0690	0.0083	605.0434	72.4406	527.8664	25.1037	899.0176	108.5458	527.1560	23.8661
401 - 8	2	1.0445	0.0693	2.5722	13.77	111.54	0.7813	0.0861	0.0856	0.0040	2.4349	0.1598	11.6804	0.5304	0.0660	0.0071	586.2090	64.6149	529.4044	24.5490	803.9396	87.1206	529.5426	24.0444
401 - 9	2	1.0282	0.0716	2.4931	13.74	105.02	0.8113	0.0906	0.0846	0.0043	2.3978	0.1556	11.8052	0.5884	0.0692	0.0077	603.1904	67.3394	523.6622	26.5834	904.2037	100.2378	524.1632	26.1234
MAD	2	1.8465	0.1952	13.7654	25.60	650.08	0.5985	0.0150	0.0755	0.0013	7.7090	0.2421	13.2628	0.2468	0.0566	0.0050	476.2954	11.9340	469.0094	7.9363	475.2640	41.9907	468.5993	8.7186
MAD	2	1.8692	0.2113	13.7753	25.10	646.93	0.6111	0.0153	0.0770	0.0013	7.6677	0.2413	12.9643	0.2412	0.0566	0.0050	484.2832	12.1341	478.4502	8.0961	473.6883	41.9038	478.9961	8.9120

MAD: Madagascar; McClure: McClure Mountains

Appendix 5 Table A1 LA-ICP-MS U-Pb apatite data collected in this study

Apatite U-Pb Standard reference materials

Sample	Analytical Session	^{206}Pb ppm	^{207}Pb ppm	^{208}Pb ppm	U ppm	Th ppm	$^{207}Pb/^{235}U$ (calc)	±2SE	$^{206}Pb/^{238}U$	±2SE	$^{208}Pb/^{206}Pb$	±2SE	$^{238}U/^{206}Pb$	±2SE	$^{207}Pb/^{206}Pb$	±2SE	$^{207}Pb/^{235}U$ (calc) Age (Ma)	±2SE	$^{206}Pb/^{238}U$ Age (Ma)	±2SE	$^{207}Pb/^{206}Pb$ Age (Ma)	±2SE	$^{238}U/^{206}Pb$ Age (Ma)	±2SE
MAD	2	1.8488	0.2149	14.2506	25.08	638.89	0.6027	0.0151	0.0763	0.0014	8.0689	0.2523	13.1076	0.2305	0.0566	0.0051	478.9445	12.0003	474.0022	8.4563	475.6768	42.6248	473.9469	8.3359
MAD	2	1.8579	0.2329	13.5528	24.92	638.61	0.6018	0.0151	0.0762	0.0014	7.6931	0.2449	13.1197	0.2308	0.0566	0.0051	478.3749	11.9861	473.4691	8.4468	475.4114	42.8179	473.5281	8.3285
MAD	2	1.8479	0.2456	13.7368	24.91	636.75	0.5899	0.0148	0.0755	0.0024	7.8874	0.2873	13.2483	0.4066	0.0566	0.0051	470.8048	11.7964	468.9823	14.7584	473.8691	42.9455	469.0919	14.3972
MAD	2	1.8124	0.1990	13.4932	24.62	635.51	0.6030	0.0151	0.0771	0.0024	7.7385	0.2913	12.9714	0.3981	0.0566	0.0051	479.1526	12.0056	478.7613	15.0662	475.3786	43.0702	478.7434	14.6935
MAD	2	1.7897	0.2063	13.3688	25.00	637.62	0.5872	0.0147	0.0750	0.0028	7.7915	0.2548	13.3204	0.4858	0.0566	0.0052	469.1028	11.7538	466.3266	17.4310	473.7603	43.4274	466.6447	17.0183
MAD	2	1.8440	0.2220	13.5598	24.77	634.38	0.6064	0.0152	0.0775	0.0029	7.7124	0.2735	12.9124	0.4709	0.0566	0.0051	481.2910	12.0591	480.9499	17.9776	474.9321	42.9227	480.8513	17.5364
MAD	2	1.8156	0.2085	13.2850	24.59	626.17	0.6073	0.0152	0.0775	0.0021	7.6361	0.2477	12.9092	0.3394	0.0566	0.0051	481.8556	12.0733	480.9816	12.8689	475.2528	42.9817	480.9670	12.6448
MAD	2	1.7697	0.2201	13.5753	24.44	631.93	0.5879	0.0147	0.0750	0.0020	8.0869	0.2969	13.3313	0.3505	0.0566	0.0052	469.5375	11.7646	466.0228	12.4687	475.0638	43.9014	466.2756	12.2585
MAD	2	1.8079	0.2256	13.5770	24.44	632.04	0.5995	0.0150	0.0763	0.0002	7.9085	0.2566	13.1089	0.0387	0.0566	0.0052	476.9250	11.9497	473.8503	1.1246	474.1864	43.3342	473.9015	1.3975
MAD	2	1.8274	0.2301	13.6879	24.64	630.93	0.5998	0.0150	0.0762	0.0002	7.9056	0.2541	13.1246	0.0387	0.0566	0.0052	477.0828	11.9537	473.4146	1.1236	475.7624	43.2947	473.3566	1.3959
MAD	2	1.9064	0.2653	13.9243	24.77	641.21	0.6126	0.0154	0.0763	0.0010	7.7980	0.2492	13.1069	0.1604	0.0566	0.0051	485.2233	12.1577	473.8478	6.0887	474.3709	42.8270	473.9738	5.8014
MAD	2	1.8152	0.2128	13.6543	24.37	626.78	0.6114	0.0153	0.0762	0.0010	7.8663	0.2503	13.1297	0.1607	0.0566	0.0051	484.4142	12.1374	473.3086	6.0818	474.8380	42.7869	473.1799	5.7917
MAD	2	1.8142	0.2050	13.8803	25.03	633.07	0.6039	0.0151	0.0768	0.0012	7.9798	0.2672	13.0182	0.2072	0.0566	0.0051	479.6832	12.0189	477.2245	7.7183	476.0708	43.0164	477.0865	7.5921
MAD	2	1.7376	0.2068	12.9749	24.16	617.47	0.5942	0.0149	0.0756	0.0012	7.8264	0.2523	13.2209	0.2104	0.0566	0.0052	473.5209	11.8645	469.8358	7.5988	475.8717	43.4743	470.0315	7.4799
MAD	2	1.8257	0.2233	13.6921	24.73	637.88	0.5977	0.0150	0.0767	0.0011	7.8919	0.2528	13.0405	0.1939	0.0566	0.0052	475.7936	11.9214	476.1898	7.0151	475.1004	43.4350	476.2999	7.0839
MAD	2	1.7552	0.2062	13.3792	24.24	626.91	0.5907	0.0148	0.0758	0.0011	7.9820	0.2585	13.1982	0.1963	0.0566	0.0052	471.3316	11.8096	470.8900	6.9370	475.4374	44.0865	470.8103	7.0022
MAD	2	1.7796	0.1966	13.1848	24.74	628.08	0.5968	0.0150	0.0768	0.0014	7.7023	0.2485	13.0249	0.2399	0.0566	0.0052	475.1862	11.9062	476.8677	8.5591	475.7205	43.5235	476.8476	8.7822
MAD	2	1.7665	0.2218	13.5002	24.40	627.33	0.5886	0.0147	0.0757	0.0014	8.0694	0.2605	13.2153	0.2434	0.0566	0.0052	469.9752	11.7756	470.1619	8.4388	475.8658	44.1148	470.2246	8.6602
MAD	2	1.7999	0.2083	13.6745	24.37	626.28	0.6097	0.0153	0.0768	0.0013	7.9484	0.2568	13.0092	0.2187	0.0566	0.0052	483.3594	12.1110	477.1508	7.9966	475.8053	43.4734	477.4028	8.0257
MAD	2	1.8026	0.2221	13.3672	24.54	621.18	0.6004	0.0150	0.0757	0.0013	7.8153	0.2550	13.2242	0.2223	0.0567	0.0052	477.4957	11.9640	470.1253	7.8789	477.4671	43.8446	469.9184	7.8998
MAD	2	1.8002	0.2255	13.5206	24.51	629.88	0.5979	0.0150	0.0758	0.0008	7.9134	0.2917	13.1913	0.1263	0.0566	0.0052	475.9268	11.9247	470.7964	4.9553	474.8131	43.8022	471.0497	4.5112
MAD	2	1.8089	0.2258	13.4185	24.32	626.11	0.6057	0.0152	0.0767	0.0008	7.8152	0.2545	13.0380	0.1249	0.0566	0.0052	480.8393	12.0478	476.6211	5.0166	474.9016	43.6778	476.3863	4.5623
MAD	2	1.8443	0.2109	13.8135	24.89	634.33	0.6112	0.0153	0.0761	0.0005	7.8107	0.2724	13.1292	0.0733	0.0566	0.0051	484.2907	12.1343	473.0240	3.4057	474.0267	43.0774	473.1973	2.6409
MAD	2	1.7919	0.1999	13.2021	24.23	627.28	0.6128	0.0154	0.0764	0.0005	7.6624	0.2642	13.1011	0.0731	0.0566	0.0052	485.3440	12.1607	474.3689	3.4154	475.5786	43.4974	474.1754	2.6463
MAD	2	1.8442	0.2561	13.5917	24.57	634.93	0.6015	0.0151	0.0759	0.0007	7.8714	0.2606	13.1563	0.1015	0.0566	0.0052	478.1626	11.9808	471.8414	4.3364	474.2416	43.7124	472.2579	3.6448
MAD	2	1.7918	0.2006	13.7364	24.57	636.54	0.6061	0.0152	0.0765	0.0007	7.9868	0.2614	13.0762	0.1009	0.0566	0.0052	481.1229	12.0549	475.4613	4.3697	476.1914	43.5153	475.0445	3.6663
MAD	2	1.7970	0.1880	13.3182	24.89	635.02	0.6038	0.0151	0.0765	0.0009	7.6607	0.2651	13.0682	0.1352	0.0566	0.0052	479.6230	12.0173	475.4949	5.4381	475.5581	43.3184	475.3247	4.9168
MAD	2	1.7822	0.1878	13.6844	24.87	632.66	0.5988	0.0150	0.0759	0.0009	7.9424	0.2825	13.1642	0.1362	0.0566	0.0052	476.4849	11.9387	471.8018	5.3959	474.4132	43.5722	471.9844	4.8823
McClure - 1	2	0.9745	0.2099	1.1107	10.32	29.53	3.1491	0.2212	0.1051	0.0040	1.1265	0.0962	9.5179	0.3711	0.2139	0.0147	1444.7852	101.4644	644.1794	24.7811	2934.3931	201.2896	644.0217	25.1104
McClure - 10	2	2.1755	0.4775	3.1968	23.18	90.52	3.2055	0.1625	0.1059	0.0040	1.4555	1.4555	0.0915	9.4455	0.3443	0.2185	0.0095	1458.4941	73.9508	25.9657	3311.5471	205.7971	699.2555	25.6299
McClure - 11	2	0.9021	0.2458	1.1059	8.84	20.84	4.3210	0.2833	0.1146	0.0043	1.2124	0.1060	8.7280	0.3199	0.2711	0.0168	1697.3677	111.2884	699.3838	24.2841	2968.7830	128.7485	648.7178	23.6471
McClure - 12	2	0.9968	0.2811	1.1825	9.44	24.32	4.6261	0.2982	0.1184	0.0042	1.1732	1.1732	0.1092	8.4382	0.2963	0.2805	0.0163	1753.9911	113.0734	25.9657	3311.5471	205.7971	699.2555	25.6299
McClure - 13	2	1.8833	0.3297	1.9039	21.49	56.47	2.3895	0.1371	0.0968	0.0029	1.0007	1.0007	0.0659	10.3326	0.2987	0.1742	0.0091	1239.4608	71.1330	25.6759	3365.2248	195.4937	721.9721	25.3515
McClure - 14	2	1.3220	0.2651	1.3921	14.19	35.25	2.9115	0.1839	0.1030	0.0036	1.0442	1.0442	0.0805	9.7220	0.3195	0.1998	0.0117	1384.9137	87.4683	17.6158	2597.7756	135.0494	595.5145	17.2176
McClure - 15	2	0.7211	0.1880	0.8112	7.28	17.50	4.0510	0.2951	0.1124	0.0049	1.1131	1.1131	0.1128	8.8697	0.3845	0.2594	0.0183	1644.5010	119.8047	22.3159	2823.4456	164.7479	631.1443	20.7405
McClure - 16	2	0.7799	0.2087	0.7910	7.88	18.65	4.1579	0.2892	0.1125	0.0047	1.0022	1.0022	0.1018	8.8578	0.3706	0.2660	0.0178	1665.7565	115.8489	29.9249	3242.4297	229.1053	688.6619	29.8546
McClure - 17	2	0.7900	0.2011	0.8840	8.46	25.03	3.6770	0.2762	0.1055	0.0044	1.1079	1.1079	0.1095	9.4771	0.2531	0.0181	1566.3887	117.6726	646.7607	26.8401	3203.2969	229.3451	646.6630	26.6853
McClure - 18	2	0.7672	0.1835	0.8335	7.56	19.22	3.7561	0.2765	0.1148	0.0049	1.0745	1.0745	0.1073	8.7064	0.2376	0.0169	1583.4162	116.5420	700.5603	29.6729	3103.1654	220.8805	700.8955	29.5166
McClure - 19	2	3.0587	0.4716	3.1142	32.90	101.29	2.2338	0.1494	0.1062	0.0037	1.0074	1.0074	0.0757	9.4207	0.3292	0.1531	0.0095	1191.7028	79.7158	650.4141	22.6759	2379.6977	148.4383	650.3425	22.7270
McClure - 2	2	0.9510	0.2284	1.0936	10.11	28.64	3.4934	0.2326	0.1044	0.0041	1.1378	0.0989	9.5692	0.3788	0.2387	0.0151	1525.7322	101.5929	640.3125	24.9985	3110.5011	196.5393	640.7331	25.3611

MAD: Madagascar; McClure: McClure Mountains

Appendix 5 Table A1 LA-ICP-MS U-Pb apatite data collected in this study

Sample	Analytical Session	^{206}Pb ppm	^{207}Pb ppm	^{208}Pb ppm	U ppm	Th ppm	^{207}Pb/^{235}U (calc)	±2SE	^{206}Pb/^{238}U	±2SE	^{208}Pb/^{206}Pb	±2SE	^{238}U/^{206}Pb	±2SE	^{207}Pb/^{206}Pb	±2SE	^{207}Pb/^{235}U (calc) Age (Ma)	±2SE	^{206}Pb/^{238}U Age (Ma)	±2SE	^{207}Pb/^{206}Pb Age (Ma)	±2SE	^{238}U/^{206}Pb Age (Ma)	±2SE
McClure - 20	2	2.5734	0.4117	2.4470	28.95	78.19	2.2160	0.4862	0.1014	0.0103	0.9403	0.0995	9.8514	0.6558	0.1588	0.0133	1186.0969	260.2138	622.5026	63.0491	2441.9017	205.2894	623.2406	41.4874
McClure - 21	2	0.8089	0.2021	0.8779	8.12	19.18	3.8964	0.2899	0.1119	0.0047	1.0721	0.1166	8.9194	0.3701	0.2484	0.0168	1612.9433	119.9865	683.6190	28.5242	3173.7117	214.2264	685.0167	28.4201
McClure - 22	2	0.8426	0.2143	0.8884	9.11	22.22	3.6812	0.2742	0.1038	0.0043	1.0425	0.1002	9.6202	0.3917	0.2530	0.0174	1567.2909	116.7515	636.6632	26.0728	3203.1410	219.6856	637.5035	25.9558
McClure - 23	2	1.3256	0.3077	1.4131	14.08	37.72	3.4107	0.2028	0.1058	0.0037	1.0540	0.0806	9.4417	0.3024	0.2308	0.0126	1506.8621	89.5911	648.4369	22.3803	3057.0094	166.6534	648.9645	20.7858
McClure - 24	2	1.4438	0.2862	1.8221	15.57	49.82	2.8707	0.1844	0.1043	0.0034	1.2490	0.0847	9.6004	0.2966	0.1972	0.0113	1374.2517	88.2788	639.3173	20.6136	2802.7591	160.8964	638.7551	19.7339
McClure - 25	2	1.5696	0.3458	2.3476	16.77	72.85	3.2165	0.1962	0.1036	0.0035	1.4794	0.0919	9.6441	0.3011	0.2190	0.0115	1461.1402	89.1449	635.3861	21.7212	2972.5737	156.3092	635.9956	19.8567
McClure - 26	2	2.4304	0.3594	2.3224	29.60	79.88	1.8947	0.1128	0.0910	0.0024	0.9458	0.0628	10.9981	0.2695	0.1470	0.0085	1079.2291	64.2479	561.4613	14.7670	2311.1223	132.9526	561.0044	13.7449
McClure - 27	2	1.1963	0.2951	1.7070	12.09	47.57	3.8223	0.2550	0.1114	0.0038	1.4112	0.1096	8.9766	0.3021	0.2453	0.0151	1597.4503	106.5623	680.9732	23.3780	3153.7704	194.2120	680.8741	22.9144
McClure - 28	2	1.8968	0.3375	2.0467	21.56	66.65	2.4487	0.1397	0.0988	0.0028	1.0689	0.0742	10.1151	0.2784	0.1771	0.0090	1257.0469	71.7216	607.6415	17.3924	2625.2224	134.0422	607.7344	16.7283
McClure - 29	2	1.4452	0.3420	1.5161	15.27	40.47	3.5030	0.2478	0.1067	0.0039	1.0386	0.0907	9.3785	0.3157	0.2357	0.0132	1527.8827	108.0955	653.8015	23.7530	3090.1511	173.4120	653.1262	21.9840
McClure - 3	2	1.0993	0.2259	1.1733	11.84	33.84	2.9544	0.1954	0.1036	0.0039	1.0586	0.1007	9.6673	0.3589	0.2047	0.0127	1395.9775	92.3485	635.3349	23.9128	2863.3350	178.2520	634.5443	23.5607
McClure - 30	2	1.6652	0.3383	1.8607	18.28	52.77	2.8930	0.2248	0.1025	0.0034	1.1062	0.0754	9.7308	0.3178	0.2023	0.0133	1380.0831	107.2182	628.8304	21.0759	2844.3776	187.5409	630.6015	20.5960
McClure - 4	2	0.7736	0.1961	0.8268	7.57	18.89	4.0108	0.2854	0.1141	0.0049	1.0584	0.1046	8.7655	0.3725	0.2522	0.0173	1636.3962	116.4577	696.2846	29.9055	3198.2179	219.5695	696.4167	29.5947
McClure - 5	2	2.2369	0.2628	2.1676	26.98	77.49	1.5046	0.0986	0.0932	0.0038	0.9589	0.0588	10.7537	0.4220	0.1170	0.0069	932.2502	61.0668	574.2462	23.1710	1909.8461	112.2852	573.2031	22.4920
McClure - 6	2	2.2776	0.2678	2.3483	27.95	82.59	1.4794	0.0907	0.0915	0.0037	1.0214	0.0604	10.9536	0.4285	0.1172	0.0065	922.0043	56.4965	564.2766	22.7016	1912.4374	106.0391	563.1856	22.0325
McClure - 7	2	1.1573	0.2105	1.2137	13.10	35.88	2.4965	0.1701	0.0997	0.0050	1.0390	0.0894	10.0461	0.4900	0.1812	0.0127	1271.0291	86.6219	612.5460	30.8946	2662.9162	186.9079	611.7201	29.8378
McClure - 8	2	1.0057	0.1990	1.0305	10.99	25.45	2.8162	0.1974	0.1035	0.0053	1.0110	0.0905	9.6461	0.4845	0.1966	0.0131	1359.8570	95.3222	634.6434	32.6221	2797.0905	186.7941	635.8750	31.9409
McClure - 9	2	2.3998	0.5034	4.8026	25.26	151.92	3.1039	0.1890	0.1074	0.0041	1.9799	0.1263	9.3144	0.3342	0.2087	0.0103	1433.6581	87.2887	657.7265	25.0057	2894.4067	142.6223	657.3999	23.5909

MAD: Madagascar; McClure: McClure Mountains

Appendix 5 Table A2: LA-ICP-MS Trace element data collected for apatite from Vulcan Prospect in this study

Included Data

Sample	Drill hole	Comment	Si	P	Ca	V	Mn	Fe	Sr	Y	Zr	Th	U
801_apatite - 10	VUD 009 801	LREE depleted	1120.84	187323.30	394000	0.11	92.12	191.86	523.89	685.99	0.01	3.27	6.60
801_apatite - 13	VUD 009 801	LREE depleted	2219.32	178638.44	394000	0.40	74.05	1926.52	660.55	536.17	<0.009	1.82	3.41
801_apatite - 14	VUD 009 801	LREE depleted	10837.80	179205.60	394000	0.20	68.79	379.30	643.64	504.37	0.26	2.70	5.63
801_apatite - 15	VUD 009 801	LREE depleted	3502.00	187250.47	394000	0.47	69.35	173.83	570.50	545.74	0.05	0.65	3.97
801_apatite - 16	VUD 009 801	LREE depleted	596.71	190242.12	394000	<0.040	72.51	81.93	835.52	460.43	0.01	1.55	1.59
801_apatite - 17	VUD 009 801	LREE depleted	15625.77	185366.68	394000	2.58	62.67	2992.89	578.18	362.17	0.14	2.57	4.25
801_apatite - 18	VUD 009 801	LREE depleted	160.97	186596.25	394000	<0.044	77.06	<44.485	544.51	646.29	<0.009	0.72	6.22
801_apatite - 19	VUD 009 801	LREE depleted	1013.96	186304.35	394000	0.18	71.43	628.67	573.04	479.13	0.01	1.59	4.29
801_apatite - 20	VUD 009 801	LREE depleted	320.69	193011.23	394000	1.17	76.22	8388.27	697.56	479.83	0.64	1.27	7.14
801_apatite - 21	VUD 009 801	LREE depleted	1268.80	190583.85	394000	0.06	86.37	163.75	721.96	569.91	<0.008	1.45	2.82
801_apatite - 23	VUD 009 801	LREE depleted	273.41	191012.87	394000	<0.050	74.29	189.28	640.30	494.88	0.51	0.77	8.49
801_apatite - 25	VUD 009 801	LREE depleted	1181.69	190938.05	394000	0.12	54.52	225.45	781.97	129.85	0.02	0.14	0.17
801_apatite - 28	VUD 009 801	LREE depleted	1762.13	192347.16	394000	0.23	75.34	334.15	560.60	729.57	0.03	1.52	10.27
801_apatite - 3	VUD 009 801	LREE depleted	961.72	183620.06	394000	2.01	73.51	147.41	521.99	595.50	0.09	0.70	6.43
801_apatite - 30	VUD 009 801	LREE depleted	391.68	186948.14	394000	0.12	73.86	299.72	592.50	543.35	<0.008	1.77	6.47
801_apatite - 31	VUD 009 801	LREE depleted	196.83	192653.26	394000	<0.044	74.62	63.18	615.43	749.28	0.02	2.70	7.03
801_apatite - 32	VUD 009 801	LREE depleted	1817.79	186085.72	394000	0.16	78.17	1148.59	549.18	734.43	0.09	3.50	8.86
801_apatite - 33	VUD 009 801	LREE depleted	<110.889	190350.36	394000	<0.061	73.86	<41.381	612.69	781.63	0.03	2.63	9.04
801_apatite - 34	VUD 009 801	LREE depleted	16523.52	188562.46	394000	2.06	74.36	1463.86	609.81	589.86	0.21	2.44	4.57
801_apatite - 35	VUD 009 801	LREE depleted	3209.48	190828.99	394000	0.38	70.37	715.53	584.28	606.93	0.12	3.28	8.13
801_apatite - 36	VUD 009 801	LREE depleted	544.78	191389.16	394000	0.15	79.28	436.01	588.89	622.70	0.30	2.41	8.38
801_apatite - 37	VUD 009 801	LREE depleted	2986.76	188521.01	394000	0.49	71.50	457.51	573.33	613.18	6.70	3.20	8.44
801_apatite - 38	VUD 009 801	LREE depleted	4503.58	187762.37	394000	1.63	76.50	393.42	585.44	563.70	0.03	2.27	5.08
801_apatite - 4	VUD 009 801	LREE depleted	2088.60	184249.13	394000	0.44	72.92	1568.47	605.34	520.55	0.04	2.56	5.41
801_apatite - 42	VUD 009 801	LREE depleted	791.42	190245.96	394000	0.15	70.91	343.80	701.41	538.93	0.02	2.62	3.49
801_apatite - 43	VUD 009 801	LREE depleted	193.22	186335.88	394000	<0.043	73.86	240.97	613.63	515.50	0.02	1.83	4.46
801_apatite - 44	VUD 009 801	LREE depleted	442.42	190532.11	394000	0.03	75.58	71.21	765.78	635.07	<0.017	2.37	3.13
801_apatite - 47	VUD 009 801	LREE depleted	2052.88	193652.61	394000	0.40	78.25	441.21	556.83	584.57	0.05	2.70	6.33
801_apatite - 48	VUD 009 801	LREE depleted	4652.77	195336.80	394000	1.07	72.86	1233.96	668.44	491.67	3.53	0.44	2.55
801_apatite - 5	VUD 009 801	LREE depleted	4916.14	184483.85	394000	2.73	68.23	620.82	583.36	496.17	0.13	1.44	4.73
801_apatite - 50	VUD 009 801	LREE depleted	2055.50	190038.62	394000	0.11	69.27	472.95	620.80	397.00	0.06	0.77	4.45
801_apatite - 51	VUD 009 801	LREE depleted	199.21	193988.86	394000	<0.041	83.73	48.54	606.91	608.18	0.01	2.56	4.49
801_apatite - 54	VUD 009 801	LREE depleted	166.77	189316.49	394000	<0.042	78.97	56.96	720.54	425.92	0.07	1.60	1.98
801_apatite - 55	VUD 009 801	LREE depleted	1129.76	190445.10	394000	0.30	83.23	1011.60	681.56	672.74	987.69	10.19	44.14
801_apatite - 6	VUD 009 801	LREE depleted	1777.35	187003.55	394000	0.95	75.45	1693.30	605.32	523.90	0.06	1.64	4.67
801_apatite - 7	VUD 009 801	LREE depleted	5575.53	185764.60	394000	0.81	75.89	653.05	536.42	474.54	0.02	1.21	4.16
801_apatite - 9	VUD 009 801	LREE depleted	544.44	188235.49	394000	0.09	83.36	324.16	624.37	689.88	0.02	3.41	5.19
852_apatite - 47	VUD 009 852		178.56	194758.64	394000	0.05	1218.61	1140.29	63.73	306.93	0.04	108.94	49.32
852_apatite - 10	VUD 009 852		239.16	176855.42	394000	0.07	673.77	2498.45	153.05	547.54	0.08	68.52	183.11
852_apatite - 2	VUD 009 852		<190.050	195393.94	394000	<0.072	127.30	2930.47	122.60	1355.15	0.07	52.11	15.52
852_apatite - 62	VUD 009 852		198.39	188955.74	394000	0.18	441.43	3363.51	102.19	481.37	0.04	317.90	120.89
852_apatite - 28	VUD 009 852		234.23	190597.75	394000	0.11	462.95	3715.63	58.53	273.16	0.03	34.68	50.69
852_apatite - 7	VUD 009 852		219.95	193323.25	394000	0.15	553.53	3719.90	98.19	489.16	0.06	193.41	213.09
852_apatite - 27	VUD 009 852		265.51	186944.27	394000	0.13	791.28	5540.77	127.79	828.77	0.15	247.12	358.24
852_apatite - 52	VUD 009 852		478.03	187060.27	394000	0.21	1060.88	8099.87	116.12	705.42	0.06	205.00	181.68
852_apatite - 40	VUD 009 852		181.44	193614.12	394000	0.20	850.28	8349.00	93.81	903.71	0.15	82.76	281.07
852_apatite - 37	VUD 009 852		307.97	189955.82	394000	0.33	776.08	8792.82	84.94	267.75	0.06	291.92	22.96
973_apatite - 11	VUD 009 973		415.75	186797.21	394000	2.04	321.66	3501.00	137.54	986.97	0.31	20.66	104.41
973_apatite - 12	VUD 009 973		640.08	191244.03	394000	1.78	163.78	8924.09	307.66	325.10	3.50	16.40	42.82
973_apatite - 13	VUD 009 973		1783.76	190028.97	394000	0.41	168.72	1623.73	372.68	318.13	11.10	11.79	28.89
973_apatite - 14	VUD 009 973		425.05	190492.89	394000	0.51	85.86	2559.89	602.89	388.73	277.35	6.30	41.87
973_apatite - 16	VUD 009 973		1179.07	189701.80	394000	1.72	224.16	6638.86	177.24	438.83	0.49	30.18	59.76
973_apatite - 18	VUD 009 973		2341.83	192874.30	394000	0.86	150.84	2748.27	410.31	357.96	3.09	13.11	46.43
973_apatite - 23	VUD 009 973		500.46	196757.57	394000	0.88	264.70	2102.15	505.98	478.31	0.11	43.98	32.08
973_apatite - 25	VUD 009 973		30097.25	162373.47	394000	0.97	116.37	3915.14	594.65	540.80	14.26	76.45	13.17
973_apatite - 27	VUD 009 973		818.61	188749.37	394000	1.14	120.69	4301.06	378.33	322.09	0.23	9.89	37.07
973_apatite - 28	VUD 009 973		3428.47	193641.19	394000	0.82	172.07	1274.22	440.55	319.48	15.29	6.76	34.85
973_apatite - 3	VUD 009 973		6696.11	188129.08	394000	4.49	110.65	8548.47	432.74	362.61	132.12	6.54	31.30
973_apatite - 30	VUD 009 973		521.87	190296.70	394000	2.13	248.54	3253.72	483.62	333.73	0.57	20.49	67.90
973_apatite - 31	VUD 009 973		1601.85	190995.19	394000	0.61	244.28	1549.97	254.94	650.96	51.14	75.36	65.70
973_apatite - 32	VUD 009 973		424.24	190057.59	394000	0.16	89.64	155.57	431.29	155.67	0.01	3.40	11.20
973_apatite - 33	VUD 009 973		339.00	191368.63	394000	0.85	259.07	1142.52	391.61	636.35	0.41	33.91	173.37
973_apatite - 36	VUD 009 973		217.29	190676.33	394000	0.26	201.32	<49.135	694.81	160.61	<0.021	13.39	21.88
973_apatite - 37	VUD 009 973		<256.459	186255.35	394000	0.14	66.96	<82.531	765.26	144.12	0.06	0.71	0.12
973_apatite - 4	VUD 009 973		800.04	190615.36	394000	0.24	285.98	135.03	176.28	368.81	<0.019	7.94	41.20
973_apatite - 41	VUD 009 973		399.37	186052.93	394000	0.33	164.83	682.60	444.63	292.50	0.09	10.50	30.39
973_apatite - 42	VUD 009 973		224.99	187927.96	394000	0.10	145.67	473.75	487.48	182.66	0.67	1.47	2.71
973_apatite - 43	VUD 009 973		423.16	193683.93	394000	0.45	126.79	1012.26	635.09	200.02	3.05	32.81	12.31
973_apatite - 44	VUD 009 973		1667.64	189660.30	394000	0.76	221.83	1416.96	266.20	362.50	0.07	52.29	58.18
973_apatite - 45	VUD 009 973		259.91	191768.89	394000	<0.047	63.22	65.32	517.27	223.04	<0.012	2.33	2.43
973_apatite - 47	VUD 009 973		4410.96	191074.43	394000	0.98	340.12	1299.39	194.41	511.03	0.79	53.51	86.27

Element concentrations in ppm
$Eu/Eu^{*} = [(Eu_{CN}/(Sm_{CN}+Gd_{CN})/2)]$
$Y/Y^{*} = [(Y_{CN}/(Dy_{CN}+Ho_{CN})/2)]$
$TCe/Ce^{*} = [(Ce_{CN}/(La_{CN} \times Pr_{CN})^{0.5})]$
$LCe/Ce^{*} = [(Ce_{CN}/((Nd_{CN})^{0.5}/Sm_{CN}))]$
CN = chondrite normalised
Normalising values from Sun and McDonough (1989)

Appendix 5 Supplementary material for Mapping hydrothermal systems in IOCG deposits using apatite geochronology and geochemsitry: An example from Vulcan Cu-Au prospect

Appendix 5 Table A2: LA-ICP-MS Trace element data collected for apatite from Vulcan Prospect in this study

Included Data

Sample	La	Ce	Pr	Nd	Sm	Eu	Gd	Tb	Dy	Ho	Er	Tm	Yb	Lu	Hf
801_apatite - 10	0.06	0.87	0.56	9.67	61.20	41.91	570.92	102.20	414.09	37.23	42.23	3.05	14.43	1.46	0.01
801_apatite - 13	0.07	0.97	0.45	9.44	51.91	38.99	481.55	83.83	331.62	30.00	31.62	2.07	10.29	0.95	<0.008
801_apatite - 14	0.33	2.04	0.90	15.84	60.01	34.45	451.58	77.91	316.83	27.94	32.10	2.34	10.33	0.91	0.06
801_apatite - 15	0.10	0.69	0.35	7.33	50.56	36.50	475.60	82.74	338.68	29.93	32.64	2.16	9.55	1.06	<0.005
801_apatite - 16	0.10	1.08	0.69	12.59	79.96	48.92	577.89	84.15	300.68	25.85	27.14	1.87	8.17	0.77	<0.004
801_apatite - 17	0.06	0.84	0.56	8.23	45.15	28.48	363.23	60.45	229.28	20.03	20.45	1.67	6.86	0.67	0.02
801_apatite - 18	0.06	0.74	0.41	8.18	56.82	38.42	533.64	96.62	387.78	35.08	40.80	3.00	13.73	1.55	<0.005
801_apatite - 19	0.34	1.37	0.50	7.70	52.75	33.84	440.34	74.27	294.70	25.74	29.63	2.15	9.65	0.96	0.02
801_apatite - 20	0.12	1.08	0.52	10.75	57.15	36.34	443.67	77.06	303.26	26.23	30.39	2.30	9.69	0.97	0.07
801_apatite - 21	0.06	0.98	0.61	10.52	65.73	44.84	554.45	91.84	361.50	31.44	34.74	2.43	10.56	1.11	0.01
801_apatite - 23	0.74	2.94	0.82	10.77	56.52	35.21	447.09	76.48	299.33	26.63	31.49	2.50	11.40	1.07	0.01
801_apatite - 25	0.03	0.42	0.27	5.86	29.98	18.96	212.90	28.93	98.08	8.05	7.63	0.47	2.09	0.16	0.00
801_apatite - 28	0.16	1.13	0.59	9.92	68.20	43.98	611.14	109.89	443.92	39.63	46.75	2.98	13.90	1.44	<0.005
801_apatite - 3	0.17	1.04	0.56	8.08	57.04	39.00	518.05	91.35	363.87	31.98	38.05	2.86	11.99	1.30	<0.005
801_apatite - 30	0.08	1.09	0.62	11.98	62.44	36.75	491.10	81.32	310.76	28.57	36.79	2.88	13.05	1.28	0.01
801_apatite - 31	0.06	0.83	0.52	9.54	68.99	47.97	658.32	114.91	463.06	40.42	45.52	3.10	12.61	1.29	0.03
801_apatite - 32	0.06	0.85	0.51	9.73	67.67	45.02	603.73	107.16	440.35	39.45	46.49	3.14	13.92	1.45	0.04
801_apatite - 33	0.06	1.07	0.73	13.66	86.77	49.68	650.55	106.18	404.94	38.40	55.27	4.59	18.32	1.87	<0.005
801_apatite - 34	0.28	1.26	0.48	8.62	55.31	39.15	511.33	91.50	365.12	32.56	36.12	2.37	10.73	1.04	0.03
801_apatite - 35	0.08	0.99	0.62	11.57	68.31	39.88	555.71	93.14	356.19	31.81	39.82	3.00	13.35	1.27	0.05
801_apatite - 36	0.06	0.98	0.67	10.83	67.91	40.44	548.64	95.75	381.03	33.91	41.08	3.01	14.00	1.38	0.06
801_apatite - 37	0.03	0.94	0.53	10.08	63.28	39.35	547.61	95.29	377.66	33.55	39.10	2.89	12.91	1.36	0.22
801_apatite - 38	0.03	0.64	0.46	7.38	53.98	37.78	501.82	87.27	351.78	31.18	36.40	2.56	10.81	1.08	<0.005
801_apatite - 4	0.08	1.17	0.71	11.11	61.10	35.25	451.76	72.57	275.37	26.23	36.41	3.09	14.61	1.38	<0.004
801_apatite - 42	0.18	1.56	0.77	11.14	57.70	40.19	504.93	85.78	340.72	29.54	31.96	2.23	9.83	0.98	<0.005
801_apatite - 43	0.07	1.32	0.75	11.51	60.85	33.46	406.72	66.76	255.37	25.09	36.22	3.24	14.94	1.55	0.02
801_apatite - 44	0.12	1.01	0.65	10.61	75.97	50.78	633.90	105.59	407.51	35.33	37.42	2.49	10.40	1.14	<0.005
801_apatite - 47	0.02	0.76	0.48	9.29	57.07	39.01	510.10	87.56	364.42	33.26	38.13	2.79	11.18	1.32	0.06
801_apatite - 48	0.12	0.88	0.54	7.91	48.65	35.86	460.25	77.87	311.03	27.62	32.15	2.07	9.33	0.88	0.16
801_apatite - 5	0.06	1.08	0.63	10.61	62.85	34.73	427.53	68.50	262.33	24.67	34.78	2.91	13.07	1.36	0.03
801_apatite - 50	0.03	0.90	0.50	8.42	47.73	29.36	379.81	62.77	244.02	21.92	25.13	1.99	9.36	0.99	0.08
801_apatite - 51	0.05	0.81	0.47	8.88	57.41	39.23	534.15	93.37	378.53	33.28	37.74	2.59	12.12	1.26	0.01
801_apatite - 54	0.05	0.85	0.58	8.33	48.71	33.23	414.11	69.64	277.99	24.16	27.44	1.85	8.94	0.91	0.02
801_apatite - 55	0.07	1.02	0.50	9.94	57.53	39.73	520.80	91.59	378.28	36.68	48.97	4.76	28.32	3.91	26.39
801_apatite - 6	0.06	1.34	0.69	11.36	63.29	33.07	412.47	66.86	257.19	25.18	37.26	3.33	15.20	1.56	0.01
801_apatite - 7	0.05	0.67	0.40	8.04	47.24	33.67	424.84	73.15	292.81	26.18	31.01	2.04	9.95	0.93	<0.005
801_apatite - 9	0.06	0.85	0.59	9.33	65.17	43.80	594.21	104.16	423.91	38.01	41.62	2.91	13.15	1.37	0.02
852_apatite - 47	25.77	129.75	37.16	252.80	94.58	13.53	103.70	14.09	87.24	15.55	38.06	3.93	20.97	2.28	0.01
852_apatite - 10	29.48	251.56	61.44	420.52	160.86	22.52	162.67	19.97	111.02	21.35	56.14	6.98	42.45	5.30	0.01
852_apatite - 2	31.06	759.52	88.41	743.63	414.03	67.55	493.02	61.14	328.31	61.07	150.79	16.59	82.47	9.88	<0.006
852_apatite - 62	14.74	147.35	38.18	300.96	132.83	19.48	152.74	19.83	102.29	20.17	50.62	6.14	35.48	4.44	<0.007
852_apatite - 28	6.64	104.13	33.00	271.86	138.06	20.82	145.23	17.27	81.98	12.91	28.24	2.93	16.87	1.95	<0.004
852_apatite - 7	38.96	199.16	60.66	405.80	157.76	23.33	167.20	21.41	116.48	21.24	53.16	5.91	32.16	4.01	0.01
852_apatite - 27	22.05	268.16	52.85	364.37	155.98	26.91	205.08	29.52	178.76	36.35	100.77	13.23	78.21	10.44	<0.004
852_apatite - 52	39.08	762.61	75.17	443.54	136.26	19.34	160.33	21.32	131.04	27.19	76.26	10.28	62.95	8.64	<0.005
852_apatite - 40	21.92	739.95	58.93	424.86	169.71	25.89	205.01	27.81	165.79	35.78	105.22	13.93	83.44	11.06	0.03
852_apatite - 37	13.24	125.06	33.38	256.63	120.29	19.19	133.20	15.42	79.80	13.37	31.87	3.44	17.48	2.02	<0.004
973_apatite - 11	44.52	146.09	14.01	52.97	17.84	7.16	88.21	26.01	196.65	37.89	89.59	8.13	37.97	4.65	<0.005
973_apatite - 12	1.02	4.10	0.75	4.87	15.80	10.57	112.04	15.50	87.28	14.57	31.94	3.08	12.63	1.41	0.07
973_apatite - 13	6.63	21.42	2.22	10.85	20.28	13.91	135.86	16.17	78.61	13.05	28.36	2.45	11.22	1.29	0.40
973_apatite - 14	1.81	4.87	1.05	8.61	29.64	21.83	223.99	20.77	83.62	14.55	38.38	4.02	27.01	3.79	8.29
973_apatite - 16	3.36	11.82	1.30	7.83	13.65	7.15	79.76	16.28	104.82	18.26	38.04	3.15	13.34	1.56	0.01
973_apatite - 18	15.84	70.44	4.70	18.79	23.10	14.75	142.43	16.67	82.71	14.23	30.83	2.75	12.12	1.49	0.11
973_apatite - 23	3.35	9.09	1.29	8.49	22.92	14.56	145.10	20.12	125.29	24.26	53.89	5.18	20.46	1.99	0.01
973_apatite - 25	37.34	115.29	4.67	19.55	27.51	18.25	184.08	22.56	118.62	22.26	51.71	4.56	19.36	1.60	0.20
973_apatite - 27	1.88	7.30	1.31	7.66	26.61	14.37	144.98	16.46	81.15	12.85	29.68	2.51	12.21	1.31	<0.006
973_apatite - 28	7.44	21.78	2.88	15.95	25.69	14.43	135.11	15.89	81.04	13.39	29.03	2.50	11.37	1.24	0.38
973_apatite - 3	6.70	19.42	2.47	10.39	29.16	18.98	181.33	19.52	83.04	14.08	34.48	3.54	20.39	3.05	5.33
973_apatite - 30	53.74	171.50	17.79	63.40	28.40	12.22	102.61	13.58	72.29	12.01	26.07	2.73	13.45	1.56	0.04
973_apatite - 31	4.60	22.98	0.84	6.42	17.48	11.34	121.25	20.55	133.09	26.87	67.33	6.91	31.48	3.80	1.46
973_apatite - 32	3.67	11.73	1.36	7.40	18.55	9.79	84.56	10.10	43.93	6.52	12.98	1.08	4.61	0.49	<0.004
973_apatite - 33	37.91	116.66	14.09	51.36	22.87	9.98	100.08	18.27	124.07	23.86	53.54	5.44	29.06	4.09	0.01
973_apatite - 36	11.64	48.97	4.73	22.37	18.78	9.09	83.73	9.47	45.64	6.74	12.90	1.14	4.93	0.49	<0.004
973_apatite - 37	0.18	1.21	0.36	6.13	43.36	27.43	242.75	17.30	50.17	6.70	10.29	1.06	4.10	0.33	<0.008
973_apatite - 4	1.40	7.20	1.22	8.62	10.41	4.90	54.34	12.77	89.48	16.22	31.86	2.58	11.93	1.07	<0.003
973_apatite - 41	1.59	7.33	1.46	11.66	24.09	15.03	138.31	15.81	73.33	12.47	26.56	2.37	9.86	1.10	<0.004
973_apatite - 42	0.22	1.56	0.46	4.99	19.10	11.24	102.28	11.43	51.48	7.70	15.13	1.27	4.99	0.57	0.04
973_apatite - 43	3.40	10.44	1.51	9.70	24.63	15.64	146.73	13.95	55.90	8.65	16.25	1.35	5.69	0.66	0.14
973_apatite - 44	4.95	17.52	2.07	9.51	17.35	9.71	100.19	15.24	89.60	16.09	33.94	3.02	13.60	1.59	0.02
973_apatite - 45	0.26	2.04	0.63	6.31	30.19	18.89	178.44	16.86	63.09	8.90	17.98	1.56	6.68	0.73	<0.003
973_apatite - 47	30.83	108.82	10.41	38.09	12.41	5.83	67.36	16.70	116.07	20.10	45.14	4.34	20.42	2.42	<0.005

Element concentrations in ppm

$Eu/Eu^{*} = [(Eu_{CN}/(Sm_{CN}+Gd_{CN})/2)]$

$Y/Y^{*} = [(Y_{CN}/(Dy_{CN}+Ho_{CN})/2)]$

$TCe/Ce^{*} = [(Ce_{CN}/(La_{CN} \times Pr_{CN})^{0.5})]$

$LCe/Ce^{*} = [(Ce_{CN}/((Nd_{CN})^{0.5}/Sm_{CN}))]$

CN = chondrite normalised

Normalising values from Sun and McDonough (1989)

Appendix 5 Supplementary material for Mapping hydrothermal systems in IOCG deposits using apatite geochronology and geochemsitry: An example from Vulcan Cu-Au prospect

Appendix 5 Table A2: LA-ICP-MS Trace element data collected for apatite from Vulcan Prospect in this study

Included Data

Sample	REE	REY	Eu/Eu*	LCe/Ce*	TCe/Ce*	Y/Y*	Ce/Lu	La/Ce	Gd/Yb	La/Sm	Gd/Yb_{CN}	La/Sm_{CN}	La/Ce_{CN}	La/Yb_{CN}
801_apatite - 10	1299.88	1985.87	0.40	0.00	1.11	0.22	0.02	0.07	39.57	0.00	32.73	0.0007	0.19	0.00
801_apatite - 13	1073.77	1609.94	0.44	0.00	1.28	0.22	0.04	0.08	46.78	0.00	38.70	0.0009	0.20	0.01
801_apatite - 14	1033.50	1537.86	0.40	0.00	0.90	0.21	0.09	0.16	43.70	0.01	36.15	0.0035	0.42	0.02
801_apatite - 15	1067.90	1613.63	0.42	0.00	0.89	0.22	0.03	0.14	49.78	0.00	41.18	0.0013	0.37	0.01
801_apatite - 16	1169.87	1630.30	0.44	0.00	0.98	0.21	0.06	0.10	70.70	0.00	58.49	0.0008	0.25	0.01
801_apatite - 17	785.97	1148.14	0.42	0.00	1.12	0.21	0.05	0.07	52.95	0.00	43.81	0.0008	0.18	0.01
801_apatite - 18	1216.81	1863.10	0.40	0.00	1.20	0.22	0.02	0.07	38.86	0.00	32.15	0.0006	0.19	0.00
801_apatite - 19	973.92	1453.05	0.41	0.00	0.80	0.22	0.06	0.25	45.63	0.01	37.74	0.0041	0.64	0.03
801_apatite - 20	999.53	1479.36	0.43	0.00	1.04	0.21	0.05	0.11	45.77	0.00	37.86	0.0014	0.29	0.01
801_apatite - 21	1210.80	1780.72	0.43	0.00	1.22	0.21	0.04	0.06	52.51	0.00	43.44	0.0006	0.16	0.00
801_apatite - 23	1003.00	1497.88	0.42	0.00	0.91	0.22	0.11	0.25	39.21	0.01	32.44	0.0085	0.65	0.05
801_apatite - 25	413.84	543.70	0.46	0.00	1.14	0.18	0.11	0.07	101.62	0.00	84.07	0.0006	0.18	0.01
801_apatite - 28	1393.63	2123.20	0.39	0.00	0.88	0.22	0.03	0.14	43.97	0.00	36.37	0.0015	0.37	0.01
801_apatite - 3	1165.36	1760.86	0.41	0.00	0.80	0.22	0.03	0.17	43.20	0.00	35.73	0.0020	0.43	0.01
801_apatite - 30	1078.72	1622.06	0.40	0.00	1.20	0.23	0.04	0.07	37.64	0.00	31.14	0.0008	0.18	0.00
801_apatite - 31	1467.14	2216.42	0.40	0.00	1.12	0.22	0.03	0.07	52.23	0.00	43.20	0.0006	0.19	0.00
801_apatite - 32	1379.52	2113.95	0.41	0.00	1.20	0.22	0.02	0.07	43.37	0.00	35.88	0.0006	0.18	0.00
801_apatite - 33	1432.09	2213.72	0.40	0.00	1.19	0.26	0.02	0.06	35.52	0.00	29.38	0.0005	0.16	0.00
801_apatite - 34	1155.87	1745.73	0.42	0.00	0.83	0.22	0.05	0.22	47.66	0.01	39.43	0.0033	0.57	0.02
801_apatite - 35	1215.74	1822.67	0.38	0.00	1.08	0.23	0.03	0.08	41.64	0.00	34.44	0.0008	0.21	0.00
801_apatite - 36	1239.70	1862.40	0.39	0.00	1.18	0.22	0.03	0.06	39.20	0.00	32.43	0.0006	0.16	0.00
801_apatite - 37	1224.59	1837.78	0.39	0.00	1.72	0.22	0.03	0.03	42.42	0.00	35.09	0.0003	0.09	0.00
801_apatite - 38	1123.17	1686.87	0.41	0.00	1.27	0.22	0.02	0.05	46.40	0.00	38.39	0.0004	0.13	0.00
801_apatite - 4	990.84	1511.39	0.41	0.00	1.17	0.25	0.04	0.07	30.92	0.00	25.58	0.0009	0.18	0.00
801_apatite - 42	1117.52	1656.45	0.43	0.00	1.02	0.21	0.07	0.11	51.37	0.00	42.50	0.0020	0.29	0.01
801_apatite - 43	917.87	1433.36	0.42	0.00	1.41	0.27	0.04	0.05	27.21	0.00	22.51	0.0007	0.13	0.00
801_apatite - 44	1372.92	2007.99	0.43	0.00	0.88	0.21	0.04	0.12	60.98	0.00	50.44	0.0010	0.30	0.01
801_apatite - 47	1155.39	1739.96	0.42	0.00	1.74	0.21	0.02	0.03	45.64	0.00	37.76	0.0003	0.08	0.00
801_apatite - 48	1015.16	1506.83	0.43	0.00	0.82	0.21	0.04	0.14	49.34	0.00	40.82	0.0016	0.36	0.01
801_apatite - 5	945.12	1441.29	0.41	0.00	1.36	0.25	0.03	0.05	32.71	0.00	27.06	0.0006	0.14	0.00
801_apatite - 50	832.92	1229.93	0.41	0.00	1.68	0.22	0.04	0.04	40.59	0.00	33.58	0.0005	0.10	0.00
801_apatite - 51	1199.89	1808.07	0.40	0.00	1.34	0.22	0.03	0.06	44.06	0.00	36.45	0.0005	0.14	0.00
801_apatite - 54	916.80	1342.72	0.43	0.00	1.16	0.21	0.04	0.06	46.34	0.00	38.33	0.0007	0.16	0.00
801_apatite - 55	1222.10	1894.84	0.42	0.00	1.31	0.24	0.01	0.07	18.39	0.00	15.21	0.0008	0.18	0.00
801_apatite - 6	928.86	1452.76	0.40	0.00	1.64	0.27	0.04	0.04	27.14	0.00	22.45	0.0006	0.11	0.00
801_apatite - 7	950.98	1425.52	0.43	0.00	1.11	0.22	0.03	0.08	42.71	0.00	35.33	0.0007	0.21	0.00
801_apatite - 9	1339.14	2029.02	0.40	0.00	1.13	0.22	0.03	0.07	45.19	0.00	37.38	0.0005	0.17	0.00
852_apatite - 47	839.40	1146.33	0.27	0.01	1.01	0.41	2.36	0.20	4.95	0.27	4.09	0.1759	0.51	0.88
852_apatite - 10	1372.26	1919.80	0.27	0.01	1.43	0.56	1.97	0.12	3.83	0.18	3.17	0.1183	0.30	0.50
852_apatite - 2	3307.49	4662.64	0.30	0.01	3.50	0.47	3.19	0.04	5.98	0.08	4.95	0.0484	0.11	0.27
852_apatite - 62	1045.25	1526.63	0.27	0.01	1.50	0.53	1.38	0.10	4.31	0.11	3.56	0.0717	0.26	0.30
852_apatite - 28	881.89	1155.05	0.29	0.01	1.70	0.40	2.22	0.06	8.61	0.05	7.12	0.0310	0.16	0.28
852_apatite - 7	1307.24	1796.40	0.28	0.01	0.99	0.48	2.06	0.20	5.20	0.25	4.30	0.1594	0.51	0.87
852_apatite - 27	1542.69	2371.46	0.31	0.02	1.90	0.51	1.07	0.08	2.62	0.14	2.17	0.0913	0.21	0.20
852_apatite - 52	1974.02	2679.45	0.26	0.05	3.40	0.59	3.66	0.05	2.55	0.29	2.11	0.1852	0.13	0.45
852_apatite - 40	2089.30	2993.00	0.28	0.04	4.97	0.59	2.78	0.03	2.46	0.13	2.03	0.0834	0.08	0.19
852_apatite - 37	864.39	1132.15	0.30	0.01	1.44	0.39	2.58	0.11	7.62	0.11	6.30	0.0710	0.27	0.54
973_apatite - 11	771.67	1758.64	0.37	0.19	1.41	0.57	1.30	0.30	2.32	2.50	1.92	1.6112	0.79	0.84
973_apatite - 12	315.55	640.65	0.48	0.02	1.13	0.44	0.12	0.25	8.87	0.06	7.34	0.0416	0.64	0.06
973_apatite - 13	362.32	680.45	0.52	0.05	1.35	0.48	0.69	0.31	12.11	0.33	10.02	0.2110	0.80	0.42
973_apatite - 14	483.92	872.66	0.51	0.01	0.86	0.54	0.05	0.37	8.29	0.06	6.86	0.0394	0.96	0.05
973_apatite - 16	320.32	759.14	0.44	0.05	1.37	0.49	0.31	0.28	5.98	0.25	4.95	0.1588	0.73	0.18
973_apatite - 18	450.86	808.81	0.51	0.12	1.97	0.50	1.96	0.22	11.75	0.69	9.72	0.4428	0.58	0.94
973_apatite - 23	455.99	934.31	0.50	0.02	1.06	0.43	0.19	0.37	7.09	0.15	5.87	0.0943	0.95	0.12
973_apatite - 25	647.36	1188.16	0.50	0.16	2.11	0.52	2.99	0.32	9.51	1.36	7.87	0.8762	0.84	1.38
973_apatite - 27	360.28	682.37	0.47	0.02	1.12	0.47	0.23	0.26	11.87	0.07	9.82	0.0457	0.67	0.11
973_apatite - 28	377.73	697.21	0.50	0.04	1.14	0.46	0.73	0.34	11.88	0.29	9.83	0.1871	0.88	0.47
973_apatite - 3	446.56	809.17	0.52	0.04	1.15	0.51	0.26	0.35	8.89	0.23	7.36	0.1483	0.89	0.24
973_apatite - 30	591.37	925.10	0.48	0.13	1.34	0.54	4.56	0.31	7.63	1.89	6.31	1.2214	0.81	2.87
973_apatite - 31	474.94	1125.90	0.48	0.09	2.83	0.54	0.25	0.20	3.85	0.26	3.19	0.1700	0.52	0.10
973_apatite - 32	216.77	372.44	0.52	0.04	1.27	0.43	0.99	0.31	18.35	0.20	15.18	0.1276	0.81	0.57
973_apatite - 33	611.28	1247.63	0.44	0.12	1.22	0.58	1.18	0.32	3.44	1.66	2.85	1.0702	0.84	0.94
973_apatite - 36	280.62	441.23	0.48	0.09	1.59	0.43	4.13	0.24	17.00	0.62	14.06	0.4001	0.61	1.70
973_apatite - 37	411.36	555.48	0.54	0.00	1.16	0.36	0.15	0.15	59.25	0.00	49.02	0.0026	0.38	0.03
973_apatite - 4	254.00	622.81	0.42	0.04	1.33	0.47	0.28	0.19	4.55	0.13	3.77	0.0871	0.50	0.08
973_apatite - 41	340.97	633.47	0.52	0.02	1.16	0.47	0.28	0.22	14.02	0.07	11.60	0.0425	0.56	0.12
973_apatite - 42	232.42	415.08	0.52	0.01	1.18	0.43	0.11	0.14	20.48	0.01	16.94	0.0076	0.37	0.03
973_apatite - 43	314.49	514.51	0.52	0.02	1.12	0.43	0.66	0.33	25.81	0.14	21.35	0.0890	0.84	0.43
973_apatite - 44	334.39	696.89	0.47	0.06	1.32	0.47	0.46	0.28	7.37	0.29	6.09	0.1842	0.73	0.26
973_apatite - 45	352.59	575.63	0.52	0.00	1.21	0.43	0.12	0.13	26.69	0.01	22.08	0.0056	0.33	0.03
973_apatite - 47	498.96	1009.99	0.41	0.24	1.47	0.51	1.86	0.28	3.30	2.48	2.73	1.6035	0.73	1.08

Element concentrations in ppm

$Eu/Eu^* = [(Eu_{CN}/(Sm_{CN}+Gd_{CN})/2)]$

$Y/Y^* = [(Y_{CN}/(Dy_{CN}+Ho_{CN})/2)]$

$TCe/Ce^* = [(Ce_{CN}/(La_{CN} \times Pr_{CN})^{0.5})]$

$LCe/Ce^* = [(Ce_{CN}/((Nd_{CN})^{0.5}/Sm_{CN}))]$

CN = chondrite normalised

Normalising values from Sun and McDonough (1989)

Appendix 5 Supplementary material for Mapping hydrothermal systems in IOCG deposits using apatite geochronology and geochemsitry: An example from Vulcan Cu-Au prospect

Appendix 5 Table A2: LA-ICP-MS Trace element data collected for apatite from Vulcan Prospect in this study

Included Data

Sample	Drill hole	Comment	Si	P	Ca	V	Mn	Fe	Sr	Y	Zr	Th	U
973_apatite - 51	VUD 009 973		646.47	189494.30	394000	0.29	114.22	642.64	591.53	255.80	53.67	14.21	25.70
973_apatite - 52	VUD 009 973		<165.100	189436.08	394000	<0.080	58.13	244.32	575.16	243.74	17.89	1.99	1.83
973_apatite - 55	VUD 009 973		541.47	190586.42	394000	0.43	210.68	173.09	387.08	499.59	<0.024	10.49	48.63
973_apatite - 57	VUD 009 973	La/Ce >1	1395.63	185192.79	394000	1.26	250.28	2276.53	243.16	584.52	1.00	47.89	97.99
973_apatite - 60	VUD 009 973	LREE enriched	787.94	187236.06	394000	0.71	257.09	997.73	1503.23	1011.31	0.74	108.97	135.84
973_apatite - 7	VUD 009 973		929.85	193658.83	394000	0.81	164.94	713.66	448.94	310.93	0.24	5.44	35.07
1084 - 1	VUD 007 1084		365.90	191863.27	393600	0.65	38.81	542.42	175.05	381.05	0.04	0.38	0.42
1084 - 12	VUD 007 1084		510.57	185888.24	393600	0.43	38.41	919.10	398.64	589.64	<0.008	8.11	0.34
1084 - 13	VUD 007 1084		938.33	192116.59	393600	0.43	60.82	1566.39	372.61	1112.10	0.03	37.02	8.74
1084 - 14	VUD 007 1084		151.57	189670.13	393600	1.51	49.16	9882.06	299.54	641.14	0.01	0.69	0.93
1084 - 15	VUD 007 1084		722.34	186729.83	393600	22.57	36.66	719.59	206.83	220.39	0.59	69.72	44.45
1084 - 16	VUD 007 1084		313.47	189273.46	393600	2.97	46.10	727.34	248.01	519.87	0.65	161.02	10.06
1084 - 17	VUD 007 1084		388.26	192699.58	393600	0.08	62.16	411.91	289.80	659.02	0.03	0.84	0.98
1084 - 18	VUD 007 1084		755.01	190021.33	393600	0.38	54.76	670.86	364.28	959.39	0.02	49.66	12.80
1084 - 19	VUD 007 1084		365.84	189894.91	393600	<0.077	41.99	219.43	329.38	512.23	0.01	0.22	0.42
1084 - 2	VUD 007 1084		623.50	193453.34	393600	0.11	74.99	449.32	326.42	946.11	0.02	25.06	3.39
1084 - 20	VUD 007 1084		572.06	193457.77	393600	<0.086	81.56	462.54	404.98	857.93	0.02	19.54	3.57
1084 - 21	VUD 007 1084		1054.18	186281.76	393600	1.01	50.13	1829.96	338.74	913.70	0.03	33.90	4.73
1084 - 22	VUD 007 1084		445.63	191969.29	393600	0.22	101.61	559.00	555.11	438.31	0.03	99.47	4.41
1084 - 25	VUD 007 1084		835.09	189494.69	393600	7.64	38.81	938.49	191.49	566.33	0.38	153.83	26.57
1084 - 26	VUD 007 1084		391.94	183436.48	393600	0.16	281.08	1216.67	315.04	723.79	0.59	2.99	1.44
1084 - 27	VUD 007 1084		780.15	190985.06	393600	0.53	36.66	1449.34	337.70	649.26	0.22	94.29	18.56
1084 - 28	VUD 007 1084		483.13	190768.28	393600	0.12	57.81	300.54	366.98	664.37	<0.007	2.95	1.92
1084 - 29	VUD 007 1084	HREE depleted	317.41	193190.95	393600	0.64	36.57	482.02	185.88	137.92	0.03	5.53	3.76
1084 - 3	VUD 007 1084		436.96	189438.21	393600	1.13	24.17	1186.64	167.63	257.03	0.19	24.03	10.52
1084 - 30	VUD 007 1084		199.34	186643.47	393600	0.31	24.67	757.22	162.80	261.27	0.09	5.63	0.33
1084 - 31	VUD 007 1084	HREE depleted	165.15	191186.64	393600	<0.077	24.50	353.40	201.77	34.31	<0.007	0.12	0.32
1084 - 33	VUD 007 1084		747.43	191758.37	393600	1.70	63.54	4146.57	436.80	679.70	0.40	94.89	25.77
1084 - 34	VUD 007 1084		759.73	188929.70	393600	3.71	30.33	2576.41	204.50	250.52	0.21	37.40	25.86
1084 - 35	VUD 007 1084		576.57	186673.76	393600	<0.090	40.92	1033.81	297.12	851.25	0.04	0.85	1.91
1084 - 36	VUD 007 1084		3240.02	189429.35	393600	3.38	91.45	6742.24	365.87	951.83	0.27	146.34	12.03
1084 - 37	VUD 007 1084		773.32	190592.41	393600	0.76	46.91	788.78	227.96	541.80	0.20	258.85	10.86
1084 - 38	VUD 007 1084		3930.93	192251.99	393600	5.49	40.66	1373.64	205.25	276.15	0.28	16.30	10.23
1084 - 39	VUD 007 1084		421.36	195000.33	393600	1.38	44.17	560.34	178.90	577.40	<0.009	16.62	2.20
1084 - 4	VUD 007 1084		563.54	190233.65	393600	0.30	45.33	626.23	337.16	638.71	0.02	29.38	4.82
1084 - 40	VUD 007 1084		2697.17	188222.46	393600	3.35	45.49	5361.00	426.44	974.65	0.13	23.65	2.10
1084 - 42	VUD 007 1084		1975.44	190212.39	393600	1.74	62.22	3937.37	502.38	519.99	<0.006	1.01	0.78
1084 - 44	VUD 007 1084		2982.50	198628.14	393600	4.04	35.47	3101.17	289.76	919.00	0.37	50.89	0.76
1084 - 46	VUD 007 1084	HREE depleted	359.74	192771.31	393600	24.66	31.18	557.51	176.28	143.56	0.05	3.24	1.78
1084 - 48	VUD 007 1084		470.51	194614.33	393600	0.28	50.59	687.74	311.51	578.45	0.01	1.05	1.16
1084 - 49	VUD 007 1084		370.25	189751.61	393600	0.78	179.78	1801.81	403.58	583.65	0.07	8.29	1.09
1084 - 5	VUD 007 1084		477.80	193379.08	393600	0.10	77.81	407.60	332.58	767.08	0.01	16.27	4.20
1084 - 50	VUD 007 1084		2175.00	188218.55	393600	4.19	39.81	9612.05	245.54	1298.63	0.34	107.02	1.58
1084 - 51	VUD 007 1084		226.88	190557.78	393600	1.42	29.12	321.66	194.20	303.29	0.02	0.56	0.32
1084 - 53	VUD 007 1084		961.58	189035.45	393600	5.31	29.50	634.59	254.04	594.18	0.48	276.15	19.80
1084 - 54	VUD 007 1084		290.05	189583.02	393600	<0.116	103.08	909.06	409.46	670.82	<0.008	3.82	3.03
1084 - 55	VUD 007 1084		763.82	193740.15	393600	2.99	41.32	688.10	208.91	485.10	0.18	76.35	94.59
1084 - 56	VUD 007 1084		458.46	191216.42	393600	0.19	38.23	682.20	308.75	558.27	0.03	15.86	8.40
1084 - 57	VUD 007 1084		293.30	195549.19	393600	2.91	118.44	702.22	430.35	265.11	0.04	14.75	4.93
1084 - 58	VUD 007 1084		426.86	188929.32	393600	0.27	27.83	449.39	171.39	531.76	0.04	11.76	3.92
1084 - 59	VUD 007 1084		226.81	193309.47	393600	0.26	44.18	716.26	181.58	251.40	0.04	8.43	6.31
1084 - 6	VUD 007 1084		768.99	188800.51	393600	6.44	24.04	1278.04	719.59	545.50	0.27	159.22	15.65
1084 - 60	VUD 007 1084		940.31	192422.23	393600	6.36	60.08	3126.74	414.65	393.61	0.07	53.56	4.33
1084 - 7	VUD 007 1084		460.08	191956.28	393600	0.81	7.80	869.61	136.44	351.71	0.02	8.18	0.10
1084 - 9	VUD 007 1084		750.96	185055.08	393600	0.22	32.85	1623.98	321.92	895.59	0.27	19.93	4.22
1183 - 1	VUD 007 1183		349.27	193122.08	393600	0.23	103.32	392.17	484.84	459.08	<0.007	4.13	2.59
1183 - 10	VUD 007 1183	LREE depleted	236.54	188963.57	393600	0.12	28.99	281.08	204.31	430.94	0.01	1.07	0.07
1183 - 11	VUD 007 1183		607.29	190833.80	393600	0.39	76.68	898.97	313.87	751.54	0.11	75.58	10.43
1183 - 12	VUD 007 1183		553.74	191087.90	393600	0.15	100.85	400.86	287.03	544.08	<0.007	2.58	3.76
1183 - 13	VUD 007 1183		525.32	193213.96	393600	1.92	110.82	437.62	503.25	506.00	0.24	63.68	5.53
1183 - 14	VUD 007 1183		684.09	195177.86	393600	0.19	108.07	509.00	522.83	625.74	0.09	151.42	8.74
1183 - 15	VUD 007 1183		186.87	195280.83	393600	0.33	75.51	285.66	217.03	451.16	<0.008	0.79	0.86
1183 - 16	VUD 007 1183		701.44	191497.79	393600	1.49	110.36	414.92	484.06	714.43	0.30	226.44	9.03
1183 - 17	VUD 007 1183		443.28	194770.52	393600	0.33	114.53	831.63	196.37	545.75	0.03	2.31	2.85
1183 - 18	VUD 007 1183		250.27	196873.75	393600	0.46	84.54	930.46	533.61	285.69	<0.007	6.81	0.36
1183 - 19	VUD 007 1183		500.48	191218.22	393600	0.25	71.39	1085.05	417.87	397.61	0.02	70.47	3.98
1183 - 2	VUD 007 1183		332.34	191211.82	393600	0.40	111.12	426.54	201.53	510.71	0.03	7.75	2.49
1183 - 20	VUD 007 1183		156.31	190783.20	393600	<0.088	85.19	305.97	303.78	498.29	0.01	0.63	0.70
1183 - 24	VUD 007 1183		535.27	192750.18	393600	0.64	100.30	425.39	430.80	581.64	0.16	28.92	3.53
1183 - 26	VUD 007 1183		272.08	192441.19	393600	0.19	57.42	283.64	266.10	480.79	0.01	23.64	1.37
1183 - 27	VUD 007 1183		527.77	192373.18	393600	2.09	81.44	1216.89	295.90	487.49	0.17	166.14	6.30

Element concentrations in ppm
$Eu/Eu^{*} = [(Eu_{CN}/(Sm_{CN}+Gd_{CN})/2)]$
$Y/Y^{*} = [(Y_{CN}/(Dy_{CN}+Ho_{CN})/2)]$
$TCe/Ce^{*} = [(Ce_{CN}/(La_{CN} \times Pr_{CN})^{0.5})]$
$LCe/Ce^{*} = [(Ce_{CN}/((Nd_{CN})^{0.5}/Sm_{CN}))]$
CN = chondrite normalised
Normalising values from Sun and McDonough (1989)

Appendix 5 Supplementary material for Mapping hydrothermal systems in IOCG deposits using apatite geochronology and geochemsitry: An example from Vulcan Cu-Au prospect

Appendix 5 Table A2: LA-ICP-MS Trace element data collected for apatite from Vulcan Prospect in this study

Included Data

Sample	La	Ce	Pr	Nd	Sm	Eu	Gd	Tb	Dy	Ho	Er	Tm	Yb	Lu	Hf
973_apatite - 51	5.05	18.95	2.26	11.44	25.95	16.65	159.14	15.87	64.37	10.07	21.89	2.12	10.61	1.56	2.02
973_apatite - 52	0.70	2.03	0.51	4.95	37.90	26.94	268.24	22.32	70.93	9.95	19.16	1.70	7.65	0.82	0.37
973_apatite - 55	0.85	5.23	0.88	5.95	11.24	6.64	72.50	17.47	122.66	22.82	46.79	3.96	19.16	1.97	0.02
973_apatite - 57	29.80	52.43	10.34	38.64	17.88	7.27	78.38	16.94	114.02	22.30	53.24	5.86	29.79	4.28	<0.006
973_apatite - 60	1236.07	1828.26	117.18	295.59	53.51	15.37	134.60	27.43	183.75	36.90	80.78	7.31	29.33	3.45	0.04
973_apatite - 7	2.88	10.24	1.68	9.53	23.12	14.88	153.68	17.03	81.15	13.14	29.59	2.51	11.76	1.08	0.01
1084 - 1	81.48	332.41	61.35	349.03	88.58	12.88	87.11	11.11	62.44	12.13	32.38	4.06	19.48	2.98	0.02
1084 - 12	235.40	712.51	113.67	558.07	147.87	29.28	159.16	19.80	103.52	18.26	40.91	4.00	23.05	2.96	<0.009
1084 - 13	1006.19	2854.75	371.71	1579.38	296.22	37.66	254.15	34.21	191.75	36.87	96.86	11.73	70.68	9.26	<0.010
1084 - 14	35.17	219.34	57.50	398.66	157.61	19.68	162.67	23.09	135.56	23.87	66.74	7.93	47.51	5.76	<0.009
1084 - 15	1338.93	3136.25	329.81	1164.84	144.98	23.16	88.57	9.31	48.82	8.46	22.34	2.76	14.17	1.68	<0.009
1084 - 16	450.34	1344.97	189.66	828.15	169.89	19.32	146.96	17.96	100.99	18.20	47.76	5.63	32.14	4.24	<0.008
1084 - 17	241.70	820.99	126.82	605.67	153.42	20.42	151.77	19.94	113.07	21.01	53.62	6.57	36.17	4.74	<0.008
1084 - 18	750.68	2075.80	276.45	1186.83	241.47	29.26	225.57	29.16	163.12	30.84	80.24	9.76	53.58	6.93	0.01
1084 - 19	142.27	516.85	84.13	432.70	117.95	19.44	119.52	15.12	82.05	14.31	36.12	4.05	23.44	3.05	<0.008
1084 - 2	699.02	2172.11	302.34	1328.12	261.39	29.34	232.69	29.86	167.93	32.10	84.38	10.01	56.59	7.22	<0.008
1084 - 20	744.45	2267.65	313.47	1368.85	260.53	31.94	223.59	28.18	158.38	30.19	81.71	9.83	55.91	7.28	0.02
1084 - 21	590.15	1728.09	247.04	1135.84	251.67	42.57	245.92	30.57	163.05	31.13	75.67	8.43	45.58	5.71	0.02
1084 - 22	547.48	1667.64	234.09	1006.28	182.92	25.99	138.62	16.26	83.32	14.32	36.83	4.52	27.58	3.44	<0.008
1084 - 25	601.71	1908.78	267.37	1147.91	195.04	23.58	150.14	17.52	96.98	18.37	50.20	6.29	35.74	4.64	0.03
1084 - 26	499.49	1469.95	202.61	872.98	178.33	25.93	165.02	21.96	131.84	24.93	72.61	9.34	53.61	8.36	0.05
1084 - 27	826.83	2097.23	265.67	1110.69	202.51	18.93	170.71	21.81	119.22	22.49	59.20	7.25	40.04	5.01	<0.009
1084 - 28	284.78	895.34	131.38	587.05	146.59	22.71	139.90	19.72	111.56	20.89	54.93	6.43	38.29	4.60	<0.009
1084 - 29	359.43	902.07	111.26	411.91	58.96	15.56	39.80	4.70	26.44	4.59	12.30	1.60	9.23	1.22	<0.007
1084 - 3	272.45	778.92	108.19	497.34	97.09	16.91	79.44	9.20	51.35	8.56	19.44	1.90	9.18	0.87	0.01
1084 - 30	109.74	386.42	63.23	316.53	80.49	15.47	75.58	10.31	53.35	9.77	22.45	2.65	14.33	1.32	0.05
1084 - 31	160.80	512.54	72.01	302.24	47.37	14.47	26.55	2.52	10.43	1.29	2.33	0.16	0.76	0.07	<0.008
1084 - 33	977.75	2737.73	347.03	1387.17	223.49	28.19	172.86	21.41	121.91	25.26	75.65	9.38	55.34	7.24	0.01
1084 - 34	606.90	1745.28	225.33	894.28	136.57	21.19	86.68	9.53	52.78	9.27	23.19	2.41	12.73	1.32	<0.010
1084 - 35	555.33	1614.02	222.08	985.18	200.90	26.74	190.62	26.23	157.19	30.94	90.39	11.69	66.89	9.77	<0.009
1084 - 36	958.56	2770.38	372.07	1572.27	305.46	41.64	261.37	34.51	184.02	34.41	88.28	10.02	58.31	7.20	0.03
1084 - 37	814.45	2369.38	314.85	1272.75	217.80	25.79	163.32	19.91	109.46	20.02	52.92	6.54	37.77	5.20	0.01
1084 - 38	455.03	1519.74	211.44	849.52	134.95	19.03	88.57	10.83	58.54	10.58	25.98	2.84	15.47	1.76	<0.012
1084 - 39	178.68	682.64	114.17	580.00	141.25	13.59	131.75	17.73	100.36	18.99	52.18	6.23	32.82	4.63	<0.011
1084 - 4	473.50	1385.61	191.47	862.05	181.95	26.15	171.02	20.20	108.15	19.68	49.14	5.64	30.36	4.23	0.01
1084 - 40	1074.64	2893.31	388.85	1768.21	365.70	72.26	340.66	42.69	223.35	37.53	84.99	8.57	40.77	5.02	0.02
1084 - 42	241.75	817.26	125.03	592.06	135.16	22.28	128.14	15.17	78.27	14.17	36.75	4.42	24.85	3.16	<0.008
1084 - 44	368.83	1220.93	204.79	1042.48	266.84	56.41	264.50	34.79	181.38	31.79	73.06	6.83	31.68	3.95	0.03
1084 - 46	368.73	1047.28	131.38	488.98	76.03	22.36	52.16	5.75	30.07	5.20	13.32	1.44	8.67	0.94	<0.008
1084 - 48	365.25	1250.69	195.08	915.71	185.64	26.11	161.75	19.47	101.98	18.35	50.87	5.90	32.91	4.74	0.01
1084 - 49	421.91	1246.46	184.53	852.71	179.42	27.39	156.89	19.01	99.11	18.22	44.85	5.49	29.66	3.97	<0.010
1084 - 5	595.76	1744.31	234.19	1011.90	201.85	25.10	179.70	23.41	133.54	25.45	67.00	8.06	45.36	5.70	<0.008
1084 - 50	579.72	1903.83	318.11	1668.08	436.74	101.97	471.37	59.93	312.54	51.43	107.20	9.03	33.97	3.20	0.06
1084 - 51	97.99	390.09	69.14	383.67	89.62	12.84	83.82	9.82	52.70	9.60	25.06	2.79	12.54	1.77	<0.008
1084 - 53	580.76	1903.08	279.85	1245.34	214.28	25.72	167.01	20.49	109.91	20.07	54.46	7.02	41.24	5.40	0.01
1084 - 54	385.84	1338.90	201.94	915.14	201.59	23.19	175.29	22.71	128.75	24.49	65.17	7.54	43.19	5.43	<0.010
1084 - 55	817.84	2172.11	274.63	1142.64	185.89	21.10	141.56	16.97	92.62	16.86	43.82	5.20	28.89	3.80	<0.010
1084 - 56	376.92	1158.15	173.31	822.22	167.86	21.78	143.97	17.80	96.41	18.28	48.25	6.04	33.70	4.48	<0.009
1084 - 57	668.57	1893.26	239.28	918.53	137.11	18.63	91.38	10.52	55.51	9.76	25.21	2.83	16.27	2.12	<0.009
1084 - 58	410.16	1291.78	188.48	888.11	173.22	11.42	152.32	18.51	104.02	18.38	50.80	5.79	31.55	3.94	<0.010
1084 - 59	430.27	1154.89	154.34	673.11	110.99	12.46	86.00	9.63	51.05	8.56	21.85	2.39	12.55	1.74	<0.010
1084 - 6	1129.09	2611.27	297.45	1168.83	209.93	27.43	163.38	20.27	103.50	18.85	46.22	5.52	30.27	3.94	<0.012
1084 - 60	779.93	1971.34	257.61	1060.61	180.47	26.14	141.56	16.34	82.16	14.49	33.35	3.87	21.64	2.63	0.01
1084 - 7	144.39	377.04	60.39	321.78	95.81	14.49	102.19	14.24	76.16	12.76	28.27	2.78	11.61	1.05	<0.010
1084 - 9	802.09	2210.33	298.59	1317.97	270.57	40.95	238.24	31.35	173.16	32.32	86.64	10.58	59.95	8.22	0.01
1183 - 1	335.36	1025.22	150.84	712.05	144.76	19.00	125.22	15.35	84.28	15.17	40.28	4.88	25.84	3.32	<0.008
1183 - 10	28.63	120.67	25.21	159.09	64.74	10.68	87.81	12.87	74.56	13.93	38.17	4.43	23.15	3.20	<0.012
1183 - 11	378.62	1310.74	202.90	959.54	216.21	32.17	198.03	25.33	140.60	25.78	64.89	7.67	42.15	5.65	<0.009
1183 - 12	548.99	1527.93	205.01	876.76	163.93	23.33	139.13	17.09	94.06	18.16	48.23	5.93	35.96	4.91	<0.008
1183 - 13	568.95	1720.11	236.25	1016.89	180.48	22.36	142.37	17.55	95.02	17.35	46.31	5.62	32.58	4.32	<0.008
1183 - 14	777.55	2241.31	302.40	1282.02	237.46	26.90	181.71	21.92	115.80	21.51	56.01	6.58	39.02	5.55	<0.009
1183 - 15	191.70	638.19	95.15	473.82	113.86	14.62	109.72	13.54	78.27	15.33	42.03	5.10	29.92	4.27	0.02
1183 - 16	607.90	1909.68	276.20	1228.53	236.74	29.21	203.28	25.46	137.84	25.16	66.26	7.98	44.72	6.06	<0.008
1183 - 17	294.23	892.67	129.58	603.80	144.99	20.24	148.05	19.00	107.77	19.05	48.66	5.82	29.29	4.02	0.02
1183 - 18	264.21	727.29	105.57	489.58	109.60	19.48	101.68	12.34	65.63	10.44	25.67	2.79	14.66	2.00	0.01
1183 - 19	425.00	1221.95	170.00	740.51	142.73	25.05	123.55	16.26	84.88	15.08	33.38	3.62	18.18	2.21	0.01
1183 - 2	399.54	1145.77	165.10	781.06	168.14	19.51	148.45	18.09	96.67	17.43	45.26	5.31	29.98	3.70	<0.009
1183 - 20	177.58	543.12	77.51	365.57	93.73	16.32	99.89	13.83	83.67	16.39	44.29	5.48	31.87	4.18	<0.009
1183 - 24	346.94	1104.79	169.94	839.05	181.62	20.37	159.74	20.16	100.40	19.62	51.68	6.46	37.11	4.99	0.02
1183 - 26	110.76	440.93	77.37	412.67	116.47	17.16	117.18	15.89	88.58	16.32	42.75	5.36	29.78	3.67	<0.008
1183 - 27	368.62	1149.23	167.87	767.04	152.07	20.84	129.39	16.45	89.76	17.16	46.40	5.76	34.78	4.89	<0.008

Element concentrations in ppm
$Eu/Eu^* = [(Eu_{CN}/(Sm_{CN}+Gd_{CN})/2)]$
$Y/Y^* = [(Y_{CN}/(Dy_{CN}+Ho_{CN})/2)]$
$TCe/Ce^* = [(Ce_{CN}/(La_{CN} \times Pr_{CN})^{0.5})]$
$LCe/Ce^* = [(Ce_{CN}/((Nd_{CN})^{0.5}/Sm_{CN}))]$
CN = chondrite normalised
Normalising values from Sun and McDonough (1989)

Appendix 5 Supplementary material for Mapping hydrothermal systems in IOCG deposits using apatite geochronology and geochemsitry: An example from Vulcan Cu-Au prospect

Appendix 5 Table A2: LA-ICP-MS Trace element data collected for apatite from Vulcan Prospect in this study

Included Data

Sample	REE	REY	Eu/Eu*	LCe/Ce*	TCe/Ce*	Y/Y*	Ce/Lu	La/Ce	Gd/Yb	La/Sm	Gd/Yb_{CN}	La/Sm_{CN}	La/Ce_{CN}	La/Yb_{CN}
973_apatite - 51	365.93	621.74	0.52	0.04	1.36	0.47	0.50	0.27	15.00	0.19	12.41	0.1256	0.69	0.34
973_apatite - 52	473.79	717.54	0.52	0.00	0.82	0.42	0.10	0.34	35.06	0.02	29.00	0.0119	0.89	0.07
973_apatite - 55	338.11	837.70	0.46	0.03	1.46	0.46	0.11	0.16	3.78	0.08	3.13	0.0486	0.42	0.03
973_apatite - 57	481.18	1065.69	0.41	0.08	0.72	0.57	0.51	0.57	2.63	1.67	2.18	1.0758	1.47	0.72
973_apatite - 60	4049.54	5060.84	0.39	0.34	1.16	0.61	21.99	0.68	4.59	23.10	3.80	14.9114	1.75	30.23
973_apatite - 7	372.25	683.19	0.49	0.02	1.12	0.45	0.39	0.28	13.07	0.12	10.81	0.0805	0.73	0.18
1084 - 1	1157.42	1538.47	0.28	0.03	1.14	0.69	4.63	0.25	4.47	0.92	3.70	0.5939	0.63	3.00
1084 - 12	2168.45	2758.09	0.37	0.03	1.05	0.66	10.00	0.33	6.90	1.59	5.71	1.0277	0.85	7.32
1084 - 13	6851.44	7963.53	0.25	0.04	1.13	0.65	12.79	0.35	3.60	3.40	2.97	2.1929	0.91	10.21
1084 - 14	1361.08	2002.23	0.24	0.01	1.18	0.55	1.58	0.16	3.42	0.22	2.83	0.1440	0.41	0.53
1084 - 15	6334.08	6554.47	0.34	0.11	1.14	0.52	77.49	0.43	6.25	9.24	5.17	5.9619	1.10	67.80
1084 - 16	3376.22	3896.09	0.23	0.05	1.11	0.59	13.15	0.33	4.57	2.65	3.78	1.7112	0.86	10.05
1084 - 17	2375.92	3034.94	0.26	0.04	1.13	0.66	7.19	0.29	4.20	1.58	3.47	1.0171	0.76	4.79
1084 - 18	5159.68	6119.07	0.24	0.04	1.10	0.67	12.44	0.36	4.21	3.11	3.48	2.0070	0.93	10.05
1084 - 19	1610.99	2123.22	0.32	0.04	1.14	0.72	7.02	0.28	5.10	1.21	4.22	0.7786	0.71	4.35
1084 - 2	5413.10	6359.21	0.22	0.04	1.14	0.64	12.49	0.32	4.11	2.67	3.40	1.7264	0.83	8.86
1084 - 20	5581.95	6439.88	0.25	0.04	1.13	0.61	12.92	0.33	4.00	2.86	3.31	1.8446	0.85	9.55
1084 - 21	4601.41	5515.11	0.33	0.03	1.09	0.63	12.56	0.34	5.40	2.34	4.46	1.5138	0.88	9.29
1084 - 22	3989.30	4427.61	0.29	0.05	1.13	0.61	20.13	0.33	5.03	2.99	4.16	1.9322	0.85	14.24
1084 - 25	4524.27	5090.60	0.25	0.05	1.15	0.66	17.07	0.32	4.20	3.09	3.48	1.9917	0.81	12.08
1084 - 26	3736.97	4460.76	0.29	0.05	1.12	0.62	7.30	0.34	3.08	2.80	2.55	1.8082	0.88	6.68
1084 - 27	4967.59	5616.85	0.19	0.05	1.08	0.62	17.38	0.39	4.26	4.08	3.53	2.6358	1.02	14.81
1084 - 28	2464.16	3128.52	0.30	0.04	1.12	0.68	8.08	0.32	3.65	1.94	3.02	1.2542	0.82	5.34
1084 - 29	1959.08	2097.00	0.56	0.13	1.09	0.61	30.60	0.40	4.31	6.10	3.57	3.9352	1.03	27.93
1084 - 3	1950.84	2207.87	0.35	0.06	1.10	0.59	37.05	0.35	8.65	2.81	7.16	1.8116	0.90	21.28
1084 - 30	1161.64	1422.91	0.38	0.05	1.12	0.56	12.16	0.28	5.27	1.36	4.36	0.8801	0.73	5.49
1084 - 31	1153.53	1187.84	0.67	0.11	1.15	0.42	298.61	0.31	34.90	3.39	28.87	2.1913	0.81	151.60
1084 - 33	6190.40	6870.11	0.26	0.06	1.14	0.61	15.69	0.36	3.12	4.37	2.58	2.8243	0.92	12.67
1084 - 34	3827.48	4078.00	0.33	0.07	1.14	0.55	54.78	0.35	6.81	4.44	5.63	2.8687	0.90	34.18
1084 - 35	4187.98	5039.23	0.26	0.04	1.11	0.61	6.85	0.34	2.85	2.76	2.36	1.7845	0.89	5.96
1084 - 36	6698.50	7650.33	0.27	0.04	1.12	0.59	15.97	0.35	4.48	3.14	3.71	2.0259	0.89	11.79
1084 - 37	5430.16	5971.96	0.24	0.05	1.13	0.57	18.91	0.34	4.32	3.74	3.58	2.4141	0.89	15.47
1084 - 38	3404.28	3680.43	0.30	0.07	1.18	0.54	35.84	0.30	5.73	3.37	4.74	2.1767	0.77	21.10
1084 - 39	2075.02	2652.42	0.19	0.03	1.15	0.65	6.13	0.26	4.01	1.27	3.32	0.8167	0.68	3.91
1084 - 4	3529.15	4167.86	0.28	0.04	1.11	0.68	13.60	0.34	5.63	2.60	4.66	1.6801	0.88	11.19
1084 - 40	7346.54	8321.19	0.39	0.03	1.08	0.51	23.90	0.37	8.36	2.94	6.91	1.8971	0.96	18.91
1084 - 42	2238.46	2758.46	0.32	0.04	1.14	0.76	10.73	0.30	5.16	1.79	4.27	1.1547	0.76	6.98
1084 - 44	3788.28	4707.28	0.41	0.02	1.07	0.59	12.84	0.30	8.35	1.38	6.91	0.8923	0.78	8.35
1084 - 46	2252.30	2395.86	0.62	0.11	1.15	0.55	46.27	0.35	6.02	4.85	4.98	3.1309	0.91	30.51
1084 - 48	3334.44	3912.89	0.28	0.04	1.13	0.65	10.96	0.29	4.92	1.97	4.07	1.2702	0.75	7.96
1084 - 49	3289.62	3873.27	0.30	0.04	1.08	0.67	13.04	0.34	5.29	2.35	4.38	1.5181	0.87	10.20
1084 - 5	4301.32	5068.40	0.25	0.05	1.13	0.65	12.69	0.34	3.96	2.95	3.28	1.9054	0.88	9.42
1084 - 50	6057.13	7355.77	0.44	0.02	1.07	0.49	24.68	0.30	13.88	1.33	11.48	0.8569	0.79	12.24
1084 - 51	1241.45	1544.74	0.28	0.04	1.15	0.66	9.13	0.25	6.68	1.09	5.53	0.7059	0.65	5.60
1084 - 53	4674.63	5268.81	0.25	0.04	1.14	0.62	14.62	0.31	4.05	2.71	3.35	1.7497	0.79	10.10
1084 - 54	3539.18	4210.00	0.23	0.04	1.16	0.59	10.24	0.29	4.06	1.91	3.36	1.2357	0.74	6.41
1084 - 55	4963.94	5449.05	0.23	0.06	1.11	0.60	23.75	0.38	4.90	4.40	4.05	2.8403	0.97	20.30
1084 - 56	3089.18	3647.44	0.26	0.04	1.09	0.66	10.73	0.33	4.27	2.25	3.53	1.4496	0.84	8.02
1084 - 57	4088.98	4354.09	0.29	0.08	1.14	0.55	37.02	0.35	5.62	4.88	4.65	3.1478	0.91	29.47
1084 - 58	3348.47	3880.23	0.13	0.04	1.12	0.59	13.59	0.32	4.83	2.37	3.99	1.5287	0.82	9.33
1084 - 59	2729.83	2981.23	0.23	0.07	1.08	0.58	27.62	0.37	6.85	3.88	5.67	2.5026	0.96	24.59
1084 - 6	5835.96	6381.46	0.27	0.06	1.09	0.60	27.50	0.43	5.40	5.38	4.46	3.4722	1.12	26.75
1084 - 60	4592.14	4985.75	0.30	0.06	1.06	0.55	31.14	0.40	6.54	4.32	5.41	2.7899	1.02	25.85
1084 - 7	1262.96	1614.67	0.29	0.04	0.98	0.54	14.92	0.38	8.81	1.51	7.28	0.9729	0.99	8.92
1084 - 9	5580.97	6476.56	0.30	0.04	1.09	0.59	11.16	0.36	3.97	2.96	3.29	1.9138	0.94	9.60
1183 - 1	2701.56	3160.65	0.26	0.05	1.10	0.63	12.83	0.33	4.85	2.32	4.01	1.4956	0.84	9.31
1183 - 10	667.14	1098.08	0.29	0.03	1.09	0.66	1.56	0.24	3.79	0.44	3.14	0.2855	0.61	0.89
1183 - 11	3610.29	4361.83	0.29	0.03	1.14	0.61	9.62	0.29	4.70	1.75	3.89	1.1305	0.75	6.44
1183 - 12	3709.43	4253.50	0.29	0.05	1.10	0.65	12.91	0.36	3.87	3.35	3.20	2.1620	0.93	10.95
1183 - 13	4106.17	4612.17	0.25	0.05	1.13	0.61	16.51	0.33	4.37	3.15	3.62	2.0352	0.85	12.53
1183 - 14	5315.73	5941.47	0.23	0.05	1.12	0.62	16.77	0.35	4.66	3.27	3.85	2.1139	0.90	14.29
1183 - 15	1825.50	2276.65	0.25	0.04	1.14	0.65	6.20	0.30	3.67	1.68	3.03	1.0869	0.78	4.60
1183 - 16	4805.02	5519.45	0.25	0.04	1.13	0.59	13.07	0.32	4.55	2.57	3.76	1.6577	0.82	9.75
1183 - 17	2467.19	3012.94	0.27	0.04	1.10	0.58	9.22	0.33	5.05	2.03	4.18	1.3101	0.85	7.20
1183 - 18	1950.94	2236.63	0.35	0.05	1.05	0.52	15.11	0.36	6.94	2.41	5.74	1.5562	0.94	12.93
1183 - 19	3022.41	3420.02	0.35	0.05	1.10	0.54	22.91	0.35	6.79	2.98	5.62	1.9222	0.90	16.77
1183 - 2	3044.01	3554.72	0.23	0.04	1.08	0.61	12.86	0.35	4.95	2.38	4.10	1.5340	0.90	9.56
1183 - 20	1573.44	2071.72	0.33	0.05	1.12	0.67	5.39	0.33	3.13	1.89	2.59	1.2231	0.84	4.00
1183 - 24	3062.88	3644.52	0.22	0.04	1.10	0.65	9.19	0.31	4.30	1.91	3.56	1.2332	0.81	6.71
1183 - 26	1494.90	1975.69	0.28	0.03	1.15	0.62	4.99	0.25	3.93	0.95	3.26	0.6139	0.65	2.67
1183 - 27	2970.26	3457.75	0.27	0.05	1.12	0.61	9.76	0.32	3.72	2.42	3.08	1.5649	0.83	7.60

Element concentrations in ppm

$Eu/Eu^{*} = [(Eu_{CN}/(Sm_{CN}+Gd_{CN})/2)]$

$Y/Y^{*} = [(Y_{CN}/(Dy_{CN}+Ho_{CN})/2)]$

$TCe/Ce^{*} = [(Ce_{CN}/(La_{CN} \times Pr_{CN})^{0.5})]$

$LCe/Ce^{*} = [(Ce_{CN}/((Nd_{CN})^{0.5}/Sm_{CN}))]$

CN = chondrite normalised

Normalising values from Sun and McDonough (1989)

Appendix 5 Supplementary material for Mapping hydrothermal systems in IOCG deposits using apatite geochronology and geochemsitry: An example from Vulcan Cu-Au prospect

Appendix 5 Table A2: LA-ICP-MS Trace element data collected for apatite from Vulcan Prospect in this study

Included Data

Sample	Drill hole	Comment	Si	P	Ca	V	Mn	Fe	Sr	Y	Zr	Th	U
1183 - 28	VUD 007 1183		495.47	190425.18	393600	1.04	95.76	382.48	473.65	658.45	0.03	31.24	2.51
1183 - 29	VUD 007 1183		845.96	190505.90	393600	0.91	91.70	1631.03	530.22	419.41	0.13	54.13	2.56
1183 - 3	VUD 007 1183		269.28	192561.94	393600	0.24	113.15	456.17	599.61	391.23	0.02	1.96	0.39
1183 - 30	VUD 007 1183		1706.31	194830.61	393600	1.68	110.26	3559.71	485.37	527.34	0.37	55.97	5.60
1183 - 31	VUD 007 1183		441.15	193744.46	393600	1.16	64.59	380.76	246.37	633.68	0.87	496.28	40.63
1183 - 32	VUD 007 1183		621.69	192582.63	393600	0.23	112.37	406.35	392.80	546.74	0.14	107.90	13.79
1183 - 33	VUD 007 1183		604.15	194192.29	393600	<0.089	101.93	385.55	353.28	518.66	0.01	26.00	4.08
1183 - 34	VUD 007 1183		480.48	193915.59	393600	0.29	90.33	727.55	356.90	569.88	0.05	42.13	6.67
1183 - 35	VUD 007 1183		805.42	193212.71	393600	<0.076	77.61	1522.57	419.16	499.78	0.13	127.63	14.58
1183 - 36	VUD 007 1183		537.11	195935.53	393600	0.17	92.07	883.11	292.32	503.35	0.07	72.03	6.17
1183 - 37	VUD 007 1183		772.91	189176.40	393600	0.37	78.65	756.57	425.29	531.31	0.22	242.98	17.72
1183 - 38	VUD 007 1183	LREE depleted	160.93	195243.23	393600	<0.068	17.78	101.16	183.60	203.43	<0.007	0.62	0.01
1183 - 4	VUD 007 1183		547.97	195102.16	393600	0.12	111.14	456.14	265.17	908.16	0.03	0.98	5.01
1183 - 40	VUD 007 1183		884.29	188874.47	393600	0.15	78.16	943.08	409.28	589.34	0.12	47.75	13.51
1183 - 43	VUD 007 1183		660.85	190447.22	393600	0.53	83.75	404.36	442.18	908.06	0.21	101.73	7.24
1183 - 44	VUD 007 1183	LREE depleted	237.85	191534.93	393600	<0.069	21.92	268.83	189.41	319.91	0.01	1.82	0.06
1183 - 46	VUD 007 1183		438.92	195737.88	393600	1.58	89.48	519.50	476.88	413.67	0.10	5.18	4.90
1183 - 47	VUD 007 1183		3282.43	189169.20	393600	3.53	71.66	7402.34	365.13	558.79	0.18	41.73	6.78
1183 - 49	VUD 007 1183		850.19	191137.82	393600	0.12	79.15	560.55	411.49	558.88	0.05	203.80	14.49
1183 - 5	VUD 007 1183		464.33	187618.90	393600	1.02	95.40	415.84	427.00	586.19	0.15	35.01	4.86
1183 - 52	VUD 007 1183		320.89	194705.10	393600	2.42	52.57	1711.77	314.74	451.77	0.27	94.44	1.51
1183 - 53	VUD 007 1183		549.97	191704.90	393600	0.29	81.07	948.92	207.70	475.29	0.02	2.00	1.03
1183 - 54	VUD 007 1183		727.94	192756.50	393600	0.51	93.81	919.11	314.69	600.52	0.41	192.87	11.99
1183 - 55	VUD 007 1183		528.15	191757.40	393600	0.91	113.62	628.39	582.40	450.29	0.06	9.90	1.38
1183 - 56	VUD 007 1183		916.63	191013.31	393600	7.29	109.01	495.07	472.20	550.50	1.01	328.11	16.29
1183 - 58	VUD 007 1183		148.90	191534.45	393600	<0.079	15.88	111.08	129.26	206.71	<0.007	0.40	0.01
1183 - 59	VUD 007 1183	LREE depleted	266.13	192176.49	393600	0.20	33.53	221.83	191.03	555.98	<0.007	0.09	0.12
1183 - 6	VUD 007 1183		371.94	195428.67	393600	0.20	97.03	823.35	535.36	486.44	0.02	6.15	2.29
1183 - 61	VUD 007 1183		713.20	180123.36	393600	0.14	93.62	684.51	359.97	502.79	0.03	1.96	2.49
1183 - 64	VUD 007 1183		263.91	193601.94	393600	<0.095	58.92	286.38	268.13	417.25	<0.008	4.78	0.69
1183 - 65	VUD 007 1183		<150.519	189702.81	393600	<0.123	39.28	581.71	216.55	387.36	0.01	7.82	0.32
1183 - 67	VUD 007 1183		496.85	193261.09	393600	<0.083	86.28	1007.31	362.97	397.98	<0.007	7.77	2.26
1183 - 68	VUD 007 1183		649.18	192769.43	393600	3.18	99.36	851.25	352.52	541.48	0.28	135.96	6.07
1183 - 7	VUD 007 1183		380.22	193475.70	393600	0.32	87.38	864.68	389.59	417.37	0.07	5.84	0.96
1183 - 71	VUD 007 1183		869.75	183693.74	393600	0.36	89.65	1849.21	392.21	598.98	0.05	120.38	11.53
1183 - 9	VUD 007 1183		597.25	194033.52	393600	0.27	96.91	919.13	280.65	571.52	0.10	74.30	5.34
1210 - 10	VUD 017 1210		521.02	195622.02	393600	0.13	70.59	658.07	408.91	442.33	0.09	65.54	8.82
1210 - 12	VUD 017 1210		625.21	189130.85	393600	18.81	29.76	153.91	328.23	345.94	0.05	34.79	6.33
1210 - 13	VUD 017 1210		422.65	192093.03	393600	<0.078	70.49	443.73	450.45	493.14	0.03	6.04	2.05
1210 - 14	VUD 017 1210		1431.13	187181.91	393600	1.32	66.42	3132.34	388.99	699.88	0.04	16.67	8.93
1210 - 16	VUD 017 1210		431.63	191028.85	393600	<0.088	82.51	747.88	470.59	535.48	0.02	10.54	3.69
1210 - 17	VUD 017 1210		335.54	195978.46	393600	0.31	44.93	1082.57	298.45	211.39	0.02	2.13	0.87
1210 - 18	VUD 017 1210		452.06	197290.51	393600	<0.082	65.97	350.12	390.11	426.41	0.01	19.18	2.27
1210 - 20	VUD 017 1210		341.25	195555.97	393600	2.27	37.13	748.86	352.55	192.71	0.03	11.41	3.65
1210 - 21	VUD 017 1210		1056.05	191617.86	393600	5.38	68.86	1781.51	357.07	601.91	0.15	15.04	32.65
1210 - 23	VUD 017 1210		351.01	195769.00	393600	<0.119	44.16	235.55	258.45	252.71	0.01	2.66	0.50
1210 - 24	VUD 017 1210		333.80	195336.09	393600	0.48	53.18	881.01	273.08	357.85	0.24	2.70	0.81
1210 - 25	VUD 017 1210		356.30	191165.69	393600	0.48	47.54	789.98	272.03	344.63	0.12	1.34	1.42
1210 - 26	VUD 017 1210		440.54	188332.07	393600	1.04	62.62	420.65	304.13	360.66	0.06	9.35	8.14
1210 - 28	VUD 017 1210		631.71	190520.00	393600	0.14	62.72	926.98	364.84	474.53	0.31	9.82	2.51
1210 - 3	VUD 017 1210		17262.37	176690.76	393600	0.40	67.78	1130.21	278.13	278.82	4.49	0.71	0.76
1210 - 33	VUD 017 1210		625.20	193909.30	393600	0.55	49.82	1109.07	326.35	201.26	0.43	8.32	3.17
1210 - 38	VUD 017 1210		964.67	167224.46	393600	4.73	68.95	714.22	299.96	450.75	0.04	7.42	27.00
1210 - 39	VUD 017 1210		721.52	192139.58	393600	5.71	83.00	1009.65	391.88	576.14	0.76	99.08	7.34
1210 - 42	VUD 017 1210		332.64	192651.02	393600	1.28	68.47	362.28	372.48	610.33	0.04	17.21	3.05
1210 - 45	VUD 017 1210		964.98	137291.05	393600	2.20	82.55	1008.80	462.12	502.47	0.46	52.99	7.66
1210 - 46	VUD 017 1210		244.39	190846.75	393600	0.21	47.21	972.07	332.46	356.71	0.14	10.30	1.17
1210 - 47	VUD 017 1210		692.63	192238.96	393600	<0.085	67.07	584.30	398.52	455.62	0.94	75.63	5.56
1210 - 48	VUD 017 1210		721.05	195483.24	393600	<0.089	75.94	524.71	394.93	507.07	0.07	83.95	7.60
1210 - 5	VUD 017 1210		1702.01	190329.56	393600	1.23	76.30	1834.46	342.92	1203.52	0.25	248.56	46.94
1210 - 52	VUD 017 1210		367.84	188619.05	393600	<0.095	64.35	752.51	353.93	422.71	0.06	31.70	3.10
1210 - 54	VUD 017 1210		844.36	187300.39	393600	6.28	68.62	429.21	353.51	593.58	0.11	22.10	22.72
1210 - 58	VUD 017 1210		775.10	196203.50	393600	0.80	82.86	798.80	662.10	570.04	0.09	40.45	4.02
1210 - 59	VUD 017 1210		398.42	192586.26	393600	3.36	79.53	1210.59	656.84	452.49	0.26	26.97	4.38
1210 - 6	VUD 017 1210		539.70	194957.55	393600	7.31	61.47	1011.47	354.11	397.82	0.36	30.04	10.24
1210 - 60	VUD 017 1210		1066.98	189425.23	393600	1.73	59.04	438.32	334.19	1134.22	0.08	33.29	16.42
1210 - 61	VUD 017 1210		242.93	195687.06	393600	2.36	62.09	564.66	411.71	409.99	0.04	0.54	0.78
1210 - 62	VUD 017 1210		1256.87	191045.60	393600	11.40	76.17	3233.68	367.21	726.80	0.39	55.96	36.23
1210 - 65	VUD 017 1210		532.28	192575.86	393600	0.19	71.33	495.29	399.99	548.08	0.04	62.60	5.86
1210 - 66	VUD 017 1210		334.97	192168.51	393600	<0.085	66.92	344.47	351.25	304.40	0.01	6.03	1.20
1210 - 67	VUD 017 1210		1164.68	193177.29	393600	6.73	70.13	423.20	324.67	675.22	0.23	159.82	25.11

Element concentrations in ppm
$Eu/Eu^* = [(Eu_{CN}/(Sm_{CN}+Gd_{CN})/2)]$
$Y/Y^* = [(Y_{CN}/(Dy_{CN}+Ho_{CN})/2)]$
$TCe/Ce^* = [(Ce_{CN}/(La_{CN} \times Pr_{CN})^{0.5})]$
$LCe/Ce^* = [(Ce_{CN}/((Nd_{CN})^{0.5}/Sm_{CN}))]$
CN = chondrite normalised
Normalising values from Sun and McDonough (1989)

Appendix 5 Supplementary material for Mapping hydrothermal systems in IOCG deposits using apatite geochronology and geochemsitry: An example from Vulcan Cu-Au prospect

Appendix 5 Table A2: LA-ICP-MS Trace element data collected for apatite from Vulcan Prospect in this study

Included Data

Sample	La	Ce	Pr	Nd	Sm	Eu	Gd	Tb	Dy	Ho	Er	Tm	Yb	Lu	Hf
1183 - 28	630.02	1871.64	261.96	1154.95	210.86	26.73	179.95	21.20	119.73	22.20	59.86	7.37	43.08	5.96	0.01
1183 - 29	416.94	1293.13	190.85	888.29	169.37	26.52	144.51	16.98	85.93	15.22	37.94	4.51	24.13	3.39	<0.008
1183 - 3	403.64	1328.73	190.03	821.26	150.78	19.62	118.18	13.93	75.16	13.59	36.34	4.31	22.83	3.09	<0.009
1183 - 30	369.97	1247.89	193.30	918.76	185.55	27.50	155.38	19.30	101.30	18.69	47.33	5.87	32.64	4.55	<0.008
1183 - 31	213.80	816.31	141.62	742.09	182.91	18.45	166.12	21.54	121.57	22.08	58.41	6.88	37.88	5.08	<0.010
1183 - 32	484.39	1526.36	221.89	1005.44	197.13	25.68	156.92	18.88	102.65	18.55	48.21	5.83	31.17	4.46	0.02
1183 - 33	455.18	1471.61	212.34	943.28	178.89	24.60	141.05	16.88	91.26	16.98	45.38	5.51	34.64	4.62	<0.008
1183 - 34	288.58	960.52	152.23	766.80	177.66	25.86	166.37	21.25	113.48	20.17	48.39	5.76	32.05	3.85	<0.008
1183 - 35	610.35	1909.01	263.02	1101.97	192.96	27.99	143.14	17.62	93.24	16.64	43.38	5.45	31.29	4.14	<0.008
1183 - 36	471.22	1380.73	198.37	897.70	171.23	22.75	140.36	17.42	94.42	17.75	45.59	5.62	32.27	4.37	<0.008
1183 - 37	561.28	1841.30	270.76	1190.19	215.23	24.75	163.69	18.83	100.68	17.62	47.58	5.69	33.15	4.37	<0.011
1183 - 38	18.95	87.21	19.85	133.58	64.49	11.37	81.15	10.34	50.29	7.82	15.88	1.42	7.18	0.75	<0.009
1183 - 4	451.76	1401.18	201.57	923.06	209.84	29.92	200.22	26.06	147.47	29.26	76.27	9.43	53.59	7.08	<0.010
1183 - 40	548.84	1862.47	274.90	1267.47	228.20	27.94	176.37	21.59	112.60	20.27	51.03	6.08	36.45	4.72	0.02
1183 - 43	634.54	2063.45	296.78	1339.07	269.26	30.76	235.52	29.39	162.71	30.64	81.52	10.31	57.95	7.73	0.01
1183 - 44	40.54	158.67	27.93	151.61	47.22	9.70	60.80	9.06	54.16	10.00	25.29	2.70	13.74	1.41	<0.008
1183 - 46	619.35	1854.54	252.08	1068.21	177.46	19.97	127.29	14.91	78.26	13.69	35.72	4.48	24.93	3.57	<0.008
1183 - 47	257.00	848.11	144.54	755.81	182.97	24.46	160.18	19.99	102.89	17.77	43.49	5.14	28.02	3.90	<0.009
1183 - 49	483.87	1642.35	247.36	1123.43	212.38	24.09	165.07	19.64	106.89	19.36	50.02	6.08	36.50	4.90	<0.008
1183 - 5	371.78	1205.98	180.98	870.47	184.17	18.04	160.10	19.83	109.30	19.97	54.02	6.76	37.77	5.01	<0.009
1183 - 52	278.30	722.98	103.60	473.79	116.30	16.49	113.40	15.89	92.91	16.78	43.46	5.12	28.29	3.59	0.02
1183 - 53	222.30	672.09	101.97	497.61	130.19	18.85	137.37	16.96	89.34	15.02	34.85	3.59	17.99	1.76	0.02
1183 - 54	570.76	1743.25	248.53	1135.99	214.28	27.41	169.67	20.50	112.78	20.85	55.42	7.14	42.03	5.79	0.03
1183 - 55	547.09	1622.98	226.01	997.29	179.86	23.80	138.88	16.40	87.62	15.85	39.39	4.82	27.15	3.45	<0.009
1183 - 56	882.04	2559.86	344.06	1455.14	238.01	30.30	168.43	19.48	104.72	19.27	51.34	6.57	38.77	5.21	<0.009
1183 - 58	25.55	94.60	16.53	99.32	38.18	8.15	56.81	7.80	43.93	6.97	15.15	1.37	5.49	0.50	<0.009
1183 - 59	21.44	111.95	23.84	160.99	66.08	8.82	91.82	14.00	88.20	18.49	52.65	6.56	37.78	5.06	0.01
1183 - 6	441.32	1264.25	181.53	830.94	166.83	25.10	147.87	18.55	96.74	17.11	42.14	4.85	27.22	3.79	<0.008
1183 - 61	390.59	1164.67	168.51	778.97	156.22	23.72	132.18	16.90	95.86	18.09	50.30	6.26	42.69	6.66	<0.011
1183 - 64	106.89	401.00	67.81	352.33	101.38	13.15	101.12	14.18	80.36	14.68	37.20	4.37	24.58	2.93	<0.010
1183 - 65	96.53	362.17	65.30	377.84	114.24	16.18	120.60	15.03	84.07	13.76	33.05	3.55	17.12	1.97	0.01
1183 - 67	485.07	1374.06	191.56	829.52	147.96	24.83	118.09	13.73	74.20	13.46	34.61	3.86	20.30	2.53	0.01
1183 - 68	458.96	1480.08	214.72	951.66	189.64	25.25	151.20	19.72	105.75	19.20	52.32	6.40	37.76	5.17	<0.010
1183 - 7	330.97	1043.16	158.60	749.76	156.43	23.72	138.03	16.96	86.32	15.25	36.07	4.08	21.74	2.74	<0.009
1183 - 71	879.37	1976.96	254.61	1093.58	211.87	34.66	184.28	21.72	114.90	20.04	49.86	5.75	33.38	4.89	<0.009
1183 - 9	595.15	1774.94	238.37	1006.80	187.01	27.69	151.37	19.53	104.18	18.97	49.89	6.23	37.21	5.31	0.01
1210 - 10	473.05	1406.92	194.32	855.24	161.02	23.75	124.41	15.87	87.38	15.30	39.89	4.96	27.62	3.70	0.01
1210 - 12	644.76	1895.48	242.29	949.56	134.33	18.84	89.13	11.14	61.70	11.28	32.35	4.17	24.85	3.54	0.01
1210 - 13	638.69	1978.04	266.57	1098.84	187.31	23.29	140.85	17.38	93.68	17.21	46.18	5.76	35.30	4.70	<0.009
1210 - 14	621.35	1956.47	273.47	1215.15	232.68	35.94	182.81	24.02	129.52	23.92	64.67	7.87	45.17	5.94	0.02
1210 - 16	849.11	2464.05	325.32	1319.99	209.54	21.89	154.64	18.74	103.01	19.60	51.97	6.36	38.93	5.19	<0.010
1210 - 17	225.08	770.60	126.03	615.44	112.55	23.99	76.37	8.64	41.91	6.91	16.23	1.76	9.54	1.04	<0.009
1210 - 18	398.15	1293.69	188.17	834.39	160.39	19.72	124.33	14.79	79.29	14.00	37.18	4.28	25.81	3.48	0.01
1210 - 20	480.40	1310.26	171.53	685.04	99.06	19.22	66.54	7.58	38.52	6.38	15.64	2.00	11.28	1.35	<0.010
1210 - 21	601.81	1629.26	220.83	955.04	182.74	37.17	149.04	18.53	102.12	17.80	45.96	5.71	34.19	4.07	<0.010
1210 - 23	117.78	404.44	62.47	308.63	69.64	13.60	68.30	8.32	44.53	7.95	18.99	2.04	10.56	1.18	<0.013
1210 - 24	151.80	457.14	73.99	382.14	95.63	19.84	94.28	12.60	68.57	11.89	29.39	3.16	17.47	1.97	0.02
1210 - 25	156.97	548.15	90.24	449.66	104.04	20.30	91.64	11.94	65.01	11.47	28.42	3.11	16.79	2.18	<0.010
1210 - 26	226.95	744.65	112.01	532.79	106.28	22.54	89.09	11.40	63.43	11.74	29.81	3.45	19.56	2.57	<0.010
1210 - 28	404.20	1309.62	194.05	904.79	180.94	27.26	148.69	18.12	95.54	16.93	41.73	4.51	26.22	3.01	0.03
1210 - 3	122.05	415.21	67.68	361.12	85.83	17.79	77.73	10.19	51.62	8.99	22.08	2.76	13.42	1.80	0.09
1210 - 33	460.14	1053.17	139.78	586.73	98.14	19.96	68.60	7.91	38.01	6.89	15.93	1.77	9.71	1.13	<0.010
1210 - 38	728.04	2173.00	274.45	1146.09	184.06	29.92	120.83	14.46	82.96	13.88	37.70	4.29	26.70	3.02	<0.016
1210 - 39	448.67	1442.93	215.32	987.34	194.74	29.51	154.39	19.05	108.57	19.45	52.31	6.18	34.95	4.68	<0.010
1210 - 42	267.93	906.33	144.24	715.15	163.02	20.78	152.98	19.43	109.66	20.26	54.12	6.39	34.49	4.20	<0.010
1210 - 45	435.38	1244.33	182.42	845.87	162.84	24.85	129.87	16.14	90.78	15.07	42.75	4.83	30.79	3.48	0.13
1210 - 46	290.93	727.63	106.56	504.27	109.35	18.74	95.48	12.60	71.86	13.44	32.94	3.64	17.38	2.26	0.02
1210 - 47	265.19	858.21	137.15	675.26	150.89	24.63	123.67	14.90	80.08	14.63	37.01	4.51	25.24	3.32	<0.009
1210 - 48	425.09	1298.32	190.78	885.35	174.28	27.92	148.00	17.63	95.53	17.74	43.49	5.13	28.30	3.75	<0.010
1210 - 5	638.43	2054.89	303.30	1424.03	311.65	51.87	271.79	36.53	208.53	38.29	102.25	12.57	71.33	8.64	0.05
1210 - 52	264.34	891.98	143.16	683.14	150.77	22.95	125.93	15.00	79.52	13.93	35.73	4.20	23.81	3.39	<0.011
1210 - 54	348.61	1212.61	194.03	933.08	195.82	39.19	157.85	20.24	103.93	19.07	50.11	6.34	35.11	4.31	<0.010
1210 - 58	764.68	2536.13	362.34	1542.01	247.70	32.53	172.07	20.65	106.39	19.64	50.34	6.02	37.61	5.15	<0.013
1210 - 59	411.85	1327.49	199.24	904.08	166.72	25.17	128.62	15.62	84.21	15.53	40.28	4.73	29.83	4.04	<0.008
1210 - 6	290.20	965.21	143.36	678.55	134.68	24.78	107.54	13.74	73.08	13.22	33.62	3.87	21.75	2.71	0.03
1210 - 60	268.47	983.02	169.58	895.29	238.27	48.18	236.73	33.39	192.86	36.06	100.55	12.46	72.16	9.88	<0.009
1210 - 61	120.88	493.72	88.29	463.72	112.30	16.20	107.19	13.98	77.12	14.10	37.25	4.88	26.90	3.61	0.02
1210 - 62	671.00	2011.81	287.07	1282.24	243.06	43.62	184.87	23.85	131.07	22.54	59.86	7.53	44.62	5.06	0.01
1210 - 65	422.39	1298.02	193.47	903.83	185.21	26.86	156.87	18.81	100.18	18.04	46.14	5.62	31.14	4.17	<0.008
1210 - 66	197.93	598.49	94.80	467.36	105.69	17.55	85.11	10.23	54.39	9.73	24.32	2.78	15.82	2.11	0.01
1210 - 67	458.47	1540.98	235.61	1091.32	214.08	35.85	169.93	21.35	115.79	20.81	53.80	6.66	37.58	4.37	<0.008

Element concentrations in ppm
$Eu/Eu^{*} = [(Eu_{CN}/(Sm_{CN}+Gd_{CN})/2)]$
$Y/Y^{*} = [(Y_{CN}/(Dy_{CN}+Ho_{CN})/2)]$
$TCe/Ce^{*} = [(Ce_{CN}/(La_{CN} \times Pr_{CN})^{0.5})]$
$LCe/Ce^{*} = [(Ce_{CN}/((Nd_{CN})^{0.5}/Sm_{CN}))]$
CN = chondrite normalised
Normalising values from Sun and McDonough (1989)

Appendix 5 Table A2: LA-ICP-MS Trace element data collected for apatite from Vulcan Prospect in this study

Included Data

Sample	REE	REY	Eu/Eu*	LCe/Ce*	TCe/Ce*	Y/Y*	Ce/Lu	La/Ce	Gd/Yb	La/Sm	Gd/Yb_{CN}	La/Sm_{CN}	La/Ce_{CN}	La/Yb_{CN}
1183 - 28	4615.53	5273.98	0.25	0.04	1.11	0.63	13.04	0.34	4.18	2.99	3.46	1.9289	0.87	10.49
1183 - 29	3317.71	3737.12	0.31	0.04	1.11	0.56	15.83	0.32	5.99	2.46	4.95	1.5892	0.83	12.40
1183 - 3	3201.47	3592.70	0.27	0.05	1.16	0.60	17.86	0.30	5.18	2.68	4.28	1.7282	0.78	12.68
1183 - 30	3328.04	3855.38	0.30	0.04	1.13	0.59	11.39	0.30	4.76	1.99	3.94	1.2872	0.77	8.13
1183 - 31	2554.75	3188.43	0.20	0.03	1.13	0.60	6.67	0.26	4.39	1.17	3.63	0.7546	0.68	4.05
1183 - 32	3847.55	4394.29	0.27	0.04	1.12	0.61	14.22	0.32	5.03	2.46	4.16	1.5863	0.82	11.15
1183 - 33	3642.23	4160.89	0.28	0.05	1.14	0.65	13.21	0.31	4.07	2.54	3.37	1.6427	0.80	9.43
1183 - 34	2782.99	3352.87	0.28	0.03	1.11	0.58	10.36	0.30	5.19	1.62	4.29	1.0486	0.78	6.46
1183 - 35	4460.20	4959.98	0.30	0.05	1.15	0.62	19.14	0.32	4.57	3.16	3.78	2.0420	0.83	13.99
1183 - 36	3499.79	4003.14	0.27	0.05	1.09	0.60	13.10	0.34	4.35	2.75	3.60	1.7766	0.88	10.48
1183 - 37	4495.12	5026.43	0.24	0.04	1.14	0.61	17.48	0.30	4.94	2.61	4.08	1.6836	0.79	12.14
1183 - 38	510.29	713.72	0.32	0.02	1.09	0.48	4.80	0.22	11.30	0.29	9.35	0.1898	0.56	1.89
1183 - 4	3766.71	4674.87	0.28	0.04	1.12	0.69	8.22	0.32	3.74	2.15	3.09	1.3898	0.83	6.05
1183 - 40	4638.94	5228.28	0.25	0.04	1.16	0.60	16.39	0.29	4.84	2.41	4.00	1.5526	0.76	10.80
1183 - 43	5249.64	6157.71	0.23	0.04	1.15	0.63	11.08	0.31	4.06	2.36	3.36	1.5214	0.79	7.85
1183 - 44	612.82	932.72	0.37	0.05	1.14	0.67	4.66	0.26	4.42	0.86	3.66	0.5542	0.66	2.12
1183 - 46	4294.48	4708.15	0.23	0.05	1.13	0.61	21.53	0.33	5.11	3.49	4.22	2.2531	0.86	17.82
1183 - 47	2594.26	3153.05	0.27	0.03	1.06	0.63	9.03	0.30	5.72	1.40	4.73	0.9068	0.78	6.58
1183 - 49	4141.93	4700.81	0.23	0.04	1.15	0.60	13.92	0.29	4.52	2.28	3.74	1.4708	0.76	9.51
1183 - 5	3244.17	3830.37	0.20	0.04	1.12	0.61	9.99	0.31	4.24	2.02	3.51	1.3032	0.80	7.06
1183 - 52	2030.91	2482.68	0.27	0.05	1.03	0.56	8.36	0.38	4.01	2.39	3.32	1.5449	0.99	7.06
1183 - 53	1959.90	2435.19	0.27	0.04	1.08	0.62	15.88	0.33	7.64	1.71	6.32	1.1023	0.85	8.86
1183 - 54	4374.38	4974.89	0.26	0.04	1.12	0.61	12.50	0.33	4.04	2.66	3.34	1.7196	0.85	9.74
1183 - 55	3930.62	4380.91	0.27	0.05	1.12	0.59	19.50	0.34	5.11	3.04	4.23	1.9637	0.87	14.45
1183 - 56	5923.19	6473.69	0.27	0.05	1.12	0.60	20.41	0.34	4.34	3.71	3.59	2.3924	0.89	16.32
1183 - 58	420.35	627.06	0.36	0.04	1.11	0.56	7.85	0.27	10.34	0.67	8.55	0.4319	0.70	3.34
1183 - 59	707.67	1263.66	0.23	0.02	1.20	0.69	0.92	0.19	2.43	0.32	2.01	0.2094	0.49	0.41
1183 - 6	3268.24	3754.68	0.30	0.04	1.08	0.58	13.85	0.35	5.43	2.65	4.49	1.7078	0.90	11.63
1183 - 61	3051.62	3554.41	0.30	0.05	1.10	0.59	7.25	0.34	3.10	2.50	2.56	1.6141	0.87	6.56
1183 - 64	1321.99	1739.24	0.25	0.04	1.14	0.59	5.67	0.27	4.11	1.05	3.40	0.6807	0.69	3.12
1183 - 65	1321.41	1708.78	0.27	0.03	1.10	0.54	7.64	0.27	7.04	0.84	5.83	0.5455	0.69	4.04
1183 - 67	3333.77	3731.75	0.34	0.06	1.09	0.62	22.50	0.35	5.82	3.28	4.81	2.1165	0.91	17.14
1183 - 68	3717.85	4259.33	0.27	0.04	1.14	0.59	11.87	0.31	4.00	2.42	3.31	1.5624	0.80	8.72
1183 - 7	2783.84	3201.21	0.30	0.04	1.10	0.56	15.82	0.32	6.35	2.12	5.25	1.3659	0.82	10.92
1183 - 71	4885.84	5484.82	0.33	0.05	1.01	0.60	16.77	0.44	5.52	4.15	4.57	2.6794	1.15	18.90
1183 - 9	4222.64	4794.15	0.30	0.05	1.14	0.63	13.87	0.34	4.07	3.18	3.37	2.0545	0.87	11.47
1210 - 10	3433.43	3875.76	0.30	0.05	1.12	0.59	15.79	0.34	4.50	2.94	3.73	1.8966	0.87	12.28
1210 - 12	4123.42	4469.36	0.30	0.08	1.16	0.64	22.22	0.34	3.59	4.80	2.97	3.0987	0.88	18.61
1210 - 13	4553.79	5046.93	0.26	0.05	1.16	0.60	17.46	0.32	3.99	3.41	3.30	2.2013	0.83	12.98
1210 - 14	4819.00	5518.88	0.32	0.04	1.15	0.62	13.67	0.32	4.05	2.67	3.35	1.7239	0.82	9.87
1210 - 16	5588.35	6123.83	0.22	0.06	1.13	0.59	19.70	0.34	3.97	4.05	3.29	2.6161	0.89	15.65
1210 - 17	2036.10	2247.48	0.45	0.05	1.11	0.59	30.75	0.29	8.00	2.00	6.62	1.2910	0.75	16.92
1210 - 18	3197.67	3624.08	0.25	0.05	1.14	0.62	15.42	0.31	4.82	2.48	3.99	1.6026	0.79	11.07
1210 - 20	2914.79	3107.50	0.41	0.09	1.10	0.59	40.38	0.37	5.90	4.85	4.88	3.1308	0.95	30.56
1210 - 21	4004.28	4606.19	0.41	0.05	1.08	0.68	16.60	0.37	4.36	3.29	3.61	2.1260	0.95	12.63
1210 - 23	1138.42	1391.13	0.38	0.06	1.14	0.65	14.20	0.29	6.47	1.69	5.35	1.0918	0.75	8.00
1210 - 24	1419.87	1777.72	0.40	0.04	1.04	0.61	9.64	0.33	5.40	1.59	4.46	1.0247	0.86	6.23
1210 - 25	1599.91	1944.54	0.39	0.04	1.11	0.61	10.46	0.29	5.46	1.51	4.52	0.9741	0.74	6.71
1210 - 26	1976.25	2336.92	0.43	0.05	1.13	0.65	12.04	0.30	4.55	2.14	3.77	1.3785	0.79	8.32
1210 - 28	3375.61	3850.13	0.30	0.04	1.13	0.57	18.05	0.31	5.67	2.23	4.69	1.4421	0.80	11.06
1210 - 3	1258.27	1537.09	0.41	0.04	1.10	0.63	9.59	0.29	5.79	1.42	4.79	0.9180	0.76	6.52
1210 - 33	2507.87	2709.13	0.43	0.08	1.00	0.61	38.82	0.44	7.07	4.69	5.85	3.0267	1.13	34.01
1210 - 38	4839.40	5290.16	0.34	0.06	1.17	0.64	29.83	0.34	4.53	3.96	3.74	2.5536	0.87	19.56
1210 - 39	3718.09	4294.23	0.31	0.04	1.12	0.61	12.81	0.31	4.42	2.30	3.65	1.4873	0.80	9.21
1210 - 42	2618.99	3229.32	0.25	0.04	1.11	0.63	8.95	0.30	4.44	1.64	3.67	1.0610	0.76	5.57
1210 - 45	3229.40	3731.88	0.31	0.04	1.07	0.65	14.83	0.35	4.22	2.67	3.49	1.7261	0.90	10.14
1210 - 46	2007.09	2363.80	0.34	0.05	1.00	0.56	13.36	0.40	5.49	2.66	4.54	1.7176	1.03	12.01
1210 - 47	2414.70	2870.31	0.33	0.04	1.09	0.65	10.71	0.31	4.90	1.76	4.05	1.1346	0.80	7.54
1210 - 48	3361.31	3868.38	0.32	0.04	1.10	0.60	14.37	0.33	5.23	2.44	4.33	1.5746	0.85	10.77
1210 - 5	5534.10	6737.62	0.33	0.03	1.13	0.66	9.87	0.31	3.81	2.05	3.15	1.3225	0.80	6.42
1210 - 52	2457.85	2880.56	0.31	0.04	1.11	0.62	10.91	0.30	5.29	1.75	4.37	1.1319	0.77	7.96
1210 - 54	3320.29	3913.87	0.41	0.03	1.13	0.65	11.69	0.29	4.50	1.78	3.72	1.1493	0.74	7.12
1210 - 58	5903.27	6473.30	0.28	0.04	1.16	0.61	20.42	0.30	4.57	3.09	3.78	1.9929	0.78	14.58
1210 - 59	3357.42	3809.92	0.31	0.05	1.12	0.61	13.65	0.31	4.31	2.47	3.57	1.5948	0.80	9.90
1210 - 6	2506.29	2904.11	0.37	0.05	1.14	0.62	14.78	0.30	4.95	2.15	4.09	1.3910	0.78	9.57
1210 - 60	3296.90	4431.12	0.39	0.02	1.11	0.67	4.13	0.27	3.28	1.13	2.71	0.7274	0.71	2.67
1210 - 61	1580.14	1990.13	0.28	0.03	1.15	0.61	5.68	0.24	3.98	1.08	3.30	0.6949	0.63	3.22
1210 - 62	5018.20	5745.00	0.37	0.04	1.11	0.65	16.50	0.33	4.14	2.76	3.43	1.7822	0.86	10.79
1210 - 65	3410.74	3958.82	0.29	0.04	1.10	0.63	12.92	0.33	5.04	2.28	4.17	1.4723	0.84	9.73
1210 - 66	1686.29	1990.69	0.34	0.04	1.06	0.64	11.79	0.33	5.38	1.87	4.45	1.2089	0.85	8.98
1210 - 67	4006.60	4681.82	0.34	0.04	1.13	0.67	14.62	0.30	4.52	2.14	3.74	1.3825	0.77	8.75

Element concentrations in ppm
$Eu/Eu^* = [(Eu_{CN}/(Sm_{CN}+Gd_{CN})/2)]$
$Y/Y^* = [(Y_{CN}/(Dy_{CN}+Ho_{CN})/2)]$
$TCe/Ce^* = [(Ce_{CN}/(La_{CN} \times Pr_{CN})^{0.5})]$
$LCe/Ce^* = [(Ce_{CN}/((Nd_{CN})^{0.5}/Sm_{CN}))]$
CN = chondrite normalised
Normalising values from Sun and McDonough (1989)

Appendix 5 Supplementary material for Mapping hydrothermal systems in IOCG deposits using apatite geochronology and geochemsitry: An example from Vulcan Cu-Au prospect

Appendix 5 Table A2: LA-ICP-MS Trace element data collected for apatite from Vulcan Prospect in this study

Included Data													
Sample	**Drill hole**	**Comment**	**Si**	**P**	**Ca**	**V**	**Mn**	**Fe**	**Sr**	**Y**	**Zr**	**Th**	**U**
1210 - 68	VUD 017 1210		707.54	190156.05	393600	0.40	67.81	1854.43	381.57	584.20	30.64	145.74	14.10
1210 - 69	VUD 017 1210		337.31	194231.80	393600	0.08	62.26	287.79	330.84	270.76	2.46	0.67	1.07
1210 - 70	VUD 017 1210		647.26	192262.83	393600	<0.077	65.41	493.72	360.16	547.33	<0.006	202.78	1.93
1210 - 71	VUD 017 1210		592.67	192964.72	393600	0.40	73.12	420.55	381.32	519.78	0.09	62.48	6.72
1210 - 72	VUD 017 1210		340.19	193420.72	393600	<0.081	58.59	446.66	336.16	331.06	0.07	3.70	1.14
1210 - 73	VUD 017 1210		558.27	188984.18	393600	2.61	69.18	498.51	368.53	532.02	0.06	123.85	12.82
1210 - 74	VUD 017 1210		534.45	189542.94	393600	0.14	67.88	989.75	379.10	484.00	0.06	54.21	5.68
1210 - 75	VUD 017 1210		182.06	196067.90	393600	0.10	47.74	473.70	336.08	145.29	0.02	2.36	0.20
1210 - 76	VUD 017 1210		509.66	189149.54	393600	2.23	70.93	5356.10	568.21	453.25	6.45	25.82	5.36
1210 - 8	VUD 017 1210		592.85	191467.27	393600	1.61	58.80	3475.27	371.62	518.67	3.04	25.66	7.59
1210 - 9	VUD 017 1210		151.40	186842.93	393600	0.23	61.59	608.53	300.29	285.45	1.48	3.55	0.94
1488 - 38	VUD 016 1488		2719.74	191279.05	393600	2.00	44.29	4435.65	266.94	308.89	0.16	0.29	4.87
1488 - 29	VUD 016 1488		3558.68	188699.64	393600	0.25	37.93	1601.16	297.64	263.76	<0.007	0.21	5.24
1488 - 32	VUD 016 1488		151.50	188409.51	393600	<0.064	42.49	82.03	242.42	377.91	0.02	0.50	7.98
1488 - 41	VUD 016 1488		18784.65	183448.33	393600	0.83	38.71	5001.27	277.88	243.78	0.12	0.43	5.75
1488 - 30	VUD 016 1488		156.95	188144.03	393600	<0.068	41.88	67.58	260.58	478.30	0.12	2.13	15.43
1488 - 21	VUD 016 1488		<117.626	188259.54	393600	<0.084	30.36	97.82	608.92	85.34	<0.007	0.39	0.40
1488 - 23	VUD 016 1488		3300.97	188228.32	393600	1.63	47.90	5239.85	252.93	388.71	0.38	0.21	8.90
1488 - 74	VUD 016 1488		39514.59	184052.79	393600	1.69	51.26	6664.67	363.42	107.27	0.11	0.80	0.45
1488 - 31	VUD 016 1488		2560.86	187248.59	393600	1.03	35.75	4448.58	292.48	295.90	0.25	0.88	7.64
1488 - 14	VUD 016 1488		8505.61	185980.92	393600	1.56	41.97	2548.25	296.42	272.14	0.11	0.49	5.16
1488 - 70	VUD 016 1488		858.89	189362.10	393600	0.29	30.62	1196.85	289.64	249.54	0.04	1.14	3.93
1488 - 63	VUD 016 1488		25168.83	178897.52	393600	9.39	45.05	2991.84	383.54	186.60	0.21	0.86	2.07
1488 - 35	VUD 016 1488		161.87	187351.68	393600	0.69	43.23	961.74	280.84	373.53	0.09	0.12	9.62
1488 - 37	VUD 016 1488		13246.38	187380.84	393600	0.97	46.95	1189.24	242.69	369.67	0.14	0.14	8.64
1488 - 44	VUD 016 1488		8622.17	187316.78	393600	4.65	44.68	8003.48	271.75	313.94	0.27	0.40	8.24
1488 - 64	VUD 016 1488		10679.69	182034.88	393600	3.10	49.98	2157.05	455.61	215.35	0.17	2.49	0.62
1488 - 69	VUD 016 1488		569.68	182912.09	393600	0.50	34.30	565.56	280.13	446.78	0.02	7.01	11.76
1488 - 17	VUD 016 1488		3087.04	186010.59	393600	1.13	36.91	1950.69	286.63	310.05	0.07	0.41	7.98
1488 - 34	VUD 016 1488		1307.79	186063.76	393600	0.67	33.22	3338.88	410.30	127.94	0.23	0.02	1.61
1488 - 54	VUD 016 1488		1444.42	189193.55	393600	0.14	40.44	436.32	257.93	272.74	0.04	0.29	6.15
1488 - 10	VUD 016 1488		431.52	188085.72	393600	0.23	38.67	1371.27	301.27	277.26	<0.011	0.62	4.49
1488 - 65	VUD 016 1488		5361.29	187202.04	393600	2.03	36.58	2587.97	308.76	242.61	0.10	1.66	6.24
1488 - 27	VUD 016 1488		345.27	186932.06	393600	0.42	32.40	4269.44	347.91	171.63	0.03	0.93	3.12
1488 - 8	VUD 016 1488		1913.85	181772.94	393600	1.06	42.45	2695.93	246.23	390.25	0.04	1.61	10.00
1488 - 66	VUD 016 1488		1722.59	189549.61	393600	0.10	34.65	2052.54	267.30	246.26	0.07	0.18	5.12
1488 - 4	VUD 016 1488		5777.72	187397.44	393600	<0.133	40.75	771.65	644.35	80.07	<0.010	0.79	0.10
1488 - 28	VUD 016 1488		1232.32	188547.30	393600	1.60	39.49	2140.47	299.72	307.75	0.05	0.18	7.46
1488 - 22	VUD 016 1488		171.45	187466.95	393600	<0.087	32.15	233.28	713.98	77.86	<0.007	1.17	0.44
1488 - 9	VUD 016 1488		787.45	187086.19	393600	1.07	31.50	3126.86	302.45	212.77	0.06	0.74	4.29
1488 - 7	VUD 016 1488		773.23	194227.41	393600	0.78	59.45	5376.40	568.60	130.46	0.19	2.32	0.41
1488 - 36	VUD 016 1488		536.97	187450.99	393600	<0.102	30.76	1124.59	277.07	138.11	0.05	0.01	1.34
1488 - 5	VUD 016 1488		4713.15	185093.97	393600	2.94	31.55	3894.66	322.86	256.58	0.17	3.50	5.83
1488 - 52	VUD 016 1488		238.70	188856.88	393600	<0.086	37.08	42.78	560.24	134.93	<0.006	0.68	2.21
1488 - 45	VUD 016 1488		13120.25	185080.46	393600	4.68	48.05	3620.36	318.28	355.08	9.60	1.21	6.97
1488 - 56	VUD 016 1488		2571.32	190939.00	393600	0.89	45.89	2171.71	264.16	318.08	0.05	0.65	4.60
1488 - 3	VUD 016 1488		4693.89	182572.85	393600	1.19	36.29	3112.41	292.58	437.17	2.52	20.66	9.03
1488 - 67	VUD 016 1488		208.90	191811.44	393600	0.12	39.37	567.44	817.82	74.09	0.01	0.76	0.03
1488 - 51	VUD 016 1488		5677.21	191078.81	393600	1.66	34.05	1817.54	313.28	276.52	0.27	0.44	7.41
1488 - 11	VUD 016 1488		1884.61	188689.64	393600	1.06	44.68	4501.36	384.59	201.61	0.13	0.54	3.26
1488 - 18	VUD 016 1488		32668.66	180874.28	393600	0.54	55.45	3357.40	567.26	174.39	0.12	1.71	0.31
1488 - 2	VUD 016 1488		31579.77	165594.83	393600	<0.101	41.50	1416.54	229.75	248.03	0.09	0.07	5.60
1488 - 13	VUD 016 1488		8477.20	183424.01	393600	3.01	50.82	3431.27	432.13	304.83	0.18	1.98	1.24
1488 - 57	VUD 016 1488		1870.15	191235.16	393600	0.36	43.78	1692.13	246.44	360.27	0.07	0.17	7.11
1488 - 46	VUD 016 1488		18354.02	186167.75	393600	0.64	47.02	2699.62	405.91	135.49	0.05	0.41	0.99
1488 - 43	VUD 016 1488		1556.76	191241.05	393600	0.90	32.96	1378.03	300.08	198.90	6.88	0.74	5.83
1488 - 19	VUD 016 1488	La/Ce >1	2727.84	186599.36	393600	1.45	33.88	4499.14	314.63	171.34	0.15	0.23	3.39
1488 - 42	VUD 016 1488	LREE enriched	196.54	189100.46	393600	0.29	48.78	2501.70	640.04	122.05	0.12	2.53	0.25
1488 - 33	VUD 016 1488	LREE enriched	3847.35	185791.60	393600	1.48	32.00	1091.93	276.30	374.92	0.29	6.43	8.61
1488 - 16	VUD 016 1488	LREE enriched	31601.80	174709.25	393600	0.38	48.43	1143.40	416.24	261.06	0.05	1.57	2.61
1488 - 49	VUD 016 1488	LREE enriched	1899.84	186577.96	393600	1.23	46.84	1506.07	279.07	410.79	0.16	1.04	10.28
1488 - 73	VUD 016 1488	LREE enriched	3253.36	186648.65	393600	1.64	46.61	3818.22	323.43	363.60	0.26	2.47	10.01
1488 - 15	VUD 016 1488	LREE enriched	20848.43	183067.63	393600	3.98	53.32	4053.44	568.24	290.72	0.32	6.29	1.56
1488 - 72	VUD 016 1488	LREE enriched	9948.12	187321.68	393600	3.60	42.65	6674.39	432.10	292.10	0.60	5.52	6.18
1488 - 48	VUD 016 1488	LREE enriched	4704.07	185286.55	393600	0.21	37.08	1501.98	948.03	209.62	0.22	23.10	6.62
1488 - 71	VUD 016 1488	LREE enriched	15663.94	182764.26	393600	1.36	37.02	3410.88	394.48	194.29	0.19	2.99	6.45
1488 - 55	VUD 016 1488	LREE enriched	10640.72	186541.88	393600	1.94	48.83	4405.14	602.06	276.33	0.25	33.24	3.67
1488 - 40	VUD 016 1488	LREE enriched	1429.24	201974.61	393600	0.61	47.22	900.20	1319.85	356.62	0.90	54.21	8.01

Element concentrations in ppm
$Eu/Eu^{*} = [(Eu_{CN}/(Sm_{CN}+Gd_{CN})/2)]$
$Y/Y^{*} = [(Y_{CN}/(Dy_{CN}+Ho_{CN})/2)]$
$TCe/Ce^{*} = [(Ce_{CN}/(La_{CN} \times Pr_{CN})^{0.5})]$
$LCe/Ce^{*} = [(Ce_{CN}/((Nd_{CN})^{0.5}/Sm_{CN}))]$
CN = chondrite normalised
Normalising values from Sun and McDonough (1989)

Appendix 5 Table A2: LA-ICP-MS Trace element data collected for apatite from Vulcan Prospect in this study

Included Data

Sample	La	Ce	Pr	Nd	Sm	Eu	Gd	Tb	Dy	Ho	Er	Tm	Yb	Lu	Hf
1210 - 68	406.14	1194.52	180.35	868.09	187.66	29.75	161.82	20.16	108.65	19.13	48.77	5.66	32.73	4.20	0.99
1210 - 69	110.19	363.69	60.62	319.42	80.80	17.59	79.91	9.72	49.19	8.49	21.21	2.40	12.41	1.51	0.11
1210 - 70	508.20	1826.85	269.18	1195.48	210.63	22.52	163.56	19.86	106.81	19.38	52.67	6.41	38.83	5.00	<0.008
1210 - 71	248.00	846.19	137.99	686.17	153.88	26.17	136.11	16.61	91.34	16.36	40.92	5.09	29.30	3.96	<0.008
1210 - 72	186.73	621.73	97.72	486.97	108.99	18.62	96.69	11.37	58.52	10.57	26.61	3.17	17.89	2.19	<0.008
1210 - 73	238.84	858.86	139.21	696.39	154.83	26.43	134.50	16.64	91.90	16.53	44.04	5.16	29.61	3.88	0.03
1210 - 74	458.22	1317.12	185.16	829.50	164.00	22.30	136.96	16.64	92.35	16.59	42.46	5.12	28.57	3.85	<0.008
1210 - 75	183.60	381.30	53.37	255.08	56.77	10.99	49.28	5.91	30.37	4.55	11.35	1.25	6.59	0.77	<0.011
1210 - 76	436.63	1357.77	199.00	872.69	161.25	24.20	129.62	16.29	86.42	15.76	40.43	4.85	28.61	3.53	0.16
1210 - 8	260.47	677.12	108.30	567.86	141.74	29.68	134.34	17.54	94.24	16.41	41.10	4.86	26.40	3.23	0.12
1210 - 9	144.65	427.15	69.73	358.68	88.52	18.36	83.10	10.28	53.20	8.70	22.41	2.56	13.26	1.58	0.08
1488 - 38	0.02	0.67	0.31	4.25	17.33	16.40	130.27	24.25	104.84	13.20	23.61	2.28	9.60	1.03	<0.011
1488 - 29	0.02	0.33	0.21	3.14	11.52	10.10	80.07	16.56	81.35	10.73	20.41	1.81	8.56	0.82	<0.010
1488 - 32	0.02	0.37	0.25	3.85	14.65	13.25	115.72	23.89	116.80	15.48	29.92	2.69	12.90	1.29	<0.008
1488 - 41	0.02	0.58	0.23	4.30	14.21	12.93	95.42	17.04	77.14	10.25	18.73	1.72	8.18	0.80	0.02
1488 - 30	0.02	0.53	0.35	5.23	15.54	13.30	116.01	24.79	135.10	19.68	38.04	3.55	16.47	1.78	<0.008
1488 - 21	0.02	0.41	0.27	3.37	8.13	6.91	47.39	8.21	37.23	4.13	6.17	0.48	1.93	0.17	<0.009
1488 - 23	0.02	0.40	0.25	4.03	14.46	13.71	120.82	24.97	124.78	16.65	31.73	2.77	13.07	1.37	<0.010
1488 - 74	0.03	0.47	0.33	4.93	20.15	19.21	140.45	18.54	56.96	5.11	9.08	0.72	2.41	0.33	<0.015
1488 - 31	0.03	0.58	0.41	5.61	16.69	12.81	91.16	17.22	88.11	12.18	22.44	1.98	9.51	0.94	<0.012
1488 - 14	0.03	0.70	0.34	5.13	18.55	17.87	131.10	23.15	97.05	11.63	21.21	2.08	9.27	0.88	<0.009
1488 - 70	0.04	0.84	0.33	6.08	15.10	12.29	88.06	14.92	78.30	10.34	18.52	1.70	6.57	0.78	0.01
1488 - 63	0.04	1.15	0.61	8.99	36.29	33.07	219.00	27.96	92.56	8.73	14.01	1.27	5.41	0.67	<0.013
1488 - 35	0.04	0.58	0.29	4.38	14.21	12.82	101.35	22.20	111.41	14.94	28.67	2.69	13.09	1.34	0.02
1488 - 37	0.04	0.58	0.29	4.49	13.71	12.80	104.71	22.29	115.77	14.60	28.78	2.65	13.08	1.21	0.05
1488 - 44	0.04	0.78	0.38	4.63	13.51	10.91	92.97	18.67	97.87	12.74	24.94	2.24	11.29	1.11	0.03
1488 - 64	0.04	1.38	0.62	12.71	48.32	49.05	341.08	44.13	126.54	11.05	15.97	1.28	5.95	0.57	0.04
1488 - 69	0.05	1.25	0.79	9.58	35.21	26.10	157.38	25.74	132.89	17.55	35.60	3.14	12.59	1.44	0.02
1488 - 17	0.05	0.47	0.25	3.58	12.86	10.81	86.48	18.05	94.32	12.97	24.09	2.06	10.63	1.04	0.02
1488 - 34	0.05	0.41	0.25	3.75	8.27	7.13	53.74	9.30	43.57	5.18	9.86	0.80	3.50	0.39	<0.010
1488 - 54	0.05	0.78	0.32	5.43	14.68	13.40	99.18	19.06	86.08	11.24	20.99	2.03	9.17	0.86	<0.011
1488 - 10	0.05	0.67	0.46	5.81	22.90	19.66	155.59	26.09	103.17	11.37	21.35	2.17	7.97	0.89	<0.014
1488 - 65	0.05	0.52	0.25	3.86	10.98	9.22	77.44	15.47	75.82	9.75	18.48	1.66	7.26	0.84	0.02
1488 - 27	0.05	0.57	0.35	4.78	9.92	7.57	60.58	10.93	55.84	7.44	12.89	1.20	5.07	0.57	<0.010
1488 - 8	0.05	0.34	0.21	3.69	12.21	11.77	114.80	24.90	121.96	15.65	31.02	2.81	12.65	1.46	0.04
1488 - 66	0.06	0.46	0.25	3.45	11.76	10.81	80.02	15.83	76.60	10.04	18.12	1.73	7.86	0.81	<0.010
1488 - 4	0.06	1.77	1.15	18.73	72.37	62.63	334.01	33.12	71.78	4.93	6.00	0.48	1.34	0.10	<0.013
1488 - 28	0.07	0.41	0.26	3.63	12.66	11.44	93.32	18.65	93.87	12.78	23.87	2.36	11.15	1.03	<0.010
1488 - 22	0.07	0.54	0.25	3.60	8.65	8.06	52.06	7.35	34.32	3.91	6.11	0.47	1.70	0.17	<0.009
1488 - 9	0.07	0.44	0.24	3.27	9.49	8.66	69.02	12.93	65.87	8.69	16.15	1.56	6.55	0.71	<0.011
1488 - 7	0.08	1.65	0.91	13.12	60.84	57.06	359.83	40.53	90.87	6.29	9.69	0.76	2.89	0.28	<0.014
1488 - 36	0.08	0.36	0.21	2.58	9.84	8.11	57.82	10.42	44.45	6.02	10.13	0.85	4.19	0.41	0.01
1488 - 5	0.09	0.78	0.56	5.71	15.20	11.92	82.83	15.52	77.11	10.34	19.06	1.65	6.90	0.70	<0.012
1488 - 52	0.11	2.02	0.91	10.00	12.72	8.14	58.61	9.88	47.56	6.09	10.21	0.84	3.39	0.32	<0.009
1488 - 45	0.12	1.37	0.72	8.16	33.20	32.28	226.70	36.36	134.08	15.21	28.60	2.48	12.52	1.13	0.23
1488 - 56	0.12	0.83	0.38	4.10	19.92	18.35	145.29	26.44	111.21	13.79	24.45	2.33	10.18	1.02	<0.009
1488 - 3	0.14	2.08	1.06	16.46	35.69	26.58	155.74	25.49	134.73	17.96	32.75	2.73	11.18	1.18	0.08
1488 - 67	0.15	2.25	1.43	23.81	83.26	72.22	389.00	35.14	75.01	4.81	5.00	0.38	1.33	0.12	<0.008
1488 - 51	0.17	0.86	0.39	4.66	12.42	9.64	80.63	15.98	83.25	11.04	21.54	1.85	9.24	0.84	0.02
1488 - 11	0.17	1.21	0.58	7.85	32.68	30.66	202.90	26.17	87.58	9.31	14.93	1.38	5.84	0.67	0.02
1488 - 18	0.17	2.69	1.36	20.49	84.58	78.60	479.10	52.45	127.65	9.31	12.09	0.89	4.02	0.31	0.04
1488 - 2	0.17	0.45	0.16	2.12	8.50	9.01	73.17	15.57	74.94	9.96	19.04	1.90	7.42	0.84	<0.012
1488 - 13	0.23	2.27	1.12	15.41	65.80	66.61	448.31	58.43	169.65	15.03	21.94	1.87	7.78	0.70	0.06
1488 - 57	0.35	1.18	0.35	4.28	13.53	11.97	106.07	22.17	107.09	15.00	27.89	2.61	12.95	1.22	<0.013
1488 - 46	0.60	2.16	0.64	8.51	30.60	29.87	194.43	24.68	74.34	6.85	9.91	0.91	3.70	0.38	<0.011
1488 - 43	0.73	3.78	0.92	9.27	12.60	9.20	64.18	12.17	62.04	7.71	15.69	1.28	6.27	0.60	0.15
1488 - 19	0.92	2.27	0.48	4.49	10.18	7.55	58.55	10.70	54.12	6.82	12.74	1.19	4.84	0.55	0.02
1488 - 42	6.80	18.55	2.82	22.23	71.86	63.63	373.39	39.08	95.05	6.63	8.55	0.67	3.11	0.25	<0.010
1488 - 33	7.12	14.91	1.76	13.21	24.54	18.70	125.90	21.13	108.51	15.18	28.18	2.46	11.02	1.21	<0.011
1488 - 16	16.53	38.21	5.29	26.15	47.66	45.33	288.59	38.01	122.56	11.77	20.34	1.62	8.01	0.77	<0.013
1488 - 49	16.76	37.54	4.45	18.05	18.16	14.84	122.04	24.88	123.50	16.53	32.41	3.06	13.42	1.43	<0.009
1488 - 73	31.27	69.74	7.53	32.55	19.35	14.51	115.75	21.61	111.26	14.48	29.24	2.75	12.74	1.27	<0.010
1488 - 15	61.81	166.20	17.71	67.97	81.25	72.90	496.44	60.29	170.39	14.41	20.60	1.80	7.00	0.72	0.03
1488 - 72	74.83	159.80	17.06	68.22	27.65	19.54	144.47	23.91	103.59	12.50	23.61	2.09	9.10	0.92	0.05
1488 - 48	134.47	219.40	18.81	64.58	17.91	12.67	72.38	12.75	67.20	8.61	15.84	1.44	6.75	0.60	0.03
1488 - 71	196.73	299.29	27.14	76.24	16.99	10.03	64.97	12.30	60.10	7.93	14.29	1.31	5.84	0.63	0.01
1488 - 55	261.46	513.05	52.82	166.29	48.78	32.62	218.78	32.28	114.49	12.31	21.41	1.86	8.59	0.84	<0.009
1488 - 40	484.59	1096.23	117.59	404.34	91.70	46.37	269.67	37.16	136.44	15.84	26.15	2.53	10.97	1.09	0.07

Element concentrations in ppm
$Eu/Eu^* = [(Eu_{CN}/(Sm_{CN}+Gd_{CN})/2)]$
$Y/Y^* = [(Y_{CN}/(Dy_{CN}+Ho_{CN})/2)]$
$TCe/Ce^* = [(Ce_{CN}/(La_{CN} \times Pr_{CN})^{0.5})]$
$LCe/Ce^* = [(Ce_{CN}/((Nd_{CN})^{0.5}/Sm_{CN}))]$
CN = chondrite normalised
Normalising values from Sun and McDonough (1989)

Appendix 5 Supplementary material for Mapping hydrothermal systems in IOCG deposits using apatite geochronology and geochemsitry: An example from Vulcan Cu-Au prospect

Appendix 5 Table A2: LA-ICP-MS Trace element data collected for apatite from Vulcan Prospect in this study

Included Data

Sample	REE	REY	Eu/Eu*	LCe/Ce*	TCe/Ce*	Y/Y*	Ce/Lu	La/Ce	Gd/Yb	La/Sm	Gd/Yb_{CN}	La/Sm_{CN}	La/Ce_{CN}	La/Yb_{CN}
1210 - 68	3267.64	3851.84	0.32	0.04	1.07	0.62	11.79	0.34	4.94	2.16	4.09	1.3971	0.88	8.90
1210 - 69	1137.14	1407.90	0.42	0.04	1.08	0.64	10.01	0.30	6.44	1.36	5.33	0.8804	0.78	6.37
1210 - 70	4445.41	4992.74	0.22	0.04	1.19	0.59	15.16	0.28	4.21	2.41	3.48	1.5576	0.72	9.39
1210 - 71	2438.08	2957.87	0.34	0.04	1.11	0.65	8.88	0.29	4.65	1.61	3.84	1.0404	0.76	6.07
1210 - 72	1747.75	2078.81	0.34	0.04	1.11	0.65	11.76	0.30	5.40	1.71	4.47	1.1060	0.78	7.49
1210 - 73	2456.83	2988.85	0.34	0.04	1.14	0.67	9.19	0.28	4.54	1.54	3.76	0.9959	0.72	5.79
1210 - 74	3318.84	3802.84	0.27	0.05	1.09	0.60	14.20	0.35	4.79	2.79	3.97	1.8037	0.90	11.50
1210 - 75	1051.19	1196.48	0.39	0.07	0.93	0.58	20.45	0.48	7.48	3.23	6.18	2.0879	1.24	19.98
1210 - 76	3377.06	3830.31	0.30	0.05	1.11	0.60	15.95	0.32	4.53	2.71	3.75	1.7480	0.83	10.95
1210 - 8	2123.28	2641.95	0.41	0.03	0.97	0.64	8.69	0.38	5.09	1.84	4.21	1.1863	0.99	7.08
1210 - 9	1302.18	1587.63	0.41	0.04	1.03	0.63	11.22	0.34	6.27	1.63	5.18	1.0549	0.87	7.83
1488 - 38	348.06	656.96	0.66	0.00	2.29	0.37	0.03	0.02	13.57	0.00	11.23	0.0006	0.06	0.00
1488 - 29	245.61	509.37	0.64	0.00	1.36	0.40	0.02	0.05	9.36	0.00	7.74	0.0009	0.13	0.00
1488 - 32	351.08	729.00	0.61	0.00	1.27	0.40	0.01	0.05	8.97	0.00	7.42	0.0009	0.14	0.00
1488 - 41	261.57	505.35	0.69	0.00	2.01	0.39	0.03	0.04	11.66	0.00	9.65	0.0010	0.09	0.00
1488 - 30	390.40	868.70	0.60	0.00	1.40	0.43	0.01	0.04	7.04	0.00	5.83	0.0010	0.12	0.00
1488 - 21	124.84	210.18	0.71	0.00	1.24	0.30	0.10	0.06	24.51	0.00	20.27	0.0019	0.15	0.01
1488 - 23	369.04	757.75	0.61	0.00	1.22	0.39	0.01	0.06	9.25	0.00	7.65	0.0011	0.16	0.00
1488 - 74	278.73	386.00	0.70	0.00	1.16	0.25	0.06	0.06	58.30	0.00	48.23	0.0009	0.16	0.01
1488 - 31	279.68	575.58	0.67	0.00	1.24	0.41	0.03	0.05	9.58	0.00	7.93	0.0012	0.14	0.00
1488 - 14	339.00	611.13	0.70	0.00	1.58	0.36	0.03	0.05	14.15	0.00	11.71	0.0012	0.12	0.00
1488 - 70	253.88	503.42	0.68	0.00	1.89	0.40	0.04	0.04	13.41	0.00	11.09	0.0015	0.11	0.00
1488 - 63	449.75	636.34	0.74	0.00	1.87	0.27	0.07	0.03	40.47	0.00	33.48	0.0006	0.08	0.00
1488 - 35	327.99	701.52	0.65	0.00	1.33	0.42	0.02	0.07	7.75	0.00	6.41	0.0017	0.17	0.00
1488 - 37	334.99	704.66	0.64	0.00	1.26	0.40	0.02	0.07	8.01	0.00	6.62	0.0020	0.19	0.00
1488 - 44	292.07	606.02	0.60	0.00	1.50	0.40	0.03	0.05	8.24	0.00	6.81	0.0020	0.14	0.00
1488 - 64	658.70	874.05	0.74	0.00	2.02	0.23	0.10	0.03	57.33	0.00	47.43	0.0006	0.08	0.01
1488 - 69	459.33	906.11	0.73	0.00	1.57	0.42	0.04	0.04	12.50	0.00	10.34	0.0009	0.10	0.00
1488 - 17	277.65	587.70	0.63	0.00	1.04	0.41	0.02	0.10	8.13	0.00	6.73	0.0024	0.26	0.00
1488 - 34	146.19	274.13	0.67	0.00	0.92	0.37	0.04	0.12	15.37	0.01	12.71	0.0037	0.30	0.01
1488 - 54	283.27	556.01	0.68	0.00	1.53	0.40	0.04	0.06	10.82	0.00	8.95	0.0021	0.16	0.00
1488 - 10	378.16	655.41	0.64	0.00	1.09	0.35	0.03	0.07	19.51	0.00	16.14	0.0014	0.19	0.00
1488 - 65	231.60	474.22	0.61	0.00	1.13	0.40	0.03	0.10	10.67	0.00	8.83	0.0029	0.25	0.00
1488 - 27	177.77	349.40	0.61	0.00	1.02	0.38	0.04	0.09	11.94	0.01	9.88	0.0034	0.23	0.01
1488 - 8	353.53	743.78	0.56	0.00	0.78	0.40	0.01	0.16	9.07	0.00	7.51	0.0028	0.40	0.00
1488 - 66	237.79	484.05	0.69	0.00	0.92	0.40	0.02	0.13	10.18	0.01	8.42	0.0033	0.33	0.01
1488 - 4	608.47	688.54	0.84	0.00	1.56	0.16	0.72	0.04	249.47	0.00	206.37	0.0006	0.09	0.03
1488 - 28	285.50	593.25	0.64	0.00	0.75	0.41	0.02	0.16	8.37	0.01	6.92	0.0034	0.42	0.00
1488 - 22	127.23	205.09	0.76	0.01	0.99	0.29	0.13	0.13	30.70	0.01	25.40	0.0051	0.33	0.03
1488 - 9	203.64	416.41	0.65	0.00	0.84	0.40	0.03	0.16	10.54	0.01	8.72	0.0047	0.40	0.01
1488 - 7	644.81	775.27	0.77	0.00	1.52	0.20	0.24	0.05	124.35	0.00	102.87	0.0008	0.12	0.02
1488 - 36	155.47	293.58	0.68	0.00	0.69	0.38	0.04	0.21	13.80	0.01	11.42	0.0050	0.54	0.01
1488 - 5	248.37	504.95	0.68	0.00	0.86	0.41	0.05	0.11	12.00	0.01	9.93	0.0037	0.29	0.01
1488 - 52	170.78	305.70	0.62	0.01	1.58	0.36	0.26	0.05	17.29	0.01	14.30	0.0054	0.14	0.02
1488 - 45	532.94	888.02	0.72	0.00	1.15	0.34	0.05	0.08	18.11	0.00	14.98	0.0023	0.22	0.01
1488 - 56	378.42	696.50	0.65	0.00	0.93	0.36	0.03	0.15	14.27	0.01	11.81	0.0040	0.38	0.01
1488 - 3	463.77	900.93	0.75	0.00	1.29	0.40	0.07	0.07	13.93	0.00	11.53	0.0026	0.18	0.01
1488 - 67	693.91	768.00	0.84	0.00	1.19	0.14	0.75	0.07	293.33	0.00	242.65	0.0011	0.17	0.08
1488 - 51	252.49	529.01	0.60	0.01	0.81	0.41	0.04	0.19	8.73	0.01	7.22	0.0086	0.50	0.01
1488 - 11	421.94	623.56	0.75	0.00	0.94	0.30	0.08	0.14	34.72	0.01	28.72	0.0033	0.36	0.02
1488 - 18	873.70	1048.09	0.79	0.00	1.35	0.19	0.36	0.06	119.19	0.00	98.60	0.0013	0.16	0.03
1488 - 2	223.27	471.30	0.67	0.01	0.65	0.41	0.02	0.38	9.86	0.02	8.15	0.0131	0.99	0.02
1488 - 13	875.15	1179.98	0.76	0.00	1.08	0.24	0.13	0.10	57.61	0.00	47.65	0.0022	0.26	0.02
1488 - 57	326.66	686.93	0.60	0.01	0.81	0.41	0.04	0.30	8.19	0.03	6.77	0.0167	0.77	0.02
1488 - 46	387.58	523.07	0.77	0.00	0.85	0.24	0.23	0.28	52.50	0.02	43.43	0.0126	0.71	0.12
1488 - 43	206.43	405.34	0.67	0.02	1.12	0.40	0.26	0.19	10.23	0.06	8.47	0.0372	0.50	0.08
1488 - 19	175.41	346.75	0.62	0.02	0.82	0.40	0.17	0.41	12.09	0.09	10.00	0.0586	1.05	0.14
1488 - 42	712.61	834.66	0.80	0.01	1.02	0.18	3.11	0.37	120.24	0.09	99.47	0.0611	0.95	1.57
1488 - 33	393.82	768.74	0.69	0.03	1.02	0.42	0.51	0.48	11.42	0.29	9.45	0.1872	1.23	0.46
1488 - 16	670.83	931.89	0.77	0.03	0.99	0.28	2.07	0.43	36.03	0.35	29.81	0.2238	1.12	1.48
1488 - 49	447.07	857.86	0.62	0.08	1.05	0.41	1.09	0.45	9.10	0.92	7.53	0.5959	1.15	0.90
1488 - 73	484.05	847.65	0.61	0.11	1.10	0.41	2.28	0.45	9.09	1.62	7.52	1.0433	1.16	1.76
1488 - 15	1239.50	1530.22	0.72	0.04	1.21	0.23	9.64	0.37	70.87	0.76	58.63	0.4911	0.96	6.33
1488 - 72	687.30	979.39	0.63	0.12	1.08	0.36	7.19	0.47	15.87	2.71	13.13	1.7472	1.21	5.90
1488 - 48	653.42	863.04	0.75	0.26	1.05	0.39	15.30	0.61	10.73	7.51	8.88	4.8466	1.58	14.30
1488 - 71	793.79	988.08	0.64	0.34	0.99	0.40	19.83	0.66	11.13	11.58	9.20	7.4761	1.70	24.17
1488 - 55	1485.58	1761.90	0.66	0.14	1.05	0.31	25.49	0.51	25.47	5.36	21.07	3.4606	1.32	21.83
1488 - 40	2740.67	3097.28	0.64	0.10	1.11	0.33	41.75	0.44	24.58	5.28	20.34	3.4117	1.14	31.69

Element concentrations in ppm

$Eu/Eu^{*} = [(Eu_{CN}/(Sm_{CN}+Gd_{CN})/2)]$

$Y/Y^{*} = [(Y_{CN}/(Dy_{CN}+Ho_{CN})/2)]$

$TCe/Ce^{*} = [(Ce_{CN}/(La_{CN} \times Pr_{CN})^{0.5})]$

$LCe/Ce^{*} = [(Ce_{CN}/((Nd_{CN})^{0.5}/Sm_{CN}))]$

CN = chondrite normalised

Normalising values from Sun and McDonough (1989)

Appendix 5 Supplementary material for Mapping hydrothermal systems in IOCG deposits using apatite geochronology and geochemsitry: An example from Vulcan Cu-Au prospect

Appendix 5 Table A2: LA-ICP-MS Trace element data collected for apatite from Vulcan Prospect in this study

Rejected Data												
Sample	**Drill hole**	**Comment**	**Si**	**P**	**Ca**	**V**	**Mn**	**Fe**	**Sr**	**Y**	**Zr**	**Th**	**U**
801_apatite - 11	VUD 009 801	LREE enriched. Ce and La inclusions.	878.37	189580.99	394000	0.09	75.52	396.62	713.96	665.73	0.01	1.73	8.51
801_apatite - 12	VUD 009 801	LREE inclusions. Ce, La, Pr inclusions.	38972.90	179146.49	394000	0.21	60.34	1368.40	631.74	259.95	0.05	1.63	1.96
801_apatite - 2	VUD 009 801	LREE depleted High Fe.	7503.80	188890.90	394000	2.63	82.74	11154.51	643.50	673.80	0.23	3.24	5.28
801_apatite - 24	VUD 009 801	LREE inclusions. Ce, La inclusions.	427.32	187979.18	394000	0.13	65.01	555.70	656.09	431.62	<0.010	1.28	4.07
801_apatite - 26	VUD 009 801	LREE inclusions.	241.58	187596.94	394000	<0.078	67.98	259.06	612.47	572.93	0.06	1.81	6.14
801_apatite - 27	VUD 009 801	LREE inclusions.	418.10	190567.71	394000	0.54	70.30	547.48	1100.54	538.58	0.09	3.89	9.45
801_apatite - 52	VUD 009 801	LREE inclusions. Fe inclusions.	4884.77	184211.07	394000	9.27	79.95	46004.99	728.90	543.40	3.83	17.16	9.05
801_apatite - 53	VUD 009 801	LREE depleted High Fe.	6688.75	190161.61	394000	10.35	67.09	17700.23	596.47	426.55	0.30	1.14	5.32
825_apatite - 26	VUD 009 825	monazite, xenotime? High P, Y, Th and U. Drilled through grain into silicate	386.73	183521.78	394000	<0.068	709.23	1534.18	123.01	898.45	0.08	261.28	506.76
825_apatite - 6	VUD 009 825	drilled through grain into Fe oxide	508.10	182949.91	394000	0.12	1083.58	3292.05	97.51	415.85	0.04	71.47	233.49
825_apatite - 25	VUD 009 825	high Th, Y, P. Drilled through grain into silicate	240.47	185303.54	394000	<0.065	206.93	3600.19	37.78	196.73	0.06	901.87	16.45
825_apatite - 51	VUD 009 825		528.92	197671.78	394000	0.44	766.87	8650.13	119.48	837.39	0.21	334.36	567.00
825_apatite - 24	VUD 009 825		275.34	186695.14	394000	0.44	167.04	9558.51	94.51	244.29	0.09	684.50	111.12
825_apatite - 31	VUD 009 825	La, Th, Sr, Ce, Pr, Nd inclusions. High Fe.	355.80	193732.47	394000	0.58	908.66	10471.46	410.61	1181.38	36.75	1087.49	427.37
825_apatite - 63	VUD 009 825	High Fe, low Ca	934.96	178061.38	394000	0.47	1023.69	10605.88	107.45	1070.99	0.19	126.65	336.37
825_apatite - 12	VUD 009 825	High Fe, low Ca	258.10	192638.12	394000	0.20	822.13	10720.14	97.68	549.65	0.07	266.49	141.02
825_apatite - 56	VUD 009 825	High Fe, low Ca	304.68	185813.04	394000	0.54	1187.94	11035.26	118.48	1061.84	0.09	133.69	287.45
825_apatite - 1	VUD 009 825	High Fe, low Ca	261.06	193188.29	394000	0.19	202.71	11605.54	75.90	206.61	0.13	274.42	7.12
825_apatite - 8	VUD 009 825	High Fe, low Ca	549.41	189439.30	394000	0.34	562.00	12758.87	77.24	510.81	0.03	135.72	141.13
825_apatite - 45	VUD 009 825	High Fe, low Ca	287.78	188446.60	394000	1.03	789.22	13019.37	215.97	1132.11	<0.009	53.14	115.64
825_apatite - 5	VUD 009 825	High Fe, low Ca	445.30	193525.19	394000	0.38	1159.19	13143.39	166.71	975.65	4.30	185.90	165.06
825_apatite - 53	VUD 009 825	High Fe, low Ca	474.35	192907.00	394000	0.61	994.94	15648.91	115.53	1178.02	0.15	209.81	592.74
825_apatite - 4	VUD 009 825	High Fe, low Ca	377.21	188265.84	394000	0.95	880.20	16238.59	98.02	700.25	0.17	177.00	232.36
825_apatite - 19	VUD 009 825	High Fe, low Ca	189.79	192272.07	394000	0.31	487.58	17274.65	85.46	532.28	0.12	313.24	196.10
825_apatite - 61	VUD 009 825	High Fe, low Ca	243.22	191879.84	394000	0.26	528.93	17299.25	134.13	1087.69	0.10	57.48	240.74
825_apatite - 54	VUD 009 825	High Fe, low Ca	366.84	191705.13	394000	0.62	755.09	17331.00	114.09	1096.15	0.16	84.46	289.71
825_apatite - 49	VUD 009 825	High Fe, low Ca	456.56	186417.48	394000	1.18	625.78	18800.08	278.91	1393.31	0.15	155.23	258.92
825_apatite - 21	VUD 009 825	High Fe, low Ca	262.06	189190.55	394000	0.30	789.98	19279.19	61.09	277.75	0.03	520.50	71.93
825_apatite - 15	VUD 009 825	High Fe, low Ca	370.94	191686.46	394000	0.60	627.41	19408.16	177.81	987.61	0.16	49.35	148.67
825_apatite - 17	VUD 009 825	High Fe, low Ca	288.78	187995.01	394000	1.22	510.30	19461.62	120.82	1116.08	2.14	353.33	132.98
825_apatite - 34	VUD 009 825	High Fe, low Ca	307.79	194657.81	394000	0.53	1146.86	19696.74	157.18	1093.85	0.21	52.55	259.90
825_apatite - 50	VUD 009 825	High Fe, low Ca	<161.456	195127.29	394000	0.92	878.81	21536.74	135.86	1233.84	0.59	40.36	215.46

Element concentrations in ppm
$Eu/Eu^{*} = [(Eu_{CN}/(Sm_{CN}+Gd_{CN})/2)]$
$Y/Y^{*} = [(Y_{CN}/(Dy_{CN}+Ho_{CN})/2)]$
$TCe/Ce^{*} = [(Ce_{CN}/(La_{CN} \times Pr_{CN})^{0.5})]$
$LCe/Ce^{*} = [(Ce_{CN}/((Nd_{CN})^{0.5}/Sm_{CN}))]$
CN = chondrite normalised
Normalising values from Sun and McDonough (1989)

Appendix 5 Supplementary material for Mapping hydrothermal systems in IOCG deposits using apatite geochronology and geochemsitry: An example from Vulcan Cu-Au prospect

Appendix 5 Table A2: LA-ICP-MS Trace element data collected for apatite from Vulcan Prospect in this study

Rejected Data

Sample	La	Ce	Pr	Nd	Sm	Eu	Gd	Tb	Dy	Ho	Er	Tm	Yb	Lu	Hf
801_apatite - 11	8.22	21.57	2.94	18.81	68.03	43.91	563.94	100.09	404.57	36.37	41.05	2.91	12.76	1.34	<0.005
801_apatite - 12	44.20	72.29	6.98	25.90	36.91	22.06	266.25	43.90	171.70	14.35	16.05	1.17	5.14	0.40	<0.006
801_apatite - 2	0.07	0.89	0.56	8.32	64.10	43.81	584.70	103.08	425.47	37.09	39.59	2.69	11.41	1.24	0.01
801_apatite - 24	2.21	6.27	1.00	12.00	52.14	29.04	343.42	57.38	215.75	21.10	30.57	2.73	11.95	1.21	0.03
801_apatite - 26	5.53	7.83	1.80	15.24	67.03	35.34	474.35	79.21	300.01	28.58	40.71	3.46	15.95	1.78	<0.007
801_apatite - 27	41.97	97.69	12.69	53.76	61.36	37.50	481.48	83.39	329.71	29.25	32.31	2.36	10.39	1.03	0.02
801_apatite - 52	77.97	170.70	18.10	63.77	63.74	37.72	475.30	84.21	336.29	30.06	35.58	2.70	10.70	1.11	0.12
801_apatite - 53	0.34	1.55	0.63	9.13	58.63	33.30	401.88	63.10	238.01	21.01	28.65	2.51	11.12	1.03	0.01
825_apatite - 26	16.84	194.46	46.11	324.99	147.75	27.03	209.43	31.65	184.60	37.61	114.11	14.30	89.60	11.88	<0.005
825_apatite - 6	24.56	228.42	57.21	393.39	145.85	18.55	148.98	17.91	102.18	18.22	44.87	4.95	28.43	3.56	<0.007
825_apatite - 25	8.24	100.22	32.26	263.80	127.51	17.72	132.70	13.80	60.31	9.48	18.08	1.58	7.14	0.74	0.01
825_apatite - 51	18.23	198.37	45.12	318.16	138.67	25.07	191.89	26.32	170.43	35.42	102.52	12.86	76.84	10.27	<0.007
825_apatite - 24	38.96	143.22	54.59	368.93	137.99	19.50	130.41	14.45	63.68	10.42	23.14	2.39	13.17	1.65	<0.004
825_apatite - 31	138.60	1201.34	78.29	421.34	161.17	27.94	230.90	34.95	223.93	48.03	151.43	21.76	136.67	17.85	1.43
825_apatite - 63	18.10	940.86	49.54	400.68	191.36	29.99	255.60	35.84	224.19	46.19	130.68	16.81	108.96	13.41	0.04
825_apatite - 12	24.45	190.84	48.07	331.44	136.46	21.86	158.31	22.09	126.48	23.79	62.26	7.23	40.48	4.88	0.01
825_apatite - 56	48.79	1608.50	93.38	605.12	200.84	28.06	228.32	32.18	190.64	41.54	125.90	17.47	109.12	15.39	0.03
825_apatite - 1	23.80	197.79	56.45	420.43	183.03	24.39	164.91	16.84	72.30	10.69	20.29	1.60	7.76	0.93	0.01
825_apatite - 8	14.67	158.09	43.86	364.41	176.16	26.41	190.54	23.71	120.81	21.34	55.58	6.47	34.37	4.41	<0.006
825_apatite - 45	20.92	1011.54	68.99	514.53	216.85	31.59	267.19	36.16	217.48	48.27	137.92	17.83	111.18	13.26	<0.008
825_apatite - 5	43.85	3106.88	81.74	528.47	191.87	29.48	252.48	36.21	229.54	47.18	143.23	18.70	120.49	15.77	0.03
825_apatite - 53	25.19	1305.52	73.34	482.46	189.28	30.37	248.54	38.68	248.22	52.62	158.63	22.01	144.62	19.44	0.02
825_apatite - 4	24.14	416.69	61.59	407.59	139.75	21.05	165.92	24.95	148.73	29.52	82.94	10.43	63.64	8.06	0.01
825_apatite - 19	33.31	271.31	65.33	453.84	172.97	24.04	174.64	22.25	124.53	22.20	58.41	6.62	37.23	4.81	0.01
825_apatite - 61	9.80	537.99	37.08	324.20	199.24	34.02	274.98	38.27	233.34	47.62	129.66	15.84	94.17	11.34	0.01
825_apatite - 54	27.58	625.36	82.69	547.44	205.54	32.10	244.88	35.10	213.19	44.45	130.38	16.99	105.40	13.97	0.03
825_apatite - 49	55.06	841.16	100.27	663.98	239.60	33.36	263.61	35.71	210.04	50.54	156.84	22.39	141.49	18.83	<0.006
825_apatite - 21	7.74	107.49	32.41	273.09	125.11	18.41	130.20	15.23	73.41	12.42	28.41	3.33	16.90	2.41	<0.005
825_apatite - 15	42.47	363.44	71.67	466.37	165.81	24.80	211.30	30.31	189.61	40.07	118.44	15.21	91.57	12.33	0.02
825_apatite - 17	31.61	698.01	89.38	695.24	346.51	52.96	390.57	51.22	284.27	51.20	132.01	15.25	83.71	9.65	0.06
825_apatite - 34	33.49	3047.03	61.15	419.72	167.45	25.90	226.05	33.68	216.62	48.33	145.83	19.48	129.86	16.69	0.00
825_apatite - 50	30.80	1317.42	76.01	553.00	249.95	36.45	313.17	44.40	251.37	52.38	158.15	21.07	132.51	16.93	0.02

Element concentrations in ppm
$Eu/Eu^{\star} = [(Eu_{CN}/(Sm_{CN}+Gd_{CN})/2)]$
$Y/Y^{\star} = [(Y_{CN}/(Dy_{CN}+Ho_{CN})/2)]$
$TCe/Ce^{\star} = [(Ce_{CN}/(La_{CN} \times Pr_{CN})^{0.5})]$
$LCe/Ce^{\star} = [(Ce_{CN}/((Nd_{CN})^{0.5}/Sm_{CN}))]$
CN = chondrite normalised
Normalising values from Sun and McDonough (1989)

Appendix 5 Table A2: LA-ICP-MS Trace element data collected for apatite from Vulcan Prospect in this study

Rejected Data												
Sample	**Drill hole**	**Comment**	**Si**	**P**	**Ca**	**V**	**Mn**	**Fe**	**Sr**	**Y**	**Zr**	**Th**	**U**
825_apatite - 3	VUD 009 825	High Fe, low Ca	265.59	192699.71	394000	1.33	586.58	22379.34	140.45	1514.07	9.34	129.27	296.31
825_apatite - 22	VUD 009 825	High Fe, low Ca	365.20	193470.55	394000	0.56	879.56	25751.20	126.82	855.74	0.24	398.59	363.85
825_apatite - 11	VUD 009 825	High Fe, low Ca	248.80	194052.18	394000	1.62	787.60	26071.22	156.05	680.32	0.11	44.88	176.40
825_apatite - 16	VUD 009 825	High Fe, low Ca	305.00	194957.16	394000	1.49	1302.11	27725.94	95.94	473.16	0.13	333.44	191.61
825_apatite - 57	VUD 009 825	High Fe, low Ca	202.76	196167.89	394000	0.91	467.56	32782.44	109.11	1266.93	0.68	53.01	630.34
825_apatite - 14	VUD 009 825	High Fe, low Ca	372.76	192979.17	394000	1.77	1013.36	33687.22	114.59	1014.76	0.31	99.96	347.03
825_apatite - 32	VUD 009 825	High Fe, low Ca	327.41	192292.44	394000	1.03	439.46	33854.44	116.39	1178.48	1.07	132.65	705.59
825_apatite - 20	VUD 009 825	High Fe, low Ca	224.68	193141.82	394000	2.31	1186.49	35819.86	54.48	470.72	0.12	371.13	215.84
825_apatite - 39	VUD 009 825	High Fe, low Ca	577.11	189800.79	394000	2.29	682.47	41507.66	151.87	809.09	0.26	115.61	140.42
825_apatite - 59	VUD 009 825	High Fe, low Ca	919.62	190207.40	394000	2.56	668.52	43871.74	111.14	452.02	0.11	106.59	125.00
825_apatite - 43	VUD 009 825	High Fe, low Ca	429.12	194725.42	394000	2.23	1044.32	47786.15	182.50	1081.43	0.51	59.47	237.42
825_apatite - 36	VUD 009 825	High Fe, low Ca	179.63	193730.24	394000	2.72	1026.60	53943.45	137.83	1081.61	0.55	305.73	316.52
825_apatite - 18	VUD 009 825	High Fe, low Ca	326.16	192970.66	394000	2.67	777.36	58540.46	114.36	589.08	0.22	556.99	102.24
825_apatite - 23	VUD 009 825	High Fe, low Ca	657.00	191324.46	394000	1.48	435.55	60422.57	92.55	270.87	0.02	764.53	31.43
825_apatite - 55	VUD 009 825	High Fe, low Ca	490.46	193709.34	394000	3.47	460.44	60669.30	107.51	1040.82	0.75	167.95	208.95
825_apatite - 46	VUD 009 825	High Fe, low Ca	368.00	195276.67	394000	2.78	1161.37	68050.49	150.45	336.79	0.17	200.79	134.14
825_apatite - 13	VUD 009 825	High Fe, low Ca	233.88	198177.77	394000	3.14	1385.73	71196.31	150.26	641.06	0.29	146.83	194.27
825_apatite - 38	VUD 009 825	High Fe, low Ca	468.31	190600.90	394000	8.92	824.70	110924.37	107.54	705.72	0.55	462.93	304.64
825_apatite - 33	VUD 009 825	High Fe, low Ca La, Ce, Sr, Pr inclusions.	435.05	188443.74	394000	5.73	878.00	127371.18	182.95	1360.35	1.96	70.55	647.48
825_apatite - 30	VUD 009 825	High Fe.	1130.83	192558.67	394000	4.32	548.29	195618.49	466.80	959.07	1.05	302.37	353.09
825_apatite - 44	VUD 009 825	High Fe, low Ca	764.82	195903.15	394000	10.63	905.25	200261.10	102.12	449.50	0.82	176.41	151.90
825_apatite - 9	VUD 009 825	High Fe, low Ca	699.63	192243.25	394000	10.91	992.59	228082.04	110.95	401.24	0.32	73.11	122.47
825_apatite - 60	VUD 009 825	High Fe, low Ca	558.52	190912.08	394000	12.51	803.89	253629.50	123.23	820.62	0.87	188.98	328.85
825_apatite - 58	VUD 009 825	High Fe, low Ca	857.41	191417.26	394000	26.91	898.92	583854.77	142.59	805.76	1.04	215.02	330.25
973_apatite - 1	VUD 009 973	La/Ce >1. La Ce inclusions. Ca P drop off.	630.46	192968.50	394000	0.28	168.78	905.24	468.67	304.78	0.24	6.00	79.28
973_apatite - 10	VUD 009 973	LREE inclusions. La, Ce, Zr inclusions. High Fe.	1238.45	194218.63	394000	39.05	285.91	98508.69	615.00	340.29	201.13	15.51	48.56
973_apatite - 15	VUD 009 973	LREE inclusion. Ce, La, Sr, Fe.	32248.33	187956.53	394000	37.31	143.44	111457.79	2282.27	484.45	602.40	75.82	83.72
973_apatite - 17	VUD 009 973	Fe and Ce La Pr Th inclusions. High Fe.	732.13	191202.42	394000	5.28	343.84	11036.27	215.33	631.60	0.54	58.72	53.36
973_apatite - 19	VUD 009 973	LREE mineral. La, Ce, Sr, Fe. Zr inclusion. High Fe.	7423.35	197281.66	394000	46.38	162.88	115109.34	3478.82	265.29	30.55	121.32	43.46
973_apatite - 2	VUD 009 973	LREE inclusion. Ce, La, Sr. High Fe.	5332.53	195585.12	394000	10.91	258.48	30248.09	1250.50	449.34	13.76	37.89	48.99
973_apatite - 20	VUD 009 973	La/Ce >1. Ce La inclusions. High Fe.	1672.31	188617.22	394000	6.23	160.48	26790.05	483.33	365.80	4.13	8.79	41.36
973_apatite - 21	VUD 009 973	La/Ce >1. Ce La Sr inclusions. High Fe.	6540.74	189075.95	394000	2.47	294.99	13404.66	236.48	532.43	1.40	40.46	87.78

Element concentrations in ppm
$Eu/Eu^{*} = [(Eu_{CN}/(Sm_{CN}+Gd_{CN})/2)]$
$Y/Y^{*} = [(Y_{CN}/(Dy_{CN}+Ho_{CN})/2)]$
$TCe/Ce^{*} = [(Ce_{CN}/(La_{CN} \times Pr_{CN})^{0.5})]$
$LCe/Ce^{*} = [(Ce_{CN}/((Nd_{CN})^{0.5}/Sm_{CN}))]$
CN = chondrite normalised
Normalising values from Sun and McDonough (1989)

Appendix 5 Supplementary material for Mapping hydrothermal systems in IOCG deposits using apatite geochronology and geochemsitry: An example from Vulcan Cu-Au prospect

Appendix 5 Table A2: LA-ICP-MS Trace element data collected for apatite from Vulcan Prospect in this study

Rejected Data															
Sample	**La**	**Ce**	**Pr**	**Nd**	**Sm**	**Eu**	**Gd**	**Tb**	**Dy**	**Ho**	**Er**	**Tm**	**Yb**	**Lu**	**Hf**
825_apatite - 3	36.38	684.23	80.36	524.26	179.80	26.24	223.56	33.04	219.93	51.73	168.59	23.28	154.65	21.70	0.16
825_apatite - 22	22.21	467.85	54.30	374.34	161.27	26.14	211.94	30.59	187.20	37.13	105.67	13.51	82.27	10.83	0.02
825_apatite - 11	24.11	326.37	60.45	401.01	150.16	22.12	174.71	25.08	143.60	27.43	76.41	9.38	54.93	7.26	0.04
825_apatite - 16	13.17	120.85	31.70	229.52	95.08	15.60	125.03	17.79	105.61	20.29	52.26	6.21	34.80	4.25	<0.004
825_apatite - 57	12.41	116.74	36.84	314.12	187.84	33.68	268.64	39.48	236.43	49.45	145.81	18.89	114.97	15.43	0.02
825_apatite - 14	38.29	781.33	105.04	615.87	168.57	23.22	180.96	27.14	173.33	37.75	120.67	17.59	120.71	16.57	0.01
825_apatite - 32	21.09	300.64	42.35	291.07	116.16	19.77	158.37	23.50	157.19	38.01	125.03	18.12	118.24	16.98	0.03
825_apatite - 20	9.54	80.15	23.35	176.33	78.20	12.91	117.07	18.33	115.79	21.02	52.29	6.04	31.43	4.20	<0.006
825_apatite - 39	16.98	761.68	42.75	315.88	143.79	22.83	181.40	24.98	153.09	32.96	97.62	13.47	81.72	10.46	<0.005
825_apatite - 59	16.62	198.45	54.21	405.10	170.34	24.74	170.60	20.53	103.55	19.25	47.49	5.68	30.04	3.72	<0.006
825_apatite - 43	30.22	2421.42	59.42	432.53	195.76	29.13	246.60	35.46	222.44	48.96	142.31	19.68	133.83	16.75	0.01
825_apatite - 36	14.07	1559.94	36.83	285.91	150.11	25.97	229.76	36.81	231.60	49.53	149.45	20.36	135.91	17.32	<0.007
825_apatite - 18	24.65	517.52	74.18	482.25	167.82	23.44	173.60	22.41	125.78	24.60	70.10	9.28	58.20	7.80	0.01
825_apatite - 23	44.01	307.25	76.05	515.59	188.97	24.72	157.29	16.67	75.66	11.94	26.31	2.44	13.25	1.57	0.03
825_apatite - 55	17.46	626.26	45.73	364.59	210.00	35.62	268.72	37.65	223.65	45.74	126.40	15.98	93.35	11.70	0.02
825_apatite - 46	11.01	124.14	37.73	293.65	125.03	18.01	130.27	16.36	79.34	14.63	34.60	4.33	21.90	2.65	<0.006
825_apatite - 13	20.31	196.57	52.23	361.40	134.33	21.27	165.84	24.53	144.34	27.43	76.05	8.62	46.79	5.85	<0.007
825_apatite - 38	21.74	438.31	50.85	357.66	157.09	25.06	191.35	27.53	162.51	32.40	90.88	12.07	71.43	8.95	<0.005
825_apatite - 33	31.23	174.39	45.93	289.83	107.68	17.19	152.20	24.49	175.92	42.39	146.96	21.44	150.00	21.60	<0.005
825_apatite - 30	136.22	683.15	69.55	361.27	111.05	18.90	140.24	18.12	116.14	28.42	93.58	13.87	96.30	14.03	0.03
825_apatite - 44	15.44	162.14	43.07	346.32	137.81	20.64	155.62	18.39	104.41	19.36	51.09	5.59	33.91	4.07	<0.008
825_apatite - 9	12.29	150.38	42.96	338.66	143.37	21.20	143.72	18.00	94.62	16.83	42.30	4.80	27.14	3.39	0.01
825_apatite - 60	23.71	358.39	48.08	329.12	142.67	25.17	199.44	28.44	179.11	36.89	102.18	13.44	83.04	10.69	<0.006
825_apatite - 58	32.20	1020.07	66.10	422.18	136.68	20.67	171.12	23.43	140.03	30.62	89.18	12.58	81.42	11.04	0.05
973_apatite - 1	10.40	14.56	1.91	9.82	24.38	15.60	149.20	16.39	78.42	12.74	27.49	2.79	11.18	1.08	0.07
973_apatite - 10	170.48	228.41	16.69	47.16	23.00	12.45	116.65	15.31	74.39	13.01	30.93	3.11	20.95	2.65	6.03
973_apatite - 15	1485.09	2184.22	160.60	364.28	80.40	32.20	268.77	24.60	94.39	17.91	48.68	6.53	42.41	6.69	17.76
973_apatite - 17	0.92	5.05	0.72	5.37	12.93	7.81	91.95	22.05	156.80	31.64	73.56	6.58	27.56	2.68	<0.004
973_apatite - 19	3047.22	4284.19	307.40	691.35	101.75	28.27	196.50	18.27	68.24	9.99	22.48	1.98	9.72	0.98	0.73
973_apatite - 2	901.45	1360.25	100.52	255.28	44.35	14.19	115.37	16.76	97.43	17.55	37.45	3.38	15.42	1.86	0.51
973_apatite - 20	45.97	99.82	6.24	22.19	26.39	16.13	148.60	17.56	85.02	14.43	33.00	3.30	14.25	1.63	0.19
973_apatite - 21	29.31	33.81	3.43	13.65	15.40	8.64	88.12	17.31	116.01	22.62	55.68	6.11	28.57	3.64	0.05

Element concentrations in ppm
$Eu/Eu^{\star} = [(Eu_{CN}/(Sm_{CN}+Gd_{CN})/2)]$
$Y/Y^{\star} = [(Y_{CN}/(Dy_{CN}+Ho_{CN})/2)]$
$TCe/Ce^{\star} = [(Ce_{CN}/(La_{CN} \times Pr_{CN})^{0.5})]$
$LCe/Ce^{\star} = [(Ce_{CN}/((Nd_{CN})^{0.5}/Sm_{CN}))]$
CN = chondrite normalised
Normalising values from Sun and McDonough (1989)

Appendix 5 Supplementary material for Mapping hydrothermal systems in IOCG deposits using apatite geochronology and geochemsitry: An example from Vulcan Cu-Au prospect

Appendix 5 Table A2: LA-ICP-MS Trace element data collected for apatite from Vulcan Prospect in this study

Rejected Data Sample	Drill hole	Comment	Si	P	Ca	V	Mn	Fe	Sr	Y	Zr	Th	U
973_apatite - 24	VUD 009 973	La/Ce >1.. Fe, Ce La inclusions. Drilled off grain. High Fe.	4326.60	193062.02	394000	15.09	212.04	49213.66	342.89	424.67	16.94	26.72	73.54
973_apatite - 29	VUD 009 973	La/Ce >1. Ce La Sr inclusions. High Fe.	6425.40	189523.94	394000	59.62	201.67	241344.33	1572.50	154.08	12.85	31.64	32.59
973_apatite - 35	VUD 009 973	La/Ce >1. La, Ce, Pr inclusions.	597.74	191562.68	394000	0.11	185.89	885.94	557.81	378.79	0.21	16.88	75.24
973_apatite - 38	VUD 009 973	La/Ce >1. La, Ce inclusions, Si inclusion.	597.19	190357.25	394000	0.77	72.85	357.96	978.86	149.77	3.55	10.32	3.54
973_apatite - 39	VUD 009 973	La/Ce >1. La, Ce inclusions. High Fe.	3000.74	188421.72	394000	7.79	100.79	27087.89	549.21	242.53	63.85	6.67	17.43
973_apatite - 40	VUD 009 973	La/Ce >1. La, C inclusions. Zr inclusion.	2611.76	195946.99	394000	0.47	155.71	922.26	451.73	293.30	65.53	5.45	42.63
973_apatite - 46	VUD 009 973	High Fe.	423.19	191261.31	394000	11.06	85.04	37467.46	902.99	357.87	284.64	5.63	30.92
973_apatite - 48	VUD 009 973	LREE inclusions. La, Ce, Fe inclusions.	567.41	193245.80	394000	0.46	267.59	1249.84	787.67	506.81	0.19	41.87	82.69
973_apatite - 49	VUD 009 973	La/Ce >1. La Ce inclusions. Fe Si inclusions. High Fe.	5880.12	185284.19	394000	26.60	60.46	25787.88	651.21	127.63	31.91	1.55	3.86
973_apatite - 5	VUD 009 973	LREE inclusion. Sr, Ce, La, Fe. P and Ca drop off. High Fe.	389.05	193767.00	394000	4.49	126.55	12952.20	851.36	190.44	0.83	4.82	16.83
973_apatite - 50	VUD 009 973	Ce, La, Sr Y inclusion. Fe inclusion.	4088.51	190100.89	394000	5.96	219.75	13225.36	1266.68	635.56	3.82	61.89	61.37
973_apatite - 53	VUD 009 973	LREE inclusions. La, Ce, Sr inclusions. Fe silicate inclusion. Zr inclusion.	2785.44	188515.48	394000	1.08	224.27	1621.95	1475.67	324.67	0.08	44.50	42.57
973_apatite - 56	VUD 009 973	La/Ce >1. Ce La Fe inclusion. High Fe.	<283.153	201116.25	394000	4.74	134.27	24914.89	903.52	255.41	1.35	20.39	47.16
973_apatite - 58	VUD 009 973	La/Ce >1. Y, Zr inclusion, La, Ce inclusion. U irregular. High Fe.	870.38	184811.05	394000	8.67	102.36	11593.20	569.75	293.29	61.24	12.79	19.47
973_apatite - 59	VUD 009 973	LREE inclusions. La, Ce, Pr inclusion. Silicate off grain.	192.48	182618.45	394000	<0.071	60.54	268.01	739.89	246.91	0.21	10.28	0.83
973_apatite - 6	VUD 009 973	Fe, Zr, Sm inclusions. LREE inclusion. Ce, La, Sr. U, P and Ca dropp off.	530.47	189372.56	394000	7.13	132.74	25337.91	584.97	286.37	23.32	4.23	38.16
973_apatite - 8	VUD 009 973	High Fe.	468.30	196221.52	394000	13.42	249.89	40614.24	944.63	264.60	9.09	16.63	65.85
1084 - 10	VUD 007 1084	High Fe	7350.68	185468.52	393600	15.34	47.10	92225.60	204.60	411.06	0.44	10.42	1.71
1084 - 11	VUD 007 1084	LREE enriched. High Fe.	202878.11	183556.54	393600	163.69	339.87	499440.54	2282.66	837.39	32.71	274.03	35.02
1084 - 41	VUD 007 1084	High Fe	81616.64	185118.10	393600	128.01	302.18	181494.77	262.26	1018.54	2.22	151.36	3.50
1084 - 47	VUD 007 1084	High Fe	262.37	195191.49	393600	1.65	55.51	14661.78	370.57	1117.95	0.02	73.06	0.58
1084 - 8	VUD 007 1084	High Fe	686.31	161528.31	393600	4.12	1849.57	10196.42	148.42	485.88	0.20	30.80	5.06
1210 - 2	VUD 017 1210	High Fe	481.95	180164.66	393600	211.93	76.75	361825.09	303.99	363.10	7.95	2.48	7.24
1210 - 7	VUD 017 1210	High Fe	5038.34	188860.28	393600	52.23	72.28	57020.04	273.59	279.21	1.19	3.54	1.95
1488 - 1	VUD 016 1488	LREE enriched. Zr U inclusions - zircon High Fe. Low Ca	36466.75	179566.78	393600	28.84	77.99	74746.04	3537.09	393.22	371.90	286.12	79.90
1488 - 12	VUD 016 1488	LREE enriched. LREE zone or inclusion. High Fe	5693.33	187223.78	393600	3.91	41.32	11136.34	847.82	280.55	0.80	29.14	8.29
1488 - 20	VUD 016 1488	LREE enriched. Th, La, Ce inclusion. High Fe. Increasing Si. Pb inclusions	4456.04	187638.27	393600	4.31	40.25	13135.14	495.54	262.68	0.98	15.93	8.75
1488 - 24	VUD 016 1488	LREE enriched. Inclusions.	6602.70	184876.96	393600	4.55	44.12	12777.01	698.21	307.06	0.91	20.52	7.09
1488 - 47	VUD 016 1488	High Fe	536.08	188502.49	393600	2.57	39.05	24330.28	257.48	409.78	0.39	4.61	13.20
1488 - 53	VUD 016 1488	LREE enriched. U signal peaks then drops off. Fe inclusions.	4933.62	188024.08	393600	4.59	44.77	15265.29	1347.56	392.27	2.44	81.47	17.63
1488 - 6	VUD 016 1488	LREE enriched. La Ce inclusion. Fe Si inclusion.	14994.54	178231.30	393600	7.23	35.55	13041.11	627.07	281.96	0.86	51.46	7.83
1488 - 68	VUD 016 1488	La/Ce >1. High Fe. La Ce inclusions.	4358.63	189450.39	393600	1.79	36.81	15174.41	295.51	417.08	0.57	24.17	10.85

Element concentrations in ppm
$Eu/Eu^{\star} = [(Eu_{CN}/(Sm_{CN}+Gd_{CN})/2)]$
$Y/Y^{\star} = [(Y_{CN}/(Dy_{CN}+Ho_{CN})/2)]$
$TCe/Ce^{\star} = [(Ce_{CN}/(La_{CN} \times Pr_{CN})^{0.5})]$
$LCe/Ce^{\star} = [(Ce_{CN}/((Nd_{CN})^{0.5}/Sm_{CN}))]$
CN = chondrite normalised
Normalising values from Sun and McDonough (1989)

Appendix 5 Supplementary material for Mapping hydrothermal systems in IOCG deposits using apatite geochronology and geochemsitry: An example from Vulcan Cu-Au prospect

Appendix 5 Table A2: LA-ICP-MS Trace element data collected for apatite from Vulcan Prospect in this study

Rejected Data

Sample	La	Ce	Pr	Nd	Sm	Eu	Gd	Tb	Dy	Ho	Er	Tm	Yb	Lu	Hf
973_apatite - 24	23.18	54.06	5.67	21.15	25.08	13.44	131.42	18.48	100.82	17.82	38.25	3.58	16.88	2.02	0.46
973_apatite - 29	569.81	853.82	55.44	145.92	47.54	24.02	227.08	16.41	45.66	5.54	12.65	0.95	4.18	0.36	0.52
973_apatite - 35	57.82	90.25	7.79	23.56	27.25	15.04	148.28	16.97	88.55	15.60	33.64	3.17	12.27	1.60	<0.005
973_apatite - 38	63.47	100.85	8.17	26.03	36.44	22.99	213.70	16.10	46.26	6.45	11.31	0.91	3.93	0.37	0.15
973_apatite - 39	15.76	17.13	2.45	11.14	27.71	17.80	153.19	15.18	64.21	10.50	25.34	2.45	12.77	1.33	2.29
973_apatite - 40	2.92	6.04	1.29	7.80	21.90	14.56	156.15	16.56	72.80	12.41	29.83	3.31	15.67	1.77	3.62
973_apatite - 46	3.14	8.39	1.38	9.66	33.74	23.19	227.08	19.53	70.67	12.17	32.74	3.94	25.39	3.98	8.67
973_apatite - 48	476.26	694.40	47.02	129.16	23.63	7.61	80.62	16.72	109.77	20.72	44.84	4.15	18.43	2.38	<0.006
973_apatite - 49	11.65	17.55	1.83	10.58	35.90	21.36	186.83	14.15	41.36	5.28	9.63	0.87	4.41	0.46	0.90
973_apatite - 5	86.72	112.12	9.37	29.26	30.85	18.09	167.33	13.81	52.23	8.39	16.31	1.27	5.92	0.51	0.04
973_apatite - 50	868.97	1299.12	81.80	211.46	42.45	15.02	137.87	21.04	133.78	25.94	60.34	5.80	27.83	3.17	0.08
973_apatite - 53	810.50	1218.03	101.62	198.79	46.43	15.66	126.06	15.45	82.66	14.69	31.16	2.36	10.86	0.97	<0.006
973_apatite - 56	15.36	28.91	2.58	13.84	32.23	18.69	182.90	16.11	65.89	11.07	23.52	2.02	10.11	0.90	0.12
973_apatite - 58	8.96	16.96	1.80	10.71	28.52	20.88	211.26	18.36	75.11	11.58	24.88	2.41	12.08	1.38	1.91
973_apatite - 59	125.42	190.07	12.81	34.82	43.26	27.16	264.24	21.62	71.58	10.00	18.99	1.59	5.47	0.62	<0.005
973_apatite - 6	0.46	2.99	0.79	6.82	26.00	17.64	174.11	17.49	72.66	12.36	27.70	2.53	11.52	1.23	0.52
973_apatite - 8	344.73	442.64	32.18	81.82	28.62	15.99	141.02	14.56	66.93	11.48	24.77	2.41	11.24	1.21	0.24
1084 - 10	210.47	519.90	78.45	357.05	97.92	15.29	99.67	13.42	74.84	13.19	33.21	4.14	20.92	2.49	0.02
1084 - 11	5661.24	10816.25	1050.29	3673.38	437.28	76.86	323.09	36.70	177.70	30.04	70.53	7.38	42.61	5.06	1.94
1084 - 41	569.39	1876.17	306.57	1561.82	420.47	96.11	440.74	50.64	242.80	38.96	79.62	6.52	26.90	2.67	0.43
1084 - 47	363.20	1351.97	248.83	1307.77	346.19	53.32	322.41	42.52	235.37	41.32	99.72	10.51	51.48	5.15	0.02
1084 - 8	291.91	1212.10	202.80	997.36	191.42	16.83	151.17	17.46	94.92	17.28	44.31	4.96	28.05	3.10	<0.011
1210 - 2	152.03	427.34	68.57	343.27	85.93	18.89	87.97	11.36	66.00	12.05	31.25	3.54	20.63	2.43	0.14
1210 - 7	121.29	388.30	63.77	346.27	87.32	16.25	83.00	9.89	50.99	9.05	21.38	2.32	12.19	1.39	0.04
1488 - 1	2563.18	5745.06	562.85	1811.39	330.71	122.66	451.63	45.00	150.37	17.33	33.99	3.34	19.79	2.72	15.93
1488 - 12	267.89	587.02	62.23	218.38	48.42	25.02	150.71	22.96	94.79	11.70	21.18	1.94	8.62	0.90	0.04
1488 - 20	71.77	155.25	16.80	60.25	22.73	14.70	100.74	16.95	84.82	10.63	19.69	1.68	8.36	0.96	0.02
1488 - 24	167.63	365.44	40.37	145.13	55.04	36.24	208.28	27.54	107.18	12.75	22.65	1.78	7.64	0.83	0.04
1488 - 47	0.06	0.86	0.43	6.72	18.28	15.13	124.56	23.69	124.39	16.89	32.48	2.99	12.81	1.42	0.02
1488 - 53	680.46	1487.19	159.16	534.18	114.04	51.87	264.97	34.54	143.34	16.39	31.25	2.49	11.41	1.11	<0.011
1488 - 6	288.62	552.67	57.33	197.68	54.50	26.50	134.74	19.10	92.13	11.72	21.44	1.85	7.98	0.79	0.05
1488 - 68	1.98	4.84	1.22	16.25	48.23	31.35	181.23	24.81	125.60	17.12	30.79	2.50	11.77	1.16	0.05

Element concentrations in ppm
$Eu/Eu^{\star} = [(Eu_{CN}/(Sm_{CN}+Gd_{CN})/2)]$
$Y/Y^{\star} = [(Y_{CN}/(Dy_{CN}+Ho_{CN})/2)]$
$TCe/Ce^{\star} = [(Ce_{CN}/(La_{CN} \times Pr_{CN})^{0.5})]$
$LCe/Ce^{\star} = [(Ce_{CN}/((Nd_{CN})^{0.5}/Sm_{CN}))]$
CN = chondrite normalised
Normalising values from Sun and McDonough (1989)

Appendix 5 Table A3: LA-ICP-MS Trace element florencite data from the Vulcan Prospect, collected in this study

Included Data

Sample	Drill hole	Mineral	Comment	O	Na	Al	Si	P	Ca	Sc	Mn	Fe	Cu	As
801_florencite - 10	VUD 009 801	Florencite		206021	1588	187020	20528	122391	52471	11.46	104.73	45954.54	20.11	250.26
801_florencite - 11	VUD 009 801	Florencite		239740	1342	242678	69274	71476	33011	16.88	70.91	50811.77	98.40	181.78
801_florencite - 12	VUD 009 801	Florencite		242798	1875	247658	196024	102321	29355	25.65	88.89	69391.67	60.33	323.65
801_florencite - 13	VUD 009 801	Florencite		273919	1711	298695	356985	44264	11628	29.66	64.10	464107.27	62.50	234.70
801_florencite - 14	VUD 009 801	Florencite		266226	1989	286164	327414	62522	18681	38.66	54.09	42696.06	<15.631	130.83
801_florencite - 15	VUD 009 801	Florencite		254643	1961	267370	248869	79607	32223	84.39	53.26	192678.88	<15.020	254.22
801_florencite - 17	VUD 009 801	Florencite		243072	2814	248175	211866	100350	30596	33.14	98.63	306056.74	62.39	293.48
801_florencite - 21	VUD 009 801	Florencite		267593	1614	288486	541860	51807	19888	66.22	84.56	361644.54	<15.737	218.60
801_florencite - 22	VUD 009 801	Florencite		242448	1803	247240	140914	99870	34696	62.23	68.92	136800.80	12.08	198.34
801_florencite - 23	VUD 009 801	Florencite		229318	1641	225363	139899	78575	28626	15.22	50.60	17547.55	13.44	195.87
801_florencite - 24	VUD 009 801	Florencite		234814	1586	234564	142081	83884	27986	24.32	81.94	188168.74	36.74	281.64
801_florencite - 26	VUD 009 801	Florencite		270255	1073	292746	354254	37792	14274	27.48	81.94	56816.77	24.94	107.75
801_florencite - 28	VUD 009 801	Florencite		230403	1886	227594	108748	102187	38732	46.85	113.38	412651.44	<13.778	319.59
801_florencite - 3	VUD 009 801	Florencite		280930	1641	310260	364823	23907	10269	28.38	35.18	145296.78	<16.131	176.40
801_florencite - 31	VUD 009 801	Florencite		224251	1304	217201	93893	95007	42246	26.45	74.55	99911.16	<13.111	267.55
801_florencite - 32	VUD 009 801	Florencite		221766	2064	213143	96609	107904	41272	22.87	93.51	160677.30	<14.151	298.10
801_florencite - 33	VUD 009 801	Florencite		268334	1714	289534	304317	43768	13499	29.74	50.64	472261.53	28.56	298.10
801_florencite - 34	VUD 009 801	Florencite		272628	1532	296614	471190	46471	13987	29.46	90.19	466513.95	62.44	242.16
801_florencite - 35	VUD 009 801	Florencite		226542	1690	220930	123784	105080	46562	21.14	96.84	58543.01	49.71	299.36
801_florencite - 36	VUD 009 801	Florencite		273479	1631	297981	378567	44835	15240	26.98	54.31	285656.66	12.73	131.67
801_florencite - 37	VUD 009 801	Florencite		247423	1171	255161	223021	66560	24072	28.66	51.11	37767.26	<14.786	166.66
801_florencite - 38	VUD 009 801	Florencite		236685	1400	237391	112139	76553	40759	30.73	67.69	257917.07	38.36	501.74
801_florencite - 39	VUD 009 801	Florencite		196823	1633	171692	5052	104854	34695	10.77	110.85	53950.18	<13.426	255.44
801_florencite - 40	VUD 009 801	Florencite		281244	1144	310731	370640	19858	7032	32.75	87.71	699626.82	35.89	194.60
801_florencite - 5	VUD 009 801	Florencite		247691	1381	255600	207011	93285	31568	29.21	72.52	298089.72	18.52	367.09
801_florencite - 6	VUD 009 801	Florencite		231215	1938	228658	163286	85926	36077	43.08	117.61	519311.88	15.15	300.63
801_florencite - 7	VUD 009 801	Florencite		251455	1618	261893	250768	80430	22201	38.89	90.16	453227.02	76.29	344.05
801_florencite - 9	VUD 009 801	Florencite		262625	1587	280238	451420	45905	21150	38.14	80.07	319706.59	121.96	168.79
852_florencite - 10	VUD 009 852	Florencite	monazite?	196952	2913	173707	2447	135810	36794	5.32	328.92	11044.36	135.17	1977.30
852_florencite - 11	VUD 009 852	Florencite	monazite?	206870	3168	189784	21193	108562	32725	4.68	287.95	12864.35	147.31	1228.86
852_florencite - 12	VUD 009 852	Florencite	monazite?	215732	3679	204177	103397	107100	31808	8.62	465.18	19009.40	148.84	1534.74
852_florencite - 13	VUD 009 852	Florencite	monazite?	199720	3518	178140	11854	121461	34482	2.62	333.17	17913.31	92.82	1031.13
852_florencite - 16	VUD 009 852	Florencite	monazite?	199842	2924	178493	3488	128742	35697	5.33	280.43	10897.56	96.97	1762.66
852_florencite - 17	VUD 009 852	Florencite	monazite?	198369	2894	176101	3115	136024	33444	5.54	294.97	14386.27	130.80	2236.88
852_florencite - 18	VUD 009 852	Florencite	monazite?	199054	2764	177321	5591	130061	37428	7.70	331.93	10776.82	120.16	2052.36
852_florencite - 19	VUD 009 852	Florencite	monazite?	194662	2572	169955	3640	132622	36654	5.73	289.06	9762.69	130.22	1856.25
852_florencite - 2	VUD 009 852	Florencite	monazite?	204293	2120	185860	4191	148260	36661	6.14	219.66	8586.25	100.00	1007.06
852_florencite - 20	VUD 009 852	Florencite	monazite?	195887	2997	172005	10556	127324	35739	5.19	317.01	25051.63	70.96	1588.75
852_florencite - 21	VUD 009 852	Florencite	monazite?	195526	3024	171365	8673	118034	32837	4.07	317.77	32548.60	72.38	1577.18
852_florencite - 23	VUD 009 852	Florencite	monazite?	196522	2937	172905	8948	154253	34297	4.72	294.21	10587.27	112.85	2303.95
852_florencite - 25	VUD 009 852	Florencite	monazite?	207776	3213	191128	109258	100711	26299	8.31	335.44	29539.24	148.75	917.56
852_florencite - 27	VUD 009 852	Florencite	monazite?	197854	3466	175073	10051	130334	34296	2.88	341.50	28040.96	119.22	1539.56
852_florencite - 28	VUD 009 852	Florencite	monazite?	202468	2979	182585	5378	123837	35224	2.99	308.34	11113.29	143.94	1570.05
852_florencite - 29	VUD 009 852	Florencite	monazite?	199340	3189	177622	10612	140636	34086	5.38	741.88	475693.98	412.82	1974.90
852_florencite - 32	VUD 009 852	Florencite	monazite?	219890	2885	210930	111590	89812	27196	8.66	304.41	72786.11	183.75	723.14
852_florencite - 33	VUD 009 852	Florencite	monazite?	200700	4600	179656	3865	92956	38270	3.83	319.41	30473.98	74.43	1302.89
852_florencite - 39	VUD 009 852	Florencite	monazite?	204118	2924	185238	26708	123339	39046	9.02	337.93	719401.69	121.38	1381.02
852_florencite - 4	VUD 009 852	Florencite	monazite?	201390	2378	180829	4027	146809	36200	4.21	573.73	559950.16	101.22	1770.96
852_florencite - 40	VUD 009 852	Florencite	monazite?	219613	6347	210673	116206	111037	27343	15.21	301.57	576371.17	85.08	445.06
852_florencite - 42	VUD 009 852	Florencite	monazite?	195178	2768	170823	5743	124828	43315	6.52	285.26	12296.05	44.85	2550.84
852_florencite - 47	VUD 009 852	Florencite	monazite?	197190	3129	174406	19501	126821	35949	9.13	335.33	17095.60	66.17	1592.61
852_florencite - 5	VUD 009 852	Florencite	monazite?	209714	3891	194588	103560	117795	33652	9.70	416.27	133039.64	166.34	602.94
852_florencite - 50	VUD 009 852	Florencite	monazite?	202669	2637	183323	16488	90518	30383	8.55	351.06	41272.32	186.51	1119.21
852_florencite - 51	VUD 009 852	Florencite	monazite?	199744	3411	178213	4312	107120	38476	4.45	359.07	12394.45	65.30	1853.80
852_florencite - 52	VUD 009 852	Florencite	monazite?	197902	2970	175395	4379	120558	37568	8.28	308.76	10725.01	72.49	1427.83
852_florencite - 54	VUD 009 852	Florencite	monazite?	206877	3866	189732	90611	118269	35352	5.85	397.88	71883.97	143.04	1439.73
852_florencite - 6	VUD 009 852	Florencite	monazite?	201864	2780	181916	22791	109824	32125	10.56	325.09	11943.45	148.50	1395.99
852_florencite - 8	VUD 009 852	Florencite	monazite?	197145	3217	174509	28732	117285	33974	4.77	311.38	12254.70	137.71	1665.90
973_florencite - 1	VUD 009 973	Florencite		222012	1292	214432	100934	103265	18302	126.63	198.90	37132.54	24.59	353.28
973_florencite - 10	VUD 009 973	Florencite		241236	670	245435	176894	71556	13455	39.74	127.91	119125.71	122.96	305.27
973_florencite - 11	VUD 009 973	Florencite		234016	958	233620	196373	97870	16959	42.28	151.32	131802.41	192.83	412.39
973_florencite - 12	VUD 009 973	Florencite		266044	1317	285954	313079	45236	8597	34.45	90.39	108140.58	143.31	196.05
973_florencite - 13	VUD 009 973	Florencite		232881	1187	231784	197074	116893	16101	34.15	158.16	174517.34	277.29	571.64
973_florencite - 14	VUD 009 973	Florencite		240494	1311	244366	252832	91199	11673	81.42	162.96	199009.87	223.15	314.59
973_florencite - 15	VUD 009 973	Florencite		231724	976	229877	136639	90366	19099	25.26	137.70	181294.65	191.70	386.96
973_florencite - 16	VUD 009 973	Florencite		214283	1136	201320	92285	144083	23416	29.45	208.00	212633.10	239.85	647.92
973_florencite - 17	VUD 009 973	Florencite		255913	1802	269450	338950	68880	13479	44.75	127.36	173541.23	204.03	257.77
973_florencite - 18	VUD 009 973	Florencite		212431	1319	198389	88674	148453	23021	34.84	196.83	181653.20	204.45	718.32
973_florencite - 19	VUD 009 973	Florencite		248241	895	256850	211606	67930	11588	34.21	117.48	103075.97	140.77	266.94
973_florencite - 2	VUD 009 973	Florencite		210264	1493	195459	67318	136655	19217	157.32	237.24	37151.08	27.81	429.66
973_florencite - 20	VUD 009 973	Florencite		259481	931	275238	266422	52430	8037	27.61	98.74	131549.38	145.04	305.97

Element concentrations in ppm
$Eu/Eu^* = [(Eu_{CN}/(Sm_{CN}+Gd_{CN})/2)]$
$Y/Y^* = [(Y_{CN}/(Dy_{CN}+Ho_{CN})/2)]$
$Ce/Ce^* = [(Ce_{CN}/(La_{CN} \times Pr_{CN})^{0.5})]$
CN = chondrite normalised
Normalising values from Sun and McDonough (1989)

Appendix 5 Supplementary material for Mapping hydrothermal systems in IOCG deposits using apatite geochronology and geochemsitry: An example from Vulcan Cu-Au prospect

Appendix 5 Table A3: LA-ICP-MS Trace element florencite data from the Vulcan Prospect, collected in this study

Included Data

Sample	Sr	Y	Zr	Nb	Ba	La	Ce	Pr	Nd	Sm	Eu	Gd	Tb	Dy
801_florencite - 10	102267.61	47.67	5.23	3.58	1776.66	27398.23	61013.28	7026.37	18807.06	3128.63	380.24	812.52	19.51	23.36
801_florencite - 11	51499.05	58.07	2.30	4.94	1113.01	18944.82	38429.39	5172.29	16492.67	1788.89	346.15	534.44	14.11	30.57
801_florencite - 12	52205.92	73.96	5.49	11.21	1597.10	15833.08	37839.35	3719.86	12860.79	1717.77	208.96	414.00	14.46	29.67
801_florencite - 13	17563.86	44.24	27.47	95.32	663.94	6805.48	13954.85	1131.61	4953.13	712.98	80.04	235.13	4.61	14.40
801_florencite - 14	23110.04	61.29	2.06	1.81	885.33	9253.87	21458.49	2317.11	7534.91	970.76	134.20	256.52	8.12	23.86
801_florencite - 15	24865.31	267.19	11.24	25.24	2624.61	18064.17	35309.96	3517.09	9704.14	1147.32	125.86	289.58	13.12	46.10
801_florencite - 17	47604.25	88.56	10.16	18.89	2044.02	19473.52	36242.11	4509.69	14193.62	1599.38	240.16	400.84	13.08	28.27
801_florencite - 21	16456.29	121.40	17.84	50.48	1467.85	11139.75	23428.47	2193.29	6547.36	826.14	94.64	207.71	10.65	29.39
801_florencite - 22	41595.90	171.75	48.27	21.04	2067.65	20282.16	43069.38	4265.51	13817.50	1889.52	214.69	423.68	13.62	46.67
801_florencite - 23	72205.50	55.60	3.42	0.86	1797.43	23370.57	43407.29	4542.45	14277.56	2296.24	223.04	566.43	15.41	23.15
801_florencite - 24	57329.98	74.31	18.65	36.19	1974.56	19757.13	46313.14	4920.45	15086.81	1803.04	204.71	408.21	14.26	41.01
801_florencite - 26	20099.57	46.81	3.41	1.45	1007.53	10267.68	15249.25	1605.52	6805.82	609.72	85.44	170.17	5.48	8.47
801_florencite - 28	50341.21	173.51	22.03	54.88	2923.29	24447.54	54062.63	5125.12	18520.48	2108.56	292.25	640.71	17.44	55.01
801_florencite - 3	8657.94	36.80	11.29	33.44	612.67	4407.18	9159.94	1067.14	3530.71	453.85	48.42	136.74	3.75	13.91
801_florencite - 31	75774.34	89.64	8.86	25.02	3065.36	20705.14	49527.75	5737.44	16817.21	2408.15	219.04	600.14	17.68	41.05
801_florencite - 32	74627.65	88.22	9.01	28.24	2921.32	22944.25	56363.38	5183.53	16343.20	2235.99	306.43	571.69	18.59	43.07
801_florencite - 33	22896.75	49.37	30.74	79.36	914.26	10017.60	18045.20	1748.23	6012.18	853.12	83.82	211.89	6.66	14.31
801_florencite - 34	17496.57	55.46	15.51	87.16	822.96	7548.32	15629.21	1552.04	5424.81	677.00	78.35	181.24	5.89	16.62
801_florencite - 35	71895.17	77.16	2.96	4.44	1839.72	22802.18	45671.47	5688.58	17474.73	2172.78	327.66	680.33	19.26	34.75
801_florencite - 36	17739.24	42.94	17.48	69.68	747.24	7355.55	14506.61	1479.03	4642.07	678.49	87.41	199.73	6.35	13.10
801_florencite - 37	51996.91	56.04	11.17	1.49	1711.10	14748.14	30587.58	3417.85	10439.65	1596.37	159.35	391.68	11.29	26.73
801_florencite - 38	73583.91	62.06	13.49	40.92	2336.63	15356.98	32577.87	3417.92	13408.52	1634.64	196.79	492.34	12.33	32.89
801_florencite - 39	124135.69	57.67	5.91	10.32	2010.21	26919.27	65238.42	5973.09	18920.31	2487.60	444.30	729.89	16.37	23.51
801_florencite - 40	7835.55	33.26	35.40	168.57	672.29	4574.12	9270.31	817.64	3369.88	349.05	43.37	200.47	3.61	11.49
801_florencite - 5	50270.57	71.56	42.39	38.58	1575.62	13351.98	32277.97	3471.41	11300.80	1451.50	185.64	363.87	11.49	33.71
801_florencite - 6	63546.93	106.32	18.17	56.99	2491.86	22066.71	44678.48	4960.51	16226.81	2028.52	210.11	572.14	17.19	48.39
801_florencite - 7	39175.47	71.42	24.33	69.18	1570.43	15829.72	31400.02	2927.83	11484.55	1275.27	173.58	414.35	13.62	31.51
801_florencite - 9	26650.63	68.26	19.34	61.71	1191.04	10616.99	24385.05	3132.39	7644.74	1180.88	142.37	303.17	9.68	18.52
852_florencite - 10	67566.12	425.40	170.09	0.16	1669.73	33995.79	77363.28	9645.62	30130.35	2956.62	265.71	750.36	37.20	125.64
852_florencite - 11	65776.56	261.06	47.20	<0.022	1201.88	26274.92	72001.15	7775.64	24661.97	2351.57	226.77	535.33	20.91	63.45
852_florencite - 12	60688.38	302.93	84.50	0.09	1240.83	22967.45	59988.16	8070.67	23698.85	3014.28	211.07	597.15	28.22	104.30
852_florencite - 13	70346.46	252.52	73.34	<0.020	1346.36	30080.56	75960.92	8601.41	28308.83	2918.21	235.42	655.11	34.78	79.01
852_florencite - 16	62665.80	421.63	110.47	0.02	1971.38	31740.21	79440.31	8901.65	29044.33	2666.74	223.16	710.40	33.31	132.79
852_florencite - 17	67754.47	433.38	101.82	0.02	1575.71	32997.35	75321.04	9148.61	28036.32	2664.80	237.38	704.91	37.04	113.63
852_florencite - 18	64753.52	636.37	199.93	0.09	1618.88	31995.59	74806.28	8982.89	28292.18	2731.26	236.43	714.78	40.80	201.60
852_florencite - 19	70637.17	499.00	136.02	0.06	1602.05	32607.51	81337.84	9301.44	30027.75	2966.00	260.95	794.67	40.49	137.32
852_florencite - 2	49779.81	544.51	110.07	0.03	5226.78	34137.70	81775.16	8891.06	28401.57	2907.11	248.06	776.03	50.97	206.52
852_florencite - 20	72243.67	447.99	79.97	0.02	1476.08	31835.53	78204.80	9156.53	28213.18	2500.38	232.59	696.85	30.70	127.34
852_florencite - 21	72190.83	386.20	65.37	0.08	1359.07	32402.26	78530.10	9132.37	29763.28	2610.58	237.17	708.75	31.38	112.95
852_florencite - 23	73411.46	333.53	54.11	<0.012	1656.29	33684.97	77034.08	9314.00	27709.07	2614.83	214.94	611.98	31.09	106.19
852_florencite - 25	72928.49	180.76	56.77	0.18	1220.62	25597.58	63451.81	8201.08	25105.43	1910.99	187.91	521.62	18.96	66.41
852_florencite - 27	73939.44	210.36	45.56	0.09	1445.68	29580.90	78039.79	8841.63	27910.72	2496.57	221.56	577.83	22.59	69.40
852_florencite - 28	66791.03	242.83	57.25	<0.014	1403.74	32157.35	72446.51	8746.80	28186.28	2631.53	235.66	646.60	22.89	83.44
852_florencite - 29	66573.19	363.96	65.55	2.53	1631.41	32735.00	75617.03	9230.87	29247.93	2716.63	235.59	639.85	31.06	99.35
852_florencite - 32	60685.43	216.56	32.15	0.16	987.43	21343.39	54085.99	7235.31	22623.96	2150.62	181.38	457.26	17.15	63.11
852_florencite - 33	73796.03	281.87	43.54	0.35	1467.89	29646.43	70001.17	8722.18	29645.23	2668.12	236.67	670.03	25.87	85.28
852_florencite - 39	58757.71	594.50	19.33	0.72	1864.74	37391.15	74129.11	8551.70	27372.05	2705.67	226.17	675.25	33.09	111.38
852_florencite - 4	55344.11	357.18	49.45	1.40	1692.58	35478.84	84578.20	9438.90	29903.47	2648.01	229.46	738.51	38.98	125.76
852_florencite - 40	54471.64	263.19	58.72	1.94	1246.67	24070.38	53764.94	7061.89	25170.42	1964.76	211.21	995.21	22.95	100.64
852_florencite - 42	68037.84	498.90	39.85	0.06	1919.18	38470.35	81233.32	8967.64	26722.55	2203.92	201.16	616.00	32.45	133.90
852_florencite - 47	66543.55	641.13	80.22	0.02	1547.69	32082.08	76889.04	8626.89	27014.69	2301.63	212.02	616.23	41.90	194.69
852_florencite - 5	58710.68	319.70	83.17	0.21	1199.55	25806.95	73263.82	7368.09	21904.93	2157.36	194.86	584.05	25.24	87.59
852_florencite - 50	68427.09	895.13	35.62	0.31	1372.57	26609.65	69965.51	7128.14	23243.79	2053.48	199.19	651.75	44.46	220.18
852_florencite - 51	71260.82	327.63	136.07	0.04	1694.19	32956.36	69992.68	8731.78	29222.25	2485.18	221.09	568.23	31.14	109.41
852_florencite - 52	71411.11	782.48	96.12	0.03	1465.35	29596.90	73296.50	8300.70	28087.41	2714.57	244.73	728.99	44.61	197.19
852_florencite - 54	69856.10	322.14	43.20	<0.039	1427.41	28747.06	65858.67	8001.66	23749.65	2271.58	223.26	566.85	26.14	94.93
852_florencite - 6	61424.52	840.97	188.41	0.23	1352.36	28773.26	74492.57	8286.02	28562.74	2379.32	228.40	716.91	48.57	251.02
852_florencite - 8	71469.13	257.20	54.95	0.08	9326.76	28836.24	75050.42	8985.64	27940.71	2600.88	230.77	629.49	24.03	112.48
973_florencite - 1	38097.23	503.34	10.15	1.48	9353.79	48934.92	67522.82	4407.21	10632.25	1112.29	153.63	487.40	21.97	70.12
973_florencite - 10	33260.64	175.93	11.60	3.55	4237.09	31936.45	49507.06	3655.35	8060.63	909.66	141.06	400.19	17.86	51.48
973_florencite - 11	39233.34	184.80	10.71	3.22	4663.84	37250.23	54701.39	3680.26	9600.41	1149.24	168.26	502.43	19.59	48.59
973_florencite - 12	18079.77	89.71	11.61	3.35	2269.43	16050.12	24320.14	1684.41	4105.43	489.80	77.97	232.53	8.01	28.30
973_florencite - 13	41020.41	174.82	16.69	5.56	5110.80	37345.96	54718.93	3893.63	9906.86	1189.55	158.15	490.82	21.24	52.87
973_florencite - 14	31339.77	230.73	15.91	5.55	5363.18	34259.89	49699.46	3266.42	8037.38	971.27	127.81	374.67	20.25	51.70
973_florencite - 15	41506.57	179.27	11.84	5.14	5169.33	36997.45	56828.00	4127.87	10583.28	1235.08	165.87	522.70	22.72	60.35
973_florencite - 16	55711.76	198.33	12.77	5.03	6143.71	49231.98	70833.26	5132.51	13181.37	1613.19	235.55	687.80	25.79	67.58
973_florencite - 17	24238.45	147.67	13.97	3.78	3453.01	23685.86	33018.15	2324.72	5773.54	664.20	98.25	260.70	13.02	31.36
973_florencite - 18	52279.19	246.42	13.23	4.85	6529.15	48288.00	79404.99	5326.04	13156.89	1474.22	218.16	681.35	27.22	71.75
973_florencite - 19	30061.41	163.86	9.51	2.34	3505.44	27027.55	41410.67	2936.63	7505.83	874.59	126.81	382.77	16.05	42.95
973_florencite - 2	42717.22	683.36	11.06	2.27	12640.50	57449.66	78851.91	5486.67	11580.66	1261.01	192.20	530.58	24.98	84.42
973_florencite - 20	22784.07	99.31	12.93	3.28	2916.17	20134.89	29750.35	2083.58	5780.22	681.16	92.11	280.58	13.48	29.15

Element concentrations in ppm
$Eu/Eu^* = [(Eu_{CN}/(Sm_{CN}+Gd_{CN})/2)]$
$Y/Y^* = [(Y_{CN}/(Dy_{CN}+Ho_{CN})/2)]$
$Ce/Ce^* = [(Ce_{CN}/(La_{CN} \times Pr_{CN})^{0.5})]$
CN = chondrite normalised
Normalising values from Sun and McDonough (1989)

Appendix 5 Table A3: LA-ICP-MS Trace element florencite data from the Vulcan Prospect, collected in this study

Included Data

Sample	Ho	Er	Tm	Yb	Lu	Hf	Ta	W	Bi	Th	U	ΣREY	Eu/Eu*	Ce/Ce*	Y/Y*
801_florencite - 10	2.08	4.36	0.62	2.06	0.15	<0.084	0.05	0.82	1.19	4049.55	26.48	118666	0.29	1.06	2.53
801_florencite - 11	2.98	5.26	0.52	2.45	0.33	0.38	0.35	0.76	0.37	2964.12	30.40	81823	0.46	0.94	0.25
801_florencite - 12	3.32	5.11	0.70	1.88	0.75	<0.082	0.27	0.24	1.79	2757.57	30.28	72724	0.29	1.19	0.32
801_florencite - 13	1.06	1.33	0.49	1.32	0.43	0.85	3.19	3.16	1.96	899.90	66.81	27941	0.26	1.22	0.43
801_florencite - 14	2.88	5.02	0.78	5.18	0.35	0.70	0.06	0.58	1.17	1391.29	14.94	42033	0.33	1.12	0.33
801_florencite - 15	7.38	15.87	1.63	9.72	2.00	1.15	1.04	0.88	1.62	1612.52	36.51	68521	0.26	1.07	0.69
801_florencite - 17	2.88	6.51	0.51	2.70	0.76	0.34	0.64	2.05	2.42	1953.54	65.43	76803	0.36	0.93	0.41
801_florencite - 21	5.13	11.73	1.02	6.62	0.78	<0.092	1.67	3.13	1.78	1044.36	77.12	44624	0.28	1.15	0.48
801_florencite - 22	5.14	12.44	1.66	6.93	1.08	1.11	0.99	0.21	1.01	2043.83	45.47	84222	0.28	1.12	0.48
801_florencite - 23	1.59	4.57	0.18	2.13	0.27	<0.055	0.04	<0.077	1.25	2326.25	31.78	88786	0.23	1.02	0.34
801_florencite - 24	3.64	6.40	0.37	3.40	0.16	0.62	0.69	1.19	1.08	2351.94	82.61	88637	0.28	1.13	0.24
801_florencite - 26	1.07	3.19	0.22	2.87	0.29	<0.086	0.15	0.65	0.29	897.17	6.30	34862	0.33	0.91	0.69
801_florencite - 28	5.37	12.81	1.24	10.64	0.71	2.96	1.33	0.84	1.06	2788.60	95.20	105474	0.33	1.17	0.42
801_florencite - 3	1.66	1.52	0.24	3.02	<0.029	0.82	0.41	<0.108	0.55	486.93	29.08	18865	0.25	1.02	0.34
801_florencite - 31	4.37	7.17	0.49	4.14	0.50	0.26	0.33	0.34	1.38	3211.10	80.42	96180	0.22	1.10	0.28
801_florencite - 32	2.75	6.43	0.60	3.66	0.43	0.60	0.43	0.50	2.56	3059.16	90.04	104112	0.33	1.25	0.29
801_florencite - 33	2.09	2.38	0.43	2.01	0.25	1.94	3.00	3.97	1.73	932.66	92.17	37050	0.24	1.04	0.42
801_florencite - 34	1.89	5.03	0.42	2.88	0.23	1.47	1.99	1.32	0.85	943.13	60.50	31179	0.28	1.10	0.43
801_florencite - 35	3.46	5.96	0.57	2.56	0.58	0.63	0.19	<0.113	1.32	3602.96	29.19	94962	0.36	0.97	0.29
801_florencite - 36	1.36	3.03	0.33	1.18	0.11	0.67	0.75	1.80	1.63	801.88	50.99	29017	0.31	1.06	0.43
801_florencite - 37	3.28	5.93	0.41	1.29	0.47	0.59	<0.017	<0.093	0.61	2048.27	20.73	61446	0.24	1.04	0.27
801_florencite - 38	3.24	6.78	0.48	3.32	0.24	0.82	0.24	1.81	2.23	2430.19	82.52	67206	0.29	1.09	0.25
801_florencite - 39	2.80	5.39	0.38	2.83	0.38	<0.073	0.07	0.30	0.58	4268.96	46.11	120822	0.42	1.24	0.31
801_florencite - 40	2.69	1.96	0.36	1.73	0.24	0.39	2.58	4.57	1.80	422.44	108.67	18680	0.27	1.16	0.31
801_florencite - 5	3.24	7.79	0.44	2.36	0.21	0.74	1.44	0.18	1.82	1974.20	76.41	62534	0.31	1.15	0.28
801_florencite - 6	7.45	7.70	0.80	4.91	0.45	0.66	0.94	4.52	1.27	2747.88	99.82	90936	0.25	1.03	0.26
801_florencite - 7	2.99	4.17	0.43	5.41	0.28	0.71	1.11	2.27	1.23	1937.35	79.86	63635	0.32	1.11	0.30
801_florencite - 9	2.47	4.27	0.08	2.53	0.76	1.65	1.08	0.37	1.09	1492.13	85.20	47512	0.29	1.02	0.46
852_florencite - 10	19.85	45.66	6.82	41.76	4.50	2.11	0.01	<0.042	7.53	23296.68	217.25	155815	0.22	1.03	0.40
852_florencite - 11	9.34	32.26	3.59	19.00	2.73	0.88	<0.012	0.22	6.72	21434.05	86.14	134240	0.23	1.22	0.50
852_florencite - 12	20.13	35.74	7.80	26.95	3.85	0.80	0.11	0.17	5.58	18260.23	209.93	119078	0.17	1.06	0.33
852_florencite - 13	12.37	41.41	5.02	26.35	3.52	0.81	<0.010	0.07	5.72	22461.44	142.03	147215	0.20	1.14	0.38
852_florencite - 16	19.69	54.39	6.30	41.77	6.63	1.54	<0.007	<0.036	9.52	22654.16	258.15	153443	0.20	1.14	0.38
852_florencite - 17	23.09	56.84	7.68	40.32	5.66	1.45	<0.007	0.18	9.34	25443.29	251.65	149828	0.21	1.05	0.42
852_florencite - 18	34.84	95.08	9.09	61.58	9.52	2.33	<0.007	0.04	10.16	27190.23	407.01	148848	0.21	1.07	0.37
852_florencite - 19	22.06	64.44	7.02	55.17	6.22	1.54	<0.007	0.05	9.66	24001.06	307.58	158128	0.21	1.13	0.43
852_florencite - 2	31.44	71.10	7.26	41.08	6.59	1.29	0.04	<0.053	17.02	15765.49	417.16	158096	0.20	1.13	0.32
852_florencite - 20	20.50	54.20	6.43	46.46	4.30	0.97	<0.007	0.04	10.03	25751.07	379.17	151578	0.22	1.11	0.42
852_florencite - 21	17.23	45.18	5.52	28.70	4.15	0.99	<0.009	<0.046	7.06	24685.93	264.25	154016	0.22	1.10	0.41
852_florencite - 23	14.86	41.76	5.17	32.45	4.57	0.86	0.01	0.09	10.22	22880.83	240.57	151754	0.20	1.05	0.39
852_florencite - 25	8.19	24.26	2.40	18.81	2.29	0.30	<0.014	<0.069	4.56	20988.61	105.52	125298	0.24	1.06	0.34
852_florencite - 27	11.44	28.10	3.33	20.80	2.50	0.60	<0.008	<0.042	6.34	22893.81	111.49	148038	0.22	1.17	0.36
852_florencite - 28	11.55	27.42	3.54	22.69	2.89	0.94	<0.008	0.11	6.03	20555.07	124.51	145468	0.22	1.04	0.36
852_florencite - 29	18.16	45.51	5.81	30.02	4.32	1.40	<0.012	0.30	30.83	22784.23	284.42	151021	0.21	1.05	0.42
852_florencite - 32	10.92	49.01	2.50	16.21	2.33	0.56	<0.012	0.16	8.40	18449.21	145.32	108456	0.21	1.05	0.40
852_florencite - 33	15.38	52.78	6.99	38.11	3.55	0.15	0.10	<0.106	7.06	21544.44	206.39	142100	0.21	1.05	0.38
852_florencite - 39	24.58	45.90	9.57	38.54	4.80	<0.142	<0.042	<0.211	38.65	17178.54	403.05	151913	0.20	1.00	0.58
852_florencite - 4	17.92	38.98	5.33	28.20	4.05	0.89	0.01	0.48	51.40	16336.53	203.75	163632	0.21	1.12	0.35
852_florencite - 40	17.28	45.01	5.29	102.32	18.12	0.80	<0.062	<0.308	9.00	19225.90	343.30	113814	0.24	1.00	0.30
852_florencite - 42	21.77	62.50	6.81	56.44	5.54	0.40	<0.008	0.21	12.56	23737.96	517.34	159233	0.22	1.06	0.44
852_florencite - 47	29.01	99.16	9.81	73.53	8.43	1.08	<0.007	<0.035	12.07	30177.95	625.27	148840	0.22	1.12	0.40
852_florencite - 5	14.43	35.81	6.25	30.84	4.02	1.86	<0.016	0.43	7.73	23109.75	168.53	131804	0.22	1.28	0.43
852_florencite - 50	37.22	94.62	15.84	84.78	11.17	0.37	<0.009	0.15	16.93	31340.23	1069.30	131255	0.23	1.23	0.48
852_florencite - 51	14.75	31.91	6.99	33.69	4.86	1.88	0.02	<0.058	5.13	23427.39	158.80	144738	0.22	1.00	0.37
852_florencite - 52	34.46	81.32	12.84	83.13	7.87	0.89	<0.008	0.05	7.79	28233.84	722.88	144214	0.22	1.13	0.46
852_florencite - 54	19.03	36.58	4.35	22.96	3.17	<0.078	<0.024	<0.117	7.06	21281.49	303.53	129948	0.24	1.05	0.38
852_florencite - 6	40.03	97.05	17.24	74.86	14.52	2.86	<0.009	0.09	8.00	27449.53	501.50	144823	0.23	1.17	0.40
852_florencite - 8	10.70	33.27	5.83	25.04	2.73	0.71	<0.010	<0.051	7.17	22053.70	159.78	144745	0.21	1.13	0.30
973_florencite - 1	13.21	41.61	4.68	22.59	2.62	0.42	0.10	0.29	46.00	1202.39	231.11	133931	0.31	1.11	0.81
973_florencite - 10	6.49	10.06	0.89	5.73	0.47	0.57	0.08	2.86	15.32	470.44	82.69	94879	0.35	1.11	0.43
973_florencite - 11	6.31	10.55	1.41	5.25	0.37	0.26	0.08	5.22	18.44	548.56	97.42	107329	0.33	1.13	0.48
973_florencite - 12	2.52	7.00	0.62	2.69	0.55	1.13	0.06	4.53	10.66	250.20	54.54	47100	0.36	1.13	0.43
973_florencite - 13	5.89	11.88	0.92	5.07	0.73	0.30	0.14	9.11	25.35	560.13	93.55	107977	0.30	1.10	0.43
973_florencite - 14	7.28	17.65	1.63	10.83	0.82	0.13	0.09	10.80	19.35	539.60	145.47	97078	0.30	1.14	0.55
973_florencite - 15	7.20	9.58	0.97	3.44	0.34	0.79	0.03	7.99	18.72	505.66	81.37	110744	0.31	1.11	0.38
973_florencite - 16	6.11	10.85	0.65	4.54	0.49	0.65	0.09	8.00	25.04	596.90	97.72	141230	0.33	1.08	0.39
973_florencite - 17	4.18	9.41	0.72	5.07	0.47	<0.073	0.09	6.90	14.64	369.85	84.09	66037	0.34	1.08	0.58
973_florencite - 18	8.73	13.42	1.72	4.71	0.74	0.29	<0.019	7.60	29.92	645.96	111.07	148924	0.33	1.20	0.44
973_florencite - 19	4.67	9.22	0.86	5.08	0.59	0.57	0.03	3.26	12.27	422.75	69.12	80508	0.33	1.12	0.49
973_florencite - 2	18.09	48.91	6.04	32.39	4.03	0.55	0.13	0.35	64.64	1413.88	307.81	156255	0.35	1.07	0.88
973_florencite - 20	3.84	6.37	0.70	3.63	0.45	0.70	0.12	3.76	12.29	291.35	51.03	58960	0.31	1.11	0.42

Element concentrations in ppm
$Eu/Eu^* = [(Eu_{CN}/(Sm_{CN}+Gd_{CN})/2)]$
$Y/Y^* = [(Y_{CN}/(Dy_{CN}+Ho_{CN})/2)]$
$Ce/Ce^* = [(Ce_{CN}/(La_{CN} \times Pr_{CN})^{0.5})]$
CN = chondrite normalised
Normalising values from Sun and McDonough (1989)

Appendix 5 Supplementary material for Mapping hydrothermal systems in IOCG deposits using apatite geochronology and geochemsitry: An example from Vulcan Cu-Au prospect

Appendix 5 Table A3: LA-ICP-MS Trace element florencite data from the Vulcan Prospect, collected in this study

Included Data

Sample	Drill hole	Mineral	Comment	O	Na	Al	Si	P	Ca	Sc	Mn	Fe	Cu	As
973_florencite - 24	VUD 009 973	Florencite		269229	933	291256	310617	38459	8083	58.35	166.88	139427.45	120.01	129.31
973_florencite - 25	VUD 009 973	Florencite		272221	1285	296140	382959	54618	8466	52.50	395.95	521849.04	203.20	255.84
973_florencite - 26	VUD 009 973	Florencite		239516	650	242925	192177	74539	11161	19.93	59.24	19790.85	11.57	198.90
973_florencite - 27	VUD 009 973	Florencite		227622	1120	223638	141613	100841	14258	22.86	64.75	10111.02	16.00	238.58
973_florencite - 28	VUD 009 973	Florencite		228644	963	225348	148231	95294	14901	32.92	70.31	9482.64	29.88	271.40
973_florencite - 29	VUD 009 973	Florencite		242130	1149	246973	219631	88684	15960	46.34	276.45	297955.16	16.07	360.33
973_florencite - 3	VUD 009 973	Florencite		241372	1778	246080	199086	89292	14472	97.82	146.99	22982.39	30.25	249.08
973_florencite - 31	VUD 009 973	Florencite		224174	1433	217757	123356	106428	19312	89.53	291.52	175037.50	70.89	387.20
973_florencite - 32	VUD 009 973	Florencite		223787	1502	217302	114025	113962	17367	113.34	225.36	78031.95	22.21	333.50
973_florencite - 33	VUD 009 973	Florencite		227464	1438	223186	130973	118429	19973	103.19	251.11	50813.60	18.14	346.51
973_florencite - 37	VUD 009 973	Florencite		268392	1220	289865	348310	38449	6018	60.60	207.25	245515.94	58.60	143.91
973_florencite - 38	VUD 009 973	Florencite		229610	1008	226560	160770	98331	18953	37.48	212.82	48350.72	28.80	445.64
973_florencite - 39	VUD 009 973	Florencite		274926	1486	300498	354424	36510	8315	36.26	915.83	947224.20	67.57	271.43
973_florencite - 4	VUD 009 973	Florencite		226643	1572	222002	155975	110497	17475	81.83	126.25	16547.73	174.11	327.81
973_florencite - 40	VUD 009 973	Florencite		272396	1770	296377	453437	45836	4758	41.30	700.96	633064.63	109.38	219.42
973_florencite - 43	VUD 009 973	Florencite		275378	1271	301222	435300	46710	6413	34.94	480.94	619638.44	82.88	360.70
973_florencite - 44	VUD 009 973	Florencite		277027	1129	303921	337962	29334	5749	32.02	803.94	987310.45	73.47	221.79
973_florencite - 46	VUD 009 973	Florencite		209132	1606	193103	58368	117045	23244	62.47	338.05	129018.62	53.77	407.17
973_florencite - 47	VUD 009 973	Florencite		218936	1654	209014	94004	99862	22703	44.42	208.61	77961.86	25.05	320.63
973_florencite - 48	VUD 009 973	Florencite		276079	1242	302430	376596	37512	6212	40.24	164.71	157391.98	51.84	177.50
973_florencite - 49	VUD 009 973	Florencite		215226	1264	202942	93842	110191	23082	39.15	346.50	112934.87	20.97	476.02
973_florencite - 50	VUD 009 973	Florencite		250802	2312	261227	298441	79978	15381	74.49	838.05	686624.27	178.66	360.09
973_florencite - 52	VUD 009 973	Florencite		270917	1140	293925	310886	35394	10133	29.18	161.87	158145.80	22.75	113.08
973_florencite - 53	VUD 009 973	Florencite		210695	1848	195676	71552	117258	24556	65.95	352.06	113895.70	15.94	426.67
973_florencite - 54	VUD 009 973	Florencite		205924	1365	188118	42910	117236	22952	130.68	220.51	14814.91	17.28	333.25
973_florencite - 55	VUD 009 973	Florencite		271688	1001	295274	322240	25588	6608	46.36	69.70	18271.60	29.97	83.56
973_florencite - 56	VUD 009 973	Florencite		211133	1097	196446	61917	108265	20972	119.66	192.10	12948.40	19.54	324.52
973_florencite - 57	VUD 009 973	Florencite		215001	1240	202844	78188	106284	21087	137.12	219.01	30065.65	23.46	314.37
973_florencite - 58	VUD 009 973	Florencite		245764	823	252810	207830	83153	15598	42.35	272.64	233849.19	19.56	370.62
973_florencite - 6	VUD 009 973	Florencite		248168	1049	256749	224985	75589	16266	37.99	148.68	185832.58	248.04	362.47
973_florencite - 60	VUD 009 973	Florencite		272265	1066	296188	484335	41073	4797	59.46	288.50	494804.96	110.19	128.22
973_florencite - 61	VUD 009 973	Florencite		211095	1292	196056	94376	160429	24347	17.02	248.64	113389.88	48.03	724.77
973_florencite - 7	VUD 009 973	Florencite		243602	1222	249309	242679	94422	13988	45.15	212.73	155144.03	549.78	522.16
973_florencite - 8	VUD 009 973	Florencite		252032	868	263123	257545	64796	12338	49.78	111.79	98131.38	121.25	249.04
973_florencite - 9	VUD 009 973	Florencite		241620	1599	246144	247044	110952	16922	46.81	171.27	196599.96	307.38	448.31

Element concentrations in ppm
$Eu/Eu^* = [(Eu_{CN}/(Sm_{CN}+Gd_{CN})/2)]$
$Y/Y^* = [(Y_{CN}/(Dy_{CN}+Ho_{CN})/2)]$
$Ce/Ce^* = [(Ce_{CN}/(La_{CN} \times Pr_{CN})^{0.5})]$
CN = chondrite normalised
Normalising values from Sun and McDonough (1989)

Appendix 5 Table A3: LA-ICP-MS Trace element florencite data from the Vulcan Prospect, collected in this study

Included Data

Sample	Sr	Y	Zr	Nb	Ba	La	Ce	Pr	Nd	Sm	Eu	Gd	Tb	Dy
973_florencite - 24	13249.42	173.94	26.96	5.83	2644.74	15065.84	21732.52	1379.93	3579.39	354.31	63.53	170.44	8.08	20.19
973_florencite - 25	11822.25	134.31	37.04	18.31	2168.98	12592.19	18807.93	1321.19	2867.12	353.36	54.72	149.43	5.81	19.48
973_florencite - 26	31570.53	675.09	4.70	1.67	8826.53	33941.26	48191.31	3363.89	8336.53	1024.35	140.37	406.07	16.44	61.89
973_florencite - 27	36904.27	814.98	3.51	1.70	11397.22	42439.95	59891.26	4071.97	10019.64	1184.13	182.49	515.86	21.11	80.41
973_florencite - 28	35726.57	808.92	4.79	0.40	11552.99	41989.38	59059.94	3994.39	9595.01	1094.15	170.51	484.19	21.83	81.28
973_florencite - 29	32102.31	211.15	21.47	22.65	4453.04	32338.83	46828.59	3180.60	8115.79	918.27	134.04	425.78	15.19	47.12
973_florencite - 3	25938.36	441.65	10.23	0.84	8074.70	35332.13	48857.61	3103.38	7666.93	768.96	113.35	335.85	15.78	54.34
973_florencite - 31	41120.46	378.90	9.24	7.40	6968.55	47944.00	62516.71	4391.72	10209.94	1134.06	173.37	530.74	23.45	64.93
973_florencite - 32	35995.66	517.96	55.44	3.99	8469.35	48357.18	66723.00	4162.46	10032.08	1128.96	152.13	474.29	22.51	82.46
973_florencite - 33	37845.24	327.90	7.43	1.96	6908.05	43045.63	62616.18	4296.21	9979.59	1073.17	165.88	470.46	20.63	61.81
973_florencite - 37	13619.19	217.16	102.90	15.19	2735.28	16483.99	21933.53	1458.38	3432.65	383.60	57.22	177.46	8.39	35.09
973_florencite - 38	40615.57	195.57	4.84	1.37	6141.37	37928.53	61317.49	4058.00	9800.91	1098.97	172.38	504.36	21.65	54.77
973_florencite - 39	11619.06	101.47	47.07	32.90	1615.81	11332.11	14573.55	1063.16	2359.70	294.70	51.20	165.77	5.84	14.02
973_florencite - 4	36865.63	550.22	7.53	0.54	9659.62	44630.19	61951.47	3932.62	9974.94	1105.74	164.79	488.50	19.04	68.40
973_florencite - 40	13297.50	77.77	27.55	25.91	1929.94	11952.91	17697.86	1346.24	3033.00	421.26	70.91	159.86	6.04	19.32
973_florencite - 43	11110.48	104.81	67.80	37.00	1605.69	9877.88	15344.94	1104.73	2657.41	337.71	44.07	126.39	7.81	14.39
973_florencite - 44	11232.98	117.68	47.76	28.30	1654.12	8104.20	12874.42	924.96	2571.37	302.02	51.83	135.94	7.60	16.76
973_florencite - 46	50747.66	374.39	13.13	3.56	7020.30	57233.93	80106.07	5325.48	11172.64	1453.80	201.34	633.46	22.50	63.22
973_florencite - 47	47704.55	275.47	13.31	2.33	4871.02	45530.79	70897.28	4995.72	11900.32	1365.32	201.62	640.88	21.35	62.09
973_florencite - 48	9544.63	115.79	56.50	8.47	2080.33	10252.66	14489.54	972.14	2642.68	343.66	35.73	143.40	6.53	20.93
973_florencite - 49	49916.98	248.23	12.36	5.12	5041.70	51395.60	71594.75	4809.97	12914.90	1415.09	212.18	668.17	24.64	55.99
973_florencite - 50	25149.56	324.16	66.04	30.47	4752.09	24904.42	40369.59	3040.01	5824.93	740.75	112.68	262.40	18.91	45.19
973_florencite - 52	13947.99	71.60	11.29	4.25	1425.85	12796.77	20403.15	1325.79	3307.44	443.36	65.60	190.54	5.87	15.60
973_florencite - 53	49670.72	245.55	8.59	4.10	6088.00	56377.77	77065.90	5022.63	12393.23	1513.09	221.90	637.13	23.41	56.93
973_florencite - 54	47001.74	507.63	11.88	0.19	9649.36	60166.16	84083.15	5378.41	13934.09	1428.46	188.09	597.71	26.11	81.90
973_florencite - 55	10641.11	141.48	4.08	<0.032	2358.37	14601.07	19275.42	1457.88	3183.00	395.74	56.23	158.84	6.30	26.61
973_florencite - 56	42649.84	333.33	7.74	0.43	6841.30	60430.46	80218.42	5032.38	12408.35	1261.70	179.29	525.69	24.88	72.59
973_florencite - 57	41266.78	381.21	13.55	0.95	7638.42	55245.50	76565.08	4953.88	11478.85	1256.44	178.21	529.95	22.05	68.38
973_florencite - 58	32078.18	213.88	20.39	12.83	3481.46	29224.49	42709.64	2806.21	7510.14	910.74	149.77	440.65	18.95	43.25
973_florencite - 6	28914.88	146.50	14.10	6.00	3479.64	28182.77	42100.57	2915.73	6991.98	856.83	123.73	400.44	17.34	39.74
973_florencite - 60	11962.60	120.08	28.80	15.93	2068.08	12756.21	19036.62	1218.60	2662.86	334.90	62.99	162.71	6.58	21.06
973_florencite - 61	60746.84	216.81	4.74	3.81	5697.49	45825.31	77885.93	4602.64	13109.66	1433.37	231.31	684.04	26.69	68.12
973_florencite - 7	33495.45	164.41	13.20	4.01	4188.98	30416.85	45122.19	3094.90	7925.99	913.39	144.54	412.26	15.85	46.20
973_florencite - 8	25544.45	146.74	12.64	2.94	3725.01	25364.30	38914.97	2489.26	6531.67	755.30	105.70	336.47	13.34	35.01
973_florencite - 9	31600.81	181.62	10.58	7.10	4552.50	31518.00	49650.11	3397.79	8448.72	958.27	134.21	449.52	18.01	39.29

Element concentrations in ppm
$Eu/Eu^* = [(Eu_{CN}/(Sm_{CN}+Gd_{CN})/2)]$
$Y/Y^* = [(Y_{CN}/(Dy_{CN}+Ho_{CN})/2)]$
$Ce/Ce^* = [(Ce_{CN}/(La_{CN} \times Pr_{CN})^{0.5})]$
CN = chondrite normalised
Normalising values from Sun and McDonough (1989)

Appendix 5 Supplementary material for Mapping hydrothermal systems in IOCG deposits using apatite geochronology and geochemsitry: An example from Vulcan Cu-Au prospect

Appendix 5 Table A3: LA-ICP-MS Trace element florencite data from the Vulcan Prospect, collected in this study

Included Data

Sample	Ho	Er	Tm	Yb	Lu	Hf	Ta	W	Bi	Th	U	ΣREY	Eu/Eu*	Ce/Ce*	Y/Y*
973_florencite - 24	5.36	13.05	1.22	7.66	0.97	1.47	0.30	1.63	18.40	627.92	110.00	42576	0.40	1.15	0.87
973_florencite - 25	3.70	13.30	0.92	5.95	1.30	0.68	1.37	21.49	30.51	699.31	122.50	36331	0.35	1.11	0.78
973_florencite - 26	15.68	54.27	6.99	35.51	3.90	0.23	<0.015	0.45	10.78	639.00	54.89	96274	0.31	1.09	1.12
973_florencite - 27	16.75	67.08	8.37	44.66	4.93	0.24	0.09	0.42	13.47	750.04	64.39	119364	0.35	1.10	1.11
973_florencite - 28	18.92	62.68	8.78	42.78	5.25	0.06	0.02	<0.059	19.77	866.07	82.05	117438	0.35	1.10	1.05
973_florencite - 29	6.03	14.18	2.31	9.39	0.82	1.70	1.07	3.02	32.51	1420.09	135.06	92248	0.33	1.12	0.56
973_florencite - 3	12.50	34.44	4.44	18.54	2.42	0.80	<0.012	<0.059	47.46	889.02	186.94	96762	0.33	1.13	0.87
973_florencite - 31	10.25	25.32	2.74	16.24	1.91	0.74	0.58	1.72	40.94	1635.34	205.82	127424	0.34	1.04	0.70
973_florencite - 32	13.32	37.23	4.07	24.81	3.81	1.39	0.34	1.98	49.62	1597.81	260.12	131736	0.31	1.14	0.74
973_florencite - 33	10.12	23.32	2.67	14.18	1.59	0.81	0.21	1.47	42.59	1489.29	231.95	122109	0.35	1.11	0.63
973_florencite - 37	5.70	24.92	1.78	13.82	1.74	2.97	0.99	3.89	18.19	603.86	127.04	44235	0.34	1.08	0.73
973_florencite - 38	6.39	12.28	1.00	5.36	0.65	0.53	0.13	0.68	18.15	1342.60	98.02	115178	0.35	1.19	0.46
973_florencite - 39	3.14	9.32	0.45	7.16	1.05	3.73	0.77	10.52	23.87	807.00	191.53	29983	0.38	1.01	0.78
973_florencite - 4	13.99	46.56	5.03	27.67	2.76	0.57	<0.015	<0.074	44.62	1034.70	162.18	122982	0.34	1.13	0.89
973_florencite - 40	3.55	7.00	0.58	2.75	<0.149	0.62	1.10	16.04	19.11	750.76	113.39	34799	0.39	1.07	0.46
973_florencite - 43	2.43	9.75	0.84	4.47	0.57	2.13	1.33	23.78	21.38	544.96	93.25	29638	0.30	1.12	0.85
973_florencite - 44	3.45	6.61	0.50	5.17	0.34	3.25	0.41	12.99	19.31	570.53	166.14	25123	0.39	1.14	0.78
973_florencite - 46	11.50	27.65	3.35	11.11	1.49	0.61	0.08	0.66	42.42	2549.66	199.76	156642	0.31	1.11	0.68
973_florencite - 47	9.80	21.24	2.16	11.11	1.45	0.21	0.03	2.57	25.67	2930.09	151.80	135937	0.33	1.14	0.53
973_florencite - 48	3.53	10.83	1.53	5.95	0.80	2.57	0.41	11.96	18.06	398.05	91.67	29046	0.24	1.11	0.65
973_florencite - 49	8.36	18.39	1.62	7.17	0.81	0.09	0.09	2.56	34.18	2850.94	140.98	143376	0.34	1.10	0.54
973_florencite - 50	7.53	16.81	1.94	12.69	2.08	4.06	1.37	10.74	46.70	1490.73	228.32	75684	0.35	1.12	0.84
973_florencite - 52	2.07	5.20	0.35	3.07	0.22	0.76	0.04	0.99	8.73	904.09	62.17	38637	0.34	1.20	0.57
973_florencite - 53	7.17	17.66	1.68	9.86	1.52	0.53	0.09	1.41	39.12	3397.31	197.14	153595	0.33	1.11	0.54
973_florencite - 54	13.78	34.97	4.24	21.85	2.57	0.36	0.01	1.56	49.73	1809.04	251.77	166469	0.30	1.13	0.73
973_florencite - 55	3.30	8.00	1.07	7.21	0.13	0.43	<0.024	<0.107	8.87	502.59	51.51	39322	0.33	1.01	0.67
973_florencite - 56	9.07	24.21	2.95	17.11	2.18	0.08	0.05	1.19	39.12	1494.60	212.91	160543	0.32	1.11	0.58
973_florencite - 57	10.46	26.04	2.82	14.83	1.80	0.66	0.01	0.06	53.00	1534.75	239.66	150735	0.32	1.12	0.67
973_florencite - 58	6.31	14.46	1.34	6.93	1.83	<0.062	0.68	2.02	30.10	1268.92	124.62	84059	0.37	1.14	0.60
973_florencite - 6	4.37	10.47	0.92	4.68	0.41	1.02	0.10	6.29	15.52	387.44	82.30	81796	0.32	1.12	0.48
973_florencite - 60	3.91	7.85	1.28	5.43	0.61	2.84	1.53	17.00	25.06	611.93	130.71	36402	0.42	1.17	0.65
973_florencite - 61	6.08	12.45	0.84	4.20	0.49	<0.069	0.10	0.71	38.48	1619.59	92.79	144108	0.36	1.30	0.43
973_florencite - 7	5.75	9.21	1.38	6.09	0.54	0.27	0.08	6.13	27.98	465.59	92.34	88280	0.36	1.12	0.45
973_florencite - 8	4.69	8.96	0.93	5.61	0.29	0.81	0.11	3.80	13.09	363.06	75.55	74713	0.32	1.18	0.52
973_florencite - 9	6.59	12.26	1.37	4.70	1.40	0.32	<0.024	12.29	22.46	528.76	108.06	94822	0.31	1.16	0.54

Element concentrations in ppm
$Eu/Eu^* = [(Eu_{CN}/(Sm_{CN}+Gd_{CN})/2)]$
$Y/Y^* = [(Y_{CN}/(Dy_{CN}+Ho_{CN})/2)]$
$Ce/Ce^* = [(Ce_{CN}/(La_{CN} \times Pr_{CN})^{0.5})]$
CN = chondrite normalised
Normalising values from Sun and McDonough (1989)

Appendix 5 Supplementary material for Mapping hydrothermal systems in IOCG deposits using apatite geochronology and geochemsitry: An example from Vulcan Cu-Au prospect

Appendix 5 Table A3: LA-ICP-MS Trace element florencite data from the Vulcan Prospect, collected in this study

Rejected Data	Drill hole	Mineral	O	Na	Al	Si	P	Ca	Sc	Mn	Fe	Cu	As
801_florencite - 16	VUD 009 801	Florencite	285840	1034	318310	407502	12900	5699	34.84	41.95	68660.88	70.77	42.15
801_florencite - 19	VUD 009 801	Florencite	270115	1838	292563	445008	52422	15224	51.02	87.89	942129.03	26.18	377.93
801_florencite - 2	VUD 009 801	Florencite	285331	1294	317441	412704	13844	3783	23.59	42.75	145440.02	45.04	86.02
801_florencite - 27	VUD 009 801	Florencite	290245	979	325479	443622	4760	4699	20.43	58.57	188328.98	39.45	65.61
801_florencite - 29	VUD 009 801	Florencite	273905	1557	298595	303742	35357	11911	30.90	135.30	1176112.65	<14.103	319.49
801_florencite - 30	VUD 009 801	Florencite	275099	1931	300291	458110	39916	14150	29.78	121.75	1878242.88	<27.994	310.97
801_florencite - 4	VUD 009 801	Florencite	289608	1328	324447	400404	5653	2767	11.98	20.02	51597.61	104.06	45.58
825_florencite - 1	VUD 009 825	Florencite	131018	1188	86450	2224	69811	20512	2.28	102.27	5644.95	50.16	716.39
825_florencite - 15	VUD 009 825	Florencite	84146	459	24163	10341	14405	12684	1.20	52.00	3889.69	60.49	181.11
825_florencite - 24	VUD 009 825	Florencite	265881	1927632	285010	6296360	77809	764402	<37.797	606.25	<10657.788	<194.495	17306.73
825_florencite - 3	VUD 009 825	Florencite	288433	3022	322554	473154	14737	21306	20.40	109.82	60955.82	408.97	120.94
825_florencite - 34	VUD 009 825	Florencite	192288	3669	166346	7979	158023	126199	9.83	556.59	18910.71	79.42	1482.49
825_florencite - 7	VUD 009 825	Florencite	168474	2409	136143	6332	95062	33995	5.61	242.34	10309.30	70.62	1204.05
973_florencite - 21	VUD 009 973	Florencite	286525	1002	319408	483673	8128	2841	16.05	45.03	62870.80	122.94	56.70
973_florencite - 22	VUD 009 973	Florencite	286238	733	318990	361941	10333	3318	35.72	97.33	167045.19	156.79	47.02
973_florencite - 23	VUD 009 973	Florencite	283921	987	315189	372733	17488	4677	32.58	300.61	380063.68	231.27	77.12
973_florencite - 30	VUD 009 973	Florencite	286945	2980	320096	463861	15898	<2728.745	59.68	1014.05	2450709.77	205.94	271.49
973_florencite - 41	VUD 009 973	Florencite	286100	1109	318717	434256	10275	3551	29.31	593.21	753855.46	71.71	81.87
973_florencite - 42	VUD 009 973	Florencite	228257	2409	224344	146910	106258	25434	153.52	2504.63	3559239.63	739.63	737.65
973_florencite - 45	VUD 009 973	Florencite	280930	1225	310264	393676	24136	2971	43.89	1584.01	1200733.67	161.51	186.62

Element concentrations in ppm
$Eu/Eu^* = [(Eu_{CN}/(Sm_{CN}+Gd_{CN})/2)]$
$Y/Y^* = [(Y_{CN}/(Dy_{CN}+Ho_{CN})/2)]$
$Ce/Ce^* = [(Ce_{CN}/(La_{CN} \times Pr_{CN})^{0.5})]$
CN = chondrite normalised
Normalising values from Sun and McDonough (1989)

Appendix 5 Supplementary material for Mapping hydrothermal systems in IOCG deposits using apatite geochronology and geochemsitry: An example from Vulcan Cu-Au prospect

Appendix 5 Table A3: LA-ICP-MS Trace element florencite data from the Vulcan Prospect, collected in this study

Rejected Data	Sr	Y	Zr	Nb	Ba	La	Ce	Pr	Nd	Sm	Eu	Gd	Tb	Dy
801_florencite - 16	3298.12	11.56	3.60	6.36	390.18	4219.20	4600.87	481.89	2228.75	286.66	28.72	68.56	1.86	3.08
801_florencite - 19	17405.41	96.58	49.16	135.81	1662.58	8576.21	18108.74	1915.54	7153.24	722.09	93.23	229.85	8.26	20.12
801_florencite - 2	5718.55	26.82	12.52	24.49	396.69	1700.33	5887.36	921.94	1645.15	433.19	30.52	86.07	3.31	9.56
801_florencite - 27	1573.85	2.05	12.64	24.77	145.15	470.11	1391.76	110.30	336.42	53.55	7.83	21.96	0.72	1.10
801_florencite - 29	17448.58	38.10	39.35	340.98	823.46	7606.18	12776.32	1354.85	4936.99	737.67	79.47	165.40	5.85	12.50
801_florencite - 30	16523.52	44.23	52.82	1121.75	1102.18	5449.38	12723.20	1247.12	4300.43	538.52	68.61	153.54	6.55	20.94
801_florencite - 4	1860.03	7.81	8.88	2.49	205.10	1061.79	1825.60	177.88	553.94	98.23	16.20	21.35	1.03	4.38
825_florencite - 1	38243.94	186.96	22.26	0.05	273010.34	18107.65	44428.34	4667.88	14891.45	1352.51	118.60	393.53	17.98	60.50
825_florencite - 15	32718.41	27.60	5.93	0.02	461200.83	3149.71	7657.66	1007.30	3129.75	338.01	30.39	73.12	2.42	8.19
825_florencite - 24	35349.92	55.37	2628.77	1.20	4221.42	4778.78	14312.55	1545.43	3816.64	386.36	103.86	54.11	1.02	23.45
825_florencite - 3	3174.96	26.09	4.64	1.27	176.68	994.70	2510.54	249.41	805.82	87.08	7.26	24.57	3.71	3.13
825_florencite - 34	75159.85	816.10	249.05	0.15	1499.98	30972.29	79114.12	9272.50	26015.11	2634.43	244.62	753.39	49.21	214.27
825_florencite - 7	55408.07	460.03	101.82	0.07	118391.83	25202.67	60875.15	7240.28	23897.38	2253.47	205.56	599.46	32.28	124.51
973_florencite - 21	3627.91	32.17	31.79	1.32	507.07	3290.64	4906.16	377.83	955.74	121.79	12.04	57.92	3.04	9.24
973_florencite - 22	2912.10	36.47	22.56	6.72	908.38	4675.54	4740.92	281.65	742.84	78.75	12.02	27.57	3.03	5.44
973_florencite - 23	5122.12	71.60	30.46	22.36	1040.72	5040.21	7125.84	527.64	1154.78	160.03	25.99	79.19	2.92	7.19
973_florencite - 30	3106.17	61.25	77.95	118.80	624.56	2546.94	4340.05	277.60	882.61	84.69	10.76	52.09	3.16	7.67
973_florencite - 41	4135.15	30.91	35.80	21.10	517.29	3184.13	5260.19	360.63	1029.21	99.86	21.91	55.10	1.73	6.30
973_florencite - 42	38439.25	437.73	128.63	354.74	6573.59	38862.40	60752.25	5003.77	10987.13	1107.02	190.27	495.51	20.11	70.65
973_florencite - 45	7789.59	85.61	87.38	49.31	1096.72	6528.70	9772.46	882.18	1319.08	210.05	32.64	80.34	3.44	14.52

Element concentrations in ppm
$Eu/Eu^* = [(Eu_{CN}/(Sm_{CN}+Gd_{CN})/2)]$
$Y/Y^* = [(Y_{CN}/(Dy_{CN}+Ho_{CN})/2)]$
$Ce/Ce^* = [(Ce_{CN}/(La_{CN} \times Pr_{CN})^{0.5})]$
CN = chondrite normalised
Normalising values from Sun and McDonough (1989)

Appendix 5 Supplementary material for Mapping hydrothermal systems in IOCG deposits using apatite geochronology and geochemsitry: An example from Vulcan Cu-Au prospect

Appendix 5 Table A3: LA-ICP-MS Trace element florencite data from the Vulcan Prospect, collected in this study

Rejected Data	Ho	Er	Tm	Yb	Lu	Hf	Ta	W	Bi	Th	U
801_florencite - 16	1.20	2.58	0.09	0.85	0.20	<0.094	0.31	0.89	<0.349	170.02	8.27
801_florencite - 19	3.18	7.32	0.90	6.98	0.53	2.62	4.26	3.76	1.04	782.78	141.51
801_florencite - 2	0.91	2.72	<0.025	0.50	<0.064	1.70	0.24	1.08	<0.760	263.89	25.96
801_florencite - 27	0.27	0.23	0.16	0.39	<0.037	<0.084	0.26	0.34	<0.372	72.04	29.89
801_florencite - 29	1.35	4.41	0.71	2.29	0.33	1.48	5.74	9.34	1.32	857.71	115.56
801_florencite - 30	1.16	3.07	0.60	0.89	0.45	0.78	23.11	15.59	1.30	916.15	160.25
801_florencite - 4	0.35	1.03	0.16	<0.048	<0.038	1.72	<0.027	<0.154	<0.876	73.91	6.58
825_florencite - 1	10.06	20.45	2.92	18.61	1.33	0.23	<0.007	<0.036	7.04	6677.54	94.61
825_florencite - 15	1.80	1.57	0.31	5.27	0.38	0.23	<0.004	<0.021	0.54	2242.63	7.11
825_florencite - 24	4.99	5.94	0.50	53.71	1.29	60.59	<0.277	<1.411	<5.408	1139.76	65.61
825_florencite - 3	0.86	2.58	0.72	1.89	0.55	0.89	<0.028	0.33	6.41	827.00	13.23
825_florencite - 34	43.51	104.43	13.47	93.26	11.44	3.71	0.02	0.30	7.95	32921.24	526.75
825_florencite - 7	20.53	53.30	7.94	57.09	8.08	0.93	0.01	0.05	7.94	19671.41	320.13
973_florencite - 21	0.77	3.61	0.23	2.23	0.11	1.95	0.07	1.03	1.84	67.63	13.90
973_florencite - 22	0.66	3.49	0.14	2.17	0.14	1.62	0.31	2.11	7.49	147.99	54.98
973_florencite - 23	2.15	3.64	0.42	5.93	0.50	0.72	1.03	8.90	11.18	219.96	93.23
973_florencite - 30	1.70	6.69	1.96	4.37	0.65	6.05	7.21	31.94	26.20	149.96	276.53
973_florencite - 41	0.70	1.91	0.09	1.43	<0.063	0.93	0.49	17.92	10.15	227.09	77.21
973_florencite - 42	13.38	37.22	2.83	14.74	1.86	3.70	4.92	157.79	77.78	2159.17	662.95
973_florencite - 45	2.01	9.48	1.52	5.84	0.52	3.45	1.65	42.30	20.70	422.89	159.16

Element concentrations in ppm
$Eu/Eu^* = [(Eu_{CN}/(Sm_{CN}+Gd_{CN})/2)]$
$Y/Y^* = [(Y_{CN}/(Dy_{CN}+Ho_{CN})/2)]$
$Ce/Ce^* = [(Ce_{CN}/(La_{CN} \times Pr_{CN})^{0.5})]$
CN = chondrite normalised
Normalising values from Sun and McDonough (1989)

Appendix 5 Supplementary material for Mapping hydrothermal systems in IOCG deposits using apatite geochronology and geochemsitry: An example from Vulcan Cu-Au prospect

Appendix 5 Table A4: Magnetite and hematite LA-ICP-MS trace element data collected at Vulcan in this study

Included Data

Sample	Drill hole	Mineral	Comment
1183 G1 - 1	VUD 007 1183	Magnetite	High V, Al and Mg
1183 G1 - 3	VUD 007 1183	Magnetite	High V and Al.
1183 G12 - 1	VUD 007 1183	Magnetite	High Al and V.
1183 G13 - 1	VUD 007 1183	Magnetite	High Al, V and Mg, Ti inclusions
1183 G15 - 3	VUD 007 1183	Magnetite	Mg Mn inclusions
1183 G19 - 3	VUD 007 1183	Magnetite	High Al and V. low Mg and P
1183 G21 - 1	VUD 007 1183	Magnetite	High Al and V. low Mg and P
1183 G23 - 2	VUD 007 1183	Magnetite	High Mg, Al, V.
1183 G24 - 1	VUD 007 1183	Magnetite	High Al an Mg.
1183 G16 - 2	VUD 007 1183	Magnetite	REE BDL.Mg inclusions
1183 G17 - 1	VUD 007 1183	Magnetite	Mg Si inclusions. REE BDL.
1183 G2 - 1	VUD 007 1183	Magnetite	High V and Al. High Mg and P. REE BDL
1183 G2 - 2	VUD 007 1183	Magnetite	High V and Al. High Mg and P. REE BDL
1183 G5 - 1	VUD 007 1183	Magnetite	High Al and V. low Mg and P. REE BDL.
1183 G6 - 1	VUD 007 1183	Magnetite	High Al and V. low Mg and P. REE BDL.
1183 G8 - 1	VUD 007 1183	Magnetite	High V and Al. High Mg and P. REE BDL
1183 G9 - 1	VUD 007 1183	Magnetite	High V and Al. High Mg and P. REE BDL
1183 G10 - 1	VUD 007 1183	Magnetite	High Al and V. low Mg and P. REE BDL.
1183 G11 - 2	VUD 007 1183	Magnetite	High V and Al. High Mg and P. REE BDL
1183 G14 - 1	VUD 007 1183	Magnetite	High Al and V. low Mg and P. REE BDL.
1183 G15 - 2	VUD 007 1183	Magnetite	High Al and V. low Mg and P. REE BDL.
1183 G16 - 1	VUD 007 1183	Magnetite	Mg Mn inclusions. REE BDL.
1183 G18 - 2	VUD 007 1183	Magnetite	High Al and V. low Mg and P. REE BDL.
1183 G19 - 1	VUD 007 1183	Magnetite	High Al and V. low Mg and P. REE BDL.
1183 G19 - 2	VUD 007 1183	Magnetite	High Al and V. low Mg and P. REE BDL.
1183 G20 - 1	VUD 007 1183	Magnetite	High Al and V. low Mg and P. REE BDL.
1183 G22 - 1	VUD 007 1183	Magnetite	High Al and V. low Mg and P. REE BDL.
1183 G23 - 3	VUD 007 1183	Magnetite	High Al and V. low Mg and P. REE BDL.
1192 Img 5 G6 - 3	VUD 007 1192	Magnetite	Mg inclusions. High Al and V.
1192 Img 6 G1 - 1	VUD 007 1192	Magnetite	High Al, V and Mg. High P and Ce. HREE BDL.
1192 no image bottom G4 - 2	VUD 007 1192	Magnetite	High Al, V, Mg, Ce and P.
1192 Img 4 G2 - 2	VUD 007 1192	Magnetite	High Al, V, Mg. High P and Ce.
1192 no image bottom R G1 - 1	VUD 007 1192	Magnetite	Mg Al inclusions. High V and Al. Mg and P
1192mag G1 - 3	VUD 007 1192	Magnetite	High Mg, Al, and V. High Ce
1192mag G6 - 4	VUD 007 1192	Magnetite	High Al, V.
1192mag G6 - 10	VUD 007 1192	Magnetite	Al Mg inclusions
1192 Img 3 G1 - 2	VUD 007 1192	Magnetite	High Al, V and Mg. High P and Ce.
1192mag G1 - 4	VUD 007 1192	Magnetite	Al inclusion. High Mg, Al, and V. High Ce and P
1192mag G6 - 7	VUD 007 1192	Magnetite	High Al, V Mg.
1192 Img 4 G2 - 1	VUD 007 1192	Magnetite	High Al, V, Mg.
1192 Img 5 G6 - 2	VUD 007 1192	Magnetite	High Al, Mg and V.
1192mag G6 - 6	VUD 007 1192	Magnetite	High Al, V Mg.
1192 no image bottom R G1 - 5	VUD 007 1192	Magnetite	High V, Al and Mg
1192mag G6 - 5	VUD 007 1192	Magnetite	High Al, V.
1192 Img 6 G1 - 3	VUD 007 1192	Magnetite	High Al, Mg and V.
1192mag G6 - 9	VUD 007 1192	Magnetite	High Al, V Mg.
1192 no image bottom R G1 - 6	VUD 007 1192	Magnetite	High V and Al.
1192mag G1 - 2	VUD 007 1192	Magnetite	High Mg, Al, and V. High Ce
1192 Img 5 G3 - 1	VUD 007 1192	Magnetite	High Al and Mg
1192 no image bottom R G1 - 7	VUD 007 1192	Magnetite	High V, Al and Mg
1192mag G1 - 1	VUD 007 1192	Magnetite	High Mg, Al, V and Ce
1192 no image bottom G7 - 2	VUD 007 1192	Magnetite	High Ag and Al.
1192 no image botton G1 - 6	VUD 007 1192	Magnetite	High Al, Mg and V. P and Ce.
1192 no image botton G1 - 5	VUD 007 1192	Magnetite	High Al, Mg and V. P and Ce.
1192 no image botton G1 - 1	VUD 007 1192	Magnetite	High Mg, Al, V.
1192 no image botton G1 - 2	VUD 007 1192	Magnetite	Ti Nb inclusions. High Mg, Al, V
1192 no image botton G1 - 8	VUD 007 1192	Magnetite	Ti Nb inclusions. High Mg, Al, V
1192 no image botton G1 - 7	VUD 007 1192	Magnetite	High Mg, Al and V. P and Ce
1192mag G4 - 2	VUD 007 1192	Magnetite	High Mg Al
1192 no image botton G1 - 9	VUD 007 1192	Magnetite	Ti Nb inclusions. High V, Al, Mg.
1192 no image bottom G7 - 1	VUD 007 1192	Magnetite	Ce inclusions. High Mg and Al.
1192 no image botton G1 - 4	VUD 007 1192	Magnetite	High Mg, Al and V.
1192mag G4 - 1	VUD 007 1192	Magnetite	High Mg Al
1192 no image botton G1 - 3	VUD 007 1192	Magnetite	High Al, Mg and V.
1192 no image bottom R G1 - 4	VUD 007 1192	Magnetite	High Al, V and Mg.
1192 Img 5 G3 - 2	VUD 007 1192	Magnetite	High Al and Mg
1192 Img 5 G3 - 3	VUD 007 1192	Magnetite	High Al and Mg
1192 Img 5 G5 - 1	VUD 007 1192	Magnetite	High vV and Al. Mn inclusion
1192mag G6 - 3	VUD 007 1192	Magnetite	High Al, V. REE BDL.
1192 no image bottom G5 - 1	VUD 007 1192	Magnetite	High V and Al. low Mg and P
1192mag G6 - 8	VUD 007 1192	Magnetite	High Al, V. REE BDL.

Element concentrations in ppm
BDL: below detection limit
NA: no analysis
$Eu/Eu^* = [(Eu_{CN}/(Sm_{CN}+Gd_{CN})/2)]$
$Y/Y^* = [(Y_{CN}/(Dy_{CN}+Ho_{CN})/2)]$
$Ce/Ce^* = [(Ce_{CN}/(La_{CN} \times Pr_{CN})^{0.5})]$
CN = chondrite normalised
Normalising values from Sun and McDonough (1989)

Appendix 5 Supplementary material for Mapping hydrothermal systems in IOCG deposits using apatite geochronology and geochemsitry: An example from Vulcan Cu-Au prospect

Appendix 5 Table A4: Magnetite and hematite LA-ICP-MS trace element data collected at Vulcan in this study

Included Data

Sample	Mg	Al	Si	P	Ca	Ti	V	Mn	Fe	Co	Ni	Cu	Zn	As
1183 G1 - 1	166	352	2069	<11.424	90	131	275	11	720000	3.12	286.46	<0.173	1.66	0.30
1183 G1 - 3	83	297	1250	<12.110	72	50	270	9	720000	2.88	278.61	0.41	2.58	0.38
1183 G12 - 1	65	288	2109	<10.035	42	50	213	9	720000	5.50	219.22	1.18	2.32	0.56
1183 G13 - 1	146	336	2504	<11.397	83	219	250	16	720000	3.91	198.59	0.56	4.70	0.80
1183 G15 - 3	750	302	341	<15.200	<55.368	79	114	180	720000	3.73	154.40	17.40	4.54	7.65
1183 G19 - 3	63	176	637	<11.408	121	35	567	8	720000	2.97	302.58	0.62	1.40	1.58
1183 G21 - 1	74	326	762	<11.930	<44.775	68	100	9	720000	7.41	121.91	<0.221	2.63	0.87
1183 G23 - 2	309	226	4068	<13.136	601	61	118	16	720000	5.26	261.04	0.98	2.72	0.49
1183 G24 - 1	1021	873	7315	<16.895	1014	85	112	14	720000	5.85	268.03	<0.299	3.82	0.82
1183 G16 - 2	3	356	184	<13.345	<47.210	51	233	9	720000	2.79	325.40	<0.230	3.49	0.91
1183 G17 - 1	4	184	160	<12.934	<52.199	28	169	8	720000	3.21	147.85	0.27	1.48	0.28
1183 G2 - 1	2	314	169	<11.687	<42.427	45	395	9	720000	3.17	270.28	0.25	1.80	0.58
1183 G2 - 2	4	316	152	<11.283	<40.780	36	412	8	720000	1.83	281.69	<0.225	0.42	0.24
1183 G5 - 1	9	119	233	<13.149	<42.353	36	138	6	720000	2.87	156.46	0.55	0.67	3.89
1183 G6 - 1	6	536	176	<11.744	<46.960	65	109	9	720000	2.72	173.41	<0.208	0.37	0.27
1183 G8 - 1	3	176	174	<11.199	<34.756	32	187	8	720000	2.21	239.85	<0.227	1.08	<0.209
1183 G9 - 1	2	230	181	<11.136	<41.288	53	109	8	720000	2.87	248.39	<0.215	1.04	0.44
1183 G10 - 1	2	133	133	<10.295	<43.619	36	112	8	720000	3.10	255.81	0.39	0.92	0.49
1183 G11 - 2	2	162	130	13	<42.574	13	11	9	720000	2.87	119.58	<0.191	1.04	0.31
1183 G14 - 1	2	75	200	<12.288	<54.792	56	158	6	720000	3.40	319.23	0.30	1.47	4.99
1183 G15 - 2	8	406	174	<11.280	<43.066	28	158	10	720000	4.00	130.51	0.27	2.60	0.67
1183 G16 - 1	3	357	160	<14.065	<56.296	46	234	9	720000	2.42	312.81	<0.222	0.44	0.25
1183 G18 - 2	2	189	198	<12.580	<42.920	29	131	8	720000	1.99	198.42	<0.185	1.22	0.34
1183 G19 - 1	30	215	583	<16.470	<62.352	38	565	8	720000	1.04	248.41	0.24	<0.274	0.44
1183 G19 - 2	24	193	637	<12.930	<42.528	35	584	9	720000	1.33	269.14	<0.243	1.06	0.41
1183 G20 - 1	3	273	186	<12.423	<45.187	49	151	9	720000	3.13	173.15	<0.210	1.73	0.29
1183 G22 - 1	4	203	189	<13.779	<49.894	144	249	8	720000	3.22	132.69	2.84	1.56	2.75
1183 G23 - 3	5	283	179	<12.198	<46.418	68	108	8	720000	3.80	249.01	0.40	3.79	1.43
1192 Img 5 G6 - 3	35	142	311	<10.475	<45.251	28	77	7	720000	3.31	158.06	0.56	2.13	2.55
1192 Img 6 G1 - 1	43	334	617	<14.128	90	28	52	9	720000	6.55	381.27	5.28	2.77	1.21
1192 no image bottom G4 - 2	165	286	1864	11	186	83	143	6	720000	16.83	181.41	<0.175	<0.224	0.34
1192 Img 4 G2 - 2	95	231	529	<12.272	168	39	131	8	720000	3.31	175.93	<0.212	1.65	0.45
1192 no image bottom R G1 - 1	191	640	1096	<13.066	69	34	628	13	720000	10.80	180.81	0.30	2.94	0.69
1192mag G1 - 3	203	385	2285	<11.630	155	71	186	8	720000	8.40	196.11	0.22	<0.193	<0.213
1192mag G6 - 4	57	632	986	<11.615	<38.414	63	116	1	720000	13.80	136.06	<0.189	<0.179	0.31
1192mag G6 - 10	830	1673	2646	14	74	38	117	10	720000	7.15	407.09	<0.199	4.04	0.58
1192 Img 3 G1 - 2	120	422	1468	<11.534	267	53	133	7	720000	10.31	190.86	<0.210	1.49	0.48
1192mag G1 - 4	249	635	2109	<9.494	387	61	188	10	720000	9.74	200.28	0.26	0.55	0.34
1192mag G6 - 7	114	543	1702	<11.467	130	31	111	5	720000	11.90	294.62	0.85	0.50	1.04
1192 Img 4 G2 - 1	103	322	824	<11.297	148	43	129	7	720000	3.57	169.89	0.24	3.10	2.60
1192 Img 5 G6 - 2	42	217	533	<10.823	104	38	78	7	720000	2.39	150.26	<0.180	0.28	0.30
1192mag G6 - 6	162	631	1471	<10.946	125	91	123	3	720000	14.00	139.62	0.18	0.20	0.29
1192 no image bottom R G1 - 5	104	484	2411	17	167	124	639	7	720000	19.63	189.20	<0.184	<0.257	0.39
1192mag G6 - 5	99	637	1855	<15.073	70	80	122	2	720000	14.27	128.52	<0.220	0.46	<0.219
1192 Img 6 G1 - 3	73	457	1008	<12.102	167	53	48	9	720000	2.84	105.11	<0.196	0.86	0.37
1192mag G6 - 9	138	722	1613	<11.557	112	67	120	5	720000	10.07	132.97	0.25	0.22	0.30
1192 no image bottom R G1 - 6	100	401	2957	16	97	54	610	6	720000	19.83	217.65	<0.190	0.38	0.38
1192mag G1 - 2	465	416	3228	16	341	97	192	6	720000	10.14	209.70	<0.174	<0.186	0.41
1192 Img 5 G3 - 1	192	184	1725	<13.016	165	14	6	11	720000	3.81	57.51	0.59	2.38	2.68
1192 no image bottom R G1 - 7	332	462	4874	<13.264	621	56	651	10	720000	6.39	203.90	0.47	1.02	0.49
1192mag G1 - 1	1142	505	5274	12	862	100	195	10	720000	11.60	219.51	0.41	<0.217	0.49
1192 no image bottom G7 - 2	387	147	2740	<10.783	177	1	4	18	720000	5.23	30.73	<0.193	1.66	0.45
1192 no image botton G1 - 6	476	450	3603	<11.550	233	150	214	11	720000	6.98	153.85	<0.208	0.93	0.70
1192 no image botton G1 - 5	464	457	3683	<9.826	230	206	214	11	720000	11.64	157.60	<0.198	1.52	0.64
1192 no image botton G1 - 1	551	458	3213	<14.284	183	247	219	16	720000	9.54	153.44	<0.288	4.34	0.60
1192 no image botton G1 - 2	579	463	3681	<10.631	316	241	200	11	720000	13.11	145.36	<0.193	0.49	0.37
1192 no image botton G1 - 8	606	443	3815	<12.371	270	241	200	13	720000	10.08	150.20	<0.196	3.40	0.67
1192 no image botton G1 - 7	657	463	3629	<12.814	326	104	211	10	720000	14.03	157.45	<0.191	<0.260	0.24
1192mag G4 - 2	370	129	3707	<10.589	256	<0.144	2	12	720000	3.47	16.29	<0.149	0.84	0.57
1192 no image botton G1 - 9	794	553	4444	<10.557	539	277	211	16	720000	8.49	158.14	<0.223	0.80	0.56
1192 no image bottom G7 - 1	585	163	3729	<12.002	313	1	4	21	720000	4.35	29.10	<0.187	1.40	0.34
1192 no image botton G1 - 4	761	572	4787	<10.894	640	353	207	18	720000	11.40	152.53	<0.255	3.37	2.25
1192mag G4 - 1	349	142	3511	<9.921	563	0	2	11	720000	3.44	16.08	<0.161	1.36	1.12
1192 no image botton G1 - 3	1304	1077	5005	<12.199	711	228	214	17	720000	7.85	153.91	0.33	4.24	0.78
1192 no image bottom R G1 - 4	710	1193	6732	<13.143	1556	95	626	12	720000	7.85	184.44	<0.231	0.87	0.40
1192 Img 5 G3 - 2	476	328	4768	14	355	6	5	17	720000	4.24	51.48	<0.226	2.06	0.65
1192 Img 5 G3 - 3	437	411	5489	13	439	17	7	22	720000	3.90	62.52	0.28	2.09	1.17
1192 Img 5 G5 - 1	4	228	223	<11.726	<41.257	47	318	11	720000	5.06	248.82	<0.186	1.38	<0.259
1192mag G6 - 3	2	612	184	<10.980	<35.736	64	114	2	720000	13.01	128.77	<0.194	0.32	<0.199
1192 no image bottom G5 - 1	3	370	210	12	<44.283	48	122	7	720000	2.72	133.43	<0.203	<0.217	0.42
1192mag G6 - 8	5	600	214	<14.682	<41.150	46	122	6	720000	12.04	135.49	<0.248	<0.211	<0.220

Element concentrations in ppm
BDL: below detection limit
NA: no analysis
$Eu/Eu^* = [(Eu_{CN}/(Sm_{CN}+Gd_{CN})/2)]$
$Y/Y^* = [(Y_{CN}/(Dy_{CN}+Ho_{CN})/2)]$
$Ce/Ce^* = [(Ce_{CN}/(La_{CN} \times Pr_{CN})^{0.5})]$
CN = chondrite normalised
Normalising values from Sun and McDonough (1989)

Appendix 5 Table A4: Magnetite and hematite LA-ICP-MS trace element data collected at Vulcan in this study

Included Data

Sample	Sr	Y	Zr	Nb	Mo	Sn	Ba	La	Ce	Pr	Nd	Sm	Eu	Gd
1183 G1 - 1	0.08	0.77	0.01	0.36	<0.028	0.22	0.17	0.25	1.09	0.14	0.64	0.14	0.02	0.17
1183 G1 - 3	0.13	0.27	<0.005	0.10	<0.058	0.13	0.07	0.13	0.77	0.08	0.47	0.05	0.01	0.06
1183 G12 - 1	0.05	0.50	0.08	0.08	0.07	0.27	<0.013	0.04	0.47	0.03	0.17	0.04	0.01	0.18
1183 G13 - 1	0.11	0.78	0.02	1.46	<0.034	0.42	0.09	0.04	0.61	0.05	0.12	0.12	0.01	0.07
1183 G15 - 3	0.22	0.06	0.05	0.52	0.57	0.15	0.11	0.01	0.08	0.01	0.05	0.01	0.01	<0.022
1183 G19 - 3	0.20	0.12	0.02	0.11	0.07	0.10	0.24	0.07	0.22	0.02	0.10	0.01	0.01	<0.011
1183 G21 - 1	0.08	0.17	0.01	0.05	0.03	0.14	0.12	0.22	0.82	0.07	0.42	0.11	0.01	0.08
1183 G23 - 2	0.25	0.60	0.04	1.56	0.06	0.21	0.13	0.45	3.81	0.24	1.40	0.32	0.03	0.21
1183 G24 - 1	1.71	3.22	0.13	3.28	0.04	0.48	0.38	1.17	4.09	0.52	2.02	0.52	0.04	0.52
1183 G16 - 2	0.03	0.01	<0.009	0.04	<0.021	0.13	0.08	0.00	0.02	0.00	0.01	<0.011	0.01	<0.022
1183 G17 - 1	<0.004	<0.003	<0.003	0.00	<0.026	0.08	<0.016	<0.002	0.01	0.00	<0.002	<0.008	<0.003	<0.033
1183 G2 - 1	<0.011	0.00	0.01	0.42	0.09	0.15	<0.013	<0.002	0.01	<0.002	0.00	<0.007	<0.003	<0.015
1183 G2 - 2	<0.007	0.01	0.00	<0.001	<0.034	0.11	<0.013	0.01	0.02	<0.002	<0.006	<0.007	<0.003	<0.016
1183 G5 - 1	0.04	0.02	0.04	0.48	0.06	0.08	0.09	0.03	0.10	0.01	0.02	<0.020	<0.003	<0.016
1183 G6 - 1	0.01	0.00	<0.009	<0.001	0.04	0.13	<0.013	0.00	<0.002	0.00	0.00	<0.007	<0.003	0.01
1183 G8 - 1	0.01	<0.002	0.01	0.02	0.03	0.05	0.04	0.01	0.01	0.00	<0.006	0.02	<0.003	<0.027
1183 G9 - 1	0.05	0.00	<0.008	<0.001	<0.032	0.15	0.12	<0.002	0.00	<0.001	0.01	0.01	<0.003	<0.010
1183 G10 - 1	<0.014	0.00	<0.002	0.00	0.02	0.09	0.07	<0.002	0.00	<0.000	0.00	<0.017	<0.003	<0.006
1183 G11 - 2	<0.007	<0.002	<0.006	0.00	<0.041	0.08	<0.012	<0.001	<0.001	<0.000	0.00	<0.009	<0.003	<0.019
1183 G14 - 1	0.06	0.01	0.10	1.18	0.86	0.13	0.11	0.07	0.09	0.01	<0.008	<0.022	<0.003	<0.019
1183 G15 - 2	1.04	0.01	<0.004	0.05	0.15	0.09	0.10	0.04	0.06	0.00	0.06	<0.004	0.01	<0.029
1183 G16 - 1	<0.006	<0.003	<0.009	0.01	<0.018	0.12	<0.018	<0.002	<0.002	0.00	<0.017	0.04	<0.004	<0.012
1183 G18 - 2	<0.009	0.00	<0.002	0.00	<0.035	0.07	0.06	0.04	0.05	0.00	0.02	<0.005	0.01	<0.017
1183 G19 - 1	0.06	0.10	0.00	0.00	<0.025	0.09	0.14	0.07	0.25	0.03	0.06	<0.010	<0.004	<0.017
1183 G19 - 2	<0.007	0.03	0.04	<0.001	0.03	0.09	0.06	0.01	0.05	0.00	0.02	<0.005	<0.003	<0.014
1183 G20 - 1	0.02	<0.002	0.02	<0.002	<0.016	0.11	<0.014	0.01	0.02	0.00	<0.012	<0.008	<0.003	0.01
1183 G22 - 1	0.03	0.03	0.20	14.37	0.21	1.66	0.02	0.03	0.09	<0.002	0.04	<0.003	<0.004	0.03
1183 G23 - 3	0.04	0.01	0.01	0.02	<0.017	0.17	0.02	0.11	0.12	0.00	0.03	<0.020	<0.003	<0.021
1192 Img 5 G6 - 3	0.32	0.04	0.05	0.51	0.21	0.15	0.18	0.07	0.17	0.02	0.06	0.04	0.00	0.02
1192 Img 6 G1 - 1	0.15	0.18	0.02	0.25	<0.035	0.23	0.09	0.31	1.00	0.07	0.33	0.07	0.02	0.08
1192 no image bottom G4 - 2	0.02	0.33	0.04	0.05	<0.029	0.17	<0.013	0.43	3.07	0.22	0.87	0.10	0.01	0.11
1192 Img 4 G2 - 2	0.05	0.19	0.03	0.02	0.04	0.20	0.06	0.43	1.15	0.10	0.41	0.04	0.00	0.06
1192 no image bottom R G1 - 1	0.09	0.18	<0.003	0.04	<0.049	0.14	0.14	0.47	1.31	0.13	0.54	0.09	<0.003	0.05
1192mag G1 - 3	0.32	0.20	0.01	0.18	0.07	0.21	0.10	0.50	2.12	0.19	0.72	0.15	0.01	0.07
1192mag G6 - 4	0.02	0.25	0.01	0.04	<0.185	0.21	<0.013	0.09	0.58	0.05	0.19	0.09	0.01	0.03
1192mag G6 - 10	0.13	0.30	0.01	0.03	0.04	0.15	0.07	0.16	1.36	0.11	0.49	0.07	0.02	0.07
1192 Img 3 G1 - 2	0.11	0.37	<0.005	0.07	0.07	0.26	0.22	0.50	1.66	0.22	0.56	0.11	0.02	0.13
1192mag G1 - 4	0.45	0.28	0.01	0.12	0.03	0.30	0.11	0.61	2.46	0.21	0.97	0.17	0.02	0.11
1192mag G6 - 7	0.37	0.37	0.26	0.06	0.04	0.14	0.40	0.27	1.23	0.11	0.48	0.13	0.02	0.07
1192 Img 4 G2 - 1	0.21	0.22	0.02	0.13	0.48	0.16	0.13	0.12	0.93	0.07	0.28	0.12	0.00	0.06
1192 Img 5 G6 - 2	0.09	0.14	0.01	0.15	<0.027	0.18	0.02	0.04	0.37	0.03	0.20	<0.016	<0.003	0.05
1192mag G6 - 6	0.02	0.43	0.02	0.05	0.01	0.24	<0.013	0.08	0.69	0.06	0.21	0.11	0.02	0.11
1192 no image bottom R G1 - 5	0.18	0.72	0.01	0.04	<0.056	0.33	0.13	0.10	1.34	0.10	0.43	0.14	0.02	0.13
1192mag G6 - 5	0.02	0.51	0.02	0.13	0.02	0.24	<0.016	0.02	0.45	0.02	0.17	0.10	0.02	0.13
1192 Img 6 G1 - 3	0.11	0.39	0.04	0.47	<0.033	0.31	0.06	0.07	0.70	0.03	0.31	0.06	0.01	0.07
1192mag G6 - 9	0.04	0.66	0.01	0.11	<0.022	0.22	0.03	0.08	0.78	0.05	0.25	0.13	0.02	0.13
1192 no image bottom R G1 - 6	0.09	0.69	0.01	0.04	<0.019	0.29	0.07	0.15	1.96	0.14	0.60	0.17	0.03	0.10
1192mag G1 - 2	0.23	0.49	0.02	0.52	<0.019	0.22	0.07	0.64	3.29	0.35	1.38	0.26	0.03	0.33
1192 Img 5 G3 - 1	0.12	1.10	0.19	1.49	0.21	0.37	0.24	0.29	1.41	0.14	0.72	0.20	0.01	0.13
1192 no image bottom R G1 - 7	0.51	1.33	0.03	0.18	<0.030	0.38	0.14	0.33	3.01	0.20	1.07	0.23	0.04	0.26
1192mag G1 - 1	0.68	0.92	0.03	0.80	<0.024	0.32	0.21	1.58	7.36	0.64	2.77	0.40	0.03	0.31
1192 no image bottom G7 - 2	0.16	1.50	0.13	2.31	0.05	0.48	0.06	0.22	0.80	0.11	0.52	0.06	0.01	0.11
1192 no image botton G1 - 6	0.39	1.84	0.07	1.80	<0.054	0.49	0.15	0.39	1.70	0.23	1.14	0.19	0.02	0.13
1192 no image botton G1 - 5	0.25	1.63	0.05	2.20	<0.040	0.62	0.08	0.39	1.50	0.17	0.80	0.21	0.02	0.18
1192 no image botton G1 - 1	0.26	1.84	0.06	2.57	0.03	0.76	0.13	0.37	1.69	0.18	0.78	0.29	0.02	0.19
1192 no image botton G1 - 2	0.30	1.82	0.09	3.85	<0.020	0.88	0.15	0.45	2.04	0.27	1.05	0.19	0.04	0.17
1192 no image botton G1 - 8	0.18	1.65	0.09	3.03	0.04	0.71	0.11	0.40	1.40	0.15	0.85	0.18	0.04	0.22
1192 no image botton G1 - 7	0.21	1.93	0.09	1.38	0.06	0.55	0.07	0.38	1.55	0.20	0.90	0.11	0.02	0.17
1192mag G4 - 2	0.21	1.73	0.13	2.75	<0.027	0.35	0.18	0.28	1.23	0.16	0.74	0.12	0.02	0.21
1192 no image botton G1 - 9	0.42	2.21	0.20	4.58	0.06	0.79	0.16	0.58	2.29	0.30	1.38	0.29	0.03	0.29
1192 no image bottom G7 - 1	0.31	2.22	0.24	3.12	<0.024	0.66	0.36	0.47	5.43	0.30	1.06	0.22	0.03	0.19
1192 no image botton G1 - 4	0.54	2.06	0.51	4.75	0.04	1.20	0.49	0.85	2.95	0.37	1.31	0.35	0.05	0.21
1192mag G4 - 1	0.42	2.03	0.27	4.02	0.05	0.48	0.45	0.94	2.34	0.34	1.14	0.26	0.04	0.25
1192 no image botton G1 - 3	0.52	2.91	0.18	5.62	0.07	0.96	0.25	1.10	3.82	0.52	2.06	0.40	0.04	0.30
1192 no image bottom R G1 - 4	2.42	2.85	0.07	0.39	<0.035	0.64	2.14	0.96	6.93	0.64	2.88	0.65	0.14	0.72
1192 Img 5 G3 - 2	0.30	3.46	0.27	3.46	<0.019	0.56	0.19	0.59	2.57	0.31	1.70	0.35	0.03	0.35
1192 Img 5 G3 - 3	0.35	3.75	0.55	3.83	0.03	0.58	0.70	0.50	2.56	0.25	1.23	0.34	0.06	0.42
1192 Img 5 G5 - 1	<0.010	<0.002	0.02	<0.001	0.04	0.06	0.04	<0.002	<0.002	<0.002	<0.010	<0.008	<0.003	0.02
1192mag G6 - 3	<0.012	0.01	<0.004	<0.001	<0.035	0.17	0.04	<0.002	0.01	0.00	<0.006	0.01	<0.003	<0.012
1192 no image bottom G5 - 1	0.01	0.01	0.01	<0.001	<0.031	0.14	<0.014	0.08	0.11	0.02	0.12	<0.019	<0.003	0.01
1192mag G6 - 8	<0.013	0.10	0.02	<0.002	<0.017	0.13	<0.016	0.02	0.01	0.00	0.01	0.01	0.01	0.03

Element concentrations in ppm
BDL: below detection limit
NA: no analysis
$Eu/Eu^* = [(Eu_{CN}/(Sm_{CN}+Gd_{CN})/2)]$
$Y/Y^* = [(Y_{CN}/(Dy_{CN}+Ho_{CN})/2)]$
$Ce/Ce^* = [(Ce_{CN}/(La_{CN} \times Pr_{CN})^{0.5})]$
CN = chondrite normalised
Normalising values from Sun and McDonough (1989)

Appendix 5 Supplementary material for Mapping hydrothermal systems in IOCG deposits using apatite geochronology and geochemsitry: An example from Vulcan Cu-Au prospect

Appendix 5 Table A4: Magnetite and hematite LA-ICP-MS trace element data collected at Vulcan in this study

Included Data

Sample	Tb	Dy	Ho	Er	Tm	Yb	Lu	Hf	Ta	W	ΣREY	Eu/Eu*	Y/Y*	Ce/Ce*
1183 G1 - 1	0.03	0.20	0.03	0.07	0.01	0.04	0.01	<0.005	0.09	0.05	3.62	0.43	0.81	1.41
1183 G1 - 3	0.02	0.08	0.01	0.02	<0.002	0.02	<0.002	<0.006	0.06	0.01	1.97	0.50	0.86	1.87
1183 G12 - 1	0.02	0.08	0.02	0.06	0.00	0.10	0.00	0.01	0.05	0.19	1.70	0.31	1.11	3.49
1183 G13 - 1	0.03	0.18	0.03	0.09	0.01	0.04	0.01	<0.006	0.09	0.08	2.18	0.43	0.83	3.59
1183 G15 - 3	<0.002	0.03	<0.002	0.01	<0.002	<0.018	<0.002	<0.007	0.01	0.03	0.27			2.24
1183 G19 - 3	0.01	0.01	0.00	0.02	0.00	0.03	0.00	0.01	0.02	<0.006	0.62		2.24	1.47
1183 G21 - 1	0.01	0.02	0.00	0.02	0.00	0.02	<0.002	<0.005	0.04	0.08	1.96	0.32	1.67	1.55
1183 G23 - 2	0.02	0.14	0.03	0.05	0.01	0.07	0.01	<0.005	0.09	0.30	7.37	0.41	0.73	2.80
1183 G24 - 1	0.08	0.64	0.10	0.42	0.03	0.17	0.04	<0.008	0.27	0.06	13.58	0.23	0.96	1.26
1183 G16 - 2	<0.002	<0.006	<0.002	0.01	0.00	<0.012	<0.002	<0.007	<0.002	<0.008	0.059			1.75
1183 G17 - 1	<0.002	<0.006	<0.002	<0.005	<0.002	<0.013	<0.002	<0.006	0.00	<0.007	0.017			
1183 G2 - 1	<0.002	0.01	<0.001	<0.004	<0.001	<0.007	<0.002	<0.005	0.01	<0.006	0.027			
1183 G2 - 2	<0.001	<0.005	<0.001	<0.004	<0.001	<0.009	<0.001	0.01	<0.002	<0.006	0.033			
1183 G5 - 1	<0.002	0.01	<0.002	<0.005	<0.001	0.02	<0.002	<0.006	0.01	0.01	0.199			1.78
1183 G6 - 1	<0.002	<0.005	<0.001	<0.004	<0.001	<0.006	<0.002	<0.005	0.00	0.01	0.028			
1183 G8 - 1	<0.002	<0.005	<0.001	<0.004	<0.001	<0.004	<0.002	<0.005	<0.002	<0.006	0.039			0.67
1183 G9 - 1	<0.002	<0.005	<0.001	<0.004	<0.001	0.01	<0.002	<0.005	0.00	0.01	0.036			
1183 G10 - 1	0.00	<0.005	<0.001	<0.004	<0.001	0.01	<0.001	<0.005	0.00	0.01	0.016			
1183 G11 - 2	<0.001	<0.005	<0.001	<0.004	<0.001	0.01	<0.001	<0.005	<0.000	<0.005	0.010			
1183 G14 - 1	<0.002	0.01	<0.002	<0.005	<0.002	<0.003	<0.002	<0.006	0.02	0.02	0.195			1.07
1183 G15 - 2	<0.002	<0.005	<0.002	<0.005	0.00	<0.019	<0.002	<0.005	0.01	0.01	0.182			1.79
1183 G16 - 1	<0.002	<0.007	<0.002	<0.006	<0.002	<0.010	<0.002	<0.007	<0.003	<0.008	0.038			
1183 G18 - 2	<0.002	<0.005	<0.001	<0.004	<0.001	<0.008	<0.002	<0.005	0.00	<0.006	0.126			1.21
1183 G19 - 1	<0.002	<0.007	<0.002	0.02	<0.002	0.02	0.00	<0.007	0.01	<0.008	0.542			1.38
1183 G19 - 2	0.00	<0.005	0.00	<0.005	<0.001	<0.004	0.00	0.01	0.01	<0.006	0.113			2.15
1183 G20 - 1	<0.002	<0.005	0.00	<0.005	<0.001	0.02	<0.002	<0.005	0.00	<0.006	0.069			0.93
1183 G22 - 1	<0.002	<0.007	<0.002	<0.006	0.00	<0.010	<0.002	<0.007	0.06	0.75	0.219			
1183 G23 - 3	<0.002	<0.005	<0.002	<0.005	<0.001	0.00	<0.002	0.01	<0.003	<0.006	0.277			2.78
1192 Img 5 G6 - 3	0.00	0.01	0.00	0.02	<0.001	0.01	<0.001	0.01	0.01	0.03	0.48	0.40	0.54	1.02
1192 Img 6 G1 - 1	0.01	0.02	0.01	0.02	<0.002	<0.005	0.01	<0.006	0.05	0.02	2.11	0.67	1.52	1.61
1192 no image bottom G4 - 2	0.01	0.05	0.01	0.02	0.01	<0.012	<0.002	<0.005	0.06	0.08	5.24	0.29	1.24	2.43
1192 Img 4 G2 - 2	0.01	0.04	0.01	0.01	<0.001	0.01	0.00	<0.006	0.01	<0.007	2.47	0.28	0.80	1.36
1192 no image bottom R G1 - 1	0.01	0.04	0.01	0.01	0.00	0.02	0.00	0.01	0.00	0.04	2.88		0.62	1.27
1192mag G1 - 3	0.01	0.03	0.01	0.01	0.01	0.03	<0.002	<0.006	0.08	0.06	4.08	0.38	0.93	1.65
1192mag G6 - 4	0.01	0.05	0.00	0.02	0.00	0.01	0.00	<0.005	0.02	0.03	1.40	0.29	1.38	1.97
1192mag G6 - 10	0.01	0.04	0.01	0.04	0.00	0.01	0.00	<0.005	0.04	0.04	2.70	0.89	1.20	2.41
1192 Img 3 G1 - 2	0.02	0.04	0.02	0.03	0.01	0.01	0.00	<0.005	0.05	0.03	3.70	0.54	1.08	1.21
1192mag G1 - 4	0.01	0.07	0.01	0.03	0.01	0.02	0.00	<0.005	0.05	0.01	4.98	0.48	0.82	1.65
1192mag G6 - 7	0.03	0.04	0.02	0.04	0.00	0.03	0.01	<0.005	0.02	0.06	2.85	0.73	1.05	1.72
1192 Img 4 G2 - 1	0.01	0.04	0.02	0.04	0.00	0.04	0.01	<0.005	0.02	0.16	1.98	0.14	0.65	2.34
1192 Img 5 G6 - 2	<0.002	0.05	0.01	0.02	0.00	0.10	0.01	<0.005	<0.003	<0.006	1.01		0.65	2.44
1192mag G6 - 6	0.01	0.08	0.02	0.03	0.01	0.05	0.00	<0.005	0.03	0.05	1.90	0.42	0.86	2.51
1192 no image bottom R G1 - 5	0.02	0.08	0.02	0.06	0.01	0.02	0.01	<0.005	0.03	0.09	3.21	0.41	1.43	3.11
1192mag G6 - 5	0.02	0.08	0.02	0.05	0.01	0.04	<0.002	<0.006	0.08	0.07	1.66	0.60	0.87	5.35
1192 Img 6 G1 - 3	0.01	0.05	0.02	0.07	0.01	0.08	0.00	<0.005	0.11	<0.006	1.87	0.66	0.97	3.70
1192mag G6 - 9	0.01	0.09	0.02	0.07	0.01	0.05	0.01	<0.005	0.07	0.06	2.35	0.50	1.22	3.05
1192 no image bottom R G1 - 6	0.02	0.11	0.02	0.06	0.00	0.05	0.01	<0.005	0.02	0.15	4.11	0.75	1.19	3.25
1192mag G1 - 2	0.03	0.11	0.02	0.07	0.00	0.08	0.01	<0.005	0.23	0.08	7.08	0.32	0.92	1.67
1192 Img 5 G3 - 1	0.02	0.15	0.03	0.11	0.02	0.11	0.01	<0.006	0.05	0.04	4.45	0.23	1.14	1.71
1192 no image bottom R G1 - 7	0.05	0.18	0.05	0.10	0.02	0.11	0.01	<0.006	0.11	0.19	6.99	0.56	1.08	2.84
1192mag G1 - 1	0.04	0.19	0.04	0.15	0.02	0.14	0.02	<0.005	0.49	0.14	14.60	0.25	0.80	1.77
1192 no image bottom G7 - 2	0.03	0.18	0.04	0.18	0.02	0.16	0.02	<0.005	0.09	0.01	3.96	0.32	1.34	1.24
1192 no image botton G1 - 6	0.03	0.20	0.06	0.16	0.01	0.15	0.03	<0.005	0.38	0.01	6.29	0.34	1.23	1.36
1192 no image botton G1 - 5	0.03	0.24	0.06	0.15	0.02	0.12	0.02	0.01	0.38	0.01	5.55	0.33	1.06	1.40
1192 no image botton G1 - 1	0.04	0.22	0.08	0.20	0.01	0.09	0.02	<0.006	0.36	<0.008	6.02	0.20	1.02	1.58
1192 no image botton G1 - 2	0.03	0.28	0.06	0.18	0.03	0.15	0.03	<0.005	0.36	0.01	6.79	0.66	1.05	1.40
1192 no image botton G1 - 8	0.03	0.34	0.07	0.19	0.02	0.13	0.02	0.02	0.31	<0.007	5.68	0.70	0.81	1.40
1192 no image botton G1 - 7	0.04	0.30	0.06	0.23	0.02	0.17	0.02	<0.005	0.37	<0.007	6.10	0.53	1.10	1.38
1192mag G4 - 2	0.05	0.27	0.07	0.14	0.04	0.27	0.04	<0.005	0.09	0.04	5.37	0.35	1.00	1.40
1192 no image botton G1 - 9	0.04	0.40	0.07	0.19	0.02	0.15	0.02	<0.006	0.49	<0.007	8.27	0.34	1.00	1.32
1192 no image bottom G7 - 1	0.07	0.33	0.09	0.20	0.04	0.27	0.03	<0.005	0.10	0.02	10.96	0.41	0.97	3.52
1192 no image botton G1 - 4	0.04	0.38	0.08	0.25	0.03	0.26	0.03	0.02	0.56	0.01	9.22	0.52	0.92	1.28
1192mag G4 - 1	0.04	0.35	0.06	0.20	0.04	0.34	0.04	<0.005	0.13	0.08	8.43	0.53	1.07	1.01
1192 no image botton G1 - 3	0.05	0.50	0.10	0.28	0.02	0.21	0.06	0.01	1.07	0.01	12.38	0.34	0.97	1.23
1192 no image bottom R G1 - 4	0.10	0.49	0.13	0.36	0.02	0.29	0.03	<0.006	0.10	0.26	17.20	0.61	0.85	2.13
1192 Img 5 G3 - 2	0.05	0.49	0.11	0.39	0.04	0.34	0.07	<0.005	0.12	0.03	10.87	0.30	1.13	1.46
1192 Img 5 G3 - 3	0.07	0.61	0.11	0.46	0.05	0.47	0.06	0.01	0.12	0.07	10.94	0.47	1.09	1.73
1192 Img 5 G5 - 1	<0.002	<0.005	<0.002	<0.005	<0.001	<0.005	<0.002	<0.005	0.00	<0.006	0.019			
1192mag G6 - 3	<0.002	0.01	<0.001	0.01	<0.001	<0.005	<0.002	0.01	<0.004	<0.006	0.038			
1192 no image bottom G5 - 1	0.01	0.01	0.00	0.01	<0.001	<0.013	<0.002	<0.005	0.00	<0.006	0.384		0.19	0.79
1192mag G6 - 8	0.00	0.02	<0.002	<0.005	<0.002	<0.022	<0.002	0.01	<0.001	<0.007	0.198	1.27		0.49

Element concentrations in ppm
BDL: below detection limit
NA: no analysis
$Eu/Eu^* = [(Eu_{CN}/(Sm_{CN}+Gd_{CN})/2)]$
$Y/Y^* = [(Y_{CN}/(Dy_{CN}+Ho_{CN})/2)]$
$Ce/Ce^* = [(Ce_{CN}/(La_{CN} \times Pr_{CN})^{0.5})]$
CN = chondrite normalised
Normalising values from Sun and McDonough (1989)

Appendix 5 Table A4: Magnetite and hematite LA-ICP-MS trace element data collected at Vulcan in this study

Included Data

Sample	Drill hole	Mineral	Comment
1192mag G6 - 1	VUD 007 1192	Magnetite	High Al, V. REE BDL.
1192mag G6 - 2	VUD 007 1192	Magnetite	Al inclusions. High Al, V. REE BDL.
1192mag G5 - 1	VUD 007 1192	Magnetite	High Al, V. REE BDL.
1192 Img 3 G1 - 1	VUD 007 1192	Magnetite	High V and Al. low Mg and P
1192mag G5 - 2	VUD 007 1192	Magnetite	High Al, V. REE BDL.
1192mag G5 - 3	VUD 007 1192	Magnetite	High Al, V. REE BDL.
1192 Img 3 G1 - 3	VUD 007 1192	Magnetite	High Al and V. REE BDL.
1192mag G5 - 4	VUD 007 1192	Magnetite	High Al, V. REE BDL.
1192 Img 5 G2 - 1	VUD 007 1192	Magnetite	High V and Al. low Mg and P.REE BDL.
1192mag G2 - 2	VUD 007 1192	Magnetite	High Al and V. low Mg and P. REE BDL.
1192 no image bottom G2 - 1	VUD 007 1192	Magnetite	High V and Al. low Mg and P.REE BDL.
1192mag G2 - 1	VUD 007 1192	Magnetite	High Al and V. low Mg and P. REE BDL.
1192 no image bottom G2 - 3	VUD 007 1192	Magnetite	High V and Al. low Mg and P.REE BDL.
1192 no image bottom G2 - 2	VUD 007 1192	Magnetite	High V and Al. low Mg and P. REE BDL.
1192 off img2 G2 - 2	VUD 007 1192	Magnetite	High V and Al. low Mg and P.REE BDL.
1192mag G3 - 3	VUD 007 1192	Magnetite	High Al and V. low Mg and P. REE BDL.
1192 img2 G1 - 1	VUD 007 1192	Magnetite	High V and Al. low Mg and P. REE BDL.
1192 off img2 G2 - 1	VUD 007 1192	Magnetite	High V and Al. low Mg and P. REE BDL.
1192mag G3 - 1	VUD 007 1192	Magnetite	High Al and V. low Mg and P. REE BDL.
1192mag G3 - 2	VUD 007 1192	Magnetite	High Al and V. low Mg and P. REE BDL.
1192 Img 6 G2 - 1	VUD 007 1192	Magnetite	High V and Al. low Mg and P.REE BDL.
1192 Img 4 G1 - 1	VUD 007 1192	Magnetite	High V and Al. low Mg and P.REE BDL.
1192 no image bottom R G1 - 3	VUD 007 1192	Magnetite	Mg Si inclusions. High V and Al. REE BDL.
1192 Img 5 G6 - 1	VUD 007 1192	Magnetite	High Al and V. REE BDL.
1192 Img 5 G1 - 1	VUD 007 1192	Magnetite	High V and Al. low Mg and P. REE BDL.
1192 Img 4 G3 - 1	VUD 007 1192	Magnetite	High V and Al. low Mg and P.REE BDL.
1192 Img 4 G3 - 3	VUD 007 1192	Magnetite	High V and Al. low Mg and P
1192 no image bottom G3 - 2	VUD 007 1192	Magnetite	High V and Al. low Mg and P.REE BDL.
1192 no image bottom G3 - 1	VUD 007 1192	Magnetite	High V and Al. low Mg and P. REE BDL.
1192 Img 5 G4 - 1	VUD 007 1192	Magnetite	REE BDL.
1192 no image bottom G6 - 1	VUD 007 1192	Magnetite	High V and Al. low Mg and P.REE BDL.
1192mag G1 - 5	VUD 007 1192	Magnetite	Cu Co inclusions. High Mg, Al, and V. High Ce and P. REE BDL.
1259 Img17 - G1 - 3	VUD 017 1259	Magnetite	High V, Al , Mg and ~Si
1259 Img17 - G3 - 2	VUD 017 1259	Magnetite	High V, Al, Mg. REE BDL.
1259 Img17 - G4 - 1	VUD 017 1259	Magnetite	High V, Al, Mg
1259 Img17 - G7 - 1	VUD 017 1259	Magnetite	High V, Al, Mg
1259 Img15- G1 - 3	VUD 017 1259	Magnetite	High V, Al, Mg and ~Si
1259 Img15- G2 - 1	VUD 017 1259	Magnetite	High V, Al , Mg and ~Si
1259 Img15- G2 - 2	VUD 017 1259	Magnetite	High V, Al , Mg and ~Si
1259 Img15- G2 - 3	VUD 017 1259	Magnetite	High V, Al , Mg and ~Si
1259 Img15- G3 - 1	VUD 017 1259	Magnetite	High V, Al, Mg and ~Si and ~P
1259 Img15- G3 - 2	VUD 017 1259	Magnetite	High V, Al , Mg and ~Si and ~P
1259 Img15- G3 - 3	VUD 017 1259	Magnetite	High V, Al, Mg
1259 Img15- G3 - 4	VUD 017 1259	Magnetite	High V, Al, Mg ~Si
1259 Img15- G4 - 1	VUD 017 1259	Magnetite	High V, Al , Mg and ~Si
1259 Img15- G5 - 2	VUD 017 1259	Magnetite	High V, Al, Mg. Si Mn inclusions
1259 Img14- G1 - 3	VUD 017 1259	Magnetite	Mg inclusions, High V and Al
1259 Img14- G1 - 4	VUD 017 1259	Magnetite	High V, Al, Mg. La, Ce, Th peak after signal
1259 Img14- G2 - 1	VUD 017 1259	Magnetite	High V, Al, Mg
1259 Img14- G2 - 2	VUD 017 1259	Magnetite	High V, Al, Mg ~Si
1259 Img14- G3 - 1	VUD 017 1259	Magnetite	High V, Al, Mg
1259 Img14- G4 - 1	VUD 017 1259	Magnetite	High V, Al, Mg ~Si
1259 Img14- G4 - 2	VUD 017 1259	Magnetite	High V, Al, Mg. Ti inclusions, ~high P and La, Ce
1259 Img14- G4 - 3	VUD 017 1259	Magnetite	Al inclusions. High V and Mg
1259 Img14- G5 - 1	VUD 017 1259	Magnetite	High V, Al, Mg.
1259 Img14- G5 - 3	VUD 017 1259	Magnetite	U inclusion. High V, Al, Mg
1259 Img14- G5 - 4	VUD 017 1259	Magnetite	High V, Al, Mg. Ce P peaks
1259 Img13- G1 - 1	VUD 017 1259	Magnetite	High V, Al , Mg and ~Si
1259 Img13- G1 - 3	VUD 017 1259	Magnetite	Cu inclusion. Ce peaks with Cu. High V, Al, Mg
1259 Img13- G2 - 1	VUD 017 1259	Magnetite	High V, Al, Mg ~Si. Ce peaks.
1259 Img13- G4 - 2	VUD 017 1259	Magnetite	208 spike. High V, Al, Mg. High P, Ca, Ce, La and U - apatite
1259 Img13- G4 - 3	VUD 017 1259	Magnetite	High V, Al, Mg. Co inclusions ~high P
1259 no img- G1 - 2	VUD 017 1259	Magnetite	Cu inclusions. High V, Al Mg. Ce peaks with Cu.
1259 no img- G2 - 6	VUD 017 1259	Magnetite	Mg Ti U inclusions. High V, Al, Mg, P
1259 mag G1 - 1	VUD 017 1259	Magnetite	High V, Al, Mg and P, Ce
1259 mag G1 - 2	VUD 017 1259	Magnetite	High V, Al, Mg. Apatite inclusion?
1259 mag G2 - 2	VUD 017 1259	Magnetite	High V, Mg and Al.
1259 mag G2 - 5	VUD 017 1259	Magnetite	High V, Mg and Al.
1259 mag G3 - 1	VUD 017 1259	Magnetite	High V, Mg and Al.
1259 mag G3 - 2	VUD 017 1259	Magnetite	High V, Mg and Al.
1259 mag G3 - 3	VUD 017 1259	Magnetite	Ti inclusions. High V, Mg and Al. High P
1259 mag G3 - 4	VUD 017 1259	Magnetite	High V, Mg and Al.

Element concentrations in ppm
BDL: below detection limit
NA: no analysis
$Eu/Eu^* = [(Eu_{CN}/(Sm_{CN}+Gd_{CN})/2)]$
$Y/Y^* = [(Y_{CN}/(Dy_{CN}+Ho_{CN})/2)]$
$Ce/Ce^* = [(Ce_{CN}/(La_{CN} \times Pr_{CN})^{0.5})]$
CN = chondrite normalised
Normalising values from Sun and McDonough (1989)

Appendix 5 Table A4: Magnetite and hematite LA-ICP-MS trace element data collected at Vulcan in this study

Included Data

Sample	Mg	Al	Si	P	Ca	Ti	V	Mn	Fe	Co	Ni	Cu	Zn	As
1192mag G6 - 1	2	580	155	<13.834	<49.694	54	118	5	720000	10.58	137.64	<0.231	0.28	0.27
1192mag G6 - 2	5	787	164	<12.543	<42.208	67	121	4	720000	12.59	139.48	<0.203	0.46	0.29
1192mag G5 - 1	3	320	149	<11.971	<47.657	46	73	6	720000	2.62	152.39	<0.183	0.38	0.35
1192 Img 3 G1 - 1	22	249	230	<9.259	42	45	130	7	720000	13.05	155.36	<0.197	<0.204	0.23
1192mag G5 - 2	3	300	147	<10.568	<33.738	43	71	4	720000	1.96	156.28	<0.186	<0.152	<0.178
1192mag G5 - 3	3	268	166	<9.613	<37.163	41	74	5	720000	2.33	157.52	<0.197	<0.161	0.21
1192 Img 3 G1 - 3	1	185	130	<11.860	<43.181	36	134	5	720000	17.70	159.70	<0.172	0.56	0.37
1192mag G5 - 4	3	318	158	<10.846	<39.767	47	76	6	720000	2.80	162.86	<0.196	<0.145	0.20
1192 Img 5 G2 - 1	4	164	203	<16.655	<54.206	46	162	10	720000	4.28	164.29	<0.303	1.14	<0.207
1192mag G2 - 2	2	219	193	<12.610	<39.921	36	152	7	720000	10.65	168.75	<0.244	0.76	0.19
1192 no image bottom G2 - 1	2	318	188	<8.754	<43.153	69	189	7	720000	6.82	169.84	<0.172	0.70	0.26
1192mag G2 - 1	2	220	143	<14.585	<48.056	38	147	7	720000	9.70	170.77	<0.228	0.41	0.35
1192 no image bottom G2 - 3	1	291	155	<10.481	<37.347	61	184	4	720000	10.26	171.86	0.23	0.14	0.45
1192 no image bottom G2 - 2	1	315	158	11	<35.472	65	196	5	720000	10.35	172.77	<0.175	0.20	0.38
1192 off img2 G2 - 2	2	199	144	<12.024	<42.065	44	70	8	720000	3.15	175.38	<0.217	0.47	0.53
1192mag G3 - 3	4	447	167	<9.839	<36.385	121	169	8	720000	4.87	175.59	<0.190	0.91	0.26
1192 img2 G1 - 1	8	189	200	<14.976	<51.058	38	190	10	720000	3.54	178.44	<0.258	1.73	0.45
1192 off img2 G2 - 1	8	139	255	<12.243	<43.678	29	72	8	720000	3.10	184.21	<0.202	0.93	0.35
1192mag G3 - 1	8	434	143	17	<39.393	128	183	6	720000	8.25	184.51	<0.176	0.22	0.30
1192mag G3 - 2	8	432	153	<10.630	<44.775	114	182	4	720000	11.43	186.86	<0.155	0.20	0.30
1192 Img 6 G2 - 1	2	213	160	<11.969	<35.827	28	286	8	720000	4.22	186.90	<0.214	1.49	0.53
1192 Img 4 G1 - 1	5	419	207	<11.869	<51.981	83	131	9	720000	6.63	187.45	<0.227	0.43	0.36
1192 no image bottom R G1 - 3	27	327	737	<13.190	<45.377	46	667	9	720000	8.26	191.34	<0.226	0.52	0.25
1192 Img 5 G6 - 1	11	211	222	<14.475	<62.160	48	117	7	720000	7.09	201.58	<0.239	2.79	2.07
1192 Img 5 G1 - 1	2	123	133	<11.364	<44.212	29	172	8	720000	12.61	210.75	<0.234	0.98	0.54
1192 Img 4 G3 - 1	3	126	168	<12.240	<50.090	22	319	8	720000	5.44	235.42	<0.242	0.94	0.34
1192 Img 4 G3 - 3	3	148	169	12	<42.990	24	338	9	720000	5.49	256.07	<0.181	1.08	0.25
1192 no image bottom G3 - 2	2	234	148	<12.372	38	45	323	10	720000	3.76	257.32	<0.182	0.94	0.32
1192 no image bottom G3 - 1	4	235	215	<11.635	<43.520	56	323	9	720000	3.73	260.81	0.24	2.01	1.77
1192 Img 5 G4 - 1	3	481	157	<9.104	<36.088	32	244	8	720000	4.47	304.17	<0.185	0.47	0.42
1192 no image bottom G6 - 1	5	519	165	<11.568	<45.237	120	288	8	720000	3.42	310.71	0.79	1.16	0.86
1192mag G1 - 5	26	271	251	<12.075	<44.897	51	196	9	720000	47.65	378.83	398.49	0.47	0.42
1259 Img17 - G1 - 3	942	598	2735	13	98	169	872	12	720000	3.42	88.29	1.24	1.52	0.58
1259 Img17 - G3 - 2	285	562	1937	<14.826	56	91	886	9	720000	5.49	82.28	1.10	6.35	0.78
1259 Img17 - G4 - 1	994	543	2319	<13.563	219	71	846	12	720000	5.10	82.46	2.21	1.64	<0.203
1259 Img17 - G7 - 1	975	609	2965	<13.280	142	135	887	13	720000	17.54	84.23	1.10	1.26	0.47
1259 Img15- G1 - 3	834	608	2320	<12.831	78	166	882	13	720000	13.71	84.42	0.25	1.42	0.34
1259 Img15- G2 - 1	1262	589	3111	<11.024	146	151	851	14	720000	7.72	78.48	0.50	<0.209	0.35
1259 Img15- G2 - 2	1073	542	2670	<10.777	162	77	889	14	720000	16.44	82.08	0.90	1.44	0.32
1259 Img15- G2 - 3	1173	613	2968	<11.426	49	105	820	15	720000	8.20	81.79	1.55	2.01	0.33
1259 Img15- G3 - 1	635	605	2024	<11.254	45	174	860	11	720000	14.12	84.55	0.45	1.05	0.36
1259 Img15- G3 - 2	1085	601	2932	11	47	194	866	14	720000	19.22	92.02	0.35	0.33	0.48
1259 Img15- G3 - 3	831	627	2280	20	<39.520	199	876	12	720000	4.51	110.00	0.79	4.90	0.87
1259 Img15- G3 - 4	1057	608	2793	14	145	184	893	13	720000	9.53	79.73	0.66	2.18	0.34
1259 Img15- G4 - 1	1002	601	2521	16	94	178	857	13	720000	3.58	93.83	0.59	5.02	0.45
1259 Img15- G5 - 2	768	652	2299	<12.091	<36.104	187	897	19	720000	2.62	81.87	0.34	12.25	0.33
1259 Img14- G1 - 3	370	551	1060	<10.699	<34.490	164	829	10	720000	4.54	76.21	<0.198	1.47	<0.186
1259 Img14- G1 - 4	516	558	1691	<16.533	<41.951	206	784	10	720000	4.54	72.15	<0.222	9.02	0.93
1259 Img14- G2 - 1	331	641	1642	<15.524	<42.902	155	866	10	720000	4.17	81.08	0.24	7.29	0.27
1259 Img14- G2 - 2	623	559	1788	<15.160	171	126	901	12	720000	5.16	88.83	2.16	4.18	0.42
1259 Img14- G3 - 1	1115	609	2585	<11.018	50	160	868	14	720000	2.31	80.65	0.23	1.02	0.48
1259 Img14- G4 - 1	656	625	1798	<11.804	63	159	900	11	720000	7.16	80.05	0.40	2.96	0.47
1259 Img14- G4 - 2	616	604	2078	<10.372	130	247	855	10	720000	8.02	77.42	0.30	0.27	0.52
1259 Img14- G4 - 3	558	674	1189	<12.086	81	225	843	17	720000	8.98	77.36	<0.227	4.65	0.77
1259 Img14- G5 - 1	601	605	2356	<11.102	<44.017	178	849	11	720000	5.51	80.28	0.78	0.23	0.42
1259 Img14- G5 - 3	368	566	1273	<10.712	73	233	853	9	720000	12.49	79.82	0.84	1.25	0.43
1259 Img14- G5 - 4	469	604	1812	<12.371	<43.893	178	816	10	720000	2.60	78.87	0.22	2.90	0.37
1259 Img13- G1 - 1	876	608	2040	<11.814	115	168	834	12	720000	10.43	79.92	2.11	1.21	0.34
1259 Img13- G1 - 3	664	582	1682	<12.821	<43.807	183	811	10	720000	4.03	78.14	2.42	0.57	0.47
1259 Img13- G2 - 1	596	603	1607	<13.444	105	125	886	11	720000	8.55	87.62	0.38	3.74	0.55
1259 Img13- G4 - 2	1026	522	2445	<11.114	332	89	853	12	720000	11.04	81.35	0.37	1.87	0.58
1259 Img13- G4 - 3	520	597	1846	12	<38.230	138	809	11	720000	4.42	76.51	0.39	2.81	0.42
1259 no img- G1 - 2	384	629	853	<12.428	123	149	915	8	720000	18.89	81.07	2.95	0.37	0.26
1259 no img- G2 - 6	431	587	1888	<11.111	56	332	920	11	720000	20.07	80.29	<0.199	2.21	0.73
1259 mag G1 - 1	1116	631	2655	<12.160	156	137	830	14	720000	22.97	78.88	0.93	0.68	0.65
1259 mag G1 - 2	243	575	1136	<11.625	51	128	789	8	720000	15.40	75.10	0.46	0.80	0.43
1259 mag G2 - 2	1075	614	3036	<12.939	111	151	843	14	720000	10.06	81.80	2.49	3.43	0.32
1259 mag G2 - 5	1033	668	2992	<12.100	218	211	929	14	720000	4.42	127.87	<0.202	2.42	0.28
1259 mag G3 - 1	488	542	1619	<11.107	66	142	862	9	720000	11.44	81.11	0.71	1.18	<0.208
1259 mag G3 - 2	808	615	2436	<12.795	108	156	869	13	720000	16.16	78.09	0.24	0.23	0.34
1259 mag G3 - 3	343	603	1553	<11.909	61	594	875	10	720000	10.09	81.59	0.25	5.39	0.41
1259 mag G3 - 4	330	562	1306	<9.571	77	170	807	9	720000	4.84	76.95	0.23	2.26	0.23

Element concentrations in ppm
BDL: below detection limit
NA: no analysis
$Eu/Eu^* = [(Eu_{CN}/(Sm_{CN}+Gd_{CN})/2)]$
$Y/Y^* = [(Y_{CN}/(Dy_{CN}+Ho_{CN})/2)]$
$Ce/Ce^* = [(Ce_{CN}/(La_{CN} \times Pr_{CN})^{0.5})]$
CN = chondrite normalised
Normalising values from Sun and McDonough (1989)

Appendix 5 Supplementary material for Mapping hydrothermal systems in IOCG deposits using apatite geochronology and geochemsitry: An example from Vulcan Cu-Au prospect

Appendix 5 Table A4: Magnetite and hematite LA-ICP-MS trace element data collected at Vulcan in this study

Included Data

Sample	Sr	Y	Zr	Nb	Mo	Sn	Ba	La	Ce	Pr	Nd	Sm	Eu	Gd
1192mag G6 - 1	0.01	<0.003	<0.003	<0.002	<0.026	0.10	<0.015	0.00	<0.002	<0.001	<0.011	<0.033	<0.003	0.01
1192mag G6 - 2	0.01	0.00	0.01	<0.001	<0.032	0.16	<0.014	0.02	0.02	0.00	<0.008	<0.007	<0.003	<0.013
1192mag G5 - 1	<0.006	<0.002	<0.001	0.00	<0.023	0.30	<0.013	0.01	0.01	0.01	<0.014	0.01	<0.003	<0.019
1192 Img 3 G1 - 1	0.03	0.04	0.00	0.02	<0.022	0.09	0.05	0.02	0.14	0.01	<0.011	0.01	<0.002	0.01
1192mag G5 - 2	0.01	<0.002	<0.003	<0.001	0.03	0.22	<0.012	<0.001	<0.001	0.00	<0.015	0.00	<0.003	<0.009
1192mag G5 - 3	0.01	<0.002	<0.003	<0.001	0.02	0.21	<0.012	<0.001	<0.001	<0.001	<0.007	<0.006	0.00	<0.006
1192 Img 3 G1 - 3	<0.003	<0.002	0.00	<0.001	0.03	0.09	<0.012	<0.002	<0.001	0.00	0.01	<0.011	0.00	<0.007
1192mag G5 - 4	<0.006	<0.002	<0.006	<0.001	0.02	0.30	<0.012	<0.001	<0.001	<0.002	0.02	<0.021	<0.003	0.02
1192 Img 5 G2 - 1	<0.014	<0.003	<0.016	0.00	<0.029	0.09	0.09	<0.002	<0.002	<0.000	<0.008	<0.005	<0.003	0.01
1192mag G2 - 2	0.01	<0.002	0.01	<0.001	0.02	0.04	<0.014	<0.002	0.02	<0.001	<0.012	<0.018	<0.003	<0.010
1192 no image bottom G2 - 1	0.01	<0.002	<0.002	<0.001	<0.030	0.21	0.03	0.01	0.01	<0.001	0.00	<0.015	<0.003	<0.006
1192mag G2 - 1	0.05	<0.002	0.00	<0.001	<0.043	0.10	0.06	0.01	0.01	0.00	<0.012	<0.021	<0.003	<0.025
1192 no image bottom G2 - 3	<0.012	0.00	0.00	<0.001	<0.030	0.14	0.01	0.00	0.00	<0.002	0.01	<0.007	<0.003	<0.020
1192 no image bottom G2 - 2	<0.008	<0.002	<0.006	<0.001	<0.034	0.19	<0.013	0.01	0.02	<0.001	0.02	0.01	0.01	<0.013
1192 off img2 G2 - 2	0.01	0.00	0.01	0.01	<0.038	0.10	<0.014	0.00	0.01	0.00	<0.010	<0.007	<0.003	<0.018
1192mag G3 - 3	<0.007	0.01	0.00	0.03	0.08	0.06	0.07	0.01	0.04	0.01	<0.017	<0.009	<0.003	<0.009
1192 img2 G1 - 1	0.10	0.01	<0.001	0.00	<0.030	0.16	<0.017	0.05	0.10	0.01	<0.016	<0.015	<0.004	<0.035
1192 off img2 G2 - 1	0.01	0.01	0.00	<0.002	<0.032	0.11	0.02	0.01	0.02	<0.002	<0.012	<0.008	0.01	<0.020
1192mag G3 - 1	<0.011	0.01	<0.005	0.00	0.01	0.13	<0.012	0.01	0.01	0.00	<0.011	0.01	<0.003	0.02
1192mag G3 - 2	<0.007	<0.002	<0.005	0.00	<0.043	0.13	<0.012	0.01	0.01	<0.001	<0.011	<0.003	<0.003	0.02
1192 Img 6 G2 - 1	0.19	<0.002	0.01	0.01	<0.034	0.09	0.06	0.02	0.02	0.00	<0.016	<0.002	<0.003	<0.014
1192 Img 4 G1 - 1	0.03	0.01	0.00	0.00	0.04	0.24	0.02	0.05	0.07	0.01	<0.017	<0.003	<0.003	<0.011
1192 no image bottom R G1 - 3	<0.005	0.12	<0.005	0.01	<0.027	0.11	<0.014	0.01	0.28	0.02	0.07	0.03	<0.003	<0.015
1192 Img 5 G6 - 1	0.11	<0.003	0.04	0.21	0.15	0.06	<0.017	0.03	0.06	0.00	<0.004	0.03	<0.004	<0.018
1192 Img 5 G1 - 1	0.01	0.01	<0.010	0.01	0.08	0.07	<0.013	0.00	0.01	<0.000	0.01	0.02	0.00	0.01
1192 Img 4 G3 - 1	<0.014	0.01	<0.007	0.00	0.04	0.03	<0.015	0.00	0.00	<0.001	0.01	<0.008	<0.003	0.03
1192 Img 4 G3 - 3	0.11	0.04	<0.004	<0.001	<0.022	0.08	0.04	0.05	0.08	0.02	<0.015	0.01	<0.002	<0.010
1192 no image bottom G3 - 2	<0.008	0.01	<0.003	0.00	<0.027	0.14	0.07	0.03	0.06	0.00	<0.018	0.01	<0.003	<0.010
1192 no image bottom G3 - 1	0.02	0.01	0.02	0.29	0.05	0.26	0.03	0.01	0.01	<0.002	<0.010	0.01	0.00	0.01
1192 Img 5 G4 - 1	<0.007	<0.002	0.04	<0.001	<0.030	0.06	<0.012	0.01	0.00	<0.001	0.01	<0.007	0.00	<0.016
1192 no image bottom G6 - 1	0.03	<0.002	0.03	5.56	0.10	1.28	<0.014	<0.002	0.01	<0.001	0.01	<0.008	<0.003	<0.024
1192mag G1 - 5	0.01	0.01	0.02	<0.001	<0.032	0.12	<0.014	0.01	0.03	0.00	<0.009	0.02	<0.003	<0.023
1259 Img17 - G1 - 3	0.06	0.38	0.01	0.01	<0.031	0.20	0.04	0.11	0.45	0.06	0.21	0.06	0.00	0.04
1259 Img17 - G3 - 2	0.03	0.09	0.03	0.00	<0.017	0.15	<0.013	0.02	0.13	0.01	0.17	0.02	<0.002	<0.017
1259 Img17 - G4 - 1	0.02	0.51	0.03	0.01	<0.023	0.14	0.03	0.06	0.43	0.06	0.18	0.03	0.01	0.04
1259 Img17 - G7 - 1	0.04	0.34	0.01	0.01	<0.015	0.23	<0.011	0.15	0.63	0.09	0.30	0.05	0.01	0.03
1259 Img15- G1 - 3	0.02	0.32	0.01	0.00	<0.040	0.23	<0.012	0.12	0.22	0.03	0.23	<0.012	0.00	0.02
1259 Img15- G2 - 1	0.02	0.55	0.02	0.01	<0.017	0.19	0.01	0.13	0.54	0.06	0.21	0.06	0.01	0.05
1259 Img15- G2 - 2	0.03	0.57	0.03	0.01	0.03	0.17	<0.011	0.15	0.54	0.05	0.22	0.07	0.01	0.07
1259 Img15- G2 - 3	0.02	0.41	0.02	0.00	<0.034	0.16	<0.011	0.07	0.33	0.03	0.15	0.03	0.00	0.03
1259 Img15- G3 - 1	<0.004	0.29	0.02	<0.001	<0.022	0.20	<0.013	0.07	0.26	0.03	0.04	0.01	0.01	0.03
1259 Img15- G3 - 2	0.01	0.39	0.02	0.01	0.02	0.26	<0.012	0.07	0.28	0.04	0.15	0.03	0.00	0.02
1259 Img15- G3 - 3	0.10	0.41	0.78	0.06	0.13	0.23	0.08	0.15	0.39	0.06	0.21	0.04	0.01	<0.028
1259 Img15- G3 - 4	0.02	0.41	0.03	0.01	0.02	0.22	0.06	0.10	0.45	0.05	0.24	0.03	0.01	0.03
1259 Img15- G4 - 1	0.09	0.42	0.29	0.02	0.05	0.37	0.03	0.13	0.48	0.07	0.25	0.05	0.01	0.03
1259 Img15- G5 - 2	0.06	0.19	0.04	<0.001	<0.021	0.23	0.02	0.03	0.07	0.01	0.05	0.01	<0.002	0.04
1259 Img14- G1 - 3	0.03	0.09	0.05	0.01	<0.021	0.30	<0.011	0.05	0.09	0.01	0.05	0.01	<0.002	0.02
1259 Img14- G1 - 4	0.13	0.22	1.05	0.08	0.62	0.48	0.03	0.10	0.24	0.02	0.08	<0.013	0.01	0.06
1259 Img14- G2 - 1	1.01	0.10	0.00	0.00	<0.035	0.21	0.24	0.01	0.05	0.00	0.03	0.01	<0.003	<0.012
1259 Img14- G2 - 2	0.06	0.29	0.00	0.01	<0.029	0.16	<0.013	0.05	0.36	0.03	0.16	0.04	0.01	0.01
1259 Img14- G3 - 1	0.01	0.34	0.02	0.00	<0.050	0.34	<0.012	0.09	0.30	0.03	0.19	0.03	0.00	0.02
1259 Img14- G4 - 1	0.14	0.22	0.01	0.01	0.04	0.23	0.06	0.08	0.22	0.04	0.08	<0.013	<0.003	<0.015
1259 Img14- G4 - 2	0.03	0.22	0.02	0.01	0.04	0.37	<0.011	0.07	0.26	0.02	0.16	0.03	<0.002	<0.037
1259 Img14- G4 - 3	0.37	0.22	0.04	0.02	<0.032	0.33	0.20	0.07	0.20	0.03	0.08	0.03	0.01	<0.401
1259 Img14- G5 - 1	0.02	0.21	<0.003	0.01	<0.026	0.21	<0.012	0.02	0.11	0.01	0.05	0.02	<0.002	<0.010
1259 Img14- G5 - 3	0.07	0.22	0.01	0.02	<0.040	0.21	0.09	0.07	0.17	0.03	0.09	<0.010	0.00	0.03
1259 Img14- G5 - 4	0.01	0.28	0.01	0.01	<0.032	0.18	0.02	0.03	0.23	0.02	0.07	<0.018	0.01	0.03
1259 Img13- G1 - 1	0.02	0.32	0.02	0.02	<0.028	0.16	0.03	0.12	0.41	0.06	0.17	<0.017	0.01	0.03
1259 Img13- G1 - 3	0.04	0.22	0.02	0.02	<0.036	0.19	<0.013	0.06	0.28	0.03	0.07	0.03	0.01	0.04
1259 Img13- G2 - 1	0.03	0.17	0.03	0.01	<0.030	0.16	<0.014	0.07	0.40	0.03	0.15	0.02	<0.003	0.04
1259 Img13- G4 - 2	0.19	0.38	0.06	0.02	<0.046	0.11	0.05	0.18	0.88	0.10	0.36	0.03	0.01	0.11
1259 Img13- G4 - 3	0.02	0.17	0.01	0.00	<0.033	0.30	<0.012	0.03	0.11	0.01	0.04	<0.016	0.00	0.04
1259 no img- G1 - 2	0.02	0.13	0.04	0.01	<0.010	0.14	<0.013	0.04	0.21	0.04	0.09	0.02	0.01	0.02
1259 no img- G2 - 6	0.37	0.28	0.10	0.03	<0.056	0.35	0.44	0.04	0.17	0.03	0.13	0.04	0.01	0.02
1259 mag G1 - 1	0.04	0.47	0.06	0.01	<0.037	0.14	0.08	0.21	0.64	0.09	0.33	0.05	0.00	0.04
1259 mag G1 - 2	0.02	0.06	<0.007	<0.001	<0.044	0.20	<0.013	0.06	0.14	0.01	0.05	0.02	<0.003	0.06
1259 mag G2 - 2	0.01	0.35	0.01	0.01	<0.016	0.21	<0.015	0.02	0.21	0.01	0.04	<0.008	0.01	<0.027
1259 mag G2 - 5	0.05	0.38	0.06	0.02	<0.018	0.34	0.06	0.24	0.68	0.08	0.44	0.04	0.02	0.05
1259 mag G3 - 1	<0.014	0.12	0.01	0.02	<0.033	0.18	<0.013	0.02	0.15	0.01	0.06	0.02	0.00	<0.015
1259 mag G3 - 2	0.10	0.22	0.07	0.00	<0.039	0.28	0.19	0.15	0.48	0.06	0.20	0.01	<0.003	0.03
1259 mag G3 - 3	0.22	0.21	0.02	0.18	<0.035	0.38	0.08	0.09	0.23	0.04	0.07	0.02	<0.003	0.03
1259 mag G3 - 4	0.23	0.09	0.01	0.01	<0.020	0.28	0.03	0.04	0.23	0.02	0.10	<0.011	0.01	<0.012

Element concentrations in ppm
BDL: below detection limit
NA: no analysis
$Eu/Eu^* = [(Eu_{CN}/(Sm_{CN}+Gd_{CN})/2)]$
$Y/Y^* = [(Y_{CN}/(Dy_{CN}+Ho_{CN})/2)]$
$Ce/Ce^* = [(Ce_{CN}/(La_{CN} \times Pr_{CN})^{0.5})]$
CN = chondrite normalised
Normalising values from Sun and McDonough (1989)

Appendix 5 Supplementary material for Mapping hydrothermal systems in IOCG deposits using apatite geochronology and geochemsitry: An example from Vulcan Cu-Au prospect

Appendix 5 Table A4: Magnetite and hematite LA-ICP-MS trace element data collected at Vulcan in this study

Included Data

Sample	Tb	Dy	Ho	Er	Tm	Yb	Lu	Hf	Ta	W	ΣREY	Eu/Eu*	Y/Y*	Ce/Ce*
1192mag G6 - 1	<0.002	<0.006	<0.002	<0.005	<0.001	<0.007	<0.002	<0.006	0.00	<0.007	0.016			
1192mag G6 - 2	<0.002	<0.005	<0.001	<0.005	<0.001	0.01	<0.002	<0.005	<0.004	<0.006	0.059			0.67
1192mag G5 - 1	<0.002	<0.005	<0.001	0.01	<0.001	<0.002	<0.002	<0.005	<0.003	0.01	0.037			0.49
1192 Img 3 G1 - 1	<0.001	0.02	0.00	<0.004	<0.001	<0.007	<0.001	0.01	0.02	<0.005	0.249		0.51	2.86
1192mag G5 - 2	<0.001	<0.004	<0.001	<0.004	<0.001	0.00	<0.001	<0.004	<0.001	<0.005	0.008			
1192mag G5 - 3	<0.001	<0.004	<0.001	<0.004	<0.001	0.00	<0.001	<0.004	0.00	0.01	0.006			
1192 Img 3 G1 - 3	<0.001	<0.005	<0.001	0.01	0.00	<0.005	<0.001	<0.005	<0.001	<0.005	0.025			
1192mag G5 - 4	<0.001	<0.004	<0.001	<0.004	<0.001	<0.001	<0.001	0.01	0.00	<0.005	0.041			
1192 Img 5 G2 - 1	<0.002	<0.007	<0.002	<0.006	<0.002	0.02	0.00	<0.006	<0.002	<0.008	0.037			
1192mag G2 - 2	<0.002	<0.005	<0.002	<0.005	<0.001	<0.015	<0.002	<0.005	<0.004	<0.006	0.017			
1192 no image bottom G2 - 1	<0.001	<0.005	<0.001	<0.004	<0.001	0.00	<0.001	<0.005	<0.002	0.01	0.023			
1192mag G2 - 1	<0.002	<0.005	<0.002	<0.005	<0.001	<0.007	<0.002	<0.005	<0.003	0.01	0.027			0.56
1192 no image bottom G2 - 3	<0.001	<0.005	<0.001	<0.004	<0.001	0.00	<0.002	<0.005	<0.000	0.01	0.026			
1192 no image bottom G2 - 2	0.00	<0.005	<0.001	<0.004	<0.001	<0.001	<0.001	<0.005	0.00	<0.006	0.079			
1192 off img2 G2 - 2	<0.002	<0.005	0.00	<0.005	<0.001	<0.007	<0.002	<0.005	<0.001	<0.006	0.017			0.49
1192mag G3 - 3	<0.002	<0.005	<0.001	<0.004	<0.001	<0.010	<0.001	<0.005	<0.001	<0.006	0.067			1.04
1192 img2 G1 - 1	<0.002	0.01	0.00	<0.006	<0.002	0.02	<0.002	<0.006	0.00	<0.007	0.200		0.07	1.13
1192 off img2 G2 - 1	<0.002	<0.006	<0.002	<0.005	<0.001	<0.008	<0.002	0.01	0.00	<0.006	0.053			
1192mag G3 - 1	<0.002	<0.005	0.00	<0.004	<0.001	<0.008	<0.001	<0.005	<0.002	<0.006	0.067			0.90
1192mag G3 - 2	<0.001	<0.005	<0.001	<0.004	<0.001	0.00	<0.001	0.01	<0.001	<0.006	0.044			
1192 Img 6 G2 - 1	<0.001	0.01	<0.001	<0.004	<0.001	0.00	<0.002	<0.005	<0.001	<0.006	0.048			0.55
1192 Img 4 G1 - 1	0.00	<0.005	0.00	<0.005	<0.001	0.01	<0.002	<0.005	0.00	0.01	0.148			1.16
1192 no image bottom R G1 - 3	<0.002	0.02	<0.002	0.01	0.00	0.00	<0.002	<0.005	0.01	<0.006	0.551			6.10
1192 Img 5 G6 - 1	<0.002	<0.007	<0.002	0.03	0.00	<0.007	<0.002	<0.006	<0.004	<0.007	0.148			1.55
1192 Img 5 G1 - 1	<0.001	<0.005	<0.001	<0.004	<0.001	<0.005	<0.002	<0.005	<0.001	<0.006	0.063	1.58		
1192 Img 4 G3 - 1	0.00	<0.006	<0.002	<0.005	<0.001	<0.007	<0.002	<0.006	<0.001	0.01	0.057			
1192 Img 4 G3 - 3	<0.001	0.01	<0.001	<0.004	0.00	0.01	0.00	<0.004	0.00	<0.005	0.219			0.69
1192 no image bottom G3 - 2	<0.002	0.01	<0.002	<0.005	<0.001	<0.010	<0.002	<0.005	0.00	0.01	0.119			1.39
1192 no image bottom G3 - 1	<0.002	<0.005	<0.001	<0.004	<0.001	<0.010	<0.002	0.02	0.01	0.11	0.051	1.08		
1192 Img 5 G4 - 1	<0.001	0.01	<0.001	<0.004	0.00	0.01	<0.001	0.01	0.00	<0.005	0.038			
1192 no image bottom G6 - 1	<0.002	<0.005	<0.002	<0.005	<0.001	<0.012	0.00	<0.005	0.02	0.54	0.030			
1192mag G1 - 5	<0.002	<0.005	0.00	<0.005	<0.001	<0.007	<0.002	<0.005	<0.002	<0.006	0.062			1.52
1259 Img17 - G1 - 3	0.01	0.05	0.01	0.05	0.01	0.07	0.02	0.00	0.00	<0.005	1.55	0.30	1.10	1.33
1259 Img17 - G3 - 2	0.00	<0.005	<0.001	0.01	0.00	<0.010	0.00	<0.005	0.01	0.01	0.45			2.48
1259 Img17 - G4 - 1	0.01	0.10	0.02	0.06	0.00	0.05	0.01	<0.004	0.00	0.02	1.56	0.70	0.83	1.73
1259 Img17 - G7 - 1	0.00	0.05	0.01	0.06	0.01	0.06	0.01	0.01	0.00	0.02	1.79	0.80	1.13	1.35
1259 Img15- G1 - 3	0.01	0.07	0.01	0.03	0.01	0.06	0.01	<0.004	0.01	0.02	1.15		0.88	0.92
1259 Img15- G2 - 1	0.01	0.08	0.01	0.07	0.00	0.08	0.02	<0.004	0.01	0.03	1.87	0.54	1.27	1.47
1259 Img15- G2 - 2	0.01	0.06	0.03	0.06	0.01	0.07	0.01	<0.004	<0.001	0.01	1.92	0.32	1.14	1.55
1259 Img15- G2 - 3	0.00	0.05	0.01	0.05	0.01	0.06	0.01	<0.004	0.00	0.01	1.24	0.48	1.31	1.79
1259 Img15- G3 - 1	0.01	0.03	0.00	0.03	0.02	0.06	0.01	<0.004	0.01	<0.005	0.89	1.23	3.23	1.37
1259 Img15- G3 - 2	0.01	0.07	0.01	0.03	0.00	0.08	0.01	<0.004	0.00	0.03	1.20	0.53	0.97	1.30
1259 Img15- G3 - 3	0.01	0.04	0.02	0.03	0.01	0.10	0.02	0.04	0.01	0.05	1.49		1.26	1.03
1259 Img15- G3 - 4	0.00	0.05	0.02	0.08	0.01	0.06	0.01	<0.004	0.01	0.02	1.54	1.15	1.16	1.61
1259 Img15- G4 - 1	0.01	0.06	0.01	0.05	0.01	0.13	0.01	0.01	0.01	0.01	1.71	0.62	1.24	1.24
1259 Img15- G5 - 2	0.00	0.04	0.01	0.03	0.00	0.02	0.01	<0.004	<0.001	<0.005	0.51		0.88	1.02
1259 Img14- G1 - 3	0.01	0.02	0.00	0.02	<0.001	0.02	0.00	0.01	<0.001	0.01	0.38		1.53	0.98
1259 Img14- G1 - 4	0.01	0.02	0.01	0.04	0.01	0.06	0.01	0.03	0.00	0.03	0.89		1.38	1.16
1259 Img14- G2 - 1	0.00	0.02	0.01	0.01	0.00	0.01	<0.002	<0.005	0.00	<0.006	0.25		0.65	3.81
1259 Img14- G2 - 2	0.01	0.08	0.01	0.03	0.00	0.02	0.01	0.01	<0.003	0.02	1.11	0.82	0.69	2.24
1259 Img14- G3 - 1	0.00	0.03	0.01	0.06	0.01	0.09	0.01	0.01	0.03	0.01	1.23	0.31	1.23	1.30
1259 Img14- G4 - 1	0.00	0.05	0.00	0.03	0.01	0.12	0.02	<0.005	0.03	0.01	0.86		1.22	1.01
1259 Img14- G4 - 2	0.00	0.02	0.01	0.03	0.01	0.03	0.01	<0.004	0.03	0.01	0.87		1.23	1.52
1259 Img14- G4 - 3	<0.001	0.05	0.01	0.01	0.00	0.10	0.01	0.01	0.05	<0.006	0.82		0.64	1.05
1259 Img14- G5 - 1	0.01	0.05	0.01	0.04	0.00	0.04	0.00	0.00	0.00	<0.005	0.59		0.76	1.43
1259 Img14- G5 - 3	0.01	0.04	0.01	0.02	0.00	0.05	0.01	<0.004	<0.002	0.02	0.74		0.82	0.99
1259 Img14- G5 - 4	0.01	0.05	0.01	0.03	0.00	<0.009	0.01	<0.004	<0.003	0.01	0.77		1.10	2.69
1259 Img13- G1 - 1	0.01	0.02	0.01	0.06	0.01	0.06	0.01	0.01	0.00	0.01	1.29		1.69	1.15
1259 Img13- G1 - 3	0.01	0.03	0.01	0.06	0.01	0.07	<0.001	<0.004	0.00	0.01	0.92	0.76	0.94	1.71
1259 Img13- G2 - 1	0.01	0.03	0.02	0.01	0.00	0.04	0.00	<0.005	<0.002	<0.006	0.99		0.55	2.11
1259 Img13- G4 - 2	0.01	0.07	0.01	0.06	0.00	0.06	0.00	<0.005	0.01	0.01	2.28	0.35	0.90	1.60
1259 Img13- G4 - 3	0.00	0.02	0.01	0.01	0.01	0.03	0.00	0.01	0.00	<0.005	0.47		0.96	1.68
1259 no img- G1 - 2	0.00	0.02	0.00	0.02	0.00	0.01	0.00	<0.004	0.00	0.02	0.62	1.30	1.82	1.17
1259 no img- G2 - 6	0.00	0.06	0.01	0.02	0.01	0.09	0.01	<0.004	0.02	0.02	0.92	0.70	0.76	1.19
1259 mag G1 - 1	0.02	0.09	0.01	0.05	0.01	0.09	0.02	0.01	0.01	0.02	2.12	0.28	1.10	1.11
1259 mag G1 - 2	<0.002	0.02	0.00	0.01	<0.001	<0.005	<0.002	<0.005	0.00	0.01	0.43		0.56	1.47
1259 mag G2 - 2	<0.002	0.06	0.01	0.04	0.01	0.09	0.01	0.01	0.01	0.02	0.86		1.05	3.40
1259 mag G2 - 5	0.00	0.06	0.01	0.05	0.02	0.11	0.02	<0.006	0.03	<0.007	2.19	1.24	1.53	1.23
1259 mag G3 - 1	0.00	0.01	0.00	0.02	0.00	0.03	0.01	0.01	0.01	0.01	0.47		1.85	3.35
1259 mag G3 - 2	0.01	0.05	0.01	0.03	0.01	0.11	0.02	0.01	0.02	<0.006	1.38		0.66	1.27
1259 mag G3 - 3	0.00	0.02	0.01	0.03	0.00	0.07	0.01	<0.005	0.02	0.01	0.85		1.05	1.00
1259 mag G3 - 4	0.00	0.02	0.01	0.03	0.00	0.02	<0.001	<0.005	0.03	<0.006	0.59		0.67	1.79

Element concentrations in ppm
BDL: below detection limit
NA: no analysis
$Eu/Eu^* = [(Eu_{CN}/(Sm_{CN}+Gd_{CN})/2)]$
$Y/Y^* = [(Y_{CN}/(Dy_{CN}+Ho_{CN})/2)]$
$Ce/Ce^* = [(Ce_{CN}/(La_{CN} \times Pr_{CN})^{0.5})]$
CN = chondrite normalised
Normalising values from Sun and McDonough (1989)

Appendix 5 Table A4: Magnetite and hematite LA-ICP-MS trace element data collected at Vulcan in this study

Included Data

Sample	Drill hole	Mineral	Comment
1259 mag G3 - 6	VUD 017 1259	Magnetite	High V, Mg and Al.
1259 mag G5 - 1	VUD 017 1259	Magnetite	High V, Mg and Al.
1259 mag G5 - 2	VUD 017 1259	Magnetite	High V, Mg and Al.
1259 mag G5 - 3	VUD 017 1259	Magnetite	Ti inclusions. High V, Mg and Al. High P
1259 mag G5 - 4	VUD 017 1259	Magnetite	High V, Mg and Al.
1259 mag G5 - 5	VUD 017 1259	Magnetite	High V, Mg and Al.
1259 mag G4 - 2	VUD 017 1259	Magnetite	High V, Mg and Al. REE BDL.
1259 Img17 - G2 - 2	VUD 017 1259	Magnetite	Co inclusion. High V, Al, Mg. REE BDL.
1259 Img17 - G5 - 2	VUD 017 1259	Magnetite	High V, Al, Mg. REE BDL.
1259 Img17 - G6 - 2	VUD 017 1259	Magnetite	Mg inclusions. High V and Al. REE BDL.
1259 Img17 - G7 - 2	VUD 017 1259	Magnetite	Hgih V, Al, Mg. REE BDL.
1259 Img15- G4 - 2	VUD 017 1259	Magnetite	High V, Al, Mg ~Si. Ce peaks. REE BDL.
1259 Img14- G2 - 5	VUD 017 1259	Magnetite	207 spike. High V, Al, Mg. REE BDL.
1259 Img14- G3 - 2	VUD 017 1259	Magnetite	High V and Al. Mg inclusions. ~high P. REE BDL.
1259 Img14- G5 - 2	VUD 017 1259	Magnetite	High V, Al, Mg. REE BDL.
1259 Img13- G1 - 2	VUD 017 1259	Magnetite	High V, Al , Mg and ~Si REE BDL.
1259 Img15- G4 - 3	VUD 017 1259	Magnetite	Mg inclusions. High V and Al. REE BDL.
1259 Img17 - G2 - 1	VUD 017 1259	Magnetite	High V, Al , Mg and ~Si
1259 Img17 - G5 - 1	VUD 017 1259	Magnetite	Mg inclusions. High V and Al
1259 Img15- G1 - 2	VUD 017 1259	Magnetite	High V, Al. Mg and Ti inclusions
1259 Img14- G2 - 3	VUD 017 1259	Magnetite	Mg Si inclusions?
1259 Img14- G5 - 5	VUD 017 1259	Magnetite	Mg Ti inclusions. U inclusion.
1259 Img14- G2 - 4	VUD 017 1259	Magnetite	High V, Al. Mg inclusions
1259 Img17 - G6 - 3	VUD 017 1259	Magnetite	High V and Al. REE BDL.
1259 Img17 - G1 - 1	VUD 017 1259	Magnetite	High V and Al. Mg inclusions? REE BDL.
1259 Img17 - G1 - 2	VUD 017 1259	Magnetite	High V and Al. Mg inclusions? REE BDL.
1259 Img17 - G6 - 1	VUD 017 1259	Magnetite	Mg inclusions. High V and Al. REE BDL.
1259 Img17 - G6 - 4	VUD 017 1259	Magnetite	Mg inclusions. High V and Al. REE BDL.
1259 Img17 - G7 - 3	VUD 017 1259	Magnetite	High V, Al, Mg. REE BDL.
1259 Img15- G1 - 1	VUD 017 1259	Magnetite	High V, Al, Mg. REE BDL.
1259 Img15- G5 - 1	VUD 017 1259	Magnetite	Mg inclusions. High V and Al. REE BDL.
1259 Img14- G1 - 1	VUD 017 1259	Magnetite	Mg inclusions. High V and Al. REE BDL.
1259 Img14- G1 - 2	VUD 017 1259	Magnetite	Mg inclusions. High V and Al. REE BDL.
1259 Img13- G1 - 4	VUD 017 1259	Magnetite	Cu inclusions. High V, Al, Mg, Ce peaks with Cu REE BDL.
1259 Img13- G2 - 2	VUD 017 1259	Magnetite	High V and Al. Mg inclusions. ~high P. REE BDL.
1259 mag G2 - 1	VUD 017 1259	Magnetite	High V, Mg and Al. REE BDL.
1259 mag G2 - 3	VUD 017 1259	Magnetite	High V, Mg and Al. REE BDL.
1259 mag G2 - 4	VUD 017 1259	Magnetite	High V, Mg and Al. REE BDL.
1259 mag G4 - 1	VUD 017 1259	Magnetite	High V, Mg and Al. REE BDL.
1259 mag G5 - 7	VUD 017 1259	Magnetite	High V, Mg and Al. REE BDL.
1268 img 8- G1 - 5	VUD 017 1268	Magnetite	Mg Mn inclusions. High V and Al and Si, P and Ce
1268 img 8- G2 - 4	VUD 017 1268	Magnetite	High V, Al, Mg and P ~Ce and La
1268 img 9- G2 - 1	VUD 017 1268	Magnetite	High Al and V. Mg inclusions. High P
1268 img 9- G2 - 2	VUD 017 1268	Magnetite	High Al and V. Mg inclusions. High P, Ce and Th
1268 img 11 G3 - 4	VUD 017 1268	Magnetite	High Al, V, Mg. High P and Ce.
1268 img 11 G3 - 5	VUD 017 1268	Magnetite	Mg inclusions. High and Al
1268 img 12 G1 - 2	VUD 017 1268	Magnetite	High Al, V and Mg. REE BDL.
1268 img 12 G2 - 3	VUD 017 1268	Magnetite	Mg inclusions, High V and Al
1268 img 12 G2 - 4	VUD 017 1268	Magnetite	Mg inclusions. High V and Al
1268 img 12 off G7 - 2	VUD 017 1268	Magnetite	High Mn Co P Ce Ti
1268 mag G2 - 3	VUD 017 1268	Magnetite	REE BDL.High A and Al. High P and Mg.
1268 mag G3 - 1	VUD 017 1268	Magnetite	High Al, V. High P and Mg
1268 mag G4 - 3	VUD 017 1268	Magnetite	High V and Al, low P and Mg.
1268 mag G10 - 3	VUD 017 1268	Magnetite	High Al, V. High Mg and P.
1268 img 12 G3 - 2	VUD 017 1268	Magnetite	Mg inclusions. High V and Al
1268 img 10 G4 - 2	VUD 017 1268	Magnetite	High V and Al. Mg inclusions. High P. REE BDL.
1268 img 12 G2 - 2	VUD 017 1268	Magnetite	Mg inclusions.High V and Al. REE BDL.
1268 mag G2 - 1	VUD 017 1268	Magnetite	High Al, V. Mg. P. HREE BDL.
1268 mag G4 - 1	VUD 017 1268	Magnetite	High Al, V. low P and Mg. REE BDL.
1268 mag G4 - 4	VUD 017 1268	Magnetite	High Mg, Al, V. REE BDL.
1268 mag G6 - 1	VUD 017 1268	Magnetite	High V and Al, low P and Mg. REE BDL.
852(1) - 3	VUD 009 852	Hematite	High Al, Mg and Mn
852(1) - 4	VUD 009 852	Hematite	High Al
852(1) - 5	VUD 009 852	Hematite	High Al and Mn
852(1) - 6	VUD 009 852	Hematite	High Al and Mg
852(1) - 7	VUD 009 852	Hematite	High Al, Mn
852(1) - 8	VUD 009 852	Hematite	High Al
852(1) - 10	VUD 009 852	Hematite	Mn inclusion.
852(1) - 12	VUD 009 852	Hematite	High Al and Mn
852(1) - 13	VUD 009 852	Hematite	High Al and Mn
852(1) - 14	VUD 009 852	Hematite	High Al and Mn and Si

Element concentrations in ppm
BDL: below detection limit
NA: no analysis
$Eu/Eu^* = [(Eu_{CN}/(Sm_{CN}+Gd_{CN})/2)]$
$Y/Y^* = [(Y_{CN}/(Dy_{CN}+Ho_{CN})/2)]$
$Ce/Ce^* = [(Ce_{CN}/(La_{CN} \times Pr_{CN})^{0.5})]$
CN = chondrite normalised
Normalising values from Sun and McDonough (1989)

Appendix 5 Supplementary material for Mapping hydrothermal systems in IOCG deposits using apatite geochronology and geochemsitry: An example from Vulcan Cu-Au prospect

Appendix 5 Table A4: Magnetite and hematite LA-ICP-MS trace element data collected at Vulcan in this study

Included Data

Sample	Mg	Al	Si	P	Ca	Ti	V	Mn	Fe	Co	Ni	Cu	Zn	As
1259 mag G3 - 6	248	607	1763	<10.062	<43.933	898	868	11	720000	16.68	82.18	0.32	1.32	0.44
1259 mag G5 - 1	939	619	2234	<12.074	108	105	852	13	720000	10.88	187.51	0.56	0.21	0.24
1259 mag G5 - 2	534	607	1840	<13.087	<47.184	149	888	11	720000	9.35	113.70	<0.208	1.32	0.49
1259 mag G5 - 3	323	621	1712	<12.191	<50.710	211	849	9	720000	8.12	112.73	0.21	0.32	<0.176
1259 mag G5 - 4	280	573	1772	<12.296	<49.694	213	832	8	720000	11.23	124.69	<0.198	0.53	0.49
1259 mag G5 - 5	449	593	1774	<16.454	144	222	854	14	720000	6.09	151.60	0.89	2.93	0.28
1259 mag G4 - 2	1073	621	2298	<11.472	74	218	870	13	720000	10.92	78.70	0.30	1.04	0.42
1259 Img17 - G2 - 2	645	622	1797	<11.404	81	197	879	12	720000	7.23	83.46	1.70	3.27	0.41
1259 Img17 - G5 - 2	489	596	1952	<13.190	77	104	855	11	720000	14.24	78.85	1.32	0.23	0.54
1259 Img17 - G6 - 2	300	630	1089	<12.624	<44.251	107	882	10	720000	32.03	84.55	4.02	<0.198	0.68
1259 Img17 - G7 - 2	566	638	1671	<13.415	<44.421	152	915	10	720000	15.82	82.37	0.72	2.11	0.29
1259 Img15- G4 - 2	529	628	1847	<13.526	<44.254	231	905	11	720000	3.29	93.31	0.47	0.87	0.40
1259 Img14- G2 - 5	600	606	1599	<11.007	<47.283	163	853	11	720000	4.55	78.58	0.48	3.21	0.31
1259 Img14- G3 - 2	226	570	957	16	66	142	871	8	720000	10.01	79.24	0.32	1.91	0.26
1259 Img14- G5 - 2	264	610	1766	<11.551	<46.648	175	876	10	720000	6.86	85.10	0.18	0.59	0.55
1259 Img13- G1 - 2	656	579	2031	<12.393	130	154	844	11	720000	7.41	83.73	0.96	4.20	0.38
1259 Img15- G4 - 3	103	578	443	19	<43.250	172	849	9	720000	1.35	82.73	0.16	5.84	0.21
1259 Img17 - G2 - 1	631	582	2149	<13.076	55	162	864	12	720000	3.39	80.47	0.71	1.28	0.35
1259 Img17 - G5 - 1	182	619	1317	<13.332	<32.977	125	892	9	720000	6.91	82.39	0.36	1.06	0.20
1259 Img15- G1 - 2	419	618	1429	<13.323	<30.997	343	875	10	720000	10.51	81.34	0.34	1.29	0.34
1259 Img14- G2 - 3	382	600	1153	<12.226	<32.958	156	877	10	720000	2.94	81.31	0.70	1.12	0.29
1259 Img14- G5 - 5	154	578	461	<11.077	79	198	862	7	720000	6.00	81.90	0.56	2.15	0.32
1259 Img14- G2 - 4	172	565	988	<13.039	38	119	826	9	720000	3.57	76.07	0.32	4.00	0.92
1259 Img17 - G6 - 3	79	612	428	<13.040	38	102	920	8	720000	28.25	84.35	0.72	0.31	<0.238
1259 Img17 - G1 - 1	56	585	1216	13	<45.250	195	857	8	720000	9.36	79.05	0.80	3.84	0.54
1259 Img17 - G1 - 2	25	603	828	<14.870	<54.799	143	928	9	720000	9.78	83.48	<0.226	2.60	0.37
1259 Img17 - G6 - 1	197	602	612	<12.535	<43.706	97	878	9	720000	28.05	78.26	0.78	0.17	0.30
1259 Img17 - G6 - 4	199	555	596	<13.141	<36.718	82	891	9	720000	15.17	84.18	3.91	0.90	<0.239
1259 Img17 - G7 - 3	137	614	1113	<13.705	<38.944	129	889	9	720000	15.46	85.99	0.96	1.08	0.57
1259 Img15- G1 - 1	295	628	1776	<15.459	<42.408	155	885	10	720000	10.79	81.66	0.49	0.20	0.44
1259 Img15- G5 - 1	186	599	1139	<12.422	<38.534	251	878	9	720000	4.84	84.47	0.30	2.28	0.24
1259 Img14- G1 - 1	54	597	536	<12.079	<34.663	202	853	9	720000	4.58	82.54	0.18	1.83	0.43
1259 Img14- G1 - 2	77	574	733	<10.724	<37.643	176	839	8	720000	5.50	80.35	0.40	1.00	0.21
1259 Img13- G1 - 4	176	588	490	<11.201	46	149	849	8	720000	4.11	78.81	1.70	2.75	0.63
1259 Img13- G2 - 2	357	632	905	<12.023	<42.970	133	902	9	720000	9.78	92.81	0.93	1.14	0.33
1259 mag G2 - 1	170	614	906	13	43	164	864	9	720000	16.89	78.24	0.55	0.82	0.24
1259 mag G2 - 3	11	605	377	<11.002	<41.685	125	864	8	720000	7.59	82.92	<0.226	1.60	0.24
1259 mag G2 - 4	101	619	1036	<10.694	<42.443	182	884	9	720000	17.15	100.60	<0.228	0.50	0.22
1259 mag G4 - 1	29	629	1617	<11.630	<43.732	251	876	9	720000	2.57	92.84	0.60	3.37	0.30
1259 mag G5 - 7	67	628	1205	<13.693	57	191	872	8	720000	5.07	89.08	<0.202	1.28	0.34
1268 img 8- G1 - 5	390	523	2121	<13.139	175	137	295	44	720000	2.16	29.68	<0.202	8.62	0.46
1268 img 8- G2 - 4	222	407	1499	<13.884	206	84	294	6	720000	5.13	35.27	0.63	9.57	1.39
1268 img 9- G2 - 1	102	407	543	<10.845	87	79	294	5	720000	1.89	31.55	0.50	1.30	0.30
1268 img 9- G2 - 2	210	425	1074	<11.273	274	84	296	7	720000	2.58	30.89	2.79	0.80	0.43
1268 img 11 G3 - 4	208	532	1073	<8.475	266	134	290	7	720000	1.05	27.16	<0.215	3.31	0.37
1268 img 11 G3 - 5	61	470	1014	<9.953	85	112	274	6	720000	0.93	26.11	0.48	2.76	0.36
1268 img 12 G1 - 2	223	356	1126	12	257	46	291	6	720000	4.90	37.51	0.39	2.11	0.51
1268 img 12 G2 - 3	25	390	359	<10.616	<46.066	62	286	5	720000	1.22	31.19	0.80	1.85	<0.182
1268 img 12 G2 - 4	63	402	571	<12.794	56	68	292	6	720000	2.63	31.99	1.13	5.49	0.74
1268 img 12 off G7 - 2	202	462	1003	<10.842	216	109	302	6	720000	2.45	29.26	0.85	3.12	0.31
1268 mag G2 - 3	88	446	867	<10.382	145	95	300	7	720000	8.35	31.89	0.32	3.85	0.39
1268 mag G3 - 1	117	550	953	<13.582	127	156	297	7	720000	2.92	28.11	0.82	2.74	0.43
1268 mag G4 - 3	18	495	458	19	<44.772	116	288	7	720000	8.94	34.15	<0.198	0.79	<0.212
1268 mag G10 - 3	190	465	892	<11.582	195	82	300	7	720000	1.50	31.79	0.43	8.84	0.47
1268 img 12 G3 - 2	41	392	456	<10.532	<40.191	78	280	5	720000	0.88	27.77	<0.163	3.05	0.30
1268 img 10 G4 - 2	39	387	381	<13.694	49	67	285	5	720000	0.79	30.86	0.36	7.92	<0.258
1268 img 12 G2 - 2	43	398	352	15	<43.511	61	289	6	720000	1.24	32.07	0.97	1.73	0.41
1268 mag G2 - 1	135	438	839	<12.050	189	83	284	7	720000	6.34	32.34	0.83	2.34	0.42
1268 mag G4 - 1	33	462	409	<14.480	<45.829	99	307	7	720000	15.82	30.25	0.52	1.09	0.26
1268 mag G4 - 4	90	397	603	<11.743	120	86	280	6	720000	1.90	31.43	0.56	18.64	0.39
1268 mag G6 - 1	22	454	263	<12.486	<52.465	81	299	6	720000	2.95	31.62	0.58	5.30	<0.258
852(1) - 3	352	638	1435	86	331	6	29	134	690000	13.72	116.35	1.83	3.16	24.38
852(1) - 4	178	967	1128	102	207	5	35	72	690000	11.16	94.95	2.85	1.90	26.23
852(1) - 5	20	848	1141	258	295	2	11	164	690000	47.09	285.45	1.46	9.23	10.28
852(1) - 6	660	353	1576	<19.571	159	6	37	28	690000	13.47	145.87	<0.644	2.12	28.89
852(1) - 7	167	899	1537	613	1349	4	16	236	690000	42.48	273.14	2.46	17.71	16.69
852(1) - 8	55	307	378	24	<65.111	6	37	35	690000	12.99	141.54	2.41	1.60	19.16
852(1) - 10	35	921	980	62	75	<0.351	3	85	690000	42.52	371.31	<0.535	4.86	9.47
852(1) - 12	138	721	987	771	1420	4	24	202	690000	19.58	173.78	3.85	15.06	11.63
852(1) - 13	146	1243	1648	796	1491	8	47	631	690000	71.22	251.40	19.52	22.28	24.35
852(1) - 14	39	790	1307	499	450	0	2	241	690000	72.59	318.30	1.55	11.98	20.37

Element concentrations in ppm
BDL: below detection limit
NA: no analysis
$Eu/Eu^* = [(Eu_{CN}/(Sm_{CN}+Gd_{CN})/2)]$
$Y/Y^* = [(Y_{CN}/(Dy_{CN}+Ho_{CN})/2)]$
$Ce/Ce^* = [(Ce_{CN}/(La_{CN} \times Pr_{CN})^{0.5})]$
CN = chondrite normalised
Normalising values from Sun and McDonough (1989)

Appendix 5 Supplementary material for Mapping hydrothermal systems in IOCG deposits using apatite geochronology and geochemsitry: An example from Vulcan Cu-Au prospect

Appendix 5 Table A4: Magnetite and hematite LA-ICP-MS trace element data collected at Vulcan in this study

Included Data

Sample	Sr	Y	Zr	Nb	Mo	Sn	Ba	La	Ce	Pr	Nd	Sm	Eu	Gd
1259 mag G3 - 6	0.07	0.19	0.02	0.01	<0.045	1.73	<0.014	0.10	0.24	0.03	0.08	0.02	<0.003	0.02
1259 mag G5 - 1	<0.011	0.30	<0.003	0.00	<0.025	0.19	0.01	0.07	0.21	0.04	0.10	0.05	<0.003	0.01
1259 mag G5 - 2	0.04	0.28	0.01	0.01	<0.028	0.20	<0.015	0.03	0.12	0.02	0.07	<0.023	<0.003	<0.023
1259 mag G5 - 3	0.04	0.13	0.00	0.00	<0.020	0.37	0.02	0.03	0.10	0.01	0.06	<0.017	<0.003	0.03
1259 mag G5 - 4	0.12	0.11	0.02	0.02	<0.033	0.39	0.06	0.05	0.26	0.03	0.08	0.01	0.01	<0.027
1259 mag G5 - 5	0.13	0.14	0.00	0.01	<0.055	0.30	<0.018	0.05	0.27	0.02	0.16	0.02	<0.004	0.05
1259 mag G4 - 2	0.03	0.48	0.02	0.01	0.02	0.25	<0.013	0.08	0.38	0.03	0.18	0.05	0.00	<0.014
1259 Img17 - G2 - 2	0.05	0.14	0.02	0.01	<0.020	0.24	0.03	0.02	0.20	0.01	0.06	0.02	<0.002	0.02
1259 Img17 - G5 - 2	0.01	0.20	0.01	<0.001	<0.031	0.15	<0.012	0.02	0.17	0.02	0.03	0.03	<0.002	<0.027
1259 Img17 - G6 - 2	<0.012	0.10	0.04	<0.001	<0.021	0.19	0.06	0.01	0.08	0.00	0.05	<0.019	<0.002	0.01
1259 Img17 - G7 - 2	0.03	0.13	0.02	0.01	<0.040	0.17	<0.012	0.03	0.17	0.02	0.08	0.03	<0.002	<0.017
1259 Img15- G4 - 2	<0.009	0.19	0.01	0.01	<0.016	0.31	<0.013	0.05	0.19	0.02	0.10	0.01	<0.002	0.03
1259 Img14- G2 - 5	<0.006	0.22	<0.004	0.01	<0.030	0.18	0.04	0.01	0.09	0.01	0.06	0.01	0.01	<0.019
1259 Img14- G3 - 2	0.38	0.12	0.01	0.01	<0.063	0.23	0.15	0.07	0.27	0.02	0.13	<0.011	<0.002	0.04
1259 Img14- G5 - 2	<0.010	0.11	0.00	0.00	<0.048	0.17	0.01	0.02	0.06	0.01	0.05	0.01	<0.002	<0.014
1259 Img13- G1 - 2	0.26	0.25	0.04	0.02	<0.038	0.15	0.01	0.11	0.33	0.04	0.17	0.02	<0.002	0.04
1259 Img15- G4 - 3	0.16	0.05	0.01	0.01	<0.016	0.26	0.01	0.01	0.05	0.01	0.01	0.03	<0.002	<0.021
1259 Img17 - G2 - 1	<0.007	0.15	0.01	0.00	<0.021	0.23	<0.012	0.01	0.09	0.01	0.06	0.02	0.00	0.01
1259 Img17 - G5 - 1	<0.005	0.06	<0.005	0.01	<0.037	0.21	<0.012	0.01	0.04	0.01	0.01	<0.016	0.00	<0.014
1259 Img15- G1 - 2	0.04	0.06	0.01	<0.001	<0.041	0.31	0.01	0.02	0.03	0.00	0.02	<0.010	<0.002	<0.013
1259 Img14- G2 - 3	0.00	0.15	<0.002	0.00	<0.015	0.23	<0.011	0.02	0.09	0.02	0.02	<0.017	0.00	0.04
1259 Img14- G5 - 5	0.01	0.04	0.02	0.01	<0.021	0.16	<0.011	0.02	0.11	0.01	<0.012	<0.014	0.00	0.02
1259 Img14- G2 - 4	0.04	0.08	0.05	0.01	0.03	0.20	0.04	0.04	0.09	0.01	0.05	<0.011	<0.002	0.01
1259 Img17 - G6 - 3	0.28	0.00	0.01	0.01	<0.019	0.20	<0.012	0.00	0.02	<0.001	0.01	<0.014	<0.002	0.01
1259 Img17 - G1 - 1	0.12	0.02	<0.001	0.00	<0.021	0.23	0.13	0.00	0.02	<0.001	<0.009	<0.010	<0.002	<0.010
1259 Img17 - G1 - 2	0.18	0.01	0.01	0.01	<0.035	0.33	0.13	0.03	0.00	<0.002	<0.007	<0.004	0.00	<0.014
1259 Img17 - G6 - 1	0.01	0.02	0.00	0.00	<0.022	0.12	<0.012	<0.001	0.03	0.00	0.04	<0.007	<0.002	<0.020
1259 Img17 - G6 - 4	0.10	0.05	0.01	0.01	<0.017	0.10	0.06	0.01	0.04	0.01	0.01	0.01	0.00	<0.002
1259 Img17 - G7 - 3	0.05	0.03	0.04	0.00	<0.046	0.15	<0.012	0.01	0.03	<0.002	0.01	<0.010	<0.002	<0.006
1259 Img15- G1 - 1	0.01	0.09	0.00	0.00	<0.033	0.20	<0.013	0.01	0.05	0.01	<0.020	<0.004	<0.002	0.01
1259 Img15- G5 - 1	0.02	0.03	0.01	0.01	<0.013	0.29	<0.012	0.01	0.01	<0.002	<0.002	<0.007	<0.002	<0.007
1259 Img14- G1 - 1	0.02	0.03	0.00	0.00	<0.032	0.33	0.01	<0.001	0.01	0.00	0.00	0.00	<0.002	0.01
1259 Img14- G1 - 2	<0.006	0.01	0.00	0.00	<0.023	0.23	<0.012	<0.001	0.01	<0.001	0.01	<0.003	<0.002	<0.010
1259 Img13- G1 - 4	0.05	0.03	0.05	0.02	0.05	0.15	0.04	0.03	0.09	<0.002	0.01	<0.007	<0.002	<0.011
1259 Img13- G2 - 2	0.18	0.07	0.01	0.01	<0.032	0.12	0.11	0.03	0.12	0.01	0.06	<0.012	<0.002	0.04
1259 mag G2 - 1	0.01	0.03	<0.004	<0.001	<0.013	0.18	<0.014	0.00	0.03	0.00	<0.022	<0.003	<0.003	<0.023
1259 mag G2 - 3	0.00	<0.002	<0.001	<0.001	<0.038	0.19	<0.013	0.00	0.00	<0.002	<0.010	<0.008	<0.003	<0.010
1259 mag G2 - 4	<0.011	0.03	0.01	<0.001	<0.036	0.21	<0.013	0.01	0.03	<0.002	0.01	0.02	<0.003	<0.007
1259 mag G4 - 1	<0.012	0.01	0.03	<0.002	<0.036	0.21	0.06	<0.002	0.01	0.00	0.03	0.03	<0.003	<0.012
1259 mag G5 - 7	<0.012	0.01	0.02	<0.002	<0.027	0.44	<0.016	<0.002	0.00	<0.002	<0.011	<0.008	<0.003	0.02
1268 img 8- G1 - 5	0.09	0.27	0.02	0.54	<0.040	0.29	0.01	0.34	1.02	0.13	0.53	0.09	0.01	0.08
1268 img 8- G2 - 4	0.03	0.17	0.11	0.19	0.12	0.25	0.02	0.17	0.49	0.07	0.20	0.05	0.01	0.03
1268 img 9- G2 - 1	0.05	0.08	0.01	0.07	<0.031	0.16	0.03	0.08	0.35	0.05	0.16	0.07	0.01	<0.031
1268 img 9- G2 - 2	0.08	0.24	0.02	0.27	<0.025	0.23	0.06	0.36	1.29	0.15	0.50	0.10	0.01	0.10
1268 img 11 G3 - 4	0.05	0.23	0.03	0.20	<0.041	0.21	<0.013	0.08	0.41	0.04	0.20	0.08	0.00	0.04
1268 img 11 G3 - 5	0.01	0.03	0.05	0.09	<0.043	0.22	0.05	0.01	0.14	0.01	0.06	0.03	0.00	0.02
1268 img 12 G1 - 2	0.02	0.21	0.02	0.11	<0.033	0.17	<0.013	0.20	0.74	0.10	0.44	0.05	0.00	<0.021
1268 img 12 G2 - 3	0.02	0.06	0.00	0.02	<0.041	0.14	<0.012	0.08	0.24	0.04	0.12	0.02	0.00	0.05
1268 img 12 G2 - 4	0.09	0.07	0.15	0.13	0.15	0.13	0.05	0.08	0.20	0.02	0.13	<0.019	<0.003	<0.012
1268 img 12 off G7 - 2	0.13	0.22	0.02	0.32	<0.056	0.23	0.38	0.31	1.38	0.15	0.56	0.09	0.01	0.10
1268 mag G2 - 3	0.05	0.12	<0.010	0.07	<0.032	0.17	<0.014	0.04	0.19	0.01	0.07	<0.008	0.01	<0.018
1268 mag G3 - 1	0.10	0.14	0.03	0.21	<0.036	0.24	0.03	0.10	0.42	0.04	0.15	0.04	0.01	0.04
1268 mag G4 - 3	<0.006	0.03	<0.003	0.03	0.02	0.20	0.02	0.01	0.08	0.01	0.02	0.02	<0.003	<0.020
1268 mag G10 - 3	0.09	0.19	0.02	0.18	<0.021	0.36	0.04	0.08	0.49	0.04	0.23	0.07	0.01	0.04
1268 img 12 G3 - 2	0.04	0.05	0.00	0.09	<0.017	0.16	0.11	0.06	0.27	0.02	0.06	0.02	0.00	<0.009
1268 img 10 G4 - 2	0.11	0.04	<0.009	0.04	<0.040	0.12	<0.015	0.04	0.16	0.01	0.03	0.03	0.01	<0.014
1268 img 12 G2 - 2	0.05	0.06	0.00	0.02	0.03	0.16	0.09	0.08	0.29	0.04	0.09	<0.007	0.00	<0.011
1268 mag G2 - 1	0.02	0.21	0.01	0.12	<0.049	0.17	0.10	0.09	0.44	0.06	0.20	0.05	0.01	0.01
1268 mag G4 - 1	0.05	0.03	0.03	0.04	<0.048	0.11	0.05	0.01	0.09	0.01	0.02	<0.013	<0.003	0.04
1268 mag G4 - 4	0.29	0.11	0.04	0.09	0.05	0.20	0.17	0.04	0.22	0.02	0.08	<0.009	0.01	<0.016
1268 mag G6 - 1	0.03	0.01	0.01	0.02	<0.020	0.17	0.09	0.01	0.06	0.01	<0.007	<0.006	<0.003	<0.020
852(1) - 3	1.62	0.30	0.60	4.80	4.83	0.48	1.53	0.35	1.30	0.19	0.64	0.13	<0.011	0.05
852(1) - 4	2.58	0.26	0.59	3.98	5.02	0.69	1.71	0.16	0.72	0.09	0.43	0.13	0.01	0.09
852(1) - 5	1.86	0.40	0.36	3.89	168.78	0.24	6.18	0.06	0.28	0.03	0.16	0.04	0.01	0.03
852(1) - 6	1.70	0.67	1.03	6.62	1.22	0.56	0.37	0.54	2.30	0.32	1.20	0.21	0.00	0.33
852(1) - 7	3.15	1.46	0.61	5.08	89.33	0.31	6.69	0.85	1.97	0.30	1.23	0.22	0.01	0.34
852(1) - 8	0.89	0.15	0.72	7.98	2.55	0.65	1.21	0.08	0.25	0.02	0.18	<0.007	<0.004	0.02
852(1) - 10	1.05	0.09	0.05	0.12	115.70	<0.032	3.58	0.03	0.16	0.04	0.12	<0.007	<0.006	<0.016
852(1) - 12	3.95	2.17	0.63	6.73	59.31	0.85	7.76	0.41	1.81	0.29	1.37	0.52	0.03	0.43
852(1) - 13	5.47	1.95	1.53	14.16	58.88	1.04	24.69	0.33	2.78	0.36	2.16	1.01	0.05	0.67
852(1) - 14	2.49	0.52	0.08	0.31	373.15	<0.032	6.47	0.10	0.44	0.06	0.31	0.08	0.01	<0.016

Element concentrations in ppm
BDL: below detection limit
NA: no analysis
$Eu/Eu^* = [(Eu_{CN}/(Sm_{CN}+Gd_{CN})/2)]$
$Y/Y^* = [(Y_{CN}/(Dy_{CN}+Ho_{CN})/2)]$
$Ce/Ce^* = [(Ce_{CN}/(La_{CN} \times Pr_{CN})^{0.5})]$
CN = chondrite normalised
Normalising values from Sun and McDonough (1989)

Appendix 5 Supplementary material for Mapping hydrothermal systems in IOCG deposits using apatite geochronology and geochemsitry: An example from Vulcan Cu-Au prospect

Appendix 5 Table A4: Magnetite and hematite LA-ICP-MS trace element data collected at Vulcan in this study

Included Data

Sample	Tb	Dy	Ho	Er	Tm	Yb	Lu	Hf	Ta	W	ΣREY	Eu/Eu*	Y/Y*	Ce/Ce*
1259 mag G3 - 6	<0.002	0.05	0.01	0.03	0.01	0.05	0.00	<0.005	0.01	<0.006	0.83		0.72	1.08
1259 mag G5 - 1	0.01	0.03	0.01	0.04	0.01	0.08	0.02	<0.005	0.01	<0.006	0.99		1.15	0.99
1259 mag G5 - 2	0.00	0.03	0.01	0.05	0.01	0.09	0.01	<0.006	0.00	<0.007	0.73		1.18	1.26
1259 mag G5 - 3	0.00	0.02	0.01	0.02	0.00	0.03	0.00	<0.005	0.02	<0.006	0.45		1.05	1.43
1259 mag G5 - 4	<0.002	0.04	0.00	0.01	0.01	0.03	0.01	<0.005	0.02	0.01	0.64		0.95	1.82
1259 mag G5 - 5	0.00	<0.007	0.01	0.02	0.01	0.02	0.01	<0.007	0.01	0.03	0.77			2.35
1259 mag G4 - 2	0.00	0.05	0.01	0.07	0.01	0.08	0.02	<0.005	0.00	0.02	1.46		1.71	1.76
1259 Img17 - G2 - 2	<0.001	0.03	0.01	0.02	0.01	0.05	0.01	<0.004	0.00	<0.005	0.61		0.77	3.17
1259 Img17 - G5 - 2	<0.001	0.05	0.01	0.03	0.00	0.03	0.01	<0.004	0.00	0.01	0.60		0.64	2.07
1259 Img17 - G6 - 2	<0.001	0.02	0.00	0.02	<0.001	0.02	0.00	<0.004	<0.002	<0.005	0.32		1.05	2.70
1259 Img17 - G7 - 2	<0.001	0.02	0.01	0.01	<0.001	0.01	0.00	0.01	<0.002	0.01	0.53		0.91	1.55
1259 Img15- G4 - 2	0.00	0.02	<0.001	0.04	<0.001	0.04	0.00	<0.004	0.01	0.01	0.71			1.27
1259 Img14- G2 - 5	<0.001	0.01	0.00	0.02	0.01	0.03	0.01	0.01	0.01	0.01	0.50		2.31	1.76
1259 Img14- G3 - 2	0.01	<0.005	0.01	0.01	0.00	0.01	0.00	0.01	0.02	<0.005	0.70			1.62
1259 Img14- G5 - 2	0.00	0.02	0.00	0.03	0.00	0.05	0.00	0.01	<0.002	<0.005	0.36		1.10	1.61
1259 Img13- G1 - 2	<0.001	0.05	0.01	0.04	0.01	0.03	0.01	<0.004	0.00	0.01	1.10		1.12	1.25
1259 Img15- G4 - 3	<0.001	<0.005	<0.001	0.01	0.00	0.01	0.00	<0.004	0.00	0.01	0.20			1.28
1259 Img17 - G2 - 1	<0.001	0.03	0.00	0.02	0.01	0.05	0.01	<0.004	0.01	0.01	0.47	0.62	1.11	3.09
1259 Img17 - G5 - 1	0.00	0.02	0.00	<0.004	0.00	0.02	0.00	<0.004	0.01	<0.005	0.18		0.52	0.90
1259 Img15- G1 - 2	0.00	0.01	0.00	0.02	<0.001	0.03	0.01	<0.004	0.01	<0.005	0.22		0.86	0.93
1259 Img14- G2 - 3	<0.001	0.02	0.01	0.02	<0.001	0.04	0.00	<0.004	<0.002	<0.005	0.41		1.00	1.27
1259 Img14- G5 - 5	0.00	0.01	<0.001	<0.003	<0.001	<0.011	<0.001	<0.004	<0.001	<0.005	0.21			1.54
1259 Img14- G2 - 4	<0.001	<0.005	0.00	0.01	<0.001	0.00	0.00	<0.004	<0.002	0.02	0.29			0.94
1259 Img17 - G6 - 3	<0.001	0.01	<0.001	<0.004	<0.001	<0.004	<0.001	<0.004	<0.001	<0.005	0.05			
1259 Img17 - G1 - 1	0.02	<0.004	<0.001	0.01	<0.001	0.02	<0.001	<0.004	0.00	<0.004	0.08			
1259 Img17 - G1 - 2	<0.001	<0.006	<0.002	<0.004	0.00	<0.007	0.00	0.01	<0.001	<0.006	0.05			
1259 Img17 - G6 - 1	<0.001	<0.005	<0.001	<0.004	0.00	0.01	<0.001	<0.004	<0.003	0.01	0.10			
1259 Img17 - G6 - 4	0.00	<0.005	<0.001	0.00	<0.001	<0.008	<0.001	<0.004	<0.001	<0.005	0.14			1.28
1259 Img17 - G7 - 3	<0.001	<0.005	<0.001	<0.004	<0.001	0.01	<0.001	<0.004	<0.002	<0.005	0.08			
1259 Img15- G1 - 1	0.00	<0.005	0.01	<0.004	0.00	<0.013	<0.001	<0.004	0.00	<0.005	0.18			2.12
1259 Img15- G5 - 1	<0.001	<0.005	<0.001	<0.004	<0.001	0.02	0.00	<0.004	0.01	<0.005	0.06			
1259 Img14- G1 - 1	<0.001	<0.005	<0.001	<0.004	<0.001	<0.005	0.00	<0.004	<0.003	0.00	0.07			
1259 Img14- G1 - 2	<0.001	<0.005	0.00	<0.004	<0.001	<0.009	<0.001	<0.004	<0.003	<0.005	0.03			
1259 Img13- G1 - 4	<0.001	<0.005	<0.001	<0.004	0.00	0.00	<0.001	<0.004	0.01	0.01	0.16			
1259 Img13- G2 - 2	0.00	<0.005	0.00	<0.004	<0.001	0.02	<0.001	<0.004	0.01	<0.005	0.34			1.73
1259 mag G2 - 1	<0.002	<0.005	0.00	<0.005	<0.001	0.01	0.00	<0.005	0.00	<0.006	0.08			2.16
1259 mag G2 - 3	<0.002	0.01	<0.001	<0.005	<0.001	<0.002	<0.002	<0.005	<0.001	<0.006	0.01			
1259 mag G2 - 4	<0.002	0.02	<0.001	<0.004	<0.001	0.01	<0.002	<0.005	<0.002	<0.006	0.13			
1259 mag G4 - 1	<0.002	<0.006	<0.002	<0.005	0.00	<0.005	0.00	<0.006	0.00	<0.007	0.09			
1259 mag G5 - 7	<0.002	<0.006	0.00	<0.005	0.00	0.01	<0.002	<0.006	0.00	<0.007	0.04			
1268 img 8- G1 - 5	0.01	0.07	0.01	0.03	0.01	0.03	0.01	<0.004	0.03	<0.005	2.62	0.24	0.68	1.17
1268 img 8- G2 - 4	0.01	0.04	0.00	0.02	0.00	0.04	0.00	0.01	0.01	0.03	1.29	0.89	1.58	1.12
1268 img 9- G2 - 1	0.00	0.01	0.00	0.02	<0.001	<0.006	<0.001	<0.004	0.01	<0.005	0.84		1.64	1.35
1268 img 9- G2 - 2	0.00	0.05	0.01	0.02	0.00	0.04	0.00	<0.004	0.02	<0.005	2.87	0.33	1.00	1.35
1268 img 11 G3 - 4	0.02	0.04	0.01	0.02	<0.001	0.02	0.00	<0.005	0.01	0.03	1.20	0.22	0.70	1.86
1268 img 11 G3 - 5	<0.001	0.01	0.00	0.01	<0.001	0.01	<0.001	0.01	0.00	<0.005	0.33	0.52	0.54	3.51
1268 img 12 G1 - 2	0.01	0.01	0.00	0.02	<0.001	<0.007	0.00	<0.005	0.01	0.05	1.80		2.11	1.27
1268 img 12 G2 - 3	0.00	0.01	0.00	<0.004	<0.001	<0.007	<0.001	0.01	0.01	0.02	0.64	0.44	0.99	1.05
1268 img 12 G2 - 4	0.00	<0.005	0.00	0.02	0.00	0.02	<0.002	<0.005	0.00	0.05	0.53			1.23
1268 img 12 off G7 - 2	0.02	0.05	0.01	0.02	<0.001	0.02	<0.002	0.01	0.01	<0.006	2.93	0.26	0.86	1.56
1268 mag G2 - 3	0.00	0.02	<0.002	0.02	<0.001	<0.008	0.00	<0.005	<0.003	0.01	0.50			2.52
1268 mag G3 - 1	0.00	0.05	0.00	0.01	0.00	0.03	<0.002	<0.007	0.01	<0.008	1.04	0.66	0.89	1.63
1268 mag G4 - 3	<0.002	<0.005	0.01	0.01	<0.001	<0.006	0.00	0.01	0.01	<0.006	0.18			2.28
1268 mag G10 - 3	0.01	0.03	0.01	0.01	<0.001	0.02	0.00	<0.005	0.01	0.02	1.23	0.41	1.08	2.22
1268 img 12 G3 - 2	0.00	0.01	0.00	0.00	<0.001	0.01	<0.001	<0.004	0.00	0.01	0.51		0.76	2.03
1268 img 10 G4 - 2	<0.002	0.01	<0.002	<0.005	<0.001	<0.007	<0.002	<0.005	0.01	<0.006	0.32			2.12
1268 img 12 G2 - 2	<0.001	<0.005	<0.001	<0.004	0.00	<0.008	<0.001	<0.004	0.01	0.03	0.56			1.27
1268 mag G2 - 1	<0.002	0.02	0.01	0.01	<0.001	0.02	0.00	<0.005	0.01	0.01	1.14	1.57	1.28	1.43
1268 mag G4 - 1	<0.002	<0.006	<0.002	0.01	<0.002	<0.005	<0.002	<0.006	0.00	<0.007	0.20			2.45
1268 mag G4 - 4	0.00	<0.005	0.00	0.01	<0.001	<0.007	<0.002	<0.005	0.01	0.03	0.49			1.91
1268 mag G6 - 1	<0.002	0.01	<0.002	<0.005	<0.002	0.01	<0.002	<0.006	<0.002	<0.007	0.10			1.68
852(1) - 3	0.02	0.04	0.01	0.04	0.03	0.14	0.01	<0.007	0.01	0.27	3.24		1.21	1.23
852(1) - 4	0.02	0.07	0.01	0.07	0.01	0.04	0.01	<0.004	0.03	0.21	2.10	0.24	0.67	1.45
852(1) - 5	0.00	0.03	0.01	0.08	0.01	0.07	0.01	<0.008	0.03	1.12	1.21	0.43	1.84	1.66
852(1) - 6	0.01	0.11	0.04	0.10	0.02	0.12	0.02	0.02	0.05	0.10	5.99	0.04	0.76	1.34
852(1) - 7	0.05	0.17	0.04	0.19	0.03	0.16	0.03	<0.006	0.07	0.18	7.05	0.10	1.29	0.95
852(1) - 8	<0.004	0.02	0.00	0.04	0.00	0.02	0.00	0.00	0.06	0.54	0.79		1.75	1.55
852(1) - 10	0.01	0.01	0.00	0.01	<0.002	0.03	0.01	<0.001	0.01	0.04	0.50		1.48	1.13
852(1) - 12	0.07	0.32	0.08	0.19	0.02	0.29	0.06	0.03	0.04	1.13	8.08	0.21	1.06	1.27
852(1) - 13	0.07	0.43	0.13	0.18	0.04	0.22	0.05	0.03	0.08	0.95	10.43	0.20	0.62	1.96
852(1) - 14	0.02	0.05	0.02	0.06	0.01	0.03	0.03	<0.002	0.00	0.10	1.75		1.33	1.35

Element concentrations in ppm
BDL: below detection limit
NA: no analysis
$Eu/Eu^* = [(Eu_{CN}/(Sm_{CN}+Gd_{CN})/2)]$
$Y/Y^* = [(Y_{CN}/(Dy_{CN}+Ho_{CN})/2)]$
$Ce/Ce^* = [(Ce_{CN}/(La_{CN} \times Pr_{CN})^{0.5})]$
CN = chondrite normalised
Normalising values from Sun and McDonough (1989)

Appendix 5 Supplementary material for Mapping hydrothermal systems in IOCG deposits using apatite geochronology and geochemsitry: An example from Vulcan Cu-Au prospect

Appendix 5 Table A4: Magnetite and hematite LA-ICP-MS trace element data collected at Vulcan in this study

Included Data

Sample	Drill hole	Mineral	Comment
852(1) - 15	VUD 009 852	Hematite	High Al
852(1) - 21	VUD 009 852	Hematite	High Al
852(1) - 22	VUD 009 852	Hematite	High Al
852(1) - 23	VUD 009 852	Hematite	High Al
852(1) - 29	VUD 009 852	Hematite	High Al and Mn
852(1) - 30	VUD 009 852	Hematite	High Al and Mg. Co inclusion
852(1) - 32	VUD 009 852	Hematite	High Al, Mn and Mg
852(1) - 33	VUD 009 852	Hematite	High Al and Mg
852(1) - 35	VUD 009 852	Hematite	High Mg and Al
852(1) - 36	VUD 009 852	Hematite	High Al and Mn
852(1) - 37	VUD 009 852	Hematite	High Al, Mn, Mg and Co
852(1) - 38	VUD 009 852	Hematite	High Al and Mg. Co and Mn inclusions
852(1) - 39	VUD 009 852	Hematite	High Al, Mg and Mn
852(1) - 40	VUD 009 852	Hematite	High Al and Mg
852(1) - 41	VUD 009 852	Hematite	High Al, Mg and Mn and P
852(1) - 42	VUD 009 852	Hematite	High Al, Mg and Mn
852(1) - 44	VUD 009 852	Hematite	High Al and Mg
852(1) - 50	VUD 009 852	Hematite	High AL and Mn
852(1) - 51	VUD 009 852	Hematite	High Al, Mn and Mg
852(1) - 52	VUD 009 852	Hematite	High Al
852(1) - 56	VUD 009 852	Hematite	Mg inclusions. High Al
852(1) - 58	VUD 009 852	Hematite	High Al, Mg
973(1) - 20	VUD 009 973	Hematite	High Al and V
973(1) - 21	VUD 009 973	Hematite	High Al and V. Ti and Mn inclusion before signal.
973(1) - 26	VUD 009 973	Hematite	
973(1) - 36	VUD 009 973	Hematite	High Al, V, Mn, U
973(1) - 43	VUD 009 973	Hematite	High Al, Mn and V
973(1) - 31	VUD 009 973	Hematite	Hi Al. REE BDL.
973(1) - 32	VUD 009 973	Hematite	W peak. REE BDL.
994(1) - 1	VUD 009 994	Hematite	High Al and Mg
994(1) - 2	VUD 009 994	Hematite	High Al and Mg
994(1) - 6	VUD 009 994	Hematite	High Al and Mg. U peak. Nb.
994(1) - 11	VUD 009 994	Hematite	Co inclusions. High Al.
994(1) - 12	VUD 009 994	Hematite	High Al and Mg
994(1) - 13	VUD 009 994	Hematite	High Al, Mg, Mn and Nb.
994(1) - 16	VUD 009 994	Hematite	High AL and Mg.
994(1) - 18	VUD 009 994	Hematite	High Al, Mn, Mg and Nb.
994(1) - 20	VUD 009 994	Hematite	High Al, Mg, Mn and Nb.
994(1) - 21	VUD 009 994	Hematite	Mn inclusions. High Al and Mg
994(1) - 22	VUD 009 994	Hematite	Mg inclusions. High Al Mg and Mn.
994(1) - 24	VUD 009 994	Hematite	Al Mg inclusion. Ni inclusion
994(1) - 25	VUD 009 994	Hematite	High Al, Mg and Mn
994(1) - 27	VUD 009 994	Hematite	Al inclusions. High Mg and Mn
994(1) - 28	VUD 009 994	Hematite	Mn and U inclusion?
994(1) - 31	VUD 009 994	Hematite	High Al and Mg
994(1) - 32	VUD 009 994	Hematite	High Al, Mn and Mg
994(1) - 33	VUD 009 994	Hematite	Mg and Mn inclusions. High Al.
994(1) - 35	VUD 009 994	Hematite	High Al, Mg and Mn
994(1) - 36	VUD 009 994	Hematite	High Al, Mg and Mn
994(1) - 38	VUD 009 994	Hematite	Al and Mg inclusions, High Al and Mg
994(1) - 40	VUD 009 994	Hematite	Mg inclusions. High Al Mg.
994(1) - 41	VUD 009 994	Hematite	High Al and Mg
994(1) - 42	VUD 009 994	Hematite	High Mg and Al
994(1) - 43	VUD 009 994	Hematite	Al Si Mn Mg inclusions
994(1) - 44	VUD 009 994	Hematite	Al Si Mn Mg inclusions
994(1) - 45	VUD 009 994	Hematite	High Al, Mn and Mg
994(1) - 47	VUD 009 994	Hematite	High Al and Mg
994(1) - 48	VUD 009 994	Hematite	High Al, Mn and Mg
994(1) - 49	VUD 009 994	Hematite	High Al, Mn and Mg
994(1) - 50	VUD 009 994	Hematite	High Al, Mn and Mg
994(1) - 51	VUD 009 994	Hematite	High Al and Mg
994(1) - 52	VUD 009 994	Hematite	High Al and Mg. Al inclusion after signal
994(1) - 53	VUD 009 994	Hematite	High Al and Mg. Ba inclusion after signal
994(1) - 55	VUD 009 994	Hematite	High Al, Mg and Nb.
994(1) - 56	VUD 009 994	Hematite	High Al, Mg and Mn
994(1) - 57	VUD 009 994	Hematite	Al inclusion after signal
994(1) - 58	VUD 009 994	Hematite	Mg inclusion
994(1) - 59	VUD 009 994	Hematite	High Al, Mg and Mn
994(1) - 60	VUD 009 994	Hematite	Mg and Al inclusions
994(1) - 61	VUD 009 994	Hematite	Mg and Al inclusions
994(1) - 62	VUD 009 994	Hematite	Mg and Al inclusions. Off hem grain after signal

Element concentrations in ppm
BDL: below detection limit
NA: no analysis
$Eu/Eu^* = [(Eu_{CN}/(Sm_{CN}+Gd_{CN})/2)]$
$Y/Y^* = [(Y_{CN}/(Dy_{CN}+Ho_{CN})/2)]$
$Ce/Ce^* = [(Ce_{CN}/(La_{CN} \times Pr_{CN})^{0.5})]$
CN = chondrite normalised
Normalising values from Sun and McDonough (1989)

Appendix 5 Supplementary material for Mapping hydrothermal systems in IOCG deposits using apatite geochronology and geochemsitry: An example from Vulcan Cu-Au prospect

Appendix 5 Table A4: Magnetite and hematite LA-ICP-MS trace element data collected at Vulcan in this study

Included Data

Sample	Mg	Al	Si	P	Ca	Ti	V	Mn	Fe	Co	Ni	Cu	Zn	As
852(1) - 15	188	904	1256	373	703	8	36	75	690000	12.76	133.84	4.55	4.25	34.90
852(1) - 21	63	396	439	<29.448	<91.532	4	22	16	690000	7.56	75.82	<0.870	0.80	9.97
852(1) - 22	34	499	611	60	106	3	29	34	690000	10.92	123.17	2.74	2.19	22.24
852(1) - 23	82	496	720	40	303	3	34	28	690000	9.15	132.16	10.13	2.52	27.29
852(1) - 29	36	470	645	206	303	3	21	84	690000	16.59	122.59	2.85	3.06	17.29
852(1) - 30	637	537	1839	78	322	6	31	80	690000	20.53	140.22	7.46	2.67	36.77
852(1) - 32	149	771	1124	77	208	7	26	55	690000	8.42	105.45	4.04	2.40	35.52
852(1) - 33	289	333	960	27	87	4	32	42	690000	14.07	94.31	<0.577	1.55	23.31
852(1) - 35	754	463	2013	28	319	7	36	93	690000	17.47	74.97	<0.659	2.93	35.41
852(1) - 36	58	1049	1564	495	827	1	6	196	690000	45.88	249.24	2.61	11.98	19.32
852(1) - 37	218	927	1068	48	105	3	27	250	690000	79.62	189.31	18.49	14.74	19.37
852(1) - 38	678	608	1607	<16.969	213	6	40	52	690000	23.68	72.06	<0.550	2.89	23.12
852(1) - 39	312	342	1068	184	147	5	28	101	690000	22.46	148.78	1.17	6.24	12.15
852(1) - 40	318	588	1270	49	208	5	32	38	690000	11.27	115.31	3.60	1.47	30.55
852(1) - 41	173	703	1191	744	1587	4	21	142	690000	9.45	78.42	3.47	6.54	19.90
852(1) - 42	321	533	1284	36	124	5	26	46	690000	11.83	112.93	1.99	2.08	29.20
852(1) - 44	460	401	1422	23	133	7	31	36	690000	16.19	126.56	1.86	2.25	26.79
852(1) - 50	70	493	687	259	431	5	27	103	690000	15.37	118.42	14.41	6.17	29.41
852(1) - 51	185	606	917	189	316	7	33	80	690000	15.86	140.13	9.48	5.85	21.85
852(1) - 52	66	492	511	<31.501	<102.291	4	30	13	690000	8.98	104.45	2.91	1.29	17.39
852(1) - 56	73	655	775	24	<98.230	7	40	13	690000	6.65	104.77	6.39	1.10	34.38
852(1) - 58	158	811	1220	121	288	8	36	40	690000	12.59	120.46	14.83	2.93	25.95
973(1) - 20	33	862	664	69	<119.688	320	337	69	690000	6.23	91.11	25.94	10.19	13.65
973(1) - 21	33	548	405	37	<124.975	245	316	45	690000	6.03	69.27	6.93	3.17	22.69
973(1) - 26	23	661	823	122	94	349	209	109	690000	6.31	129.91	35.86	11.39	17.66
973(1) - 36	45	1051	1390	237	213	433	247	118	690000	12.08	113.42	81.72	13.17	13.81
973(1) - 43	32	605	810	103	151	3473	275	286	690000	168.72	122.27	36.55	23.89	5.73
973(1) - 31	32	675	442	<29.512	<99.475	251	110	62	690000	10.85	43.92	1.32	6.94	0.80
973(1) - 32	21	511	522	36	<67.059	243	249	56	690000	8.89	52.07	<0.543	7.38	1.09
994(1) - 1	691	555	2474	<19.753	171	12	19	50	690000	12.57	87.87	3.51	3.93	31.18
994(1) - 2	581	290	1450	<20.541	<81.017	54	25	41	690000	14.66	91.67	2.31	2.36	31.98
994(1) - 6	459	461	1802	35	144	11	22	25	690000	5.82	87.46	<0.523	2.90	46.58
994(1) - 11	64	279	484	<28.502	<59.994	130	23	16	690000	40.15	111.14	17.97	1.37	26.53
994(1) - 12	328	222	1280	21	62	7	17	37	690000	11.44	87.20	1.68	1.97	38.19
994(1) - 13	361	314	1642	28	79	21	13	44	690000	4.54	96.65	1.15	1.73	48.98
994(1) - 16	346	253	1015	<23.751	245	227	26	33	690000	12.06	104.29	10.05	2.06	28.42
994(1) - 18	480	648	2040	<33.607	<100.417	98	33	38	690000	10.06	91.02	5.61	4.15	46.99
994(1) - 20	555	396	2215	<21.166	340	9	30	45	690000	9.76	91.83	<0.460	9.13	51.06
994(1) - 21	682	410	1853	23	137	8	23	90	690000	9.16	86.77	0.85	3.68	20.75
994(1) - 22	519	378	1484	<15.582	<72.838	6	20	58	690000	11.10	94.57	3.63	3.49	26.27
994(1) - 24	332	379	1514	<23.113	<95.376	11	21	49	690000	11.52	93.31	<0.740	3.06	45.97
994(1) - 25	269	440	1212	127	106	5	18	112	690000	7.85	62.23	12.92	13.46	21.64
994(1) - 27	496	428	1852	61	284	56	18	89	690000	11.79	83.36	8.67	3.67	38.61
994(1) - 28	252	570	1201	179	91	379	24	129	690000	13.26	55.69	24.43	7.56	33.68
994(1) - 31	439	669	1248	<41.205	<132.589	20	38	57	690000	14.22	50.84	<0.932	2.48	32.97
994(1) - 32	218	631	2047	<22.823	576	7	28	49	690000	5.90	43.66	<0.586	3.62	30.83
994(1) - 33	195	633	880	<22.646	1479	4	18	50	690000	7.31	41.57	2.59	2.32	28.10
994(1) - 35	743	515	2476	144	220	112	25	92	690000	9.55	89.80	10.84	6.56	36.59
994(1) - 36	1124	487	2749	112	332	183	27	89	690000	12.64	100.04	20.15	4.72	33.68
994(1) - 38	654	404	1928	<21.001	160	6	23	52	690000	13.97	94.32	1.51	3.37	38.28
994(1) - 40	492	219	1413	<20.496	217	9	19	33	690000	12.88	90.82	1.09	4.44	31.12
994(1) - 41	89	208	573	<19.365	<72.933	20	21	31	690000	19.54	105.26	1.44	1.21	22.82
994(1) - 42	690	372	1870	45	316	73	20	59	690000	11.16	89.68	3.75	4.05	28.62
994(1) - 43	814	1660	4798	164	170	170	19	117	690000	10.56	98.71	16.98	22.87	33.11
994(1) - 44	570	1325	3880	122	179	124	20	76	690000	9.37	94.47	13.27	12.95	33.89
994(1) - 45	550	538	2436	185	210	302	20	233	690000	18.57	107.24	44.22	10.94	28.86
994(1) - 47	358	606	1552	39	<76.672	18	25	65	690000	13.31	64.04	5.09	4.30	40.88
994(1) - 48	649	793	2667	45	225	80	25	117	690000	19.82	53.07	7.04	9.00	15.66
994(1) - 49	646	409	2213	160	194	322	30	125	690000	11.78	114.03	17.85	10.55	24.78
994(1) - 50	587	668	2663	462	244	69	23	253	690000	12.95	109.44	47.73	34.82	10.60
994(1) - 51	544	233	1770	24	77	25	24	41	690000	9.81	94.24	0.72	4.07	21.77
994(1) - 52	312	700	1563	<24.583	145	45	23	54	690000	9.14	50.70	3.20	3.42	38.29
994(1) - 53	146	995	1304	113	114	128	21	63	690000	7.72	34.00	7.26	4.07	33.56
994(1) - 55	270	893	1433	<18.601	<65.096	28	33	23	690000	9.22	55.37	1.21	1.39	27.60
994(1) - 56	692	580	2432	177	187	401	26	143	690000	14.83	62.71	24.59	9.47	41.23
994(1) - 57	690	656	1883	58	149	198	67	248	690000	20.58	99.45	17.32	7.28	34.18
994(1) - 58	469	394	1571	30	165	48	29	79	690000	9.07	86.32	6.72	2.17	35.11
994(1) - 59	555	605	1739	75	245	54	25	102	690000	11.55	61.57	8.43	5.28	32.58
994(1) - 60	343	532	1329	<25.531	92	13	17	41	690000	10.45	68.51	1.96	2.70	25.21
994(1) - 61	242	700	1872	66	<84.636	157	24	62	690000	13.47	91.57	7.92	3.89	41.55
994(1) - 62	352	999	2361	90	162	58	21	68	690000	7.19	76.65	8.10	6.66	63.33

Element concentrations in ppm
BDL: below detection limit
NA: no analysis
$Eu/Eu^* = [(Eu_{CN}/(Sm_{CN}+Gd_{CN})/2)]$
$Y/Y^* = [(Y_{CN}/(Dy_{CN}+Ho_{CN})/2)]$
$Ce/Ce^* = [(Ce_{CN}/(La_{CN} \times Pr_{CN})^{0.5})]$
CN = chondrite normalised
Normalising values from Sun and McDonough (1989)

Appendix 5 Table A4: Magnetite and hematite LA-ICP-MS trace element data collected at Vulcan in this study

Included Data

Sample	Sr	Y	Zr	Nb	Mo	Sn	Ba	La	Ce	Pr	Nd	Sm	Eu	Gd
852(1) - 15	2.23	1.18	1.49	9.68	19.03	0.92	3.40	0.36	1.89	0.29	1.48	0.37	0.05	0.24
852(1) - 21	0.89	0.07	0.65	2.01	0.43	5.66	1.16	0.08	0.34	0.02	0.17	0.07	<0.007	0.06
852(1) - 22	0.85	0.22	0.30	2.65	15.27	0.58	1.83	0.12	0.46	0.06	0.29	0.01	0.02	0.03
852(1) - 23	1.75	0.28	0.47	4.89	5.68	0.34	2.68	0.92	2.33	0.22	1.19	0.22	0.02	0.08
852(1) - 29	1.07	0.57	0.18	1.49	29.64	0.30	3.02	0.09	0.42	0.06	0.28	0.04	0.01	0.11
852(1) - 30	2.68	0.65	0.86	8.37	8.30	0.68	2.97	0.77	2.96	0.33	1.45	0.21	0.02	0.18
852(1) - 32	1.79	0.51	0.58	6.26	10.64	0.57	2.07	0.67	2.48	0.22	0.93	0.16	0.01	0.19
852(1) - 33	1.52	0.23	0.67	3.19	2.28	0.38	0.76	0.15	0.56	0.05	0.19	0.05	0.01	0.02
852(1) - 35	2.80	0.80	0.79	7.00	2.85	0.88	0.90	0.35	2.14	0.16	1.29	0.24	0.02	0.10
852(1) - 36	4.37	1.03	0.16	0.81	138.37	0.06	7.59	0.12	0.63	0.10	0.49	0.16	0.02	0.11
852(1) - 37	2.45	0.25	0.20	1.74	12.47	0.22	15.75	0.43	1.03	0.09	0.42	0.13	0.01	0.04
852(1) - 38	4.94	0.36	0.54	6.07	0.29	0.81	1.01	0.35	1.13	0.16	0.70	0.10	0.00	0.09
852(1) - 39	1.65	0.44	0.87	7.40	17.42	0.47	2.60	0.07	0.55	0.07	0.30	0.03	0.00	0.07
852(1) - 40	2.12	0.44	0.92	7.41	7.24	0.63	2.33	0.93	2.63	0.25	1.09	0.12	0.02	0.15
852(1) - 41	4.39	1.90	0.51	3.40	14.64	0.52	3.40	0.42	1.91	0.33	1.46	0.26	0.07	0.30
852(1) - 42	1.52	0.50	0.50	4.20	3.36	0.47	1.69	0.33	1.27	0.16	0.42	0.17	0.02	0.07
852(1) - 44	2.46	0.43	0.47	4.78	1.46	0.40	1.29	0.90	2.73	0.38	1.70	0.36	0.02	0.05
852(1) - 50	1.15	0.82	0.50	6.38	25.75	0.93	4.36	0.20	1.12	0.17	0.86	0.20	0.03	0.24
852(1) - 51	2.02	0.58	0.71	9.19	23.42	0.54	3.07	0.33	1.27	0.16	0.71	0.21	0.01	0.06
852(1) - 52	0.79	0.09	0.30	2.87	1.23	1.58	0.80	0.14	0.47	0.05	0.20	0.03	<0.002	0.06
852(1) - 56	1.93	0.21	0.62	6.31	1.17	0.70	0.97	0.58	1.57	0.20	0.76	0.12	0.01	0.11
852(1) - 58	1.48	0.56	0.76	15.02	9.54	0.77	1.43	1.27	3.08	0.38	1.44	0.31	<0.001	0.25
973(1) - 20	2.17	0.54	0.50	1.15	3.11	0.83	4.40	2.35	3.25	0.27	0.89	<0.011	<0.005	0.07
973(1) - 21	1.08	0.37	0.39	0.42	1.95	0.84	1.50	2.91	5.47	0.37	1.12	0.11	<0.002	0.04
973(1) - 26	1.59	0.75	0.88	0.39	16.86	0.76	5.88	0.57	1.49	0.06	0.32	0.09	0.03	0.03
973(1) - 36	3.93	0.90	3.61	1.53	23.02	1.78	8.40	0.44	1.06	0.08	0.24	0.04	0.03	0.07
973(1) - 43	1.42	1.38	26.23	37.08	7.57	10.26	8.60	0.19	0.67	0.05	0.24	<0.009	<0.010	0.19
973(1) - 31	0.32	0.01	<0.002	<0.003	<0.050	0.85	0.68	0.04	0.05	0.01	<0.010	<0.011	<0.008	<0.024
973(1) - 32	0.04	0.03	0.01	0.00	0.12	0.84	0.09	0.01	0.03	<0.001	<0.006	<0.007	<0.003	<0.016
994(1) - 1	2.15	0.88	0.33	11.32	0.62	0.81	1.10	0.57	2.13	0.30	1.11	0.26	0.02	0.13
994(1) - 2	1.27	0.88	0.65	18.43	2.26	1.28	0.90	0.31	1.17	0.15	0.73	0.18	0.02	0.11
994(1) - 6	1.94	0.81	1.15	18.31	1.26	0.79	1.24	0.45	1.66	0.25	0.90	0.22	0.02	0.17
994(1) - 11	0.62	0.17	1.20	6.98	3.63	1.73	0.56	0.12	0.46	0.04	0.28	<0.008	<0.003	0.04
994(1) - 12	1.00	0.81	0.26	13.15	0.62	0.85	1.23	0.54	2.18	0.30	1.65	0.32	0.03	0.19
994(1) - 13	1.40	0.84	0.66	16.96	0.94	0.50	0.97	0.39	1.80	0.19	1.00	0.27	0.03	0.11
994(1) - 16	1.46	0.57	0.99	17.73	4.03	2.25	1.06	0.50	1.61	0.15	0.61	0.14	0.02	0.09
994(1) - 18	1.38	0.61	0.70	20.55	3.32	1.26	1.98	0.35	1.71	0.13	0.68	0.35	<0.002	0.08
994(1) - 20	3.13	0.69	0.52	20.03	0.22	0.91	3.74	0.29	1.07	0.17	0.74	0.14	0.03	0.11
994(1) - 21	1.11	0.81	0.35	18.13	0.24	0.92	0.76	0.33	1.60	0.22	0.92	0.22	0.03	0.07
994(1) - 22	0.74	1.00	0.35	11.53	0.21	0.87	1.43	0.42	1.41	0.20	1.03	0.25	0.02	0.19
994(1) - 24	1.16	0.79	0.44	10.76	1.22	1.03	0.30	0.46	1.82	0.27	0.92	0.27	0.03	0.16
994(1) - 25	1.26	0.84	0.24	7.47	0.81	0.64	2.28	0.29	1.17	0.14	0.69	0.13	0.01	0.06
994(1) - 27	1.78	1.11	0.63	11.15	2.38	0.77	3.86	0.93	3.36	0.47	1.83	0.41	0.03	0.18
994(1) - 28	2.18	0.78	2.04	10.25	8.61	1.88	3.54	0.34	1.06	0.12	0.70	0.18	0.04	0.18
994(1) - 31	3.11	0.41	0.48	10.16	5.44	1.30	2.38	0.37	1.21	0.12	0.38	0.07	0.02	0.05
994(1) - 32	3.63	0.62	0.68	13.90	4.69	1.20	2.81	0.17	0.52	0.08	0.30	0.02	0.00	0.03
994(1) - 33	2.48	0.38	0.31	7.27	4.29	0.90	1.22	2.09	6.14	0.94	3.50	0.56	0.03	0.30
994(1) - 35	2.57	1.52	1.26	21.38	4.71	0.76	2.92	0.82	2.92	0.38	1.67	0.33	0.02	0.20
994(1) - 36	2.33	1.35	1.77	30.11	4.42	1.37	2.90	1.93	5.56	0.59	2.41	0.36	0.04	0.18
994(1) - 38	2.21	0.60	0.34	13.52	1.80	0.67	1.73	0.42	1.48	0.21	0.70	0.14	0.00	0.14
994(1) - 40	2.76	0.62	0.24	16.30	0.66	0.71	1.17	0.71	2.28	0.25	1.06	0.12	0.02	0.13
994(1) - 41	0.74	0.14	0.50	0.64	2.29	0.56	0.25	0.12	0.35	0.03	0.15	0.06	<0.004	<0.018
994(1) - 42	2.02	1.12	0.77	10.47	2.00	0.67	1.12	0.76	2.48	0.31	1.67	0.30	0.03	0.18
994(1) - 43	1.75	1.34	1.34	15.31	4.11	0.95	2.50	0.79	3.47	0.49	1.74	0.41	0.06	0.27
994(1) - 44	2.16	1.03	1.57	15.76	4.76	0.91	3.21	0.28	1.25	0.17	0.78	0.17	0.04	0.17
994(1) - 45	3.11	1.43	2.63	13.84	9.56	1.02	6.32	1.15	4.33	0.45	2.08	0.35	0.05	0.23
994(1) - 47	1.78	0.69	0.82	23.31	2.18	1.15	1.63	0.99	2.51	0.34	1.06	0.31	0.03	0.18
994(1) - 48	1.67	0.86	1.01	12.12	13.08	1.29	4.11	0.77	2.72	0.38	1.41	0.27	0.03	0.13
994(1) - 49	1.82	1.25	2.15	21.98	6.36	1.91	4.22	1.33	4.36	0.53	2.36	0.64	0.03	0.37
994(1) - 50	2.41	1.71	0.88	24.45	4.45	0.89	7.75	0.75	2.95	0.39	1.85	0.28	0.03	0.17
994(1) - 51	0.89	0.94	0.64	26.39	2.39	1.14	0.70	0.47	2.07	0.28	1.32	0.17	0.04	0.25
994(1) - 52	2.12	0.88	0.80	26.65	4.87	1.59	1.54	0.42	1.76	0.20	0.78	0.22	<0.002	0.20
994(1) - 53	2.28	0.54	0.78	9.97	8.23	1.33	1.81	0.20	0.66	0.07	0.30	0.09	0.01	0.05
994(1) - 55	1.07	0.42	1.08	83.73	3.80	5.60	0.74	0.18	0.80	0.09	0.43	0.07	0.01	0.11
994(1) - 56	19.28	1.36	2.86	17.53	9.90	1.91	4.28	1.02	3.77	0.51	2.10	0.40	0.02	0.29
994(1) - 57	2.15	1.31	3.45	24.01	18.03	1.88	3.19	0.52	2.59	0.35	1.09	0.45	0.09	0.25
994(1) - 58	1.86	1.01	1.20	25.06	4.69	1.88	1.38	0.50	1.77	0.24	1.43	0.27	0.03	0.15
994(1) - 59	3.92	0.98	1.13	14.23	4.42	1.03	6.39	1.11	3.44	0.41	1.80	0.45	0.01	0.23
994(1) - 60	1.76	0.44	1.19	7.74	1.03	0.77	0.72	0.28	1.03	0.13	0.40	0.03	0.01	0.15
994(1) - 61	1.97	0.57	1.21	22.88	4.72	1.84	1.72	0.48	1.29	0.13	0.58	0.11	0.02	0.14
994(1) - 62	3.87	0.99	1.09	27.84	2.54	1.07	2.54	1.62	5.40	0.61	2.17	0.42	0.04	0.23

Element concentrations in ppm
BDL: below detection limit
NA: no analysis
$Eu/Eu^* = [(Eu_{CN}/(Sm_{CN}+Gd_{CN})/2)]$
$Y/Y^* = [(Y_{CN}/(Dy_{CN}+Ho_{CN})/2)]$
$Ce/Ce^* = [(Ce_{CN}/(La_{CN} \times Pr_{CN})^{0.5})]$
CN = chondrite normalised
Normalising values from Sun and McDonough (1989)

Appendix 5 Supplementary material for Mapping hydrothermal systems in IOCG deposits using apatite geochronology and geochemsitry: An example from Vulcan Cu-Au prospect

Appendix 5 Table A4: Magnetite and hematite LA-ICP-MS trace element data collected at Vulcan in this study

Included Data

Sample	Tb	Dy	Ho	Er	Tm	Yb	Lu	Hf	Ta	W	ΣREY	Eu/Eu*	Y/Y*	Ce/Ce*
852(1) - 15	0.04	0.24	0.04	0.21	0.01	0.13	0.02	0.01	0.08	0.90	6.54	0.52	0.87	1.42
852(1) - 21	<0.006	0.02	0.01	<0.006	<0.002	0.02	0.01	0.07	0.02	3.49	0.86		0.36	2.26
852(1) - 22	0.00	0.05	0.01	0.04	0.02	0.02	0.01	0.01	0.03	1.25	1.35	5.19	0.94	1.31
852(1) - 23	0.01	0.09	0.02	0.07	0.01	0.03	0.01	0.02	0.04	0.35	5.50	0.56	0.53	1.25
852(1) - 29	0.01	0.12	0.02	0.06	0.02	0.09	0.02	<0.001	0.01	0.83	1.91	0.37	0.84	1.42
852(1) - 30	0.02	0.09	0.02	0.12	0.02	0.17	0.01	0.01	0.08	0.54	7.03	0.38	1.05	1.42
852(1) - 32	0.02	0.11	0.02	0.09	0.01	0.07	0.02	0.01	0.07	0.21	5.51	0.14	0.82	1.55
852(1) - 33	0.01	0.05	0.01	0.06	0.01	0.02	0.00	<0.007	0.02	1.29	1.44	1.39	0.93	1.51
852(1) - 35	0.04	0.14	0.03	0.11	0.01	0.27	0.03	<0.006	0.08	0.23	5.74	0.45	0.97	2.19
852(1) - 36	0.02	0.06	0.04	0.17	0.02	0.12	0.02	0.01	0.01	0.10	3.11	0.56	1.68	1.39
852(1) - 37	0.01	0.07	0.02	0.07	0.01	0.10	0.01	<0.012	0.01	0.41	2.68	0.44	0.59	1.26
852(1) - 38	0.02	0.10	0.01	0.05	0.01	0.04	0.02	0.01	0.06	0.20	3.15	0.12	0.84	1.15
852(1) - 39	0.01	0.05	0.02	0.07	0.01	0.12	0.02	0.02	0.07	0.62	1.83	0.28	1.16	1.86
852(1) - 40	0.01	0.10	0.03	0.06	0.02	0.09	0.02	0.02	0.04	1.64	5.95	0.48	0.66	1.31
852(1) - 41	0.04	0.32	0.10	0.34	0.04	0.26	0.04	0.01	0.02	0.44	7.78	0.79	0.82	1.24
852(1) - 42	0.02	0.05	0.02	0.09	0.01	0.09	0.01	0.04	0.02	0.16	3.21	0.58	1.31	1.36
852(1) - 44	0.05	0.05	0.03	0.08	0.03	0.08	0.02	0.03	0.04	0.16	6.90	0.52	0.85	1.13
852(1) - 50	0.02	0.16	0.04	0.09	0.01	0.11	0.01	0.01	0.04	1.50	4.10	0.41	0.76	1.47
852(1) - 51	0.03	0.05	0.02	0.08	0.01	0.05	0.02	0.02	0.06	3.20	3.59	0.40	1.42	1.34
852(1) - 52	0.00	0.02	0.00	<0.006	<0.000	0.02	0.01	<0.002	0.03	2.19	1.09		0.77	1.33
852(1) - 56	0.02	0.05	0.01	0.02	0.01	0.02	0.01	0.02	0.05	0.76	3.71	0.39	0.70	1.12
852(1) - 58	0.01	0.14	0.01	0.08	<0.001	0.10	0.01	0.01	0.17	0.50	7.64		0.98	1.07
973(1) - 20	0.02	0.04	0.02	0.12	0.02	0.15	0.01	<0.007	0.02	15.20	7.73		1.42	0.99
973(1) - 21	0.02	0.07	0.02	0.07	0.01	0.16	0.03	0.07	0.01	27.55	10.77		0.74	1.27
973(1) - 26	0.01	0.08	0.02	0.09	0.02	0.13	0.03	0.01	0.03	105.33	3.73	2.03	1.35	1.93
973(1) - 36	0.01	0.11	0.03	0.09	0.02	0.09	0.03	0.11	0.08	1.34	3.24	1.67	1.20	1.36
973(1) - 43	0.02	0.23	0.04	0.22	0.01	0.24	0.01	1.13	0.45	3.95	3.48		1.05	1.67
973(1) - 31	<0.004	<0.004	0.00	<0.006	<0.002	0.01	<0.002	<0.003	<0.002	0.87	0.12			0.70
973(1) - 32	<0.002	0.01	0.00	<0.004	<0.001	<0.005	<0.001	<0.002	0.02	1.20	0.08		0.42	
994(1) - 1	0.03	0.08	0.04	0.19	0.02	0.18	0.04	0.01	0.02	0.28	5.98	0.39	1.13	1.24
994(1) - 2	0.04	0.23	0.04	0.13	0.03	0.21	0.04	<0.004	0.08	0.23	4.27	0.44	0.74	1.29
994(1) - 6	0.02	0.15	0.04	0.15	0.04	0.16	0.03	0.04	0.07	0.88	5.05	0.28	0.85	1.20
994(1) - 11	<0.002	0.05	0.01	0.00	0.01	0.05	0.01	0.05	0.05	2.16	1.24		0.72	1.54
994(1) - 12	0.02	0.13	0.03	0.15	0.02	0.23	0.04	0.00	0.04	0.32	6.63	0.35	0.97	1.32
994(1) - 13	0.03	0.11	0.03	0.16	0.04	0.27	0.06	0.01	0.06	0.33	5.33	0.47	1.02	1.61
994(1) - 16	0.02	0.14	0.01	0.09	0.02	0.10	0.04	0.04	0.11	0.78	4.10	0.42	1.00	1.43
994(1) - 18	0.02	0.19	0.02	0.14	0.00	0.25	0.02	<0.009	0.10	1.67	4.56		0.69	1.91
994(1) - 20	0.02	0.13	0.04	0.13	0.02	0.13	0.04	0.01	0.04	0.28	3.74	0.79	0.77	1.14
994(1) - 21	0.02	0.21	0.05	0.16	0.02	0.22	0.04	0.02	0.04	0.29	4.92	0.63	0.60	1.43
994(1) - 22	0.05	0.24	0.03	0.15	0.02	0.16	0.03	0.01	0.04	0.28	5.21	0.34	0.89	1.16
994(1) - 24	0.03	0.16	0.03	0.14	0.03	0.20	0.01	0.02	0.02	0.47	5.33	0.38	0.90	1.25
994(1) - 25	0.04	0.13	0.04	0.12	0.02	0.16	0.04	0.01	0.02	0.36	3.87	0.38	0.90	1.39
994(1) - 27	0.03	0.24	0.05	0.22	0.03	0.33	0.05	0.01	0.04	0.52	9.27	0.33	0.75	1.23
994(1) - 28	0.03	0.23	0.03	0.13	0.03	0.19	0.02	0.05	0.11	0.76	4.06	0.65	0.70	1.26
994(1) - 31	0.01	0.06	0.01	0.06	0.01	0.14	0.02	<0.003	0.04	3.72	2.94	0.93	1.13	1.39
994(1) - 32	0.00	0.06	0.00	0.06	0.00	0.10	0.01	0.02	0.00	2.38	1.97	0.64	4.38	1.11
994(1) - 33	0.02	0.09	0.02	0.06	0.01	0.03	0.02	<0.005	0.01	2.21	14.18	0.24	0.76	1.06
994(1) - 35	0.04	0.25	0.09	0.16	0.04	0.31	0.04	0.04	0.06	1.44	8.80	0.27	0.79	1.25
994(1) - 36	0.05	0.24	0.05	0.28	0.02	0.34	0.02	0.02	0.15	1.02	13.43	0.54	0.91	1.26
994(1) - 38	0.01	0.17	0.03	0.10	0.01	0.14	0.02	0.00	0.05	0.25	4.18	0.06	0.70	1.21
994(1) - 40	0.02	0.17	0.03	0.11	0.02	0.12	0.02	0.01	0.04	0.65	5.68	0.42	0.62	1.32
994(1) - 41	<0.001	0.01	0.01	0.03	<0.002	0.02	0.01	0.04	0.00	0.29	0.94		0.97	1.32
994(1) - 42	0.04	0.20	0.05	0.15	0.03	0.19	0.03	0.02	0.06	0.32	7.54	0.37	0.87	1.24
994(1) - 43	0.04	0.27	0.09	0.26	0.04	0.27	0.06	0.07	0.08	0.30	9.59	0.53	0.68	1.35
994(1) - 44	0.03	0.29	0.05	0.22	0.03	0.32	0.04	0.06	0.09	0.47	4.88	0.76	0.68	1.41
994(1) - 45	0.06	0.26	0.07	0.18	0.04	0.37	0.04	0.10	0.13	0.93	11.09	0.55	0.83	1.45
994(1) - 47	0.02	0.10	0.02	0.10	0.03	0.13	0.02	0.01	0.07	3.64	6.55	0.43	1.10	1.05
994(1) - 48	0.03	0.13	0.05	0.14	0.03	0.24	0.02	0.01	0.02	0.69	7.21	0.53	0.84	1.21
994(1) - 49	0.05	0.26	0.05	0.12	0.04	0.33	0.04	0.05	0.13	1.13	11.75	0.18	0.81	1.26
994(1) - 50	0.04	0.33	0.06	0.21	0.05	0.36	0.06	0.03	0.09	0.40	9.25	0.38	0.90	1.32
994(1) - 51	0.03	0.20	0.03	0.13	0.01	0.29	0.04	0.02	0.06	1.11	6.26	0.58	0.92	1.38
994(1) - 52	0.03	0.22	0.05	0.18	0.03	0.19	0.02	0.03	0.11	0.36	5.18		0.63	1.49
994(1) - 53	0.02	0.07	0.02	0.09	0.01	0.14	0.02	0.06	0.07	1.87	2.28	0.59	1.13	1.37
994(1) - 55	0.02	0.06	0.03	0.11	0.02	0.13	0.00	0.03	0.15	9.41	2.47	0.51	0.75	1.54
994(1) - 56	0.04	0.28	0.08	0.22	0.02	0.32	0.05	0.12	0.11	1.27	10.49	0.22	0.68	1.27
994(1) - 57	0.03	0.22	0.07	0.17	0.04	0.30	0.07	0.09	0.10	1.97	7.54	0.82	0.81	1.47
994(1) - 58	0.04	0.18	0.04	0.16	0.02	0.22	0.03	0.06	0.05	0.98	6.08	0.48	0.94	1.23
994(1) - 59	0.03	0.21	0.05	0.13	0.04	0.24	0.03	0.02	0.02	1.46	9.17	0.09	0.73	1.23
994(1) - 60	0.04	0.07	0.02	0.08	0.02	0.11	0.01	0.01	0.03	1.00	2.82	0.37	0.96	1.31
994(1) - 61	0.01	0.10	0.02	0.10	0.02	0.12	0.02	0.03	0.13	1.13	3.70	0.40	0.95	1.22
994(1) - 62	0.05	0.28	0.04	0.20	0.01	0.24	0.04	<0.007	0.05	1.15	12.34	0.36	0.69	1.31

Element concentrations in ppm
BDL: below detection limit
NA: no analysis
$Eu/Eu^* = [(Eu_{CN}/(Sm_{CN}+Gd_{CN})/2)]$
$Y/Y^* = [(Y_{CN}/(Dy_{CN}+Ho_{CN})/2)]$
$Ce/Ce^* = [(Ce_{CN}/(La_{CN} \times Pr_{CN})^{0.5})]$
CN = chondrite normalised
Normalising values from Sun and McDonough (1989)

Appendix 5 Supplementary material for Mapping hydrothermal systems in IOCG deposits using apatite geochronology and geochemsitry: An example from Vulcan Cu-Au prospect

Appendix 5 Table A4: Magnetite and hematite LA-ICP-MS trace element data collected at Vulcan in this study

Included Data

Sample	Drill hole	Mineral	Comment
994(1) - 63	VUD 009 994	Hematite	Al inclusions. Ba inclusion after signal.
994(1) - 64	VUD 009 994	Hematite	High Al and Mg
994(1) - 66	VUD 009 994	Hematite	High Al and Mg
994(1) - 67	VUD 009 994	Hematite	HighAl and Mg
994(1) - 69	VUD 009 994	Hematite	High Al and Mg
994(1) - 70	VUD 009 994	Hematite	High Al
994(1) - 72	VUD 009 994	Hematite	High Al, Mn and Mg
994(2) - 1	VUD 009 994	Hematite	High Al, Mn and Mg
994(2) - 2	VUD 009 994	Hematite	High Al, Mn, Mg and Nb.
994(2) - 3	VUD 009 994	Hematite	High Al, Mn
994(2) - 4	VUD 009 994	Hematite	High Al
994(2) - 7	VUD 009 994	Hematite	High AL and Mg
994(2) - 11	VUD 009 994	Hematite	High AL and Mg
994(2) - 16	VUD 009 994	Hematite	High Al. Ba peak after signal
994(2) - 17	VUD 009 994	Hematite	High Al and Mn
994(2) - 19	VUD 009 994	Hematite	High Al
994(2) - 21	VUD 009 994	Hematite	Mn inclusion.
994(2) - 22	VUD 009 994	Hematite	High Al and Mg
994(2) - 23	VUD 009 994	Hematite	High Al and Mg
994(2) - 25	VUD 009 994	Hematite	High Al and Mg
994(2) - 26	VUD 009 994	Hematite	High Al and Mg
994(2) - 28	VUD 009 994	Hematite	High Al
994(2) - 29	VUD 009 994	Hematite	High Al.
994(2) - 30	VUD 009 994	Hematite	High Al, Mn and V
994(2) - 31	VUD 009 994	Hematite	High Al and Mg
994(2) - 32	VUD 009 994	Hematite	High Al and Mg
994(2) - 33	VUD 009 994	Hematite	Mn inclusion.
994(2) - 35	VUD 009 994	Hematite	High Al and Mg
994(2) - 36	VUD 009 994	Hematite	High Al, Mn and V
994(2) - 37	VUD 009 994	Hematite	High Al, Mn and Mg
994(2) - 39	VUD 009 994	Hematite	
994(2) - 42	VUD 009 994	Hematite	High AL and Mg
994(2) - 44	VUD 009 994	Hematite	High Al and Mn
994(2) - 46	VUD 009 994	Hematite	High Al
994(2) - 47	VUD 009 994	Hematite	Mg Al inclusions
994(2) - 48	VUD 009 994	Hematite	High Al
994(2) - 49	VUD 009 994	Hematite	High Al and Mg
994(2) - 50	VUD 009 994	Hematite	High Al and Mn

Element concentrations in ppm
BDL: below detection limit
NA: no analysis
$Eu/Eu^* = [(Eu_{CN}/(Sm_{CN}+Gd_{CN})/2)]$
$Y/Y^* = [(Y_{CN}/(Dy_{CN}+Ho_{CN})/2)]$
$Ce/Ce^* = [(Ce_{CN}/(La_{CN} \times Pr_{CN})^{0.5})]$
CN = chondrite normalised
Normalising values from Sun and McDonough (1989)

Appendix 5 Supplementary material for Mapping hydrothermal systems in IOCG deposits using apatite geochronology and geochemsitry: An example from Vulcan Cu-Au prospect

Appendix 5 Table A4: Magnetite and hematite LA-ICP-MS trace element data collected at Vulcan in this study

Included Data

Sample	Mg	Al	Si	P	Ca	Ti	V	Mn	Fe	Co	Ni	Cu	Zn	As
994(1) - 63	347	479	1063	<16.095	292	8	19	42	690000	12.84	83.97	1.42	2.64	26.86
994(1) - 64	705	379	2033	<17.097	198	10	19	45	690000	10.82	90.23	1.33	2.71	27.05
994(1) - 66	987	264	2639	<18.648	226	11	19	52	690000	13.29	96.18	1.71	3.44	38.54
994(1) - 67	377	266	1247	20	137	6	18	33	690000	11.22	69.30	<0.484	2.06	43.59
994(1) - 69	809	356	1958	<19.046	221	8	19	99	690000	11.79	88.22	3.93	2.86	23.35
994(1) - 70	242	1885	2852	171	<113.090	1340	94	172	690000	11.46	48.09	35.38	9.86	23.73
994(1) - 72	376	404	1351	38	1919	63	26	83	690000	12.21	57.44	4.00	3.30	37.26
994(2) - 1	480	1517	2439	239	318	204	51	193	690000	8.00	32.58	27.10	10.02	60.39
994(2) - 2	605	1478	3184	121	335	145	44	127	690000	6.27	34.47	18.06	8.38	54.57
994(2) - 3	130	1232	1266	37	92	108	145	234	690000	22.98	46.87	23.11	6.52	36.16
994(2) - 4	343	3060	5403	241	130	487	32	172	690000	7.78	27.06	40.71	15.51	33.11
994(2) - 7	569	1913	3285	36	541	183	39	85	690000	5.01	25.84	8.66	5.61	55.64
994(2) - 11	473	1783	3504	31	195	126	95	119	690000	21.23	64.42	11.00	3.64	28.77
994(2) - 16	345	1178	2117	23	331	169	54	173	690000	11.84	47.81	28.80	6.05	44.03
994(2) - 17	463	1467	2975	108	334	987	181	908	690000	72.93	68.12	97.62	17.11	35.23
994(2) - 19	185	966	1639	130	172	164	51	181	690000	9.60	38.50	43.48	6.38	36.61
994(2) - 21	807	917	2586	33	696	73	36	235	690000	8.42	40.81	23.81	4.68	51.58
994(2) - 22	624	1633	2723	67	712	183	34	112	690000	6.09	27.55	19.82	7.86	49.78
994(2) - 23	677	1516	3006	255	328	603	32	196	690000	7.98	35.42	58.23	13.64	62.02
994(2) - 25	936	1810	3404	103	466	245	48	203	690000	11.56	40.72	35.59	9.65	60.92
994(2) - 26	760	1683	2809	54	993	121	55	180	690000	7.69	33.82	18.15	7.54	60.02
994(2) - 28	123	785	927	<27.632	120	22	23	34	690000	4.29	44.76	5.16	2.30	36.13
994(2) - 29	523	1567	2805	166	351	256	76	309	690000	13.34	40.11	43.97	10.02	38.49
994(2) - 30	151	1490	1682	46	<71.307	156	158	317	690000	31.86	67.13	31.19	8.47	23.82
994(2) - 31	866	1426	3273	18	1597	53	20	47	690000	4.11	46.94	<0.530	4.20	57.06
994(2) - 32	619	907	2251	<19.641	449	52	26	49	690000	3.74	38.83	1.76	3.76	51.84
994(2) - 33	428	1278	1911	77	448	298	65	101	690000	6.04	34.94	11.76	5.12	54.81
994(2) - 35	334	1028	1457	27	110	68	51	79	690000	3.94	34.93	4.11	2.71	40.74
994(2) - 36	82	1752	1469	26	<96.847	653	346	348	690000	94.06	117.56	34.18	19.13	19.28
994(2) - 37	523	487	1936	<22.566	463	249	33	233	690000	17.86	60.79	124.53	4.36	52.28
994(2) - 39	104	162	422	<24.040	<101.823	19	15	16	690000	2.96	57.84	<0.669	3.16	18.77
994(2) - 42	768	1400	3085	<23.320	255	53	45	71	690000	6.71	39.40	20.03	4.43	64.67
994(2) - 44	257	2137	2836	266	514	557	40	283	690000	11.53	33.30	60.95	9.32	36.00
994(2) - 46	350	1330	1903	153	154	178	35	136	690000	5.79	27.53	45.61	7.22	47.66
994(2) - 47	486	1687	2442	234	120	306	58	173	690000	9.37	29.31	31.84	8.81	70.22
994(2) - 48	33	728	663	22	<73.309	670	37	47	690000	3.66	43.86	5.75	1.95	19.68
994(2) - 49	501	726	1953	<24.256	383	105	30	88	690000	13.28	57.48	30.91	2.35	19.29
994(2) - 50	250	1112	1636	24	205	480	109	464	690000	46.34	51.10	60.69	12.04	37.08

Element concentrations in ppm
BDL: below detection limit
NA: no analysis
$Eu/Eu^* = [(Eu_{CN}/(Sm_{CN}+Gd_{CN})/2)]$
$Y/Y^* = [(Y_{CN}/(Dy_{CN}+Ho_{CN})/2)]$
$Ce/Ce^* = [(Ce_{CN}/(La_{CN} \times Pr_{CN})^{0.5})]$
CN = chondrite normalised
Normalising values from Sun and McDonough (1989)

Appendix 5 Supplementary material for Mapping hydrothermal systems in IOCG deposits using apatite geochronology and geochemsitry: An example from Vulcan Cu-Au prospect

Appendix 5 Table A4: Magnetite and hematite LA-ICP-MS trace element data collected at Vulcan in this study

Included Data														
Sample	**Sr**	**Y**	**Zr**	**Nb**	**Mo**	**Sn**	**Ba**	**La**	**Ce**	**Pr**	**Nd**	**Sm**	**Eu**	**Gd**
994(1) - 63	1.57	0.56	0.64	13.37	0.94	0.69	3.87	0.37	1.51	0.23	0.70	0.25	0.02	0.04
994(1) - 64	2.12	1.06	0.60	10.02	0.66	0.68	1.02	1.39	4.05	0.52	2.05	0.31	0.02	0.25
994(1) - 66	2.12	1.57	0.44	14.08	0.77	0.48	1.89	1.35	4.99	0.56	2.54	0.38	0.02	0.28
994(1) - 67	1.23	0.58	0.28	9.39	0.79	0.66	0.39	0.16	0.81	0.11	0.48	0.10	0.01	0.07
994(1) - 69	1.87	1.01	0.25	7.59	1.52	0.75	1.54	0.86	3.12	0.41	1.57	0.43	0.02	0.20
994(1) - 70	1.53	0.84	5.17	21.49	25.34	8.18	4.62	0.87	2.23	0.26	1.20	0.14	<0.002	0.09
994(1) - 72	2.48	1.10	0.61	16.54	2.36	1.40	1.31	0.57	1.80	0.24	0.82	0.27	0.03	0.29
994(2) - 1	5.33	1.15	3.61	45.53	11.85	2.40	4.22	0.76	2.58	0.36	1.22	0.21	0.02	0.17
994(2) - 2	5.05	1.17	3.48	55.58	9.37	2.27	3.11	1.42	4.62	0.59	2.48	0.41	0.04	0.34
994(2) - 3	2.83	0.55	4.22	35.86	14.26	2.24	4.89	0.32	0.94	0.10	0.37	0.06	0.00	0.05
994(2) - 4	9.37	1.15	3.18	49.76	12.59	3.19	5.43	2.29	5.57	0.55	1.87	0.20	0.04	0.26
994(2) - 7	6.45	1.28	3.02	58.86	7.03	2.19	4.01	2.30	6.63	0.71	2.55	0.43	0.03	0.26
994(2) - 11	3.32	0.61	3.42	38.33	14.28	2.52	4.79	0.49	2.33	0.30	1.20	0.14	0.01	0.20
994(2) - 16	3.08	1.01	3.74	61.21	4.33	3.64	4.51	1.44	3.97	0.53	1.85	0.18	0.03	0.24
994(2) - 17	3.69	2.00	17.43	103.10	24.50	6.57	11.26	1.41	4.20	0.51	2.05	0.51	0.05	0.29
994(2) - 19	2.99	0.82	3.10	46.13	9.18	2.37	4.52	1.18	3.14	0.37	1.33	0.14	0.04	0.11
994(2) - 21	3.62	1.66	2.34	41.43	2.99	1.86	2.34	2.68	7.64	0.92	3.69	0.59	0.05	0.52
994(2) - 22	4.12	0.98	2.62	48.31	8.59	2.66	2.19	1.14	3.74	0.43	1.43	0.33	0.04	0.33
994(2) - 23	5.65	1.54	3.50	68.65	11.64	2.96	5.02	1.46	4.81	0.59	2.31	0.34	0.04	0.30
994(2) - 25	5.87	1.61	4.05	48.54	7.53	2.42	4.43	2.42	6.67	0.84	3.09	0.50	0.03	0.35
994(2) - 26	5.19	1.38	3.92	48.67	5.39	2.07	2.75	1.35	5.56	0.62	2.38	0.33	0.08	0.25
994(2) - 28	2.19	0.18	0.45	7.40	2.55	1.33	0.85	0.62	1.30	0.11	0.27	0.07	0.02	<0.023
994(2) - 29	3.22	1.23	4.40	62.53	13.89	3.80	6.03	1.56	4.80	0.55	2.50	0.57	0.05	0.19
994(2) - 30	2.08	0.65	4.20	34.11	17.00	2.09	7.39	0.39	1.23	0.12	0.47	0.09	0.03	0.11
994(2) - 31	4.51	1.65	0.94	28.82	0.80	1.29	2.17	1.52	5.74	0.80	3.30	0.57	0.05	0.37
994(2) - 32	4.11	0.91	1.31	27.49	1.66	1.46	2.93	1.11	3.95	0.57	2.07	0.43	0.02	0.17
994(2) - 33	3.89	1.11	3.49	47.65	12.11	3.45	3.03	0.72	2.65	0.29	1.24	0.25	0.01	0.21
994(2) - 35	2.07	0.75	2.11	47.84	3.66	3.02	1.37	0.59	1.98	0.27	0.91	0.19	0.04	0.15
994(2) - 36	1.83	0.74	16.30	42.23	56.79	5.36	11.38	0.30	0.76	0.11	0.33	0.07	0.02	0.11
994(2) - 37	5.14	1.66	3.47	17.30	3.65	1.92	12.51	3.17	8.10	0.65	2.75	0.38	0.04	0.46
994(2) - 39	1.45	0.09	0.14	6.53	0.21	0.15	0.98	0.11	0.22	0.06	0.13	0.03	0.01	0.04
994(2) - 42	4.64	1.30	1.84	48.40	1.89	1.96	2.95	3.33	9.34	1.18	4.69	0.47	0.09	0.50
994(2) - 44	5.53	1.22	3.16	71.70	17.27	4.15	6.99	3.44	7.99	1.01	2.99	0.56	0.06	0.43
994(2) - 46	4.52	0.94	3.14	84.01	10.12	3.68	4.37	3.03	8.15	0.95	3.99	0.52	0.04	0.25
994(2) - 47	4.82	1.08	3.50	87.02	15.06	3.13	3.11	1.59	5.01	0.52	1.69	0.42	0.04	0.13
994(2) - 48	2.15	0.21	0.40	2.66	4.72	1.95	0.98	0.19	0.72	0.04	0.48	<0.008	<0.005	<0.019
994(2) - 49	1.50	0.68	1.44	20.96	2.76	1.35	2.55	0.80	2.07	0.21	1.09	0.17	0.02	0.18
994(2) - 50	3.19	1.19	10.02	39.71	12.79	3.87	8.43	0.42	1.51	0.20	0.64	0.10	0.02	0.14

Element concentrations in ppm
BDL: below detection limit
NA: no analysis
$Eu/Eu^* = [(Eu_{CN}/(Sm_{CN}+Gd_{CN})/2)]$
$Y/Y^* = [(Y_{CN}/(Dy_{CN}+Ho_{CN})/2)]$
$Ce/Ce^* = [(Ce_{CN}/(La_{CN} \times Pr_{CN})^{0.5})]$
CN = chondrite normalised
Normalising values from Sun and McDonough (1989)

Appendix 5 Supplementary material for Mapping hydrothermal systems in IOCG deposits using apatite geochronology and geochemsitry: An example from Vulcan Cu-Au prospect

Appendix 5 Table A4: Magnetite and hematite LA-ICP-MS trace element data collected at Vulcan in this study

Included Data

Sample	Tb	Dy	Ho	Er	Tm	Yb	Lu	Hf	Ta	W	ΣREY	Eu/Eu*	Y/Y*	Ce/Ce*
994(1) - 63	0.01	0.13	0.04	0.07	0.01	0.17	0.02	0.01	0.04	0.74	4.14	0.58	0.58	1.27
994(1) - 64	0.04	0.24	0.04	0.16	0.02	0.23	0.04	0.03	0.03	0.22	10.40	0.25	0.88	1.16
994(1) - 66	0.05	0.30	0.06	0.29	0.05	0.26	0.05	0.01	0.03	0.18	12.76	0.18	0.86	1.38
994(1) - 67	0.01	0.15	0.02	0.07	0.02	0.11	0.02	<0.004	0.03	0.16	2.72	0.37	0.79	1.48
994(1) - 69	0.05	0.29	0.04	0.17	0.03	0.25	0.04	<0.005	0.01	0.10	8.49	0.24	0.76	1.28
994(1) - 70	0.04	0.19	0.04	0.06	0.01	0.10	0.03	0.18	0.13	3.02	6.09		0.70	1.14
994(1) - 72	0.03	0.22	0.04	0.19	0.04	0.17	0.03	0.02	0.06	0.47	5.85	0.34	0.90	1.16
994(2) - 1	0.03	0.25	0.06	0.16	0.04	0.27	0.05	0.11	0.13	7.31	7.34	0.38	0.68	1.19
994(2) - 2	0.05	0.22	0.06	0.21	0.05	0.23	0.06	0.07	0.16	5.67	11.94	0.35	0.79	1.23
994(2) - 3	0.02	0.10	0.02	0.10	0.02	0.11	0.03	0.10	0.06	9.21	2.79	0.29	0.86	1.27
994(2) - 4	0.04	0.15	0.04	0.12	0.02	0.21	0.03	0.09	0.21	8.37	12.56	0.54	1.08	1.20
994(2) - 7	0.03	0.17	0.06	0.21	0.03	0.16	0.05	0.05	0.17	7.43	14.89	0.25	0.94	1.26
994(2) - 11	0.04	0.16	0.05	0.10	0.03	0.16	0.03	0.06	0.03	5.15	5.86	0.18	0.52	1.46
994(2) - 16	0.02	0.23	0.05	0.20	0.04	0.24	0.04	0.06	0.11	4.88	10.06	0.42	0.72	1.10
994(2) - 17	0.07	0.44	0.08	0.34	0.05	0.26	0.05	0.54	0.17	9.43	12.31	0.39	0.83	1.20
994(2) - 19	0.01	0.11	0.03	0.18	0.01	0.15	0.03	0.04	0.16	3.04	7.64	0.93	1.15	1.14
994(2) - 21	0.05	0.20	0.08	0.26	0.03	0.37	0.06	0.06	0.11	2.17	18.80	0.29	1.02	1.17
994(2) - 22	0.03	0.19	0.04	0.14	0.03	0.29	0.03	0.08	0.11	7.67	9.18	0.37	0.82	1.29
994(2) - 23	0.05	0.28	0.08	0.29	0.04	0.36	0.06	0.12	0.28	2.96	12.55	0.40	0.79	1.25
994(2) - 25	0.06	0.27	0.08	0.26	0.04	0.38	0.05	0.08	0.11	3.99	16.67	0.24	0.85	1.13
994(2) - 26	0.03	0.28	0.06	0.16	0.03	0.24	0.04	0.14	0.09	6.77	12.79	0.79	0.83	1.46
994(2) - 28	0.00	0.03	0.01	0.03	<0.001	0.06	0.00	0.01	0.02	4.77	2.70		0.87	1.20
994(2) - 29	0.03	0.23	0.07	0.18	0.03	0.35	0.08	0.06	0.08	5.12	12.43	0.42	0.73	1.25
994(2) - 30	0.02	0.12	0.03	0.10	0.01	0.15	0.01	0.08	0.07	6.77	3.53	0.92	0.82	1.39
994(2) - 31	0.07	0.37	0.07	0.25	0.04	0.30	0.10	0.04	0.08	1.30	15.20	0.33	0.79	1.26
994(2) - 32	0.02	0.20	0.05	0.14	0.02	0.14	0.03	0.02	0.07	2.00	9.83	0.24	0.72	1.20
994(2) - 33	0.04	0.24	0.03	0.17	0.02	0.20	0.03	0.11	0.14	7.47	7.21	0.09	0.94	1.39
994(2) - 35	0.02	0.12	0.03	0.10	0.01	0.15	0.01	0.03	0.06	8.66	5.30	0.83	1.00	1.20
994(2) - 36	0.02	0.14	0.03	0.10	0.01	0.17	0.01	0.32	0.10	11.48	2.92	0.69	0.80	1.01
994(2) - 37	0.05	0.43	0.06	0.15	0.03	0.25	0.03	0.07	0.18	1.69	18.23	0.28	0.76	1.36
994(2) - 39	0.01	0.03	0.01	0.01	0.01	0.02	0.01	<0.003	0.01	0.18	0.79	0.55	0.45	0.65
994(2) - 42	0.03	0.34	0.05	0.13	0.05	0.30	0.04	0.01	0.11	3.39	21.85	0.58	0.73	1.14
994(2) - 44	0.04	0.29	0.05	0.15	0.03	0.23	0.03	0.10	0.16	3.22	18.53	0.40	0.76	1.04
994(2) - 46	0.04	0.19	0.03	0.15	0.03	0.26	0.03	0.07	0.20	6.49	18.62	0.37	0.91	1.16
994(2) - 47	0.01	0.30	0.07	0.27	0.01	0.13	0.04	0.08	0.25	6.23	11.31	0.49	0.58	1.33
994(2) - 48	0.01	0.03	0.02	0.03	0.01	0.03	<0.001	0.01	0.02	6.58	1.77		0.73	1.98
994(2) - 49	0.02	0.09	0.05	0.06	0.01	0.12	0.02	<0.002	0.06	2.29	5.58	0.33	0.79	1.22
994(2) - 50	0.03	0.24	0.04	0.13	0.03	0.11	0.04	0.21	0.17	6.41	4.85	0.49	0.89	1.26

Element concentrations in ppm
BDL: below detection limit
NA: no analysis
$Eu/Eu^* = [(Eu_{CN}/(Sm_{CN}+Gd_{CN})/2)]$
$Y/Y^* = [(Y_{CN}/(Dy_{CN}+Ho_{CN})/2)]$
$Ce/Ce^* = [(Ce_{CN}/(La_{CN} \times Pr_{CN})^{0.5})]$
CN = chondrite normalised
Normalising values from Sun and McDonough (1989)

Appendix 5 Supplementary material for Mapping hydrothermal systems in IOCG deposits using apatite geochronology and geochemsitry: An example from Vulcan Cu-Au prospect

Appendix 5 Table A4: Magnetite and hematite LA-ICP-MS trace element data collected at Vulcan in this study

Rejected Data

Source Filename	Drill hole	Mineral	Comment
1259 Img17 - G3 - 1	VUD 017 1259	Magnetite	La Ce, Th inclusions. Delete
1259 Img13- G3 - 1	VUD 017 1259	Magnetite	High V, Al, Mg. High Ca, P, Ce and La - apatite. High U.
1259 Img13- G3 - 2	VUD 017 1259	Magnetite	High V, Al, Mg. High Ca, P, Ce and La - apatite. High U.
1259 Img13- G4 - 1	VUD 017 1259	Magnetite	High V, Al, Mg. High Ca, P, Ce and La - apatite. High U. Co inclusions
1259 no img- G1 - 1	VUD 017 1259	Magnetite	High V, Al, Mg. High Ca, P, Ce and La - apatite. High U.
1259 no img- G1 - 3	VUD 017 1259	Magnetite	High V, Al, Mg. High Ca, P, Ce and La - apatite. High U.
1259 no img- G2 - 1	VUD 017 1259	Magnetite	High V, Al, Mg. High Ca, P, Ce and La - apatite. High U.
1259 no img- G2 - 2	VUD 017 1259	Magnetite	High V, Al, Mg. High Ca, P, Ce and La - apatite? High U.
1259 no img- G2 - 3	VUD 017 1259	Magnetite	High V, Al, Mg. High Ca, P, Ce and La - apatite? High U.
1259 no img- G2 - 4	VUD 017 1259	Magnetite	High V, Al, Mg. High Ca, P, Ce and La - apatite. High U.
1259 no img- G2 - 5	VUD 017 1259	Magnetite	High V, Al, Mg. High Ca, P, Ce and La - apatite. High U.
1268 img 8- G1 - 1	VUD 017 1268	Magnetite	High V, Mg, Al. High P, Ce ~high Th and La.
1268 img 8- G1 - 2	VUD 017 1268	Magnetite	High V, Al, Mg. High Ce, P, La, Th, Ca, U - apatite
1268 img 8- G1 - 3	VUD 017 1268	Magnetite	High V, Al. Mg. High Ce, P, La and Th, Ca and U
1268 img 8- G1 - 4	VUD 017 1268	Magnetite	Ti inclusions. High V, Al, Mg. High Ce and P.
1268 img 8- G2 - 1	VUD 017 1268	Magnetite	High V, Al, Mg and Ce, P, Th and La
1268 img 8- G2 - 2	VUD 017 1268	Magnetite	Monazite inclusion. Mg Mn inclusions
1268 img 8- G2 - 3	VUD 017 1268	Magnetite	High Al, V, Mg, Si, Ce P La and Th, Ca and U
1268 img 8- G2 - 5	VUD 017 1268	Magnetite	High V, Al, Mg. High Ce, Th, P, La, Ca - apatite?
1268 img 8- G2 - 6	VUD 017 1268	Magnetite	High V, Al, Mg. High Ca, P, Ce and La - apatite. High U.
1268 img 8- G2 - 7	VUD 017 1268	Magnetite	Mg Mn inclusions. High V, Al. High Ce, La, Th, Ca, U
1268 img 8- G2 - 8	VUD 017 1268	Magnetite	High Mg, Al, V, Si, Ce, Th, La, P, Ca - apatite inclusions
1268 img 9- G1 - 1	VUD 017 1268	Magnetite	High Mg, Al, V, Si, Ce, Th, La, P, Ca - apatite inclusions
1268 img 9- G1 - 2	VUD 017 1268	Magnetite	Cu inclusions. High Mg, V, Al. High Ce, P, La, Th, Ca
1268 img 9- G2 - 3	VUD 017 1268	Magnetite	High Mg, Al, V, Si. High Cem P, La, Ca, Th
1268 img 9- G3 - 1	VUD 017 1268	Magnetite	La inclusion. High Mg, Al, V, Ce, Th, P and Ca - apatite, monazite
1268 img 9- G3 - 2	VUD 017 1268	Magnetite	High V, Al, Mg, Si. High Cem P, La
1268 img 9- G4 - 1	VUD 017 1268	Magnetite	High Mg, Al, V, Si, Mn and Ce. High La, Th, Ca - apatite
1268 img 9- G4 - 2	VUD 017 1268	Magnetite	High Mg, Al, V, Si, Ce, Th, La, P, Ca - apatite inclusions
1268 img 9- G4 - 3	VUD 017 1268	Magnetite	Monazite inclusion.
1268 img 9- G5 - 1	VUD 017 1268	Magnetite	Mn inclusions. High Mg, Al, V, Si. High Ce, Th, La, Ca.
1268 img 9- G6 - 1	VUD 017 1268	Magnetite	High V, Al, Mg. ~Si. High Ce, P, La, Th
1268 img 9- G6 - 2	VUD 017 1268	Magnetite	High V, Al. Mg. ~Si. High Ce, P, La, Th
1268 img 9- G6 - 3	VUD 017 1268	Magnetite	High V, Al , Mg ~Si. High Ce, P, La, Th
1268 img 9- G6 - 4	VUD 017 1268	Magnetite	High Y P Ce Si apatite inclusion. High V, Al, Mg.
1268 img 9- G6 - 5	VUD 017 1268	Magnetite	LREE Th inclusions monazite
1268 img 9- G6 - 6	VUD 017 1268	Magnetite	High Al, V, Mg. High Si, Ce, P, La, Th
1268 img 9- G6 - 7	VUD 017 1268	Magnetite	LREE Th inclusions monazite. High V, Al, Mg
1268 img 9- G6 - 8	VUD 017 1268	Magnetite	Cu inclusion. High V, Al, Mg. Si, Ce, P, La, Th.
1268 img 9- G6 - 9	VUD 017 1268	Magnetite	High V, Al, Mg. Ce, P, La, Th, Ca - apatite?
1268 img 10 G1 - 1	VUD 017 1268	Magnetite	High V, Al, Mg, Si, Ce. La, Th P Ca - apatite?
1268 img 10 G1 - 2	VUD 017 1268	Magnetite	High V, Al, Mg, Si, Ce. La, Th P Ca - apatite?
1268 img 10 G1 - 3	VUD 017 1268	Magnetite	High V, Al, Mg, Si, Ce. La, Th P Ca - apatite?
1268 img 10 G1 - 4	VUD 017 1268	Magnetite	High V, Al, Mg, Si, Ce. La, Th P Ca - apatite?
1268 img 10 G1 - 5	VUD 017 1268	Magnetite	High V, Al, Mg, Si, Ce. La, Th P Ca - apatite?
1268 img 10 G1 - 6	VUD 017 1268	Magnetite	High V, Al, Mg, Si, Ce. La, Th P Ca - apatite?
1268 img 10 G1 - 7	VUD 017 1268	Magnetite	High V, Al, Mg, Si, Ce. La, Th P Ca - apatite?
1268 img 10 G1 - 8	VUD 017 1268	Magnetite	High V, Al, Mg, Si, Ce. La, Th P Ca - apatite?
1268 img 10 G1 - 9	VUD 017 1268	Magnetite	High V, Al, Mg, Si, Ce. La, Th P Ca - apatite?
1268 img 10 G1 - 10	VUD 017 1268	Magnetite	High V, Al, Mg, Si, Ce. La, Th P Ca - apatite?
1268 img 10 G1 - 11	VUD 017 1268	Magnetite	High V, Al, Mg, Si, Ce. La, Th P Ca - apatite?
1268 img 10 G2 - 1	VUD 017 1268	Magnetite	Ce P inclusions. High Al and V.
1268 img 10 G2 - 2	VUD 017 1268	Magnetite	High V, Al, Mg, Si, Ce. La, Th P Ca - apatite?
1268 img 10 G2 - 3	VUD 017 1268	Magnetite	Mg Ce inclusions. High Al and V.
1268 img 10 G2 - 4	VUD 017 1268	Magnetite	High V, Al, Mg, Si, Ce. La, Th P Ca - apatite?
1268 img 10 G2 - 5	VUD 017 1268	Magnetite	High V, Al, Mg, Si, Ce. La, Th P Ca - apatite?
1268 img 10 G3 - 1	VUD 017 1268	Magnetite	High V, Al, Mg. Monazite inclusions.
1268 img 10 G3 - 2	VUD 017 1268	Magnetite	Cu inclusion. High Mg, V, Al, Ce, La, Th, P
1268 img 10 G3 - 3	VUD 017 1268	Magnetite	High Mg, Al, V. High Ce, Th, La, Ca, P - apatite?
1268 img 10 G3 - 4	VUD 017 1268	Magnetite	High Mg, Al, V. High Ce, Th, La, Ca, P - apatite?
1268 img 10 G4 - 1	VUD 017 1268	Magnetite	High Mg, Al, V. High Ce, Th, La, Ca, P - apatite?
1268 img 10 G4 - 3	VUD 017 1268	Magnetite	Co Cu inclusions. High Ce, La, Th, P, Ca, U - monazite and apaite?
1268 img 10 G4 - 4	VUD 017 1268	Magnetite	Mn inclusions. High Mg, Al, V. High Ce, Th, La, P and Ca = apatite and monazite?
1268 img 11 G1 - 1	VUD 017 1268	Magnetite	Al-Mg inclusion. Co inclusions. Cu inclusions. High Ce, La, P, Th
1268 img 11 G1 - 2	VUD 017 1268	Magnetite	High Mg, Al, V. High Ce, Th, La, Ca, P - apatite?
1268 img 11 G1 - 3	VUD 017 1268	Magnetite	High Mg, Al, V. High Ce, Th, La, Ca, P - apatite?
1268 img 11 G1 - 4	VUD 017 1268	Magnetite	High Mg, Al, V. High Ce, Th, La, Ca, P - apatite? Cu inclusion
1268 img 11 G1 - 5	VUD 017 1268	Magnetite	High Mg, Al, V. High Ce, Th, La, Ca, P - apatite?
1268 img 11 G1 - 6	VUD 017 1268	Magnetite	High Mg, Al, V. High Ce, Th, La, Ca, P - apatite?
1268 img 11 G1 - 7	VUD 017 1268	Magnetite	Monazite inclusion.
1268 img 11 G2 - 1	VUD 017 1268	Magnetite	High Mg, Al, V. High Ce, Th, La, Ca, P - apatite?

Element concentrations in ppm
BDL: below detection limit
NA: no analysis
$Eu/Eu^* = [(Eu_{CN}/(Sm_{CN}+Gd_{CN})/2)]$
$Y/Y^* = [(Y_{CN}/(Dy_{CN}+Ho_{CN})/2)]$
$Ce/Ce^* = [(Ce_{CN}/(La_{CN} \times Pr_{CN})^{0.5})]$
CN = chondrite normalised
Normalising values from Sun and McDonough (1989)

Appendix 5 Supplementary material for Mapping hydrothermal systems in IOCG deposits using apatite geochronology and geochemsitry: An example from Vulcan Cu-Au prospect

Appendix 5 Table A4: Magnetite and hematite LA-ICP-MS trace element data collected at Vulcan in this study

Rejected Data														
Source Filename	**Mg**	**Al**	**Si**	**P**	**Ca**	**Ti**	**V**	**Mn**	**Fe**	**Co**	**Ni**	**Cu**	**Zn**	**As**
1259 Img17 - G3 - 1	2262	553	1282	<14.728	1649	90	884	237	720000	3.17	88.48	0.82	13.78	1.49
1259 Img13- G3 - 1	1588	639	3842	<11.443	414	198	863	15	720000	12.44	78.72	<0.198	0.73	0.34
1259 Img13- G3 - 2	1228	640	3107	<10.986	294	136	860	14	720000	6.63	78.42	<0.190	0.61	0.22
1259 Img13- G4 - 1	979	560	2321	<12.965	146	95	814	12	720000	34.47	97.09	2.08	8.16	0.68
1259 no img- G1 - 1	508	606	1233	<11.578	257	146	878	10	720000	13.07	79.80	0.63	0.88	0.29
1259 no img- G1 - 3	538	526	1267	13	159	112	888	9	720000	7.62	81.38	0.59	4.00	0.39
1259 no img- G2 - 1	641	610	1703	<12.969	52	297	889	11	720000	21.98	78.86	0.59	0.21	0.65
1259 no img- G2 - 2	256	620	1048	<12.077	<37.222	134	895	10	720000	24.62	78.97	0.58	<0.182	0.39
1259 no img- G2 - 3	360	592	1621	<10.714	45	144	844	9	720000	17.01	79.03	0.20	<0.233	0.36
1259 no img- G2 - 4	1002	634	2534	<10.140	103	148	857	13	720000	12.62	80.57	<0.187	1.16	0.31
1259 no img- G2 - 5	706	602	2444	<10.548	97	217	858	11	720000	5.35	75.29	0.35	0.20	0.40
1268 img 8- G1 - 1	305	598	2698	<11.617	281	252	314	8	720000	3.63	29.89	0.57	2.43	0.47
1268 img 8- G1 - 2	749	680	4012	12	793	238	294	8	720000	4.36	27.80	0.60	0.30	0.41
1268 img 8- G1 - 3	368	563	2810	<9.870	398	171	302	8	720000	9.17	28.68	0.30	<0.146	0.41
1268 img 8- G1 - 4	328	550	2614	<13.226	266	144	303	7	720000	5.71	28.96	<0.176	1.80	0.37
1268 img 8- G2 - 1	575	598	3732	<12.689	526	190	279	7	720000	3.06	27.73	0.23	0.21	0.58
1268 img 8- G2 - 2	1789	498	1603	16	133	138	322	103	720000	8.80	30.80	0.65	10.42	3.21
1268 img 8- G2 - 3	640	545	3285	<11.667	568	182	271	8	720000	2.07	24.67	0.50	1.93	0.25
1268 img 8- G2 - 5	495	561	3187	<10.468	508	115	295	9	720000	3.49	31.16	0.55	0.16	0.43
1268 img 8- G2 - 6	599	531	2864	<11.076	506	112	276	8	720000	2.32	25.57	0.47	6.94	<0.209
1268 img 8- G2 - 7	1701	576	2288	<11.755	290	145	313	156	720000	2.31	30.01	0.25	9.06	0.51
1268 img 8- G2 - 8	1603	613	5699	16	1567	122	294	10	720000	2.53	31.73	0.77	2.07	0.38
1268 img 9- G1 - 1	312	421	2109	12	317	67	289	6	720000	1.18	35.03	0.73	2.95	0.53
1268 img 9- G1 - 2	816	571	5797	<11.357	859	87	298	10	720000	3.19	37.49	71.65	12.14	0.66
1268 img 9- G2 - 3	646	478	3556	<12.016	686	75	293	7	720000	3.11	36.34	0.69	6.06	0.56
1268 img 9- G3 - 1	1931	784	8006	<12.141	2541	116	288	14	720000	5.13	46.86	1.32	7.85	0.70
1268 img 9- G3 - 2	497	461	1714	15	477	53	276	22	720000	6.16	35.72	23.23	5.67	0.41
1268 img 9- G4 - 1	1736	792	7249	<10.713	2048	137	298	18	720000	3.86	47.58	1.39	12.63	0.65
1268 img 9- G4 - 2	2954	1326	10020	15	2887	204	295	49	720000	6.40	37.83	2.09	22.80	1.06
1268 img 9- G4 - 3	8078	834	9150	26	3449	122	299	631	720000	6.05	53.54	2.55	19.50	0.80
1268 img 9- G5 - 1	1228	633	4681	<8.974	1346	103	283	11	720000	2.87	40.46	2.08	8.02	0.48
1268 img 9- G6 - 1	676	589	4103	<11.264	754	129	289	9	720000	4.56	29.50	0.61	0.39	0.49
1268 img 9- G6 - 2	794	556	4100	<10.603	898	118	296	8	720000	4.36	31.07	0.94	0.19	0.42
1268 img 9- G6 - 3	766	630	4004	<9.879	813	142	291	9	720000	5.06	27.95	0.61	0.21	0.52
1268 img 9- G6 - 4	686	577	3735	2462	7674	132	279	9	720000	4.16	27.60	1.66	0.30	0.55
1268 img 9- G6 - 5	2315	658	5602	20	1443	155	297	89	720000	3.37	35.83	1.16	29.35	0.66
1268 img 9- G6 - 6	610	582	3835	<11.403	623	129	286	8	720000	3.10	30.05	0.56	<0.236	0.63
1268 img 9- G6 - 7	1154	667	4503	<16.638	1409	122	308	9	720000	2.86	33.55	4.27	6.58	0.43
1268 img 9- G6 - 8	700	551	3715	<11.099	811	110	292	10	720000	1.99	30.41	1.90	1.05	0.76
1268 img 9- G6 - 9	544	488	3161	11	544	104	276	9	720000	1.45	32.28	4.82	6.15	0.45
1268 img 10 G1 - 1	1930	1040	7662	14	2379	196	298	12	720000	4.80	31.10	1.05	8.07	0.68
1268 img 10 G1 - 2	2190	996	8600	22	2335	190	293	12	720000	6.94	28.16	1.85	1.47	0.87
1268 img 10 G1 - 3	2009	946	7946	19	1973	217	292	11	720000	10.42	29.99	0.47	0.33	0.60
1268 img 10 G1 - 4	1521	806	7152	26	1511	173	289	10	720000	7.47	28.18	5.97	<0.228	0.50
1268 img 10 G1 - 5	1471	821	6497	<11.816	1431	190	293	10	720000	11.95	29.14	0.59	<0.171	0.59
1268 img 10 G1 - 6	1177	693	5219	37	1135	132	294	9	720000	3.82	30.43	6.34	1.55	0.56
1268 img 10 G1 - 7	1268	739	5935	<11.308	1347	144	290	10	720000	5.19	30.01	0.44	0.37	0.51
1268 img 10 G1 - 8	1150	577	4951	<11.903	1404	86	296	10	720000	3.85	46.22	1.28	7.23	0.53
1268 img 10 G1 - 9	1360	667	5682	19	1618	99	296	11	720000	3.00	29.84	0.24	7.27	0.52
1268 img 10 G1 - 10	1297	768	6423	14	1178	185	288	9	720000	15.16	29.86	0.54	<0.216	0.43
1268 img 10 G1 - 11	1286	798	6008	21	1248	222	295	9	720000	16.49	27.14	0.51	<0.178	0.44
1268 img 10 G2 - 1	66	593	645	<13.317	122	181	282	6	720000	8.92	28.72	4.98	7.10	0.31
1268 img 10 G2 - 2	657	523	2911	<11.207	763	109	285	10	720000	1.78	33.91	2.05	18.85	<0.233
1268 img 10 G2 - 3	153	424	755	<9.840	90	89	295	5	720000	1.28	30.30	<0.210	1.47	0.22
1268 img 10 G2 - 4	1702	970	7509	<11.003	2111	203	282	13	720000	3.60	30.93	30.99	17.48	0.38
1268 img 10 G2 - 5	1335	839	5718	<12.395	1333	165	311	16	720000	3.15	31.92	1.27	17.36	0.77
1268 img 10 G3 - 1	259	486	1588	<10.416	335	66	282	7	720000	2.65	38.18	10.92	5.22	0.47
1268 img 10 G3 - 2	1025	697	4218	<11.109	1281	101	313	9	720000	4.45	36.43	27.71	5.08	0.58
1268 img 10 G3 - 3	1649	623	5400	<13.790	1757	97	291	12	720000	2.41	35.22	10.66	9.62	0.72
1268 img 10 G3 - 4	1858	712	6730	33	2210	137	282	24	720000	3.09	33.55	5.88	16.86	0.41
1268 img 10 G4 - 1	742	475	4024	<11.932	923	62	285	8	720000	3.26	41.67	0.52	2.98	0.39
1268 img 10 G4 - 3	1450	522	5974	93	1898	45	274	8	720000	282.51	148.85	1020.03	6.11	0.97
1268 img 10 G4 - 4	1875	576	6278	19	2359	61	307	49	720000	3.11	47.12	1.21	8.18	0.60
1268 img 11 G1 - 1	1345	1300	4933	18	716	85	291	16	720000	5.35	36.63	25.95	18.97	0.47
1268 img 11 G1 - 2	2094	944	8339	<12.570	2306	252	308	22	720000	4.54	33.46	0.73	12.46	0.74
1268 img 11 G1 - 3	2129	973	8627	<14.451	2677	260	318	24	720000	4.58	36.73	1.29	23.10	0.73
1268 img 11 G1 - 4	398	564	2246	<11.006	398	121	297	9	720000	3.67	27.94	4.49	0.68	0.57
1268 img 11 G1 - 5	412	747	2699	<11.794	295	137	293	8	720000	1.86	27.96	<0.207	18.41	0.28
1268 img 11 G1 - 6	1029	743	4917	<11.201	1077	193	285	12	720000	2.48	27.92	2.86	11.14	0.49
1268 img 11 G1 - 7	339	572	2714	<10.211	405	128	276	6	720000	1.71	27.07	3.34	6.61	0.60
1268 img 11 G2 - 1	1021	553	5226	<10.697	1153	84	298	13	720000	3.12	47.00	1.41	9.20	0.48

Element concentrations in ppm
BDL: below detection limit
NA: no analysis
$Eu/Eu^* = [(Eu_{CN}/(Sm_{CN}+Gd_{CN})/2)]$
$Y/Y^* = [(Y_{CN}/(Dy_{CN}+Ho_{CN})/2)]$
$Ce/Ce^* = [(Ce_{CN}/(La_{CN} \times Pr_{CN})^{0.5})]$
CN = chondrite normalised
Normalising values from Sun and McDonough (1989)

Appendix 5 Supplementary material for Mapping hydrothermal systems in IOCG deposits using apatite geochronology and geochemsitry: An example from Vulcan Cu-Au prospect

Appendix 5 Table A4: Magnetite and hematite LA-ICP-MS trace element data collected at Vulcan in this study

Rejected Data														
Source Filename	**Sr**	**Y**	**Zr**	**Nb**	**Mo**	**Sn**	**Ba**	**La**	**Ce**	**Pr**	**Nd**	**Sm**	**Eu**	**Gd**
1259 Img17 - G3 - 1	1.28	0.90	0.37	0.05	0.05	0.10	0.11	5.29	12.56	1.29	5.09	0.82	0.11	0.46
1259 Img13- G3 - 1	0.16	0.61	0.10	0.03	<0.033	0.45	0.06	0.70	2.31	0.33	1.20	0.18	0.03	0.09
1259 Img13- G3 - 2	0.28	0.45	0.04	0.03	<0.036	0.39	0.04	0.40	1.29	0.18	0.61	0.13	0.01	0.02
1259 Img13- G4 - 1	0.07	0.40	0.04	0.02	<0.043	0.17	0.05	0.22	0.68	0.08	0.26	0.01	<0.003	0.09
1259 no img- G1 - 1	0.01	0.31	0.51	0.01	<0.027	0.16	0.01	0.10	0.39	0.04	0.16	0.05	0.00	0.04
1259 no img- G1 - 3	0.02	0.19	0.06	0.01	<0.029	0.08	<0.013	0.05	0.23	0.02	0.08	0.02	0.01	0.03
1259 no img- G2 - 1	0.02	0.29	0.02	0.00	<0.044	0.20	0.02	0.12	0.28	0.04	0.07	0.06	<0.002	0.02
1259 no img- G2 - 2	0.05	0.11	0.00	0.00	<0.027	0.16	0.04	0.01	0.09	0.01	0.05	<0.007	<0.002	<0.018
1259 no img- G2 - 3	0.02	0.12	0.01	0.00	<0.017	0.15	<0.012	0.03	0.10	0.02	0.07	0.02	<0.002	0.02
1259 no img- G2 - 4	0.06	0.52	0.01	0.01	<0.016	0.19	0.03	0.17	0.48	0.08	0.27	0.01	<0.002	0.05
1259 no img- G2 - 5	0.03	0.28	0.01	0.01	<0.043	0.23	0.01	0.13	0.44	0.06	0.18	0.04	0.01	0.03
1268 img 8- G1 - 1	0.11	0.42	0.02	0.58	<0.045	0.47	0.14	0.45	1.88	0.25	1.03	0.14	0.01	0.16
1268 img 8- G1 - 2	0.19	1.12	0.07	1.12	0.04	0.65	0.06	1.86	6.77	0.90	3.34	0.55	0.05	0.31
1268 img 8- G1 - 3	0.15	0.51	0.03	0.66	0.02	0.42	<0.012	0.86	3.49	0.40	1.52	0.22	0.02	0.24
1268 img 8- G1 - 4	0.08	0.36	0.03	0.57	<0.031	0.40	<0.013	0.65	2.33	0.35	1.33	0.16	0.01	0.07
1268 img 8- G2 - 1	0.20	0.67	0.01	0.96	<0.039	0.62	0.01	1.42	4.68	0.67	2.84	0.39	0.02	0.24
1268 img 8- G2 - 2	1.09	1.25	2.28	1.22	0.73	0.32	0.04	4.80	9.44	1.06	3.67	0.37	0.10	0.31
1268 img 8- G2 - 3	0.24	0.52	0.04	1.12	<0.023	0.43	0.10	1.57	4.74	0.65	2.36	0.50	0.03	0.25
1268 img 8- G2 - 5	0.18	0.55	0.02	0.83	<0.032	0.42	0.10	1.28	5.00	0.61	2.39	0.45	0.03	0.29
1268 img 8- G2 - 6	0.29	0.65	0.06	0.73	<0.032	0.32	0.05	1.65	5.17	0.69	2.79	0.37	0.05	0.34
1268 img 8- G2 - 7	0.10	0.66	0.46	0.85	0.51	0.29	0.04	0.80	3.09	0.35	1.56	0.21	0.03	0.14
1268 img 8- G2 - 8	0.72	1.63	0.13	2.21	0.05	0.69	0.70	4.58	15.89	1.94	7.30	1.26	0.08	0.85
1268 img 9- G1 - 1	0.09	0.26	0.06	0.26	<0.027	0.23	0.07	0.54	2.19	0.30	1.05	0.15	0.01	0.11
1268 img 9- G1 - 2	0.49	1.10	0.06	1.12	<0.033	0.47	0.54	1.20	4.31	0.48	2.22	0.37	0.03	0.28
1268 img 9- G2 - 3	0.32	0.61	0.05	0.52	<0.033	0.38	0.11	0.57	2.49	0.29	1.15	0.17	0.01	0.10
1268 img 9- G3 - 1	1.25	2.33	0.17	2.07	<0.036	0.84	1.13	5.08	13.59	1.91	7.60	1.07	0.11	0.70
1268 img 9- G3 - 2	1.11	0.47	0.16	0.40	<0.034	0.25	1.26	1.34	4.63	0.54	1.77	0.37	0.02	0.17
1268 img 9- G4 - 1	0.97	2.20	0.16	2.06	0.08	0.93	0.64	2.80	10.15	1.32	5.41	0.72	0.10	0.60
1268 img 9- G4 - 2	1.80	3.75	0.87	4.14	<0.041	1.45	1.04	7.29	21.91	2.69	10.24	1.63	0.16	1.26
1268 img 9- G4 - 3	4.30	4.32	1.25	2.73	<0.087	1.20	1.73	21.86	48.98	5.52	20.48	3.29	0.40	1.72
1268 img 9- G5 - 1	0.66	1.15	0.10	1.23	<0.031	0.59	0.49	2.15	7.24	0.97	3.94	0.61	0.07	0.41
1268 img 9- G6 - 1	0.18	0.87	0.07	1.39	<0.022	0.48	0.04	1.59	5.40	0.73	3.07	0.48	0.05	0.33
1268 img 9- G6 - 2	0.25	0.90	0.07	1.46	<0.032	0.42	0.04	1.94	7.10	0.94	3.93	0.58	0.06	0.40
1268 img 9- G6 - 3	0.28	1.12	0.07	1.60	<0.010	0.44	0.05	1.74	6.56	0.85	3.57	0.57	0.05	0.36
1268 img 9- G6 - 4	5.57	27.71	0.09	1.71	<0.019	0.48	1.12	7.07	31.00	5.00	23.54	3.91	0.45	3.67
1268 img 9- G6 - 5	1.60	2.02	0.45	2.29	<0.028	0.90	2.47	12.56	28.55	3.06	11.44	1.38	0.21	1.17
1268 img 9- G6 - 6	0.22	0.83	0.08	1.33	<0.025	0.55	0.08	1.39	5.45	0.66	2.54	0.39	0.04	0.25
1268 img 9- G6 - 7	0.64	1.26	0.14	1.41	<0.056	0.61	0.06	2.90	10.14	1.36	4.87	1.06	0.09	0.54
1268 img 9- G6 - 8	0.32	0.88	0.04	1.11	<0.015	0.41	0.39	1.60	5.69	0.78	3.25	0.49	0.04	0.44
1268 img 9- G6 - 9	0.25	0.62	0.05	0.83	<0.023	0.39	0.10	1.28	4.62	0.59	2.44	0.34	0.03	0.24
1268 img 10 G1 - 1	1.10	3.01	0.27	4.19	<0.037	1.49	0.66	3.64	12.92	1.75	7.07	1.36	0.13	0.88
1268 img 10 G1 - 2	1.01	4.18	0.42	4.52	0.04	1.36	0.43	6.21	20.05	2.64	10.48	1.70	0.17	1.18
1268 img 10 G1 - 3	0.71	4.36	0.35	4.82	<0.028	1.30	0.32	6.47	20.55	2.63	10.15	1.70	0.13	1.21
1268 img 10 G1 - 4	0.49	2.89	0.16	3.25	<0.035	0.89	0.14	4.46	14.41	1.77	8.02	1.19	0.11	0.91
1268 img 10 G1 - 5	0.45	2.80	0.15	3.12	<0.029	0.91	0.23	3.64	12.01	1.51	6.23	0.98	0.09	0.79
1268 img 10 G1 - 6	0.39	2.06	0.06	1.83	<0.018	0.57	0.06	2.71	9.19	1.18	4.27	0.71	0.08	0.50
1268 img 10 G1 - 7	0.50	2.40	0.12	2.43	<0.026	0.62	0.21	4.01	13.07	1.53	6.26	0.92	0.11	0.74
1268 img 10 G1 - 8	0.56	1.26	0.12	1.05	0.02	0.50	0.25	1.65	6.17	0.87	3.18	0.55	0.05	0.39
1268 img 10 G1 - 9	0.65	1.91	0.20	1.88	0.04	0.61	0.31	5.39	17.19	2.07	7.88	0.99	0.12	0.85
1268 img 10 G1 - 10	0.41	2.86	0.17	3.30	<0.019	0.83	0.14	3.14	11.39	1.32	5.55	0.90	0.07	0.63
1268 img 10 G1 - 11	0.37	2.71	0.20	3.34	<0.043	1.01	0.14	3.80	12.95	1.53	5.76	0.91	0.10	0.81
1268 img 10 G2 - 1	0.82	0.13	0.03	0.50	<0.056	0.37	1.34	0.37	1.10	0.10	0.34	0.04	<0.003	<0.014
1268 img 10 G2 - 2	0.67	0.88	0.10	1.19	<0.028	0.52	0.44	1.26	4.89	0.54	2.46	0.35	0.03	0.31
1268 img 10 G2 - 3	0.03	0.14	0.01	0.19	<0.019	0.19	0.05	0.12	0.65	0.06	0.23	0.04	0.01	0.03
1268 img 10 G2 - 4	2.06	2.54	0.35	3.24	0.05	1.18	2.86	3.30	11.91	1.43	5.72	1.05	0.09	0.73
1268 img 10 G2 - 5	0.59	2.02	0.23	2.18	0.13	1.12	0.24	2.18	7.93	1.03	3.98	0.65	0.07	0.58
1268 img 10 G3 - 1	0.35	0.31	0.03	0.39	<0.015	0.30	2.28	0.71	2.77	0.29	1.25	0.14	0.01	0.10
1268 img 10 G3 - 2	0.59	1.18	0.12	1.18	<0.032	0.54	0.69	1.68	6.21	0.80	2.92	0.66	0.05	0.35
1268 img 10 G3 - 3	0.92	1.94	0.52	1.81	<0.038	0.64	0.44	2.80	8.24	1.02	4.04	1.00	0.07	0.61
1268 img 10 G3 - 4	0.93	2.69	0.69	3.13	0.02	1.00	0.49	4.60	17.37	1.83	7.58	1.27	0.16	0.90
1268 img 10 G4 - 1	0.34	0.91	0.10	0.62	<0.019	0.38	0.12	1.21	3.63	0.51	2.03	0.31	0.04	0.24
1268 img 10 G4 - 3	1.96	1.98	0.14	1.04	<0.035	0.52	0.54	7.29	21.39	2.66	10.84	1.11	0.17	0.76
1268 img 10 G4 - 4	0.96	1.80	0.14	0.94	0.04	0.53	0.42	3.49	10.92	1.43	5.40	0.92	0.05	0.49
1268 img 11 G1 - 1	0.85	0.75	0.08	0.64	<0.023	0.49	0.97	1.32	4.61	0.56	2.30	0.33	0.05	0.21
1268 img 11 G1 - 2	1.19	2.69	0.18	3.66	<0.017	1.44	0.68	3.93	13.55	1.81	6.75	1.11	0.12	0.89
1268 img 11 G1 - 3	1.13	2.91	0.29	3.70	0.03	1.51	0.90	4.23	13.88	1.88	7.92	1.21	0.12	1.08
1268 img 11 G1 - 4	0.50	0.43	0.03	0.52	<0.026	0.33	0.73	0.76	2.67	0.29	1.14	0.21	0.03	0.21
1268 img 11 G1 - 5	0.37	0.50	0.06	0.73	<0.038	0.34	0.29	0.89	3.52	0.41	1.44	0.24	0.01	0.13
1268 img 11 G1 - 6	0.51	1.71	0.11	2.52	<0.047	0.85	0.31	1.91	8.01	0.93	3.87	0.54	0.08	0.42
1268 img 11 G1 - 7	0.32	0.57	0.03	0.86	<0.030	0.53	0.08	2.20	6.89	0.57	2.52	0.32	0.03	0.25
1268 img 11 G2 - 1	0.35	1.18	0.05	0.73	<0.042	0.51	0.06	2.20	6.98	0.88	3.48	0.53	0.04	0.35

Element concentrations in ppm
BDL: below detection limit
NA: no analysis
$Eu/Eu^* = [(Eu_{CN}/(Sm_{CN}+Gd_{CN})/2)]$
$Y/Y^* = [(Y_{CN}/(Dy_{CN}+Ho_{CN})/2)]$
$Ce/Ce^* = [(Ce_{CN}/(La_{CN} \times Pr_{CN})^{0.5})]$
CN = chondrite normalised
Normalising values from Sun and McDonough (1989)

Appendix 5 Table A4: Magnetite and hematite LA-ICP-MS trace element data collected at Vulcan in this study

Rejected Data

Source Filename	Tb	Dy	Ho	Er	Tm	Yb	Lu	Hf	Ta	W
1259 Img17 - G3 - 1	0.03	0.23	0.05	0.09	0.01	0.13	0.05	0.02	0.00	0.05
1259 Img13- G3 - 1	0.02	0.09	0.02	0.08	0.02	0.15	0.04	<0.004	0.07	0.01
1259 Img13- G3 - 2	0.00	0.09	0.02	0.07	0.01	0.17	0.02	<0.004	0.04	<0.005
1259 Img13- G4 - 1	0.01	0.03	0.02	0.04	0.01	0.08	0.01	<0.005	0.01	<0.006
1259 no img- G1 - 1	0.01	0.02	0.01	0.03	0.01	0.05	0.01	0.02	0.01	0.01
1259 no img- G1 - 3	0.01	0.02	0.01	0.02	0.00	0.04	0.00	<0.004	0.00	0.02
1259 no img- G2 - 1	0.00	0.04	0.01	0.04	0.01	0.06	0.01	0.01	0.00	0.01
1259 no img- G2 - 2	0.00	0.02	0.00	0.01	0.00	0.02	0.01	<0.004	0.00	0.02
1259 no img- G2 - 3	<0.001	0.02	0.01	0.02	0.01	0.03	0.00	<0.004	0.00	<0.005
1259 no img- G2 - 4	0.01	0.08	0.01	0.07	0.01	0.12	0.02	0.01	0.01	<0.005
1259 no img- G2 - 5	0.00	0.02	0.00	0.06	0.01	0.09	0.00	<0.004	0.03	<0.005
1268 img 8- G1 - 1	0.03	0.06	0.01	0.03	<0.001	0.03	0.01	<0.004	0.04	0.01
1268 img 8- G1 - 2	0.04	0.22	0.03	0.07	0.01	0.07	0.01	0.01	0.06	0.01
1268 img 8- G1 - 3	0.02	0.07	0.02	0.04	0.00	0.02	0.00	<0.004	0.03	<0.005
1268 img 8- G1 - 4	0.01	0.08	0.01	0.02	0.00	0.02	0.00	<0.005	0.03	0.01
1268 img 8- G2 - 1	0.03	0.14	0.02	0.05	0.01	0.04	0.01	<0.004	0.05	0.01
1268 img 8- G2 - 2	0.07	0.33	0.05	0.20	0.03	0.18	0.02	0.04	0.03	0.10
1268 img 8- G2 - 3	0.03	0.11	0.02	0.03	0.01	0.06	0.01	<0.004	0.06	0.04
1268 img 8- G2 - 5	0.02	0.14	0.01	0.05	0.00	0.07	0.01	<0.004	0.05	0.01
1268 img 8- G2 - 6	0.03	0.08	0.03	0.04	0.00	0.03	0.01	<0.004	0.03	0.01
1268 img 8- G2 - 7	0.04	0.16	0.02	0.08	0.01	0.03	0.01	<0.005	0.03	0.02
1268 img 8- G2 - 8	0.08	0.34	0.06	0.17	0.01	0.14	0.02	<0.005	0.11	0.01
1268 img 9- G1 - 1	0.01	0.08	0.01	0.02	<0.001	0.01	<0.001	<0.005	0.02	<0.006
1268 img 9- G1 - 2	0.04	0.19	0.04	0.10	0.02	0.12	0.01	0.01	0.07	0.10
1268 img 9- G2 - 3	0.02	0.07	0.02	0.06	0.00	0.08	0.01	0.01	0.03	0.05
1268 img 9- G3 - 1	0.08	0.41	0.08	0.17	0.03	0.22	0.03	0.01	0.14	0.20
1268 img 9- G3 - 2	0.02	0.05	0.02	0.05	<0.001	0.07	0.00	0.02	0.02	0.02
1268 img 9- G4 - 1	0.08	0.35	0.09	0.20	0.03	0.23	0.03	0.01	0.12	0.21
1268 img 9- G4 - 2	0.15	0.83	0.10	0.37	0.04	0.38	0.07	<0.005	0.19	<0.006
1268 img 9- G4 - 3	0.17	0.94	0.15	0.46	0.06	0.46	0.08	0.02	0.15	0.23
1268 img 9- G5 - 1	0.04	0.27	0.04	0.09	0.01	0.15	0.01	<0.004	0.07	0.14
1268 img 9- G6 - 1	0.06	0.19	0.03	0.06	0.01	0.10	0.01	<0.005	0.09	<0.006
1268 img 9- G6 - 2	0.04	0.19	0.02	0.06	0.01	0.08	0.02	<0.005	0.08	0.01
1268 img 9- G6 - 3	0.03	0.18	0.04	0.09	0.01	0.06	0.01	<0.004	0.07	<0.005
1268 img 9- G6 - 4	0.56	4.63	0.92	2.00	0.23	1.18	0.16	0.00	0.09	0.01
1268 img 9- G6 - 5	0.13	0.47	0.07	0.19	0.03	0.19	0.03	<0.005	0.10	<0.006
1268 img 9- G6 - 6	0.03	0.20	0.03	0.04	0.01	0.06	0.01	<0.005	0.07	<0.005
1268 img 9- G6 - 7	0.08	0.23	0.04	0.15	0.01	0.14	0.01	<0.007	0.08	0.01
1268 img 9- G6 - 8	0.05	0.20	0.03	0.07	0.01	0.08	0.01	0.01	0.06	0.03
1268 img 9- G6 - 9	0.02	0.12	0.02	0.05	0.00	0.04	0.01	<0.004	0.06	0.02
1268 img 10 G1 - 1	0.11	0.61	0.10	0.26	0.03	0.26	0.04	0.01	0.17	<0.006
1268 img 10 G1 - 2	0.17	0.80	0.16	0.30	0.04	0.21	0.04	0.01	0.23	0.01
1268 img 10 G1 - 3	0.18	0.80	0.14	0.32	0.04	0.18	0.05	0.01	0.21	<0.005
1268 img 10 G1 - 4	0.12	0.63	0.11	0.25	0.03	0.14	0.02	0.01	0.17	<0.006
1268 img 10 G1 - 5	0.10	0.60	0.10	0.20	0.02	0.15	0.03	<0.005	0.18	<0.006
1268 img 10 G1 - 6	0.09	0.42	0.06	0.15	0.01	0.12	0.01	0.01	0.10	0.01
1268 img 10 G1 - 7	0.10	0.47	0.08	0.17	0.02	0.17	0.02	0.01	0.12	0.01
1268 img 10 G1 - 8	0.06	0.24	0.06	0.12	0.03	0.17	0.01	<0.005	0.09	0.12
1268 img 10 G1 - 9	0.09	0.45	0.06	0.10	0.02	0.14	0.02	0.01	0.11	0.11
1268 img 10 G1 - 10	0.09	0.61	0.10	0.22	0.04	0.14	0.02	<0.004	0.16	<0.005
1268 img 10 G1 - 11	0.09	0.54	0.06	0.17	0.03	0.19	0.03	0.02	0.17	0.01
1268 img 10 G2 - 1	0.00	0.06	0.01	0.02	<0.001	0.02	<0.002	<0.005	0.03	<0.006
1268 img 10 G2 - 2	0.04	0.22	0.03	0.10	0.01	0.10	0.01	<0.005	0.06	0.01
1268 img 10 G2 - 3	0.00	0.02	0.00	0.01	0.00	0.01	<0.001	<0.004	0.01	<0.005
1268 img 10 G2 - 4	0.10	0.59	0.09	0.17	0.03	0.15	0.02	0.01	0.15	0.01
1268 img 10 G2 - 5	0.08	0.44	0.06	0.16	0.01	0.11	0.02	0.03	0.09	0.02
1268 img 10 G3 - 1	0.01	0.05	0.01	0.02	0.01	0.01	0.00	<0.005	0.03	0.06
1268 img 10 G3 - 2	0.04	0.19	0.03	0.13	0.02	0.10	0.00	0.01	0.07	0.04
1268 img 10 G3 - 3	0.05	0.51	0.10	0.14	0.01	0.13	0.04	0.02	0.11	0.12
1268 img 10 G3 - 4	0.11	0.55	0.10	0.25	0.04	0.22	0.05	0.05	0.14	0.02
1268 img 10 G4 - 1	0.02	0.12	0.03	0.09	0.01	0.10	0.01	0.01	0.04	0.14
1268 img 10 G4 - 3	0.05	0.41	0.07	0.16	0.02	0.20	0.03	0.01	0.07	0.28
1268 img 10 G4 - 4	0.05	0.31	0.06	0.17	0.02	0.25	0.03	0.02	0.08	0.20
1268 img 11 G1 - 1	0.02	0.14	0.01	0.08	0.01	0.08	0.01	0.01	0.04	0.07
1268 img 11 G1 - 2	0.12	0.61	0.09	0.21	0.03	0.23	0.04	<0.005	0.15	0.03
1268 img 11 G1 - 3	0.13	0.60	0.09	0.33	0.06	0.28	0.07	0.02	0.17	0.03
1268 img 11 G1 - 4	0.02	0.09	0.02	0.03	0.01	0.05	0.01	<0.004	0.02	0.01
1268 img 11 G1 - 5	0.02	0.10	0.02	0.03	0.00	0.01	0.01	<0.005	0.03	<0.006
1268 img 11 G1 - 6	0.06	0.34	0.06	0.16	0.02	0.10	0.02	<0.005	0.11	<0.005
1268 img 11 G1 - 7	0.03	0.12	0.03	0.05	0.00	<0.021	0.01	<0.004	0.04	<0.005
1268 img 11 G2 - 1	0.03	0.19	0.04	0.12	0.01	0.15	0.01	0.01	0.06	0.17

Element concentrations in ppm
BDL: below detection limit
NA: no analysis
$Eu/Eu^* = [(Eu_{CN}/(Sm_{CN}+Gd_{CN})/2)]$
$Y/Y^* = [(Y_{CN}/(Dy_{CN}+Ho_{CN})/2)]$
$Ce/Ce^* = [(Ce_{CN}/(La_{CN} \times Pr_{CN})^{0.5})]$
CN = chondrite normalised
Normalising values from Sun and McDonough (1989)

Appendix 5 Supplementary material for Mapping hydrothermal systems in IOCG deposits using apatite geochronology and geochemsitry: An example from Vulcan Cu-Au prospect

Appendix 5 Table A4: Magnetite and hematite LA-ICP-MS trace element data collected at Vulcan in this study

Rejected Data

Source Filename	Drill hole	Mineral	Comment
1268 img 11 G2 - 2	VUD 017 1268	Magnetite	High Mg, Al, V. High Ce, Th, La, Ca, P - apatite?
1268 img 11 G2 - 3	VUD 017 1268	Magnetite	High Mg, Al, V. High Ce, Th, La, Ca, P - Monazite? apatite?
1268 img 11 G2 - 4	VUD 017 1268	Magnetite	Monazite and apatite inclusions.
1268 img 11 G3 - 1	VUD 017 1268	Magnetite	Monazite and apatite inclusions before signal.
1268 img 11 G3 - 2	VUD 017 1268	Magnetite	High Mg, Al, V. High Ce, Th, La, Ca, P - apatite?
1268 img 11 G3 - 3	VUD 017 1268	Magnetite	High Mg, Al, V. High Ce, Th, La, Ca, P - apatite?
1268 img 11 G3 - 6	VUD 017 1268	Magnetite	High Mg, Al, V. High Ce, Th, La, Ca, P - apatite?
1268 img 12 G1 - 1	VUD 017 1268	Magnetite	High Mg, Al, V. High Ce, Th, La, Ca, P - apatite?
1268 img 12 G1 - 3	VUD 017 1268	Magnetite	Apatite inclusion.
1268 img 12 G1 - 4	VUD 017 1268	Magnetite	High Mg, Al, V. High Ce, Th, La, Ca, P - apatite?
1268 img 12 G2 - 1	VUD 017 1268	Magnetite	Monazite inclusion.
1268 img 12 G2 - 5	VUD 017 1268	Magnetite	High Al, Mg and V.
1268 img 12 G3 - 1	VUD 017 1268	Magnetite	High Mg, Al, V. High Ce, Th, La, Ca, P - apatite?
1268 img 12 G3 - 3	VUD 017 1268	Magnetite	High Mg, Al, V. High Ce, Th, La, Ca, P - apatite?
1268 img 12 off G4 - 1	VUD 017 1268	Magnetite	High Mg, Al, V. High Ce, Th, La, Ca, P - apatite?
1268 img 12 off G4 - 2	VUD 017 1268	Magnetite	High Mg, Al, V. High Ce, Th, La, Ca, P - apatite?
1268 img 12 off G4 - 3	VUD 017 1268	Magnetite	High Mg, Al, V. High Ce, Th, La, Ca, P - apatite?
1268 img 12 off G4 - 4	VUD 017 1268	Magnetite	High Mg, Al, V. High Ce, Th, La, Ca, P - apatite?
1268 img 12 off G4 - 5	VUD 017 1268	Magnetite	Monazite apatite inclusions.
1268 img 12 off G5 - 1	VUD 017 1268	Magnetite	High Mg, Al, V. High Ce, Th, La, Ca, P - apatite?
1268 img 12 off G5 - 2	VUD 017 1268	Magnetite	High Mg, Al, V. High Ce, Th, La, Ca, P - apatite?
1268 img 12 off G5 - 3	VUD 017 1268	Magnetite	High Mg, Al, V. High Ce, Th, La, Ca, P - apatite?
1268 img 12 off G5 - 4	VUD 017 1268	Magnetite	High Mg, Al, V. High Ce, Th, La, Ca, P - apatite?
1268 img 12 off G6 - 1	VUD 017 1268	Magnetite	High Mg, Al, V. High Ce, Th, La, Ca, P - apatite?
1268 img 12 off G6 - 2	VUD 017 1268	Magnetite	High Mg, Al, V. High Ce, Th, La, Ca, P - apatite?
1268 img 12 off G6 - 3	VUD 017 1268	Magnetite	High Mg, Al, V. High Ce, Th, La, Ca, P - apatite?
1268 img 12 off G6 - 4	VUD 017 1268	Magnetite	High Mg, Al, V. High Ce, Th, La, Ca, P - apatite?
1268 img 12 off G7 - 1	VUD 017 1268	Magnetite	High Al, V and Mg, High Cem Th, P, La, Ca - apaptite? Ti inclusions
1268 img 12 off G7 - 3	VUD 017 1268	Magnetite	High V, Al, Mg. High Ce, High U, Th, P, Ca and La
1268 img 12 off G7 - 4	VUD 017 1268	Magnetite	High Mg, Al, V. High Ce, Th, La, Ca, P - apatite?
1268 img 12 off G7 - 5	VUD 017 1268	Magnetite	High Mg, Al, V. High Ce, Th, La, Ca, P - apatite?
1268 img 12 off G7 - 6	VUD 017 1268	Magnetite	High Mg, Al, V. High Ce, Th, La, Ca, P - apatite?
1268 img 12 off G7 - 7	VUD 017 1268	Magnetite	High Mg, Al, V. High Ce, Th, La, Ca, P - apatite?
1268 img 12 off G7 - 8	VUD 017 1268	Magnetite	High Mg, Al, V. High Ce, Th, La, Ca, P - apatite?
1268 img 12 off G7 - 9	VUD 017 1268	Magnetite	High Mg, Al, V. High Ce, Th, La, Ca, P - apatite?
1268 img 12 off G7 - 10	VUD 017 1268	Magnetite	Monazite inclusion.
1268 no image top G1 - 1	VUD 017 1268	Magnetite	High Mg, Al, V. High Ce, Th, La, Ca, P - apatite?
1268 no image top G1 - 2	VUD 017 1268	Magnetite	High Mg, Al, V. High Ce, Th, La, Ca, P - apatite?
1268 no image top G1 - 3	VUD 017 1268	Magnetite	Monazite inclusions.
1268 no image top G1 - 4	VUD 017 1268	Magnetite	Cu inclusion. High La, Ce, Th - monazite
1268 no image top G1 - 5	VUD 017 1268	Magnetite	Cu inclusion. High La, Ce, Th - monazite
1268 no image top G1 - 6	VUD 017 1268	Magnetite	High Mg, Al, V. High Ce, Th, La, Ca, P - monazite? apatite?
1268 no image top G1 - 7	VUD 017 1268	Magnetite	High Mg, Al, V. High Ce, Th, La, Ca, P - apatite?
1268 no image top G1 - 8	VUD 017 1268	Magnetite	Pr spike. High Mg, Al, V. High Ce, Th, La, Ca, P - monazite? apatite?
1268 no image top G1 - 9	VUD 017 1268	Magnetite	Monazite inclusion.
1268 no image top G1 - 10	VUD 017 1268	Magnetite	High Mg, Al, V. High Ce, Th, La, Ca, P - monazite? apatite?
1268 no image top G1 - 11	VUD 017 1268	Magnetite	High Mg, Al, V. High Ce, Th, La, Ca, P - monazite? apatite?
1268 no image top G1 - 12	VUD 017 1268	Magnetite	High Mg, Al, V. High Ce, Th, La, Ca, P - monazite? apatite?
1268 no image top G2 - 1	VUD 017 1268	Magnetite	High Mg, Al, V. High Ce, Th, La, Ca, P - monazite? apatite?
1268 no image top G2 - 2	VUD 017 1268	Magnetite	Monazite inclusions.
1268 no image top G2 - 3	VUD 017 1268	Magnetite	High Mg, Al, V. High Ce, Th, La, Ca, P - monazite? apatite?
1268 no image top G2 - 4	VUD 017 1268	Magnetite	High Mg, Al, V. High Ce, Th, La, Ca, P - monazite? apatite?
1268 no image top G2 - 5	VUD 017 1268	Magnetite	High Mg, Al, V. High Ce, Th, La, Ca, P - monazite? apatite?
1268 no image top G2 - 6	VUD 017 1268	Magnetite	High Mg, Al, V. High Ce, Th, La, Ca, P - monazite? apatite?
1268 no image top G2 - 7	VUD 017 1268	Magnetite	High Mg, Al, V. High Ce, Th, La, Ca, P - monazite? apatite?
1268 no image top G2 - 8	VUD 017 1268	Magnetite	High Mg, Al, V. High Ce, Th, La, Ca, P - monazite? apatite?
1268 no image top G2 - 9	VUD 017 1268	Magnetite	High Mg, Al, V. Mn inclusion, Monazite inclusion?
1268 no image top G2 - 10	VUD 017 1268	Magnetite	High Mg, Al, V. High Ce, Th, La, Ca, P - monazite? apatite?
1268 no image top G2 - 11	VUD 017 1268	Magnetite	High Mg, Al, V. High Ce, Th, La, Ca, P - monazite? apatite?
1268 no image top G2 - 12	VUD 017 1268	Magnetite	High Mg, Al, V. High Ce, Th, La, Ca, P - monazite? apatite?
1268 no image top G2 - 13	VUD 017 1268	Magnetite	High Mg, Al, V. High Ce, Th, La, Ca, P - monazite? apatite?
1268 no image top G2 - 14	VUD 017 1268	Magnetite	High Mg, Al, V. High Ce, Th, La, Ca, P - monazite? apatite?
1268 no image top G2 - 15	VUD 017 1268	Magnetite	High Mg, Al, V. High Ce, Th, La, Ca, P - monazite? apatite?
1192 Img 4 G3 - 2	VUD 007 1192	Magnetite	Mg inclusions. High P, Ce and La
1192 Img 5 G3 - 4	VUD 007 1192	Magnetite	Off haem grain Fe drop
1192 Img 6 G1 - 2	VUD 007 1192	Magnetite	High Al, Mg and V. Apatite inclusion,
1192 Img 3 G2 - 1	VUD 007 1192	Magnetite	Monazite inclusions.
1192 no image bottom G4 - 1	VUD 007 1192	Magnetite	High V and Al. low Mg and P
1192 no image bottom G7 - 3	VUD 007 1192	Magnetite	Al-Mg inclusions. Ce inclusions
1192 off img2 G3 - 1	VUD 007 1192	Magnetite	Mg Al inclusions. High V and Al. Mg and P
1192 no image bottom R G1 - 2	VUD 007 1192	Magnetite	High V, Al, Mg. P and Ce

Element concentrations in ppm
BDL: below detection limit
NA: no analysis
$Eu/Eu^* = [(Eu_{CN}/(Sm_{CN}+Gd_{CN})/2)]$
$Y/Y^* = [(Y_{CN}/(Dy_{CN}+Ho_{CN})/2)]$
$Ce/Ce^* = [(Ce_{CN}/(La_{CN} \times Pr_{CN})^{0.5})]$
CN = chondrite normalised
Normalising values from Sun and McDonough (1989)

Appendix 5 Supplementary material for Mapping hydrothermal systems in IOCG deposits using apatite geochronology and geochemsitry: An example from Vulcan Cu-Au prospect

Appendix 5 Table A4: Magnetite and hematite LA-ICP-MS trace element data collected at Vulcan in this study

Rejected Data

Source Filename	Mg	Al	Si	P	Ca	Ti	V	Mn	Fe	Co	Ni	Cu	Zn	As
1268 img 11 G2 - 2	739	478	2993	<10.916	917	82	292	9	720000	2.11	37.67	1.62	5.56	0.31
1268 img 11 G2 - 3	1547	569	5568	12	1652	81	285	9	720000	3.07	37.76	1.15	7.34	0.41
1268 img 11 G2 - 4	2518	688	6594	214	1895	106	297	172	720000	3.91	45.85	1.98	19.64	1.37
1268 img 11 G3 - 1	702	517	3083	<14.905	740	83	258	19	720000	2.81	40.41	0.87	13.97	0.55
1268 img 11 G3 - 2	916	665	3928	<8.305	1059	137	287	12	720000	3.19	34.04	0.40	3.14	0.37
1268 img 11 G3 - 3	831	587	3687	<8.814	1023	144	276	15	720000	3.97	40.54	0.96	13.13	0.47
1268 img 11 G3 - 6	3240	797	5919	<14.605	1594	208	272	249	720000	4.35	33.83	1.09	21.08	0.83
1268 img 12 G1 - 1	905	502	4246	22	1058	71	280	14	720000	2.44	50.03	1.33	8.66	0.68
1268 img 12 G1 - 3	1625	1363	7190	530	2391	168	281	22	720000	4.54	36.70	1.15	18.36	1.18
1268 img 12 G1 - 4	1589	822	7090	<10.368	2074	142	280	20	720000	8.42	38.32	0.99	7.60	0.81
1268 img 12 G2 - 1	516	952	3234	36	812	75	287	11	720000	12.59	36.68	3.81	2.73	1.02
1268 img 12 G2 - 5	501	386	2286	<12.669	609	46	300	7	720000	3.09	48.11	0.91	4.29	0.93
1268 img 12 G3 - 1	1603	748	6279	18	2112	119	283	10	720000	3.89	32.11	0.38	4.03	0.79
1268 img 12 G3 - 3	1570	519	5160	19	1794	64	288	10	720000	3.28	36.51	0.62	3.26	0.72
1268 img 12 off G4 - 1	1109	606	5028	<10.554	1216	129	292	18	720000	3.76	44.23	1.45	8.41	0.53
1268 img 12 off G4 - 2	1457	745	6464	13	1705	168	288	23	720000	4.54	39.91	1.28	3.64	0.73
1268 img 12 off G4 - 3	1362	699	6545	12	1691	179	282	26	720000	4.75	42.39	1.83	3.53	0.38
1268 img 12 off G4 - 4	1190	684	5383	9	1608	148	277	24	720000	4.11	46.27	1.40	8.43	0.60
1268 img 12 off G4 - 5	1837	933	8171	16	2126	173	303	26	720000	4.84	44.82	1.39	20.01	2.25
1268 img 12 off G5 - 1	825	564	3225	<10.869	760	95	290	11	720000	7.39	31.98	1.01	0.59	0.54
1268 img 12 off G5 - 2	2459	1001	9787	28	2636	150	298	15	720000	7.46	32.09	1.38	1.13	0.80
1268 img 12 off G5 - 3	2550	1156	10672	41	3113	150	291	15	720000	9.13	29.84	2.89	6.18	1.21
1268 img 12 off G5 - 4	2977	1088	11405	46	2942	123	285	14	720000	7.84	34.60	3.39	4.12	1.05
1268 img 12 off G6 - 1	1932	838	7889	25	2227	108	290	12	720000	3.78	35.36	2.01	6.56	0.87
1268 img 12 off G6 - 2	2914	936	10401	29	2828	136	277	12	720000	4.65	30.67	1.70	5.72	0.85
1268 img 12 off G6 - 3	2686	911	9621	33	2754	140	289	12	720000	4.97	26.94	1.42	0.72	0.83
1268 img 12 off G6 - 4	2638	1043	8695	24	2269	128	289	46	720000	4.86	29.15	2.10	20.42	0.88
1268 img 12 off G7 - 1	718	589	3787	14	790	135	287	8	720000	3.06	28.93	0.55	1.32	0.36
1268 img 12 off G7 - 3	739	621	4034	<10.549	666	160	293	9	720000	3.26	30.45	0.82	<0.216	0.44
1268 img 12 off G7 - 4	867	636	4344	43	958	140	299	9	720000	4.33	29.39	0.51	1.36	0.54
1268 img 12 off G7 - 5	921	607	4368	<9.349	855	158	280	9	720000	4.27	28.21	0.71	<0.204	0.40
1268 img 12 off G7 - 6	809	663	4620	22	708	178	283	7	720000	2.35	30.20	0.26	1.74	0.64
1268 img 12 off G7 - 7	530	580	3713	15	479	158	290	8	720000	3.14	29.01	0.58	3.59	0.53
1268 img 12 off G7 - 8	445	600	3139	11	332	186	299	7	720000	1.95	27.54	0.32	1.16	0.43
1268 img 12 off G7 - 9	318	582	2958	<8.880	197	272	285	8	720000	1.97	30.44	0.36	0.97	0.33
1268 img 12 off G7 - 10	2375	1051	4744	27	905	147	295	136	720000	4.08	31.73	<0.244	47.72	0.69
1268 no image top G1 - 1	2294	704	7656	<11.999	2376	132	286	12	720000	4.18	31.18	1.44	2.98	0.72
1268 no image top G1 - 2	2354	852	8484	16	2321	146	289	12	720000	4.57	30.70	0.43	2.05	0.82
1268 no image top G1 - 3	2023	817	8028	48	1710	146	289	11	720000	4.67	30.69	19.84	4.95	0.92
1268 no image top G1 - 4	2225	1295	7807	455	3568	170	278	29	720000	3.89	28.95	367.18	15.99	0.85
1268 no image top G1 - 5	2678	817	8596	144	3124	149	295	12	720000	6.06	30.54	31.13	11.47	0.77
1268 no image top G1 - 6	2565	828	8886	47	2945	118	286	14	720000	5.40	34.37	4.26	2.83	0.71
1268 no image top G1 - 7	2732	856	8952	28	2757	145	300	13	720000	8.49	37.64	11.49	2.18	0.93
1268 no image top G1 - 8	1869	471	5786	19	2210	50	289	50	720000	2.76	45.50	1.43	12.49	0.81
1268 no image top G1 - 9	1303	621	4645	<11.128	1519	112	282	10	720000	2.81	28.53	99.16	3.47	0.73
1268 no image top G1 - 10	2325	690	7754	14	2102	123	270	12	720000	3.86	31.77	4.35	1.07	0.83
1268 no image top G1 - 11	2880	768	8959	18	2659	129	310	14	720000	3.91	32.25	2.36	2.42	1.28
1268 no image top G1 - 12	2354	937	8469	19	2555	154	302	24	720000	4.18	30.14	3.40	11.47	0.63
1268 no image top G2 - 1	2958	2188	10213	32	2392	149	285	19	720000	4.54	34.75	2.14	26.66	2.27
1268 no image top G2 - 2	3154	943	7116	66	2017	135	272	169	720000	4.77	31.36	1.74	35.06	1.16
1268 no image top G2 - 3	2320	740	7950	147	2541	146	275	11	720000	4.34	30.93	0.98	4.18	0.54
1268 no image top G2 - 4	2493	825	8470	26	2310	161	300	13	720000	5.16	29.92	1.76	0.25	0.67
1268 no image top G2 - 5	2226	854	8588	17	2259	156	277	13	720000	7.04	33.12	2.04	0.90	0.87
1268 no image top G2 - 6	2399	1095	8781	12	2656	212	291	14	720000	6.04	31.20	1.63	11.20	0.81
1268 no image top G2 - 7	2487	924	9040	20	2527	197	311	12	720000	19.25	30.56	2.16	0.18	0.97
1268 no image top G2 - 8	2584	1035	9742	31	2819	198	314	14	720000	4.15	33.62	2.15	4.06	1.36
1268 no image top G2 - 9	2328	626	3040	<12.666	1099	298	294	158	720000	2.94	28.61	<0.260	21.12	1.19
1268 no image top G2 - 10	2556	946	8842	12	2458	223	270	12	720000	7.40	27.87	1.51	0.75	0.53
1268 no image top G2 - 11	3226	1483	9489	27	2607	195	299	15	720000	3.94	31.38	0.85	16.82	1.02
1268 no image top G2 - 12	3163	797	9342	15	2766	156	280	184	720000	3.88	30.24	2.38	10.11	3.08
1268 no image top G2 - 13	2383	890	8962	18	2551	212	283	14	720000	4.19	27.59	1.75	1.73	0.64
1268 no image top G2 - 14	2053	859	7492	31	2314	163	281	12	720000	4.15	28.98	1.84	33.31	0.58
1268 no image top G2 - 15	3092	1677	9196	33	2388	146	304	25	720000	3.84	30.78	1.29	32.49	1.12
1192 Img 4 G3 - 2	67	173	650	<9.086	148	25	311	9	720000	6.72	252.50	<0.235	0.93	0.79
1192 Img 5 G3 - 4	258837	65566	3276805	422	468811	834	21	209	720000	8.48	69.36	20.74	38.07	7327.80
1192 Img 6 G1 - 2	238	1073	1605	<15.675	227	54	52	12	720000	3.62	103.61	<0.227	8.22	1.17
1192 Img 3 G2 - 1	204	384	3053	<13.351	240	105	84	19	720000	2.77	169.34	<0.205	2.32	5.40
1192 no image bottom G4 - 1	NA	NA	NA	NA	NA	NA	NA	NA	NA	NA	NA	NA	NA	NA
1192 no image bottom G7 - 3	251	272	2056	<12.433	56	32	19	18	720000	4.33	31.94	<0.236	2.32	3.14
1192 off img2 G3 - 1	1212	2211	2756	<13.197	<44.104	74	47	14	720000	4.10	121.58	0.44	7.89	1.52
1192 no image bottom R G1 - 2	358	283	3053	<14.814	567	24	701	11	720000	7.91	218.72	0.41	2.65	0.97

Element concentrations in ppm
BDL: below detection limit
NA: no analysis
$Eu/Eu^* = [(Eu_{CN}/(Sm_{CN}+Gd_{CN})/2)]$
$Y/Y^* = [(Y_{CN}/(Dy_{CN}+Ho_{CN})/2)]$
$Ce/Ce^* = [(Ce_{CN}/(La_{CN} \times Pr_{CN})^{0.5})]$
CN = chondrite normalised
Normalising values from Sun and McDonough (1989)

Appendix 5 Table A4: Magnetite and hematite LA-ICP-MS trace element data collected at Vulcan in this study

Rejected Data

Source Filename	Sr	Y	Zr	Nb	Mo	Sn	Ba	La	Ce	Pr	Nd	Sm	Eu	Gd
1268 img 11 G2 - 2	0.38	0.83	0.07	0.82	<0.047	0.45	0.21	1.49	5.40	0.67	2.77	0.40	0.03	0.34
1268 img 11 G2 - 3	0.61	1.52	0.18	1.47	<0.025	0.43	0.35	3.87	13.15	1.68	7.23	0.98	0.10	0.66
1268 img 11 G2 - 4	1.61	8.87	0.61	1.83	0.03	0.72	0.89	240.76	492.29	46.56	153.59	17.63	3.18	8.84
1268 img 11 G3 - 1	0.73	0.89	0.11	0.89	0.08	0.48	0.26	1.04	3.57	0.48	1.84	0.23	0.04	0.16
1268 img 11 G3 - 2	0.51	1.33	0.08	1.33	<0.017	0.64	0.39	1.70	5.42	0.75	3.13	0.57	0.07	0.48
1268 img 11 G3 - 3	0.49	1.21	0.09	1.21	0.23	0.62	0.32	1.64	5.39	0.80	2.95	0.39	0.05	0.36
1268 img 11 G3 - 6	1.38	2.29	0.83	3.12	0.75	0.99	0.24	5.94	13.62	1.85	7.12	0.95	0.09	0.66
1268 img 12 G1 - 1	0.33	1.01	0.04	0.42	0.05	0.26	<0.013	0.87	3.52	0.39	1.61	0.34	0.05	0.25
1268 img 12 G1 - 3	2.25	3.19	0.37	1.73	0.63	0.85	0.83	7.10	20.43	2.17	8.78	1.56	0.17	0.92
1268 img 12 G1 - 4	0.95	2.17	0.16	1.76	<0.027	0.88	0.48	3.46	11.64	1.66	6.22	1.03	0.11	0.78
1268 img 12 G2 - 1	3.09	2.20	0.05	1.22	0.02	0.61	4.64	7.68	18.73	2.10	7.57	1.09	0.14	0.72
1268 img 12 G2 - 5	0.22	0.51	0.14	0.54	0.06	0.26	0.13	0.63	2.25	0.30	1.47	0.14	0.04	0.12
1268 img 12 G3 - 1	0.82	1.76	0.14	2.19	<0.030	0.84	0.46	3.04	9.57	1.41	5.42	0.98	0.12	0.66
1268 img 12 G3 - 3	0.91	1.98	0.12	1.31	<0.029	0.45	0.53	5.47	18.62	2.33	9.10	1.32	0.16	0.72
1268 img 12 off G4 - 1	0.43	1.37	0.09	1.44	<0.034	0.66	0.20	2.02	7.08	0.95	3.93	0.57	0.05	0.42
1268 img 12 off G4 - 2	0.70	2.06	0.13	2.14	<0.028	1.01	0.34	2.88	10.68	1.37	5.22	0.90	0.11	0.70
1268 img 12 off G4 - 3	0.76	1.85	0.15	2.18	<0.016	1.00	0.39	2.86	9.98	1.31	5.30	0.93	0.08	0.53
1268 img 12 off G4 - 4	0.55	1.78	0.09	1.59	<0.021	0.76	0.31	2.20	7.88	1.13	4.28	0.77	0.08	0.44
1268 img 12 off G4 - 5	1.92	2.80	0.67	2.83	1.75	1.11	0.41	12.82	31.18	3.22	12.07	1.84	0.25	1.20
1268 img 12 off G5 - 1	0.36	1.31	0.10	1.02	<0.039	0.72	0.19	2.85	9.16	1.10	4.47	0.80	0.07	0.58
1268 img 12 off G5 - 2	1.58	4.09	0.26	3.61	<0.020	1.54	0.82	9.95	31.92	3.98	16.21	2.51	0.23	1.77
1268 img 12 off G5 - 3	2.47	5.58	0.45	4.57	0.06	1.82	2.90	11.88	37.17	4.70	19.44	3.34	0.35	2.35
1268 img 12 off G5 - 4	2.24	4.84	0.34	3.97	<0.025	1.44	1.83	13.16	42.06	5.28	20.75	3.69	0.33	2.54
1268 img 12 off G6 - 1	2.17	3.34	0.18	2.34	<0.021	1.13	3.80	7.89	26.57	3.11	13.08	2.17	0.19	1.40
1268 img 12 off G6 - 2	1.47	4.54	0.24	4.38	<0.026	1.36	0.73	12.56	37.49	4.77	18.95	3.17	0.27	2.14
1268 img 12 off G6 - 3	1.18	4.42	0.27	3.70	<0.016	1.20	0.58	9.71	32.06	4.10	14.62	2.71	0.25	1.95
1268 img 12 off G6 - 4	1.76	3.72	0.25	3.03	0.04	1.19	1.98	9.32	29.66	3.58	14.96	2.36	0.23	1.60
1268 img 12 off G7 - 1	0.19	0.87	0.03	0.92	<0.039	0.44	0.06	1.42	5.20	0.66	2.95	0.43	0.03	0.38
1268 img 12 off G7 - 3	0.23	0.94	0.06	1.24	<0.015	0.53	0.04	1.44	5.63	0.65	2.74	0.43	0.06	0.39
1268 img 12 off G7 - 4	0.25	1.18	0.16	1.18	<0.044	0.49	0.10	1.66	6.31	0.78	2.82	0.53	0.06	0.43
1268 img 12 off G7 - 5	0.18	0.94	0.05	1.44	<0.045	0.51	0.13	1.79	6.34	0.83	3.53	0.67	0.06	0.40
1268 img 12 off G7 - 6	0.32	1.07	0.09	1.46	<0.027	0.64	0.08	1.73	5.90	0.78	3.00	0.39	0.04	0.45
1268 img 12 off G7 - 7	0.17	0.75	0.05	0.69	<0.015	0.52	<0.013	0.91	3.14	0.42	1.71	0.31	0.01	0.26
1268 img 12 off G7 - 8	0.10	0.68	0.03	0.73	0.02	0.48	<0.013	0.65	2.28	0.27	1.04	0.26	0.01	0.15
1268 img 12 off G7 - 9	0.03	0.44	0.03	0.88	<0.034	0.55	0.01	0.34	1.28	0.15	0.67	0.13	0.01	0.14
1268 img 12 off G7 - 10	2.93	2.17	1.46	1.30	0.08	0.69	0.45	30.80	56.00	6.13	21.36	2.99	0.47	1.64
1268 no image top G1 - 1	1.20	2.87	0.12	2.89	<0.038	0.65	0.70	8.50	26.38	3.38	13.45	1.88	0.16	1.51
1268 no image top G1 - 2	1.05	3.66	0.19	2.68	0.05	0.98	0.44	9.04	27.86	3.58	13.87	2.13	0.18	1.40
1268 no image top G1 - 3	3.56	3.26	0.05	2.50	<0.027	0.84	0.49	43.70	94.81	11.10	40.03	4.13	0.76	2.63
1268 no image top G1 - 4	3.41	4.99	0.42	3.86	<0.029	1.00	4.56	12.97	37.82	4.73	18.92	2.83	0.30	1.87
1268 no image top G1 - 5	2.27	3.62	0.15	3.33	0.04	0.88	1.96	12.28	37.89	4.74	20.00	2.14	0.20	1.50
1268 no image top G1 - 6	1.43	3.25	0.17	2.61	<0.023	0.97	0.77	11.33	36.60	4.57	17.71	2.42	0.18	1.76
1268 no image top G1 - 7	1.66	3.62	0.85	3.33	0.04	1.31	0.87	11.41	37.93	4.42	17.12	2.10	0.20	1.49
1268 no image top G1 - 8	1.83	1.78	0.34	0.77	<0.035	0.53	2.41	6.54	21.16	4.33	9.47	1.52	0.14	0.75
1268 no image top G1 - 9	1.07	1.84	0.17	4.72	<0.038	0.49	1.33	10.77	26.03	2.95	10.69	1.40	0.18	0.96
1268 no image top G1 - 10	1.27	2.64	0.15	2.45	<0.036	0.78	0.77	8.88	29.66	3.57	13.94	1.77	0.16	1.53
1268 no image top G1 - 11	1.19	2.71	0.23	3.08	<0.057	0.79	0.62	10.35	32.71	4.00	16.20	2.24	0.21	1.60
1268 no image top G1 - 12	2.00	4.92	0.23	4.31	<0.038	1.01	1.75	10.49	33.75	4.06	15.45	2.38	0.19	1.41
1268 no image top G2 - 1	2.11	3.92	0.39	3.47	<0.034	1.23	1.25	14.76	42.31	4.68	19.09	2.71	0.32	1.57
1268 no image top G2 - 2	6.96	3.72	1.08	2.40	0.27	0.78	2.27	61.56	128.01	12.94	45.44	6.23	0.83	3.43
1268 no image top G2 - 3	1.31	4.19	0.09	2.08	<0.008	0.90	0.54	8.59	29.80	3.59	14.36	2.19	0.19	1.30
1268 no image top G2 - 4	1.25	3.38	0.15	2.93	0.03	0.83	0.56	9.97	32.50	3.99	15.55	2.20	0.19	1.62
1268 no image top G2 - 5	1.30	3.70	0.16	3.12	<0.026	1.08	1.08	10.56	34.05	3.99	15.13	2.13	0.17	1.68
1268 no image top G2 - 6	1.56	5.16	0.28	4.07	<0.028	1.42	0.84	10.84	35.21	4.13	16.82	2.68	0.23	1.60
1268 no image top G2 - 7	1.20	4.06	0.22	3.29	<0.044	1.32	0.46	10.45	33.12	4.04	15.73	2.07	0.26	1.54
1268 no image top G2 - 8	1.52	4.74	0.25	4.01	0.07	1.54	1.00	11.55	37.71	4.53	17.49	2.56	0.26	1.67
1268 no image top G2 - 9	1.84	1.99	1.63	2.93	1.11	0.61	1.06	4.51	13.04	1.57	6.27	0.91	0.09	0.69
1268 no image top G2 - 10	1.18	5.63	0.24	4.27	0.05	1.45	0.75	10.25	33.27	3.88	15.52	2.28	0.24	1.53
1268 no image top G2 - 11	1.43	4.24	0.18	3.19	0.04	1.00	1.36	10.17	33.93	3.98	15.78	2.21	0.19	1.34
1268 no image top G2 - 12	1.23	3.03	0.84	2.70	0.03	0.75	1.56	9.22	29.95	3.70	14.50	2.16	0.22	1.87
1268 no image top G2 - 13	0.99	6.76	0.36	6.08	<0.021	1.22	0.42	9.35	29.70	3.77	14.60	2.32	0.25	1.56
1268 no image top G2 - 14	1.83	4.17	0.21	3.21	<0.035	1.24	1.18	9.04	28.69	3.49	13.63	1.97	0.19	1.46
1268 no image top G2 - 15	2.56	3.65	0.13	3.43	<0.027	0.76	3.32	13.71	38.55	4.89	18.16	2.52	0.28	1.23
1192 Img 4 G3 - 2	0.28	0.11	0.12	0.09	<0.032	0.10	0.43	0.58	1.19	0.14	0.37	0.05	0.01	0.03
1192 Img 5 G3 - 4	333.22	17.60	2113.39	7.13	<0.668	3.49	1953.43	21.64	39.44	4.45	16.19	2.09	1.60	1.79
1192 Img 6 G1 - 2	0.24	0.25	0.03	0.51	0.05	0.28	0.50	0.37	1.18	0.11	0.57	0.05	<0.004	0.09
1192 Img 3 G2 - 1	0.45	1.07	0.29	3.31	0.35	0.67	0.21	1.03	4.62	0.36	1.65	0.37	0.06	0.23
1192 no image bottom G4 - 1	NA	NA	NA	NA	NA	NA	NA	NA	NA	NA	NA	NA	NA	NA
1192 no image bottom G7 - 3	0.67	1.30	1.31	3.70	2.32	0.62	0.34	1.20	2.82	0.25	0.67	0.12	0.02	0.23
1192 off img2 G3 - 1	0.06	0.01	0.24	0.30	<0.044	0.19	0.15	0.01	0.02	0.00	<0.011	0.01	<0.003	<0.016
1192 no image bottom R G1 - 2	0.54	0.47	0.06	0.13	<0.040	0.37	0.34	1.03	2.89	0.31	1.26	0.11	<0.004	0.11

Element concentrations in ppm
BDL: below detection limit
NA: no analysis
$Eu/Eu^* = [(Eu_{CN}/(Sm_{CN}+Gd_{CN})/2)]$
$Y/Y^* = [(Y_{CN}/(Dy_{CN}+Ho_{CN})/2)]$
$Ce/Ce^* = [(Ce_{CN}/(La_{CN} \times Pr_{CN})^{0.5})]$
CN = chondrite normalised
Normalising values from Sun and McDonough (1989)

Appendix 5 Table A4: Magnetite and hematite LA-ICP-MS trace element data collected at Vulcan in this study

Rejected Data

Source Filename	Tb	Dy	Ho	Er	Tm	Yb	Lu	Hf	Ta	W
1268 img 11 G2 - 2	0.02	0.18	0.04	0.08	0.01	0.12	0.02	<0.004	0.04	<0.005
1268 img 11 G2 - 3	0.05	0.32	0.04	0.14	0.02	0.14	0.02	<0.004	0.07	0.02
1268 img 11 G2 - 4	0.76	2.70	0.32	0.65	0.06	0.33	0.03	0.02	0.12	0.14
1268 img 11 G3 - 1	0.02	0.20	0.02	0.11	0.01	<0.020	0.01	<0.006	0.05	0.12
1268 img 11 G3 - 2	0.05	0.27	0.04	0.13	0.01	0.15	0.02	<0.004	0.07	0.02
1268 img 11 G3 - 3	0.03	0.19	0.03	0.08	0.02	0.12	0.02	<0.005	0.06	0.11
1268 img 11 G3 - 6	0.09	0.38	0.06	0.24	0.02	0.22	0.03	0.04	0.10	0.12
1268 img 12 G1 - 1	0.03	0.22	0.03	0.11	0.01	0.13	0.02	<0.005	0.03	0.24
1268 img 12 G1 - 3	0.10	0.56	0.12	0.24	0.04	0.17	0.03	0.01	0.11	0.13
1268 img 12 G1 - 4	0.07	0.38	0.08	0.16	0.02	0.17	0.03	<0.005	0.12	0.17
1268 img 12 G2 - 1	0.08	0.42	0.06	0.20	0.03	0.29	0.02	<0.005	0.05	0.16
1268 img 12 G2 - 5	0.02	0.12	0.03	0.03	0.01	0.05	<0.002	<0.005	0.03	0.21
1268 img 12 G3 - 1	0.07	0.34	0.06	0.20	0.02	0.19	0.02	<0.005	0.13	0.06
1268 img 12 G3 - 3	0.10	0.47	0.07	0.16	0.02	0.14	0.03	<0.005	0.08	0.11
1268 img 12 off G4 - 1	0.05	0.22	0.05	0.13	0.02	0.09	0.02	<0.004	0.08	0.10
1268 img 12 off G4 - 2	0.07	0.47	0.05	0.18	0.03	0.22	0.03	<0.004	0.10	0.11
1268 img 12 off G4 - 3	0.08	0.38	0.05	0.17	0.03	0.19	0.03	0.01	0.12	0.22
1268 img 12 off G4 - 4	0.06	0.32	0.09	0.17	0.01	0.19	0.02	<0.005	0.10	0.15
1268 img 12 off G4 - 5	0.12	0.63	0.11	0.22	0.05	0.30	0.04	0.02	0.14	0.18
1268 img 12 off G5 - 1	0.07	0.31	0.04	0.09	0.01	0.09	0.01	<0.005	0.05	<0.006
1268 img 12 off G5 - 2	0.21	1.15	0.14	0.31	0.04	0.21	0.05	0.01	0.13	0.02
1268 img 12 off G5 - 3	0.32	1.43	0.17	0.43	0.05	0.35	0.04	0.03	0.21	0.03
1268 img 12 off G5 - 4	0.28	1.24	0.17	0.30	0.05	0.32	0.06	0.02	0.21	0.07
1268 img 12 off G6 - 1	0.17	0.81	0.09	0.24	0.04	0.21	0.02	0.02	0.13	0.06
1268 img 12 off G6 - 2	0.30	1.17	0.16	0.28	0.04	0.30	0.04	<0.005	0.26	0.02
1268 img 12 off G6 - 3	0.24	1.17	0.14	0.28	0.03	0.21	0.03	0.02	0.18	0.02
1268 img 12 off G6 - 4	0.18	1.06	0.10	0.27	0.03	0.21	0.03	<0.005	0.17	0.01
1268 img 12 off G7 - 1	0.04	0.20	0.03	0.09	0.01	0.05	0.01	<0.005	0.05	0.02
1268 img 12 off G7 - 3	0.04	0.23	0.03	0.07	0.01	0.06	0.01	<0.005	0.07	<0.005
1268 img 12 off G7 - 4	0.05	0.29	0.04	0.11	0.01	0.08	0.01	<0.005	0.07	<0.006
1268 img 12 off G7 - 5	0.05	0.26	0.03	0.11	0.01	0.06	0.01	<0.004	0.06	<0.005
1268 img 12 off G7 - 6	0.06	0.21	0.04	0.09	0.01	0.05	0.01	<0.005	0.08	<0.006
1268 img 12 off G7 - 7	0.03	0.13	0.02	0.05	0.01	0.06	0.01	0.01	0.04	<0.006
1268 img 12 off G7 - 8	0.02	0.11	0.02	0.06	0.01	0.06	0.01	<0.005	0.04	<0.005
1268 img 12 off G7 - 9	0.02	0.07	0.02	0.05	<0.001	0.04	<0.002	<0.005	0.04	<0.006
1268 img 12 off G7 - 10	0.16	0.68	0.11	0.26	0.03	0.18	0.03	0.03	0.04	<0.007
1268 no image top G1 - 1	0.16	0.64	0.08	0.26	0.01	0.15	0.02	<0.006	0.12	0.05
1268 no image top G1 - 2	0.15	0.81	0.11	0.28	0.04	0.21	0.03	0.02	0.11	0.23
1268 no image top G1 - 3	0.23	0.86	0.12	0.28	0.02	0.20	0.02	<0.005	0.11	0.02
1268 no image top G1 - 4	0.21	1.27	0.17	0.47	0.04	0.33	0.05	0.01	0.17	0.16
1268 no image top G1 - 5	0.14	0.85	0.13	0.34	0.04	0.20	0.03	<0.005	0.15	0.03
1268 no image top G1 - 6	0.14	0.63	0.09	0.25	0.04	0.27	0.04	0.02	0.11	0.05
1268 no image top G1 - 7	0.16	0.87	0.14	0.34	0.05	0.27	0.05	<0.006	0.15	0.02
1268 no image top G1 - 8	0.06	0.32	0.06	0.18	0.03	0.21	0.02	0.01	0.05	0.19
1268 no image top G1 - 9	0.09	0.45	0.05	0.20	0.03	0.11	0.03	0.01	0.08	0.10
1268 no image top G1 - 10	0.15	0.52	0.10	0.24	0.02	0.18	0.03	0.01	0.10	0.05
1268 no image top G1 - 11	0.20	0.72	0.10	0.23	0.03	0.24	0.04	0.01	0.18	0.09
1268 no image top G1 - 12	0.20	1.14	0.15	0.32	0.05	0.27	0.04	0.01	0.20	0.03
1268 no image top G2 - 1	0.18	0.88	0.12	0.24	0.02	0.25	0.01	0.02	0.16	0.05
1268 no image top G2 - 2	0.25	0.96	0.13	0.32	0.03	0.26	0.04	0.04	0.12	0.03
1268 no image top G2 - 3	0.13	0.77	0.15	0.34	0.04	0.35	0.04	<0.005	0.10	0.05
1268 no image top G2 - 4	0.18	0.65	0.12	0.30	0.03	0.33	0.03	0.02	0.13	0.01
1268 no image top G2 - 5	0.20	0.84	0.13	0.41	0.03	0.15	0.03	<0.005	0.13	0.05
1268 no image top G2 - 6	0.22	0.96	0.16	0.42	0.06	0.29	0.03	0.01	0.15	0.02
1268 no image top G2 - 7	0.20	0.95	0.13	0.29	0.03	0.16	0.04	0.02	0.15	0.03
1268 no image top G2 - 8	0.20	1.05	0.15	0.38	0.07	0.26	0.04	0.01	0.17	0.01
1268 no image top G2 - 9	0.08	0.45	0.09	0.21	0.03	0.12	0.02	0.09	0.10	0.10
1268 no image top G2 - 10	0.19	1.26	0.17	0.35	0.05	0.27	0.05	0.01	0.17	0.05
1268 no image top G2 - 11	0.17	0.79	0.16	0.35	0.04	0.30	0.03	0.01	0.14	0.11
1268 no image top G2 - 12	0.16	0.68	0.09	0.20	0.03	0.22	0.02	0.02	0.14	0.03
1268 no image top G2 - 13	0.30	1.51	0.25	0.50	0.05	0.32	0.05	0.02	0.25	0.01
1268 no image top G2 - 14	0.20	0.90	0.15	0.28	0.03	0.19	0.03	<0.005	0.14	0.02
1268 no image top G2 - 15	0.16	0.92	0.16	0.24	0.05	0.19	0.02	<0.007	0.17	0.16
1192 Img 4 G3 - 2	0.01	0.05	0.01	0.01	<0.001	0.03	<0.002	0.01	0.01	0.02
1192 Img 5 G3 - 4	0.44	3.59	0.49	1.64	0.24	2.48	0.48	45.16	0.54	0.47
1192 Img 6 G1 - 2	0.03	0.06	0.01	0.04	0.00	0.08	0.00	<0.006	0.11	0.03
1192 Img 3 G2 - 1	0.02	0.22	0.05	0.08	0.02	0.19	0.02	0.02	0.05	0.19
1192 no image bottom G4 - 1	NA	NA	NA	NA	NA	NA	NA	NA	NA	NA
1192 no image bottom G7 - 3	0.02	0.18	0.03	0.10	0.01	0.17	0.03	0.04	0.03	0.12
1192 off img2 G3 - 1	<0.002	0.01	<0.002	<0.005	0.00	0.00	0.00	<0.006	0.01	<0.007
1192 no image bottom R G1 - 2	0.02	0.06	0.01	0.09	0.02	0.04	0.01	<0.006	0.01	0.12

Element concentrations in ppm
BDL: below detection limit
NA: no analysis
$Eu/Eu^* = [(Eu_{CN}/(Sm_{CN}+Gd_{CN})/2)]$
$Y/Y^* = [(Y_{CN}/(Dy_{CN}+Ho_{CN})/2)]$
$Ce/Ce^* = [(Ce_{CN}/(La_{CN} \times Pr_{CN})^{0.5})]$
CN = chondrite normalised
Normalising values from Sun and McDonough (1989)

Appendix 5 Supplementary material for Mapping hydrothermal systems in IOCG deposits using apatite geochronology and geochemsitry: An example from Vulcan Cu-Au prospect

Appendix 5 Table A4: Magnetite and hematite LA-ICP-MS trace element data collected at Vulcan in this study

Rejected Data

Source Filename	Drill hole	Mineral	Comment
1183 G1 - 2	VUD 007 1183	Magnetite	Monazite inclusions,
1183 G1 - 4	VUD 007 1183	Magnetite	High V, Al, Mg . P, Th, and Ce
1183 G3 - 1	VUD 007 1183	Magnetite	High V, Mg Al. High Ce and P.
1183 G4 - 1	VUD 007 1183	Magnetite	High Al, Mg and V. High Ce and P
1183 G7 - 1	VUD 007 1183	Magnetite	Mg-Al-Si inclusion.
1183 G11 - 1	VUD 007 1183	Magnetite	Mg-Al-Si inclusion.
1183 G11 - 3	VUD 007 1183	Magnetite	Off haem grain Fe drop
1183 G15 - 1	VUD 007 1183	Magnetite	High Al, Mg and V. High Ce and P
1183 G18 - 1	VUD 007 1183	Magnetite	High V, Al, Mg. High P and Ce.
1183 G22 - 2	VUD 007 1183	Magnetite	Mg-Si-Al inclusion
1183 G22 - 3	VUD 007 1183	Magnetite	High Al, Mg, V and P. Apatite inclusion?
1183 G23 - 1	VUD 007 1183	Magnetite	Mg Al inclusions
1268 mag G1 - 1	VUD 017 1268	Magnetite	High Mg, Al, V. Ce, Th, La, Ca, P
1268 mag G1 - 2	VUD 017 1268	Magnetite	High Mg, Al, V. Ce, Th, La, Ca, P
1268 mag G2 - 2	VUD 017 1268	Magnetite	Monazite inclusions,
1268 mag G3 - 2	VUD 017 1268	Magnetite	High Mg, Al, V and Ce
1268 mag G4 - 2	VUD 017 1268	Magnetite	High Mg, Al, V. High Ce, Th, La, Ca, P - monazite? apatite?
1268 mag G5 - 1	VUD 017 1268	Magnetite	High Mg, Al, V. High Ce and P
1268 mag G7 - 1	VUD 017 1268	Magnetite	High Mg, Al, V. High Ce.
1268 mag G7 - 2	VUD 017 1268	Magnetite	High Mg, Al, V. High Ce.
1268 mag G7 - 3	VUD 017 1268	Magnetite	High Mg, Al, V. High Ce.
1268 mag G8 - 1	VUD 017 1268	Magnetite	Monazite inclusions,
1268 mag G8 - 2	VUD 017 1268	Magnetite	High Mg, Al, V. High P, Ca, Ce, Th, La.
1268 mag G9 - 1	VUD 017 1268	Magnetite	High Mg, Al, V. High P, Ca, Ce, Th, La.
1268 mag G9 - 2	VUD 017 1268	Magnetite	High Mg, Al, V. High P, Ca, Ce, Th, La.
1268 mag G9 - 3	VUD 017 1268	Magnetite	High Mg, Al, V. High P, Ca, Ce, Th, La.
1268 mag G10 - 1	VUD 017 1268	Magnetite	High Mg, Al, V. High P, Ca, Ce, Th, La.
1268 mag G10 - 2	VUD 017 1268	Magnetite	High Mg, Al, V. High P, Ca, Ce, Th, La.
1268 mag G10 - 4	VUD 017 1268	Magnetite	High Mg, Al, V and Ce
1259 mag G3 - 5	VUD 017 1259	Magnetite	Apatite inclusion.
1259 mag G5 - 6	VUD 017 1259	Magnetite	Apatite inclusions.
994(1) - 3	VUD 009 994	Hematite	High Al and Mg. Cu inclusion. La Ce Th inclusion
994(1) - 4	VUD 009 994	Hematite	High Al Mn and Mg. Ce and La inclusion
994(1) - 5	VUD 009 994	Hematite	High Al and Mg. Si inclusions.Th Ce La
994(1) - 7	VUD 009 994	Hematite	High Al Mg and Mn. Si Ti inclusions. La Ca P inclusions after signal.
994(1) - 8	VUD 009 994	Hematite	High Al and Mg. Possible apatite inclusions
994(1) - 9	VUD 009 994	Hematite	High Al and Mg. Possible apatite inclusions
994(1) - 10	VUD 009 994	Hematite	High Al and Mg. Possible apatite inclusions
994(1) - 14	VUD 009 994	Hematite	High Al, Mn and Mg. High La, Ce P and Th
994(1) - 15	VUD 009 994	Hematite	Florencite inclusion. Delete
994(1) - 17	VUD 009 994	Hematite	High Al, Ti, Mn, Mg, Co Ni, V
994(1) - 19	VUD 009 994	Hematite	High Al, Mg, Mn and Nb. La, Ce, P Th inclusions
994(1) - 23	VUD 009 994	Hematite	Monaztite inclusion before signal. High Al and Mg
994(1) - 26	VUD 009 994	Hematite	La Ce Th, P inclusions
994(1) - 29	VUD 009 994	Hematite	High Al, Mg and Nb, Apatite inclusion after signal
994(1) - 30	VUD 009 994	Hematite	High AL and Mg. Possible monazite inclusions (high La, Ce, Th, P)
994(1) - 34	VUD 009 994	Hematite	Florencite inclusion.
994(1) - 37	VUD 009 994	Hematite	Al Si inclusion.
994(1) - 39	VUD 009 994	Hematite	High Al and Mg. Cu inclusion. La Ce Th inclusion
994(1) - 46	VUD 009 994	Hematite	High Al and Mg. Ce inclusions
994(1) - 54	VUD 009 994	Hematite	Al Mg Mn and Pb inclusions.
994(1) - 65	VUD 009 994	Hematite	Florencite inclusion before signal.
994(1) - 68	VUD 009 994	Hematite	Co and Ce peaks
994(1) - 71	VUD 009 994	Hematite	Florencite inclusions
994(1) - 73	VUD 009 994	Hematite	Florencite inclusion before and after signal.
994(2) - 5	VUD 009 994	Hematite	Florencite inclusions.
994(2) - 6	VUD 009 994	Hematite	Florencite inclusions after signal
994(2) - 8	VUD 009 994	Hematite	Florencite inclusions,
994(2) - 9	VUD 009 994	Hematite	La Ce inclusions?
994(2) - 10	VUD 009 994	Hematite	La, Ce, Th inclusions
994(2) - 12	VUD 009 994	Hematite	La inclusions? High Al
994(2) - 13	VUD 009 994	Hematite	Florencite, apatite inclusion after signal.
994(2) - 14	VUD 009 994	Hematite	High Al and Mg. Ce peaks.
994(2) - 15	VUD 009 994	Hematite	High Al, Mn and Mg. La Ce peak after signal
994(2) - 18	VUD 009 994	Hematite	Monazite inclusions Th Ce and La.
994(2) - 20	VUD 009 994	Hematite	Monazite inclusion after signal. High Al
994(2) - 24	VUD 009 994	Hematite	Florencite inclusion after signal
994(2) - 27	VUD 009 994	Hematite	Monazite inclusion after signal. High Al, Mn and V
994(2) - 34	VUD 009 994	Hematite	High Al. Ca peak before signal.
994(2) - 38	VUD 009 994	Hematite	High Al
994(2) - 40	VUD 009 994	Hematite	Cu inclusion. Ba inclusion. Pb inclusion. La and Ce inclusions

Element concentrations in ppm
BDL: below detection limit
NA: no analysis
$Eu/Eu^* = [(Eu_{CN}/(Sm_{CN}+Gd_{CN})/2)]$
$Y/Y^* = [(Y_{CN}/(Dy_{CN}+Ho_{CN})/2)]$
$Ce/Ce^* = [(Ce_{CN}/(La_{CN} \times Pr_{CN})^{0.5})]$
CN = chondrite normalised
Normalising values from Sun and McDonough (1989)

Appendix 5 Table A4: Magnetite and hematite LA-ICP-MS trace element data collected at Vulcan in this study

Rejected Data														
Source Filename	**Mg**	**Al**	**Si**	**P**	**Ca**	**Ti**	**V**	**Mn**	**Fe**	**Co**	**Ni**	**Cu**	**Zn**	**As**
1183 G1 - 2	70	378	1141	<11.832	229	53	286	10	720000	4.62	302.57	1.61	4.15	1.19
1183 G1 - 4	331	511	2819	<14.660	126	48	263	12	720000	3.63	275.02	0.53	2.81	0.40
1183 G3 - 1	179	288	2106	<11.400	235	56	119	12	720000	3.31	107.19	<0.224	2.41	0.46
1183 G4 - 1	77	292	426	<11.855	152	77	110	9	720000	3.17	93.22	1.74	1.66	0.55
1183 G7 - 1	374	885	855	<19.360	<65.112	38	146	11	720000	3.11	219.95	0.76	3.01	<0.349
1183 G11 - 1	20	200	208	<11.801	<51.730	14	11	9	720000	3.29	114.33	0.27	1.24	0.32
1183 G11 - 3	220530	56883	2742582	<233.244	401295	770	20	163	720000	4.29	123.32	37.70	37.89	6166.72
1183 G15 - 1	150	293	3307	<10.369	152	61	148	9	720000	3.84	203.41	<0.188	2.30	0.87
1183 G18 - 1	103	230	1256	<13.350	161	53	212	8	720000	1.30	267.40	<0.285	0.58	0.29
1183 G22 - 2	2199	4196	6579	<13.256	99	71	130	22	720000	4.51	343.06	7.51	9.90	3.16
1183 G22 - 3	154	339	1532	<15.002	185	69	121	16	720000	4.93	209.76	3.92	3.04	1.53
1183 G23 - 1	61	291	312	<13.877	<56.564	40	109	6	720000	3.68	248.11	2.04	1.93	3.49
1268 mag G1 - 1	2321	1129	9084	<11.410	2326	358	294	31	720000	5.70	29.47	0.94	9.85	0.86
1268 mag G1 - 2	1920	925	7680	<12.102	1826	286	289	25	720000	4.66	29.21	1.41	13.95	0.64
1268 mag G2 - 2	308	541	1328	<11.384	283	109	291	8	720000	1.84	27.03	3.39	18.12	<0.254
1268 mag G3 - 2	982	616	3345	<12.172	928	157	299	30	720000	3.30	32.33	0.68	14.56	0.66
1268 mag G4 - 2	1499	801	5714	<12.649	1514	168	280	12	720000	12.01	29.12	<0.224	1.57	0.45
1268 mag G5 - 1	664	550	5452	<15.912	555	73	287	15	720000	4.89	36.82	3.81	2.62	<0.294
1268 mag G7 - 1	1706	838	7595	13	1925	162	292	19	720000	4.22	32.90	1.13	20.18	0.84
1268 mag G7 - 2	1302	796	7507	<14.088	1416	167	300	23	720000	3.68	33.67	5.29	8.03	1.16
1268 mag G7 - 3	1510	776	8280	<11.400	1502	149	286	22	720000	4.10	32.58	0.59	9.96	0.85
1268 mag G8 - 1	2830	982	8174	<12.944	2382	180	278	73	720000	5.40	30.68	1.17	38.71	0.91
1268 mag G8 - 2	2667	1029	8952	<13.108	2729	250	290	23	720000	6.10	31.21	1.26	21.10	0.76
1268 mag G9 - 1	2373	1114	8921	<12.357	2381	370	276	34	720000	5.43	27.50	2.19	11.70	0.78
1268 mag G9 - 2	2272	1226	9442	<12.679	2447	404	290	30	720000	5.21	27.78	1.73	4.16	0.54
1268 mag G9 - 3	2054	922	9595	<14.106	2415	247	305	31	720000	5.21	50.12	3.69	8.37	0.55
1268 mag G10 - 1	2286	1088	9218	<14.754	2597	257	299	24	720000	6.33	31.32	1.63	9.65	0.63
1268 mag G10 - 2	1982	1078	7079	<10.899	2068	271	293	26	720000	5.06	29.43	1.71	1.79	0.77
1268 mag G10 - 4	2071	949	8234	<15.460	2647	202	289	25	720000	5.66	35.26	1.38	13.48	1.49
1259 mag G3 - 5	1657	825	4669	<14.948	3511	141	885	236	720000	2.25	84.50	2.68	18.05	0.46
1259 mag G5 - 6	602	1016	2674	<13.561	<56.556	187	904	13	720000	3.34	199.08	0.69	19.82	0.70
994(1) - 3	424	418	1398	<23.247	333	47	28	43	690000	13.96	113.82	108.35	1.67	30.23
994(1) - 4	145	371	905	<25.202	219	5	17	46	690000	10.87	93.41	2.17	3.06	32.91
994(1) - 5	246	382	1402	<28.548	<86.309	8	19	53	690000	11.86	88.33	5.32	1.94	28.46
994(1) - 7	749	799	2677	160	403	494	29	183	690000	11.14	84.06	21.98	13.62	44.25
994(1) - 8	751	380	2022	<21.413	142	5	23	45	690000	11.65	84.75	1.15	2.94	26.41
994(1) - 9	519	348	1728	<24.656	178	8	19	30	690000	7.87	89.81	0.77	2.53	56.90
994(1) - 10	391	308	1415	<24.880	161	93	23	36	690000	12.07	97.93	1.10	2.31	30.07
994(1) - 14	322	348	1363	205	231	111	17	88	690000	6.13	90.48	9.97	7.34	51.07
994(1) - 15	457	1953	5100	372	199	503	22	154	690000	9.03	86.53	37.91	21.53	53.81
994(1) - 17	195	515	1225	256	102	3139	44	137	690000	53.73	56.73	19.04	14.92	28.52
994(1) - 19	171	397	1078	130	110	659	24	73	690000	13.75	90.09	13.11	4.94	48.07
994(1) - 23	589	275	1714	<21.543	<98.975	9	21	31	690000	12.49	104.83	0.91	2.45	30.33
994(1) - 26	1042	487	2626	<33.408	220	12	26	111	690000	15.92	61.50	21.03	7.53	13.42
994(1) - 29	339	588	1383	86	195	130	26	84	690000	11.58	58.61	11.11	4.60	41.42
994(1) - 30	551	361	1605	<25.901	<81.680	36	21	49	690000	11.98	69.51	7.75	2.31	32.31
994(1) - 34	304	755	1528	213	169	305	25	129	690000	11.73	70.82	26.19	8.95	35.15
994(1) - 37	669	8381	13844	188	292	261	24	114	690000	15.30	96.43	47.11	9.17	35.97
994(1) - 39	618	333	1795	27	212	18	22	38	690000	8.72	92.33	1.09	2.78	29.71
994(1) - 46	723	631	2337	32	474	16	27	47	690000	16.62	107.83	39.18	4.52	47.97
994(1) - 54	870	453	2521	<16.998	1301	3	19	96	690000	22.85	80.04	1.25	4.56	28.62
994(1) - 65	620	326	1705	<28.431	<106.704	3	19	126	690000	12.13	93.60	16.88	4.59	18.34
994(1) - 68	462	456	1686	91	175	270	27	83	690000	17.39	60.12	11.72	5.60	28.82
994(1) - 71	228	653	1364	310	151	581	42	238	690000	15.28	81.19	62.33	59.95	26.13
994(1) - 73	411	295	1294	<20.430	219	9	24	28	690000	22.76	92.00	34.96	1.50	27.99
994(2) - 5	625	2229	3446	30	491	69	37	67	690000	5.20	37.18	5.19	6.16	65.61
994(2) - 6	435	824	1308	<25.526	881	38	26	46	690000	6.78	45.41	5.14	3.85	24.99
994(2) - 8	667	2080	4186	171	557	460	91	120	690000	27.73	145.91	186.60	7.56	31.94
994(2) - 9	187	3420	5402	55	359	536	180	61	690000	10.81	80.13	5.47	6.48	60.53
994(2) - 10	422	2677	4000	54	255	3467	117	360	690000	143.91	71.26	63.53	17.52	20.03
994(2) - 12	293	1222	2121	27	594	173	48	105	690000	6.83	40.62	14.15	4.43	46.46
994(2) - 13	200	2237	2254	63	<121.380	312	36	43	690000	4.85	90.86	4.31	3.70	43.43
994(2) - 14	268	1149	1906	32	1296	297	36	38	690000	4.67	95.64	3.14	3.90	63.15
994(2) - 15	487	939	1988	37	302	234	49	178	690000	11.65	51.35	24.06	5.06	24.60
994(2) - 18	406	825	1691	247	302	521	35	144	690000	6.93	37.52	35.71	6.79	25.67
994(2) - 20	444	2277	2904	36	271	141	90	344	690000	16.94	36.59	30.23	6.77	46.30
994(2) - 24	806	1422	2813	58	356	772	40	248	690000	27.82	29.77	97.81	9.47	52.46
994(2) - 27	23	1263	951	227	643	190	310	349	690000	54.36	84.32	41.71	20.61	24.26
994(2) - 34	226	966	1253	44	<92.460	98	55	56	690000	3.86	32.23	7.01	2.95	44.51
994(2) - 38	308	1622	2454	380	366	775	68	176	690000	10.39	63.72	32.31	12.90	70.41
994(2) - 40	126	121	692	48	133	17	14	33	690000	7.24	88.14	253.90	1.46	32.48

Element concentrations in ppm
BDL: below detection limit
NA: no analysis
$Eu/Eu^* = [(Eu_{CN}/(Sm_{CN}+Gd_{CN})/2)]$
$Y/Y^* = [(Y_{CN}/(Dy_{CN}+Ho_{CN})/2)]$
$Ce/Ce^* = [(Ce_{CN}/(La_{CN} \times Pr_{CN})^{0.5})]$
CN = chondrite normalised
Normalising values from Sun and McDonough (1989)

Appendix 5 Supplementary material for Mapping hydrothermal systems in IOCG deposits using apatite geochronology and geochemsitry: An example from Vulcan Cu-Au prospect

Appendix 5 Table A4: Magnetite and hematite LA-ICP-MS trace element data collected at Vulcan in this study

Rejected Data														
Source Filename	**Sr**	**Y**	**Zr**	**Nb**	**Mo**	**Sn**	**Ba**	**La**	**Ce**	**Pr**	**Nd**	**Sm**	**Eu**	**Gd**
1183 G1 - 2	2.27	0.15	<0.005	0.10	<0.033	0.15	0.67	2.53	3.46	0.40	1.22	0.11	0.01	0.05
1183 G1 - 4	0.15	0.82	0.00	0.11	<0.065	0.21	0.39	0.48	2.33	0.26	1.08	0.27	0.04	0.20
1183 G3 - 1	0.14	0.73	0.02	0.18	<0.016	0.17	0.23	0.23	2.48	0.15	0.74	0.19	0.02	0.14
1183 G4 - 1	0.05	0.14	0.01	0.03	<0.014	0.15	<0.013	0.24	1.21	0.09	0.32	0.05	0.02	<0.010
1183 G7 - 1	<0.005	<0.004	0.02	<0.002	<0.014	0.06	<0.021	<0.003	0.00	<0.001	<0.009	<0.006	<0.004	<0.020
1183 G11 - 1	<0.017	<0.002	0.01	0.01	0.04	0.11	<0.014	0.00	<0.002	<0.001	<0.003	<0.007	<0.003	0.01
1183 G11 - 3	281.01	12.43	1681.23	3.12	<0.461	3.11	1644.92	10.35	19.50	2.28	7.52	0.73	0.72	1.03
1183 G15 - 1	0.09	0.51	<0.004	0.91	0.09	0.22	0.06	0.16	2.79	0.16	0.93	0.31	0.05	0.22
1183 G18 - 1	0.05	0.27	0.01	0.07	<0.029	0.11	<0.015	0.15	1.46	0.10	0.55	0.19	0.04	0.11
1183 G22 - 2	0.28	2.40	0.10	1.67	0.10	0.33	0.18	0.39	1.36	0.18	0.73	0.19	0.03	0.22
1183 G22 - 3	0.16	0.55	0.03	0.52	0.08	0.32	0.03	0.17	0.48	0.06	0.38	0.03	0.00	0.04
1183 G23 - 1	0.14	0.00	0.01	0.11	0.13	<0.034	0.07	0.01	0.02	0.01	<0.014	<0.014	<0.004	<0.032
1268 mag G1 - 1	1.42	3.86	0.26	5.44	<0.021	2.15	1.35	3.74	13.67	1.78	7.54	1.33	0.15	1.14
1268 mag G1 - 2	0.94	2.58	0.09	3.51	0.05	1.46	0.79	2.87	10.34	1.49	5.61	0.88	0.12	0.69
1268 mag G2 - 2	0.34	0.42	0.02	0.77	<0.066	0.27	0.46	0.39	1.46	0.14	0.74	0.13	0.02	0.08
1268 mag G3 - 2	0.46	0.99	0.30	1.67	0.40	0.64	0.26	1.46	4.93	0.68	3.08	0.40	0.04	0.37
1268 mag G4 - 2	0.63	1.86	0.15	2.26	<0.019	0.91	0.36	2.75	10.37	1.35	5.72	0.99	0.10	0.57
1268 mag G5 - 1	0.39	0.81	0.05	0.65	<0.033	0.41	0.54	0.55	2.66	0.35	1.36	0.23	0.03	0.22
1268 mag G7 - 1	0.95	2.60	0.13	2.43	0.03	1.01	0.84	2.13	7.96	1.12	4.81	0.70	0.08	0.67
1268 mag G7 - 2	0.37	2.10	0.09	1.98	<0.037	0.98	0.17	1.48	7.12	0.81	3.29	0.52	0.05	0.76
1268 mag G7 - 3	0.54	2.16	0.10	2.28	<0.044	0.94	0.14	1.82	7.25	0.98	4.46	0.72	0.09	0.81
1268 mag G8 - 1	1.58	3.32	0.23	3.88	<0.028	1.43	0.85	5.98	20.35	2.41	11.54	1.43	0.19	0.93
1268 mag G8 - 2	1.35	3.37	0.21	4.59	0.04	1.77	0.94	4.76	16.58	2.14	9.46	1.69	0.14	1.21
1268 mag G9 - 1	1.26	3.71	0.20	6.19	<0.014	2.15	0.82	4.83	16.50	2.12	9.21	1.54	0.15	1.35
1268 mag G9 - 2	1.26	4.52	0.27	6.82	<0.047	2.33	1.07	4.49	15.08	2.03	8.93	1.44	0.13	1.25
1268 mag G9 - 3	1.15	2.80	0.14	3.26	<0.048	1.68	0.72	4.43	14.38	1.93	8.35	1.53	0.11	0.97
1268 mag G10 - 1	1.15	3.31	0.17	4.22	<0.051	1.64	0.69	4.94	16.84	2.23	9.09	1.54	0.17	1.26
1268 mag G10 - 2	1.06	2.64	0.19	3.59	0.04	1.60	0.59	4.12	14.33	1.91	7.99	1.22	0.11	1.01
1268 mag G10 - 4	1.49	2.91	0.17	3.89	<0.046	1.34	0.93	4.23	15.57	2.02	8.41	1.20	0.12	1.30
1259 mag G3 - 5	0.55	1.10	0.01	0.01	<0.057	0.13	0.25	0.22	0.87	0.11	0.43	0.19	0.03	0.18
1259 mag G5 - 6	0.26	0.20	0.46	0.06	0.24	0.42	0.06	0.62	1.72	0.20	1.19	0.09	0.04	0.09
994(1) - 3	1.22	0.57	0.50	14.28	5.76	1.38	1.38	0.66	1.90	0.24	0.81	0.20	0.04	0.16
994(1) - 4	1.63	0.38	0.09	4.71	1.15	0.40	2.65	0.16	0.56	0.05	0.22	0.06	0.00	0.03
994(1) - 5	0.86	0.75	0.33	10.66	<0.067	0.94	1.69	0.26	1.02	0.12	0.54	0.21	0.01	0.16
994(1) - 7	4.35	1.52	2.97	22.31	13.03	1.85	5.75	0.83	2.84	0.34	1.69	0.26	0.03	0.32
994(1) - 8	2.63	1.04	0.34	10.85	0.54	0.62	1.13	0.63	2.12	0.24	1.21	0.42	0.04	0.21
994(1) - 9	2.60	0.96	0.63	14.22	2.83	0.78	1.07	0.74	2.64	0.38	1.58	0.22	0.02	0.20
994(1) - 10	1.93	0.80	0.53	9.65	4.96	1.00	2.41	0.65	2.36	0.30	1.21	0.38	0.01	0.18
994(1) - 14	1.41	1.03	1.03	15.29	4.28	0.83	2.87	1.18	4.04	0.47	1.74	<0.012	0.04	0.19
994(1) - 15	2.63	1.48	2.21	26.07	10.02	1.34	3.31	2.16	8.76	1.05	4.07	0.63	0.09	0.49
994(1) - 17	2.39	0.75	12.23	46.47	15.40	10.41	5.53	0.49	1.87	0.22	0.89	0.25	0.01	0.14
994(1) - 19	1.93	0.70	3.31	21.67	12.86	1.72	6.74	0.27	1.18	0.19	0.92	0.29	<0.007	0.15
994(1) - 23	1.22	0.81	0.33	16.94	0.32	0.87	1.08	0.44	1.86	0.20	0.94	0.14	<0.005	0.29
994(1) - 26	3.02	1.45	0.36	14.23	1.94	1.23	3.33	1.29	4.13	0.59	2.27	0.49	0.05	0.16
994(1) - 29	1.92	0.88	1.43	45.52	6.43	2.55	1.75	0.43	1.55	0.18	0.84	0.25	0.02	0.20
994(1) - 30	1.32	0.99	0.52	18.90	2.00	1.11	1.16	0.71	2.40	0.25	1.35	0.25	0.01	0.25
994(1) - 34	4.59	1.45	2.21	17.90	8.97	1.31	4.43	18.79	40.03	3.49	11.07	1.45	0.14	0.79
994(1) - 37	2.86	1.20	2.00	19.18	5.71	1.50	4.72	1.63	5.16	0.65	2.35	0.42	0.05	0.37
994(1) - 39	1.52	0.98	0.57	15.27	2.95	0.75	0.93	1.05	3.57	0.41	1.71	0.23	0.03	0.21
994(1) - 46	5.02	1.16	0.83	22.80	1.07	0.97	6.87	5.27	16.53	1.75	6.95	1.01	0.07	0.52
994(1) - 54	3.46	1.02	0.15	7.11	0.25	0.66	1.57	0.39	2.10	0.24	1.00	0.27	0.01	0.14
994(1) - 65	1.04	1.06	0.28	7.29	0.30	0.79	3.97	0.57	2.16	0.35	1.37	0.14	0.04	0.15
994(1) - 68	1.89	0.87	1.53	20.76	7.57	2.32	2.42	0.59	2.55	0.31	1.31	0.26	0.03	0.12
994(1) - 71	3.87	1.07	3.63	14.76	16.46	3.13	7.53	3.72	9.46	0.95	3.16	0.39	0.05	0.34
994(1) - 73	1.77	0.55	0.39	20.55	1.13	1.39	3.69	1.36	3.60	0.26	1.33	0.34	0.02	0.05
994(2) - 5	10.23	1.37	2.61	42.93	4.54	1.74	3.10	7.70	16.17	1.40	3.88	0.73	0.02	0.27
994(2) - 6	2.77	1.08	0.87	31.37	1.76	0.95	4.69	1.37	3.41	0.29	1.72	0.09	0.04	0.21
994(2) - 8	15.01	1.26	3.80	12.04	7.21	2.08	12.13	14.34	37.32	2.51	13.92	1.17	0.08	0.34
994(2) - 9	13.20	0.83	2.91	10.60	11.63	3.61	47.46	14.06	15.65	1.87	3.63	1.19	0.11	0.33
994(2) - 10	6.60	1.68	25.80	65.27	33.68	9.47	20.32	4.44	11.69	0.99	2.42	0.18	0.04	0.16
994(2) - 12	3.06	1.18	4.11	61.85	4.40	3.38	2.79	2.43	3.85	0.50	1.81	0.29	0.02	0.19
994(2) - 13	11.21	1.82	2.92	8.61	3.83	1.77	6.10	5.94	9.98	1.22	5.23	0.42	0.08	0.54
994(2) - 14	6.72	0.94	1.41	20.20	4.58	2.18	2.27	1.59	5.95	0.44	1.97	0.19	0.03	0.19
994(2) - 15	3.57	1.22	3.44	37.31	6.58	3.14	13.95	1.19	3.31	0.42	1.62	0.36	0.02	0.17
994(2) - 18	3.09	1.68	2.36	22.82	15.20	2.61	9.94	7.78	16.55	1.37	4.89	0.55	0.07	0.47
994(2) - 20	4.44	1.25	6.09	67.94	11.45	2.96	5.77	1.32	4.01	0.43	2.00	0.26	0.03	0.19
994(2) - 24	5.38	1.38	6.30	62.72	11.64	3.30	11.11	2.08	6.68	0.86	2.49	0.40	0.17	0.30
994(2) - 27	1.35	1.14	7.69	8.98	27.41	2.44	8.75	0.04	0.17	0.04	0.23	0.04	0.00	0.13
994(2) - 34	2.27	0.51	2.60	86.85	4.36	4.41	1.58	0.26	0.94	0.15	0.52	0.10	0.01	0.07
994(2) - 38	8.41	2.39	4.92	18.25	11.10	3.41	7.94	5.66	12.69	1.66	5.24	0.81	0.10	0.60
994(2) - 40	2.17	0.37	0.16	17.81	0.12	0.33	4.78	1.55	3.01	0.34	1.24	0.11	0.01	0.11

Element concentrations in ppm
BDL: below detection limit
NA: no analysis
$Eu/Eu^* = [(Eu_{CN}/(Sm_{CN}+Gd_{CN})/2)]$
$Y/Y^* = [(Y_{CN}/(Dy_{CN}+Ho_{CN})/2)]$
$Ce/Ce^* = [(Ce_{CN}/(La_{CN} \times Pr_{CN})^{0.5})]$
CN = chondrite normalised
Normalising values from Sun and McDonough (1989)

Appendix 5 Supplementary material for Mapping hydrothermal systems in IOCG deposits using apatite geochronology and geochemsitry: An example from Vulcan Cu-Au prospect

Appendix 5 Table A4: Magnetite and hematite LA-ICP-MS trace element data collected at Vulcan in this study

Rejected Data										
Source Filename	**Tb**	**Dy**	**Ho**	**Er**	**Tm**	**Yb**	**Lu**	**Hf**	**Ta**	**W**
1183 G1 - 2	0.01	0.05	0.00	0.02	0.00	0.01	0.00	0.01	0.03	0.02
1183 G1 - 4	0.05	0.21	0.03	0.08	0.00	0.02	0.01	0.02	0.16	0.14
1183 G3 - 1	0.02	0.12	0.03	0.10	0.01	0.04	0.01	<0.005	0.16	0.02
1183 G4 - 1	0.00	0.05	0.00	0.01	0.00	<0.011	0.00	<0.005	0.04	0.01
1183 G7 - 1	<0.002	<0.008	<0.002	<0.007	0.00	<0.007	0.01	<0.008	0.00	<0.009
1183 G11 - 1	<0.002	<0.005	<0.002	<0.005	<0.001	<0.007	<0.002	<0.005	<0.001	<0.006
1183 G11 - 3	0.23	1.62	0.33	0.92	0.17	1.28	0.28	37.39	0.37	0.50
1183 G15 - 1	0.02	0.10	0.02	0.03	0.01	0.03	0.00	<0.005	0.05	0.13
1183 G18 - 1	0.01	0.06	0.02	0.04	0.00	<0.009	<0.002	<0.006	0.04	0.01
1183 G22 - 2	0.03	0.44	0.07	0.17	0.03	0.16	0.02	0.01	0.11	0.07
1183 G22 - 3	0.01	0.05	0.03	0.04	0.01	0.07	0.01	<0.007	0.05	<0.008
1183 G23 - 1	0.00	<0.007	<0.002	0.01	<0.002	<0.006	<0.002	<0.007	<0.001	0.06
1268 mag G1 - 1	0.17	0.90	0.14	0.36	0.05	0.35	0.04	0.02	0.23	0.03
1268 mag G1 - 2	0.09	0.49	0.07	0.21	0.03	0.20	0.03	0.01	0.18	0.04
1268 mag G2 - 2	0.01	0.07	0.02	0.03	0.01	0.04	0.00	<0.006	0.02	<0.007
1268 mag G3 - 2	0.03	0.19	0.02	0.05	0.01	0.11	0.01	0.01	0.06	0.07
1268 mag G4 - 2	0.06	0.38	0.06	0.16	0.02	0.13	0.03	<0.005	0.11	0.02
1268 mag G5 - 1	0.04	0.20	0.04	0.10	0.01	0.12	0.01	<0.007	0.06	0.16
1268 mag G7 - 1	0.08	0.49	0.10	0.24	0.04	0.35	0.04	<0.006	0.10	0.05
1268 mag G7 - 2	0.07	0.31	0.09	0.18	0.03	0.19	0.03	0.01	0.08	0.02
1268 mag G7 - 3	0.07	0.41	0.07	0.24	0.04	0.18	0.02	0.01	0.11	0.01
1268 mag G8 - 1	0.12	0.68	0.11	0.25	0.03	0.24	0.03	0.02	0.16	<0.007
1268 mag G8 - 2	0.18	0.72	0.13	0.29	0.04	0.32	0.05	0.01	0.18	0.01
1268 mag G9 - 1	0.16	0.71	0.08	0.30	0.03	0.25	0.05	<0.005	0.23	0.01
1268 mag G9 - 2	0.16	1.08	0.13	0.41	0.04	0.35	0.04	0.03	0.24	0.02
1268 mag G9 - 3	0.11	0.53	0.09	0.27	0.02	0.30	0.03	0.02	0.13	0.05
1268 mag G10 - 1	0.11	0.73	0.15	0.24	0.05	0.28	0.05	0.01	0.18	0.01
1268 mag G10 - 2	0.11	0.52	0.10	0.26	0.03	0.27	0.04	0.01	0.15	0.08
1268 mag G10 - 4	0.12	0.55	0.12	0.36	0.05	0.26	0.03	<0.007	0.16	0.06
1259 mag G3 - 5	0.03	0.17	0.05	0.13	0.02	0.13	0.02	<0.007	0.01	<0.008
1259 mag G5 - 6	0.01	0.02	0.00	0.05	0.01	0.05	0.01	0.03	0.01	0.04
994(1) - 3	0.02	0.17	0.03	0.12	0.01	0.13	0.01	0.02	0.05	0.74
994(1) - 4	0.01	0.10	0.03	0.07	0.00	0.08	0.02	<0.005	0.00	0.91
994(1) - 5	0.03	0.18	0.05	0.14	0.01	0.18	0.03	0.01	0.03	0.10
994(1) - 7	0.05	0.37	0.08	0.22	0.05	0.29	0.07	0.15	0.17	1.52
994(1) - 8	0.02	0.25	0.06	0.19	0.03	0.21	0.03	0.03	0.03	0.12
994(1) - 9	0.04	0.18	0.04	0.13	0.03	0.22	0.06	0.04	0.04	0.20
994(1) - 10	0.03	0.13	0.04	0.13	0.02	0.14	0.03	0.01	0.04	0.32
994(1) - 14	0.04	0.31	0.08	0.10	0.03	0.44	0.06	<0.004	0.08	0.71
994(1) - 15	0.06	0.26	0.06	0.18	0.05	0.41	0.06	0.09	0.15	0.81
994(1) - 17	0.03	0.19	0.04	0.11	0.03	0.33	0.03	0.51	1.03	1.43
994(1) - 19	0.01	0.21	0.04	0.12	0.03	0.21	0.03	0.11	0.15	1.00
994(1) - 23	0.02	0.21	0.04	0.06	0.02	0.27	0.04	0.01	0.03	0.35
994(1) - 26	0.06	0.25	0.06	0.12	0.05	0.32	0.05	0.03	0.03	0.40
994(1) - 29	0.04	0.12	0.04	0.11	0.03	0.19	0.01	0.02	0.12	3.36
994(1) - 30	0.03	0.18	0.05	0.18	0.02	0.14	0.03	<0.002	0.06	1.47
994(1) - 34	0.05	0.42	0.05	0.25	0.04	0.28	0.05	0.09	0.16	2.20
994(1) - 37	0.04	0.26	0.06	0.19	0.05	0.31	0.04	0.10	0.14	0.84
994(1) - 39	0.04	0.18	0.04	0.16	0.03	0.23	0.03	0.00	0.05	0.85
994(1) - 46	0.06	0.17	0.05	0.23	0.03	0.21	0.03	0.03	0.08	0.78
994(1) - 54	0.03	0.22	0.04	0.21	0.02	0.26	0.03	<0.001	0.03	0.18
994(1) - 65	0.03	0.20	0.04	0.18	0.04	0.25	0.05	0.01	0.02	0.94
994(1) - 68	0.03	0.18	0.04	0.18	0.02	0.23	0.05	0.06	0.09	1.06
994(1) - 71	0.04	0.28	0.05	0.16	0.03	0.24	0.03	0.19	0.08	1.61
994(1) - 73	0.02	0.12	0.02	0.06	0.02	0.12	0.02	0.02	0.05	0.70
994(2) - 5	0.04	0.31	0.05	0.15	0.04	0.29	0.04	0.06	0.11	5.88
994(2) - 6	0.03	0.28	0.02	0.18	0.01	0.19	0.02	0.02	0.10	1.17
994(2) - 8	0.04	0.17	0.04	0.18	0.03	0.25	0.02	0.13	0.21	2.35
994(2) - 9	0.02	0.15	0.04	0.11	0.01	0.11	0.01	0.07	0.25	8.09
994(2) - 10	0.06	0.12	0.09	0.21	0.02	0.20	0.03	0.93	0.34	9.64
994(2) - 12	0.03	0.16	0.06	0.18	0.04	0.25	0.02	0.12	0.19	5.92
994(2) - 13	0.04	0.20	0.07	0.15	0.10	0.33	0.06	0.03	0.11	0.76
994(2) - 14	0.01	0.17	0.04	0.09	0.01	0.18	0.01	0.01	0.23	1.69
994(2) - 15	0.04	0.21	0.06	0.12	0.03	0.28	0.02	0.05	0.11	3.28
994(2) - 18	0.07	0.38	0.06	0.17	0.02	0.19	0.03	0.08	0.15	8.60
994(2) - 20	0.05	0.26	0.08	0.21	0.04	0.27	0.03	0.08	0.16	7.85
994(2) - 24	0.06	0.31	0.06	0.31	0.03	0.32	0.06	0.14	0.32	3.51
994(2) - 27	0.01	0.09	0.05	0.11	0.02	0.15	0.02	0.12	0.01	6.29
994(2) - 34	0.03	0.09	0.02	0.10	0.02	0.15	0.03	0.06	0.05	6.15
994(2) - 38	0.07	0.40	0.12	0.36	0.05	0.47	0.10	0.14	0.35	2.39
994(2) - 40	0.01	0.08	0.02	0.06	0.01	0.06	0.00	<0.006	0.03	1.32

Element concentrations in ppm
BDL: below detection limit
NA: no analysis
$Eu/Eu^* = [(Eu_{CN}/(Sm_{CN}+Gd_{CN})/2)]$
$Y/Y^* = [(Y_{CN}/(Dy_{CN}+Ho_{CN})/2)]$
$Ce/Ce^* = [(Ce_{CN}/(La_{CN} \times Pr_{CN})^{0.5})]$
CN = chondrite normalised
Normalising values from Sun and McDonough (1989)

Appendix 5 Supplementary material for Mapping hydrothermal systems in IOCG deposits using apatite geochronology and geochemsitry: An example from Vulcan Cu-Au prospect

Appendix 5 Table A4: Magnetite and hematite LA-ICP-MS trace element data collected at Vulcan in this study

Rejected Data

Source Filename	Drill hole	Mineral	Comment
994(2) - 41	VUD 009 994	Hematite	La and Ce inclusions
994(2) - 43	VUD 009 994	Hematite	La Ce Th inclusion
994(2) - 45	VUD 009 994	Hematite	Florencite inclusion after signal
973(1) - 1	VUD 009 973	Hematite	Florencite.
973(1) - 2	VUD 009 973	Hematite	Florencite. Small part of signal kept
973(1) - 3	VUD 009 973	Hematite	Florencite. Small part of signal kept
973(1) - 4	VUD 009 973	Hematite	Florencite inclusion after signal
973(1) - 5	VUD 009 973	Hematite	High U and Pb. High La, Ce Ba. Small part of signal kept
973(1) - 6	VUD 009 973	Hematite	High U and Pb. Ti inclusions.
973(1) - 7	VUD 009 973	Hematite	Ti inclusion in florencite
973(1) - 8	VUD 009 973	Hematite	Florencite.
973(1) - 9	VUD 009 973	Hematite	Florencite.
973(1) - 10	VUD 009 973	Hematite	Florencite. Small part of signal kept
973(1) - 11	VUD 009 973	Hematite	Florencite. Small part of signal kept
973(1) - 12	VUD 009 973	Hematite	Florencite.
973(1) - 13	VUD 009 973	Hematite	Florencite.
973(1) - 14	VUD 009 973	Hematite	High Al. ?Florencite inclusion, Small part of signal kept.
973(1) - 15	VUD 009 973	Hematite	Florencite.
973(1) - 16	VUD 009 973	Hematite	Florencite. Small part of signal kept
973(1) - 17	VUD 009 973	Hematite	Florencite.
973(1) - 18	VUD 009 973	Hematite	Florencite. Small part of signal kept
973(1) - 19	VUD 009 973	Hematite	? Florencite. High W and U. SMall part of signal kept.
973(1) - 22	VUD 009 973	Hematite	Florencite.
973(1) - 23	VUD 009 973	Hematite	Florencite.
973(1) - 24	VUD 009 973	Hematite	Florencite. Small part of signal kept
973(1) - 25	VUD 009 973	Hematite	Florencite.
973(1) - 27	VUD 009 973	Hematite	Florencite.
973(1) - 28	VUD 009 973	Hematite	Florencite. Small part of signal kept
973(1) - 29	VUD 009 973	Hematite	Small part signal kept before florencite inclusion.
973(1) - 30	VUD 009 973	Hematite	High Al. Ti inclusions
973(1) - 33	VUD 009 973	Hematite	Florencite.
973(1) - 34	VUD 009 973	Hematite	Very high Al. ? Florencite
973(1) - 35	VUD 009 973	Hematite	Very high Al. ? Florencite
973(1) - 37	VUD 009 973	Hematite	Florencite.
973(1) - 38	VUD 009 973	Hematite	Florencite. Small part of signal kept
973(1) - 39	VUD 009 973	Hematite	Florencite.
973(1) - 40	VUD 009 973	Hematite	Florencite inclusion after signal. Small part of signal kept
973(1) - 41	VUD 009 973	Hematite	Florencite inclusion before signal.
973(1) - 42	VUD 009 973	Hematite	Florencite.
973(1) - 44	VUD 009 973	Hematite	High Al. Small part of signal kept.
852(1) - 1	VUD 009 852	Hematite	High Al, Mn, Mg and P (La, and Ce). V peak
852(1) - 2	VUD 009 852	Hematite	High Al. Mn, Mg and P. SMall part of signal kept.
852(1) - 9	VUD 009 852	Hematite	High Al, Mn, Mg and PO
852(1) - 11	VUD 009 852	Hematite	Apatite inclusion after signal - P and Ce peak
852(1) - 16	VUD 009 852	Hematite	Ce, La, Th inclusion before and after signal
852(1) - 17	VUD 009 852	Hematite	Ce, La, P inclusion after signal
852(1) - 18	VUD 009 852	Hematite	Florencite inclusion before and after signal
852(1) - 19	VUD 009 852	Hematite	Florencite or apatite.
852(1) - 20	VUD 009 852	Hematite	Florencite or apatite.
852(1) - 24	VUD 009 852	Hematite	High Al, La, Ce, Th
852(1) - 25	VUD 009 852	Hematite	Monazite inclusions Th Ce and La. Delete
852(1) - 26	VUD 009 852	Hematite	High Al and Mn. P inclusion after signal
852(1) - 27	VUD 009 852	Hematite	High P and Ce
852(1) - 28	VUD 009 852	Hematite	Th, P, La and Ce inclusions
852(1) - 31	VUD 009 852	Hematite	Apatite inclusion after signal - P, La and Ce peak
852(1) - 34	VUD 009 852	Hematite	High Al, Mn, P and Pb after apatite inclusion
852(1) - 43	VUD 009 852	Hematite	High Al and Mn. La, Ce, Th, P inclusion before signal
852(1) - 45	VUD 009 852	Hematite	Apatite inclusion before signal - P Ca, La and Ce peak
852(1) - 46	VUD 009 852	Hematite	Apatite inclusion after signal - P, Ca, La and Ce peak
852(1) - 47	VUD 009 852	Hematite	Florencite? Also high P, Al
852(1) - 48	VUD 009 852	Hematite	Apatite or monazite inclusion before signal.
852(1) - 49	VUD 009 852	Hematite	Florencite? Also high Mn, Mg and Al
852(1) - 53	VUD 009 852	Hematite	Apatite or monazite inclusions
852(1) - 54	VUD 009 852	Hematite	Monazite inclusion before signal
852(1) - 55	VUD 009 852	Hematite	Apatite or monazite inclusions,
852(1) - 57	VUD 009 852	Hematite	Monazite or apatite inclusions?
852(1) - 59	VUD 009 852	Hematite	Monazite or apatite inclusions?

Element concentrations in ppm
BDL: below detection limit
NA: no analysis
$Eu/Eu^* = [(Eu_{CN}/(Sm_{CN}+Gd_{CN})/2)]$
$Y/Y^* = [(Y_{CN}/(Dy_{CN}+Ho_{CN})/2)]$
$Ce/Ce^* = [(Ce_{CN}/(La_{CN} \times Pr_{CN})^{0.5})]$
CN = chondrite normalised
Normalising values from Sun and McDonough (1989)

Appendix 5 Table A4: Magnetite and hematite LA-ICP-MS trace element data collected at Vulcan in this study

Rejected Data														
Source Filename	**Mg**	**Al**	**Si**	**P**	**Ca**	**Ti**	**V**	**Mn**	**Fe**	**Co**	**Ni**	**Cu**	**Zn**	**As**
994(2) - 41	51	1428	1702	96	106	1050	38	113	690000	7.20	74.92	12.69	6.46	40.14
994(2) - 43	437	1465	2205	29	251	56	30	60	690000	7.52	26.28	3.34	4.25	42.24
994(2) - 45	476	1498	2265	84	401	146	29	90	690000	4.89	29.17	26.62	7.83	60.63
973(1) - 1	257	8747	10332	1389	358	1482	194	105	690000	12.44	124.65	9.50	6.66	21.56
973(1) - 2	381	12698	15486	180	226	6334	218	164	690000	23.18	105.39	15.26	14.27	35.31
973(1) - 3	25	543	1428	23	327	718	190	74	690000	1.11	66.27	2.10	3.61	43.08
973(1) - 4	578	23023	23845	4711	965	1621	192	178	690000	19.57	92.26	22.84	11.06	35.58
973(1) - 5	10	286	663	<23.299	<79.914	456	200	34	690000	2.48	211.42	<0.706	1.21	33.43
973(1) - 6	14	354	655	<14.776	120	3477	247	61	690000	2.97	211.31	0.72	1.57	52.57
973(1) - 7	13	311	608	<26.771	<88.951	8394	237	39	690000	3.14	215.47	<0.898	2.95	42.91
973(1) - 8	1528	39714	52569	3492	3255	2785	259	474	690000	63.00	120.11	87.92	27.52	29.27
973(1) - 9	303	4473	8490	337	372	3387	282	537	690000	91.73	130.59	91.33	25.16	18.70
973(1) - 10	349	2416	3817	297	234	1787	284	513	690000	50.52	125.44	103.76	26.55	19.10
973(1) - 11	410	1583	3231	525	836	1265	313	587	690000	49.12	143.74	101.14	26.14	16.24
973(1) - 12	196	4650	5653	977	290	4367	244	756	690000	94.49	113.29	129.87	31.49	16.29
973(1) - 13	431	21812	24666	4005	776	4116	226	746	690000	97.51	100.66	137.27	27.52	28.70
973(1) - 14	448	4522	7742	302	349	2236	305	638	690000	62.73	123.74	129.55	40.46	11.92
973(1) - 15	360	10084	11169	2595	604	4245	270	721	690000	84.88	120.65	127.65	31.83	21.25
973(1) - 16	49	1235	1613	231	<117.263	342	305	196	690000	9.76	153.72	75.16	26.27	6.05
973(1) - 17	336	13181	15132	61155	134550	4440	235	354	690000	27.59	130.98	43.05	16.09	32.98
973(1) - 18	258	5273	7087	663	797	3297	256	235	690000	24.10	98.71	39.24	14.34	35.86
973(1) - 19	23	597	499	<24.195	142	1667	179	93	690000	2.46	61.49	3.45	4.24	28.47
973(1) - 22	899	36176	47339	1806	507	3564	182	394	690000	49.88	141.11	58.51	25.74	31.32
973(1) - 23	197	2921	5362	481	225	2278	186	502	690000	59.82	170.18	83.23	30.16	22.84
973(1) - 24	216	1872	4125	289	402	2614	185	454	690000	47.60	131.76	91.86	34.41	17.18
973(1) - 25	1315	30674	40075	1725	514	1699	195	149	690000	32.70	153.27	41.82	18.60	28.91
973(1) - 27	1102	33441	43013	1852	2653	3298	240	281	690000	52.68	155.06	34.79	16.36	27.99
973(1) - 28	87	1041	1733	132	<141.164	566	306	161	690000	16.88	117.51	53.42	20.69	13.26
973(1) - 29	47	793	826	133	<111.439	291	316	135	690000	8.46	103.83	41.60	18.92	4.46
973(1) - 30	48	1041	1368	254	<78.297	408	302	228	690000	8.56	85.08	66.85	26.03	9.61
973(1) - 33	4431	179738	205962	15808	4038	10175	245	285	690000	57.82	314.07	41.97	26.98	71.61
973(1) - 34	333	11144	14566	228	296	615	197	115	690000	12.47	69.54	13.56	10.23	82.03
973(1) - 35	264	7852	9862	284	184	520	161	90	690000	8.30	53.61	11.13	13.14	64.20
973(1) - 37	3423	129835	176576	741	816	1641	215	197	690000	43.71	216.24	48.91	31.81	24.87
973(1) - 38	155	4372	5072	80	<106.930	8615	117	325	690000	240.19	100.20	41.18	20.68	11.15
973(1) - 39	2226	82221	97210	48321	84893	4540	199	301	690000	62.30	141.38	34.94	26.63	77.64
973(1) - 40	22	667	507	135	<109.139	233	226	60	690000	10.44	178.02	16.55	5.09	12.93
973(1) - 41	654	2233	7890	649	921	2466	125	493	690000	56.08	111.83	97.77	46.65	7.36
973(1) - 42	644	19961	26543	2937	644	4610	157	620	690000	92.74	94.08	110.13	38.85	24.97
973(1) - 44	131	3591	4896	91	129	875	274	114	690000	8.46	125.78	13.53	8.26	21.60
852(1) - 1	219	655	1064	1452	3727	8	41	210	690000	21.51	168.22	29.18	10.53	27.41
852(1) - 2	201	965	1282	1271	2651	1	14	141	690000	37.43	256.18	7.87	9.27	14.97
852(1) - 9	329	1124	2112	2416	4708	5	20	534	690000	47.78	276.73	49.48	25.91	26.96
852(1) - 11	281	1108	1492	765	1839	9	32	196	690000	39.61	267.25	4.54	15.15	16.95
852(1) - 16	290	722	1504	<24.057	93	7	41	15	690000	5.80	103.90	<0.778	<0.555	38.16
852(1) - 17	151	947	1276	<29.417	131	8	38	15	690000	4.79	79.34	<0.865	1.78	33.82
852(1) - 18	365	670	1743	239	615	9	39	160	690000	17.61	114.59	12.09	6.95	29.40
852(1) - 19	125	915	1103	423	821	2	22	136	690000	21.00	224.09	7.07	10.31	24.65
852(1) - 20	136	1070	1343	84	293	5	35	78	690000	22.07	134.88	6.80	5.58	25.88
852(1) - 24	109	747	927	155	335	4	23	85	690000	15.11	134.50	4.04	4.85	25.21
852(1) - 25	94	944	1301	443	607	4	23	135	690000	20.71	179.84	11.19	8.83	26.54
852(1) - 26	28	493	831	100	<78.796	4	27	113	690000	15.34	116.10	10.76	6.45	16.29
852(1) - 27	191	890	1316	316	578	5	32	105	690000	16.54	153.09	7.24	5.33	29.54
852(1) - 28	165	964	1112	78	<131.303	3	41	70	690000	12.00	111.94	4.41	3.25	27.95
852(1) - 31	162	807	1187	31	<71.723	6	29	63	690000	7.19	87.27	2.60	1.66	29.29
852(1) - 34	191	1356	2262	1075	1557	16	33	373	690000	51.24	263.76	5.36	28.40	22.32
852(1) - 43	77	862	1146	485	728	5	30	135	690000	16.75	134.58	17.94	6.47	30.43
852(1) - 45	336	665	1466	59	273	5	38	17	690000	7.23	106.07	2.20	1.41	40.91
852(1) - 46	173	926	1644	1242	2709	4	21	241	690000	33.84	224.77	7.42	23.60	23.96
852(1) - 47	68	464	775	356	964	3	30	66	690000	15.82	137.72	0.91	3.67	29.69
852(1) - 48	109	1158	1859	725	1040	2	11	278	690000	46.56	308.98	5.68	16.29	19.71
852(1) - 49	1365	453	3147	39	478	2	32	281	690000	30.08	129.86	32.59	7.16	17.41
852(1) - 53	212	752	1295	38	225	5	33	17	690000	6.32	84.86	2.56	1.04	38.02
852(1) - 54	324	887	1444	54	278	8	26	56	690000	10.13	113.65	2.72	1.45	29.36
852(1) - 55	126	917	1253	462	835	4	23	134	690000	21.92	180.06	9.89	7.02	30.69
852(1) - 57	140	639	791	82	174	6	30	40	690000	9.16	105.75	7.59	2.49	26.67
852(1) - 59	89	911	999	265	498	3	24	112	690000	16.16	156.66	7.37	3.84	24.93

Element concentrations in ppm
BDL: below detection limit
NA: no analysis
$Eu/Eu^* = [(Eu_{CN}/(Sm_{CN}+Gd_{CN})/2)]$
$Y/Y^* = [(Y_{CN}/(Dy_{CN}+Ho_{CN})/2)]$
$Ce/Ce^* = [(Ce_{CN}/(La_{CN} \times Pr_{CN})^{0.5})]$
CN = chondrite normalised
Normalising values from Sun and McDonough (1989)

Appendix 5 Supplementary material for Mapping hydrothermal systems in IOCG deposits using apatite geochronology and geochemsitry: An example from Vulcan Cu-Au prospect

Appendix 5 Table A4: Magnetite and hematite LA-ICP-MS trace element data collected at Vulcan in this study

Rejected Data														
Source Filename	**Sr**	**Y**	**Zr**	**Nb**	**Mo**	**Sn**	**Ba**	**La**	**Ce**	**Pr**	**Nd**	**Sm**	**Eu**	**Gd**
994(2) - 41	2.53	0.52	2.24	7.61	8.16	1.48	3.84	0.93	3.65	0.26	0.63	0.17	0.05	0.14
994(2) - 43	5.25	1.23	1.49	39.96	4.82	1.94	9.03	6.64	14.85	1.71	6.49	1.01	0.03	0.46
994(2) - 45	5.46	1.38	2.23	85.80	7.99	3.20	13.73	2.72	7.67	0.87	4.06	0.69	0.07	0.54
973(1) - 1	504.22	6.51	7.89	5.75	85.80	3.98	83.32	473.07	682.29	53.39	124.37	12.29	2.41	6.36
973(1) - 2	14.69	3.03	12.05	24.19	43.65	16.08	10.83	28.56	37.43	3.75	4.84	0.43	0.16	0.39
973(1) - 3	11.51	7.60	0.26	10.18	495.35	2.71	10.99	112.98	202.55	18.14	60.43	5.57	0.68	2.90
973(1) - 4	1614.10	43.76	31.52	9.84	47.02	5.28	284.62	1767.02	2791.01	191.75	463.07	50.24	7.43	25.74
973(1) - 5	0.88	4.90	0.20	0.64	93.18	0.78	2.16	6.28	19.09	2.21	8.29	1.03	1.25	0.84
973(1) - 6	2.62	3.55	0.44	5.55	114.29	6.22	1.11	9.32	21.22	1.96	5.60	0.83	0.82	0.60
973(1) - 7	1.54	1.09	0.42	7.07	94.35	13.91	0.59	2.56	3.98	0.35	1.10	<0.012	0.13	0.18
973(1) - 8	802.63	11.64	19.56	16.10	27.36	8.13	129.85	931.52	1327.92	92.13	241.16	27.94	3.78	13.35
973(1) - 9	24.76	2.03	19.27	21.47	28.43	9.22	19.54	19.45	30.90	1.77	4.87	0.71	0.10	0.46
973(1) - 10	92.18	2.33	14.75	12.10	21.38	5.63	33.01	84.00	130.02	9.63	22.50	2.46	0.32	0.96
973(1) - 11	29.08	3.07	13.69	8.92	21.72	4.44	22.54	25.79	44.06	4.01	9.42	1.81	0.16	0.64
973(1) - 12	315.69	8.93	26.55	24.36	34.74	10.38	132.07	341.03	556.21	41.87	91.31	10.85	1.30	4.80
973(1) - 13	1510.84	25.75	27.14	24.32	40.54	10.96	328.11	1631.77	2534.53	173.88	420.69	49.72	7.18	20.00
973(1) - 14	12.96	2.59	19.63	12.64	23.87	6.34	27.76	5.18	10.20	0.97	3.97	0.38	0.03	0.42
973(1) - 15	805.77	18.08	24.26	19.89	29.88	9.93	239.81	885.48	1267.41	87.79	208.18	22.38	3.71	10.37
973(1) - 16	3.33	1.51	2.27	0.50	5.27	0.65	11.62	5.97	12.28	0.96	1.83	0.11	0.03	0.41
973(1) - 17	495.87	137.10	19.38	21.81	21.54	13.08	62.51	331.14	485.84	39.68	79.66	20.57	5.06	43.95
973(1) - 18	68.01	49.10	113.07	19.94	29.22	10.28	22.70	85.55	125.90	11.02	29.46	6.82	2.69	10.01
973(1) - 19	5.70	4.32	0.35	7.61	61.64	4.29	4.41	36.68	69.75	6.53	22.45	2.42	0.32	1.12
973(1) - 22	543.13	11.56	14.53	27.36	22.55	9.30	160.36	534.63	834.26	56.73	147.93	15.97	2.48	6.96
973(1) - 23	91.46	4.48	13.76	18.68	20.59	5.98	66.15	101.99	173.00	9.50	23.58	2.92	0.45	1.44
973(1) - 24	30.06	3.12	15.23	21.03	23.20	6.80	30.06	23.82	38.79	2.37	7.04	0.68	0.12	0.46
973(1) - 25	625.59	14.42	14.06	9.63	20.50	5.10	103.56	682.71	901.18	63.48	164.74	19.80	2.61	8.10
973(1) - 27	225.45	9.60	21.76	17.76	42.97	13.26	40.53	182.64	303.25	18.42	47.56	4.99	1.18	4.52
973(1) - 28	1.73	2.48	0.64	1.12	6.53	1.03	8.17	4.97	9.65	0.90	3.41	0.81	0.03	0.36
973(1) - 29	0.86	0.87	1.12	0.08	1.76	0.67	6.47	0.44	1.21	0.15	0.72	0.16	0.02	0.10
973(1) - 30	3.95	1.33	2.82	0.66	24.86	1.00	13.82	1.05	1.44	0.14	0.48	0.07	0.02	0.09
973(1) - 33	6592.89	247.23	232.83	29.71	32.74	20.17	1338.56	8712.29	12440.68	732.98	1807.29	196.57	29.89	93.20
973(1) - 34	5.93	0.80	3.99	8.68	16.66	11.08	8.33	1.24	3.28	0.33	0.62	0.11	0.04	0.12
973(1) - 35	3.75	1.01	4.12	10.26	13.04	8.82	5.96	1.06	2.49	0.16	0.73	0.28	0.01	0.30
973(1) - 37	308.77	50.95	90.76	7.81	13.18	6.07	67.41	380.45	417.70	32.56	100.80	11.44	1.72	9.17
973(1) - 38	2.69	1.34	46.85	65.81	20.37	19.49	15.84	0.80	2.27	0.10	0.60	0.03	0.06	0.13
973(1) - 39	4416.12	102.10	27.76	25.31	32.36	12.49	635.13	3877.59	6051.27	419.36	969.85	120.85	22.97	90.93
973(1) - 40	0.70	0.50	0.51	0.41	20.45	0.41	2.28	0.87	1.87	0.28	1.15	0.04	<0.001	0.09
973(1) - 41	107.76	6.28	16.40	21.17	18.56	10.64	50.41	81.24	119.46	8.84	19.26	2.80	0.79	1.55
973(1) - 42	906.20	24.35	30.15	29.15	38.43	14.44	367.04	975.44	1519.22	106.81	265.33	24.97	4.00	14.12
973(1) - 44	1.91	0.52	2.24	3.74	9.05	2.78	5.91	0.61	1.23	0.10	0.21	<0.009	0.01	0.08
852(1) - 1	5.30	4.41	0.86	11.50	38.69	0.81	5.93	1.19	4.73	0.78	4.07	1.15	0.15	1.03
852(1) - 2	4.81	4.00	0.39	3.59	84.12	0.33	7.22	0.51	2.80	0.49	2.33	0.62	0.10	0.71
852(1) - 9	10.07	7.17	0.69	6.95	91.21	0.48	19.13	1.35	6.49	0.97	5.15	1.45	0.21	1.36
852(1) - 11	7.38	2.40	1.63	15.74	100.85	0.85	8.19	0.48	1.98	0.40	1.53	0.25	0.05	0.37
852(1) - 16	1.90	0.49	0.74	7.27	1.45	0.70	1.38	0.60	2.61	0.31	0.94	0.11	0.01	0.04
852(1) - 17	2.74	0.48	1.07	8.38	1.75	0.28	3.00	0.70	1.78	0.28	0.64	0.11	0.03	0.04
852(1) - 18	5.42	2.22	1.10	8.52	6.43	0.80	7.00	5.15	10.05	1.74	6.38	1.00	0.09	0.80
852(1) - 19	2.22	0.92	0.68	3.38	50.25	0.28	6.20	1.26	4.93	0.65	3.18	0.35	0.09	0.43
852(1) - 20	4.75	0.80	0.93	3.62	22.46	0.27	6.62	1.16	2.83	0.43	0.86	0.08	<0.013	0.16
852(1) - 24	2.02	1.09	0.33	3.81	21.61	0.41	3.83	5.74	20.55	2.56	9.19	1.47	0.11	0.47
852(1) - 25	2.99	1.39	0.57	5.54	40.69	0.61	7.79	6.95	19.77	2.48	8.34	1.27	0.12	0.59
852(1) - 26	0.92	0.87	0.34	3.39	7.97	0.60	1.95	0.23	0.65	0.11	0.43	0.23	0.01	0.08
852(1) - 27	2.15	1.20	0.53	4.04	28.98	0.53	5.14	1.79	5.68	0.67	2.61	0.51	0.07	0.27
852(1) - 28	1.65	0.56	0.43	5.50	19.51	0.77	2.65	0.87	2.71	0.23	1.24	0.19	0.02	0.17
852(1) - 31	2.59	0.48	0.55	5.61	7.18	0.48	8.21	0.69	2.12	0.38	1.03	0.11	0.02	0.17
852(1) - 34	6.77	2.42	2.38	27.72	126.91	1.04	12.17	0.41	1.56	0.25	1.25	0.19	0.07	0.39
852(1) - 43	2.93	1.22	1.01	10.35	33.29	0.77	4.17	4.51	15.88	1.61	8.28	1.00	0.06	0.53
852(1) - 45	2.12	0.72	0.98	5.57	0.88	0.59	1.64	0.61	2.29	0.24	1.03	0.08	0.04	0.24
852(1) - 46	6.81	3.94	1.41	7.56	84.62	0.29	9.05	0.88	3.83	0.58	2.81	0.91	0.10	0.75
852(1) - 47	2.55	1.10	0.08	0.71	27.19	0.62	3.79	0.17	1.02	0.19	0.74	0.21	0.01	0.19
852(1) - 48	3.74	1.25	0.14	0.77	128.86	0.36	10.45	0.32	1.38	0.18	1.34	0.38	0.01	0.42
852(1) - 49	3.25	1.05	0.47	4.36	4.48	0.34	3.05	5.26	15.03	1.94	5.85	0.95	0.07	0.45
852(1) - 53	1.93	0.52	0.61	8.46	0.71	0.60	1.63	1.17	3.45	0.25	1.69	0.10	0.03	0.09
852(1) - 54	1.51	0.66	0.67	9.83	21.79	0.87	1.52	0.72	2.59	0.40	0.98	0.32	<0.003	0.34
852(1) - 55	2.52	1.19	0.41	5.65	46.69	0.48	5.87	4.99	18.89	2.06	7.32	1.34	0.05	0.59
852(1) - 57	1.73	0.37	0.51	6.65	8.49	0.51	2.07	1.04	3.00	0.74	1.56	0.26	0.03	0.10
852(1) - 59	2.11	0.73	0.74	5.69	30.16	0.79	3.95	1.38	3.64	0.31	1.64	0.29	0.04	0.15

Element concentrations in ppm
BDL: below detection limit
NA: no analysis
$Eu/Eu^* = [(Eu_{CN}/(Sm_{CN}+Gd_{CN})/2)]$
$Y/Y^* = [(Y_{CN}/(Dy_{CN}+Ho_{CN})/2)]$
$Ce/Ce^* = [(Ce_{CN}/(La_{CN} \times Pr_{CN})^{0.5})]$
CN = chondrite normalised
Normalising values from Sun and McDonough (1989)

Appendix 5 Table A4: Magnetite and hematite LA-ICP-MS trace element data collected at Vulcan in this study

Rejected Data										
Source Filename	**Tb**	**Dy**	**Ho**	**Er**	**Tm**	**Yb**	**Lu**	**Hf**	**Ta**	**W**
994(2) - 41	0.01	0.17	0.03	0.10	0.01	0.09	0.02	0.13	0.23	0.86
994(2) - 43	0.04	0.17	0.05	0.07	0.03	0.25	0.05	0.02	0.12	7.79
994(2) - 45	0.08	0.17	0.08	0.24	0.05	0.15	0.05	0.02	0.41	4.17
973(1) - 1	0.31	1.00	0.21	1.38	0.09	0.62	0.07	0.21	0.28	167.70
973(1) - 2	0.08	0.36	0.15	0.46	0.06	0.59	0.11	0.55	0.98	121.18
973(1) - 3	0.36	1.74	0.36	1.06	0.13	1.14	0.18	0.03	0.14	1355.86
973(1) - 4	1.43	6.71	1.48	4.86	0.58	4.54	0.66	0.90	0.54	142.82
973(1) - 5	0.18	0.95	0.18	0.54	0.10	0.93	0.22	0.01	0.01	155.73
973(1) - 6	0.08	0.65	0.18	0.70	0.11	1.33	0.20	0.01	0.03	305.31
973(1) - 7	<0.004	0.21	0.05	0.12	0.06	0.49	0.14	<0.007	0.06	246.77
973(1) - 8	0.64	2.28	0.32	1.03	0.11	0.88	0.11	0.86	0.95	10.67
973(1) - 9	0.03	0.41	0.11	0.31	0.04	0.28	0.04	0.98	0.57	3.62
973(1) - 10	0.09	0.54	0.11	0.40	0.05	0.37	0.07	0.49	0.28	4.55
973(1) - 11	0.08	0.54	0.11	0.39	0.03	0.43	0.04	0.47	0.18	3.13
973(1) - 12	0.23	1.08	0.26	1.07	0.10	0.63	0.08	0.95	1.18	3.55
973(1) - 13	0.95	3.40	0.70	2.01	0.26	1.20	0.16	0.92	1.06	3.44
973(1) - 14	0.05	0.27	0.12	0.27	0.08	0.38	0.09	0.76	0.38	2.26
973(1) - 15	0.54	1.93	0.53	1.74	0.18	1.20	0.13	0.86	0.82	2.99
973(1) - 16	0.03	0.33	0.08	0.20	0.04	0.24	0.02	0.05	0.02	0.44
973(1) - 17	5.86	33.89	6.25	14.98	1.36	6.22	0.66	0.69	0.84	13.14
973(1) - 18	2.15	17.44	11.63	14.26	1.86	10.28	1.02	11.75	0.57	219.49
973(1) - 19	0.18	0.76	0.17	0.59	0.11	0.68	0.10	0.05	0.04	649.06
973(1) - 22	0.32	1.36	0.28	0.96	0.13	0.60	0.09	0.48	1.15	8.06
973(1) - 23	0.12	0.57	0.14	0.50	0.14	0.53	0.05	0.54	0.97	3.92
973(1) - 24	0.05	0.48	0.12	0.51	0.05	0.16	0.09	0.57	0.93	3.04
973(1) - 25	0.42	1.87	0.40	1.25	0.21	0.94	0.17	0.47	0.54	3.71
973(1) - 27	0.32	1.88	0.32	0.76	0.13	0.77	0.13	0.79	1.10	196.53
973(1) - 28	0.07	0.37	0.11	0.28	0.03	0.30	0.03	0.05	0.03	5.46
973(1) - 29	0.06	0.15	0.04	0.20	0.03	0.02	0.02	<0.008	0.02	9.19
973(1) - 30	0.01	0.22	0.08	0.18	0.03	0.25	0.05	0.08	0.05	248.92
973(1) - 33	6.09	31.02	6.83	26.02	2.86	26.68	4.33	10.56	1.69	8.62
973(1) - 34	0.02	0.14	0.03	0.22	0.01	0.13	0.03	0.12	0.13	18.21
973(1) - 35	0.04	0.18	0.06	0.21	0.02	0.23	0.03	0.14	0.16	18.51
973(1) - 37	1.13	6.84	1.70	9.29	0.95	5.20	0.85	2.38	0.35	2.69
973(1) - 38	0.01	0.28	0.04	0.23	0.02	0.13	0.04	2.05	3.04	4.94
973(1) - 39	6.96	22.57	3.69	8.86	0.84	4.60	0.99	1.38	1.39	31.78
973(1) - 40	<0.006	0.11	0.02	0.07	0.01	0.03	0.01	<0.011	0.03	1.08
973(1) - 41	0.13	0.81	0.23	0.65	0.08	0.97	0.10	0.67	0.71	1.14
973(1) - 42	0.68	2.81	0.69	2.35	0.28	1.74	0.18	1.04	1.17	3.77
973(1) - 44	0.02	0.12	0.01	0.14	0.03	0.11	0.02	0.08	0.16	4.03
852(1) - 1	0.15	0.77	0.17	0.44	0.05	0.63	0.07	0.03	0.07	0.42
852(1) - 2	0.14	0.50	0.13	0.51	0.08	0.51	0.05	0.01	0.04	0.30
852(1) - 9	0.17	1.07	0.23	0.75	0.12	0.99	0.13	<0.002	0.05	0.36
852(1) - 11	0.07	0.64	0.09	0.23	0.03	0.24	0.05	0.04	0.07	0.62
852(1) - 16	0.00	0.21	0.03	0.13	<0.004	0.14	0.01	0.01	0.04	0.32
852(1) - 17	0.02	0.15	0.02	0.09	0.05	0.10	0.01	0.02	0.09	1.33
852(1) - 18	0.07	0.39	0.09	0.28	0.07	0.19	0.03	<0.003	0.08	0.51
852(1) - 19	0.03	0.44	0.07	0.29	0.02	0.10	0.02	<0.032	0.11	0.60
852(1) - 20	0.01	0.10	0.04	0.03	<0.001	0.16	<0.003	<0.005	0.01	0.10
852(1) - 24	0.06	0.25	0.07	0.12	0.02	0.08	0.01	<0.005	0.04	0.50
852(1) - 25	0.05	0.26	0.05	0.15	0.02	0.17	0.03	0.00	0.04	0.39
852(1) - 26	0.01	0.15	0.01	0.07	0.02	0.12	0.02	<0.008	0.03	3.54
852(1) - 27	0.04	0.20	0.06	0.11	0.02	0.16	0.03	<0.007	0.04	0.35
852(1) - 28	0.01	0.06	0.02	0.08	0.02	0.07	0.02	<0.002	0.06	1.00
852(1) - 31	0.01	0.06	0.01	0.04	0.01	0.08	0.01	0.01	0.06	0.63
852(1) - 34	0.04	0.38	0.07	0.30	0.04	0.36	0.04	0.03	0.20	0.17
852(1) - 43	0.04	0.28	0.04	0.14	0.03	0.26	0.03	<0.010	0.07	2.40
852(1) - 45	0.01	0.06	0.01	0.11	0.01	0.20	0.01	0.02	0.03	0.71
852(1) - 46	0.09	0.63	0.11	0.45	0.05	0.62	0.08	0.01	0.04	0.93
852(1) - 47	0.04	0.16	0.03	0.07	0.01	0.07	0.03	<0.003	<0.001	0.86
852(1) - 48	0.02	0.24	0.06	0.27	0.04	0.24	0.01	<0.005	0.01	0.71
852(1) - 49	0.04	0.21	0.05	0.10	0.02	0.14	0.03	<0.009	0.05	0.35
852(1) - 53	0.02	0.14	<0.002	0.04	0.04	0.16	0.03	<0.007	0.08	0.31
852(1) - 54	0.02	0.32	0.05	0.02	0.03	0.08	0.02	<0.015	0.14	0.41
852(1) - 55	0.06	0.22	0.04	0.13	0.03	0.17	0.02	0.02	0.09	0.35
852(1) - 57	0.02	0.11	0.01	0.05	0.01	0.04	0.01	0.00	0.08	0.62
852(1) - 59	0.03	0.15	0.03	0.10	<0.001	0.15	0.02	0.02	0.08	0.34

Element concentrations in ppm
BDL: below detection limit
NA: no analysis
$Eu/Eu^* = [(Eu_{CN}/(Sm_{CN}+Gd_{CN})/2)]$
$Y/Y^* = [(Y_{CN}/(Dy_{CN}+Ho_{CN})/2)]$
$Ce/Ce^* = [(Ce_{CN}/(La_{CN} \times Pr_{CN})^{0.5})]$
CN = chondrite normalised
Normalising values from Sun and McDonough (1989)

Appendix 5 Figure A1 Back scatter electron (left) and mineral liberation analysis (right) maps for thin sections analysed in this study

VUD 017 1259

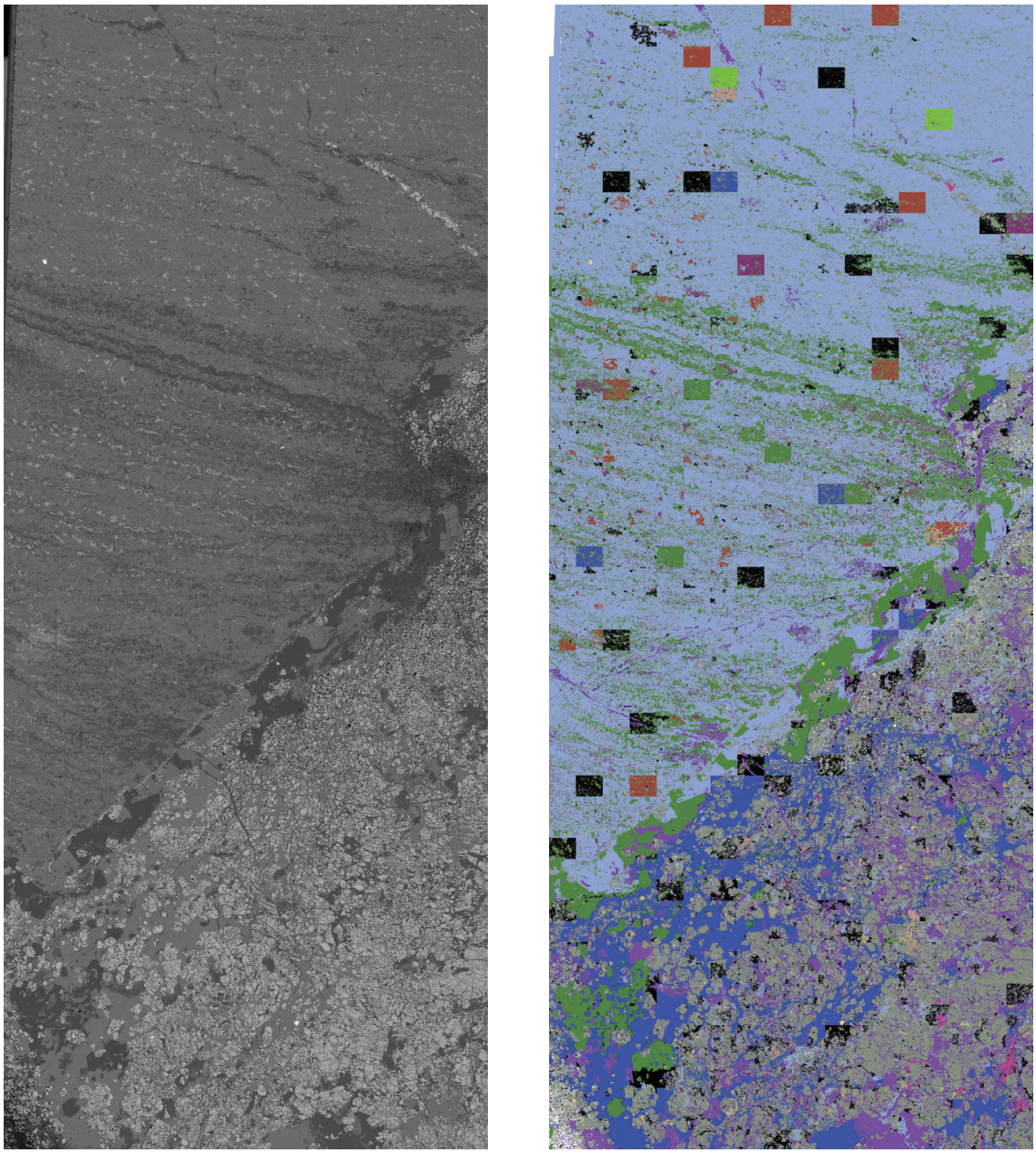

Appendix 5 Figure A1 Back scatter electron (left) and mineral liberation analysis (right) maps for thin sections analysed in this study

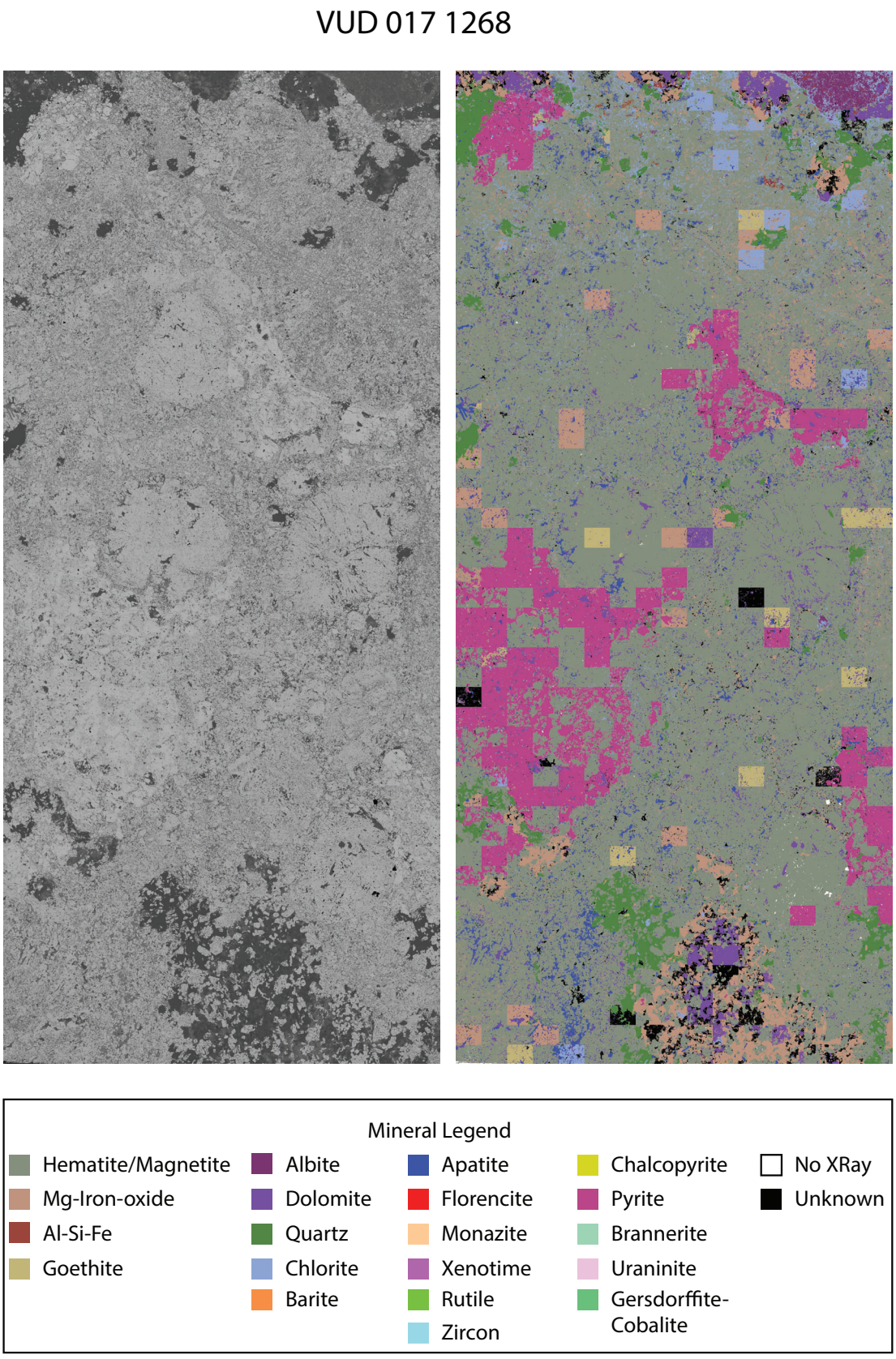

Appendix 5 Figure A1 Back scatter electron (left) and mineral liberation analysis (right) maps for thin sections analysed in this study

VUD 007 1192

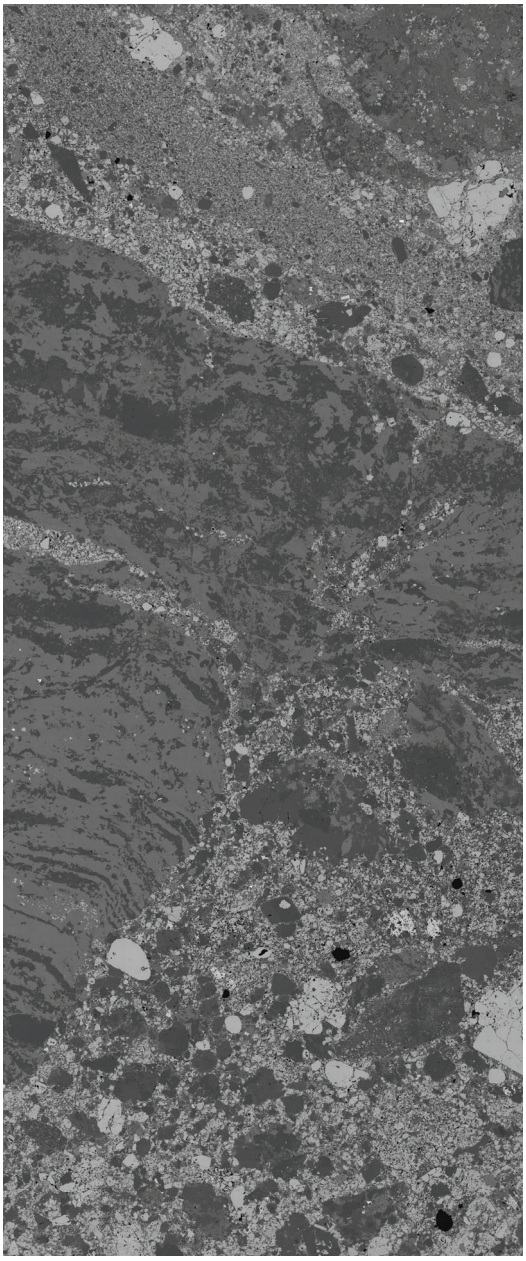

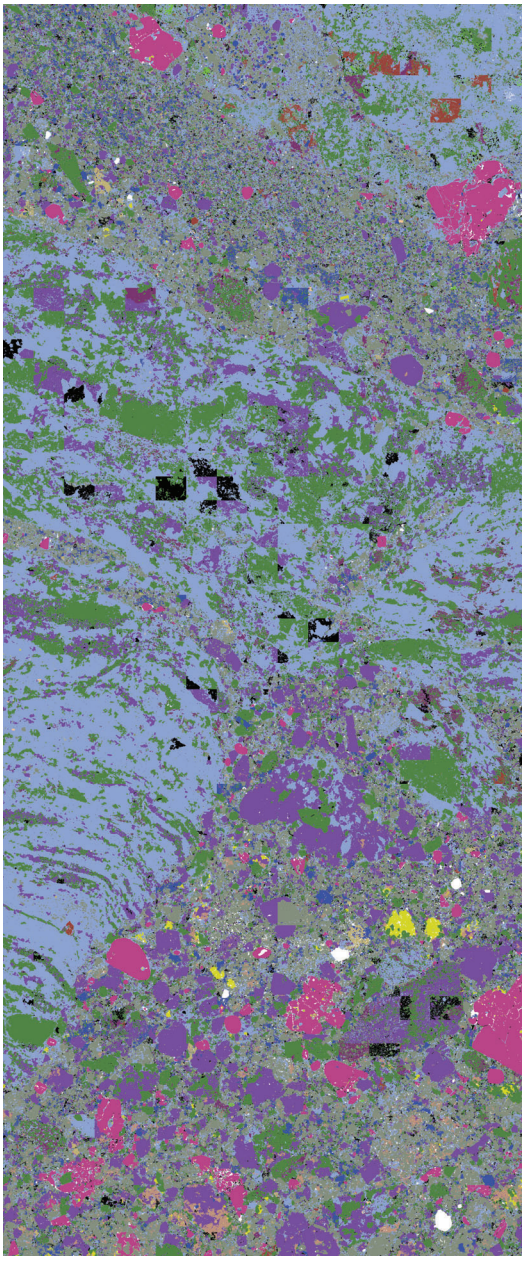

Mineral Legend

Hematite/Magnetite	Albite	Apatite	Chalcopyrite	No XRay
Mg-Iron-oxide	Dolomite	Florencite	Pyrite	Unknown
Al-Si-Fe	Quartz	Monazite	Brannerite	
Goethite	Chlorite	Xenotime	Uraninite	
	Barite	Rutile	Gersdorffite-Cobalite	
		Zircon		

Appendix 5 Figure A1 Back scatter electron (left) and mineral liberation analysis (right) maps for thin sections analysed in this study

VUD 007 1183

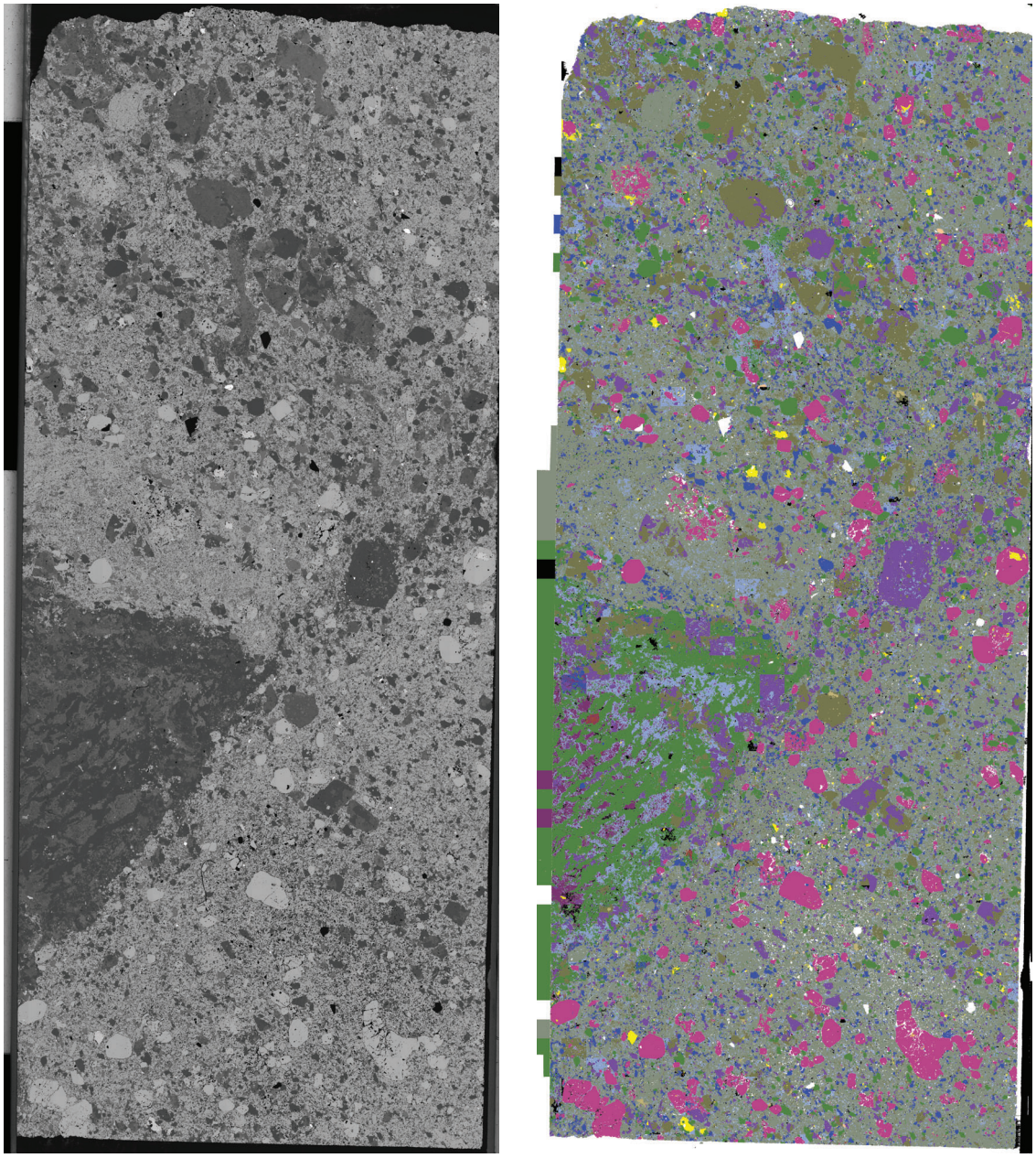

Appendix 5 Figure A1 Back scatter electron (left) and mineral liberation analysis (right) maps for thin sections analysed in this study

VUD 009 852

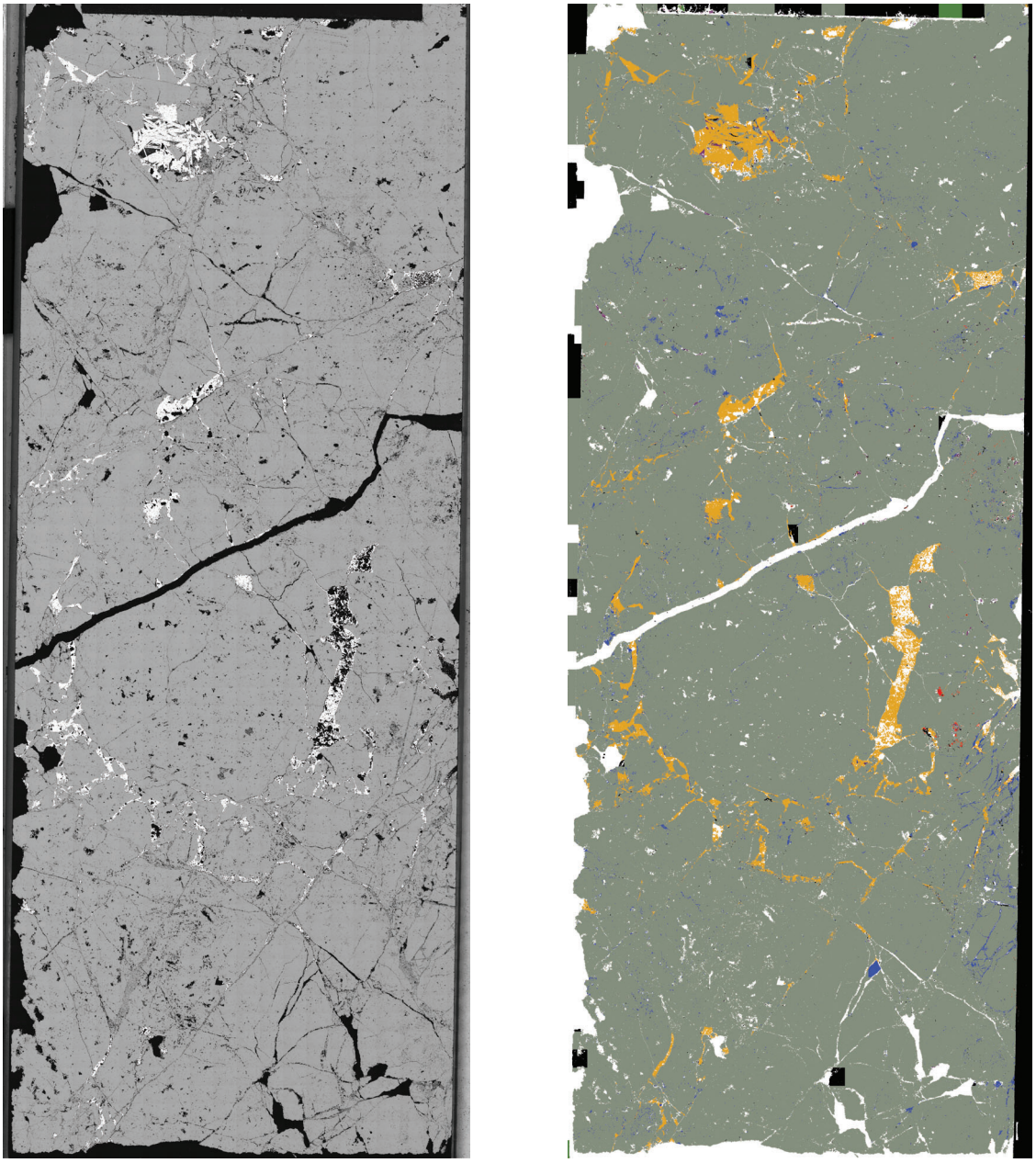

Appendix 5 Figure A1 Back scatter electron (left) and mineral liberation analysis (right) maps for thin sections analysed in this study

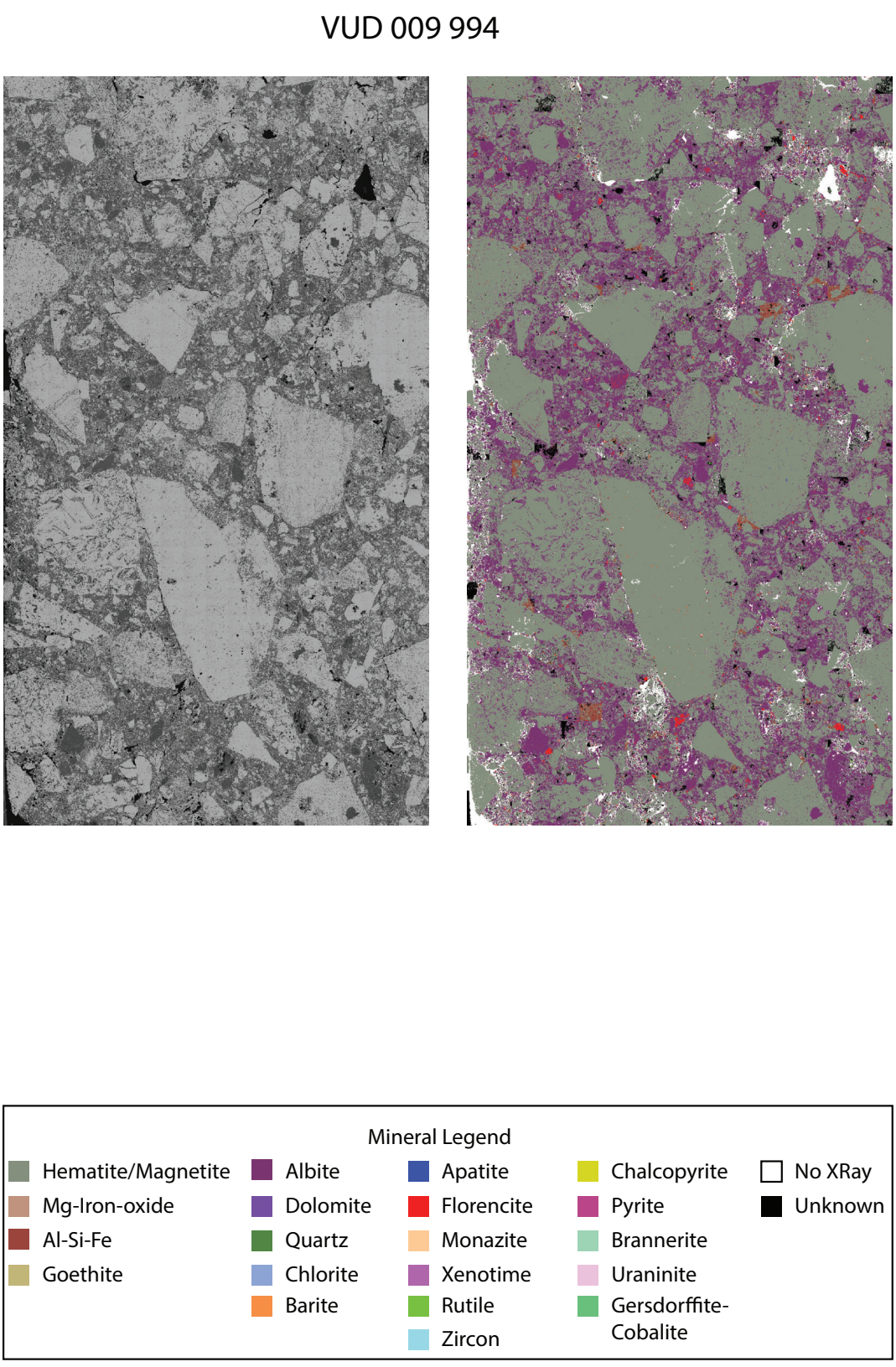

Appendix 5 Figure A1 Back scatter electron (left) and mineral liberation analysis (right) maps for thin sections analysed in this study

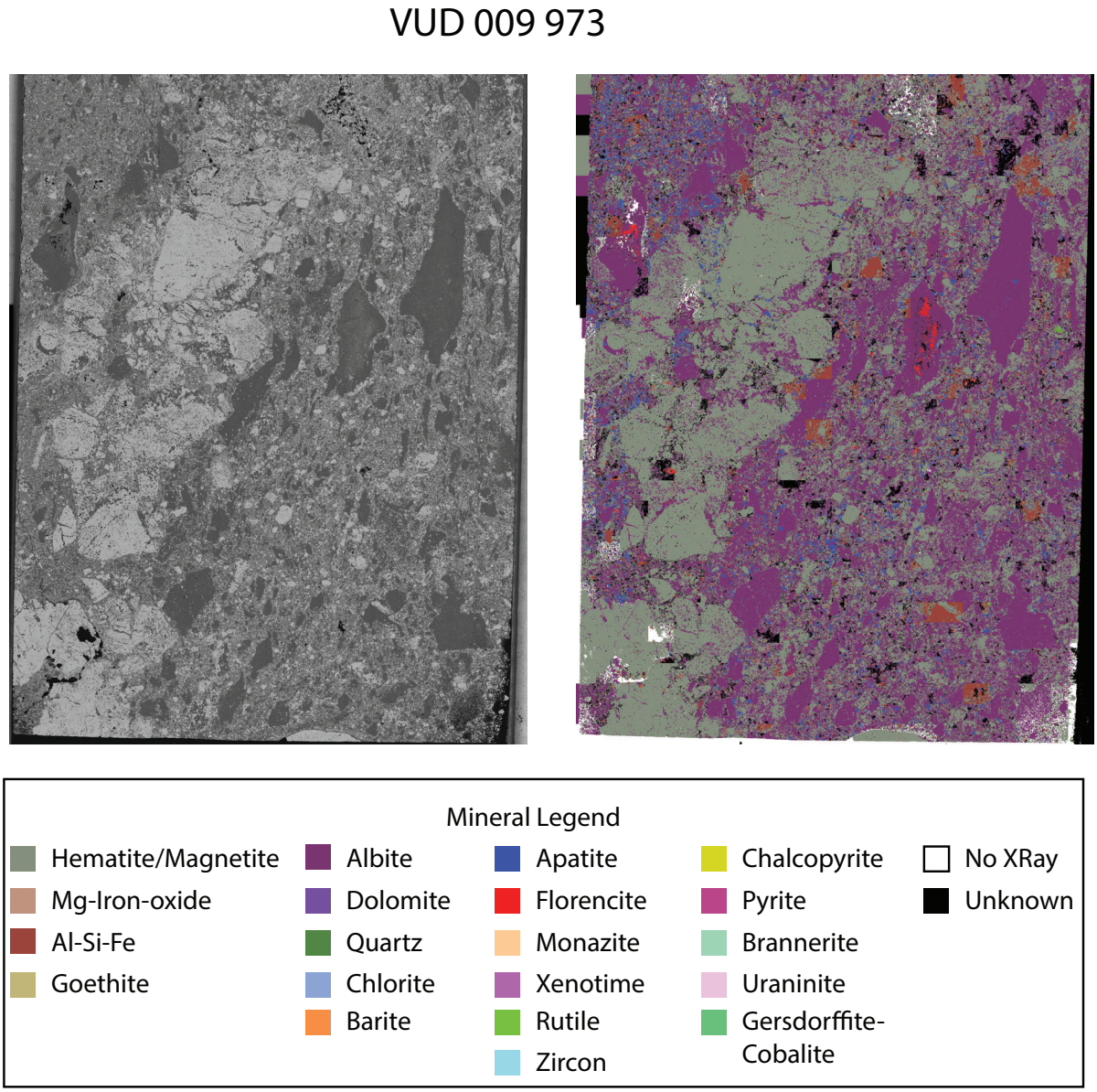

Appendix 5 Figure A1 Back scatter electron (left) and mineral liberation analysis (right) maps for thin sections analysed in this study

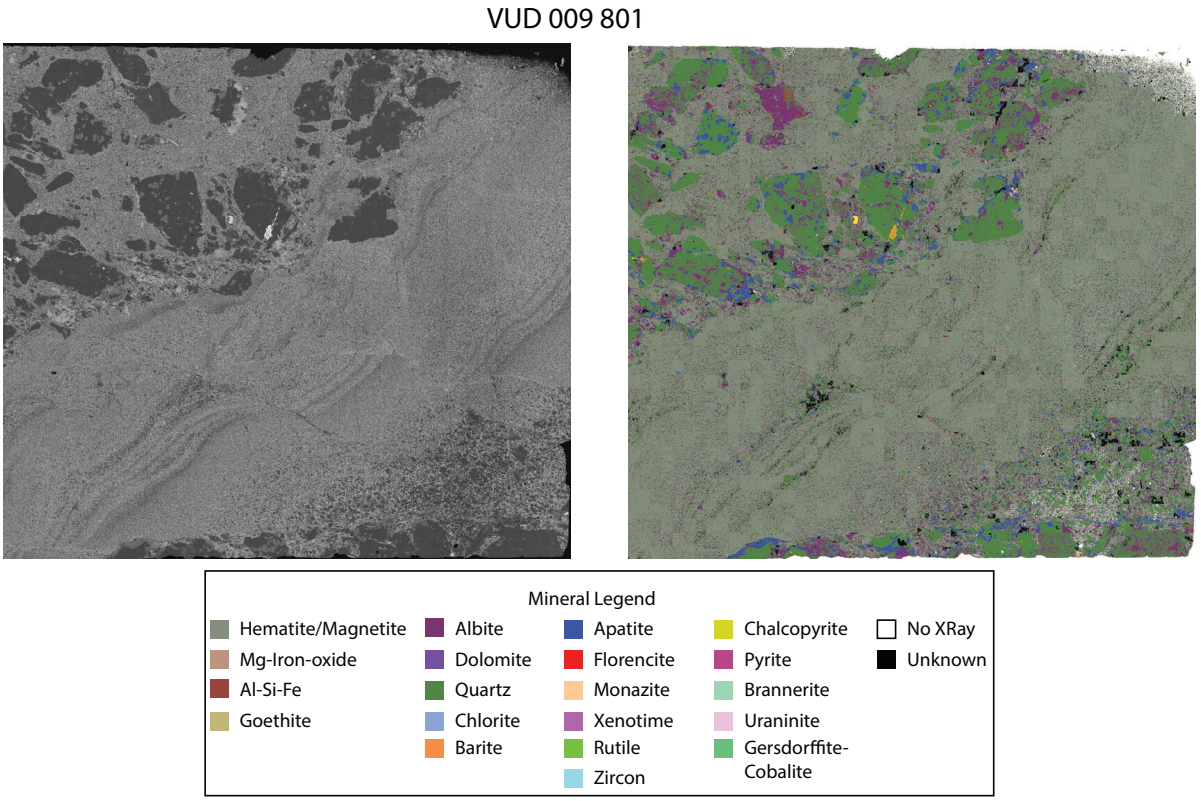

Appendix 5 Figure A1 Back scatter electron (left) and mineral liberation analysis (right) maps for thin sections analysed in this study

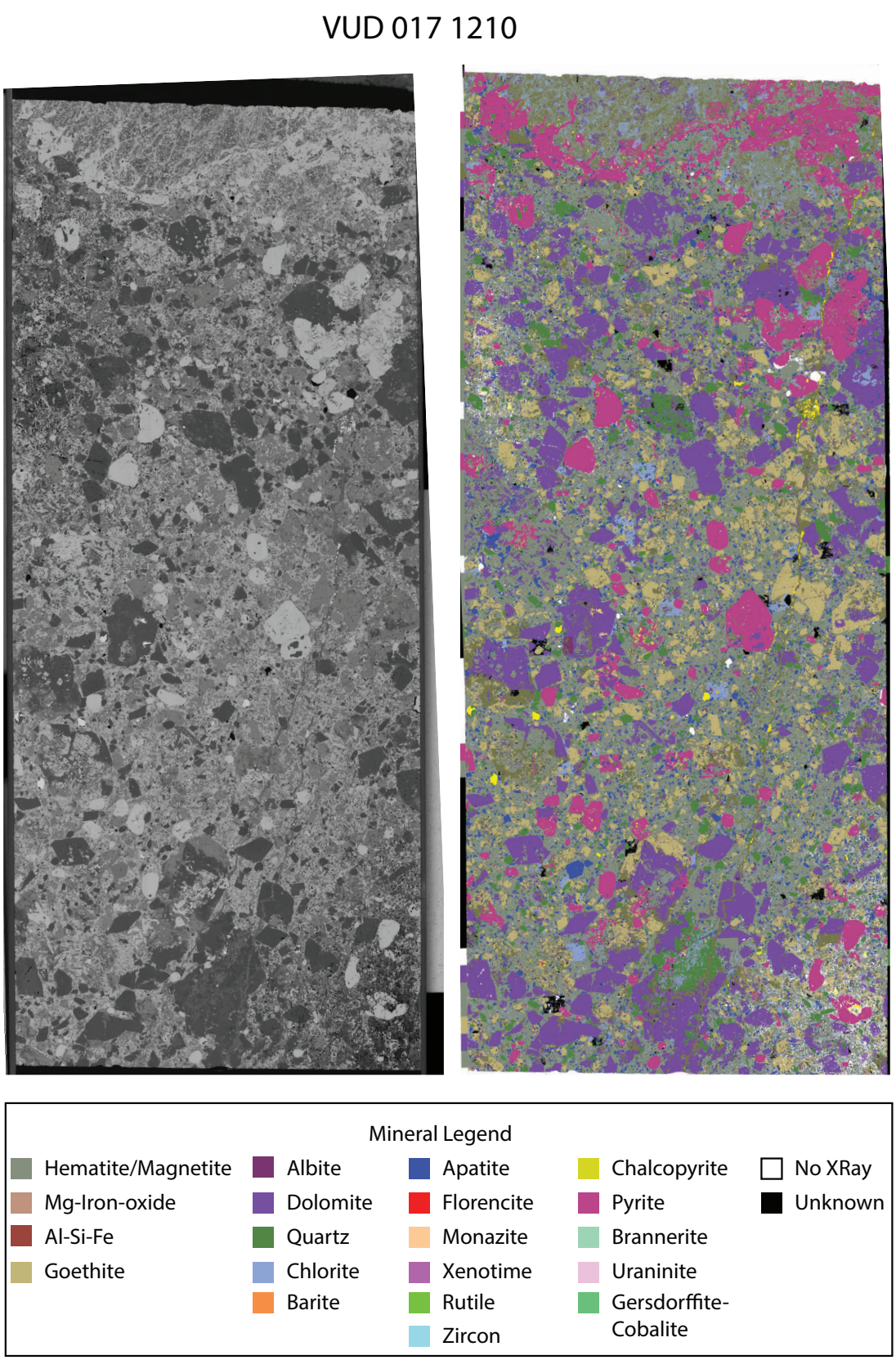

Appendix 5 Figure A1 Back scatter electron (left) and mineral liberation analysis (right) maps for thin sections analysed in this study

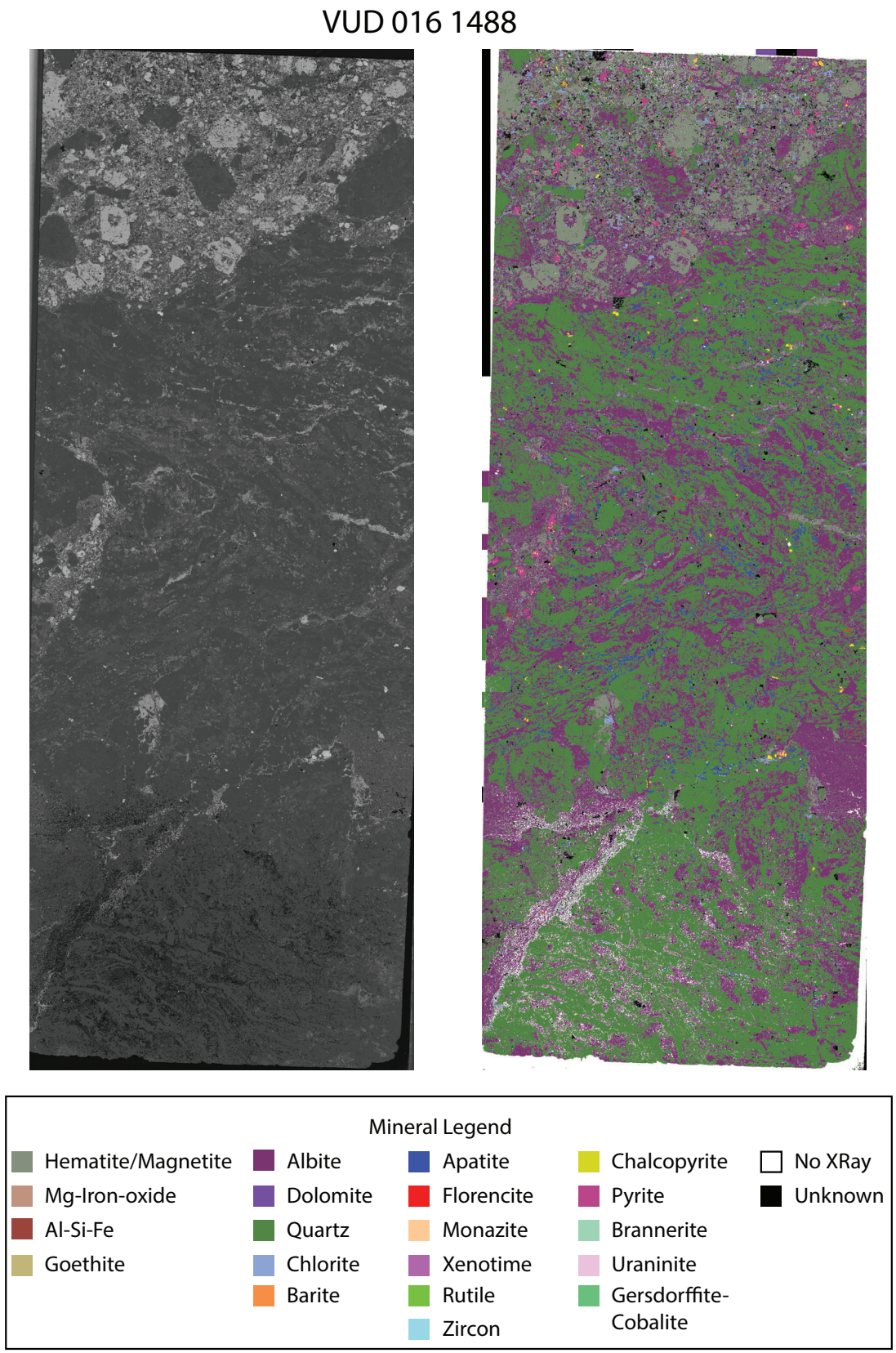

Appendix 5 Figure A1 Back scatter electron (left) and mineral liberation analysis (right) maps for thin sections analysed in this study

VUD 007 1084

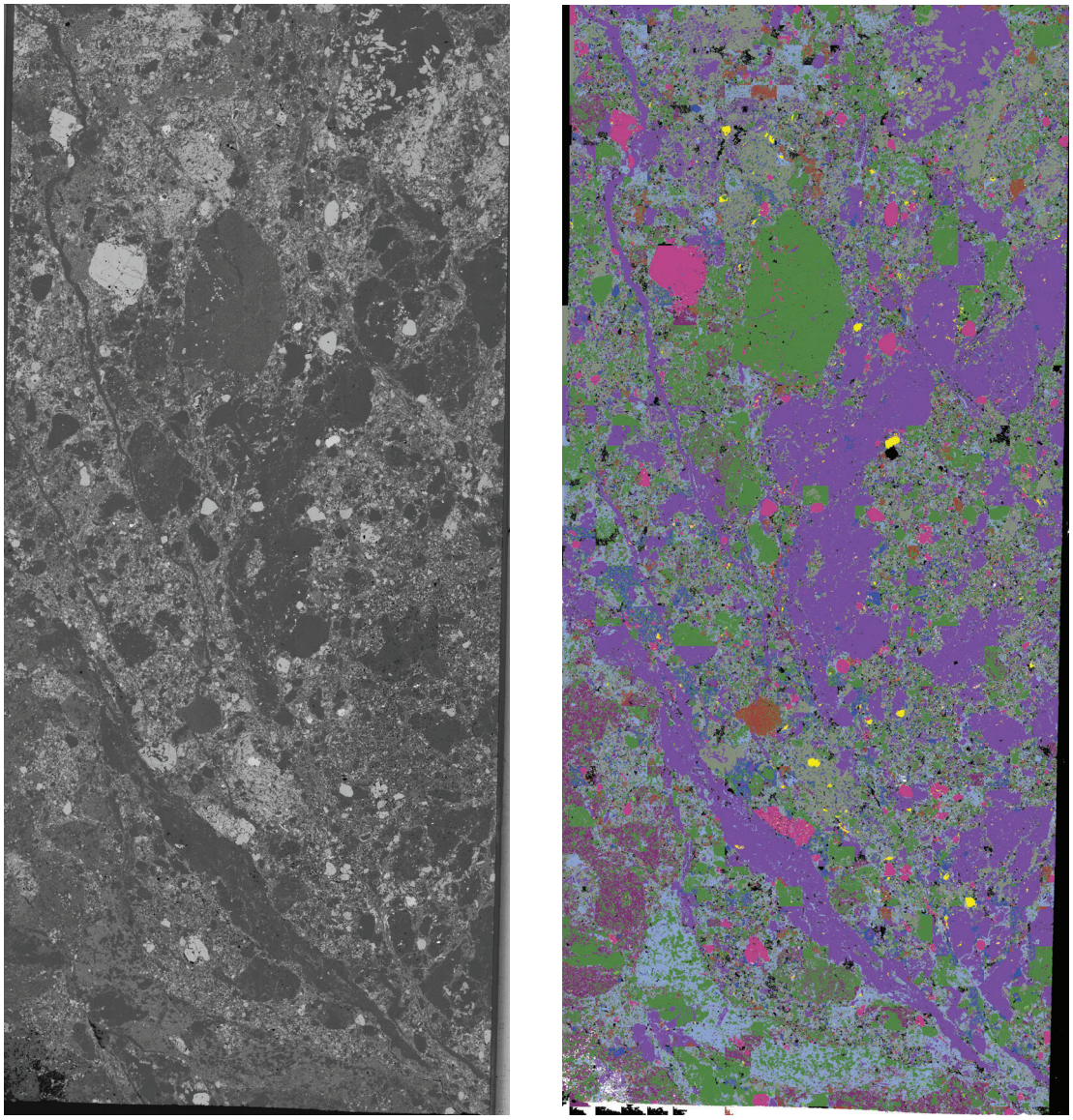

Appendix 5 Figure A2 Time-resolved profiles for representative apatite, magnetite, hematite and florencite from the Vulcan Prospect

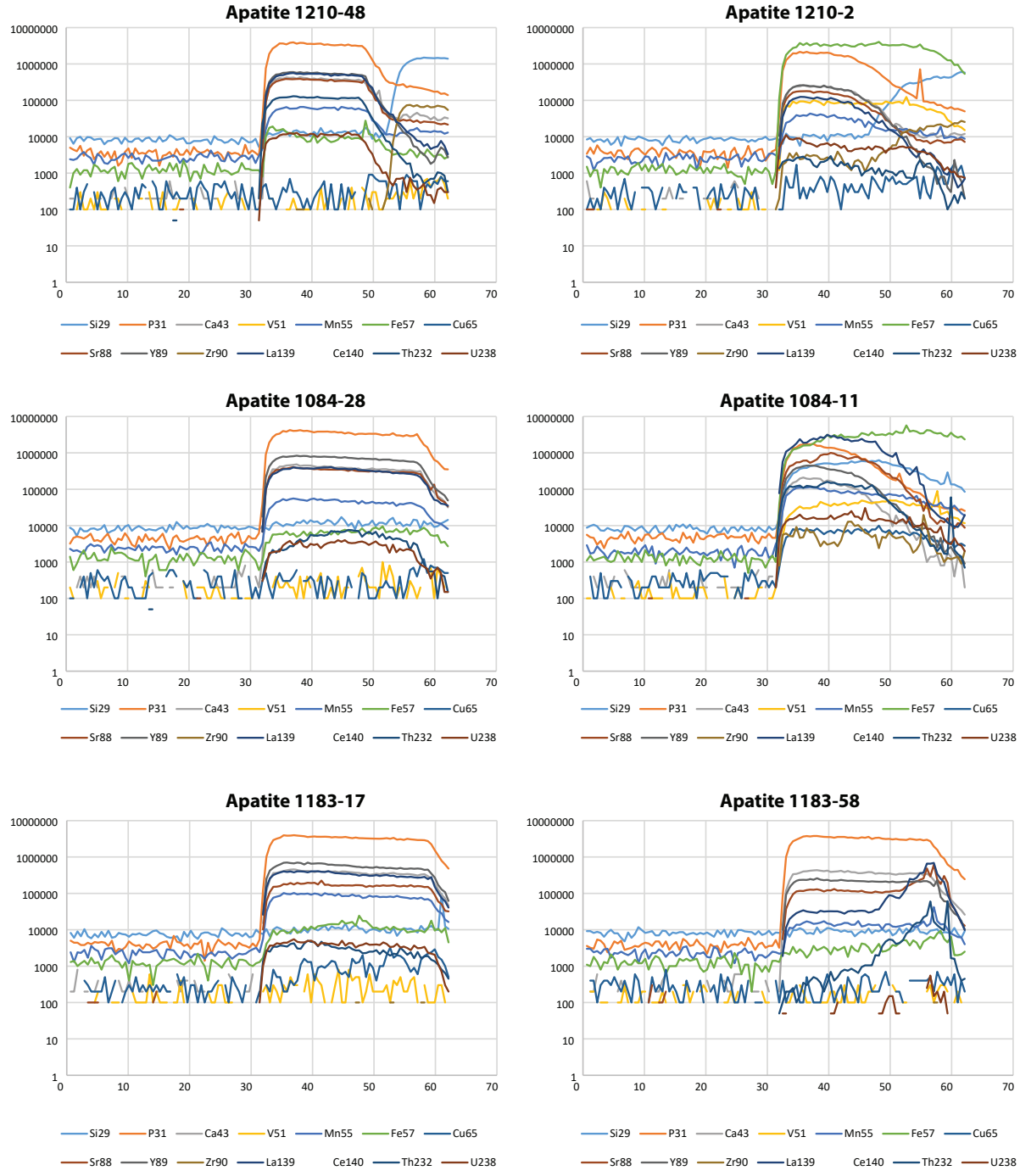

Appendix Figure A2-1: Representative time-resolved profiles for ca. 1600 Ma magnetite-associated apatite. Profiles on the left are analyses that were included in U-Pb geochronology calculations (1210-48, 1084-28 and 1183-17), and profiles on the right were discarded due to the presence of inclusions or the grain not being apatite.

Appendix 5 Figure A2 Time-resolved profiles for representative apatite, magnetite, hematite and florencite from the Vulcan Prospect

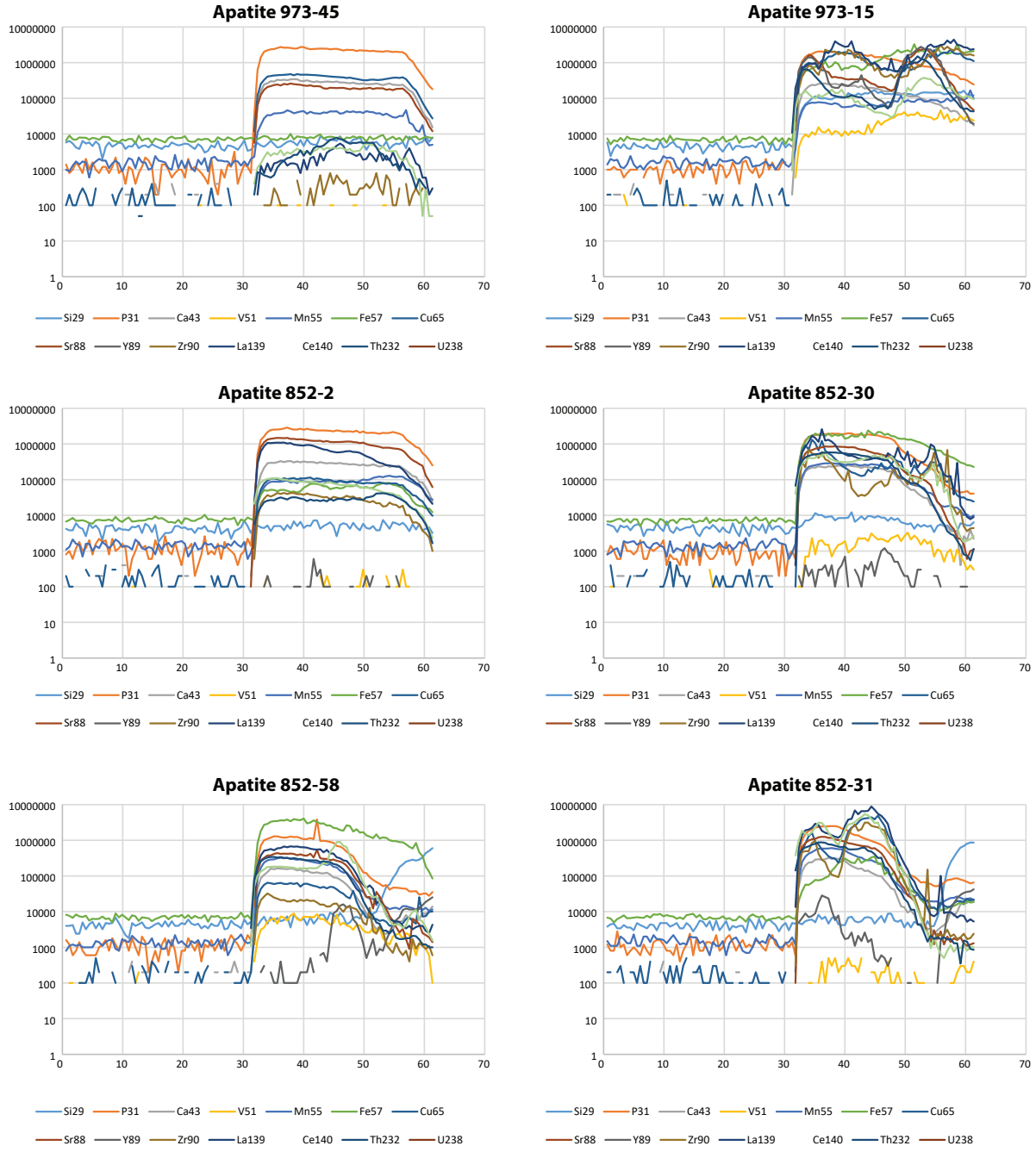

Appendix Figure A2-2: Representative time-resolved profiles for ca. 1100 Ma hematite-associated apatite. Profiles for samples 973-45 and 825-2 were included in U-Pb geochronology calculations, and profiles for samples 973-15, 825-30, 825-58 and 825-31 were discarded due to the presence of inclusions or the grain not being apatite (e.g. 825-58).

Appendix 5 Figure A2 Time-resolved profiles for representative apatite, magnetite, hematite and florencite from the Vulcan Prospect

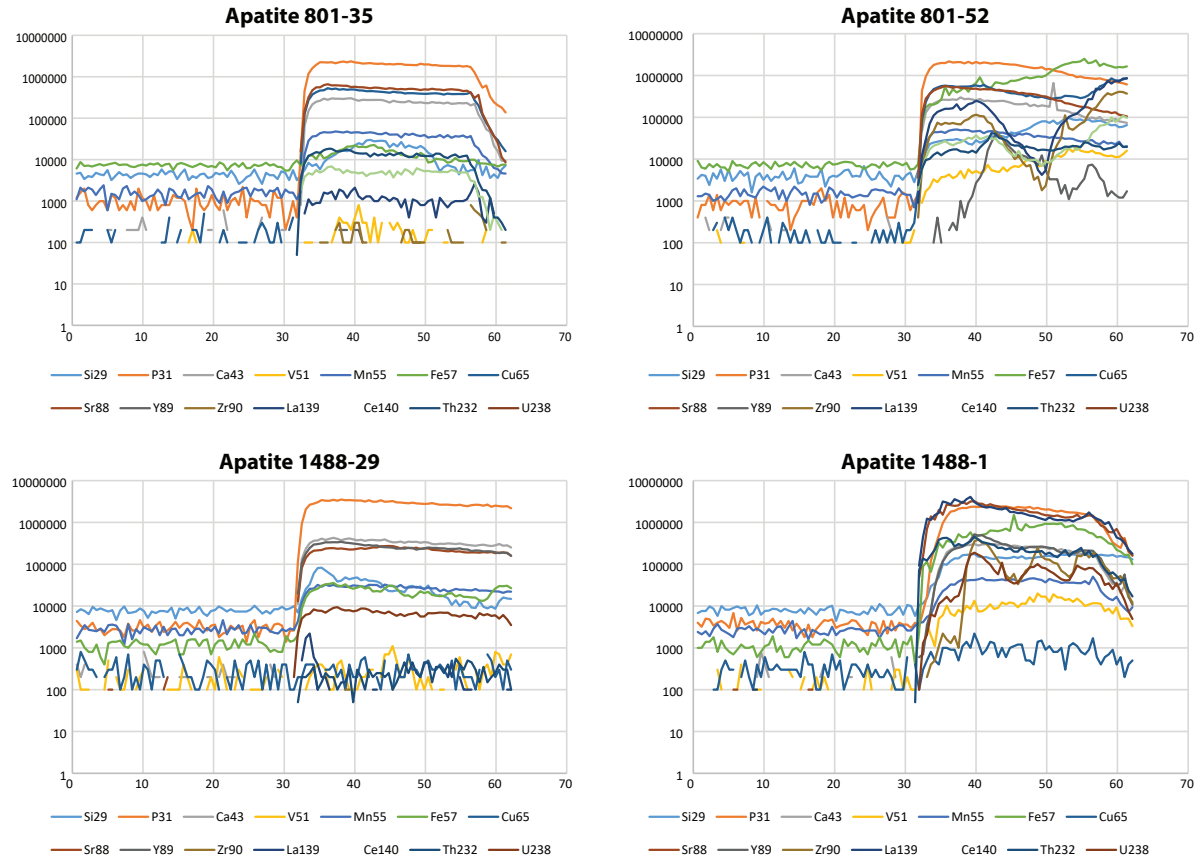

Appendix Figure A2-3: Representative time-resolved profiles for ca. 450 Ma hematite-associated apatite. Profiles on the left are analyses that were included in U-Pb geochronology calculations (801-35 and 1488-29), and profiles on the right were discarded due to the presence of inclusions or the grain not being apatite.

Appendix 5 Figure A2 Time-resolved profiles for representative apatite, magnetite, hematite and florencite from the Vulcan Prospect

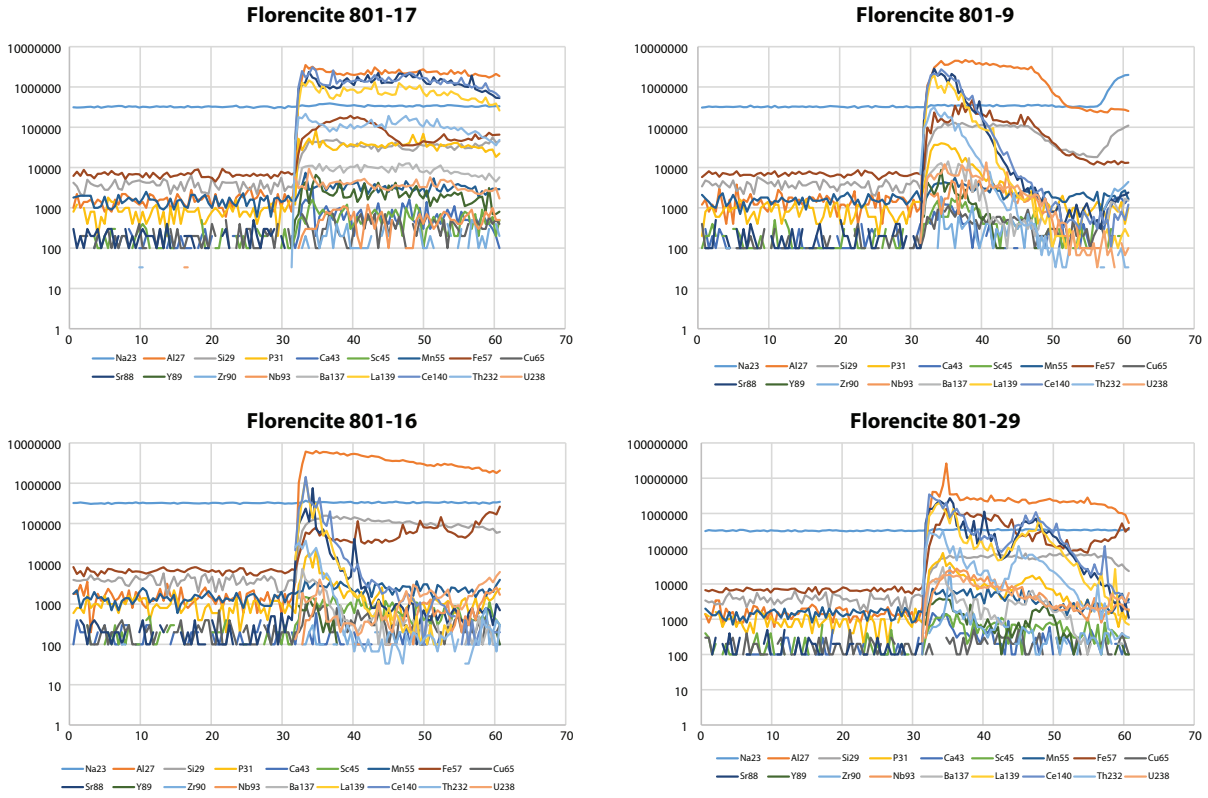

Appendix Figure A2-4: Representative time-resolved profiles for florencite from sample VUD 009 801. The profiles for sample 801-17 was included in discussion and the profiles for 801-9, 801-16 and 801-29 were discarded due to the presence of inclusions.

Appendix 5 Figure A2 Time-resolved profiles for representative apatite, magnetite, hematite and florencite from the Vulcan Prospect

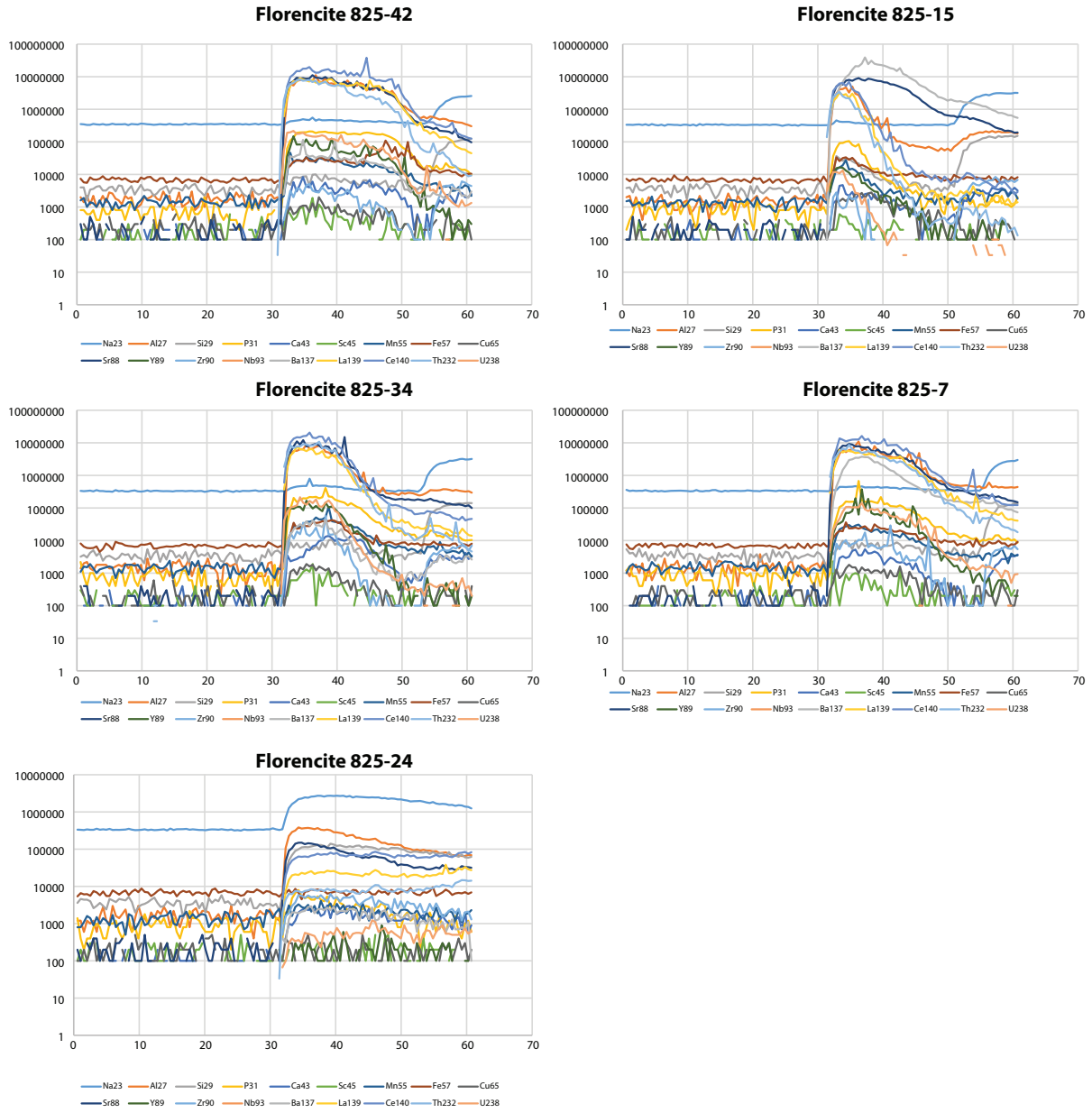

Appendix Figure A2-5: Representative time-resolved profiles for florencite from sample VUD 009 825. The profile for sample 825-42 was included in discussion, excluding the signal from 50 seconds onwards, and the profiles for 825-15, 825-34, 825-7 and 825-24 were discarded due to the presence of inclusions or the grain not being florencite.

Appendix 5 Figure A2 Time-resolved profiles for representative apatite, magnetite, hematite and florencite from the Vulcan Prospect

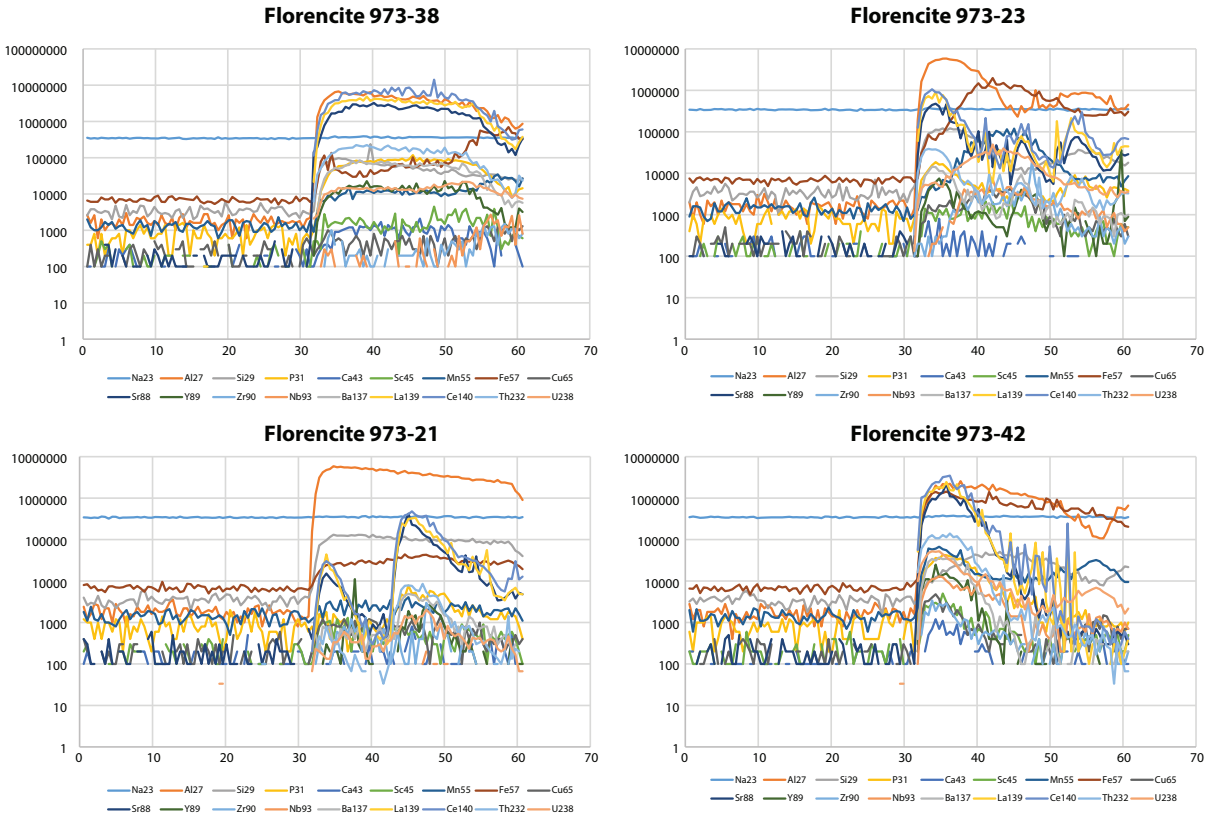

Appendix Figure A2-6: Representative time-resolved profiles for florencite from sample VUD 009 973. The profiles for sample 973-38 was included in discussion and the profiles for 973-23, 973-21 and 973-42 were discarded due to the presence of inclusions or the grains not being florencite.

Appendix 5 Figure A2 Time-resolved profiles for representative apatite, magnetite, hematite and florencite from the Vulcan Prospect

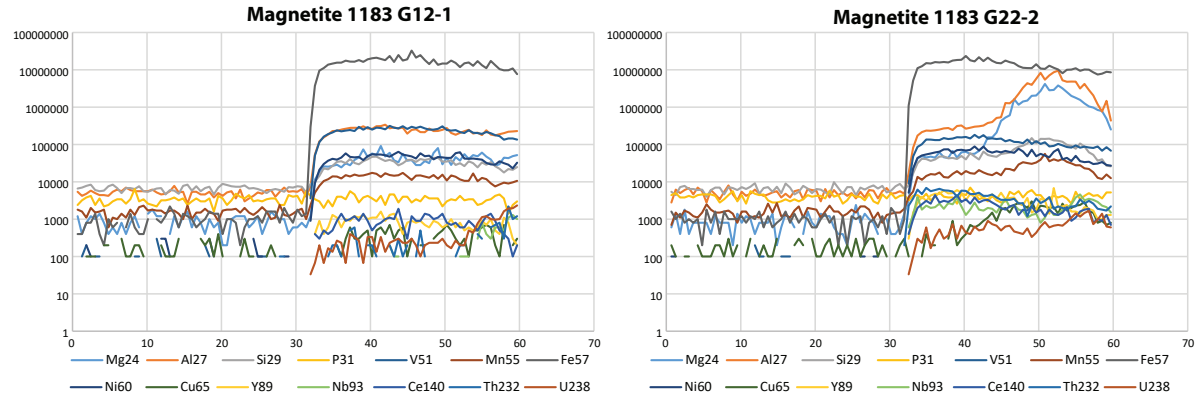

Appendix Figure A2-7: Representative time-resolved profiles for magnetite from drill hole VUD007 1183. The profiles on the left was included for discussion and the profiles on the right was discarded due to the presence of inclusions.

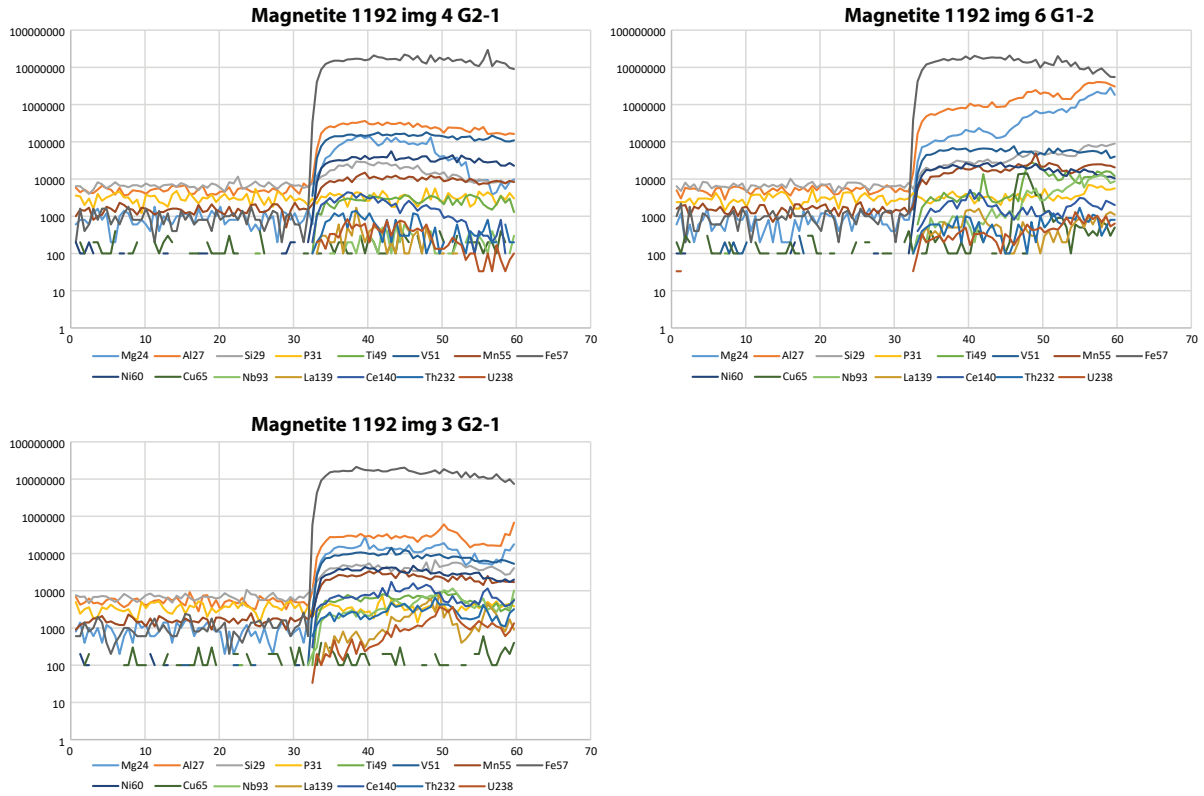

Appendix Figure A2-8: Representative time-resolved profiles for magnetite from drill hole VUD007 1192. The profile for sample 1192 img 4 G2-1 was included in discussion and profiles for 1192 img 6 G1-2 and 1192 img 3 G2-1 were discarded due to the presence of inclusions.

Appendix 5 Figure A2 Time-resolved profiles for representative apatite, magnetite, hematite and florencite from the Vulcan Prospect

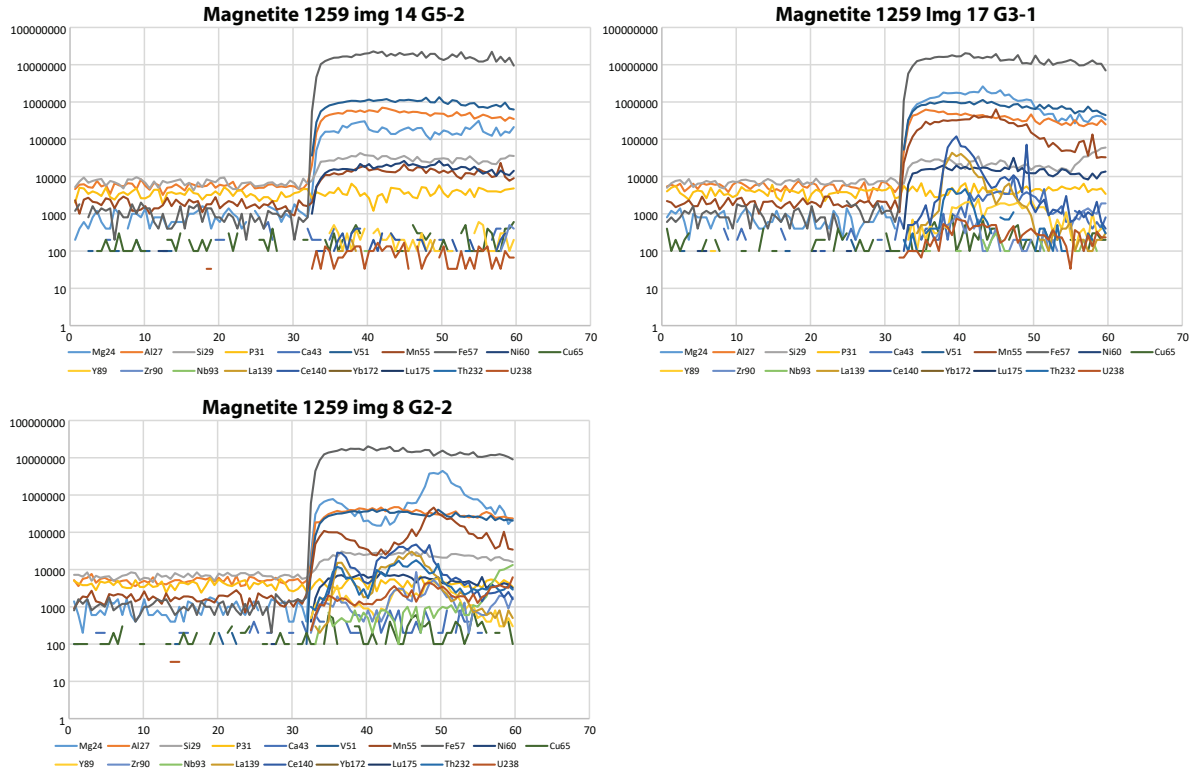

Appendix Figure A2-9: Representative time-resolved profiles for magnetite from drill hole VUD017 1259. The profile for sample 1259 img 14 G5-2 was included in discussion and profiles for 1268 img 17 G3-1 and 1259 img 8 G2-2 were discarded due to the presence of inclusions.

Appendix 5 Figure A2 Time-resolved profiles for representative apatite, magnetite, hematite and florencite from the Vulcan Prospect

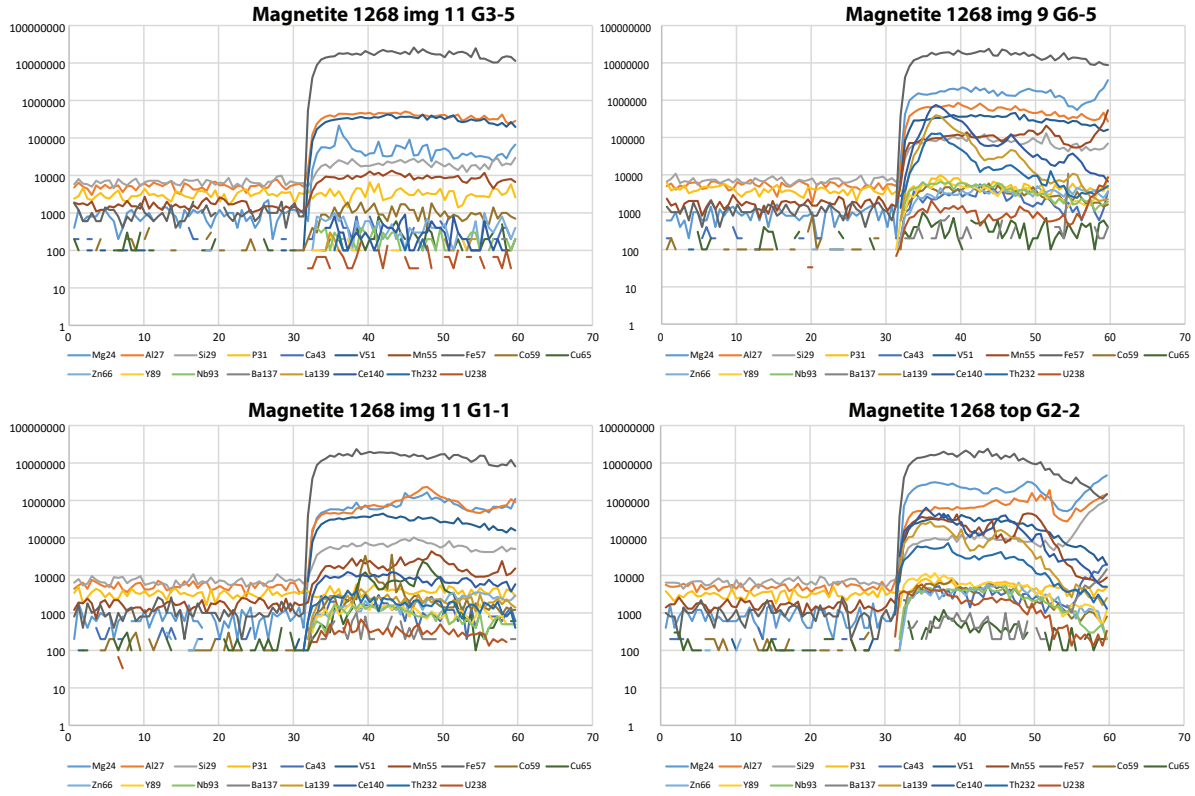

Appendix Figure A2-10: Representative time-resolved profiles for magnetite from drill hole VUD017 1268. The profile for sample 1268 img 11 G3-5 was included in discussion and profiles for 1268 img 9 G6-5, 1268 img 11 G1-1 and 1268 top G2-2 were discarded due to the presence of inclusions.

Appendix 5 Figure A2 Time-resolved profiles for representative apatite, magnetite, hematite and florencite from the Vulcan Prospect

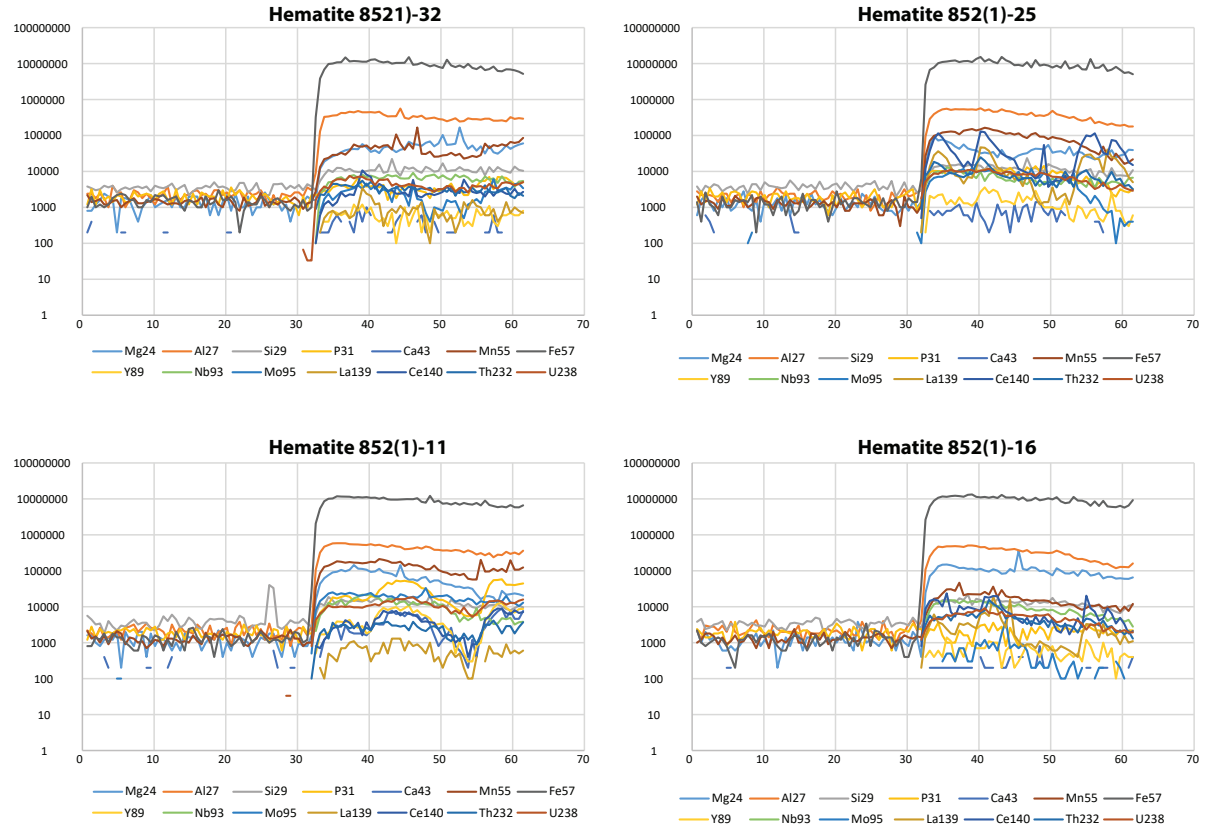

Appendix Figure A2-11: Representative time-resolved profiles for hematite from sample VUD 009 852. The profiles for sample 852(1)-32 was included in discussion and the profiles for 852(1)-25, 852(1)-11 and 852(1)-16 were discarded due to the presence of inclusions.

Appendix 5 Figure A2 Time-resolved profiles for representative apatite, magnetite, hematite and florencite from the Vulcan Prospect

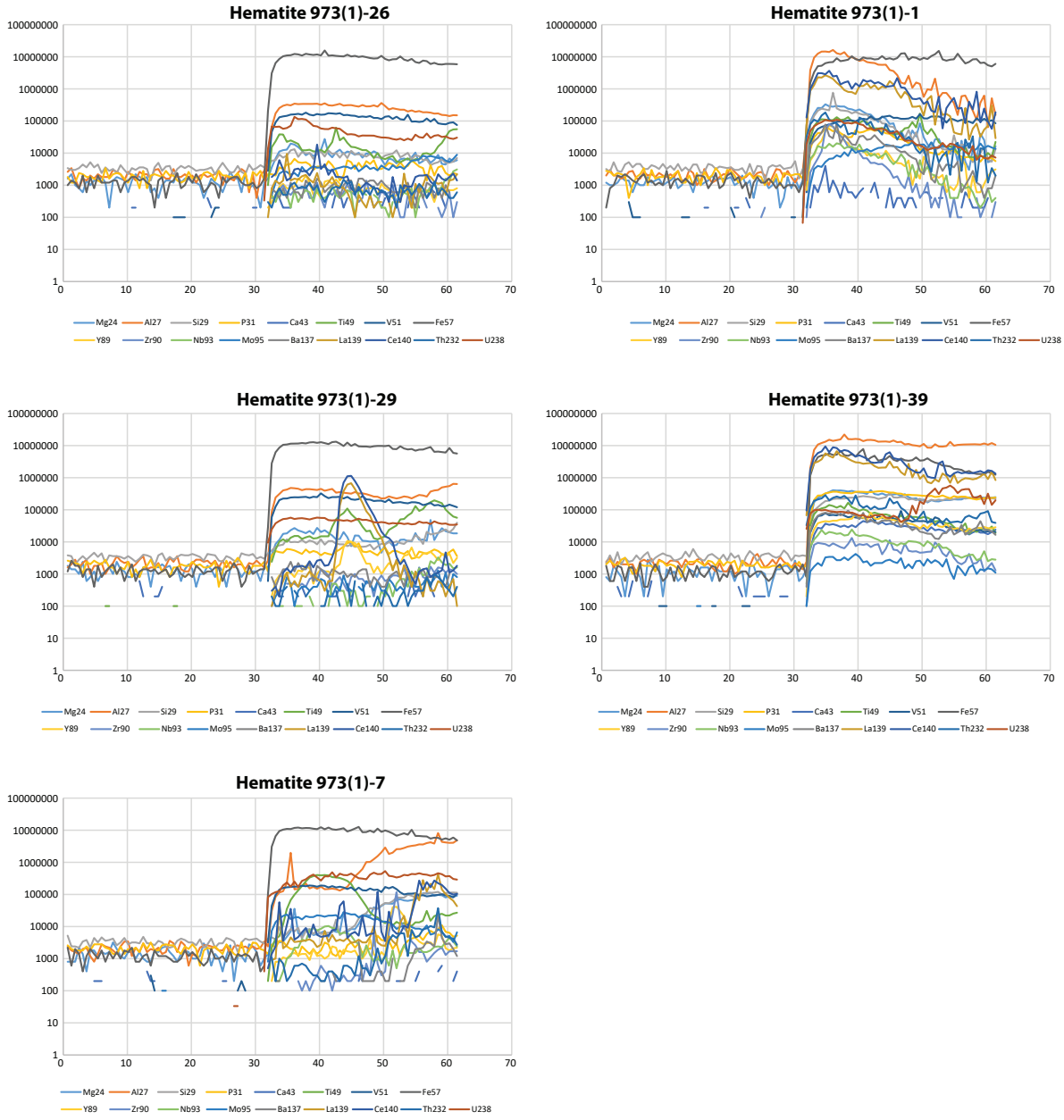

Appendix Figure A2-12: Representative time-resolved profiles for hematite from sample VUD 009 973. The profiles for sample 973(1)-26 was included in discussion and the profiles for 973(1)-1, 973(1)-29, 973(1)-39 and 973(1)-7 were discarded due to the presence of inclusions.

Appendix 5 Figure A2 Time-resolved profiles for representative apatite, magnetite, hematite and florencite from the Vulcan Prospect

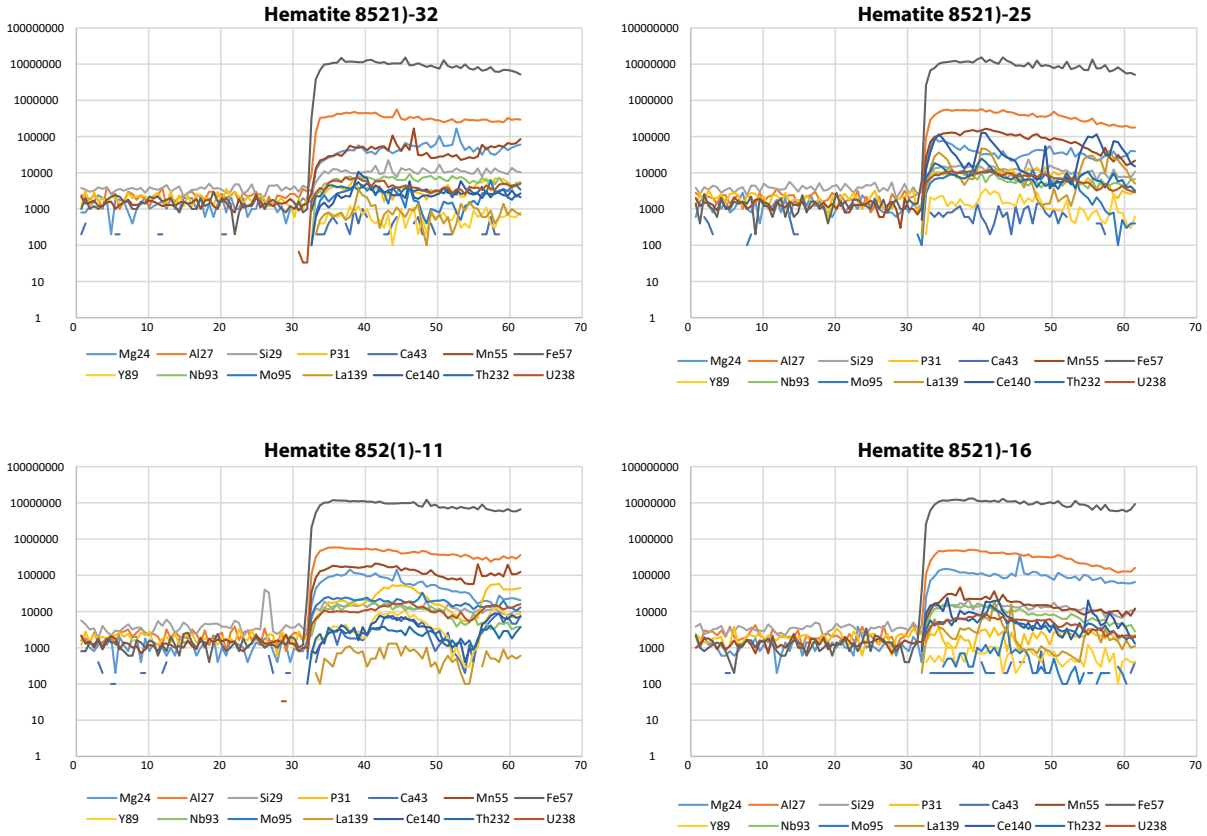

Appendix Figure A2-13: Representative time-resolved profiles for hematite from sample VUD 009 994. The profiles for sample 994(1)-11 was included in discussion and the profiles for 994(1)-30, 944(1)-71 and 994(2)-5 were discarded due to the presence of inclusions.

Appendix Figure A3 Chondrite-normalised REY plots and transition metals vs total REY including samples below the detection limit

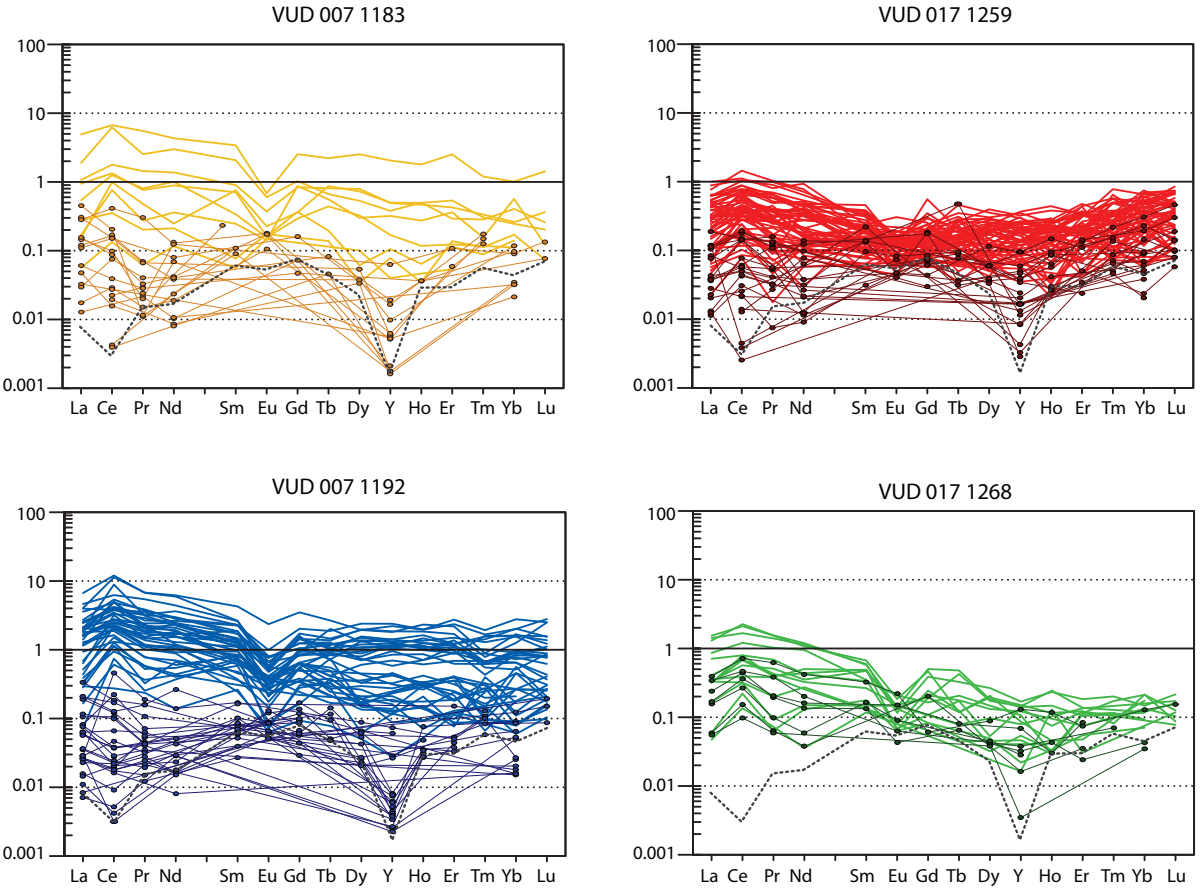

Appendix Figure A3-1: REY plots for magnetite samples including analyses below the detection limit, as indicated by the darker lines and points. Dark grey dashed line represents the detection limit for each element.

Appendix Figure A3 Chondrite-normalised REY plots and transition metals vs total REY including samples below the detection limit

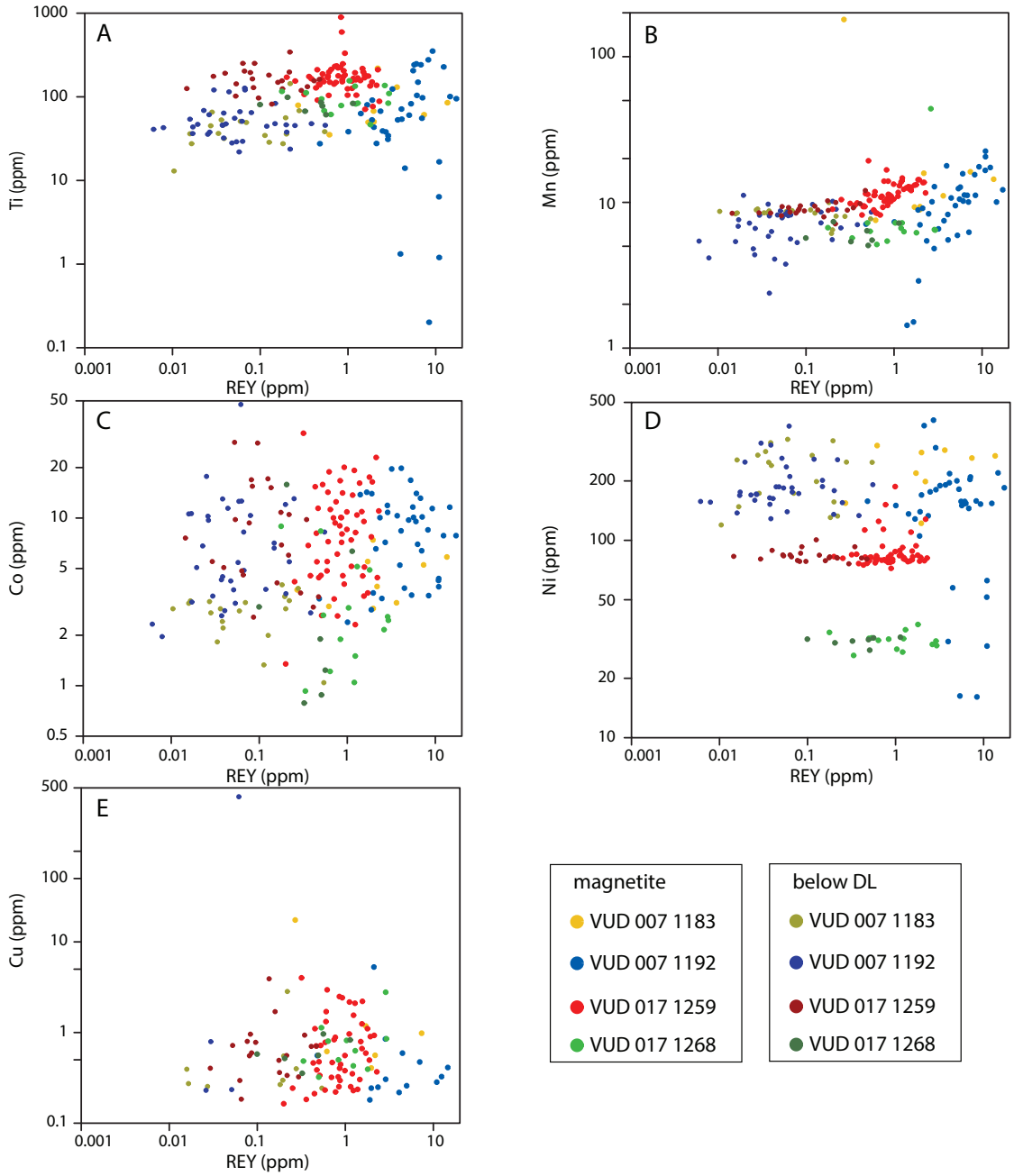

Appendix Figure A3-2: REY plots for hematite samples including analyses below the detection limit for sample VUD009 973, as indicated by darker lines and points. Dark grey dashed line represents the detection limit for each element. Analyses below the detection limit are indicated by the darker symbols of the same colour for each magnetite sample.

Appendix Figure A3 Chondrite-normalised REY plots and transition metals vs total REY including samples below the detection limit

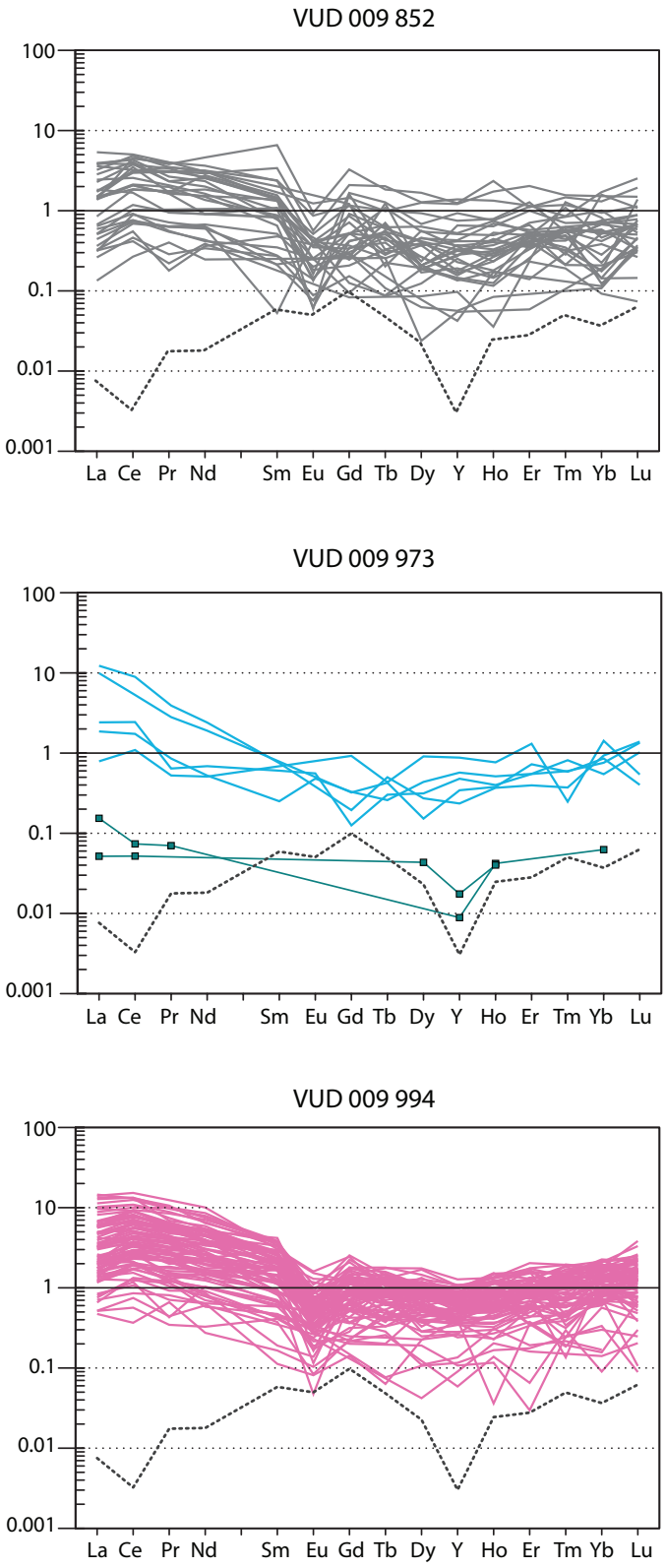

Appendix Figure A3-3: REY plots for hematite samples including analyses below the detection limit for sample VUD009 973, as indicated by darker lines and points. Dark grey dashed line represents the detection limit for each element.

Appendix 6

Publications arising from the project

New geology

The link is in the geochemistry: how we know a metasomatised mantle underlies the mineral systems of the Gawler Craton

Claire Wade[1, 2], Anthony Reid[1, 2] Justin Payne[3] and Karin Barovich[2]
1 Geological Survey of South Australia, Department for Energy and Mining
2 School of Physical Sciences, University of Adelaide
3 School of Natural and Built Environments, University of South Australia

Introduction

A coherent and related system of Mesoproterozoic magmatism, hydrothermal alteration and deformation extends from the western Gawler Craton to eastern Curnamona Province, South Australia. This system produced the Olympic Dam iron oxide – copper–gold (IOCG) orebody and the Olympic Cu–Au Province metallogenic system in addition to gold-dominant deposits of the Central Gawler Gold Province and related prospects across the Gawler Craton and Curnamona Province (Budd and Skirrow 2007; Skirrow et al. 2018; Reid 2019). Such an extensive system requires the input of an enormous amount of energy, and energy on such a scale can only be delivered into the crust from the mantle. Therefore, understanding the composition and evolution of the mantle lithosphere beneath the Gawler Craton is a key component towards understanding the evolution of the Mesoproterozoic mineral systems in this region.

Recently we have been working on a major new geochemical and isotopic dataset that focuses on the mafic rocks of the Gawler Craton. This dataset includes 132 surface and drill core samples from across the Gawler Craton (Fig. 1). For each sample we have analysed the whole-rock major and trace element geochemistry. Selected samples have also been analysed for Sm–Nd isotopic composition. This dataset has now been published and fully described (Wade et al. 2019). In this paper we describe the major patterns evident in the new dataset in relation to a subset of samples associated with IOCG and gold mineral deposits and prospects. We also discuss the implications of the recognition of compositional heterogeneity and evidence for metasomatism in the source regions for the Mesoproterozoic mafic rocks of the Gawler Craton. We conclude that the IOCG and related mineral systems were fundamentally influenced by the mantle composition in terms of both its ability to melt and the magmas and metals thus released during this melting event.

Mafic geochemistry dataset: samples and methods

Mafic rocks provide a window into the lower crust and mantle as they are most often the product of melting of these source regions. In particular, when geochemical data are filtered to exclude samples that have undergone crustal assimilation during magma ascent and evolution, the geochemistry of primitive mafic rocks is indicative of the type of mantle from which they were derived (Walter 2014).

The new mafic rock dataset of 132 samples were selected from IOCG and gold-dominated deposits and prospects. Samples representative of the IOCG prospects include gabbros and aphanitic mafic dykes from drill cores located in the vicinity of Olympic Dam and Chianti prospect (Fig. 2a), samples from the White Hill region (Fig. 2b), and samples from the Hillside deposit (Fig. 2c). Samples that were taken from prospects related to gold mineralisation include mafic dykes collected from the region around Tarcoola, including from the Perseverance Mine (Fig. 2d), and also from several gold prospects across the Central Gawler Gold Province.

Geochemical analyses were performed by Bureau Veritas Minerals, Perth, Western Australia. Major elements and chlorine were analysed using X-ray fluorescence (XRF) spectrometry, while trace elements

Gawler Craton geochemistry

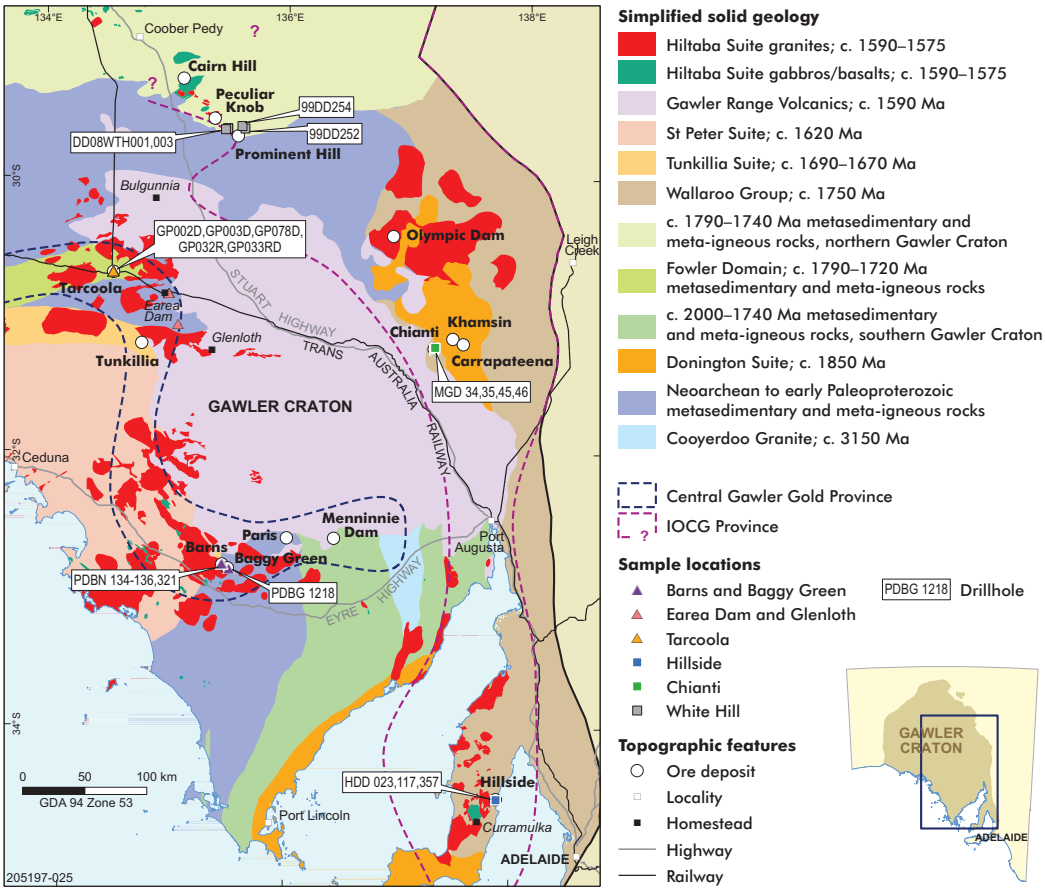

Figure 1 *Simplified solid geology location diagram of the study area within the Gawler Craton showing the sample locations in this study.*

were determined by laser ablation - inductively coupled plasma - mass spectrometry (LA-ICP-MS) and Au, Pt and Pd were analysed using fire assay ICP-MS. FeO was determined volumetrically and fluorine was determined using specific ion electrode. Whole-rock analyses for Sm–Nd isotopic compositions were performed at the University of Adelaide.

Summary of results

Of the 132 analysed, a subset of 50 samples from gold deposits Barns, Baggy Green, Earea Dam, Glenloth and Tarcoola, and IOCG deposits Chianti, Hillside and White Hill (Fig. 1) were used to compare geochemical and isotopic compositions of mafic rocks related to the different mineralisation styles. Silica values are low to intermediate, 42.7–61.8 wt% SiO_2 (Fig. 3a), and Mg# (calculated as molar Mg# = (Mg/ [Mg+Fe] x100)) range from 25 to 67. In general, the gold deposit samples have higher Mg# (34–67) compared with the IOCG deposit samples (25–49). Coherent trends are formed between Fe_2O_{3t} and TiO_2 with Mg# in the IOCG samples, while the gold samples have lower Fe_2O_{3t} and TiO_2 abundances and form flatter trends, with the exception of samples from Earea Dam and Glenloth (Figs 3b, c). Ni, Th and Cr (not shown) contents are highest in the Barns samples and form coherent trends with Mg# (Figs 3d, e).

Three clear groupings have emerged from the data (Figs 3, 4). The samples from the IOCG province have moderate to high Cr and Ni; are generally enriched in high field strength elements including Zr, Nb, Th and Y (Fig. 4a); and have moderate light rare earth element enrichment (Fig. 4b). Samples associated with gold deposits or prospects have

Gawler Craton geochemistry

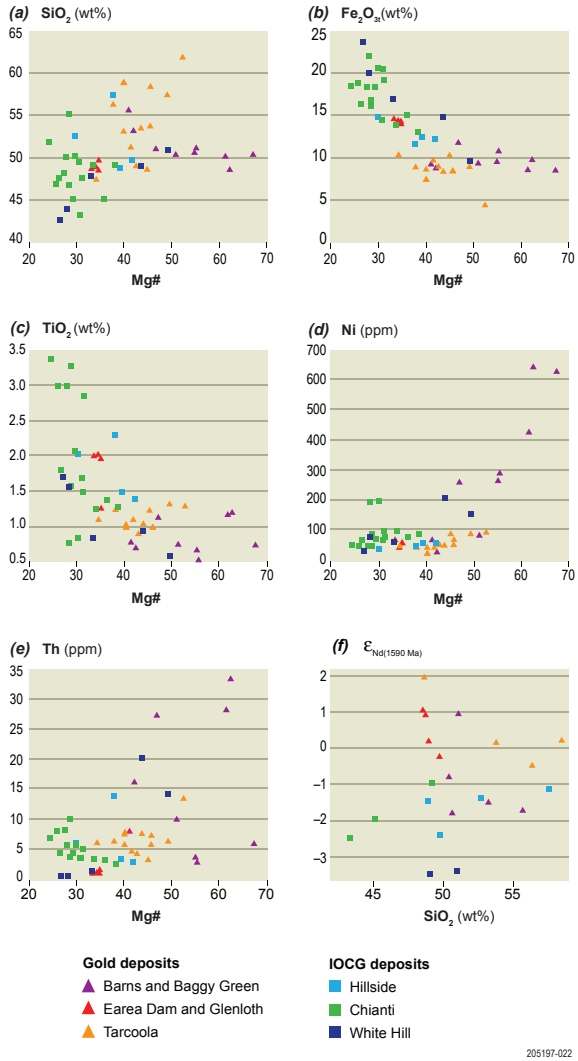

Figure 3 *Major element and trace element variation diagrams vs Mg#, and $\varepsilon_{Nd(1590\ Ma)}$ vs SiO_2 for mafic Hiltaba Suite dykes associated with gold and IOCG deposits. Includes geochemical data from Budd (2006) and Frost (2009).*

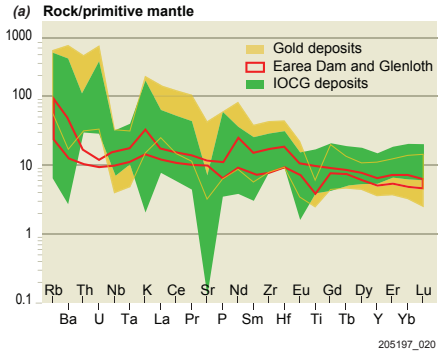

Figure 4(a) *Primitive mantle normalised trace element diagram for mafic Hiltaba Suite dykes associated with gold and IOCG deposits.*

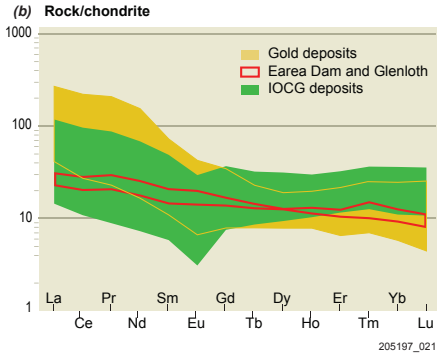

Figure 4(b) *Chondrite normalised rare earth diagram for mafic Hiltaba Suite dykes associated with gold and IOCG deposits.*

by subduction processes and was therefore hydrated, or partly hydrated mantle (Fig. 5; e.g. Goodenough, Upton and Ellam 2002; Sandeman, Cousens and Hemmingway 2003; Cai et al. 2013; Pearce, Ernst and Peate 2015; and Condie and Shearer 2017). This subduction-modified source is evident across most of the Hiltaba Suite and includes samples from both the IOCG district (Hillside, White Hill and Chianti) as well as from gold deposits (Barns, Baggy Green and Tarcoola).

Mantle input from c. 1590 Ma magmatic rocks is considered to be important for metals in the Olympic Dam Cu–Au Province and the Central Gawler Gold Province, as evidenced by the association of juvenile isotopes with increasing Cu and Au abundance (Budd and Skirrow 2007; Skirrow et al. 2007). Our new data suggest that a metasomatised, subduction-modified subcontinental lithospheric mantle is the most prominent geochemical group and appears to be associated with both IOCG and gold-dominated mineralisation styles.

Subduction and metasomatism have been recognised as being important processes to generate metal enrichment in the mantle (Richards 2009; Groves et al. 2010; Tassara et al. 2017), resulting in residual siderophile and chalcophile-rich zones or veins in the subcontinental lithospheric mantle. These zones or veins may constitute a viable source

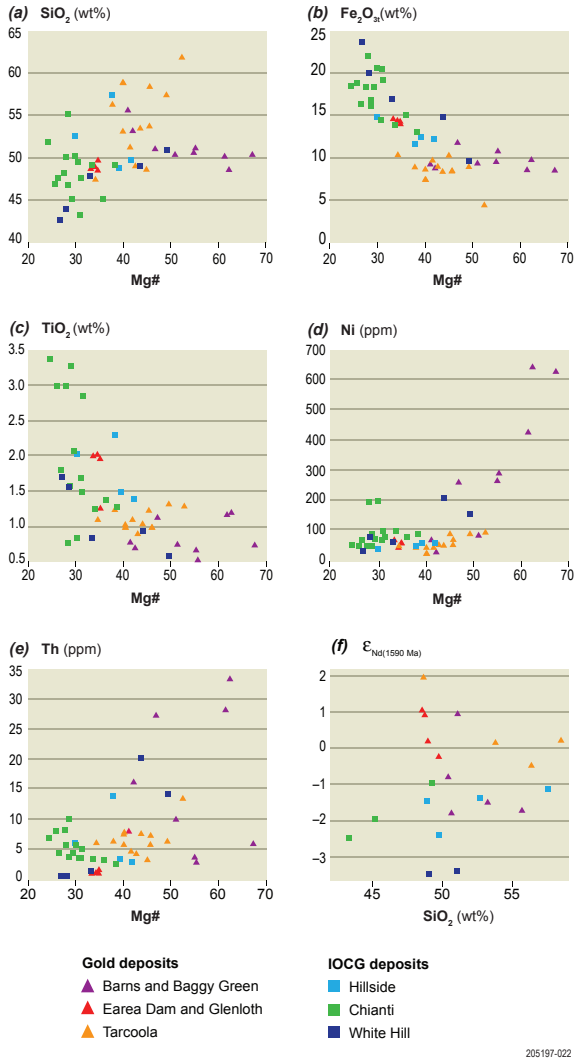

Figure 3 Major element and trace element variation diagrams vs Mg#, and $\varepsilon_{Nd(1590\ Ma)}$ vs SiO_2 for mafic Hiltaba Suite dykes associated with gold and IOCG deposits. Includes geochemical data from Budd (2006) and Frost (2009).

by subduction processes and was therefore hydrated, or partly hydrated mantle (Fig. 5; e.g. Goodenough, Upton and Ellam 2002; Sandeman, Cousens and Hemmingway 2003; Cai et al. 2013; Pearce, Ernst and Peate 2015; and Condie and Shearer 2017). This subduction-modified source is evident across most of the Hiltaba Suite and includes samples from both the IOCG district (Hillside, White Hill and Chianti) as well as from gold deposits (Barns, Baggy Green and Tarcoola).

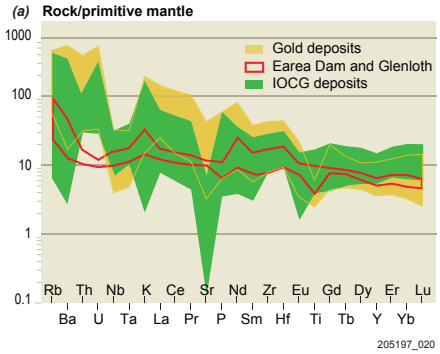

Figure 4(a) Primitive mantle normalised trace element diagram for mafic Hiltaba Suite dykes associated with gold and IOCG deposits.

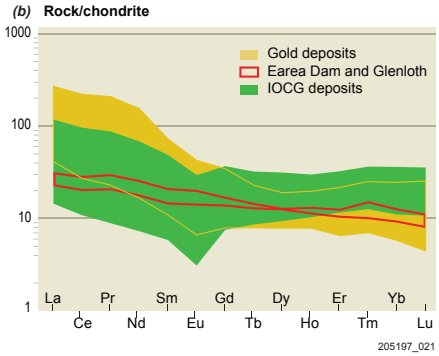

Figure 4(b) Chondrite normalised rare earth diagram for mafic Hiltaba Suite dykes associated with gold and IOCG deposits.

Mantle input from c. 1590 Ma magmatic rocks is considered to be important for metals in the Olympic Dam Cu–Au Province and the Central Gawler Gold Province, as evidenced by the association of juvenile isotopes with increasing Cu and Au abundance (Budd and Skirrow 2007; Skirrow et al. 2007). Our new data suggest that a metasomatised, subduction-modified subcontinental lithospheric mantle is the most prominent geochemical group and appears to be associated with both IOCG and gold-dominated mineralisation styles.

Subduction and metasomatism have been recognised as being important processes to generate metal enrichment in the mantle (Richards 2009; Groves et al. 2010; Tassara et al. 2017), resulting in residual siderophile and chalcophile-rich zones or veins in the subcontinental lithospheric mantle. These zones or veins may constitute a viable source

New geology

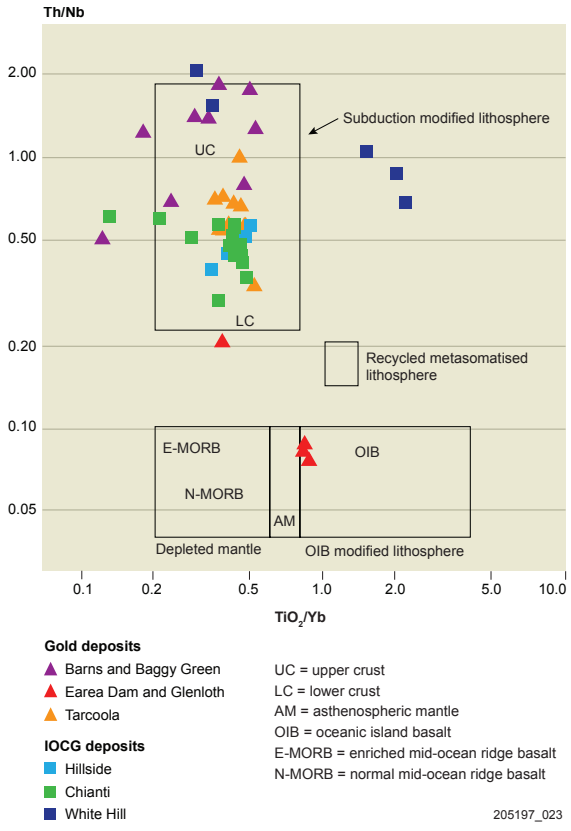

Figure 5 *Th/Nb vs TiO_2/Yb plot of Pearce, Ernst and Peate (2015) showing different mantle source regions and the association of mafic Hiltaba Suite dykes correlated with gold and IOCG deposits in a subduction-modified lithosphere.*

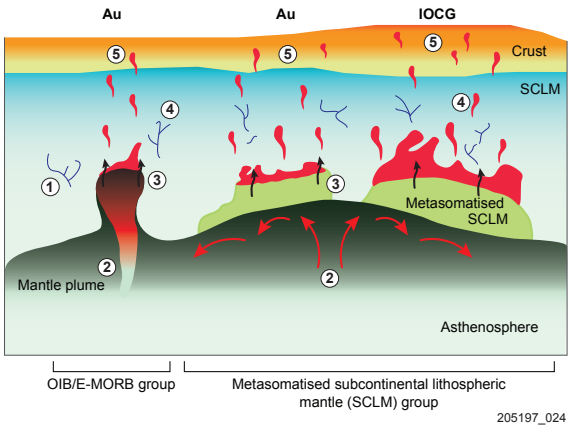

for Cu and Au, which are able to be remobilised by fertile and hydrous magmas (e.g. Hiltaba Suite) during partial melting of the subcontinental lithospheric mantle (Fig. 6). Generation of the IOCG and gold-dominated mineralisation in the Gawler Craton may be related to remelting of such a long-lived, subduction-modified metasomatised subcontinental lithospheric mantle (Fig. 6).

In contrast, the gold-related Earea Dam and Glenloth samples have low Th/Nb ratios (<0.10) and geochemical compositions consistent with an oceanic island basalt (OIB) source (Fig. 5). These samples may in fact represent a juvenile mantle source such as would be expected of a mantle plume (Paces and Bell 1989; Hart et al. 1992; Hastie et al. 2016). Although not as widespread or as strongly linked to economically significant mineralisation, the presence of these juvenile and OIB-like mafic rocks may be indicative of the occurrence of a mantle plume or lithospheric delamination event that may have affected the Gawler Craton (Skirrow et al. 2018). Such major geodynamic events could have been responsible for the melting of the pre-existing, subduction-modified subcontinental lithospheric mantle and the associated migration of metals and magmas into the crust to form the mineral deposits of the Gawler Craton.

Further work is underway to focus on determining metal sources by combining trace and rare earth element chemistry of minerals and in situ mineral isotope analysis to assess magma petrogenesis and an indicator of magmatic potential to contribute to deposit formation in the Gawler Craton.

Acknowledgements

This research is a part of PhD project (C Wade) in the Source to Spectrum Australian Research Council Linkage Project (LP160100578) supported by the Geological Survey of South Australia, Fortescue Metals Group, Minotaur Exploration Ltd, Investigator Resources Ltd and Rex Minerals Ltd.

Figure 6 *Conceptual model for the formation of c. 1590 Ma Gawler Craton Au and IOCG mineral systems.*

1 *Multiple previous metasomatic events create siderophile and chalcophile-rich zones or veins in the SCLM.*
2 *Upwelling asthenospheric mantle and a mantle plume invoke partial melting of metasomatised SCLM and SCLM respectively.*
3 *Subsequently hydrous and fertile magmas (mafic Hiltaba Suite) are produced by such partial melting.*
4 *Au and Cu stored in the SCLM are remobilised by mafic magmas of the Hiltaba Suite.*
5 *Formation of Au and IOCG mineral deposits in upper crust.*

References

Budd A 2006. The Tarcoola Goldfield of the Central Gawler Gold Province, and the Hiltaba Association Granites, Gawler Craton, South Australia. PhD thesis, Australian National University, Canberra.

Budd AR and Skirrow RG 2007. The nature and origin of gold deposits of the Tarcoola Goldfield and implications for the Central Gawler Gold Province, South Australia. *Economic Geology* 102:1541–1563.

Cai Y-C, Fan H-R, Santosh M, Liu X, Hu F-F, Yang K-F, Lan T-G, Yang Y-H and Liu Y 2013. Evolution of the lithospheric mantle beneath the southeastern North China Craton: constraints from mafic dikes in the Jiaobei terrain. *Gondwana Research* 24:601–621.

Condie KC and Shearer CK 2017. Tracking the evolution of mantle sources with incompatible element ratios in stagnant-lid and plate-tectonic planets. *Geochimica et Cosmochimica Acta* 213:47–62.

Frost A 2009. Petrogenesis, modelling and characterisation of layered mafic intrusions White Hill and Peculiar Knob North within the Mount Woods Inlier, South Australia. Hons thesis, Macquarie University, Sydney.

Goodenough KM, Upton BGJ and Ellam RM 2002. Long-term memory of subduction processes in the lithospheric mantle: evidence from the geochemistry of basic dykes in the Gardar Province of South Greenland. *Journal of the Geological Society* 159:705–714.

Groves DI, Bierlein FP, Meinert LD and Hitzman MW 2010. Iron oxide copper-gold (IOCG) deposits through earth history: implications for origin, lithospheric setting, and distinction from other epigenetic iron oxide deposits. *Economic Geology* 105:641–654.

Hart SR, Hauri EH, Oschmann LA and Whitehead JA 1992. Mantle plumes and entrainment: isotopic evidence. *Science* 256:517–520.

Hastie AR, Fitton JG, Kerr AC, McDonald I, Schwindrofska A and Hoernle K 2016. The composition of mantle plumes and the deep earth. *Earth and Planetary Science Letters* 444:13–25.

Paces JB and Bell K 1989. Non-depleted sub-continental mantle beneath the Superior Province of the Canadian Shield: Nd-Sr isotopic and trace element evidence from midcontinent rift basalts. *Geochimica et Cosmochimica Acta* 53:2023–2035.

Pearce JA, Ernst RE and Peate DW 2015. A geochemical proxy approach to LIP forensics. *Abstracts - Geological Association of Canada* 38.

Reid A 2019. The Olympic Cu-Au Province, Gawler Craton: a review of the lithospheric architecture, geodynamic setting, alteration systems, cover successions and prospectivity. *Minerals* 9(6), 371. (Open access)

Richards JP 2009. Postsubduction porphyry Cu-Au and epithermal Au deposits: products of remelting of subduction-modified lithosphere. *Geology* 37:247–250.

Sandeman HA, Cousens BL and Hemmingway CJ 2003. Continental tholeiitic mafic rocks of the Paleoproterozoic Hurwitz Group, Central Hearne sub-domain, Nunavut: insight into the evolution of the Hearne sub-continental lithosphere. *Canadian Journal of Earth Sciences* 40:1219–1237.

Skirrow R, van der Wielen SE, Champion DC, Czarnota K and Thiel S 2018. Lithospheric architecture and mantle metasomatism linked to iron-oxide Cu-Au ore formation: multidisciplinary evidence from the Olympic Dam region, South Australia. *Geochemistry, Geophysics, Geosystems* 19.

Skirrow RG, Bastrakov E, Barovich K, Fraser G, Fanning CM, Creaser R and Davidson G 2007. Timing of iron oxide Cu-Au-(U) hydrothermal activity and Nd isotope constraints on metal sources in the Gawler Craton, South Australia. *Economic Geology* 102:1441–1470.

Tassara S, González-Jiménez JM, Reich M, Schilling ME, Morata D, Begg G, Saunders E, Griffin WL, O'Reilly SY, Grégoire M, Barra F and Corgne A 2017. Plume-subduction interaction forms large auriferous provinces. *Nature communications* 8:843–843.

Wade CE, Payne JL, Barovich KM and Reid AJ 2019. Heterogeneity of the sub-continental lithospheric mantle and 'non-juvenile' mantle additions to a Proterozoic silicic large igneous province. *Lithos* 340-341:87–107.

Walter MJ 2014. 3.10 - Melt extraction and compositional variability in mantle lithosphere. In HD Holland and KK Turekian eds, *Treatise on geochemistry.* 2nd edn. Elsevier, pp. 393–419.

FURTHER INFORMATION

Claire Wade
Claire.Wade@sa.gov.au